



GEOLOGICAL SURVEY OF CANADA
COMMISSION GÉOLOGIQUE DU CANADA

PAPER
ÉTUDE 80-1A

This document was produced
by scanning the original publication.

Ce document est le produit d'une
numérisation par balayage
de la publication originale.

**CURRENT RESEARCH
PART A**

**RECHERCHES EN COURS
PARTIE A**



Energy, Mines and
Resources Canada

Énergie, Mines et
Ressources Canada

1980

Notice to Librarians and Indexers

The Geological Survey's thrice-yearly *Current Research* series contains many reports comparable in scope and subject matter to those appearing in scientific journals and other serials. All contributions to the Scientific and Technical Report section of *Current Research* include an abstract and bibliographic citation. It is hoped that these will assist you in cataloguing and indexing these reports and that this will result in a still wider dissemination of the results of the Geological Survey's research activities.

Avis aux bibliothécaires et préparateurs d'index

La série Recherches en cours de la Commission géologique paraît trois fois par année; elle contient plusieurs rapports dont la portée et la nature sont comparable à ceux qui paraissent dans les revues scientifiques et autres périodiques. Tous les articles publiés dans la section des rapports scientifiques et techniques de la publication Recherches en cours sont accompagnés d'un résumé et d'une bibliographie, ce qui vous permettra, nous l'espérons, de cataloguer et d'indexer ces rapports, d'où une meilleure diffusion des résultats de recherche de la Commission géologique.

Technical editing and compilation *Rédaction et compilation techniques*

R.G. Blackadar
P.J. Griffin
H. Dumych
E.R.W. Neale

Production editing and layout *Préparation et mise en page*

Leona R. Mahoney
Lorna A. Firth
Michael J. Kiel

Typed and checked by *Dactylographie et vérification*

Debby Busby
Judy Côté
Jane Desautels
Susan Gagnon
Janet Gilliland
Sharon Parnham



**GEOLOGICAL SURVEY
PAPER 80-1A
COMMISSION GÉOLOGIQUE
ÉTUDE 80-1A**

CURRENT RESEARCH PART A

RECHERCHES EN COURS PARTIE A

1980

© Minister of Supply and Services Canada 1980

Available in Canada through

authorized bookstore agents
and other bookstores

or by mail from

Canadian Government Publishing Centre
Supply and Services Canada
Hull, Québec, Canada K1A 0S9

and from

Geological Survey of Canada
601 Booth Street
Ottawa, Canada K1A 0E8

A deposit copy of this publication is also available
for reference in public libraries across Canada

Cat. No. M44-80/1AE Canada: \$7.50
ISBN-- 0-660-10481-4 Other Countries: \$9.00

Price subject to change without notice

Geological Survey of Canada – *Commission géologique du Canada*

D.J. McLAREN
Director General
Directeur général

J.G. FYLES
Chief Geologist
Géologue en chef

E. HALL
Scientific Executive Officer
Agent exécutif scientifique

M.J. KEEN
Director, Atlantic Geoscience Centre, Dartmouth, Nova Scotia
Directeur du Centre géoscientifique de l'Atlantique, Dartmouth (Nouvelle-Écosse)

J.A. MAXWELL
Director, Central Laboratories and Technical Services Division
Directeur de la Division des laboratoires centraux et des services techniques

R.G. BLACKADAR
A/Director, Geological Information Division
Directeur intérim. de la Division de l'information géologique

D.F. STOTT
Director, Institute of Sedimentary and Petroleum Geology, Calgary, Alberta
Directeur de l'Institut de géologie sédimentaire et pétrolière, Calgary (Alberta)

J.E. RIESOR
Director, Precambrian Geology Division
Directeur de la Division de la géologie du Précambrien

A.G. DARNLEY
Director, Resource Geophysics and Geochemistry Division
Directeur de la Division de la géophysique et de la géochimie appliquées

J.S. SCOTT
Director, Terrain Sciences Division
Directeur de la Division de la science des terrains

G.B. LEECH
Director, Economic Geology Division
Directeur de la Division de la géologie économique

R.B. CAMPBELL
Director, Cordilleran Geology Division, Vancouver, British Columbia
Directeur de la Division de la géologie de la Cordillère, Vancouver (Colombie-Britannique)

Separates

A limited number of separates of the papers that appear in this volume are available by direct request to the individual authors. The addresses of the Geological Survey of Canada offices follow:

601 Booth Street,
OTTAWA, Ontario
K1A 0E8

Institute of Sedimentary and Petroleum Geology,
3303-33rd Street N.W.,
CALGARY, Alberta
T2L 2A7

Cordilleran Geology Division
100 West Pender Street,
VANCOUVER, B.C.
V6B 1R8

Atlantic Geoscience Centre,
Bedford Institute of Oceanography,
P.O. Box 1006,
DARTMOUTH, N.S.
B2Y 4A2

When no location accompanies an author's name in the title of a paper, the Ottawa address should be used.

Tirés à part

On peut obtenir un nombre limité de "tirés à part" des articles qui paraissent dans cette publication en s'adressant directement à chaque auteur. Les adresses des différents bureaux de la Commission géologique du Canada sont les suivantes:

*601, rue Booth
OTTAWA, Ontario
K1A 0E8*

*Institut de géologie sédimentaire et pétrolière
3303 N. - O., 33rd, ST. N.W.,
CALGARY, Alberta
T2L 2A7*

*Division de la géologie de la Cordillère
100 West Pender Street
VANCOUVER, Colombie-Britannique
V6B 1R8*

*Centre géoscientifique de l'Atlantique
Institut océanographique de Bedford
B.P. 1006
DARTMOUTH, Nouvelle-Ecosse
B2Y 4A2*

Lorsque l'adresse de l'auteur ne figure pas sous le titre d'un document, on doit alors utiliser l'adresse d'Ottawa.

SCIENTIFIC AND TECHNICAL REPORTS RAPPORTS SCIENTIFIQUES ET TECHNIQUES

ECONOMIC GEOLOGY/GÉOLOGIE ÉCONOMIQUE

	Page
M.L. ATKINSON and D.H. WATKINSON: Copper mineralization and hydrothermal alteration of volcanic rocks at Bedford Hill, Noranda area, Québec	119
A.R. MILLER and J.A. KERSWILL: Elemental associations within Aphebian clastic redbeds, northern half of the Richmond Gulf area, New Quebec	271
S.I. SAIF: Petrographic and geochemical investigation of iron formation and other iron-rich rocks in Bathurst District, New Brunswick	309

GEOCHRONOLOGY/GÉOCHRONOLOGIE

G.P. BEAKHOUSE and R.H. McNUTT: Geochronological investigation of granitoid rocks at Redditt, northwestern Ontario: A preliminary report	57
H. GABRIELSE, R.K. WANLESS, R.L. ARMSTRONG, and L.R. ERDMAN: Isotopic dating of early Jurassic volcanism and plutonism in north-central British Columbia	27

GEOPHYSICS/GÉOPHYSIQUE

J.G. CONAWAY: Uranium concentrations and the system response function in gamma ray logging	77
R.L. GRASTY: Skyshine and the calibration of ground gamma ray spectrometers	133
A.K. SINHA: Electromagnetic resistivity mapping of the area around Alfred, Ontario, with Geonics EM 34 System	293

MARINE GEOSCIENCE/ÉTUDES GÉOSCIENTIFIQUE DU MILIEU MARIN

J.R. HARPER: Coastal processes on Graham Island, Queen Charlotte Islands, British Columbia	13
--	----

MINERALOGY/MINÉRALOGIE

J. RIMSAITE: Mineralogy of radioactive occurrences in the Grenville structural province, Bancroft area, Ontario: A progress report	253
--	-----

PALEONTOLOGY/PALÉONTOLOGIE

N.S. IOANNIDES and D.J. McINTYRE: A preliminary palynological study of the Caribou Hills outcrop section along the Mackenzie River, District of Mackenzie	197
T.P. POULTON: Trigoniid bivalves from the Bajocian (middle Jurassic) rocks of central Oregon	187
E.T. TOZER: New genera of Triassic Ammonoidea	107

PETROLOGY/PÉTROLOGIE

	Page
R.F. EMSLIE, B. COUSENS, C. HAMBLIN, and J. BIELECKI: The Mistastin Batholith, Labrador-Québec: An Elsonian composite rapakivi suite	95
E. FROESE: A reaction grid for medium grade mafic rocks	53
R.H. SUTCLIFFE and J.J. FAWCETT: Petrological studies on the Rainy Lake granitoid complex, northwestern Ontario: A preliminary evaluation	335

QUATERNARY GEOLOGY/GÉOLOGIE DU QUATERNAIRE

S.M. COSTACHUK: Heavy mineral analysis of southern Beaufort Sea sediments	241
T.J. DAY: A study of initial motion characteristics of particles in graded bed material ...	281
S.A. EDLUND: Vegetation of Lougheed Island, District of Franklin	329
P.A. EGGINTON: Determining river ice frequency from the tree record	265
J. ROSS MACKAY: Deformation of ice-wedge polygons, Garry Island, Northwest Territories	287

REGIONAL GEOLOGY/GÉOLOGIE RÉGIONALE

Appalachian Region/Région des Appalaches

K.L. CURRIE, G.E. PAJARI, JR., and R.K. PICKERILL: Comments on the boundaries of the Davidsville Group, northeastern Newfoundland	115
G.R. DUNNING and R.K. HERD: The Annieopsquotch ophiolite complex, southwest Newfoundland, and its regional relationships	227
D.P. KENNEDY: Geology of the Corner Brook Lake area, western Newfoundland	235
H. WILLIAMS and S.C. GODFREY: Geology of Stephenville map area, Newfoundland ...	217

Arctic Islands/Archipel Arctique

ULRICH MAYR, T.T. UYENO, R.S. TIPNIS, and C.R. BARNES: Subsurface stratigraphy and conodont zonation of the Lower Paleozoic succession, Arctic Platform, southern Arctic Archipelago	209
--	-----

Cordilleran Region/Région de la Cordillère

R.G. ANDERSON: Satellitic stocks, volcanic and sedimentary stratigraphy, and structure around the northern and western margins of the Hotailuh batholith, north-central British Columbia	37
R.L. BROWN: Frenchman Cap Dome, Shuswap Complex, British Columbia: A progress report	47
H. GABRIELSE and J.L. MANSY: Structural style in northeastern Cry Lake map area, north-central British Columbia	33
P.B. READ: Stratigraphy and structure: Thor-Odin to Frenchman Cap "Domes", Vernon east-half map area, southern British Columbia	19
J.G. SOUTHER: Geothermal reconnaissance in the central Garibaldi Belt, British Columbia	1

Precambrian Shield/Bouchier Précambrien	Page
K. ATTOH: Stratigraphic relations of the volcanic sedimentary successions in the Wawa greenstone belt, Ontario	101
W.R.A. BARAGAR and C.G. LAMONTAGNE: The Circum-Ungava belt in eastern Hudson Bay: The geology of Sleeper Islands and parts of the Ottawa and Belcher islands	89
H.H. BOSTOCK: Reconnaissance geology of the Fort Smith-Hill Island Lake area, Northwest Territories	153
K.D. CARD, J.A. PERCIVAL, and KENNETH COE: Progress report on regional geological synthesis, central Superior Province	61
F.W. CHANDLER, B.W. CHARBONNEAU, A. CIESIELSKI, Y.T. MAURICE, and S. WHITE: Geological studies of the Late Precambrian supracrustal rocks and underlying granitic basement, Fury and Hecla Strait area, Baffin Island, District of Franklin	125
J.B. HENDERSON and P.H. THOMPSON: The Healey Lake map area (northern part) and the enigmatic Thelon Front, District of Mackenzie	165
J.R. HENDERSON and C.R. TIPPETT: Foxe Fold belt in eastern Baffin Island, District of Franklin	147
P.F. HOFFMAN: Conjugate transcurrent faults in north-central Wopmay Orogen (early Proterozoic) and their dip-slip reactivation during post-orogenic extension, Hepburn Lake map area, District of Mackenzie	183
P.F. HOFFMAN: On the relative age of the Muskox Intrusion and the Coppermine River basalts, District of Mackenzie	223
P.F. HOFFMAN, M.R. ST-ONGE, R.M. EASTON, J. GROTZINGER and D.E. SCHULZE; Syntectonic plutonism in north-central Wopmay Orogen (early Proterozoic), Hepburn Lake map area, District of Mackenzie	171
G.D. JACKSON, T.R. IANNELLI, and B.J. TILLEY: Rift-related late Proterozoic sedimentation and volcanism on northern Baffin and Bylot islands, District of Franklin ..	319
A.N. LeCHEMINANT, A.R. MILLER, G.W. BOOTH, M.J. MURRAY, and G.A. JENNER: Geology of the Tebesjuak Lake map area, District of Keewatin: A progress report with notes on uranium and base metal mineralization	339
A.P. LICHTBLAU and E. DIMROTH: Stratigraphy and facies at the south margin of the Archean Noranda caldera, Noranda, Québec	69
VICTOR OWEN, E. DIMROTH and GERARD WOUSSEN: The old gneiss complex east of Chicoutimi, Québec	137
M.R. ST-ONGE and P.F. HOFFMAN; "Hot-side-up" and "hot-side-down" metamorphic isograds in north-central Wopmay Orogen, Hepburn Lake map area, District of Mackenzie	179
R. TIRRUL and I. BELL: Geology of the Anialik River greenstone belt, Hepburn Island map area, District of Mackenzie	157

GENERAL/GÉNÉRALITÉS

W.H. FRITZ: International Precambrian-Cambrian Boundary Working Group's 1979 field study to Mackenzie Mountains, Northeast Territories	41
T.M. GORDON: Manipulation and display of digital cartographic data	301

SCIENTIFIC AND TECHNICAL NOTES
NOTES SCIENTIFIQUES ET TECHNIQUES

	Page
H. GABRIELSE: Operation Dease	347
H. GABRIELSE: Operation Finlay	348
S. LEAMING: Studies of ultramafic rocks in Dease Lake area, British Columbia	349
J.L. MANSY: Structure of the Turnagain River pendant in northeastern Cry Lake map area, British Columbia	351
S.P. GORDEY: Stratigraphic cross-section, Selwyn Basin to Mackenzie Platform, Nahanni map area, Yukon Territory and District of Mackenzie	353
J.J. CASEY and C.M. SCARFE: Summary of the petrology of the Heart Peaks volcanic centre, northwestern British Columbia	356
DIRK TEMPELMAN-KLUIT: Highlights of field work in Laberge and Carmacks map areas, Yukon Territory	357
M.L. McARTHUR, R.S. TIPNIS, and C.I. GODWIN: Early and Middle Ordovician conodont fauna from the Mountain Diatrema, northern Mackenzie Mountains, District of Mackenzie	363
D.C. KAMINENI, P.A. BROWN, and DENVER STONE: Fracture filling material in the Atikokan area, northwestern Ontario	369
N.R. GADD: Iceflow patterns, Montreal-Ottawa Lowland areas	375
CLAUDE GAUTHIER: Existence of a central New Brunswick ice cap based on evidence of northwestward-moving ice in the Edmundston area, New Brunswick	377
P.A. BROWN, D.C. KAMINENI, DENVER STONE, and R.H. THIVIERGE: General geology of the Eye-Dashwa lakes pluton, Atikokan, northwestern Ontario	379
O.R. ECKSTRAND: Mineral assemblage polarity in magmatic sulphide blebs in a komatiitic nickel deposit	385
G.R. LACHANCE and R.M. ROUSSEAU: Theoretical aspects of enhancement coefficients in X-ray spectrometry	390

DISCUSSIONS AND COMMUNICATIONS
DISCUSSIONS ET COMMUNICATIONS

J.S. COLVILLE: A theoretical estimation of ion mobilities through glaciolacustrine sediments – Diffusion down a concentration gradient: Discussion	391
Note to Contributors	393
Author Index	395

SCIENTIFIC AND TECHNICAL REPORTS

RAPPORTS SCIENTIFIQUES ET TECHNIQUES

1. GEOTHERMAL RECONNAISSANCE IN THE CENTRAL GARIBALDI BELT, BRITISH COLUMBIA

Projects 730067, 770001

J.G. Souther
Cordilleran Geology Division, Vancouver

Souther, J.G., Geothermal reconnaissance in the central Garibaldi Belt, British Columbia; in Current Research, Part A, Geological Survey of Canada, Paper 80-1A, p.1-11, 1980.

Abstract

The central part of the Cenozoic Garibaldi Belt includes seven volcanic complexes that extend south from Meager Mountain. They have erupted lavas ranging in composition from augite, olivine basalt through hypersthene andesite and dacite, to biotite rhyodacite. Many of the centres are characterized by subglacial, ice-contact features but preglacial and postglacial phases are also present. The north-northwesterly trend of the belt reflects young structures in the underlying Mesozoic to Tertiary plutonic and metamorphic rocks of the Coast Plutonic Complex. Hydrothermal alteration associated with these structures plus the discovery of thermal springs near Mt. Cayley suggest that reservoirs of residual heat, similar to those being developed at Meager Mountain, may also be present in the central Garibaldi Belt.

Introduction

The Cenozoic Garibaldi volcanic belt is a continuation of the High Cascades of the western United States. It extends from Mount Garibaldi, at the head of Howe Sound, northward for 120 km to Meager Mountain near the head of Lillooet River, a region underlain by Mesozoic to Tertiary granitic and metamorphic rocks of the Coast Plutonic Complex. The volcanic belt includes at least twelve complexes which range in composition from high-alumina basalt to rhyolite and in structure from isolated single flows to complex multiple domes, stratovolcanoes, clusters of pyroclastic cones, spines, tuyas and other subglacial forms. Much of the activity occurred during the Pleistocene but the oldest stages are known to go back at least to Pliocene time, and the most recent activity, eruption of the Bridge River ash from Meager Mountain, occurred about 2400 years ago (Nasmith et al., 1967; Read, 1978).

The possibility of an active geothermal system related to Garibaldi group volcanoes was recognized as early as 1973 (Nevin et al., 1975; Souther, 1975; Lewis and Souther, 1978) when both the Geological Survey and British Columbia Hydro and Power Authority independently began reconnaissance programs. Mount Garibaldi itself and the cluster of centres that surround it lie within Garibaldi Provincial Park and are thus excluded from direct geothermal exploration. However, this part of the belt has received the most intense geological, petrographic and chemical study (Mathews, 1958; Green, 1977) and thus provides a useful model of the style and setting of volcanism in the belt as a whole. The main focus of geothermal exploration has been at Meager Mountain where in 1978 the Energy, Mines and Resources and B.C. Hydro programs were combined into a unified, joint venture. During the early years of the program geological mapping (Read, 1978), water geochemistry and geothermometry (Hammerstrom and Brown, 1977), self-potential, resistivity (Shore, 1978) and magnetotelluric (Ngoc, 1976) surveys confirmed the possibility of anomalously high subsurface temperatures. Subsequently more detailed resistivity studies and shallow drilling have defined two thermal reservoirs each with temperatures known to be above 100°C at less than 500 m below the surface. Drilling in 1979 encountered water at 140°C at a depth of less than 150 m. The threshold temperature for production of steam at turbine pressure is 150°C, thus the possibility of power generation at Meager Mountain appears to be good enough to warrant the drilling of a deep (± 1200 m) test well.

With Meager Mountain approaching the final exploration stage, this study was initiated to examine the potential of other young volcanic centres that lie between Garibaldi Park and Meager Mountain. Little work has been done on this central part of the belt which includes at least seven young volcanic piles. This preliminary report is based on two weeks' field work and a cursory examination of one or two thin sections from each of the piles visited. Further work, including detailed surface mapping, hydrological, geochemical and isotope studies, is planned for the summer of 1980.

The seven complexes described here (Fig. 1.1) lie in a north-south belt along the ice-covered height of land between Cheakamus and Squamish River valleys. Logging roads provide access to within a few kilometres of most of the centres, but extreme local relief and precipitous slopes on the volcanics edifies themselves pose severe restrictions on future exploration and development.

Basement Rocks

The geological map of Pemberton area (Woodsworth, 1977) shows the entire central Garibaldi Belt to be underlain by plutonic rocks, mainly quartz diorite of unknown age. No attempt was made, during the present study, to further subdivide these rocks except in the vicinity of Mt. Cayley (Fig. 1.2). There, the basement rocks can be grouped into three distinct assemblages. The oldest (unit 1) comprises a large pendant of metasediments including quartz mica schist, greenstone, amphibolite gneiss and crystalline limestone. The latter is intensely deformed but provides a useful horizon marker that can be traced around the crests of near-isoclinal, east-west trending folds.

The metasediments are closely associated with and appear to be gradational with a hornblende-rich complex (unit 2) of quartz diorite, diorite and minor amphibolite. These rocks are commonly foliated, contain numerous mafic inclusions and dyke swarms, and locally have distinct gneissic layering. Contacts between unit 2 and hornblende, biotite granodiorite (unit 3) are sharp. The granodiorite is a relatively uniform, poorly foliated, medium-grained rock that underlies much of the northern part of the volcanic belt. It is cut by a large pluton (unit 4) of clean, pinkish white, coarse- to medium-grained quartz monzonite.

The only basement structures that appear to be related to the volcanic belt are north-northwesterly trending, gouge-filled fractures. These are best developed near Mount Cayley, where they are associated with hydrothermal alteration, but fractures having similar orientation were noted south of Mount Fee and between Mount Cayley and Cauldron Dome.

Mount Fee Complex

Mount Fee (Fig. 1.2) is a narrow elliptical spine of rhyodacite about 1.0 kilometre long and 0.25 kilometre across at its widest point. The massive, sparsely jointed rock forms a series of near-vertical towers that rise 100 to 150 m above the ridge itself. Most of the summit ridge is a denuded neck of intrusive, pale grey porphyritic rhyodacite with abundant randomly oriented phenocrysts of glassy feldspar and sparse

tiny books of biotite. The mantle of pyroclastics that must once have enclosed it has been completely stripped away except for a small remnant on the western side and along the northern end where the lip of the conduit is exposed in cross-section. Contacts are nearly vertical. Along them the granitic wall rock has been shattered and granulated for several feet and the adjacent rhyodacite is quenched to a narrow (40-50 cm) selvage of granular, porphyritic glass.

At its northern end the intrusive spine wedges out and appears to cut a coarse, blocky tuff-breccia which, in turn, is overlain by thick flows. The extrusive rock is similar to that of the central spine except for slightly greater oxidation which gives it a faint purplish cast that contrasts with the nearly white rock of the neck itself. The root-zone of these flows is well exposed on the headwall of a small cirque on the east side of the summit ridge. On the southern spur of the cirque massive rhyodacite of the central spine extends down to the glacier ice, whereas basement quartz diorite, exposed on the north spur to within 30 m of the ridge crest, must be the northern rim of the main conduit. It is overlain successively by 2 to 4 m of angular colluvium comprising blocks of basement rocks only; about 2 m of brown, altered lapilli and ash; and 5 to 6 m of punky breccia comprising dark angular chunks of rhyodacite in a pale grey, lightly welded matrix. The breccia is overlain by columnar-jointed, purplish grey, rhyodacite lava flows. These extend eastward into the head of Brandywine Creek, dropping from an elevation of 2225 m on the ridge to 945 m in less than 2 km. They are confined to a single, steep-sided ridge which, from the pattern of jointing, appears to comprise a single cooling unit about 150 m thick, plus two or three much thinner flows near the base. On the south side of this ridge the lava is underlain by and interlayered with steep, northerly dipping beds of coarse blocky breccia similar to the basal breccia on the northern rim of the summit ridge. Both are probably part of a steep-sided pyroclastic cone which formed during the initial stages of activity and later acted as a barrier that diverted the massive effusion of viscous lava into a channel around the north edge of the cone. Intrusion of the central spine of viscous rhyodacite appears to have been the culminating event in the Mount Fee activity. It cuts the early-formed breccia and was probably initially completely enclosed by it. Pelean spines may have projected above the pyroclastic pile during intrusion of the neck but none are preserved. The existing towers and spires are erosional remnants bounded by joint planes. The absence of quench features as well as the absence of a till layer under the Mount Fee flows, suggest that they are preglacial. A relatively old age is also consistent with the nearly complete denudation of the central spine.

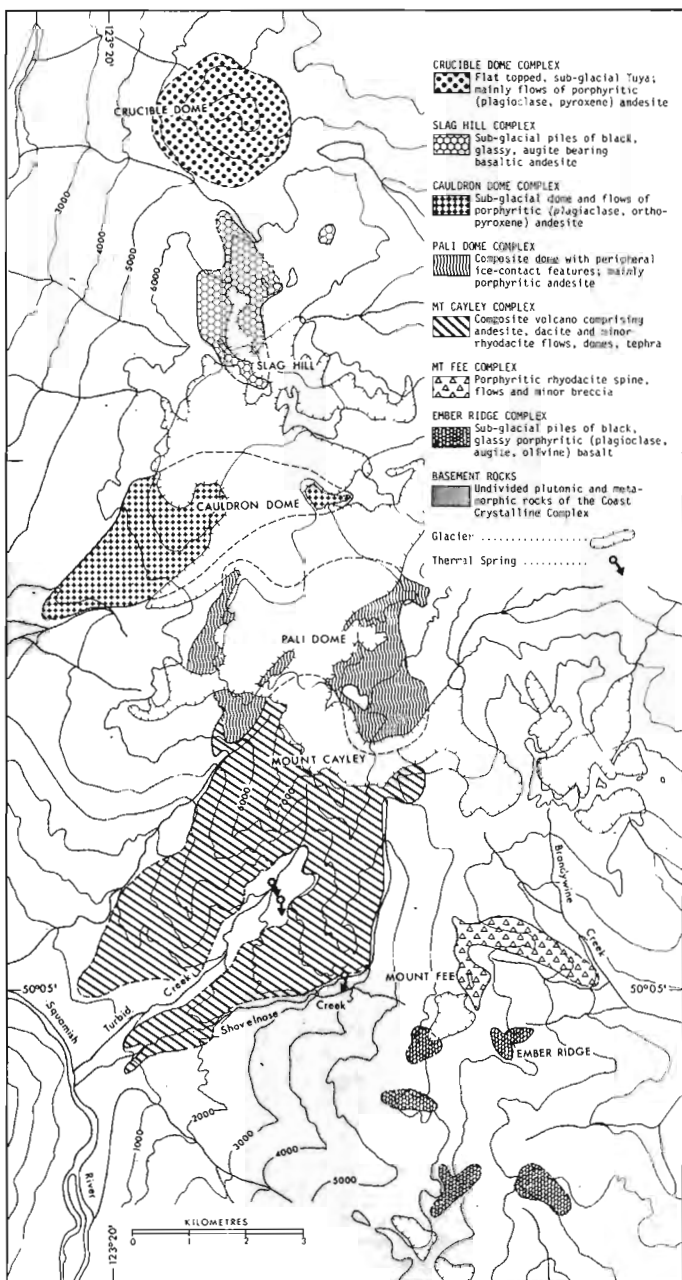


Figure 1.1. Location map showing the distribution of Cenozoic volcanic rocks in the central Garibaldi Belt.

Ember Ridge Complex

Five small patches of medium grey, aphanitic to vitreous, hornblende-bearing basalt outcrop on the ridge south of Mount Fee. Each is characterized by an unique colloform surface, resulting from the overlapping and interfingering of large steeply inclined bulbous cooling units (Fig. 1.3). Individual flows, up to 60 m thick, are separated by deep furrows which locally well out into small elliptical glass-lined caverns. Jointing, though extremely complex, is approximately normal to the bulbous flow surfaces defined by the furrows. The columns are uniformly small, from 7 to 20 cm across, and tend toward three-dimensional polygonal forms typical of quenched lavas (Fig. 1.4). The similarity in lithology and structure suggests that the five piles are approximately coeval and that they originated from a common source at depth. However, they are believed to have issued from separate vents. The activity almost certainly occurred during a period of extensive ice cover causing the rapidly quenched lava to pile up in the form of steep-sided exogenous domes directly over the vents.

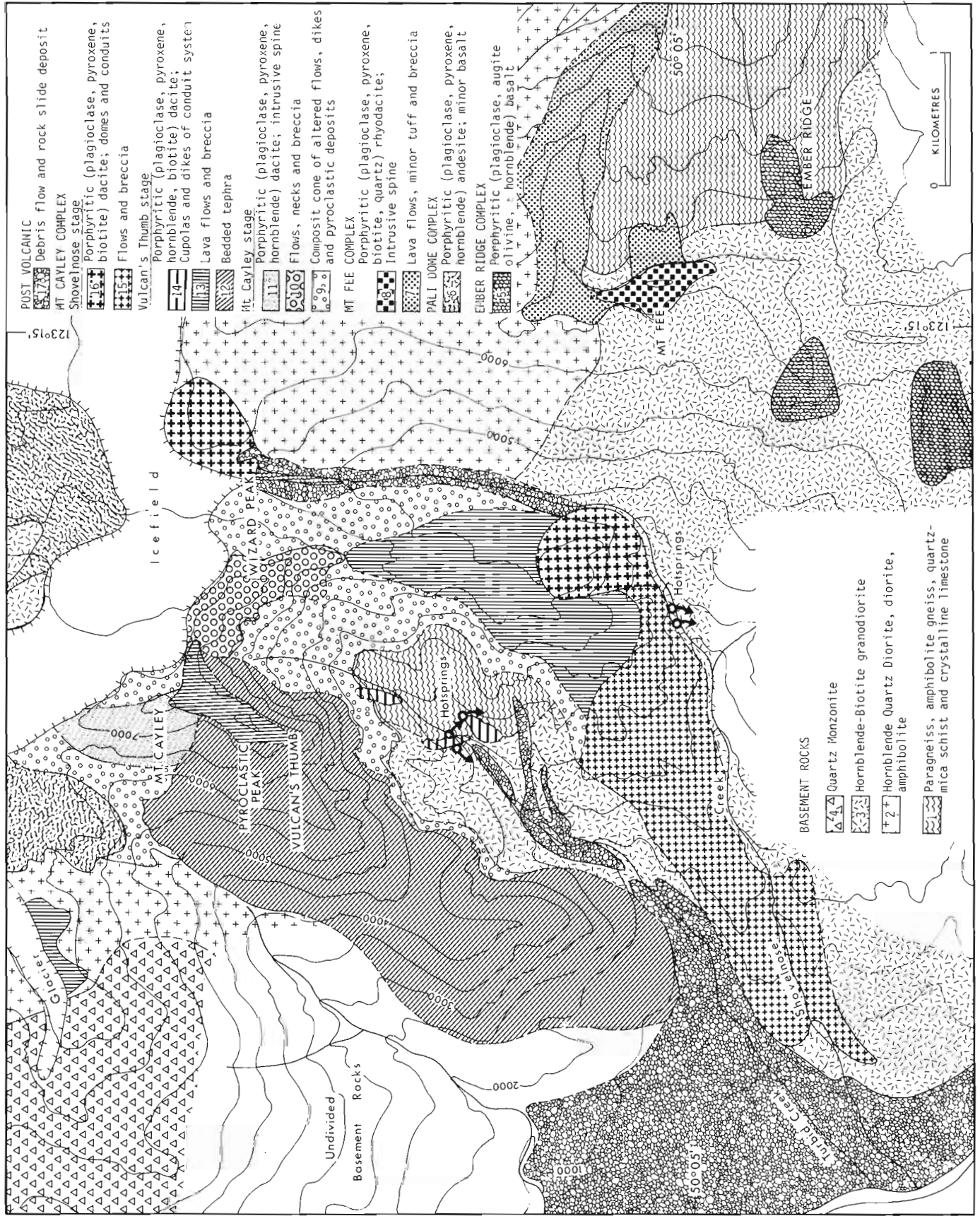


Figure 1.2. Geological map of Mount Cayley and adjacent areas.



Figure 1.4. Detail of jointing in glassy basalt of Ember Ridge. Note small, polygonal forms typical of quenched lava.



Figure 1.3. View of Ember Ridge showing bulbous, overlapping masses of quenched basalt.



Figure 1.5. Stereogram of Phyroclastic Peak (left) and Wizard Peak (right). Prominent spire in foreground is the Vulcan's Thumb. The light coloured rocks in upper Turbid Creek (lower right) are altered flows and breccias of unit 9. Note the sharp contact with overlying massive flows of Wizard Peak (unit 10) and Pyroclastic Peak (unit 13).

The largest of the three domes is exposed through a vertical distance of about 300 m at the head of Brandywine Creek. It rests on complexly folded crystalline limestone and amphibolite gneiss (unit 1) which is intensely fractured, silicified and pyritized along a prominent east-west zone parallel to the southern contact of the truncated dome. Fractures in the deeper part of this zone are mainly filled with colloform silica and minor calcite, and the adjacent rock is bleached and pyritized. Higher in the zone the percentage of open, calcite-lined fractures increases and silica is less abundant. Near the top of the ridge the old pre-volcanic surface is exposed beneath flows that spread laterally from the top of the dome. There the upward extension of the fracture system is expressed as subvertical solution channels in the marble. These are from a few centimetres to more than 30 cm across and can be traced one or two metres below the old surface. If this karst-like topography is a surface expression of the deeper fractures, then the hydrothermal system that formed them must have been active immediately prior to and possibly after eruption of the adjacent dome. It seems probable that the heat source driving the hydrothermal system was, in fact, the rising column of basalt that eventually erupted to form the dome.

Mount Cayley Complex

Mount Cayley, the largest volcano in the central Garibaldi belt, is a composite pile formed during at least three distinct stages of activity.

Mount Cayley Stage

The earliest or Mount Cayley stage, produced a composite pile of porphyritic dacite flows, tephra and breccia. The lower unit (No. 9) comprises a thick south-westerly dipping prism of flows and tephra cut by numerous dykes and sills. The rock has undergone varying degrees of hydrothermal alteration which impart a light yellow, ochre or red colour to most outcrops (Fig. 1.5). On the northwest side of Turbid Creek the basal flow of this unit is separated from unaltered basement granodiorite by about 25 m of well-indurated, unstratified fossil colluvium. Clasts in the lower 15 m of this deposit are derived entirely from basement and include subrounded boulders up to one metre across. Most of the closely packed clasts are 5 to 20 cm across, subrounded to angular, and randomly oriented. The sparse matrix comprises sand-sized rock fragments rather than clay or silt, suggesting that the deposit is not of glacial origin but rather a mixture of talus, outwash and slide debris that mantled the western-sloping, prevolcanic surface. The first volcanic clasts, small chips of white altered rhyolite, appear about 10 m from the top of the deposit. These increase in size and number upward, grading into a volcanic breccia comprising angular chips and clasts of white to reddish brown layered rhyolite. The basal flow, a thick pale grey dacite flecked with rusty alteration spots, rests directly on the bleached upper surface of this breccia. No glass or colonnade is developed along its base.

The altered rocks of unit 9 are overlain by massive flows of fresh porphyritic (plagioclase, hypersthene, hornblende) dacite (unit 10) which forms the upper 500 m of Wizard Peak (Fig. 1.5). Individual cooling units are up to 150 m thick and dip steeply southeast away from Mount Cayley (Fig. 1.6). The narrow serrated ridge of Mount Cayley itself is an intrusive spine of similar porphyritic dacite (unit 11) which cuts pyroclastic deposits of unit 9 (Fig. 1.7). The nearly vertical contacts are well exposed along the eastern and northern faces of the summit ridge, where the pyroclastic beds have either been truncated or more commonly tilted up to conform with the intrusive contact (Fig. 1.8). The pyroclastics are stained red for about 50 cm

along the contact and the adjacent rhyodacite is quenched to black vitreous glass. At several places the enclosing pyroclastics have fallen away from the intrusive contact revealing a smooth convex vitreous surface with prominent horizontal crenulations from 3 to 4 cm across (Fig. 1.9). The quenched zone, which varies from 1 to 3 m thick, is characterized by concentric fractures parallel to the convex outer surface. These are from 10 to 30 cm apart and give the outcrop a layered aspect resembling the skin of a giant onion. Well-developed rectangular joints have formed within each layer normal to its bounding surfaces. Intrusion of this spine of dacite is believed to be the culminating event of the Mount Cayley stage of activity.

Vulcan's Thumb Stage

Vulcan's Thumb is the largest in a cluster of slender pinnacles that rise from the precipitous summit ridge of Pyroclastic Peak (Fig. 1.5). It is a remnant of vent breccia deposited in the upper part of a composite volcano that was superimposed on the steep southwestern flank of the older Mount Cayley edifice during the Vulcan's Thumb stage of activity. Massive lavas and blocky, agglutinated breccias of porphyritic (plagioclase, hypersthene, hornblende, biotite) dacite (unit 13) form most of the lower and central part of the pile. Massive cooling units, up to 130 m thick cling precariously to 60° slopes on the northwest side of the peak, whereas nearly vertical fluted cliffs on the southeast, Turbid Creek, side truncate both flows and breccias in the central conduit region of the volcano. There the base of the Vulcan's Thumb pile rests on a steep westerly dipping surface that truncates older, Mount Cayley stage deposits, and laps onto the old basement surface.

The central pile of Vulcan's Thumb lavas and breccia is overlain and flanked by patches of unconsolidated, bedded tephra (unit 12). These are believed to be remnants of a once extensive tephra cone that formerly mantled most of the Vulcan's Thumb edifice and the surrounding older rocks. An 130 m thick section of blocky tuff breccia in the saddle between Mount Cayley and Wizard Peak laps unconformably against these two older piles and grades into agglutinated, poorly stratified breccia on the summit of Pyroclastic Peak. It consists of angular blocks of porphyritic, biotite-bearing dacite up to 50 cm across, suspended in a nearly white matrix of lapilli and ash. Bedding, due mainly to size-sorting, is prominent both in the summit ridge deposits and in a much larger remnant on the east side of Turbid Creek where at least 600 m of alternately coarse and fine tephra forms steep, unstable slopes.

Rapid erosion in upper Turbid Creek has cut through the volcanic pile and excavated a 300 m deep canyon into the underlying basement rocks. Within this canyon three cupolas and several smaller tabular bodies of biotite-bearing porphyritic dacite (unit 14) are exposed. Contacts with the basement rocks are sharp, planar or broadly convex surfaces along which the basement gneiss and granodiorite are intensely fractured or granulated over a width of 5 to 15 cm and the adjacent dacite is quenched to black vitreous glass. The vitreous selvage varies from a few centimetres to more than a metre thick and, like the outer skin of the Mount Cayley spire, its smooth glassy surface is ribbed with subhorizontal crenulations. The presence of biotite in these subvolcanic intrusions suggests that they are related to the biotite-bearing, Vulcan's Thumb dacite.

Shovelnose Stage

Two small domes (unit 16) each slightly more than half a kilometre in diameter, are exposed in the upper part of Shovelnose valley, and related flows (unit 15) extend down Shovelnose Creek almost to Squamish River.

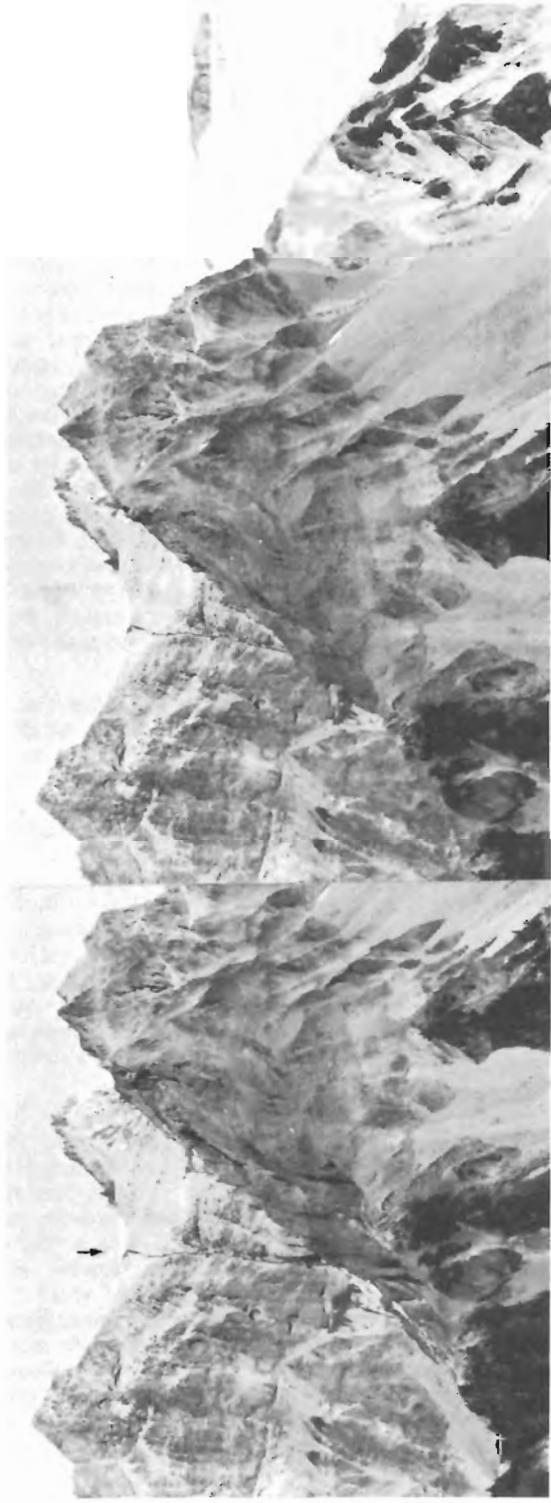


Figure 1.6. Stereogram of Pyroclastic Peak (left), Mount Cayley (centre), and Wizard Peak (right). The small stream (arrow) that cuts across unconsolidated tephra beds between Mount Cayley and Pyroclastic Peak drains a small lake perched on the ridge and descends into upper Turbid Creek. (see text, geological hazards.)



Figure 1.7. View of Mount Cayley showing contact between massive, intrusive dacite of the summit ridge (unit 11) and pyroclastic deposits (unit 9) in foreground and on eastern face.



Figure 1.8. Contact between dacite (right) of Mount Cayley intrusive spine and pyroclastic deposits of unit 9 (left). A 30 cm layer of black glass with transverse joints lies along contact.



Figure 1.9

Detail of quenched selvage of the Mount Cayley intrusive spine showing horizontal crenulations. Surface to right of hammer is the actual vitreous surface of the intrusion from which the enclosing pyroclastic deposits have fallen away.

The more northerly dome is a steep-sided symmetrical exogenous mass of porphyritic (plagioclase, hypersthene, biotite) dacite. A prominent colonnade is developed in quenched dacite along the southern base of the dome. It rests on blocky, bedded tephra which in turn is separated from basement diorite by up to 12 m of boulder till comprising only basement clasts.

The second dome, an endogenous mass of similar dacite, has been dissected by Shovelnose Creek, revealing complex tiers of radiating, small diameter, columns throughout the entire 400 m high cliffs on its eastern side. Most of the remaining mass of the dome is intrusive into, and quenched against, tephra deposits of unit 12. However, its missing eastern side may have breached the surface during its emplacement. The age relationship of this dome to flows of similar composition (unit 15) in Shovelnose Creek is not known. It seems probable that the eruptive event began with effusion of the flows and culminated with emplacement of the dome.

Thermal Springs

Two groups of thermal springs were discovered within the Mount Cayley complex. A group of three springs and numerous seeps in upper Turbid Creek are associated with cupolas of Vulcan's Thumb dacite. In fact, each of the three major springs issue from fractures in the contact zones of cupolas. Numerous additional cold seeps issue from hydrothermally altered, gouge-filled fractures in the surrounding basement rock. These fractures, which consistently trend between 150° and 180°, are abundant in upper Turbid Creek but are less common elsewhere. They are probably due to expansion of the roof-rocks above intrusive masses of dacite. The group of two springs and associated seeps in Shovelnose Creek issue from basement rocks near the southern intrusive margin of the Shovelnose endogenous dome.

Each of the main thermal springs has built extensive tufa and sinter deposits, whereas the cold seeps are precipitating bright red ferruginous ochre. Preliminary temperature measurements indicate a range from about 18°C to 40°C. Water samples for major and minor element chemistry, isotope study and geothermometry have been collected and are being processed by the University of Waterloo hydrology laboratory.

Pali Dome Complex

The source area of the Pali Dome flows is almost completely ice covered. However, its morphology and the dominance of lava flows rather than pyroclastic deposits in isolated nunataks suggests that it is a composite lava dome. Peripheral lobes of lava on both the east and west sides rest directly on basement, except for one large lobe on the southwestern corner which overlaps Mount Cayley tephra and flows. The proximal portion of most flows appears to be subaerial. Large diameter columns form well developed vertical colonnades which are underlain by scoriaceous, oxidized flow breccia. In contrast the distal flows are clearly quenched. Columns decrease in diameter to less than 30 cm and are commonly either horizontal or form fantastic radiating masses. Most flows terminate in nearly vertical, ice-contact cliffs from 100 to 200 m high (Fig. 1.10). The bounding cliffs on the southeastern side of the pile are flanked by over 70 m of granular glass which must have spalled off the advancing flow front and accumulated in the moat between lava and ice.

The Pali Dome lava is a coarsely porphyritic (plagioclase, hypersthene, ± hornblende) andesite.

Cauldron Dome Complex

The edifice of Cauldron Dome (Fig. 1.11) is a nearly flat-topped elliptical pile of thick porphyritic andesite flows. It has the classical form of a tuya, but if the steep bounding cliffs originated as ice-contact margins subsequent erosion has removed all direct evidence of quenching. Tiers of thick, nearly vertical, columns are separated by oxidized scoria and no glass was found in or adjacent to the pile.

Two very thick (100 to 130 m) complexly jointed lava flows extend 2 km southwest from the bounding cliffs of the main pile. Their surface is 300 m below the flat-topped summit of Cauldron Dome, yet both are identical, coarsely porphyritic, plagioclase, orthopyroxene andesite. It seems likely that Cauldron Dome itself formed as a subglacial pile and that the lower flows were directed into a meltwater channel that breached the enclosing barrier of ice during the latter stages of activity.



Figure 1.10

Complexly jointed, ice-contact terminus of andesite flow lobe on the southeast side of Pali Dome. Note well-defined colonnade at base of 125 m cliffs. Creek canyon in front of flow exposes 70 m of granular glass.



Figure 1.11

Flat-topped edifice of Cauldron Dome, probably a subglacial tuya.

Slag Hill Complex

The structure of the Slag Hill pile resembles that of Ember Ridge. Black, glassy, augite-bearing, basaltic andesite lava forms steep-sided, bulbous masses with complex, small diameter, curved and radiating columns. In thin section the rock is seen to comprise over 50 per cent brown glass. It is obviously a quenched, subglacial pile, but except for a small flat-topped bluff at the extreme upper (southern) end of the pile, it lacks the classical tuya form. The pile rests directly on a steep northwesterly sloping basement surface. Outflow channels probably developed on this slope shortly after the eruption started, thus only a small amount of lava was initially ice-ponded to form the flat-topped bluff in the source area. Most of it was channeled, along with meltwater, into subglacial caverns where it was quenched and solidified into its present bulbous forms.

Crucible Dome Complex

Crucible Dome is a nearly circular flat-topped pile of porphyritic (plagioclase, hypersthene) andesite. Its lower contact is completely obscured by talus and its original outer margins have been greatly modified by erosion. The flat upper surface is a clinkery red scoria strewn with bomb-like chunks of vesicular oxidized lava. It is probably a modified tuya on which the upper flows at least were subaerial.

Geothermal Potential

Until dates have been obtained on samples collected for radiometric dating, the relative ages of various centres in the central Garibaldi belt can only be estimated. Two samples, believed to be from the Slag Hill complex gave ages of 0.3 and 0.7 Ma but their stratigraphic position within the pile is not known (Green, 1977; erroneously reported as Mount Cayley ages). The widespread presence of subglacial structures suggests that some activity in the central belt was roughly coeval with that of Mount Garibaldi, 0.1 to 1.3 Ma, whereas relatively advanced erosion of Mount Fee indicates a somewhat older age.

The predominance of acid to intermediate, and hence relatively viscous magma favours the emplacement of subvolcanic intrusions. Indeed the recognition of endogenous domes and cupolas in the deeply dissected Mount Cayley pile confirms their presence. Thus, both the age and style of activity are such that a reservoir of residual heat might logically be expected somewhere beneath the central volcanic belt. This is strongly supported by the presence of thermal springs associated with the domes and cupolas of Mount Cayley.

The similarity between Mount Cayley and parts of the Meager Mountain complex is striking. The lithology, age, internal structure, morphology and proximity to thermal



Figure 1.12. Stereogram of upper Turbid Creek valley, showing area devastated by recent debris flows.

springs is remarkably similar. Moreover, the northerly to northwesterly trend of the volcanic belt between Mount Cayley and Meager Mountain is reflected by anisotropy of resistivity at Meager Mountain, by the orientation of elliptical intrusive spines on Mount Cayley and Mount Fee, and by the hydrothermally altered basement fractures in upper Turbid Creek. The possibility that this trend reflects a fundamental structure related to the young thermal history of the region should be investigated further. It would seem reasonable that geothermal exploration, presently focused on Meager Mountain, should be extended south into the central Garibaldi belt.

Geological Hazards

Any engineering development in the mountains must take into account the risk of landslides, flash floods and avalanches, but in young volcanic terrane, where poorly consolidated and intensely fractured flows and tephra are much less stable than comparable slopes on competent rock, the need for caution is paramount. The oversteepened slopes of the Mount Cayley complex, particularly on the Turbid Creek side, are swept by repeated small rock-avalanches during the summer and mixed, rock and snow avalanches in the winter. This material accumulates in the narrow canyons and is periodically flushed out during times of flood or by catastrophic debris flows that may be triggered by a single violent storm, a temporary upstream blockage or a strategically placed rock or ice fall. Debris-flow deposits up to 15 m thick (unit 17) fill much of lower Turbid Creek valley and fan out to form a benchland in Squamish River valley. There they support a growth of mature forest, indicating that flash floods and debris flows descending lower Turbid Creek for the last 100 to 200 years have not overflowed the 10 m-deep U-shaped channel that has been cut into the old deposits. However, a much younger slide above the 600 m-elevation has swept away the forest and buried 30 to 45 cm-diameter logs under as much as 10 m of debris. The area affected by this younger slide is defined by prominent trimlines that extend high above the present level of debris (Fig. 1.12). The event was probably triggered by a mixed rock and snow avalanche from steep, tephra cliffs on the southeast side of Turbid Creek. Older valley fill was remobilized and added to the volume of the flow which stripped away all but a few patches of mature forest. The present morphology of the slide area suggests that the initial, catastrophic event, was followed by successive small slides that locally stripped the older debris-flow deposits down to bedrock. The remaining debris stands as sinuous steep-sided ridges and mounds from 8 to 15 m high. Large buried logs which project from these banks show no evidence of decay and only the outer few centimetres have been bleached by groundwater action.

In addition to these deposits of older slide debris, both upper Turbid Creek and the unnamed creek northwest of Pyroclastic Peak contain large volumes of unstable young fill. The susceptibility of this material to sliding was actually observed on August 17, 1979 when a series of torrential thunderstorms passed over the Mount Cayley area. Countless small debris flows (Fig. 1.13) were initiated on the steep upper talus slopes. These started as small slumps on steep water-saturated slopes of fine talus and granular ash-rich colluvium. Once started they rapidly gained momentum and size, rushing down the slope as a slurry of mud and suspended blocks contained by marginal levees and a mobile, crescent-shaped terminal ridge. The presence of this terminal ridge of blocks seems to play a key role in the mobility of the flow. By containing the fluidized slurry of water and fine particles, debris on the slope in front of the flow is literally pushed aside by the weight and momentum of the advancing terminal ridge rather than overridden by the more fluid central portion of the flow. In this way the terminal ridge is maintained by



Figure 1.13: Small debris flow started by torrential rain on August 17, 1979. Multiple small flows from this slope coalesced to trigger a large debris flow that ran for nearly one kilometre down the creekbed northwest of Pyroclastic Peak.

continuous addition of new material at its advancing front and simultaneous dispersal of debris from its edges to form the lateral levees. Thus, the levee-bounded channel left by these flows was never occupied by a continuous stream of debris but rather by a relatively small volume of fluidized slurry trapped behind an advancing barrier of larger blocks.

After running for several hundred metres, most of these small flows either branched out into several distributary lobes, each too small to sustain further movement, or the central mass of fluidized debris spilled over the terminal ridge and dispersed on the slope below the flow. However, several of these small flows coalesced in the creek northwest of Pyroclastic Peak and triggered a large debris flow that ran for nearly one kilometre. This was visited two days after the storm at which time sharp-crested levees of blocks and silt up to one metre high bounded a smooth, U-shaped channel up to 3 m across. This was lined with a gelatinous layer of mud, which at the slightest disturbance slumped into a small stream of fluidized debris. At several places along the course of this flow loose material had been stripped from the steep walls of the creek canyon and carried away by the flow. At one point a slab of talus, 1.5 m thick, 100 m long and 20 m high, was stripped to bedrock leaving the upper part of the truncated talus cone hanging precariously to smooth granitic outcrop 20 m above the creek bed.

The threat of a large debris flow in Turbid Creek is posed by the formation of a small lake in the saddle between Pyroclastic Peak and Mount Cayley (Fig. 1.6). The saddle is underlain by more than 100 m of unconsolidated, blocky

tephra and the lake is ponded on this material between a small receding glacier on the northwestern side and the sharp crest of the ridge. Outflow from the lake, estimated at 250 to 300 L per minute, spills over the narrow lip of the ridge and cascades down a 70° to 80° slope into upper Turbid Creek. Despite its small size the lake is considered to pose a serious hazard. Not only is it ponded on unconsolidated material, it is also perched over 500 m vertically above deposits of unstable debris that fill the steep tributary canyons of Turbid Creek. If the present barrier should fail the resulting flood of water would probably trigger a series of progressive slides that could coalesce into a major debris flow comparable with those that formed the extensive debris deposits preserved in the lower part of Turbid Creek valley. The possibility of draining the lake should be considered if any extended work is undertaken in the Turbid Creek valley.

Acknowledgments

The writer is grateful to Dr. J.J. Clague (Terrain Sciences Division, Vancouver) for observations and discussion pertaining to the older, Turbid Creek, debris flow deposits. Special thanks are due to M.E.K. Souther who assisted with the field work on a voluntary basis.

References

Green, N.L.

1977: Multistage Andesite Genesis in the Garibaldi Lake Area, Southwestern British Columbia; unpublished Ph.D. thesis, University of British Columbia.

Hammerstrom, L.T., and Brown, T.H.

1977: The Geochemistry of Thermal Waters from the Mount Meager Hot Springs Area, British Columbia; Geological Survey of Canada, Open File 532.

Lewis, T.J. and Souther, J.G.

1978: Meager Mountain, British Columbia – A possible Geothermal Energy Resource; Canada, Earth Physics Branch, Geothermal Series No. 9.

Mathews, W.H.

1958: Geology of the Mount Garibaldi map-area, southwestern British Columbia. II. Geomorphology and Quaternary volcanic rocks; Geological Society America Bulletin, v. 69, p. 179-198.

Nasmith, H., Mathews, W.H., and Rouse, G.E.

1967: Bridge River Ash and some other Recent ash beds in British Columbia; Canadian Journal of Earth Sciences, v. 4, p. 163-170.

Nevin Sadlier-Brown Goodbrand Ltd.

1975: Detailed Geothermal Investigation at Meager Creek; 2 volumes, A report to B.C. Hydro and Power Authority, Vancouver, British Columbia.

Ngoc, Pham Van

1976: Reconnaissance Survey in the Lillooet Valley, British Columbia; Canada, Earth Physics Branch, Open File 77-20.

Read, P.B.

1978: Geology, Meager Creek Geothermal Area, British Columbia; Geological Survey of Canada, Open File 603.

Shorc, G.A.

1978: Meager Creek Geothermal System, British Columbia, Part III: Resistivity Methods and Results; in Transactions, Geothermal Resources Council, v. 2, sec. 2, p. 593-596.

Souther, J.G.

1975: Geothermal Potential of Western Canada; in Proceedings, Second United Nations Symposium on the Development and Use of Geothermal Resources, v. 1, p. 259-267, 1975.

Woodsworth, G.L.

1977: Pemberton (92J) Map-Area; Geological Survey of Canada, Open File 482.

COASTAL PROCESSES ON GRAHAM ISLAND, QUEEN CHARLOTTE ISLANDS, BRITISH COLUMBIA

Project 750108

John R. Harper¹
Cordilleran Geology Division

Harper, John R., *Coastal processes on Graham Island, Queen Charlotte Islands, British Columbia; in Current Research, Part A, Geological Survey of Canada, Paper 80-1A, p. 13-18, 1980.*

Abstract

A wide (up to 2 km) and long (40 km) beach-ridge plain is actively evolving on the northeast coast (McIntyre Bay) of the Queen Charlotte Islands. The coast is anomalous for British Columbia in that the beaches are wide and sandy; an extensive dune system is present (dunes up to 10 m in height); and the shore is prograding at about 0.4 m/a. The source of the deposited sediment appears to be offshore, and the net movement of sediment onshore may be a result of recent uplift which has raised an offshore platform. This platform provides source material and modifies normal physical processes (such as shoaling wave characteristics) that move material landward.

Introduction

Graham Island is the more northerly of the two major islands which form the Queen Charlotte Island Group (Fig. 2.1). Much of the Graham Island coast is irregular and rocky, similar to most of the coast in British Columbia. However, the northeastern corner is a broad, roughly triangular, sedimentary plain (the Argonaut Plain; Fig. 2.1) which supplies abundant material to the nearshore system. The shallow nearshore (< 20 m depth) is mostly sand covered and gradients are low (Fig. 2.2). Beaches are wide, composed of sand and gravel, and except for a few rock outcrops, are continuous for more than 120 km (Clague and Bornhold, in prep.). An extensive dune system has developed landward of the beaches, and fluctuating sea levels during the Holocene (Fladmark, 1974; Clague, 1975; Alley and Thomson, 1978) have distributed recent sediments over a wide band along the present coast.

The McIntyre Bay coastline represents the largest segment of prograding coastline in British Columbia and for that reason is of unique geological interest. The source of the accreting sediment is unclear as are the paths of sediment movement and the salient transport mechanism. Interactive effects between recent tectonic activity (uplift) and sediment-transport processes are also uncertain. Studies are underway of (1) the recent sea level changes and Holocene shoreline progradation rates, (2) the nearshore sediment distribution in McIntyre Bay, (3) the circulation in the bay, and (4) the paths of nearshore sediment movement. This paper reports preliminary results from these studies.

Physical Processes

The Queen Charlotte Islands are characterized by a strongly seasonal wind pattern with moderate northwesterlies common in summer and frequent southeasterly gales predominating in winter.

Waves are predominantly locally generated and thus follow a similar pattern to the seasonal wind variation. The southeasters drive a strong south to north longshore drift along the east coast of Graham Island; the moderate summer northwesterlies combine with Pacific swell to produce at present a net easterly drift along the McIntyre Bay shore. However, easterly components during both the summer and winter may cause drift reversals on the north coast; that is, drift from east to west.

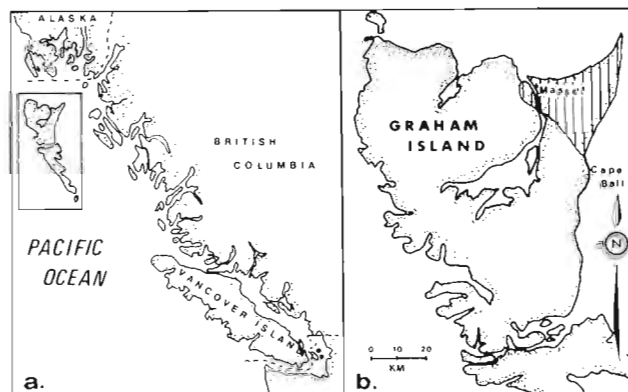
Tides, which are mixed semidiurnal (range 5-7 m), may also be important in transporting sediment, especially when reinforced by strong winds blowing over the shallow nearshore

zones. Hydraulic model studies (Bell and Boston, 1962; Bell, 1963) show that the tide floods strongly to the east through McIntyre Bay and that the ebb tide is much weaker, thus producing a net easterly coastal boundary current. The model results also suggest that along the east coast a net southerly tidal current may exist.

Recent Sea Level Changes

Sea level data for the Queen Charlotte Islands are summarized in Clague (1975) and are being refined from additional collections taken during 1978 (Clague, personal communication). Important features of the recent sea level changes are: (1) a possible postglacial minimum of 20-30 m below present sea level prior to 11000 B.P. (Fladmark, 1974), (2) a rapid rise to a postglacial maximum near 13 m above present sea level around 9000 B.P., (3) an apparently long still-stand near 12 m above present sea level until at least 4500 B.P. (Alley and Thomson, 1978) and (4) a gradual emergence from 4500 B.P. to present.

The latter two events have had the most significant effect on recent coastal morphology. The high sea level stand near 12 m produced a prominent marine scarp along much of the north coast of Graham Island (Fig. 2.3). As the shoreline emerged the system changed from dominantly erosional to a dominantly accretionary, as shown by the presence of a wide (up to 2 km) beach-ridge plain fronting the scarp (Fig. 2.3).



a. Location map of the Queen Charlotte Islands
b. Graham Island and the Argonaut Plain (lined)

Figure 2.1

¹Pacific Geoscience Centre, Sidney, B.C.

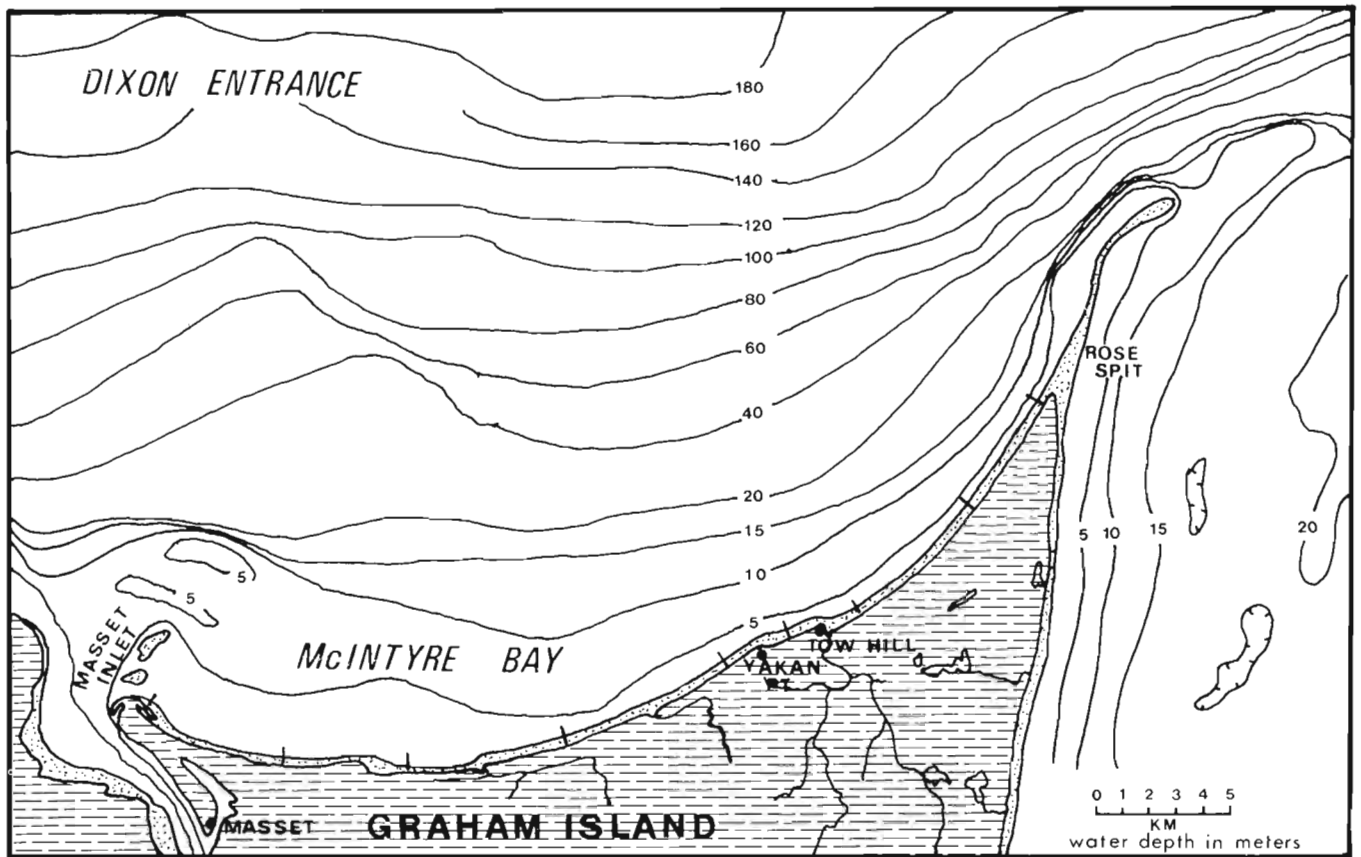


Figure 2.2. Bathymetric map of northeastern Graham Island, showing locations of beach profiles.

Geomorphic Description

There are two distinct segments to the Argonaut Plain shoreline, the east-facing shore extending from Cape Ball northward to Rose Spit (48 km) and the north-facing segment between Rose Spit and Massey Inlet (40 km). The two segments are geomorphically dissimilar. The east coast is generally eroding. Large sea cliffs are cut into unconsolidated Pleistocene material at Cape Ball (60 m high) and Eagle Hill (30 m high), and farther north, smaller cliffs are cut into dunes and old recurved spits. Erosion of the coast has continued throughout the Holocene leaving a very wide, shallow offshore platform (Fig. 2.2). Only the most northerly section of this coast, near Rose Spit, is accretionary. Most of the northern portion of the shoreline is fronted by one or two offshore bars. The intertidal zone is narrow (generally less than 50 m) except where offshore bars attach obliquely to the beaches (Fig. 2.4). On the backshore, an extensive system of blow-out or parabolic dunes (Bird, 1969) is developed with vertical relief over 10 m (Fig. 2.4).

In contrast, the north coast along McIntyre Bay is rapidly accreting, has a wide intertidal zone (generally greater than 200 m) and lacks offshore bars. Dunes are primarily the fore dune type and because of the progradation, have produced an extensive Holocene beach-ridge plain. A well-defined abandoned marine scarp occurs behind the beach-ridge plain.

Quaternary History

Field studies undertaken in 1978 and 1979 have provided additional information on shoreline progradation, the nearshore sediment distribution and sediment transport paths. Detailed analysis of airphotos combined with the field information has helped define the recent geomorphic history.

Prior to 5000 B.P., during higher sea level stands (10 to 13 m), a prominent marine scarp was cut into unconsolidated sediments. A typical section of local sediments near Massey consists of: a thick (> 1500 m) marine/nonmarine fossiliferous sandstone, the Skonun Formation, which lies at and below sea level (two rock outcrops occur along the coast); 7 m of stiff clayey sandy silt overlying the Skonun Formation; 4 m of finely crossbedded outwash sands; and capping the sequence, 2-5 m of cobbly till. This sequence appears to be widespread on the Argonaut Plain; the lower silt unit probably correlates with Sutherland Brown's (1968, p. 32) "stony marine till" observed near Cape Ball. Observation dives in McIntyre Bay indicate that much of the bottom (inside the 10 m depth contour and west of Yakan Point) is boulder covered; at one dive site a cobbly boulder lag rested on a clay silt outcrop. The observations suggest that at least the silt unit extends 2 to 3 km seaward of the abandoned marine scarp. The cobble boulder material is apparently ice-drop material derived from the 'marine till'.

Coastal Evolution

During the high sea level stand, material eroded from the cliff face was moved to the east to form an older set of recurved spits east of Tow Hill (Fig. 2.4); material may also have accumulated near the mouth of Massey Inlet as intertidal bars. The coarsest sediment, cobbles and boulders would likely have formed a transgressive lag deposit, possibly the lag identified during the scuba dives.

Emergence began about 5000 B.P. and has continued to present. Since the emergence began, a wide beach-ridge plain has evolved. The attachment angle and orientation of the older beach ridges (old foredune ridges) suggests that initially longshore transport was westerly, west of Yakan Point and

easterly east of Tow Hill. The drift divergence indicates that sediment was supplied either from offshore or from local stream runoff. A large inlet shoal at the present location of Masset and Haida and similar to the present drying bank east of Masset Inlet (Fig. 2.2) emerged as a small island.

Subtle changes in beach-ridge orientation and size define a number of beach-ridge 'packages' (Fig. 2.4) which reflect temporary reversals in drift direction or fluctuations in sediment supply as the shoreline evolved. Discontinuous uplift (causing relative sea level fluctuations) could also be a factor, and in general it is difficult to separate the effects of progradation and uplift. The nearly complete aeolian cover which averages about 2 m thick on the beach-ridge plain indicates that the beach-ridge plain is a net sediment sink, i.e. an accretionary feature as opposed to just an uplifted platform. A profile across the ridges (Fig. 2.5) indicates the general elevation changes, the thickness of aeolian deposits and the marine limit (as determined by augering). The landward break-in-slope (11 m) is the edge of the colluvial deposits from the abandoned scarp. Seaward of that, elevations gradually decrease with the landwardmost dune crest at 11 m and the present active foredune crest at 6.8 m. The relict beach sediments are distinguished from the dune material by changes in sorting and in size of the sand fraction or by the presence of well-rounded pebbles and shells. The marine limit also dips seaward from a maximum elevation around 7 m (hole 11) to a local maximum at 5 m near the present foredune (hole 18). Definition of the marine limit landward of auger hole 10 becomes problematic because of interfingering with colluvium. Although Sangán Creek appears to separate two beach-ridge 'packages', the gradual slope of the beach deposits suggests that the emergence has been relatively uniform. Shell pavements were encountered in holes 1, 16, 17, 18 at elevations from 4 to 5 m; shells were absent from other holes presumably because of leaching. In trenches and auger holes dug in the active beach, these pebble/shell pavements usually formed at or slightly above the high water elevation (approximately 2.5 to 3.5 m). The presence of shell pavements between 4 and 5 m near the active beach may be related to relatively recent high water storm events (HHWL is 3.7 m) but also could suggest recent and substantial uplift. Additional radiocarbon dates of collected shell material should clarify the amount of recent uplift. The problem illustrates the complexity of reconstructing sea level changes in a macrotidal region.

A shell date (GSC-2815) of 930 ± 60 B.P. from an old beach ridge (Clague, personal communication) gives a mean

progradation rate of 0.4 m/a for the central section of this coast (see Fig. 2.3). If one assumes that the relict scarp, which lies 1.5 km inland of the active beach, was abandoned about 5000 B.P. (Alley and Thomson, 1978), a mean progradation rate of 0.3 m/a at the same site results. The agreement between the two estimates suggests a relatively uniform progradation rate.

Sediment Sources

Since the beach-ridge plain represents a significant sediment sink to the coastal system, a sizeable sediment source is required; that source is not readily apparent. Possible sources are (1) sediment moved from the east coast, westward around Rose Spit, (2) material introduced by local creek runoff, (3) relict offshore sand deposits moving onshore or (4) sediment deposited on the Masset Inlet ebb-tidal delta and subsequently moved eastward and onshore.

There is no evidence for the first alternative; it is unlikely that sediment moves from Rose Spit westward. The longshore drift is dominantly to the east and tidal currents also show a net easterly component.

Local creek discharge obviously contributes some material to the beaches and during the early phases of uplift, may have contributed a significant proportion of the accumulated sediment. At present however, suspended and bed load contributions are small, in part due to the heavy forest and peat cover.

Seabed drifter studies show that a mechanism exists for moving offshore sands onshore. Fifty-three (of 100) bottom drifters dropped at two sites in February (1979) were recovered onshore between March and May (Fig. 2.6). The recoveries indicate that not only can sediment be moved onshore but also significantly alongshore, one drifter having moved 20 km eastward and several having moved 16 km westward. Sand offshore is abundant as indicated by offshore sediment samples (Fig. 2.7) and could conceivably be the source of onshore material. The boulder cobble lags noted during the dives indicates that the clayey sandy silt matrix of the 'marine till' (Sutherland Brown, 1968) has gone somewhere, presumably onshore. Eventually, however, as the lag cover becomes more complete (100% coverage was noted on one of the dives) the supply would be expected to gradually diminish. The meager data available suggest however a constant or increasing progradation rate, i.e., a relatively continuous supply.

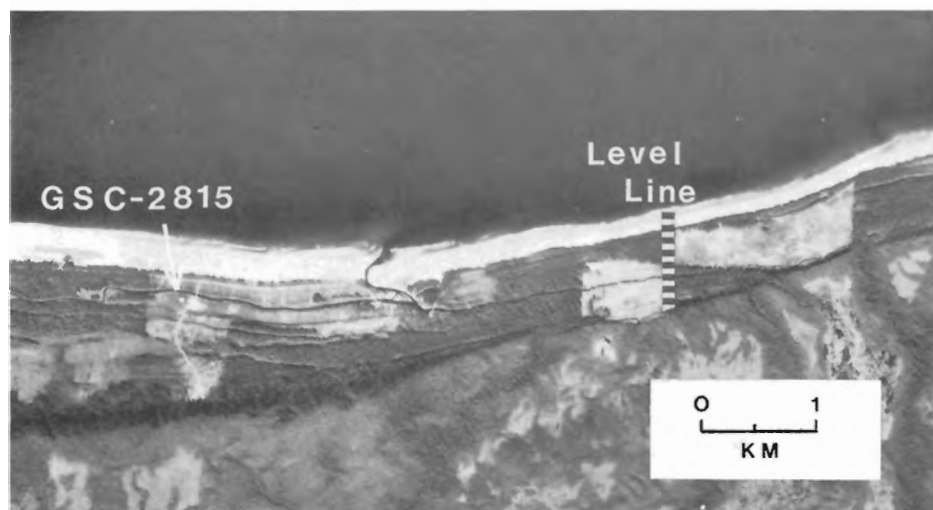


Figure 2.3.

Vertical airphoto showing the abandoned marine scarp and the beach-ridge plain near the mouth of Sangán Creek. The location of the dated shell sample (GSC-2815) is shown (BC 5630 195).

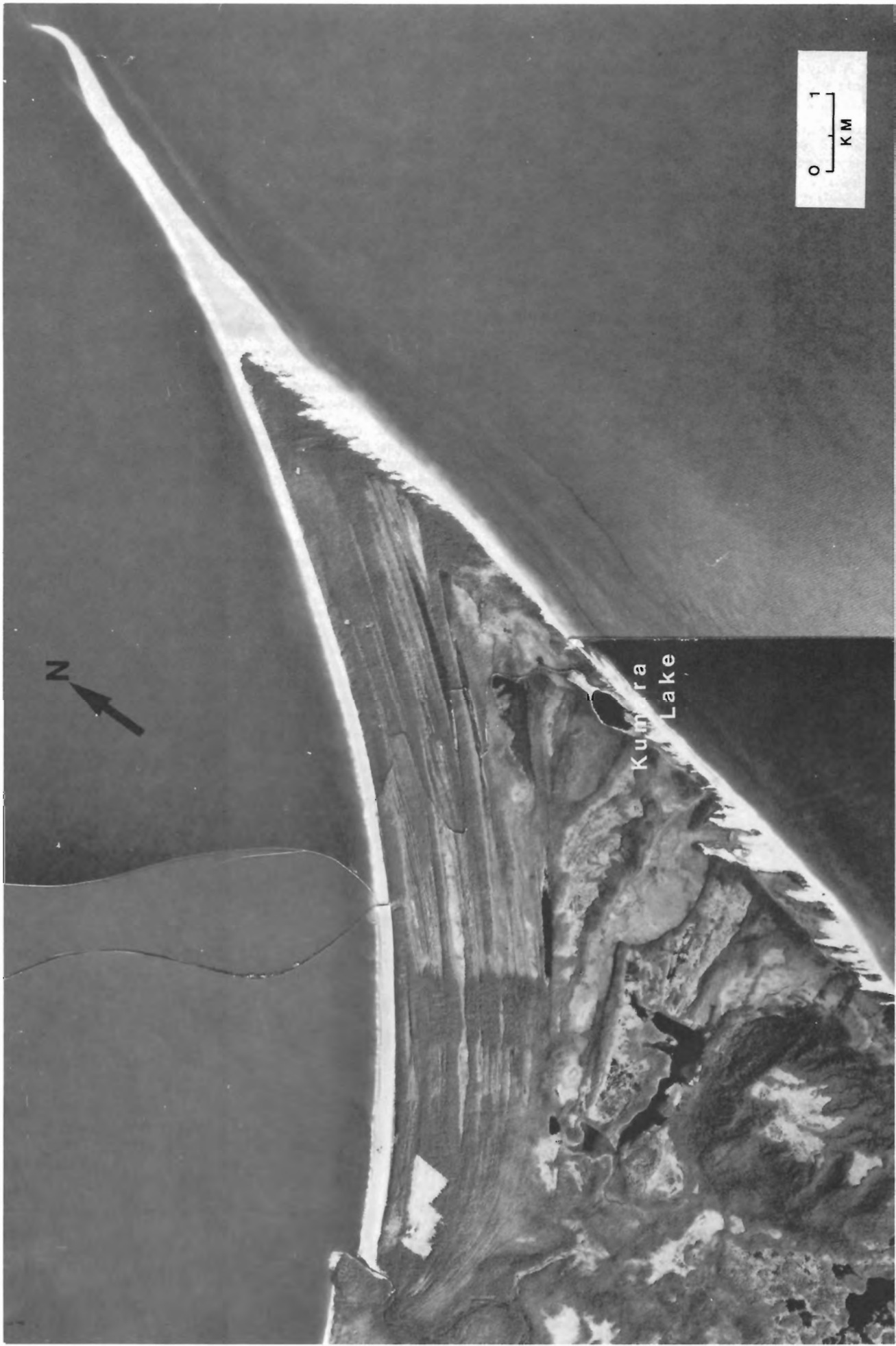


Figure 2.4. Vertical airphoto showing the beach-ridge plain east of Tow Hill. Older recurves are apparent near Kumara Lake. Off shore bars attach to the beach near Kumara Lake and near Rose Point (BC 5630 190).

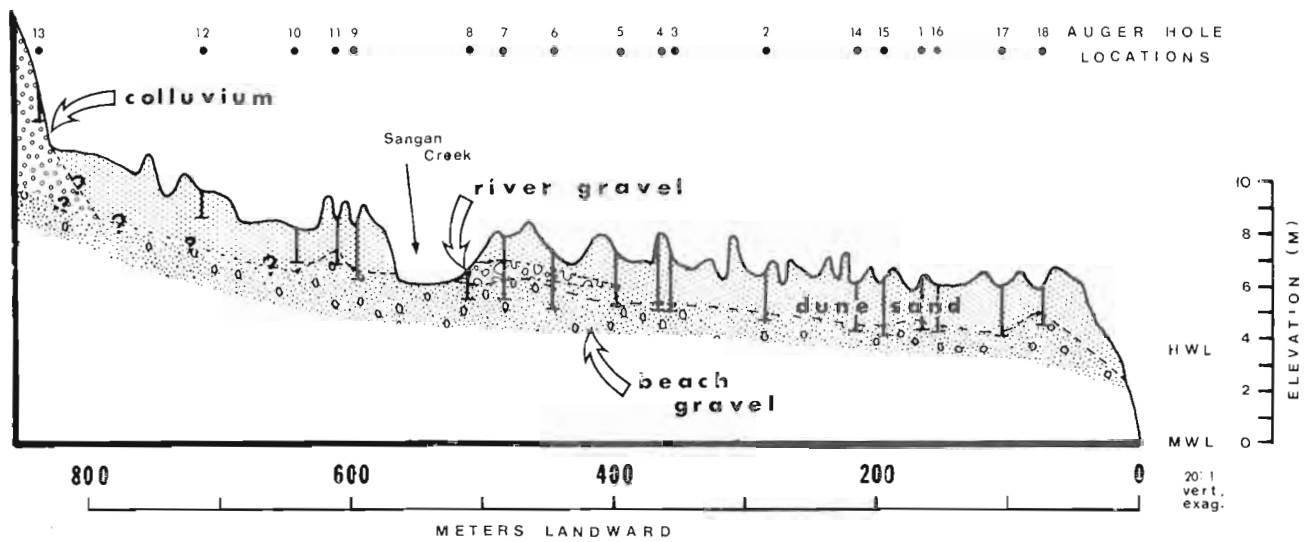


Figure 2.5. A survey line and section across the beach-ridge plain, 2.5 km east of the mouth of Sangan Creek (see Fig. 2.3 for location).

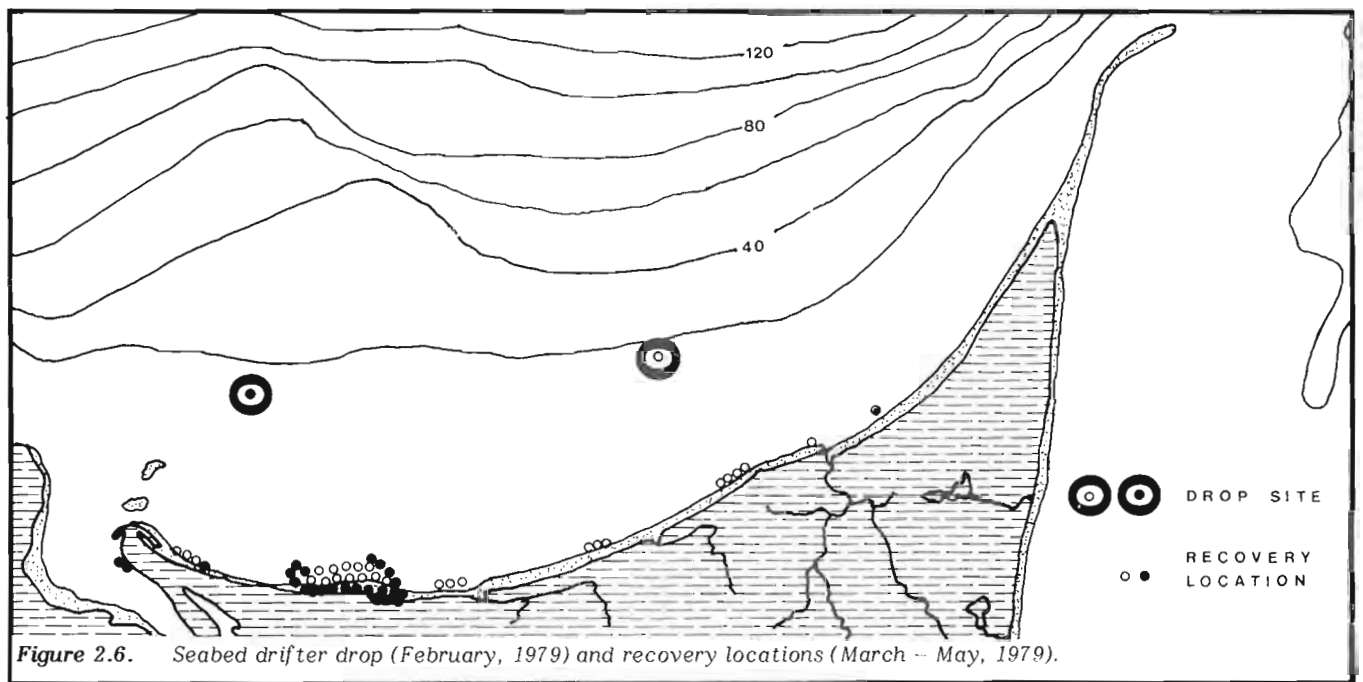


Figure 2.6. Seabed drifter drop (February, 1979) and recovery locations (March – May, 1979).

One additional source may be material from the Masset Inlet ebb-tidal delta. Twenty-six (of 50) bottom drifters dropped on the ebb-tidal delta reached shore (Fig. 2.6); thus a mechanism apparently exists for moving material from the delta to the shore. This sediment source is likely to be continuously renewed and is unlikely to be diminished by the formation of lag deposits.

A combination of the latter two sources appears to be the most likely supply of the sand being deposited onshore. The sediment is known to be available and easily moved and there is evidence that a transport mechanism exist. The occurrence of boulder and cobble lags clearly indicates that large amounts of fines have already been eroded. Further analysis of mineral suites and sediment texture from offshore and onshore samples should help define the source.

Active Beach Processes

In an attempt to define the seasonal variability (such as classic "winter-summer" beach cycles) ten beach profiles

were established between Masset Inlet and Rose Spit (Fig. 2.2). Profiles were surveyed in August (1978), February (1979) and July (1979). Total volumetric changes were small and no systematic pattern was apparent. Most profiles showed no change or slight erosion. It is notable however that all profiles were stable or accretionary between February and July (1979), suggesting some seasonality in the beach changes. Only two profiles showed a net accretion during the study period.

Additional Problems

Several geological and oceanographic problems warrant further consideration before the conceptual evolution of the coast can be considered complete. These problems include: (a) the ultimate destination of the very large amount of sediment eroded from the east coast, transported north and presumably lost offshore; (b) the actual transport mechanism for moving the sand onshore, probably a combination of shoaling waves and tides; (c) the cause of beach-ridge "packages", possibly

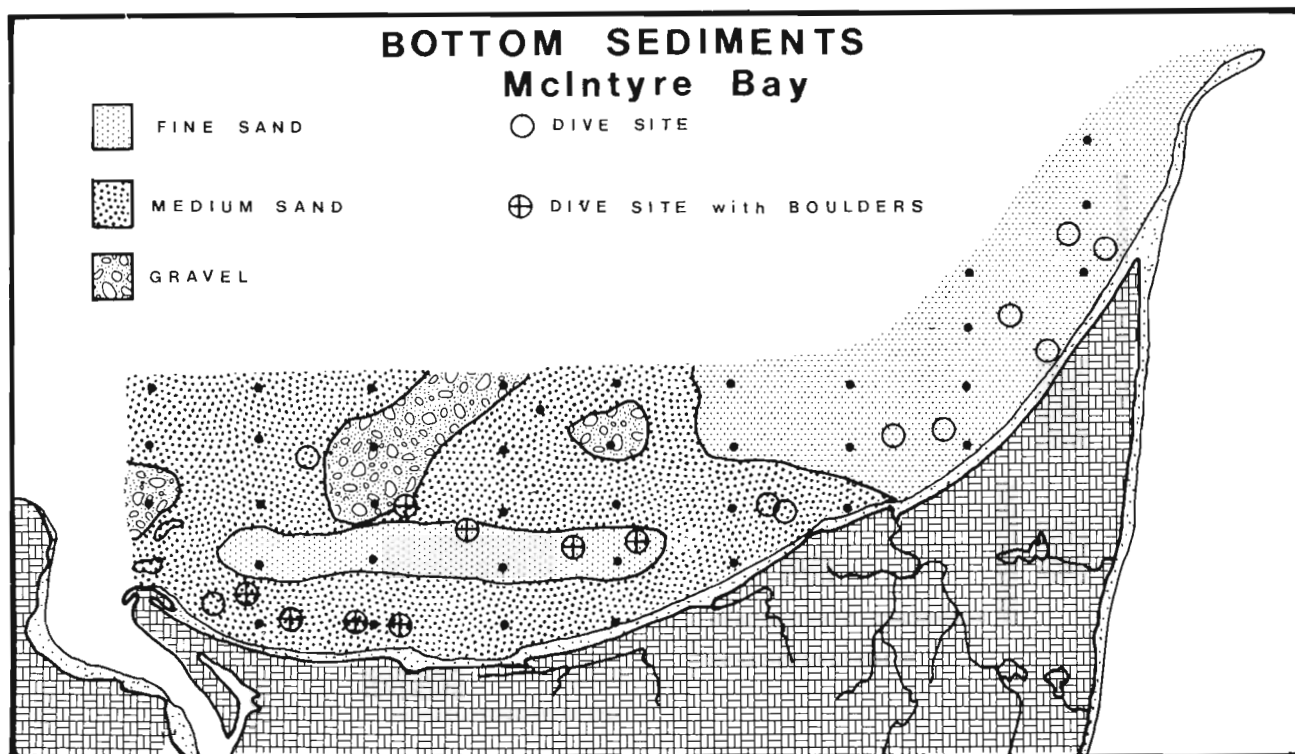


Figure 2.7. Sediment distribution in McIntyre Bay based on field descriptions of grab samples (sample grid shown by black dots). Scuba dive sites shown by open circles. At dive sites where boulders were noted, the circles are crossed.

the result of drift reversals, supply fluctuations or sea level fluctuations; and (d) the presence of a very distinct tree line along the McIntyre Bay coast. In front of this line is a wide (generally greater than 50 m) aeolian apron where dune ridges are indistinct and which is almost totally devoid of trees or shrubs. The apron is morphologically dissimilar to older portions of the beach-ridge plain. One possible explanation (supported by auger holes through the deposit) is that the accumulation of driftwood, largely a result of recent logging, is an effective sediment trap and has created an anomalously high progradation rate within the last few decades.

Summary

The northeast coast of Graham Island, Queen Charlotte Islands, is a dynamic, rapidly evolving coastal system. Recent uplift and oceanographic processes have produced a large progradational (regressive) beach-ridge plain along the McIntyre Bay shoreline. Progradation rates along the narrower part of the plain are on the order of 0.3 to 0.4 m/yr. The sediment source appears to be offshore. Material is transported onshore by some combination of shoaling waves, tides and wind-driven currents. The transport mechanism which is a key to understanding the evolution of the coastal system, is only poorly understood at present.

Acknowledgments

Brian Bornhold, Graham Riley and Bob Spitzer assisted in the field and their help is greatly appreciated. P.A. Collins, S.R. Collison, N. Leffler, R. Leffler, R.H. Poll and R. Schatz of Masset kindly provided location information on the seabed drifters. The Ministry of Fisheries and Oceans graciously provided a vessel and crew for the collection of offshore sediment samples. B.D. Bornhold and R.D. Gillie of the Geological Survey reviewed the manuscript.

References

- Alley, N.F. and Thomson, B.
1978: Queen Charlotte Islands, aspects of environment geology; British Columbia Ministry of Environment, Resource Analysis Branch, Bulletin no. 2, p. 64.
- Bell, W.H.
1963: Surface current studies in the Hecate model; Fisheries Research Board, M.S. Report Series (Oceanography and Limnology), no. 159, p. 27.
- Bell, W.H. and Boston, N.
1962: The Hecate Model; Fisheries Research Board, M.S. Report Series (Oceanography and Limnology), no. 110, p. 35.
- Bird, E.C.F.
1969: Coasts. Massachusetts Institute of Technology Press, Cambridge (Massachusetts), p. 246.
- Clague, J.J.
1975: Late Quarternary sea level fluctuations, Pacific coast of Canada and adjacent areas; in Report of Activities Part C, Geological Survey of Canada Paper 75-1C, p. 17-21.
- Clague, J.J. and Bornhold, B.D.
Morphology and littoral processes of the Pacific coast of Canada; in McCann (editor), The coastline of Canada, Geological Survey of Canada Paper 80-10. (in prep.)
- Fladmark, K.R.
1974: A paleoecological model for northwest coast prehistory; unpublished Ph.D. Dissertation, University of Calgary (Archaeology Department), p. 319.
- Sutherland Brown, A.
1968: Geology of the Queen Charlotte Islands, British Columbia; British Columbia Department of Mines and Petroleum Resources, Bulletin no. 54, p. 226.

**STRATIGRAPHY AND STRUCTURE:
THOR-ODIN TO FRENCHMAN CAP "DOMES",
VERNON EAST-HALF MAP AREA, SOUTHERN BRITISH COLUMBIA**

EMR Contract 95708

Peter B. Read¹
Cordilleran Geology Division, Vancouver

Read, Peter B., Stratigraphy and structure: Thor-Odin to Frenchman Cap "domes", Vernon east-half, map area, southern British Columbia; in Current Research, Part A, Geological Survey of Canada, Paper 80-1A, p. 19-25, 1980.

Abstract

The Mantling Zone consists of a basal quartzite, an overlying unit of pelitic, psammitic and calc-silicate gneiss with one or more quartzites, a thin white marble and rare carbonatite lenses which together comprise a shelf sequence, and an upper thick unit of psammitic and some pelitic gneiss. The top of the uppermost quartzite defines the base of the upper unit. Subdivision of the shelf sequence into units based on the continuity of quartzite layers permits stratigraphic correlation of units of the Mantling Zone between Thor-Odin and Frenchman Cap "domes". The shelf sequence probably correlates with the Belt-Purcell Supergroup and the overlying psammitic unit with the Horsethief Creek Group.

Of the three phases of penetrative deformation affecting the Shuswap Metamorphic Complex, the first two produced isoclinal, reclined to recumbent folds. The first phase probably consists of northerly trending folds with anticlines verging eastward. The second phase has a curvilinear fold axis lying in a southwesterly dipping axial plane. These two phases produced simple to complexly deformed structures more akin to nappes than domes and Thor-Odin and Pinnacle Peaks are accordingly renamed nappes. Because probably the same basal quartzite layer forms the base of the Mantling Zone in Thor-Odin and Frenchman Cap, significant diapiric movement of the Core Zone into the Mantling Zone is unlikely. Extensive development of pegmatite and leucogranitic intrusions west of Frenchman Cap and northwest of Thor-Odin indicates that thermal culminations associated with the highest grade of metamorphism do not necessarily coincide with extensive areas of core gneiss. The nappe structure, lack of diapirism, and noncoincidence of thermal culminations with extensive areas of core gneiss do not support a gneiss dome concept.

The Columbia River fault zone bounds the Shuswap Metamorphic Complex on the east, forms the base of klippen lying on the complex, and may bound the complex on the west. The fault zone records a long history of movement from the mid-Jurassic to Early Cretaceous décollement between complex and cover to fracturing and the development of clay gouge along the eastern side of the complex in the Tertiary.

Introduction

Three months were devoted mainly to unravelling the stratigraphy and structure of the stratified metamorphic rocks between the Core Zones of Thor-Odin and Frenchman Cap "domes" in the Shuswap Metamorphic Complex. This work is a continuation of earlier work (Read, 1979a and 1979b) and supplements the published work of Reesor (1973) and unpublished investigations of Craig (1966) and Hill (1975). A week was spent south of the Jordan River area (Fyles, 1970) with R.L. Brown resolving problems in stratigraphic correlations between Thor-Odin and Frenchman Cap "domes". Southeast of Revelstoke, further work better defined the distribution of amphibolite in the south end of Clachnacudainn Salient. West of Pinnacle Peaks "dome", a brief examination substantiated the fault (Jones, 1959) separating moderate- to high-grade metamorphic rocks of the "dome" from low-grade Upper Paleozoic to Lower Mesozoic rocks southwest of the "dome".

Two major faults delimit three tectonic elements which underlie the map area in part. From west to east, the Columbia River fault zone separates the Shuswap Metamorphic Complex to the west from the Kootenay Arc and Clachnacudainn Salient to the east. East of Revelstoke, Standfast Creek slide sets Clachnacudainn Salient against Kootenay Arc. West of Upper Arrow Lake, klippen composed of low-grade Lower Mesozoic rocks lie on the complex, and farther west these rocks are faulted against the western edge of the complex (Fig. 3.3).

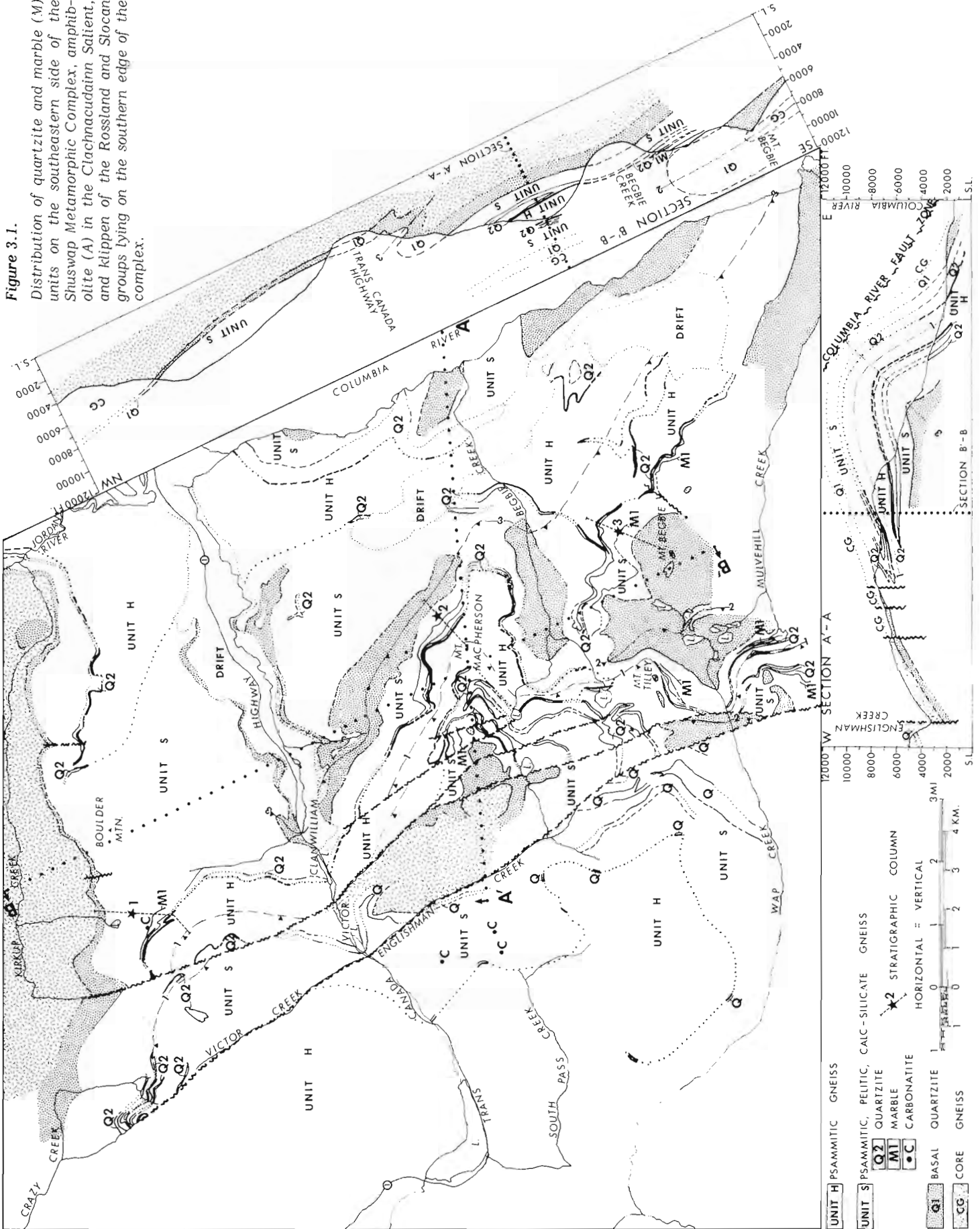
Stratigraphy of the Shuswap Metamorphic Complex

Schist and gneiss of the Shuswap Metamorphic Complex are divided into Core Zone and overlying, autochthonous Mantling Zone. The base of the lowest persistent quartzite (Q1) defines the contact between the Core and Mantling zones (Fig. 3.3). Within the map area, a few thousand metres of stratified rocks of the amphibolite facies form Thor-Odin and the southern flank of Frenchman Cap "domes". The rocks are predominantly metasedimentary, lie mainly in the sillimanite zone, and, on the western and southern sides of Thor-Odin, contain abundant quartz-feldspar pegmatites and leucogranitic sills and dykes. Stratigraphic facing of the succession depends upon sedimentary structures measured in a few localities (Fig. 3.2).

With an increase in mica and feldspar, the basal quartzite (Q1) passes downward into biotite-muscovite paragneiss of the Core Zone. Deeper in the Core Zone, hornblende becomes characteristic, and sillimanite and garnet are absent. Extensive areas of Core Zone gneiss outcrop in the centres of Thor-Odin and Frenchman Cap "domes" (Reesor, 1970), but this summer's work outlined areas on the flanks of the "domes" (Fig. 3.1) and substantiated Höy and McMillan's (1979) suggestion that unit 10 at the south end of the Jordan River area (Fyles, 1970) is gneiss of the Core Zone, and unit 9 is the basal quartzite. The remaining stratigraphic correlations are more complicated than those suggested by Höy and McMillan and need further work. Quartz monzonite gneiss with feldspar augen forms sills up to 10 km long in the paragneiss.

¹ Consulting Geologist; Geotex Consultants Ltd., 1000-100 W. Pender St., Vancouver, B.C., V6B 1R8.

Figure 3.1.
 Distribution of quartzite and marble (M) units on the southeastern side of the Shuswap Metamorphic Complex, amphibolite (A) in the Clachnacudainn Saitent, and klippen of the Rossland and Slovan groups lying on the southern edge of the complex.



★1 BOULDER MTN. ★2 MT. MACPHERSON ★ MT. BEGBIE

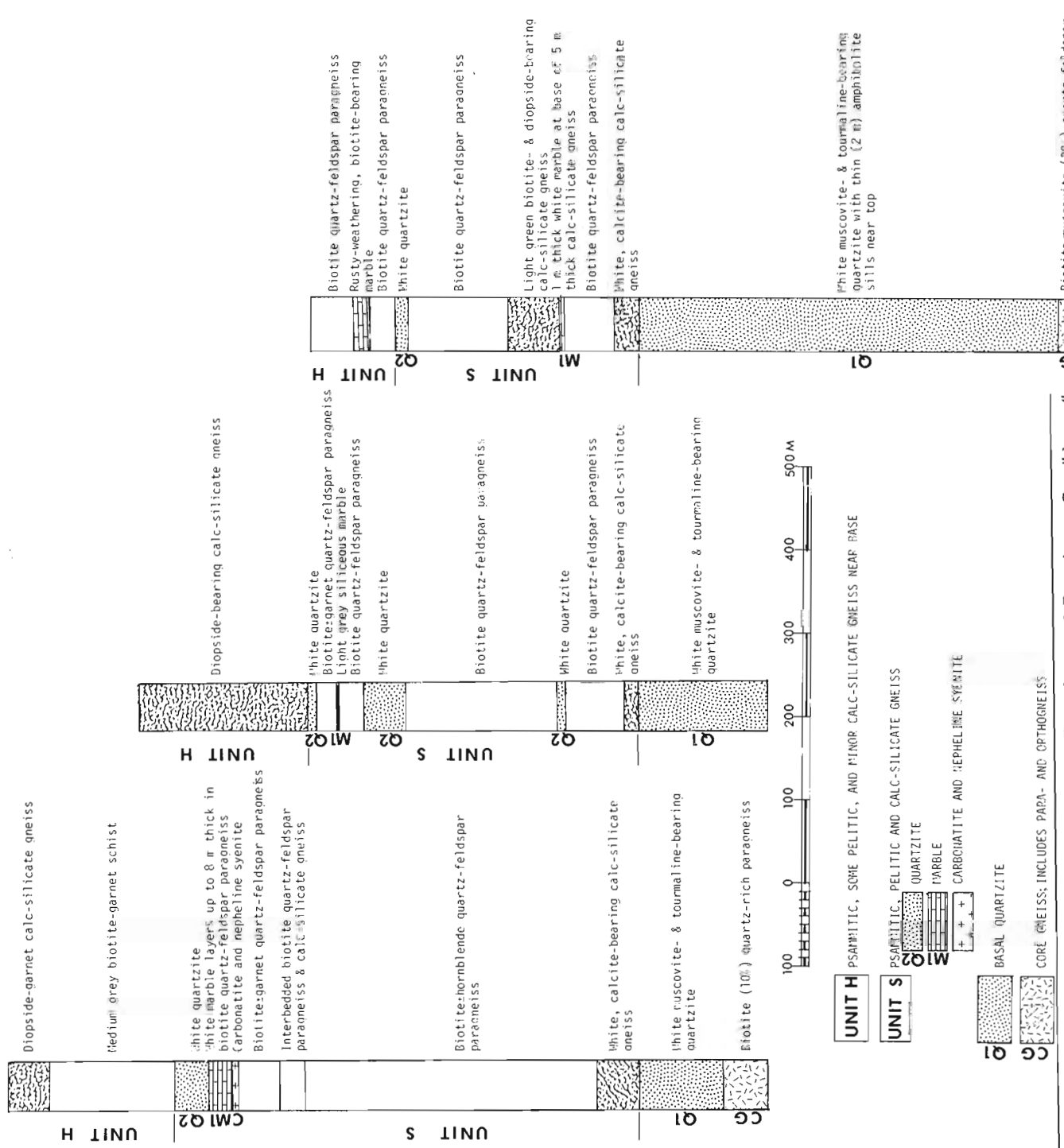
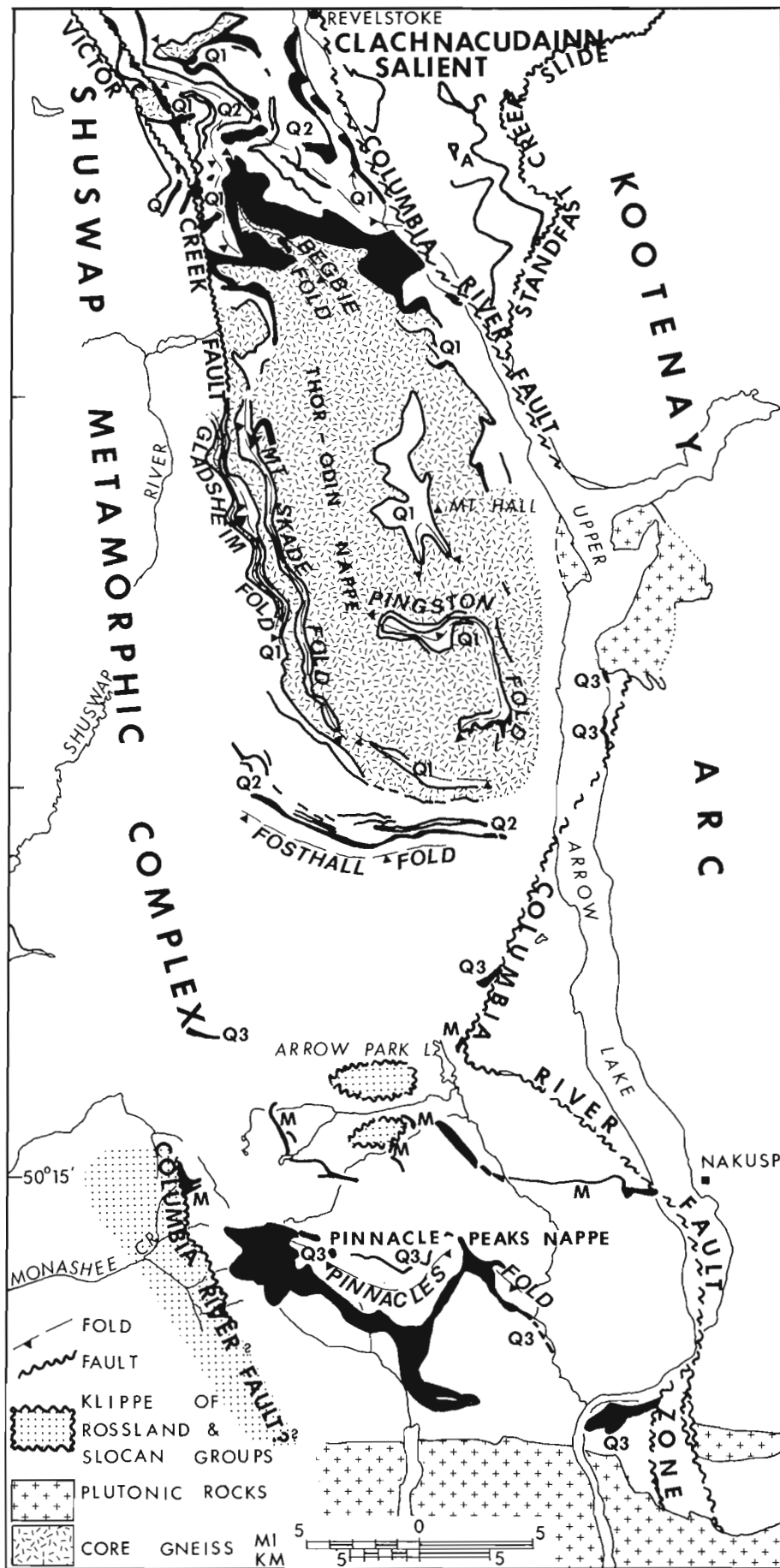


Figure 3.2. Stratigraphic columns of the Mantling Zone between Thor-Odin and Frenchman Cap "domes". See Figure 3.1 for location of columns.



- Q = undifferentiated
- Q1 = basal quartzite
- Q2 = second quartzite
- Q3 = quartzite in Pinnacle Peaks "dome"

Figure 3.3. Distribution of quartzite and marble (M) units on the southeastern side of the Shuswap Metamorphic Complex, amphibolite (A) in the Clachnacudainn Salient, and klippen of the Rossland and Slocan groups lying on the southern edge of the complex.

A muscovite- and tourmaline-bearing quartzite (Q1) overlies paragneiss of the Core Zone and locally, as in Kirkup Creek, the orthogneiss. The basal quartzite ranges in thickness from 30 m to as much as 500 m on Mount Begbie or at the head of Crazy Creek. Variations in thickness are probably mainly of sedimentary rather than tectonic origin.

Overlying the basal quartzite is a unit of heterogeneous, metasedimentary schist and gneiss. Biotite-quartz-feldspar paragneiss, locally with garnet and/or sillimanite, and diopside-biotite-bearing calc-silicate gneiss with some impure marble predominate. Thin quartzite layers (Q2), here and there up to 100 m thick, a 1- to 2 m-thick white marble (M1) and rare lenses of carbonatite (C) are minor components of major stratigraphic importance. Horizontal facies changes among the psammitic, pelitic, and calc-silicate gneisses result in a lenticular and interfingering distribution. Only the quartzite and white marble form relatively continuous horizons. The top of the basal quartzite defines the lower contact of the unit overlying the basal quartzite, and the top of the second, or in places uppermost quartzite, defines the top of the unit. Typical stratigraphic columns in Figure 3.2 show that within 30 m above the basal quartzite is a 10- to 30 m-thick, white calc-silicate gneiss with calcite, diopside and biotite. One hundred to two hundred metres above the base is a 2- to 15 m-thick white calc-silicate gneiss with a 1 m to locally 5 m-thick white marble. On Boulder Mountain carbonatite lenses are spatially associated with the marble. One or more quartzite layers from 5 to 100 m thick lie up to 200 m above the white marble. Although for tectonic or sedimentary reasons the quartzites are not continuous, sufficient continuity allows the top of the uppermost quartzite to define the top of the unit. Throughout the map area, the top of the unit is close to, but not necessarily at the same stratigraphic level. Above the uppermost quartzite are up to 300 m of grey-green, diopside-bearing, calc-silicate gneiss or grey garnetiferous mica schist such as that exposed near the peak of Mount MacPherson.

In Wap Creek west of Victor Creek fault, quartzite layers up to 200 m thick, which are interbedded with biotite-sillimanite-garnet paragneiss, lie near the base of an upright section more than 1500 m thick. Near the head of South Pass Creek, a few thin carbonatite lenses lie close to the uppermost thin quartzite. Above the quartzite is a thick sequence of biotite ± sillimanite ± garnet paragneiss (Fig. 3.5) hosting abundant pegmatite, alaskite, amphibolite and foliated granitic sills. This section contains the transition

from a shelf sequence of pelitic, psammitic and calcareous sediments with thick quartzite and thin limestone layers which envelops the Core Zone to an overlying thick succession of psammite and some pelite devoid of quartzite and limestone.

Stratigraphy of Clachnacudainn Salient

Read (1979a, 1979b), following Thompson (1978) showed only one amphibolite (A) in the south end of Clachnacudainn Salient. Further work indicates a second amphibolite 10 to 50 m thick is structurally 300 m beneath that shown by Thompson.

Folding

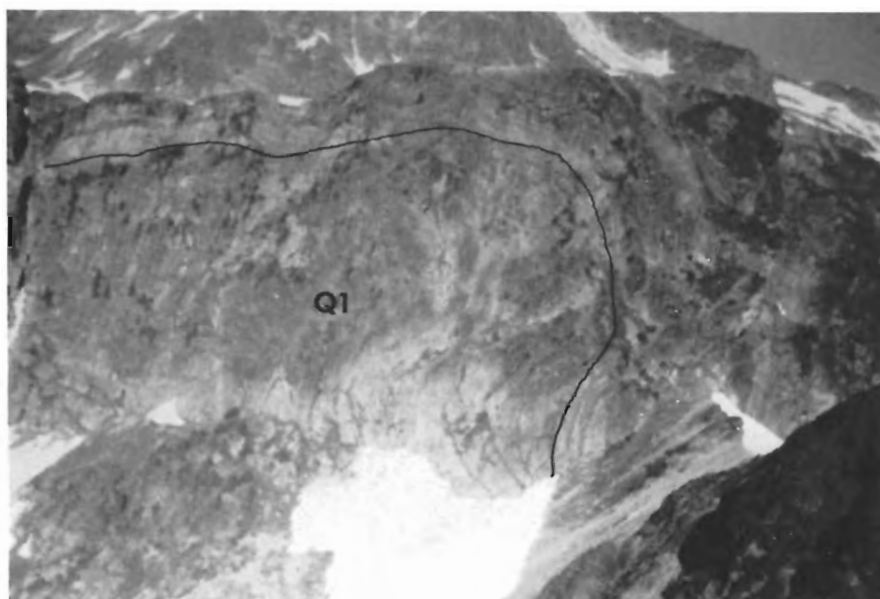
Polyphase, noncoaxial deformation pervades the Shuswap Metamorphic Complex and produces the so-called gneiss "domes" which characterize the eastern part of the complex. The first two phases are isoclinal. Evidence for the first phase rests on mesoscopic structures folded around macroscopic folds, such as Figure 3.4, which Reesor (1973; personal communication, 1978) mistook as first phase, and the outcrop distribution of quartzite, particularly on the west flank of Thor-Odin, which is compatible with northerly trending folds. Scant data suggest that first-phase folds trend northerly and anticlines verge to the east. This phase is responsible for the largely eroded recumbent anticline which overlies the preserved syncline of Mantling Zone between Frenchman Cap and Thor-Odin (Fig. 3.1).

Second-phase folds usually obliterate earlier mesoscopic structures. Their fold axis is curvilinear but lies in a southwesterly dipping axial plane foliation. Northeast of Thor-Odin, second-phase folds plunge southeasterly, north of the "dome" they trend easterly and are flat, and northwest of the "dome" they plunge southwesterly. The folds are isoclinal and recumbent to reclined.

A northwest-trending, third-phase fold starts north of the Trans-Canada Highway near Clanwillian, crosses the lower part of Begbie Creek and plunges southeasterly before truncation by the Columbia River fault zone. The fold exposes gneiss of the Core Zone on Trans-Canada Highway and basal quartzite in Begbie Creek, and it folds down the inverted limb of the largely eroded first-phase anticline so that it outcrops on the west bank of Columbia River (Fig. 3.1).

Figure 3.4.

A down-plunge view of a second phase anticline on the west ridge of Mount Tilley shows the upper limb and hinge outlined by a thin-bedded calc-silicate gneiss which overlies the basal quartzite exposed in massive cliffs.



A broad arching postdates all phases of penetrative folding and probably the mid-Jurassic to Early Cretaceous movement of the Columbia River fault zone.

Structural analysis indicates that gneiss of the Core Zone probably overlay the area between Thor-Odin and Frenchman Cap but has since been eroded to yield an apparent structural depression between two apparent domes (Fig. 3.1). At the north end of Thor-Odin, large-scale superposed folds control the outcrop distribution of core gneiss. These folds form an isoclinal, complexly deformed nappe centred by core gneiss. In the southern part of Thor-Odin (Reesor and Moore, 1971), mantling gneiss is infolded into core gneiss in isoclinal, upright to recumbent folds, such as Gladshiem Lake and Mount Skade infolds, and Pingston fold and its northern continuation towards Mount Hall (Read, 1979b). In Pinnacles Peak the dominant structure is an east-trending, open to tight antiform verging northwards. Thor-Odin and Pinnacle Peaks are geometrically more akin to simple to complexly deformed nappes than domes and have accordingly been renamed Thor-Odin nappe and Pinnacle Peaks nappe.

Although stratigraphic correlations between Frenchman Cap and Thor-Odin nappe are incomplete, the basal quartzite surrounding the core gneiss of both is probably the same layer. If, as Reesor (1970, p. 80) suggested, the Core Zone moved "as a diapiric unit relative to the mantling gneisses", then in Frenchman Cap and Thor-Odin the Core Zone stopped at precisely the same stratigraphic level. Such coincidence seems unlikely and negates the concept of significant diapirism of the Core Zone. Furthermore, Reesor (1970, p. 73) described the "gneiss dome" as "related to culminations of large north-verging east-west folds and coincident culminations in the thermal structure". In the northern half of Thor-Odin and throughout Frenchman Cap (R.L. Brown, personal communication, 1979), the highest grade of metamorphism and extensive development of pegmatite and leucogranitic intrusions lie west of the Core Zone and are not coincident with it.



Figure 3.5. On the Trans Canada Highway 0.4 km west of Victor Lake, a roadcut of biotite-hornblende paragneiss with quartz-feldspar augen is typical of rocks in the second sillimanite zone.

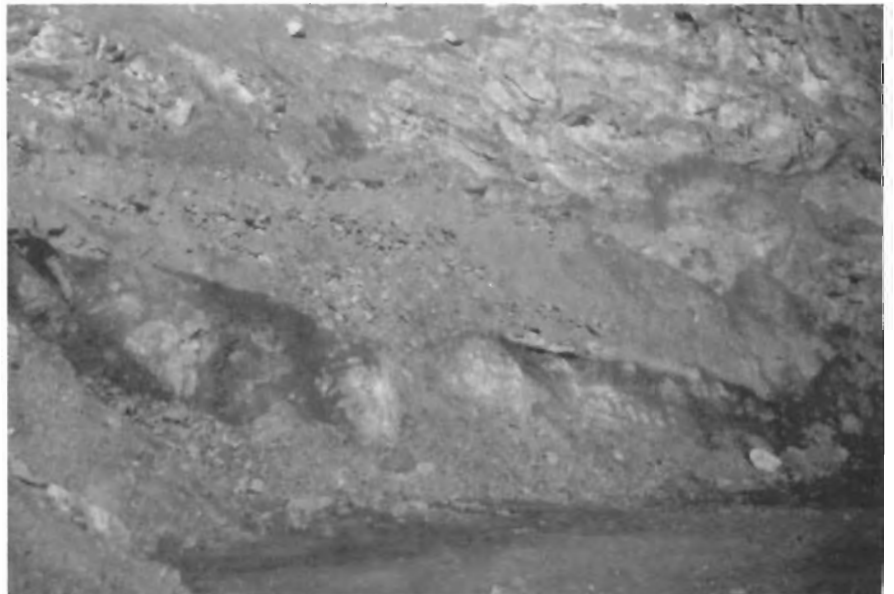


Figure 3.6. On the east side of Columbia River 8.3 km southeast of the bridge across the Illecillewaet River, a roadside quarry exposes mylonite and gently eastward dipping gouge zones up to 2 m thick. The person stands on a gouge zone which seeps water.

Faulting

In Vernon east-half, map area, the Columbia River fault zone bounds the Shuswap Metamorphic Complex on the east, forms the base of klippen lying on the complex, and may bound the complex on the west. The fault zone has a long movement-history from mid-Jurassic to Early Cretaceous, when development of mylonite and fault breccia records décollement between complex and cover, to the Tertiary when fracturing of mylonite and breccia and development of clay gouge record movement along the east side of the complex (Fig. 3.6) and beneath the klippen. On the western edge of the complex, blastomylonite and metamorphosed monomictic breccia form an undisturbed zone 15 to 60 m thick which dips westerly at 40 to 60 degrees. The zone represents either a metamorphosed fault or a metamorphosed angular unconformity cutting previously deformed and metamorphosed rocks. The change from Upper Triassic rocks of the chlorite zone in the hanging wall of the zone to garnet or staurolite zone rocks of Pinnacle Peaks nappe in the footwall, and the difference in structural trends and fabric of the rocks across the zone are more easily explained by a fault than by an unconformity. In addition, the probable fault cuts off a distinctive marble (M) (Fig. 3.3) in the stratigraphy of Pinnacle Peaks Nappe and may truncate a layer of volcanoclastic rocks in the cover.

In the north part of the map area, a set of north-northwest striking, subvertical faults lies along and east of Victor Creek (Jones 1959). Oblique-slip displacements are in the order of 300 m or less except for the main strand along Victor Creek, Englishman Creek, and the headwaters of Shuswap River where movement is unsolved but must exceed 300 m. Mylonite and healed fault breccia define the faults, and Tertiary (?) dykes intrude them.

Stratigraphic Correlation

A few sedimentary structures indicate that the assumed upright stratigraphic order in Read (1979a, 1979b) is correct. In the Mantling Zone, the lower heterogeneous shelf-succession with quartzites passes upward into a thick monotonous sequence of psammite and some pelite. The latter sequence extends northward along the western side of Frenchman Cap as unit E (Wheeler, 1965). It lies above a décollement described by Brown (personal communication, 1979) and northeast of Frenchman Cap it joins the Horsethief Creek Group (Wheeler 1965, p. 9; Brown, personal communication, 1979). In Vernon east-half map area, no décollement separates the shelf from the overlying sequence as it does to the north, and the area provides additional support to the correlation of units of the Mantling Zone, up to the uppermost quartzite, with the Belt-Purcell Supergroup as suggested by Read (1979a and 1979b) and Brown and Psutka (1979).

References

- Brown, R.L.
1980: Frenchman Cap dome, Shuswap Complex, British Columbia: a progress report; in *Current Research, Geological Survey of Canada, Part A, Paper 80-1A*, p. 47-51.
- Brown, R.L. and Psutka, J.F.
1979: Stratigraphy of the east flank of Frenchman Cap dome, Shuswap Complex, British Columbia; in *Current Research, Part A, Geological Survey of Canada, Paper 79-1A*, p. 35-36.
- Craig, D.B.
1966: Structure and petrology within Shuswap Metamorphic Complex Revelstoke, British Columbia; unpublished Ph.D. thesis, Department of Geology, University of Wisconsin, 130 p.
- Fyles, J.T.
1970: The Jordan River area near Revelstoke, British Columbia; *British Columbia Department of Mines and Petroleum Resources, Bulletin 57*, 64 p.
- Hill, R.P.
1975: Structural and petrological studies in the Shuswap Metamorphic Complex near Revelstoke, British Columbia; unpublished M.Sc. thesis, Department of Geology, University of Calgary, 147 p.
- Höy, T. and McMillan, W.J.
1979: Geology in the vicinity of Frenchman Cap gneiss dome; in *Geological Fieldwork 1978*, British Columbia Ministry of Energy, Mines and Petroleum Resources, Paper 79-1, p. 24-30.
- Jones, A.G.
1959: Vernon map-area, British Columbia; Geological Survey of Canada, Memoir 296, 186 p.
- Read, P.B.
1979a: Relationship between the Shuswap Metamorphic Complex and Kootenay Arc, Vernon east-half, southern British Columbia; in *Current Research, Part A, Geological Survey of Canada, Paper 79-1A*, p. 37-40.
1979b: Geology and mineral deposits, eastern part of Vernon east-half, British Columbia; Geological Survey of Canada, Open File 658.
- Reesor, J.E.
1970: Some aspects of structural evolution and regional setting in part of the Shuswap Metamorphic Complex; in *Structure of the southern Canadian Cordillera*, Geological Association of Canada, Special Paper 6, p. 73-86.
1973: Blanket Mountain area, British Columbia; in *Report of Activities, Part A, Geological Survey of Canada, Paper 73-1*, p. 38.
- Reesor, J.E. and Moore J.M.
1971: Petrology and structure of Thor-Odin gneiss dome, Shuswap Metamorphic Complex, British Columbia; Geological Survey of Canada, Bulletin 195, 149 p.
- Thompson, R.I.
1978: Geology of the Akolkolex River area; British Columbia Ministry of Energy, Mines and Petroleum Resources, Bulletin 60, 77 p.
- Wheeler, J.O.
1965: Big Bend map-area, British Columbia; Geological Survey of Canada, Paper 64-32, 37 p.

ISOTOPIC DATING OF EARLY JURASSIC VOLCANISM AND PLUTONISM IN NORTH-CENTRAL BRITISH COLUMBIA

Project 770016

H. Gabrielse¹, R.K. Wanless², R.L. Armstrong³, and L.R. Erdman³
Precambrian Geology Division

Gabrielse, H., Wanless, R.K., Armstrong, R.L., and Erdman, L.R., Isotopic dating of Early Jurassic volcanism and plutonism in north-central British Columbia, in Current Research, Part A, Geological Survey of Canada, Paper 80-1A, p. 27-32, 1980.

Abstract

Thick sequences of Lower and Middle Jurassic andesitic volcanic rocks flank Bowser Basin in the Intermontane Belt of north-central British Columbia. Distinctive Early Jurassic volcanics in the northern part of the region have been dated by the Rb-Sr whole-rock method at 191 ± 9 and 189 ± 13 Ma. Presumed correlative rocks on the northeastern flank of the basin (Toodoggone volcanics) have given Rb-Sr isochrons of 185 ± 5 and 185 ± 3 Ma and K-Ar dates of 182 ± 8 , 179 ± 8 and 189 ± 6 Ma. Approximately coeval granitic rocks give K-Ar dates ranging from 181 to 207 Ma. Initial $^{87}\text{Sr}/^{86}\text{Sr}$ ratios (0.7036 to 0.7043) are like those of modern andesitic volcanic arc suites.

Introduction

During the past ten years geological reconnaissance mapping has shown the distribution of Lower and Middle Jurassic volcanic rocks on the flanks of Bowser Basin, a large successor basin in the Intermontane Belt of north-central British Columbia (see Fig. 4.1; Souther, 1972; Tipper and Richards, 1976; Richards, 1975; Gabrielse, 1976, 1979; L.R. Erdman, 1978). Meagre data suggest that the present distribution of these volcanics approximates the locii of major eruptive centres during Early and Middle Jurassic time. Oweegee Dome within the northwestern part of the basin includes strata of pre-Permian(?) to Late Jurassic age with little, if any, Jurassic volcanic rock (Monger, 1977). Lower and Middle Jurassic rocks along the northeastern flank of the basin are predominantly volcanic whereas coeval strata farther southwest are predominantly sedimentary (Tipper, 1976; personal communication, 1977). It appears, therefore, that Early and Middle Jurassic volcanism (and related plutonism) was a major factor in the tectonic development of the Bowser Basin. Relative to other regional tectonic elements Jurassic volcanism was concentrated along Stikine and Skeena arches, the east side of the Coast Plutonic Complex and the west side of the Omineca Crystalline Belt.

Volcanic Rocks

In the northern part of Bowser Basin flanking volcanic terranes include abundant and distinctive maroon, grey and green weathering, well-layered andesite with lesser amounts of basalt, dacite and rhyolite. The rocks include vesicular flows, agglomerate, tuff and epiclastic sandstone. Spherulitic and flow-banded rhyolite, which weathers from cream to rusty brown and occurs as lenses or domes, is a relatively minor but conspicuous lithology within sequences dated paleontologically as Early Jurassic. Thicknesses of the volcanics commonly exceed 500 m. Unconformably overlying the Lower Jurassic volcanics along the northern margin of Bowser Basin are intercalated andesitic volcanics, commonly weathering pastel shades of purple, and fine grained to conglomeratic sedimentary rocks. Vesicular lava is most abundant but tuff and agglomerate are common. The sedimentary strata contain abundant clasts derived from the late Paleozoic Cache Creek Group to the north. Locally, strata believed correlative with those noted above contain a rich Middle Bajocian (lower Middle Jurassic) fauna. The Jurassic volcanic rocks have been affected by regional lower greenschist facies metamorphism with common development of albite, epidote, chlorite and calcite.

Plutonic Rocks

Stocks and batholiths of biotite-hornblende granodiorite to quartz monzonite are spatially related to the Lower Jurassic volcanic rocks and are believed to be genetically related to them. Less certain is the relationship between Bajocian(?) volcanic rocks and pink weathering hornblende-biotite quartz monzonite plutons that have given K-Ar ages ranging from 159 to 171 Ma.

Geochronometry

Five different suites of Lower Jurassic igneous rocks from the northern perimeter of the Bowser Basin have been selected for Rb, Sr, and Sr isotopic composition. Four were analyzed entirely at the University of British Columbia, and one jointly at U.B.C. and the Geological Survey of Canada in Ottawa (Table 4.1).

Rb-Sr Age Determinations

Erdman (1978) studied the petrology, chemistry, and geochronometry of three volcanic suites from the north end of the Bowser Basin. From that study two acceptable Rb-Sr isochrons were obtained. The third suite was altered, perhaps younger (Middle Jurassic) and thus is not included in this report. On the basis of structure, lithology, and stratigraphic continuity, correlation of rocks between the two areas with Lower Jurassic isochrons seems certain. In the southern locality marine fine grained clastic sedimentary rocks form a member about 15 m thick within the volcanics. Fossils include *Weyla* sp. and belemnoids dated as Early Jurassic by H.W. Tipper (personal communication, 1978). Sedimentary rocks have not been noted in the northern locality (near Mount Sister Mary), but about 5 km farther north volcanic-bearing sedimentary strata are abundantly fossiliferous. There, ammonites indicate a lower Toarcian age. No middle or upper Toarcian rocks have been recognized in the northern Bowser Basin region. The most accurate Rb-Sr whole rock isochron, obtained on samples from near Mount Sister Mary, is 191 ± 9 Ma (Fig. 4.2, 4.3). The age obtained from the southern locality, although not as accurate, is 189 ± 13 Ma (Fig. 4.4).

Nathan Green provided a suite of volcanic and granitic rocks of presumably Early Jurassic age (Toodoggone volcanics of Carter, 1972) from near Oxide Peak. Eight of these samples define an isochron of 185 ± 5 Ma (Fig. 4.5). Two of the volcanics lie distinctly above the isochron and were not

¹Cordilleran Geology Division, Vancouver.

²Precambrian Division, Ottawa.

³Department of Geological Sciences, University of British Columbia, Vancouver.

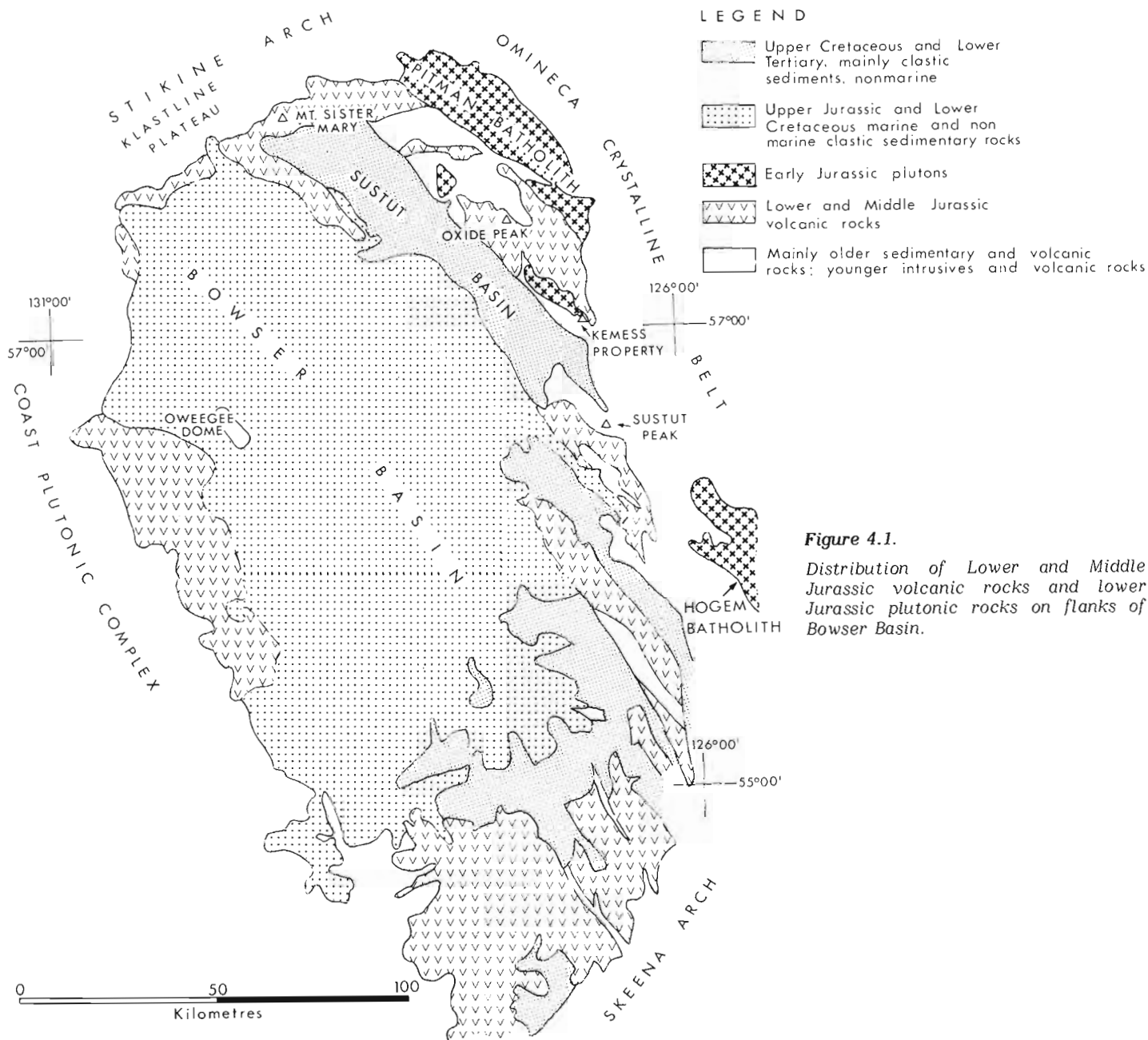


Figure 4.1.
Distribution of Lower and Middle Jurassic volcanic rocks and lower Jurassic plutonic rocks on flanks of Bowser Basin.

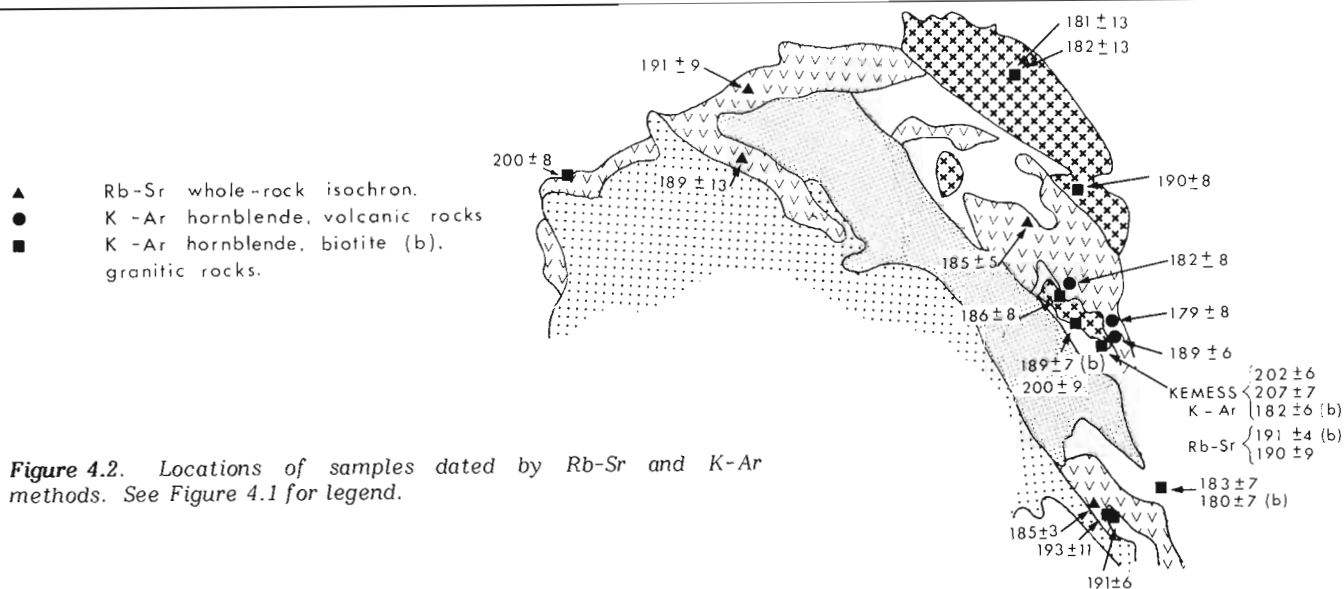


Figure 4.2. Locations of samples dated by Rb-Sr and K-Ar methods. See Figure 4.1 for legend.

Table 4.1
Sample data for Rb and Sr analyses and Sr isotopic composition

Sample Number	Latitude	Longitude	ppm Sr	ppm Rb	$^{87}\text{Sr}/^{86}\text{Sr}$
A: Mount Sister Mary 191 ± 9 Ma with initial $^{87}\text{Sr}/^{86}\text{Sr} = 0.7036 \pm 0.0001$					
GAE 119B	58°00'53"	129°05'17"	782	20.6	.7039
GAE 118B	58°00'47"	129°05'54"	1183	42.0	.7038
GAE 117C	58°00'32"	129°06'30"	772	55.2	.7042
SPHERY	58°00'26"	129°03'27"	284	89.7	.7061
B: South of Mount Sister Mary 189 ± 13 Ma with initial $^{87}\text{Sr}/^{86}\text{Sr} = 0.7043 \pm 0.0001$					
GAE 124B	57°41'34"	129°05'14"	403	22.3	.7046
GAE 121B	57°41'14"	129°05'29"	476	47.5	.7053
GAE 124	57°41'32"	129°05'20"	168	21.6	.7053
GAE 125	57°41'37"	129°05'08"	216	82.7	.7076
FLOW RHY	57°42'24"	129°04'56"	157	106.0	.7093
C: Oxide Peak 185 ± 5 Ma with initial $^{87}\text{Sr}/^{86}\text{Sr} = 0.7041 \pm 0.0001$					
348	57°20'23"	127°19'45"	336	64.5	.7075
348	57°20'23"	127°19'45"	316	124.0	.7071
353	57°20'11"	127°19'27"	369	27.0	.7047
433	57°14'23"	127°50'35"	571	73.9	.7051
SOM-1	57°19'52"	127°17'14"	515	85.8	.7054
OX-9	57°28'39"	127°23'33"	237	99.6	.7073
OX-5	57°28'36"	127°23'50"	258	89.8	.7068
OX-4	57°28'37"	127°23'59"	380	92.5	.7061
OX-8*	57°28'	127°23'	495	77.1	.7056
OX-1*	57°28'	127°24'	334	72.3	.7062
D: Southwest of Sustut Peak 185 ± 3 Ma with initial $^{87}\text{Sr}/^{86}\text{Sr} = 0.7040 \pm 0.0001$					
M75-205A	56°33'00"	126°48'00"	552	68.9	.7049
M75-207D	56°33'00"	126°50'00"	258	21.8	.7047
Wn-101-75A	56°30'30"	126°46'15"	60.97	143.6	.7215
Wn-101-75C	56°30'30"	126°46'15"	56.50	87.40	.7166
Wn-101-75D	56°30'30"	126°46'15"	74.70	122.1	.7165
Wn-101-75H	56°30'30"	126°46'15"	56.28	134.9	.7222
Wn-101-75I	56°30'30"	126°46'15"	60.59	142.4	.7215
Wn-101-75K*	56°30'30"	126°46'15"	63.47	163.8	.7222
Wn-101-75L	56°30'30"	126°46'15"	61.29	146.0	.7224
E: Southeast of Telegraph Creek 180 ± 109 Ma with initial $^{87}\text{Sr}/^{86}\text{Sr} = 0.7039 \pm 0.0005$					
GJ 75	57°39'	130°14'	677	67.6	.7044
GJ 90	57°40'	130°14'	696	68.6	.7049
GJ 62	57°39'	130°15'	564	83.3	.7050
GJ 87	57°40'	130°14'	698	58.0	.7047
GJ 84	57°40'	130°14'	686	90.6	.7051
<p>At U.B.C. Rb and Sr concentrations were determined by replicate analyses of pressed powder pellets using X-ray fluorescence. U.S. Geological Survey rock standards were used for calibration; mass absorption coefficients were obtained from Mo Kα Compton scattering measurements. Rb/Sr ratios have a precision of 2% (1σ) and concentrations a precision of 5% (1σ). Sr isotopic composition was measured on unspiked samples prepared using standard ion exchange techniques. The mass spectrometer (60° sector, 30 cm radius, solid source) is of U.S. National Bureau of Standards design, modified by H. Faul. Data acquisition is digitized and automated using a NOVA computer. Experimental data have been normalized to a $^{86}\text{Sr}/^{88}\text{Sr}$ ratio of 0.1194 and adjusted so that the NBS standard SrCO₃ (SRM987) gives a $^{87}\text{Sr}/^{86}\text{Sr}$ ratio of 0.71022 ± 0.0002 and the Eimer and Amend Sr a ratio of 0.70800 ± 0.0002. The precision of a single $^{87}\text{Sr}/^{86}\text{Sr}$ ratio is 0.00013 (1σ). Rb-Sr dates are based on a Rb decay constant of $1.42 \times 10^{-11} \text{ a}^{-1}$. The regressions are calculated according to the technique of York (1967, 1969). Much of the analytical work was done by Krista Scott. Analytical procedures in use at the Geological Survey laboratory in Ottawa were described by Wanless and Loveridge (1972).</p> <p>* Sample not used for isochron calculation.</p>					

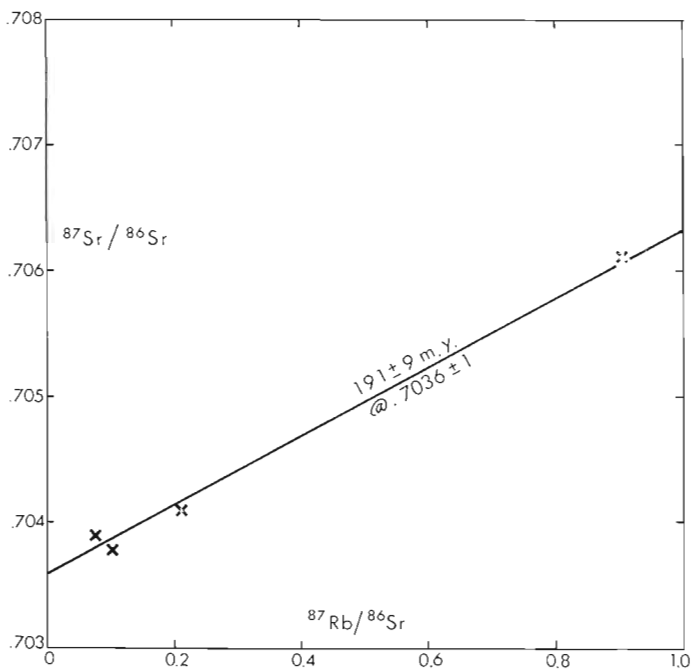


Figure 4.3. Rb/Sr whole rock isochron for volcanics near Mount Sister Mary.

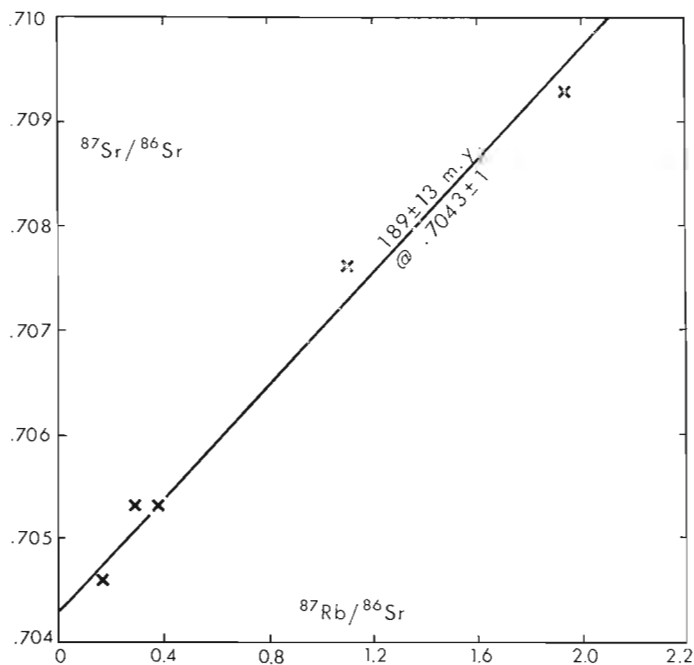


Figure 4.4. Rb/Sr whole rock isochron for volcanics south of Mount Sister Mary.

used in its calculation. This type of discordance is expectable in any volcanic suite that has been altered in the presence of sea water (as observed in the Nicola volcanics by Preto et al., in press).

J.W.H. Monger provided samples of Hazelton Group volcanics from southwest of Sustut Peak of both University of British Columbia and Geological Survey of Canada laboratories for Sr isotopic analyses. The samples

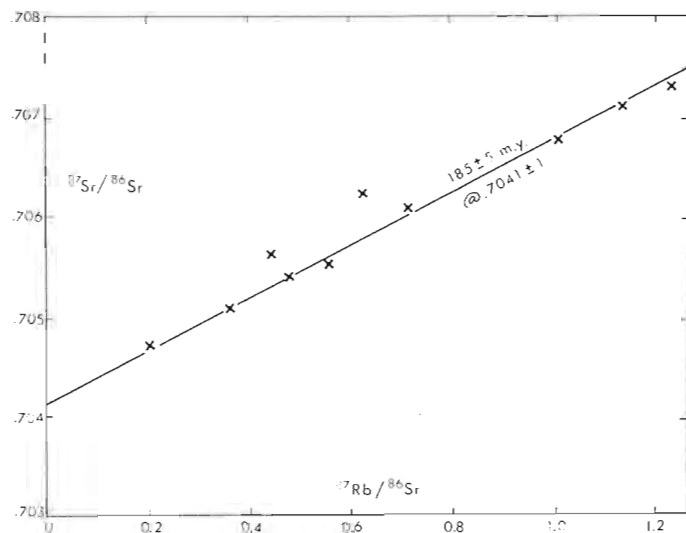


Figure 4.5. Rb/Sr whole rock isochron for volcanics near Oxide Peak.

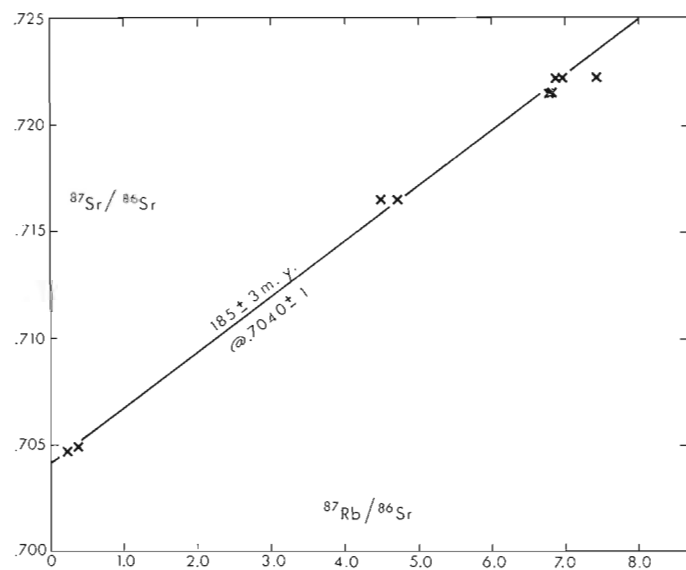


Figure 4.6. Rb/Sr whole rock isochron for volcanics southwest of Sustut Peak.

representing rocks tentatively correlated with the Telkwa Formation (Richards, 1975) give an isochron of 185 ± 3 Ma (Fig. 4.6). In the type area the Telkwa Formation is of Sinemurian to earliest Pliensbachian age (Tipper and Richards, 1976).

Schmitt (1977) analyzed a sample suite from a pluton at the southwest end of the Klastline plateau on the northwest margin of the Bowser Basin. A precise isochron date was unattainable because of limited range in Rb/Sr ratio. The result obtained, 180 ± 109 Ma, is fortuitously close to our other isochron dates.

Cann and Godwin (in press) report Rb-Sr whole rock and mineral (predominantly biotite) isochron dates for granitic rocks on the Kemess property of 190 ± 9 and 191 ± 4 Ma, respectively (see Fig. 4.2).

Initial $^{87}\text{Sr}/^{86}\text{Sr}$ Ratios

The different whole-rock Rb-Sr isochrons discussed above give initial ratios of 0.7036 ± 0.0001 , 0.7043 ± 0.0001 , 0.7041 ± 0.0001 , 0.7040 ± 0.0001 , 0.7039 ± 0.0005 and 0.7042 ± 0.0001 , respectively. These are typical of the values for modern volcanic arcs (Faure and Powell, 1972) where the mantle source region is dominant but the magma-genesis system is slightly contaminated with more radiogenic crustal Sr.

K-Ar Age Determinations

Volcanic rocks, mainly well-layered andesite and dacite characterized by free quartz, underlie sedimentary strata of the Sustut Group along the northeast margin of Bowser Basin. Three samples of hornblende analyzed from the volcanics have given ages of 182 ± 8 , 179 ± 8 and 189 ± 6 Ma (Table 4.2). The volcanics underlie rocks containing Bajocian fossils and are lithologically identical to those dated by the Rb-Sr method to the northwest.

Granodiorite and quartz monzonite plutons of similar chemistry to the Early Jurassic volcanics and spatially related to them occur along the northeast margin of Sustut Basin. Ages obtained by the K-Ar method on hornblende and biotite are: 181 ± 13 , 182 ± 13 , 186 ± 8 , 190 ± 8 , 189 ± 7 and 200 ± 9 Ma. The last two are from the same sample and represent ages derived from biotite and hornblende, respectively. Related to these are hornblende K-Ar dates of 202 ± 6 and 207 ± 7 Ma and biotite K-Ar date of 182 ± 6 Ma for granitic rocks on the Kemess property (Cann and Godwin, in press).

Two granitic stocks in the area near Sustut Peak have yielded K-Ar ages of 193 ± 11 and 191 ± 6 Ma on hornblendes and 183 ± 7 and 180 ± 7 Ma on a hornblende-biotite pair (Church, 1974, 1975).

A hornblende K-Ar date of 200 Ma was provided for Schmitt (1977) for a similar pluton on the northwestern margin of the Bowser Basin.

Table 4.2
Sample data for K and Ar analyses* on hornblende and biotite

Sample Number	Latitude	Longitude	K%	$\text{Ar}^{40}/\text{K}^{40}$	Radiogenic Argon %	Age Ma
<u>Volcanic rocks</u>						
GSC 76-77	57°08'00"	126°42'18"	0.864	0.01119	75.5	179 ± 8
GSC 78-24	57°16'30"	127°01'00"	0.787	0.01113	56.9	182 ± 8
Carter, 1972	57°07'36"	126°43'00"	0.873	0.01158	91.3	189 ± 6
<u>Granitic rocks</u>						
GSC 76-74	57°14'36"	127°02'54"	0.447	0.01166	78.8	186 ± 8
GSC 76-75 (biotite)	57°09'54"	127°02'12"	6.40	0.01184	94.6	189 ± 7
GSC 76-76	57°09'54"	127°02'12"	0.459	0.01256	83.8	200 ± 9
GSC 78-21	57°36'12"	126°53'06"	0.851	0.01162	83.6	190 ± 8
GSC 77-88	58°03'48"	127°16'48"	0.820	0.01106	53.3	181 ± 13
GSC 77-88	58°03'48"	127°16'48"	0.820	0.01115	78.7	182 ± 13
Schmitt, 1977	57°40'00"	130°14'00"	0.602	0.01227	80.0	200 ± 8
Church, 1975 (Asitka)	56°36'00"	126°26'00"	2.60	0.0116	88.1	183 ± 7
Church, 1975 (biotite)	56°36'00"	126°26'00"	0.379	0.01097	56.7	180 ± 7
Church, 1974 (Day)	56°30'00"	126°46'00"	0.367	0.01183	49.3	193 ± 11
Church, 1975 (Pat)	56°28'00"	126°42'30"	0.589	0.01169	88.9	191 ± 6

At U.B.C. K is determined by Krista Scott in duplicate by atomic absorption using a Techtron AA4 spectrophotometer and Ar by J.E. Harakal by isotope dilution using an AEI MS-10 mass spectrometer and high purity ^{38}Ar spike (White et al., 1967). Analytical procedures used by the GSC laboratory in Ottawa are outlined in the Geological Survey's papers on Age Determinations and Geological Studies. Errors are for two standard deviations. The constants used are:

$$\lambda^{40}\text{K}_e = 0.581 \times 10^{-10} \text{a}^{-1}, \lambda^{40}\text{K}_\beta = 4.962 \times 10^{-10} \text{a}^{-1},$$

$$^{40}\text{K} = 0.01167 \text{ atom per cent}$$

* Sample numbers with the prefix GSC were analyzed at the Geological Survey of Canada laboratory in Ottawa. All others were analyzed at University of British Columbia with the exception of Sample Church, 1974 (Day) analyzed by Geochron Laboratories.

Summary

Lower Jurassic volcanic rocks near the northern and northeastern margins of Bowser Basin have given ages by Rb-Sr and K-Ar methods ranging from 179 to 191 Ma. Ages on spatially related granitic plutons support the contention that they are essentially coeval with the volcanic rocks, but some may be attributable to earlier igneous activity during deposition of Hazelton volcanic rocks along the eastern and southern parts of the Bowser Basin (Tipper and Richards, 1976).

References

- Cann, R.M. and Godwin, C.I.
1972: Geology, Rb-Sr and K-Ar dating of the Kemess porphyry copper-molybdenum deposit, north-central British Columbia; Canadian Institute of Mining and Metallurgy, Bulletin. (in press)
- Carter, N.C.
1972: Toodoggone River area; in *Geology, Exploration and Mining in British Columbia, 1971*; British Columbia Department of Mines and Petroleum Resources, p. 63-70.
- Church, B.N.
1974: Geology of the Sustut area; in *Geological Fieldwork 1974*; British Columbia Department of Mines and Petroleum Resources, p. 51-55.
1975: Geology of the Sustut Area; in *Geology Exploration and Mining in British Columbia, 1974*; British Columbia Department of Mines and Petroleum Resources, p. 305-309.
- Erdman, L.R.
1978: Petrology, geochronology, and geochemistry of Jurassic volcanic and granitic rocks on the Cry Lake and Spatsizi map-area; unpublished B.Sc. thesis, University of British Columbia, 63 p.
- Faure, G. and Powell, J.L.
1972: *Strontium Isotope Geology*; Springer-Verlag, Berlin, 188 p.
- Gabrielse, H.
1976: Toodoggone River map-area; Geological Survey of Canada, Open File 306 (map).
1979: Cry Lake map-area; Geological Survey of Canada, Open File 610 (map).
- Monger, J.W.H.
1977: Upper Paleozoic rocks of northwestern British Columbia; in *Report of Activities, Part A, Geological Survey of Canada, Paper 77-1A*.
- Preto, A.V., Osatenko, M.J., McMillan, W.V., and Armstrong, R.L.
Isotopic dates and strontium isotopic ratios for plutonic and volcanic rocks in the Quesnel Trough and Nicola Belt, south-central British Columbia; Canadian Journal of Earth Sciences. (in press)
- Richards, T.A.
1975: McConnell Creek map-area; Geological Survey of Canada, Open File 342 (map).
- Schmitt, H.R.
1977: A Triassic-Jurassic granodiorite monzodiorite pluton southeast of Telegraph Creek, B.C.; unpublished B.Sc. thesis, University of British Columbia, 91 p.
- Souther, J.G.
1972: Telegraph Creek map-area, British Columbia; Geological Survey of Canada, Paper 71-44.
- Tipper, H.W.
1976: Biostratigraphic study of Mesozoic rocks in Intermontane and Insular belts of the Canadian Cordillera, British Columbia; in *Report of Activities, Part A, Geological Survey of Canada, Paper 76-1A*.
- Tipper, H.W. and Richards, T.A.
1976: Jurassic stratigraphy and history of north-central British Columbia; Geological Survey of Canada, Bulletin 270.
- Wanless, R.K. and Loveridge, W.D.
1972: Rubidium-strontium isochron age studies, Report 1; Geological Survey of Canada, Paper 72-23.
- White, H., Erickson, G.P., Northcote, K.E., Dirom, G.E., and Harakal, J.E.
1967: Isotopic dating of the Guichon batholith, B.C.; Canadian Journal of Earth Sciences, v. 4, p. 677-690.
- York, D.
1967: The best isochron; *Earth and Planetary Science Letters*, v. 2, p. 479-482.
1969: Least-squares fitting of a straight line with correlated errors; *Earth Planetary Science Letters*, v. 5, p. 320-324.

**STRUCTURAL STYLE IN NORTHEASTERN CRY LAKE MAP AREA,
NORTH-CENTRAL BRITISH COLUMBIA**

Project 770016

H. Gabrielse and J.L. Mansy¹
Cordilleran Geology Division, Vancouver

Gabrielse, H. and Mansy, J.L., Structural style in northeastern Cry Lake map area, north-central British Columbia, in Current Research, Part A, Geological Survey of Canada, Paper 80-1A, p. 33-35, 1980.

Abstract

Klippen of Devonian-Mississippian (?) and younger rocks of oceanic type overlie typical miogeoclinal strata in northeastern Cry Lake map area. Their age of emplacement appears to have been during Late Jurassic or Early Cretaceous time.

Introduction

For many years it has been recognized that two contrasting assemblages of rocks in Cassiar Mountains presented a major problem in paleogeographic interpretation. A miogeoclinal assemblage comprising clastic and carbonate strata of Late Proterozoic to Late Devonian age clearly represents a depositional environment along the western margin of the North American craton. On the other hand, an overlying assemblage of chert, limestone, shale, basic volcanics and ultramafic rocks is of oceanic aspect and represents an environment of deposition with no apparent close relationship to the craton. Field work in 1979 supports the concept that most of the Devonian to Permian volcanic and related rocks in northeastern Cry Lake map area are allochthonous.

Stratigraphy

The largest of the presumed allochthonous masses comprises most of the Sylvester Group (Gabrielse, 1979). Excluded are the autochthonous black shales, commonly pyritic, that have been mapped as the basal unit. Farther north, in McDame map area the black shale is overlain by chert-pebble conglomerate and chert arenite also interpreted as autochthonous. Conodonts from the shale indicate a Late Devonian, late Frasnian or Famennian age (B.E.B. Cameron, personal communication, 1978).

Overlying the shale in Cry Lake map area is an intensely folded sequence of well-bedded chert. South of Major Hart River the unit occurs in folds with flat-lying axial planes and amplitudes of a few metres to tens of metres (Fig. 5.1). Great differences in thickness and character of



Figure 5.1. *Folded chert south of Major Hart River. Exposure is about 15 m high.*

¹University of Lille, France

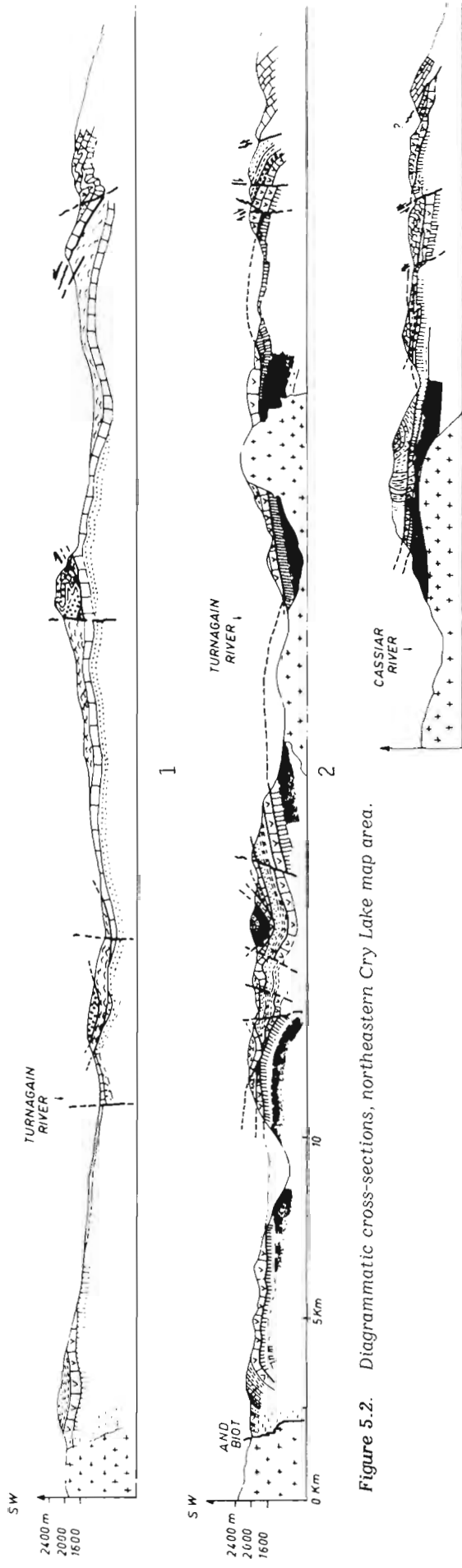


Figure 5.2. Diagrammatic cross-sections, northeastern Cry Lake map area.



Figure 5.3. View looking north, north of Turnagain River, showing interformational fault contact between Espee Formation and truncated Tsaydiz Formation.

strata beneath the chert suggest that it occurs directly above the sole of a thrust plate. The upper part of the Sylvester Group includes thick units of basic volcanics and a number of alpine-type ultramafic bodies.

Two small klippen, one underlying the peak of a mountain centred on 128°17'30"W, 58°45'30"N and the other at 128°14'W, 58°44'30"N were mapped in 1979. The former, comprising well-layered tuff, in part possibly mylonitic, minor sandy limestone in beds to 7 m thick and feldspar-quartz porphyry dykes, rests on or against strata of the Kechika and Atan groups. The latter, possibly 150 m long and 100 m wide, rests on carbonates of the Atan and Kechika groups. It consists of poorly bedded to well-bedded black, nodular cherty argillite.

A third probable klippe outcrops north of the big bend of Turnagain River northeast of the mouth of Three Forks Creek (Gabrielse, 1979). There, autochthonous rocks of Middle and Late Devonian age are apparently structurally overlain by breccia containing clasts of limestone and strongly pyritized acid volcanics in turn overlain by basic volcanics.

Structure

Study of structural style in the Sylvester Group requires much further work. The lower, autochthonous strata have been involved in westerly verging folding and thrusting followed by northeasterly directed thrust faulting (Gabrielse and Mansy, 1978). It is not clear that the upper part of the

Group has undergone the same two deformations. Northeasterly directed thrusts are evident and locally it seems as if the earlier formed southwesterly verging structures have been truncated along the sole of the allochthon.

The klippe at 128°17'30"W, 58°45'30"N is intensely deformed and is characterized by a flat foliation along which original layering has been transposed. The structure is similar to that involving chert at the base of the major allochthon to the northwest.

Structural style in the miogeoclinal strata in northeastern Cry Lake map area is fairly well known. Dominant structures are southwesterly verging folds and associated thrust faults (Fig. 5.2). Flat-lying faults that have placed nappes of younger strata on older are particularly common in the Turnagain River area (Fig. 5.3). Only near Major Hart River are the later easterly directed thrust faults clearly defined.

References

Gabrielse, H.

1979: Geological map of Cry Lake map area; Geological Survey of Canada, Open File Report 610.

Gabrielse, H. and Mansy, J.L.

1978: Structure style in northeast Cry Lake map area, north-central British Columbia; in Current Research, Part A, Geological Survey of Canada, Paper 78-1A, p. 33-34.

**SATELLITIC STOCKS, VOLCANIC AND SEDIMENTARY STRATIGRAPHY,
AND STRUCTURE AROUND THE NORTHERN AND WESTERN MARGINS OF
THE HOTAILUH BATHOLITH, NORTH-CENTRAL BRITISH COLUMBIA**

Project 770016

R.G. Anderson¹
Cordilleran Geology Division, Vancouver

Anderson, R.G., Satellite stocks, volcanic and sedimentary stratigraphy, and structure around the northern and western margins of the Hotailuh Batholith, north-central British Columbia; in Current Research, Part A, Geological Survey of Canada, Paper 80-1A, p. 37-40, 1980.

Abstract

Radiometric ages on the oldest phase of the Hotailuh Batholith and on cobbles in basal conglomerate nonconformably overlying the batholith indicate that emplacement and unroofing of the oldest phase took place in Late Triassic time. On the basis of regional correlations with rocks in McConnell Creek and Tulsequah map areas the distinctive maroon-weathering volcanics north and east of Hotailuh Batholith are thought to be Early Jurassic and possibly Late Triassic.

Introduction

The purpose of the 1979 season was to examine three outlying satellitic stocks north and west of the Hotailuh Batholith, to establish a stratigraphy in volcanic and sedimentary rocks along the northern margin of the batholith and to elucidate some of the structure in the nongranitoid rocks. Field work was carried out with the aid of helicopter support provided by the Operation Dease base on the Tanzilla River. Tentative identification of fossils was made by Dr. H.W. Tipper.

Pallen Creek and Tanzilla Stocks

The Pallen Creek and Tanzilla stocks underlie areas of 17.8 km² and 2.3 km² respectively, east of the Tanzilla River in the southeastern corner of Dease Lake map area (104 J). The Pallen Creek Stock was first discovered by mineral exploration companies and its eastern, northern and western contacts later verified by officers of the Geological Survey of Canada (H. Gabrielse, personal communication, 1979). The Tanzilla Stock is outlined on the preliminary geological map of Dease Lake (Gabrielse and Souther, 1962). Both granitic bodies are characterized by aeromagnetic highs (Geological Survey of Canada, 1978b).

The Pallen Creek Stock underlies the headwaters of Pallen Creek 4 km west and southwest of peak 6256 feet and 23.5 km northeast of the confluence of the Tanzilla and Stikine rivers. A distinctive, homogeneous and massive, pink potassium-feldspar megacryst-bearing, biotite-hornblende monzodiorite to quartz monzodiorite forms most of the stock. Near its northeast end is a small exposure of

irregular, equigranular hornblende gabbro and biotite-hornblende monzodiorite. Intrusive relationships indicate that the equigranular monzodiorite intrudes the gabbro and that both lithologies are intruded by thin, irregular hornblende-biotite syenite dykes. Along its eastern margin all phases of the Pallen Creek Stock intrude locally-pillowed augite porphyry volcanics or shale and siltstone underlying the volcanics. The contact is not exposed along the western margin of the batholith and the southern margin of the stock is poorly exposed. Discordant hornblende-biotite potassium-argon ages of 161 Ma (hornblende) and 141 Ma (biotite) have been determined for the megacryst-bearing phase of the Pallen Creek Stock (H. Gabrielse, personal communication, 1979).

The Tanzilla Stock is located 11 km east-southeast of the abandoned settlement of Cariboo Meadows and 19 km north-northeast of the confluence of the Tanzilla and Stikine rivers. It consists of a massive, homogeneous, fresh, melanocratic hornblende-biotite quartz monzodiorite, monzodiorite and diorite with sphene, euhedral fresh biotite and a distinctive slabby outcrop appearance due to vertical and horizontal joints. This jointing pattern is visible on airphotos of the body as a set of northeast- and southeast-trending lineaments. The monzodiorite-quartz monzodiorite is intruded at one locality by a stockwork of syenitic dykes. Contacts are apparently only well exposed at one locality, along the northern margin of the stock, where tough, massive augite-plagioclase porphyry volcanics(?) appear to be hornfelsed adjacent to the contact. No radiometric ages have yet been determined from the Tanzilla Stock.

Lithologies, intrusive relationships, radiometric ages and aeromagnetic signatures of the Pallen Creek and Tanzilla stocks suggest they may be correlative with the Three Sisters Plutons (mafic, quartz monzodiorite-monzodiorite and potassic marginal phases) of the Hotailuh Batholith described in earlier papers (Anderson, 1978, 1979).

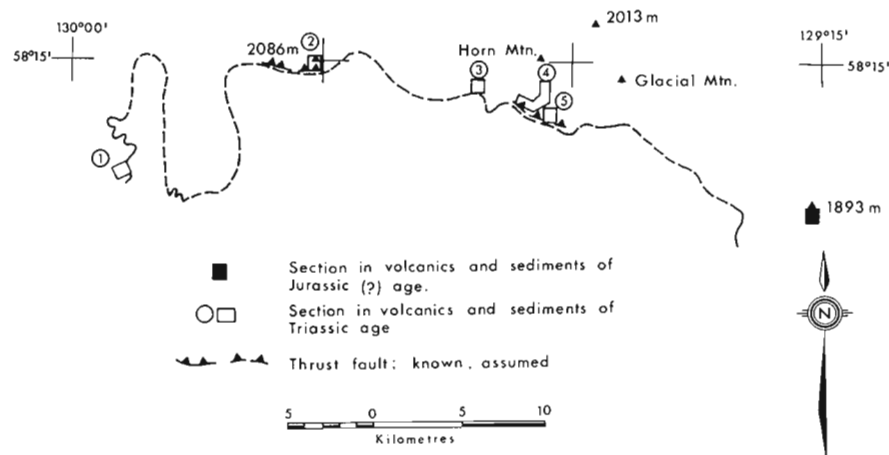
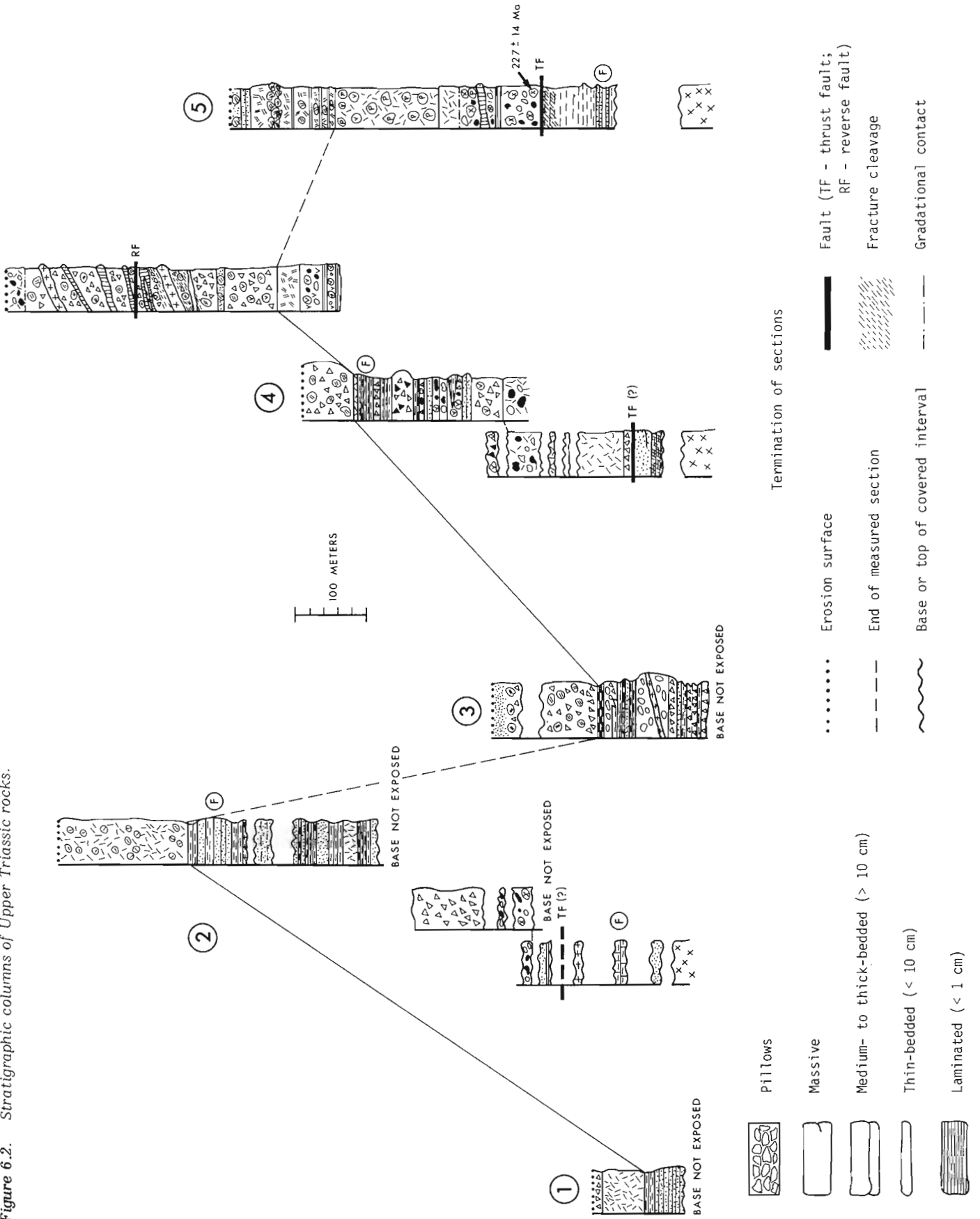


Figure 6.1

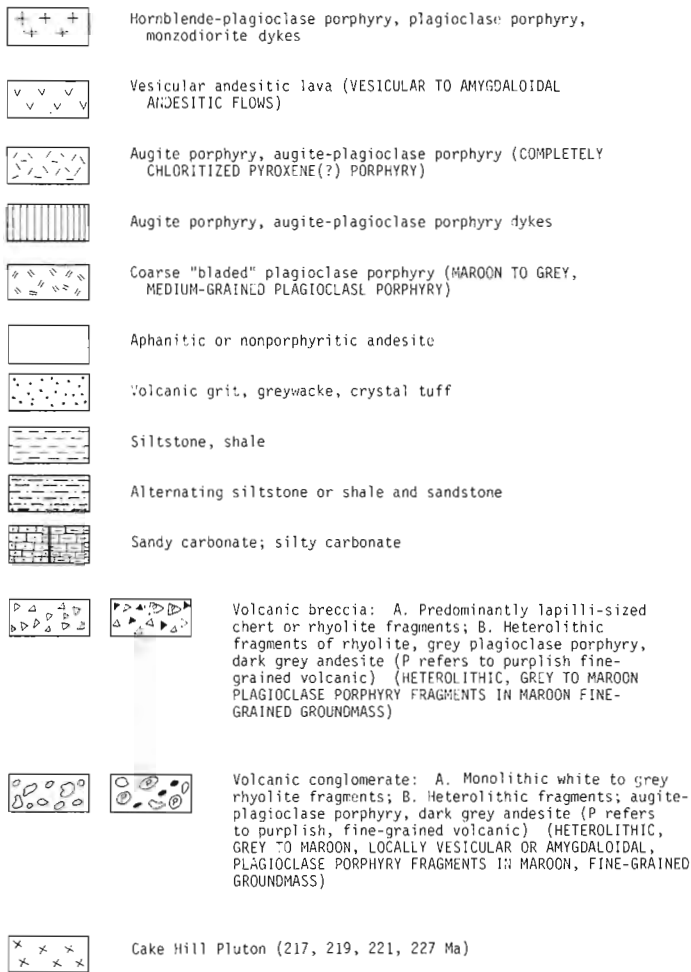
Locations of stratigraphic sections measured in Upper Triassic and Lower Jurassic rocks on north side of Hotailuh Batholith (contact indicated by dashed line).

¹Carleton University, Ottawa, Ontario.

Figure 6.2. Stratigraphic columns of Upper Triassic rocks.



STRATIGRAPHIC SECTION LEGEND¹



1. Capitalized explanation in parentheses refers to symbols used in the Lower Jurassic (?) section (Figure 6.3).

Snowdrift Creek Stock

The Snowdrift Creek Stock is exposed as numerous large outcrops, separated by large areas of cover, within and along Snowdrift Creek, 3 to 5 km north of Horn Mountain and Glacial Mountain. If these outcrops are correlative, the stock has an area of approximately 67 km². The main outcrop areas are seen on the preliminary and revised Cry Lake map areas (Gabrielse, 1962, 1979). In two main exposures examined, the stock consists of faintly to moderately foliated, slightly heterogeneous (uncommon, small, rounded, fine grained dioritic inclusions and elongate schlieren), fresh biotite-hornblende quartz monzodiorite. It clearly intrudes, includes and metamorphoses augite porphyry and arkosic(?) sediments at one location and may intrude, alter and deform argillites of probable Pliensbachian age along its western margin (Gabrielse, personal communication, 1977). A preliminary potassium-argon age on biotite from the Snowdrift Creek Stock gives an age of 147 ± 5 Ma (R.K. Wanless, written communication, 1978).

Features such as its euhedral hornblende, greater quartz content, more common sphene, less common inclusions and negative aeromagnetic anomaly (Geological Survey of Canada, 1978a) distinguish the Snowdrift Creek Stock from the lithologically similar quartz monzodiorite-monzodiorite phase of the Three Sisters Plutons of the Hotailuh Batholith.

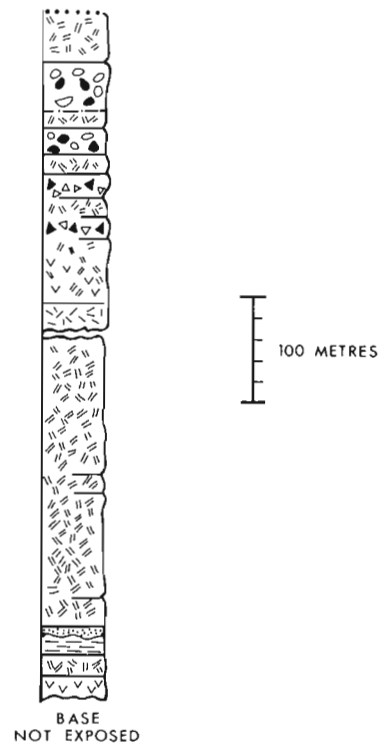


Figure 6.3. Stratigraphic column for Upper Triassic and/or Lower Jurassic maroon-weathering volcanics.

The Snowdrift Creek Stock greatly resembles the McBride River Pluton in lithology and distribution relative to the main batholith.

Stratigraphy and Structure

The best exposures of sections through the Triassic and Jurassic volcanic and sedimentary rocks around the Hotailuh Batholith occur along its northern margin where these rocks dip uniformly off the batholith at 35 to 45 degrees. It was reported by Anderson in 1978 that along this northern margin volcanic and sedimentary rocks of probable Triassic age nonconformably overlie the Cake Hill Pluton and at the contact contain cobbles and boulders of this pluton. Monger and Thorstad (1978) briefly described the Triassic and Jurassic volcanics around the Hotailuh Batholith. Insufficient time prevented detailed mapping of the volcanics and sediments. Representative sections through the Triassic sediments and volcanics and Lower Jurassic(?) maroon volcanics and sediments are presented, however, in Figures 6.2 and 6.3, respectively. The location of these sections is given in Figure 6.1.

The exposed bases of the Triassic sections generally consist of heterolithic volcanic breccias and conglomerates with minor to significant thicknesses of interbedded greywacke, arenite, siltstone, and shale. Locally, recessive, 10-15m-thick, moderately to thinly bedded greywacke and siltstone units alternate with the resistant, massive volcaniclastic units. These sedimentary units are commonly scoured and convolutedly bedded at their contact with the base of a thick volcaniclastic unit. Volcanic breccias and volcanic conglomerates are generally poorly sorted, massive, matrix-supported, medium to coarse and dark green to grey. The fragments are predominantly volcanic and may range in size from 0.5 to 60 cm. The exception is the large concentration of rounded granitic cobbles and boulders of Cake Hill Pluton found at the base of the Triassic part of

section 5. Hornblende from these cobbles has been dated at 227 ± 14 Ma by the K-Ar method (R.K. Wanless, written communication, 1979). In some units, fragments may be angular or rounded. Except for monolithic volcanic conglomerates containing whitish, pyritiferous, locally flow-layered rhyolitic fragments, generally the fragments are dark grey to green feldspar porphyries best distinguished on weathered surfaces. Vesicular and (or) amygdaloidal lava fragments appear in volcaniclastic units near the base of major flow units, are useful for local correlation of volcaniclastic units and indicate derivation from a nearby source. The groundmass for many of the units is dark grey, fine grained and apparently volcanic or reworked volcanic rock. One especially useful volcaniclastic unit is the white rhyolite-fragment breccia-conglomerate. This is a heterolithic unit of bimodal fragment-size consisting of small (1 cm) angular to squarish, white, uncommonly flow-layered and porphyritic (rounded quartz and plagioclase phenocrysts), pyritiferous, fine grained rhyolitic fragments and larger (10-25 cm), rounded, light grey (uncommonly with a brownish weathering(?) rind), medium- to coarse-grained, "bladed"-plagioclase-porphyry fragments. The thickness of this unit changes dramatically, thickening to the west from 5 m in section 5 to at least 120-200 m in sections 3 and 4. Its distinctive lithology (especially the "bladed"-plagioclase-porphyry fragments) and position relative to tentatively dated sediments makes it a useful marker horizon.

Augite porphyry, hornblende-plagioclase-porphyry syenite (of the last pulse of Three Sisters Plutons' activity) and minor massive andesite dykes intrude the Triassic sections and produce a fracture cleavage in the distinctive white-rhyolite-fragment breccia-conglomerate parallel to dyke contacts.

The flows generally are massive, thick and restricted to the top of the measured sections. Augite porphyry or "bladed" plagioclase porphyry are the predominant flow lithologies. In section 2, fragments of augite porphyry are found within an augite porphyry groundmass. Locally, as in section 5, the "bladed" plagioclase porphyry is pillowed and down dip these pillows appear to be broken and intercalated with green coarse greywacke.

The age of the Triassic part of sections 1 through 5 is fairly well known. Cobbles in the basal part of section 5 are dated at 227 ± 14 Ma and give a maximum age for the sections since similar granitic-cobble-bearing, volcanic conglomerates are seen nonconformably overlying the Cake Hill Pluton. Fossil localities in section 4 and above the thrust fault in section 2 contain a similar ammonite genus which indicates a Late Triassic age. This is the basis for the correlation between sections 2 and 3. A minimum age is suggested near the location of section 1 where the volcanics are intruded by quartz syenite of the potassic marginal phase dated at 164 ± 5 Ma (biotite) and 169 ± 11 Ma (hornblende) (R.K. Wanless, written communication, 1978).

At the base of three sections, nonconformably overlying the Cake Hill Pluton, are thin sedimentary units of Toarcian age. These units consist of clean, buff quartzite to quartzofeldspathic arenite and intercalated black shale and minor rusty tan micrite. A recent study by Henderson (1978) on fauna from the lower fossil locality shown in section 2 indicates an Early Toarcian age for that locality. Tentative identification of at least five ammonite genera and *Weyla* pelecypods from the fossil locality in section 5 establishes the age of that unit as Toarcian (H.W. Tipper, personal communication, 1979). The correlation between the basal sedimentary unit of section 4 and the Toarcian unit of section 5 is based on lithological similarity.

The Lower Jurassic(?) section (Fig. 6.3) differs from the Triassic sections in that volcaniclastics are much subordinate to flows and the flows are more commonly vesicular or amygdaloidal in the Lower Jurassic(?) section. The most distinctive field criterion for the Lower Jurassic volcanics is

their reddish to maroon groundmass. This is caused by oxidation of the fine- to medium-grained magnetite phenocrysts in many of the flows to hematite and consequent reddish staining of all or part of the groundmass. Individual flows may be distinguished with difficulty by the concentration and size of the fine- to medium-grained plagioclase phenocrysts, rarely by groundmass texture and by varying resistance to weathering. Fragments in the volcaniclastics are rounded to angular, poorly sorted, from 1 to 45 cm across and consist of plagioclase porphyry similar to flows above and below the volcaniclastic units. The matrix is fine grained, maroon and tuffaceous(?). No fossils were collected from this section and its designated Early Jurassic(?) age is based on lithological similarities to Lower Jurassic volcanics in the Tulsequah map area (J.W.H. Monger and H.W. Tipper, personal communication, 1979) and correlation with the Telkwa Formation of the Hazelton Group (Monger and Thorstad, 1978).

A southerly directed thrust along part of the northern margin of the Hotailuh Batholith brings Upper Triassic volcanics and sediments over Toarcian calcareous sediments and limestones (Fig. 6.1, and sections 2, 4 and 5 of Fig. 6.2). Little deformation in the Toarcian sediments is seen except for a well developed fracture in shale beds beneath the thrust fault. The presence of near-to-source fragments, such as the very large Cake Hill Pluton boulders in the basal part and fragile vesicular or amygdaloidal lava fragments in the middle part of the thrusted Upper Triassic section, indicates that the section has not been thrust very far. Locally, small-scale, northerly directed reverse faults also occur in the thrust plate of Upper Triassic volcanics. Near section 1, intrusion of the potassic marginal phase of the Three Sisters Plutons has warped, block-faulted and drag-folded the sediments of the Lower Triassic section.

References

- Anderson, R.G.
 1978: Preliminary report on the Hotailuh Batholith; its distribution, age and contact relationships in the Cry Lake, Spatsizi and Dease Lake map areas, north-central British Columbia; in Current Research, Part A, Geological Survey of Canada, Paper 78-1A, p. 29-31.
 1979: Distribution and emplacement history of plutons within the Hotailuh Batholith in north-central British Columbia; in Current Research, Part A, Geological Survey of Canada, Paper 79-1A, p. 393-395.
- Geological Survey of Canada
 1978a: Cry Lake (104 I); aeromagnetic map 7797G.
 1978b: Dease Lake (104 J); aeromagnetic map 7798G.
- Gabrielse, H.
 1962: Cry Lake map area; Geological Survey of Canada, Map 29-1962.
 1979: Geological map of Cry Lake map area; Geological Survey of Canada, Open File 610.
- Gabrielse, H. and Souther, J.G.
 1962: Dease Lake map area; Geological Survey of Canada, Map 21-1962.
- Henderson, C.
 1978: Paleontology and Paleoecology of a Lower Jurassic Bryozoan biotic association, Turnagain Lake (Cry Lake map-area, 104 I), British Columbia; unpublished B.Sc. thesis, University of British Columbia. 88 p.
- Monger, J.W.H. and Thorstad, L.
 1978: Lower Mesozoic stratigraphy, Cry Lake and Spatsizi map areas, British Columbia; in Current Research, Part A, Geological Survey of Canada, Paper 78-1A, p. 21-24.

Project 650024

W.H. Fritz
Institute of Sedimentary and Petroleum Geology, Ottawa

Fritz, W.H., *International Precambrian-Cambrian Boundary Working Group's Field Study to Mackenzie Mountains, Northwest Territories, Canada; in Current Research, Part A, Geological Survey of Canada, Paper 80-1A, p. 41-45, 1980.*

Abstract

During the 1979 field season thirteen Working Group members studied five stratigraphic sections in the west-central Mackenzie Mountains, and selected a tentative boundary interval within map unit 12 of the Sekwi Mountain map area in order to focus Canadian research. Map unit 12 is part of a thick succession of late Precambrian and early Lower Cambrian interbedded shale, siltstone and quartzite, the upper portion of which is mainly dated by the use of trace fossils. The overlying late Lower Cambrian succession was also inspected. These strata belong to the Sekwi Formation, and consist of platform carbonates to the east and laterally equivalent slope and basin deposits to the west. Trilobites are the principal fossils used in correlating these younger strata.

Introduction

During the summer of 1979 the Working Group (IUGS-IGCP Project 29) inspected boundary strata and fossils in two areas, eastern Newfoundland and the Mackenzie Mountains. Because some members visited but one of the two areas, there was only a partial overlap of personnel on the two excursions. Members on the Mackenzie trip were as follows: J.D. Aitken (Canada), S. Conway Morris (U.K.), J.W. Cowie (U.K.), M. Fedonkin (USSR), T.P. Fletcher (U.K.), W.H. Fritz (Canada), H.J. Hofmann (Canada), J.L. Kirschvink (U.S.A.), C.A. Nelson (U.S.A.), A. Yu. Rozanov (USSR), V.E. Savitsky (USSR), B.W. Webby (Australia), and Xing Yusheng (People's Republic of China). Aitken and Fritz acted as hosts and guides, and early scheduling and planning was accomplished by the Working Group's leader J.W. Cowie and secretary A. Yu. Rozanov. The trip took place between July 31 and August 9, 1979, and was based at a field camp on June Lake, west-central Mackenzie Mountains, Northwest Territories. The campsite was a short distance east of centre on the Sekwi Mountain map sheet (105 P), the geology of which was published by S.L. Blusson in 1971. The numbered map units referred to in the following text and figures are informal formations erected by Blusson for use on his geological map.

Late Precambrian and Early Lower Cambrian

A planned inspection of the tillite-bearing Rapitan Group was cancelled due to bad weather. Late Precambrian glacial deposits continue to be of interest to the Working Group as a reference horizon below the boundary, and reports of a low stratigraphic occurrence in the Mackenzie Mountains reinforces a growing belief that considerable time passed after one or more late Precambrian glacial events and deposition of the boundary strata. Between the Mackenzie tillite (map unit 6 or Shezal Formation) and the oldest Precambrian strata inspected are siltstone and shale assigned to map unit 7 (Twitya Formation) which Eisbacher (1978, p. 12) found to be 400 m to 900 m thick in nearby sections.

The oldest strata examined belong to map unit 8 (correlated with Keele Formation) in section 38 (Fig. 7.1, 7.3). Abundant carbonate clasts and interbedded siltstone in this map unit were interpreted by many members as belonging to a second, young tillite. Although similar clasts have been reported in unit 8 and equivalent strata elsewhere (Blusson, 1971; Eisbacher, 1978) without mention of a glacial origin, it was suggested by the Working Group that these strata be studied further in order to resolve the "second tillite" controversy.

The overlying map unit 9 is a thick (± 1000 m) succession of dark shale and siltstone with interbedded quartzite at the top. Blusson (1971, map and p. 9) showed map unit 9 to be older than map unit 10b on his map legend, and in the text he has described map unit 9 as a unit that "...coarsens upward, containing more silty and sandy bands in the upper part, grading conformably into overlying quartzites of unit 10". By his mapping of map unit 12 directly over map unit 9 at the site of section 38, Blusson has implied that an unconformity exists at the contact between the two. Observations by the Working Group strengthen this interpretation, as no trace fossils were seen in map unit 9, but they were noted to appear abruptly in the lowest siltstone interbeds of map unit 12. In Figure 7.3 the mentioned unconformity is shown as passing westward under map units 10b and 11 in accordance with the relationships implied by Blusson's map and text. In describing map unit 11 Blusson (1971, p. 9) stated, "Thinning and eventual disappearance to the north is apparently primary as the upper contact is conformable with overlying quartzites of unit 12". A second interpretation was expressed by J.D. Aitken (personal communication), who stated that his current investigations have led him to believe that map unit 11 has also been removed by erosion at section 38, and that the same unconformity is present between map units 11 and 12 at sections 37 and 33.

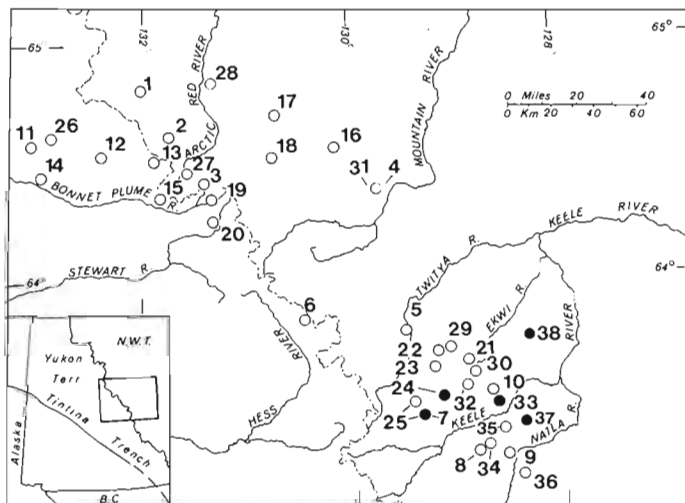


Figure 7.1. Index map showing sections inspected by members of Working Group (solid circles) and other published Lower Cambrian sections (open circles). For description of some sections and references to others see Fritz (1979).

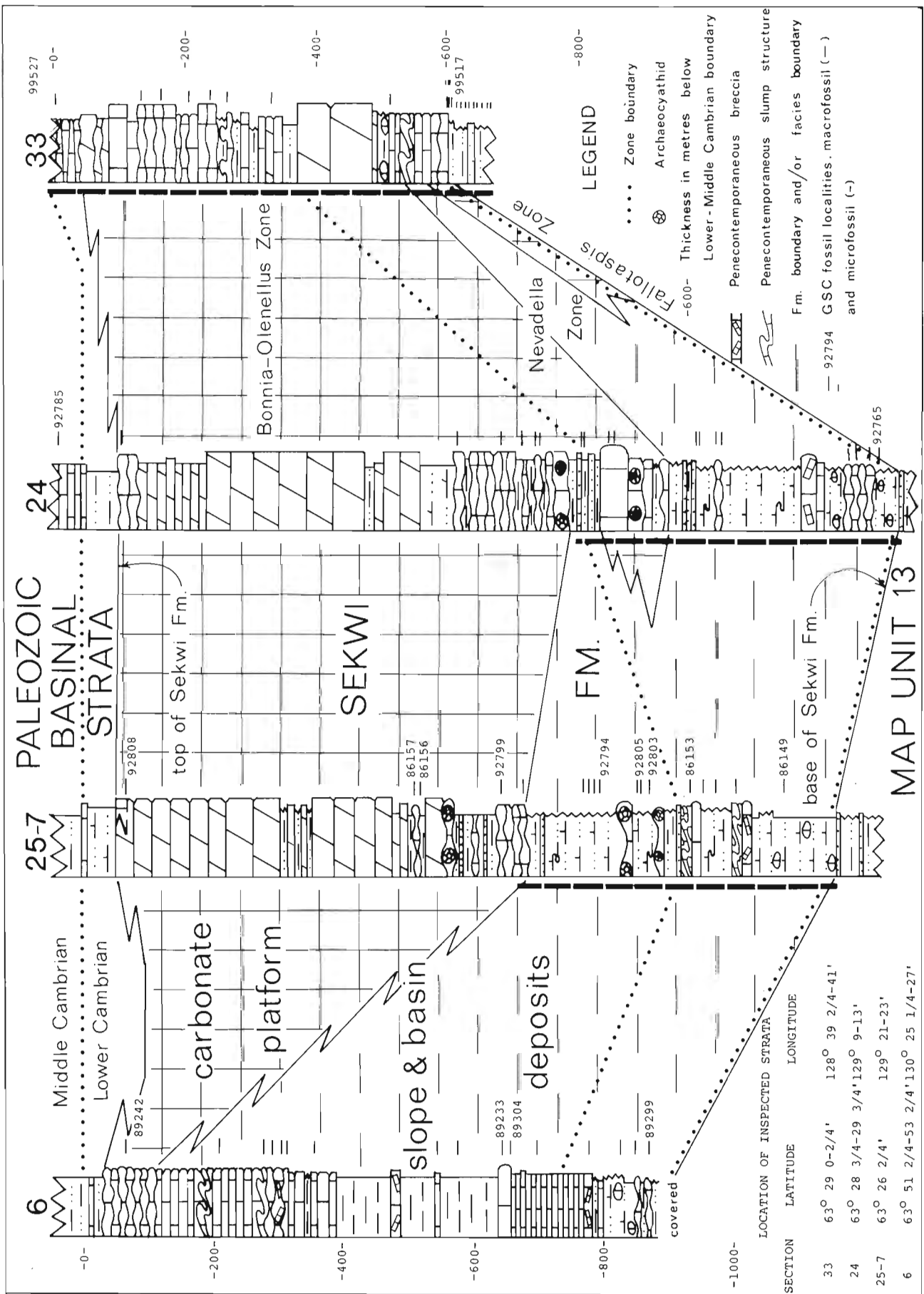


Figure 7.2. Stratigraphic sections showing late Lower Cambrian strata. Heavy dashed line adjacent to sections locates strata studied by Working Group. Sections are located in Figure 7.1. Figure modified from Fritzt, 1976, Text-figure 1.

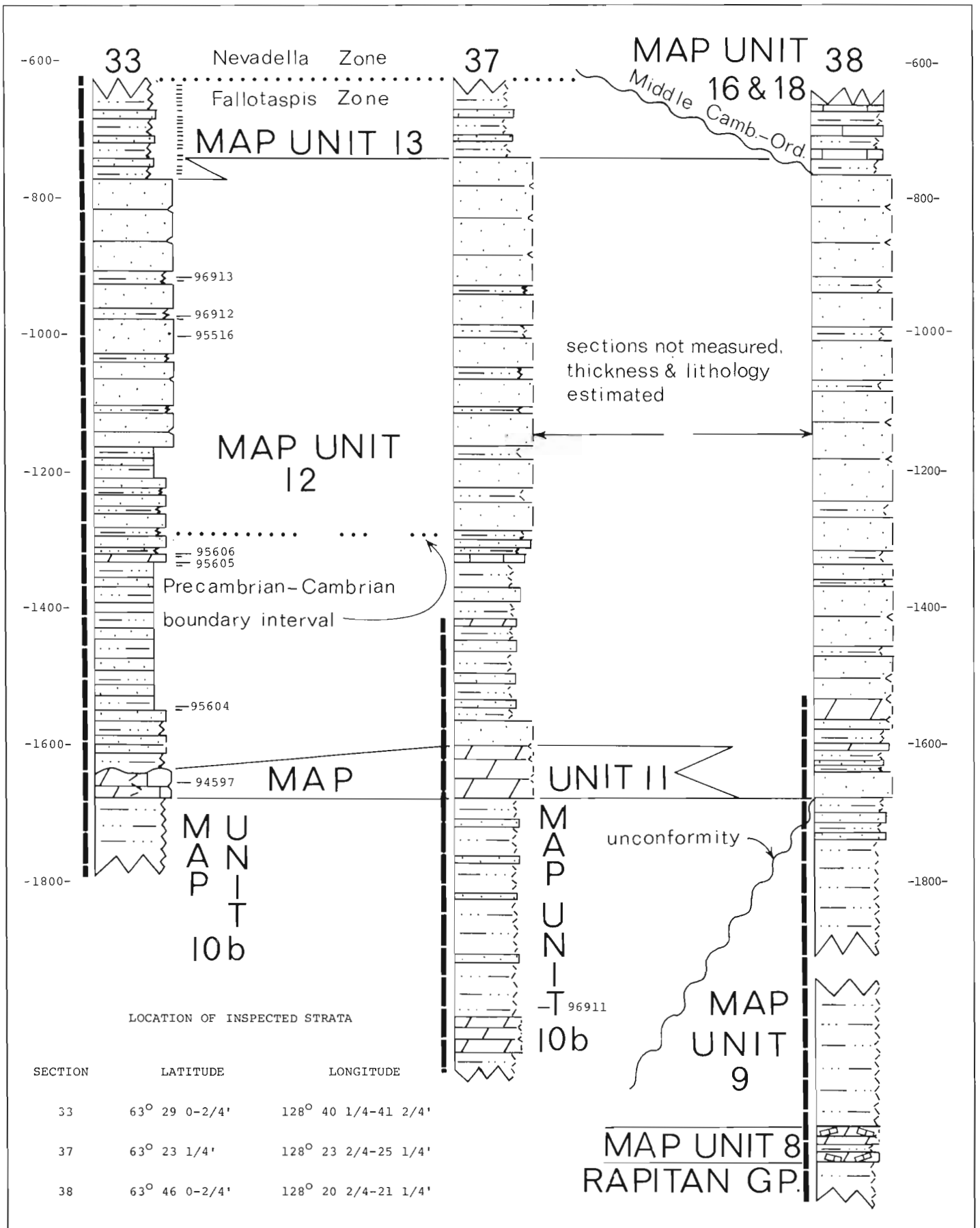


Figure 7.3. Stratigraphic sections showing late Precambrian and early Lower Cambrian strata. Heavy dashed line adjacent to sections locates strata studied by Working Group. Sections are located in Figure 7.1. See Figure 7.2 for legend.

Strata belonging to map unit 10b were inspected at basinward sections 33 and 37. These strata are composed almost exclusively of dark shale and siltstone at section 33 and of a similar shale and siltstone with minor interbedded quartzite plus a prominent dolomite subunit at section 37. Small (1 to 1.5 mm wide) trails are scattered throughout the upper part of map unit 10b, and sparse larger but simple trails are also present. Spheres 4 mm in diameter and "zebra stripes" that angle across bedding (cf. *Newlandia frondosa* Walcott) were inspected in the dolomite subunit at section 37, but the significance or even organic origin of the two types of structures remains uncertain. A single, large Ediacara-type fossil (cf. *Inkrylovia* sp.) was found in local float 40 m above the dolomite subunit (GSC loc. 96911) in the same section.

Overlying map unit 10b at sections 33 and 37 is map unit 11, a dolomite unit that changes colour and bedding rapidly over a short lateral distance. At section 37 the map unit is thick bedded at section 33 it is thin to thick bedded, interfingers with limestone, and the uppermost beds form large (3 m high) mounds. It was reported that a sample from map unit 11 taken 12 km south (Fig. 7.1, section 35) of section 33 produced shell microfossils consisting of *Protohertzina* cf. *P. anabarica*, an undetermined dome shaped form, and an undetermined multilayered form (S. Conway Morris, personal communication).

Brief excursions were made over the lower part of map unit 12 at sections 37 and 38, but the main interest was focused on section 33. Here map unit 12 has an abundance and wide vertical distribution of trace fossils that enabled members to agree on a tentative level for the Precambrian-Cambrian boundary. The selected interval lies 350 m to 370 m above the base of map unit 12 (15-35 m above base of stratigraphic unit 3, Section 33, Fritz, 1979). The interval lies within a uniform succession of interbedded shale, siltstone and quartzite that includes sparse, thin carbonate beds. Strata of this lithology extend from the base of the map unit to a level well above the middle. In and below the boundary interval are trace fossils consisting of trails 1 to 1.5 mm wide, *Planolites* sp., and rare traces with parallel grooves. Within the interval and above are the trace fossils *Gyrolithes polonicus*, *Didymaulichnus* sp. and *Phycodes* sp., whereas slightly above the interval is *Treptichnus* sp. Thick bedded quartzite dominates the upper part of map unit 12,

but thin siltstone interbeds are present which contain the trace fossils *Didymaulichnus* sp., *Phycodes pedum*, *Planolites* sp., *Neonorites* sp., *Treptichnus* sp., and various escape structures. Long, narrow sponge-like structures were collected at two horizons (GSC locs. 96912, 96913) and a hyolithid was collected with the sponges(?) at the higher locality.

Map unit 13, the highest in a predominantly clastic succession, is composed of dark siltstone and interbedded very fine grained quartzite. The trace fossils *Bergaueria* sp., *Teichichnus* sp., *Rusophycus* sp., and *Scolicia* sp. are present. Three thin (5 mm) phosphatic beds located 6-6.3 m below the top of the map unit contain *Chancorella* sp., hyolithids, brachiopods, and *Volborthella*(?) sp. Map unit 13 was sampled by Aitken and Fritz at 7 m intervals for acritarchs in 1977, and only one collection from near the top contained specimens adequately preserved for close determination. This sample contains forms known from the Lower Cambrian *Holmia* and *Protolenus* Zones as understood from the Acado-Baltic Faunal Province (personal communication, M. Vanguetstaine). Sampling done at the same time in map units 12, 9, and in the middle and upper Rapitan yielded only unsatisfactory material.

Late Lower Cambrian

Strata of this age have been assigned to the Sekwi Formation (Handfield, 1968), a formation that changes laterally from platform carbonates in the east to slope and basin deposits of siltstone and platy limestone to the west (Fig. 7.2). As a whole, these late Lower Cambrian strata contain far more carbonate than do the late Precambrian and early Lower Cambrian rocks. This vertical change, from carbonate poor (late Precambrian to early Lower Cambrian) to carbonate rich (late Lower Cambrian) takes place at the base of the Sekwi Formation and is accompanied by a major change in the fossils. Below, trace fossils are well preserved, abundant, and shelly fossils are very rare. Above, trace fossils are less diagnostic (often destroyed by bioturbation) and shelly fossils are both abundant and diverse.

At section 33 the shelly fossils in the Sekwi Formation are representative of the North American Faunal Province. The occurrences and ranges of genera such as *Parafallotaspis*, *Nevadella*, *Fremontella*, *Wanneria*, *Proliostracus*, *Salterella*, and *Olenellus* were checked against a detailed range chart (Fritz, 1972) compiled from a section (Fig. 7.1, section 10) 5 km north of section 33. Of particular interest at section 33 was the boundary between the *Fallotaspis* Zone and the *Nevadella* Zone. This boundary represents one of the best time lines in the Lower Cambrian and has been correlated (Fritz, 1972) with the base of the *Callavia* Zone in England, the boundary between Zones 4 and 5 in Morocco, and the boundary between the Kenyada and Atdaban Horizons in Siberia. Working Group members found *Parafallotaspis* sp., *Helcionellida* sp., and *Palagiella* sp. below the boundary and *Keeleaspis* sp., *Nevadella* sp., and *Holmiella* sp. above.

Sekwi strata deposited under slope and basin conditions were seen at sections 24 and 25-7. At section 24 it was noted that *Judomia*, a Siberian index fossil for the upper Adaban and until now believed to be rare in North America, dominates the slope deposits. These deposits are the lateral equivalent of the *Nevadella* Zone deposits in the carbonate platform facies. Platform edge and high slope deposits at sections 24 and 25-7 contain abundant archaeocyathids, demonstrating the affinity of these animals for these two marginal environments. Diverse and unusual forms are also present here, such as the archaeocyathid(?) *Tabulaconus* sp., and the trilobites *Bradyfallotaspis* sp. and *Sekwiaspis* sp. Strata belonging to the basinal facies were examined at section 25-7, and here the deeper water trilobites *Pagetides* sp., *Ekwipagetia* sp., *Yukonides* sp. and *Serrodiscus* sp. were collected.

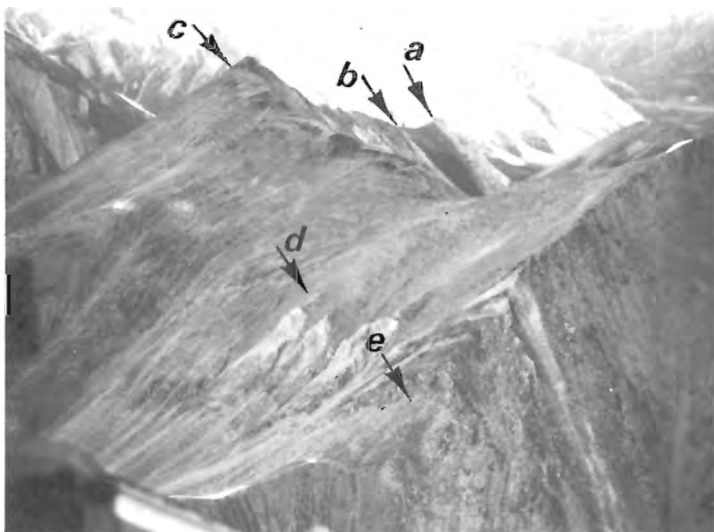


Figure 7.4. View looking northeast at section 33. Base of Sekwi Formation is at "a", base of map unit 13 is at "b", base of thick bedded quartzite in map unit 12 is at "c", base of map unit 12 is at "d", base of map unit 11 is at "e". (GSC 203474)



Standing from left, T.P. Fletcher, H.J. Hofmann, V.E. Savitsky, W.H. Fritz, S. Conway Morris, P.W. Webby.

Sitting from left, Xing Yusheng, J.L. Kirschvink, J.W. Cowie, A. Yu. Rozanov, M. Fedonkin.

Members not shown are J.D. Aitken and C.A. Nelson.

Figure 7.5 Members of Precambrian-Cambrian Boundary Working Group at June Lake, Mackenzie Mountains, Northwest Territories, August 9, 1979.

Magnetostratigraphy

The number and location of samples taken by J.L. Kirschvink are as follows: 18 samples, map unit 8, section 38; 5 samples, map unit 11, section 33; 8 samples, map unit 11, section 37; 14 samples across **Fallotaspis-Nevadella** Zone boundary, section 33; 16 samples across **F.-N.** Zone boundary, section 24; 12 samples within **Nevadella** Zone, section 24. Objectives are to determine the polarity position at numerous stratigraphic levels, to determine the presence or absence of a polarity reversal across the **F.-N.** Zone boundary at two different sections, and to demonstrate either a retention or loss of polarity direction in strata that have been consolidated on an unstable slope and were shortly thereafter rotated by slumping into the basin.

Conclusions and Recommendations

A tentative boundary interval has been delineated by the Working Group and is recommended for further boundary studies. Within this interval trace fossils change from small forms accompanied by sparse larger but simple forms to abundant and complex forms. The interval is located 350 m to 370 m above the base of map unit 12 in section 33. Map unit 11, which changes lithology laterally and has produced a small shelly microfauna, should be sampled for more fossils, and the thin carbonate interbeds extending upsection and across the boundary interval should also be sampled. The Sekwi Formation, with its diversity of faunas and depositional environments, should be brought to the attention of other working groups that will be studying intra-Cambrian correlation.

References

- Blusson, S.L.
1971: Sekwi Mountain map-area, Yukon Territory and District of Mackenzie; Geological Survey of Canada, Paper 71-22.
- Eisbacher, G.H.
1978: Re-definition and subdivision of the Rapitan Group, Mackenzie Mountains; Geological Survey of Canada, Paper 77-35.
- Fritz, W.H.
1972: Lower Cambrian trilobites from the Sekwi Formation type section, Mackenzie Mountains, northwestern Canada; Geological Survey of Canada, Bulletin 212.
1976: Lower Cambrian stratigraphy, Mackenzie Mountains, northwestern Canada; Brigham Young University, Geological Studies, v. 23, pt. 2, p. 7-22.
1979: Eleven stratigraphic sections from the Lower Cambrian of the Mackenzie Mountains, Northwestern Canada; Geological Survey of Canada, Paper 78-23.
- Handfield, R.C.
1968: Sekwi Formation, a new Lower Cambrian formation in the southern Mackenzie Mountains, District of Mackenzie; Geological Survey of Canada, Paper 68-47.

**FRENCHMAN CAP DOME, SHUSWAP COMPLEX, BRITISH COLUMBIA:
A PROGRESS REPORT**

Richard L. Brown¹
EMR Research Agreement 142-4-79
Cordilleran Geology Division

Brown, Richard L., Frenchman Cap Dome, Shuswap Complex, British Columbia; in Current Research, Part A, Geological Survey of Canada, Paper 80-1A, p. 47-51, 1980.

Abstract

Frenchman Cap dome is underlain by an Apehbian sialic basement upon which rests a platform facies of clastic and calcareous metasediments. These autochthonous cover rocks lie beneath a décollement that separates them from overlying allochthonous strata. The décollement wraps around the northern end of the dome and has been observed on the western flank as well as to the east where it coincides with the Columbia River fault.

Deformation and metamorphism of autochthonous and allochthonous cover may be related to the closing of a marginal basin that lay between Shuswap Terrane and the cratonic margin of North America. Movement on the décollement and Columbia River fault outlasted Middle Jurassic metamorphism. In the Columbia River valley clay gouge zones indicate easterly displacement of allochthonous cover rocks relative to basement and autochthonous cover of Frenchman Cap dome. Most recent movements probably occurred in the Tertiary and may be related to a time of crustal extension.

Introduction

Frenchman Cap dome (Fig. 8.1) was initially mapped on a scale of 1:253 440 by Wheeler (1965) and several detailed studies have been reported recently (Fyles, 1970; McMillan, 1973; Psutka, 1978; Hoy, 1979; Höy and McMillan, 1979; Brown and Psutka, 1979).

A stratigraphic succession in part of the autochthonous cover rocks of the dome was first established by Psutka (1978) and extended along the eastern and northern margins by Brown and Psutka (1979); a similar succession for the western and southern margins has been proposed by Höy and McMillan (1979).

These results together with new mapping by the author have been compiled and a regional stratigraphy for the cover succession is presented in Figure 8.2. The following discussion considers structural elements, geometry and tectonic setting of Frenchman Cap dome.

Structural Elements

Core Gneiss

The feldspar augen gneiss characterizes the deepest exposed levels of the dome; it is overlain by paragneiss composed of semipelite, psammite, and amphibolite. The contact is generally gradational and no intrusive relationships have been observed.

Four localities spread along the eastern side of the dome in the paragneisses and five within the augen gneiss have been sampled and radiometrically dated by the Rb-Sr whole rock method. All localities from both augen gneiss and paragneiss give an Apehbian age (2.10 ± 0.09 Ga, Armstrong and Brown, in preparation).

The internal structure and stratigraphy of the core gneiss is only poorly understood; detailed mapping will get underway this summer.

Autochthonous Cover

Apehbian gneisses of the dome are overlain by an autochthonous cover composed primarily of clastics and carbonates. Basal quartzite rests with apparent structural conformity upon the basement gneisses and has been traced with minor breaks around the flanks of the dome (Brown and Psutka, 1979; Höy and McMillan, 1979). The autochthonous succession extends southwards and outcrops about the domes

of Thor-Odin and Valhalla (Reesor, 1965; Reesor and Froese, 1969; Reesor and Moore, 1971; Read, 1979; Brown and Read, 1979).

Work this past year has demonstrated that the simple breakdown into stratigraphic units proposed for the eastern flank of the dome by Brown and Psutka (1979) is complicated by facies changes. Rocks overlying the basal quartzite are usually calcilicites and these metasediments contain a distinctive thin white marble (known to some as the "virgin marble"). This marble (unit 4m, Fig. 8.2) to the northwest and west is locally associated with a strata-bound carbonatite (unit 4CT) recognized in the Perry River area by McMillan (1973) and McMillan and Moore (1974). The marble-carbonatite bearing horizon is locally host for sulphide mineralization (Fyles, 1970; Höy, 1979). Persistence of the marble (unit 4m) around the dome, and its recognition to the south in Thor-Odin area (P.B. Read, personal communication, 1978) demonstrates that unit 4 may be considered a formation of regional significance. Other units mapped on the eastern flank of Frenchman Cap and described by Brown and Psutka (1979) are less persistent. For example, local separation of pelitic rocks from calcilicites is possible but on a regional scale these lithologies may be facies equivalents. The northern end of Frenchman Cap dome is particularly instructive (Fig. 8.2). The axial surface trace of Kirbyville syncline (KS, Fig. 8.2) is located by well defined tops in graded grit beds and by change in asymmetry of minor folds; calcilicites (unit 4c) above the basal quartzite (unit 3) on the southern limb correlate with grit-bearing pelitic rocks (unit 4p) on the northern limb. The Sibley Creek syncline (SS, Fig. 8.2) is also well defined, in this case the closure involves crossbedded quartzite (unit 4q) that become interdigitated with amphibolites (unit 4a) some of which are clearly metavolcanics. These amphibolites are thick and persistent on the northern limb of the fold, but give way to pelite (unit 4p) and quartzite (unit 4q) on the southern limb. The recognition of these facies changes requires that local subdivisions be lumped into a single formation (unit 4).

The age of the autochthonous cover rocks is yet to be determined; the presence of quartzites and marbles has led some workers to propose correlation with Cambrian rocks exposed in the miogeocline to the east (Wheeler et al., 1972; Reesor, 1970; Höy and McMillan, 1979) however, Brown and Psutka (1979) and Brown and Read (1979) have suggested that a Proterozoic (Belt-Purcell) age should be considered as an alternative hypothesis.

¹Department of Geology, Carleton University, Ottawa, Ontario.

Frenchman Cap Décollement

At the northern end of the dome, autochthonous cover rocks dip northward beneath migmatitic rocks that appear to correlate with strata of the Selkirk allochthon. North of the Columbia River fault zone (Fig. 8.3), marker horizons in the Selkirk Mountains cross the Columbia River and continue northwestward without offset into the Monashee Mountains (Fig. 8.1, 8.3; Campbell, 1968; Brown et al., 1977). These markers include the Middle Marble and Lower Pelitic members of the Upper Proterozoic Horsethief Creek Group (Brown and Tippett, 1978).

The contact of probable Horsethief Creek Group against autochthonous cover is well exposed at the northwest end of Frenchman Cap dome (Fig. 8.2). Postmetamorphic shearing has disrupted stratigraphy and locally generated

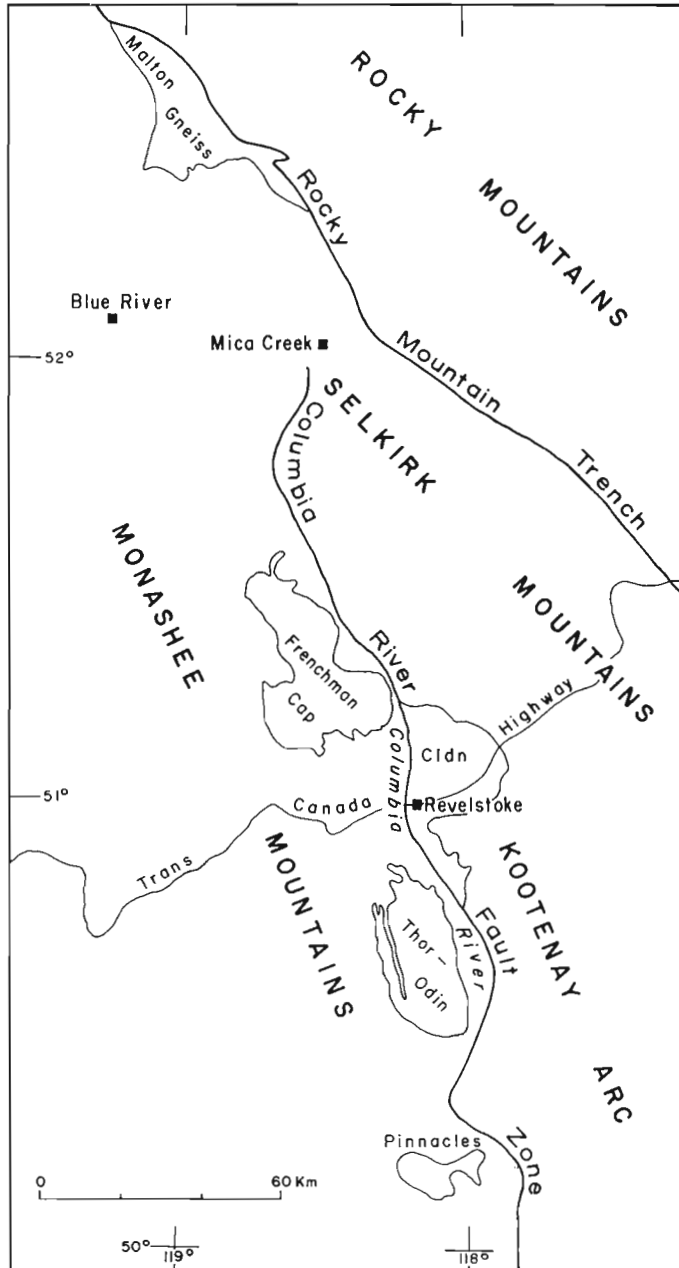


Figure 8.1. Location and setting of Frenchman Cap dome. Cldn indicates clachnacudainn salient (allochthon).

tectonic breccias. Quartzite (unit 4q), pelite (unit 4p), calcisilicate (unit 4c) and carbonatite (unit 4CT) units are variously involved in the footwall of the décollement. Abundant kyanite with minor sillimanite occurs in pelitic rocks below the décollement; pegmatite is generally restricted to discordant dykes. Semipelitic migmatite, psammite, amphibolite boudins, together with pervasive concordant and discordant pegmatite characterize the rocks of the hanging wall; kyanite is absent and sillimanite is generally present as coarse fibrous knots.

Detailed petrological and structural analysis across the contact will be started this summer; the available information indicates that strata above the décollement were displaced after the peak of metamorphism, and that higher grade rocks of the allochthonous cover have been displaced onto lower grade autochthonous rocks.

Similar contact relationships have been observed between Anstey River and the head of Perry River on the western flank of the dome (Fig. 8.2). Continuation around the western part of the dome appears most likely, and the boundary has been extrapolated on the basis of lithologic descriptions by Wheeler (1965). The décollement has been traced northeastward to the vicinity of Hoskins Creek where it swings eastward into the Columbia River valley toward the Columbia River fault zone (Fig. 8.2, 8.3).

Columbia River Fault

Autochthonous cover rocks on the eastern margin of Frenchman Cap dome are truncated in the Columbia River valley by the Columbia River fault zone. This shallow (20°) easterly dipping fault has been traced for over 200 km (Fig. 8.1); it isolates the autochthonous cover of the Shuswap Metamorphic Complex from metamorphic rocks of the Selkirks and Kootenay Arc (Brown and Read, 1979; Read, 1979; Brown and Psutka, 1979).

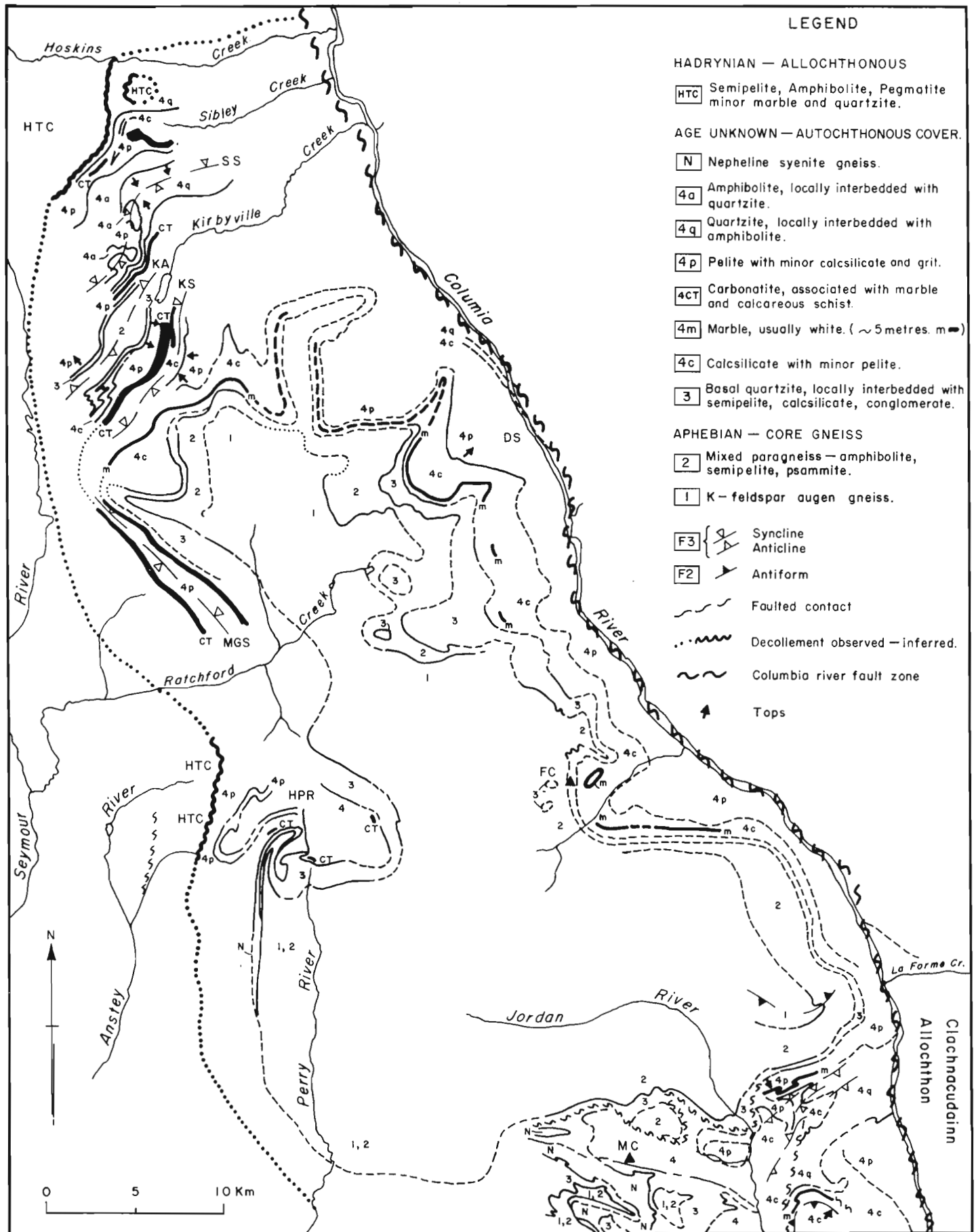
To the north of Frenchman Cap dome the Columbia River fault continues beyond Hoskins Creek, but either dies out or swings back toward the southeast before reaching the vicinity of Soards Creek where, as previously mentioned, Campbell (1968) has traced an unfaulted marble horizon and a sillimanite isograd across the Columbia River valley (Fig. 8.3).

Most recent movement along the Columbia River fault is postmetamorphic and has disrupted igneous plutons that are at least as young as Late Cretaceous (Armstrong and Brown, in preparation). Slickensides, fibre growth and cleavage in clay gouge zones indicate that movement has been normal to high angle oblique slip. The Selkirk allochthon has been displaced eastward relative to Shuswap basement (Fig. 8.3). The magnitude of the displacement is not known, but has been sufficient to juxtapose rocks with metamorphic grade as low as greenschist against footwall rocks of upper amphibolite grade.

Relationships between the Frenchman Cap décollement and the fault zone in the Columbia River require clarification: the early detachment of the Selkirk allochthon is marked by the décollement that wraps around the northern end of Frenchman Cap dome and coincides to the east with the Columbia River fault zone, the northward extension of the fault in the valley (Fig. 8.3) is probably related to more recent displacement.

Structural Geometry

Polyphase deformation in the autochthonous cover has been described in the Mount Copeland-Jordan River area (Fyles, 1970), at the head of Perry River (McMillan, 1973), and in the Downie slide area (Psutka, 1978).



M.C. - (Mount Copeland area) after Fyles (1970)

HPR - (Head of Perry River area) after McMillan (1973)

MGS - (Mount Grace Syncline) after Höy (1979)

DS - (Downie Slide area) after Psutka (1978)

Figure 8.2. Stratigraphy of Frenchman Cap dome. See text for further explanation.

The geometry of autochthonous cover and basement gneisses at the northwestern end of the dome appears to be relatively straight forward. Major closures are late to postmetamorphic anticlines and synclines with axial surfaces that dip away from the dome toward the northwest and southwest at moderate to shallow angles (Fig. 8.2; Kirbyville-Mount Grace Syncline, Kirbyville anticline, Sibley syncline). Late metamorphic folds are also dominant along the eastern margin; axial surfaces dip northwesterly toward the dome and hinge lines vary through the horizontal with moderate plunges to the northwest and southeast, however complexities develop adjacent to the Columbia River fault zone.

Interference patterns are evident to the south in the Jordan river region (Fyles, 1970). Large refolded isoclinal folds deform both basement and cover in this southern region which lies between Frenchman Cap and Thor-Odin dome.

Doming of the basement and cover appears to be a late stage postmetamorphic event that has been superimposed after nappe style folding.

Recognition of Aphebian basement (units 1 and 2) implies that a precover geometry and metamorphic history may be preserved. Structure of allochthonous cover rocks of the Selkirk Terrane is fairly well known to the east of the Columbia River fault zone (Brown and Tippett, 1978; Brown, 1978), but has yet to be investigated to the west where these strata approach the Frenchman Cap décollement. At the moment it is not certain whether or not the structural and metamorphic events recorded in the autochthonous cover rocks correlate with the middle Jurassic deformation and metamorphism recorded in the allochthonous cover.

Tectonic Setting

Frenchman Cap is one of several domes in the Shuswap metamorphic complex, and similar terranes occur along much of the axial zone of the North American Cordillera (cf. Davis and Coney, 1979). Agreement on the origin or origins of these "core complexes" is yet to be obtained.

The Aphebian age for sialic basement rocks in Frenchman Cap and similar or older ages from core gneisses in Thor-Odin (Wanless and Reesor, 1975; Duncan, 1978) indicate that much of the Shuswap Terrane is probably underlain by sialic basement that is at least two billion years old. Is this basement part of cratonic North America or does it have an exotic origin.

Primary sedimentary features are only locally preserved in the autochthonous cover rocks but the presence of crossbedded sandstone, rapid facies changes of calcareous muds and clastics, together with the laterally continuous limestone horizon suggests a shallow marine platform environment; locally interdigitated volcanic rocks imply a tectonically active setting. It has been argued on both geological and geophysical grounds that cratonic North America at this latitude probably does not extend west of the Rocky Mountain trench (for summary discussion see Monger and Price, 1979), and that a marginal basin separated the Shuswap Terrane from the craton (Brown, 1979, in press). These arguments imply that the Shuswap Terrane lay offshore North America in Proterozoic to Paleozoic times, and that the tectonic setting was "Pacific type" rather than "Atlantic type".

Basement gneisses, autochthonous and allochthonous cover record a protracted history of deformation. The main metamorphism to have affected the allochthonous cover appears to have occurred in the Jurassic, but significant deformation took place before and after this event. It is suggested that the deformations and metamorphism are related to the closing of the marginal basin that lay between the Shuswap Terrane and North America.

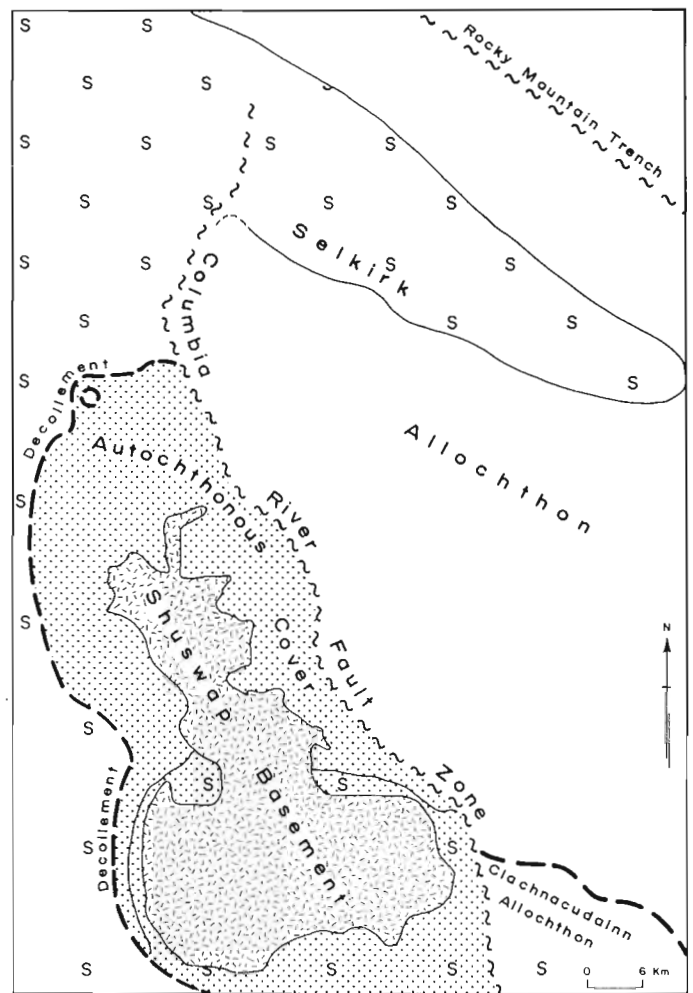


Figure 8.3. Structural elements in the vicinity of Frenchman Cap dome. S = terrane of sillimanite grade. See text for further explanation.

Acknowledgments

This investigation is part of a continuing study of the Shuswap and Selkirk terranes. Since 1972 the program has been funded primarily by grants from Energy, Mines and Resources (research agreements) and NSERC (operating grant A2693). During the summers of 1977 and 1978 this work was also supported by the British Columbia Hydro and Power Authority as part of a geological investigation of the Revelstoke reservoir.

References

Brown, R.L.
 1978: Structural evolution of the southeast Canadian Cordillera: A new hypothesis; *Tectonophysics*, v. 48, p. 133-151.
 1979: Convergence of Shuswap Arc and North American Cratonic Margin, southern British Columbia; *Geological Society of America, Annual Meeting, Abstracts with Programs*, v. 11, no. 7, p. 395.
 Metamorphic complex of southeast Canadian Cordillera and relationship to Foreland thrusting; in *Thrust and Nappe Tectonics*, Geological Society of London. (in press)

- Brown, R.L. and Read, P.B.
1979: Basement-cover interaction: Shuswap Metamorphic complex and the Kootenay Arc – Northern Selkirks; in *Evolution of the Cratonic Margin and Related Mineral Deposits, Cordilleran Section*, Geological Association of Canada, Program and Abstracts, v. 9.
- Brown, R.L. and Psutka, J.F.
1979: Stratigraphy of the east flank of Frenchman Cap dome, Shuswap complex, British Columbia; in *Current Research, Part A*, Geological Survey of Canada, Paper 79-1A, p. 35-36.
- Brown, R.L. and Tippett, C.R.
1978: The Selkirk Fan Structure of the Southeastern Canadian Cordillera; Geological Society of America Bulletin, v. 89, p. 548-558.
- Brown, R.L., Perkins, M.J., and Tippett, C.R.
1977: Structure and stratigraphy of the Big Bend area, British Columbia; in *Report of Activities, Part A*, Geological Survey of Canada, Paper 77-1A.
- Campbell, R.B.
1968: Canoe River, British Columbia; Geological Survey of Canada Map 15-1967.
- Davis, G.H. and Coney, P.J.
1979: Geologic development of the Cordilleran metamorphic core complexes; *Geology*, v. 7, p. 120-124.
- Duncan, I.J.
1978: Rb/Sr whole-rock evidence for three Precambrian events in the Shuswap complex, southeast British Columbia; in *Program with Abstracts*, Geological Association of Canada, v. 3, p. 392-393.
- Fyles, J.T.
1970: The Jordan River area near Revelstoke, British Columbia, British Columbia Department of Mines and Petroleum Resources, Bulletin 57, p. 1-64.
- Höy, T.
1979: Cotton Lead/Zinc deposit; in *Geological Fieldwork, 1978*, British Columbia Department of Mines and Petroleum Resources, Paper 1979-1, p. 19-24.
- Höy, T. and McMillan, W.J.
1979: Geology in the vicinity of Frenchman Cap Gneiss dome; in *Geological Fieldwork 1978*, British Columbia Department of Mines and Petroleum Resources, Paper 1979-1, p. 25-30.
- McMillan, W.J.
1973: Petrology and structure of the west flank, Frenchman's Cap dome, near Revelstoke, British Columbia; Geological Survey of Canada, Paper 71-29.
- McMillan, W.J. and Moore, J.M.
1974: Gneissic alkalic rocks and carbonatites in Frenchman's Cap Gneiss dome, Shuswap complex, British Columbia; *Canadian Journal of Earth Sciences*, v. 11, p. 304-318.
- Monger, J.W.H. and Price, R.A.
1979: Geodynamic evolution of the Canadian Cordillera – progress and problems; *Canadian Journal of Earth Sciences*, v. 16, p. 770-792.
- Psutka, F.J.
1978: Structural setting of the Downie slide, northeast flank of Frenchman Cap Gneiss dome, Shuswap complex, southeastern British Columbia; unpublished M.Sc. thesis, Carleton University, Ottawa, Ontario, 70 p.
- Read, P.B.
1979: Relationship between the Shuswap Metamorphic complex and Kootenay Arc, Vernon east-half, southern British Columbia; in *Current Research, Part A*, Geological Survey of Canada, Paper 79-1A, p. 37-40.
- Reesor, J.E.
1965: Structural evolution and plutonism in Valhalla Gneiss complex, British Columbia; Geological Survey of Canada, Bulletin 129, 128 p.
1970: Some aspects of structural evolution and regional setting in part of the Shuswap Metamorphic complex; in Wheeler, J.O. (Ed.) *Structure of the Southern Canadian Cordillera* in J.O. Wheeler, ed., Geological Association of Canada, Special Paper 6, p. 73-86.
- Reesor, J.E. and Froese, E.
1969: Structural and petrological study of Pennacle Peaks gneiss dome, British Columbia; in *Report of Activities, Part A*, Geological Survey of Canada, Paper 69-1A, p. 139-140.
- Reesor, J.E. and Moore, J.M.
1971: Petrology and structure of Thorodin Gneiss Dome, Shuswap Metamorphic complex, British Columbia; Geological Survey of Canada, Bulletin 195, 149 p.
- Wanless, R.K. and Reesor, J.E.
1975: Precambrian zircon age of orthogneiss in the Shuswap Metamorphic complex, British Columbia; *Canadian Journal of Earth Sciences*, v. 12, p. 326-332.
- Wheeler, J.O.
1965: Big Bend map-area, British Columbia (82 M east-half); Geological Survey of Canada, Paper 64-32, 37 p.
- Wheeler, J.O., Campbell, R.B., Reesor, J.E., and Mountjoy, E.W.
1972: Structural style of the southern Canadian Cordillera; 24th International Geological Congress Guidebook A-C 01.

Project 780011

E. Froese
Precambrian Geology DivisionFroese, E., *A reaction grid for medium grade mafic rocks; in Current Research, Part A, Geological Survey of Canada, Paper 80-1A, p. 53-55, 1980.***Abstract**

Many reactions in medium grade mafic rocks take place in the presence of quartz, plagioclase, magnetite, and ilmenite. A proposed reaction grid accommodates many common mineral assemblages, which can be conveniently represented on the biotite composition surface.

Mineral reactions in mafic rocks lend themselves to a broad subdivision of metamorphic conditions. This fact and the widespread occurrence of mafic rocks presumably prompted Eskola (1939) to choose mineral compatibilities in mafic rocks as facies boundaries. Extensive work in pelitic rocks has demonstrated a multitude of reactions, particularly in medium and high grade rocks. Thus Winkler (1976) decided to use reactions in pelitic rocks as boundaries between his divisions of low, medium, and high grade metamorphism. Reactions in pelitic rocks have become particularly useful as indicators of metamorphic grade since they were linked to form petrogenetic grids. A recent version by D.M. Carmichael combines reactions in muscovite-bearing rocks with those in muscovite-free rocks (see Bailes and McRitchie, 1978). However, the rarity of pelitic rocks in some terranes makes it worthwhile also to consider mafic rocks as indicators of metamorphic grade. In particular, a reaction grid will be helpful in drawing attention to pertinent reactions in mafic rocks.

At a grade of metamorphism somewhat below the appearance of staurolite in biotite- and muscovite-bearing rocks (beginning of medium grade metamorphism), oligoclase-andesine becomes stable. Clinopyroxene, hornblende, and cummingtonite are stable at these conditions; various reactions will lead to the coexistence of these three minerals with plagioclase. These reactions mark the traditional boundary between the greenschist and amphibolite facies (Turner, 1968). The amphiboles remain stable over a large range of metamorphic conditions until the beginning of the granulite facies. Cummingtonite plays an interesting role in amphibolites. Shidô (1958) suggested that cummingtonite, which is common in amphibolites of the Abukuma region, typically develops in low-pressure metamorphism. On the other hand, almandine amphibolites occur in terranes of high pressure metamorphism. And in some areas of intermediate pressure (e.g. Snow Lake, Manitoba), almandine and cummingtonite occur together with hornblende (Bailes and McRitchie, 1978). These observations suggest phase relations shown schematically in Figure 9.1.

Traditionally the metamorphism of mafic rocks has been discussed with the aid of ACF diagrams (Eskola, 1939; Turner, 1968; Froese, 1973; Winkler, 1976). This approach makes it difficult to consider reactions involving biotite and obscures the effect of FeO and MgO as separate components. Therefore, the biotite surface (Froese, 1978) has been used here as a means of showing mineral compatibilities. Many mafic rocks contain small amounts of biotite and, therefore, a subdivision of the biotite composition surface into mineral fields is a suitable method of representing mineral assemblages. In fact, such phase relations remain valid in K₂O-free rocks if biotite is compatible with the indicated mineral assemblages. Various associations of mineral assemblages are shown as insets in a grid (Fig. 9.2). The grid has been constructed by incorporating reactions deduced from common mineral assemblages in mafic rocks together

with basic requirements of reaction grids (Zen, 1966). The grid connects at higher temperature with two reactions from a grid proposed for granulites (Froese and Jen, 1979). It is of interest to note that the grid allows the coexistence of muscovite and hornblende at high pressures, restricts the assemblage epidote-hornblende to relatively high pressures, and accounts for the decomposition of epidote in the presence of biotite.

The grid has several inherent limitations. In order to represent the indicated reactions as lines, the following restrictions have been assumed:

- the activity of H₂O is a smoothly-varying function of pressure and temperature.
- Plagioclase of constant composition is present.
- Quartz, magnetite, and ilmenite are present.

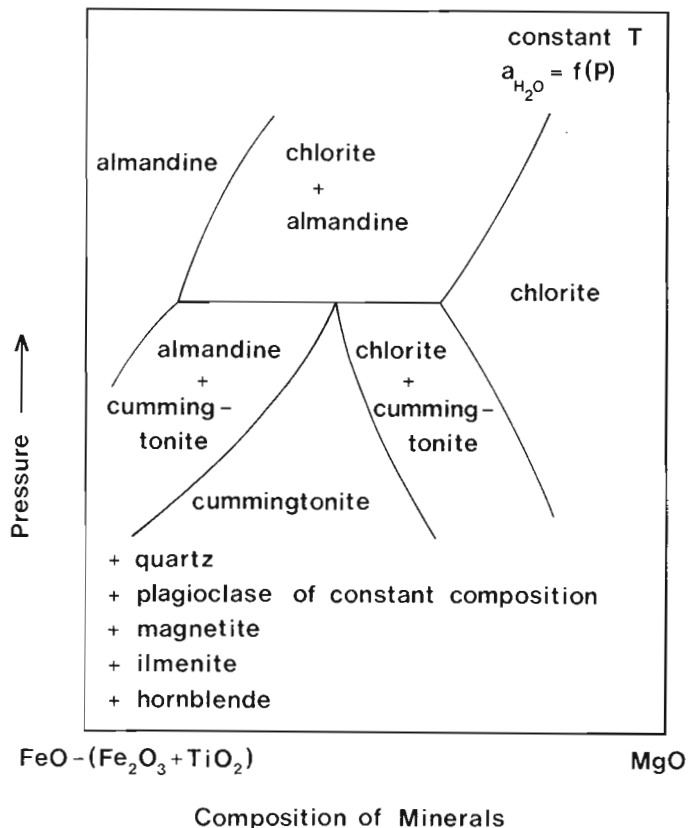


Figure 9.1. Schematic phase relations among chlorite, almandine, and cummingtonite.

Table 9.1

Mineral assemblages in metamorphosed mafic rocks

1. Central Abukuma Plateau (Shidô, 1958)	chlorite-hornblende-epidote hornblende-epidote-clinopyroxene hornblende-clinopyroxene hornblende-cummingtonite hornblende-clinopyroxene-cummingtonite-orthopyroxene
2. Broken Hill district (Binns, 1964)	hornblende-epidote-almandine hornblende-cummingtonite hornblende-almandine-clinopyroxene hornblende-clinopyroxene-orthopyroxene
3. Snow Lake - Wimapedi Lake area (Bailes, 1975; Bailes, and McRitchie, 1978; Froese and Moore, 1979)	chlorite-hornblende-almandine epidote-hornblende hornblende-cummingtonite-almandine epidote-hornblende-clinopyroxene hornblende-clinopyroxene-K feldspar
4. Bessi-Ino district (Banno, 1964)	hornblende-almandine-muscovite-epidote (no biotite) hornblende-clinopyroxene-muscovite-epidote (no biotite)

If these restrictions are not realized, the reaction boundaries of the grid broaden into bands and the pattern of associated mineral assemblages could be obscured. Of particular concern is the fact that it is necessary to consider rocks with plagioclase ranging in composition from An_{15} to An_{70} . Only practical testing will show how serious the effect of this variation of the plagioclase composition is. As a preliminary effort to this end, four pressure-temperature paths are shown (Fig. 9.2), which can accommodate diagnostic mineral assemblages from four areas, listed in Table 9.1.

The Abukuma Plateau is a well-known area of low-pressure metamorphism. The plagioclase composition varies from An_{15} to An_{70} . Typically cummingtonite and clinopyroxene coexist at high grade.

The Broken Hill district probably was metamorphosed at somewhat higher pressure. The plagioclase composition ranges from An_{33} to An_{90} . Because of the very calcic plagioclase, this example was chosen with hesitation. However, it demonstrates the typical coexistence of almandine and clinopyroxene at relatively low pressure.

In the Snow Lake-Wimapedi Lake area, the metamorphic zonation was developed at intermediate pressure (about 5-6 kb). The plagioclase composition ranges from An_{30} to An_{60} .

Metamorphism in the Bessi-Ino district is typical of the high pressure Sanbagawa belt. The glaucophane schist facies is succeeded, at higher grade, by the epidote amphibolite facies. Of particular interest is the coexistence of hornblende and clinopyroxene with muscovite. The associated plagioclase is oligoclase. The epidote-bearing mineral assemblages listed in Table 9.1 cannot be shown on the biotite composition surface because, at these conditions, biotite and epidote are incompatible.

References

- Bailes, A.H.
1975: Geology of the Guay-Wimapedi Lakes area; Manitoba Geological Services Branch, Publication 75-2.
- Bailes, A.H. and McRitchie, W.D.
1978: The transition from low to high grade metamorphism in the Kiseynew sedimentary gneiss belt, Manitoba; Geological Survey of Canada, Paper 78-10, p. 155-178.
- Banno, S.
1964: Petrologic studies on Sanbagawa crystalline schists in the Bessi-Ino district, central Sikoku, Japan; Journal of the Faculty of Science, University of Tokyo, sec. II, v. 15, p. 203-319.
- Binns, R.D.
1964: Zones of progressive regional metamorphism in the Willyama Complex, Broken Hill district, New South Wales; Journal of the Geological Society of Australia, v. 11, p. 283-330.
- Eskola, P.
1939: Die metamorphen Gesteine; in Die Entstehung der Gesteine, Springer-Verlag, Berlin.
- Froese, E.
1973: Metamorphism of basic rocks; Geological Survey of Canada, Open File 164, p. 57-64.
1978: The graphical representation of mineral assemblages in biotite-bearing granulites; in Current Research, Part A, Geological Survey of Canada, Paper 78-1A, p. 323-325.
- Froese, E. and Jen, L.S.
1979: A reaction grid for biotite-bearing mafic granulites; in Current Research, Part A, Geological Survey of Canada, Paper 79-1A, p. 83-85.
- Froese, E. and Moore, J.M.
1979: Metamorphism in the Snow Lake area, Manitoba; Geological Survey of Canada, Paper 78-27.
- Shidô, F.
1958: Plutonic and metamorphic rocks of the Nakoso and Iritôno districts in the Central Abukuma Plateau; Journal of the Faculty of Science, University of Tokyo, Sec. II; v. 11, p. 131-217.
- Turner, F.J.
1968: Metamorphic petrology; McGraw-Hill Book Company, New York.
- Winkler, H.G.F.
1976: Petrogenesis of metamorphic rocks, 4th edition; Springer-Verlag, New York.
- Zen, E-an
1966: Construction of pressure-temperature diagrams for multicomponent systems after the method of Schreinemakers - a geometric approach; United States Geological Survey, Bulletin 1225.

EMR Research Agreement 178-4-79

G.P. Beakhouse¹ and R.H. McNutt¹
Precambrian Geology Division

Beakhouse, G.P. and McNutt, R.H., Geochronological investigation of granitoid rocks at Redditt, Northwestern Ontario: A preliminary report; in Current Research, Part A, Geological Survey of Canada, Paper 80-1A, p. 57-60, 1980.

Abstract

Most rocks in the Redditt area of the Lount Lake batholith can be assigned to either an earlier, megacrystic granodiorite or a later, equigranular granite; both are massive, nonfoliated, retain their igneous texture, and are considered to postdate regional metamorphism associated with the Kenoran orogeny.

The age of the megacrystic granite is 2631 ± 63 Ma ($R_i = 0.70223 \pm 44$, $MSWD = 1.35$). This is similar to the nearby Dalles and Melick intrusions and falls within the range of other relatively potassic plutonic rocks from the Winnipeg batholithic belt.

Introduction

As part of a larger study of crustal development in the English River subprovince, a series of felsic plutonic rocks near the village of Redditt in northwestern Ontario is being investigated.

Felsic plutonic rocks at Redditt form a lobe of a much larger batholithic complex (termed the Lount Lake batholith by Breaks et al., 1978) which occupies the central portion of the Winnipeg River batholithic belt (Beakhouse, 1977). The relatively potassic plutonic rocks, which characterize the Lount Lake batholith, are interpreted to represent the last major plutonic event in the English River subprovince (Beakhouse, 1977; Breaks et al., 1978).

General Geology

The oldest major rock unit in the Redditt area is banded orthogneiss which outcrops in the southern part of the study area (Fig. 10.1). A Rb-Sr whole-rock isochron for presumably correlative orthogneiss 15 km south of this area has yielded an age of 2725 ± 55 Ma; $R_i = 0.7010 \pm 3$ (Wooden, 1978). The relative age of amphibolitized mafic volcanic rocks in the northwestern portion of the Redditt area (Fig. 10.1) is uncertain, although metavolcanic rocks are known to pre-date development of the orthogneiss (Beakhouse, 1977; Gower, 1978).

The Ena Lake stock (Fig. 10.1) is a multi-phase intrusion with predominant quartz diorite and subordinate diorite, quartz monzodiorite and tonalite. Igneous rock terminology used in this report is after Streckeisen (1976). No attempt to map individual phases within this intrusion has been made.

Most rocks in the Redditt area of the Lount Lake batholith can be assigned to either an earlier, megacryst-bearing granodiorite phase or a later, equigranular granite phase. Reconnaissance investigations indicate that similar lithologies are abundant throughout the Lount Lake batholith. Both the megacrystic granodiorite and equigranular granite are massive, nonfoliated, and retain their igneous texture. They are interpreted to postdate regional metamorphism associated with the Kenoran orogeny.

Petrology

Megacrystic Granodiorite

Large areas of the Redditt lobe of the Lount Lake batholith are underlain by biotite granodiorite containing microcline megacrysts. The degree of development of the

microcline megacrysts dominates the textural and mineralogical variability of this phase.

Plagioclase, quartz and microcline constitute 90 per cent or more of the modal and mesonormative mineralogy (Fig. 10.2). Plagioclase (An_{18-25}) is weakly to moderately intensely sericitized and rarely exhibits weak, normal zoning. Biotite is the predominant mafic mineral and is rarely accompanied by subordinate hornblende. Magnetite, epidote, zircon, apatite and sericite (alteration product of plagioclase) are ubiquitous accessory minerals. Minor sphene, allanite, chlorite (alteration product of biotite), muscovite and carbonate are present in some samples.

Optically continuous, poikilitic, micro-perthitic microcline megacrysts up to 4 cm in longest dimension, modify an otherwise uniform, hypidiomorphic equigranular texture. These megacrysts poikilitically enclose plagioclase, quartz and biotite and, although often subhedral, the margins are irregular in detail. Adjacent myrmekite and albitic (?) rims on plagioclase inclusions are common. All stages of development from concentrations of clearly intergranular, late microcline to well formed subhedral crystals occur.

These observations, together with the unmetamorphosed character of the rock, suggest that the megacrysts represent late magmatic concentrations of microcline and not phenocrysts or porphyroblasts. This conclusion is consistent with the position of the megacrystic granodiorite in the salic (An-Ab-Or-Qz) tetrahedron (Presnall and Bateman, 1973). It lies in the primary phase volume of plagioclase, near the quartz saturation surface and well removed from the cotectic line. The crystallization sequence for such a liquid composition would be plagioclase (+ biotite), plagioclase + quartz (+ biotite), and plagioclase + quartz + orthoclase (+ biotite).

Granite

The youngest rocks in the Redditt area have granitic compositions (Fig. 10.2). Medium grained, equigranular granite predominates in both the larger granite stock at Birch Lake (Fig. 10.1) and within numerous plugs and dykes occurring throughout the study area. Locally, the equigranular phase contains irregularly shaped pods of a pegmatitic phase having similar mineralogy which are clearly co-magmatic. Late pegmatitic dykes have similar mineralogy and may or may not be related to the equigranular granite.

Plagioclase (An_{12-18}), microcline, and quartz in sub-equal proportions (Fig. 10.2) constitute at least 95 per cent of the equigranular granite. Biotite is the predominant mafic

¹ Department of Geology, McMaster University, Hamilton, Ontario L8S 4M1

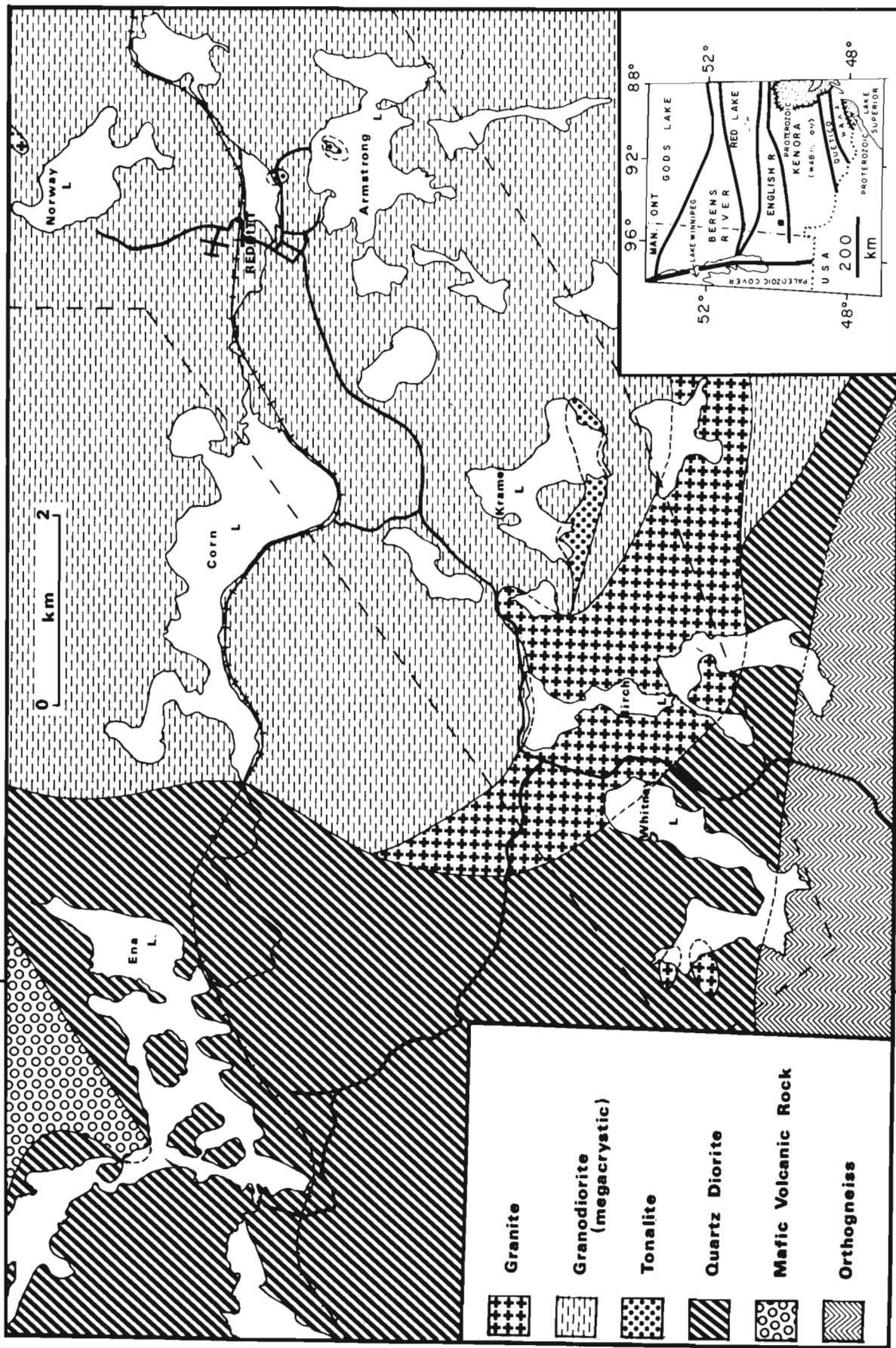


Figure 10.1 Generalized geologic map of the Redditt area.

mineral but magnetite and muscovite are common. Trace amounts of epidote, apatite, zircon, sphene, allanite, chlorite, and sericite are present in most rocks. Abundant myrmekitic inter-growths and relatively intense plagioclase sericitization suggest extensive deuteritic activity.

Geochronology

Analytical Procedures

All strontium isotopic measurements were performed on a 90° sector, 25.4 cm radius of curvature, solid source, single filament (Ta), Nier-type mass spectrometer. Rb, Sr and the Rb/Sr values were determined by X-ray fluorescence

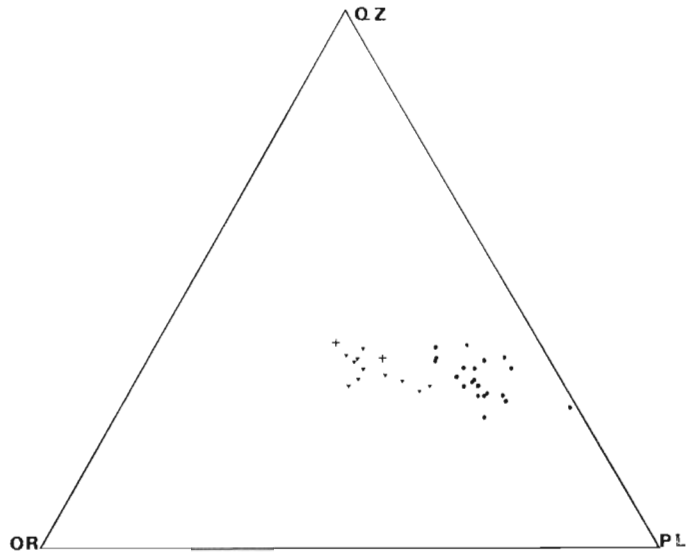


Figure 10.2 Mesonormative mineralogy of granitoid rocks at Redditt with plagioclase + K-feldspar + quartz recalculated to 100 per cent. Dots correspond to megacrystic granodiorite samples; triangles to granite samples, crosses to pegmatite samples.

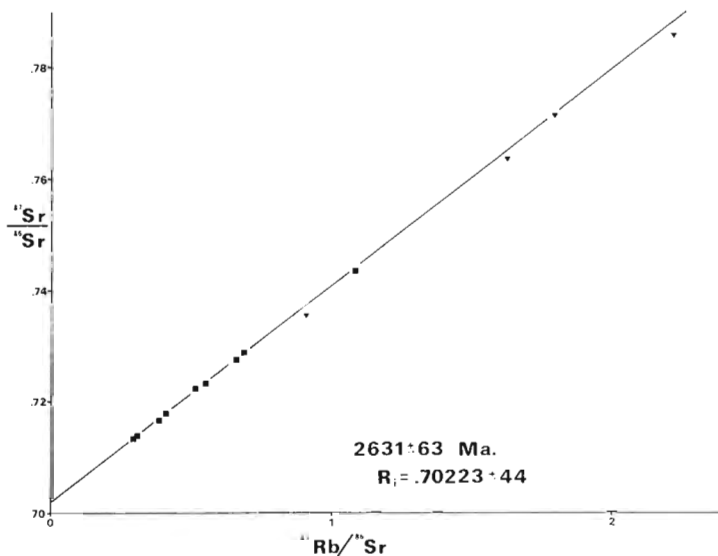


Figure 10.3 Whole-rock Rb-Sr isochron for granitoid rocks at Redditt. The isochron is calculated using only the megacrystic granodiorite samples. Squares correspond to megacrystic granodiorite samples; triangles to granite samples ($\lambda = 1.42 \times 10^{-11} \text{ a}^{-1}$).

spectrometry using the Mo-Compton peak method, developed at McMaster University by Marchand (1973).

Strontium for mass spectrometric analysis was collected in the standard way from ion exchange columns following HF digestion in teflon bombs. The total blank (chemistry and loading) is 40 ng. The precision of a mass spectrometer analysis, based on duplicate analyses, is 0.02 per cent. Six analyses of E and A SrCO_3 averaged 0.70804 ± 14 (2 σ). For XRF analyses, at least six separate pellets were prepared for each sample used on the isochron and precision based on these replicate analyses is generally better than 1 per cent. Accuracy, based on analyses of standard rocks, is generally better than 2 per cent.

Results

The data are tabulated in Table 10.1 and presented graphically in Figure 10.3. Isochron parameters are calculated using the multiple regression program REGROSS (Brooks et al., 1972). The megacrystic granodiorite data yield McIntyre I parameters (2 σ errors) of 2631 ± 63 Ma; $R_1 = 0.70223 \pm .44$; MSWD = 1.35. Inclusion of equigranular granite data decreases the isochron errors (2589 ± 33 Ma; $R_1 = 0.70246 \pm .28$) but increases the MSWD (2.10). Examination of preliminary trace element data suggests it is unlikely that the equigranular granite can be produced by fractional crystallization of the megacrystic granodiorite and, for this reason, the former isochron calculation is preferred. More isotopic and trace element analyses are planned to further evaluate this problem.

Table 10.1

Isotopic data for Redditt area granitoid rocks. $^{87}\text{Sr}/^{86}\text{Sr}$ is normalized to $^{86}\text{Sr}/^{88}\text{Sr} = .1194$ and errors quoted are sigma (mean) for individual runs

Sample	Rock Type	Rb/Sr	$^{87}\text{Rb}/^{86}\text{Sr}$	$^{87}\text{Sr}/^{86}\text{Sr}$
R-5	Megacrystic granodiorite	.1065	.3684	.71387 ± 12
R-45	"	.1008	.2921	.71347 ± 17
R-48	"	.1328	.3848	.71652 ± 5
R-52	"	.2288	.6636	.72736 ± 15
R-53	"	.2376	.6894	.72873 ± 7
R-60	"	.1776	.5132	.72229 ± 6
R-70	"	.1911	.5540	.72311 ± 9
R-71	"	.1413	.4094	.71785 ± 26
R-75	"	.3747	1.0884	.74327 ± 16
R-27	Birch Lake granite	.6218	1.8113	.77114 ± 12
R-35	"	.7666	2.2363	.78561 ± 4
R-36	Granitic dyke	.5615	1.6345	.76349 ± 4
R-37A	"	.3150	.9143	.73557 ± 16

Table 10.2

Summary of Rb-Sr isochron studies of plutonic rocks from the Winnipeg River batholithic belt

Unit	Age (Ma)	R_1	Reference
Redditt Granodiorite	2631 ± 63	.70223 ± .44	This work
Dalles Granodiorite	2630 ± 10	.7014 ± 1	Wooden (1978)
Melick Tonalite	2630 ± 70	.7012 ± 3	"
Pink Granodiorite	2664 ± 30	.7001 ± 16	Farquharson and Clark (1971)
Rennie Batholith	2603 ± 320	.7009 ± 31	" *
Whiteshell Porphyritic Granodiorite	2610 ± 113	.7071 ± 38	" *
Caddy L. Quartz Monz.	2558 ± 12	.7087 ± 15	" *
West Hawk microgranite	2620 ± 83	.7026 ± 62	" *

* These ages were calculated using the $1.39 \times 10^{-11} \text{ a}^{-1}$ decay constant which yields ages approximately 2 per cent higher than for the $1.42 \times 10^{-11} \text{ a}^{-1}$ decay constant used in the other age calculations.

Discussion

The megacrystic granodiorite at Redditt is similar in age to the nearby, more sodic, Dalles and Melick intrusions and falls within the range of other relatively potassic plutonic rocks from the Winnipeg River batholithic belt (Table 10.2). All but two of the units listed in Table 10.2 have R_i values that fall near, or marginally above, most upper mantle growth curves (Faure, 1977). The interpretation of this observation is hampered by the presence of several potential source rocks (e.g. amphibolite, diorite, depleted [?] lower crust) with low Rb/Sr ratios. These sources would diverge slowly with time from upper mantle growth curves. Further isotopic and trace element analyses are planned to evaluate the origin of the Redditt granodiorite and the significance of the relatively low initial ratio.

Acknowledgments

L. Heaman and R. Bowens provided invaluable advice and assistance with various aspects of chemistry and mass spectrometry.

References

- Beakhouse, G.P.
1977: A subdivision of the western English River subprovince; Canadian Journal of Earth Sciences, v. 14, p. 1481-1489.
- Breaks, F.W., Bond, W.D., and Stone, D.
1978: Preliminary geological synthesis of the English River subprovince, northwestern Ontario and its bearing upon mineral exploration; Ontario Geological Survey Miscellaneous Paper 72, 55 p.
- Brooks, C., Hart, S.R., and Wendt, W.
1972: On the realistic use of two-error regression treatments as applied to Rb-Sr data; Reviews of Geophysics and Space Physics, v. 10, p. 551-578.
- Farquharson, R.B. and Clark, G.S.
1971: Rb-Sr geochronology of some granitic rocks in southeastern Manitoba; in Geoscience Studies in Manitoba, A.C. Turnock, ed., Geological Association of Canada, Special Paper 9, p. 111-117.
- Faure, G.
1977: Principles of Isotope Geology; John Wiley and Sons, New York, 464 p.
- Gower, C.F.
1978: The tectonic and petrogenetic history of Archean rocks at Kenora; Unpublished Ph.D. Thesis, McMaster University, Hamilton, 622 p.
- Marchand, M.
1973: Determination of Rb, Sr and Rb/Sr by XRF; McMaster University Technical Memo 73-2, 15 p.
- Presnall, D.C. and Bateman, P.C.
1973: Fusion relations in the system $\text{NaAlSi}_3\text{O}_8$ - $\text{CaAl}_2\text{Si}_2\text{O}_8$ - KAlSi_3O_8 - SiO_2 - H_2O and generation of granitic magmas in the Sierra Nevada batholith; Bulletin of the Geological Society of America, v. 84, p. 3181-3202.
- Streckeisen, A.
1976: To each plutonic rock its proper name; Earth-Science Reviews, v. 12, p. 1-33.
- Wooden, J.L.
1978: Rb-Sr isotopic studies of the Archean rocks of the eastern Lac Seul and Kenora areas, English River subprovince, Ontario; in Proceedings, 1978 Archean Geochemical Conference, ed., I.E.M. Smith and J.G. Williams, p. 131-149.

PROGRESS REPORT ON REGIONAL GEOLOGICAL SYNTHESIS,
CENTRAL SUPERIOR PROVINCE

Project 770070

K.D. Card, John A. Percival¹, and Kenneth Coe²
Precambrian Geology Division

Card, K.D., Percival, John A., and Coe, Kenneth, Progress report on regional geological synthesis, central Superior Province; in Current Research, Part A, Geological Survey of Canada, Paper 80-1A, p. 61-68, 1980

Abstract

Reconnaissance field work, combined with existing geological data, permits preliminary subdivision of the rocks of the central Superior Province into broad categories, including greenstone belt metavolcanic-metasedimentary sequences and associated migmatite, gneiss of plutonic origin, paragneiss, and massive to foliated felsic plutons. Some tentative lithotectonic subdivisions of parts of the Wawa, Quetico, and Wabigoon subprovinces are given and the rock characteristics, structural and metamorphic aspects, and location and nature of the boundaries of these subdivisions are described. Progress reports are presented on studies being carried out on parts of the Kapuskasing Structural Zone and the Round Lake Batholith.

Introduction

The program of reconnaissance field work initiated in the central Superior Province in 1978 (Card, 1979) was continued during 1979. Data were gathered along several sections utilizing road and water access for the most part. Work was concentrated in areas that have hitherto received little attention, mainly the areas shown on existing maps as predominantly granitic. The objectives of the work include reconnaissance subdivision of these rocks, which combined with petrologic, structural, and radiometric age studies, will permit a more complete synthesis of the geology of the central Superior Province.

Another objective is the definition of areas and problems requiring further study, and in this context investigations were initiated in several areas. J.A. Percival is investigating the nature and evolution of part of the "Kapuskasing Structural Zone" in the Chapeau-Foley area,

Ontario. The results of the summer's field work by Percival and Dr. K. Coe, University of Exeter, England, are presented as Part II of this report. Percival's work on the Kapuskasing structure will form the basis of a Ph.D. thesis at Queen's University, Kingston.

The second area of study involves the Round Lake Batholith south of Kirkland Lake, Ontario. J. Lafleur has undertaken a study of this body to improve our understanding of its age relationships, petrogenesis, and mechanisms of emplacement. This work will be the topic of his M.Sc. thesis at the University of Ottawa.

Dr. K. Attah, University of Ghana, a postdoctoral fellow at the Geological Survey of Canada, is comparing greenstone belt assemblages in the West African and Canadian Precambrian shields. He conducted field studies in selected parts of the Wawa greenstone belt under the auspices of R.P. Sage of the Ontario Geological Survey.

**PART I. RESULTS OF RECONNAISSANCE INVESTIGATIONS AND STUDIES
OF IGNEOUS INTRUSIONS**

K.D. Card

Reconnaissance Investigations

Major rock units and lithotectonic subdivisions were outlined in parts of the Wawa, Quetico, and Wabigoon subprovinces of the Superior Province (Stockwell, 1970) in the region bounded by 48°30'N to 50°30'N and 85°20'W to 88°20'W (Fig. 11.1).

The Wabigoon and Wawa subprovinces are typical "greenstone-granite" terranes consisting of greenstone belt metavolcanic-metasedimentary supracrustal sequences, migmatitic rocks derived from the supracrustal rocks, orthogneiss of tonalite-granodiorite composition, and massive to foliated felsic plutons. The felsic plutons form several distinctive petrologic suites, including simple granite, syenite, granodiorite, trondhjemite, and quartz diorite intrusions, and batholithic complexes consisting of several of the foregoing rock types.

The structure of the greenstone-granite terranes is complex. The rocks of the greenstone belts commonly show steeply dipping, polyphase deformation structures and greenschist to lower amphibolite facies metamorphic mineral assemblages. The gneiss domains typically display domal

structures of diapiric origin and amphibolite facies metamorphism. The felsic plutonic rocks, mainly of syntectonic and posttectonic origin, commonly truncate and distort earlier formed structures in the country rocks.

The Quetico subprovince is a linear belt of highly deformed, highly metamorphosed supracrustal rocks some 40 km wide lying between the Wabigoon and Wawa subprovinces. The rocks are mainly immature clastic sediments (quartz wacke) metamorphosed under upper amphibolite and lower granulite facies conditions to a variety of paragneiss and migmatite. These rocks are isoclinally folded about east-west axes and pervasively invaded by granitic bodies, many of which are anatectic in origin. The granitic rocks contain abundant paragneiss inclusions in various stages of digestion and have minerals such as muscovite, garnet, and cordierite. Locally these are bodies of tonalite-granodiorite gneiss and thin units of mafic gneiss, possibly metavolcanics or mafic intrusions.

In the area shown in Figure 11.1, the northern and southern boundaries of the Quetico subprovince are, in part at least, faulted. South and east of Longlac, Ontario, the Gravel River Fault constitutes the boundary between well bedded,

¹ Department of Geology, Queen's University, Kingston, Ontario.

² Department of Geology, University of Exeter, England.

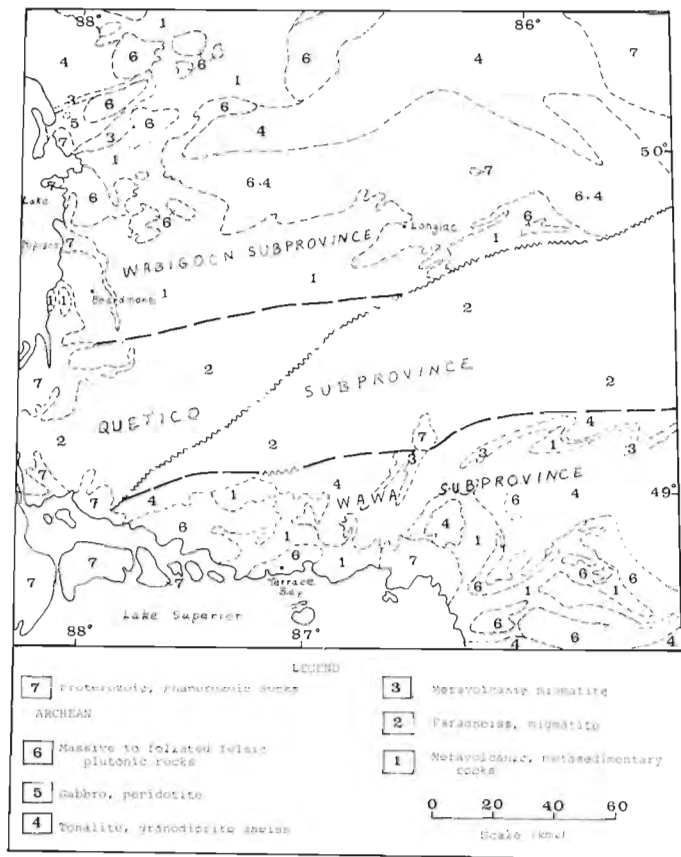


Figure 11.1. Distribution of major lithotectonic units in part of the Superior Province.

low rank metamorphic (greenschist facies) wacke of the Wabigoon subprovince to the north and high rank metamorphic (amphibolite facies) migmatitic paragneiss of the Quetico subprovince to the south. Immediately north of the fault, the low grade metasediments are cut by numerous muscovite-rich pegmatite and granite dykes. The migmatitic rocks immediately south of the fault display biotite-garnet mineral assemblages and several kilometres to the south cordierite and pyroxenes also appear.

The southern boundary of the Quetico subprovince north of Terrace Bay, Ontario is similar, comprising: 1) interbedded metasediments (quartz wacke) and metavolcanic rocks of the Wawa subprovince; 2) a unit approximately 3 km in outcrop width of low grade metasediments cut by numerous muscovitic pegmatite and granite dykes; 3) a narrow zone of mylonitic rock, probably marking a fault; 4) migmatitic paragneiss with abundant biotite, but no garnet, approximately 2 km wide; 5) migmatitic paragneiss with biotite-garnet assemblages and abundant anatectic granite and pegmatite (approximately 10 km in outcrop width); and 6) migmatitic paragneiss with biotite-garnet-cordierite-pyroxene assemblages and abundant anatectic granitic material.

The contact between the Wabigoon and Quetico subprovinces along Highway 11 is masked by Proterozoic Logan Diabase sills. However, the contact as defined by the transition from low rank metasediments to high rank migmatitic paragneiss is more than 14 km south of Beardmore, Ontario. At this locality there is an excellent exposure of the unconformity between flat lying Proterozoic sandstone of the Sibley Group and vertically dipping, low rank metamorphic metasediments of the Wabigoon subprovince.

Studies of Various Igneous Intrusions

Investigations are being conducted of various felsic plutons and mafic dyke swarms in an attempt to classify them petrologically, to deduce their ages relative to tectono-metamorphic events, and to determine their absolute ages by radiometric methods. With the presently available data it is possible to group some of the felsic plutons and mafic dykes into chemical-petrographic suites, and to deduce the general age relationships between these units and tectono-metamorphic events. However, for many intrusions, the data are insufficient or relationships are so equivocal that further studies are required. The Round Lake Batholith in the Kirkland Lake, Ontario area is probably typical of the latter group.

Round Lake Batholith

The origin, age, and mechanism of emplacement of the Round Lake Batholith have been interpreted in various ways. Moorhouse (1944) and Lovell (1972) concluded that it is of magmatic origin and intrusive into the metavolcanic rocks of the Abitibi Belt. Ridler (1975) suggested that the batholith, in part at least, is basement to the Abitibi metavolcanic rocks, remobilized during the Kenoran Orogeny, and reintroduced into its present setting.

The batholith is composite, consisting of an outer zone of cataclastically foliated, locally gneissic tonalite-granodiorite, and an interior, northeast-trending body of massive granite that contains xenoliths of the tonalite-granodiorite and of the surrounding metavolcanic rocks. The batholith occupies the core of an antiformal structure in the surrounding metavolcanic rocks. The contact of the batholith and cataclastic foliation within the batholithic rocks are generally concordant with the structure of country rocks. Granitic dykes extending from the batholith into the country rocks are rare, and there is little evidence for a contact metamorphic aureole about the intrusion.

The batholith could represent a basement diapir, as postulated by Ridler (1975). However, it could also represent a late Archean "magmatic diapir", a post-Abitibi magmatic intrusion that cooled and partly solidified while still moving diapirically upward in the dense mafic volcanic sequence.

It is expected that Lafleur's work, including completion of the mapping of the body coupled with petrographic, chemical, and structural studies, will provide the basic data required to decide which, if any, of the foregoing models is most likely.

PART II. GEOLOGY OF THE KAPUSKASING STRUCTURAL ZONE IN THE CHAPLEAU-FOLEYET AREA, ONTARIO

John A. Percival and Kenneth Coe

Introduction

This report is one of a series in a project (Card, 1979) aimed at establishing and clarifying relationships among Archean greenstone belts, gneissic and plutonic terranes in the central Superior Province. The Kapuskasing Structural Zone, a northeast-trending zone of structural discontinuity, extends from beneath the south end of James Bay (Gibb, 1978) to Lake Superior (Card, 1979) (Fig. 11.2). The zone is best exposed between latitudes 47°45'N and 48°30'N, where it separates the Abitibi subprovince to the east from the Wawa subprovince to the west (Thurston et al., 1977). In the study area, approximately between Foleyet and Chapleau, Ontario, the three subareas have distinctive characteristics which are outlined below.

Abitibi Subprovince

The eastern extremity of the Abitibi subprovince (Stockwell, 1970) (Fig. 11.2) is underlain by low grade greenstone belt rocks characterized by the preservation of primary textures in supracrustal rocks, greenschist to low amphibolite facies metamorphism, east-west structural trends and predominantly discordant, late- to post-tectonic plutons.

The Swayze-Deloro belt (Fig. 11.3), part of the Abitibi subprovince, is made up of mafic metavolcanic rocks with minor intercalated felsic metavolcanics and interstratified fine to coarse metasediments of probably volcanic parentage.

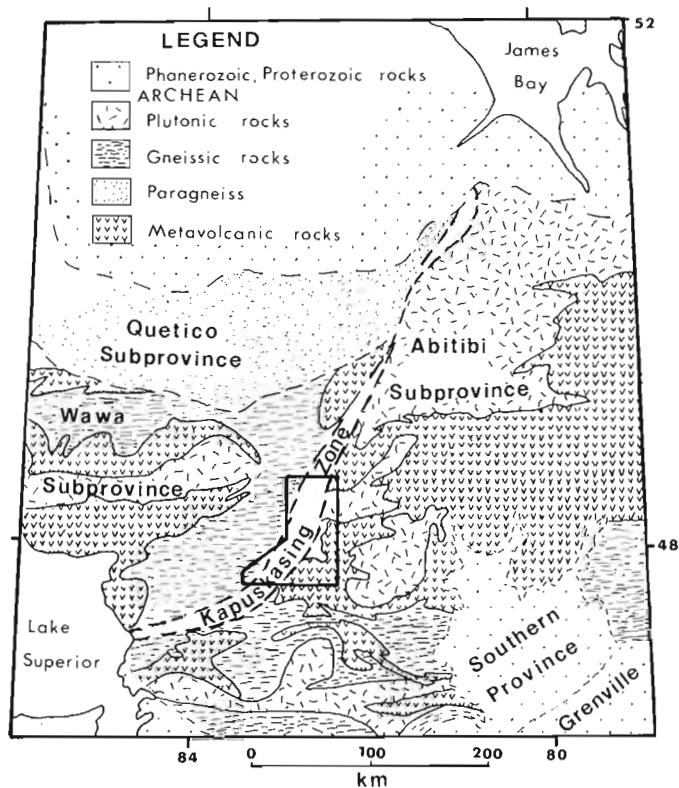


Figure 11.2. Generalized geological map showing subprovinces and major lithological units in the central Superior Province (after Card, 1979). The study area is outlined.

The supracrustal rocks are intruded by mafic and ultramafic sheets and concordant lenses, all of which are deformed, and massive to marginally xenolithic, foliated or lineated tonalite, granodiorite and granite plutons. At the eastern boundary of the Kapuskasing Structural Zone west of Foleyet (Fig. 11.3) an elongate, lineated, composite intrusion of monzonite-syenite, containing peridotite, pyroxenite, and hornblende inclusions, lies within granitic rocks.

Deformational effects are best observed in meta-sedimentary rocks. At Denyes Lake, sedimentary layering in metaconglomerate, meta-arkose, slaty and cherty rocks is at an oblique angle to an east-west to northeast-southwest trending axial planar cleavage which is associated with a tight fold system. The folds are slightly overturned to the southeast and plunge at a low angle to the west. A flat lying crenulation cleavage is locally present in the fine grained rock types. At Slate Rock Lake (Fig. 11.3), muscovite alignment parallel to sedimentary layering forms slaty cleavage. East-west lineations plunge at low angles. Step folds with axial planar cleavage warp the slaty cleavage. Locally developed, small-scale open folds with flat axial surfaces deform the axial planar cleavage.

Granitic rocks are medium grained and locally porphyritic, foliated or lineated. Some bodies have sparse but ubiquitous mafic xenoliths while others have marginal zones of inclusions. Structural trends are east-west to southeast-northwest. A 1 km-wide cataclastic zone with fracture cleavage is present in granitic rocks at Ivanhoe Lake.

The metamorphic grade appears to be lowest in meta-sedimentary rocks where muscovite-chlorite assemblages predominate. In close proximity to the lower grade rocks, metavolcanic rocks commonly contain garnet, amphibole and plagioclase. One isolated metavolcanic outcrop near the eastern margin of the Kapuskasing Structural Zone has steep east-west foliation, typical of low grade metavolcanics, but contains garnet-clinopyroxene locally. This high grade assemblage is anomalous and may be the result of proximity to the structural zone.

Chapleau Area High Grade Greenstone Belt

This subarea, part of the Wawa subprovince (Stockwell, 1970), is characterized by the abundance of xenolithic orthogneiss, paragneiss and amphibolite. Metamorphism to amphibolite and locally granulite facies was accompanied by the development of east-west, steeply dipping structures and syntectonic igneous and migmatitic rocks.

Supracrustal rocks are exposed in a 2 km-wide belt around Borden Lake (Fig. 11.3). These consist of mafic tuff-breccias, amphibolitic metavolcanics and metasediments, including muscovite-bearing arkosic paragneiss and stretched-pebble metaconglomerate. Clasts in the metaconglomerate are, in order of decreasing abundance, felsic metavolcanics, metasediments, granodiorite, plagioclase porphyritic metandesite, amphibolite and rare hornblende and quartzite. Felsic metavolcanic fragments are by far the most constricted, with long axes up to 1.5 m and short axes of 0.07 m. The belt is intruded on the south side by granodiorite with xenolithic gneissic margins and by massive pink granite. Gneissic tonalite occurs south of the granodiorite and is locally present as inclusions in granodiorite. A flaser-textured syenogabbro composite intrusion northeast of Chapleau has northwest-southeast striking fabric and is cut near its margins by tonalite.

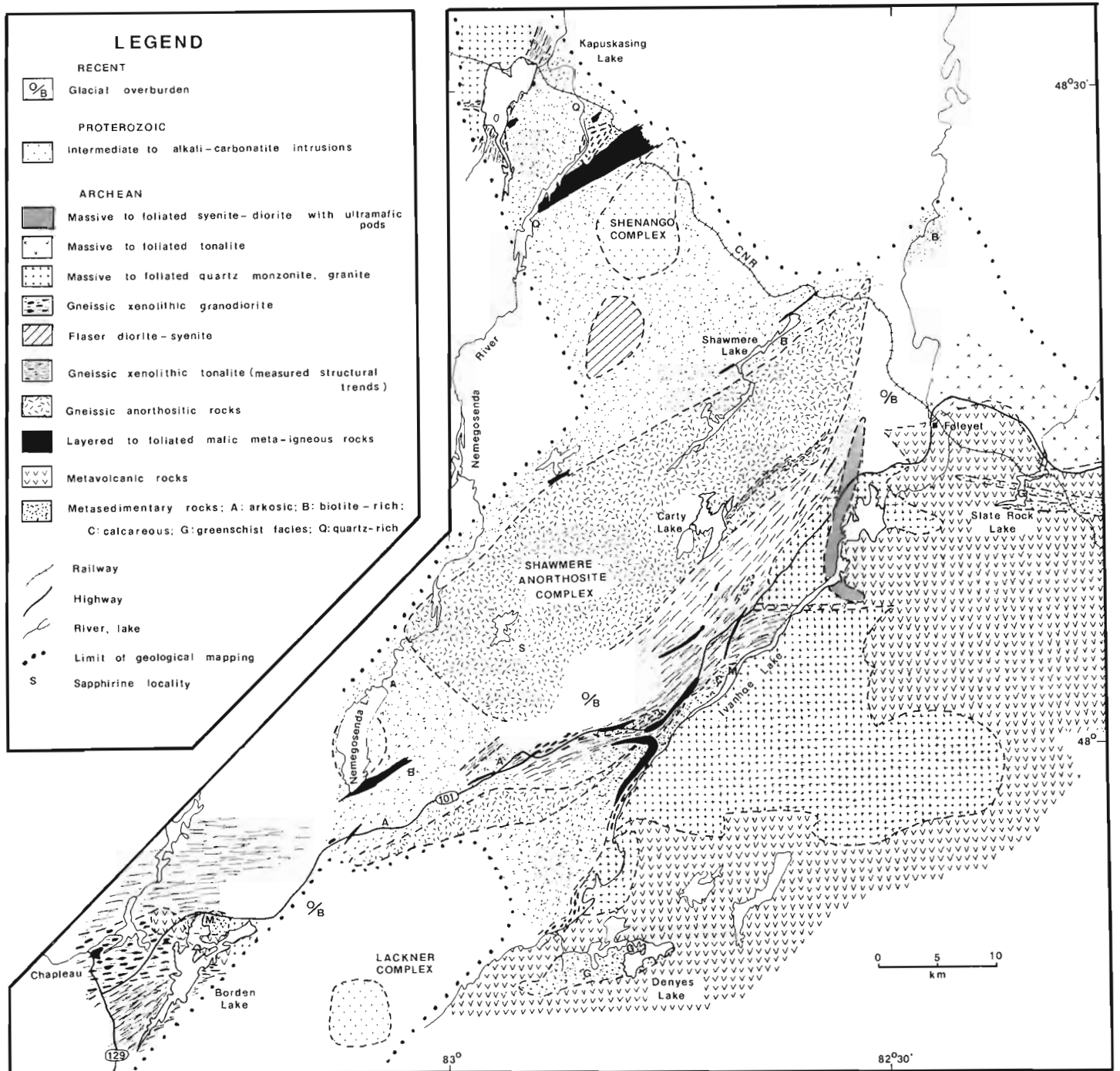


Figure 11.3. Geological sketch map of the Kapuskasing Structural Zone and adjacent areas. Geology of most of the area bounded by Slate Rock Lake, Denyes Lake and Ivanhoe Lake is after Thurston et al. (1977).

A planar fabric, generally with east-west strike, is developed as gneissic layering in granitic rocks and quartz-feldspar segregations in paragneiss and amphibolite. Small folds of the layering have gentle (0-20°) plunges to east or west. Mineral and rodding lineations are parallel to fold axes. Tonalitic rocks at the south end of Borden Lake have a flat lying foliation, locally folded about upright axial surfaces.

Amphibolite facies assemblages predominate in the Chapleau area gneiss. Mafic xenoliths generally have amphibole-plagioclase ± clinopyroxene composition.

Migmatitic paragneiss is garnet-biotite-quartz-plagioclase ± muscovite ± sillimanite(?). Granulite facies assemblages (orthopyroxene-clinopyroxene and garnet-clinopyroxene-quartz-plagioclase) are locally developed in mafic rocks around Borden Lake. The high grade assemblages at Borden Lake may be the result of proximity to the structural zone, however, poor exposure east of the lake prevents location of the boundary.

Kapuskasing Structural Zone

Lithology and Structure

Rocks in this zone are paragneiss, mafic and tonalitic orthogneiss and members of the Shawmere anorthosite complex (Thurston et al., 1977). All are metamorphosed to granulite or amphibolite facies and generally have northeast striking, gently northwest dipping structural elements. Lithological mapping is complicated by the similarity between tonalitic paragneiss and tonalitic orthogneiss. In general, the paragneiss is characterized by its heterogeneity and association with biotite-rich rocks.

Metasedimentary gneiss is biotite-quartz-plagioclase rock with or without garnet and amphibole. Variations in grain size, mafic mineral content and concentration of small pegmatitic veinlets occur on a 10 cm to 2 m scale. Regional compositional variation may indicate original sedimentary facies changes. For example, paragneiss east of Kapuskasing Lake contains up to 50 per cent quartz, in addition to garnet, biotite and plagioclase, whereas south and northeast of Shawmere Lake, biotite-rich paragneiss is common. Finely layered metasedimentary rocks of arkosic composition are the dominant rock type southeast and northeast of Nemegosenda Lake. Graphitic, biotite-rich paragneiss occurs in a small area west of Ivanhoe Lake. Layers and enclaves of mafic gneiss are present within the metasedimentary units. Confusing rounded enclaves of amphibole-plagioclase ± garnet ± clinopyroxene ± quartz rock may be boudinaged remnants of tuffaceous layers or basaltic sheet intrusions.

Orthotonalite is garnet-biotite-amphibole-quartz-plagioclase gneiss, homogeneous on the outcrop scale. Units up to 1 km wide occur within metasedimentary gneiss, for example, 10 km east of Nemegosenda Lake (Fig. 11.2). The main outcrop area of orthotonalitic gneiss is southeast of the Shawmere anorthosite complex, extending toward Ivanhoe Lake (Fig. 11.3). Here it is characterized by its uniform mineralogy and by the presence of 10 to 20 per cent mafic and ultramafic (amphibole-clinopyroxene) rounded xenoliths. In places the xenoliths have granulite facies cores (garnet-clinopyroxene-plagioclase-quartz) with amphibole-plagioclase rims. In several exposures foliation in mafic xenoliths is at a high angle to the foliation of the tonalite. Orthotonalite also occurs within the outcrop area of the Shawmere anorthosite. It is a homogeneous, foliated, medium grained garnet-biotite-amphibole-quartz-plagioclase rock injected with late tonalitic veinlets. Except for its lack of xenoliths, this rock is similar in texture and mineralogy to the tonalite south of the anorthosite.

Mafic meta-igneous rocks occur mainly within meta-sedimentary sequences but are also present in tonalitic rocks and meta-anorthosite. The fabric in the metagabbroic gneiss is made up of more or less regular layers of hydrous and anhydrous mineralogy (amphibole-plagioclase and garnet-clinopyroxene-quartz-plagioclase respectively) with tonalitic veinlets.

The Shawmere anorthosite complex is a metamorphosed deformed body of Archean age (Watkinson et al., 1972). Detailed mapping of the anorthosite by the Ontario Geological Survey is currently underway. Deformed megacrystic anorthosite (*sensu stricto*) and gabbroic anorthosite make up the bulk of the complex, but a small area centred on Carty Lake is underlain by layered anorthosite and gabbro with some ultramafic bands (L. Riccio, personal communication, 1979). Small xenoliths of anorthosite occur in mafic gneiss included as large xenoliths in orthotonalite sheets that intrude metasedimentary gneiss at Shawmere Lake. Except in a few places, compositional layering in anorthositic rocks is parallel to amphibole alignment.

Other meta-igneous rocks that intrude the zone include a xenolithic granodiorite body with quartz monzonite veinlets that intrudes metasediments east of Kapuskasing Lake on the Nemegosenda River and a foliated to flaser-textured syenodiorite and quartz diorite body south of the Shenango Complex (Fig. 11.3).

Small folds that postdate layering are present in all rock units. These are generally isoclinal and have axial planes parallel to the regional foliation, but near the western margin of the structure ortho- and paragneiss have a vertical fabric refolded about flat axial planes. Fold axes and associated mineral and rodding lineations of constant trend (240-260°) plunge gently (0-20°) either east or west. A weak axial-planar fabric is associated with isoclinal folds. In metasedimentary rocks north of the anorthosite, east-northeast structures are gentle warps of foliation and layering. Late gentle warps about northwest axes are probably responsible for the variation in plunge direction of small folds and lineations.

Metamorphism

Rocks of the Kapuskasing Zone have been metamorphosed to high-pressure granulite (de Waard, 1965; Green and Ringwood, 1967) or amphibolite facies. Paragneisses contain the assemblages:

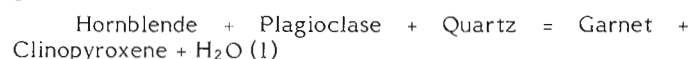
Garnet-biotite-quartz-plagioclase ± amphibole

Garnet-clinopyroxene-biotite-quartz-plagioclase ± amphibole

Garnet-biotite-hypersthene-K feldspar-quartz-plagioclase

An occurrence of sillimanite-garnet-orthopyroxene-biotite-quartz-plagioclase was reported by Thurston et al. (1977).

Mafic rocks generally have mineralogy typical of both amphibolite and granulite facies. In some mafic rocks, amphibolite/granulite layering on a scale of ten centimetres is developed and this appears to correspond to a balanced dehydration reaction marking the lower boundary of the granulite facies (Carmichael, 1974):



Mineral assemblages in mafic gneiss include:

Garnet-amphibole-plagioclase

Clinopyroxene-amphibole-plagioclase

Garnet-clinopyroxene-amphibole-sphene-plagioclase-quartz-scapolite

Garnet-clinopyroxene-orthopyroxene-amphibole-sphene-quartz-plagioclase

One mafic gneiss specimen examined in thin section shows a complex overgrowth-corona structure; symplectitic orthopyroxene-plagioclase rims surround garnet and clinopyroxene grains. Some garnets contain plagioclase inclusions which themselves contain orthopyroxene. Garnet-clinopyroxene geothermometry (Raheim and Green, 1974) and garnet-orthopyroxene geobarometry (Wood and Banno, 1973) on ten specimens indicate equilibration at ca. 600-650°C and 7.5-9.5 kb.*

Mineral assemblages in meta-anorthosite include:

Amphibole-plagioclase

Garnet-amphibole-plagioclase

Mafic layers contain garnet-clinopyroxene-amphibole-plagioclase. Garnet-amphibole rims commonly overgrow large orthopyroxene grains and amphibole overgrows clinopyroxene. One magnesian gabbro from the west end of the complex (Fig. 11.3) contains the assemblage garnet (pyrope 50)-amphibole-orthopyroxene (4.7 wt% Al₂O₃)-plagioclase (An₉₄)-sapphirine.

* 1 kb = 10⁵ k Pa

Boundary Features of the Kapuskasing Structure

Cataclastic Features

Zones of cataclasis are developed near the eastern boundary of the structural zone. Pseudotachylite veinlets with maximum width of 10 cm are common in a 1 km-wide zone of high grade rocks. These generally lack strong directional orientation and veins may be seen crosscutting others of the same origin. Even where pseudotachylite is abundant the veins are only a few tens of centimetres long and have irregular shapes. The veinlets consist of crypto-crystalline rock flour, with some porphyroclasts of amphibole and plagioclase. No glass or devitrification textures have been observed in the limited number of thin sections so far examined.

Augen gneiss with strong rodding of feldspars is present in monzonitic rocks north of Ivanhoe Lake. Ubiquitous north-northeast striking alteration veinlets in anorthositic rocks are probably associated with granulation. Granite, migmatite and a mafic dyke at one locality west of Ivanhoe Lake are of hematite-cemented protomylonite.

Marginal Features

The boundaries of the structural zone are relatively well-exposed in a few localities. East of Ivanhoe Lake (Fig. 11.4) massive or fractured granitic rocks intrude metavolcanics of the Swayze-Deloro belt. Lithology in the Kapuskasing Zone west of Ivanhoe Lake is variable. Cataclastic effects are only locally developed in rocks west of the lake, but major faults may underlie Ivanhoe Lake itself. A migmatitic 'screen' consisting of mafic gneiss and massive to foliated granite and quartz monzonite separates the Abitibi subprovince from high grade rocks in at least two places, suggesting an intrusive contact. To the north (Fig. 11.4) arkosic metasedimentary rocks (locally muscovite-bearing) with east-west, north-dipping structures appear to be continuous into migmatitic granulite facies paragneiss with northeast striking foliations at Highway 101. Northwest of Ivanhoe Lake massive granite and quartz monzonite may be correlative with gneissic granite with northeast striking, northwest-dipping fabric to the west.

The western margin of the structure is exposed at Kapuskasing Lake, where granulite facies mafic gneiss and paragneiss are separated from massive to foliated granite by xenolithic gneissic tonalite and granodiorite. Foliation in the boundary zone strikes generally north-northwest and dips east toward the structural zone. Lineations are particularly abundant in mafic gneiss, gneissic tonalite and foliated granite, generally plunging at a moderate angle to the east. Massive granite west of the lake may be intrusive into rocks of the structural zone or faulted into juxtaposition. However, a line may be drawn here to separate massive rocks or those with east-trending structures from those with generally north- to northeast-striking fabrics.

Another transition zone along the western margin is exposed south of Nemegosenda Lake on Highway 101. Here, mafic gneiss with granulite assemblages can be traced westward through a migmatitic zone approximately 2 km wide in which granulite assemblages survive in mafic xenoliths, to xenolithic granodiorite in which mafic enclaves show amphibole-plagioclase mineralogy.

Post-Archean Intrusive Rocks

Massive, fresh, medium grained mafic dykes trending 070° ($\pm 15^\circ$) up to 10 m wide are common in the Kapuskasing Structural Zone. A few of the dykes contain up to 5 per cent

plagioclase phenocrysts in a matrix similar to that of the nonporphyritic dykes. On the Goose Range fire tower road cataclastic veinlets and minor offsets were observed cutting the chilled margin of a mafic dyke which strikes 070°. A few olivine diabase dykes of the Abitibi swarm were noted, also with east-northeast trends.

Alkalic-carbonatite complexes at Lackner Lake and Nemegosenda Lake (dated by K-Ar at 1090 and 1010 Ma respectively (Gittins et al., 1967)) cut high grade rocks of the structural zone. The Shenango complex, a syenodiorite-anorthosite body, is also of late Proterozoic age (Thurston et al., 1977).

Lamprophyre dykes with an average width of about 10 cm are common in the Kapuskasing Structural Zone and also in the Chapleau area. They are vertical but trends are variable, between 360° and 090°. One such dyke has a diatreme margin containing locally derived gneissic and exotic ultramafic fragments.

Discussion and Preliminary Conclusions

The sequence of events in the Kapuskasing Structural Zone, as determined by field observations, is summarized in Table 11.1. The major differences between the Kapuskasing zone and the adjacent subprovinces are:

- the presence of granulite facies paragneiss and anorthosite in the zone;
- the lack of posttectonic (unfoliated) rocks in the zone (excepting northeast mafic dykes, 1090 and 1010 Ma plutons); and
- the predominance of northeast striking, gently northwest dipping foliations in the structure.

In addition, structures within some units change their orientation to northeast in the zone and massive rocks are tentatively correlated with foliated rocks in the structure. This suggests that some plastic movement in the zone postdates the massive plutons of the adjacent terranes. The lines marking the change of foliation trend, lithological discontinuity, increase in metamorphic grade, and zone of cataclasis are not coincident. These facts suggest that the structure formed in the following manner. Sediments were deposited in a narrow elongate (fault-bounded?) intracratonic basin, were subsequently intruded by anorthosite, deformed and metamorphosed under infrastructural conditions. In adjacent terranes, volcanic rocks were extruded, metamorphosed and intruded by syn- to post-tectonic plutons. Left lateral movement continued at depth in the Kapuskasing Structural Zone, warping structures into northeast trends. In the late Archean or early Proterozoic, reactivation of faults along the eastern boundary of the structure accommodated tilting (east side up), bringing granulite facies rocks into juxtaposition with lower grade rocks to the east. This sequence would explain the abrupt (cataclastic) transition on the east and more gradational margin to the west. The noncoincidence of boundary features on the eastern margin may be the result of continual reactivation along a zone approximately 2 km wide within which the marginal features developed and partially overlapped during different stages in the evolution of the zone.

A test for the model might be to establish similarity of radiometric ages between the Kapuskasing structure and adjacent terranes. Furthermore, an increase in metamorphic grade from west to east is to be expected if the model is correct.

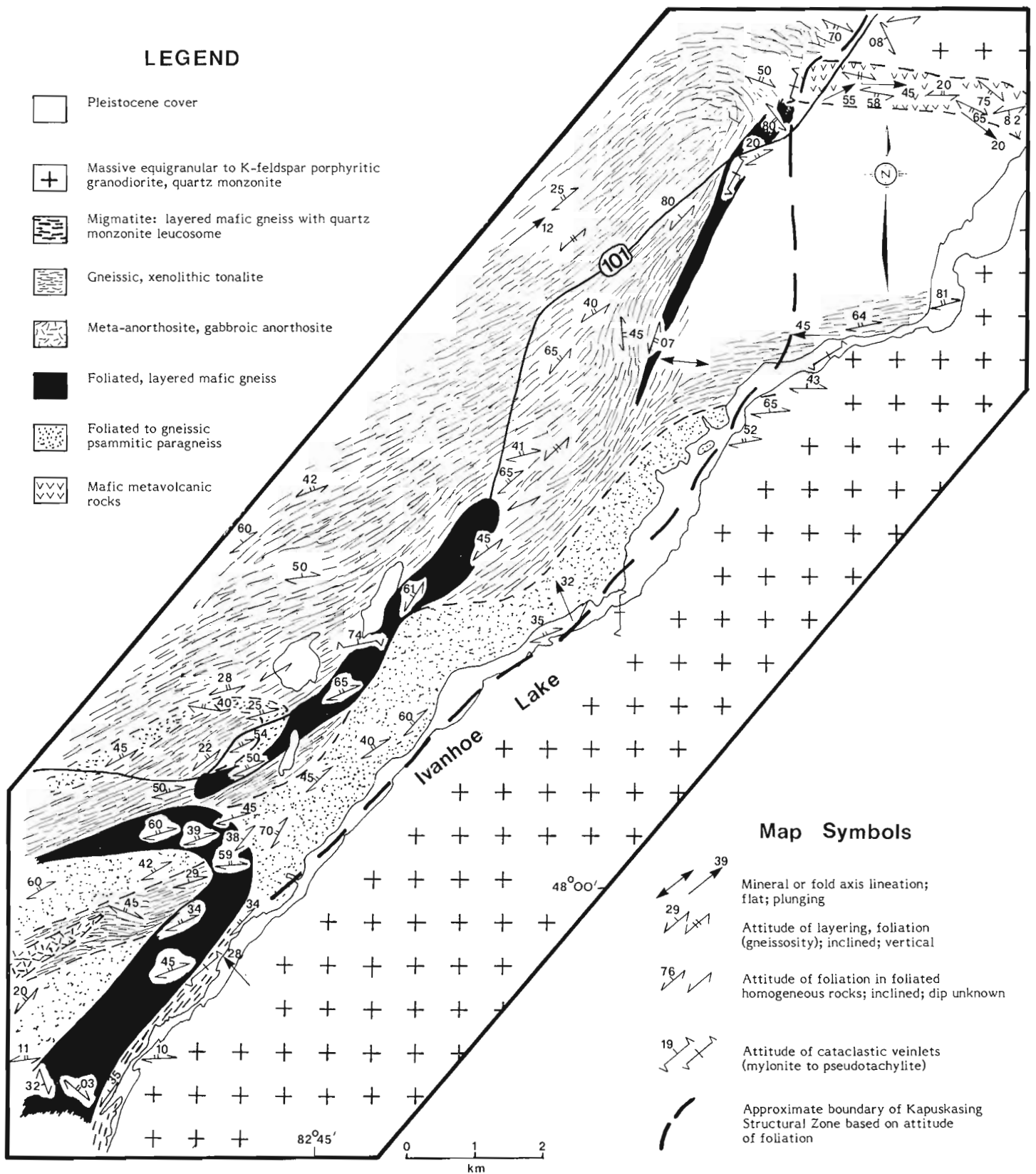


Figure 11.4. Detailed geological map of the eastern margin of the Kapuskasing Structural Zone.

Table 11.1
Sequence of geological events in the Kapuskasing Structural Zone

	S ₀	D ₁	D ₂	D ₃	Pseudotachylite
Metamorphism		-----			
Migmatisation		-----	-----		
Deformation		planar fabric	isoclinal folds (flat axes)	warps	
		tonalite -----			
Intrusion	anorthosite ----- mafic rocks (?) -----				alkalic-carbonatite ----- complexes
	Mafic rocks (?) -----				
Deposition	Sediments -----				

Acknowledgments

The authors were capably assisted in the field by J. Lafleur and J.B. Percival. The work of K. Coe, in conjunction with J. Percival, has contributed significantly to our knowledge of the Kapuskasing structure. The support provided to K. Attoh by R.P. Sage and the Ontario Geological Survey is gratefully acknowledged. The authors also acknowledge assistance and information from S. Amukun, Ontario Geological Survey, H. Lovell, Resident Geologist, Ontario Ministry of Natural Resources, Kirkland Lake, L. Riccio, Ontario Geological Survey, S.B. Lumbers, Royal Ontario Museum, and Ontario Ministry of Natural Resources staff, Chapleau District.

References

- Card, K.D.
1979: Regional geological synthesis, central Superior Province; in *Current Research, Part A, Geological Survey of Canada, Paper 79-1A*, p. 87-90.
- Carmichael, D.M.
1974: Mineral equilibria in mafic granulites (abstract); *Canadian Mineralogist*, v. 12, p. 429-430.
- de Waard, D.
1965: The occurrence of garnet in the granulite-facies terrain of the Adirondack Highlands; *Journal of Petrology*, v. 6, p. 165-191.
- Gibb, R.A.
1978: A gravity survey of James Bay and its bearing on the Kapuskasing Gneiss Belt, Ontario; *Tectonophysics*, v. 45, p. T7-T13.
- Gittins, J., MacIntyre, R.N., and York, D.
1967: The ages of carbonatite complexes in eastern Canada; *Canadian Journal of Earth Sciences*, v. 4, p. 651-655.
- Green, D.H. and Ringwood, A.E.
1967: An experimental investigation of the gabbro to eclogite transformation and its petrological applications; *Geochimica et Cosmochimica Acta*, v. 31, p. 767-834.

Lovell, H.

- 1972: Geology of Eby and Otto Townships, District of Timiskaming, Ontario; Ontario Department of Mines and Northern Affairs, GR 99, 30 p.

Moorhouse, W.W.

- 1944: Geology of the Bryce-Robillard area; Ontario Department of Mines, Annual Report, v. 50, pt. 4.

Raheim, A. and Green, D.H.

- 1974: Experimental determination of the temperature and pressure dependence of the Fe-Mg partition co-efficient for co-existing garnet and clinopyroxene; *Contributions to Mineralogy and Petrology*, v. 48, p. 179-203.

Ridler, R.H.

- 1975: Regional metallogeny and volcanic stratigraphy of the Superior Province; in *Report of Activities, Part A, Geological Survey of Canada, Paper 75-1A*, p. 353-358.

Stockwell, C.H.

- 1970: Geology of the Canadian Shield - Introduction; in *Geology and Economic Minerals of Canada*, R.J.W. Douglas (ed.), Geological Survey of Canada, Economic Geology Report 1 (5th ed.), p. 44-54.

Thurston, F.C., Siragusa, G.M., and Sage, R.P.

- 1977: Geology of the Chapleau area, Districts of Algoma, Sudbury and Cochrane; Ontario Division of Mines, Geological Report 157, 293 p.

Watkinson, D.H., Thurston, P.C., and Shafiquillah, M.

- 1972: The Shawmere anorthosite of Archean age in the Kapuskasing Belt, Ontario; *Journal of Geology*, v. 80, p. 736-739.

Wood, B.J. and Banno, S.

- 1973: Garnet-orthopyroxene and orthopyroxene relationships in simple and complex systems; *Contributions to Mineralogy and Petrology*, v. 42, p. 109-124.

STRATIGRAPHY AND FACIES AT THE SOUTH MARGIN
OF THE ARCHEAN NORANDA CALDERA, NORANDA, QUÉBEC

EMR Research Agreement 71-4-79

A.P. Lichtblau¹ and E. Dimroth²
Precambrian Geology Division

Lichtblau, A.P., and Dimroth, E., *Stratigraphy and facies at the south margin of the Archean Noranda caldera, Noranda, Québec; in Current Research, Part A, Geological Survey of Canada, Paper 80-1A, p. 69-76, 1980.*

Abstract

Pyroclastic rocks permit correlation of stratigraphic units across the southern margin of the Archean Noranda caldera. Caldera subsidence was not a sudden, unique event, but took place in several successive steps which coincided with periods of volcanic activity.

Seven facies of pyroclastic deposits were defined by their geometry and the sequence of their sedimentary structures, as follows: (1) lag deposits left behind at the site of eruption by a collapsing submarine eruption column; (2) filling of pit craters by steam explosion breccia; (3) pyroclastic debris flow; (4) pyroclastic turbidite or similar mass-flow; (5) pyroclastic air-fall, settled through water; (6) pyroclastic air-fall, coarse grained, redeposited by offshore currents in a shallow marine environment; (7) pyroclastic air-fall, fine grained, redeposited by shallow marine currents.

Introduction

The Blake River Group at Noranda has been subdivided (Gélinas et al., 1977; Dimroth and Rocheleau, 1979) into four subgroups, namely the Pelletier, Reneault, Dufault, and Dufresnoy subgroups. The Pelletier subgroup, composed of tholeiitic basalt, forms an extensive basalt plain. The calc-alkalic Reneault and Dufault subgroups are correlative and comprise a complex array of central volcanic complexes, the largest of which is Noranda central volcano.

De Rosen-Spence (1976) established the stratigraphic sequence in Noranda central volcano and reconstructed the large lines of its evolution. She found that a caldera, or a volcano-tectonic depression, 15 km wide, formed at a certain stage in the evolution of the complex. The caldera is bounded

in the north by the Hunter Creek fault, in the south by the Quemont feeder dyke and formed in the interval between the eruption of the Northwest and Brownlee rhyolites and the Héré Creek rhyolites. Most of the ore bodies in Rouyn-Noranda area are within or at the margin of this caldera, and formed during caldera subsidence.

The present work is a detailed study of the stratigraphy and of the sedimentary facies of tuffs at the south margin of the caldera. After some initial work by E. Dimroth, the area was mapped on a scale of 1:2400 by A.P. Lichtblau as an M.Sc. project at the University of Quebec at Chicoutimi. The general geology of the area is shown in Figure 12.1. A detailed stratigraphic map of the Powell andesite is shown as Figure 12.2.

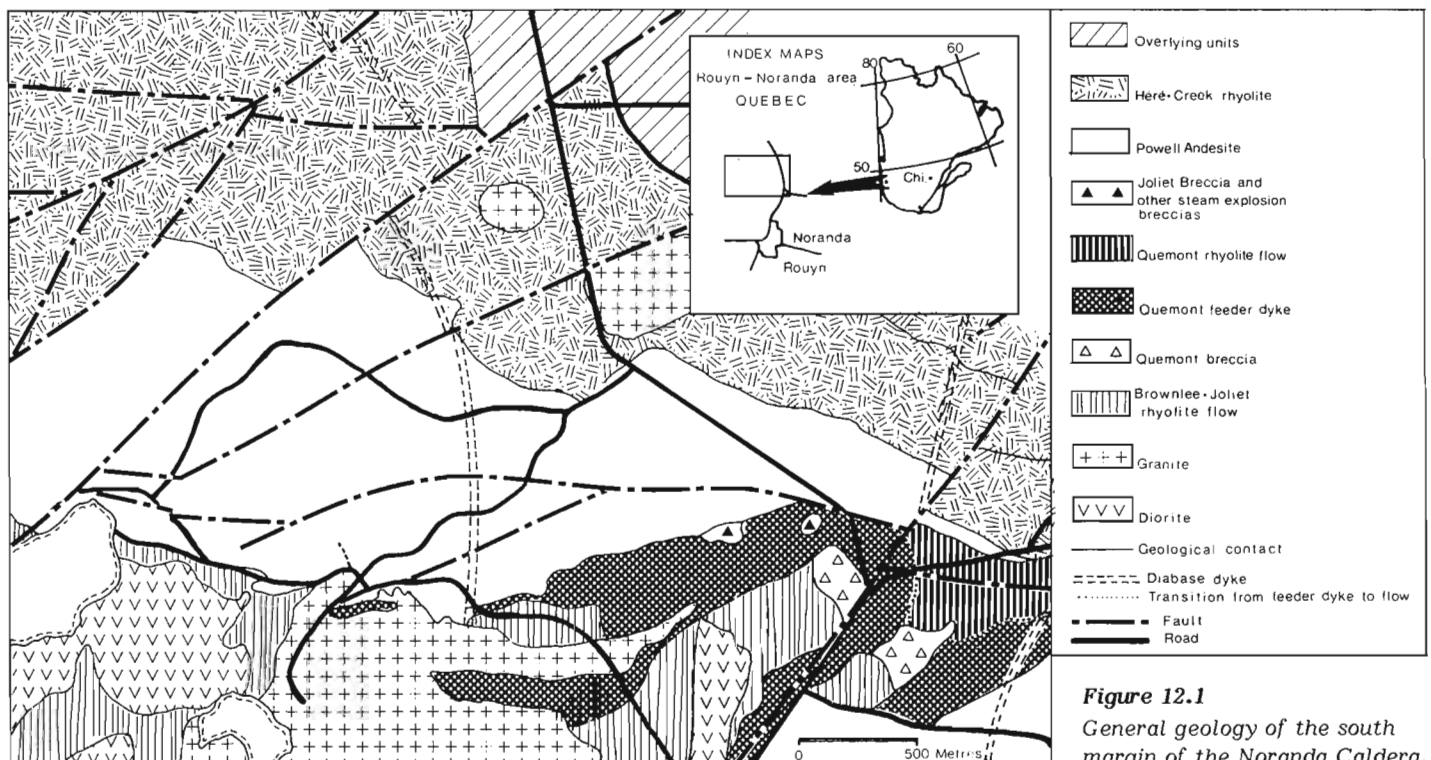


Figure 12.1
General geology of the south margin of the Noranda Caldera.

¹ Falconbridge Copper Ltd. (Lake Dufault Division), Noranda, Québec.

² Sciences de la Terre, Université du Québec à Chicoutimi, 930 est, rue Jacques-Cartier Chicoutimi, Québec G7H 2B1

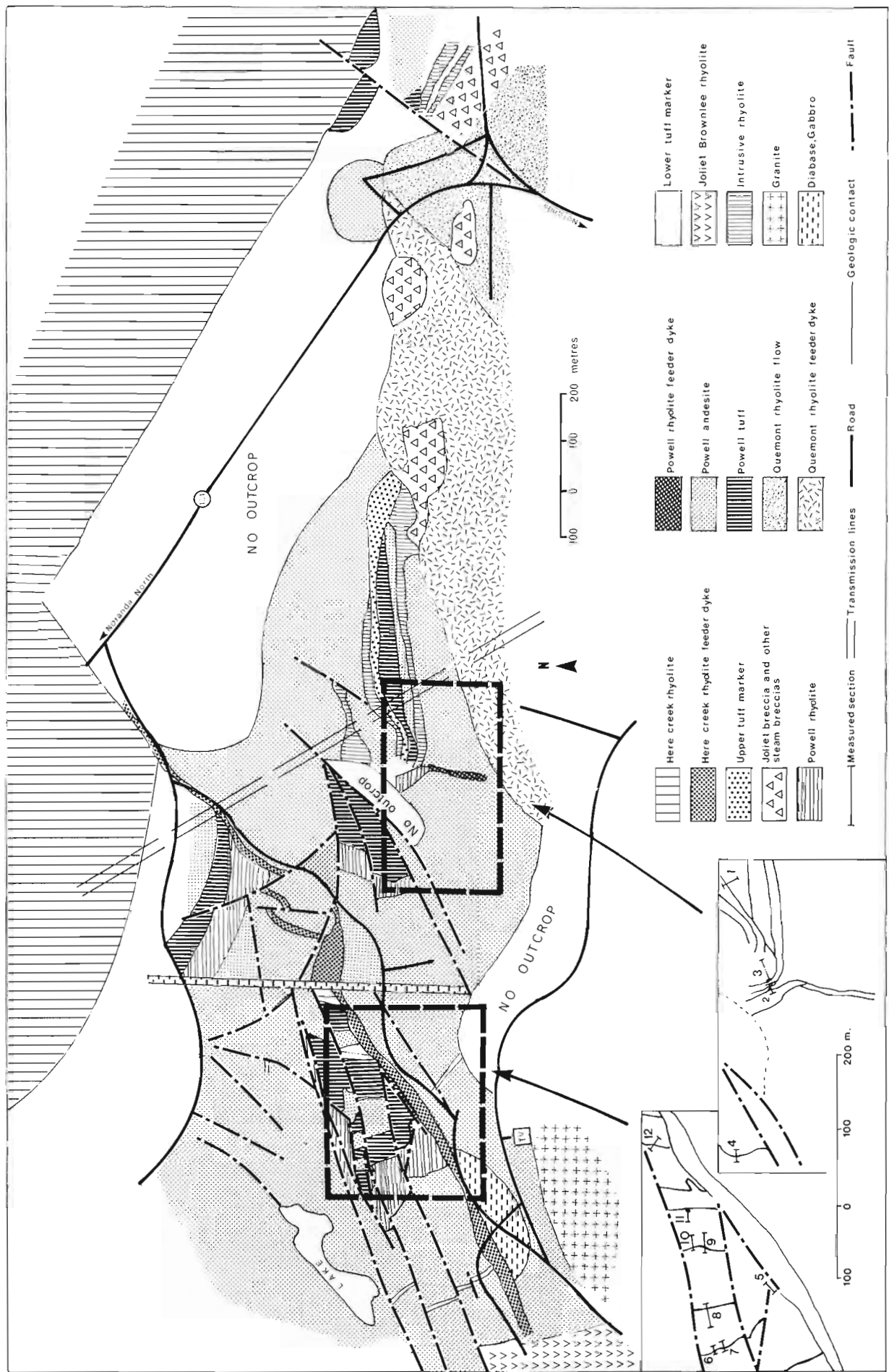


Figure 12.2 Map of the Powell andesite at the south margin of Noranda Caldera.

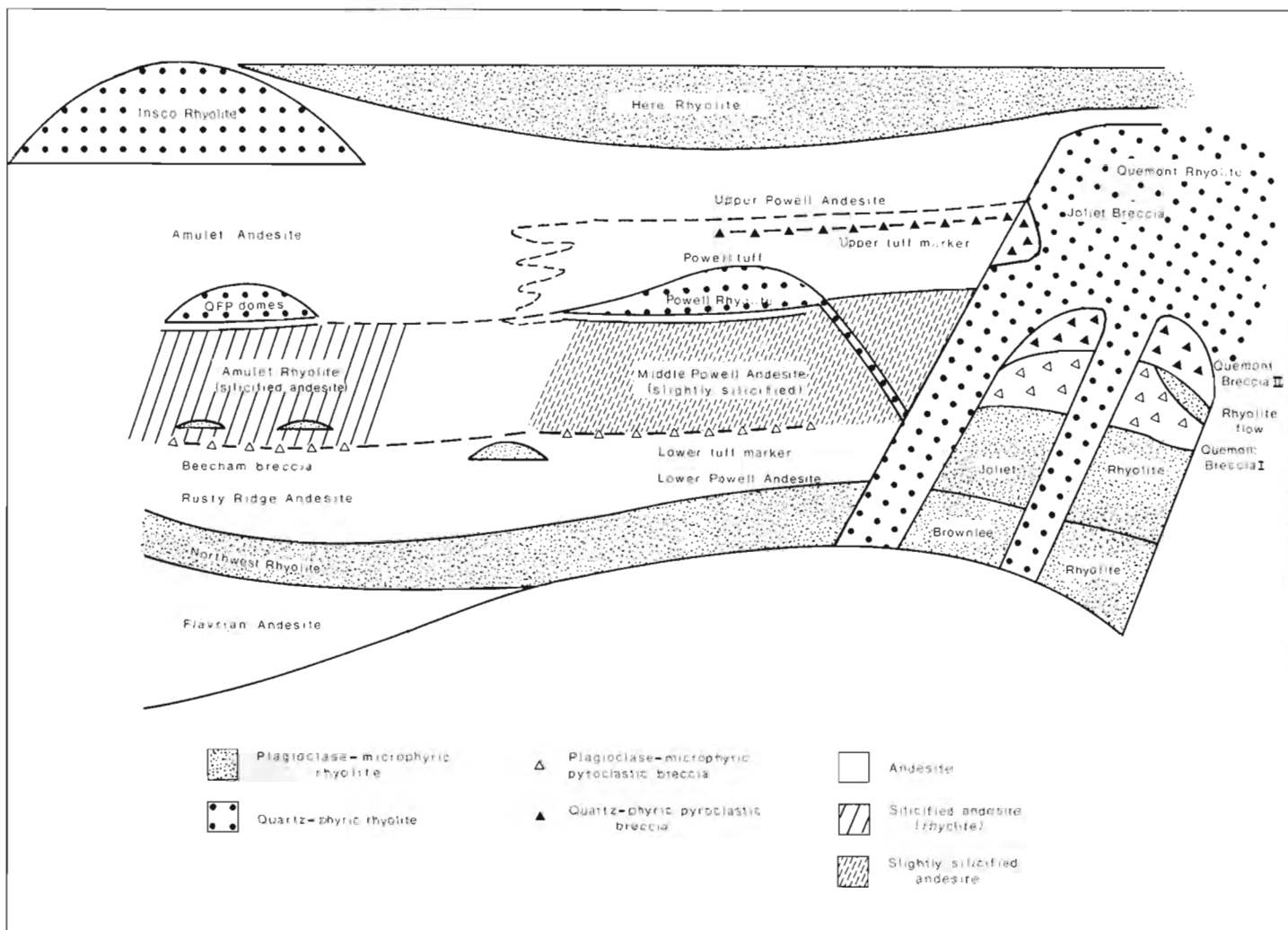


Figure 12.3 Stratigraphic correlation across the south margin of Noranda Caldera.

The area consists of four fault blocks (Fig. 12.2) sliced by numerous secondary faults. Most faults trend to the northeast. The eastern fault block includes the Quemont rhyolite flow, Quemont feeder dyke, and the Joliet/Brownlee rhyolite flows east of the Noranda TV-tower. Strata strike to the east and dip steeply to the north. Blocks 2 and 3 form a northeast-trending zone northeast of the Noranda TV station. Strikes are to the west to north in block 2, and to the north in block 3; dips are steeply north or east. Strike is again to the west in the western block and dips are steeply to the north. Internal strain of rocks is fairly strong, but primary structures are well preserved. One and, locally, two cleavages are present.

Stratigraphy and Facies

The stratigraphic sequence and its lateral correlation are shown as Figure 12.3. Four marker units permit correlation across the Quemont feeder dyke: (1) the plagioclase-microphyric Brownlee rhyolite; (2) the Beecham breccia, lower tuff marker and Quemont breccia I (essential fragments: plagioclase microphyric rhyolite); (3) the upper tuff marker and Joliet breccia (essential fragments Quemont rhyolite = quartz phyric, crystals 1-3 mm, 2 crystals/cm²); (4) the plagioclase microphyric Héré rhyolite.

The Powell rhyolite (quartz-phyric, phenocrysts 2-4 mm, 4 phenocrysts/cm²) provides a local marker in the south of the caldera; it probably correlates with quartz-porphry domes to the north. The Amulet "rhyolite" (in fact a silicified andesite, Gibson and Watkinson, 1979) probably correlates with the slightly silicified middle Powell andesite. Powell tuff is thickest in fault blocks 2 and 3 and interfingers with andesite flows. Its essential fraction is Powell rhyolite, except for the upper tuff marker (Quemont rhyolite) and a few metres of tuff below the Héré rhyolite (essential fragments: Héré rhyolite plagioclase-microporphyritic rhyolite).

The Quemont breccia I (Fig. 12.4) consists of two upward-coarsening-then fining cycles separated by a thin flow of plagioclase-microporphyritic rhyolite; it forms a wedge-shaped deposit centred at the Quemont feeder dyke. The Joliet breccia (Fig. 12.5) occupies a pit crater in the north of the Quemont feeder dyke. Brecciated rhyolite at the base and in the east of the crater formed in situ. It grades upward first in monomict rhyolite breccia, then in oligomict breccia composed of fragments of Quemont rhyolite and Powell andesite.

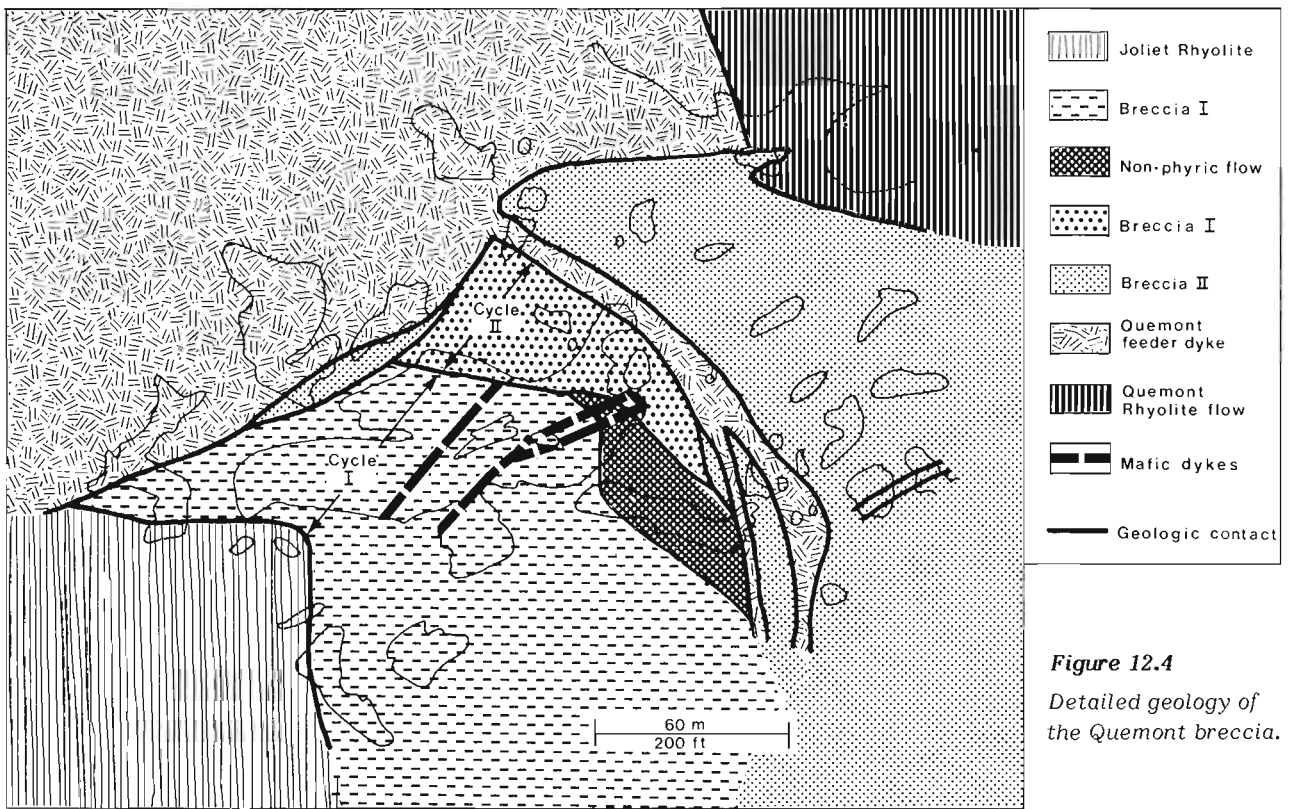


Figure 12.4
Detailed geology of the Quemont breccia.

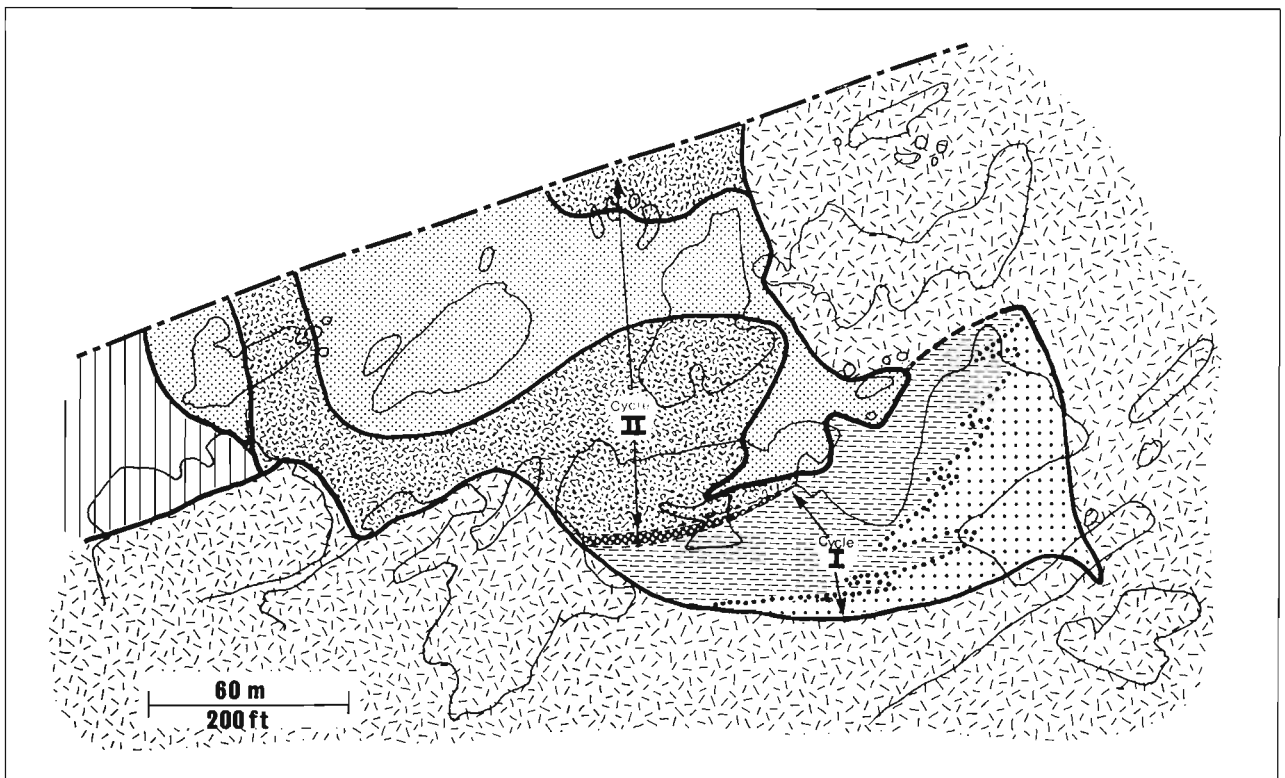


Figure 12.5 Detailed geology of the Joliet breccia.

Facies Transitions

The facies of pyroclastic rocks is described in Table 12.1; sections typical of facies 4-7 are shown in Figures 12.6-12.9. Lag deposits (facies 1, Quemont breccia I) and crater fillings (facies 2, Joliet Breccia) grade first into debris flows (facies 3), then into turbidites (facies 4) away from the caldera margin. The transition of debris flows to turbidites takes place over less than 30 m in the upper tuff marker. Turbidites grade from reversed-to-normal graded beds to normal graded beds to upward-fining beds with parallel lamination away from the caldera margin.

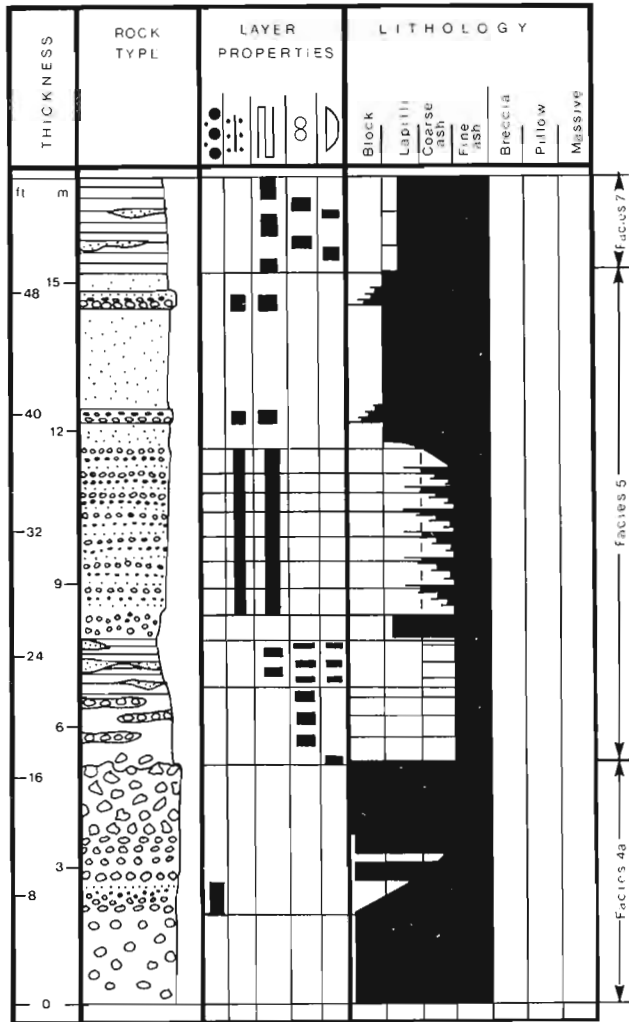
Largest grain size of the debris flow facies of the upper tuff marker coarsens from 50 cm to 200 cm away from the caldera margin. Thus, the large blocks in this debris flow were transported in an inertial regime, as in avalanches. Coarsening away from the source also has been observed in the reversed-to-normally graded facies of the lower tuff marker. Otherwise, turbidites (facies 4) coarsen toward the source.

Trough crossbeds in facies 6 consistently indicate transport away from the caldera margin. Sedimentation patterns exclude transport by tidal currents or in a fluvial environment. Thus, we suggest that transport took place by offshore rip currents induced by waves.

Synvolcanic Faults, Breccia Dykes, Hydrothermal Alteration

Many of the faults are filled by feeder dykes or are the site of abrupt changes of thickness of the Powell tuff; these faults clearly are synvolcanic. Fault block 3 is a narrow, synvolcanic graben. Breccia dykes are common, particularly at the base of the sequence; some breccia dykes cut the Héré rhyolite feeder dyke and, thus, were formed relatively late.

"Spotted alteration" and "network silicification" are common alteration effects. Spots, 5-15 mm across, composed of sericite and quartz form halos around fractures and fragment boundaries. The spots probably are derived from alkali feldspar-quartz spherulites that formed by hydrothermal devitrification. "Network silicification and albitization" (see de Rosen-Spence et al., in press) proceeded from cracks and fractures; the end product of silicification and albitization of andesite is a rock which, commonly, has been named "rhyolite" (for example the Amulet rhyolite); of course, network silicification and albitization also affected rhyolites.



- | | | | |
|--|---|--|--|
| | graded bedding | | ripples < 10 cm wavelength |
| | upward coarsening or upward fining sequence | | isolated blocks or lapilli with sediment draping, impact structure |
| | parallel lamination | | convolute bedding |
| | scour filled with trough cross beds | | pull-apart |
| | scour | | pseudo nodules and sand balls |
| | long-lenticular bedding | | |

Figure 12.6 Measured stratigraphic section across parts of Powell tuff (section 6 of Fig. 12.2).

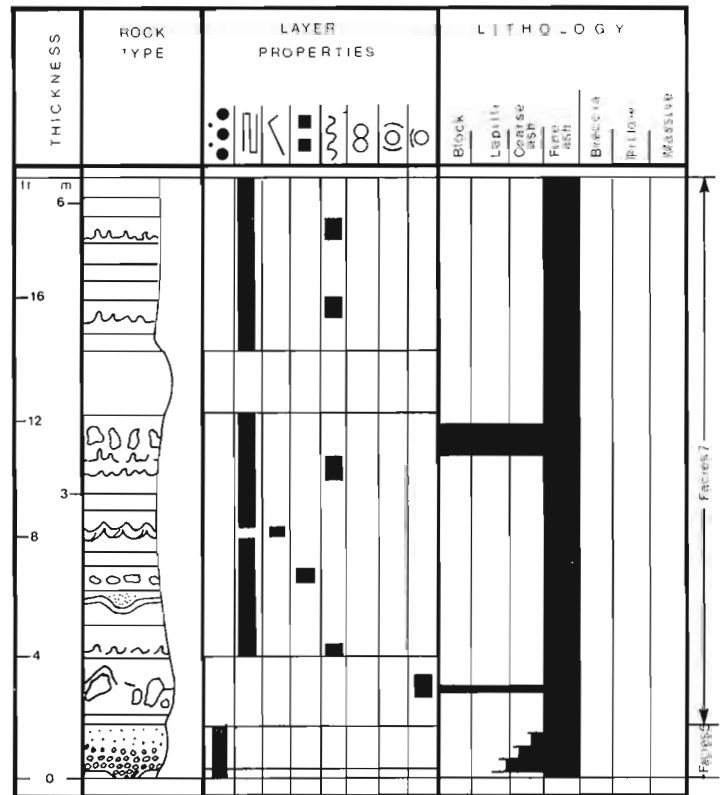


Figure 12.7 Measured stratigraphic section across parts of Powell tuff (section 7 of Fig. 12.2).

Table 12.1
Facies of pyroclastic rocks

Facies 1: Wedge-shaped deposits 50-100 m thick at feeding vent, thinning to beds less than 5 m thick over 300 m-500 m. Directly associated to feeding vent. Very poorly sorted lapilli and block tuff. Large-scale (50 m) upward coarsening and upward fining sequences. Orientation of elongated blocks and lapilli. Some parallel laminae at top of upward fining sequence are only sedimentary structure.

Polymict lithic debris, angular, poorly vesiculated. No pumice. Example: Quemont breccia I.

Interpretation: pyroclastic flow lag deposits dumped at the site of eruption, produced by phreatic explosion at a vent.

Facies 2: Filling of excavation pits in Quemont feeder dyke. Three subfacies as follows. Subfacies 2a: Monomict in situ breccia of same composition as feeder dyke. Absence of sedimentary structures. Fractures cemented by quartz and chlorite. Fills dykes and forms transition at bottom and at wall of the excavation pit. Subfacies 2b: Monomict parautochthonous block breccia. All fragments derived from Quemont feeder dyke. Blocks angular. Absence of sedimentary structures except orientation of blocks. Absence of ash matrix. Pore space filled by quartz and chlorite. Overlies subfacies 2a. Subfacies 2c: Oligomict allochthonous block breccia. Fragments of Quemont feeder dyke and overlying Powell andesite. Blocks angular, re-entrant angles common. Absence of sedimentary structures except for orientation of elongated blocks. Overlies subfacies 2b.

Interpretation: Subfacies 2a: brecciated dyke rock, more or less in situ. Subfacies 2b: brecciated dyke rock, jumbled by rising steam. Subfacies 2c: brecciated dyke and overlying rock, thrown out by steam explosion and fallen back. Example: Joliet breccia and other steam explosion breccias at Quemont feeder dyke.

Facies 3: Tabular beds, 5-30 m thick, traceable for 300 m. Large blocks (up to 2 m), angular, set in fine lapilli and coarse ash. Very poor sorting. Absence of sedimentary structures. Subfacies 3a: composition as facies 2c. Example: upper tuff marker; Subfacies 3b: composition as facies 4b. Example: rhyolite breccias at top of Powell rhyolite flow.

Interpretation: Pyroclastic debris flows originating by the steam explosion (subfacies 3a) or by collapse of a rhyolite dome (subfacies 3b).

Facies 4: Tabular beds, 0.4 to 5 m thick; lower tuff marker traceable for up to 1500 m. Small blocks and coarse lapilli set in coarse ash or fine lapilli. Very poor sorting. Reversed-to-normal graded bedding or normal graded bedding. Top of bed may be lapilli or ash with parallel laminations. Some large rip-up clasts of underlying flow may be present. Pumice absent.

Interpretation: Pyroclastic flows deposited by turbidity currents. Several subfacies are defined by composition as follows.

Subfacies 4a: Composition as facies 1 – pyroclastic flows correlating with facies 1 lag deposits.

Subfacies 4b: Monomict coarsely quartz-plagioclase-phyric rhyolite - pyroclastic flows produced by collapse of a rhyolite dome or of rhyolite spines. Subfacies 4c: Polymict tuff breccias - pyroclastic flows produced by phreatic explosion.

Facies 5: Polymict lapilli and coarse ash tuff. Thin bedded. Parallel and long-lenticular stratification, strata one lapilli diameter thick. Large isolated lapilli and blocks, commonly in nests with impact structures and erosion scours in lee. Here and there upward coarsening sequences 30-50 cm thick. Closely associated with facies 7.

Interpretation: Air fall, settled through water, little transport by marine currents. Large isolated lapilli or blocks and block nests are air-fall bombs, settled through water.

Facies 6: Polymict lapilli and coarse ash tuff. Thin bedded. Parallel stratification, generally one lapilli thickness thick, numerous erosion scours, trough crossbeds in sets 10-30 cm high, occasionally with bottomset, foreset and topset preserved. Occasionally very fine grained ash filling bottom of erosion scours and trough of crossbeds. Large isolated lapilli or blocks, not uncommonly in nests. Closely associated with facies 7. Trough crossbeds indicate offshore movement.

Interpretation: Air-fall, settled through water, and redeposited by marine offshore currents. Current directions suggest transport by shallow marine rip currents induced by waves. Isolated block and block nests are fall-back.

Facies 7: Ash tuff. Thin bedded. Parallel stratification on a millimetre-centimetre scale, rare graded beds 5 cm thick (not Bouma cycled). Current ripples. Strong syndimentary deformation: load casts, pinch and swell, sand pockets, convolute lamination, convoluted currents ripples. Isolated large lapilli and blocks, not uncommonly in nests.

Interpretation: Air-fall, settled through water, redeposited by shallow marine currents. Isolated lapilli and blocks and nests of lapilli and blocks are air-fall blocks.

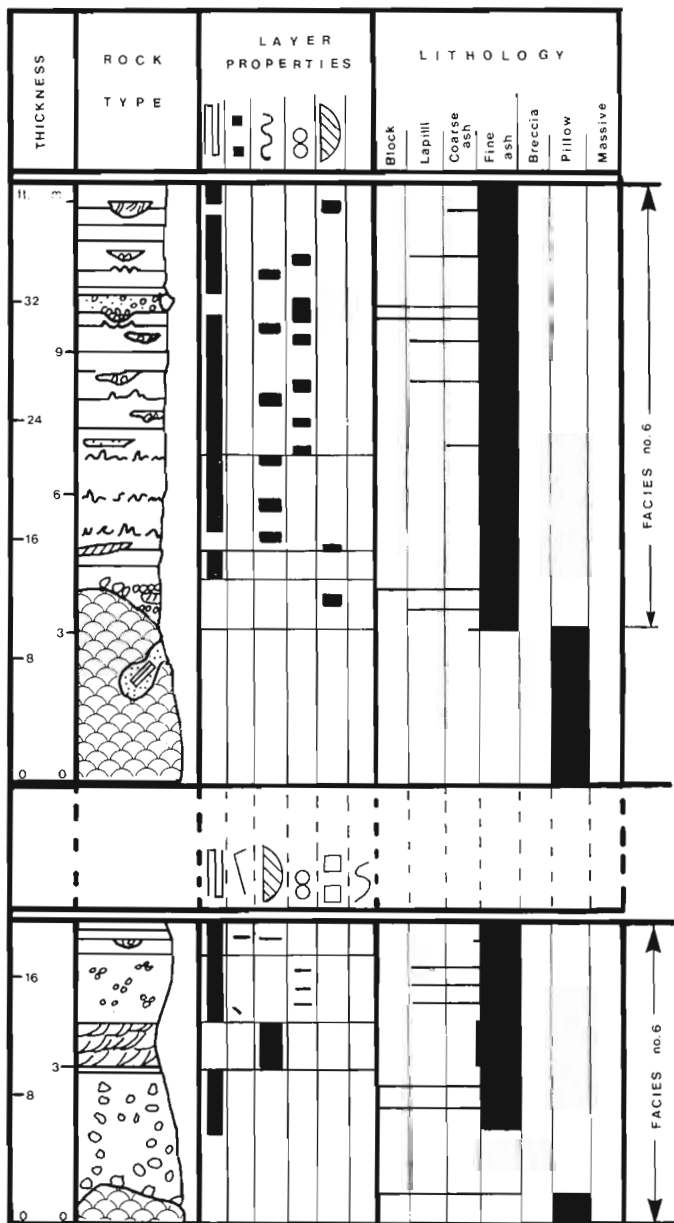


Figure 12.8 Measured stratigraphic section across parts of Powell tuff (sections 9 and 10 of Fig. 12.2).

History of Caldera Collapse

Caldera collapse began after the emplacement of the Northwest and Brownlee rhyolite flows. Mafic flows (lower Powell and Rusty Ridge andesites) built shield volcanos within the caldera, whereas the southern caldera margin was quiescent. Activity at the caldera margin resumed with extrusion of the Joliet rhyolite and its phreatic explosion (Quemont breccia I, lower tuff marker). Absence of pyroclastic falls and the very small volume of pyroclastic rocks at this level suggest that the caldera margin was in relatively deep (~200 m) water. Mafic shield volcanos (Amulet "rhyolite", middle Powell andesite) then filled the caldera.

A second period of pyroclastic activity (Quemont breccia II), intrusion of the Quemont feeder dyke and extrusion of the Quemont flow initiated renewed caldera

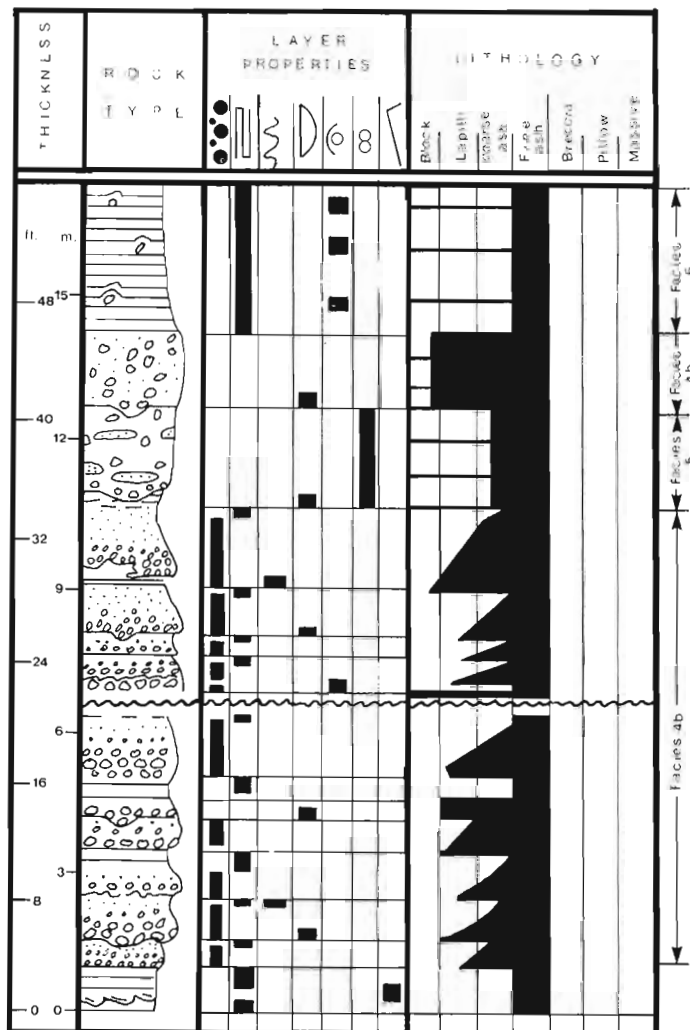


Figure 12.9 Measured stratigraphic sections across parts of Powell tuff (section 11 of Fig. 12.2).

collapse. The Powell rhyolite and quartz porphyry domes extruded within the caldera, giving rise to continuing phreatic explosions (main part of Powell tuff). Abundance of air fall tuffs suggests that the southern caldera margin was either above water level or in very shallow water (~10 m). Emplacement of mafic shields (Amulet and upper Powell andesites) continued.

Caldera collapse was completed at the time of eruption of the lowermost Héré rhyolite flow. Eruption of this flow was preceded by minor phreatic explosions. The flow is ponded in the southern part of the caldera but is not faulted at the caldera margin.

Acknowledgments

We are deeply indebted to D. Comba of Falconbridge Copper Ltd. (Lake Dufault Division) who pointed out this interesting subject of research and participated in many discussions. Victor Owen studied the petrography of the Quemont breccia I and the Joliet breccia, and Marc Tremblay did the drawings. This work has been supported by successive grants by NSERC and by successive EMR research agreements.

References

- Dimroth, E. and Rocheleau, M.
1979: Volcanology and sedimentology of Rouyn-Noranda area; Geological Association of Canada/Mineralogical Association of Canada, Quebec 1979 field trip A1, Québec, Université Laval.
- Gélinas L., Brooks C., Perreault G., Carignan J., Trudel P., and Grasso F.
1977: Chrono-stratigraphic divisions within the Abitibi volcanic belt, Rouyn-Noranda, district, Québec; in, Volcanic Regimes in Canada, Baragar, W.R.A., Coleman, L.C. and Hall, J.M., ed. Geological Association of Canada, Special Paper 16, p. 297-310.
- Gibson H.L. and Watkinson D.H.
1979: Silicification in a detailed section of the Amulet rhyolite, Noranda, P.Q.; in Abstracts with Programs, Geological Association of Canada, v. 4, p. 53.
- Rosen-Spence A.F. (de)
1976: Stratigraphy, development and petrogenesis of the central Noranda volcanic pile, Noranda, Québec; Unpublished Ph.D. thesis, University of Toronto.
- Rosen-Spence A.F. (de), Provost G., and Dimroth E.
Archean subaqueous rhyolite flows at Noranda, Quebec; Precambrian Research. (in press)

**URANIUM CONCENTRATIONS AND THE SYSTEM RESPONSE FUNCTION
IN GAMMA RAY LOGGING**

Project 740085

John G. Conaway
Resource Geophysics and Geochemistry Division

Conaway, John G., Uranium concentrations and the system response function in gamma ray logging; in Current Research, Part A, Geological Survey of Canada, Paper 80-A, p. 77-87, 1980.

Abstract

A change in certain formation parameters (density, per cent water in pore spaces, concentration of heavy elements such as uranium) with depth along a borehole can result in errors in grade-thickness product computed on the basis of gamma ray logs. Because large changes in uranium concentration and commonly density are associated with high grade uranium ore zones, grade-thickness calculations for such zones may be grossly in error. Such errors vary nonlinearly with grade and thickness of the ore zone, and therefore are not amenable to simple correction factors. Use of properly designed logging equipment which discriminates against low energy gamma rays (below about 1 MeV in high grade situations) should largely avoid these errors.

Introduction

The theoretical basis for quantitative interpretation of gamma ray logs is expressed by the equation

$$\bar{G}T = KA \quad (1)$$

first given by Scott et al. (1961). Here T is the thickness of a radioactive zone having average grade (radioelement concentration) \bar{G} , A is the area beneath the corresponding gamma ray log curve, and K is the constant of proportionality ('K-factor'). Ideally, if the gamma ray log is deconvolved (e.g. Scott, 1963; Conaway and Killeen, 1978) the amplitude of the processed log becomes directly proportional to grade or

$$G = KY \quad (2)$$

where Y is the amplitude of the deconvolved log at a given depth, G is the grade at that depth, and K is the same constant as in equation (1). Equations (1) and (2) assume that all gamma rays detected are from the radioelement decay series of interest, and also that the decay series is in radioactive equilibrium or that suitable equilibrium corrections are applied.

In their comprehensive review of borehole logging techniques for uranium, Dodd and Eschliman (1972) demonstrated that for conventional total count logging equipment equations (1) and (2) are valid only when uranium concentrations are less than about one per cent. Figure 13.1, reproduced from that paper, shows computed uranium concentration (determined from gamma ray logs in model boreholes) as a function of actual concentration, for several different probes. The breakdown of equations (1) and (2) at grades above roughly 1 per cent U_3O_8 , indicated by the nonlinearity of curves 1-6 in that region, is attributed by Dodd and Eschliman to the increased attenuation of gamma rays due to the presence of the heavy uranium atoms. This phenomenon is referred to as the 'Z-effect', where Z is the symbol for atomic number.

It is clear from Figure 13.1 that the nonlinear error in computed grade based on equations (1) and (2) can become a serious problem in the evaluation of high grade deposits. Dodd and Eschliman (1972) mentioned two approaches to solving this problem. One approach is to design the logging equipment so that it discriminates against the low energy gamma rays which are largely responsible for the Z-effect (as will be discussed later); curve 7 in Figure 13.1 demonstrates the apparent validity of this technique for grades up to about 3 per cent U_3O_8 . A second approach is to apply corrections to field logs, based on measurements in model boreholes similar to Figure 13.1.

The purpose of this paper is to examine further the ramifications of the Z-effect and related problems. It will be shown, for instance, that the error in computed grade caused by the Z-effect is not only nonlinear with grade as shown in Figure 13.1, but also with thickness of the radioactive zone.

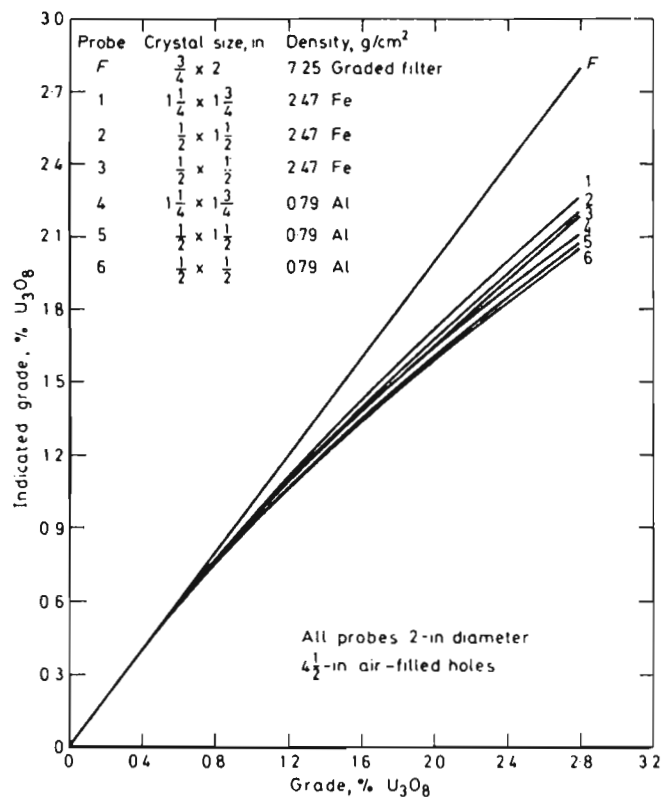


Figure 13.1. Graph showing the nonlinear relationship between computed grade and true grade for typical uranium logging probes (curves 1-6). The increasing error with increasing grade is due to the attenuation of gamma rays by the heavy uranium atoms (the 'Z-effect'). Curve F shows the improvement in linearity obtained by using a graded filter to discriminate against low energy gamma rays, which are primarily responsible for this problem. (From Dodd and Eschliman, 1972).

Thus, of the two techniques suggested by Dodd and Eschliman to correct for the Z-effect, only the technique of discriminating against low energy gamma rays will produce essentially the desired result. It will be shown here also that a nonlinear error similar to that caused by the Z-effect can result from other physical property contrasts (density or free water in the formation) between the ore zone and the barren zone, even for low grades. This paper illustrates in relatively simple terms what causes these problems, and how they can best be avoided.

Errors Resulting from Variation of the System Response Function

In earlier work by Suppe and Khaykovich (1960), Davydov (1970), Czubeck (1971), and Conaway and Killeen (1978), it has been assumed for the sake of mathematical simplicity that the response $\phi(z)$ of a point detector to a thin planar radioactive zone (the geologic impulse response or GIR) could be approximated in a homogeneous medium by

$$\phi(z) = \frac{\alpha}{2} e^{-\alpha|z|} \quad (3)$$

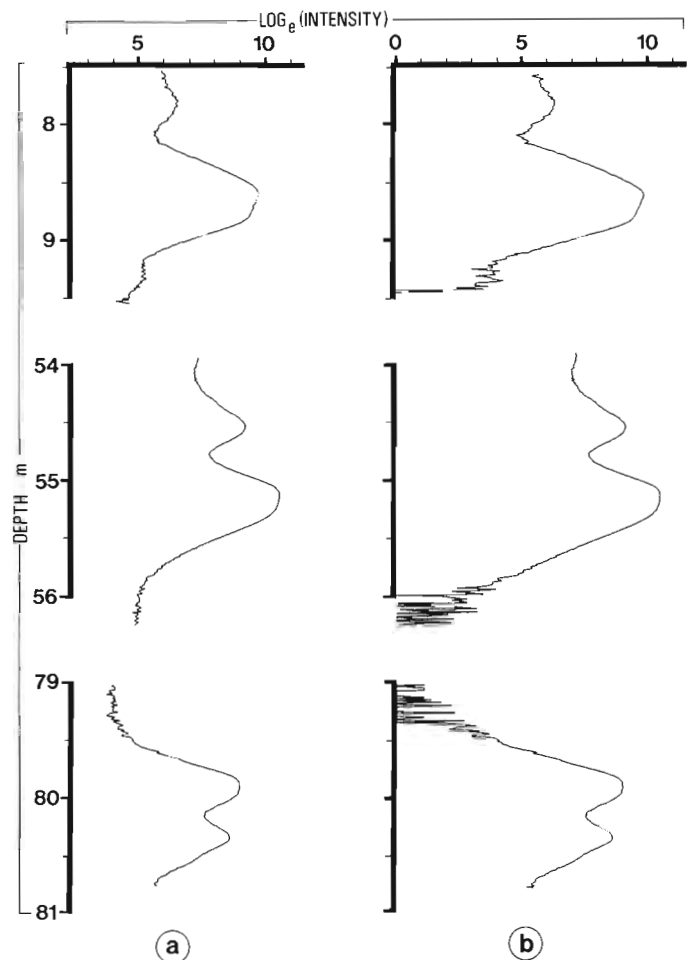
where z is the distance along the borehole from the radioactive zone and α is a constant which determines the shape of the GIR. Based on the above approximation the following 3-coefficient exact inverse filter has been developed

$$\left[\frac{e^{-\alpha\Delta z}}{(1-e^{-\alpha\Delta z})^2}, \frac{1+e^{-2\alpha\Delta z}}{(1-e^{-\alpha\Delta z})^2}, -\frac{e^{-\alpha\Delta z}}{(1-e^{-\alpha\Delta z})^2} \right] \quad (4)$$

where Δz is the sampling interval along the borehole (Conaway, in press (a)).

Four possible methods of determining the constant α have been suggested in the literature.

1. Davydov (1970) determined the value of α by a least-squares fit of the experimentally determined system response function to the double sided exponential [equation (3)]. This technique can introduce distortion into the processed log because the effect of the detector length is not taken into account (e.g. Conaway and Killeen, 1978).
2. Czubeck (1971) has suggested that the value of α might be obtained from the amplitude of the experimentally determined system response function (normalized to have unit area) at the centre of the thin zone. From equation (3) it can be seen that the height of the double sided exponential at $z = 0$ is $\alpha/2$. Thus, by Czubeck's method, α is approximated as being equal to twice the height of the normalized experimentally determined system response function at $z = 0$.
3. Conaway and Killeen (1978) suggested that α be determined from families of type curves generated for various values of α and detector length L . The type curves are overlaid on the experimentally determined system response function; the best fitting type curve for the appropriate value of L gives the desired value of α .
4. Conaway (in press (a)) gives a method for determining the value of α in model boreholes or, under favourable conditions, directly from field boreholes. For this it is necessary that there be a radioactive zone adjacent to a less radioactive zone (referred to here as the "ore" zone and the "barren" zone, respectively). The barren zone must be essentially homogeneous and at least about 1.5 m thick. The average radioactive intensity in the barren zone well away from the ore zone is subtracted from each



- (a) Plot of 3 radioactive zones from a field borehole showing the natural logarithm of the total count channel as a function of depth.
- (b) Same as in (a), but with the average gamma ray intensity in the barren zone well away from the ore zone subtracted from each value on the log before taking the natural logarithm.

Figure 13.2

datum value in the digital gamma ray log. The natural logarithm of the resulting corrected intensities are plotted against depth (Fig. 13.2), and the slope of the linear flank of the anomaly outside of the ore zone is equal to α regardless of the thickness of the ore zone or the radioelement distribution within it. The value of α given by this method will generally be close to the value given by the type curve technique described in (3) above.

For convenience it will be assumed in this section that equation (3) is a good approximation of the true GIR; this will be discussed further in the next section. The GIR shape constant α depends on the angle of dip of the radioactive strata relative to the borehole, borehole diameter, borehole fluid, casing type and thickness, and linear attenuation coefficients of the material through which the borehole passes. This last factor depends on fluid content of the pore spaces in the rock, rock density, effective atomic number and atomic weight of the rock, and gamma ray energy. Variations of α by up to nearly a factor of 2 have been noted in some holes (Conaway, in press (b)).

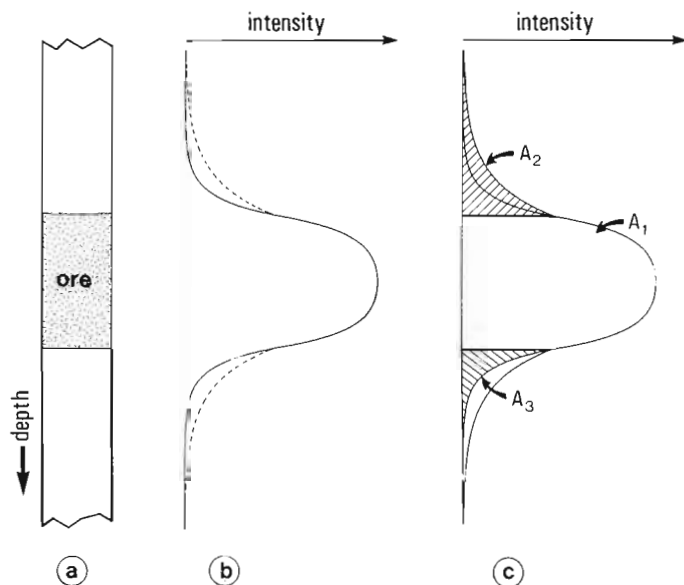
There are several types of errors which can rise from a change in formation or borehole parameters. These errors result from a change in the system response function (i.e. a change in α), a change in the system calibration factor or K-factor, or a combination of these. Several different cases may be considered:

1. If the system calibration factor is constant for a given borehole, use of an incorrect value of K in equations (1-2) clearly causes a linearly proportional error in GT or G.
2. If an incorrect value of α is used in the inverse filter [equation (4)] the shape of the processed log will be distorted and equation (2) will be invalid, but equation (1) is still valid provided the system response function remains unchanged along the borehole (Conaway et al., in press).
3. If a change in α and/or K occurs somewhere in a barren zone, at least one metre or so away from the nearest radioactive zone, then compensating corrections can be applied provided that α and K are always known. Such a change could occur in passing from an uncased region into a cased region, or from below the water table into the air-filled upper portion of the hole.
4. A change in α and/or K at the edge of or inside of an ore zone will result in an error in the computed value of GT; this error varies nonlinearly with α and T. This type of error is the subject of the present paper.

In this paper we are concerned primarily with changes in α and K due to changes in the physical properties of the rock with depth along the borehole. The effects of dip have been considered elsewhere by Suppe (1957), Roesler (1965), Moore (1978), and Conaway (1979, in press (c)). The effects of borehole diameter, fluids and casing have been considered by Czubek (1961, 1962, 1969), McDonald and Palmatier (1969), Dodd and Eschliman (1972), Wilson (1979), Conaway et al. (1979), and Rhodes and Mott (1966).

If a significant change occurs in the physical properties of the rock with depth, it is likely to occur at the interface between nonradioactive and strongly radioactive lithologic units. Clearly, the addition of uranium (or any other heavy element) in significant proportion will affect the physical properties of the rock. This will be discussed in the next section of this paper, where it will be shown that α and K can change significantly at the interfaces between the ore zone and the barren zone due to the addition of uranium. In this section it will be assumed that this is true, and the problem will be examined to determine how this can cause errors in G or GT.

Consider first the case where α undergoes a step change at the ore zone boundary. Figure 13.3a shows the geologic configuration. In Figure 13.3b, the solid line shows the gamma ray anomaly curve as it might appear if conditions such as equivalent atomic number* (Z_{eq}), density, etc., were constant along the borehole. The dashed lines show the anomaly as it might appear assuming lower (Z_{eq}) and/or density outside of the ore zone. Clearly, now, computations based on equation (1), using a K-factor valid either for the barren zone (K_{barren}) or the ore zone (K_{ore}) will give an erroneous grade-thickness product, because the total measured area under the gamma ray anomaly curve is not linearly proportional to the grade-thickness product under these conditions. The resulting error depends on the thickness of the ore zone, and the degree to which conditions inside and outside the ore zone differ. Although this is a complex phenomenon, a good idea of the magnitude of errors which may be involved can be obtained empirically by application of digital signal theory. Assuming the double sided exponential geologic impulse response function given in equation (3) to be reasonable, a change in Z_{eq} or density may be accompanied



- (a) Homogeneous ore zone of uniform grade G and thickness T between thick barren zones.
- (b) Solid line shows the shape of the gamma ray anomaly resulting from the radioactive zone shown in (a), assuming α is constant along the borehole. If α in the barren zone is smaller than α in the ore zone, the anomaly outside the ore zone would be represented by the dashed lines.
- (c) Area A_1 (no cross-hatching) is the area beneath the gamma ray log curve inside the ore zone. Area A_2 (large cross-hatched area) is the log area outside the ore zone (on one side of the anomaly) assuming α in the barren zone to be different from α in the ore zone. Area A_3 (small cross-hatched area) is the area outside the ore zone (on one side of the anomaly) assuming α is constant in the ore zone and the barren zone.

Figure 13.3

by a change in the constant α , giving the situation shown in Figure 13.3. Using the notation shown in Figure 13.3c we may develop the following expressions for true grade, computed grade, and ratio of computed grade to true grade.

$$G_{true} = \frac{K_{ore} (2A_3 + A_1)}{T} \quad (5)$$

$$G_{computed} = \frac{K_{barren} (2A_2 + A_1)}{T} \quad (6)$$

$$\frac{G_{computed}}{G_{true}} = \frac{K_{barren} (2A_2 + A_1)}{K_{ore} (2A_3 + A_1)} \quad (7)$$

Note that because the area A_3 cannot be determined from a gamma ray log, G_{true} cannot be calculated under these conditions. Note also that if K_{ore} and K_{barren} are different, K_{ore} can only be determined in the centre of an ore zone of comparable grade, which is effectively infinitely thick. We will return to these equations later in the paper after developing some idea of how K and α are affected by changes in density or uranium concentrations.

*The equivalent atomic number, Z_{eq} , of a complex medium is defined by Czubek (1966) as the atomic number of the element having the same ratio of Compton attenuation to photoelectric attenuation (for a given photon energy) as the complex medium.

What about deconvolution under these conditions? This, too, is adversely affected by changes in α . Referring to Figure 13.4, the GIR (normalized to give constant peak amplitude) is shown for thin radioactive zones at various positions relative to a barren zone-ore zone interface; in this figure $\alpha_{\text{barren}} = 0.5 \alpha_{\text{ore}}$. Note that the shape of the system response function changes continuously across the interface. Thus, the problem of deconvolving logs under these conditions is nonlinear and is not readily amenable to solution.

In order to understand the significance of the error shown in Figure 13.3 it is necessary to determine how sensitive the system response function and K-factor are to changes in borehole and formation parameters. This subject will be discussed briefly in the next section of this paper.

Dependence of the System Response Function on Formation Parameters

It was shown above that a change in the shape of the system response function at or near the ore zone boundaries would result in an error in the computed grade-thickness product. The system response function depends on borehole diameter, borehole fluid content, casing, and relative dip of the radioactive zones; these are parameters which lend themselves readily to studies in specially constructed model boreholes. Formation factors such as density and equivalent atomic number of the rock, which are of primary interest in this paper, would be difficult to study in this manner. In the absence of suitable model boreholes, or for corroboration of results from model boreholes and extension of those results over a wider range of variation of the relevant parameters, use of Monte Carlo computer simulation is a useful technique. Unfortunately, this technique imposes considerable demands in terms of computer time and core memory if any but the simplest geometry is to be considered, and a study of that type was beyond the means of this investigation. In this section the variation of α and K with changes in formation parameters will be discussed based on existing theory.

Czubek's Response Function

A number of theoretical and empirical formulations have been proposed to describe the system response function in gamma ray logging. Most of these have appeared in the eastern European and Russian literature (e.g. Suppe, 1957; Suppe and Khaykovich, 1960; Czubek, 1961; 1962; 1971; Roesler, 1965; see also Rhodes et al. 1961, and Rhodes and Mott, 1966). The theory of Czubek (1961) has been compared with Monte Carlo results using the same assumptions, in the case of a 15 cm diameter water-filled borehole, with excellent agreement (McDonald and Palmatier, 1969).

Czubek's analytical expression for the response ϕ_0 of a point detector to a thin planar zone of radioactive material located at $z = 0$ along the borehole (Czubek, 1971) may be written as follows

$$\phi_0(\mu z) = \frac{E_1 \left[\mu \sqrt{R^2 + z^2} \right]}{2\mu R \left[K_1(\mu R) - \int_0^\infty \frac{K_0(x) dx}{\mu R} \right]} \quad (8)$$

where μ is the linear attenuation coefficient, R is borehole radius, $K_0(x)$ and $K_1(x)$ are modified Bessel functions of the second kind, and $E_1(x)$ is the exponential integral of order 1 defined by

$$E_1(x) = \int_x^\infty \frac{e^{-t}}{t} dt \quad (9)$$

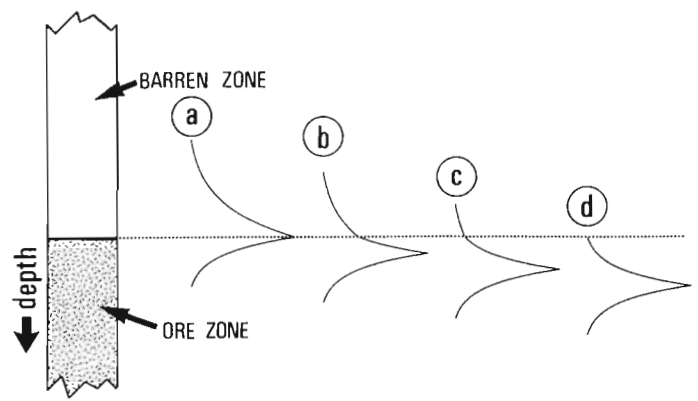


Figure 13.4. The effect on the GIR of a change of α at the ore zone-barren zone boundary. An elementary layer of ore located at the edge of the ore zone would give the asymmetrical response function shown as curve (a). A similar layer in the ore zone well away from the barren zone would give approximately the normal symmetrical double-sided exponential shown as curve (d). Intermediate positions of the thin layer would give distorted response curves of other shapes (curves b and c).

Both the exponential integral and the modified Bessel functions of the second kind are tabulated in Abramowitz and Stegun (1964). Equation (8) assumes unscattered radiation only (e.g. counts in the 1.76 MeV uranium window in the absence of thorium). This equation will be used here in a relative sense to study the effects of μ on the GIR. Rather than develop an inverse operator for his theoretical response function [equation (8)], Czubek (1971) suggested approximating this function with the double sided exponential function [equation (3)] earlier used by Suppe and Khaykovich (1960) and Davydov (1970). Czubek (1971) gave an expression for variation of α [equation (3)] with changes in borehole radius R and linear attenuation coefficient μ , based on his expression for the GIR [equation (8)]:

$$\alpha = \frac{E_1(\mu R)}{\mu R \left[K_1(\mu R) - \int_0^\infty \frac{K_0(x) dx}{\mu R} \right]} \quad (10)$$

Czubek determined his value of α based on the value of his response function (8) at $z = 0$ (i.e. at the peak of the anomaly curve), as can be seen by comparing equations (8) and (3). Equation (8) is plotted along with equation (3) (dashed and solid curves respectively), in Figure 13.5 for a range of values of μ and R, for comparison. In Figure 13.6 equation (8) is plotted along with equation (3) on semi-logarithmic axes for several of the values of μ and R shown in Figure 13.5. In general, Czubek's function behaves nearly exponentially except in the central region (i.e. in the vicinity of the thin zone). Here, the function exhibits a rounded peak due to the finite borehole diameter.

Note that the value of α given by Czubek's method based on the value of $\phi_0(z)$ at $z = 0$ in general will be different from the value of α given by the semi-logarithmic slope method described earlier, and thus the appearance of the deconvolved logs will be different (Fig. 13.7, 13.8). Figure 13.7a shows a plot of equation (8) for $R = 3$ cm and $\mu = 0.2$ cm⁻¹. For these values, equation (10) gives $\alpha = 0.204$ cm⁻¹, where as the semi-logarithmic slope method, applied to the region outside of the central distorted region, gives $\alpha = 0.27$ cm⁻¹. The inverse filter (4) has been applied to curve (a) using α values of 0.27

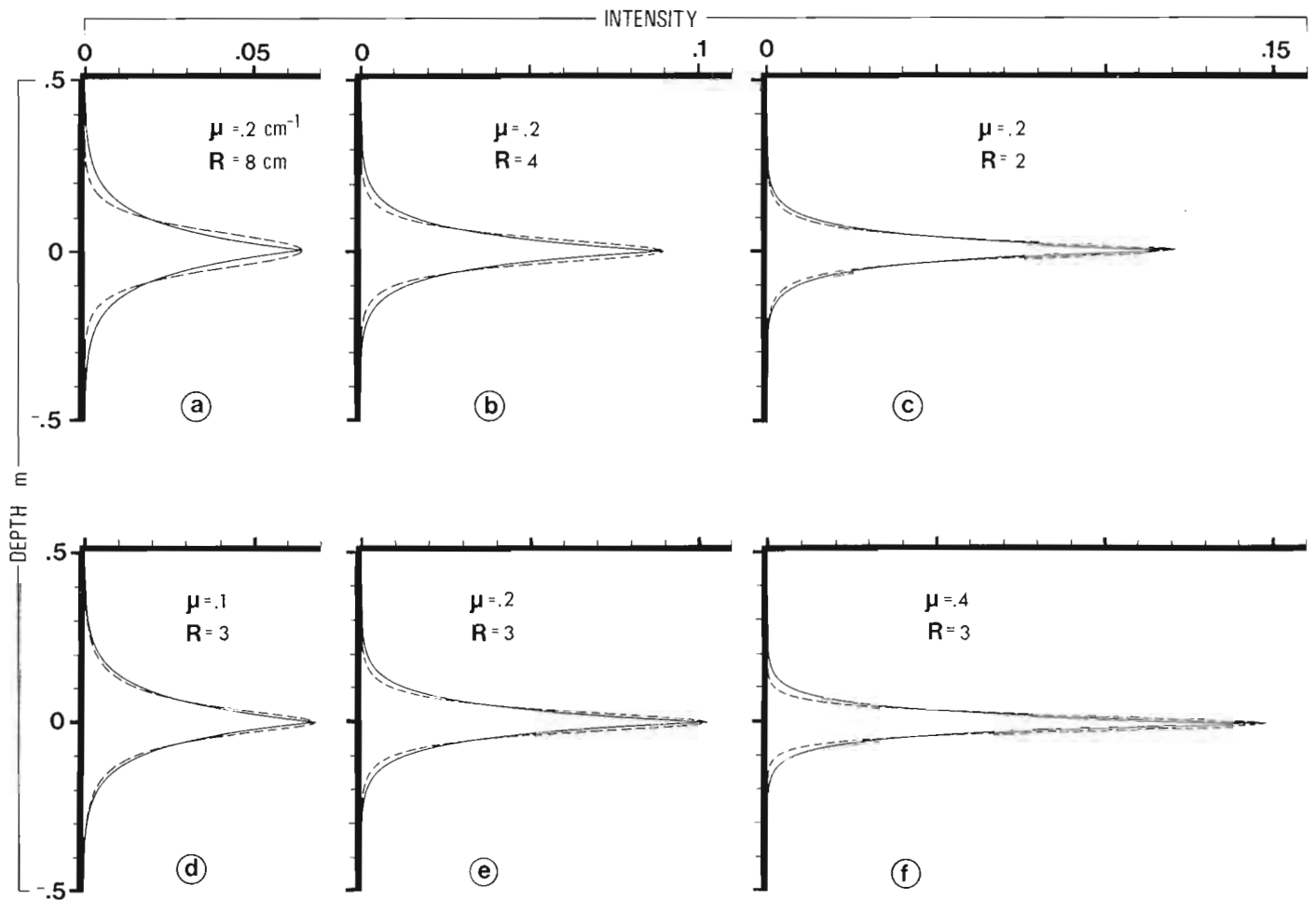


Figure 13.5. Comparison of Czubek's analytical response function [equation (8)], which includes the effect of finite borehole diameter, with the double-sided exponential GTR [equation (3)] for several values of μ and R . Czubek's response function is shown dashed.

and 0.204 cm^{-1} to produce curves (b) and (c) respectively. If curve (a) were a double sided exponential [equation (3)] with $\alpha = 0.27 \text{ cm}^{-1}$, then curve (b) would be a spike. Instead, curve (b) may be called a residual response function with some loss of spatial resolution compared to a spike, although it is a significant improvement over curve (a) and better behaved than curve (c) (i.e. no overshoot or ripple).

Figure 13.8a shows a simulated radioelement distribution. In Figure 13.8b this has been convolved digitally with Czubek's response function (shown in Fig. 13.7a) to produce the noise-free simulated gamma ray log with $\Delta z = 0.5 \text{ cm}$. Deconvolving curve (b) with the inverse filter with $\alpha = 0.204 \text{ cm}^{-1}$ produces curve (c), which ideally should be identical to curve (a). In fact, curve (c) exhibits considerable distortion; peak amplitudes are exaggerated, and there is significant overshoot. Deconvolving curve (b) using $\alpha = 0.27 \text{ cm}^{-1}$ gives curve (d). This curve is a good approximation of the radioelement distribution (curve a) with a slight loss of spatial resolution, and is a clear improvement over curves (b) and (c). Based on this evidence it is recommended that α be determined from the semi-logarithmic slope of the response function rather than by normalization. The lesson learned from these examples also applies to the determination of α from experimentally determined response functions. The semi-logarithmic slope method gives a value of α which will produce the best-behaved deconvolved logs, as shown in Figure 13.8.

The Linear Attenuation Coefficient

In borehole logging we are concerned largely with two types of interactions between gamma radiation and matter: Compton scatter, and the photoelectric effect. A third interaction, pair production, only occurs with gamma rays having energies higher than 1.022 MeV, and even then not in significant proportion except for large values of Z_{eq} of the medium surrounding the borehole. The proportion in which these three interactions occur depends on gamma ray energy and Z_{eq} (Fig. 13.9).

Given the linear attenuation coefficient due to Compton scatter in element 1, $[\mu_c]_1$, the attenuation due to that same mechanism in element 2 is given by

$$[\mu_c]_2 = [\mu_c]_1 \frac{\rho_2 A_1 Z_2}{\rho_1 A_2 Z_1} \quad (11)$$

where ρ is density, A is atomic weight, and Z is atomic number (see e.g. Evans, 1955). Similarly for photoelectric interactions

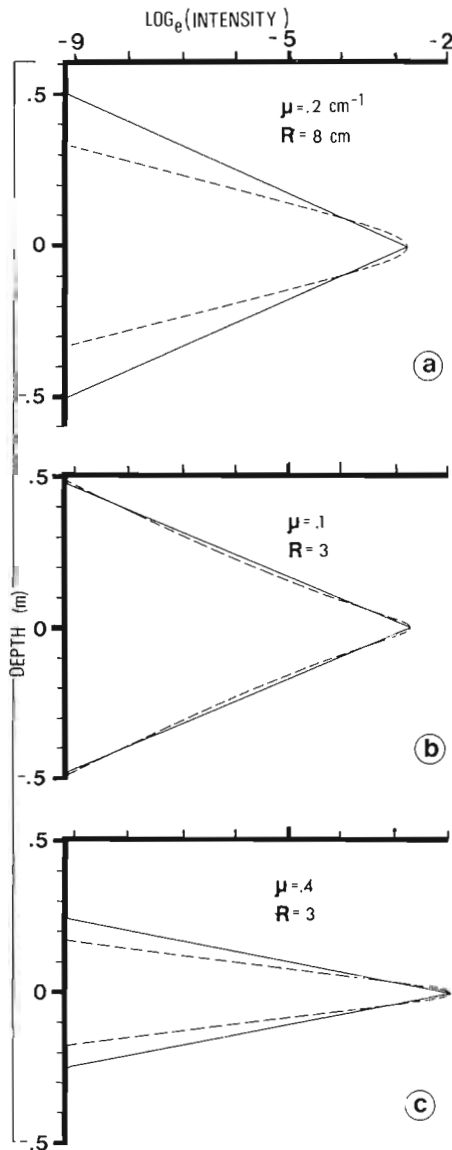
$$[\mu_{pe}]_2 = [\mu_{pe}]_1 \frac{\rho_2 A_1}{\rho_1 A_2} \left[\frac{Z_2}{Z_1} \right]^m \quad (12)$$

where m is approximately 4 for 0.1 MeV photons, rising to about 4.6 for 3 MeV photons (Evans, 1955). For interactions of the pair production type, the conversion is

$$\left[\mu_{pp} \right]_2 = \left[\mu_{pp} \right]_1 \frac{\rho_2 A_1}{\rho_1 A_2} \left[\frac{Z_2}{Z_1} \right]^2 \quad (13)$$

The approximate relationship between A and Z for the elements is given in Figure 13.10. Given the values of the linear attenuation coefficient for each of these mechanisms, the total or composite coefficient μ is given by

$$\mu = \mu_c + \mu_{pe} + \mu_{pp} \quad (14)$$



(a) corresponds with Figure 13.5a.
 (b) corresponds with Figure 13.5d.
 (c) corresponds with Figure 13.5f.

Figure 13.6. Semi-logarithmic plot of Czubek's analytical response function [equation (8)] and the double-sided exponential GIR [equation (3)]. Czubek's function is shown dashed.

From the above relationships (11-14) it can be seen that, although μ_c varies linearly with the equivalent atomic number of the medium Z_{eq} (and that variation is largely compensated by the nearly constant A/Z ratio seen in Fig. 13.10), μ_{pe} is highly sensitive to variations in Z_{eq} . Adding uranium (or other heavy element) raises the equivalent atomic number and density of the formation. Increasing Z_{eq} , in turn, affects the mode of gamma ray attenuation by the medium, altering the proportion between photoelectric absorption, Compton scatter, and pair production as shown in Figure 13.9. Furthermore, it has been pointed out by Czubek (1966) that Z_{eq} is somewhat dependent upon photon energy, as well as composition of the material; this is an added complication. This "Z-effect" is discussed by Dodd and Eschliman (1972), who presented a graph of the count rate versus ore grade for a range of uranium concentrations and several probes (Fig. 13.1). It would seem to be a simple matter to determine the grade-thickness product as shown in equation (1) by application of a simple correction factor based on plots such as the one given by Dodd and Eschliman (1972) (see Figure 13.1). It will be shown later in this paper, however, that the error is dependent on bed thickness (Fig. 13.3), and thus is difficult to correct for.

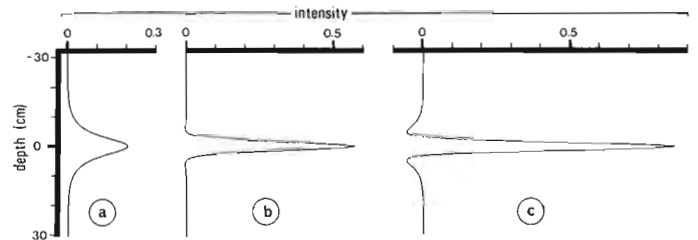


Figure 13.7. (a) Czubek's analytical response function [equation (8)] for $R = 3$ cm and $\mu = 0.2$ cm⁻¹. This has been deconvolved using the inverse filter given in equation (4), with the value of α determined by the semi-logarithmic slope method (curve b), and determined by equation (10) (curve c).

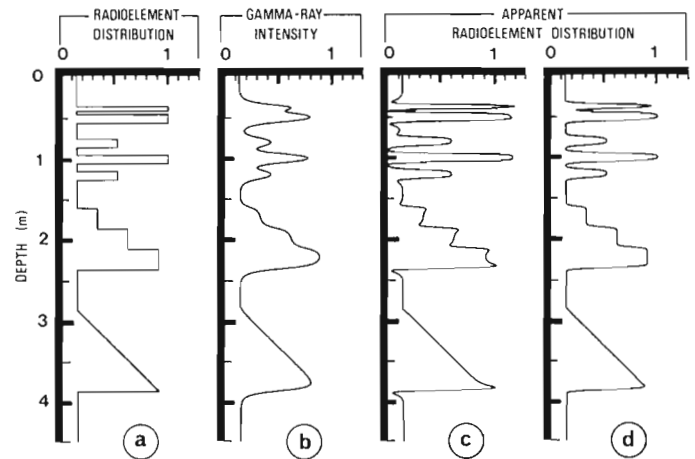


Figure 13.8. Example of a simulated radioelement distribution (a), and the corresponding synthetic gamma ray log (b), assuming the same response function shown in Figure 13.7a. Curve (b) was deconvolved using the value of α given by equation (10) to produce curve (c) and using the value of α given by the semi-logarithmic slope method to produce curve (d).

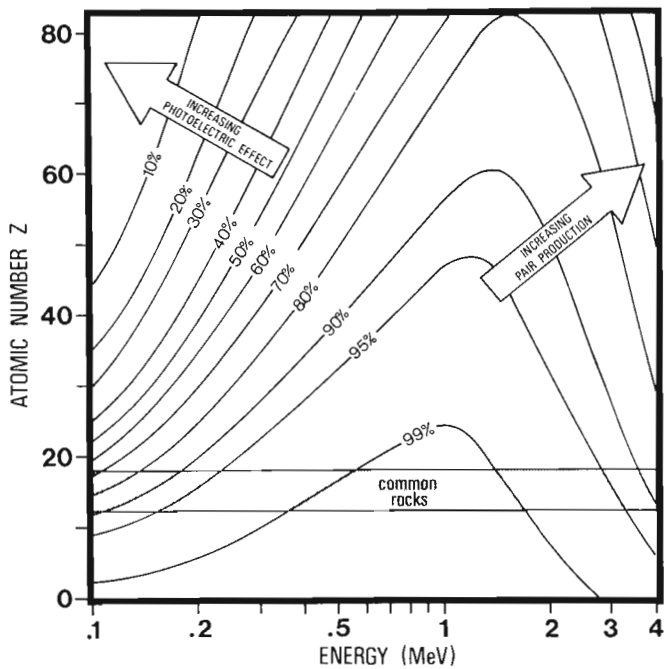


Figure 13.9. Percentage of the interactions between photons and matter which are due to Compton scattering, as a function of photon energy and atomic number of the medium. Based on data given by Davisson and Evans (1952).

Using the semi-logarithmic slope method of determining α as described earlier, equation (8) can be used to give an indication of how the parameter α varies with the linear attenuation coefficient μ of the formations through which the borehole passes (Fig. 13.11). Also shown in this figure is a plot of α against μ based on equation (10), for comparison.

The Effect of Density and Pore Fluids

The mass attenuation coefficient μ/ρ varies less between materials than does μ , and is independent of state (solid, liquid, gas) of the absorbing medium, depending only on composition. Thus, μ/ρ is, for a given formation composition, essentially independent of porosity in a dry formation. For materials of a given composition, then, μ varies linearly with ρ . In a mixture of materials for which the individual mass attenuation coefficients are known (e.g. Table 13.1), the mass attenuation coefficient of the mixture may be found from

$$\frac{\mu}{\rho} = \frac{\mu_1}{\rho_1} W_1 + \frac{\mu_2}{\rho_2} W_2 + \dots \quad (15)$$

where the subscripts 1, 2, etc. refer to materials 1, 2, etc., and W is the weight fraction of each material (Evans, 1955).

Equation (15) may be utilized to give an indication of the variation of μ/ρ for a mixture of U and barren rock (concrete) varying from 0 to 100 per cent U. An example is plotted for several energies in Figure 13.12. Of special interest in this figure is the observation that for low gamma ray energies (say, 0-0.4 MeV) the mass attenuation coefficient is relatively sensitive to uranium content of the rock, whereas at higher energies (1-2 MeV) there is little dependence of μ/ρ on uranium concentration.

It has been pointed out by Czubek (1961) that the system calibration factor K is proportional to μ/ρ

$$K = k \left(\frac{\mu}{\rho} \right) \quad (16)$$

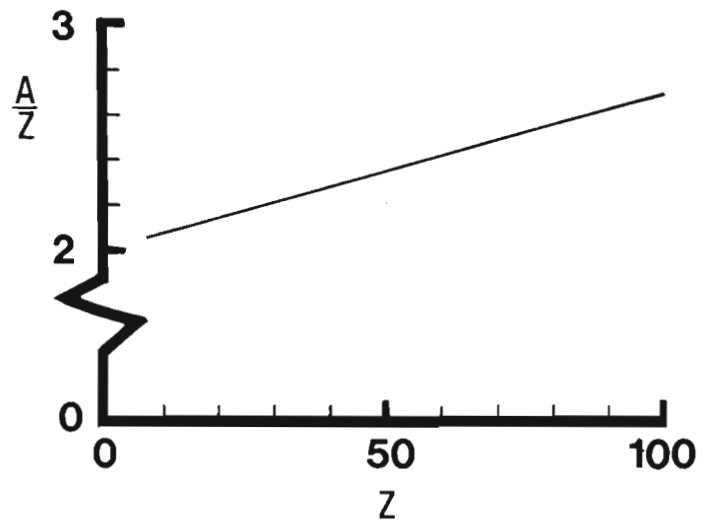


Figure 13.10. Ratio of atomic weight (A) to atomic number (Z), as a function of atomic number, for the elements. This graph shows only the general trend; there is considerable scatter about this trend, especially at large values of Z .

(Czubek's K -factor is the inverse of the one commonly used in North America, and used here) where k is a factor which includes all parameters affecting the calibration (e.g. detector efficiency and instrument low-energy threshold), other than the mass attenuation coefficient μ/ρ . Equation (16) allows us to re-plot the data shown in Figure 13.12 as the ratio of K_{ore}/K_{barren} against per cent U (Fig. 13.13).

Referring to Figure 13.13 it can be seen that for photon energies on the order of 1-2 MeV the calibration factor K can be expected to remain nearly constant in any grade of ore. Thus, the suggestion by Dodd and Eschliman (1972) and others that a graded filter be used around the detector to help discriminate against low energy gamma rays is apparently a good one when high grades are involved. This technique has the added advantage that the count rate is considerably reduced, thus making the task of the associated instrumentation easier.

Making use of the relationship between α and μ (determined by the semi-logarithmic slope method) shown in Figure 13.11, the data shown in Figure 13.12, and equation (15), we can go one step farther and plot α as a function of uranium content as shown in Figure 13.14, and $\alpha_{ore}/\alpha_{barren}$ as a function of uranium content in Figure 13.15.

It is of interest to determine the effect on μ of water in the pore spaces for rock of a given porosity. Because the mass attenuation coefficients of air and water are similar (Table 13.1), it may be seen from equation (15) that μ/ρ will be similar for dry rock or water saturated rock. This has also been demonstrated by Czubek and Zorski (1976), who showed that the variation of μ/ρ with per cent free water in the pore spaces will generally be only a few per cent. The variation in μ , then, will be essentially linear with the variation of density between wet and dry rock of a given composition and porosity. This approximation may be written as:

$$\frac{\mu_{wet}}{\mu_{dry}} = \frac{\rho_{wet}}{\rho_{dry}} \quad (17)$$

where the subscripts "wet" and "dry" denote the water content of pore spaces of a given rock matrix. On the other hand it is clear that, although the mass attenuation

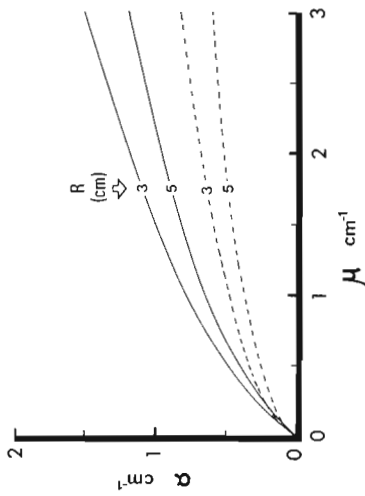


Figure 13.11. Variation of α with the linear attenuation coefficient μ for boreholes of radius 3 and 5 cm. Solid lines were determined using the semi-logarithmic slope method on Czubek's response function [equation (8)]; dashed lines were derived from equation (10).

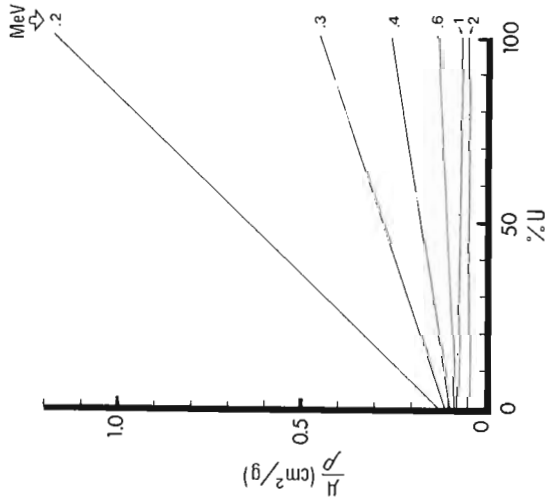


Figure 13.12. Relationship between mass attenuation coefficient (μ/ρ) and uranium concentration based on data from Fano et al. (1962). The matrix is assumed to be concrete with a density of 2.35 g/cm^3 .

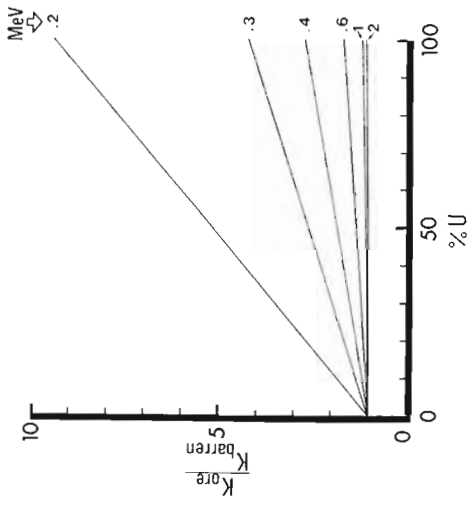


Figure 13.13. Plot of $K_{\text{ore}}/K_{\text{barren}}$ as a function of uranium concentration in concrete, based on data from Fano et al. (1962).

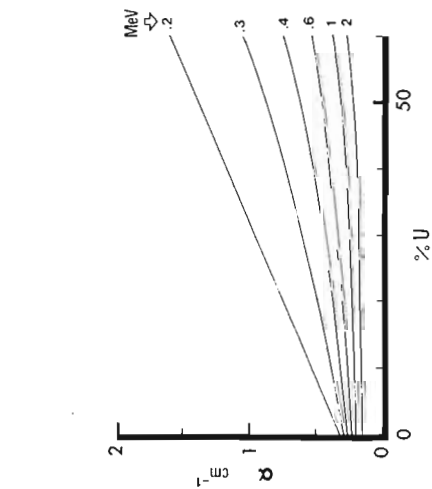


Figure 13.14. Plot of α as a function of uranium concentration in concrete, based on data from Fano et al. (1962) and Figure 13.11, for a 6 cm diameter borehole.

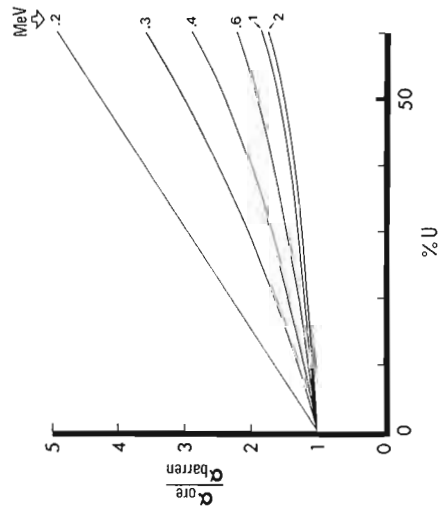


Figure 13.15. Plot of $\alpha_{\text{ore}}/\alpha_{\text{barren}}$ as a function of uranium concentration in concrete, based on data from Fano et al. (1962) and Figure 13.11, for a 6 cm diameter borehole.

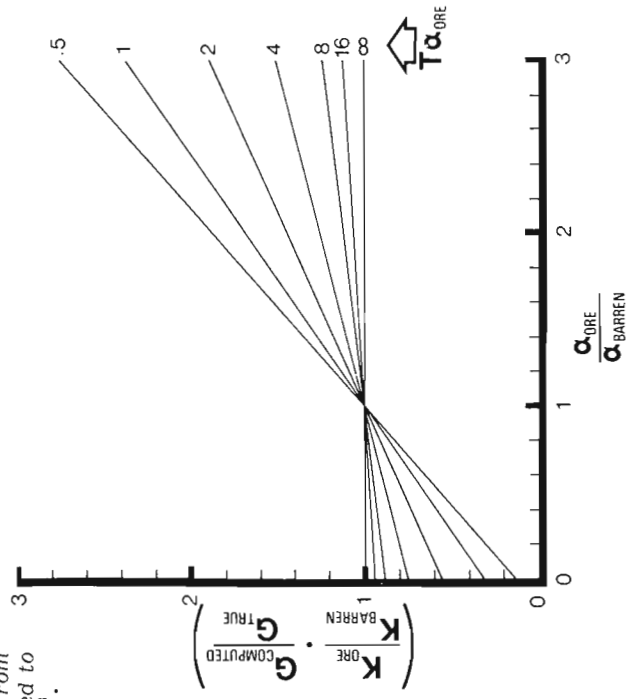


Figure 13.16. Error in computed grade based on equation (1) plotted as a function of α and K in the ore zone and in the barren zone for seven values of the product $T\alpha_{\text{ore}}$. This figure was derived digitally from equations (5) to (7), assuming a double-sided exponential GIR [equation (3)].

Table 13.1
Total gamma ray mass attenuation coefficients (cm^2/g) for various materials (data from Fano et al., 1962, except as noted).

Material	ρ [$\frac{\text{g}}{\text{cm}^3}$]	$\frac{\mu}{\rho}$ (cm^2/g) at gamma ray energies:				
		0.2 MeV	0.4 MeV	0.6 MeV	1.0 MeV	2.0 MeV
Uranium	19.0*	1.17	0.259	0.136	0.0757	0.0484
Concrete	2.35	0.124	0.0954	0.0804	0.0635	0.0445
Water	1.0*	0.136	0.106	0.0896	0.0706	0.0493
Air	.0012*	0.123	0.0953	0.0804	0.0635	0.0445

*Handbook of Chemistry and Physics, Chemical Rubber Company, 50th edition, 1969, Cleveland Ohio. Densities for air and water are at standard temperature and pressure.

coefficient is largely unaffected by changes in water content of a formation of a given porosity, the linear attenuation coefficient μ changes proportionally to the change in density [equation (17)]. Thus, a change in the shape of the system response function is predicted by equation (8).

In borehole logging a range of gamma ray energies will be observed, the range depending on specific energy window settings on spectral logging equipment, or on the lower energy threshold of total count equipment. In addition, the energy characteristics of the detector modify the energy distribution of the detected gamma rays. No attempt has been made in this paper to incorporate these instrument response characteristics into the theory, and therefore graphs such as Figures 13.12-13.15 are useful only as qualitative guides, at specific gamma ray energies. It should be emphasized also that Czubek's theory [equation (8)] assumes unscattered gamma rays only.

It is interesting to note from equation (16) that, in homogeneous rock, K is a function of the mass attenuation coefficient, and therefore is independent of density for a given composition. On the other hand, equation (8) shows that the shape of the system response function (and therefore α is a function of the linear attenuation coefficient, and therefore density [see equations (11)-(13)].

Now we are in a position to determine approximately the range of errors which will be encountered under various conditions of uranium concentration, density, and gamma ray energy. Assuming the GIR to be represented adequately by equation (3), equations (5) to (7) have been used to predict the error which will result for a range of values of $\alpha_{\text{ore}}/\alpha_{\text{barren}}$, $K_{\text{ore}}/K_{\text{barren}}$, and $T\alpha_{\text{ore}}$ (i.e. the product of α_{ore} and T) (Figure 13.16). This figure was derived digitally assuming that the probe has been calibrated in the centre of an infinitely thick model ore zone having characteristics similar to the one being simulated. Furthermore, the change in the flux of radiation backscattered from the barren zone back into the radioactive zone due to the altered physical properties of the barren zone was assumed to be insignificant, as was the effect of the borehole.

As an example of how this figure is used, consider the case of a 10 cm thick bed of 10 per cent U, and the 0.352 MeV gamma ray emitted by ^{214}Pb in the ^{238}U decay series. From Figure 13.13 we see that $K_{\text{ore}}/K_{\text{barren}}$ is about 1.2; from Figure 13.14 we see that in a 6 cm diameter borehole $\alpha_{\text{ore}} = 0.4 \text{ cm}^{-1}$; from Figure 13.15 we find that $\alpha_{\text{ore}}/\alpha_{\text{barren}}$ is about 1.3. Referring now to Figure 13.16 we move across the horizontal axis to 1.3, vertically to the $T\alpha_{\text{ore}} = 4$ line, and project horizontally to the left from that point to find a value on the vertical axis of 1.07. Multiplying this by $K_{\text{barren}}/K_{\text{ore}} = 1/1.2$ we see that $G_{\text{computed}}/G_{\text{true}}$ is 0.89, or an 11 per cent error in G in the

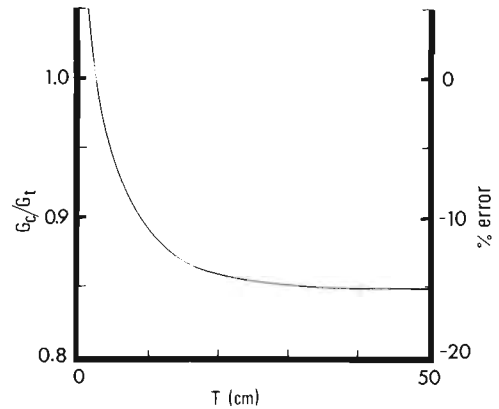


Figure 13.17. Example of how the error in the computed grade-thickness product for a radioactive stratum varies nonlinearly with the thickness of the stratum, as described in text.

evaluation of equation (1). This error increases with decreasing thickness T , with increasing ore grade G , and in general increases with decreasing gamma ray energy. Figure 13.16 should not be used for correcting radioelement concentrations derived from field logs, because α and K are generally not known for conditions both inside and outside a high-grade uranium zone, and because gamma ray logs usually include considerable scattered radiation, whereas equation (8) was derived assuming unscattered radiation.

Consider now the same example (10 per cent U and 0.352 MeV gamma rays) but with various thicknesses of the radioactive zone. Working from Figure 13.16 we can produce a plot of $G_{\text{computed}}/G_{\text{true}}$ (or % error) against thickness for these parameters (Fig. 13.17). The reason for the nonlinearity of the error in computed grade as a function of zone thickness shown in Figure 13.17 can be visualized easily from Figure 13.3 and equations (5) to (7). This nonlinear error should be taken into account in interpreting field logs, and also in calibrating a probe in a high-grade model borehole. In the latter case, a K -factor derived based on the area of the gamma ray anomaly obtained in the model borehole [equation (1)] is valid only for a uranium zone of that thickness and concentration, if α changes significantly at the model ore zone boundary. Note that the value of K will be a weighted average of K_{ore} and K_{barren} . To determine K_{ore} alone the model ore zone should be effectively infinitely thick, and the K -factor derived using equation (2) based on the average radioelement intensity in the centre of the ore zone.

It is generally assumed in gamma ray logging that the computed grade-thickness product is independent of rock density because grade is determined as percent uranium by weight (or similar units) and thus includes the effect of density. It has been shown here that this is true only when the system response function is unchanged across the ore zone boundaries. A change in rock density unaccompanied by a change in composition will result in a linearly proportional change in μ , but no change in K [equation (16)]. The corresponding change in α can be determined from Figure 13.11, and the error found from Figure 13.16 as before.

Discussion and Conclusions

Changes in certain physical parameters of the rock (e.g. density, Z_{eq} , per cent water in the pore spaces) with depth can introduce errors into quantitative radioelement determinations based on gamma ray logs. Such variations are particularly insidious when they are spatially associated with the radioactive material itself, as the data in such cases will in general be confounded. It has been pointed out by Dodd and Eschliman (1972) and others that the computed grade thickness product for a uranium ore zone can be in error because of self attenuation of the gamma radiation by the uranium itself (the Z-effect). In this paper it has been demonstrated that this error varies nonlinearly with ore zone thickness and thus is not amenable to the application of simple correction factors. Errors due to changes in density or Z_{eq} at the ore zone/barren zone interface cannot in general be removed from the data. Instead, they must be avoided as much as possible by using suitably designed instrumentation. From Figures 13.12-13.16 it is evident that such errors will be minimized by restricting instrument sensitivity to gamma radiation above 1 MeV. This can be done by using a lower energy discriminator set at 1 MeV. In high count rate zones it is also helpful or essential to use a graded filter (usually concentric sleeves of lead, cadmium and copper, or similar metals) around the detector, as described by Dodd and Eschliman (1972). This filter will attenuate many of the low energy gamma rays which might otherwise saturate the electronic circuitry.

In ordinary gross-count gamma ray logging systems the lower energy threshold is generally 100 keV or lower. Because gamma radiation detectors of the small sizes usually used in borehole applications are inefficient at high gamma ray energies, these gross count systems are heavily biased towards the low energies. Thus, any attempt to make such instruments applicable to evaluation of high grade ore deposits by incorporation of high speed counting circuits, pulse dividing circuits etc., to enable the system to handle the enormous count rates involved attacks only part of the problem. Rather than count all of these low energy gamma rays, and compute erroneous grade thickness values based on them, it is clearly better to use equipment which will discriminate against the low energy gamma rays, thus minimizing the nonlinear errors described in this paper.

Acknowledgments

I am grateful to R.L. Grasty, K.A. Richardson, and Q. Bristow for their helpful comments and suggestions regarding the manuscript. I would also like to thank P.H. Dodd for permission to use Figure 13.1.

References

- Abramowitz, M. and Stegun, I.A.
1964: Handbook of Mathematical Functions with Formulas, Graphs, and Mathematical Tables; National Bureau of Standards, Applied Math Series, No. 55.
- Conaway, J.G.
1979: Problems in gamma-ray logging: The effect of dipping zones on the accuracy of ore grade determinations; in *Current Research, Part A*, Geological Survey of Canada, Paper 79-1A, p. 41-44.
Exact inverse filters for the deconvolution of gamma-ray logs; *Geoexploration*. (in press(a))
Direct determination of the gamma ray logging system response function in field boreholes, *Geoexploration*. (in press(b))
Deconvolution of gamma ray logs in the case of dipping radioactive zones, *Geophysics*, v. 45. (in press(c))
- Conaway, J.G., Allen, K.V., Blanchard, Y.B., Bristow, Q., Hyatt, W.G., and Killeen, P.G.
1979: The effects of borehole diameter, borehole fluid, and casing thickness on gamma ray logs in large diameter boreholes; in *Current Research, Part C*, Geological Survey of Canada, Paper 79-1C, p. 37-40.
- Conaway, J.G., Bristow, Q., and Killeen, P.G.
Optimization of gamma-ray logging techniques for uranium; *Geophysics*, v. 45. (in press)
- Conaway, J.G. and Killeen, P.G.
1978: Quantitative uranium determinations from gamma-ray logs by application of digital time series analysis; *Geophysics*, v. 43, p. 1204-1221.
- Czubek, J.A.
1961: Some problems of the theory and quantitative interpretation of the gamma-ray logs; *Acta Geophysica Polonica*, v. 9, p. 121-137.
1962: The influence of the drilling fluid on the gamma-ray intensity in the borehole; *Acta Geophysica Polonica*, v. 10, p. 25-30.
1966: Physical possibilities of gamma-gamma logging; in *Radioisotope Instruments in Industry and Geophysics*, volume 2, International Atomic Energy Agency Proceedings Series, IAEA, Vienna.
1969: Influence of borehole construction on the results of spectral gamma-logging; in *Nuclear Techniques and Mineral Resources*, International Atomic Energy Agency Proceedings Series, IAEA, Vienna.
1971: Differential interpretation of gamma-ray logs: I. Case of the static gamma-ray curve; Report No. 760/I, Nuclear Energy Information Center, Polish Government Commissioner for Use of Nuclear Energy, Warsaw, Poland.
- Czubek, J.A. and Zorski, T.
1976: Recent advances in gamma-ray log interpretation; International Atomic Energy Agency Advisory Group Meeting on Evaluation of Uranium Resources, Rome, Italy.
- Davisson, C.M. and Evans, R.D.
1952: Gamma ray absorption coefficients; *Reviews of Modern Physics*, v. 24, No. 2, p. 79-107.

- Davydov, Y.B.
1970: Odnomernaya obratnaya zadacha gamma-karotazha skvazhin (One dimensional inversion problem of borehole gamma logging); *Izvestiya Vysshoye Uchebnoye Zavedeniya Geologiya i Razvedka*, No. 2, p. 105-109 (in Russian).
- Dodd, P.H. and Eschliman, D.H.
1972: Borehole logging techniques for uranium exploration and evaluation; in *Uranium Prospecting Handbook*, S.H.U. Bowie, M. Davis, and D. Ostle, ed., Institute of Mining and Metallurgy, London.
- Evans, R.D.
1955: *The Atomic Nucleus*; McGraw Hill, New York.
- Fano, U., Zerby, C.D., and Berger, M.J.
1962: Gamma-ray attenuation; in *Reactor Handbook*, E.P. Blizard and L.S. Abbott, ed., Interscience Publishers, John Wiley and Sons, New York.
- McDonald, W.J., and Palmatier, E.D.
1969: Predicting nuclear log response; *Journal of Petroleum Technology*, v.21, p. 1421-1426.
- Moore, D.C.
1978: Problems associated with calibration of radiation detectors for measurements in thin and dipping ore zones; Paper Presented at 48th Annual Meeting of the Society of Exploration Geophysicists, San Francisco, Oct. 29-Nov. 2.
- Rhodes, D.F. and Mott, W.E.
1966: Quantitative interpretation of gamma-ray spectral logs; *Geophysics*, v. 28, p. 410-418.
- Rhodes, D.F., Stalwood, R.A., and Mott, W.E.
1961: Intensity of unscattered gamma-rays inside cylindrical selfabsorbing sources; *Nuclear Science and Engineering*, v. 9, p. 41-46.
- Roesler, R.
1965: Ein neues Auswerteverfahren für radiometrische Bohrlochmessungen unter besonderer Berücksichtigung der K₂O-Bestimmung aus Messungen der natürlichen Gammastrahlung in Bohrlochern; *Freiberger Forschungshefte, C180, Geophysik*, VEB Deutscher Verlag für Grundstoffindustrie, Leipzig.
- Scott, J.H.
1963: Computer analysis of gamma-ray logs; *Geophysics*, v. 28, p. 457-465.
- Scott, J.H., Dodd, P.H., Drouillard, R.F., and Mudra, P.J.
1961: Quantitative interpretation of gamma-ray logs; *Geophysics*, v. 26, p. 182-191.
- Suppe, S.A.
1957: Gamma-ray borehole logging; in *Radiometric Methods in the Prospecting of Uranium Ores*, V.V. Alekseev, A.G. Grammakov, A.I. Nikonov, and G.P. Tafeev, ed., Translation available as AEC-tr-3738 (Book 2), U.S. Atomic Energy Agency.
- Suppe, S.A. and Khaykovich, I.M.
1960: Resheniye pryamoi zadachi gamma-karotazha v sluchaye slozhnogo raspredeleniya radioaktivnogo elementa v aktivnykh plastakh (Solution of the linear problem of gamma logging in the case of a complex distribution of the radioactive element in the active strata); *Voprosy Rudnoi Geofiziki*, Issue 1 (in Russian).
- Wilson, R.D.
1979: Log deconvolution with the inverse digital filter; *Spectral Gamma-Ray Logging Technical Note 9*, Bendix Field Engineering Corp., Grand Junction, Colorado.

THE CIRCUM-UNGAVA BELT IN EASTERN HUDSON BAY:
THE GEOLOGY OF SLEEPER ISLANDS AND PARTS OF
THE OTTAWA AND BELCHER ISLANDS

Project 780012

W.R.A. Baragar and C.G. Lamontagne¹
Precambrian Geology Division

Baragar, W.R.A. and Lamontagne, C.G., The Circum-Ungava Belt in eastern Hudson Bay: The geology of Sleeper Islands and parts of the Ottawa and Belcher islands; in Current Research, Part A, Geological Survey of Canada, Paper 80-1A, p. 89-94, 1980.

Abstract

Volcanic rocks of the Aphebian Circum-Ungava Belt were mapped and sampled at three localities in eastern Hudson Bay; near Sanikiluaq in the northern part of the Belcher Islands, on the Sleeper Islands, and on Gilmour and Perley islands of the Ottawa Islands. Volcanic rocks of the Sleeper Islands appear to be correlative with the Flaherty Formation of the Belcher Islands but compared to the section measured near Sanikiluaq they form a thicker (+2000 m compared to 1460 m), more diversified (six mappable lithologies) sequence with a notably lower vesicularity. This is consistent with their position west of the Sanikiluaq section where they presumably formed in deeper water farther offshore. Gabbroic sills with a rich basal concentration of coarse feldspar phenocrysts occur beneath the exposed volcanic sequence on the Sleeper Islands and may be equivalent to the feldsparphyric Haig Intrusions subjacent to the Flaherty Formation on the Belcher Islands.

The volcanic succession of Gilmour and Perley islands is divisible into two broad groupings; a sequence of variolitic pillowed basalts and an ill-defined assemblage of mixed komatiitic and tholeiitic lavas. The latter includes peridotitic komatiite flows of which two types are notable: 1) spinifex-textured flows virtually identical to the Munro Township model, and 2) differentiated flows with peridotite base, doleritic top and breccia capping. An uncertain proportion of the remaining flows is believed to be basaltic komatiites on the basis of colour, pillow form and jointing. The Ottawa Islands komatiites are presumed to be correlative with komatiites of the Cape Smith Belt. Their projected position west of the Sleeper Islands, their virtual lack of vesicles, and their thickness (possibly 4500 m) are consistent with a view that they are deep water effusions, sited even farther from the cratonic mass than the volcanics of the Sleeper Islands.

Introduction

The Circum-Ungava Belt was assumed to extend from the Cape Smith Belt through eastern Hudson Bay to the Belcher Islands at least partly on the basis of its reported presence in the intervening islands, the Ottawa and Sleeper islands (Dimroth et al., 1970). Yet these islands had never been mapped. The Ottawa Islands were visited briefly by Bell (1879) and Manning (1947) who reported on some aspects of their geology, including the presence in the Ottawa Islands of ultramafic rocks. Following discovery of ultramafic lava flows (komatiites) in the Cape Smith Belt (Schwarz and Fujiwara, 1977) with their attendant economic and scientific interest, a closer look at the small islands of eastern Hudson Bay became imperative. Hence, about two months were spent this past summer examining the volcanic stratigraphy of a northern part of the Belcher Islands, the Sleeper Islands and part of the Ottawa Islands (Fig. 14.1). Regretably, we had only sufficient time to map on the major islands of the Ottawa group, Gilmour and Perley islands.

In each of the three localities a surveyed line was chained across the volcanic successions and the geology mapped along the line at a scale of 400 feet to the inch. Samples for chemical analyses were taken at stratigraphic intervals of 100-150 m. On the Sleeper and Ottawa Islands, where no previous mapping had been done, traversing was extended to the rest of the islands, or as far as possible within the time available.

The age of the Circum-Ungava Belt is assumed to be late Aphebian but age determinations vary from 2150 Ma (Schimmann, 1978) to 1590 Ma (Brooks and Arndt, quoted in Schmidt, in press) with the most commonly accepted age of 1700-1800 Ma being that of Fryer (1972).

We are grateful for the very able assistance in the field of Isabelle Cadieux and Robert Houde, supplemented from time to time by our associates K. Clark and D.G. Rose, who were engaged in a related paleomagnetic study of these rocks. To the captain and crew of the Peterhead Tooluk, Johnny Inukpuk, Simeonie Elijassoiopik, Sam Elijassiatuk, and Daniel Weetiluktuk, we give our acknowledgments with thanks for safe and pleasant passages around the rather treacherous waters of eastern Hudson Bay. We would also like to acknowledge our indebtedness to Barry MacDonald of the R.C.M.P. and Alister MacGregor and David Purchess of the Hudson's Bay Co., Sanikiluaq and to Richard Jones and Bob Janes of the Hudson's Bay Co., Inoucdjouac for help and much pleasant hospitality.

Belcher Islands

Section lines across the Eskimo and Flaherty formations at distances of about 3 km south and southwest of Sanikiluaq village were mapped and sampled in the present study. Knowledge of the geology of the islands is attributable mainly to Jackson (1960 and in Dimroth et al., 1970), but more detailed work on the volcanic formations was done by Leggett (1974), Ware (1978), and Ricketts (1979) on the Flaherty Formation, and by Stirbys (1975) on the Eskimo Formation. The Eskimo is one of the older and the Flaherty one of the younger formations on the Belcher Islands, and in this region they are separated by about 1350 m of mainly carbonates, quartzites, and iron formation. The Flaherty Formation evidently marks the change from mio- to eugeosynclinal conditions.

The Eskimo Formation along the line of section is 970 m thick and is composed essentially of massive basaltic flows generally ranging in thickness from 20 to 100 m. One

¹Département de Géologie et Minéralogie, Université Laval, Québec.

agglomeratic member in the middle of the formation is of special interest in that it contains a few felsic as well as mafic bombs. Very thin interlayers of chert and quartzite occur intermittently through the succession. Flow tops are highly amygdaloidal and it is difficult to escape Stirbys' (1975) conclusion that eruption was subaerial.

The Flaherty Formation along the section measured is 1460 m thick but the upper contact is not exposed. It is composed of pillowed and massive basalts, both markedly amygdaloidal, and three separate beds of lapilli tuff ranging in thickness from 10 to 35 m. Immediately below the formation is one of the Haig sills containing segregations of closely spaced plagioclase phenocrysts of 1-2 cm diameter. Very similar are segregations of plagioclase phenocrysts in the upper part of one of the lowermost Flaherty flows, and it is reasonable to suppose that the two are comagmatic. In the case of the flow, segregation of phenocrysts was evidently by flotation.

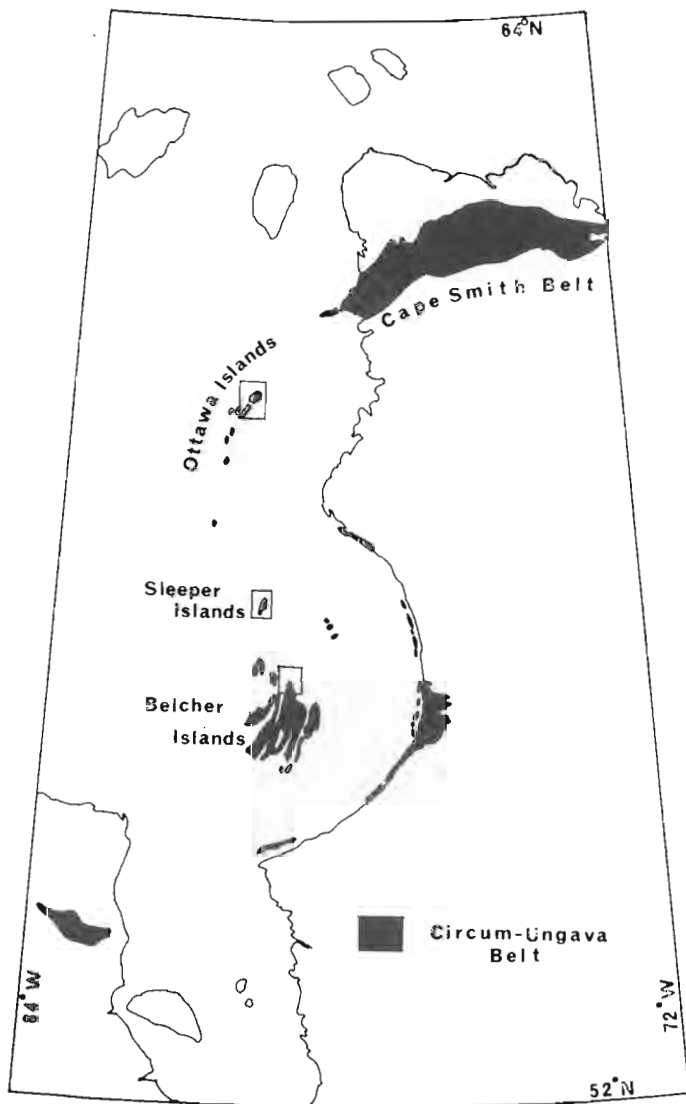


Figure 14.1. Location map showing the areas referred to in the present report in relation to their position in the Circum-Ungava Belt.

Sleeper Islands

The Sleeper Islands consist of two major and innumerable small islands which rise very little above sea level, and in consequence are almost devoid of drift and nearly free of lichen.

The volcanic succession is subdivided into six lithologies of varying distinctiveness (Fig. 14.2). The lowermost unit consists of a number (at least six to eight) of thin basaltic flows generally ranging in thickness from 5 to 10 m. Typically, each flow comprises pillow lava at the bottom, massive lava above and a thin (10-20 cm) hyaloclastite top. The unit is a minimum of about 260 m thick. It is overlain by a thin (50-100 m) but laterally persistent member composed of two or three flows of mainly pillowed basalts. These are distinguished from neighbouring flows in the stratigraphic succession by a content of 10 to 15 per cent feldspar phenocrysts ranging generally from 2 to 4 mm in diameter. Following this unit is an undistinguished sequence of aphyric, dark grey basalts. They are mainly pillowed, but invariably the pillows branch upward into massive tops capped by a few centimetres or metres of pillow breccia. Locally, they are variolitic, but inasmuch as the variolites seem to be related to fractures as well as pillow margins, it is difficult to be sure whether and to what degree they may be secondary. Individual flows are from 10 to 50 m and the sequence from 400 to 600 m thick. Contained within the sequence of aphyric pillow lavas is a unit composed of one or more distinctive massive flows. It is typically columnar jointed, is dark grey, and has a uniform, finely doleritic texture. A fresh surface of the rock is spotted with sparsely distributed, rounded pyrite blebs of 2 to 5 mm diameter. The unit is about 250 m thick and is capped by 2 or 3 m of breccia.

The large feldsparphyric member is the most distinctive of the Sleeper Islands assemblage. It is composed of sparsely scattered, blocky white feldspar phenocrysts ranging between about 0.5 and 3 cm across in a slightly pinkish weathering, dark grey groundmass. In the north island (Kidney Island) the member is divided into lower (a) and upper (b) units on the basis of a difference in phenocryst content of from 10-20 per cent and less than 5 per cent, respectively. This distinction is not apparent in the southern island. The flows are mainly pillowed, but as in other units, they pass into massive phases near their tops and are capped by 1 to 3 m of pillow breccia. The pillows are extraordinarily large in comparison with those of other units - commonly 3 to 4 m long, 1-2 m thick - and the flows are typically thick, 100 m or more. The total thickness of the member on the northern island is from 600 to 800 m, but it appears to be thinner on the southern island. They are named the Kidney Flows after the island on which they are best exposed.

Associated with the Kidney Flows are agglomerate lenses at three stratigraphic levels. These are composed of irregular lava masses ranging from a few centimetres to a few metres across (commonly 10 to 30 cm) set in a matrix of lapilli tuff. All the constituent materials appear to be of similar composition, probably the same as the large feldsparphyric lava, but feldspar phenocrysts are prominent in only one of the lenses. Angular lithic fragments are at the cores of many of the lava masses, reminiscent of the accretionary bombs described by Heiken (1978). The agglomerate lenses are reasonably interpreted as sections of volcanic cones and are indicative of shallow water or subaerial eruption.

Above the Kidney Flows are aphyric pillowed and massive basalts generally similar to the sequence which underlies them. The overall thickness of the volcanic assemblage on Kidney Island is about 2000 m.

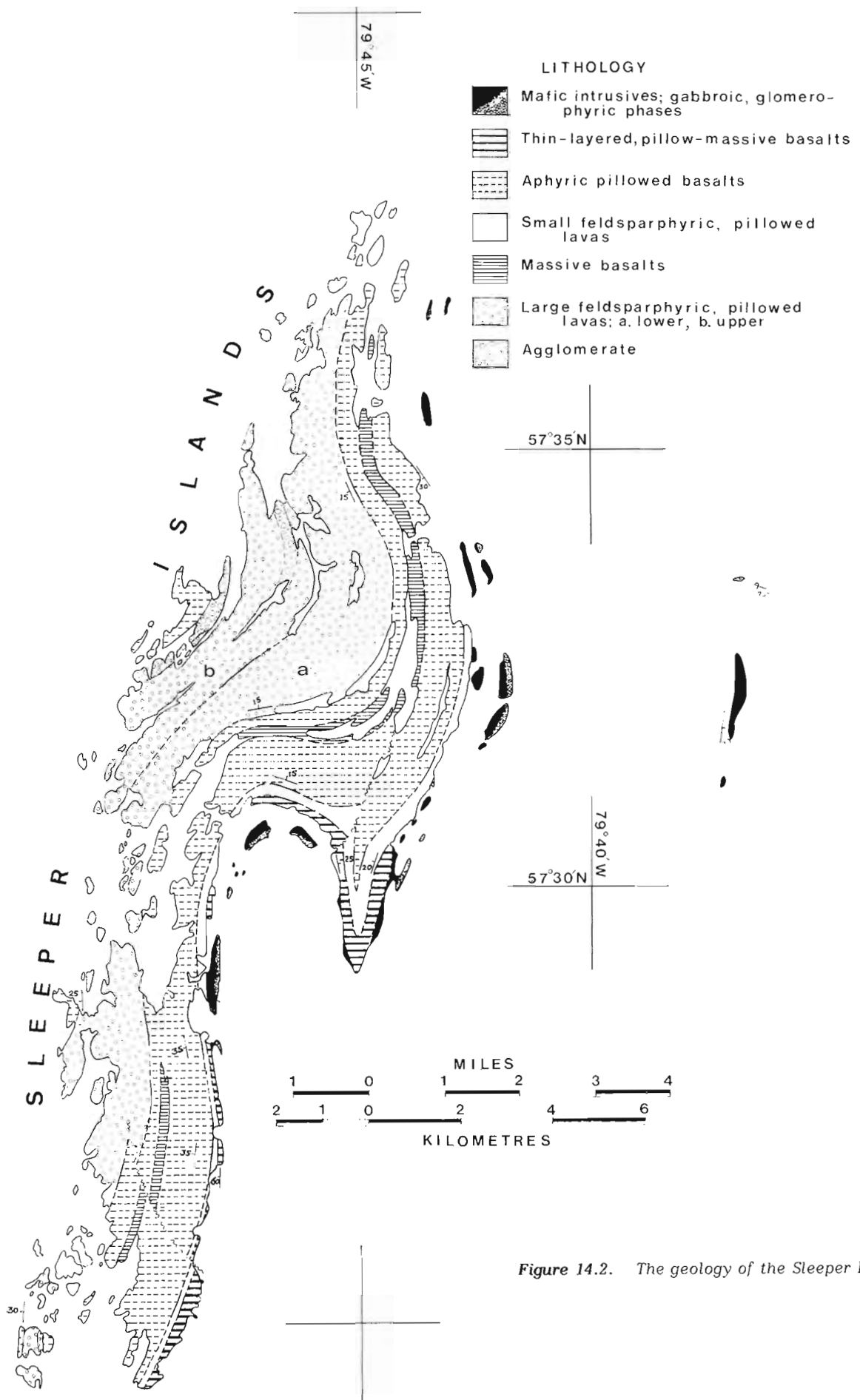
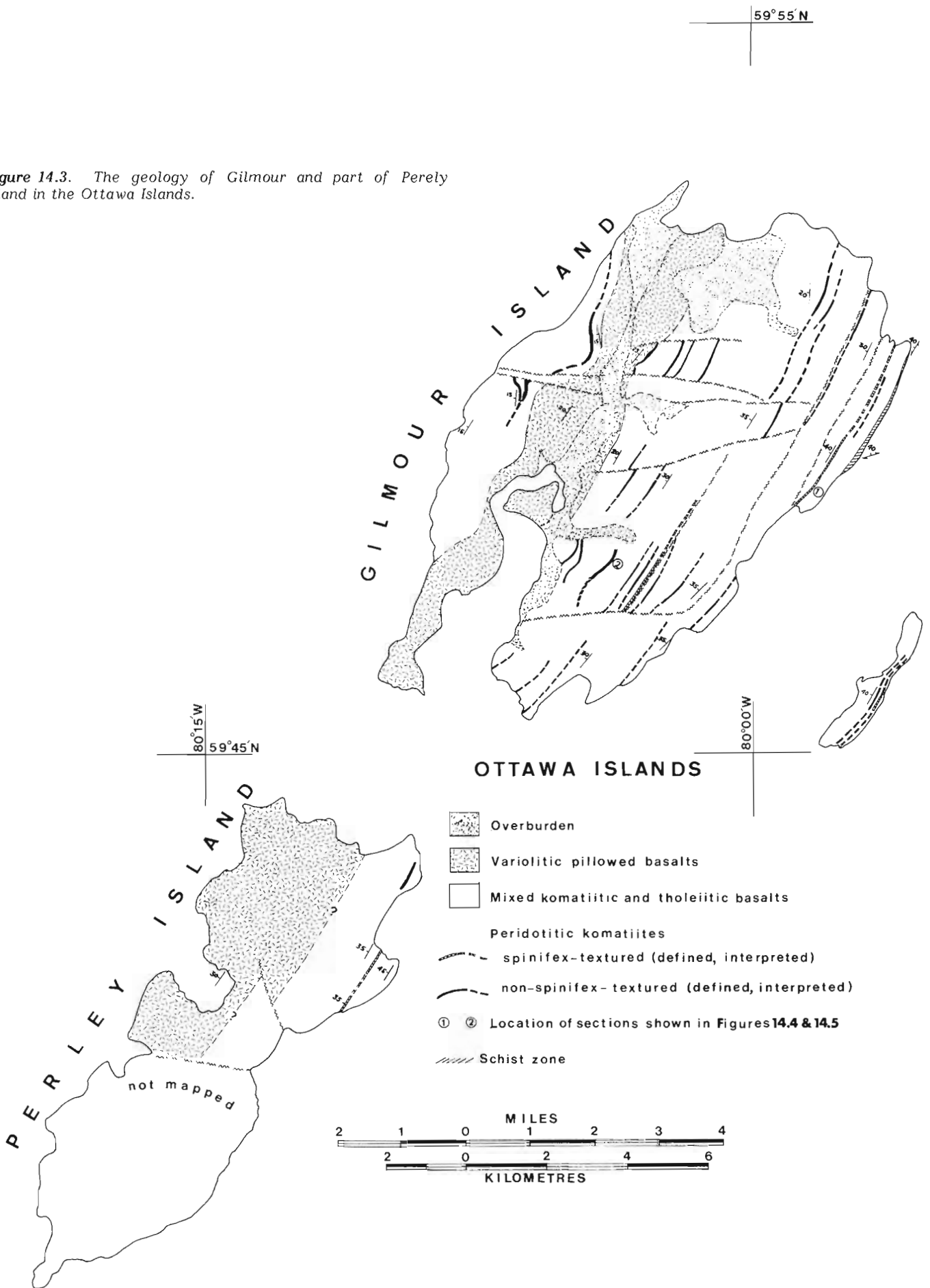


Figure 14.2. The geology of the Sleeper Islands.

Figure 14.3. The geology of Gilmour and part of Perley Island in the Ottawa Islands.



At the base of the volcanic sequence exposed on the Sleeper Islands parallel chains of coarse grained mafic rocks outcrop on the headlands, peninsulas and offshore islands of the eastern shore. Contacts with country rocks are not exposed but the mafic rocks are thought to belong to two sills intrusive into sedimentary rocks underlying the volcanic sequence. The outer sill contains a remarkable segregation of closely spaced, coarse (2 to 5 cm) feldspar phenocrysts on its lower side and a differentiated gabbroic mass in its upper part. In one place (the peninsula on the eastern side of the anticlinal point) two graded layers, each several metres thick and showing decreasing feldspar concentration upward, succeed one another and then pass into overlying gabbro. These sills may be correlative with the Haig Intrusions of the Belcher Islands which, as we have seen, also contain feldspathic segregations. Their stratigraphic position relative to the Sleeper Islands sequence is equivalent to that of the Haig Intrusions relative to the Flaherty Formation. Gabbro also outcrops on islands about 5 km east of Kidney Island where it dips steeply east in contrast to dips on the Sleeper Islands.

Ottawa Islands

Gilmour and Perley islands of the Ottawa group of islands are composed of volcanic rocks which, on the basis of field observations, can be divided into two broad groupings; komatiites and associated lavas and variolitic pillowed basalts (Fig. 14.3). In the first group peridotitic komatiites can be separated but further subdivision may only be possible after extensive laboratory study. Age relationships are not certain. The rocks all dip and face westward but strike faults, some of which are readily interpretable from air photographs, are inconspicuous on the ground and age relationships based upon superposition cannot be accepted with great confidence.

The variolitic pillow lavas are a fairly uniform assemblage of rocks. They are typically green weathering, dark greenish grey basalts and are mostly pillowed. Pillows are well formed and generally marked with a zone of light coloured variolites lying a few centimetres inward of the rim. Variolites range from about 1 to 5 mm in diameter. Tiers of quartz-filled, flat, tabular cavities in pillow interiors, representing successive levels of lava within the pillow as it was repeatedly drained, are a common phenomenon in this group, particularly near the tops of flows. Individual flows are thick (100-300 m) and generally topped with a thin layer (2-10 m) of massive basalt. Overall thickness of the variolitic flows appears to be about 800 m.

Peridotitic komatiites are conspicuous among flows of the komatiitic grouping in that they weather to a deep orange or chocolate-brown colour. They occur singly or in closely associated pairs and are widely distributed through the sequence. Two major types which can be singled out among the peridotitic komatiites are illustrated in Figures 14.4 and 14.5. Figures 14.4, drawn from a field sketch made at locality 1 (Fig. 14.3) shows a profile which is virtually identical to spinifex-textured flows in Munro Township, Ontario (Pyke et al., 1973). The flow is about 14 m thick and comprises an upper chilled zone, a spinifex zone with blades radiating and increasing in dimension downward, a thin laminar zone parallel to flow boundaries, a thick equigranular zone with conspicuous brown weathering, and a lower chilled zone. The other type, shown in Figure 14.5, is a fractionated flow that grades from a lower peridotitic to an upper doleritic zone and is capped by flow-top breccia. It is much thicker (50 m) than the spinifex flow and was evidently formed from a less mafic magma. Most of the other non-spinifex textured flows are variants of the differentiated type but commonly thinner and with a greater proportion of the peridotitic phase.

Apart from the peridotitic komatiites, lavas of the komatiitic grouping are pillowed and massive basaltic flows. Those which are believed with most confidence to be basaltic komatiites are characterized by thin rimmed, irregularly shaped and commonly discontinuous pillows, and by polygonal jointing in both pillowed and massive phases. In some cases they show a brownish weathered surface. The over- and underlying flows of Figure 14.4 are illustrative of some of the pillows and jointing which are thought to be indicative of basaltic komatiites. Sketches of jointing in massive and pillowed ultramafic flows given by Arndt et al. (1979) can be readily duplicated in this sequence. However, the physical characteristics of flows vary widely within this grouping from those with the appearance of basaltic komatiites as interpreted above to those judged to be typical of tholeiitic basalts, and subdivision on the basis of field work alone was not possible.

The succession on Gilmour Island declines in dip from east to west across the island from about 40 to 15 degrees westerly. If repetition by faulting is discounted the total thickness of the assemblage would be about 4500 m. Apart from faulting the rocks are little deformed except for a schist zone, at least 100 m wide, that parallels the strike along the northeast coast of Gilmour Island. Minor pyrrhotite mineralization occurs along the tops of two or three flows on the eastern side of Gilmour Island, but nothing that is likely to be of economic interest was observed.

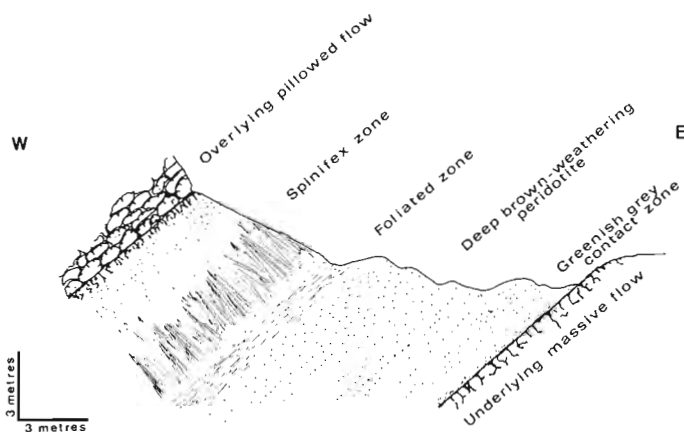


Figure 14.4. Cross-section of a spinifex-textured, peridotitic komatiite flow from Gilmour Island. Locality 1, Figure 14.3.

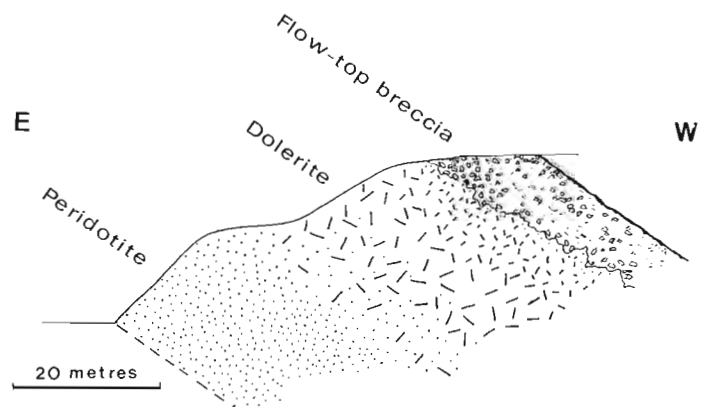


Figure 14.5. Cross-section of a differentiated, peridotitic komatiite flow from Gilmour Island. Locality 2, Figure 14.3.

Correlation

Although units established on the Sleeper Islands cannot be correlated directly with any part of the Flaherty Formation observed on the Belcher Islands, there is an overall similarity between the two assemblages. Rocks on the Sleeper Islands are on strike with Flaherty volcanics on the North Belcher Islands mapped in part by Jackson (1960). These lie west of the section measured near Sanikiluaq and might be expected to be farther offshore and in deeper water than the latter. Consistent with this view is the greater thickness of the Sleeper Islands assemblage (minimum 2000 m) compared with that of the Flaherty Formation near Sanikiluaq (1460 m) and a markedly lower degree of vesicularity. One of the Haig Intrusions at the base of the Flaherty Formation may have a counterpart in the richly feldsparphyric sill at the base of the Sleeper Islands succession.

The komatiitic grouping of the Ottawa Islands undoubtedly correlates with komatiites of Cape Smith Island (Schwarz and Fujiwara, 1977) with which they are on strike. Their projected position southward along the Circum-Ungava Belt would place them west of the Sleeper and Belcher Islands and presumably more remote from the craton. An almost total lack of vesicles in rocks of the Ottawa Islands and a thickness of possibly 4500 m or more is again consistent with this interpretation.

References

- Arndt, N.T., Francis, D., and Hynes, A.J.
1979: The field characteristics and petrology of Archean and Proterozoic komatiites; *Canadian Mineralogist*, v. 17, p. 147-163.
- Bell, R.
1879: Report on an exploration of the east coast of Hudson's Bay; Geological Survey of Canada, Report of Progress, 1877-78, p. 1C-37C.
- Dimroth, E., Baragar, W.R.A., Bergeron, R., and Jackson, G.D.
1970: The filling of the Circum-Ungava geosyncline; in Baer, A.J., ed., *Basins and Geosynclines of the Canadian Shield*; Geological Survey of Canada, Paper 70-40, p. 45-142.
- Fryer, B.J.
1972: Age determinations in the Circum-Ungava geosyncline and the evolution of Precambrian banded iron formations; *Canadian Journal of Earth Sciences*, v. 9, p. 652-664.
- Heiken, G.
1978: Characteristics of tephra from Cinder Cone, Lassen Volcanic National Park, California; *Bulletin Volcanologique*, v. 41, No. 2, p. 119-130.
- Jackson, G.D.
1960: Belcher Islands, Northwest Territories; Geological Survey of Canada, Paper 60-20.
- Leggett, S.R.
1974: A petrographic and stratigraphic study of the Flaherty Formation, Belcher Islands, Northwest Territories; unpublished B.Sc. Thesis, Brock University.
- Manning, T.H.
1947: Explorations on the east coast of Hudson Bay; *Geographical Journal*, London, v. 109, p. 58-75.
- Pyke, D.R., Naldrett, A.J., and Eckstrand, O.R.
1973: Archean ultramafic flows in Munro Township, Ontario; *Geological Society of America*, v. 84, p. 955-978.
- Ricketts, B.D.
1979: Sedimentology and stratigraphy of eastern and central Belcher Islands, Northwest Territories; unpublished Ph.D. Thesis, Carleton University.
- Schimann, K.
1978: Geology of the Wakeham Area eastern end of the Cape Smith Belt, New Quebec; unpublished Ph.D. Thesis, University of Alberta.
- Schmidt, P.W.
Paleomagnetism of igneous rocks from the Belcher Islands, N.W.T., Canada; *Canadian Journal of Earth Sciences*. (submitted)
- Schwarz, E.J. and Fujiwara, Y.
1977: Komatiitic basalts from the Proterozoic Cape Smith range in northern Quebec, Canada; in Baragar, W.R.A., Coleman, L.C., and Hall, J.M. eds., *Volcanic Regimes in Canada*, Special Paper 16, Geological Association of Canada.
- Stirbys, A.F.
1975: A petrographic and geochemical study of the Eskimo Formation, Belcher Islands, Northwest Territories; unpublished B.Sc. Thesis, Brock University.
- Ware, M.T.
1978: Volcaniclastic sediments of the Flaherty Formation, Belcher Islands, Northwest Territories; unpublished B.Sc. Thesis, Carleton University.

**THE MISTASTIN BATHOLITH, LABRADOR-QUEBEC:
AN ELSONIAN COMPOSITE RAPAKIVI SUITE**

Project 750011

R.F. Emslie, B. Cousens¹, C. Hamblin², and J. Bielecki³
Precambrian Geology Division

Emslie, R.F., Cousens, B., Hamblin, C., and Bielecki, J.; The Mistastin Batholith, Labrador-Quebec: an Elsonian composite rapakivi suite; in Current Research, Part A, Geological Survey of Canada, Paper 80-1A, p. 95-100, 1980.

Abstract

The Mistastin Batholith is a composite Elsonian intrusion of Helikian age in central Labrador. Two rock types, pyroxene-hornblende quartz monzonite and biotite-hornblende granite underlie much of the batholith and coarse, alkali feldspar ovoids mantled with plagioclase (wiborgite texture) are widespread in both types. Older anorthositic rocks, probably mainly megaxenoliths, are enclosed by pyroxene-hornblende quartz monzonite. Other xenoliths include a group that can be correlated with the wall rock lithologies and another group of granulitic xenoliths, perhaps from a deeper source. Small intrusions of pyroxene monzonite, biotite granite, and alaskite also form local parts of the batholith. Fluorite is a widespread accessory mineral in biotite-hornblende granites in the southern and western parts of the batholith.

Introduction

The suite of Elsonian intrusive rocks in central Labrador consists of dominant bodies of anorthositic, monzonitic and granitic (adamellite) composition, together with lesser amounts of gabbroic rocks and minor ferrodiorite. The apparent crystallization ages of these rocks lie in a range from about 1350 to 1500 Ma. The igneous activity postdates the Hudsonian Orogeny in the region by some 200 to 300 Ma and is considered to be essentially anorogenic in nature. Rapakivi textures and rapakivi-like chemistries characterize the granitic intrusions (Emslie, 1978) and their association with penecontemporaneous anorthositic rocks is like that of the classic rapakivi intrusions of the Baltic Shield (Vorma, 1976) which have ages in the range of about 1400 to 1700 Ma. (Vaasjoki, 1977).

The Mistastin Batholith underlies about 5000 km² on the Labrador-Quebec boundary about 240 km east-northeast of Schefferville, Quebec. It is one of the largest discrete Elsonian granitic masses in the region. Reconnaissance mapping by Taylor (1975) outlined the batholith and recognized its similarity to other Elsonian granitic masses. He also noted the occurrence of fluorite in the southern part of the batholith (Taylor, 1972). Previous studies within the batholith have been directed primarily toward interpretation of the fossil crater at Mistastin Lake (Taylor and Dence, 1969; Currie, 1971; Grieve, 1975; Marchand and Crocket, 1977).

Elsonian granitic rocks have been relatively neglected by comparison with the efforts expended on the anorthositic and basic rocks. This has been due in part to preoccupation with the fascinating petrological problems presented by the latter but also perhaps due to their generally better exposure. Wheeler (1955; 1969) was the only person to have made extensive field and petrographic observations on the granitic intrusions that form part of the Nain complex. He was able to define subdivisions based mainly upon the mafic silicate assemblages (olivine facies, hornblende facies, biotite facies). He reported fluorite as an accessory mineral in biotite facies of the Tessiarsuyungoakh intrusion.

Present investigations of the Mistastin Batholith are directed toward assessing the geochemical and petrological evolution of the intrusive rocks with a view toward establishing constraints on the sources of the magmas and interpreting the processes and conditions under which they crystallized. Recent geochemical reconnaissance surveys of

waters and lake and stream sediments (Geological Survey of Canada, 1979) show that anomalously high concentrations of U, F, and Mo are localized within the batholith. The nature of processes leading to concentration of these and other economically significant elements will form an integral part of the study.

The initial step of the program, mapping and sampling of the batholith, was begun during the 1979 field season. Work was carried out from June 20 to August 31 by a four-man team, supported by helicopter for two weeks during July.

Geology of the Mistastin Batholith

Distribution of the major rock units of the batholith is indicated on the LANDSAT image in Figure 15.1. Roughly 40 per cent of the batholith is underlain by a dark pyroxene-hornblende quartz monzonite. A younger pale facies biotite-hornblende granite underlies a further 50 per cent. The remaining 5 to 10 per cent of the batholith is composed of anorthositic rocks, including leucotroctolite and minor gabbro, and relatively small masses of pyroxene monzonite, biotite granite and alaskite, most of which are not indicated separately on Figure 15.1.

Country Rocks

Gneisses surrounding the Mistastin Batholith were examined only within a few kilometres of the contact. The gneisses (amphibolite facies) are rather similar around much of the batholith. Regularly-layered biotite- (\pm hornblende)-quartz-plagioclase assemblages are characteristic of much of the rock at the western margin of the batholith. Gneisses at the remaining periphery are, for the most part, distinctly migmatitic carrying up to 50 per cent granitic leucosome. In general, exposure of the wall rock at the contact is poor and a clearly defined contact aureole is not apparent in the field. However, occurrences of garnet, sillimanite, and cordierite (?) were noted close to the contact in several places. Mineral layering and foliation in wall rocks is steeply dipping to subvertical near most contacts; strikes of gneissosity tend to be subparallel to the contact.

Anorthositic Rocks

Several masses of anorthositic rocks occur within the batholith; the largest (about 60 km²) lies immediately south and southeast of Mistastin Lake. All anorthositic rocks so far discovered lie within pyroxene-hornblende quartz monzonite

¹ University of British Columbia, Vancouver

² Concordia University, Montreal

³ McGill University, Montreal



which is commonly medium- to fine-grained near contacts between the two rocks. A considerable range of compositions and textures is present in the anorthositic – rocks from very coarse grained anorthosite with blue iridescent plagioclase to leuconorite, leucotroctolite and local fine- to medium-grained gabbro. Mineral layering and plagioclase lamination occurs sporadically. Fine- to medium-grained granite and quartz monzonite dykes are common locally. The nature and distribution of the anorthositic rocks suggests that most or all of them may be isolated blocks brought up from greater depths by invading pyroxene-hornblende quartz monzonite.

Pyroxene-hornblende Quartz Monzonite

This rock typically has a distinctive coarse grained to porphyritic texture with up to 60 per cent (20 to 40 per cent is the common range) ovoid alkali feldspars with white weathering plagioclase rims (Fig. 15.2, 15.3). The ovoids are typically 2 to 4 cm across with scattered rarer individuals up to 7-8 cm, and less commonly 15-20 cm, across. Plagioclase rims on alkali feldspar ovoids (wiborgite texture) are commonly 1 to 2 mm thick but it is not unusual to find a range of thicknesses up to 5 mm or more in a single exposure. Unrimmed ovoids may occur in the same hand specimen with rimmed ones. Multiple rims may occur on some of the larger individuals. Ovoid cores are commonly speckled with small mafic mineral inclusions which may define or emphasize internal zonal patterns. Quartz is commonly about 15 to 20 per cent of the rock but ranges widely from about 5 to 25 per cent. Quartz grains are usually rounded to subhedral, sometimes showing crystal faces. Colour index normally varies between about 10 and 20. Hornblende is usually the dominant mafic mineral with pyroxene subordinate, in the form of cores within hornblende; locally, however, pyroxene dominates. Opaque oxides are common accessories and biotite is usually present in small amounts. Fresh rocks are dark olive shades but many outcrops are deeply weathered to reddish brown or chocolate brown grus.

Biotite-hornblende Granite

These rocks underlie the largest part of the batholith. Most fresh samples are pale shades of pink or grey but exposed surfaces are commonly stained light to medium rusty brown. Plagioclase-mantled ovoids are typically 2 to 4 cm across but range up to about 15 cm (Fig. 15.4). These commonly comprise 5 to 60 per cent of the rock although local areas are free of mantled ovoids. Quartz normally ranges from 20 to 40 per cent of these granites and typically occurs as small (2 to 4 mm) subhedral to euhedral terminated crystals surrounding large feldspar ovoids. Colour index is mostly in the range 10 to 20 with biotite and hornblende the typical mafic silicates; the ratio of these two minerals is variable but hornblende is more commonly dominant. Small cores of pyroxene occur in hornblende in some rocks which may be transitional to pyroxene-hornblende quartz

Figure 15.1

LANDSAT image of Mistastin Batholith and surroundings. Scale is about 1:500 000. The batholith is outlined in black. Internal subdivisions between pyroxene-hornblende quartz monzonite to north and east and biotite-hornblende granites to south and west (smaller body occurs on eastern side) are indicated by solid white lines. Main outcrop areas of anorthositic rocks are enclosed by dotted white lines. The tadpole-shaped body in the southwest quadrant is pyroxene monzonite. Note that the biotite-hornblende granite areas have generally more subdued relief than areas underlain by pyroxene-hornblende quartz monzonites. Black arrow points north.

monzonites; dykes of biotite-hornblende granite, however, cut typical pyroxene-hornblende quartz monzonites at a number of localities. Disseminated purple fluorite occurs widely in biotite-hornblende granite in the southern and western parts of the batholith. Most occurrences of fluorite appear to be associated with granites having higher than usual biotite:hornblende ratios.

Other Intrusive Rocks

A tadpole-shaped body of pyroxene monzonite and/or syenite intrudes biotite-hornblende granite in the south-western quadrant of the batholith (Fig. 15.1). Most of the rock is coarse grained and carries rimmed and unrimmed alkali feldspar ovoids; medium- and fine-grained facies occur near the margins and fine grained dykes cut the adjacent granite. A well defined strong positive aeromagnetic anomaly coincides with this intrusion.

Smaller bodies of alaskitic granite, equigranular biotite granite and biotite-hornblende granite occur within the batholith but are not shown separately in Figure 15.1. They occur as segregations, dykes, and small intrusive masses.

Dyke Rocks

Granitic dykes including ovoid-bearing granites and quartz monzonites, equigranular biotite and biotite-hornblende granites, and aplites occur widely within the batholith and adjacent to its contacts but are nowhere abundant and most are but a few centimetres to a metre thick. Very rare small pods or seams of quartz and of pegmatitic material were observed locally but true pegmatites are rare or absent.

Small diabase dykes of diverse orientations were mapped at a number of localities within the batholith. Two of the larger olivine diabase dykes noted (5 m and 30 m thick) are vertical and strike northeasterly, subparallel to the swarm cutting the Harp Lake Complex to the southeast.

Xenoliths

Xenoliths, although only rarely abundant, are widely distributed within the Mistastin Batholith. Within a kilometre or so of contacts with country rock gneisses, rotated subrounded to subangular inclusions of wall rock are often present and may be very abundant within a few hundred metres of the walls. At many contacts, however, the granitic rocks are virtually inclusion-free.

In the interior of the batholith a variety of xenoliths were mapped and sampled. These included cordierite- and sillimanite-bearing paragneisses, amphibolite, biotite-quartz-plagioclase gneisses, and granitic gneisses together with a substantial suite of fine- to medium-grained, mafic to felsic granulites. This latter group cannot be readily related to nearby country rock lithologies. Most inclusions are less than 2 m in maximum dimension but masses more than 10 m across are not uncommon. Rounded outlines with sharp boundaries are characteristic of most xenoliths (Fig. 15.5).

Discussion

Anorogenic magmatic suites can be favourable assemblages for providing insights into the processes of magma generation and subsequent differentiation as they are relatively uncomplicated by severe tectonic mixing and contamination. For example, pyroxene-hornblende quartz monzonite forms one of the early large plutons of the Mistastin Batholith. Large blocks of anorthositic rocks contained within this unit are like those closely associated with similar granitic rocks in other Elsonian complexes.

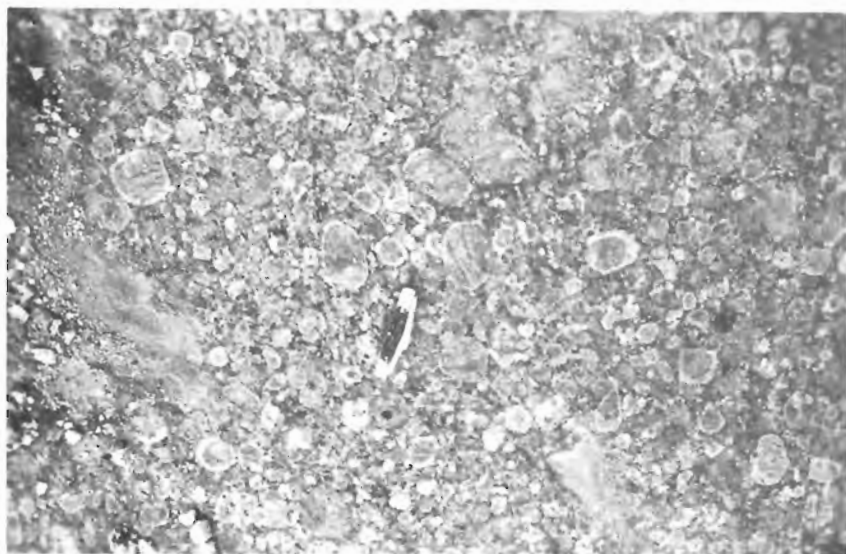


Figure 15.2

Mantled ovoid alkali feldspars in pyroxene-hornblende quartz monzonite. Note the wide range in sizes of ovoids and varying thicknesses of white-weathered plagioclase rims. (GSC 203423-A)

Figure 15.3

Pyroxene-hornblende quartz monzonite with small angular gneiss inclusion (to left and slightly above pocketknife). Note the range of alkali feldspar sizes and of the thicknesses of plagioclase rims. Most are rounded to ovoidal but rare subhedral tablets occur (below knife). (GSC 203423-F)



Their presence implies an earlier stage of basic magmatism perhaps closely related to the production of the subsequent granitic magmas. Granulitic inclusions are widely dispersed in pyroxene-hornblende quartz monzonite and because they are of a higher metamorphic grade than the contiguous wall rocks of the batholith, they are presumably samples of some deeper terrane. It is possible that these xenoliths are samples of the source rocks for the parent magmas of the granitic assemblage. The common richness of the pyroxene-hornblende quartz monzonite in mantled and unmantled large alkali feldspar ovoids seems to imply that these rocks are unlikely to have been liquids but rather are a fraction enriched in early-formed crystals. The younger biotite-hornblende granite is probably a significantly more fractionated rock judging by the higher content of volatile bearing minerals and the presence of fluorite in some facies; common ovoid-rich facies in the unit suggest that crystal accumulation also played some role. Medium- and fine-grained equigranular biotite-hornblende granites, biotite granites, and alaskitic granites that occur as small intrusions and dykes may more closely approximate true liquid compositions.

Anomalously high values of U, F, and Mo in waters, and lake and stream sediments (Geological Survey of Canada, 1979) inside the batholith appear to be localized within, or close to, the biotite-hornblende granites. This is additional evidence that these granites, or parts of them, are relatively more fractionated. Economically interesting mineral occurrences have not yet been identified.

Mineral assemblages in the monzonites, quartz monzonites and granites are capable of providing estimates of a number of intensive variables such as T , P_{solid} , $f_{\text{H}_2\text{O}}$, f_{O_2} , and f_{F_2} and the ranges of variation in these. Such estimates together with analytical data on trace element concentrations in minerals should be useful to monitor and interpret rates and degrees of trace element enrichment or depletion with differentiation. This kind of information can form a quantitative basis for interpretation of ore-forming processes in granitic rocks.



Figure 15.4

Biotite-hornblende granite. Scattered mantled ovoids are common but mantling may be less distinct than in most pyroxene-hornblende quartz monzonites. (GSC 203423-E)



Figure 15.5 *Large rounded inclusion of granitic gneiss in pyroxene-hornblende quartz monzonite. Rounded outlines are typical of many xenoliths. (GSC 203423-B)*

A number of corrections have been made to the geology shown on the published detailed outcrop map of the area around Mistastin Lake (Currie, 1971) both in terms of rock nomenclature and rock distribution. Most notable perhaps is that anorthositic rocks underlie more than double the area previously indicated south and southeast of the lake (see Fig. 15.1).

The weight of evidence and opinion is now heavily in favour of the interpretation that the Mistastin Lake crater is a product of impact by an extraterrestrial object. The main exposures of impact melt rock around the lake were examined and sampled during the field season. In our opinion the preserved remnant outcrops are consistent with a sub-horizontal tabular form for the original melt sheet or sheets; evidence to support a steeply dipping ring dyke or cone sheet structure is not convincing.

References

- Currie, K.L.
1971: Geology of the resurgent cryptoexplosion crater at Mistastin Lake, Labrador; Geological Survey of Canada, Bulletin 207.
- Emslie, R.F.
1978: Anorthosite massifs, rapakivi granites, and Late Proterozoic rifting of North America; *Precambrian Research*, v. 7, p. 61-98.
- Grieve, R.A.F.
1975: Petrology and chemistry of the impact melt at Mistastin Lake crater, Labrador; *Geological Society of America Bulletin*, v. 86, p. 1617-1629.
- Geological Survey of Canada
1979: Regional lake sediment and water reconnaissance data, Labrador, 1978, NTS 13L(N/2), 13M; Geological Survey of Canada Open File 557.
- Marchand, M., and Crocket, J.H.
1977: Sr isotopes and trace element geochemistry of the impact melt and target rocks at the Mistastin Lake crater, Labrador; *Geochimica et Cosmochimica Acta*, v. 41, p. 1487-1495.
- Taylor, F.C.
1972: Reconnaissance geology of a part of the Precambrian Shield, northeastern Quebec and northern Labrador (Part III); Geological Survey of Canada, Paper 71-48, 14 p.

Taylor, F.C. (cont'd)

1975: Geology, Mistastin Lake area, Newfoundland-Quebec; Geological Survey of Canada, Map 1442A.

Taylor, F.C., and Dence, M.R.

1969: A probable meteorite origin for Mistastin Lake; Canadian Journal of Earth Sciences, v. 6, p. 39-45.

Vaasjoki, M.

1977: Rapakivi granites and other postorogenic rocks in Finland: their age and the lead isotopic composition of certain associated galena mineralizations; Geological Survey of Finland Bulletin 294, 64 p.

Vorma, A.

1976: On the petrochemistry of rapakivi granites with special reference to the Laitila massif, southwestern Finland; Geological Survey of Finland Bulletin 285, 98 p.

Wheeler, E.P.

1955: Adamellite intrusive north of Davis Inlet, Labrador; Geological Society of America Bulletin, v. 66, p. 1031-1060.

Wheeler, E.P. II

1969: Minor intrusives associated with the Nain anorthosite; in Origin of Anorthosite and Related Rocks, ed. Y.W. Isachsen; New York State Museum and Science Service Memoir 18, p. 189-206.

**STRATIGRAPHIC RELATIONS OF THE VOLCANIC SEDIMENTARY SUCCESSIONS IN
THE WAWA GREENSTONE BELT, ONTARIO**

Projects 780012 and 770070

K. Attoh
Precambrian Geology Division

Attoh, K., *Stratigraphic relations of the volcanic sedimentary successions in the Wawa greenstone belt, Ontario; in Current Research, Part A, Geological Survey of Canada, Paper 80-1A, p. 101-106, 1980.*

Abstract

A preliminary correlation model for the Wawa greenstone belt is presented from which it is inferred that the following sequences of volcanic and sedimentary rocks can be identified. 1. A basal sequence of epiclastic sediments that appear to have been deposited on a pre-existing granitoid crust is overlain by minor felsic volcanic rocks with local iron formation. 2. A sequence of mafic to felsic volcanic rocks that is locally overlain by iron formation (predominantly carbonate). In the Michipicoten Harbour area this cycle is preceded by a sequence of intermediate-felsic flows which is structurally discontinuous with an overlying succession of mafic flows. 3. Clastic sediments, typified by the Dore Formation, were unconformably deposited on the mafic-felsic volcanic cycle. 4. The sequence that overlies these clastic sediments is dominantly composed of felsic volcanics and associated sediments. In the Josephine Lake-Mildred Lake area mafic volcanic rocks overlie the sediments.

The estimated total thickness of the succession is about 8000 m.

Introduction

The Wawa greenstone belt is located in District of Algoma and extends east-northeast from Lake Superior to the western part of the Sudbury District (Fig. 16.1). General geological features of the belt are shown on the compilation map of Wawa-Manitouwadge sheet (O.D.M., 1972). On this scale and also because of lack of recent mapping, the stratigraphic relationships between the volcanic and sedimentary successions are obscure.

During June and August 1979, the writer examined some sections in the Wawa volcanic belt. Because of lack of accessibility due to thick forest it was found most profitable to study sections along the main access routes. The areas studied are:

1. A "fume-burnt" area with little vegetation located north-east of Wawa and between Highways 17 and 101. The area is herein referred to as the Lena Lake-Mildred Lake-Josephine Lake area.

2. About 10 km of section on Highway 101, which also provides access to the "fume-burnt" area above.
3. A beach section along the northeast shore of Lake Superior between Michipicoten Harbour and the estuary of Michipicoten River.
4. Nearly 40 km of discontinuous sections along Highway 17 between Wawa and White River.
5. An area of poor outcrop along the northeastern margin of the belt between Dubreuilville and Lochalsh.

Previous stratigraphic studies in the Wawa greenstone belt were largely concerned with origin of iron formation in relation to volcanic stratigraphy (Goodwin, 1962). It was recognized in these studies that iron formations terminate cycles of mafic-felsic volcanism and this was found useful in correlating stratigraphic units over broad areas. On the other hand, volcanic successions without iron formation or even distinct mafic-felsic volcanic cycles, are difficult to correlate. One objective of the present study is to identify sequences that could be used in correlating units within the volcanic succession.

**Lena Lake-Mildred Lake-Josephine Lake
("fume-burnt") Area**

The lithologic units in this area show well preserved stratigraphic relations and many units can be traced throughout the entire area (Fig. 16.2). The pillow facing in mafic flows is generally consistent with "top" directions in clastic sediments and the identification of a syncline suggests that the local stratigraphy has considerable continuity (Columns A and B, Fig. 16.3).

Section A: East of Goetz Lake

South of Josephine Lake, pillowed lavas belonging to the mafic volcanic unit are present. The base of this unit is not exposed so the thickness represented in Column A, Figure 16.3 is that exposed east of Wawa Lake on Highway 101.

The felsic volcanic unit above the mafic volcanic unit lacks primary stratification, but exhibits a cleavage which is parallel to the lithologic boundary. The rock is fragmental,

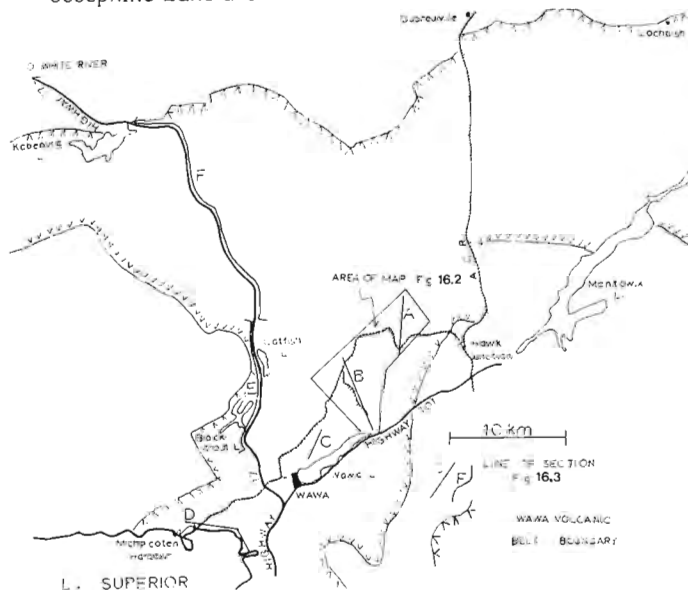


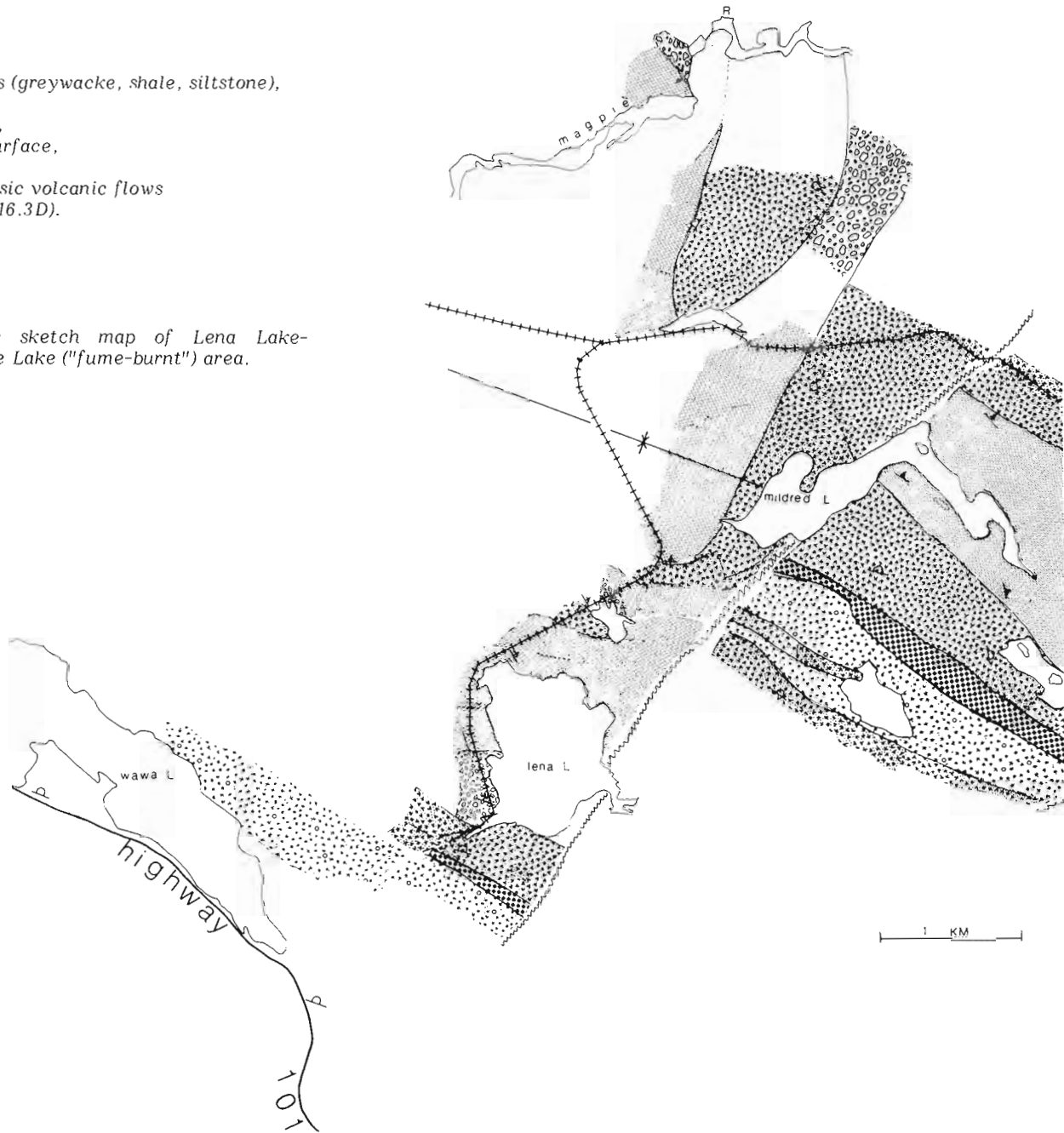
Figure 16.1. Index map of the Wawa greenstone belt showing the sections described.

1. = mafic volcanics,
2. = felsic volcanics,
3. = iron formation,
4. = clastic sediments (greywacke, shale, siltstone),
5. = conglomerate,
6. = volcanic breccia,
7. = synclinal axial surface,
8. = fault,
9. = intermediate-felsic volcanic flows (used in Figure 16.3D).

Facing Directions

- pillows
- sediments

Figure 16.2. Geologic sketch map of Lena Lake-Mildred Lake-Josephine Lake ("fume-burnt") area.



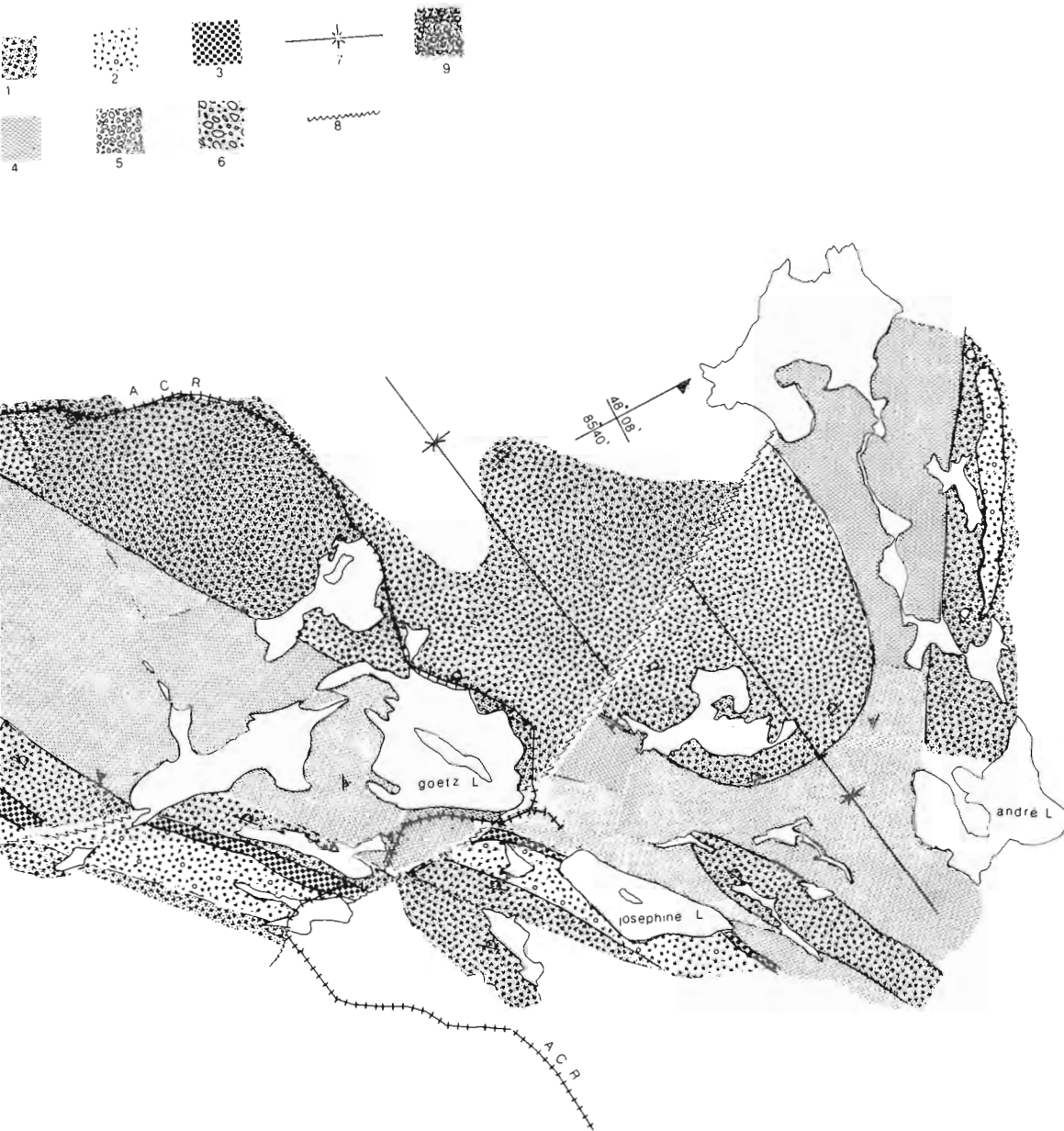
with distinct felsic volcanic fragments of lapilli size, and does not appear to have been welded. The unit thickness is variable (Fig. 16.2), ranging from less than 300 m to over 700 m. The contact is conformable with the underlying mafic volcanic unit, but because the cleavage is subparallel to the lithic interface it may be in part tectonic.

Iron formation overlies the fragmental felsic volcanic unit. Close to the contact, iron formation appears to be in part produced by replacement of fragmental felsic volcanics by iron carbonate. The resulting breccia consists of angular fragments of felsic volcanics and finely bedded sediments in an iron carbonate matrix. The iron formation unit in the area is dominantly steel-grey micritic iron carbonate which weathers dark brown. Sulphide-rich horizons occur locally near the top of the iron formation. The iron formation varies in thickness from less than 50 to over 200 m; thinner zones corresponding to thicker underlying felsic volcanics.

The mafic volcanic unit (MV2), which overlies the iron formation, is well exposed in the area and increases in thickness westward from 0 to over 700 m. It consists of alternating pillowed and massive flows. Hyaloclastite and pillow breccia zones are associated with the pillowed flows, in both lateral and vertical facies changes. An estimate of total number of flows was not possible because it was not always possible to recognize flow unit boundaries. The boundaries of the pillow flow units conform crudely with the boundaries of the lithologic unit (unit MV2), and with the pillow stratification.

Epiclastic Sediments. Clastic sediments overlying the mafic volcanics comprise greywacke, siltstone and shale, which have variously developed and preserved Bouma cycles. Soft sediment deformation in the form of convoluted and disrupted strata occur within these sediments northeast of

Figure 16.2. (cont'd)



André Lake, and locally, conglomerate zones consisting of clasts of iron formation occur near the base. Tops based on crossbedding, migrating ripples and graded bedding are consistent with those of the underlying units and suggest that the sequence is conformable. However, local fold structures are present as well as a penetrative north-trending cleavage which is not related to regional structure. Thickness ranges from 400 to 1500 m.

Mapping of the sedimentary strata has revealed the presence of a syncline which plunges westward and is overturned to the north. Although the underlying iron formation could not be traced to the north limb of the syncline, the stratigraphy is roughly the same on the two limbs of the syncline (Fig. 16.2).

A mafic volcanic unit (MV3), which forms the core of the syncline, is the youngest unit in Section A. Around the nose of the fold the pillow facing in the unit is conformable with the synclinal structure. In the western parts of the same unit, the pillows strike consistently north-south and face west, suggesting a structural break between the mafic

volcanic unit (MV3) and the underlying sediments. The trend of the pillows in the mafic volcanic unit is parallel to the cleavage in the underlying sediments, indicating that the pillow orientations may in part be tectonic

Section B: Lena Lake-Mildred Lake

The sequence west of Mildred Lake fault differs from that described above in the following ways: (i) the preserved thickness of clastic sediments west of the fault is much greater than east of the fault, and (ii) conglomerate zones are more extensive in the clastic sediments west of the fault than east of the fault (Fig. 16.2).

However, the succession mafic volcanics-felsic volcanics-iron formation-mafic volcanics is identical on both sides of the fault and the units can readily be correlated (Fig. 16.3). A more or less complete sedimentary cycle is preserved along the Algoma Central Railway tracks from Lena Lake to the main tracks.

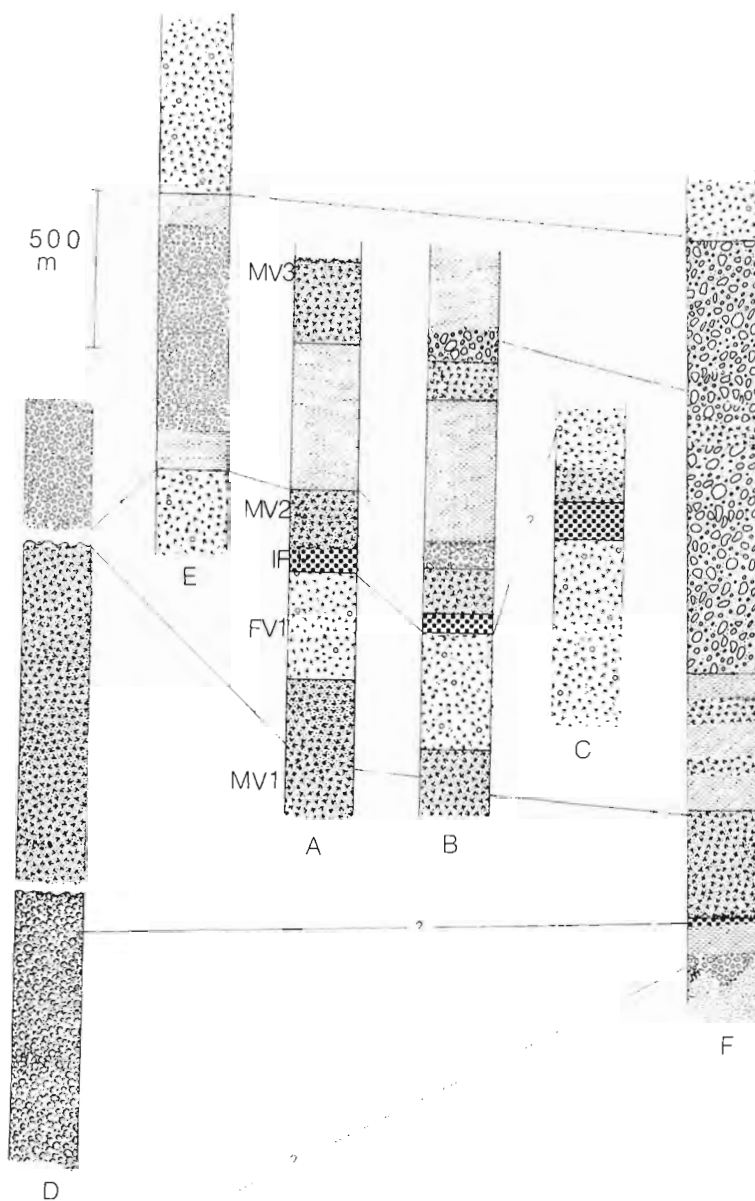


Figure 16.3. A stratigraphic correlation chart for the Wawa greenstone belt. The locations of sections are shown on Figure 16.1. Lithic symbols are the same as in Figure 16.2.

Clastic Sedimentary Cycle. At the base, the sediments consist of rounded pebble to boulder clasts in a sand to granular matrix. Some of the clasts are mafic volcanic and the material is largely unsorted and unstratified. This unit is overlain by a coarse wacke-sediment interbedded with micaceous sandstone, thin carbonate-bearing layers, and green micaceous siltstone. Some greywackes show well developed turbidite features. Crossbedded quartz-arenites occur above the turbidite facies. The arenites, which outcrop just below the mafic volcanic rocks (MV3), mark the top of a lower sedimentary cycle.

The conglomerate above the mafic volcanic unit (MV3) marks the beginning of a second cycle of clastic sedimentation. Locally, the mafic flows are interbedded with the clastic sediments, and the sediments can be traced into coarse volcanic breccia. Along the Magpie River the sediments sharply overlie volcanic breccia, but elsewhere volcanic breccia appears to grade into the sediments.

It is very likely that the lower clastic sequence of Column B is the equivalent of the Dore Formation, whose type section lies farther west in the Wawa Belt.

Section C: Wawa Lake – Helen Mine Area

This section is located about 7 km west of Mildred Lake fault and is labelled C on Figure 16.1. It is chiefly a felsic fragmental volcanic unit consisting of crystal tuffs (welded tuffs with spherulitic structures near the base) and lapilli tuffs with agglomerate zones containing bomb-size fragments, some of which preserve fusiform shapes. Mesoscopic folds occur in the unit, but they are unlikely to have increased the apparent thickness, which is 2000 m. This unit in Section C is a more proximal facies equivalent of the felsic fragmental unit in Section B.

The iron formation in Section C is not the same as that shown in Sections A and B. Another iron formation unit, which occurs above the one shown in Section C, can be traced into the iron formation in Sections A and B. This illustrates the problem of using iron formation horizons for correlations.

Lake Superior–Michipicoten Harbour Area: Section D

The section was studied to determine the relationship between the volcanic sequences and the Dore Formation near its type locality. The succession is shown in Section D, and location of section on Figure 16.1.

Felsic-intermediate Volcanic Sequence

The rocks exposed between Sandy Beach and Michipicoten River include pillowed mafic-intermediate flows and felsic flows. Fragmental felsic rocks are only exposed off the coast line and include tuff breccias and lithic tuffs. Tops are consistently to the southwest. Some pillow structures are amoeboid and can be traced into fragments of vesicular leucocratic lava enclosed in hyaloclastic debris. The felsic rocks include finely laminated "flow rocks" and coarser fragmental rocks with smeared-out lapilli-size leucoclasts.

The conformable succession of felsic-intermediate volcanic rocks is structurally discontinuous with a mafic volcanic succession to the west. The contact between the two sequences is not exposed, being in part intruded by a quartz monzonite stock, and appears to be faulted. However, because the sequence decreases in age westward, it is inferred that the felsic succession is older than the mafic sequence (see below). The felsic sequence is over 2000 m thick.

Mafic Volcanic Sequence

This sequence, exposed west of Sandy Beach, almost exclusively comprises pillowed and massive mafic flows. The pillows are generally well formed and rarely vesicular. Some large, elongated pillows suggest lava toes origin, but no bifurcation was observed. In some places the elongation of pillows is clearly tectonic, being parallel to the cleavage in the fine interpillow sediments. "Cherty" rocks occur and are considered to be primary chemical precipitates. Felsic volcanic rocks interbedded with the iron formation occur only as beds a few metres thick. The massive mafic flows are strongly cleaved and the cleavage is subparallel to pillow stratification, especially near the contact with the Dore Formation.

The contact with Dore Formation is exposed at Michipicoten Harbour, and is marked by strongly deformed zones in which mafic schists at the base of the Dore

sediments are isoclinally folded. The volcanic rocks strike north here, while the contact strikes northeast, and the Dore conglomerate contains clasts of mafic volcanics. This angular unconformity is evidence that pre-Dore volcanics were deformed before the deposition of the Dore sediments.

Dore Formation

The base of the Dore Formation is exposed at Michipicoten Harbour and can be traced about 2 km west to the shore of Lake Superior. In the Michipicoten Harbour area the Dore Formation is a conglomerate with rounded clasts ranging from pebble to boulder size. The clasts include quartz-feldspar pegmatoid rocks, amphibole-bearing granitoid rocks and black chert (iron formation?). Clasts of mafic volcanic rocks occur but are not abundant. The matrix is a mafic (chloritic) rock which is strongly cleaved and folded. Stratification features are rare, and tops could not be determined.

The Dore Formation is correlated with the clastic sediments in Lena Lake-Mildred Lake-Josephine Lake area (Fig. 16.3). The pre-Dore volcanic succession in Sections B and D are quite different and the angular unconformity between the Dore sediments and volcanics in the Michipicoten Harbour area is absent to the northeast (e.g. Section B). The distinct pre-sediment iron formation is absent from the Michipicoten Harbour section. For this reason, the pre-Dore sequences in the Michipicoten area are correlated with the lower part of the Lena Lake-Mildred Lake section, as shown on Figure 16.3.

Highway 17 (Trans-Canada area)

Highway 17 provides a useful access to the major lithologic units in the Wawa belt. For convenience, the section along Highway 17 is divided into (1) a southern portion ending about 25 km north of Wawa, and (2) a northern portion which ends in the granitic rocks north of the belt. The sections are respectively labelled E and F on Figure 16.1.

Section E: Southern Portion of Highway 17

The section begins about 10 km north of Wawa. The succession is shown on Section E and its correlations with previously described sections are indicated. Tops could not be determined in this section except by comparing the section with nearby sequences.

Felsic Volcanics (post-Dore). This unit outcrops between Black Trout Lake and the northern end of the section. It is characterized by a penetrative foliation which is conformable with the southeast dipping foliation in the underlying Dore sediments. The felsic volcanics contain discontinuous bands of smeared-out fragments which may represent original volcanic fragments, but unequivocal evidence of primary stratification was not observed. Irregular chloritoid zones are present and weather out to give pseudo-folding structures. Fine grained "glassy" felsic lenses may represent cherty sediments, as suggested by the lack of fragmental textures. At the northern end of the section west of Catfish Lake the felsic rocks are interbedded with mafic rocks containing euhedral prismatic crystals of actinolite(?) randomly oriented on the cleavage/bedding surface. The interface between the felsic rocks and the actinolite-bearing rocks is sharp and does not suggest an intrusive relationship.

West of Catfish Lake (Fig. 16.1) an antiformal structure is defined by change in dip of the layering and is considered to be a localized closure in the regional synclinorium (Fig. 16.3). The core of this regional synclinorium plunges west (Fig. 16.2) and in this area is occupied by felsic volcanics which overlie the Dore sediments.

Section F: Northern Section Along Highway 17

The succession along this portion of Highway 17 is shown in Section F.

Volcanic Belt and Granitoid Basement Relation. The contact between metasediments of the Wawa belt and weakly foliated intrusive granodiorite is exposed 40 km north of Wawa along the new Dubreuilville road. At the contact, the metasediments have been amphibolitized and cut by granitoid veins producing an intrusive breccia. The granodiorite is more weakly foliated farther away from the contact and the metasediment is well stratified farther away from this contact. A quartz monzonite stock is intrusive into the contact zone on Highway 17 near Kabenung Lake. The contact is not exposed, but blocks of partially digested mafic volcanic fragments are enclosed in unfoliated quartz monzonite.

Earliest Sedimentary Unit. The altered metasediments described above can be traced into less metamorphosed greywacke and conglomerate which consists of distinct granitoid pebbles and cobbles up to 30 cm in diameter in a recrystallized greenish matrix. Stratification in the conglomerate is deflected around the bigger undeformed cobbles, whereas the smaller pebble-granule clasts are stretched out, grading into augen schists. Crossbedded strata indicate considerable movement along localized horizons within the unit. The transposed beds with deformed crossbedding (rotated to steep angles to stratification) show "rootless" tight isoclinal folds preserved between shear zones. These shear zones are parallel to the regional lithologic boundary. Graded bedding is preserved and provides general facing of the unit. As this unit occurs at the core of an anticline and contains granitoid fragments, it is interpreted to be the basal sediments in the Wawa belt. The preserved estimated thickness of the unit is 600 m.

The boundary between the basal sediments and the overlying mafic volcanic unit is marked by a 100 m thick felsic volcanic unit with interbedded iron formation. This is another situation where iron formation terminates clastic sedimentation rather than a mafic-felsic volcanic cycle.

Mafic Volcanics. A mafic volcanic unit composed of pillowed flows, pillow breccia, hyaloclastic breccia layers and minor massive flows and thin beds of clastic sediments, overlies the lowermost sediments. The pillows are generally well formed, grading into smaller equant pillows (pilloids) and pillow breccia. This unit forms open folds with upright axial surfaces which to the south are overturned. Estimated thickness is 600 m.

Interbedded Clastic Sediments and Mafic Volcanic Rocks. The lower mafic volcanics are overlain by a unit consisting of interbedded clastic sediments and mafic volcanics. Its boundary with the underlying mafic volcanic unit is conformable, and the unit is characterized by a high proportion of clastic sediments interbedded with coarse grained massive mafic flows. A hyaloclastic breccia zone was the only primary stratification observed in the interbedded mafic volcanics. Some of the massive mafic rocks may represent sills. The unit is an estimated 800 m thick.

Volcanic Breccia. The preserved thickness of this unit is about 2000 m (Fig. 16.3) and a petrographic study of the volcanic breccia is in progress, with a view to identifying its environment of deposition.

This rock is coarsely fragmental, with some of the angular fragments well over 30 cm in maximum dimension. These appear to form discs which lie in a shallow dipping penetrative cleavage. Most of the fragments are aphyric felsic volcanic rocks. The matrix is a coarse greywacke tuff-breccia which is darker than the "clasts". There is a continuous gradation between fragments and matrix, such that it is difficult at places to differentiate between matrix and fragments. Size zonation of fragments occurs - large clasts are concentrated in certain zones along the strike of "strata". The shallow dipping foliation surface is parallel to stratification in the rare, finely laminated, cherty, rocks and interbedded crystal-rich layers. The axial surface of mesoscopic isoclinal folds is also parallel to the stratification surface.

Near the contact with the underlying unit, the volcanic breccia is intruded by a thick diabase dyke. The enclosed blocks of sediment have been partially fused to produce a pink felsite rock with preserved "ghost" stratification. The volcanic breccia unit is interbedded with the mafic volcanic rocks. The boundaries and dominant cleavage surface are conformable with the underlying mafic volcanic-sedimentary unit.

Conclusions

The lithostratigraphic units described here include the major rock units exposed in the Wawa greenstone belt. On the basis of the sections studied, it is concluded that iron formation horizons are of limited use in correlation because

they occur at various stratigraphic levels and are absent or obscure in some successions. Thus, correlation based on identification of similar sequences is more reliable. In the Wawa belt, some distinct sequences are recognized on the basis of structural discontinuity. In addition, sequences may be inferred from changes in characteristics of lithologic units such as from predominantly epiclastic sedimentation to volcanism or vice versa.

Acknowledgments

The Ontario Geological Survey, Ministry of Natural Resources, provided logistic support for the field work. I am especially grateful to R.P. Sage of O.G.S. for all his help during the summer. I am also grateful to K.D. Card for recommending the area and visiting me in the field. I also wish to thank W.F. Fahrig and K.D. Card for reading and improving the manuscript.

References

- Goodwin, A.M.
1962: Structure, stratigraphy and origin of iron formations, Michipicoten area, Algoma District, Ontario, Canada; Geological Society of America Bulletin, v. 73, p. 561-586.
- Ontario Division of Mines
1972: Manitowadge-Wawa sheet; Ontario Division of Mines, Geological Compilation series, Map 2220.

NEW GENERA OF TRIASSIC AMMONOIDEA

Project 670576

E.T. Tozer

Institute of Sedimentary and Petroleum Geology, Ottawa

Tozer, E.T., *New genera of Triassic Ammonoidea*; in *Current Research, Part A, Geological Survey of Canada, Paper 80-1A*, p. 107-113, 1980.

Abstract

Eoprotrachyceras, *Pterosirenites*, *Pseudotibetites*, *Pleurodistichites*, and *Neohimavatites* are proposed as new genera of Triassic Ammonoidea. Type species of *Neohimavatites* is *Himavatites canadensis* McLearn. Type species of the others are new and are described (*Eoprotrachyceras matutinum*, *Pterosirenites auritus*, *Pseudotibetites pax*, *Pleurodistichites stotti*).

Superfamily TRACHYCERATACEAE (Haug 1894)

Family ARPADITIDAE Hyatt 1900

Subfamily PROTRACHYCERATINAE Tozer 1971

Genus *Eoprotrachyceras* Tozer n. gen.Type species: *Eoprotrachyceras matutinum* n. sp.Diagnosis: Protrachyceratinid like *Protrachyceras* but with a ceratitic, not ammonitic suture line.

Discussion: Mojsisovics (1882, p. 119) described the saddles of *Ammonites archelaus* Laube (type species of *Protrachyceras* Mojsisovics) as denticulate, although this conclusion evidently was not based on data provided by the holotype, which is from the Wengen Beds of what is now northern Italy. A specimen from Hungary, identified by Mojsisovics (1882, pl. 31, fig. 1) as "*Trachyceras*" *archelaus* definitely has an ammonitic suture. In northeast British Columbia a clear succession of Ladinian zones has been defined (Tozer, 1967, p. 27-30; 1971, p. 1018). The protrachyceratinids from the Subasperum Zone, at the base of the sequence (e.g. *Eoprotrachyceras matutinum* n. sp.) unquestionably have ceratitic suture lines. Those from the younger zones (Poseidon, Meginae, Maclearni) have ammonitic suture lines. Most or all of the specimens from the younger zones are referable to *Protrachyceras sikanianum* McLearn. Krystyn and Mariolakos (1975, p. 187) described what appears to be a comparable situation in Greece, where they noted that "*Protrachyceras*" with ceratitic suture lines occurs below *Protrachyceras archelaus*. A succession of protrachyceratinids, the earlier with ceratitic, the later with ammonitic suture lines, thus seems established. The generic designation *Eoprotrachyceras* is accordingly proposed to accommodate the earlier forms. Except for the suture lines *Eoprotrachyceras* and *Protrachyceras* are similar as regards lateral tuberculation and ventral sculpture (moderately deep sulcus bordered by more or less clavate tubercles).

Composition of the genus: *Eoprotrachyceras matutinum* n. sp., *Trachyceras judicarium* var. *subasperum* Meek, *Trachyceras meeki* Mojsisovics, *Trachyceras americanum* Mojsisovics, *Trachyceras* (*Protrachyceras*) *lahontanum* Smith, *Trachyceras* (*Protrachyceras*) *dunni* Smith, *Trachyceras margaritosum* Mojsisovics, *Trachyceras curionii* Mojsisovics.

Age and distribution: Early Ladinian, Subasperum Zone, British Columbia, Nevada; Buchenstein and equivalent beds, Tethys.

Eoprotrachyceras matutinum n. sp.

Plate 17.1, figures 1-7

Figure 17.1a

Protrachyceras cf. *P. meeki* Mojsisovics; Tozer, 1967, p. 27, 68, pl. 8, fig. 1,2.

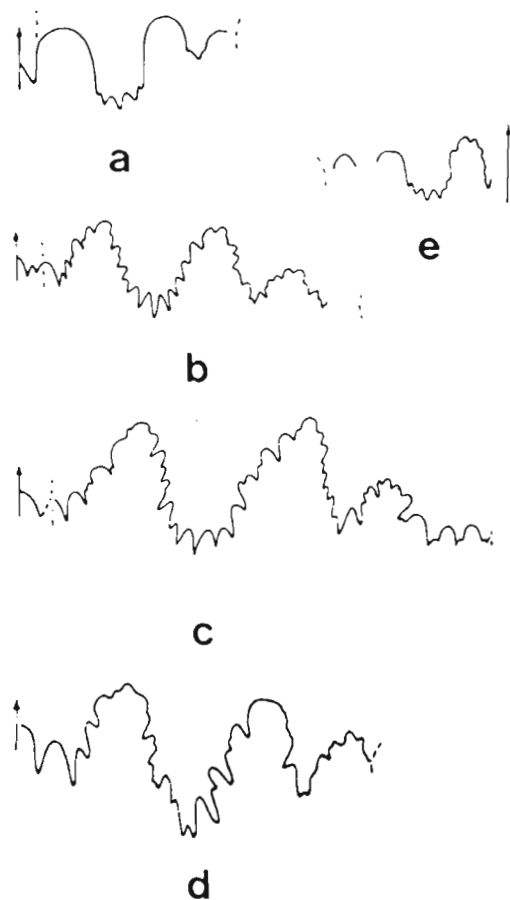
Registered material: Holotype GSC 28632, paratype GSC 28633, GSC locality 83862.¹ GSC 18900, GSC 18901 (topotypes ?), GSC locality 46484.

Diagnosis: *Eoprotrachyceras* at least 40 mm in diameter, at which size umbilical width about 35 per cent. Outer whorl with up to 6 spirals of tubercles; one weak umbilical, 2 or 3 lateral, one marginal and one ventral.

¹ All GSC localities referred to in this paper are described in Table 17.1

Table 17.1

GSC Localities	(All British Columbia)
9161	Pardonet Formation, talus block, south bank Peace River near west end of Pardonet Hill. NTS Ne-Parle-Pas Rapids 94 B/3 E. F.H. McLearn, 1917. Probably from locality 64606. (McLearn, 1960, p. 116). Lower Norian, Dawsoni Zone.
9373	Pardonet Formation, talus block, Juvavites Gully, Pardonet Hill. NTS Ne-Parle-Pas Rapids 94 B/3 E. F.H. McLearn, 1937. Probably from locality 64606. (McLearn, 1960, p. 7) Lower Norian, Dawsoni Zone.
46484	Sulphur Mountain Formation, Llama Member, unit 3, section 11 (Pelletier 1963, p. 41), east flank of high hill (elevation 6483 feet) 8 miles north of Lower Blue Lake, NTS Wapiti Lake 93 I/10 W. B.R. Pelletier, 1961. (Tozer, 1967, p. 68) Ladinian, Subasperum Zone.
64606	Pardonet Formation, section high on west side of Pardonet Hill, between localities 6 and 10 (Tozer, 1965, fig. 1), NTS Ne-Parle-Pas Rapids 94 B/3 E. Lower Norian, Dawsoni Zone (Malayites bococki bed).
66027	Pardonet Formation, north of Nevis Creek, 57° 23' N, 123° 23' W, NTS Mount Withrow 94 G/6 W. D.F. Stott, 1964. (Tozer, 1967, p. 60) Middle Norian, Columbianus Zone.
68180	Pardonet Formation, section 1 km southwest of summit of Mount McLearn, NTS Eight Mile Creek 94 N/3. E.T. Tozer, 1965. (Tozer, 1967, p. 59-61) Lower Norian, Kerri Zone.
68305	Pardonet Formation, spur on west side of Mount Ludington, NTS Nabesche River 94 B/6. E.T. Tozer, 1965 (Tozer, 1967, p. 54) Middle Norian, Columbianus Zone.
83862	Sulphur Mountain Formation, Llama Member, section on east limb of syncline 20 km north of Wapiti Lake, NTS Wapiti Lake 93 I/10 W. E.T. Tozer, 1969. Ladinian, Subasperum Zone. About 45 m below bed with Progonoceratites poseidon Tozer (Poseidon Zone) (Tozer, 1971, p. 1018).



- a. *Eoprotrachyceras matutinum* n. sp. (X 2) GSC 28632 (Plate 17.1, figures 4, 5)
- b. *Pterosirenites auritus* n. sp. (X 2) GSC 28735 (Plate 17.1, figures 18-20)
- c. *Pterosirenites auritus* n. sp. (X 2) GSC 28734 (Plate 17.1, figures 21, 22)
- d. *Pseudotibetites pax* n. sp. (X 4) GSC 28745 (Plate 17.1, figures 8, 9)
- e. *Pleurodistichites stotti* n. sp. (X 4) GSC 28921 (Plate 17.1, figures 15-17)

Figure 17.1. Suture lines.

Plate 17.1

Figures are natural size

Arrows indicate position of last septum

Numbers in parentheses are of GSC localities (Table 17.1)

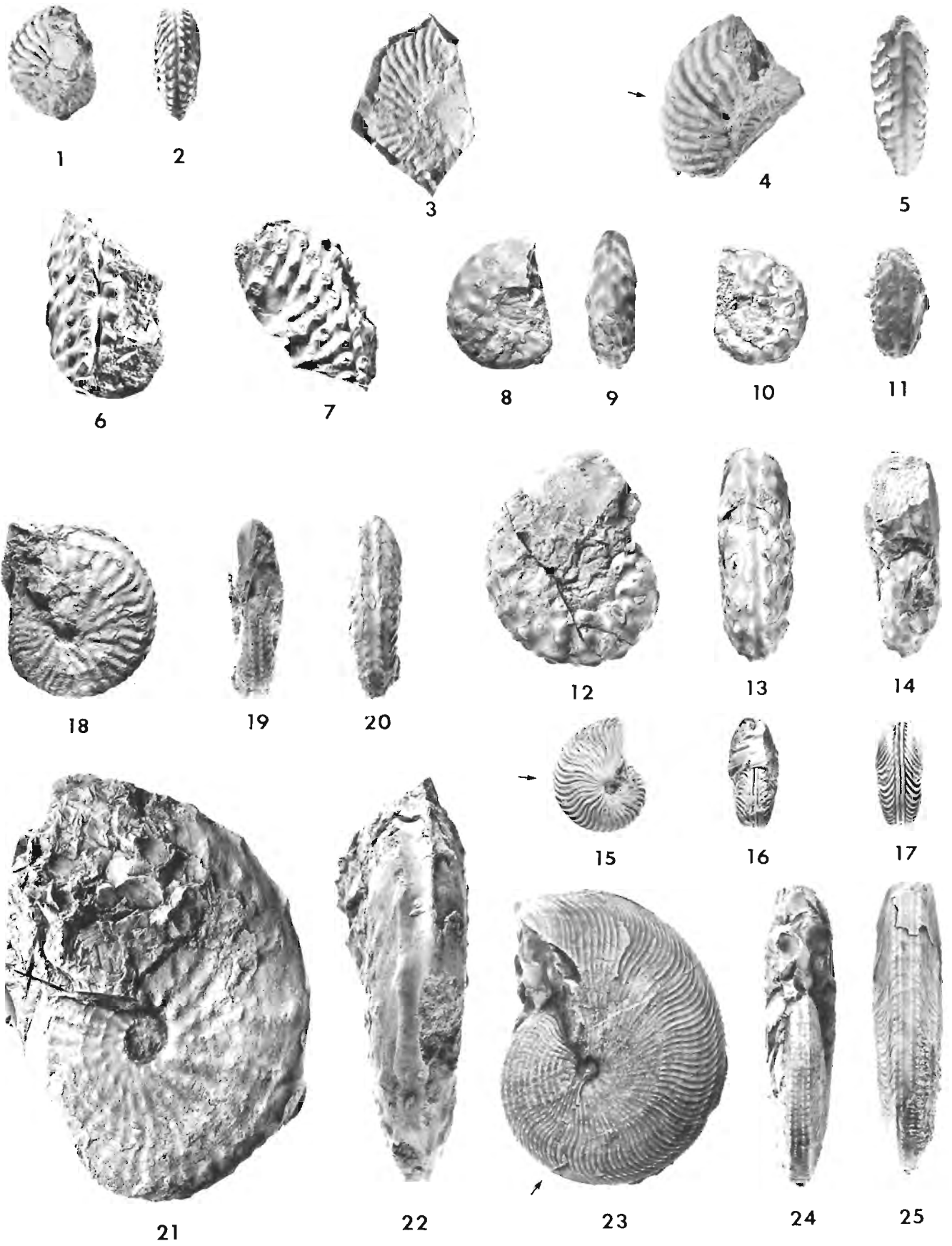
Figures 1-7 **Eoprotrachyceras matutinum** n. gen., n. sp.
1, 2, GSC 18900 (46484). 3, GSC 28633, rubber mould of paratype (83862).
4, 5, holotype, GSC 28632 (83862).
6, 7, GSC 18901 (46484).

Figures 8-14 **Pseudotibetites pax** n. gen., n. sp.
8, 9, holotype, GSC 28745. 10, 11, paratype, GSC 28747. 12-14, paratype, GSC 28746. All from GSC locality 9373. All appear to be septate.

Figures 18-22 **Pterosirenites auritus** n. gen., n. sp.
18-20, paratype, GSC 28735, phragmocone.
21, 22, holotype, GSC 28734, an apparently complete phragmocone. (68180).

Figures 15-17 **Pleurodistichites stotti** n. gen., n. sp.
Holotype, GSC 28921 (66027).

Figures 23-25 **Neohimavavites canadensis** (McLearn).
GSC 28877 (68305).



Discussion: The holotype (Plate 17.1, figures 4,5), the remains of an individual estimated to have attained a diameter of at least 40 mm, has umbilical, 2 lateral, marginal and ventral tubercle-spirals. It is preserved as internal mould and the tuberculation is subdued, evidently reflecting the development of a preseptal layer. GSC 28633 (Plate 17.1, figure 3) and GSC 18901 (Plate 17.1, figures 6, 7) do not preserve the umbilical edge. They, unlike the holotype, have 3 lateral spirals. On GSC 18901 the inner spiral is of larger tubercles than the outer two. This specimen is the remains of an individual appreciably larger than the holotype. GSC 18900 (Plate 17.1, figures 1,2) has two lateral spirals, like the holotype, but barely perceptible umbilical tuberculation. The suture line (Fig. 17.1a) is shown only by the holotype. Although the 4 specimens assigned to this species differ from one another in details, because they are evidently from the same level at the same place, they are interpreted as representing one species of **Eoprotrochyceras**, comparable with **E. meeki** (Mojsisovics), but more compressed and with less pronounced umbilical tuberculation.

Subfamily SIRENITINAE Tozer 1971

Genus **Pterosirenites** Tozer n. gen.

Type species: **Pterosirenites auritus** n. sp.

Diagnosis: Inner whorls like those of **Sirenites** except for having a more angular umbilical shoulder; outer whorls with the braided keels replaced by large clavi arranged **en echelon**.

Discussion: Affinity with **Sirenites**, an older (Carnian) genus, is obvious from the similarity of the phragmocones. **Pterosirenites** is distinguished by the acquisition of modified ventral sculpture on the outer whorl. **Neosirenites** also has modified ventral sculpture on the outer whorl but of a different nature, being alternating clavi and spines, not calvi alone.

Composition of the genus: Certainly known only by the type species. The inner whorls of **Pseudosirenites auritus**, although obviously **Sirenites**-like, differ from those of **Sirenites** and **Striatosirenites** (Carnian) and **Argosirenites** (Middle Norian) in having a distinctly angular umbilical shoulder. "**Sirenites**" **nabeschi** McLearn, and the specimens from northeastern USSR identified by Bychkov et al. (1976, plates 51, 52) as **Argosirenites obrucevi** (Bajarunas), **A. obrucevi** f. **nabeschi** McLearn, **A. nelgehensis** (Arkhipov) and **A. kiparisovae** (Zharnikova), have umbilical shoulders similar to that of **Pterosirenites auritus**. None of the specimens concerned show clavi, but this is probably a consequence of incomplete preservation. All are probably representatives of **Pterosirenites**.

Age and distribution: Lower Norian, Kerri Zone, northeast British Columbia; **Pinacoceras verchojanicum** Zone, northeast USSR (?).

Pterosirenites auritus n. sp.

Plate 17.1, figures 18-22

Figures 17.1 b, c.

Sirenites nabeschi McLearn; Tozer, 1967, p. 60 (only), non McLearn, 1939, p. 53.

Registered material: Holotype GSC 28734, 4 paratypes, GSC 28735-28738, GSC locality 68180.

Diagnosis: **Pterosirenites** with phragmocone attaining a diameter of about 85 mm, at which whorl height about 55 per cent, width about 30 per cent, umbilical width about 15 per cent of diameter. Six tubercle-spirals on whorl side (umbilical, four lateral, marginal). Clavi on outer whorl spaced at about five to a quarter whorl.

Discussion: The holotype (Plate 17.1, figures 21, 22) has braided keels, with two or three ventral tubercles adjacent to each marginal tubercle, at the beginning of the outer whorl. Adorad, at a whorl height of about 25 mm, the small ventral tubercles are replaced by clavi. Lateral sculpture comprises a tubercle spiral on the umbilical shoulder; three relatively prominent spirals on the inner half of the flank; a faint spiral on the outer half; and a prominent marginal spiral. Where the clavi are developed the marginal spiral is of large tubercles, matching the clavi in distribution. GSC 28735 (Plate 17.1, figures 18-20) clearly shows the **Sirenites**-like sculpture that characterizes much of the phragmocone. On this specimen there are only two spirals on the inner flank. Incomplete specimens from the type locality indicate that some individuals attained a size appreciably larger than the holotype. **Pseudosirenites auritus** and "**Sirenites**" **nabeschi** McLearn are probably congeneric, as mentioned above, but they are probably not conspecific in that the tuberculation on the outer flank of "**S.**" **nabeschi** is more prominent than on **P. auritus**.

Genus **Pseudotibetites** Tozer n. gen.

Type species: **Pseudotibetites pax** n. sp.

Diagnosis: Sirenitinid like **Pterosirenites** but inner whorls thicker, with notched rather than braided keels, and with more discrete clavi on the outer whorl.

Discussion: The clavi arranged **en echelon** and the absence of a deep notch on the outer side of the external saddle indicate affinity with **Pterosirenites** rather than with **Tibetitidae**, which have adventitious elements in the external saddle and clavi arranged opposite one another.

Composition of the genus: **Pseudotibetites pax** n. sp., probably also **Paratibetites ? seimkanensis** Bychkov (see below).

Age and distribution: Lower Norian, Dawsoni Zone, northeast British Columbia; upper part of **Pinacoceras verchojanicum** Zone, northeast USSR (?) (Bychkov, 1975, p. 10).

Pseudotibetites pax n. sp.

Plate 17.1, figures 8-14

Figure 17.1d.

"**Tibetites**" sp., McLearn, 1960, p. 57, pl. 5, fig. 9a, b (only); Tozer, 1967, p. 57.

Registered material: Holotype GSC 28745, paratypes GSC 28746, 28747, GSC locality 9373. Paratype GSC 12583 (McLearn, 1960, pl. 5, fig. 9a, b), GSC locality 9161. Paratype (not figured) GSC 28749, GSC locality 64606.

Diagnosis: Phragmocone diameter at least 40 mm, at which whorl height about 45 per cent, width about 35 per cent, and umbilical width about 28 per cent of diameter. Ribs are barely perceptible. Commonly there are four tubercle spirals on the whorl side (umbilical, two lateral, marginal). Umbilical tubercles are rounded; lateral tubercles are initially rounded, adrad they become clavate; marginal tubercles are clavate at a small diameter. Keels on the inner whorls have spirally arranged tubercles matching or slightly exceeding the number at the margin. At larger diameters the density of marginal and ventral clavi is the same.

Discussion: Notched keels, more or less pointed lateral tubercles and clavate marginal tubercles are apparent at a diameter of 22 mm (GSC 28747, Plate 1, figures 10, 11). At larger diameters (GSC 28745, 28746, Plate 17.1, figures 8, 9, 12-14) the ventral tubercles are distinctly clavate. The holotype (Plate 17.1, figures 8, 9) has an extra spiral of very small tubercles immediately inside the marginal spiral. GSC 12583 (McLearn, 1960, plate 5, figure 9a, b) is wholly septate at a diameter of about 40 mm.

Paratibetites ? seimkanensis Bychkov is probably congeneric with this species, being similar in mode of coiling, style of tuberculation, ventral sculpture and suture line but differing in having more spirals of lateral tubercles. The significance of this resemblance was recognized by Bychkov (1974), who compared his specimens with those described by McLearn.

Family **DISTICHITIDAE** Diener 1920

Genus **Pleurodistichites** Tozer n. gen.

Type species: **Pleurodistichites stotti** n. sp.

Diagnosis: Distichitid with strong, dense, branched, falcoid, non-tuberculate ribs. Marginal spines absent, umbilical shoulder with or without nodes. Suture line ammonitic.

Discussion: The smooth ventral keels are taken to indicate close affinity with contemporary Distichitidae rather than with the superficially similar Carnian genus **Dittmarites** (Arpaditidae) which differs in having granular keels, at least at a small diameter. **Distichites** and **Paradistichites** differ in having relatively weak ribbing and strong marginal tubercles or spines. The ribs of **Trachyleuraspides** are comparable in strength and style but differ in being tuberculate. Similarities in sculpture suggest that there may be affinity with "**Anasirenites**" **aristotelis** Mojsisovics, but not with the type species of **Anasirenites** (**A. ekkehardi** Mojsisovics), which has lateral tuberculation. The suture line of "**A.**" **aristotelis** resembles that of **Pseudosirenites**, not that of Distichitidae but in view of the other similarities it seems possible that "**A.**" **aristotelis** may represent a new genus linking **Pseudosirenites** with Distichitidae.

Composition of the genus: **Pleurodistichites stotti** n. sp., **Arpadites** (**Dittmarites**) **hindei** Mojsisovics, **Dittmarites trailli** Diener, **Ammonites lilli** Gumbel (?), **Dittmarites** ex. gr. **lilli** (Gumbel) of Arkhipov (1974, pl. 16, fig. 3-6).

Age and distribution: Middle Norian, Columbianus Zone, British Columbia, Tethys; **Otapiria ussuriensis** Zone, northeast USSR.

Pleurodistichites stotti n. sp.

Plate 17.1, figures 15-17

Figure 17.1 e

Named for D.F. Stott, who discovered the type specimens.

Registered material: Holotype, GSC 28921, paratype GSC 28922, GSC locality 66027.

Diagnosis: **Pleurodistichites** attaining a diameter of about 25 mm with whorl height about 55 per cent, width about 40 per cent and umbilical width about 10 per cent of diameter. Ribs falcoid; on the phragmocone they bifurcate on the inner flank at a small diameter; near the mid-flank at larger diameters; some on the body chamber are unbranched. Umbilical shoulder rounded, without tuberculation.

Discussion: "**Arpadites (Dittmarites)**" **hindei** Mojsisovics is probably the most closely related species. It differs in having umbilical tuberculation.

Family CYRTOPLEURITIDAE Diener 1925

Genus **Neohimavatites** Tozer n. gen.

Type species: **Himavatites canadensis** McLearn, 1940, p. 115, plate 3, figure 3; 1960, p. 52, plate 4, figures 5a, b.

Diagnosis: Cyrtopleuritid like **Himavatites** but smooth in comparison, tuberculation being reduced on the body chamber, periodic umbilical, lateral and marginal nodes being absent, periodic external ears also absent and the number of lateral tubercle-spirals being 12 or less.

Composition of the genus: **Neohimavatites canadensis** (McLearn), **Himavatites burlingi** McLearn.

Discussion: GSC 28877 (Plate 17.1, figures 23-25), a nearly complete, apparently mature specimen, shows the characters of the type species better than the holotype (McLearn, 1960, plate 4, figures 5a, b), which preserves the body chamber, but little of the phragmocone. The close similarity between the body chambers of GSC 28877 and the holotype leaves no doubt that the two are conspecific. The ultimate part of the phragmocone of GSC 28877 has 11 spirals of tubercles between the umbilicus and the outer of the two ventral rows that lie each side of the barely perceptible sulcus. Most of these ribs bear two spine bases, a feature not shown by the holotype on which the comparable part of the shell is not preserved. At this stage the ventral spirals are of clavate, denticulate tubercles, one per rib, separated from one another. This type of sculpture clearly indicates affinity with **Himavatites**. On the body chamber of GSC 28877 the lateral spirals become increasingly obscure at the aperture only eight rows are barely perceptible (as on the holotype). Concurrent with the change in lateral sculpture the four ventral spirals cease to be discrete clavi and are replaced by more or less evenly spaced denticles, two of which lie at the termination of each of the imbricate ribs.

The type species of **Himavatites** (**H. watsoni** Diener), and also the closely related species **H. multiauritus** McLearn, differ from the species assigned to **Neohimavatites** in being much more prominently sculptured, with large periodic clavi (ears) on the outer of the two ventral spirals, large periodic nodes (umbilical, lateral, marginal), and in having many more lateral tubercle spirals (about 30 in **H. watsoni**, about 20 in **H. multiauritus**). Judging from the specimen identified as **H. cf. watsoni** by McLearn (1960, plate 4, figure 7), which is a large body chamber fragment, rough, unchanged sculpture persists on the body chamber of true **Himavatites**, another difference, in comparison with **Neohimavatites**.

Three species of **Himavatites**, each in its own way, form links between the type species of **Himavatites** and that of **Neohimavatites**. They are **Himavatites hogarti** (Diener) (Tatzreiter, 1978, p. 123, plate 1, figures 1, 2); **H. columbianus** McLearn (McLearn, 1960, p. 51, plate 5, figures 6, 7); and **H. indigiricus** Bychkov (Bychkov and Polubotko, 1970, p. 118, text-figures 1a-c). **Himavatites hogarti** has numerous lateral spirals, like **H. watsoni**, but lacks large nodes and clavi, in common with **Neohimavatites**. As noted by Tatzreiter (1978, p. 123), **Acanthinites excelsior** Mojsisovics, known only from imperfect specimens, is possibly conspecific with **Himavatites hogarti**. **Himavatites columbianus** has about the same number of lateral spirals as on the phragmocone of **Neohimavatites canadensis** but has large periodic umbilical and lateral nodes, in partial conformity with **H. watsoni**. **Himavatites indigiricus** has very few lateral spirals (eight or nine) on what is probably the body chamber and would be assigned to **Neohimavatites** were it not for the fact that it has periodic lateral nodes. Bychkov, it may be noted, regarded **H. indigiricus** as a subspecies of **Neohimavatites canadensis** (Bychkov and Polubotko, 1970). A case might be made for regarding these three species as representing a new genus, linking **Himavatites** and **Neohimavatites**, but for the time being they are retained in **Himavatites**.

"**Himavatites**" **burlingi** McLearn (See McLearn, 1960, p. 52, plate 4, figures 9a, b), being without large nodes and clavi, and having relatively few (about 10) spirals of lateral tubercles, clearly has the character of **Neohimavatites** rather than **Himavatites**. The specimens of **Neohimavatites burlingi** are not completely preserved but it would appear that this species differs from **N. canadensis** in having a more prominently sculptured body chamber, retaining distinct lateral spirals and ventral clavi.

Age and distribution: Middle Norian, Columbianus Zone, upper subzones, Pardonet Formation, British Columbia; Heiberg Formation, Axel Heiberg Island.

As noted previously (Tozer, 1971, p. 1020) the Columbianus Zone, as originally defined (Tozer, 1965, p. 222; 1967, p. 37) is amenable to subdivision into at least three, probably four subzones. **Himavatites multiauritus** McLearn is restricted to the basal subzone; **Himavatites columbianus** to the next higher; **Neohimavatites canadensis** and **N. burlingi** to the upper subzone (or subzones). Recent work by Tatzreiter (1978) indicated that divisions of the Columbianus Zone are of world-wide significance. In Timor Tatzreiter has distinguished four subzones (I-IV in ascending order). **Himavatites watsoni** characterizes Subzone I, **H. hogarti** Subzone II. Subzones III and IV lack **Himavatites** and **Neohimavatites** but have other ammonoids (**Steinmannites**, **Alloclionites** etc.) that indicate correlation with the upper subzones of Canada. The distinction between **Himavatites** and **Neohimavatites** evidently serves to characterize two major divisions of the Columbianus Zone.

References

- Arkipov, Yu. V.
1974: Stratigraphy of Triassic Deposits of Eastern Yakutia; Ministry of Geology USSR, Yakutsk. (In Russian.)
- Bychkov, Yu. M.
1974: First Tibetitids in the Northeastern USSR; *Kolymia*, v. 8, p. 42, 43. (In Russian.)
1975: Norian **Sirenites** of the northeast of the USSR and some aspects of Trachyceratid systematics; *Palaeontological Journal USSR Academy of Sciences*, v. 4, p. 9-19. (In Russian.)
- Bychkov, Yu. M., Dagys, A.S., Efimova, A.F., and Polubotko, I.V.
1976: Atlas of Triassic Fauna and Flora of Northeast USSR; Moscow, Nedra. (In Russian.)
- Bychkov, Yu. M. and Polubotko, I.V.
1970: First discovery of Triassic **Himavatites** in northeast Asia; *Palaeontological Journal USSR Academy of Sciences*, v. 2, p. 114-119. (In Russian.)
- Krystyn, L. and Mariolagos, I.
1975: Stratigraphie und Tektonik der Hallstätterkalk-Scholle von Epidauros (Griechenland); *Sitzungsberichte der Österreichische Akademie der Wissenschaften, Mathem. - naturw. Klasse*, Band 184, p. 181-195.
- McLearn, F.H.
1939: Some species of the Neo-Triassic Genera **Juvavites**, **Isculites**, **Sirenites**, **Himavatites**, **Cyrtopleurites** and **Pterotoceras**; *Transactions Royal Society of Canada, Series 3, Section IV*, v. 33, p. 51-56, 1 plate.
1940: Preliminary study of some Triassic Pelecypods and Ammonoids from the Peace River Foothills, B.C.; *Canadian Field Naturalist*, v. 54, p. 111-116, plates I-IV.
1947: Upper Triassic Faunas of Pardonet Hill, Peace River Foothills, British Columbia; *Geological Survey of Canada, Paper 47-14*.
1960: Ammonoid Faunas of the Upper Triassic Pardonet Formation, Peace River Foothills, British Columbia; *Geological Survey of Canada, Memoir 311*.
- Mojsisovics, E.V.
1882: Die Cephalopoden der mediterranen Triasprovinz; *Abhandlungen der Kaiserlich-Königlichen Geologischen Reichsanstalt*, Bd. 10.
- Pelletier, B.R.
1961: Triassic Stratigraphy of the Rocky Mountains and Foothills, northeastern British Columbia; *Geological Survey of Canada, Paper 61-8*.
- Tatzreiter, F.
1978: Zur Stellung der **Himavatites columbianus** Zone (höheres Mittelnor) in der Tethys; *Schriftenreihe der Erdwissenschaftlichen Kommissionen, Österreichische Akademie der Wissenschaften*, Bd. 4, p. 105-139.
- Tozer, E.T.
1965: Upper Triassic ammonoid zones of the Peace River Foothills, British Columbia, and their bearing on the classification of the Norian Stage; *Canadian Journal of Earth Sciences*, v. 2, p. 216-226.
1967: A Standard for Triassic Time; *Geological Survey of Canada, Bulletin 156*.
1971: Triassic Time and Ammonoids: Problems and Proposals; *Canadian Journal of Earth Sciences*, v. 8, p. 989-1031, 1611.

Project 730044

K.L. Currie, G.E. Pajari Jr.¹, and R.K. Pickerill¹
Precambrian Geology Division

Currie, K.L., Pajari, G.E., Jr., and Pickerill, R.K., *Comments on the boundaries of the Davidsville Group, northeastern Newfoundland; in Current Research, Part A, Geological Survey of Canada, Paper 80-1A, p. 115-118, 1980.*

Abstract

The Davidsville Group for the most part lies unconformably upon the obducted Gander River ultramafic belt. Where the ultramafic belt is absent, the base of the group can be arbitrarily defined within a continuous section as the lowest conglomerate horizon containing ultramafic debris. This definition implies that some units of the Gander Group – Davidsville Group sequence must be diachronous. The Davidsville Group unconformably underlies the Silurian Indian Islands Group west of Gander Bay. Regional correlation shows that the Indian Islands Group is equivalent to the Botwood Group, and suggests that the Davidsville Group is at least partially equivalent to the Exploits Group. These correlations suggest that the northeastern part of the Dunnage zone must be broadly synclinal.

The supracrustal rocks of northeastern Newfoundland can be divided into four distinctive units: a lower unit rich in psammite with lesser amounts of pelite and mafic igneous rocks (lower and middle Gander Lake Group of Jenness (1963)), an allochthonous slab of ophiolite (Gander River ultramafic belt of Jenness (1963), a unit rich in black pelite (upper Gander Lake Group of Jenness (1963)), and an upper unit rich in siltstone with basal coralline limestone (Botwood and Indian Island groups of Williams (1964)). Kennedy and McGonigal (1972a) noted that the lower and middle Gander Lake Group commonly appeared to be more deformed and metamorphosed than the upper part. On this basis they re-named the upper part of the Gander Lake Group the Davidsville Group. McGonigal (1973) and Kennedy (1975) completed the revision in terminology by proposing the name Gander Group for the lower and middle parts of Jenness's (1963) Gander Lake Group. The interpretation attached by Kennedy and McGonigal (1972a) to the distinction between Gander and Davidsville groups has been shown to be erroneous (Pickerill et al., 1978a; Currie et al., 1979). However, the terminology is useful, and has become normative, despite considerable controversy (Jenness 1972; Brückner 1972, 1978; Kennedy and McGonigal 1972b; Pickerill et al., 1978a, b).

Kennedy and McGonigal (1972a) implicitly chose the Gander River ultramafic belt to separate the Gander and Davidsville groups. The simplicity and effectiveness of this criterion has recently been emphasized by Blackwood (1978). However, this definition fails where the Gander River Belt is absent, as it is southeast of Island Pond (Fig. 18.1), here called the continuous succession, and northeast of the Shoal Pond Raft. Where the sedimentary record is continuous (Currie et al., 1979), some other criterion must be chosen.

The stratigraphic record shows that emplacement of the obducted Shoal Pond ophiolitic slab was immediately followed by erosion and deposition of mafic, ultramafic and plagiogranite debris. Therefore a workable, though arbitrary, criterion for the base of the Davidsville Group can be established by choosing the stratigraphically lowest (Fig. 18.1) occurrence of clastic rocks containing ultramafic or plagiogranite debris (F. Blackwood, personal communication, 1976-79). The age of this base has been determined to lie on the Llanvirn-Llandeilo boundary by conodont assemblages from limestone immediately overlying ultrabasic rocks (Blackwood 1978, Currie et al., 1979).

Although this definition of the base of the Davidsville Group (top of the ultramafic belt or lowest clastic unit containing ultramafic and associated debris) is certainly workable from Ragged Harbour southwest to Weirs Pond, it contains a number of potential problems. First, within the continuous succession southeast of Island Pond, sediments containing the ultramafic and associated debris lie below a thinly bedded grey slate-siltstone unit and above a redbed unit. A few kilometres to the southwest, however, the debris lies within the redbed unit, and 15 km farther to the southwest on the Gander-Gander Bay highway, the redbeds lie above the ophiolitic rocks and their debris. This stratigraphic succession is the product of at least two separate sedimentary dispersal patterns, one due to normal transport of sediment down the continental slope and the other representing debris shed from local topographic highs composed of Gander River ophiolitic rocks. The foregoing observations show that one or both of the resulting sedimentary blankets must be slightly diachronous. Hence, the same lithologic unit (redbeds) can be found in different positions relative to the obducted slabs and derived debris. Hence, the same lithologic unit falls into the Gander or Davidsville Group, depending on its location. A further difficulty arises where the obducted plates, or derived debris, are completely absent, as they are in southern Newfoundland where Gander-type lithologies pass gradationally into Davidsville-type lithologies (Coleman-Sadd, 1978). Despite similarities to the continuous section south of Island Pond, different terminology is required. These difficulties emphasize the nomenclatural problems introduced by allochthonous slices.

The top of the Davidsville Group is spectacularly exposed along the west coast of Gander Bay, and on islands near Dog Bay Point (Fig. 18.2). An angular unconformity occurs between black pelite of the Davidsville Group and an overlying grey siltstone rich in limestone lenticles containing **Favosites**, crinoid debris and unidentifiable solitary corals. The state of deformation of the younger rocks varies from almost completely undeformed, through shattered, to intensely stretched and folded, but deformation is always less than that in the underlying pelite beds where the two can be observed in close proximity. The map pattern shows that the unconformity must be folded with wave lengths varying upward from a few hundred metres.

¹ Department of Geology, University of New Brunswick, Fredericton, N.B. E3B 5A3

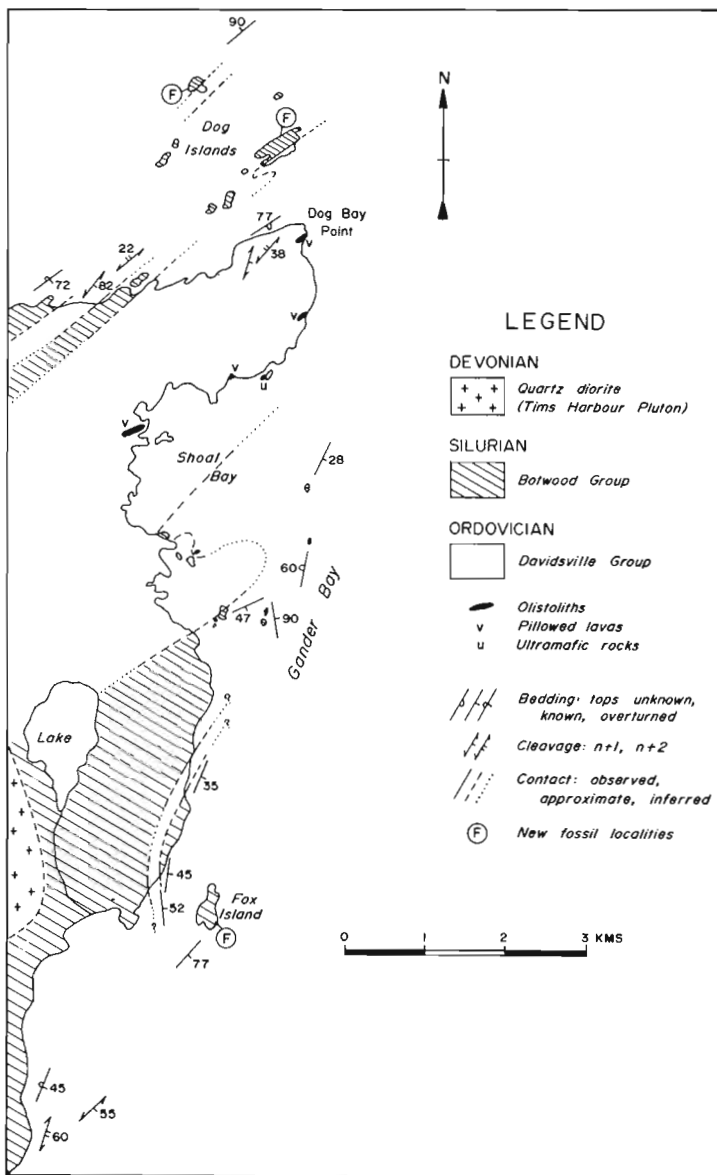


Figure 18.1. Generalized map of northeastern Newfoundland showing the relationship of the Gander, Davidsville and Botwood groups (Geology in part adapted from Williams, 1964; McCann and Kennedy, 1974; Currie et al., 1979).

The recent recognition and tracing of the unconformity permits the possible interpretation of a number of other geological features of this region (Fig. 18.1). The youngest fossils recovered from the Davidsville Group are of Caradoc age (Bergström et al., 1974). Fossils recovered from the overlying limestone lenses have been reported to be of Llandoveryan age (Williams, 1972). Since the Davidsville Group was deformed, and the sedimentary environment changed from deep water turbiditic, to shallow water, stable shelf during the time interval represented by the unconformity, it seems probable that the unconformity is of major significance and probably represents much of Ashgill time. Some deformation of the Davidsville Group, therefore, must be of this age (Taconic).

On the west side of the harbour at Port Albert, a diamictite, interpreted as glaciomarine in origin by McCann and Kennedy (1974), is overlain disconformably by siltstone

with fossiliferous (**Favosites**) limestone lenticles. The latter is overlain by an ignimbrite unit mapped by Williams (1964) as part of the Botwood Group. Because of the presence of the ignimbrite, the surrounding units were included in the Botwood Group, although they are identical to material on the west side of Gander Bay mapped by Williams (1964) as the Indian Island Group. Our observations strongly suggest that the Botwood and Indian Island groups are indistinguishable.

Williams (1967, p. 104) suggested that Silurian rocks lie unconformably upon the Davidsville Group south of Gander Bay. We believe this relation to be impossible in the sections observed by us, because the sedimentary environments of the two groups appear totally different. The Davidsville Group was marked by deep water turbidite and olistostrome formation throughout all of its later development (Pajari et al., 1979). The Silurian rocks contain wind-derived millet seed quartz grains, coral colonies and other features suggestive of stable, shallow water deposition. We suggest this change was not gradational but resulted from the closure of the Iapetus Ocean, and stabilization of the collapsed sedimentary prisms as stable shallow water to subaerial shelves. On our model this collapse and stabilization took place in late Ordovician (Caradoc-Ashgill) time.

The Dunnage Mélange strongly resembles mélange horizons within the Davidsville Group (Pajari et al., 1979). Hibbard and Williams (in press) showed that the Dunnage Mélange forms part of the Exploits Group. The probability is therefore high that the Davidsville Group is, in part, equivalent to the Exploits Group, and that the northeastern part of the Dunnage Zone has a broadly synclinal structure.

References

- Bergström, S.M., Riva, J., and Kay, M.
1974: Significance of conodonts, graptolites and shelly faunas from the Ordovician of western and north central Newfoundland; Canadian Journal of Earth Sciences, v. 11, p. 1625-1660.
- Blackwood, R.F.
1978: Northeastern Gander Zone, Newfoundland; Mineral Development Division, Newfoundland Department of Mines and Energy, Report of Activities for 1977, p. 72-79.
- Brückner, W.D.
1972: The Gander Lake and Davidsville groups of northeastern Newfoundland: New date and geotectonic implications: Discussion; Canadian Journal of Earth Sciences, v. 9, p. 1778-1779.
- 1978: Carmanville map area, Newfoundland; the northeastern end of the Appalachians - Discussion; in Current Research, Part C, Geological Survey of Canada, Paper 78-1C, p. 127-129.
- Coleman-Sadd, S.P.
1978: Gaultois Map Area (1M/12), Newfoundland; Mineral Development Division, Newfoundland Department of Mines and Energy, Report of Activities for 1977, p. 90-96.
- Currie, K.L., Pajari, G.E., and Pickerill, R.K.
1979: Tectono-stratigraphic problems in the Carmanville Area, Northeastern Newfoundland; in Current Research, Part A, Geological Survey of Canada, Paper 79-1A, p. 71-76.
- Hibbard, J.P. and Williams, H.
The regional setting of the Dunnage Mélange in the Newfoundland Appalachians; American Journal of Science. (in press)

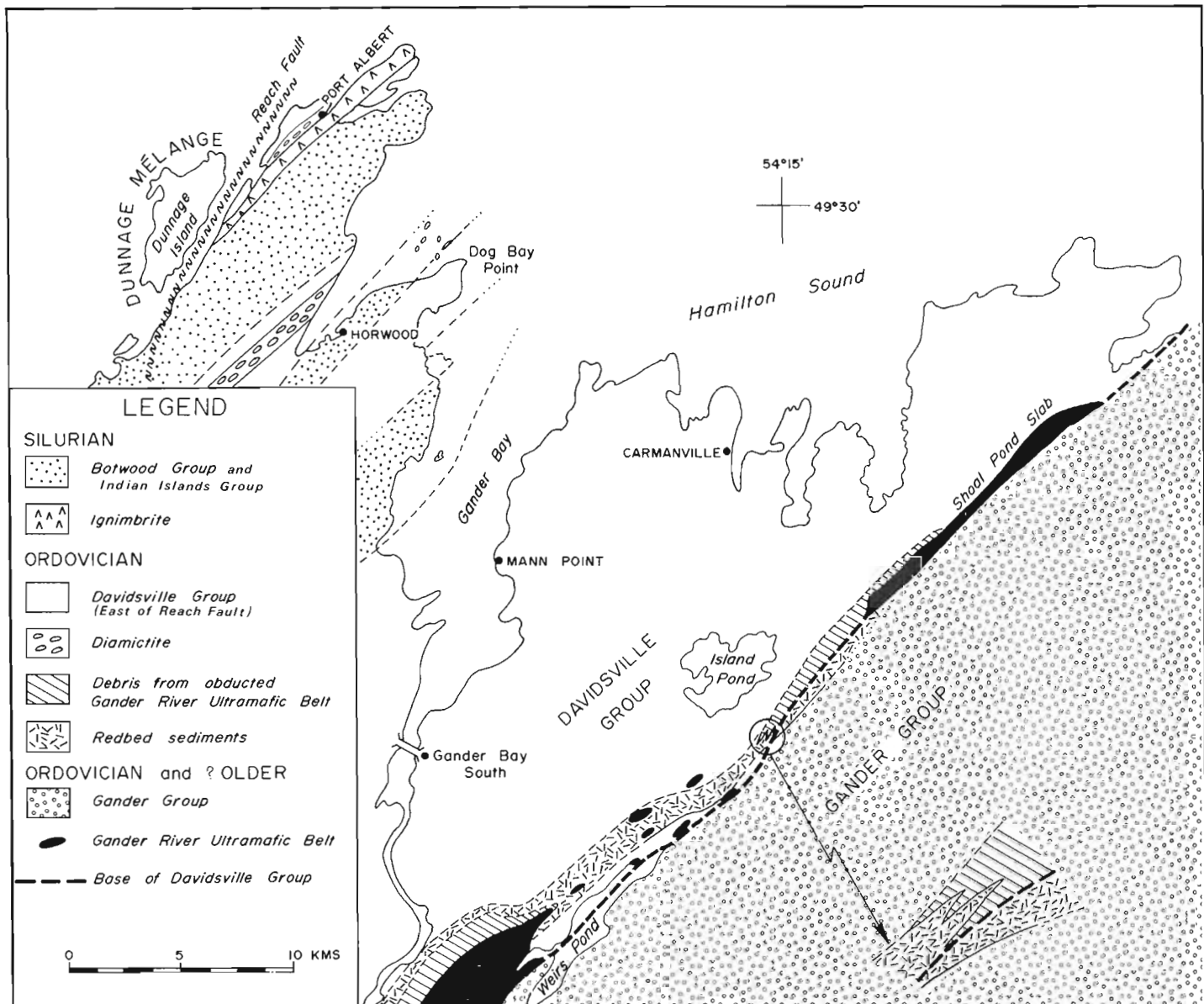


Figure 18.2. Preliminary map of the distribution of Ordovician and Silurian strata on the west side of Gander Bay.

Jenness, S.E.

1963: Terra Nova and Bonavista map-areas, Newfoundland; Geological Survey of Canada, Memoir 327.

1972: The Gander Lake and Davidsville Groups of Northeastern Newfoundland: New data and geotectonic implications: Discussions; Canadian Journal of Earth Sciences, v. 9, p. 1779-1781.

Kennedy, M.J.

1975: Repetitive orogeny in the northeastern Appalachians - new plate models based upon Newfoundland examples; Tectonophysics, v. 28, p. 29-87.

Kennedy, M.J. and McGonigal, M.H.

1972a: The Gander Lake and Davidsville Groups of north-eastern Newfoundland: New data and geotectonic implications; Canadian Journal of Earth Sciences, v. 9, p. 453-459.

Kennedy, M.J. and McGonigal, M.H. (cont'd)

1972b: The Gander Lake and Davidsville Groups of north-eastern Newfoundland: New data and geotectonic implications: Reply; Canadian Journal of Earth Sciences, v. 9, p. 1781-1783.

McCann, A.M. and Kennedy, M.J.

1974: A probable glacio-marine deposit of Late Ordovician - Early Silurian age from the north central Newfoundland Appalachian Belt; Geological Magazine, v. 111, p. 549-564.

McGonigal, M.H.

1973: The Gander and Davidsville Groups: major tectonostratigraphic units in the Gander Lake area, Newfoundland; unpublished M.Sc. thesis Memorial University of Newfoundland, St. John's, Newfoundland, 121 p.

- Pajari, G.E., Jr., Pickerill, R.K., and Currie, K.L.
1979: The nature, origin and significance of the Carmanville ophiolitic mélange, northeastern Newfoundland; *Canadian Journal of Earth Sciences*, v. 16, p. 1439-1451.
- Pickerill, R.K., Pajari, G.E., Currie, K.L., and Berger, A.R.
1978a: Carmanville map area, Newfoundland; the north-eastern end of the Appalachians; in *Current Research, Part A*, Geological Survey of Canada, Paper 78-1A, p. 209-216.
1978b: Carmanville Map Area, Newfoundland; the north-eastern end of the Appalachians - Reply; in *Current Research, Part C*, Geological Survey of Canada, Paper 78-1C, p. 129-132.
- Williams, H.
1964: Botwood, Newfoundland; Geological Survey of Canada, Map 60-1963.
1967: Silurian Rocks of Newfoundland; in *Collective Papers on Geology of the Atlantic Region*, E.R.W. Neale and H. Williams, ed., Geological Association of Canada, Special Paper Number 4, p. 93-137.
1972: Stratigraphy of Botwood map area, northeastern Newfoundland; Geological Survey of Canada, Open File 113.

**COPPER MINERALIZATION AND HYDROTHERMAL ALTERATION OF VOLCANIC ROCKS
AT BEDFORD HILL, NORANDA AREA, QUEBEC**

EMR Research Agreement 146-4-79

M.L. Atkinson¹ and D.H. Watkinson¹
Economic Geology Division

Atkinson, M.L. and Watkinson, D.H., Copper mineralization and hydrothermal alteration of volcanic rocks at Bedford Hill, Noranda area, Québec; in Current Research, Part A, Geological Survey of Canada, Paper 80-1A, p. 119-123, 1980.

Abstract

Bedford Hill is composed of a dacitic dome and overlying andesitic flows, interpreted to be part of the Amulet rhyolite formation. The rocks contain stringers rich in chalcopyrite and are hydrothermally altered. Alteration is concentrically zoned in the dacite with an inner core of intense chloritization along fractures in a zone of pervasive chloritization, in turn enclosed by an incomplete zone of sericitic alteration in spots and fractures. Silicification in the andesite was overprinted by chloritic spots in breccia-dykes and other highly permeable areas. Chalcopyrite, pyrite and minor sphalerite occur as stringers in irregular fractures in dacite. Pyrite and sphalerite occur in the matrix of fragmental andesite and in permeable andesitic vitrophyre and perlite.

The stringer mineralization and alteration at Bedford Hill are interpreted to be features typical of volcanogenic base metal deposition resulting from effects of an active hydrothermal system in a dacitic dome with activity continuing after deposition of the overlying andesite.

Introduction

Copper mineralization at Bedford Hill was discovered in the early 1920s and the area was subsequently trenched and drilled by several mining companies. The area has been mapped by Lewis (1975), and Sethuraman (personal communication from W. Hogg, Noranda Mines Ltd.). The volcanic rocks are interpreted to be part of the Amulet rhyolite formation, bounded on the north and west by the Flavrian Lake granitic complex (Goldie, 1976) and on the east by complexly faulted rocks of the Amulet rhyolite formation (Comba, 1977), as shown in Figure 19.1. Recent mapping of a section of Amulet rhyolite formation southwest of Bedford Hill has shown that its lower member is a rhyolitic flow-dome and the upper member, silicified andesite flows (Comba, 1977; Gibson, 1979; Gibson and Watkinson, 1979). The formation was interpreted to be the third of five episodes of felsic volcanism in the Noranda camp (Spence and de Rosen-Spence, 1975). The third zone of "rhyolitic" activity underlies many important economic copper-zinc deposits, three of which are within 3 km of Bedford Hill. These deposits have been recognized as volcanogenic (Gilmour, 1965) with massive sulphide lenses overlying alteration pipes with contained stringer mineralization. The alteration pipes are interpreted as conduits for hydrothermal fluids. Comba (1977) and Lewis (1975) suggested that the Cu-rich and altered rocks at Bedford Hill may have been a stringer zone underlying a massive sulphide body that is not evident because of erosion or faulting. An evaluation of the mineralization by Falconbridge Copper Limited geologists indicated that 92 000 tons of 0.89% Cu might be recoverable by open pit.

Detailed mapping of Bedford Hill was undertaken during the summer of 1979 to determine relationships between the volcanic stratigraphy, hydrothermal alteration and Cu mineralization. Petrographic and chemical studies are in progress.

Geology of Bedford Hill

The two members of the Amulet rhyolite formation recognized by Comba (1977) and Gibson (1979) in the Turcotte Lake area may also be distinguished at Bedford Hill. However, the complete section from basal Beecham breccia to silicified conformable breccias at the top is not exposed.

The Bedford Hill rocks apparently represent the upper part of the lower Amulet rhyolite and the lower part of the upper Amulet rhyolite.

The most intensely altered and mineralized unit is a dacitic dome which extends from the westernmost edge of the map area to a point near the eastern edge (Fig. 19.2). It is quartz-amydaloidal, spherulitic and has rare plagioclase phenocrysts pseudomorphed by a mosaic of quartz. No quartz phenocrysts were observed. Amygdules are flattened and are

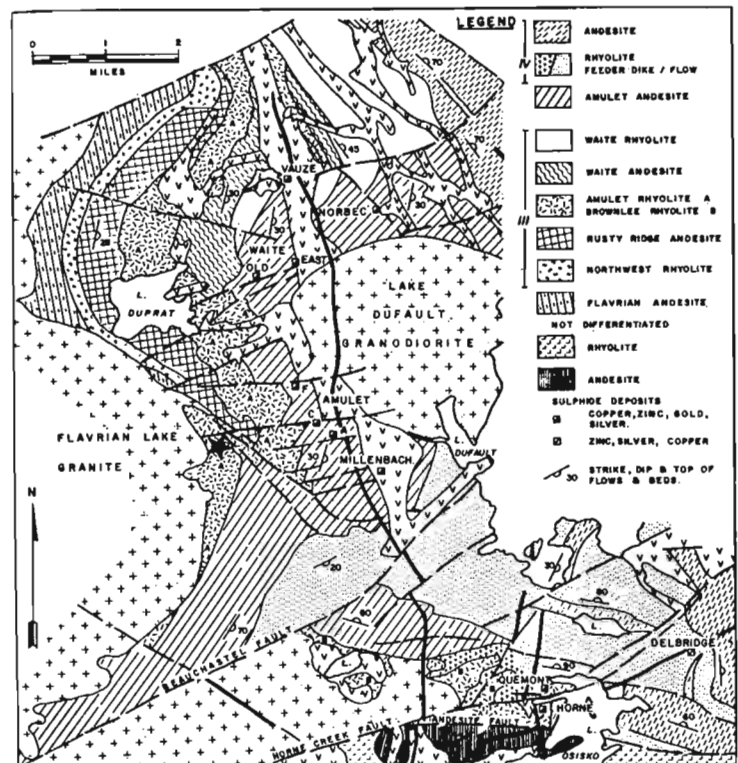
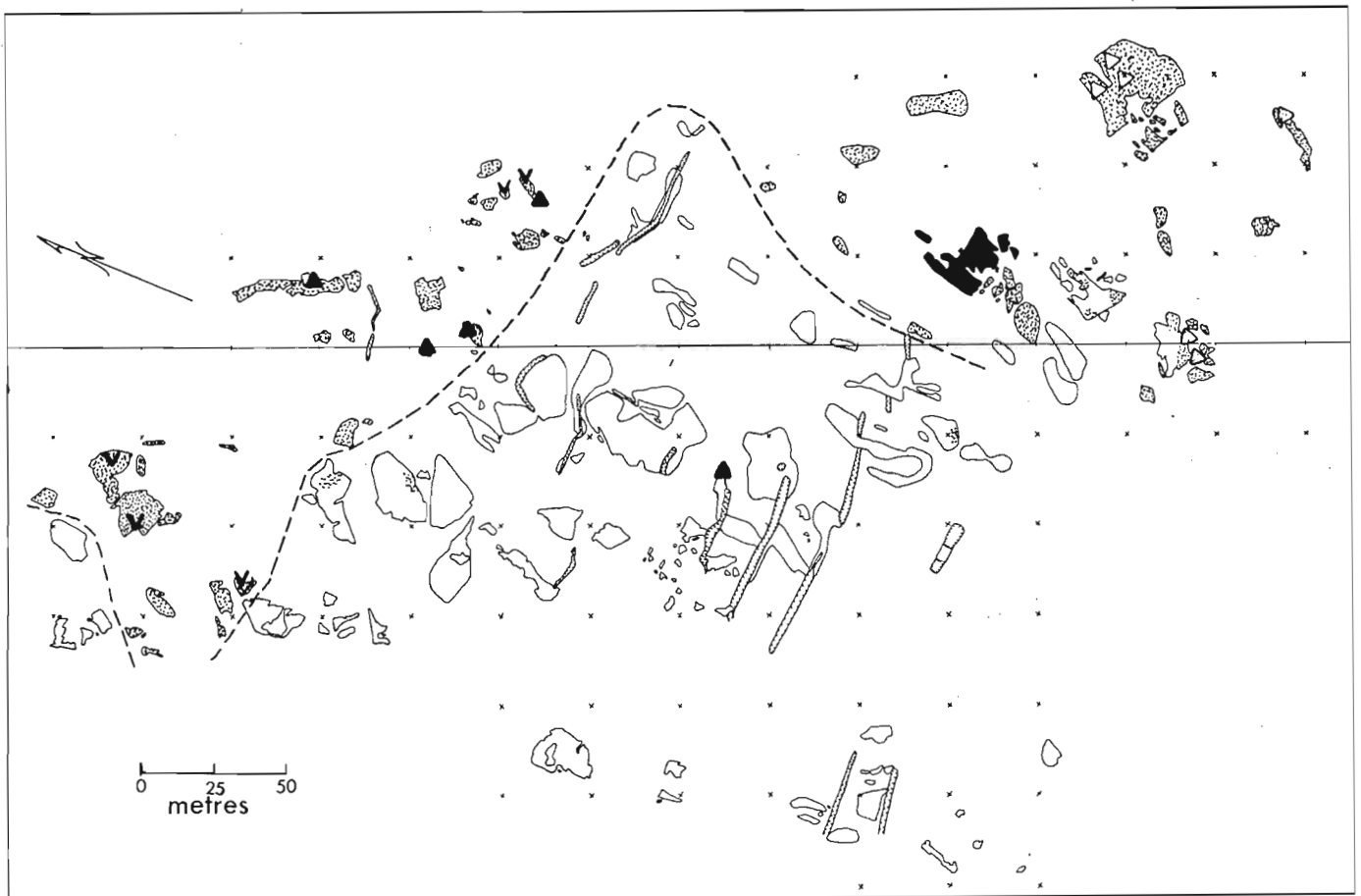


Figure 19.1. Geology of the central part of the Noranda area, after Spence and de Rosen-Spence (1975), with star showing location of Bedford Hill.

¹Department of Geology, Carleton University, Ottawa, Canada.



- | | | | |
|---|--|---|---|
|  | Andesite; massive, porphyritic, amygdaloidal |  | Vitrophyric andesite, flow-banded |
|  | Andesite; pillowed, amygdaloidal |  | Brecciated andesite, amygdaloidal fragments |
|  | Dacite; amygdaloidal, spherulitic, flow-banded |  | Breccia dike |

Figure 19.2. Geology of volcanic rocks at Bedford Hill.

locally concentrated in planes of inconsistent orientation, probably related to flow banding. Spherulites may form up to 30 per cent of the rock. They are completely recrystallized to aggregates of sericite, quartz and feldspar. Most of the primary textures in the dacite have been obliterated by recrystallization and alteration.

Overlying the dacite are andesitic flows and fragmental units. The lowermost of these is a flow banded, amygdaloidal, porphyritic, locally vitrophyric and perlitic andesite that has been variably silicified. It is exposed in the north and south of the map area. The position of the southern contact of this andesite and dacite was difficult to delineate within several metres; this is due in part to irregular erosion of the contact surface and also to intrusion of a spherulitic dyke at the contact. The zone of contact of the dacite and andesite in the central part of the map area is marked by a silicified, andesitic breccia angular silicified fragments set in a fine grained fragmental matrix. The matrix contains as much as 50 per cent pyrite and 3 per cent sphalerite.

An isolated outcrop of pillowed andesite is exposed above the lowermost silicified andesitic flows. It has a general northwesterly trend and 30° easterly dip. This unit, the Bedford andesite, may represent an erosional remnant of a once more continuous pillowed flow or may be an isolated flow filling a topographic depression in the top of the lower Amulet rhyolite (Comba, 1977).

The pillowed andesite is overlain by flows of massive, porphyritic andesite. In the southeastern corner of the map area these are cut by silicified breccia dykes. The best exposed body is pipe-like and plunges 030° at 40° . Similar breccia dykes were described by Gibson (1979) near the top of the upper Amulet rhyolite.

Pyrite-Chalcopyrite-Sphalerite Mineralization

Irregular stringer and fracture systems occur in the dacite. Trenching from early exploration work has displaced much of the mineralized rocks from its original position; however, the general east-west trend of the trenches appears to reflect the gross orientation of a fracture system containing the mineralized material. Sulphides present are pyrite, chalcopyrite and sphalerite in order of decreasing abundance. Fracturing is most intense in the trenched areas and a random orientation of the fractures is evident. The dacite also contains 2 - 3% disseminated pyrite and pyrite in amygdules.

In the overlying andesitic flows, pyrite is the most abundant sulphide and sphalerite is more abundant than chalcopyrite. Sphalerite is disseminated in the matrix of the fragmental andesite and is rarely present in stringers with pyrite and chalcopyrite. Pyrite occurs in amygdules and as disseminations in the massive rocks; it forms as much as 40 per cent of the perlitic andesite.

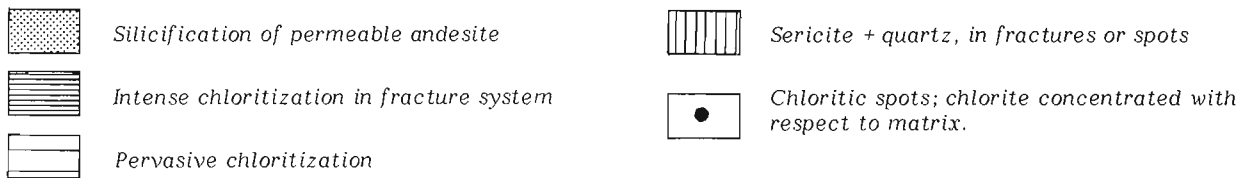
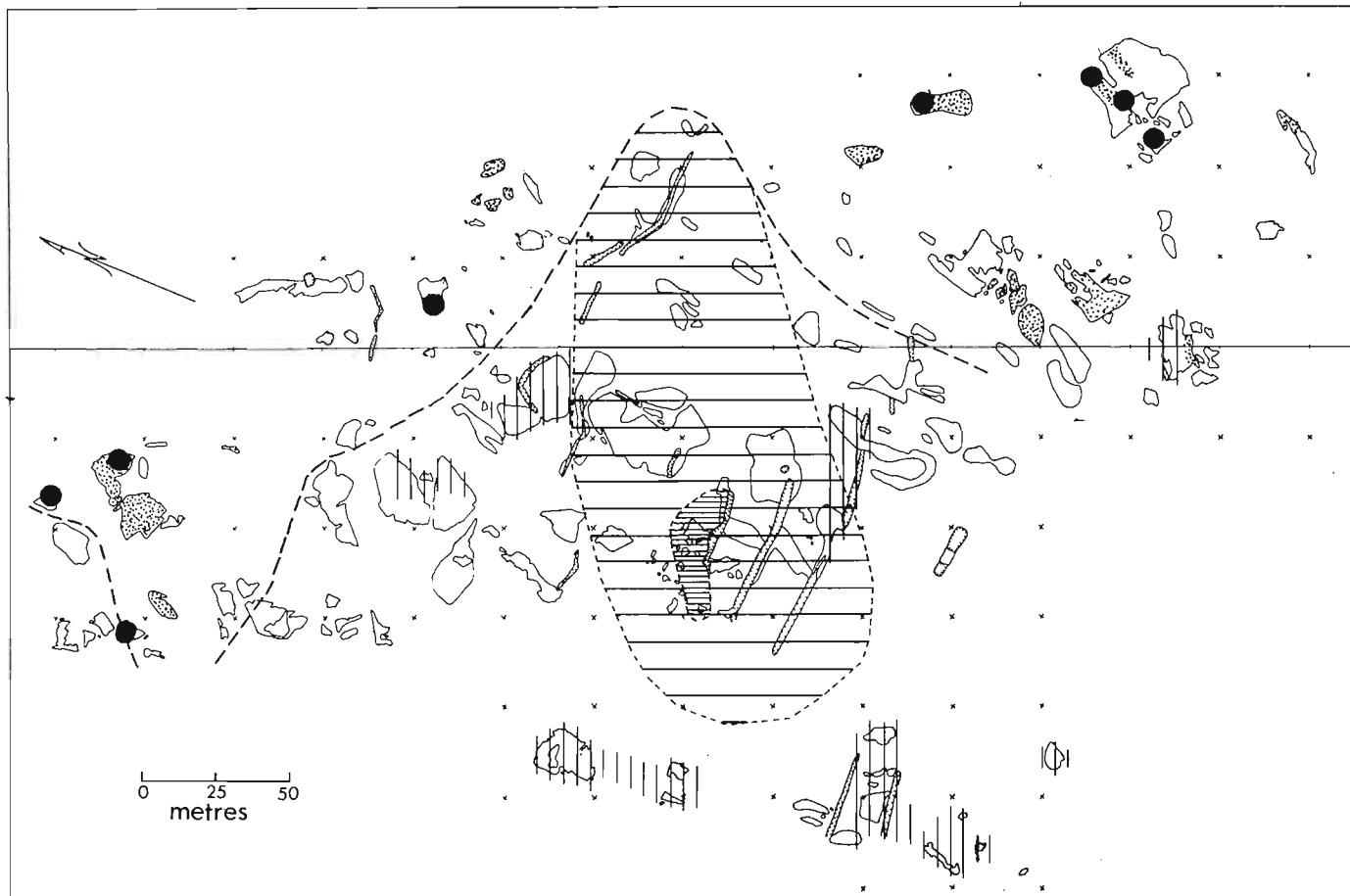


Figure 19.3. Hydrothermal alteration of volcanic rocks at Bedford Hill.

Near the contact of the dacitic dome and the overlying andesitic flows, conformable pods of massive pyrite were found. Angular, altered volcanic fragments of possible tuffaceous origin occur in some pods. These massive pyritic pods may represent small areas of discharge for hydrothermal solutions at or near the seafloor.

Hydrothermal Alteration: Chloritization, Sericitization, Silicification

Alteration at Bedford Hill occurs in three main styles; pervasive alteration, alteration along fractures and spotted alteration.

Pervasive alteration is best exemplified in the chloritic alteration zone (Fig. 19.3). Some thin sections contain as much as 60 per cent chlorite, but large areas in the field appeared even more chloritic.

The most intense alteration is in the central part of the dacitic unit. The rock here is highly fractured and marked by nearly complete chloritization. This has produced a pseudobreccia, as the unaltered areas form rounded "fragments" in the chloritic zone. The intensely altered rock forms a thin band, about 5 m wide and 25 m long. Less intense but pervasive chlorite alteration extends 25 to 100 m beyond this central core.

Sericitic alteration in a fracture system occurs in dacite and andesite as a zone around the pervasive chlorite zone. Sericite (and quartz) in fractures has produced a boxwork pattern (Fig. 19.4a) or formed along isolated fractures.

In the andesite to the north and south of the dacitic dome, the predominant alteration is silicification. Carbonate and epidote in the andesite and epidote in thin veins and amygdules are probably also products of hydrothermal alteration.

Some sericite alteration occurs as low-weathering ovoid to circular spots of variable diameter. In the field the spots are difficult to distinguish from spherulites. In many cases spherulites are mantled by a soft, grey rim, accentuating their size. These spots are enriched in mixed sericite and quartz and depleted in chlorite, relative to their matrix. They appear to have formed where the products of hydrothermal alteration nucleated on earlier formed structures such as spherulites.

Sericite-quartz concentrations also occur in elongated lath-shaped areas in a chloritic matrix. These areas are similar to the ovoid spots but may be pseudomorphs now composed of sericite + quartz + chlorite.



Figure 19.4.

Altered andesitic rocks at Bedford Hill.

- a - *Sericite and quartz along boxwork fractures in andesite. Apparent chloritic spots within boxwork.*



- b - *Silicified andesitic breccia-dyke. Chloritic porphyroblasts after chlorite alteration.*



- c - *Detail of Figure 19.4b showing apparent fracture control on chloritic spots in fragments and matrix.*

Chloritic alteration also occurs as spots with irregular to polygonal outlines in andesite. Spots with irregular shapes occur in flow banded vitrophyric andesite and are superimposed on the silicified, vitrophyric textures. In thin section, they are characterized by slightly coarser grain size and higher chlorite content than the enclosing rock.

Within and close to the andesitic breccia dykes in the southeast corner of the map area, chloritic spots have rectangular to square outlines. These spots occur in the silicified fragments, in the matrix to the fragments and within the massive andesite adjacent to the breccia dykes (Fig. 19.4b). The distribution of these chloritic spots appears to be controlled by fractures (Fig. 19.4c) and by primary permeability in the fragmental dykes. The euhedral outlines of these spots suggest they were porphyroblasts formed from chloritic alteration along fractures that are now chloritic pseudomorphs. A possible source of heat for the metamorphism is the Flavrian Lake granitic complex which outcrops 300 m from this location, and underlies Bedford Hill at about 200 m (Comba, 1977).

The two types of chloritic spots discussed here are both superimposed on silicified primary textures in the andesite. This indicates that silicification took place before the main hydrothermal alteration but the genetic relationship of the two processes is not clear.

An apparent chloritic spotting is produced in silicified andesite as a result of the silicification process. Irregularly shaped chloritic spots were produced in a silicified groundmass. In some areas, however, fracture-control of the silicification is apparent and the chlorite spots are actually unsilicified relicts of the original rock.

Discussion and Conclusions

An early alteration event in the Bedford Hill rocks was pervasive silicification of the andesite overlying the dacitic dome. Alteration of volcanic glass to chlorite could release silica and also cause volume reduction (Gibson and Watkinson, 1979). Dacitic and andesitic glass may thus have been the source of silica for silicification of the andesite in discharge channels. The permeability produced by the volume reduction in this transformation probably contributed a major part of the permeability necessary for the passage of hydrothermal fluids through the volcanic pile.

Silicified breccia dykes and pipes crosscutting the andesite may represent discharge conduits for solutions responsible for silicification as proposed by Gibson (1979). The permeability produced during brecciation might also have facilitated the passage of later hydrothermal solutions as would be required by the presence of chloritic spotting in one of the breccia dykes.

The pipe-shaped nature of the alteration zones may be inferred from the roughly concentric disposition of the sericite alteration about the chloritic alteration zone (Fig. 19.3) within the dacitic dome. If the alteration zone originally formed vertically beneath essentially horizontal volcanic rocks on the seafloor then it probably now plunges approximately 60° to the southwest as inferred from the altitude obtained for the overlying pillowed andesite.

Hydrothermal alteration is most intense within the dacitic dome where primary textures have been virtually destroyed or overprinted by the alteration. Some chloritic spotting is also present in localized areas of high permeability in the overlying andesite, but there the dominant alteration is earlier silicification. Primary features of the andesite such as vitrophyre, tuff-breccia and microlites have been silicified but the textures are preserved. Because the most intense alteration is below the dacite-andesite contact, any significant sulphide mineralization might be expected at the contact. The presence of silicified breccia dykes and associated chloritic alteration in the overlying andesite indicates that a hydrothermal system existed in the andesite also and fluids could have deposited sulphide minerals at stratigraphic levels above andesite exposed at Bedford Hill.

Acknowledgments

We are grateful to Falconbridge Copper Limited for permission to study their property and for their co-operation throughout the field season. In particular, discussions and field trips with H.L. Gibson and C.D.A. Comba were most helpful. L. Radburn and R. Conlon provided capable field assistance. The project was financed by EMR research agreement 146-4-79 and by NRC grant A7874 to D.H. Watkinson.

References

- Comba, C.D.A.
1977: Summary Report on the Waite Dufault Mines Ltd. option, Duprat Township, Noranda, Quebec; Falconbridge Copper Ltd., unpublished internal report, 44p.
- Gibson, H.L.
1979: Geology of the Amulet Rhyolite Formation, Turcotte Lake Section, Noranda Area, Quebec; unpublished M.Sc. thesis, Carleton University, Ottawa, 154p.
- Gibson, H.L. and Watkinson, D.H.
1979: Silicification in the Amulet "Rhyolite" Formation, Turcotte Lake Section, Noranda Area, Quebec, in Current Research, Part B, Geological Survey of Canada, Paper 79-1B, p. 111-120.
- Gilmour, P.
1965: The Origin of the Massive Sulphide Mineralization in the Noranda District, Northwestern Quebec; Geological Association of Canada Proceedings, v. 16, p. 63-81.
- Goldie, R.J.
1976: The Flavrian and Powell Plutons, Noranda Area, Quebec; unpublished Ph.D. thesis, Queen's University, Kingston.
- Lewis, T.D.
1975: Alteration Study of the Bedford Hill Deposit, Noranda, Quebec, Canada; unpublished B.Sc. thesis, Queen's University, Kingston, 44p.
- Spence, C.D. and de Rosen-Spence, A.F.
1975: The place of sulphide mineralization in the volcanic sequence at Noranda, Quebec; Economic Geology, v. 70, p. 90-101.

**GEOLOGICAL STUDIES OF THE LATE PRECAMBRIAN SUPRACRUSTAL ROCKS AND
UNDERLYING GRANITIC BASEMENT, FURY AND HECLA STRAIT AREA,
BAFFIN ISLAND, DISTRICT OF FRANKLIN**

Projects 790016, 760045, 790029, and 760047

F.W. Chandler¹, B.W. Charbonneau², A. Ciesielski¹, Y.T. Maurice², and S. White³

Chandler, F.W., Charbonneau, B.W., Ciesielski, A., Maurice, Y.T., and White, S., Geological studies of the Late Precambrian supracrustal rocks and underlying granitic basement, Fury and Hecla Strait area, Baffin Island, District of Franklin; in Current Research, Part A, Geological Survey of Canada, Paper 80-1A, p. 125-132, 1980.

Abstract

For about 150 km along the north shore of Fury and Hecla Strait, and extending up to 50 km inland lies a belt of mainly clastic sedimentary rocks. This unmetamorphosed Helikian and/or Hadrynian sequence, about 6000 m thick, is divided into five conformable units, described in ascending stratigraphic order. The lowest unit consists of red sandstone and shale with minor quartz-pebble conglomerate and stromatolitic dolomite passing up into white quartzite. The second unit consists of a coarsening-upward sequence of red shale and sandstone, with black shale and stromatolitic dolomite at its base. A westward-thinning pink quartzite unit is followed by a varicoloured sandstone-shale unit, transitional into a black shale unit. Both alluvial and marine depositional environments are represented in the sediments, and paleocurrents flowed broadly westward. Deformation is limited to faulting and gentle southward tilting.

Lying nonconformably beneath the sediments are granitic and gneissic rocks of Archean and/or Apebian age. Mapping, concentrated about two large radiometric anomalies situated in the east and west of the area, showed them to be broadly coincident with weakly-deformed pink biotite-hornblende granite, cut by granitic pegmatite. The granite, present as a batholith in the east, is also present as smaller bodies in the west. The eastern granite is margined by pre- to syntectonic porphyritic monzonite(?) that cuts widespread surrounding mesocratic tonalitic gneiss. A thick sequence of orthogneiss and paragneiss, partly of sedimentary origin in the western area is varied in composition and fabric. Deformation in both areas is intense except in the case of the granite and pegmatite. Geochronological and paleomagnetic studies of these rocks are in progress.

Ground radiometric and geochemical analyses show that the two previously discovered large uranium-thorium radiometric anomalies are caused by underlying pink basement granite. Whereas surrounding gneisses and late Precambrian supracrustal rocks give a weak radioactive response. Proximity of the anomalies to an Early Helikian(?) unconformity is significant for mining exploration. A core zone and some other locations within the eastern granite batholith are considerably more radioactive than the bulk of the body. Uranium and thorium concentrations are also present in pegmatite bodies, filling shear zones in the basement near and within the Proterozoic sediments and associated with quartz-pebble conglomerate in the sediments.

Introduction

In 1979 a multidisciplinary study of Late Precambrian sedimentary rocks and nearby subjacent gneiss of the Churchill Province was undertaken in the region of Fury and Hecla Strait. The sedimentary rocks were examined as part of a continuing Geological Survey of Canada study of redbeds. The study of the basement rocks will contribute to an international study of granites, jointly sponsored by the Nuclear Energy Agency (N.E.A.) and the International Atomic Energy Agency (I.A.E.A.). The aim of this study is to establish criteria that will help recognize granitoids likely to contain economic mineralization, particularly uranium mineralization.

The area is of particular interest because the nonconformity separating the sedimentary rocks and gneiss is broadly similar in age to the sub-Athabasca nonconformity of Saskatchewan—one so productive of uranium. Added impetus came from identification of large-scale radiometric uranium and thorium anomalies (Fig. 20.2) in the gneiss adjacent to the nonconformity as a result of the Canadian Uranium Reconnaissance Program. Recent geological work in the area includes that of Blackadar (1958) and Blackadar et al. (1968a, b). Blackadar (1970) summarized early work.

The supracrustal rocks were studied by F. Chandler, A. Legun, B. Zaitlin, Q. Gall, and G. Griesbach. The basement rocks were examined by A. Ciesielski, J. Maley, J. MacManus, and R. Christie. Radiometric studies were carried out by B.W. Charbonneau, G. Bernius, K. Ford, and R. Shives, and geochemical work by Y.T. Maurice and M. Wadleigh. Samples of dykes, sills and redbeds were collected for paleomagnetic study by S. White and H.C. Palmer. Organization was handled by F.W. Chandler, and R. Senneville cooked ably at base camp.

The field season lasted through July and the first half of August. A Twin Otter aircraft from Bradley Air Services was used for transporting fuel and equipment. A Bell Jet Ranger 206B helicopter from Okanagan Helicopters Ltd. provided daily transport of personnel. These aircrafts were chartered through the Polar Continental Shelf Project of the Department of Energy, Mines and Resources. Logistical support was also given by Dr. Andris Rode of the Eastern Arctic Research Laboratory of the Department of Indian and Northern Affairs at Igloodik about 150 km to the southeast.

¹ Resource Geophysics and Geochemistry Division

² Precambrian Geology Division

³ Graduate Student, Department of Geophysics, University of Western Ontario

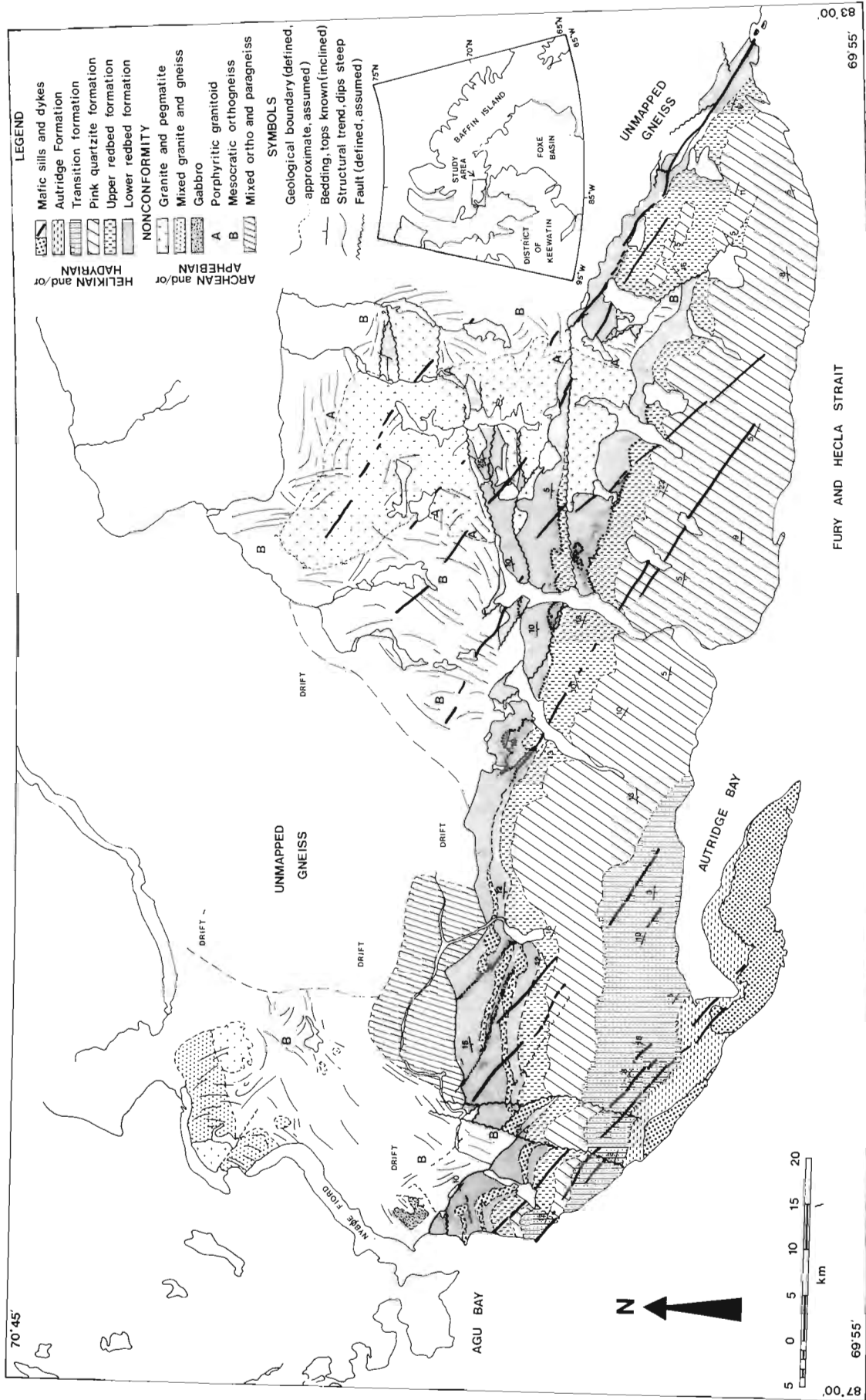


Figure 20.1. Sketch map of the geology of the Fury and Hecla Strait area, north Baffin Island, by F.W. Chandler (supracrustal rocks) and A. Ciesielski (basement gneiss).

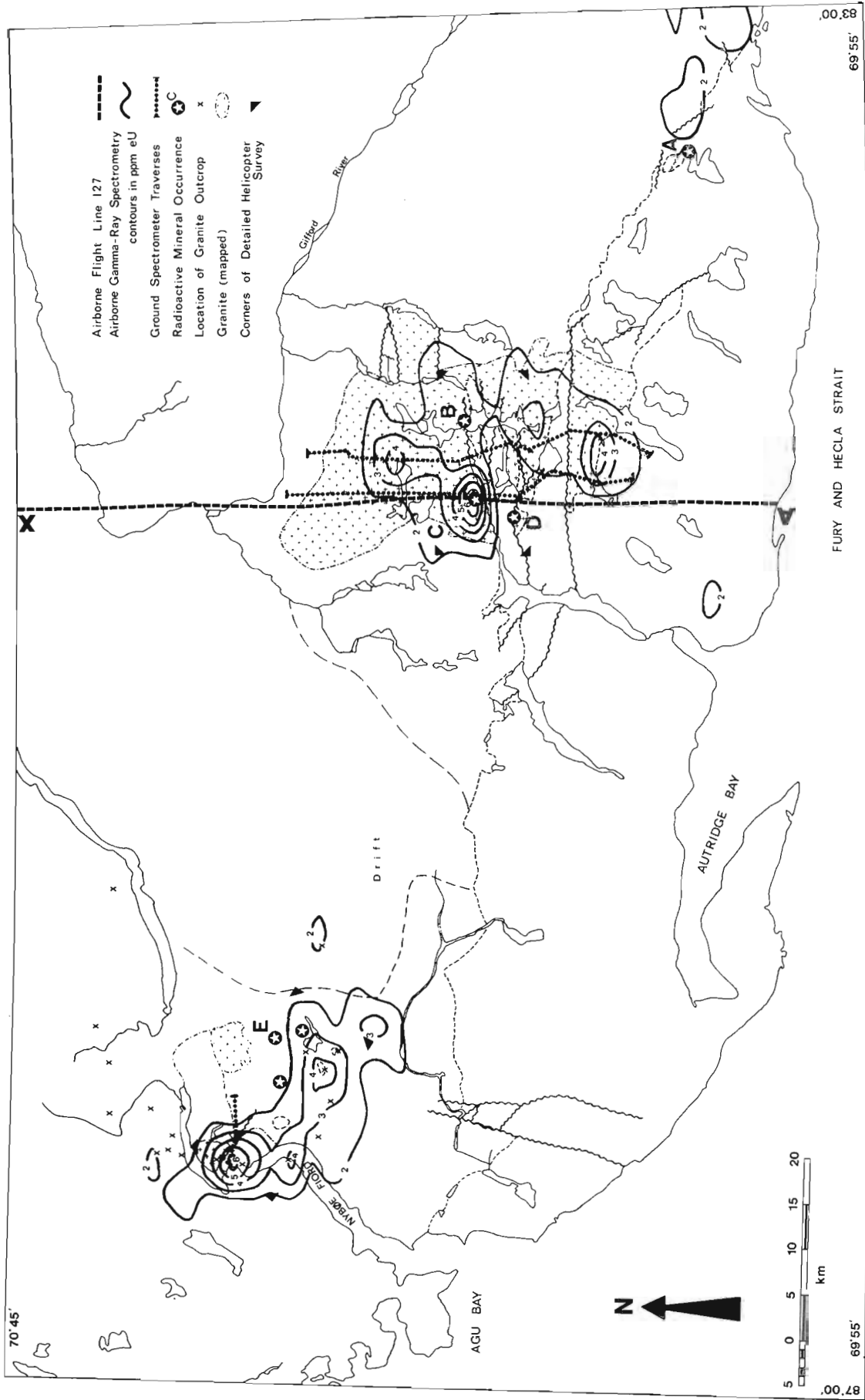


Figure 20.2. Regional airborne radiometric pattern in uranium superimposed on the major geological contacts and showing the locations of detailed studies and type-examples of radioactive mineralization.

Geology of the Supracrustal Rocks¹

The area underlain by the supracrustals is thickly blanketed by felsenmeer. Consequently many geological boundaries were traced by drift and feature mapping. Although only five sedimentary units are mappable with reasonable confidence (Fig. 20.1), subdivisions into members were made where outcrop permitted. The roughly calculated thickness of 6000 m is not greatly different from the 4575 m estimated by Blackadar (1970) who also assumed an average dip southward of 10°. The boundary with the underlying gneiss in general appears undisturbed, although in the central part of the area it is repeated by east-striking faults.

The basal sedimentary unit, the lower redbed formation is about 700 m thick and commences with red sandstone or grit. Basal polymictic breccia in two localities at the western end of the area might be fault-related. In the eastern part of the area the lower redbed formation consists of a red sandstone member overlain by a white quartzite member. Separation of these two members becomes more difficult westward. The red sandstone member consists of friable crossbedded grit and sandstone with interlayered units several metres thick of friable mudcracked red siltstone – shale. White, cream, and orange weathered sandstone and quartzite are also present. About 15 m of oligomictic hematitic quartz-cobble to boulder-orthoconglomerate in the upper part of the red sandstone member, thins and fines westward to possibly 15 cm of pebble conglomerate. Clasts include some from a previous cycle of quartz-pebble conglomerate deposition. In the east the conglomerate is unstratified or crudely size-stratified. Clast imbrication of a₁b₁ type, typical of alluvial environments (Harms et al., 1975) is common and indicates paleotransport from the southeast. Above the conglomerate, within the red sandstone member lies a zone about 60 m thick rich in red crossbedded and wave-rippled dolomitic sandstone beds. Stromatolites were found in this zone at two localities. The white quartzite member is white to pink, fine- to coarse-grained and abundantly wave rippled.

The upper redbed formation, about 500 m thick, consists mainly of a coarsening-upward red shale – red sandstone megacycle including similar second order cycles. The base of the megacycle is marked by discontinuous development of a stromatolitic dolomite member overlain by a continuous black shale member. The dolomite member, at most 5 m thick contains stromatolites of LLH type (Logan et al., 1964), some oval and oriented along azimuth 060°. Associated sediments include mudcracked shale and oolitic and oncolitic carbonate. The overlying black shale member, about 60 m thick contains minor red shale and isolated units of rippled black siltstone and grey sandstone. Trough crossbeds in the upper redbed formation indicate westward paleotransport.

Interbedded pink quartzite, bright red sandstone, and shiny red mudcracked shale mark transition to the overlying pink quartzite formation. This resistant formation is about 2800 m thick in the centre of the area, thins westward, and underlies a range of hills that runs east-west through the area. It is generally quartz-rich and may be fine grained to gritty with scattered quartz pebbles. Slack-water clay drapes are absent from the quartzite. Minor colours include white, puce, red and cream. Sedimentary structures include ripples and crossbeds, the latter indicating paleotransport to the southwest.

The pink quartzite formation is overlain by a transition formation, about 1500 m thick and composed of shale, siltstone and crossbedded sandstone. Recessive weathering of the finer grained clastics gives the unit a ribbed appearance in outcrop. The unit is strongly colour layered in white, grey, pink, red, green, and black. Sediment transport was to the southwest.

The sedimentary units described above comprise the Fury and Hecla Formation of Blackadar (1970). The overlying unit, the Autridge Formation of Blackadar (1970), is the highest stratigraphic unit in the area. It is composed of about 500 m of fissile black shale, with several per cent of grey rippled siltstone and sandstone beds dispersed through it. Syneresis cracks are common in the shale.

Two mafic sills are present in the western and central part of the area. The lower sill, about 6 m thick, consists of fine grained diabase with chlorite amygdules, and occurs close to the dolomitic sandstone zone of the lower redbed formation. The upper sill, possibly up to 30 m thick, occurs within the white quartzite member of the lower redbed formation. A third, mafic sill overlies the Autridge Formation on Autridge Peninsula and on the nearby coast to the west. Northwest-striking magnetic mafic dykes cut the sediments and may be of Franklin age (Fahrig et al., 1971).

Apart from local contact effects from the mafic intrusives, the sedimentary rocks are unmetamorphosed. Strata dip gently southward except adjacent to faults. Some of the faults strike east-west and are upthrown to the south, repeating the basement gneiss and part of the basal redbed formation. The basement is generally unaltered but adjacent to one of these faults it is strongly hematized. Two other faults contain uranium mineralization in quartz-cemented quartzite stockwork. Near these the gneiss is friable and rusty-weathered. Thorium is present in sand beds inter-layered with quartz cobble-boulder conglomerate in the lower redbed formation. Mineralization is dealt with at greater length in subsequent sections of this paper.

Blackadar (1970) commented on lithological similarity between the sequence at Fury and Hecla Strait and one 300 km to the north but was reluctant to support their correlation on account of the great separation of the sequences. Later work (Geldsetzer, 1973; Jackson et al., 1978) on the northern sequence reaffirms the similarity. Specifically, the basal redbed formation is similar to the basal Nauyat Formation of the northern area. Likewise the pink quartzite formation, transition formation and Autridge Formation have features in common with the younger Adams Sound and Arctic Bay formations to the north. Paleocurrent directions from trough crossbeds in the two areas are also similar.

Geology of the Basement Gneisses²

Mapping was carried out over the areas surrounding the two radiometric anomalies (Fig. 20.1, 20.2). The better exposed eastern area comprises a central part of granitic composition, surrounded by mesocratic gneisses probably of tonalitic composition (B, Fig. 20.1). The unusually radioactive pink granite is medium grained and contains as mafic minerals rare biotite and hornblende. Nearly all outcrops are cut by dykes of usually coarse grained and commonly quartz-rich pegmatite. In wide shear zones the pink granite acquires a gneissic texture and is normally biotite-bearing. The presence of other femic minerals arises from assimilation of more mafic inclusions. Within the pink granite deformation is weak, however one phase of folding and foliation is apparent. Outcrop of the granite is extended southward of the basal contact of the Proterozoic sediments by several east-striking faults. The pink granite contains at least five types of inclusions: (a) porphyritic monzonite, (b) mesocratic tonalitic gneiss, (c) paragneiss, (d) amphibolite, and (e) ultrabasic rocks of varied composition. Within the first two types of inclusion lie smaller inclusions of the last three lithologies. In the western area the pink granite is present as batholiths and also is widespread as mappable stocks and bodies or dykes of outcrop scale. In certain places the granite pegmatite dykes

¹ by F.W. Chandler (Project 790016)

² by André Ciesielski (Project 790029)

are very thick and abundant. These and pink granite dykes both parallel and transect the foliation of the surrounding gneisses and are probably of syn- and late-tectonic origin.

Within and mostly at the margin of the pink granite batholith of the eastern area there is a granitoid of probable monzonitic composition (A, Fig. 20.1). This medium-to coarse-grained rock contains potash feldspar phenocrysts and a significant amount of biotite. Well-developed foliation locally makes the rock an augen gneiss. This rock type has mainly amphibolite inclusions and is likely to be pre- and syntectonic. Surrounding the massive pink granite there is a widespread gneiss (B, Fig. 20.1) that is intruded by the above monzonitic granitoid. Generally it is mesocratic, fine- to medium-grained, strongly foliated and has many types of inclusions. Schlieren and other signs of assimilation of more mafic material are numerous. As in the case of the pink granite, inclusions include paragneiss of varied composition and thickness, and various amphibolitic and ultrabasic rocks. The rock also contains masses of differing size of dioritic or hybrid affinity.

In the western area the above gneisses show varied composition and fabric, including lit-par-lit layering involving biotite and hornblende, fine foliation or augen structure. Masses or dykes of amphibolite are numerous. The gneisses are in general highly deformed and migmatoid in some places. Small scale folds are common though some with dimensions greater than 12 m were seen. Structural data indicate at least two phases of deformation. Present only in the western area is a unit of mixed orthogneiss and paragneiss, differing in texture and structure from the mesocratic orthogneiss (B). This unit (Fig. 20.1) is a very thick sequence partly of sedimentary origin, with a fine compositional layering and includes banded iron formation incorporated within felsic rocks. No marker units were found that would suggest repetition of the sequence by folding. Amphibolite, gabbro and ultrabasic rocks are also interbedded within the unit. In the field distinction between the orthogneiss and paragneiss of this unit is difficult because of the fine parallel layering. Deformation is marked by vertical foliation planes and asymmetrical folds.

Generally, deformation in the eastern and western areas is intense except in the granite and pegmatite. Folds are uncommon and lineations are absent. A stratigraphic column is shown in Table 20.1.

Table 20.1

Stratigraphic column to show the relative age and deformation of the basement rocks

Diabase dykes and sills			
Proterozoic sediments	-----		
Pink granite and pegmatite	-----		
Gabbro and porphyritic monzonite	-----		
Basic dykes			
Tonalite/granodiorite (mesocratic gneiss)			
Gabbro and diorite			
Volcanic/sedimentary series			
Greywackes (paragneiss)			
Basic volcanics (amphibolites)			
Ultrabasics			
Katarchean basement??			

----- : discordance
 γ_{1-2} : deformation phase

Radiometric Studies¹

General

During 1977, an airborne gamma ray spectrometric survey was carried out in the area in accordance with Uranium Reconnaissance Program specifications (Darnley et al., 1975). The results were published in 1979 as Geophysical Series Maps 35647-G - Agu Bay and 35547-G - Erichsen Lake. Results for each sheet comprise seven contoured maps: K%, eU ppm, eTh ppm, eU/eTh, eU/K, eTh/K and Total Count. Data along the individual flight lines were published as stacked profiles of the seven parameters listed above as well as a magnetometer trace.

Regional Pattern

The reconnaissance airborne radiometric survey revealed two major anomalies (Fig. 20.2), one in the eastern part of the area and the other, in the west. Both the eastern and western anomalies are predominantly underlain by bodies of granite described in the previous section. The mapped contacts of these granites are shown on Figure 20.2. A number of granite outcrops found by helicopter landings outside the area of detailed mapping in the western area are also shown on Figure 20.2. The 2 ppm eU contour shown in Figure 20.2 outlines the southwest quarter of a ring shaped anomaly which is clearly delineated by contours on the equivalent thorium and total count maps (not included in this paper). The distribution of granite outcrops coincides with this ring of high radioactivity. The areas inside and outside the ring appear to be underlain by mesocratic to mafic gneiss with considerable drift cover. The southern half of the ring is more uraniumiferous than the northern half (Fig. 20.2).

The area situated between the two anomalies is extensively drift covered, however, geological mapping suggests that this region is underlain by the gneiss. Thus the low radiometric response is thought to be due to generally low radioactivity of the rocks and the associated glacial detritus. The southern part of the area is generally low in radioactivity because of the low overall radioelement concentrations in the sediments.

The proximity of the anomalously radioactive granites to the probably Helikian nonconformity accentuates the favourability of this area for uranium exploration. The proximity of the anomalous granite basement to the nonconformity is illustrated by the eastern anomaly. Figure 20.3, an airborne radiometric profile from the regional survey, cuts across the most radioactive portion of the eastern granite (see A-X, Fig. 20.2). This profile shows values as high as 10 ppm eU. The area of maximum radioactivity lies within the granite near the nonconformity. A sharp drop in radiometric levels occurs at the contact with the overlying sedimentary rocks. The uranium levels on the profile (> 10 ppm) are higher than on the contour maps, the latter showing maximum values of > 6 ppm. This discrepancy results from smoothing of the data in the computer contouring process. For this reason the contour maps should always be examined in combination with the profiles. The contour pattern outlines the regional picture whereas the profiles give more detailed information about the area along the flight path. Cameron et al. (1976) and Charbonneau et al. (1976) have discussed the above relationships.

Detailed Studies

Detailed studies carried out in the Fury and Hecla Strait area consisted of:

1. Three ground traverses, totalling about 80 km, along which gamma ray spectrometry, scintillometry and geological sampling were carried out. Two of the traverses were in the east and the other in the west (see dotted lines, Fig. 20.2). Stations were located at 100 m intervals.

¹ B.W. Charbonneau (Project 760045)

LINE 127(1) AGU BAY 47F NORTHWEST TERRITORIES 1977

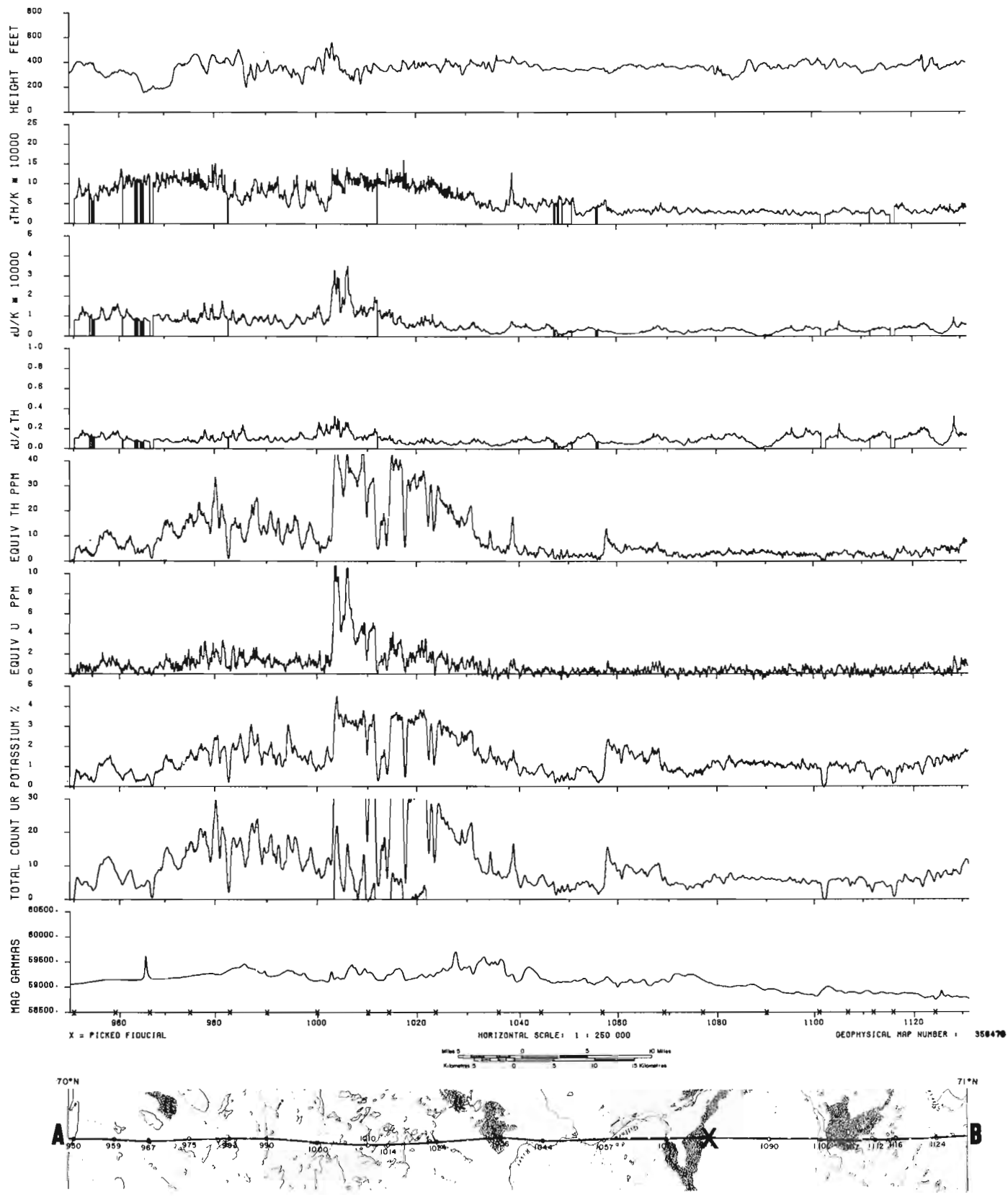


Figure 20.3. Regional airborne radiometric profile across the most radioactive portion of the granite basement.

Table 20.2

Uranium Content* of Granitic and Other
Radioactive Rocks in the Fury and Hecla Strait Area
(see Fig. 20.2 for locations)

Rock Type	Area km ²	Number of Samples	Uranium in ppm Arith. Mean	Range
Eastern granite				
- regional	≈500	23	8.2	1 - 26
- intermediate area	1	17	13.0	3 - 31
- core (Loc. C)	0.1	17	22.2	6 - 42
Western granite (regional)	≈500	14	7.2	1 - 15
Pegmatites and related rocks (Loc. E)		35	-	1 - 10 400
Shear zone (Loc. B)		3	-	127 - 302
Shear zone (Loc. D)		1	-	1490
Conglomerate (Loc. A)		1	-	32
*Determined by delayed neutron activation.				

2. Two 200 km² detailed airborne gamma spectrometry surveys flown over the most eastern and western anomalies to locate the most radioactive portions. These surveys were flown at 30 m terrain clearance with a crystal volume of 1.6 Litres, and a line spacing of 1 km (0.5 km in the area of greatest interest). The locations of the surveys are indicated on Figure 20.2 by corner marks.

3. Spot landings, to examine specific features and search for uranium enrichment.

In all, about 1000 in situ radioelement determinations were made and about 200 samples were collected.

Results of the ground traversing will enable a relationship between the radiometric response over the granites and their petrology to be established. Compilation of in situ determinations of potassium, uranium, and thorium values has not yet been completed. Initial indications based on preliminary reduction of the data show that the granites underlying the eastern and western anomalies contain about twice the concentration of uranium and thorium of average granite, whereas levels in the gneissic complex are below average granite values (Clarke et al., 1966).

Some portions of the granites are considerably more radioactive than the above levels. For example, the core of the eastern radiometric anomaly (eU > 6 ppm, Fig. 20.2) averages about five times the Clarke values for uranium and thorium. An average value of 22 ppm equivalent uranium and 104 ppm equivalent thorium was calculated across 3 km of the core zone on the ground. Values of equivalent uranium and equivalent thorium across 3 km of the core of the western granite (eU > 6 ppm, Fig. 20.2) average 12 ppm eU and 65 ppm eTh, nearly three times Clarke values. The uranium concentrations reported here have been substantiated by chemical analyses (see section on geochemistry).

Radioactive Occurrences

Various types of uranium and thorium occurrences were found and the locations of type examples are shown on Figure 20.2.

- A. Clastic (placer type) concentrations in the basal Helikian conglomerates.
- B. Veins in shear zones associated with quartz stockwork in the uppermost basement.
- C. Zones of enrichment within the granitoid bodies in the basement.
- D. Veins in shear zones associated with quartz stockwork in the Helikian sediments.
- E. Pegmatites associated with the granitoids.

Mineralogical studies and autoradiography have not yet been completed on samples from these occurrences. The concentrations reported below are based on in situ gamma spectrometric analyses and thus represent large sample volumes (> 100 kg of rock). Direct uranium determinations on some of these showings are presented in the section on geochemistry (see Table 20.2).

Locality A is a thorium occurrence in conglomerate. Low concentrations of uranium (a few tens of ppm) and up to 170 ppm eTh have been found.

Locality B is a uranium occurrence along approximately 30 m of a shear zone in the granite. This zone is filled with a quartz stockwork and hydrothermal alteration of the granite wall rock was noted. Maximum values measured were 270 ppm eU and 90 ppm eTh. The thorium concentration is probably derived from the host granite.

Locality C is in the core of the eastern granite. The rock is a subporphyritic pink granite. Maximum radioelement concentrations measured were 80 ppm eU and 160 ppm eTh. Hydrothermal alteration was noted in places.

Locality D is a uranium occurrence which is localized along 40 m of a major fault cutting Helikian sandstone. This shear zone also contains a well developed quartz stockwork and is hydrothermally altered. Maximum in situ values recorded were 660 ppm eU and 100 ppm eTh.

Locality E is representative of a number of radioactive pegmatites near the western granite. These bodies typically are up to 30 m in length by 1-2 m in width. Maximum radioelement values measured in situ were 2300 ppm eU and 1200 ppm eTh.

The results of this work illustrate the general relationship of uranium occurrences to areas of anomalous radioactivity as discussed by Darnley et al. (1977).

In addition to the above types of uranium occurrences concentrations in structural and lithological traps under the Helikian basement nonconformity might be expected as well as concentrations within the Helikian sediments in reduced facies. However no indications of the latter two types were found in this study.

Geochemistry¹

Systematic sampling of the various types of radioactive rocks occurring in the area was carried out in an attempt to characterize them chemically. The eastern granite was sampled with the sample density increasing towards the core of the radiometric anomaly (Locality C, Fig. 20.2). The sampling scheme was designed to investigate the chemical variance within outcrops (3 to 10 m) and between outcrops (30 to 50 m) and compare these with the regional variance. The analytical variance will also be estimated by means of blind duplicate samples.

The western granite was sampled in the same way as the eastern granite but with a slightly wider interval. Denser sampling of the eastern granite was carried out by foot traverses. Widely spaced sampling was done by helicopter, using information from a mapping crew.

¹ by Y.T. Mauricé (Project 760047)

The zones of anomalous radioactivity associated with quartz pebble conglomerates (Locality A, Figure 20.2), shearing (Localities B and D), and pegmatites (Localities E) were also sampled. The main radioactive shear zone associated with the eastern granite (Locality B, Fig. 20.2) was sampled along a traverse running at a right angle to the strike of the mineralization to investigate the nature and extent of the alteration that is associated with this zone. Other less radioactive zones that display similar alteration near the core of the eastern anomaly were also sampled.

In the western anomaly, 35 pegmatite bodies and related rocks, some radioactive, others barren, have been examined and sampled.

All samples collected will be analyzed for the major elements, uranium and thorium. A selection will also be analyzed for other elements including, Sn, W, Pb, Mo, F, Rb, Ba, Sr, Y, La, rare earth elements, and Zr. Microprobe analyses of selected specimens will also be carried out.

Preliminary Results

Uranium values are being determined by neutron activation/delayed neutron counting at Atomic Energy of Canada Limited. Available data (Table 20.2) are in agreement with the ground radiometric measurements. With an average uranium content of 8.2 ppm and 7.2 ppm respectively, both the eastern and the western granites are anomalously high in uranium. The substantial increase in the uranium content (22 ppm) of the rocks towards the core of the eastern granite is noteworthy. It has yet to be determined whether this pattern in the uranium distribution corresponds to variations in the major element composition of the rock and whether minor and trace elements show distributions that are sympathetic to that of uranium. These observations along with a study of samples from the radioactive shear zones and associated alterations will help to determine the mechanism responsible for the uranium enrichment of the granites and fault zones. The major and trace element concentrations of the radioactive pegmatites should establish their genetic derivation.

Paleomagnetic Studies¹

Samples were collected from the lower and upper redbed formations, from the pink quartzite formation, from the two lower mafic sills, and from mafic dykes. Twenty-two sites were drilled, each usually composed of six cores. Each core subsequently gave two paleomagnetic specimens. Two block samples taken from one site yielded five individual cores which were drilled vertically in the lab. The horizontal component of orientation was obtained in the field by all or two of the following methods: sun bearing, magnetic bearing or land sight. All cores were sawn into one inch specimens of which 235 are ready for measurement.

This study was undertaken to find the age and correlation of the sedimentary and igneous rocks and the paleo-latitude of deposition of the sedimentary rocks.

References

Blackadar, R.G.

1958: Fury and Hecla Strait, District of Franklin, Northwest Territories; Geological Survey of Canada, Map 3-1958.

1970: Precambrian geology of Northwest Baffin Island, District of Franklin; Geological Survey of Canada, Bulletin 191, 89 p.

Blackadar, R.G., Davison, W.L., and Trettin, M.P.

1968a: Geology, Agu Bay - Easter Cape, District of Franklin; Geological Survey of Canada, Map 1240A, Scale 1 in. to 4 miles.

1968b: Geology Erichsen Lake, District of Franklin; Geological Survey of Canada, Map 1242A scale 1 in. to 4 miles.

Cameron, G.W., Elliot, B.E., and Richardson, K.A.

1976: Effects of line spacing on contoured airborne gamma-ray spectrometry data; in "Exploration for Uranium Ore Deposits", IAEA, Vienna, 1976.

Charbonneau, B.W., Killeen, P.G., Carson, J.M., Cameron, G.W., and Richardson, K.A.

1976: Significance of radioelement concentration measurements made by airborne gamma-ray spectrometry over the Canadian Shield; in "Exploration for Uranium Ore Deposits", IAEA, Vienna, 1976.

Clarke, S.P., Jr., Peterman, A.E., and Heier, K.S.

1966: Abundances of uranium, thorium, potassium; Geological Society of America, Memoir 97, Section 24.

Darnley, A.G., Cameron, E.M., and Richardson, K.A.

1975: The Federal-Provincial Uranium Reconnaissance Program; in Uranium Exploration '75, Geological Survey of Canada; Paper 75-26, p. 49-71.

Darnley, A.G., Charbonneau, B.W., and Richardson, K.A.

1977: Distribution of uranium in rocks as a guide to the recognition of uraniferous regions in Recognition and evaluation of uraniferous areas, IAEA, Vienna, 1975.

Fahrig, W.F., Irving, E., and Jackson, G.D.

1971: Paleomagnetism of the Franklin diabases; Canadian Journal of Earth Sciences, v. 8, p. 455-467.

Geldsetzer, H.

1973: The tectono-sedimentary development of an algal-dominated Helikian succession on northern Baffin Island, N.W.T.; in Symposium on the Geology of the Canadian Arctic, Proceedings, Saskatoon, May, 1973, p. 99-126.

Harms, J.C., Southard, J.B., Spearing, D.R., and Walker, R.G.

1975: Depositional environment as interpreted from primary sedimentary structures and stratification sequences, lecture notes for short Course No. 2; Society of Economic Paleontologists and Mineralogists, 161 p.

Jackson, G.D., Ianelli, T.R., Narbonne, G.M., and Wallace, P.J.

1978: Upper Proterozoic sedimentary and volcanic rocks of northwestern Baffin Island; Geological Survey of Canada, Paper 78-14, 15 p.

Logan, B.W., Rezak, R., and Ginsburg, R.N.

1964: Classification and environmental significance of algal stromatolites; Journal of Geology, v. 72, p. 68-83.

¹ by S. White

SKYSHINE AND THE CALIBRATION OF GROUND GAMMA RAY SPECTROMETERS

Project 720084

R.L. Grasty

Resource Geophysics and Geochemistry Division

Grasty, R.L., Skyshine and the calibration of ground gamma ray spectrometers; in Current Research, Part A, Geological Survey of Canada, Paper 80-1A, p. 133-135, 1980.

Abstract

In any field measurement with a gamma ray spectrometer a component of the detected gamma ray flux originates from Compton scattering in the air above the detector. This downward scattered flux, commonly called 'skyshine', is not correctly represented when a field spectrometer is calibrated using large concrete calibration pads. Experiments carried out on calibration pads to simulate the skyshine component have shown that the standard procedure of calibrating a field gamma ray spectrometer yields reliable results except in areas with unusual radioelement ratios.

Introduction

In the past few years radioactive concrete pads have been constructed in a number of countries for calibrating field gamma ray spectrometers. Two sets of these calibration pads have been constructed by the Geological Survey of Canada at Uplands Airport, Ottawa and by the U.S. Department of Energy at Walker Field, Grand Junction, Colorado. The Ottawa pads measure 7.6 x 7.6 x 0.5 m thick and the Grand Junction pads 12.2 x 12.2 x 0.5 m. It is generally believed that these calibration pads are sufficiently large that the potassium, uranium and thorium gamma ray spectra at their surface adequately represent the spectra from an infinite homogeneous source. However, in any field measurement some fraction of the total gamma ray flux incident on the detector originates from gamma rays emitted by the ground, Compton scattered in the air above the point of detection, and deflected back towards the ground. In the course of the scattering process, these gamma rays lose energy. The amount of energy lost is dependent on the angle through which the gamma rays are scattered and on the initial energy of the gamma ray. Thallium-208 gamma rays at 2.62 MeV have the highest energy in the natural spectrum and travel approximately 140 m before half of them suffer a Compton collision. The downward scattered flux or skyshine can therefore originate from sources in the ground up to several hundred metres from the point of detection. Because of the small size of the calibration pads, virtually no downward scattered flux that originates from the pads can be detected on them.

In the energy range 0.4 to 2.62 MeV, Compton scattering is the predominant absorption process occurring in the air. This is also true for materials such as water or wood, because air, water and wood consist of elements with low atomic numbers. To produce a skyshine component that can be detected on the calibration pads, it is not necessary to have pads several hundred metres across. By placing plywood over the top of the detector as illustrated schematically in Figure 21.1, gamma rays from the pad can be scattered downwards from the plywood and be detected on the pad. The plywood simulates a concentrated mass of air thereby producing a radiation field with the same angular distribution as that obtained over an infinite source. The plywood also shields the detector from scattered gamma rays originating from the ground surrounding the pads.

The Experiment and Analysis of Results

In November 1978 experiments were carried out on the calibration pads at Grand Junction, Colorado to investigate the gamma ray spectrum of the skyshine component of the gamma ray flux, and in particular to determine the effect of skyshine on the calibration results. These experiments were

carried out in conjunction with a series of intercalibration experiments between the Ottawa and Grand Junction pads which have been reported elsewhere (Carson et al., in press).

A package of four prismatic 101.6 x 101.6 x 406.4 mm NaI(Tl) crystals was placed at the centre of each of the Grand Junction calibration pads on 150 mm of polystyrene and covered with plywood sheets 2.44 m square with a total thickness of 30 cm (12 inches). The weight of the plywood was found to be equivalent to a layer of air 112 m thick. Spectral data were recorded in 256 channels covering the energy range from 0 to 3.0 MeV using a multi-channel analyzer mounted in a borehole logging truck. The borehole logging truck and its equipment have been described by Bristow and Killeen (1978). Approximately 30 ten second spectra were recorded on each of the five pads, first with the plywood over the top and then with the plywood removed.

The spectral data were corrected for dead time and energy calibrated by monitoring the position of the potassium-40 peak at 1.46 MeV and the thallium-208 peak at 2.62 MeV in the thorium decay series. Data from the corrected spectra were accumulated into the three commonly used windows. These are 1.36-1.56 MeV for potassium-40, 1.66-1.86 MeV for bismuth-214 in the uranium decay series and 2.41-2.81 MeV for thallium-208 in the thorium decay series. Data were also accumulated into twelve, 200 keV-wide windows from 0.4 to 2.8 MeV in order to produce individual spectra of potassium, uranium and thorium. This was achieved by fitting the count rate, N_I , in channel I, by a least-squares technique to the equation

$$N_I = \epsilon_{KI} \times K_{\text{conc}} + \epsilon_{UI} \times U_{\text{conc}} + \epsilon_{TI} \times T_{\text{conc}} + B_I \quad (1)$$

where K_{conc} , U_{conc} and T_{conc} are the concentrations of each pad and ϵ_{KI} , ϵ_{UI} and ϵ_{TI} the sensitivities of channel I measured as counts per second per unit radioelement concentration. B_I is the background count rate for channel I, which arises from the radioactivity of the equipment and the air, cosmic radiation and radiation from the ground surrounding the pad. The values of ϵ_{KI} , ϵ_{UI} and ϵ_{TI} are shown in Figures 21.2, 21.3, and 21.4 as potassium, uranium and thorium spectra with and without a skyshine component.

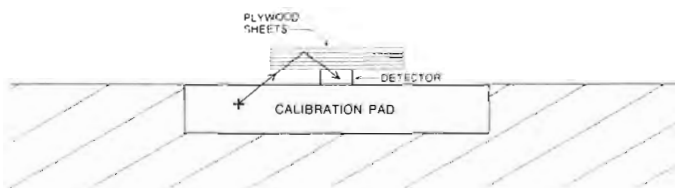


Figure 21.1. Schematic diagram of skyshine experiment.

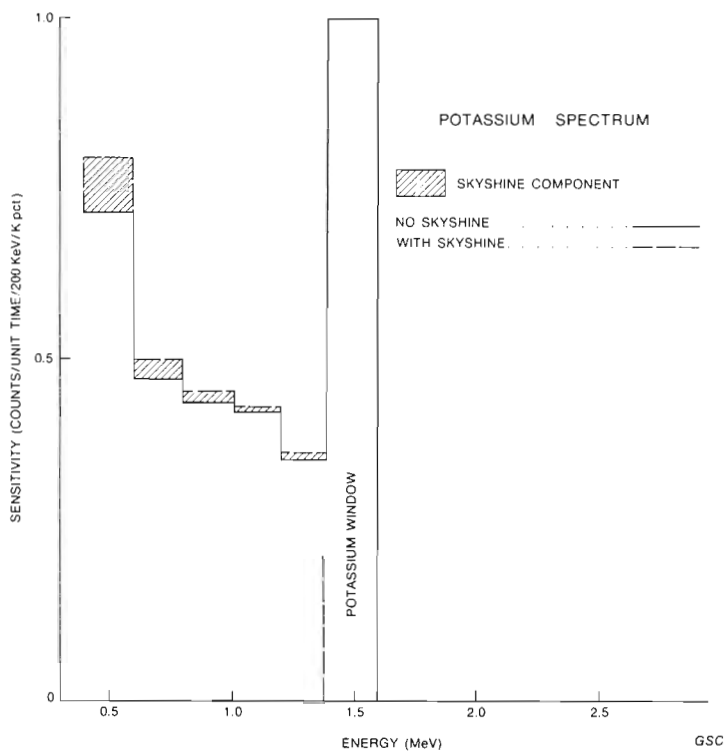


Figure 21.2. Potassium spectrum from the calibration pads with and without a skyshine component.

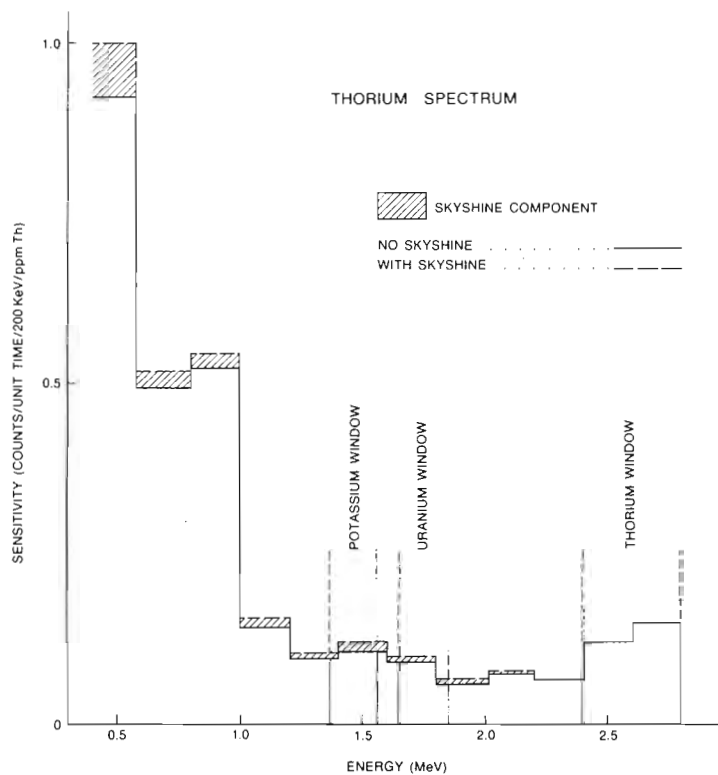


Figure 21.4. Thorium spectrum from the calibration pads with and without a skyshine component.

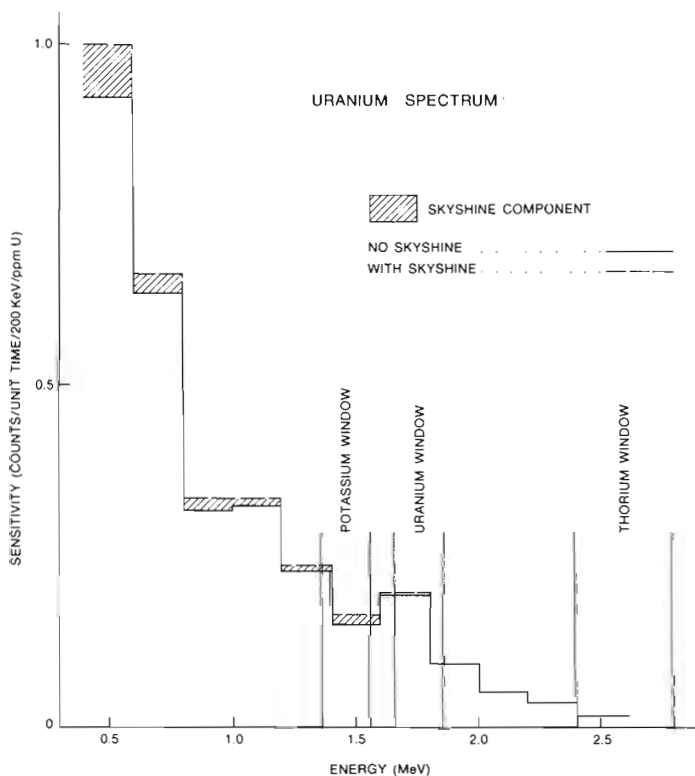


Figure 21.3. Uranium spectrum from the calibration pads with and without a skyshine component.

Table 21.1
Calibration constants

	Without Plywood on Top (No Skyshine)	With Plywood on Top (with Skyshine)
Thorium Sensitivity (Counts/sec/ppm Th)	6.60 ± 0.01	6.50 ± 0.01
Uranium Sensitivity (Counts/sec/ppm U)	11.51 ± 0.01	11.53 ± 0.01
Potassium Sensitivity (Counts/sec/K pct)	134.3 ± 0.1	134.6 ± 0.1
Thorium Background (Counts/sec)	6.2 ± 0.1	6.1 ± 0.1
Uranium Background (Counts/sec)	6.9 ± 0.2	3.0 ± 0.2
Potassium Background (Counts/sec)	25.3 ± 0.4	14.2 ± 0.5
α	0.260 ± 0.001	0.273 ± 0.001
β	0.365 ± 0.002	0.409 ± 0.002
γ	0.815 ± 0.002	0.851 ± 0.002
A	0.066 ± 0.001	0.070 ± 0.001
G	0.0064 ± 0.0004	0.0099 ± 0.0004

α is the ratio of the counts in the uranium window to the counts in the thorium window from a pure thorium source

β is the ratio of the counts in the potassium window to the counts in the thorium window from a pure thorium source

γ is the ratio of the counts in the potassium window to the counts in the uranium window from a pure uranium source

A is the ratio of the counts in the thorium window to the counts in the uranium window from a pure uranium source

G is the ratio of the counts in the uranium window to the counts in the potassium window from a pure potassium source

The count rates in the three standard windows were also fitted to equation 1 and the window sensitivities (ϵ) used to give calculated values of the stripping ratios α , β , γ , A and G (defined in Table 21.1) in a similar manner to that described by Grasty (1977). In the calculation it was assumed that there were no counts in the thorium window from a pure potassium source. The potassium, uranium and thorium sensitivities in the standard windows and calculated background count rates are shown in Table 21.1. The errors indicated are one standard deviation and were calculated by a Monte Carlo technique based on probable errors in the counts accumulated for each pad, and assuming that the pad concentrations had no errors associated with them.

Discussion and Significance of Results

In Compton scattering, a gamma ray collides with an electron and is deflected from its original direction. From momentum and energy considerations, the gamma ray will lose more energy to the electron, the greater the angle through which the gamma ray is scattered. The theory of Compton scattering shows that the probability of scattering increases as the scattering angle increases. Consequently, when gamma rays are scattered, there are more low energy than high energy gamma rays produced.

From Table 21.1 it can be seen that the potassium, uranium and thorium sensitivities, with and without the plywood on top of the detector, have similar values. This should be expected because very few thallium-208 gamma rays at 2.62 MeV will be scattered at small angles thereby still retaining sufficient energy to be detected in the thorium window. Similarly, very few scattered potassium and uranium gamma rays will retain sufficient energy to be counted in their respective windows.

A comparison of the calculated background values shows that the thorium background has remained unchanged with the addition of plywood, whereas the uranium and potassium values have been reduced by approximately 50 per cent. This can be explained by the shielding effect of the plywood on the downward scattered radiation from the ground surrounding the pads. This downward scattered radiation will be predominantly of low energy and consequently the addition of plywood will preferentially reduce the count rate in the lower energy potassium and uranium count rates by shielding the detector from bismuth-214 in the air.

Of particular interest in Table 21.1 is the difference between the stripping ratios. It is found that α , β , and γ increase by approximately 5, 12 and 4 per cent respectively with the addition of a skyshine component. Although these increases were much greater than was originally expected, a study of the theoretical proportions of downward directed gamma ray flux to total flux at ground level using tables presented by Løvborg and Kirkegaard (1975) shows that these increases are not unreasonable. For instance in the energy region covering the potassium and uranium windows the ratio of downward to total flux for a thorium source can vary anywhere from one to nine per cent. Low values of this ratio occur at energies where there are primary (and consequently upward directed) gamma rays emitted in the thorium decay series which will then dominate the spectrum at that particular energy.

It should be noted that the results presented in this paper are for measurements at ground level. At aircraft altitudes the angular distribution of upward directed flux is quite different from the distribution at ground level. As the altitude increases the high energy upward-directed flux becomes much more strongly peaked in the upward direction, i.e. few high energy gamma rays can reach the detector at

angles close to the horizontal. Consequently, there are fewer gamma rays which can be scattered at small angles and be detected in the potassium and uranium windows. The proportion of downward-to-total flux at energies above the potassium window is therefore reduced as the aircraft altitude increases and the problems of skyshine also become less significant.

An examination of the potassium, uranium and thorium spectra shown in Figures 21.2, 21.3, and 21.4 serves to aid in the interpretation of the results. Although the total skyshine component increases at low energy, the variation in the stripping ratio will be dependent on the proportions of skyshine to total flux detected. For instance in Figure 21.4 for a thorium source, although the skyshine component at the potassium window is quite small and less than at lower energies, it is still a significant proportion of the detected flux.

It is of interest to evaluate the effects of the changes in the stripping ratios on the calculation of concentrations using the values shown in Table 21.1. For a typical rock with a concentration of 8 ppm thorium and 2 per cent potassium, the calculated potassium concentration using the pad results with no skyshine will overestimate the potassium concentration by 1 per cent to give a potassium value of 2.02 per cent. This error in potassium increases as the thorium to potassium ratio increases and will give a 10 per cent error for a rock of 80 ppm thorium and 2 per cent potassium. Analysis of the change in the stripping ratios α and γ showed similarly that the uranium and potassium concentrations will only be in error in areas where the thorium-to-uranium and uranium-to-potassium values are unusually high.

In spite of the lack of downward scattered radiation on the calibration pads, the standard procedure of calibrating a field gamma ray spectrometer is therefore found to provide reliable results except in areas with unusual radioelement ratios.

Acknowledgments

This work could not have been carried out without the help of Ken Kosanke of Bendix Field Engineering Corporation who kindly provided the detector package. Peter Holman, Yves Blanchard and Bill Hyatt provided moral and physical support in moving the 1 ton of plywood, and United Air Lines Inc. generously provided an airline baggage trolley to transport the plywood.

References

- Bristow, Q. and Killeen, P.G.
1978: A new computer based gamma-ray spectral logging system; Paper presented at the Society of Exploration Geophysicists Annual Meeting, San Francisco.
- Carson, J.M., Holman, P.B., and Grasty, R.L.
1979: Airborne gamma-ray spectrometer experiments – intercalibration and variation of calibration constants with altitude; Transactions, American Nuclear Society, Atlanta.
- Grasty, R.L.
1977: A general calibration procedure for airborne gamma-ray spectrometers; Geological Survey of Canada, Paper 77-1C, p. 61-62.
- Løvborg, L. and Kirkegaard, P.
1975: Numerical evaluation of the natural gamma radiation field at aerial survey heights; Risø Report No. 317.

Victor Owen¹, Erich Dimroth¹ and Gerard Woussen¹
Precambrian Geology Division

Owen, Victor, Dimroth, Erich, and Woussen, Gerard, *The Old Gneiss Complex east of Chicoutimi, Quebec; in Current Research, Part A, Geological Survey of Canada, Paper 80-1A, p. 137-146, 1980.*

Abstract

The chronological and deformational history of the Precambrian paragneisses and orthogneisses east of Chicoutimi, Québec, has been determined by evaluation of intrusive relationships and of the relationships of anatectic veins to tectonic structures. Rocks of three age groups are defined as follows: 1) paragneiss, associated amphibolite I and granite I, all affected by anatexis I; 2) granite II, cut by dykes of amphibolite II, all affected by anatexis II and by deformation phases I and II; 3) granite III, dykes of amphibolite III, affected by anatexis III and by deformation III. Metatects of anatexis II formed chiefly in situ, whereas metatects of anatexis III are allochthonous.

Introduction

Woussen et al. (1979 a, b) presented a tentative chronology of the evolution of the bedrock in the upper Saguenay district of the Grenville Province. The purpose of this report is to document the stratigraphy of the old gneiss complex at St-Fulgence and along Rang St-Martin, east of Chicoutimi, Québec. The stratigraphy is based on 1) intrusive relationships, particularly as displayed by two generations of mafic dykes, and 2) the relationship of rock units to phases of deformation and anatexis. Apart from the present work, stratigraphic method 1 after Sederholm (1967) has yet to be systematically employed in the Grenville; it has however been used successfully in Greenland by Watterson (1965, 1968). The constituents of the old gneiss complex are subdivided into three main age groups as follows (see Table 22.1, Fig. 22.1):

1. Paragneisses, associated amphibolites (amphibolite I), and a first generation of granite (granite I) underwent a first anatexis (anatexis I). Very likely these rocks were deformed during or prior to anatexis I; all traces of such a deformation, however, have been destroyed by three later phases of folding.
2. Rocks of age group 1 were intruded by a second generation of granite (granite II) and by mafic dykes (amphibolite II). A complex deformation (deformations I and II) was accompanied by a second phase of anatexis (anatexis II).
3. Rocks of age groups 1 and 2 were intruded by a third generation of granite (granite III) and by mafic dykes (amphibolite III). Finally, all rocks were affected by a third phase of deformation and anatexis (deformation III, anatexis III).

Style of Deformation

In all likelihood rocks of age group 1 were folded before the intrusion of granite II because anatexis has never been observed to affect flat-lying, undeformed sedimentary rocks. However, all physical traces of this earliest deformation have been erased by the subsequent F_1 -folding, except, perhaps, for rare, very strongly flattened folds in the paragneiss sequence (Fig. 22.2). These intrafolial folds of layers in the paragneiss sequence and of metatects I (Fig. 22.3a) now have S_1 as the axial plane; they may be F_1 -folds, but alternatively they could be older folds rotated into the axial plane during F_1 -folding.

F_1 -folding is the dominant penetrative deformation at Rang St-Martin. It produced the regional schistosity S_1 in the gneisses of age groups 1 and 2. Flattening associated with F_1 -folding is extremely strong; rare relicts of such folds can be traced by dykes of amphibolite II.

F_2 -folds affect the regional schistosity S_1 ; they are moderately to extremely flattened. Their axial plane here is named S_2 ; it trends generally 45 to 90° and dips steeply. An axial plane schistosity parallel to S_2 is generally absent; strong lineations, however, are common in the hinge zone of F_2 -folds (Fig. 22.3c, 22.4). Most of the folds observed in the area belong to this fold generation. F_2 -folding appears to have affected all rocks of the area, except for those of age group 3.

Table 22.1
Stratigraphy of the Old Gneiss Complex

Mylonite, Carbonatite, Lamprophyre	
Metatect III	Deformation III
Amphibolite III	
Granite III	
Metatect II	Deformations I and II
Amphibolite II	
Granite II	
Metatect I	Deformation ?
Granite I	
Paragneiss and Amphibolite I	

¹ Sciences de la Terre, Université du Québec à Chicoutimi, Chicoutimi, Québec G7H 2B1

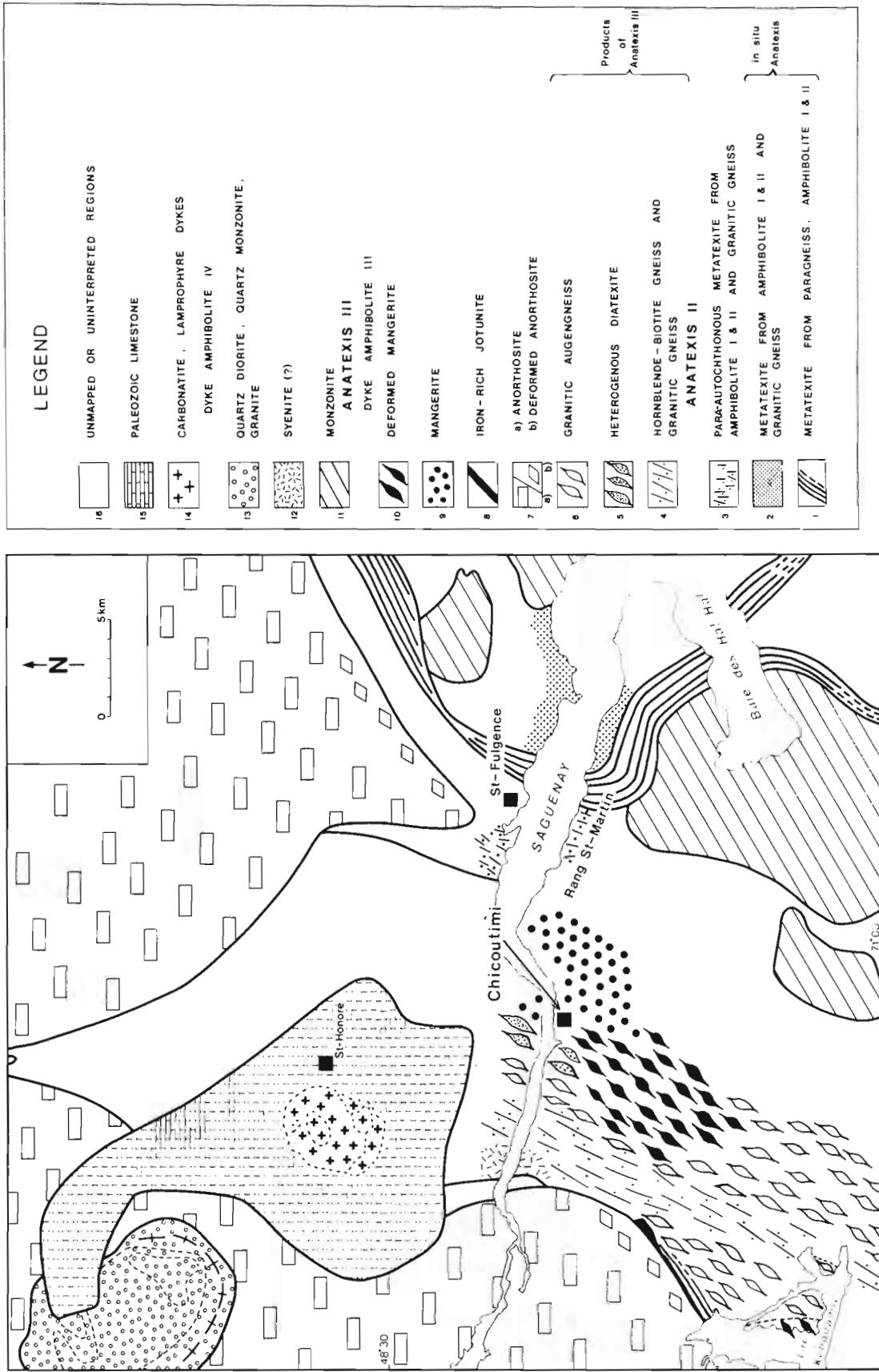


Figure 22.1 Preliminary geological map of the upper Saguenay area, Quebec revised from Woussen et al. (1979a).

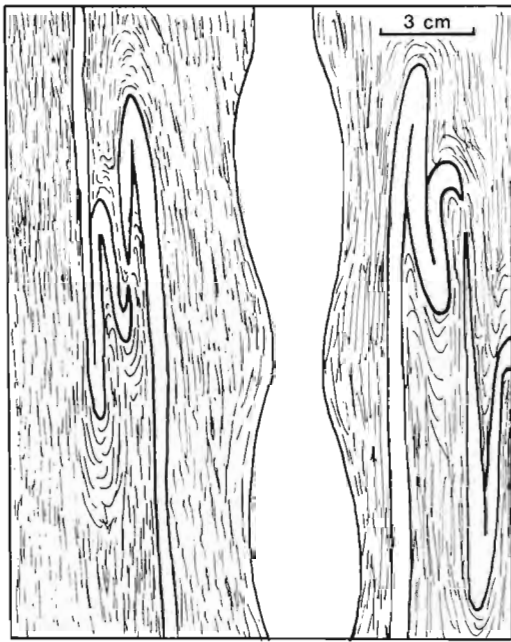


Figure 22.2 Thin metatect I veins thrown into strongly flattened folds, in the St-Fulgence paragneiss sequence. A thicker, coarser grained and garnetiferous vein of metatect II material, showing pinch and swelling, is axial planar to these folds, which possibly predate F_1 -folding.

Deformation III did not affect the area homogeneously. In wide zones it has the style of "gleitbrett" tectonics: zones 500 m to 1 m wide are separated by shear zones in which a new schistosity S_3 developed (Fig. 22.5). Zones of gleitbrett tectonics grade laterally into zones where S_1 (and the folds- F_2) are refolded into F_3 -folds with S_3 as the axial plane. Locally, anatectic veins follow slip-cleavage surfaces associated with this folding episode (Fig. 22.6). A new schistosity rarely formed in the older rocks; however, the hinges of folds axial-planar to S_3 are generally lineated. Schistosity S_3 , trending 010 to 030° and dipping steeply, forms a schistosity in the rocks of age group 3. Intensity of this deformation increases westward toward the Chicoutimi mangerite and toward the Lac St-Jean anorthosite. Furthermore, S_3 parallels the contact of the Lac St-Jean anorthosite in the area between lac Kenogami and St-Jean-Eudes. Schistosity S_3 is the only tectonic structure present in the anorthosite and mangerite and thus it very likely formed during the batholithic rise of these units.

Paragneiss, Amphibolite I, Granite I

Paragneiss, amphibolite I and granite I are the oldest constituents of the old gneiss complex. Metaquartzite, meta-arkose, and metapelite (sillimanite-garnet gneiss, sillimanite-cordierite gneiss) are relatively uncommon, having been observed mainly in the paragneiss zone followed from St-Fulgence to Ha! Ha! Bay and beyond (Fig. 22.1). Biotite-plagioclase paragneiss is more widespread; thin intercalations or inclusions of this rock are found in the terrane underlain mainly by granite I and granite II, and commonly are associated with amphibolite I.

Amphibolite I is a very heterogenous rock assemblage, occurring widely as inclusions or intercalations within the granitic sequence. Most amphibolite I is vaguely to distinctly layered and some is lensoid; massive, structureless varieties exist that are virtually identical to the amphibolite II. Most of it is mafic, but transitions into biotite-plagioclase

paragneiss exist and more leucocratic layers are not uncommon. Locally, boudinaged diopside-bearing "calc-silicate" layers are present.

Granite I is homogeneous, fine grained (about 1 mm), leucocratic and commonly quartz-rich. It contains minor biotite and, locally, hornblende. Its original coarser grain size is recognized from platy aggregates of quartz and feldspar, giving the rock a laminate to long-lensoid foliation. Laminae and lenses are defined by variable, but always low, biotite content. Obvious intrusive contacts of granite I have not been observed, but the great homogeneity of the rock, and the absence of gradations into the meta-arkoses, suggest an intrusive origin. Furthermore, a pegmatite gneiss is associated locally with granite I. Strong foliation in the pegmatite gneiss is defined by quartz plates.

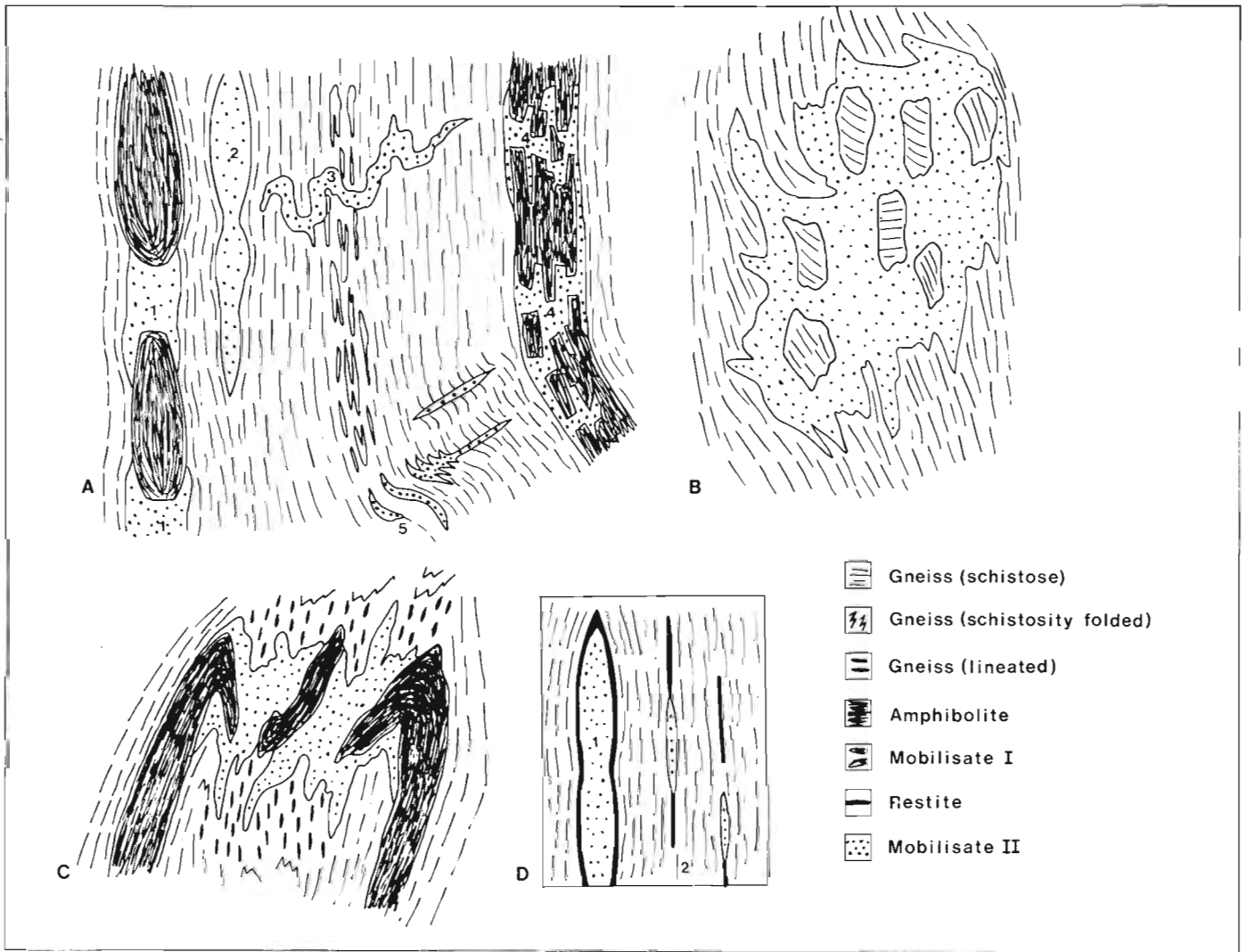
All these units underwent an early anatexis which did not affect the rocks described below. Metatectics form thin (1 to 10 mm) lenses and strongly flattened intrafolial folds parallel to S_1 (Fig. 22.2, 22.3a). Metatect I has been intensely granulated and now is grey, fine grained (less than 1 mm) quartzofeldspathic material; biotite, where present, is oriented parallel to S_1 . Thin, fine grained leucocratic layers and lenses parallel to S_1 in granite I are probably metatectics related to anatexis I as they are bounded by seams slightly enriched in biotite. However, the coarser grained (less granulated) veins with a well defined restite (Mehnert, 1968) and frequently with a central quartz vein probably result from anatexis II. Petrographic parameters offer indirect evidence for the chronology of anatectic veins; crosscutting relationships seen locally allow particular veins to be attributed to a specific anatectic episode (see Fig. 22.7 inset).

Granite II, Amphibolite II

The gneisses described above have been intruded first by two well defined types of granite and then by mafic dykes. The predominant variety of granite II is a streaky-textured, medium grained hornblende granite locally with orthopyroxene. Grain size of quartz and feldspar (plagioclase and potash feldspar) is 2 to 3 mm. The rock is characterized by aggregate streaks, 1 to 3 cm long and 1 mm thick, of 1 mm amphibole crystals, defining the schistosity S_2 . The rock acquired a strong lineation in the hinges of S_2 -folds by transformation of amphibole streaks into linear aggregates of amphibole. Intrusive contacts of this granite into amphibolite I, paragneiss and granite I are well exposed at several localities.

The second variety of granite II is a plagioclase-phyric biotite granite. Plagioclase phenocrysts are 1 to 2 cm long, 3 to 8 mm thick, are oriented parallel to the oldest schistosity, and have been partly granulated. The phenocrysts appear to be largely of primary igneous origin, and are set in a fine- to medium-grained groundmass of quartz, feldspar (plagioclase and potash feldspar), and biotite. Biotite is oriented parallel to S_2 . This granite is intrusive into the paragneiss, granite I and, especially, amphibolite I, as subconcordant dykes several tens of centimetres thick to metre-scale units. However, its relationship to the streaky hornblende granite has not yet been defined.

The paragneiss, amphibolite I, granite I and granite II have been intruded by closely spaced mafic dykes now transformed to amphibolite. Three varieties of these amphibolites have been recognized, namely 1) amphibole-phyric metagabbro amphibolite, 2) even grained metagabbro amphibolite, and 3) metadiorite amphibolite. Amphibole-phyric amphibolite contains amphibole crystals 3 to 5 mm across, in a millimetre-grained amphibole-plagioclase matrix. Even grained amphibolite has a grain size of 0.5 to 1 mm.



- A1 - Mobilizate II material filling dilation zones between dyke amphibolite boudins.
- 2 - Pinch and swell in a mobilizate II vein.
- 3 - Mobilizate II vein crosscutting S_1 and isoclinally-folded mobilized I material.
- 4 - Mobilizate II material filling interstices between dyke amphibolite breccia fragments.
- 5 - Mobilizate II material filling dilational "leaves" and following slip cleavage surfaces.

- B - Mobilizate II in dilational zones of S_2 -folding, note that layering of gneiss is continuous between rafts.
- C - Metatect accumulating in dilation zones associated with displaced fold hinges. The gneiss is lineated in the hinge zone.
- D1 - Restite forming border of anatectic vein where direction of mobilization was perpendicular to the length of the vein.
- 2 - Restite streaks forming between/within anatectic veins in which mobilization direction was parallel to the length of the vein.

Figure 22.3 Schema of typical occurrences and features of anatectic veins.

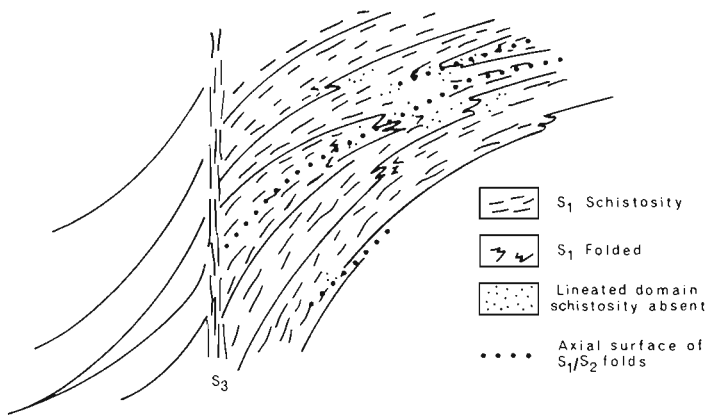


Figure 22.4 S_3 -shear surface offsetting strongly developed S_2 schistosity. Note the mineral lineation developing in the hinge zone of the F_2 -folds.

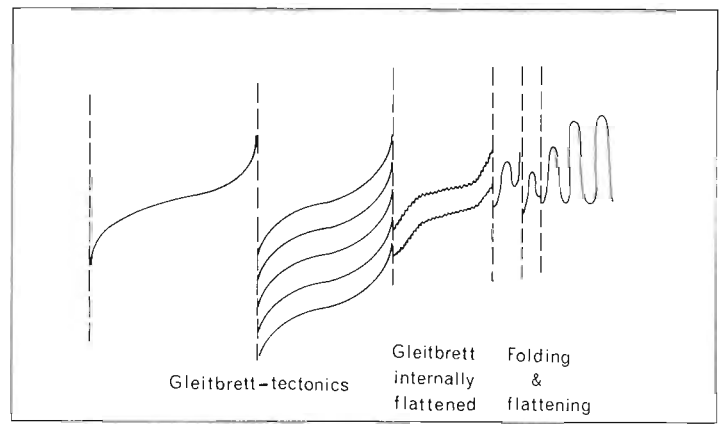


Figure 22.5 Development of a new (S_3) schistosity in shear zones cutting across older (S_1, S_2) schistositities. Where shear zones are closely spaced, the older schistosity is deformed.

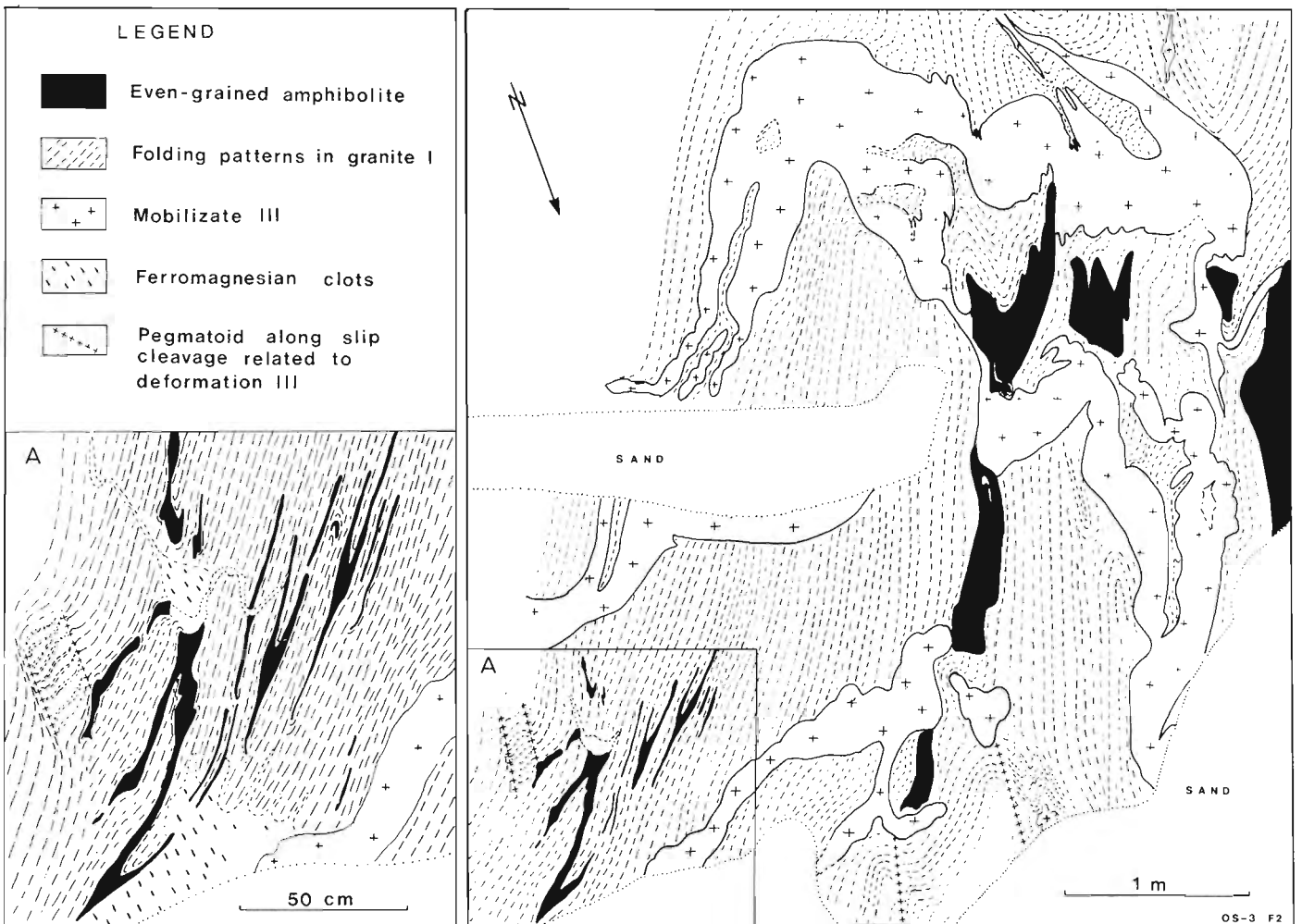


Figure 22.6 Relatively large volumes of coarse grained pegmatoid crosscutting and filling the noses of S_2 folds, in granite I, shoreline along Rang St-Martin. Enlargement shows relation of the incipient refolding of the isoclinal S_2 folds to the development of slip cleavage, which trends N10E.

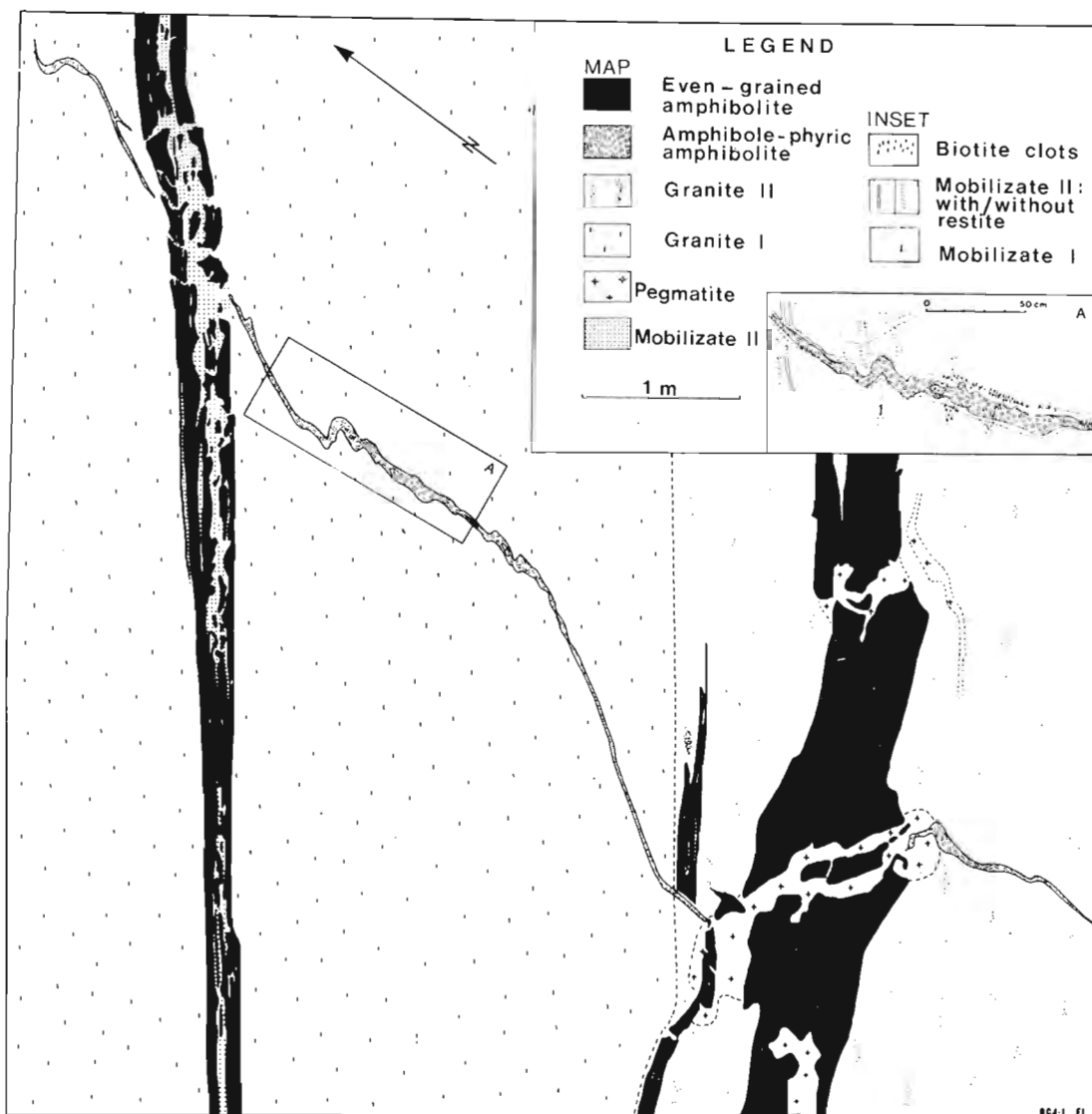


Figure 22.7 Amphibole-phyric amphibolite dyke being cut by even grained amphibolite dykes. The dyke at the left has been partly brecciated, with coarse grained mobilizate II material filling interfragmental interstices. The dyke at the right has been boudinaged, with pegmatite (mobilizate III) occurring between boudins. The contact between granites I and II is subconcordant. The inset shows mobilizate II material following the porphyritic dyke, crosscutting concordant mobilizate I veins.

Both consist of about 50-70 per cent amphibole and 30-50 per cent plagioclase. Metadiorite consists of about 20-30 per cent amphibole, 70-80 per cent plagioclase, and is fine grained (0.3 to 0.5 mm).

Dykes are 1 cm to 5 m thick; contacts with older rocks, are sharp, but reaction zones are locally present – these are described below. In general, grain size does not vary across the dykes, although coarsening from contacts to centres of dykes has been observed locally. Most dykes are subconcordant with the layering of the schistosity S_2 but crosscutting relationships were noted in places. Figure 22.7 shows subconcordant dykes of evengrained amphibolite cutting an amphibole-phyric amphibolite dyke, and Figure 22.8 shows a metadiorite dyke cutting subconcordant dykes of evengrained amphibolite.

Anatexis II

All rocks described above underwent an anatexis which coincides with the last stage of deformation I and the beginning stage of deformation II. Metatects fill dilational zones; typically they occur as pinching-and-swelling veins, and occasionally as boudinaged, rather thick lenses parallel to S_1 (Fig. 22.2, 22.3a), also characteristic and common in their emplacement in extensional zones between amphibolite boudins (Fig. 22.3a, 22.6) in breccia zones in amphibolite (Fig. 22.3a, 22.7), in axial planes of F_2 -folds and in dilational zones related to F_2 -folding (Fig. 22.3a). Typically, much metatect II material is present in the hinges of F_2 -folds (Fig. 22.3c), and in breccia zones close to the contact of rock units of very different mechanical properties (breccia zones in granite I or amphibolite, close to the contact with sillimanite-garnet paragneiss).

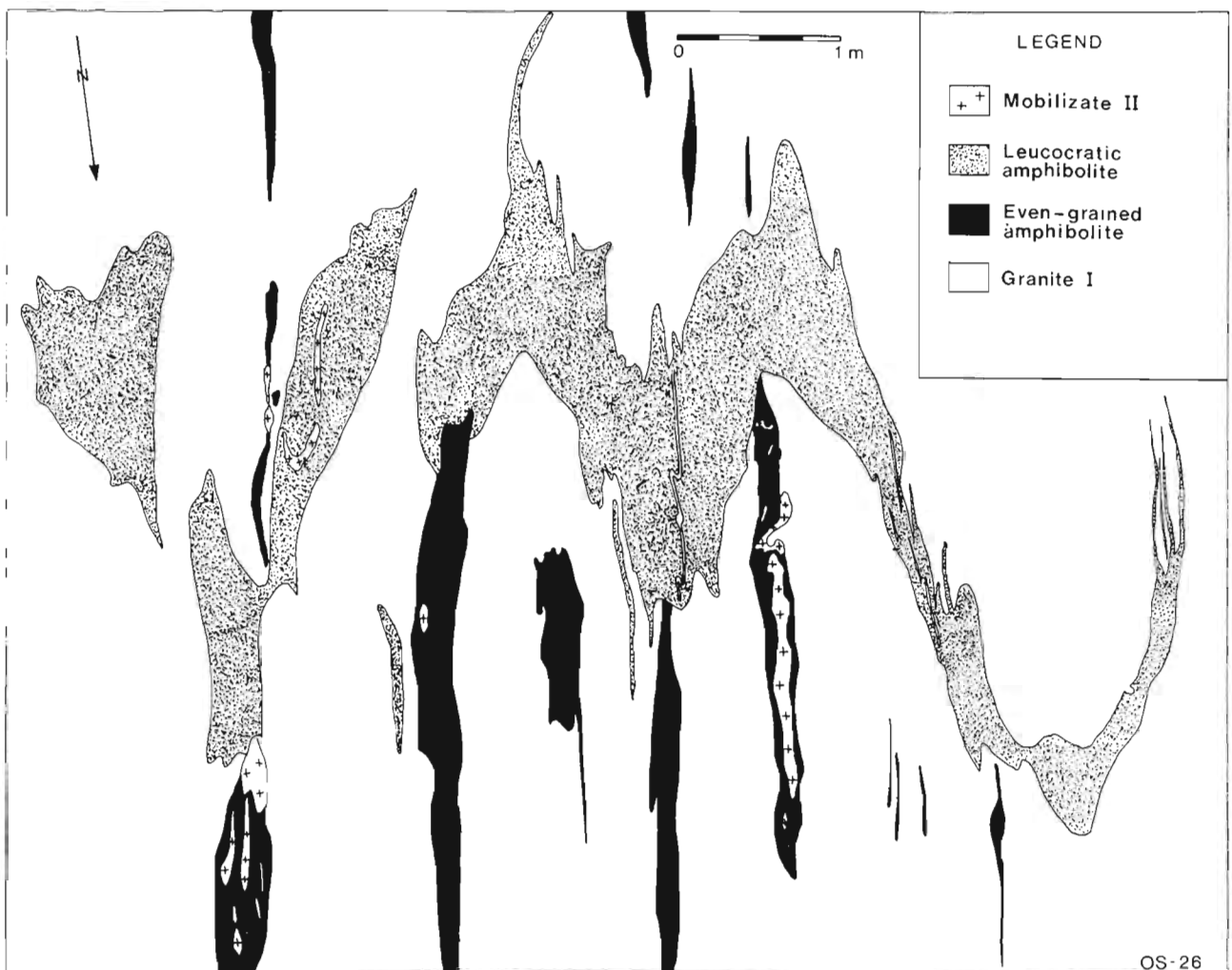


Figure 22.8 *Folded leucocratic amphibolite ("metadiorite") dyke crosscutting concordant even-grained amphibolite dykes in granite I, shoreline along Rang St-Martin. The even-grained amphibolite dykes were boudinaged by the folding episode (F_2) which folded the leucoamphibolite.*

Metatect II generally are coarse grained pink pegmatoids; thick pegmatoids commonly contain a quartz core, a centrally located quartz vein, or graphic intergrowth of quartz and feldspar. All metatect, however, have been somewhat granulated, apparently by movements related to F_2 -folding. Intensity of this granulation increases westward, and locally the metatect II have been transformed to grey, fine grained quartzofelspathic veins. The growth of feldspar porphyroblasts locally in gneisses and in amphibolites is related to anatexis II.

The following observations indicate that anatexis II generally took place in situ, and that metatect II are of local derivation:

1. In general, amphibolite II dykes are mappable as continuous units, even though boudinaged, folded, and cut by numerous veins of mobilizate II. This is true even in strongly dilational fold hinges, where the continuity of S_1 and of layering can be demonstrated (Fig. 22.3c).
2. Metatect II usually contain the same mafic minerals as do their host rocks. Thus, the predominant mafic mineral of metatect II is amphibole in amphibolite or in amphibole granite, biotite in biotite paragneiss and in biotite granite, and garnet in garnetiferous gneiss.

3. Metatect are rimmed by restite which consists always of the mafic mineral of the host rock. The direction of movement of anatectic melts can be related to the relation of movement in the metatect: where the restite rims anatectic veins parallel to S_1 ; movement was parallel to S_1 where streaks of restite grade laterally into lenses of mobilizate II (Fig. 22.3d).

Exceptions to these three rules further confirm the local derivation of metatect:

1. In the thinly layered sequence of the area, it is normal that metatect derived from one rock type should locally intrude a different rock type. In particular, layers of amphibolite and granite I in sillimanite-garnet paragneiss commonly have been strongly brecciated and have been invaded by metatect derived from the paragneiss (Fig. 22.9). These metatect contain garnet as the mafic mineral, and in the case of the amphibolite layers, the metatect are rimmed by a reaction zone where amphibole of the amphibolite has been converted to biotite, to garnet, or to both. Such zones of metatect reactions extend no more than 1 or 2 m from the source rock of the metatect and are present only at the contact of paleosomes of very different composition. For example, along amphibolite-paragneiss interfaces, garnets commonly form a mineral lineation parallel to the fold axes of F_1 -folding.

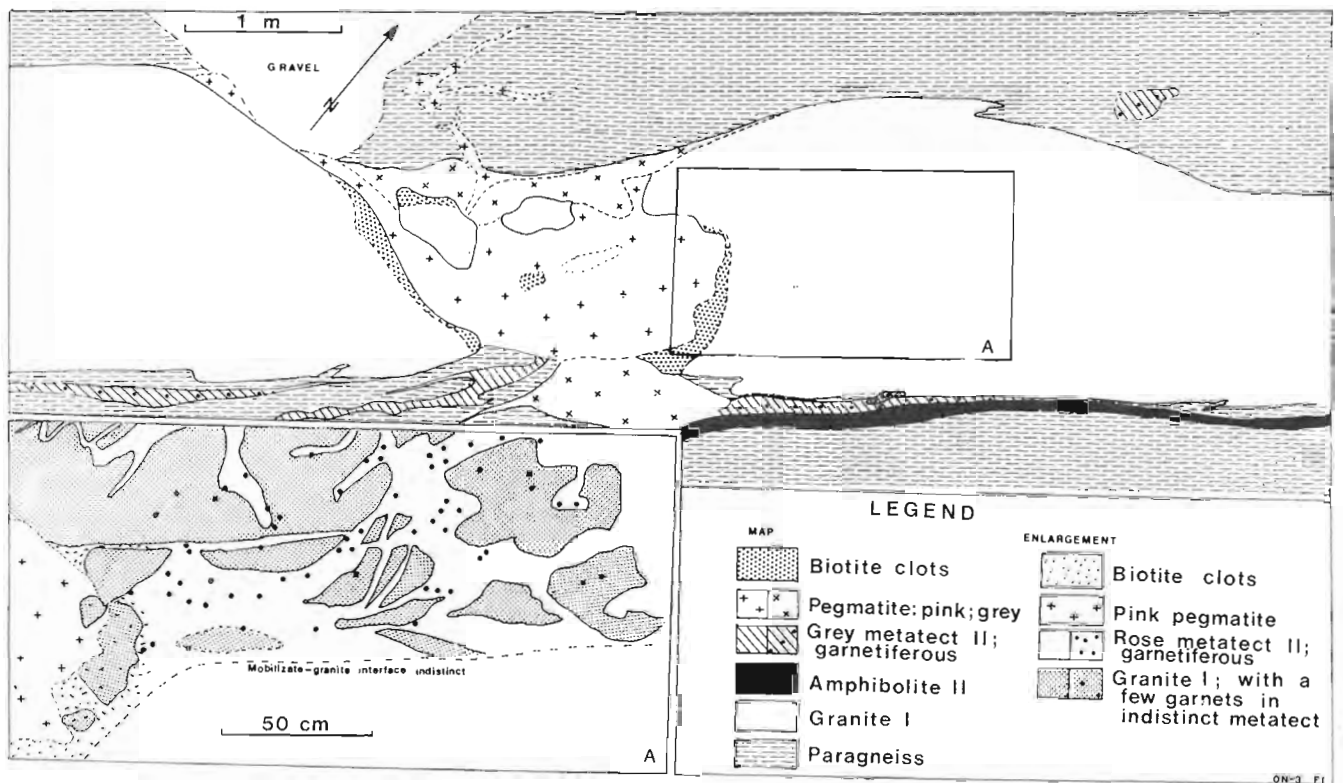


Figure 22.9 Pegmatite (mobilizate III) filling dilation zone between large boudins of brecciated granite I material, within the paragneiss sequence at St-Fulgence. The granite has been infiltrated by allochthonous garnetiferous mobilizate II material from the adjacent paragneisses. The mobilizate III material recrystallizes the granitic material, and especially the leucocratic mobilizate II material; biotite clots advance up to 25 cm along veins of the latter. Some of the mobilizate II veins in the paragneiss have also been granitized by the pegmatite: these veins are exceptionally quartz-rich and contain potash feldspar porphyroblasts up to 5 cm across.

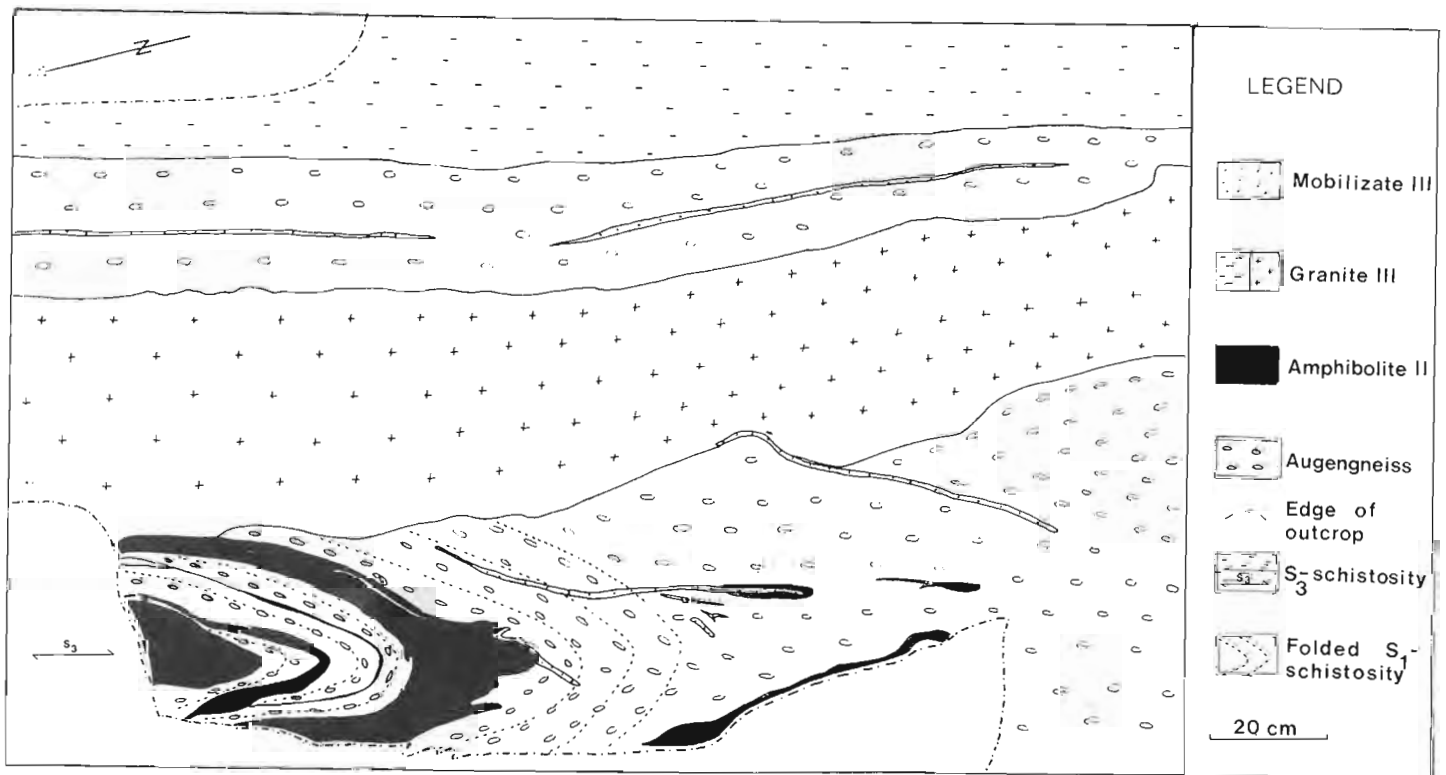


Figure 22.10 Granites III (medium grained syenitic granite (crosses) and weakly foliated medium grained granite) cut folded S_1 schistosity of porphyritic granite II and amphibolite II. The granites III are weakly foliated parallel to S_3 . Mapping and draughting by M. Elgner and C. Schroeder.

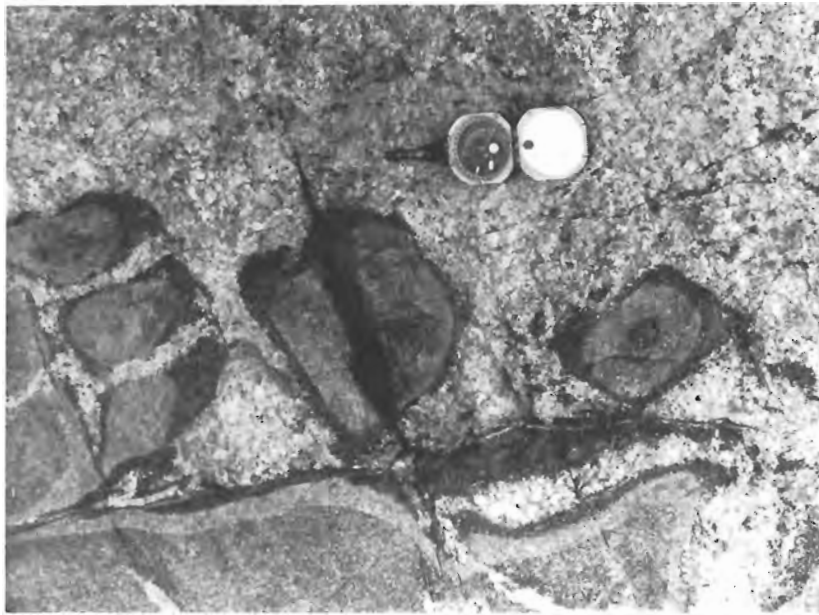


Figure 22.11 Recrystallization of amphibolite I inclusions in pegmatitic mobilizate III. A biotite-rich rim surrounds a pale, relatively fine grained zone; medium grained, essentially unaltered material occurs at the centre. Small inclusions are completely altered to biotite; intermediate sized enclaves lack the unaltered central core. Paragneiss sequence at St-Fulgence.

2. Locally, anatexis is advanced enough to destroy the original continuity of layers. In such cases, amphibolite layers can be traced for only short distances, and reaction zones rim many of the amphibolite inclusions; presumably, most of the metatect in these rocks was derived from the granitic gneiss and converted the amphibolite amphibole into biotite in a marginal reaction zone. Similar reactions occur in inclusions within the pegmatitic veins resulting from anatexis III, described below.

Granite III, Amphibolite III

Very few dykes of granite III and of amphibolite III are present in the old gneiss complex; however, these dykes appear to become more common toward the Chicoutimi mangerite. Dykes of granite III have various compositions and textures, and granite III obviously comprises a heterogeneous group of rocks. Figure 22.10 documents a medium grained (~4 mm) syenitic granite intrusive into the older sequence. S_3 is the only structure present in this dyke.

Dykes of amphibolite III are fairly common in the westernmost sector of Rang St-Martin, close to the contact of the gneiss complex and the mangerite. Amphibolite III, a fine grained (≤ 1 mm) rock of basaltic composition, crosscuts the axial plane S_2 and contains veins of metatect III, sheared by S_3 . Its relationship to granite III is unknown.

Anatexis III

Anatexis III produced pegmatitic veins. The very few veins present in the area unaffected by deformation III crosscut the older structure and form straight dykes. These dykes are not of local derivation; they are not rimmed by restites and furthermore they caused a strong recrystallization of the older gneisses (Fig. 22.11).

Anatectic veins related to anatexis III are more common in the terrane where deformation II is represented by discrete shear zones (Fig. 22.12). In these areas, anatectic veins intrude the shear zones, show a weak foliation parallel

to S_3 , and are somewhat granulated. As in the case above, some recrystallization of the old gneiss fabric is evident at vein contacts.

Where deformation III resulted in pervasive folding of the S_3 -schistosity, anatectic veins related to anatexis III are most common; here they intrude dilational zones related to F_3 -folding, as in Figure 22.12. Metatects III generally are somewhat deformed by the F_3 -folding.

Uncorrelated Rock Types

Charnockites in the eastern part of Rang St-Martin and the porphyritic diorite of Cap des Roches have not been correlated. The charnockites are very coarse grained (1 to 4 cm) rocks of dioritic composition, containing amphibole-mantled orthopyroxene crystals up to 4 cm across. Their relationship to the other rocks in the area is still unclear.

The porphyritic diorite contains about 50 per cent feldspar phenocrysts 1 to 2 cm long, set in a mafic-rich, fine grained groundmass. It is moderately to strongly deformed (schistosity S_2 ?) and is cut by numerous pegmatitic dykes and veins (metatect III, undeformed?).

References

- Mehnert, K.R.
1968: Migmatites and the Origin of Granitic Rocks; Elsevier Pub. Co., 393 p.
- Sederholm, J.J.
1967: Selected works; Granites and Migmatites; Oliver and Boyd, 607 p.
- Watterson, J.
1965: Plutonic development of the Ilordleg area, South Greenland, Part I Chronology, and the occurrence and significance of metamorphosed basic dykes; Meddelelser om Grønland, Bd. 172 Nr. 7, 147 p.

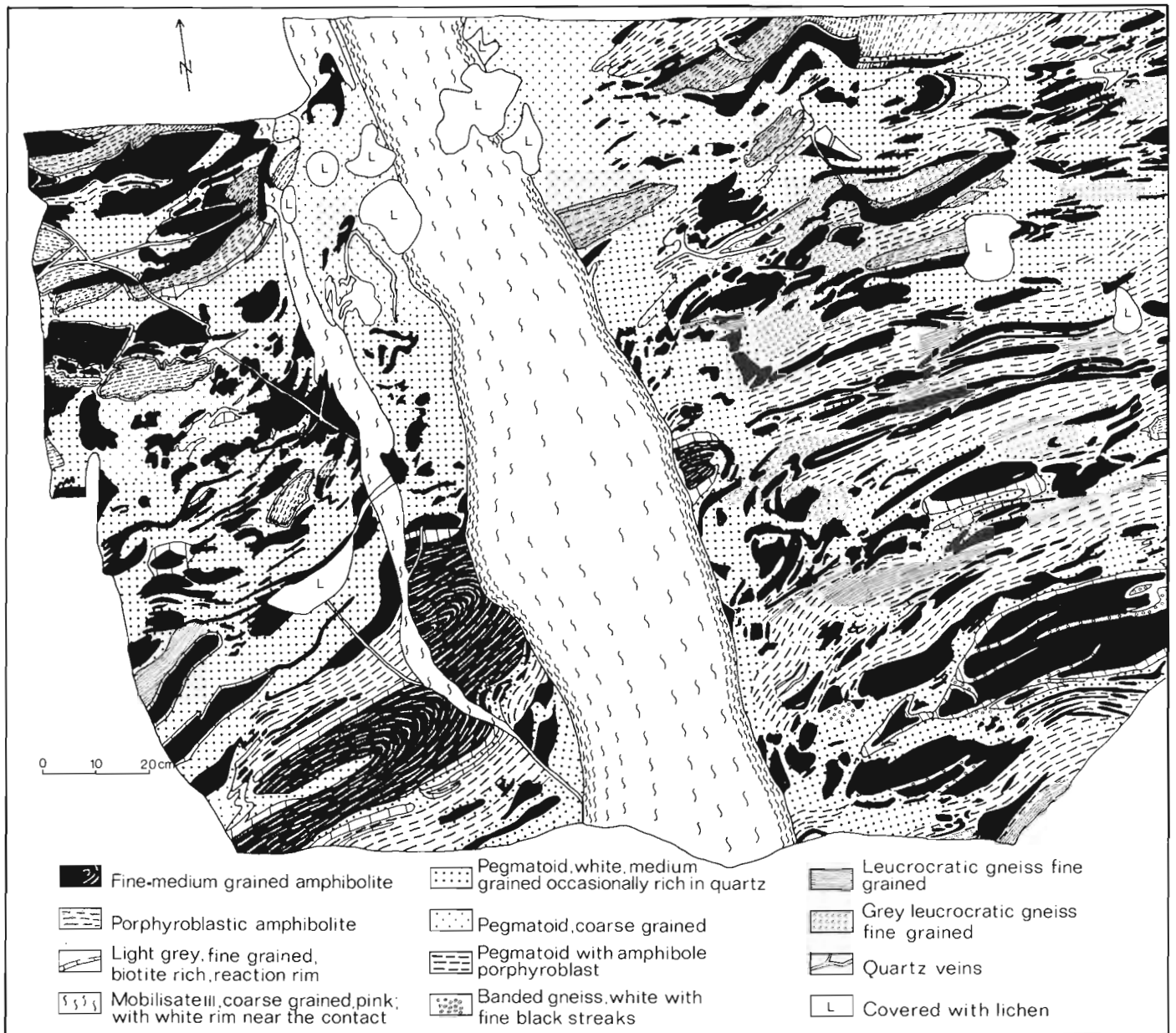


Figure 22.12 Para-autochthonous metatexite II after layered amphibole gneiss and amphibolite II, cut by mobilisate III. Note (1) folded S_1 schistosity with axial plane parallel to S_2 (lower left) in amphibolite I, cut by mobilisate III with internal schistosity S_3 , and (2) the large volume of mobilisate II, reaction rims at the margins of amphibolite inclusions and the discontinuous layering of para-autochthonous metatexites. Mapping by M. Elgner and C. Schroeder; drafting by B. Tremblay and A.-M. Wawrzakow.

Watterson, J. (cont'd.)

1968: Plutonic development of the Ilordleg area, South Greenland, Part II, late kymatic basic dykes; Meddelelser om Grønland, Bd. 185 Nr. 3, 103 p.

Woussen, G., Dimroth, E., and Roy, D.W.

1979a: Evolution chronologique des roches précambriennes du haut Saguenay; GEOS, summer 1979.

Woussen, G., Gagnon, G., Bonneau, J., Bergeron, A., Dimroth, E., Roy, D.W., and Thivierge, S.

1979b: Lithologie des roches précambriennes et des carbonatites du Saguenay-Lac-St-Jean; dans Lithologie et tectonique des roches précambriennes et des carbonatites du Saguenay-Lac-St-Jean Livret-guide, Congrès de l'Association géologique du Canada et de l'Association minéralogique du Canada, Québec, Université Laval, p. 1-8.

Project 790024

J.R. Henderson and C.R. Tippett¹
Precambrian Geology Division

Henderson, J.R. and Tippett, C.R., *Foxe Fold Belt in eastern Baffin Island, District of Franklin*; in *Current Research, Part A, Geological Survey of Canada, Paper 80-1A*, p. 147-152, 1980.

Abstract

Foxe Fold Belt, a late Aphebian (Hudsonian) mobile belt, contains polydeformed Archean and Aphebian rocks ranging from greenschist to granulite facies of metamorphism. Within the Home Bay map area (NTS 27 SE and SW) Aphebian Piling Group supracrustal rocks are divided into four lithostratigraphic units. A basal unit of mainly quartzite in the south part of the region is overlain by an interbedded marble and calcium-silicate gneiss unit towards the apparent north margin of the sedimentary basin. Locally in the interior of the basin in the southwest part of the Home Bay map area a stratiform complex of mafic and ultramafic metavolcanics overlies the quartzite. The upper unit, composing the major part of Piling Group, is made up of a succession of metaturbidites.

The first appearance of anatectic leucogranite occurs near the base of Piling Group in the southwest part of the Home Bay map area, and cuts higher into the metaturbidite succession farther east. In the south, east and north parts of the map area metamorphic conditions were highest; granulite grade rocks occur in the southeast part of the region.

Four fold sets deform Aphebian and older rocks in the region. The first two sets (F_1 and F_2) are recumbent isoclines: the largest single structure in the region appears to be a northeast-striking F_1 or F_2 anticlinal nappe. F_3 and F_4 folds are mainly horizontal normal folds developed on the recumbent fold limbs. The F_3 set strikes east-northeast and is dominant northwest of the apparent crest of the anticlinal nappe, whereas the F_4 set strikes west-northwest and is dominant southeast of the apparent crest of the nappe. Foxe Fold Belt undergoes an abrupt regional strike change across the zone where the fold sets interfere.

Anatexis apparently antedates F_4 folding in the region.

Introduction

Bedrock mapping in Home Bay map area (NTS 27SE, SW) was completed during 1979; this was the final field season devoted to studies of the stratigraphy, structure and metamorphism of rocks in Foxe Fold Belt in Baffin Island. Other studies done in relation to this project are described by Morgan et al. (1975, 1976), Tippett (1978, 1979), and Henderson et al. (1979).

Figure 23.1 outlines the Home Bay map area and indicates mapping reported upon previously. Contributions to the mapping in 1979 were made by Robert Anderson, Steven Aungst, Derek Brown, Mariette Henderson, Patrick McLellan, and Ginny Peterson, in addition to the writers. Traversing was done mainly on foot from daily excursions with a helicopter from base camps at Cape Hooper (FOX-4 DEW Line site), the head of Inugsuin Fiord, and Dewar Lakes (FOX-3 DEW Line site). Camp moves were facilitated by use of DC-3 and Twin Otter aircraft chartered from Frobisher Bay.

Much of eastern Baffin Island is nearly inaccessible except by helicopter. Local relief exceeds 1000 m in the fiords and most of the upland is covered by permanent ice and snow. In addition, prevailing easterly winds in the region produce abundant orographic cloud cover and precipitation. In this regard, we greatly appreciate the help of Alan Stacey, pilot of Aero Trades' Bell 206-A, who was constantly aware of the special difficulties presented to us in mapping the country.

Summary of Regional Relations in Foxe Fold Belt

Foxe Fold Belt is a 100-200 km wide zone of late Aphebian deformation characterized by generally gently plunging, east-west striking normal folds superposed on recumbently folded Aphebian supracrustal rocks and their

Archean granitoid basement rocks. Jackson and Taylor (1972) drew the boundaries of the deformed zone from the Canada mainland southwest of Melville Peninsula to the east coast of central Baffin Island. South of Barnes Ice Cap in central Baffin Island, Foxe Fold Belt changes strike from the east-northeast-west-southwest trend characteristic in western Baffin Island and Melville Peninsula to west-northwest-east-southeast in the short eastern segment that terminates in Home Bay.

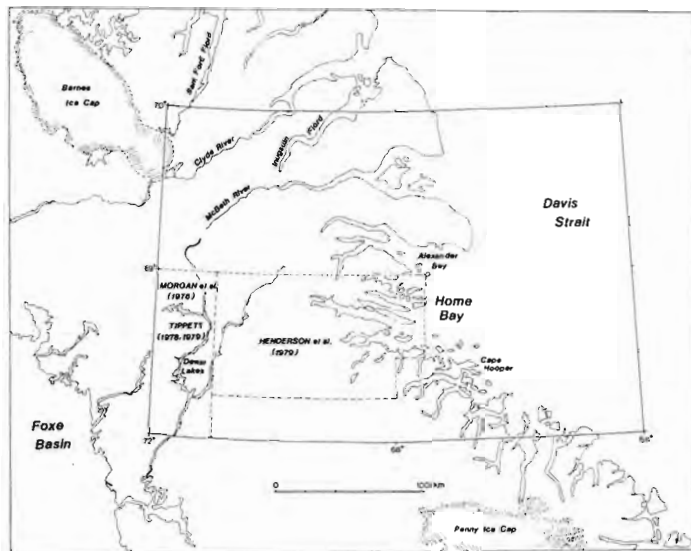


Figure 23.1. Index map of areas referred to in central Baffin Island. Home Bay map area (NTS 27 SE and SW) is outlined; parts of the area reported upon previously by Henderson et al. (1979), Morgan et al. (1976) and Tippett (1978, 1979) are indicated.

¹Department of Geological Sciences, Queen's University, Kingston, Ontario, K7L 3N6

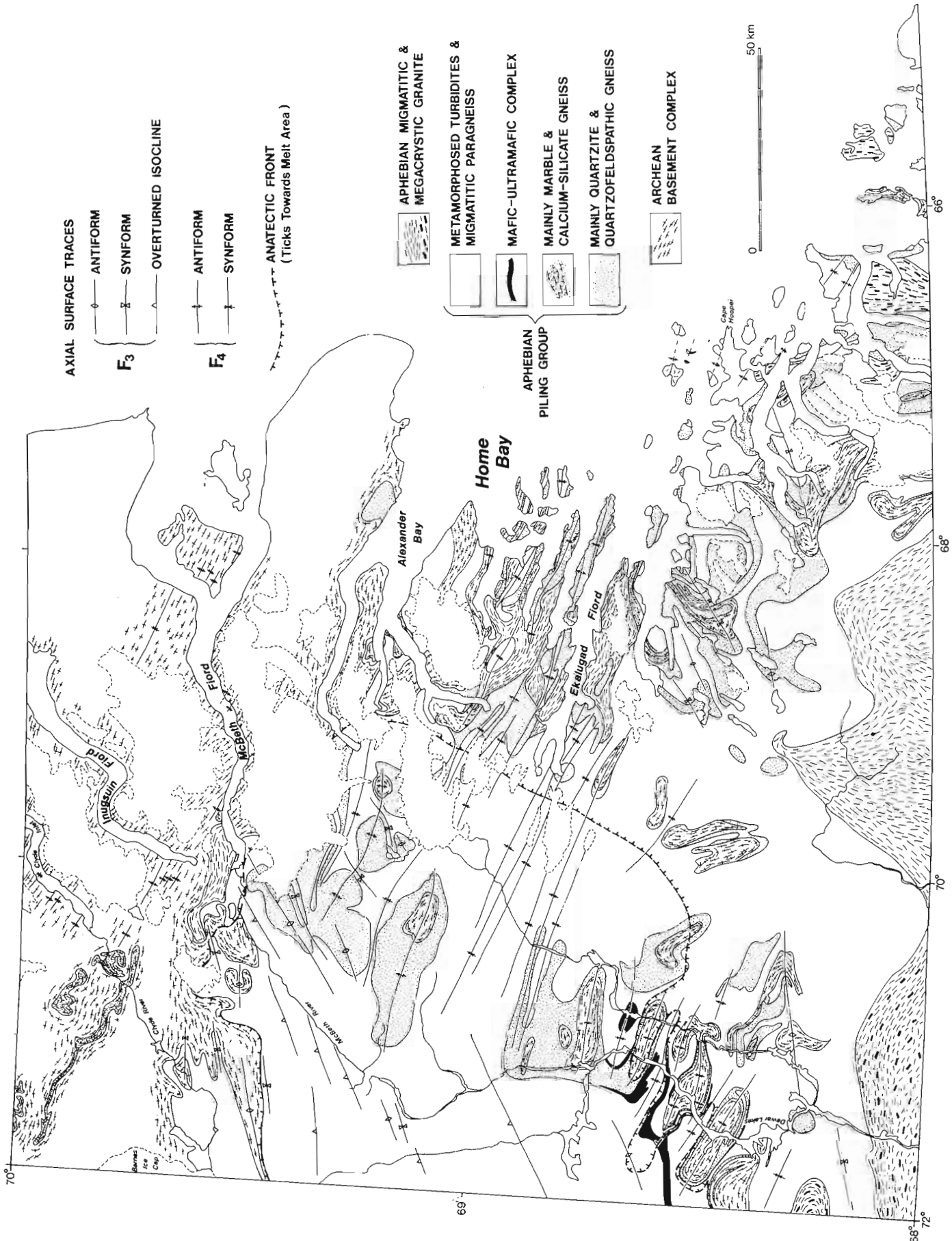


Figure 23.2. Geological sketch map of the Home Bay map area. Geology west of 70° and south of 69° by W.C. Morgan, A.V. Okuitch, P.H. Thompson, P. Chernis, 1976, and by C.R. Tippett, 1978-79. Compilation by J.R. Henderson and C.R. Tippett, 1979.

Metamorphism in the belt on Baffin Island increases outwards from greenschist grade in the central Piling Basin to granulite grade north and south of Foxe Fold Belt (Jackson and Morgan, 1978). In the high grade terranes extensive Hudsonian migmatization made it difficult to distinguish between Aphebian and Archean supracrustal and plutonic rocks. Final folding of the rocks in Foxe Fold Belt on Melville Peninsula took place before the metamorphic culmination about 1800 Ma ago (Henderson, in press); folding in the belt on Baffin Island outlasted the metamorphic climax which, according to Jackson and Morgan (1978), may have occurred about 1670 Ma ago.

Stratigraphy and Lithology

Rocks in the Home Bay map area (Fig. 23.2) may be divided on the basis of relative age and lithology into four major categories: (1) Archean (Kenoran) granitoid basement complex; (2) Piling Group supracrustal succession assumed to be Aphebian in age; (3) Late Aphebian (Hudsonian) granitoid rocks; and (4) post-Aphebian (Hadrynian) diabase dykes (not shown on Fig. 23.2).

Archean Basement Complex

A continuous expanse of granitoid basement gneiss occurs in the region northeast of a line from Alexander Bay to Barnes Ice Cap. South of this line basement rocks occur largely in west-northwest trending elliptical domes in the Dewar Lakes region, and in north trending isoclinal anticlines in the Cape Hooper region.

Basement rocks are mainly medium grained, pink-grey, layered granite-granodiorite with locally abundant folded amphibolite boudins. Layering is developed on a scale of 1-10 cm in the gneiss; mineral foliation and lineation (where developed) parallel layering in limbs and hinges of mesoscopic folds. Identification of basement rocks in the high grade terranes north and east of the anatectic front shown in Figure 23.2 commonly is based on negative mineralogical criteria, such as absence of graphite, iron oxide, garnet, sillimanite and cordierite, although presence of allanite may be a positive criterion for identification of basement rocks.

The pre-Piling relative age of the basement rocks was established by Morgan et al. (1975, 1976) and Tippett (1978, 1979) based on the regional occurrence of granitoid gneiss beneath Piling Group graded turbidites northwest of Dewar Lakes. Jackson (1978) obtained Rb-Sr "errorchron" ages of 2605 Ma and 1964 Ma from 12 samples of basement gneiss collected near the mouth of McBeth River (Fig. 23.2). The Rb-Sr values obtained from the suite according to Jackson (1978) show significant geological variation, but do, however, provide evidence for at least two periods of igneous-metamorphic activity, the earlier representing the Kenoran orogeny and the later possibly indicative of the time of metamorphism of the Piling Group.

Piling Group

In the Home Bay map area Piling Group is divided into four lithostratigraphic units. In ascending order the sequence of units is (1) micaceous quartzite or quartzofeldspathic gneiss, (2) marble and calcium silicate gneiss, (3) amphibolite and ultramafic rocks, and (4) turbidite or paragneiss. The brief descriptions of field aspects which follow emphasize regional variations within the map area. Tippett (1978, 1979) and Henderson et al. (1979) presented some additional data on the megascopic features of Piling Group rocks in the Home Bay map area. Morgan et al. (1976) described some aspects of Piling Group rocks in the west of the Home Bay map area. Piling Group is given an Aphebian age and probably is correlative with Penrhyn Group in Melville Peninsula.

Micaceous Quartzite or Quartzofeldspathic Gneiss The basal unit of Piling Group varies with increase in metamorphic grade from micaceous quartzite and schist to quartzofeldspathic gneiss. The anatectic front drawn on Figure 23.2 marks the approximate position of the transition. Pure quartzite is a minor but characteristic component of the unit throughout the region. The basal unit is most widespread in the region immediately south of McBeth River; north of the river the unit is not represented on the map, although in places northwest of Clyde River thin quartzite occurs between marble and basement gneiss. Thickness estimates are valueless, due to the imprecise knowledge of structural complexities in the region. However, the virtual disappearance of quartzite and the appearance of marble as a map unit north of McBeth River probably reflect a transition from dominantly clastic sedimentation in the interior of the basin to chemical sedimentation near the basin margin.

Marble and Calcium-Silicate Gneiss North of McBeth River, marble and calcium-silicate gneiss occurs in several narrow west-northwest striking bands in contact with basement gneiss. In places the unit overlies a thin quartzite or pelitic gneiss in contact with basement rocks. Elsewhere in the Home Bay map area the marble unit is absent or is too thin to map separately from the quartzite-quartzofeldspathic gneiss unit (e.g. north of Ekalugad Fiord).

Typically the unit is coarse grained calcite marble with scattered layers, lenses and pods of finer grained diopside-feldspar-quartz gneiss. Dispersed grains of graphite, forsterite, humite, diopside and scapolite occur in some marble outcrops. White pegmatitic granite commonly occurs with marble and may make up most of the exposure.

Marble seems to occur in Piling Group only near the north margin of the basin on Baffin Island. Morgan et al. (1975, 1976) mapped a marble-rich unit overlying quartzite in the keels of several northeast striking synclines along the north margin of the basin in the Lake Gillian map area (37 D) southwest of Barnes Ice Cap. In the region west of the Home Bay map area they noted that carbonate rocks occur in Piling Group only near the north margin of the basin.

Amphibolite and Ultramafic Rock A stratiform complex composed mainly of amphibolite and hornblende layers occurs around several of the elliptical domes near Dewar Lakes. In this region the unit overlies the basal quartzite or occurs within the turbidite-paragneiss unit. The latter occurrence may be allochthonous if the complex forms a single conformable volcanogenic sequence overlying the quartzite unit. Amphibolite occurring east of the Dewar Lakes region is too thin and discontinuous to map separately from the quartzite unit. Tippett (1978) suggested that the amphibolite and ultramafic rock unit found around Dewar Lakes may be a lateral facies equivalent of extensive sulphide facies iron formation and rusty schists, which apparently occupy the same stratigraphic position in Piling Group to the north.

Turbidite or Paragneiss Unit The principal unit of Piling Group in the Home Bay map area is a flyschoid sequence that varies with increase in metamorphic grade from a succession of recognizably distal turbidites to migmatitic biotite-graphite paragneisses. Where they occur in their lowest grade condition (e.g. the upper McBeth River and upper Dewar Lakes drainage areas), the rocks composing the turbidite unit of the group are rusty shales, siltstones and greywackes; where their metamorphic grade is higher, they are mainly rusty graphitic schists and paragneisses. In the region inside the anatectic front drawn in Figure 23.2, granitic leucosome is a significant component of the paragneiss unit and in the highest grade terranes (e.g. south and southwest of Cape Hooper) the paragneiss unit is difficult to separate from Hudsonian plutonic rocks.

Granitic Rocks

Based on their relative age and mode of occurrence, three varieties of granitic rocks (*sensu lato*) were distinguished in the Home Bay map area. Pegmatitic leucogranite occurs most abundantly; it forms the leucosome in migmatitic paragneiss and is the principal component of the migmatitic granite mapped inside the anatectic front. Several foliated megacrystic quartz monzonite plutons occur south of Cape Hooper. These rocks were emplaced after some of the leucogranites formed. Postkinematic granite pegmatite dykes compose the third variety of granitic rock distinguished in the region; they indicate that some granitic magmatism outlasted the dynamothermal Hudsonian metamorphism.

Leucogranite Inside the anatectic front drawn on Figure 23.2, Piling Group paragneiss contains conformable leucocratic laminae produced *in situ* by anatexis of the turbidites. In addition, deformed sills and dykes of leucocratic granite intrude the migmatitic paragneiss. These discordant leucogranites are slightly more mobile products of local anatexis. Mainly along the south margin of the Home Bay map area leucogranite forms the major component of the migmatite and is distinguished on the map as migmatitic granite. The migmatitic granite contacts are located approximately where Piling Group rocks could no longer be distinguished from Archean basement rocks or Hudsonian granites.

Where leucogranite is intimately associated with Piling Group paragneiss, it commonly contains schistose biotite-fibrolite lenses, except in the region south of Ekalugad Fiord where sillimanite is absent and the leucogranite contains dispersed garnet and cordierite.

Charnockitic granite southwest of Cape Hooper gave a Rb-Sr isochron age of 1670 ± 30 Ma, probably recording the time of high grade Hudsonian metamorphism in the region (Jackson and Morgan, 1978).

Megacrystic Quartz Monzonite Several north-south trending plutons and many smaller sills and dykes of foliated biotite quartz monzonite with coarse feldspar augen occur south of Cape Hooper. The plutons are semiconformable but locally the dykes crosscut leucogranite in migmatitic paragneiss. Quartz monzonite contains a few xenoliths of apparent derivation from the Archean basement complex, suggesting the magmas may have been generated by fusion of basement rocks.

Megacrystic quartz monzonite probably is a member of the quartz monzonite-monzocharnockite suite (Jackson and Morgan, 1978) covering tens of thousands of kilometres of the granulite facies terrane south of Home Bay map area. Similar rocks near Pangnirtung gave a U-Pb zircon age of 1900 ± 20 Ma, interpreted as recording the pre-granulite facies igneous activity in the region (Pidgeon and Howie, 1975).

Pegmatite Dykes Postkinematic granite pegmatite dykes occur near and inside the anatectic front throughout the Home Bay map area. The dykes commonly intrude Archean basement rocks or the Piling Group quartzite unit. They have diverse trends and range up to 30 m wide and 1000 m long. These dykes are not shown on the geologic map (Fig. 23.2).

Diabase Dykes

Vertical northwest-southeast striking diabase dykes crosscut all other rocks in the region. The dykes are widespread but not common; they are generally less than

50 m wide but may be 50 km long. Their trend is parallel to the Hadrynian Franklin dykes of north Baffin Island (Fahrig et al., 1971), but the possibility exists that some of them may be related to Tertiary rifting in Davis Strait. They are not shown on the geologic map (Fig. 23.2).

Metamorphism

In the Home Bay map area metamorphic conditions ranged from greenschist to granulite facies. Greenschist facies is evident in rocks of the upper McBeth River and Dewar Lakes drainage areas where fine grained chlorite-biotite-quartz schist (metaturbidite) and muscovite quartzite occur. Because of the restricted composition of the rocks few indicator minerals occur in the Home Bay map area, signifying lower amphibolite facies metamorphism: andalusite and staurolite are very rare; one occurrence of andalusite-sillimanite was found in the Dewar Lakes region (Tippett, 1979).

The disappearance of muscovite and appearance of sillimanite in the presence of K feldspar is the first obvious indication that the rocks have reached upper amphibolite facies. Appearance of abundant sillimanite in quartz-rich rocks is closely followed in the field by a virtual "explosion" of anatectic leucosome in metaturbidites, transforming them into migmatitic paragneisses. The assemblage biotite-sillimanite-garnet is common in the schistose restite layers in the migmatite.

Note that the anatectic front drawn on Figure 23.2 signifying the appearance of migmatitic paragneiss occurs near the base of the Piling Group succession at Dewar Lakes, and rises stratigraphically in the sequence to the south and east. Careful mapping in the Dewar Lakes region shows that the anatectic front generally follows the trace of F_4 folds in the formational contacts. Farther east and north of Dewar Lakes the location of the front is less precisely drawn, but it does appear to swing northeast towards Alexander Bay and intersect the Piling basal quartzite unit. The front remains near the base of the Piling Group as it describes a broad arc north and west from Alexander Bay towards Barnes Ice Cap.

Granulite facies is achieved in at least some of the region of migmatitic granite along the south part of Home Bay map area. Especially south and east of Cape Hooper, the feldspars show the greasy lustre and grey-green colour typical of granulites. Here also, the leucocratic layers in migmatitic paragneiss contain cordierite and garnet; and sillimanite appears to be absent from the rocks.

The sequence of metamorphic changes observed in the Home Bay map area seems to be typical of the Abukuma facies series, suggesting a high thermal gradient and relatively shallow depth of orogenic activity in Foxe Fold Belt.

Structure

Four sets of folds may be observed directly or may be inferred to be present from map patterns of Archean and Aphebian rocks in the Home Bay map area. Tippett (1978, 1979) and Morgan et al., 1976 reasoned that a pre-Piling deformation (Kenoran?) affected the Archean basement gneiss, but folds related to this (gneissosity-forming?) event were not recognized. The two earliest fold sets (F_1 and F_2) are isoclines that originally were recumbent, whereas the two latest sets (F_3 and F_4) are mainly horizontal normal folds with oppositely-dipping limbs.

F_1 and F_2 Folds

The earliest folds directly observed in the region are isoclines exhibiting axial-planar mineral foliation: these

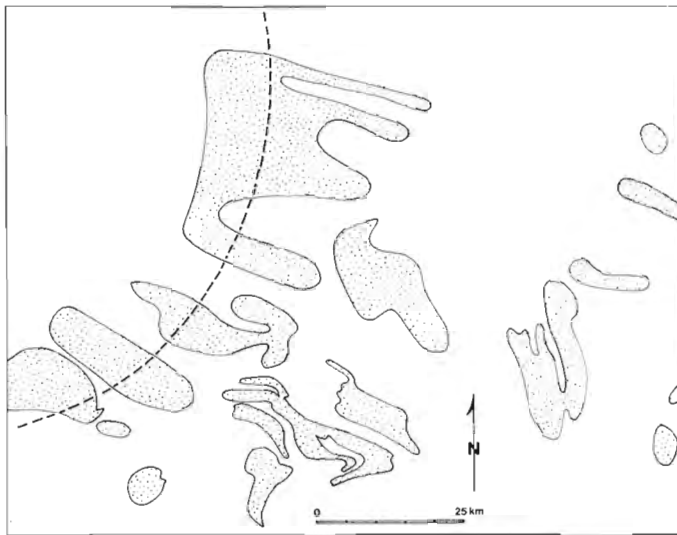


Figure 23.3. Geological sketch map of the region around Dewar Lakes. Patterned areas are underlain by Piling basal quartzite and Archean basement gneiss. The heavy-dash line shows the apparent trace of an early (F_1 or F_2) anticlinal nappe hinge.

F_1 folds occur mainly in basement-cover contact surfaces exposed near Dewar Lakes (D_2 folds of Tippett, 1978, 1979). The great majority of mesoscopic isoclinal folds observed are classified as F_2 folds because both lithological layering and mineral foliation are folded isoclinally. Some very large recumbent folds drawn by Kranck (1955) from direct observations in McBeth, Clyde and Sam Ford fiords are F_2 structures.

Henderson et al. (1979) outlined some macroscopic isoclinal folds in the region southwest of Ekalugad Fiord where overprinting relationships indicate that both F_1 and F_2 fold sets are present. Tippett (1978, 1979) correlated macroscopic imbrication of basement and cover rocks, as well as development of mineral foliation and lineation around Dewar Lakes with the F_1 set of folds. Because hinge zones of isoclinal folds are seldom seen the distinction between macroscopic F_1 and F_2 folds is not apparent unless the two sets interfere.

F_3 and F_4 Folds

Both F_3 and F_4 folds typically are horizontal normal folds (i.e. folds with nonplunging axes and vertical axial surfaces) with oppositely-dipping limbs. They are set apart mainly by their different trends in regions of non-interference: F_4 folds strike northwest-southeast, and are developed best in the region between Dewar Lakes and Alexander Bay; F_3 folds strike northeast-southwest, and are developed best in the region between Barnes Ice Cap and McBeth Fiord. The dome-and-basin map pattern southeast of McBeth River resulted from type I interference (Ramsay, 1967) of nearly orthogonal macroscopic F_3 and F_4 folds. The order of the two-fold sets is rather arbitrarily defined because mesoscopic folds belonging to either set are rare, and no regionally consistent observations on their sequential development were made: perhaps they are coeval.

In previous reports (e.g. Tippett, 1978, 1979, and Henderson et al., 1979) no distinction between F_3 and F_4 folds was made. It is clear now that the change in regional strike of Foxe Fold Belt in Baffin Island from northeast-southwest to northwest-southeast resulted from different strikes of the two latest fold sets rather than a progressive change in strike of a single set of folds.

Geometric Significance of Fold Interference Patterns

The en échelon arrangement of F_4 domes northwest of Dewar Lakes may be controlled by their localization on the crest of an F_1 or F_2 basement-gneiss cored anticlinal nappe. Figure 23.3 shows the trace of the contact between lower and upper Piling Group lithologies. The dentate appearance of the aligned F_4 domal culminations terminating west of the heavy-dash line resembles outcrop patterns produced by superposition of late normal folds on an early recumbent fold nappe. The heavy-dash line parallels the apparent trend of the nappe hinge. An interference pattern of this sort was described by Reynolds and Holmes (1954) and classified as a type 2 interference pattern by Ramsay (1967). Farther north along the apparent nappe crest F_3 and F_4 folds interfere to produce the type I interference pattern previously mentioned.

References

- Fahrig, W.F., Irving, E., and Jackson, G.D.
1971: Paleomagnetism of the Franklin diabases; Canadian Journal of Earth Sciences, v. 8, no. 4, p. 455-467.
- Henderson, J.R.
Structure and metamorphism of Aphebian Penrhyn Group and its basement in the Lyon Inlet area, Melville Peninsula, District of Franklin; Geological Survey of Canada, Bulletin 324. (in press)
- Henderson, J.R., Shaw, D., Mazurski, M., Henderson, M., Green, R., and Brisbin, D.
1979: Geology of part of Foxe Fold Belt, central Baffin Island, District of Franklin; in Current Research, Part A, Geological Survey of Canada, Paper 79-1A, p. 95-99.
- Jackson, G.D.
1978: McBeth Gneiss Dome and associated Piling Group, central Baffin Island, District of Franklin; in Wanless, R.K. and Loveridge, W.D., Rubidium-Strontium isotopic age studies, Report 2; Geological Survey of Canada, Paper 77-14, p. 14-17.
- Jackson, G.D. and Morgan, W.C.
1978: Precambrian metamorphism on Baffin and Bylot Islands; in Metamorphism in the Canadian Shield; Geological Survey of Canada, Paper 78-10, p. 249-267.
- Jackson, G.D. and Taylor, F.C.
1972: Correlation of Major Aphebian rock units in the northeastern Canadian Shield; Canadian Journal of Earth Sciences, v. 9, p. 1650-1669.
- Kranck, E.H.
1955: The bedrock geology of Clyde area in northeastern Baffin Island; Acta Geographica, v. 14, p. 226-248.
- Morgan, W.C., Bourne, J., Herd, R.K., Pickett, J.W., and Tippett, C.R.
1975: Geology of the Foxe Fold Belt, Baffin Island, District of Franklin; in Report of Activities, Part A, Geological Survey of Canada, Paper 75-1A, p. 343-347.
- Morgan, W.C., Okulitch, A.V., and Thompson, P.H.
1976: Stratigraphy, structure and metamorphism of the west half of the Foxe Fold Belt, Baffin Island; in Report of Activities, Part A, Geological Survey of Canada, Paper 76-1A, p. 387-391.

Pidgeon, R.T. and Howie, R.A.

- 1975: U-Pb age of zircon from a charnockitic granulite from Pangnirtung on the east coast of Baffin Island; Canadian Journal of Earth Sciences, v. 12, p. 1046-1047.

Ramsay, J.G.

- 1967: Folding and Fracturing of Rocks; McGraw-Hill, Inc., N.Y., 568 p.

Reynolds, D.L. and Holmes, A.

- 1955: The superposition of Caledonoid folds on an older fold-system in the Dalradians of Malin Head, Co. Donegal; Geological Magazine, v. XCI, p. 417-444.

Tippett, C.R.

- 1978: A detailed cross-section through the southern margin of the Foxe Fold Belt in the vicinity of Dewar Lakes, Baffin Island, District of Franklin; in Current Research, Part A, Geological Survey of Canada, Paper 78-1A, p. 169-173.

- 1979: Basement-supracrustal rock relationships on the southern margin of the Foxe Fold Belt, central Baffin Island, District of Franklin; in Current Research, Part A, Geological Survey of Canada, Paper 79-1A, p. 101-105.

**RECONNAISSANCE GEOLOGY OF THE FORT SMITH-HILL ISLAND LAKE
AREA, NORTHWEST TERRITORIES**

Project 790011

Hewitt H. Bostock
Precambrian Geology Division

Bostock, Hewitt H.; Reconnaissance geology of the Fort Smith-Hill Island Lake area, Northwest Territories; in Current Research, Part A, Geological Survey of Canada, Paper 80-1A, p. 153-155, 1980.

Abstract

Reconnaissance mapping of the Fort Smith-Hill Island Lake region began in 1979 with examination of scattered local areas throughout the region. This work suggests the following regional relationships.

In the Fort Smith area the oldest rocks comprise massive, leucocratic, garnet-bearing granitic rocks with associated high grade metasediments and metagabbro. These are inferred to be intruded by megacrystic granite. In the Hill Island Lake area the oldest rocks likely comprise an extensive plutonic complex which is the northern continuation of similar rocks in Saskatchewan. All of these rocks have been deformed and retrograded, and locally they have been mylonitized in zones that are commonly north-south trending.

Sediments of low metamorphic grade, which occur in the central part of the region, are of two groups: the older consists predominantly of slate siltstones and greywacke and has been intruded by granite, whereas the younger consists mostly of conglomerate and sandstone (Nonacho Group) and is not known to be intruded by granite.

The youngest rocks are northwest trending basalt to gabbro dykes.

Molybdenite occurs in association with a plagioclase rich breccia at Tsu Lake.

Introduction

The Fort Smith-Hill Island Lake area (75C, D, and part of 86A) is part of an extensive region of Precambrian rocks lying between Great Slave Lake and the southern border of the District of Mackenzie. Within this area most of the comprehensive geological mapping (Henderson, 1939; Wilson, 1941; Mulligan and Taylor, 1969; Taylor 1971) was carried out 20 or more years ago at a time when rapid preliminary reconnaissance was a prime objective. Since then a radiometric survey (Darnley and Grasty, 1972) followed by geological reconnaissance (Charboneau personal communication, 1979) and the present work have shown that regional thorium and uranium anomalies are associated with granitic rocks northeast of Fort Smith. Extensive prospecting has led to the discovery of numerous uranium occurrences farther east. The present project, involving a more thorough examination of the southern part of this area at 1:250 000 scale, is concerned with providing a more detailed and up-to-date geological framework in which these and other economic mineral occurrences may be placed. The initial field season (1979) was planned to cover a corridor across the entire area perpendicular to regional trends to provide an overview of geological units and problems that will be encountered as mapping progresses. The coverage reported here (Fig. 24.1) however, is more random than was originally planned because of widespread forest fires in this area during the 1979 field season.

Surficial Geology

Drift cover, except in the valley of Slave River, is minimal in the western part of the project area and increases eastward. The last major ice movement was from the east-northeast and is responsible for the major grain of the country. A few scattered occurrences of chattermark and fine striae suggest that a late southward drawdown of ice occurred. Distinctive erratics of high grade, garnet-bearing gneiss are widely scattered throughout the area and are probably derived from granulite facies terrain in the Penylan (Taylor, 1959) and Abitau (Hoadley, 1955) areas to the

northeast and east. Concentrations of conglomerate and sandstone erratics derived from the Nonacho Group were encountered at Tsu Lake some 80 km down ice from their nearest known outcrop.

General Geology

Rocks of the Fort Smith-Hill Island Lake areas are provisionally classified in the Table of Formations (Table 24.1).

Massive Granite

Massive, leucocratic, medium grained granitic rocks have been encountered extensively in the southwestern part of the Fort Smith area. They commonly contain scattered garnets rimmed and penetrated along fractures by chlorite. Near contacts with the Tsu Lake metasediments layers and schlieren of metasediment are present within the granite and irregular masses of granite intrude the metasediments; however it is not clear whether these intrusive relations truly represent the relative ages of the adjacent units or whether an older granite has been remobilized along its contacts with the metasediments.

Tsu Lake Metasediments

Metasediments of granulite facies metamorphic grade (containing various combinations of orthopyroxene, garnet, cordierite, and sillimanite) are extensively and excellently exposed in the vicinity of Tsu Lake near the west margin of Fort Smith area (75 D). Similar rocks are widespread as remnants within the granites at least as far east as Largepike Lake. Rocks of possible sedimentary origin and comparable metamorphic grade occur at Vandyck Lake and similar rocks may be present still farther east. West of Largepike Lake these rocks have undergone variable greenschist facies alteration commonly associated with late shearing. Farther east retrogression of the high grade metasediments is more pervasive.



Figure 24.1.

Table 24.1
Provisional Table of Formations

Group or site of major exposure	Lithology	
Sparrow dykes	basalt, gabbro, minor felsite breccia.	
Intrusive Contact		
Nonacho Group	conglomerate, arkosic sandstone, siltstone.	
Unconformity inferred		
Granite	locally fluorite-bearing.	
Intrusive contact		
Hill Island Lake sediments	greywacke, slate, chlorite schist, silty impure quartzite, arkosic siltstone, calcareous siltstone, conglomerate.	
Unconformity inferred		
Gneisses	gneisses and minor granite bodies derived from shearing and remobilization of older rocks (below).	
Megacrystic granite	megacrystic, locally garnet-bearing.	
Intrusive contact		
Metagabbro	plagioclase, hornblende, orthopyroxene, ± biotite. (commonly retrograded)	
Intrusive contact inferred		
Tsu Lake meta-sediments	psammitic to pelitic metasediments; some quartzite and iron formation. (granulite facies variously retrograded)	
Remobilized contact inferred		
Massive granite	medium grained, leucocratic, locally garnet-bearing.	

Granite-Diorite Complex including the northern continuation of the Granodiorite-Diorite Series of Koster and Baadsgaard, (1970). (Possibly related to Metagabbro)

Metagabbro

Small bodies of metagabbro up to about 2000 m wide are present throughout the area examined. In the Tsu Lake area metagabbro consists primarily of granular, coarsely twinned plagioclase with variable proportions of amphibole and orthopyroxene. Red-brown biotite is present near intrusion margins. Elsewhere and particularly in the eastern part of the area the gabbro is retrograded to hornblende gabbro and amphibolite. Megacrystic granitic rocks intrude a small body of metagabbro east of Leland Lake. Crosscutting relations between high grade metasediments and metagabbro have not been clearly established, but sill-like bodies of metagabbro are present locally within the metasediments and fine- to medium-grained metabasic dykes locally intrude them.

Megacrystic Granite

Megacrystic granite of more variable colour index than the massive granite occurs extensively to the northeast of the massive granite. Smaller bodies of similar rock intrude the gneisses and are locally deformed with them in the eastern part of the Hill Island Lake area. Most of the megacrystic granitic rocks contain either flattened or stretched quartz and potash feldspar megacrysts 2 to 3 cm in length. More rarely the rock is essentially free of foliation and lineation. In most areas examined, chiefly in the Fort Smith area (75 D), the two regional granites are separated by a zone of shearing in which remnants of metasediments, basic dykes, and granitic rocks have been hybridized and, in places mylonitized. Locally potash feldspar megacrysts occur within the massive granite especially near its margins. At Tsu Lake massive granite containing inclusions of metasediment is gradational over a short interval to megacrystic granite free of inclusions. These relations suggest that the megacrystic granite has locally developed from massive granite and is probably the younger.

Granite-Diorite Complex

Rocks of dioritic to granitic composition extend at least as far north as Grampus Lake and form a plutonic complex that is continuous with the Granodiorite-Diorite series of Koster and Baadsgaard (1970) in Saskatchewan. These rocks are apparently surrounded by a hybrid gneiss-migmatite terrane that may include remnants of high grade metasediments similar to those at Tsu Lake. Koster and Baadsgaard (1970) reported that their granodiorite diorite series postdates isoclinal early folding in the paragneiss but predates granulite facies metamorphism.

Tectonic History of Older Rock Units

The high grade metasedimentary remnants have been closely folded and severely stretched about subhorizontal fold axes producing many minor folds and fold mullions. Two sets of later steeply dipping faults intersect these axes roughly symmetrically and have associated steeply plunging minor folds. Thus it appears that east-west compression of these rocks persisted from the regime of folding and stretching into later more brittle deformation.

Subsequent deformation throughout the area appears to have consisted primarily of shearing and was accompanied by retrogression of granulite facies mineral assemblages to amphibolite and greenschist facies. Zones of mylonite are common particularly within the Fort Smith area. These are up to a hundred metres wide and commonly grade outward through foliated mafic gneiss, gneisses rich in mafic schlieren and inclusions, and foliated granite. In some areas inclusions appear to be largely of sedimentary origin and minor folding shows gentle plunge whereas in others more steeply plunging

minor folds are present and a high proportion of inclusions are of mafic dyke material. Such steeply dipping minor folds are particularly well exposed in the vicinity of Largepike Lake and more detailed study of their type (S or Z) may contribute to understanding of displacements evident in these zones of shearing. This later deformation of the basement was probably in part accompanied by faulting and folding of the overlying sedimentary cover.

Hill Island Lake Sediments

Remnants of sedimentary rocks whose metamorphic grade is mostly greenschist facies or lower, were encountered in the central part of the project area between lines drawn north and south through Kidder Lake and through Lady Grey Lake. These rocks consist of two assemblages. The older, Hill Island Lake sediments, consist of greywacke, slate, chlorite schist, fine grained impure quartzite, pink arkosic siltstone and minor conglomerate and calcareous siltstone beds, and have been intruded by granite at Thekulthili Lake. The presumably younger, Nonacho Group, is not known to be intruded by granite. The two sedimentary assemblages are likely in contact near MacInnis Lake north of the project area (Henderson, 1939).

The Hill Island Lake sediments are in fault contact with gneiss at most places where they have been examined. At the southwest end of Thekulthili Lake however, purple grey siltstone with sandstone beds has been intruded by fluorite-bearing granite that is presumably related to the granite pluton immediately to the west. Pink massive arkosic siltstone, locally with sand and pebble beds or black sand lamellae, lies on either side of the siltstones and may persist in a large roof pendant (?) of pink siltstone (or fine grained granite) within the adjacent pluton.

Nonacho Group

The Nonacho Group clearly lies unconformably on granitic basement in the Thekulthili Lake area where a distinctive conglomerate-breccia containing abundant blocks of gneiss is commonly present at the base. Higher within the group the rocks are predominantly granite pebble conglomerate, arkosic sandstones and siltstone. At the west end of Thekulthili Lake, northeastward decrease in clast size, increase in abundance of crossbedded sands, and current direction indicators support observations by McGlynn (1970) that derivation of sediment in this area was from the southwest. Top determinations and cleavage-bedding intersections indicate that the structure is complex and a large part of the southern margin of the group is overturned to the south-southeast.

Some 16 km east-southeast of Thekulthili Lake an outlier of Nonacho Group consists of interbedded conglomerate and sandstone near its base passing upward into massive foliated sandstone with occasional conglomerate beds. Granite pebbles are abundant in conglomerate near the base but dark siltstone fragments become increasingly abundant in conglomerate higher in the section. Crossbeds indicate that the west margin of the outlier faces east with dips up to 70 degrees east. Near the centre of the outlier bedding is gently dipping but cleavage remains eastward dipping at close to 70 degrees. These relations suggest that the east margin, which has not yet been mapped, may be overturned to the west.

Sparrow Dykes

The Nonacho Group and older rocks are intruded by widely scattered northwesterly trending Sparrow dykes (McGlynn et al., 1974) that are chiefly basaltic and commonly 3 m or less thick. Thicker dykes do occur however, and some of gabbro are more than 30 m thick. One forms the backbone of part of the large northwesterly trending peninsula at the

southeast end of Thekulthili Lake. A second more irregular gabbro dyke of unknown thickness but with chilled margin up to 10 m thick crosses the central part of Tsu Lake where it is accompanied by small amounts of felsic breccia. This breccia contains fragments of chilled gabbro and occurs with fine grained offshoots or in association with the chilled margin. It presumably results from remobilization of rocks of granitic composition along the dyke contacts together with slight shearing and shrinkage of the chilled margin.

Economic Geology

Much of the project area is currently being prospected for uranium and small amounts of yellow uranium stain are commonly associated with pegmatites in this area. A small galena vein has been trenced near the south shore of Thekulthili Lake (lat. 60° 47' 00"; long. 110° 15' 35"). Molybdenite mineralization was found on a small point on the west shore of Tsu Lake approximately 4.8 km north of the outlet of Taltson River (lat. 60° 41' 20"; long. 111° 56' 10"). Thumb-nail-sized patches of molybdenite occur locally in a breccia composed of blocky to folded fragments of high grade gneiss and fragments of quartz vein in a white, medium grained, matrix consisting chiefly of plagioclase. The breccia is about 8 m wide and lies between high grade metasediments to the east and mylonite along the contact with granite to the west. To north and south the breccia is covered by the lake but similar plagioclase-rich rocks outcrop locally near the granite contact along strike.

References

- Darnley, A.G. and Grastey, R.L.
1972: Airborn radiometric survey Fort Smith area, N.W.T.; Geological Survey of Canada, Open File 101.
- Henderson, J.F.
1939: Taltson Lake, Geological Survey of Canada, Map 525A.
- Hoadley, J.W.
1955: Abitau Lake, N.W.T.; Geological Survey of Canada, Paper 55-10.
- Koster, F. and Baadsgaard, H.
1970: On the geology and geochronology of northwestern Saskatchewan, I. Tazin Lake region; Canadian Journal of Earth Sciences, v. 7, p. 919-930.
- McGlynn, J.C.
1970: Study of the Nonacho Group of sedimentary rocks Nonacho Lake, Taltson and Reliance areas, District of Mackenzie (75E,F,K); in Report of Activities, Part A, Geological Survey of Canada, Paper 70-1A, p. 154-155.
- McGlynn, J.C., Hanson, G.N., Irving, E., and Park, J.K.
1974: Paleomagnetism and age of Nonacho Group sandstones and associated Sparrow Dykes, District of Mackenzie; Canadian Journal of Earth Sciences, v. 11, p. 30-42.
- Mulligan, R. and Taylor, F.C.
1969: Hill Island Lake, Geological Survey of Canada, Map 1203A.
- Taylor, F.C.
1959: Penylan Lake - Firedrake Lake, N.W.T.; Geological Survey of Canada, Map 8-1959.
- 1971: Nonacho Lake; Geological Survey of Canada, Map 1281A.
- Wilson, J.T.
1941: Fort Smith, Geological Survey of Canada, Map 607A.

**GEOLOGY OF THE ANIALIK RIVER GREENSTONE BELT, HEPBURN ISLAND
MAP AREA, DISTRICT OF MACKENZIE**

Contract 95799

R. Tirrul¹ and I. Bell²
Precambrian Geology Division

Tirrul R. and Bell, I., Geology of the Anialik River greenstone belt, Hepburn Island map area, District of Mackenzie; in Current Research, Part A, Geological Survey of Canada, Paper 80-1A, p. 157-164, 1980.

Abstract

The Anialik River greenstone belt at the northern margin of the Slave Province consists of a thick succession of Archean pillow basalts and andesites with significant but restricted accumulations of dacitic to rhyolitic volcanic rocks. The belt has been subjected to intense horizontal northwest-southeast compression punctuated by the emplacement of synkinematic and postkinematic granitic plutons. Concordant early foliations are interpreted to be related to the rise of the oldest granitoid plutons contemporaneous with regional compression. A second pervasive foliation is related to the regional compression alone. The unroofing of the early plutons during this deformation is recorded by clasts of these granitic rocks in boulder conglomerate at the top of the supracrustal succession.

Introduction

The Anialik River belt is the northwestern extension of the High Lake belt of Archean volcanic rocks in the northernmost part of the Slave Province. This project begins the mapping of these belts at 1:50 000 scale to define stratigraphic relations of the volcanic complex and to study its deformation, plutonic and metamorphic history.

The High Lake and Anialik River belts were first outlined by reconnaissance mapping in 1962 (Fraser, 1964). The High Lake 1:50 000 quadrangle (76 M/7) has been mapped by Padgham et al. (1974) and Baragar (1975) and Henderson (1975a) examined small areas of the belt.

P.A. MacKay provided superb field assistance and is responsible for some of the mapping.

Supracrustal Rocks of the Anialik Belt

The supracrustal rocks of the Anialik belt comprise thick accumulations of metabasalt and andesite with subordinate amounts of felsic volcanic and sedimentary rocks. No basement to the succession has been recognized. The sequence is intensely deformed so that bedding is difficult to recognize and reliable top determinations could only be made in a few areas. Because of the structural complications, regional stratigraphy was not established in detail. It is clear, however, that the facies relations are complex and that thick 'mafic' sections overlie, underlie, and interfinger with felsic volcanic rocks that were extruded from geographically separated centres.

Unit 1 (Fig. 25.1) consists of basalts and andesites. Basalts, distinguished by high specific gravity (S.G. 2.85+, see Lambert, 1977), where they are least metamorphosed, are typically medium green, aphanitic, aphyric and weakly to strongly foliated. Primary microscopic textures are largely obliterated, but megascopic features such as pillows, pillow breccia and amygdules up to 5 cm in diameter are common. Southeast of Turtle Lake, thin rimmed digital pillow tubes were mapped in nonamygdular flows. In a few localities transitions from massive to pillowed zones are discernible in single flows. Massive basalts are thought to be mostly flows, but may include some fine grained intrusions. Andesites are distinguished by their lower specific gravities, their brecciated nature, and locally, by the presence of plagioclase phenocrysts up to 5 mm in diameter. Breccias containing pumice fragments form distinctive horizons. Andesites are common southeast of Run Lake and are also associated with the apparent transition from mafic to felsic volcanism.

Large bodies of massive dacite and rhyolite with subordinate breccia (Unit 2) are found near Joy and Mistake lakes. An interpretation based on variable amounts or absence of quartz and feldspar phenocrysts suggests that each mass is composed of a number of flows. The flows weather light grey, pink or green, and are typically much less foliated than associated fragmental rocks.

Unit 3 comprises a wide variety of predominantly dacitic breccias and tuffs whose genesis is generally not easy to determine (Fig. 25.3f). Breccia, apparently unbedded, with blocks up to 60 cm in diameter is present northwest of Joy Lake in the same general horizon which contain massive flows of Unit 2. They are poorly sorted, and except for textural variations, monomict with a fine quartzofeldspathic, probably tuffaceous matrix. In most other areas the unit is characterized by layering, and smaller or streaky fragments, and rare crystal-rich horizons. This is especially true where the major felsic piles interfinger with more mafic volcanics. These zones are characterized by a predominance of thinly banded or laminated tuff. Ash flows were not recognized. Differentially flattened lithic clasts were observed, but in no place could this foliation be shown to be a primary feature. The presence of a number of widely spaced thin amygdular and occasionally pillowed flows throughout the unit indicates that the tuffs and breccias are subaqueous deposits.

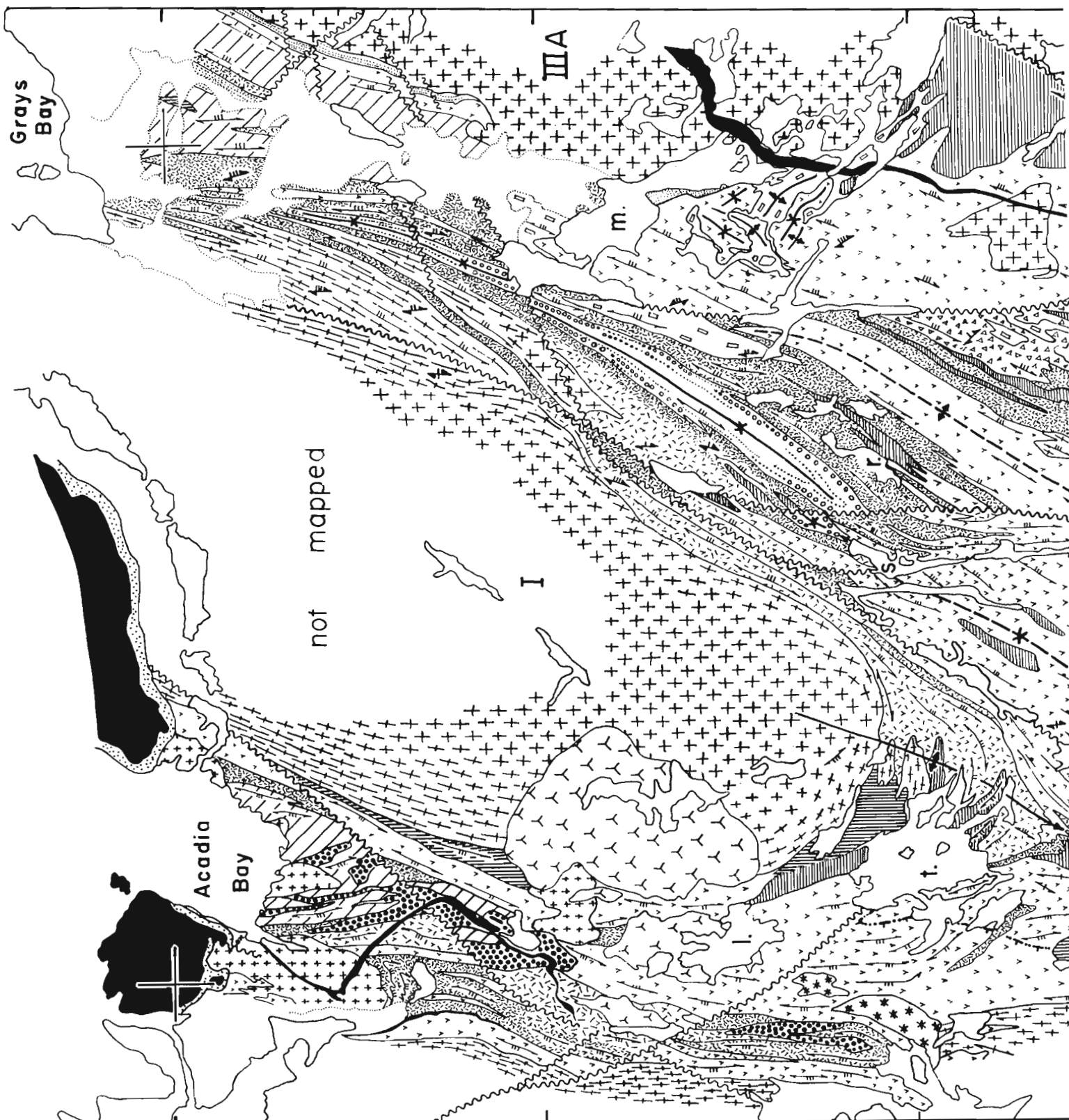
The upper part of the felsic succession northwest of Joy Lake consists of dolomitic breccias and fine volcanoclastics (Unit 4). The dolomite is now largely redistributed but occasionally cements bedded breccia, comprises laminations in breccia blocks, or is interbedded with fine volcanoclastics. Dolomitic layers are also common in the felsic belts west of Locanna Lake and north of Mistake Lake.

Strongly deformed felsic porphyry and breccia, and intermediate pumice breccia (Unit 5) is found along the southeastern margin of pluton I. It includes abundant, more mafic schists of uncertain origin.

On the south shore of Acadia Bay, a large body of light grey quartz-plagioclase porphyry intrudes the amphibolites and felsic schists. These masses of felsic porphyry are grouped in Unit 6. Similar porphyry, in most places strongly foliated, and with minor microcline as a phenocryst phase, occurs south of Grays Bay. It has concordant contacts, dolomitic tuffs on its upper(?) margin, and is transitional into fragmental zones, suggesting that it may be a large rhyodacite dome.

¹ Department of Geological Sciences, University of California, Santa Barbara U.S.A. 93016,

² Watts, Griffis and McQuat Limited, Toronto, Ontario



67° 45'

Grays Bay

Acadia Bay

not mapped

III

I

m.

S

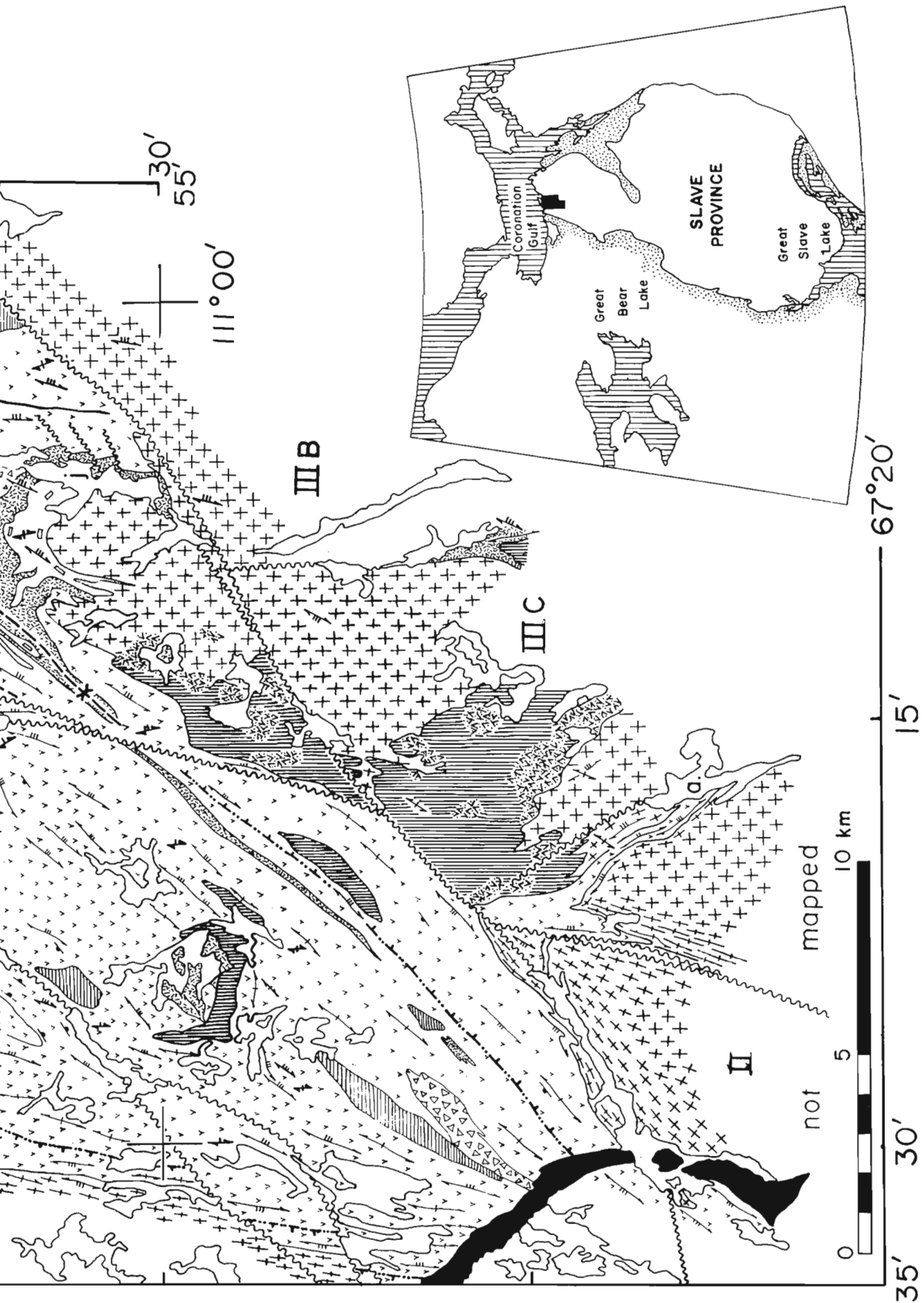
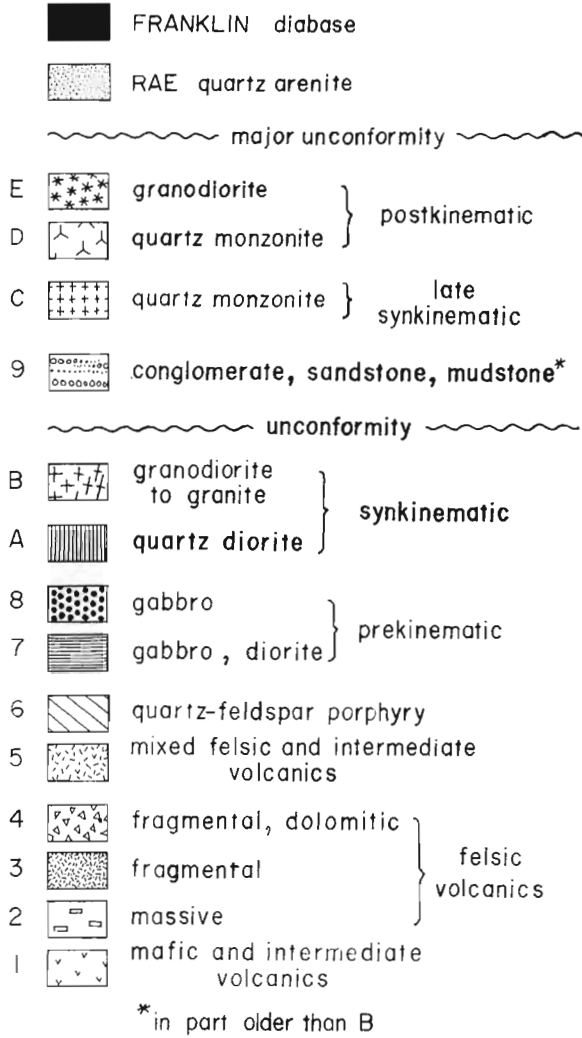
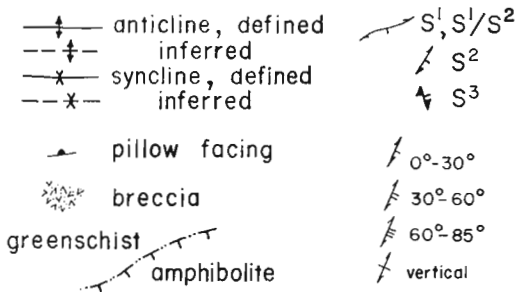


Figure 25.1. Geology of the Aniak River greenstone belt, Heppburn Island sheet (76 M).

LEGEND FOR FIGURE 25.1



- | | |
|----------------|---------------|
| a.-Aldose Lk. | r.-Run Lk. |
| j.-Joy Lk. | s.-String Lk. |
| l.-Locanna Lk. | t.-Turtle Lk. |
| m.-Mistake Lk. | |



A large number of irregular-shaped metagabbro to metadiorite (Unit 7) and metagabbro (Unit 8) intrusions are found throughout the volcanic succession. Only the larger ones are shown on Figure 25.1. They commonly have strongly foliated chilled margins, with massive, occasionally coarse grained centres, typically composed of equigranular plagioclase and amphibole. Pyroxene is recognizable in some intrusions in low grade areas, and rare intrusions contain plagioclase megacrysts. These intrusions are probably related to the mafic and intermediate flows.

One of the highlights of the field season was the discovery of a spectacular polymict conglomerate, associated with feldspathic sandstones, minor mudstone, and dolomite (Unit 9), preserved in a syncline northeast of String Lake (Fig. 25.3d, e). At the southern closure of the syncline, on the north shore of String Lake, the basal contact of coarse conglomerate truncates felsic and intermediate fragmental rocks, gabbro and amygdular flows with pronounced unconformity accentuated by tectonic deformation. At other localities, lithologic contacts are parallel or subparallel to the tectonic foliation, but the detailed map pattern of underlying units suggests that the unconformity continues northward for at least 8 km.

At the southern outcrops the conglomerate appears to be a monomict poorly sorted granitoid conglomerate with very well rounded boulders up to 0.75 m in diameter. It is actually polymict, with abundant deformed mafic to felsic volcaniclasts in the 'matrix'. In thin section, the granitic rocks are mafic-poor, nonfoliated medium- to coarse-grained quartz diorites and granodiorites, indistinguishable from the synkinematic plutons which intrude the volcanics. No metamorphic clasts are present. Interbedded sandstones, common farther north, are probably lithic and feldspathic arenites, but due to deformation and metamorphism the amount of matrix material is difficult to estimate. The original thickness of the sedimentary succession must have been at least one kilometre, with coarse conglomerate zones up to several hundred metres in thickness.

The sediments are probably shallow water deposits, based on their stratigraphic location, their overall character, and the lack of features characteristic of turbidites. They are thought to be analogous to the Jackson Lake Formation (Henderson, 1975b) in the Yellowknife Belt.

Thin zones of interbedded pelites and psammites in the northern arms of the belt are difficult to correlate because both the structure and the stratigraphy in these areas is not defined.

In general, the felsic volcanics of the east-central part of the map area north of Joy Lake and northwest of Mistake Lake are interpreted to overlie and interfinger with mafic flows of Unit 1. On the basis of their position on opposing limbs of a major syncline, the volcanic strata of Unit 5 appear to be correlative with the felsic volcanics southeast of Mistake Lake. The sequence of Unit 5 continues southwestward, around the nose of an anticline and pluton I, where it is overlain by a minimum of 2 km of basalt.

The fault between Mistake and Joy lakes separates volcanics with distinct characteristics. Felsic volcanics on the east side are largely massive, with no dolomite and minor breccia. The overlying flows are nonamygdular and contain pillows, with thin selvages. There are few volcaniclastic layers. These features are indicative of volcanism in deep water. The inverse is true of the volcanics on the east side of the fault, whose character is compatible with deposition in shallower water. One possible interpretation of these relationships is that the present fault coincides with a west side up synvolcanic structure.

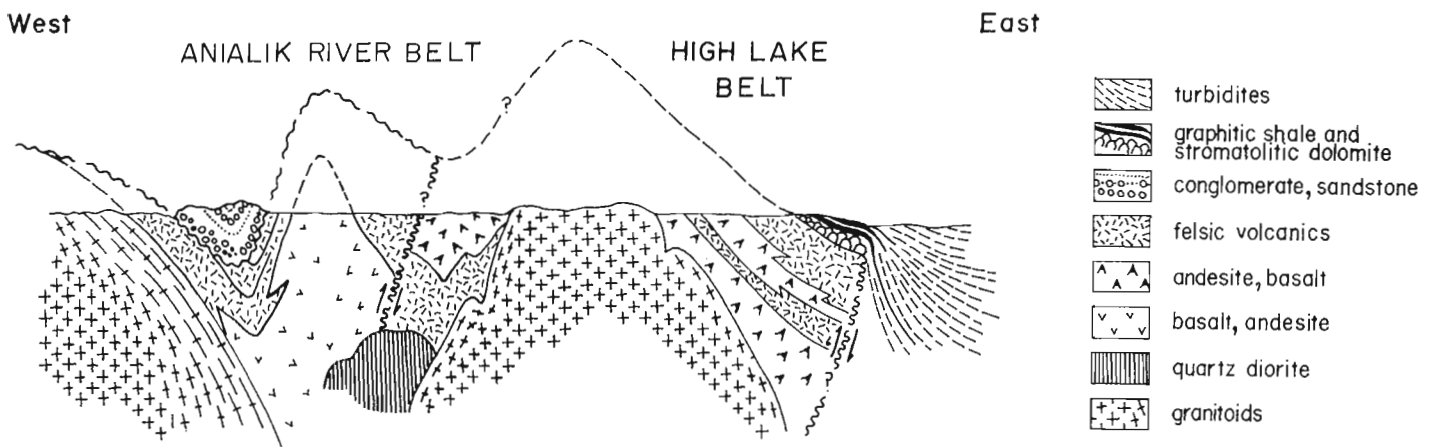


Figure 25.2. Cartoon depicting major elements of the Anialik River and High Lake belts and their possible relations. Structures have been opened for clarity.

The apparent anomalously high proportions of felsic volcanic rocks in the High Lake and Anialik belts, when compared with other Slave Province greenstones, can be in part reconciled if the two belts are considered to be parts of a once continuous belt. A very schematic cross-section through the belts, to be considered as a working model only, is shown in Figure 25.2. It was constructed by incorporating the observed and inferred lithologic and structural features into a section that suggests a higher, more normal proportion of mafic material in the belt.

Plutonic Rocks

At least two generations of plutons have been defined on the basis of crosscutting relations and timing of emplacement relative to deformation. Those of the oldest suite are mildly discordant with the volcanic stratigraphy, and concordant with the earliest tectonic foliation. They display complete compositional range from quartz diorite to granite. Medium grained hornblende quartz diorite bodies (Unit A) are the oldest of this suite. More felsic plutons of this suite always intrude quartz diorites. These relationships are well displayed north of Aldose Lake, where extensive intrusive breccia is developed. Pluton II contains alkali feldspar megacrysts, and is probably granite, as is much of the plutonic terrane along the western margin of the belt. Pluton I is mostly hornblende biotite quartz diorite to granodiorite; plutons(s) III A, III B, and III D are biotite granodiorite to quartz monzonite.

Several weakly foliated discordant biotite quartz monzonite plutons (Unit C) along the south shore of Acadia Bay do not appear to be affected by the earliest phase of deformation, and are therefore younger than the strongly foliated plutons immediately to the east and west. They may be temporarily equivalent to other quartz monzonite plutons along the eastern margin of the belt.

The youngest suite comprises nonfoliated, strongly discordant biotite granodiorite (Unit D) and quartz monzonite (Unit E) plutons north and west of Turtle Lake.

Metamorphism

The inner zone of the supracrustal belt is of greenschist facies characterized in mafic rocks by the mineral assemblage chlorite and/or actinolite + albite + epidote ± carbonate. In these rocks the transition to amphibolite facies is marked by a change from light green recessive schist to a dark green more massive and recrystallized rock, whose distribution appears to conform to the margins of the older plutons. In felsic rocks the transition is more difficult to

recognize. Both northern arms of the belt are in amphibolite facies. Pelitic assemblages in those areas include, with quartz, muscovite and plagioclase, staurolite + cordierite + garnet + biotite and andalusite + garnet + biotite.

Tectonic History

Most of the rocks in the area are affected by a prominent schistosity with a general northerly or northeasterly trend and steep inclination. At the northeast and southwest end of the early plutons, it can be resolved into one foliation (S_1) which wraps around and dips away from the plutons, and a second (S_2) which maintains a northeasterly trend and steep dip, and is axial planar to folded S_1 . At most other localities they are difficult to separate. A third crenulation cleavage (S_3) with an easterly to northeasterly dip is widespread. The three generations of foliations and associated structures are attributed to two probably related phases of deformation (D_1 and D_2) and a third distinct event.

The first phase was the most profound. The foliation (S_1) is often a plane of pronounced flattening (Fig. 25.3a to 25.3f), but because of its inhomogeneous nature, estimates of bulk strain are difficult to make. Massive flows and intrusives are often weakly foliated adjacent to strongly deformed tuff or breccia, and there is considerable meandering of foliations around competent bodies. In some areas almost all lithologies are highly strained. Unit 9, with its spheroidal granitoid clasts provides good, although differentially strained markers. At the southernmost exposure virtually undeformed granitic boulders contrast with moderate to strongly flattened clasts of volcanic origin (Fig. 25.3d). Farther north, granitic clasts too are progressively deformed into discoids and 'pancakes'. At latitude $67^{\circ}40'$ clasts have dimensions corresponding to axial strain ratios ($\sqrt{\lambda^2/\lambda^3}$) of >25 (Fig. 25.3e). This represents combined D_1 - D_2 shortening since S_1 and S_2 in the area are co-planar, but most of the shortening is due to D_1 based on the relative strains where they can be distinguished (Fig. 25.3f).

F_1 folds are difficult to recognize, partly because of the lack of well bedded units, and partly because S_2 is often co-planar with S_1 . The presence of the large-scale folds southeast of the syncline which preserves the conglomerate is based largely on lithologic distribution, since bedding determinations oblique to foliation are scarce. It is not clear whether they should be ascribed to D_1 or D_2 .

The peak of metamorphism is tentatively interpreted to be syndeformational with D_1 . Garnets from both northern arms of the belt display pronounced helicitic texture and schistosity is bent around all porphyroblasts.



Figure 25.3d. Polymict conglomerate, northeast of String Lake. Feisic clast has been highlighted.



Figure 25.3e. Very strongly flattened conglomerate, west of Mistake Lake. The conglomerate of Figure 25.3d can be traced across continuous outcrop to this locality.

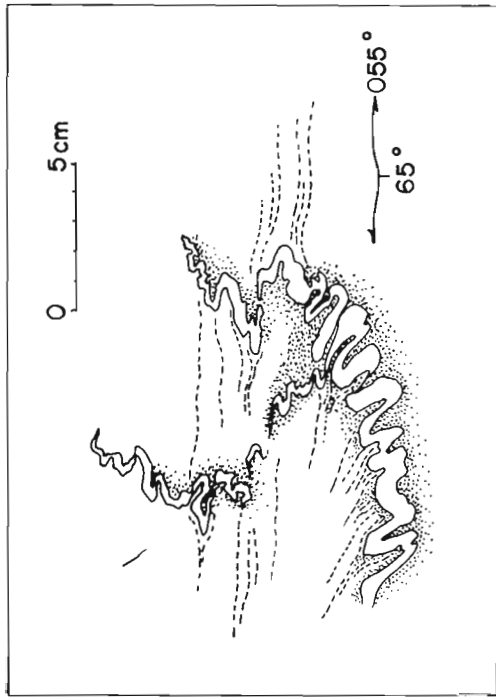


Figure 25.3a. Profile of F_1 folds in quartz veins crosscutting quartzfeldspar porphyry, Unit 5, east of Turtle Lake. D_2 does not affect this outcrop.

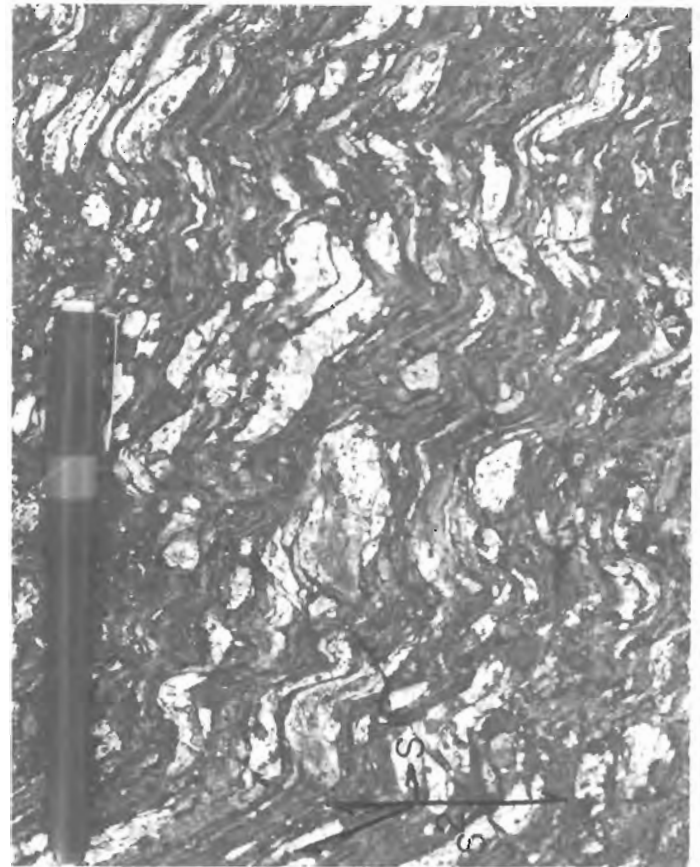


Figure 25.3b. F_2 folding strongly flattened dacite breccia, south nose of pluton I.

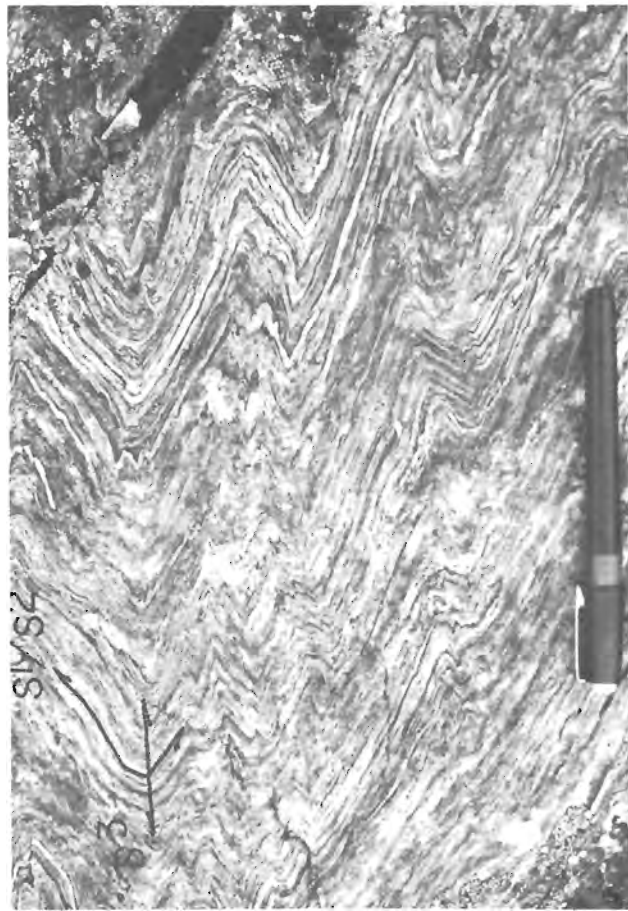


Figure 25.3f. F_3 folds north of Mistake Lake. The rock is thought to have been a felsic breccia. Each lamination is discontinuous.



Figure 25.3c. Crenulated metagranodiorite north of Aldose Lake.

Figure 25.3. Deformation in the Anialik River Belt.

Throughout the area during the second deformation (D_2), S_1 is crenulated or tightly to isoclinally folded into structures with wavelengths up to several hundred metres. At the northeast and southwest noses of plutons, the hinges of the second folds plunge away from the plutons, a feature inherited from early folds. Fold geometry is highly dependent on the rock type which is deformed. Similar folds are usually made up of buckled competent layers alternating with less competent flow-folded layers. The folds are axial planar to a crenulation cleavage which realigns phyllosilicates. The metamorphic grade during the second deformation is unclear.

Rocks well foliated by the first two deformations are often kinked or folded about conjugate axial surfaces consistent with northeast-southwest compression (D_3). North-northwesterly folds and related crenulation cleavage (S_3) predominate. Locally, inclined folds with wavelengths over 10 m are developed; chlorite is recrystallized in the hinge zones. The northwesterly trending upright folds responsible for the dome and basin interference fold pattern south of Mistake Lake may be related to this episode.

The effects of the first and second deformations on synkinematic plutons are of special interest. Two very elongate bodies of homogeneous coarse quartz-eye schist northwest of Mistake Lake are interpreted to be plutons upon which a retrogressive fabric was superimposed. Similar foliation locally developed parallel to plutonic margins north of Aldose Lake are crenulated by S_2 (Fig. 25.3c). Therefore the foliation in the masses northwest of Mistake Lake are considered to be S_1 . The southern body is gradational into a holocrystalline granitic rock. The margin of pluton I is marked by a concordant foliation which is most strongly developed along its northwestern and southeastern margins. This is also true of pluton II, but in this mass the foliation does not clearly follow contours of the northeastern contact. The foliation is often mylonitic, associated with very poorly developed lineations and featuring large K feldspar and smaller plagioclase porphyroclasts in a streaky quartz-rich matrix which bends around the crystals. This foliation does not transect the amphibolites, but its orientation is axial planar to second folding of amphibolite banding (S_1) concentric with the pluton. It is evident at this stage of the study that these plutons were emplaced during the first deformation, and subsequently modified by regional northwest compression.

Distinctly younger features are steeply-dipping right-lateral northeast trending strike-slip faults and a less well-developed northwesterly trending complementary set. They have the same orientation and sense of displacement as the late Apebian faults which crosscut the Bear Province to the west. Some may be continuous with them. Some dip-slip movement is indicated along the northeast trending fault south of Joy Lake because the extensive outcrop of mafic volcanics and gabbro on the north side does not appear in the south block. The northeast faults offset two north trending faults of unknown age. The western one has about 2 km of right lateral displacement; the offset on the eastern fault is unknown.

The area is cut by a swarm of northwest trending Mackenzie diabase dykes, and fewer dykes with easterly and northeasterly trends. A single northeasterly trending syenite porphyry dyke, which postdates the Proterozoic strike-slip faults, can be traced for over 25 km to a position north of Locanna Lake. The youngest intrusives are variably dipping sheets of Franklin diabase and gabbro.

References

Baragar, W.R.A.

1975: Miscellaneous data from volcanic belts at Yellowknife, Wolverine Lake, and James River, N.W.T.; in Report of Activities, Part A, Geological Survey of Canada, Paper 75-1A, p. 281-286.

Fraser, J.A.

1964: Geological notes on northeastern District of Mackenzie; Geological Survey of Canada, Paper 63-40.

Henderson, J.B.

1975a: Sedimentological studies of the Yellowknife Supergroup in the Slave Structural Province; in Report of Activities, Part A, Geological Survey of Canada, Paper 75-1A, p. 325-330.

Henderson, J.B. (cont'd)

1975b: Sedimentology of the Archean Yellowknife Supergroup at Yellowknife, District of Mackenzie; Geological Survey of Canada, Bulletin 246.

Lambert, M.B.

1977: Anatomy of a Greenstone Belt, Slave Province, N.W.T.; W.R.A. Baragar, ed., Volcanic Regimes in Canada; Geological Association of Canada, Special Paper No. 16, p. 331-340.

Padgham, W.A. et al.

1974: Geology High Lake 76 M/7, District of Mackenzie, Preliminary Edition, Canadian Department of Indian and Northern Development, Open File 208.

THE HEALEY LAKE MAP AREA (NORTHERN PART) AND THE ENIGMATIC
THELON FRONT, DISTRICT OF MACKENZIE

Project 780009

John B. Henderson and Peter H. Thompson
Precambrian Geology Division

Henderson, John B., and Thompson, Peter H.; *The Healey Lake Map Area (northern part) and the enigmatic Thelon Front, District of Mackenzie*; in *Current Research, Part A, Geological Survey of Canada, Paper 80-1A*, p. 165-169, 1980.

Abstract

Yellowknife Supergroup rocks occur throughout the area and include a major sequence of migmatitic intermediate volcanics and metasediments along the eastern border. Extensive plutonic and gneiss units range from granodiorite to diorite. The structural pattern produced by polyphase ductile deformation changes from complex and curvilinear in the west to north-trending linear zones in the east. Metamorphic grade of the low pressure type increases eastward from greenschist to upper amphibolite facies with relict kyanite indicating the greatest uplift in the highest grade zone. No changes in lithology, metamorphic grade, or structural style in the zone previously delineated as the Thelon Front were found. Completion of mapping in the area is required before a revised definition and location of the structural province boundary can be proposed.

Introduction

The Healey Lake area lies across part of the boundary, as presently mapped, between the Slave Structural Province and the Queen Maude Block (Heywood and Schau, 1978) of the Churchill Province. Geological mapping of the area at 1:250 000 scale begun in 1978 (Henderson, 1979) continued in the northern part of the area in an attempt to follow the low grade, less deformed Archean Yellowknife supracrustal rocks and intrusive rocks of the Slave Province that occur in the northwest corner of the area eastward to the Thelon Front (Wright, 1967), and across to the highly deformed and metamorphosed rocks of the western Churchill Province (Fraser, 1978). In addition to providing a 1:250 000 scale map where none is available currently, a major goal of the project is the better understanding of the nature and significance of the Thelon Front - the boundary between the two structural provinces.

General Geology

The area mapped to date at 1:250 000 scale or better is outlined in Figure 26.1. Wright described the Thelon Front in this vicinity as a zone that is "...gradational, probably over some miles...". The boundary as he defined it passes just west of the lake northwest of Tourgis Lake (Fig. 26.1) in a north-south direction and then curves southwesterly through the central part of the area mapped north of Healey Lake. No evidence was found in this zone of a pronounced change in lithology, metamorphic grade or structural style. A more precise definition of the front will be attempted when the mapping of the whole area is completed.

The area mapped can be divided into two parts based on structural style. West of about 107°W longitude the terrane is similar to much of the Slave Province, with abundant supracrustal rocks with irregular structural trends and several more or less equidimensional lobate plutonic bodies. To the east, however, the proportion of high grade metasediments and metavolcanics is much lower. The metamorphosed intrusive rocks occur as strongly aligned lensoid to linear bodies. Almost all units have a pronounced north to northeast-trending foliation.

Yellowknife Supergroup

The Yellowknife Supergroup has been defined as "any Archean volcanic and sedimentary assemblage within the Slave Province" (Henderson, 1970). The eastward extension of the Yellowknife rocks as defined in the Healey Lake area depends on the location of the Slave Province boundary which is a postdepositional structural marker; the Thelon Front. Because the precise location is uncertain, all the meta-sedimentary and metavolcanic rocks that occur throughout the area will be considered to be part of the Yellowknife Supergroup. This is reasonable as the rocks are similar to Yellowknife rocks elsewhere in the Slave Province.

The lowest grade, least-deformed Yellowknife rocks occur in the northwest corner of the area mapped. Part of a major volcanic complex composed dominantly of intermediate to felsic tuffs, breccias, lava flows and domes, occurs north and west of the Back River. It has been mapped in detail by Lambert (1976, 1977, 1978), who has recognized both subaerial and subaqueous environments in the evolution of the complex that culminated in the collapse of a large cauldron. The major part of the complex is essentially flat lying.

Surrounding the volcanic complex and at least to some extent interfingering with it, are greywacke-mudstone turbidites and their more highly metamorphosed equivalents that are typical of the Yellowknife sediments so abundant throughout the Slave Province. East of the complex the sediments are generally medium- to fine-grained, medium- to thin-bedded, with the greywacke-siltstone component dominating over the argillaceous component. Graded bedding is commonly preserved. South of the complex and two large plutons, the metasediments are mainly pelitic. Thin iron formation layers and lenses in the sediments are most abundant near the volcanic complex but also occur up to 15 km to the east of it.

Intermediate to felsic volcanoclastic units occur within the sedimentary sequence beyond the volcanic complex (Fig. 26.1). One such unit consists of a poorly sorted, poorly bedded breccia with angular clasts up to 8 cm where it is crossed by the Back River. To the east, the unit is made up of thin bedded, fine grained volcanoclastic sediments. A wider, more extensive felsic volcanoclastic unit occurs along the southwest shore of the large lake near the southeast corner of Figure 26.1 (west half). This unit consists of thin to medium bedded, fine grained, commonly graded beds.

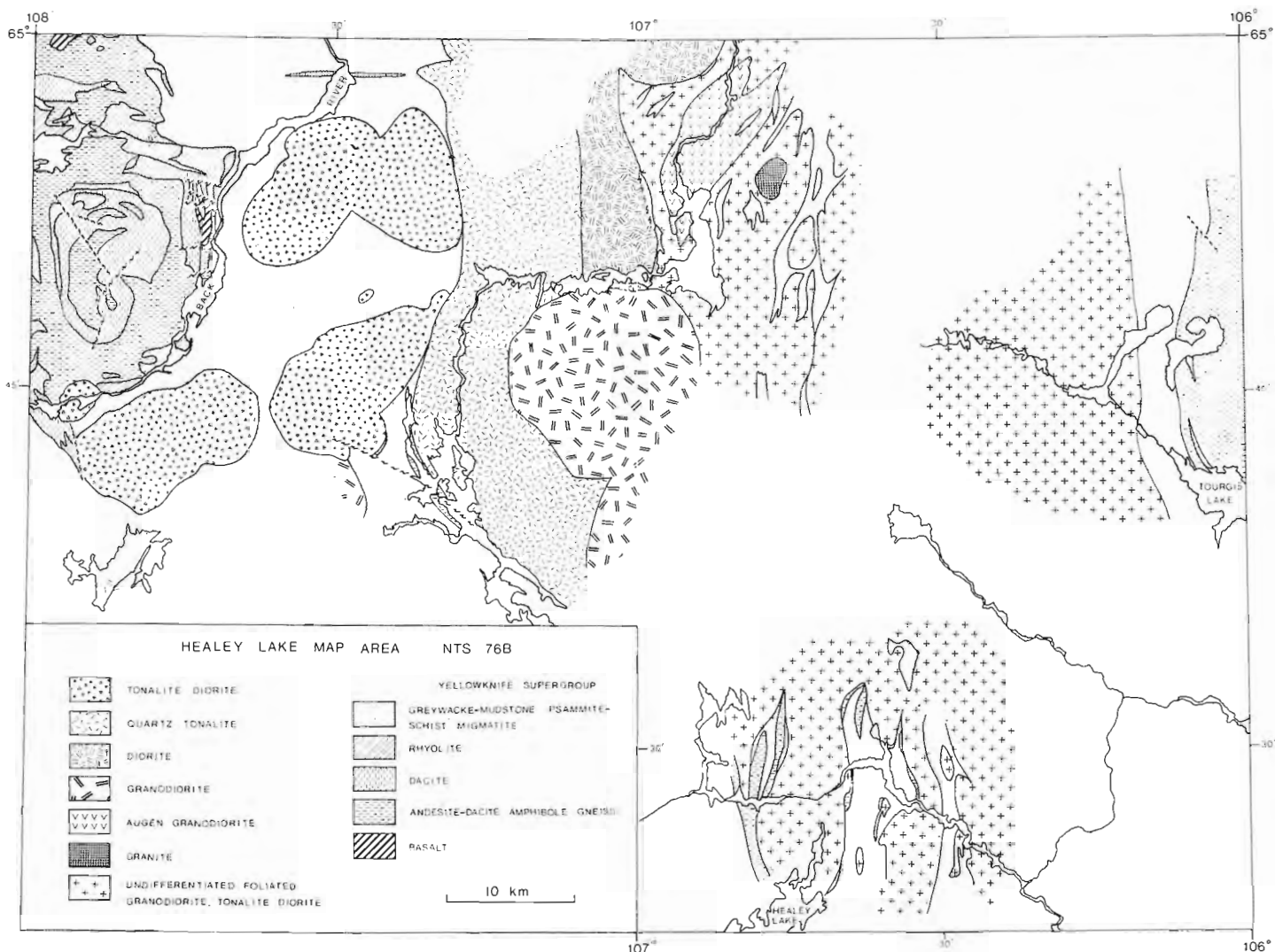


Figure 26.1 Geology of parts of the north half of the Healey Lake map area (NTS 76B). Geology of volcanic rocks west of the Back River is after Lambert (1976, 1977, 1978). Order of units in legend has no stratigraphic or age implication.

East of 107° (Fig. 26.1) the Yellowknife rocks are more highly metamorphosed and deformed so that all primary features other than gross compositional variations are lost.

Metavolcanic units in the east part of the area include a major unit of amphibole gneiss which occurs along the east border of the area mapped north of Tourgis Lake. This unit consists of layers one centimetre to a few decimetres thick which are defined by variations in texture and proportion of plagioclase, amphibole and garnet. Interlayered with them are discontinuous centimetre scale lenses to layers of white, coarser grained quartz plagioclase leucosome. This unit is thought to represent a highly metamorphosed, partly melted volcanic sequence of probable andesitic to dacitic composition. Thin but mappable units of metasediment occur within the unit and one calc-silicate rich zone up to 50 m wide extends over 3 km.

Other volcanic units, much smaller although better preserved, occur north of Healey Lake. There andesitic to dacitic metavolcanics are dominantly moderately foliated, fine grained, grey green to dark green, plagioclase amphibole rocks that are texturally and compositionally layered on a 10 to 30 cm scale. Layering is accentuated by centimetre scale units of darker, more mafic material separating the slightly coarser, thicker, more feldspathic layers. No primary

clastic outlines are preserved. Locally associated with these intermediate metavolcanics are white weathering, quartz-bearing metarhyolite units a few tens of metres thick. In some of these, layering is accentuated by carbonate-rich laminae.

The volcanics are everywhere associated with pelitic to psammitic schists that are presumably equivalent to the lowest grade greywacke-mudstone turbidites in the western part of the map area. Metasedimentary units (Fig. 26.1) vary from continuous metasediment as northwest of Tourgis Lake to the terrane in the northwest corner of Figure 26.1 (east half) where the metasediments are extensively intruded by granodioritic phases and the surrounding granodiorite contains abundant metasedimentary inclusions. The migmatitic metasediments west of the contact with the intermediate metavolcanics near Tourgis Lake contain abundant layers of coarse garnet amphibolite generally less than one metre thick that have been tightly folded with the metasediments and are thought to be metamorphosed mafic intrusions.

Granodiorite, Tonalite and Diorite

Several intrusive units have been recognized within the area mapped and they range from massive plutons in the west to gneissic units to the east. The intrusive rocks are unusual

compared to those in most other parts of the Slave Province in that there are no major granite units; most are granodioritic or more mafic in composition.

In the west, three large and two smaller, tonalitic to dioritic undeformed plutonic bodies intrude the sediments. They are massive, medium grained, dark pinkish grey, equigranular and hornblende- and biotite-rich. Locally, they are as felsic as granodiorite and as mafic as gabbro. Their contacts with the sediments are sharp and they form few or no dykes in the sediments and their contact zones contain only minor inclusions of country rock.

The quartz tonalite (Fig. 26.1) is a massive to locally weakly foliated, grey, coarse grained, biotite-rich pluton which is quite homogeneous throughout most of its outcrop area. It is characterized by abundant coarse masses of typically iridescent quartz up to one centimetre or more in size. This pluton contains only minor inclusions near its contact with the metasediments. Its relationship with the tonalite-diorite to the west is unknown, but it is intruded by the large granodiorite on its southeastern side, as shown by abundant dykes in the contact area.

The diorite that occurs east of the quartz-tonalite is a rather heterogeneous massive but more commonly foliated, dark grey, equigranular, medium grained body whose contact with the quartz-tonalite was not observed but which may be gradational. It also is intruded by the granodiorite to the south and is in fault contact with the rocks to the east.

The granodiorite to the south, which occurs as parts of two large circular plutons, is a fairly homogeneous, massive to weakly foliated, commonly buff coloured, equigranular, medium grained, with moderate to low biotite content. It commonly contains muscovite of varied grain size. It contains few inclusions and intrudes all surrounding units.

To the east is a large unit of undivided granodiorite, tonalite and locally, diorite. These rocks are almost everywhere strongly foliated and locally contain abundant small inclusions to mappable units of Yellowknife rocks. East of the large lake near the northwest corner of Figure 26.1 (east part) the unit consists of a heterogeneous assemblage of small deformed inclusion-free plutons with intervening, more foliated, granodioritic rocks with abundant meta-sedimentary inclusions. The plutons are for the most part white, medium grained, equigranular, mafic moderate to poor granodiorites and tonalites. North of the lake a well foliated, biotite-rich, augen granodiorite body lies within the granodiorite. A single pluton of massive light pink, medium fine grained, mafic-poor granite intrudes the granodiorite.

In the vicinity of Tourgis Lake the foliated granodioritic to tonalitic rocks are similar although the proportion of inclusions is smaller than farther west. The rocks are locally cataclastically deformed. Southwest of Tourgis Lake they have a very complex structural pattern. North of Healey Lake the more leucocratic granodioritic rocks are commonly rather gneissic. They are bordered on the east and west by more mafic tonalites and diorites.

Mafic Intrusions

Three diabase dyke sets of presumed post-Archean age occur within the area. The oldest set has a 090° trend and has been recognized as far west as Point Lake in the central Slave Province. These dykes are relatively unaltered in the Back River area (Fig. 26.1), but in the eastern part of the area they are metamorphosed and although the trend of the dykes is not seriously distorted, they develop a distinct northerly trending foliation. The second set has a 60° trend and is common in adjacent areas. It is not particularly abundant in the eastern part of the area mapped. The third set is the northwesterly-trending Mackenzie set.

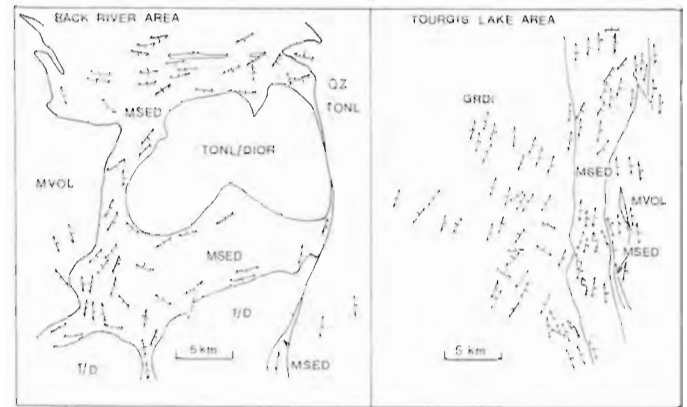


Figure 26.2 Orientation of the principal foliation in the Back River (a) and Tourgis Lake (b) areas. Rock unit abbreviations: metasedimentary (MSED) and metavolcanic (MVOL) rocks of the Yellowknife Supergroup; TONL/DIOR, tonalite/diorite; QZ TONL, quartz tonalite; GRDI, foliated granodiorite.

Structural Geology

There is a striking change in structural style across the map area. The orientation of the principal foliation and major lithologic contacts change from a complex curvilinear pattern in the west to a northerly-trending linear pattern in the east half of the area mapped (Fig. 26.1, 26.2).

In the west half the main part of the large volcanic complex is flat-lying (Lambert, 1978) but along the southern contact with the adjacent complexly deformed metasediments the dip of layering in the foliated metavolcanics is steep and locally refolded. East and south of the Back River the foliation in the metasedimentary rocks wraps around the unfoliated tonalite/diorite masses. In the east, rock units, the principal foliation and an older isoclinally folded foliation strike north to northeast and dip moderately to steeply eastward. Both intrusive and supracrustal rocks are strongly deformed in this trend; the only exception being the single pluton of massive granite (Fig. 26.1) about which the dominant foliation is deflected.

The structural pattern can be discussed in terms of three phases of ductile deformation. In the east and west the principal foliation is the product of a second phase of deformation as it is axial planar to isoclinal folds that deform both an earlier foliation and bedding/compositional layering. The variable orientation of the principal foliation in the west may be due to either diapiric rise of the plutons into the metasedimentary rocks or heterogeneous strain of relatively ductile metasediments squeezed between the more rigid plutonic and metavolcanic rock masses during horizontal compression. In the east horizontal compression resulted in the flattening of earlier structures into the present strong north to northeast orientation. The steep to moderate mainly easterly dip of the principal foliation may indicate that third phase folds are overturned to the west.

Several northwesterly-trending faults with right lateral displacements presumed to be post-Archean have been mapped. In the area west of Tourgis Lake narrow north-trending mylonite zones indicate faults parallel to the regional foliation.

Metamorphism

Widespread occurrence of andalusite, cordierite and sillimanite, with or without staurolite, in rocks of the Yellowknife Supergroup indicates low pressure type regional metamorphism. Similar low pressure mineral assemblages were produced throughout the Slave Province during a late

Archean tectonic event (Thompson, 1978). In the area mapped (Fig. 26.1, 26.3) metamorphic grade increases eastward from greenschist facies metagreywacke and meta-volcanic rocks (west of Back River) to upper amphibolite facies biotite-sillimanite-garnet-migmatite and garnet-amphibole gneiss (north and northwest of Tourgis Lake). Four zones are outlined on the basis of field observations and earlier petrographic work (Fig. 26.3). Cordierite and staurolite occur in the upper part of the biotite-chlorite zone, throughout the andalusite and andalusite-sillimanite zones, and locally in the sillimanite zone. Garnet is present locally below the sillimanite isograd but commonly in migmatitic rocks. Kyanite occurs in both the neosome and paleosome of the migmatite in the sillimanite zone, where it appears to be older than coexisting sillimanite. If the displacement along the Proterozoic Bathurst Fault is removed (approximately 140 km (Campbell and Cecile, 1979)), the kyanite localities in the map area (Fig. 26.3) line up with those described by Fraser (1968, 1972, 1978) and Thompson (1978). One locality also in the sillimanite zone with kyanite rimmed by cordierite and sillimanite, occurs north of the map area away from the main line of occurrences (Fig. 26.3a) (Padgham et al., 1974; Percival, 1979).

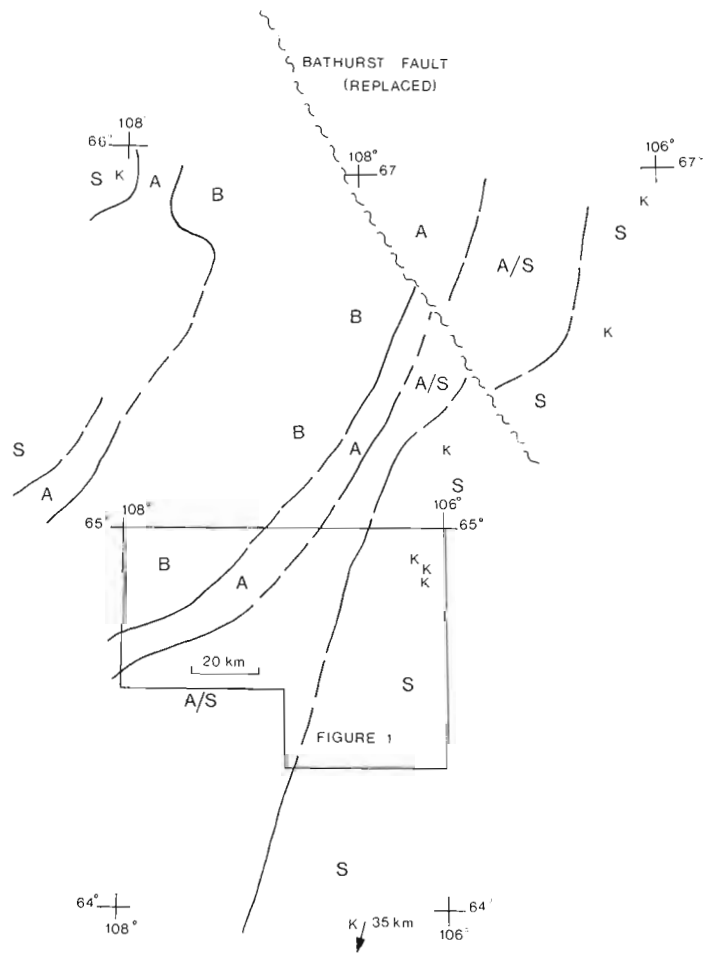


Figure 26.3 Aluminosilicate mineral zones in the area mapped and adjacent map areas. Removal of Bathurst Fault displacement according to Campbell and Cecile (1979). Zones are based on field observations and petrographic data (Fraser, 1968, 1972, 1978; Padgham et al., 1975; Percival, 1979; Thompson, 1978). Mineral name abbreviations:

B — Biotite-chlorite; S — Sillimanite;
 A — andalusite; K — kyanite.
 A/S — andalusite/sillimanite;

An erosion surface P-T curve consistent with the mineral zones does not intersect the kyanite stability field (Fig. 26.4) so either the kyanite is the product of an older relatively high pressure metamorphic event or it is a relict of an earlier stage in the development of the thermal high that produced the dominant cordierite-andalusite/sillimanite-migmatite metamorphism. In the absence of evidence for more than one metamorphism of the Yellowknife Supergroup both elsewhere in the map area and to the north (Fig. 26.3), the second possibility is preferred. That is, rocks in a thermal high which produced kyanite at intermediate pressures and temperatures were overtaken by rising isotherms (T increasing) as they were uplifted (P decreasing) (P-T time curve 2, Fig. 26.4). Two more extreme cases that would have a similar effect are the following: (i) temperature increasing at constant pressure (P-T time curve 1, Fig. 26.4), (ii) pressure decreasing at approximately constant temperature (P-T time curve 3, Fig. 26.4). Curve 3 implies that kyanite formed in equilibrium with the liquid leucosome in the migmatite prior to uplift. In all three cases, however, the presence of kyanite-bearing rocks at the surface in the eastern part of the area requires a greater degree of erosion in that area than is required to bring the cordierite-staurolite-andalusite rocks to the surface in the western part of the map area.

In the western part of the map area porphyroblasts that have overgrown the principal foliation indicate peak metamorphic conditions outlasted the main phases of deformation, as is generally the case in the Slave Province (Thompson, 1978). The leucosome in migmatite in the eastern part of the map area is intensely deformed, with sillimanite aligned parallel to axial surfaces of isoclinal folds. Peak metamorphic conditions were attained somewhat earlier than the last major phase of deformation.

Locally, retrogression is indicated by the alteration of sillimanite segregations and possibly andalusite to white mica, along with chloritization of biotite and cordierite.

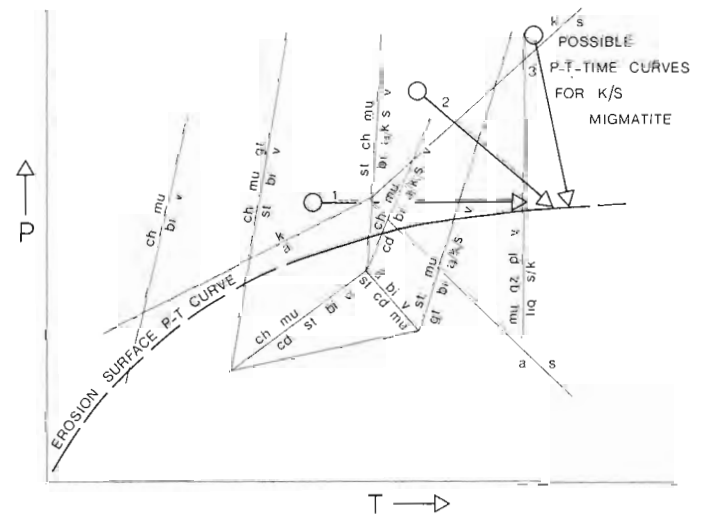


Figure 26.4 P-T diagram with estimated erosion surface P-T curve for the northern half of Healey Lake area and possible P-T time curves for kyanite-bearing rocks. Mineral name abbreviations:

ch - chlorite mu - muscovite
 bi - biotite gt - garnet
 st - staurolite a - andalusite
 k - kyanite s - sillimanite
 cd - cordierite qz - quartz
 pl - plagioclase liq - liquid
 v - vapour

Relatively coarse grained secondary white mica and chlorite is prominent in certain linear zones in the eastern half of the area mapped.

Conclusions

The results of the mapping program in the northern part of the Healey Lake area are summarized in the following conclusions:

- Deformed and metamorphosed supracrustal rocks similar to Yellowknife Supergroup rocks found elsewhere in the Slave Province occur throughout the area mapped. A major unit of highly metamorphosed metavolcanics and metasediments of unknown extent to the north or south occurs at the eastern boundary.
- All the volcanic units within the area mapped are of andesitic or more felsic composition.
- Major intrusive units are of granodioritic, tonalitic and dioritic composition. Except for one relatively small pluton, no major granitic bodies were recognized.
- Three phases of ductile deformation are proposed, with the third becoming increasingly dominant in the eastern part of the area, resulting in a regional northerly striking, moderately to steeply dipping trend being imposed on both intrusive and supracrustal rocks.
- Metamorphism is the low pressure type, with grade increasing from greenschist facies in the west to upper amphibolite facies in the east. The occurrence of relict kyanite in the higher grade assemblages implies greater uplift in the easternmost part of the area.

Previous reconnaissance mapping in the region (Wright, 1967) resulted in the placing of the Thelon Front through the eastern half of the area mapped. At that time, at the 1:1 000 000 scale of the mapping, the front was considered to be a zone several kilometres wide rather than a sharply defined line. The current more detailed mapping program has thus far failed to locate within the area mapped the zone that "...by contrasts in structure, lithology and metamorphic rank..." (Wright, 1967) defines the Thelon Front. The apparent break at 107°W longitude (Fig. 26.1) might be considered as a front as the structural style to the east and west is clearly different. On a more regional scale, however, the metamorphic gradient north of the Healey Lake area trends northeasterly (Fig. 26.3) while the structural trend as indicated by the orientation of intrusive units and structural data in the metasediments (Tremblay, 1971), suggested the structural trend continues northerly for a while but begins to swing more northwesterly as the grade drops. With the structural and metamorphic trends diverging as they do to the north, it seems unlikely the break at 107° longitude within the Healey Lake area is as regionally an important feature as the Thelon Front can be expected to be. In addition, in the southeast part of the Healey Lake area which has not as yet been mapped, there is a prominent zone of north-northeasterly trending lineaments that are coincident with an abrupt change in the magnetic anomaly pattern and roughly equivalent to part of the steep gravity gradient in the region. It is premature to speculate any further on the position and nature of the Thelon Front within the Healey Lake map area before the remainder of the area is mapped.

Acknowledgments

The mapping of the area was greatly facilitated by the enthusiastic and stimulating assistance of Alain Leclair, Léopold Nadeau and Glenn Seim. The Geology Office of the Department of Indian and Northern Affairs in Yellowknife assisted the party in many ways, but most importantly, by providing suitable boats without which the field work could not have been done. The comments of W.F. Fahrig, J.R. Henderson, J.C. McGlynn and M. Schau improved an earlier version of this report.

References

- Campbell, F.H.A. and Cecile, M.P.
1979: The northeastern margin of the Aphebian Kilohigok Basin, Melville Sound, Victoria Island, District of Franklin; in *Current Research, Part A, Geological Survey of Canada, Paper 79-1A*, p. 91-94.
- Fraser, J.A.
1968: Geology across Thelon Front, District of Mackenzie; in *Report of Activities, Part A, Geological Survey of Canada, Paper 68-1A*, p. 134.
1972: Artillery Lake map area; *Geological Survey of Canada, Paper 71-38*.
1978: Metamorphism in the Churchill Province, District of Mackenzie; in *Metamorphism in the Canadian Shield, Geological Survey of Canada, Paper 78-10*, p. 195-202.
- Henderson, J.B.
1970: Stratigraphy of the Yellowknife Supergroup, Yellowknife Bay-Prosperous Lake area, District of Mackenzie; *Geological Survey of Canada, Paper 70-26*.
1979: Healey Lake map area, District of Mackenzie; in *Current Research, Part A, Geological Survey of Canada, Paper 79-1A*, p. 400.
- Heywood, W.W. and Schau, Mikkel
1978: A subdivision of the northern Churchill Structural Province; in *Current Research, Part A, Geological Survey of Canada, Paper 78-1A*, p. 139-143.
- Lambert, M.B.
1976: The Back River Volcanic Complex, District of Mackenzie; in *Report of Activities, Part A, Geological Survey of Canada, Paper 76-1A*, p. 363-367.
1977: The southwestern margin of the Back River Volcanic Complex, District of Mackenzie; in *Report of Activities, Part A, Geological Survey of Canada, Paper 77-1A*, p. 179-180.
1978: The Back River Complex - a cauldron subsidence structure of Archean age; in *Current Research, Part A, Geological Survey of Canada, Paper 78-1A*, p. 153-158.
- Padgham, W.A., Bryan, M.P.D., Jefferson, C.W., Ronayne, E.A., and Sterenberg, V.Z.
1975: Geology Index Lake, 76-G-13, preliminary edition, E.G.S. map 1975-2 (2 inch : 1 mile map with marginal notes); Department of Indian Affairs and Northern Development, Ottawa.
- Percival, J.A.
1979: Kyanite-bearing rocks from the Hackett River area, N.W.T.: Implications for Archean geothermal gradients; *Contributions to Mineralogy and Petrology*, v. 69, p. 177-184.
- Thompson, P.H.
1978: Archean regional metamorphism in the Slave Structural Province - a new perspective on some old rocks; in *Metamorphism in the Canadian Shield, Geological Survey of Canada, Paper 78-10*, p. 95-102.
- Tremblay, L.P.
1971: Geology of Beechey Lake map-area, District of Mackenzie; *Geological Survey of Canada, Memoir 365*.
- Wright, G.M.
1967: Geology of the southeastern barren grounds, parts of the Districts of Mackenzie and Keewatin (Operations Keewatin, Baker, Thelon); *Geological Survey of Canada, Memoir 350*.

Project 770019

P.F. Hoffman, M.R. St-Onge¹, R.M. Easton²,
J. Grotzinger³, and D.E. Schulze⁴
Precambrian Geology Division

Hoffman, P.F., St-Onge, M.R., Easton, R.M., Grotzinger, J. and Schulze D.E., Syntectonic plutonism in north-central Wopmay Orogen (early Proterozoic), Hepburn Lake map area, District of Mackenzie; in Current Research, Part A, Geological Survey of Canada, Paper 80-1A, p. 171-177, 1980.

Abstract

Syn- to post-tectonic plutons in the area are clustered to form the composite Hepburn and Wentzel batholiths. Although granite is most abundant, the overall compositional range is from granite to pyroxenite. In general, the plutons become more basic and less deformed with time. The peak of metamorphism is related to the earliest granites, younger plutons being discordant with respect to the metamorphic isograds. Wentzel Batholith is the roof of a plutonic complex exposed in the core of a major anticlinorium. Hepburn Batholith comprises the floor and feeders to a pancake-shaped plutonic complex preserved in the keel of a synclinorium. The batholiths were emplaced during closure of these folds and after craton-vergent thrusting. Their setting is comparable to that of Cenozoic continental collision zones.

Introduction

Hepburn Lake map area spans the main tectonic zone (Fig. 27.1) of Wopmay Orogen. To the west are the younger calc-alkaline volcanic and plutonic rocks of Great Bear Batholith (Hoffman and McGlynn, 1977) and to the east is the foreland fold and thrust belt (Hoffman, 1973). Within this zone, syn- to post-tectonic plutons are clustered in two composite batholiths (Fig. 27.2), Hepburn Batholith (*sensu stricto*) in the middle of the zone and Wentzel Batholith (new name) on the west side. Each batholith has a distinct prograde metamorphic envelope, which ranges upward in grade from regional chlorite (below biotite) to well above orthoclase + sillimanite in pelites (St-Onge and Carmichael, 1979). The metamorphism belongs to bathozones 2 and 3 of Carmichael (1978), indicating that the batholiths were emplaced at 10-12 km depth. Structurally, Hepburn Batholith occupies the keel of a major synclinorium, whereas Wentzel Batholith appears to be in the core of an anticlinorium, most of the west limb of which has been truncated by the Wopmay Fault. Significantly, metamorphic isograds dip toward Hepburn Batholith and are "hot-side-up", whereas they dip away from Wentzel Batholith and are "hot-side-down" (St-Onge and Hoffman, 1980). The regional tectonic setting of the batholiths is interpreted as a continent-microcontinent collision zone (Hoffman, 1979).

This preliminary report was prepared by P.F. Hoffman based on mapping by all authors. D.E. Schulze is undertaking petrological studies of the gabbros. In addition, D.R.M. Pattison (Queen's University) is doing microprobe work on garnet-bearing plutons and W.R. Van Schmus (University of Kansas) has sampled a range of plutons for zircon geochronology.

Compositional Units

Most of the 150 or so plutons mappable at 1:100 000 scale are shown in Figure 27.2. It is noteworthy that the plutons vary greatly in size and are generally homogeneous in composition. Zoned plutons are uncommon. The overall compositional range is extreme, from granite to pyroxenite, but granite is areally by far the most abundant. In compositional nomenclature, we try to follow the recommendations of Streckheisen (1967). The following brief descriptions are meant to amplify the legend of Figure 27.2.

Protomylonitic Granite

The oldest and many of the largest plutons consist of medium grained, leucocratic, biotite monzogranite with an intense tectonic foliation and/or lineation. Fine grained, mafic xenoliths are locally abundant and may be so tectonically deformed as to impart a gneissic banding. Orthoclase porphyroblasts occur sparingly and this unit may grade into or be cut by porphyroblastic granite.

Porphyroblastic Granite

Strongly foliated, mesocratic, biotite syenogranite with abundant, very coarse, orthoclase porphyroblasts occurs gradationally toward marginal salients in the main granite pluton of the north lobe of Hepburn Batholith. Elsewhere, as in the remarkably elongate Keskarrah Granite (new name), similar porphyroblastic granites are sharply intrusive into protomylonitic granite.

Garnet Granite

Although accessory garnet occurs in nearly all the more felsic plutons, it is extraordinarily abundant (more than 5%) in certain plutons of Wentzel Batholith. They typically have abundant orthoclase porphyroblasts as well and in other respects resemble the porphyroblastic granites. It may be significant that both garnet and orthoclase porphyroblasts are abundant in Akaitcho Group migmatite adjacent to Wentzel Batholith but are almost absent adjacent to Hepburn Batholith.

Granodiorite

Although the overall composition of the batholiths is granodioritic, rocks of this composition are surprisingly uncommon. Even the large granodiorite pluton in the south half of Wentzel Batholith exhibits, in detail, a bimodal granite-tonalite tendency. It consists of prevailing medium grained, biotite tonalite, throughout which there are abundant gradational patches of coarse grained syenogranite. The granodiorite in the south half of Hepburn Batholith would be tonalitic were it not for poikilitic orthoclase porphyroblasts. The outer zone of the Rib Granite (new name) is highly variable in plagioclase/orthoclase ratio but its mean composition is granodioritic. Unlike the others, it is unfoliated and comes later in the intrusive sequence.

¹Department of Geological Sciences, Queen's University, Kingston, Ontario, K7L 3N6

²Department of Geology, Memorial University of Newfoundland, St. John's, Newfoundland, A1B 3X5

³Department of Geology, University of Montana, Missoula, Montana, U.S.A. 59812

⁴Program for Geosciences, University of Texas at Dallas, Richardson, Texas, U.S.A. 75080

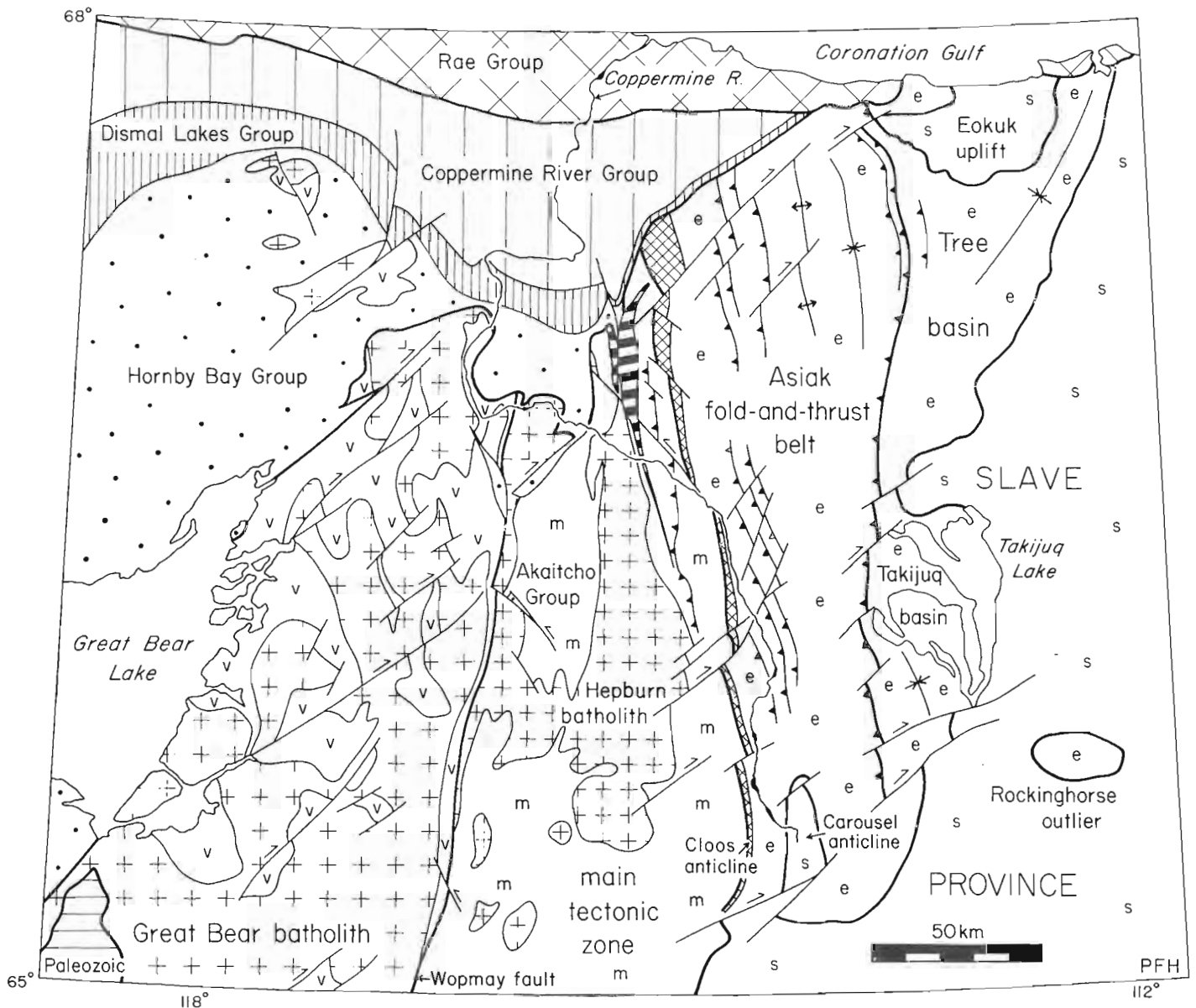


Figure 27.1. North end of Wopmay Orogen, showing the regional setting of Hepburn Batholith (centre) and the main tectonic zone.

Tonalite

The tonalites are strongly foliated, medium grained, quartz-rich rocks. Biotite is the main or only mafic mineral, in spite of the near absence of potassium feldspar. The tonalite in the north part of Wentzel Batholith is unusually rich in garnet. Varied xenoliths and globular quartz porphyroblasts are very common. Small irregular intrusions of leucogranite with sharp contacts typically occur within the tonalite but are not considered in the overall composition.

Quartz Diorite

These plutons are generally smaller and less numerous than the tonalites but are similar in being strongly foliated and in having biotite, not hornblende, as the main mafic mineral. Their intrusive contacts with protomylonitic granite are easily misinterpreted. What at first appear to be inclusions of quartz diorite in granite are, in fact, boudins of quartz diorite dykes.

Leucogranite

There are many small plutons of fine grained, very leucocratic, biotite granite, a rock which is typically variable in composition within single outcrops. Some are weakly foliated but most are massive. Leucogranite on the west side of the Squatarola Gabbro (new name) may result from melting of country rock during intrusion of the gabbro. Leucogranites within many of the most basic plutons may have a similar origin.

"Younger" Granite

There are several massive, very coarse grained, biotite syenogranites, especially near the Wopmay Fault, which closely resemble the late granites ("G3" plutons of Hoffman, 1978) of Great Bear Batholith. One of them actually intrudes the fault itself and is weakly foliated, although it obviously postdates the main fault movement. All the "younger" granites in the north half of the area intrude sedimentary and volcanic rocks, only slightly metamorphosed,

of the Dumas Group (Hoffman, 1978). The Dumas Group unconformably overlies protomylonitic granite and granodiorite of Wentzel Batholith, and is intruded by Great Bear Batholith. In the south half of the area, there are three "younger" granites in a line about 5 km east of the Wopmay Fault, the most northern of which contains large xenoliths of slightly metamorphosed Dumas Group rocks. All of these "younger" granites are probably of Great Bear Batholith age. A problem arises with the Rib Granite, spatially associated with Hepburn Batholith, which lithologically resembles the other "younger" granites but is located far from the Wopmay Fault and contains no xenoliths or other direct evidence of its age relative to the Dumas Group. Unlike the other "younger" granites, it is intruded by diorites and gabbros, so if it is as young as the Great Bear Batholith, so must the diorites and gabbros. Late diorites do occur ("G4" plutons of Hoffman, 1978) in Great Bear Batholith, although they are generally biotite-free. But if all the diorites and gabbros east of the Wopmay Fault are related to Great Bear Batholith, then it is strange indeed that they show such a remarkable spatial affinity for Hepburn Batholith.

Diorite

There are close to forty diorite bodies, none more 5 km across, and virtually all are within a narrow strip, 75 km by 15 km, trending north-south through Hepburn Lake. Characteristically, the diorite contains both hornblende and biotite, is highly variable in texture and grain size, and undergoes abrupt and extreme changes in colour index. Many of the diorites are intimately admixed with leucogranite and, although most are massive, a few have foliated zones within them.

Gabbro

There are forty or more bodies of nonfoliated, orthopyroxene ± biotite gabbro in a 100 km long strip, parallel that of the diorites but displaced about 10 km westward. Most are small but the Squatarola Gabbro, the largest, is 25 km long. One important concentration of bronzite gabbros is just west of the Muskox Intrusion (middle Proterozoic), an association which led us initially to the erroneous belief that the gabbros are coeval with it. However, in another important concentration, east of Wentzel Lake, the gabbros appear to have undergone transcurrent displacement along splays of the Belleau Fault system (Hoffman, 1980, Fig. 27.1). As the Muskox Intrusion postdates regional transcurrent faulting, the gabbros cannot be coeval with it. They are included in the Hepburn Batholith primarily because of the close spatial association. Moreover, the gabbros and diorites share a propensity for wild variation in texture, grain size and colour index. The gabbros also contain abundant leucogranite admixture, a feature common to all the more basic intrusions of Hepburn Batholith and conspicuously absent, in our experience, from the Muskox Intrusion. If the leucogranite is melted country rock, then the P-T conditions during emplacement of Hepburn Batholith would certainly be more conducive for its formation than those of Muskox Intrusion. There remains the possibility, discussed above, that the gabbros, diorites and "younger" granites are all related to the Great Bear Batholith, which also predates regional transcurrent faulting. Diorites in Great Bear Batholith do contain admixed leucogranite. There are no plutonic gabbros in Great Bear Batholith but just east of the Wopmay Fault, northwest of Akaitcho Lake, an outlier of Dumas Group is intruded by an elongate biotite gabbro, somewhat more altered than the others and lacking leucogranite. This may be the largest of an impersistent

swarm of mafic dykes, best developed west of Wentzel Lake, that parallels with Wopmay Fault. Their localization suggests that they may be feeders to Dumas Group basalts, which also occur only near the Wopmay Fault, and they are perhaps unrelated to the gabbros of Hepburn Batholith.

Ultramafic Rocks

Among the petrologic curios of the area is a small cigar-shaped body of hornblendite, grouped with the diorites in Figure 27.2, which intrudes granodiorite about 25 km south of Hepburn Lake. Another is a relatively large body of pyroxenite; with minor gabbro, which transgresses the contact between the Rib Granite and Niknark Tonalite (new name). A minor cluster of pyroxenite bodies, grouped with the gabbros in Figure 27.2, occurs on the south rim of the Coppermine River valley about 5 km east of the Wopmay Fault.

Emplacement Mechanism

The following observations indicate that magmatic stoping, not diapirism, is the dominant emplacement mechanism:

- The intrusions are highly variable in shape and size.
- The contacts are sharp and irregular in detail.
- Near contacts, dykes intrude the wall rocks and inclusions of wall rocks are common in the intrusions.
- There are no concentric, wall-parallel, flowage structures in the intrusions. Foliations and lineations are regionally coextensive with structures in the country rocks.

These observations do not preclude the possibility that the magmas melted from rising diapirs at deeper levels.

Intrusive Sequence

The intrusive sequence derived from crosscutting relations evident in Figure 27.2 shows, with complications, a general trend in composition with time. Aside from the recurrence of certain granites, younger intrusions become progressively more basic (Fig. 27.3). They also become smaller and more numerous. Only the leucogranites, "younger" granites and possibly the garnet granites are out of step with this trend. Among the major plutons of Hepburn Batholith, the protomylonitic Headnet Granite (new name) is the oldest and largest. It is cut by the porphyroblastic Keskarrah Granite, which cuts the large unnamed granodiorite south of Hepburn Lake, which in turn is cut by the Niknark Tonalite. The "younger" Rib Granite intrudes the Niknark Tonalite and is intruded by several small diorites and by the Squatarola Gabbro. The intrusive sequence of Wentzel Batholith is not so well known, the principal uncertainty being the relation of the garnet granites to the granodiorite. The overall compositional trend is dissimilar to that in Great Bear Batholith (Hoffman and McGlynn, 1977), which evolves from quartz monzodiorite through granodiorite to syenogranite and finally to diorite.

Internal deformation becomes progressively less intense in general agreement with the intrusive sequence. However, there is a marked jump in the progression, quartz diorite and older plutons being well foliated and younger ones being mostly massive. Composition must also be considered in assessing the degree of deformation. The quartz-rich tonalites deform more readily than the orthoclase-rich granites for example. Another complication is shearing, accompanied by retrograde alteration, which variably affects all intrusions within about 5 km of the Wopmay Fault.

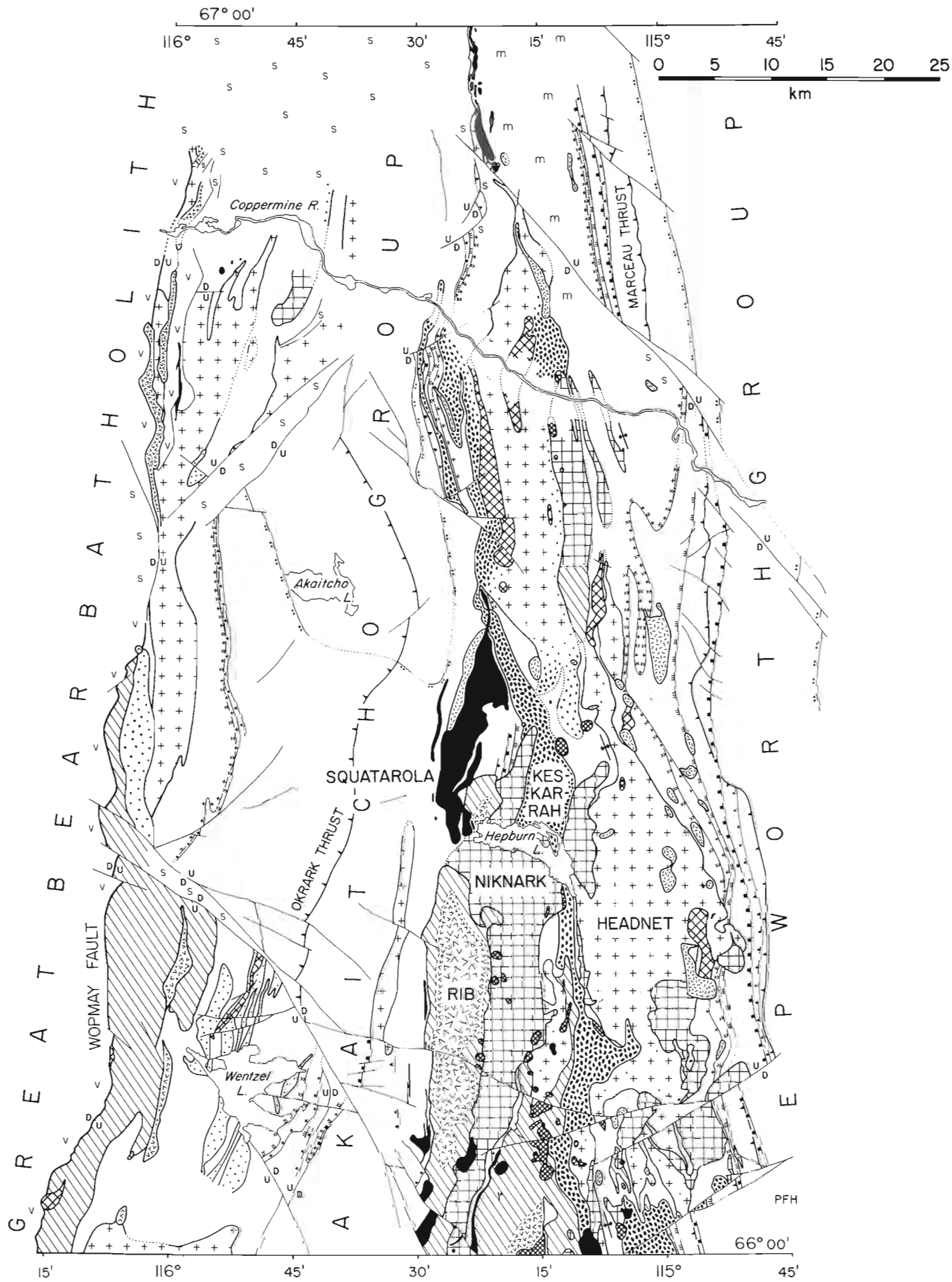


Figure 27.2. Plutons, metamorphic isograds and major faults in the Hepburn Lake map-area. The medial cluster of plutons comprises Hepburn Batholith and the western cluster, truncated by Wopmay Fault, comprises Wentzel Batholith.

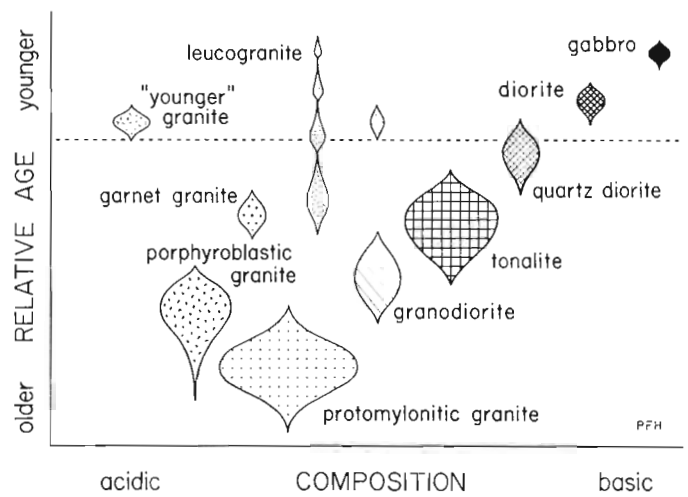
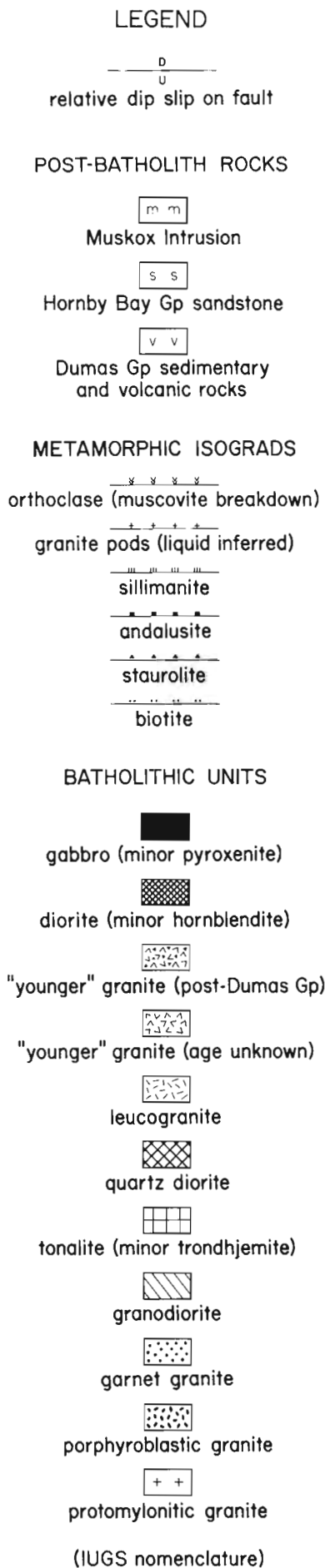


Figure 27.3. Compositional trend of plutons in Hepburn and Wentzel Batholiths with time. Units below the dashed line are strongly foliated whereas those above it are not.

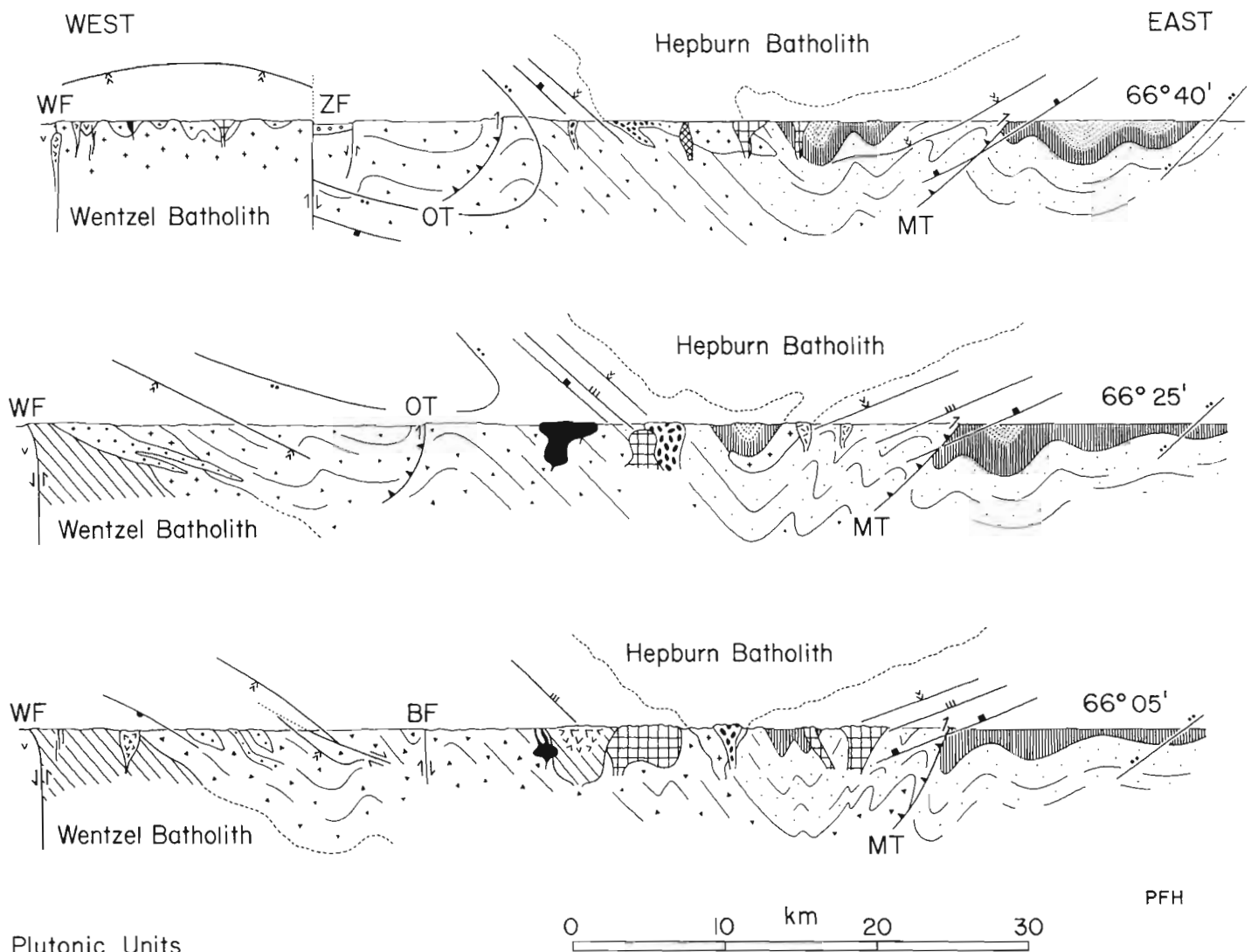
Relation to Metamorphic Isograds

The metamorphic isograds (Fig. 27.2) reflect extreme east-west variation in temperature with little or no change in pressure (St-Onge and Carmichael, 1979). The isograds are generally concentric with respect to the batholiths, the obvious heat sources. In detail, however, many plutons are discordant with the isograds, and the discordance is not simply related to the size or composition of the plutons. The Niknark Tonalite, Rib Granite and Squatarola Gabbro, for example, are grossly discordant. The isograds are best related to the large protomylonitic granites, suggesting that the peak of metamorphism occurred very early in the intrusive sequence. The only exceptions to this relationship are the narrow protomylonitic granite southwest of Hepburn Lake and the extreme eastern protuberance of the Headnet Granite, which is less deformed than the main part of that pluton and may be a separate intrusion.

In a separate paper (St-Onge and Hoffman, 1980), the dips of the isograds are deduced from structural relief provided by the dip-slip component of movement on transcurrent faults. The isograds are found to dip gently toward Hepburn Batholith and away from Wentzel Batholith. A similar analysis of intrusive contacts indicates that many plutons in Hepburn Batholith have walls that dip more steeply than the isograds. Those in Wentzel Batholith, however, seem to be generally parallel. A possible explanation is that the Hepburn plutons are feeders to a much larger, pancake-shaped body, responsible for the metamorphism, which has largely been eroded away. Wentzel Batholith could be similar but is lacking in feeder plutons because it is the roof, not the floor, of the batholith that is exposed. These relations are depicted in Figure 27.4.

Relation to Regional Structure

Hepburn and Wentzel batholiths occupy the axial zones of a paired synclinorium and anticlinorium respectively (Fig. 27.4). These are first order structures which congruently involve the well-established (Hoffman et al., 1978) stratigraphic succession, the foliation within the batholiths and the metamorphic isograds. Stratigraphic mapping of all the migmatite bands between plutons of Hepburn Batholith shows that the structurally deepest parts of the synclinorium, where the Fontano and Recluse formations are preserved, occur in three en echelon (right-handed) hinge areas, shown in Figure 27.2 and through which



Plutonic Units

- gabbro
- "younger" granite
- leucogranite
- quartz diorite
- tonalite
- granodiorite
- garnet granite
- porphyroblastic granite
- protomylonitic granite

Metamorphic Isograds

(ornament on high temperature side)

- cordierite
- orthoclase
- sillimanite
- andalusite
- biotite

Stratigraphic Units

- Hornby Bay Group (sandstone)
- Dumas Gp (calc-alkaline volcanics)
- Recluse Fm (orogenic flysch)
- Fontano Fm (black shale)
- Odjick Fm (cratogenic flysch)
- Akaitcho Gp (bimodal volcanics)

Figure 27.4. Schematic cross-sections through Wentzel and Hepburn Batholiths showing their relationship to metamorphic isograds, stratigraphic units and regional structures. Faults (see Hoffman, 1980; Easton, 1980; St-Onge and Hoffman, 1980):

- BF - Belleau Fault
- WF - Wopmay Fault
- MT - Marceau Thrust
- ZF - Zephyr Fault
- OT - Okrark Thrust

the cross-sections in Figure 27.4 are drawn. The middle cross-section is the most interesting because of the two gaping holes in the batholith between the Headnet, Keskarrah and Squatarola plutons. The eastern hole contains the deepest synclinal hinge area and the western hole is the only place in the map area where a stratigraphic contact between the Akaitcho Group and Odjick Formation (Epworth Group) can be seen (Easton, 1980). North and south of the eastern hole, the synclinorium can still be seen in the foliation of the plutonic rocks. In the north cross-section, Hepburn Batholith is well off the axis of the synclinorium and Wentzel Batholith is exposed in the cores of several secondary anticlines at the crest of what may have been a major anticlinorium, the west limb of which was subsequently translated, probably northward, and covered by the Dumas Group. In the southern cross-section, Hepburn Batholith is notable for the many discordant plutons, mostly tonalite, in which the foliation is congruent with the regional synclinorium. A simple interpretation would be that the batholiths intruded a subhorizontal succession, at different stratigraphic levels, and were subsequently folded. In this case, a difference in depth of emplacement of roughly 5 km should be reflected by differences in metamorphic pressure between the two batholiths. It is not. In the middle cross-section, where there are no major dip-slip faults to complicate matters, bathozonal data (St-Onge and Carmichael, 1979) do not permit more than about 1 km difference in depth at the peak of metamorphism. Therefore, it is more likely that the batholiths were emplaced during, rather than before, closure of the major regional folds.

Marceau Thrust (Fig. 27.2), on the east limb of the Hepburn synclinorium, and minor folds associated with it are definitely crossed by the metamorphic isograds. This is probably true also of Okrark Thrust, on the west limb of the synclinorium, where the metamorphic control is not nearly so good. Therefore, regional thrusting predated the batholiths and was followed by broad upright folding of the thrust complex, during which time the batholiths were emplaced. This seems to be exactly the structural and plutonic sequence found in Cenozoic continental collision zones (eg. Roeder, 1978). It is interesting to speculate that emplacement of syntectonic batholiths in collision zones is favoured in the hinge areas of late folds. This hypothesis cannot really be proved in the Hepburn Lake area but will be tested as mapping continues southward in Wopmay Orogen.

Acknowledgments

We are grateful to the Resident Geologist, Department of Indian and Northern Affairs, Yellowknife for logistical support. D.M. Carmichael (Queen's University) visited us in the field and contributed both mapping and encouragement.

References

- Carmichael, D.M.
 1978: Metamorphic bathozones and bathograds: a measure of the depth of post-metamorphic uplift and erosion on the regional scale; *American Journal of Science*, v. 278, p. 769-797.
- Easton, R.M.
 1980: Stratigraphy and geochemistry of the Akaitcho Group, Hepburn Lake map-area (86J): an early Proterozoic rift succession in the Wopmay Orogen; in *Current Research, Part B*, Geological Survey of Canada, Paper 80-1B, report.
- Hoffman, P.F.
 1973: Evolution of an early Proterozoic continental margin: the Coronation geosyncline and associated aulacogens of the northwestern Canadian shield; *Philosophical Transactions of the Royal Society of London, Series A*, V. 273, p. 547-581.
 1978: Sloan River map-area (86K), District of Mackenzie; Geological Survey of Canada, Open File Map 535.
 1979: Wopmay Orogen: continent-microcontinent-continent collision of early Proterozoic age, Bear Province, Canadian Shield; in *Geological Association of Canada, Program with Abstracts*, v. 4, p. 58.
 1980: Conjugate transcurrent faults in north-central Wopmay Orogen (early Proterozoic) and their dip-slip reactivation by post-orogenic extension; in *Current Research, Part A*, Geological Survey of Canada, Paper 80-1A, report 29.
- Hoffman, P.F. and McGlynn, J.C.
 1977: Great Bear Batholith: a volcano-plutonic depression; in *Volcanic Regimes in Canada*, ed. W.R.A. Baragar, L.C. Coleman and J.M. Hall, Geological Association of Canada, Special Paper 16, p. 169-192.
- Hoffman, P.F., St-Onge, M.R., Carmichael, D.M., and de Bie, I.
 1978: Geology of the Coronation Geosyncline (Aphebian), Hepburn Lake sheet (86J), Bear Province, District of Mackenzie; in *Current Research, Part A*, Geological Survey of Canada, Paper 78-1A, p. 147-151.
- Roeder, Dietrich
 1978: Three Mediterranean orogens: a geodynamic synthesis; in *Alps, Apennines, Hellenides*, ed. H. Closs, D. Roeder, and K. Schmidt, Inter-Union Commission on Geodynamics Scientific Report No. 38, Schweizerbart., Stuttgart, p. 589-620.
- St-Onge, M.R. and Carmichael, D.M.
 1979: Metamorphic conditions, northern Wopmay Orogen, N.W.T.; in *Geological Association of Canada, Program with Abstracts*, v. 4, p. 81.
- St-Onge, M.R. and Hoffman, P.F.
 1980: "Hot-side-up" and "hot-side-down" metamorphic isograds, Hepburn Lake map-area (86J), north-central Wopmay Orogen, District of Mackenzie; in *Current Research, Part A*, Geological Survey of Canada, Paper 80-1A, report 28.
- Streckheisen, A.L.
 1967: Classification and nomenclature of igneous rocks (final report of an inquiry); *Neues Jahrbuch für Mineralogie Abhandlungen*, v. 107, p. 144-214.

**"HOT-SIDE-UP" AND "HOT-SIDE-DOWN" METAMORPHIC ISOGRADS IN
NORTH-CENTRAL WOPMAY OROGEN, HEPBURN LAKE MAP AREA, DISTRICT OF MACKENZIE**

Project 770019

M.R. St-Onge¹ and P.F. Hoffman
Precambrian Geology Division

St-Onge, M.R. and Hoffman, P.F., "Hot-side-up" and "hot-side-down" metamorphic isograds in north-central Wopmay Orogen, Hepburn Lake map area, District of Mackenzie; in Current Research, Part A, Geological Survey of Canada, Paper 80-1A, p. 179-182, 1980.

Abstract

Of the three prograde metamorphic sequences in the area, two are related to Hepburn Batholith and one to Wentzel Batholith. All three are cut by postmetamorphic faults with significant vertical movement. The structural relief thus provided permits the determination that isograds on either side of Hepburn Batholith dip gently toward the batholith and are "hot-side-up". Isograds associated with Wentzel Batholith are "hot-side-down" and dip away from the batholith. It is concluded that the shape of Hepburn Batholith is a broad funnel fed from depth. Wentzel Batholith is the arched roof of an intrusive complex of unknown shape at depth.

Introduction

There are three north-trending prograde metamorphic sequences in early Proterozoic rocks of north-central Wopmay Orogen, Hepburn Lake map area (86 J). The eastern sequence is developed along the east side of Hepburn Batholith in pelite and flysch of the Epworth Group (Hoffman et al., 1978). The central sequence is developed along the west side of Hepburn Batholith in pelite and bimodal volcanic rocks of the upper Akaitcho Group (Easton, personal communication). The western sequence is developed along the east side of Wentzel Batholith in pelite and arkose of the lower Akaitcho Group. The metamorphic isograds and intrusive units are shown in Figure 27.2 of Hoffman et al. (1980).

In order to get an idea of the overall shapes of the batholiths, we attempted to determine the dips of the metamorphic isograds. Topographic relief in the area is generally insufficient to do this but the metamorphic sequences are cut by major faults, the vertical displacements across which provide significant structural relief. Most of the faults originated as conjugate transcurrent faults but the main vertical movements occurred later, during post-orogenic extension (Hoffman, 1980). By comparing the apparent offsets of the isograds with structural elements of known attitude, the dips of the isograds can be inferred, provided that the sense of dip-slip is also known. This has been done in each of the three metamorphic sequences and the results have been corroborated by independent structural evidence.

Eastern Metamorphic Sequence: "hot-side-up"

This metamorphic sequence ranges upward from quartz-muscovite-plagioclase-chlorite to sillimanite-orthoclase-garnet-cordierite-granitic melt (inferred) toward Hepburn Batholith. The sequence is cut by Sinister Fault (Fig. 28.1; see also Hoffman, 1980, Fig. 27.1 for fault locations), a northwest-trending left-lateral transcurrent fault that underwent dip-slip reactivation following deposition of the post-orogenic Hornby Bay Group (middle Proterozoic). An outlier of Hornby Bay sandstone, about 1200 m thick, is preserved along the south side of the fault, indicating that the south side moved down.

The east-vergent Marceau Thrust does not displace the isograds (Hoffman et al., 1978) and therefore must predate metamorphism. Tight pre-metamorphic folds near the thrust are generally upright or east-vergent, suggesting that the fault plane is steep or dips to the west.

The difference in offset between the isograds and Marceau Thrust across Sinister Fault is dramatic. All the isograds, even biotite, are offset much more than the thrust and the andalusite isograd shifts from the hanging wall to the footwall of the thrust. Geometry dictates that the isograds dip to the west and dip more gently than Marceau Thrust. As metamorphic grade increases to the west, the isograds are "hot-side-up".

The "hot-side-up" metamorphism is corroborated in areas of postmetamorphic folding (Fig. 28.1). These are open upright folds, in which higher metamorphic grades are found in synforms than in antifolds. It should be noted that these folds do not cause the isograds to be inverted by a structural rotation. Not only are the folds upright but the correct stratigraphic order is maintained (see cross-sections in Hoffman et al., 1980, Fig. 27.4).

Central Metamorphic Sequence: "hot-side-up"

This metamorphic sequence is similar to the eastern sequence in character but is less continuously exposed because of truncation by plutons in the south and by normal faults in the north and because pelite is less abundant in the Akaitcho Group.

Where the sequence crosses the Coppermine River, southeast of Zephyr Fault, it is cut by an unnamed northeast-trending fault (Fig. 28.2). In the absence of Hornby Bay sandstone, relative metamorphic pressures interpreted from mineral assemblages north and south of the fault are used to determine the sense of vertical displacement. The three critical isograds are as follows:

1. quartz ± muscovite + staurolite = garnet + biotite + sillimanite
2. quartz ± muscovite = orthoclase + sillimanite
3. quartz + plagioclase + orthoclase = granitic melt (inferred from granitic pods)

The presence of isograd (1) and the absence of kyanite indicate that both sides of the fault are in bathozone 3 of Carmichael (1978) (Fig. 28.3). North of the fault, isograds (2) and (3) coincide, corresponding to the muscovite-melt bathograd of St-Onge and Carmichael (1979) and to the invariant point (labelled "A" in Fig. 28.3) that separates bathozones 3a and 3b. South of the fault, however, isograd (2) is well downgrade from (3), indicating a decrease in pressure and a position within bathozone 3a. By this reasoning the fault, like nearby Zephyr and Sinister faults, must be south-side-down.

¹ Department of Geological Sciences, Queen's University, Kingston, Ontario K7L 3N6

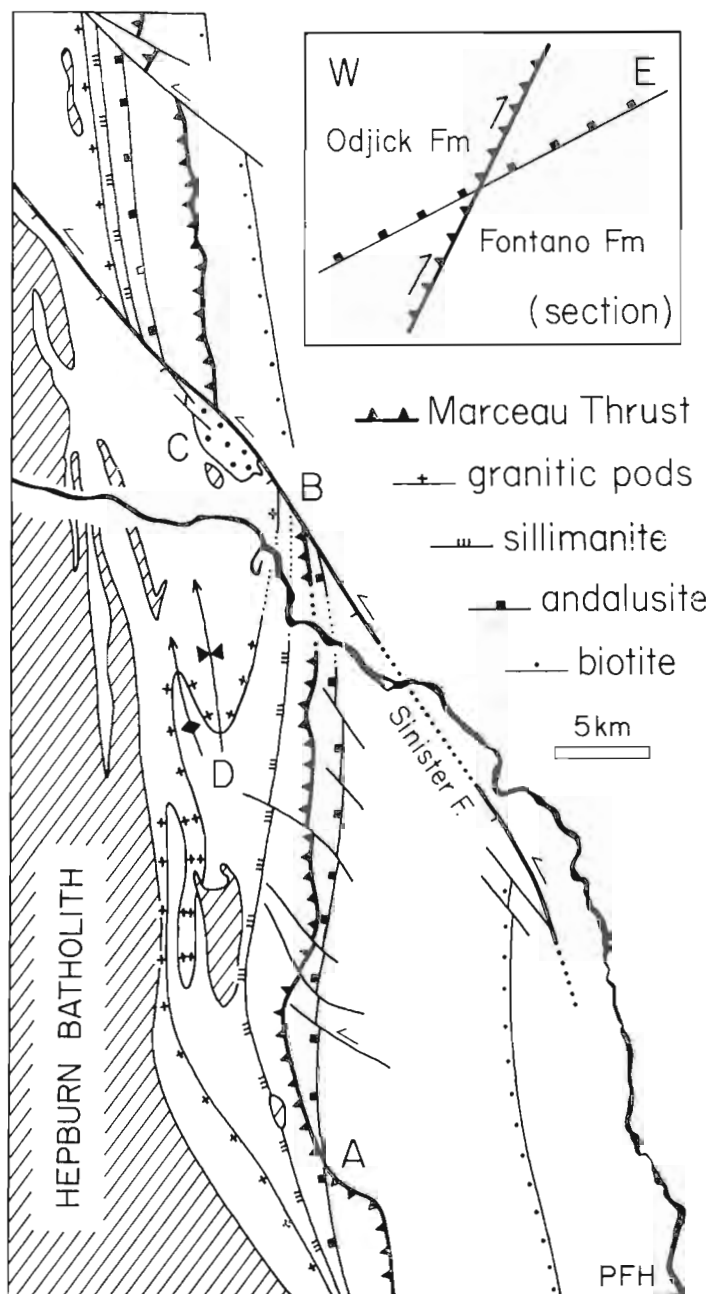


Figure 28.1. "Hot-side-up" metamorphic isograds on the east side of Hepburn Batholith. At location "A", the andalusite isograd crosses and, therefore, must postdate the Marceau Thrust. At location "B", both the thrust and the isograds are offset by Sinister Fault, a left-lateral transcurrent fault that underwent post-orogenic dip-slip (south-side-down), as can be seen by the half-graben of Hornby Bay sandstone (stippled) at location "C". The difference in offset between the thrust and the isograds requires that the isograds dip to the west more gently than the thrust plane, as shown in the section (inset). That the isograds are "hot-side-up" is corroborated at location "D", where postmetamorphic folds have higher grade rocks in synforms than in antiforms.

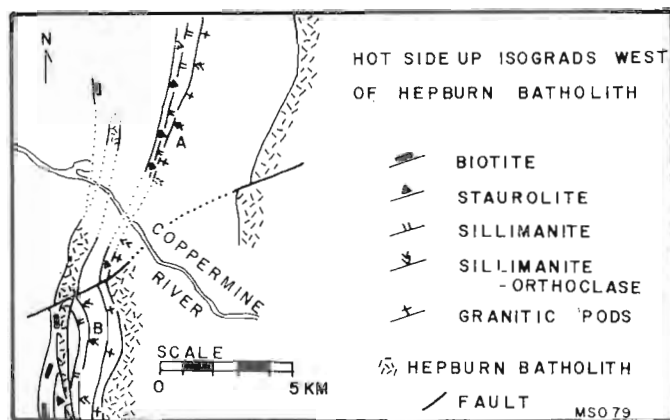


Figure 28.2. "Hot-side-up" isograds on the west side of Hepburn Batholith. North of the fault, isograds representing the first appearance of granitic pods and sillimanite + orthoclase coincide, corresponding to the muscovite-melt bathograd, which defines the bathozone 3a-3b boundary. South of the fault, the sillimanite + orthoclase isograd is well downgrade from the first appearance of granitic pods, indicating lower metamorphic pressure, within bathozone 3a.

The fault being short (10 km), transcurrent movement cannot have been great. Tentative correlation of felsic tuff units suggests less than 1 km of apparent right-lateral offset. There is no offset of the large granite dyke but its dip is unknown. The isograds are offset 1-2 km overall, significantly more than the felsic tuffs. The difference is probably an effect of the vertical component of movement. Given that the south side went down and that the felsic tuffs dip to the east (40-60°), geometry dictates that the isograds also dip to the east, even more gently than the tuffs. Therefore, these isograds must also be "hot-side-up".

This conclusion is supported by two short and strongly curved faults, shown in Figure 27.2 of Hoffman et al. (1980), that cut the metamorphic sequence north of the Coppermine River. Hornby Bay sandstone shows both to be south-side-down. The isograds and felsic tuffs are strongly and equally offset. The right-lateral offsets of 2.5 and 1.0 km surely exceed the transcurrent movement on these faults but are readily accounted for by the known dip-slip, provided that the tuffs and isograds dip concordantly to the east.

Western Metamorphic Sequence: "hot-side-down"

The western sequence is similar in character to the other two except that andalusite is generally absent. The sequence is cut by two major faults, the northeast-trending Zephyr Fault in the north and the southeast-trending Belleau Fault in the south (see Hoffman, 1980, Fig. 29.1; Hoffman et al., 1980, Fig. 27.2). Outliers of Hornby Bay sandstone indicate that Zephyr Fault is south-side-down and Belleau Fault is north-side-down.

Both the isograds and the edge of Wentzel Batholith have apparent offsets of about 20 km right-lateral across Zephyr Fault and 20 km left-lateral across Belleau Fault. The Wopmay Fault (Hoffman et al., 1980, Fig. 27.2), which predates the conjugate transcurrent faults, has less than 2 km of offset. This discrepancy can be easily explained if the isograds and the edge of the batholith dip gently to the east. As metamorphic grade increases to the west, the isograds are therefore "hot-side-down".

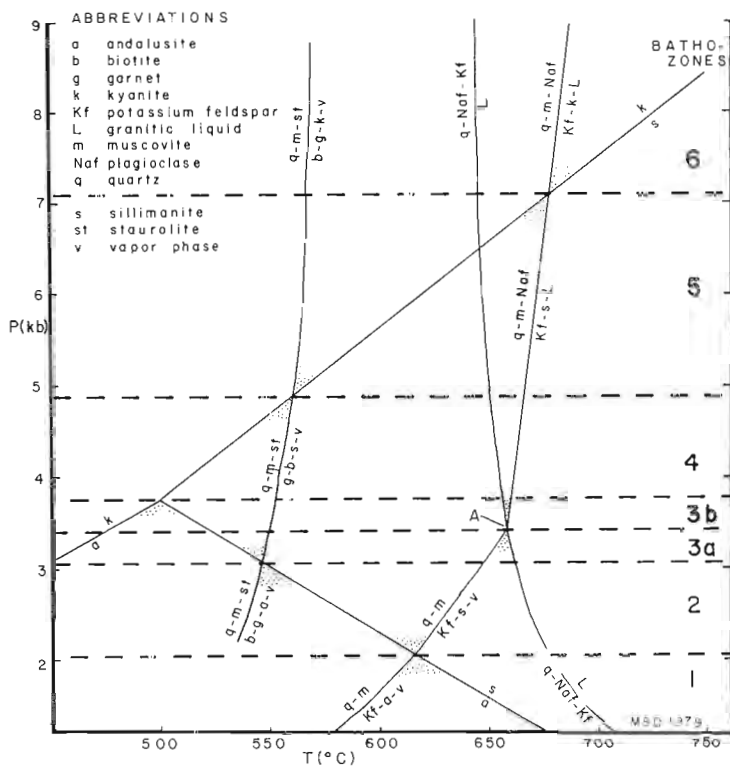


Figure 28.3. *P-T petrogenetic grid for part of the ideal pelitic system $\text{SiO}_2\text{-Al}_2\text{O}_3\text{-FeO-MgO-Na}_2\text{O-K}_2\text{O-H}_2\text{O}$, showing the bathozone scheme of Carmichael (1978) modified by St-Onge and Carmichael (1979).*

This conclusion is corroborated north of Zephyr Fault, where a number of postmetamorphic folds reveal batholithic rocks in the cores of antiforms and metamorphic rocks in synforms. The batholithic rocks, presumably the metamorphic heat source, must be generally below the metamorphic rocks, implying that the metamorphic grade increases downward.

The north-trending Kapvik Fault (Fig. 28.4; see also Hoffman, 1980, Fig. 27.1) deserves special mention because it repeats part of the metamorphic sequence south of the Belleau Fault. No Hornby Bay sandstone is present but a difference in metamorphic pressure, deduced from the pattern of isograds, indicates that the fault is east-side-down. East of the fault, isograds (2) and (3), as designated above, are coincident, indicating a metamorphic pressure corresponding to the bathozone 3a-3b boundary (Fig. 28.3). West of the fault, isograd (3) is well downgrade from (2), indicating that metamorphic pressure, in the absence of kyanite, lies within bathozone 3b. Although the fault is east-side-down, rocks on the west side are of lower metamorphic grade, seemingly inconsistent with the isograds being "hot-side-down". This discrepancy can be resolved only if the fault dips to the east more gently than the isograds, as shown in Figure 27.4 of Hoffman et al. (1980).

Shapes of the Batholiths

The eastern and central metamorphic sequences are "hot-side-up" and dip toward Hepburn Batholith. Therefore, the exposed edges of the batholith must be the floor of either a rootless synform or a broad funnel with a feeder conduit at depth. The funnel shape is favoured because the presence of garnet in most of the batholithic units points to an origin by

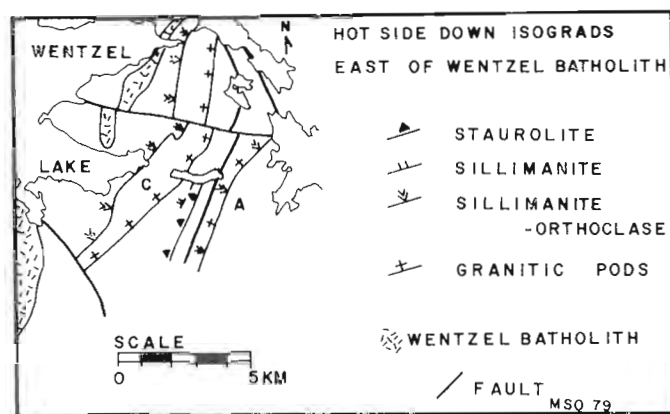


Figure 28.4. "Hot-side-down" isograds on the east side of Wentzel Batholith repeated by Kapvik Fault. At location "A", east of the fault, the first appearance of granitic pods and sillimanite + orthoclase coincide. At location "C", west of the fault, granitic pods appear well downgrade from the sillimanite + orthoclase isograd, indicating higher metamorphic pressure, within bathozone 3b.

anatectic melting at depths greater than 10 km (Green and Ringwood, 1968; Brown and Fyfe, 1970; Flood and Shaw, 1975; Green, 1976), the depth at which the batholith was emplaced (St-Onge and Carmichael, 1979). A microprobe study of garnets in various batholithic units is being undertaken by D.R.M. Pattison at Queen's University.

The western metamorphic sequence is "hot-side-down" and dips gently away from Wentzel Batholith. Therefore, it must be the roof of Wentzel Batholith that is exposed. Whether or not Wentzel and Hepburn batholiths are connected at depth cannot be deduced at present but may be revealed as this type of analysis is extended southward in Wopmay Orogen. We hope that this study serves as an example of how three-dimensional structures can be deduced even in the topographically flat areas of the Canadian Shield, and how detailed mapping of metamorphic isograds combined with experimental data on mineral stabilities can be used to resolve problems in regional tectonics.

References

- Brown, G.C. and Fyfe, W.S.
1970: The production of granitic melts during ultra-metamorphism; *Contributions to Mineralogy and Petrology*, v. 28, p. 310-318.
- Carmichael, D.M.
1978: Metamorphic bathozones and bathograds: a measure of the depth of post-metamorphic uplift and erosion on the regional scale; *American Journal of Science*, v. 278, p. 769-797.
- Flood, R.H. and Shaw, S.E.
1975: A cordierite-bearing granite suite from the New England batholith, N.S.W., Australia; *Contributions to Mineralogy and Petrology*, v. 18, p. 163-174.
- Green, T.H.
1976: Experimental generation of cordierite- or garnet-bearing granitic liquids from a pelitic composition; *Geology*, v. 4, p. 85-88.
- Green, T.H. and Ringwood, A.E.
1968: Origin of garnet phenocrysts in calc-alkaline rocks; *Contributions to Mineralogy and Petrology*, v. 18, p. 163-174.

Hoffman, P.F.

1980: Conjugate transcurrent faults in north-central Wopmay Orogen (early Proterozoic) and their dip-slip reactivation during post-orogenic extension, Hepburn Lake map area, District of Mackenzie; in Current Research, Part A, Geological Survey of Canada, Paper 80-1A, report 29.

Hoffman, P.F., St-Onge, M.R., Carmichael, D.M., and de Bie, I.

1978: Geology of the Coronation Geosyncline (Aphebian), Hepburn Lake sheet (86J), Bear Province, District of Mackenzie; in Current Research, Part A, Geological Survey of Canada, Paper 78-1A, p. 147-151.

Hoffman, P.F., St-Onge, M.R., Easton, R.M., Grotzinger, J., and Schulze, D.E.

1980: Syntectonic plutonism in north-central Wopmay Orogen (early Proterozoic), Hepburn Lake map area, District of Mackenzie; in Current Research, Part A, Geological Survey of Canada, Paper 80-1A, report 27.

St-Onge, M.R., and Carmichael, D.M.

1979: Metamorphic conditions, northern Wopmay Orogen, N.W.T.; in Program with Abstracts, Geological Association of Canada, v. 4, p. 81.

29. CONJUGATE TRANSCURRENT FAULTS IN NORTH-CENTRAL WOPMAY OROGEN (EARLY PROTEROZOIC) AND THEIR DIP-SLIP REACTIVATION DURING POST-OROGENIC EXTENSION, HEPBURN LAKE MAP AREA, DISTRICT OF MACKENZIE

Project 770019

P.F. Hoffman
Precambrian Geology Division

Hoffman, P.F., Conjugate transcurrent faults in north-central Wopmay Orogen (early Proterozoic) and their dip-slip reactivation during post-orogenic extension, Hepburn Lake map area, District of Mackenzie; in Current Research, Part A, Geological Survey of Canada, Paper 80-1A, p. 183-185, 1980.

Abstract

Conjugate sets of northeast (right-slip) and northwest (left-slip) transcurrent faults are the youngest structures related to east-west compression in the orogen. Postorogenic east-west extension resulted in dip-slip reactivation of the transcurrent faults and initiation of northerly-trending normal faults in middle Proterozoic cover rocks.

Introduction

Five major episodes of faulting are well documented in north-central Wopmay Orogen (Fig. 29.1). From oldest to youngest, they are:

1. The extensional Lupin Fault, on the west limb of Cloos Anticline (Hoffman et al., 1978), which was active during preflysch (Fontano Formation) sedimentation.
2. The belt of east-vergent thrust faults, 120 km wide, which continues east of the Hepburn Lake map area (86 J) and which formed during collisional underthrusting (Hoffman, 1979) of the Slave Craton.
3. The longitudinal Wopmay Fault, most of which is west of the Hepburn Lake map area and which is the eastern boundary of Great Bear Batholith (Hoffman and McGlynn, 1977).
4. The conjugate northeast and northwest transcurrent faults, formed during the final period of east-west compression in the orogen.
5. The northerly-trending normal faults and dip-slip reactivation of the conjugate transcurrent faults resulting from postorogenic east-west extension, mainly after deposition of the Hornby Bay Group and before the Rae Group (both middle Proterozoic).

It is the two youngest episodes that are described and illustrated in this report.

Conjugate Transcurrent Faults

The term "transcurrent fault" is used here, following Freund (1974), for strike-slip faults that are not transform faults. In the Hepburn Lake map area (Fig. 29.1), there are two sets of transcurrent faults. Almost without exception, the northeast-trending faults are right-slip and the northwest ones left-slip. So far as can be determined, all are of the same general age. They are therefore considered to comprise two sets of conjugate faults, produced as a result of east-west compression.

Conjugate transcurrent faults have been discussed in detail by Freund (1970, 1974), who illustrated how fault planes rotate about vertical axes away from the compressive axis during deformation. In the Hepburn Lake area, this phenomenon is shown by the clockwise rotation of northerly-trending structures within sets of northwest-trending faults and by counter-clockwise rotation of the same structures within sets of northeast-trending faults. Such rotations will require correction in paleomagnetic or other studies of directional properties.

The conjugate transcurrent faults are the youngest compressional structures in the orogen. The impressive set of northeast right-slip faults in Great Bear Batholith (Hoffman et al., 1976; McGlynn, 1977) postdates even the youngest plutons ("G4" plutons of Hoffman, 1978). Although conclusive evidence is lacking, it appears that most if not all strike-slip displacement occurred before deposition of the Hornby Bay Group sandstone. Strike-slip certainly predates the 1400 ± 75 Ma (Wanless et al., 1970) Western Channel Diabase, the Muskox Intrusion and the Mackenzie Dyke Swarm.

Postorogenic Normal Faults

Northerly-trending normal faults cut the middle Proterozoic cover rocks in the northwest corner of the Hepburn Lake area (Fig. 29.1), producing a series of horsts and grabens. The Canoe Lake Fault (Irvine, 1970; Hoffman, 1980), which displaces the Muskox Intrusion, is a prominent example, as is the Herb Dixon Fault (Baragar and Donaldson, 1973) in the Dismal Lakes area. Because of the northward-dipping, homoclinal nature of the cover sequence, these faults are exposed in oblique cross-section. Northward, and stratigraphically upward, the termination of these faults is generally within, or at the base of, the Coppermine River Group basalts (Baragar and Donaldson, 1973). To the south, many of these faults curve and join northeast-trending transcurrent faults in the early Proterozoic "basement".

Three of the major transcurrent faults in the Hepburn Lake area flank grabens or half-grabens of Hornby Bay Group sandstone (Fig. 29.1). Paleocurrents in the sandstones are generally south-eastward, conglomerate is rare and there is little evidence that faulting was active during sandstone deposition. In the Sloan River area, this is true also of the St. Germain Lake graben (86 K/9) but not of the Fault River Fault (86 K/11), where fanglomerate indicates movement, northwest-side-down, during early Hornby Bay Group sedimentation.

The northerly trending faults indicate east-west extension, perhaps culminating immediately before and during effusion of the Coppermine River Group basalts. In the "basement", this extension is manifested by dip-slip reactivation of the conjugate transcurrent faults. The structural relief provided by these vertical movements is invaluable in, for example, determining gently-dipping, "hot-side-up" and "hot-side-down", metamorphic isograds (St-Onge and Hoffman, 1980).

67°

Hornby Bay Group
sandstone

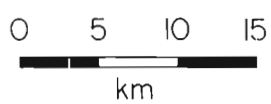
KEY

7	
6	
5	
4	
3	
2	
1	

*not
mapped*

Coppermine R.

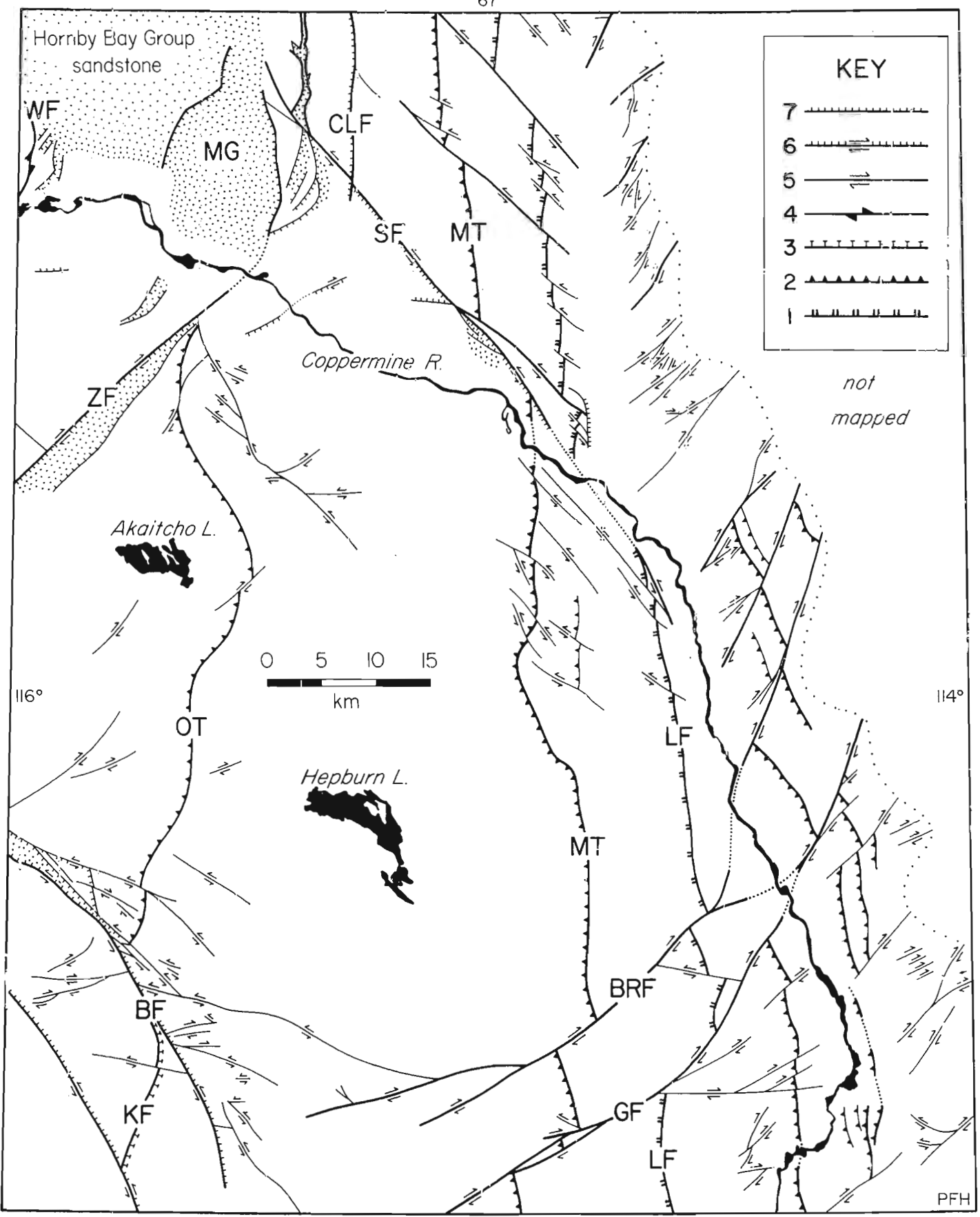
Akaitcho L.



116°

114°

Hepburn L.



66°

Figure 29.1. Faults in the Hepburn Lake map-area (86 J) and their relation to post-orogenic Hornby Bay Group sandstone (stippled).

BF - Belleau Fault	MG - Mouse Graben
BRF - Belanger Fault	MT - Marceau Thrust
CLF - Canoe Lake Fault	OT - Okrark Thrust
GF - Glen Field's Toes Fault	SF - Sinister Fault
KF - Kapvik Fault	WF - Wopmay Fault
LF - Lupin Fault	ZF - Zephyr Fault

Key (from youngest to oldest)

- 1 - Extension fault on the west limb of Cloos Anticline. Ticks on the down-thrown side.
- 2 - Thrust faults (premetamorphic). Teeth on the upper plate.
- 3 - Low-angle extension fault (postmetamorphic). Age uncertain, possibly related to (7). Ornament on down-thrown side.
- 4 - Longitudinal fault. Barbs give sense of probable strike-slip.
- 5 - Conjugate transcurrent faults (pre-Hornby Bay Group). Arrows give sense of strike-slip.
- 6 - Transcurrent faults as (5) but with significant dip-slip related to (7). Ticks on the down-thrown side.
- 7 - Extension faults (post-Hornby Bay Group). Ticks on the down-thrown side.

References

- Baragar, W.R.A. and Donaldson, J.A.
1973: Coppermine and Dismal Lakes map areas; Geological Survey of Canada, Paper 71-39, 20 p., Maps 1337A and 1338A.
- Freud, Raphael
1970: Rotation of strike-slip faults in Sistan, southeast Iran; *Journal of Geology*, v. 78, p. 188-200.
1974: Kinematics of transform and transcurrent faults; *Tectonophysics*, v. 21, p. 93-134.
- Hoffman, P.F.
1978: Sloan River map-area (86 K); Geological Survey of Canada, Open File Map 535.
1979: Wopmay Orogen: continent-microcontinent-continent collision of early Proterozoic age, Bear Province, Canadian Shield; in Geological Association of Canada, Program with Abstracts, v. 4, p. 58.

- Hoffman, P.F. (cont'd)
1980: On the relative age of the Muskox Intrusion and the Coppermine River basalts, District of Mackenzie; in Current Research, Part A, Geological Survey of Canada, Paper 80-1A, report 34.
- Hoffman, P.F. and McGlynn, J.C.
1977: Great Bear Batholith: a volcano-plutonic depression; in Volcanic Regimes in Canada, ed. W.R.A. Baragar, L.C. Coleman and J.M. Hall, Geological Association of Canada, Special Paper 16, p. 169-192.
- Hoffman, P.F., Bell, I.R. and Tirrul, R.
1976: Sloan River map-area (86 K), Great Bear Lake, District of Mackenzie; in Report of Activities, Part A, Geological Survey of Canada, Paper 76-1A, p. 353-358.
- Hoffman, P.F., St-Onge, M.R., Carmichael, D.M. and de Bie, I.
1978: Geology of the Coronation Geosyncline (Aphebian), Hepburn Lake sheet (86 J), Bear Province, District of Mackenzie; in Current Research, Part A, Geological Survey of Canada, Paper 78-1A, p. 147-151.
- Irvine, T.N.
1970: Geologic age and structural relations of the Muskox Intrusion; in Report of Activities, Part A, Geological Survey of Canada, Paper 70-1A, p. 149-153.
- McGlynn, J.C.
1977: Geology of the Bear-Slave structural provinces, District of Mackenzie; Geological Survey of Canada, Open File Map 445.
- St-Onge, M.R. and Hoffman, P.F.
1980: "Hot-side-up" and "hot-side-down" metamorphic isograds in north-central Wopmay Orogen, Hepburn Lake map-area (86 J), District of Mackenzie; in Current Research, Part A, Geological Survey of Canada, Paper 80-1A, report 28.
- Wanless, R.K., Stevens, R.D., Lachance, G.R. and Delabio, R.N.
1970: Age determinations and geological studies, K-Ar isotopic ages, report 9; Geological Survey of Canada, Paper 69-2A.

TRIGONIID BIVALVES FROM THE BAJOCIAN (MIDDLE JURASSIC)
ROCKS OF CENTRAL OREGON

Project 760042

T.P. Poulton
Institute of Sedimentary and Petroleum Geology, Calgary.

Poulton, T.P., Trigoniid Bivalves from the Bajocian (middle Jurassic) rocks of central Oregon; in Current Research, Part A, Geological Survey of Canada, Paper 80-1A, p. 187-196, 1980.

Abstract

Twelve species of trigoniid bivalves occur in the Bajocian Weberg Member of the Snowshoe Formation of central Oregon. Two of them are described as new species, *Myophorella lupheri*, and *M. taylori*. The presence of *M. taylori* in northern Vancouver Island, British Columbia suggests the occurrence of Bajocian rocks there.

Introduction

The rich shelly faunas of the Bajocian Weberg Member of the Snowshoe Formation of central Oregon contain twelve species of trigoniid bivalves. Because they are well dated by ammonites in this member, they provide valuable data for interpreting the age of similar or identical species which occur in Jurassic rocks of Canada. Two of the species, *Myophorella freboldi* Poulton and *M. sp. cf. M. argo* (Crickmay) were described previously (Poulton, 1979). The remainder, *Myophorella lupheri* n. sp., *M. argo* (Crickmay), *M. tuxedniensis* Poulton, *M. taylori* n. sp., *M. sp. aff. M. taylori*, *M. sp. aff. M. dawsoni* (Whiteaves), *Trigonia sp. aff. T. costata* Sowerby, *Vaugonia sp. cf. V. kobayashii* Alencaster, *V.(?) sp. aff. V. sharpiana* (Lycett), and *Orthotrigonia(?) sp.*, are described for the first time from Oregon in this report. Two small specimens, questionably identified as *Trigonia sp. aff. T. costata* and *Orthotrigonia(?) sp.*, from undifferentiated beds of the Snowshoe Formation, also are described.

Most of the fossils were collected by the writer in 1972. D.G. Taylor led him to some of the localities, made available many specimens collected by him, and freely provided stratigraphic information on his localities. R.W. Imlay loaned specimens already available in the U.S. Geological Survey collections, most of which were collected by him, by R. Lupher, or by L.W. Vigrass, and provided invaluable advice on the stratigraphy and access to the localities. The stratigraphic and biostratigraphic framework has been described by Lupher (1941), Dickinson and Vigrass (1965), and Imlay (1973). J.A. Jeletzky and D.G. Taylor critically read this manuscript.

Age of Fossils

The Weberg Member contains ammonites that indicate it is late Early and Middle Bajocian in age as shown by Imlay (1973). A more detailed study is currently being conducted by D.G. Taylor, who has generously provided much of the unpublished biostratigraphic data that is reproduced here.

The upper part of the Murchisonae Zone recognized by D.G. Taylor (personal communication) contains *Myophorella tuxedniensis*, *M. lupheri* in abundance, *M. taylori*, *M. freboldi*, *M. sp. aff. M. dawsoni*, *Vaugonia sp. cf. V. kobayashii*, and *Trigonia sp. aff. T. costata*. *M. lupheri* and *T. sp. aff. T. costata* also occur lower in the zone (D.G. Taylor, personal communication). The associated ammonites include *Tmetoceras scissum* (Benecke), *Praestrigites sp. cf. P. deltatus* (Buckman) and *Eudmetoceras* spp. (Imlay, 1973).

The upper part of the Concavum Zone, recognized by Taylor, contains *M. lupheri*, *M. sp. indet.*, *Trigonia sp. aff. T. costata*, and other undeterminable trigoniids. *Myophorella tuxedniensis* and *M. freboldi* occur lower in the zone.

The Laeviuscula Subzone of the Middle Bajocian, recognized by Taylor, contains *M. lupheri*, *M. freboldi*, *M. argo*, *M. sp. indet.* and *Trigonia sp. aff. T. costata*. Taylor also identified *M. lupheri* in the Discites Zone and Ovalis Subzone. The rich variety of Middle Bajocian ammonites has already been demonstrated by Imlay (1973).

In summary, *Myophorella lupheri*, *M. freboldi*, and *Trigonia sp. aff. T. costata* range throughout the Weberg Member; a lower fauna including *M. tuxedniensis*, *M. taylori*, and *Vaugonia sp. cf. V. kobayashii* appears to be restricted to the upper Murchisonae and Concavum Zones as recognized by Taylor; and *M. argo* occurs only in the Laeviuscula Zone.

The two small specimens of *T. sp. aff. T. costata* and *Orthotrigonia(?) sp.* designated as coming from the Snowshoe Formation (undivided; USGS Mesozoic locality 29414) are not associated with diagnostic ammonites, but are questionably dated as Middle Bajocian because of the similarity of one specimen to *T. sp. aff. T. costata* from the Weberg Member, and of the other to *Orthotrigonia(?) sp.* from the Middle Bajocian of central British Columbia, described by Poulton (1979).

Descriptive Paleontology

Trigonia sp. aff. T. costata Sowerby

Plate 30.1, figures 1-10

Description

Shell of medium size, those 2 cm high are longer than high, reaching 2.8 cm long. Larger specimens (e.g. Plate 30.1, fig. 8, 9), which attain 6 cm in length, become higher than long in late growth stages.

Marginal carina of right valve high, either narrow, sharp and very finely tuberculate (Plate 30.1, fig. 5, 6) or rounded and with tubercles that are coarser, but more finely spaced than the costae of flank (Plate 30.1, fig. 4). That of left valve (one specimen only) intermediate in sharpness and strength of tuberculation (Plate 30.1, fig. 1-3).

Area with indistinct concentric costellae intersecting radial costellae that are irregular in their strength and spacing. Area subdivided into more or less equal ventral and dorsal halves by a particularly strong ridge (left valve) or groove (right valve).

Inner carina sharp, finely tuberculate. Escutcheon short, relatively broad, strongly concave. With poorly defined reticulate pattern of intersecting fine radial and concentric costellae.

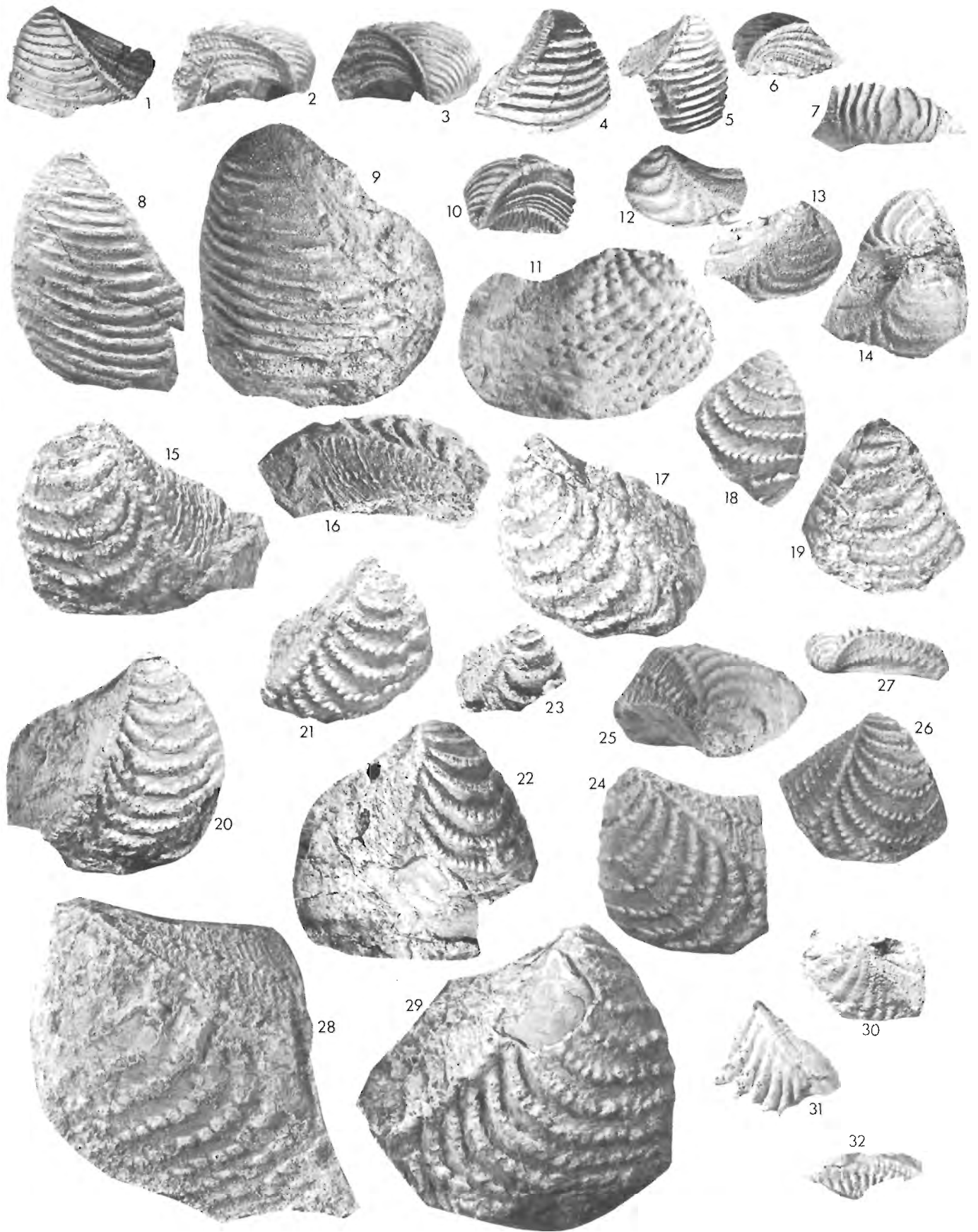


PLATE 30.1

All figures except 10, 31 and 32 from Weberg Member; 10, 31 and 32 from Snowshoe Formation, undifferentiated.

All figures except 10 and 23 natural size, 10 x3; 23 x2.

Figured specimens are stored in the collections of the Geological Survey of Canada, Ottawa (GSC), United States National Museum, Washington (USNM), and University of California Museum of Paleontology, Berkeley (UCMP).

Figures 1-10. *Trigonia* sp. aff. *T. costata* Sowerby.

- 1-3. Lateral posterodorsal and umbonal views respectively of latex cast of hypotype GSC 58932 from GSC locality 89387.
4. Lateral view of hypotype GSC 58933 from GSC locality 89387.
- 5,6. Lateral and posterior views of latex cast of hypotype GSC 58934 from GSC locality 89345.
7. Anterolateral view of latex cast of hypotype GSC 58935 from GSC locality 89387.
8. Lateral view of hypotype GSC 58936 from GSC locality 89389.
9. Lateral view of hypotype USNM 251979 from Stanford University locality 56-121F (Field number).
10. Oblique view of latex cast of hypotype USNM 251980 from USGS Mesozoic locality 29414, x3.

Figure 11. *Myophorella* sp. aff. *M. taylori* n. sp. Lateral view of latex cast of hypotype GSC 58937 from GSC locality 89382.

Figures 12-14. *Vaugonia*(?) sp. aff. *V. sharpiana* (Lycett). Lateral views of hypotypes USNM 251981, 251984, 251985 all from USGS locality 56-235 (field number).

Figures 15-29. *Myophorella lupheri* n. sp.

- 15,16. Lateral and posterior views of holotype GSC 58938 from GSC locality 89345.
17. Lateral view of paratype GSC 58940 from GSC locality 89387.
18. Anterolateral view of paratype GSC 58941 from GSC locality 89345.
19. Lateral view of paratype GSC 58942 from GSC locality 89387.
20. Lateral view of paratype GSC 58943 from GSC locality 89345.
21. Lateral view of paratype GSC 58945 from GSC locality 89345.
22. Lateral view of paratype GSC 58948 from GSC locality 89387.
23. Lateral view of juvenile paratype GSC 58947 from GSC locality 89345, x2.
- 24,25. Lateral and umbonal views of paratype UCMP 16068 from locality D7904.
- 26,27. Lateral and postero-umbonal views of paratype UCMP 16069 from locality D7904.
28. Lateral view of paratype UCMP 16029 from locality D6754.
29. Lateral view of paratype UCMP 16028 from locality D6731.

Figure 30. *Myophorella* sp. aff. *M. dawsoni* (Whiteaves). Lateral view of hypotype USNM 251982 from USGS Mesozoic locality 29822.

Figures 31, 32. *Orthotrigonia*(?) sp. Lateral and posterodorsal views of latex cast of hypotype USNM 251983 from USGS Mesozoic locality 29414.

Flank with strong, regularly spaced concentric costae that extend directly to anterior margin which they meet at right angles. They become coarser spaced with growth, but are finer spaced again near ventral margin of large specimens. Minor irregularity is seen at the locus of flexure in one specimen (Plate 30.1, fig. 7). Costae high and sharp or rounded, and somewhat steeper on their umbonal side, particularly along the anterior end of the shell. Right valve with narrow ante-carinal groove; groove of left valve somewhat broader.

Discussion

This species closely resembles British Middle Bajocian *Trigonia costata* Sowerby, as restricted and interpreted by Lycett (1872-79, p. 147-152, Plate 29) in its general sculpture, large size when adult, irregularity of the radial costellae of the flank, and non-concentric ornament of the escutcheon. The Oregon specimens differ from *T. costata* of Lycett, however, in their outline, being significantly longer than high when young and higher than long when adult, if indeed, the largest Oregon specimens (Plate 30.1, fig. 8, 9) belong to the same species as do the smaller ones. Also, the ornament of the escutcheon is finer and more regular in the Oregon specimens, although these apparent differences may be due to the different styles of preservation and stages of growth represented.

The specimens from Oregon are only questionably distinguishable at equivalent growth stages from *Trigonia* sp. described by Poulton (1976) from western Vancouver Island, because of the small number of specimens available and poor preservation of the latter. The Vancouver Island specimens apparently have more and finer radial costellae on the ventral half of the area, and the marginal carina is broader. The Pliensbachian age suggested for those specimens by Poulton (1976) on the basis of associated trigoniid species has been confirmed by restudy of the ammonites by H. Frenbold (unpublished).

The irregularity of the radial costellae on the area separate the Oregon specimens from most other *Trigonia* species, and particularly from the contemporary, otherwise similar North American species *T. americana* Meek (Imray, 1964) and *T. erbeni* Alencaster (1963). It is because of this irregularity, and the fine reticulate pattern on the escutcheon, that an unusual juvenile specimen (Plate 30.1, fig. 10) from the Snowshoe Formation is tentatively assigned to the same species.

The poor preservation of the specimen illustrated as *T. sp. cf. denticulata* by Sanborn (1960) and the lack of description or illustration of *T. sp. aff. T. costata* identified by Hyatt (1892), both from the Bajocian of California, precludes their meaningful comparison with other species.

T. sculpta Lycett (1872-79, Plate 34, fig. 1-4) from the Middle Bajocian of England is similar but is more coarsely ornamented on the area and different in outline when adult.

Material and Occurrence

Many poorly to moderately well preserved specimens from the Weberg Member, including hypotypes GSC 58932, 58933 and 58935 from GSC locality 89387; GSC 58936 from GSC locality 89389; GSC 58934 from GSC locality 89345; USNM 251979 from uncatalogued USGS Mesozoic locality 56-121F, as well as unfigured specimens from USGS Mesozoic localities 29400 and 29402, and uncatalogued USGS Mesozoic locality 56-65; one juvenile specimen from the Snowshoe Formation, hypotype USNM 251980 from USGS Mesozoic locality 29414.

Ammonites that occur directly associated with poorly preserved specimens assigned to *Trigonia* sp. aff. *T. costata* are *Eudmetoceras* (*Euaptetoceras*) sp. cf. *E. (E.) hauthali*, *E. (E.)* sp. cf. *E. (E.) klimakomphalum* (USGS Mesozoic locality 29400), and *Sonninia* (*Euhoplloceras*) sp. cf. *S. (E.) dominans* (USGS Mesozoic locality 29402) (Imlay, 1973). D.G. Taylor (personal communication) identified this species from the Murchisonae through Laeviuscula Zones.

Vaugonia sp. cf. *V. kobayashii* Alencaster

Plate 30.2, figures 1, 2

Trigonia sp. cf. *T. v-costata* Lycett. Sanborn, 1960, p. 26, Plate 2, fig. 15, 20.

cf. *Vaugonia kobayashii* Alencaster, 1963, p. 27, Plate 2, fig. 19, Plate 3, fig. 1-6.

Vaugonia sp. cf. *V. kobayashii* Alencaster. Poulton, 1979, Plate 10, fig. 29-31.

Discussion

Two specimens probably represent the same species that was described by Poulton (1979) from the Potem Formation of northern California. They exhibit the same variations as those specimens and differ in the same ways from *Vaugonia kobayashii* Alencaster (1963) and other species listed by Poulton (1979).

Material and Occurrence

Two specimens, hypotypes UCMP 16035 and 16036 from upper part of Murchisonae Zone, locality D7902 of D.G. Taylor.

Vaugonia(?) sp. aff. *V. sharpiana* (Lycett)

Plate 30.1, figures 12-13

Discussion

The costae on the flanks of these small shells change orientation abruptly along a locus near the marginal carina. They meet the marginal carina at angles of approximately 60 to 75° near the umbo, decreasing to 45° near the postero-ventral margin, but the main parts of the costae are nearly, although not precisely, concentric with the growth lines. The closest affinities are with *Vaugonia sharpiana* (Lycett, 1872-79) which, however, appears to be less distinctly rostrate at its posterior end and to have the locus of v-flexure of the costae somewhat less well defined.

The V-shape of the costae, and the posterior rostration is more pronounced than in *Trigonia impressa* Sowerby of England and Mexico (Alencaster, 1963). The costae are more coarsely spaced, their posterior parts less closely parallel with each other, and their anterior parts less closely concentric with growth lines, than are those of Lower Jurassic *Vaugonia oregonensis* Poulton and *V. sp. cf. V. vancouverensis* Poulton, from the Suplee Formation of Oregon, and the Sunrise Formation of Nevada, respectively. The present specimens may possibly be juveniles of the same species as larger specimens from probably Bajocian beds of the Potem Formation of northern California described by Poulton (1979) as *V. sp. cf. V. kobayashii* Alencaster, but the type material of *V. kobayashii*, is significantly coarser ribbed (Alencaster, 1963).

Material and Occurrence

Three poorly preserved specimens, hypotypes USNM 251981, 251984 and 251985 from uncatalogued USGS locality 56-235. Ammonites with *V. (?) sp. aff. V. sharpiana* (Lycett) are *Witchellia* (*Latiwitchellia*) *evoluta* (USGS loc. 56-235, 56-241), *Fontansesia costula*, and *Sonninia* (*Euhoplloceras*) *modesta* (both USGS localities 56-241) (Imlay, 1973).

Myophorella freboldi Poulton

Plate 30.2, figures 7, 8

Discussion

Besides the holotype (Poulton, 1979, Plate 2, fig. 11), the row of nodes along the anterior end of the shell is well preserved in only one other of the Oregon specimens (Plate 30.2, fig. 8). In another (hypotype UCMP 16066), the anterior ornament near the umbos comprises fine ribs that are much closer spaced than those of the main part of the flank. The anterior row of costal segments and the larger angle at which they meet the marginal carina separate *M. freboldi* from *M. lupheri*.

Material and Occurrence

No ammonites occur in the same collection as the holotype of *M. freboldi* (uncat. USGS loc. 56-153F), although it is probably from one of the Discites through Laeviuscula Zones. Other specimens collected by D.G. Taylor and assigned by him to the Concavum, Laeviuscula, and upper part of the Murchisonae Zones, include hypotypes UCMP 16066 (loc. D7903), and 16067 (loc. D7689).

PLATE 30.2

All figures except 13 from Weberg Member; 13 from northern Vancouver Island, British Columbia.

All figures natural size.

Abbreviations as in explanation of Plate 30.1.

Figures 1,2. *Vaugonia* sp. cf. *V. kobayashii* Alencaster.

1. Lateral view of hypotype UCMP 16036 from locality D7902.
2. Lateral view of hypotype UCMP 16035 from locality D7902.

Figures 3-6. *Myophorella argo* (Crickmay).

- 3,4. Lateral and umbonal views of hypotype UCMP 16033 from locality D7901.
5. Lateral view of hypotype UCMP 16032 from locality D7900.
6. Lateral view of hypotype UCMP 16034 from locality D7901.

Figures 7, 8. *Myophorella freboldi* Poulton.

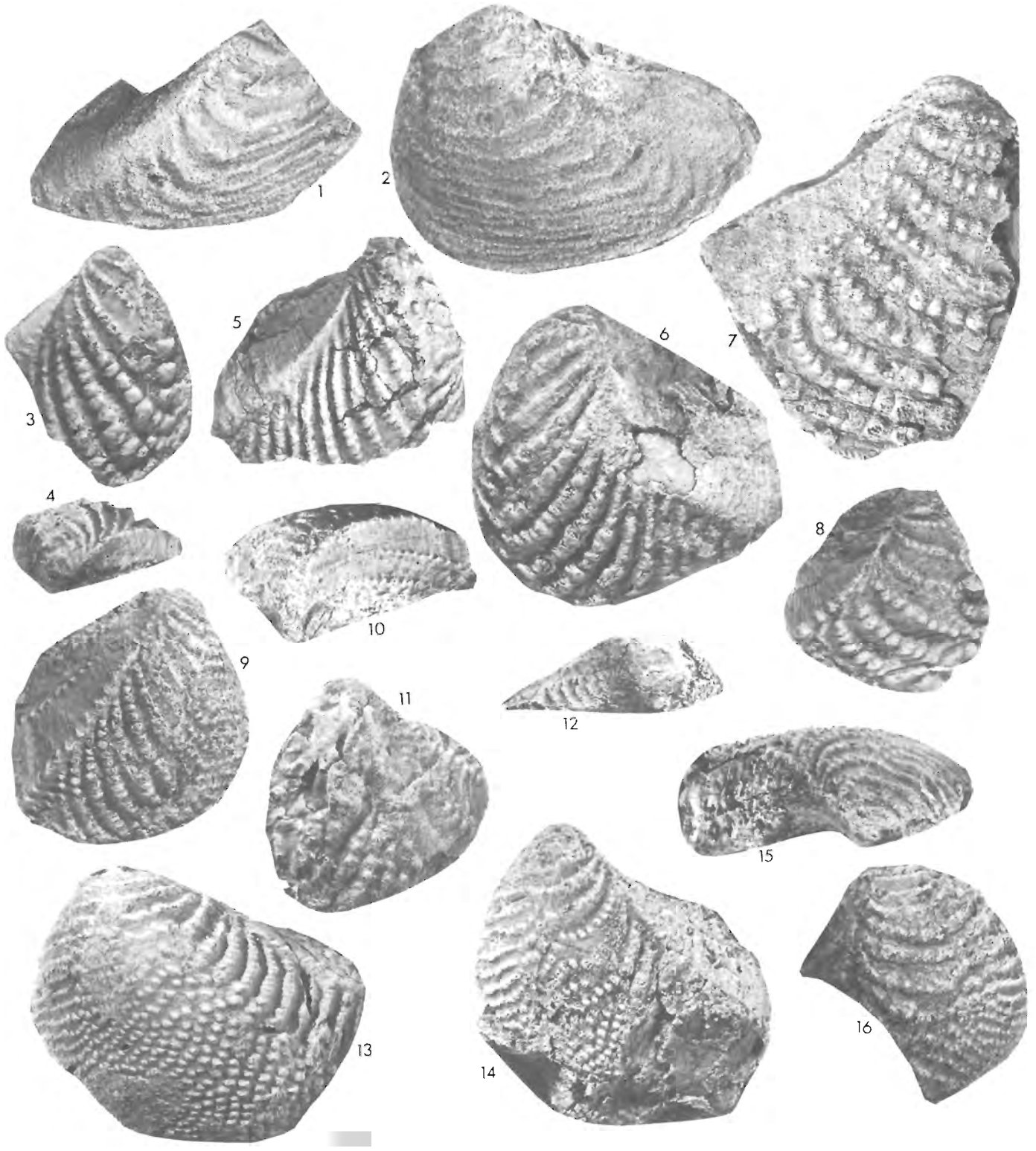
7. Lateral view of hypotype UCMP 16066 from locality D7903.
8. Lateral view of hypotype UCMP 16067 from locality D7689.

Figures 9-12. *Myophorella tuxedniensis* Poulton.

- 9,10. Lateral and postero-umbonal views of hypotype UCMP 16030 from locality D7689.
- 11,12. Lateral and umbonal views of hypotype 16031 from locality D7689.

Figures 13-16. *Myophorella taylori* n. sp.

13. Lateral view of paratype GSC 62965 from GSC locality C-80878.
- 14,15. Lateral and umbonal views of holotype UCMP 16025 from locality D7689.
16. Lateral view of paratype UCMP 16026 from locality D7689.



Myophorella argo (Crickmay)

Plate 30.2, figures 3-6

Scaphogonia argo Crickmay, 1930, p. 52, Plate 5, fig. a, b.

Myophorella argo Crickmay, Poulton, 1979, Plate 4, fig. 9-17.

Discussion

This species, previously described from Middle Bajocian units from Alaska, British Columbia, and California (Crickmay, 1930; Poulton, 1979), is represented in Oregon by 4 well preserved specimens and several that are poorly preserved. The smooth space separating anterior costal segments from those of the main part of the flank is narrower than in the holotype or is nearly absent. After the shell is about 2.5 cm high, the anterior and the main costal segments of the flank begin to meet each other, either in an irregular, V-pattern (Plate 30.2, fig. 5) or a sharp curve (Plate 30.2, fig. 6). In some of the Oregon specimens (Plate 30.2, fig. 5), the anterior ends of the main segments of the costae continue tapering anteroventrally into the narrow smooth space that lies posterior to the anterior costal segments, and a slight sinuosity is thus imparted to the costae. Both of these last characters are also seen in some of the Alaskan representatives of the species (eg. Poulton, 1979, Plate 4, fig. 14). The last character, furthermore, allies *M. argo* with *Scaphotrigonia navis* (Lamarck) of the Lower Bajocian of Europe (eg. Lebküchner, 1932) and with *Myophorella tipperi* Poulton (1979) from the Middle Bajocian of Alaska and British Columbia. None of the specimens reaches the size of adult *M. tipperi* but on the largest ones the posteriormost costae approach those of that species, becoming closer spaced and more nearly dorso-ventrally oriented than is typical of *M. argo*. *S. navis* is more coarsely ribbed, the posteriormost costae meet the marginal carina at a smaller angle, and the separation of the anterior costal segments from the remainder is more extreme than in *M. argo*.

The specific affinities of poorly preserved *M. sp. cf. M. argo* (Poulton, 1979, Plate 4, fig. 22) from the Weberg Member remain unresolved.

Material and Occurrence

Several moderately well preserved specimens, including hypotypes UCMP 16032 (loc. D7900), UCMP 16033 (loc. D7901), and UCMP 16034 (loc. D7901) from the Laeviuscula Zone (D.G. Taylor, personal communication). *Myophorella sp. cf. M. argo* of Poulton (1979, Plate 4, fig. 22) occurs directly associated with *Sonninia* (*Euhoplceras*) *modesta* and *S. (Papilliceras) sp. cf. S. (P.) espinazitensis* (uncatalogued USGS loc. 56-120), which represent the Discites through Laeviuscula Zones (Imlay, 1973).

Myophorella lupheri n. sp.

Plate 30.1, figures 15-29

Trigonia cf. T. spinulosa Young and Bird. Sanborn, 1960, p. 25, Plate 2, fig. 23.

?*Trigonia undulata* Fromherz. Sanborn, 1960, p. 26, Plate 2, fig. 28.

?*Myophorella dawsoni* Whiteaves. Poulton, 1979, Plate 1, fig. 12.

?*Myophorella sp. aff. M. frebaldi* Poulton, 1979, Plate 8, fig. 3.

Description

Shells of medium size, at least as long as 8 cm; outline rounded subtrigonal to semicircular. Umbos near anterior end, weakly to moderately opisthogyrous. Shell gently convex but anterior end and umbonal part of area descend perpendicularly to plane of commissure.

Marginal carina at same level or raised above costae of flank, with small, sharp, transversely elongate tubercles, evenly spaced at intervals increasing to 2.5 mm at postero-ventral corner. Area comprises 1/4 to 1/3 (approx.) area of shell, ornamented with fine wavy costellae. The strongest of these costae join the tubercles of the marginal carina and the ventral row of a double, irregular, median row of tubercles. These two parts of the median row of tubercles are separated from each other by a median furrow in some specimens. Finer costellae or growth lines occur between the coarser ones. Umbonal parts of shell with very finely and evenly spaced tubercles on marginal carina, sharp and regularly spaced, straight transverse costellae on area, and sharp median groove which may be close to dorsal side of area. Escutcheon carina a sharply raised ridge of strong, finely spaced tubercles which may be stronger than those of marginal carina. Escutcheon depressed, about 5/6 length of shell, smooth, or with fine growth lines.

A very narrow ante-carinal depression separates costae of flank from marginal carina. Costae of flank meet marginal carina at intervals of about 1.5 mm near umbo, increasing to about 3 mm near posteroventral margin, and meet marginal carina at angles of nearly 70° near umbos in most specimens, decreasing to about 30° near posteroventral margin.

Costae of flank are attenuated at their posterior ends. Those nearest umbos are fine, sharp, raised, concentric ridges, later ones are rows of small and finely spaced, sharp, elongated tubercles. Over central part of flank, costae form smooth, subconcentric curves in most specimens; in others, they radiate from marginal carina and curve sharply along a locus near the marginal carina. They are narrow relative to the inter-spaces, which are covered with fine growth lines. At their anterior ends the costae become thin, and descend perpendicularly to plane of commissure, and the tubercles disappear. In most specimens an indistinct node occurs near anterior end of each costa, and these nodes are aligned to form a locus running down the anterior end of the shell where its degree of convexity increases abruptly. In anteroventral region of large shells, anteroventral portions of costae swing more strongly anteriorward becoming irregular, broken, or nearly concentric with growth lines. Tubercles on costae near umbos, and on adult shell near marginal carina, aligned subradially, but a well defined radial striation is not apparent.

Discussion

The holotype (Plate 30.1, fig. 15, 16) and some paratypes (Plate 30.1, fig. 17; 21, 22, 24) are typical forms of this species, which serve best to distinguish it from closely related species. Most localities or stratigraphic units in western Canada and United States yield more or less homogeneous assemblages of species of *Myophorella*; there are, however, a small number of specimens in some collections of *M. lupheri*, and in other *M.* species, that are transitional with other species, but which do not invalidate the concepts of the species within the group.

Myophorella lupheri n. sp. is differentiated from most other North American Middle Jurassic *Myophorella* species, and particularly from its close relative, *M. dawsoni* Whiteaves, by the orientation of the ribs of the flank, and their somewhat finer, beadlike, ornamentation. In *M. lupheri*,

the costae are continuously curved anteriorward so that they intersect the growth lines at low angles, or are nearly concentric with them, in ventral parts of the adult shell. Those of *M. dawsoni*, in the same part of the shell, intersect the growth lines nearly at right angles, and in the anterior part of the shell, are commonly separated from the anterior-most portions of the costae, which extend as a discrete row of short costal segments to the anterior margin. One specimen, figured by Poulton (1979, Plate 1, fig. 12), from G.M. Dawson's original collection upon which *Trigonia dawsoni* Whiteaves was based, differs from the others of that collection in the orientation of its ribs and may possibly represent *M. lupheri*, although infraspecific variation of this nature occurs to a minor degree in this group of species.

Myophorella freboldi Poulton generally has more widely spaced and more coarsely tuberculate costae which meet the marginal carina without a marked curve toward the umbo, and which are separated from a row of tubercles along the anterior margin of the shell. *M. sp. aff. M. freboldi* (Poulton, 1979, Plate 8, fig. 3) may be a distorted specimen of *M. lupheri*.

Myophorella lupheri is similar to British Bajocian *M. (?) spinulosa* (Young and Bird) as already pointed out by Sanborn (1960), particularly to the specimen figured by Lycett (1872-79, Plate III, fig. 6). However, the tendency in that species for the costae to become concentric with the growth lines at early or intermediate growth stages (Lycett, op. cit., p. 44, Plate III, fig. 4, 5), is a significant difference from *M. lupheri*, in which species this occurs uncommonly. *M. lupheri* differs in the same way from *Vaugonia kobayashii* Alencaster (1963), and *V. sp. cf. V. kobayashii* which also are more coarsely and strongly ribbed, although one poorly preserved specimen figured by Poulton (1979, Plate 10, fig. 31) is closely similar and may well represent *M. lupheri*.

The poorly preserved, probably juvenile specimen called *Trigonia undulata* Fromherz by Sanborn (1960), lacks the V-shaped costae of that species, is probably not specifically identifiable, but may possibly represent *M. lupheri*.

In its small to intermediate size, the fineness and orientation of costation, and fine tuberculation, *M. lupheri* differs from most other *Myophorella* species. *Myophorella striata* Miller (Lycett, 1872-79, Plate V, fig. 3 or 6', 7, 8), *M. formosa* (Lycett, op. cit.), both from the Bajocian of England, and specimens from the Bajocian of Mexico identified as *M. formosa* by Alencaster (1963) are commonly somewhat larger, and have costae which radiate more strongly from the marginal carina. The British specimens have a broader, and more finely and evenly costellate area than either the Mexican form or *M. lupheri*.

The costae of South American Lower Jurassic *Myophorella catenifera* (Hupe) (Perez and Reyes, 1977, Plate III, fig. 6) radiate more strongly away from the marginal carina. Japanese species of Kobayashi and Tamura (1955) which are similar to *M. lupheri* are differentiated as follows. *M. sigmoidalis* has the characteristic sigmoidal twist of the costae on the anterior end of the flank. *M. subcircularis* has more strongly marked radial striae across the costae of the flank, is finer ribbed and more finely tuberculate. *M. sugayensis* is finer ribbed, more finely tuberculate, and has costae which meet the marginal carina at a smaller angle at equivalent growth stages. *M. sugayensis* var. *geniculata* has costae which are distinctly flexed toward the anterior margin of the shell. These costae, as in the other Japanese species, are therefore not smoothly concentric as they are in the typical forms of the Oregon species. *M. orientalis*, which also occurs in the Callovian of Alaska (Poulton, 1979), has ribs which converge more strongly toward the marginal carina, and thus present a more strongly radiating appearance.

Material and Occurrence

Abundant poorly to moderately well preserved specimens, including holotype GSC 58938 and paratypes 58941, 58943, 58945, and 58947 from GSC locality 89345; paratypes 58940, 58942, and 58948 from GSC locality 89387, and paratypes UCMP 16029 (loc. D6754), UCMP 16028 (loc. D6731), UCMP 16068, and 16069 (loc. D7904). Other unfigured specimens include those from GSC localities 89389, 89349, and 89379, from USGS Mesozoic localities 27581, 29405, and from uncatalogued USGS localities 56-3a, 56-120, 56-159, 8-20-11 (field numbers). Ammonites that occur in the same collections with *M. lupheri* include *Docidoceras sparsicostatum* (USGS Mesozoic locality 27581), *Sonninia (Euhoplloceras) modesta*, and *S. (Papilliceras) sp. cf. S. (P.) espinazitensis* (both USGS Mesozoic loc. 56-120) (Imlay, 1973). *M. lupheri* has been recognized in the upper Murchisonae through Laeviuscula Zones, most abundantly in the former.

Myophorella tuxedniensis Poulton

Plate 30.2, figures 9-12

Discussion

This species is represented by 3 specimens. Two preserve the tuberculate escutcheon that, together with the more dorsoventral orientation of the costae, broader area, and absence of a distinctively ornamented ventral region of the flank, distinguish the species from associated *M. taylori*. The Oregon specimens exhibit gradual rotation of the costae with increasing size of shell, to a nearly dorsoventral orientation, suggesting that this feature is not seen in the Alaska or British Columbia specimens (Poulton, 1979, Plate 7) only because of nonpreservation.

Material and Occurrence

Five specimens, including hypotypes UCMP 16030 and UCMP 16031 (loc. D7689) from the upper Murchisonae and middle Concavum Zones.

Myophorella taylori n. sp.

Plate 30.2, figures 13-16

Description

Shell of medium size, reaching 5 cm long; outline rounded, subtriangular. Shell gently convex but umbonal parts of shell descend perpendicularly to plane of commissure.

Marginal carina at same level or raised above costae of flank with small, sharp or rounded tubercles, evenly spaced, at intervals increasing to 3 mm in adult shell. Area narrow, apparently with very fine growth lines, a median row of small nodes, and a poorly developed groove or narrow depression dorsal to that. Escutcheon carina a row of nodes. Escutcheon depressed, apparently smooth.

A very narrow ante-carinal depression separates costae of flank from marginal carina.

Costae of posterior part of flank in umbonal 3 cm smoothly curved, concave umbonally, becoming attenuated toward marginal carina. In the 1.5 to 2 cm nearest umbo, these costae appear to extend to anterior margin which they meet at right angles, although there may be some offset of costae along anterior edge of shell. In later growth stages they become clearly separated from a more closely spaced anterior set of finely tuberculate costal segments which are approximately anteroventrally-posterodorsally oriented.

Posterior from the anteroventral corner of the shell another set of nearly dorsoventrally oriented, closely spaced, finely tuberculate costal segments appears between the two previously described sets and this becomes the predominant ornament along the ventral margin on its posterior half. Thus the flank is divided into three regions each of approximately equal area, and each with distinct ornamentation, separated from one another along radial loci: posterior region; anterior region; and central region together with ventral subregion, in the terminology of Poulton (1979).

Discussion

Although only two specimens from Oregon are referred to *M. taylori*, its formal naming as a species is justified, beyond its distinctive ornamentation, by its occurrence also in British Columbia. In particular, its presence serves to date as probably Bajocian, the beds in which it occurs at the Island Copper mine, northern Vancouver Island, British Columbia (Plate 30.2, fig. 13). This is the first suggestion that rocks of this age occur on Vancouver Island.

The intersection of anterior and posterior sets of costae resulting in V-shaped costae even in the earliest growth stages, clearly separates Yukon specimens of *Vaugonia(?) yukonensis* Poulton (1979) from *M. taylori*.

Myophorella sp. A described by Poulton (1979, Plate 8, fig. 2) from probably Lower Callovian rocks of British Columbia is closely similar but the costae meeting the marginal carina in the umbonal 3 to 4 cm are more widely spaced.

Two Bajocian species of Europe are similar to *M. taylori* but both have a broader, smooth anterior slope on the marginal carina toward which the costae taper more strongly and a less well differentiated anterior set of costal segments, which also are coarser. In neither is the marginal carina tuberculate. One is *Trigonia guisei* Lycett, assuming the specimen which was influential in the erection of the species (Lycett, 1881-1883, Plate III, fig. 3, 3a) and others from the same area (*ibid.*, fig. 5, 6) to properly represent the species. They are different from some that were also included by Lycett (*ibid.*, fig. 1, 2, 4). The other is *T. lycettensis* Strand (1928) named for those specimens illustrated by Lycett (1872-1879) in his Plate 14, figures 5 and 6. Only the specimen in his Figure 5 resembles *M. taylori*.

Trigonia leckenbyi Lycett (1872-1879, Plate 16, fig. 1) of the Toarcian of England also is similar but is larger, and more coarsely sculptured at an equivalent size. *Trigonia incurva* Benett of the Upper Oxfordian through Upper Portlandian, but particularly the specimen figured by Lycett (1872-1879, p. 43 and Plate IX, fig. 5) and that figured earlier as *T. heberti* by Munier-Chalmas (1865, Plate IV, fig. 5) are also similar. However, the marginal carina in that species is more rounded and the costae are more dorsoventrally oriented, especially their anterior and ventral portions, which results in a sinuous curvature. Also, the posterior end of the shell appears to be more rostrate and there is a greater dorsally-concave curvature of the dorsal margin. These two specimens are sufficiently unlike the remainder of those figured by Lycett (1872-1879, Plate IX) as *T. incurva*, in the ornament of the anteroventral part of the shell, to question their being assigned to the same species.

Material and Occurrence

Two specimens from Oregon, holotype UCMP 16025 and paratype UCMP 16026 (loc. D7689) from the upper part of the Murchisonae Zone, and paratype GSC 62965 (GSC loc. C-80878) from Vancouver Island, British Columbia.

Myophorella sp. aff. *M. taylori* n. sp.

Plate 30.1, figure 11

Vaugonia(?) yukonensis Poulton, 1979, Plate 8, figs. 10, 11; not Plate 8, figs. 6-9.

Discussion

The record of the possible occurrence of *Vaugonia(?) yukonensis* Poulton in the Weberg Member is amended, and the partial specimen (Plate 30.1, fig. 11) on which this suggestion was made by Poulton (1979) is now thought to represent a new, still insufficiently well understood species of *Myophorella*. The same is true of the two apparently identical specimens from the Potem Formation of northern California (Poulton, 1979, Plate 8, fig. 10, 11). These last two specimens differ from *V. (?) yukonensis* in the smoothly curved, rather than V-shaped costae in the umbonal portions of the flank and the less well developed differentiation of anterior and posterior costal segments. The Weberg specimen, whose umbonal parts are not preserved, most closely resembles the California specimen in its posterior and ventral parts.

The new unnamed species differs from *M. taylori* in the less clearly developed differentiation of the flank into regions with different styles of ornamentation and the coarser costation of the ventral and anterior portions of the flank.

Material and Occurrence

A partial right valve, hypotype GSC 58937 from GSC locality 89382.

Myophorella sp. aff. *M. dawsoni* (Whiteaves)

Plate 30.1, figure 30

Discussion

The orientation of the ribs and the broad, finely and apparently regularly costellate area of this small shell together distinguish it from the other species described in this report, and most of those described previously, from the Jurassic of North America. The closest similarities are with *Myophorella dawsoni* (Whiteaves; Poulton, 1979), and *M. argo* (Crickmay) although those species are characteristically Middle, rather than Lower, Bajocian in age.

Material and Occurrence

One poorly preserved left valve, hypotype 251982 from USGS Mesozoic locality 29822. Associated ammonites indicating the Murchisonae Zone are *Tmetoceras scissum* (Benecke), *Praestrigites* sp. cf. *P. deltatus* (Buckman) and *Eudmetoceras* spp. (Imlay, 1973).

Orthotrigonia(?) sp.

Plate 30.1, figures 31, 32

Discussion

This fragment, whose generic affinities are not at all certain is similar to *Orthotrigonia(?)* sp. described from Bajocian rocks of British Columbia and California by Poulton (1979) in the strength and fine concentric corrugation of the costae of the flank and the angle at which they meet the marginal carina. The area appears to be somewhat narrower, and is more coarsely and irregularly costellate than in those previously described specimens. The escutcheon, whose ornamentation is unknown in those specimens, is ornamented in the Oregon specimen with fine but prominent transverse costellae.

Material and Occurrence

One part of a left valve, hypotype USNM 251983 from USGS Mesozoic locality 29414, Snowshoe Formation.

References

- Alencaster, G.
1963: Pelecipodos del Jurásico medio del noreste de Oaxaca y noreste de Guerrero; Universidad Nacional Autónoma de México, Instituto de Geología; Paleontología Mexicana, Número 15.
- Crickmay, C.H.
1930: The Jurassic rocks of Ashcroft, British Columbia; University of California Geological Publications, v. 19.
- Dickinson, W.R., and Vigrass, L.W.
1965: Geology of the Suplee-Izee area Crook, Grant, and Harney Counties, Oregon; State of Oregon, Department of Geology and Mineral Industries, Bulletin 58.
- Hyatt, A.
1892: Jura and Trias at Taylorsville, California; Geological Society of America, Bulletin, v. 3, p. 395-412.
- Imlay, R.W.
1964: Marine Jurassic pelecypods from central and southern Utah; Contributions to Paleontology, United States Geological Survey, Professional Paper 483-C, p. C1-C42 and 4 Plates.
1973: Middle Jurassic (Bajocian) ammonites from eastern Oregon; United States Geological Survey, Professional Paper 756.
- Kobayashi, T., and Tamura, M.
1955: The Myophorellinae from north Japan. Studies on the Jurassic Trigonians in Japan, Part IV; Japanese Journal of Geology, Geography, v. 26, n. 1-2, p. 89-103, Plates 6, 7.
- Lebküchner, R.
1932: Die Trigonien des Süddeutschen Jura; Palaeontographica, v. 77, p. 1-119.
- Lupher, R.L.
1941: Jurassic stratigraphy of central Oregon; Geological Society of America, Bulletin, v. 52, p. 219-270.
- Lycett, J.
1872- A monograph of the British fossil trigoniae;
1879: Palaeontographical Society, London.
1881- Supplement to a monograph of the British fossil
1883: trigoniae; Palaeontographical Society, London.
- Munier-Chalmas, M.
1865: Quelques espèces nouvelles du genre *Trigonia*; Société Linnéenne de Normandie, Bulletin, v. 9, p. 415-421, Plate IV.
- Perez, d'A.E., and Reyes, B.R.
1977: Las trigonias jurásicas de Chile y su valor cronoe-stratigráfico; Instituto de Investigaciones Geológicas - Chile, Boletín 30.
- Poulton, T.P.
1976: Some Lower Jurassic trigoniid bivalves from southwestern British Columbia; Geological Survey of Canada, Bulletin 256, p. 41-53.
1979: Jurassic trigoniid bivalves from Canada and western United States; Geological Survey of Canada, Bulletin 282.
- Sanborn, A.F.
1960: Geology and paleontology of the southwest quarter of the Big Bend Quadrangle, Shasta County, California; California Division of Mines, Special Report 63.
- Strand, E.
1928: Miscellanea nomenclatorica zoologica et palaeontologica, I, II; Archiv für Naturgeschichte Jahrgang xcii, Abt. A, Heft 8, p. 30-75.

APPENDIX: LIST OF FOSSIL LOCALITIES

Geological Survey of Canada Localities

89345. T.P. Poulton, 1972. Long sandstone outcrop 1.05 km northeast of Mowich Spring, near southwest end of outcrop; north boundary of section 2, 0.24 km east of west boundary, T19S, R26E. Delintment Lake map-sheet, Oregon.
89349. T.P. Poulton, 1972. Limestone rubble at top of east-facing slope; 0.48 km east of west boundary of section 29, 0.48 km south of north boundary, T18S, R26E. Delintment Lake map-sheet, Oregon.
89379. T.P. Poulton, 1972. Road outcrop 0.56 km north-northwest of Boundary Spring. Lowest 3.6 m of sandstone at south end of outcrop. 0.8 km west of east boundary of section 29, 0.16 km north of south boundary, T18S, R26E. Oregon.
89382. Locality described by Poulton (1979). Oregon.
89387. T.P. Poulton, 1972. Road cut 0.4 km north of Mowich Spring. 9 m of sandstone at base of exposure at north end of outcrop. 0.24 km west of east boundary of section 3, 0.48 km south of north boundary, T19S, R26E. Oregon.

89389. T.P. Poulton, 1972. Small sandstone outcrop on a bend on blocked-off fire access road about 0.32 km northwest of Mowich Spring, 0.38 km west of east boundary of section 3, 0.64 km south of north boundary, T19S, R26E. Oregon.
- C-80878. J. Lamb, 1979. Mine pit, Island Copper mine, Quatsino Inlet, northern Vancouver Island, British Columbia.

United States Geological Survey Mesozoic Localities

27581. Locality 67 of Imlay (1973, p. 48).
29400. Locality 88 of Imlay (1973, p. 49).
29402. Locality 22 of Imlay (1973, p. 44).
29405. R.W. Imlay and W.O. Ross, 1966. East side of Dobson Creek, SE1/4SE1/4 section 28, T18S, R26E, Grant County.
29414. W.O. Ross and R.W. Imlay, 1966. Bulldozer cut east of junction of Gold Creek with Myrtle Creek, slightly north of Centre of section 36, T18S, R30E, west Myrtle Butte quadrangle, Grant County.
29822. Locality 13 of Imlay (1973, p. 44).
29824. Locality 43 of Imlay (1973, p. 45).

Uncatalogued Localities, USGS

- 8-20-11. On west slope of Little Mowich Mountain; the butte lying northeast of the top of the pass on the road from Freeman Creek to Howard Valley.
- 56-3a. (= V3a). L.W. Vigrass, 1956. On ridge 180 m south of north end of ridge which lies east of creek entering Beaver Creek from the south at J. Robertson ranch house; near centre of SE1/4SE1/4SE1/4 section 28, T18S, R26E, Grant County.
- 56-65. L.W. Vigrass, 1956. On narrow elongate spur extending westward into the meadows along Freeman Creek southwest of the Jim Harris ranch house.
- 56-120. Locality 20 of Imlay (1973, p. 44); redescribed by Poulton (1979).
- 56-121F. Same as locality 20 of Imlay (1973, p. 44).
- 56-153F. Locality described by Poulton (1979).
- 56-159. L.W. Vigrass, 1956. Southwest facing slope 75-m northeast of old Harris ranch house; SE1/4SW1/4, section 26, T17S, R26E.
- 56-235. Locality 28 of Imlay (1973, p. 44).
- 56-236. L.W. Vigrass, 1956. Summit of pyramidal hill immediately south of South Ammonite Hill; SE1/4SW1/4, section 29, T18S, R26E.
- 56-241. Locality 28 of Imlay (1973, p. 44).

Localities of D.G. Taylor

- D6731. Robertson Draw section; approx. Lat. 43°59'N, Long. 119°38'W; S1/2NW1/4NW1/4 sec. 29, T18S, R26E; Delintment Lake quadrangle; Grant County.
- D6754. Irrigation ditch along east side of road about 30 m north of old corral; NW1/4NE1/4 sec. 17, T18S, R26E; Dayville Quadrangle.
- D7689. Old Harris Place; near locality D7903; Lat. 44°03'58"N, Long. 119°33'55"W.
- D7897. Collected loose near Mowich Spring; Lat. 43°57'18"N, Long. 119°34'46"W; Harney County.
- D7900. Swamp Creek section; 2700 m (approx.) south-southeast, bearing 193.5° from summit of Funny Butte; approx. Lat. 44°02'50"N, Long. 119°35'45"W; E. centre of SE1/4 sec. 33, T17S, R26E; Dayville Quadrangle, Grant County.
- D7901. Same as locality D7900.
- D7902. 1430 m northwest of 'Lupher Draw' section; Lat. 43°59'49"N, 119°39'24"W; W1/2SW1/4NW1/4 sec. 19, T18S, R26E and E1/2SE1/4NE1/4 sec. 24, T18S, R25E; Delintment Lake quadrangle, Grant and Crook Counties.
- D7903. Harris Place section; 3000 m (approx.) east-south-east, bearing 257°20' from summit of Funny Butte; Lat. 44°03'54-57"N, Long. 119°33'55"W; centre of sec. 26, T17S, R26E; Dayville Quadrangle.
- D7904. Old Harris Place; near locality D7903; Lat. 44°03'58"N, Long. 119°33'55"W.

**A PRELIMINARY PALYNOLOGICAL STUDY OF THE CARIBOU HILLS OUTCROP
SECTION ALONG THE MACKENZIE RIVER, DISTRICT OF MACKENZIE**

Project 780030

N.S. Ioannides and D.J. McIntyre¹
Institute of Sedimentary and Petroleum Geology, Calgary

Ioannides, N.S. and McIntyre D.J., A preliminary palynological study of the Caribou Hills outcrop section along the Mackenzie River, District of Mackenzie; in Current Research, Part A, Geological Survey of Canada, Paper 80-1A, p. 197-208, 1980.

Abstract

Fifty-eight samples from the Upper Cretaceous and Lower Tertiary sediments of the Caribou Hills section in the Mackenzie Delta yielded diversified and well preserved microfloras. Four palynological associations have been recognized. By comparison with known assemblages, mainly from Western Canada, Campanian, Paleocene, Eocene and Oligocene ages are indicated. The microfloral transition between Paleocene and Eocene appears to be gradational whereas the break between Eocene and Oligocene is distinct.

Introduction

Since drilling began in the Mackenzie Delta in the mid-1960s the Caribou Hills outcrop section has attracted the attention of paleontologists from both government and industry. This is because of proximity to the Mackenzie Delta-Beaufort Sea Basin.

Only fragmentary published information exists on the stratigraphy and biostratigraphy of the Caribou Hills, with the works of Mountjoy (1967) and Doerenkamp et al. (1976) being the most important. Ages remain controversial, particularly for the upper pebbly sands and conglomerates, but it appears likely that all epochs of the Lower Tertiary are at least partly represented. Similarities do exist between the microflora of this sequence and those of the subsurface; thus, the section is important for subsequent biostratigraphic comparisons in the region.

The Caribou Hills section was originally designated by Mountjoy (1967, p. 10) as the type section of the Reindeer Formation. He stated that "The upper limit of the formation is considered to be the top of the quartzite and chert conglomerate exposed at the north end of the hills. The lower limit was not observed but it is inferred to be the base of the nonmarine beds which presumably overlie Cretaceous shales or older beds near the south end of the Caribou Hills".

Young (1975, Table 5) referred to the Reindeer Formation in the Mackenzie Delta as a sandstone, conglomerate, siltstone and coal sequence including sediments of Paleocene and Eocene ages and extended his definitions into the subsurface. In a later publication Young et al. (1976, p. 35) excluded from the Reindeer Formation the upper conglomeratic unit and stated "The Reindeer Formation is overlain abruptly and probably unconformably, by lithic gravel and sand of probable Neogene age". They assigned this part questionably to the Beaufort Formation.

In addition to the present investigation, parallel stratigraphic studies are concurrently being carried out by Young and McNeil (in preparation) on the subsurface of the Mackenzie Delta and by Price et al. (in preparation) on the Caribou Hills composite section. These studies constitute a continuation of a Geological Survey of Canada project in the Mackenzie Delta region which commenced in 1969. In the summer of 1978 Price et al. (in preparation) measured and described the outcrops along the Mackenzie River. More than 1250 m of sediments were estimated with the strata dipping northwards at about two degrees. However, a dip of about 4 degrees, calculated at the Cretaceous/Tertiary unconformity between wells adjacent to the outcrop, indicates that the actual total thickness of the Caribou Hills section may be more than 2500 m. The latter thickness is

herein adopted as it is more compatible with known subsurface thicknesses. In summary, the section consists of conglomeratic sands at the base, successively followed by coaly and fine grained shaly units. Cyclical conglomerates overlain by coalinitic clays and loose pebbly sands and conglomerates make up the northern part of the section. The sequence overlies Campanian strata and is overlain by probable Pleistocene surficial deposits.

Previous Palynology

Palynological studies on the Cenozoic of the Mackenzie Delta region consist mainly of subsurface investigations by various oil companies and consulting firms. Most of this information is not available in published form but Staplin (1976) discussed an investigation from four exploration wells. Additional information is found on Geological Survey of Canada Open File. Limited comparative data are available from studies of outcrop material from both sides of the Mackenzie Delta, particularly the east, but few detailed determinations have been published. On the basis of palynological evidence Rouse (in Mountjoy, 1967) considered sections 3 and 4 (respectively 32 and 15 of Price et al., in preparation) of the Reindeer Formation in the Caribou Hills to be of possible Paleocene age. Hills and Wallace (1969) agreed with the Paleocene age suggested by Rouse. Young (1975) discussed the age of the Reindeer Formation and noted that Brideaux considered the type in the Caribou Hills to be younger than the type Aklak in the Yukon Coastal Plain. Doerenkamp et al. (1976) briefly discussed microfloras from the Caribou Hills section, indicated ranges of selected taxa, and compared the assemblages with those from Banks Island. They noted four assemblages, three being of undifferentiated Paleocene-Lower Eocene age and the other Miocene to Recent. They recorded the genera *Wetzeliiella* and *Apectodinium* from approximately the same levels as in the present study and interpreted their presence as indicative of littoral conditions. Rouse and Srivastava (1972) have described Paleocene pollen and spore assemblages from the Bonnet Plume Basin to the west. Sweet (personal communication) is currently studying the Paleocene microfloras from the Bonnet Plume Basin and Aklak Creek.

Present Work

The present study expands on the work of Doerenkamp et al. (1976) but is still of a preliminary nature and much detail remains to be added.

At present, fifty-eight samples are treated, and their distribution as shown in Figure 31.1 demonstrates distinct microfloral changes within the sequence (see Plates 31.1 to 31.5).

¹Petro-Canada, P.O. Box 2844, Calgary, Alberta, T2P 2M7

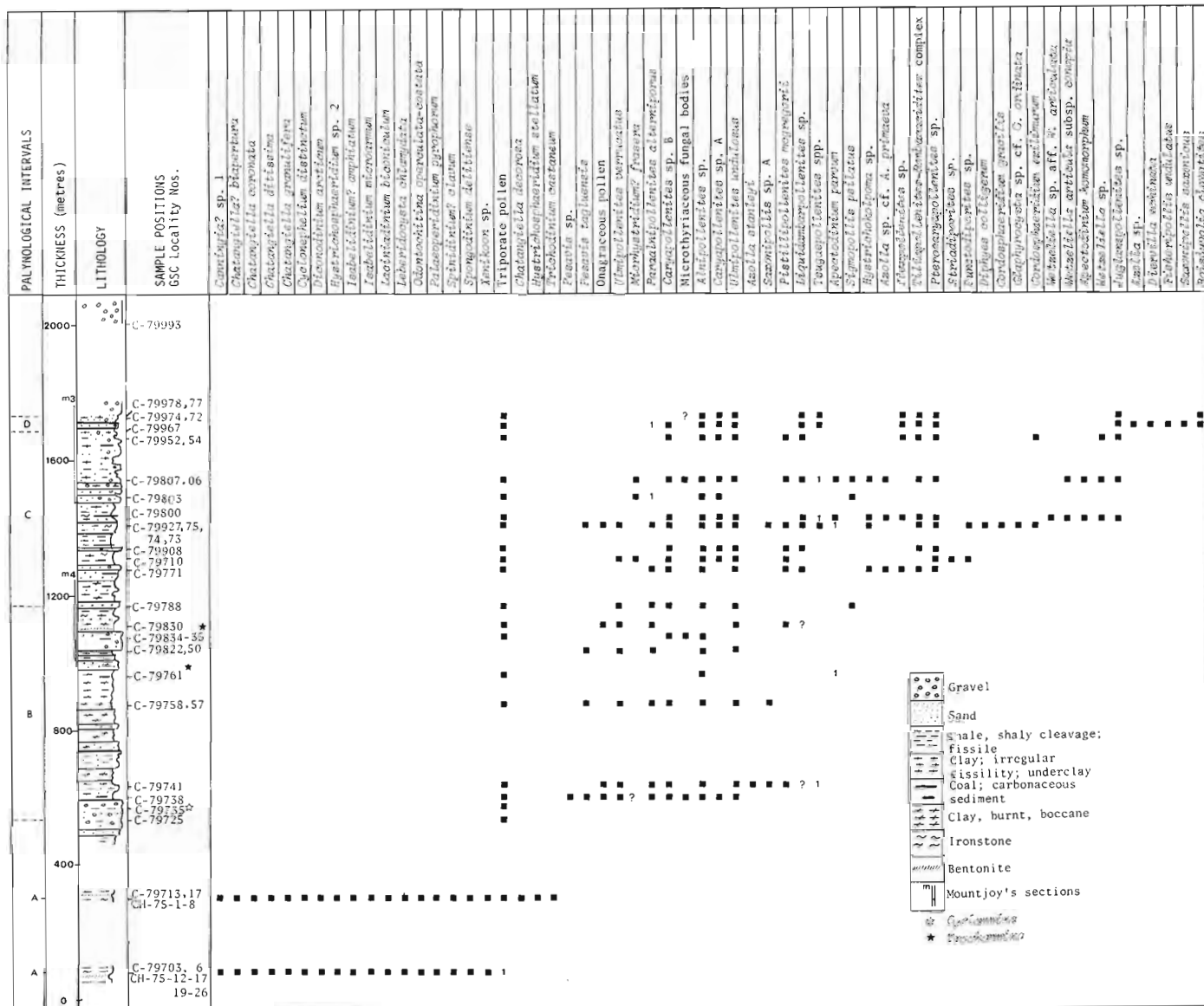
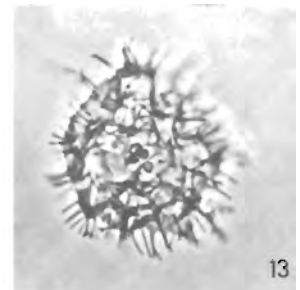
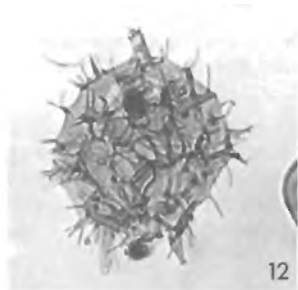
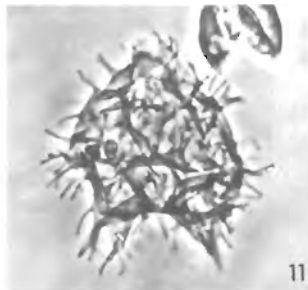
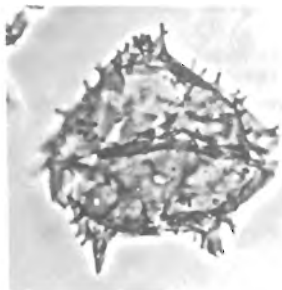
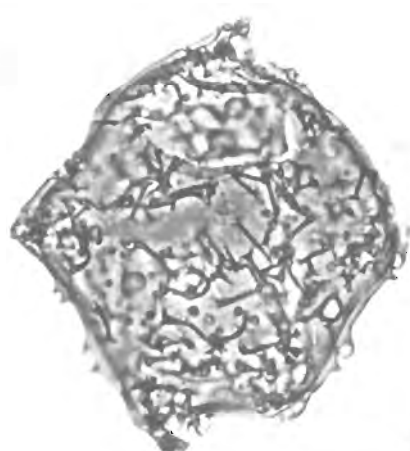
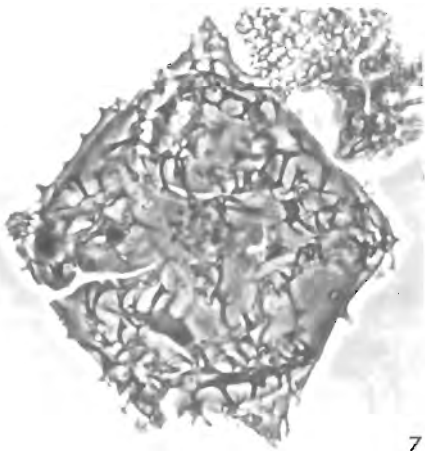
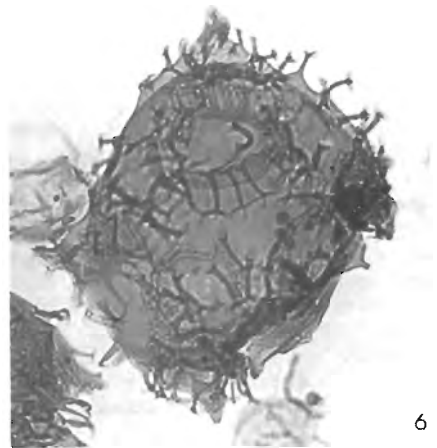
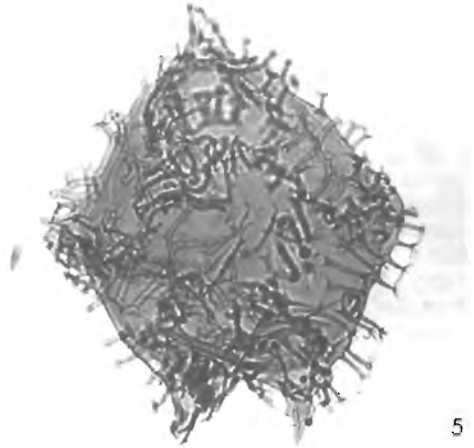
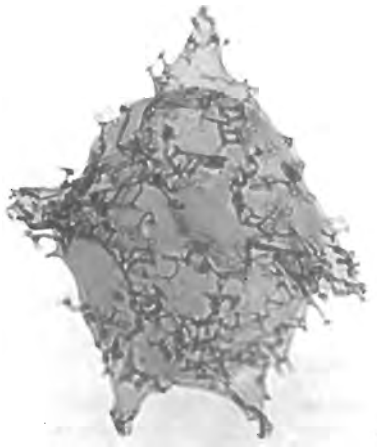
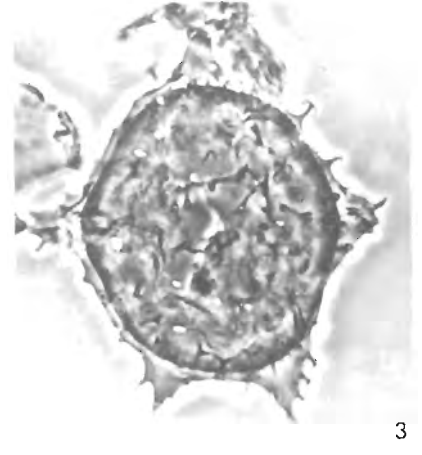
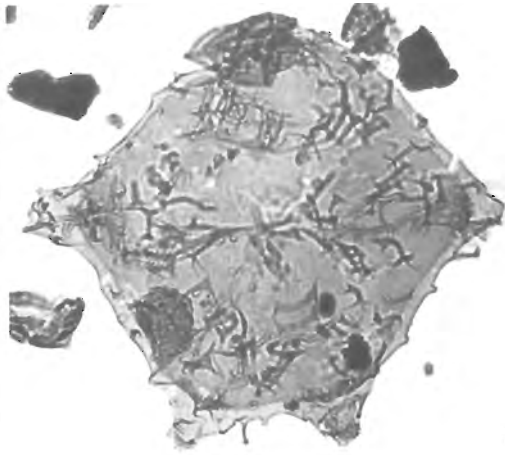
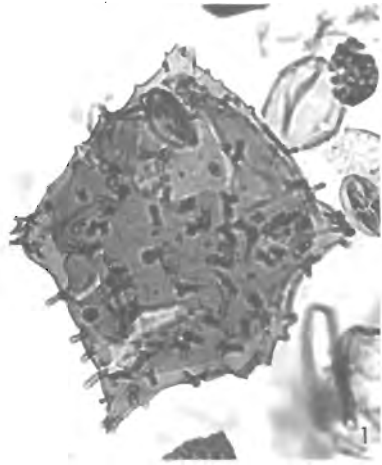


Figure 31.1. Selected palynomorph occurrences in Caribou Hills Section. (Upper portion of the conglomeratic unit not shown - total thickness subject to revision).

PLATE 31.1

All figures x 500

1. *Wetzeliella* sp. aff. *W. articulata* Eisenack. C-79800, GSC 62654; a form with same but sparser ornament than *W. articulata*, and sometimes with less ovoid endocyst.
- 2, 4-9. *Wetzeliella* sp.
 - 2, C-79954, GSC 62656;
 - 4, C-79954, GSC 62657;
 - 5, C-79954, GSC 62658;
 - 6, C-79954, GSC 62659;
 - 7, C-79954, (phase contrast), GSC 62660;
 - 8, C-79954, (phase contrast), GSC 61661;
 - 9, C-79954, GSC 62662; note variability in horn structure, form and distribution of ornament, grana on periphery of endocyst, and wall relationship.
3. *Wetzeliella articulata* subsp. *conopia* (Williams and Downie in Davey et al., 1966) Lentin and Williams. C-79800 (phase contrast), GSC 62655; a form ranging into *Wetzeliella* sp. with regard to type and distribution of ornament.
- 10-13. *Apectodinium parvum* (Alberti) Lentin and Williams
 - 10, C-79800, (phase contrast), GSC 62663;
 - 11, C-79800, (phase contrast), GSC 62664;
 - 12, C-79807, GSC 62665;
 - 13, C-79800, (phase contrast), GSC 62666; note variability in shape of cyst and horn development.



Our results should be considered in conjunction with Price et al. (in preparation) whose detailed sampling and description have given a more complete analysis of the stratigraphy of the Caribou Hills section than any previously available.

Interval A (C-79703- C-79717); (and samples from an earlier collection); Campanian.

Microfloral Composition Assemblages in this interval are characterized by the presence of abundant dinoflagellates with rare pollen and spores. The most conspicuous and dominant member of the assemblages is the large dinocyst species *Chatangiella coronata*. Other species which are consistently present and often abundant are *Chatangiella? biapertura* (McIntyre) Lentin and Williams 1976, *Isabelidium microarmum* (McIntyre) Lentin and Williams 1977, *Laciniadinium biconiculum* McIntyre 1975, *Hystrichosphaeridium* sp. 2 of McIntyre (1974) *Canningia?* sp. 1 of McIntyre (1974), *Cyclonephelium distinctum* Deflandre and Cookson 1955, *Fromea fragilis* (Cookson and Eisenack) Stover and Evitt 1978, *Palambages* spp. and *Palaeoperidinium pyrophorum* (Ehrenberg) Deflandre emend. Sarjeant 1967. Many other species occur consistently but are not abundant. Among these are *Chatangiella ditissima* (McIntyre) Lentin and Williams 1976, *C. granulifera* (Manum) Lentin and Williams 1976, *Spongodinium delitiense* (Ehrenberg) Deflandre 1936, *Diconodinium arcticum* Manum and Cookson 1964, *Pterodinium* sp. 1 of McIntyre (1974), *Leberidocysta chlamydata* (Cookson and Eisenack) Stover and Evitt 1978, *Exochosphaeridium striolatum* (Deflandre) Davey 1964, *Cleistosphaeridium? aciculare* Davey 1969, *Impletosphaeridium whitei* (Deflandre and Courteville) Morgenroth 1966, *Cyclonephelium compactum* Deflandre and Cookson 1955, *Odontochitina operculata* (O. Wetzell) Deflandre and Cookson 1955 and *Hystrichosphaeridium? difficile*. Species which occur less commonly include *Chatangiella decorosa* (McIntyre) Lentin and Williams 1976, *C. spectabilis* (Alberti) Lentin and Williams 1976, *Isabelidium? amphiatum* (McIntyre) Lentin and Williams 1977, *I. acuminatum* (Cookson and Eisenack 1976) Stover and Evitt 1978, *Alterbia minor* (Alberti) Lentin and Williams 1976, *Spinidium? clavum* Harland 1973, *Gingiodinium ornatum* (Felix and Burbridge) Lentin and Williams 1976, *Canningia? ringnesiorum* Manum and Cookson 1964, *Hystrichosphaeropsis* sp., *Chlamydochorella nyei* Cookson and Eisenack 1958, *Oligosphaeridium pulcherrimum* (Deflandre and Cookson) Davey and Williams in Davey et al. 1966, *Caligodinium aceras* (Manum and Cookson) Lentin and Williams 1977, *Trichodinium castaneum* (Deflandre) Clarke and Verdier 1967, *Hystrichosphaeridium stellatum* Maier 1959, *Wallodinium lunum* (Cookson and Eisenack) Lentin and Williams 1973 and *Xenikoon* sp. (= *Nelsoniella aceras* of McIntyre, 1974 and *Nelsoniella* sp. AE of Brideaux, 1976). Ovoid cysts, which are probably endocysts of a peridinioid dinoflagellate, are common in some samples. Reworked Late Albian - Cenomanian dinoflagellates, especially *Luxadinium propatulum* Brideaux and McIntyre 1975, *Spinidium vestitum* Brideaux 1971 and *Ovoidinium scabrosum* (Cookson and Hughes) Davey 1970 are present in most samples. A few rare dinoflagellates and spores of Hauterivian to Barremian age occur in some of the samples examined.

Pollen and spores are not abundant in any of the samples but bisaccate conifer pollen are generally present as well as some Taxodiaceous pollen. Some tricolpate pollen, rare triporate pollen, and a few spores occur in most samples but none of these are particularly diagnostic.

PLATE 31.2

All figures x 500

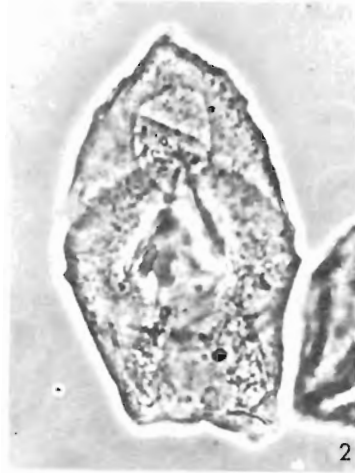
- 1, 3. *Canningia?* sp. 1
 - 1, C-79703, GSC 62638; note displaced operculum.
 - 3, C-79703, GSC 62639; operculum attached.
- 2, 9. *Isabelidium microarmum* (McIntyre) Lentin and Williams
 - 2, C-79703, (phase contrast), GSC 62640; the punctae and irregularly distributed grana may be the result of preservation.
 - 9, GSC 62646.
4. *Cordosphaeridium exilimum* Davey and Williams, in Davey et al. (1966), C-79954, (phase contrast), GSC 62641.
- 5, 6. Ovoid cysts
 - 5, GSC 62642; specimen showing faint grana.
 - 6, GSC 62643; specimen showing smooth wall.
7. *Xenikoon* sp., GSC 62644; a form similar to *Nelsoniella aceras* Cookson and Eisenack 1960 but with a smaller apical pericoel.
8. *Chatangiella? biapertura* (McIntyre) Lentin and Williams, 1976 GSC 62645.
10. *Spongodinium delitiense* (Ehrenberg) Deflandre C-79800, GSC 62647; a reworked specimen.
11. *Exochosphaeridium striolatum* (Deflandre) Davey C-79703, GSC 62648.
12. *Palaeoperidinium?* sp., C-79807, (phase contrast), GSC 62649. No archeophyle observed.
- 13, 14. *Hystrichokolpoma* sp.
 - 13, C-79771, (phase contrast), GSC 62650;
 - 14, C-79800, (phase contrast), GSC 62651.
15. *Alterbia* sp., C-79800, (phase contrast), GSC 62652. Archeophyle appears intercalary.
16. *Diconodinium arcticum* Manum and Cookson, C-79703, (phase contrast), GSC 62653.

Discussion The Tent Island Formation (Young, 1975) of the Mackenzie Delta and the Mason River Formation (Yorath et al., 1975) of the Anderson Plain are considered to be lateral equivalents (Young et al., 1976). The microfloral assemblages from the Cretaceous shales in the Caribou Hills are similar to Division H2 assemblages (McIntyre, 1974, 1975) of the Mason River Formation from the Horton River section. The Division H2 microfloras were dated as Campanian by McIntyre (1974, 1975) and the similar microfloras from the Caribou Hills section are also considered to be Campanian.

McIntyre (1974, 1975) noted that the Horton River Division H2 assemblages were characterized by an abundance of *Chatangiella coronata* and *Laciniadinium biconiculum*, both of which are restricted to Division H2. These two taxa are abundant in the Caribou Hills samples which also contains *Canningia?* sp. 1 (of McIntyre, 1974) which is restricted to Division H2 in the Horton River section. *Isabelidium microarmum* is common in the assemblages from both sections, but is not restricted to Division H2 of the Horton River section. Species, which have their first appearance in Division H2 of the Horton River section and also occur in the Caribou Hills section, are *Hystrichosphaeridium* sp. 2,



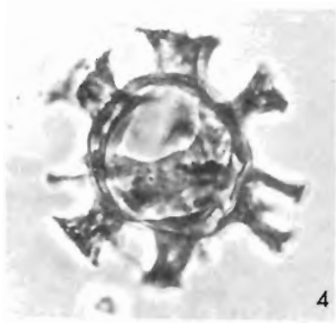
1



2



3



4



5



7



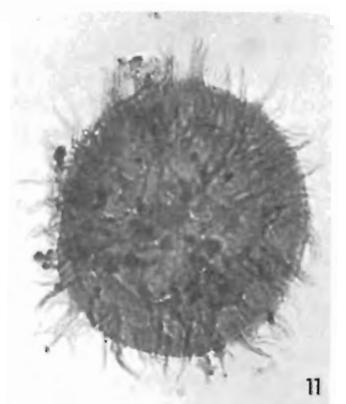
8



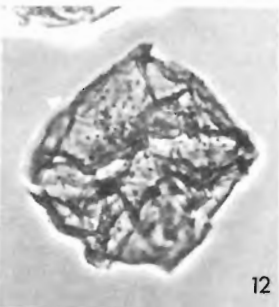
9



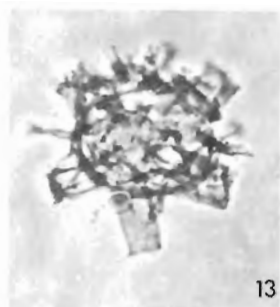
10



11



12



13



14



15



16

Isabelidium? *amphiatum*, *Chatangiella?* *biapertura* and *Palaeoperidium pyrophorum*. In the Horton River section *Exochosphaeridium striolatum*, *Chatangiella spectabilis* and *Impletosphaeridium whitei* last appear in Division H2 whereas *Gingiodinium ornatum* makes its last appearance at the top of Division H1. These four species also occur in the Caribou Hills assemblages. All other species recorded from the Caribou Hills section have also been noted in the Horton River section. The strong similarity between the Caribou Hills and Horton River assemblages suggests that the Cretaceous shales in the Caribou Hills are correlative with the base of the Mason River Formation in the Horton River section. The microfloras, which contain abundant dinoflagellates but scarce pollen, are placed in Division H2 of McIntyre (1974, 1975) and are of Campanian age.

The Cretaceous/Tertiary unconformity is abruptly defined by major microfossil changes, especially the disappearances of all Campanian dinocysts and the influx of abundant triporate pollen in the Early Tertiary.

Interval B (C-79725-C-79788); Upper Paleocene - (?) Lower Eocene

Microfloral Composition Diversity of assemblages in terms of number of species recorded is lower in this interval than the one above. However, several taxa are numerically important elements. These include *Paraalnipollenites alterniporus* (Simpson) Srivastava 1975, *Ulmipollenites verrucatus* Norton, in Norton and Hall 1969, and *Caryapollenites* sp. B. Associated forms, intermittently present within this interval, are *Pistillipollenites mcgregorii* Rouse 1962, *Saxonipollis* sp. (intectate), common *Nudopollis* sp. as in Doerenkamp et al., 1976, onagraceous pollen, the fungal spores *Pesavis tagluensis* Elsik and Jansonius 1974 and *Pesavis* sp., a single specimen of *Apectodinium parvum* (Alberti) Lentini and Williams 1977 (sample C-79761), and rare specimens of the fresh water fern *Azolla stanleyi* Jain and Hall 1969.

Discussion *Azolla stanleyi* is known only from Upper Paleocene rocks whereas *Pistillipollenites mcgregorii* is not known to range into the Lower Paleocene. This latter species was reported by Rouse and Srivastava (1972) from the Paleocene of the Bonnet Plume Formation, and by Sweet from the upper lignite of the same formation, in northeastern Yukon, together with *Saxonipollis* sp. and *Nudopollis* sp. (unpublished information). *P. mcgregorii* was also recorded by Sweet (1978) from above the Boundary coal zone in southeastern Saskatchewan, and by Nichols and Ott (1978) from zone 5 (towards the top of the Paleocene) of the Fort Union Formation in Wyoming. Rouse (1977) gave the range of the species in the Arctic as Late Paleocene to Middle Eocene. Doerenkamp et al. (1976) have shown *Nudopollis* sp. to be present in the uppermost Paleocene and Eocene Eureka Sound Formation on Banks Island, and Rouse and Srivastava (1972) have recorded it from the Paleocene of the Bonnet Plume Formation (as *Extratripoporipollenites* sp.). The presence of *Apectodinium parvum* is of significance as this species has not yet been reported from rocks older than Upper Paleocene. The scarcity of marine elements in this interval and the development of coaly beds would indicate mainly terrestrial sedimentation interrupted by minor marine incursions.

Micropaleontological evidence suggests a Paleocene age, at least for the lower part of this interval. Foraminifera attributable to *Cyclammina* have been extracted from a horizon at C-79735; they are morphologically similar to forms which commonly occur in the Paleocene and less commonly in the Campanian and Maastrichtian of the Western Siberian Lowlands. In addition, a *Trochammina* sp. has been observed both at the C-79835 and C-79761 horizons.

PLATE 31.3

All figures x 500

- 1 - 3. *Chatangiella coronata* (McIntyre) Lentini and Williams
 1. GSC 62630, dorsal view, high focus.
 2. C-79703, (phase contrast), GSC 62634, dorsal view, high focus.
 3. GSC 62632; ventral view, high focus.
4. *Odontochitina costata* Alberti, C-79703, (phase contrast), GSC 62633.
5. *Glyphrocysta* sp. cf. *G. ordinata* (Williams and Downie in Davey et al., 1966) Stover and Evitt, C-79774, (phase contrast), GSC 62634.
6. *Chatangiella decorosa* (McIntyre) Lentini and Williams, GSC 62635; dorsal view, high focus.
7. *Hystriochosphaeridium* sp. 2, in McIntyre 1974, GSC 62636
8. *Pterodinium* sp. 2, in McIntyre 1974, C-79706, GSC 62637.

This taxon occurs in the type Aklak Member of the Reindeer Formation in the Yukon Coastal Plain and has been reported in the subsurface (McNeil, personal communication).

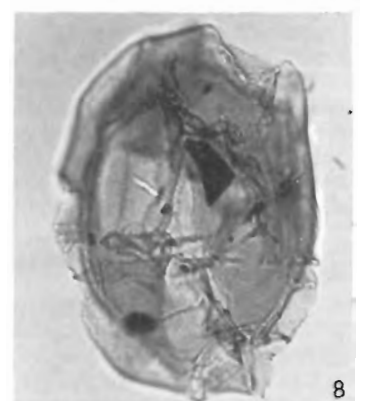
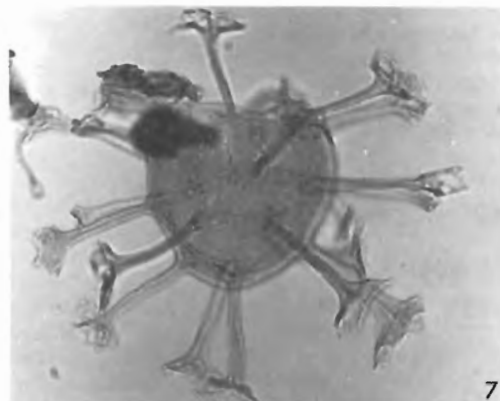
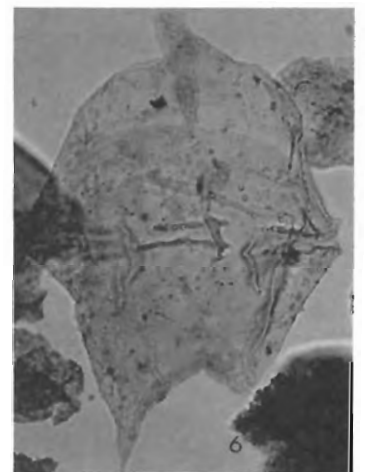
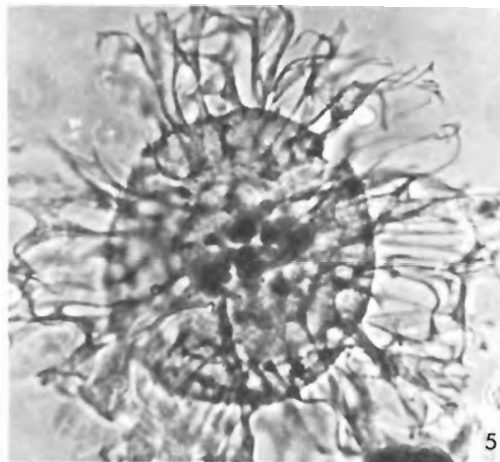
From the data discussed, a Paleocene age would appear logical for interval B. Nevertheless, because of the incompletely known ranges of microfossils at these latitudes, and because of the lack of supporting chronostratigraphic control it is not yet desirable to draw a Paleocene-Eocene boundary.

Interval C (C-79788-C-79954): Eocene, probably Lower to early Middle Eocene.

Microfloral Composition The assemblages within this interval appear to be more diversified than those lower in the section as additional taxa are added to the general microfloral composition. With the exception of *Azolla stanleyi*, all elements observed below are also present here. *Paraalnipollenites alterniporus* decreases progressively up-section, but the sporadic highest occurrences can probably be attributed to reworking.

The most important pollen elements comprise *Pterocaryapollenites* sp., *Ilexpollenites* sp., *Caryapollenites* sp. A., the *Tiliapollenites-Bombacacidites* complex, and in the upper half of the interval *Juglanspollenites* sp. A number of fungal spores are first documented at these levels which together with *Pesavis tagluensis* have the top of their ranges in the lower half of this interval. These include *Fusiformisporites* sp., *Punctodiporites* sp., and *Striadiporites* sp. Although these occurrences may signify a local microfloral change, the complex pattern of the deltaic-coastal plain sedimentation may have played an important role in their distribution. Therefore, the possibility of an extension of some of these ranges cannot be excluded.

An important feature of this interval is the invariable presence of marine microplankton which, at certain levels, constitutes 15 to 20 per cent of the assemblages. Nevertheless, despite the abundance of the dinocysts, their diversity is strikingly limited. This probably reflects a specific depositional environment (see later discussion) and perhaps to some degree, the boreal character of the assemblages. Elements exclusive to the lower half of the interval are *Glyphrocysta* sp. cf. *G. ordinata* (Williams and Downie) Stover and Evitt 1978, *Cordosphaeridium gracilis*



(Eisenack) Davey and Williams 1966, and *Diphyes colligerum* (Deflandre and Cookson) Cookson 1965. The upper half of this interval is dominated by members of the related genera *Wetzeliella* and *Apectodinium*. These are: *W.* sp. aff. *W. articulata* Eisenack 1978, *W. articulata* subsp. *conopia* (Williams and Downie) Lentin and Williams 1973, *Wetzeliella* sp., *A. homomorphum* (Deflandre and Cookson) Lentin and Williams 1977, and *A. parvum* (Alberti) Lentin and Williams 1977. Species ranging through this interval are as follows: *Cordosphaeridium exilimum* Davey and Williams 1966, *Hystrichokolpoma* sp., *Michrystidium?* *frasera* Piel 1971 (questionably assigned to the genus but probably related to *Sigmopollis*; from unpublished records known to occur in nonmarine sediments, and during this study observed in a shaly coal), *Sigmopollis psilatus* Piel 1971, *Pistillipollenites mcgregorii*, *Azolla* sp. cf. *A. primaeva* (Penhallow) Arnold 1955 (nine floats, massulae glochidiate), and a variety of microthyriaceous fungal grains.

Discussion The association of *Pistillipollenites mcgregorii*, a pollen not certainly reported from sediments younger than Middle Eocene (Rouse 1977), with such fungal spores as *Pesavis tagluensis* and *Striadiporites* sp. may suggest an Early to Middle Eocene age. Corroborative evidence is provided by the common occurrence of *Apectodinium homomorphum* and *A. parvum* with occasional records of *Wetzeliella* sp. aff. *W. articulata*. Costa and Downie (1976) in their work on the distribution of *Wetzeliella* in northeastern Europe have demonstrated that the mutual occurrence of the above dinocysts would indicate an Early Eocene age. In offshore eastern Canada, abundant *Apectodinium* is known to occur in Lower Eocene sediments (G.L. Williams, personal communication). Staplin (1976) also noted that *W. articulata* [including specimens attributed to *W. hampdenensis* Wilson 1967 - a form apparently close to *W. articulata* subsp. *conopia* (Williams and Downie) Lentin and Williams 1973], and *A. homomorphum* indicate a late Early to Middle Eocene age in the subsurface of Mackenzie Delta. Brideaux and Myhr (1976) reported *W. articulata*, *A. homomorphum*, *A. parvum* and *W. articulata* subsp. *conopia* from an interval of the Reindeer Formation in the Gulf-Mobil Parsons N-10 well dated as Early to Middle Eocene.

As in the case of the London Clay, *A. homomorphum* and *A. parvum* have been observed in fair abundance and in the Caribou Hills constitute 5 to 6.5 per cent of the assemblages. Their occurrence probably reflects a hyposaline marine environment of nearshore to estuarine deposition, as suggested by Downie et al. (1971). Doerenkamp et al. (1976) proposed a similar interpretation. The authors have observed a similar situation during subsurface studies in offshore wells in the Mackenzie Delta-Beaufort Sea region. The associated low-diversity assemblage of agglutinated foraminifers is compatible with the above environmental interpretation. Significantly, from within this interval at Caribou Hills no foraminifers have been recorded. Probably their absence is due to facies changes related to close proximity to the shore.

Interval D (C-79967 - C-79978): Probably Oligocene

Microfloral Composition This interval, collectively, yielded a rich association of pteridophyte spores, gymnosperm and angiosperm pollen, dominated by ericoid tetrads. Angiosperm pollen include the following arboreal elements: *Alnipollenites verus* (Potonie) Potonie 1937, *Betula claripites* Wodehouse 1933, *Caryapollenites* sp., *A.*, *Caryapollenites* sp. B., *ilexpollenites* sp., *Juglanspollenites* sp., *Liquidambarpollenites* sp., *Pterocaryapollenites* sp., *Ulmipollenites undulosus* Wolfe 1974, and members of the *Tiliapollenites-Bombacacidites* complex. Except for *B. claripites*, all forms are present in the underlying interval. Additional elements are *Diervilla echinata* Piel 1971, the

PLATE 31.4

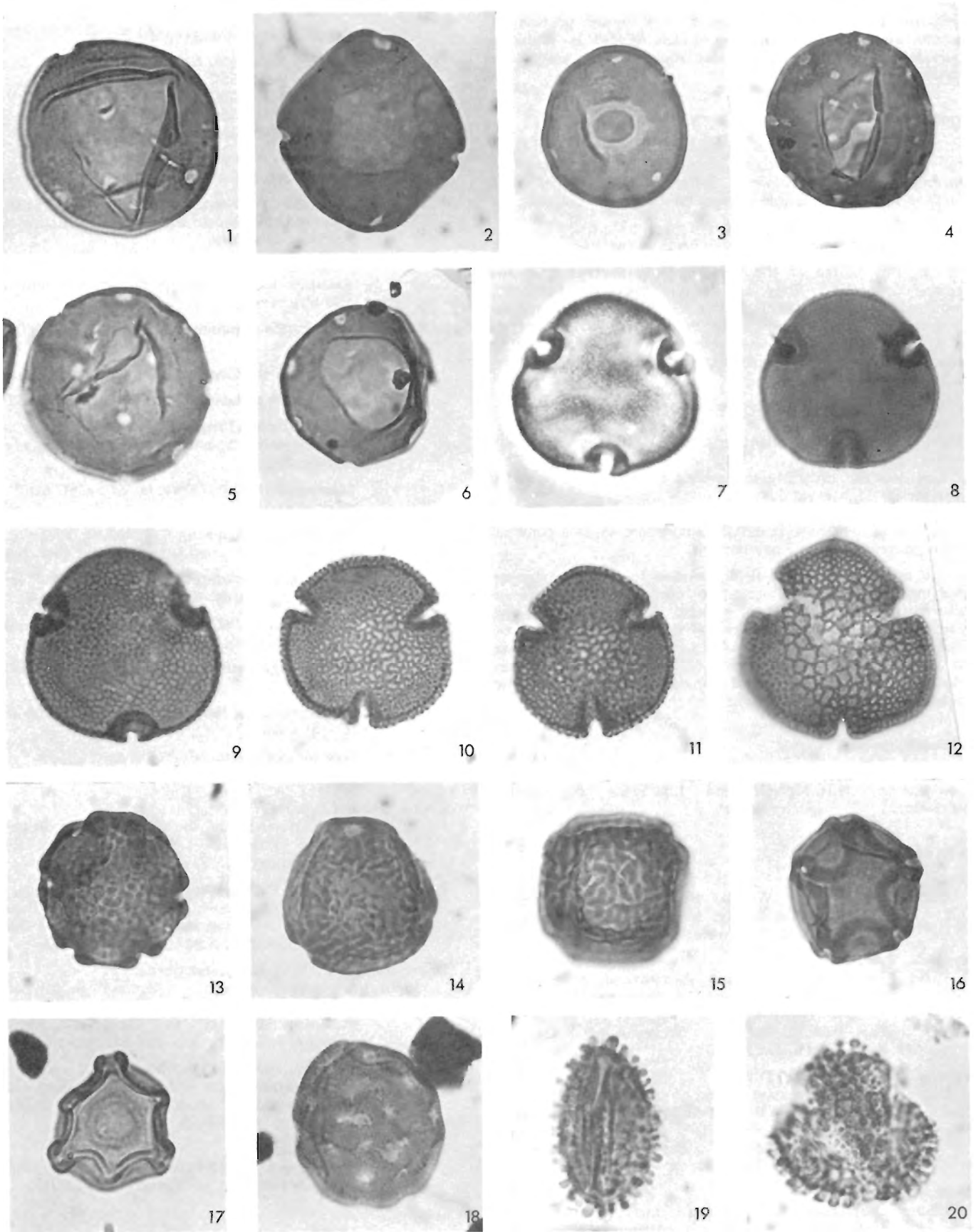
All figures x 1000

- 1, 2. *Caryapollenites* sp. A.
 - 1, C-79954, GSC 62593;
 - 2, C-79771, GSC 62594. Specimens showing three and four pores respectively.
3. *Caryapollenites* sp. B., C-79906, GSC 62595.
- 4, 5. *Juglanspollenites* sp.
 - 4, C-79954, GSC 62596
 - 5, C-79954, GSC 62597.
6. *Pterocaryapollenites* sp., C-79954, GSC 62598.
- 7-12. *Tiliapollenites-Bombacacidites* complex
 - 7, C-79800, GSC 62599; (phase contrast).
 - 8, C-79954, GSC 62600;
 - 9, C-79954, GSC 62601;
 - 10, C-79954, GSC 62602;
 - 11, C-79954, GSC 62603;
 - 12, C-79954, GSC 62604.

Specimens showing variable degree of reticulation and of inner wall thickening around the aperture.
13. *Ulmipollenites* sp., C-79954, GSC 62605. A verrucate form present with *U. verrucatus*.
- 14, 15. *Ulmipollenites undulosus* Wolfe
 - 14, C-79710, GSC 62606
 - 15, C-79954, GSC 62607.
16. *Alnipollenites* sp., C-79954, GSC 6260. Specimens with 6 pores have been observed.
17. *Paraalnipollenites alterniporus* (Simpson) Srivastava, C-79788, GSC 62609.
18. *Liquidambarpollenites* sp., C-79771, GSC 62610.
- 19, 20. *Ilexpollenites* sp.
 - 19, C-79974, GSC 62611; equatorial view.
 - 20, C-79974, GSC 62612; oblique polar view.

onagraceous *Boisduvalia clavatites* Piel 1971, the highly evolved tectate pollen *Saxonipollis saxonicus* Krutzsch 1970, *Fisheripollis undulatus* Krutzsch 1970, and species of the gymnosperm genus *Tsugaepollenites*. The occurrence of *Azolla* sp. (nine floats, with collar, massulae aglochidiate) may prove stratigraphically important in the Mackenzie Delta region (see Fowler 1975). Dinoflagellate cysts or acritarchs have not been encountered in this interval.

Discussion The assemblage described by Peil (1971) from the central interior of British Columbia compares closely with the microfloras of interval D. His assemblages contain most of the components observed here including the significant occurrences of *Boisduvalia clavatites* and *Diervilla echinata*, which have not yet been definitely recorded from pre-Oligocene rocks. The presence of *Azolla* sp. is important for the same reasons (see Fowler 1975). The early Oligocene (0-1) palynozone of Rouse (1977) contains *B. clavatites* and *D. echinata*, the latter confined to south-central British Columbia and the former represented both there and in Arctic Canada. A further comparable assemblage has been described by Hopkins et al. (1972) from the northern Rocky Mountain Trench of British Columbia. This is essentially similar to that of Peil (1971). Krutzsch (1970) reported *Saxonipollis saxonicus* from the Eocene and Miocene, and *Fisheripollis undulatus* from the Miocene of Western Europe, Central Asia and the Middle East.



An Oligocene age is favoured for this interval based on the evidence discussed above, but slightly older or younger ages cannot be excluded because the ranges of the species identified are imperfectly known. The upper portion of assemblage 2b of Doerenkamp et al. (1976) is probably equivalent to the interval discussed above but was assigned a probable Early Eocene age.

Sample C-79973

This sample, essentially a kaolinitic clay, obtained from the upper gravels yielded common wood fragments, extremely rare tricolpate pollen of a generalized morphology, and possible modern contaminants (?algal).

Conclusions and Summary

In the course of the investigation, several problems became apparent. They are largely chronostratigraphic, amplified by (1) the complexity of the deltaic facies, (2) reworking, and (3) low specific diversity of marine forms. As a result, the ages proposed are tentative and subject to future refinement. The most significant conclusions may be summarized as follows:

1. Marked qualitative differences between the Cretaceous and Tertiary intervals.
2. Introduction of abundant triporate pollen in the Early Tertiary.
3. Low specific diversity in interval B versus high specific diversity in interval C.
4. Repetition and sudden changes of palynofacies, which are typical of nearshore to deltaic environments, is a common characteristic of the palynoflora.

It may be possible in future studies to evaluate changes resulting from climatic fluctuations during the Paleogene or those reflecting evolutionary trends. For instance, if the hypothesis of a cooling climate from Late Cretaceous through Paleocene and of a subsequent warm period during the Eocene (Wolfe and Hopkins, 1967) is accepted, one may anticipate some reflections of the climatic changes on the microfloras in the section studied.

Acknowledgments

The writers are grateful to their colleagues A.R. Sweet, W.S. Hopkins, D.H. McNeil and L.L. Price for useful discussions.

References

- Arnold, C.A.
1955: A Tertiary *Azolla* from British Columbia. Michigan University, Museum of Paleontology, Contributions, Ann Arbor, v. 12(4), p. 33-45.
- Brideaux, W.W.
1976: Taxonomic notes and illustrations of selected dinoflagellate cyst species from the Gulf-Mobil Parsons N-10 well; in Report of Activities, Part B, Geological Survey of Canada, Paper 76-1B, p. 251-257.
- Brideaux, W.W. and Myhr, D.W.
1976: Lithostratigraphy and dinoflagellate cyst succession in the Gulf-Mobil Parsons N-10 well, District of Mackenzie; in Report of Activities, Part B, Geological Survey of Canada, Paper 76-1B, p. 235-249.
- Cookson, I.C.
1965: Cretaceous and Tertiary microplankton from southeastern Australia; Royal Society of Victoria, Proceedings, v. 78, p. 85-93.

PLATE 31.5

All figures x 1000 unless otherwise stated

1 - 5. *Pistillipollenites mcgregorii* Rouse

1. C-79771, GSC 62613,
2. C-79927, GSC 62614,
3. C-79710, GSC 62615,
4. C-79771, GSC 62616,
5. C-79710, GSC 62617.

Specimens showing diversity in ornament distribution and development.

6. Onagraceous pollen, C-79830, GSC 62618; specimens observed have shown an ornament ranging from verrucae to spines.
7. *Boisduvalia clavatites* Piel, C-79974, GSC 62619; specimen larger than type but smaller individuals also observed.
- 8, 14. *Saxonipollis saxonicus* Krutzsch, C-79967, (x 500), GSC 62620
14, detail showing tectum (phase contrast).
9. *Sigmopollis psilatus* Piel, C-79788, GSC 62621.
10. *Michrystidium? fraseri* Piel, C-79803, GSC 62629. Note sigmoidal aperture; probably a species of *Sigmopollis*.
11. *Saxonipollis* sp., C-79741, (x 500), GSC 62623; intectate.
12. *Diervilla echinata* Piel, C-79967, (x 500), GSC 62624; specimen slightly larger than type.
13. *Fisheripollis undulatus* Krutzsch, C-79967, (x 500), GSC 62625; tetrad of polyporate pollen.
15. *Pesavis* sp., C-79738, GSC 62626; a form showing larger cells than those of *P. tagluensis*
16. *Pesavis tagluensis* Elsik and Jansonius, C-79738, GSC 62627.
17. *Striadipores* sp., C-79710, GSC 62628; note weak reticulation.
18. *Punctodiporites* sp., C-79710, GSC 62629.

Costa, L.I. and Downie, C.

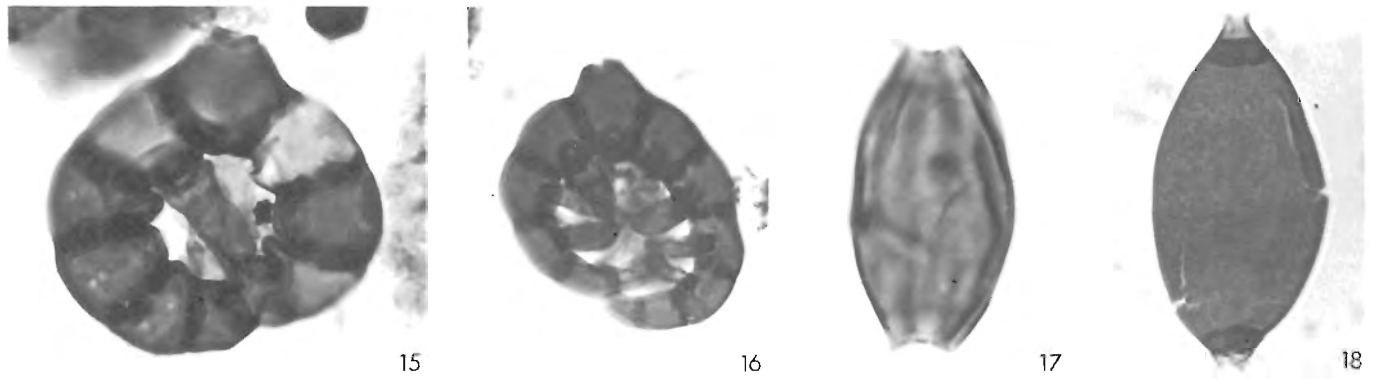
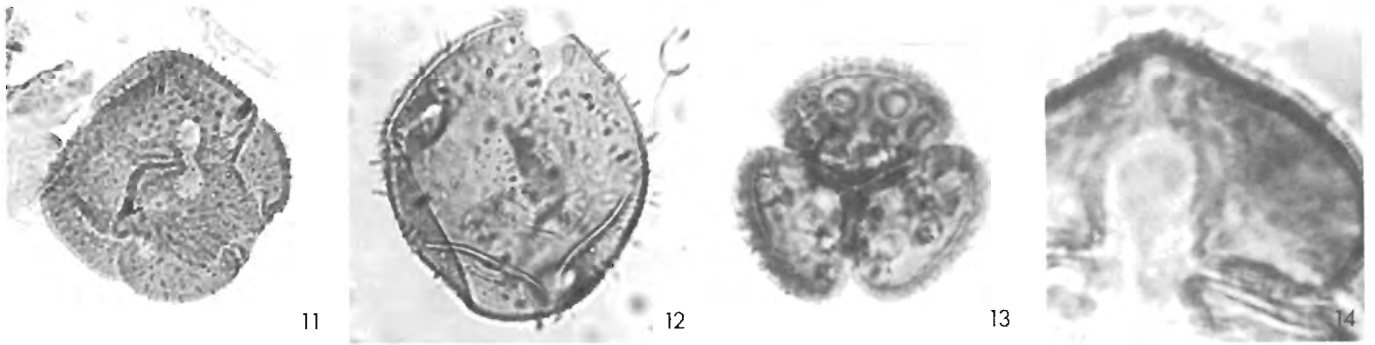
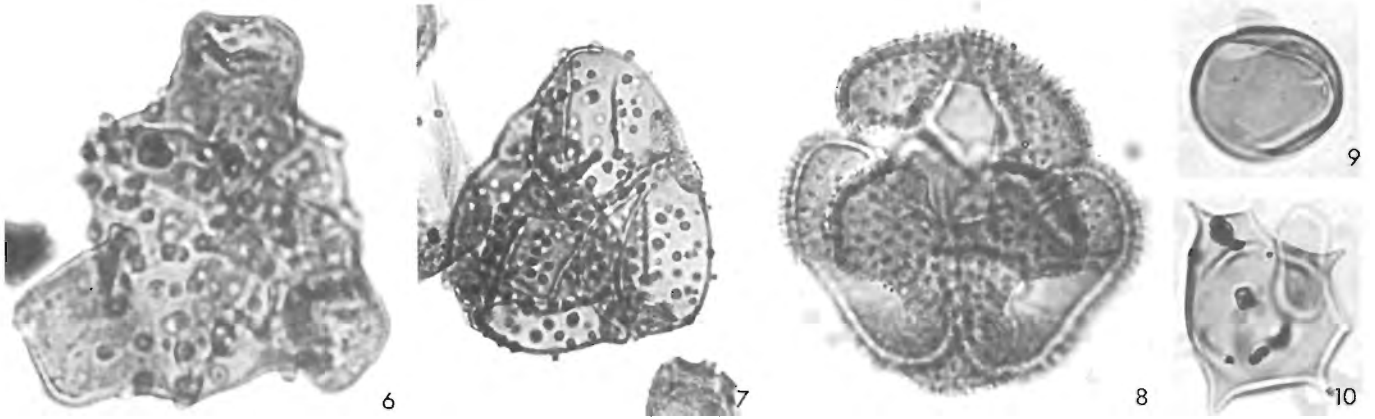
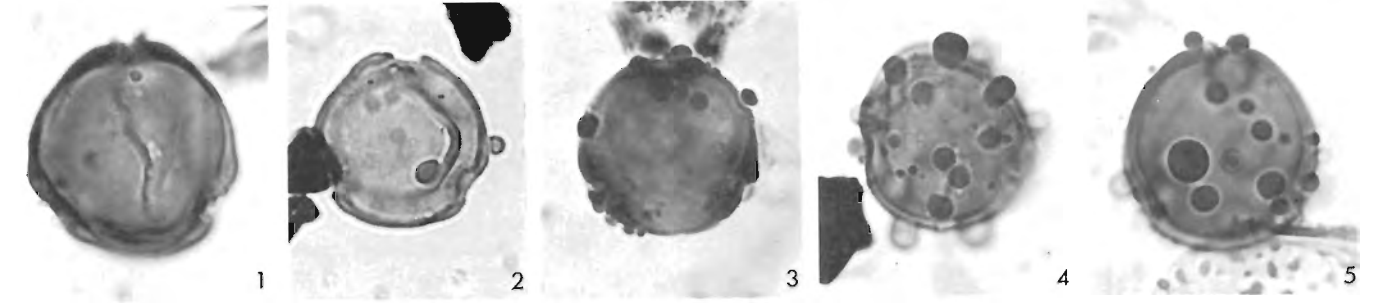
1976: The distribution of the dinoflagellate *Wetzeliella* in the Paleogene of northwestern Europe; *Palaeontology*, v. 19, p. 591-614.

Davey, R.J., Downie, C., Sarjeant, W.A.S. and Williams, G.L.
1966: Studies of Mesozoic and Cainozoic dinoflagellate cysts; *British Museum (Natural History) Bulletin*, London, Geology, Supplement 3, p. 1-248.

Doerenkamp, A., Jardiné, S., and Moreau, P.
1976: Cretaceous and Tertiary palynomorph assemblages from Banks Island and adjacent areas (N.W.T.); *Bulletin of Canadian Petroleum Geology*, v. 24, no. 3, p. 312-417.

Downie, C., Hussain, M.A., and Williams, G.L.
1971: Dinoflagellate cyst and crinarch associations in the Paleogene of southeast England; *Geoscience and Man*, v. 3, p. 29-35.

Elsik, W.C. and Jansonius, J.
1974: New genera of Paleogene fungal spores; *Canadian Journal of Botany*, v. 52, no. 5, p. 953-958.



- Eisenack, A.
1938: Die phosphoritknollen der Bernsteinformation als Überlieferer tertiären Planktons; Schriften Physikalisch-ökonomischen Gesellschaft zur Königsberg, v. 70, p. 181-188.
- Fowler, K.
1975: Megaspores and massulae of *Azolla prisca* from the Oligocene of the Isle of Wight; *Palaeontology*, v. 18, p. 483-507.
- Hills, L.V. and Wallace, S.
1969: **Paraalnipollenites**, a new form genus from uppermost Cretaceous and Paleocene rocks of Arctic Canada and Russia; *Geological Survey of Canada, Bulletin 182*, p. 139-145.
- Hopkins, W.S., Rutter, N.W., and Rouse, G.E.
1972: Geology, Paleoecology, and Palynology of some Oligocene rocks in the Rocky Mountain Trench of British Columbia; *Canadian Journal of Earth Sciences*, v. 9, p. 460-470.
- Jain, R.K., and Hall, J.W.
1969: A contribution of the early Tertiary fossil record of the Salviniaceae; *American Journal of Botany*, v. 56, p. 527-539.
- Krutzsch, W.
1970: Zur Kenntnis fossiler disperser Tetradenpollen; *Paläontologische Abhandlungen B.*, v. 314, p. 399-433.
- Lentin, J.K., and Williams, G.L.
1973: Fossil dinoflagellates - index to genera and species; *Geological Survey of Canada, Paper 73-42*, 176 p.
1977: Fossil dinoflagellates - index of genera and species, 1977 edition; *Bedford Institute of Oceanography Report Series B1-R-77-8*, 209 p.
- McIntyre, D.J.
1974: Palynology of an Upper Cretaceous section, Horton River, District of Mackenzie, N.W.T.; *Geological Survey of Canada, Paper 74-14*, 57 p.
1975: Morphologic changes in *Deflandrea* from a Campanian section, District of Mackenzie, N.W.T., Canada; *Geoscience and Man*, v. 11, p. 61-76.
- Mountjoy, E.W.
1967: Upper Cretaceous and Tertiary stratigraphy, northern Yukon Territory and northwestern District of Mackenzie; *Geological Survey of Canada, Paper 66-16*, 70 p.
- Nichols, D.J. and Ott, H.L.
1978: Biostratigraphy and evolution of the **Momipites-Caryapollenites** lineage in the early Tertiary in the Wind River Basin, Wyoming; *Palynology*, v. 2, p. 93-112.
- Norton, N.J., and Hall, J.W.
1969: Palynology of the Upper Cretaceous and Lower Tertiary in the type locality of the Hell Creek Formation, Montana, U.S.A.; *Palaeontographica*, v. 125 (B), p. 1-64.
- Piel, K.M.
1971: Palynology of Oligocene sediments from central British Columbia; *Canadian Journal of Botany*, v. 49, p. 1885-1920.
- Price, L.L., McNeil D.H., and Ioannides, N.S.
Revision of the Tertiary Reindeer Formation in the Caribou Hills, District of Mackenzie. (in preparation)
- Rouse, G.E.
1977: Paleogene palynomorph ranges in western and northern Canada; *Palynology, Contribution Series no. 5A*; v. 1, *Cenozoic Palynology*, p. 48-65.
- Rouse, G.E., and Srivastava, S.K.
1972: Palynological zonation of Cretaceous and Early Tertiary rocks of the Bonnet Plume Formation, northwestern Yukon, Canada; *Canadian Journal of Earth Sciences*, v. 9, no. 9, p. 1163-1179.
- Srivastava, S.K.
1975: Maastrichtian microspore assemblages from the interbasaltic lignites of Mull, Scotland; *Palaeontographica*, v. 150 (B), p. 125-156.
- Staplin, F.L., ed.
1976: Tertiary biostratigraphy, Mackenzie Delta region, Canada; *Bulletin Canadian Petroleum Geology*, v. 24, no. 1, p. 117-136.
- Stover, L.E. and Evitt, W.R.
1978: Analyses of pre-Pleistocene organic-walled dinoflagellates; *Stanford University Publications, Geological Sciences*, v. 15, p. 1-300.
- Sweet, A.R.
1978: Palynology of the Ravenscrag and Frenchman Formations; in *Coal Resources of Southern Saskatchewan: A model for Evaluation Methodology*, Prepared by J.A. Irvine, S.H. Whitaker, and P.L. Broughton; *Geological Survey of Canada, Economic Geology Report 30*, p. 29-39.
- Wilson, G.J.
1967: Some species of **Wetzeliella** Eisenack (Dinophyceae) from New Zealand Eocene and Paleocene strata; *New Zealand Journal of Botany*, v. 5, no. 4, p. 469-497.
- Wodehouse, R.P.
1933: Tertiary pollen - II. The oil shales of the Eocene Green River Formation; *Torrey Botanical Club Bulletin*, v. 60, no. 7, p. 479-535.
- Wolfe, J.A. and Hopkins, D.M.
1967: Climatic changes recorded by Tertiary and land floras in northwestern North America; *Tertiary Correlations and Climatic Changes in the Pacific*, p. 67-76.
- Yorath, C.J., Balkwill, H.R. and Klassen, R.W.
1975: Franklin Bay and Malloch Hill map-areas, District of Mackenzie; *Geological Survey of Canada, Paper 74-36*, 35 p.
- Young, F.G.
1975: Upper Cretaceous stratigraphy, Yukon Coastal Plain and northwestern Mackenzie Delta; *Geological Survey of Canada, Bulletin 249*, p. 1-83.
- Young, F.G. and McNeil, D.H.
Cenozoic stratigraphy of the Mackenzie Delta; *Geological Survey of Canada*. (in preparation)
- Young, F.G., Myhr, D.W., and Yorath, C.J.
1976: Geology of the Beaufort-Mackenzie Basin; *Geological Survey of Canada, Paper 76-11*, 65 p.

Projects 750017, 680101 and 500029

Ulrich Mayr, T.T. Uyeno, R.S. Tipnis¹, and C.R. Barnes²
Institute of Sedimentary and Petroleum Geology, Calgary

Mayr, Ulrich, Uyeno, T.T., Tipnis, R.S., and Barnes, C.R.; *Subsurface Stratigraphy and Conodont Zonation of the Lower Paleozoic Succession, Arctic Platform, Southern Arctic Archipelago*; in *Current Research, Part A, Geological Survey of Canada, Paper 80-1A*, p. 209-215, 1980.

Abstract

Lower Paleozoic strata of the Arctic Platform penetrated by four wells located in the southern part of the Arctic Archipelago (Murphy Alminex Victoria Island F-36 on northwestern Victoria Island; Sun Panarctic Russell E-82 on Russell Island; KMG Decalta Young Bay F-62 on east-central Prince of Wales Island; and Panarctic Deminex Garnier 0-21 on northeastern Somerset Island), range in age from Middle Cambrian to Early Devonian. For ease in discussion, the formations included in this study are grouped into four sequences (in ascending order): 1) pre-Allen Bay (conodonts ranging from late Tremadocian, Fauna C of Ethington and Clark, 1971, to Late Ordovician in age); 2) Allen Bay and Cape Storm formations (late Llandoveryan, *celloni* Zone, to Ludlovian); 3) Read Bay - Drake Bay - Peel Sound complex (Ludlovian, *ploeckensis* Zone, to Pragian, *sulcatus* Zone); and 4) Eids Formation (Zlichovian-Dalejan, *inversus* Zone). A major unconformity is present below the Allen Bay Formation.

Introduction

The present report correlates the stratigraphical sequences of four wells that penetrate the lower Paleozoic succession of the Arctic Platform. The wells, which are located on northwestern Victoria Island, Russell Island, east-central Prince of Wales Island, and northeastern Somerset Island, are:

- 1) Murphy Alminex Victoria Island F-36 (72°45'18"N, 117°11'13"W);
- 2) Sun Panarctic Russell E-82 (73°51'29"N, 98°56'49"W);
- 3) KMG Decalta Young Bay F-62 (72°41'23"N, 96°49'34"W); and
- 4) Panarctic Deminex Garnier 0-21 (73°40'52"N, 90°36'45"W).

The geographic locations of these wells are shown on Figure 32.1. The stratigraphy of two of these wells, Russell E-82 and Garnier 0-21, has been described earlier (Mayr, 1978) and some alternate nomenclature and revision of the earlier stratigraphic scheme are proposed here. Discussion of correlation is by Mayr, and biostratigraphic studies of Siluro-Devonian conodonts are by Uyeno, and of Ordovician conodonts by Tipnis and Barnes.

Stratigraphy and Conodont Biostratigraphy

The Phanerozoic succession encountered in the wells ranges in age from Cambrian to Devonian (Fig. 32.1, Table 32.1), and some of the more biostratigraphically significant conodonts from this succession are illustrated on Plate 32.1. For convenience of discussion the succession is divided into four stratigraphic sequences. The lowermost sequence of this succession consists of Cambrian and Ordovician formations which are overlain disconformably by the Allen Bay Formation. The second sequence, of latest Ordovician to Late Silurian age, contains the Allen Bay and Cape Storm formations. It is overlain gradationally by the Read Bay-Drake Bay-Peel Sound complex of formations, which, in contrast to the uniform lithologies of the underlying strata, exhibit intricate facies changes. The formations of this sequence are of Late Silurian and Early Devonian age. The uppermost sequence is represented by the Lower Devonian Eids Formation which overlies disconformably the Read Bay Formation.

Pre-Allen Bay Sequence

This sequence consists of massive, pure carbonate rocks deposited in a normal marine, subtidal environment alternating with carbonate rocks that contain relatively large amounts of terrigenous material and were deposited in a restricted, highly saline environment. The Cape Clay, Eleanor River, Thumb Mountain and Irene Bay formations belong to the first group, whereas the Cass Fjord Formation, the unnamed carbonates and the Bay Fiord Formation comprise the second group of restricted origin. The Garnier well allows the comparison of the various sets of stratigraphic nomenclature. Previously, the nomenclature derived from the Franklinian Geosyncline and from Baffin Island were used to designate the formations (Mayr, 1978). In the present work, nomenclature from the edge of the Arctic Platform, as used by Christie (1967, 1977), is applied.

The position of the lower boundary of the Cape Clay Formation in the Young Bay well is tentative. It may be picked higher, at 1185.7 m (3890 ft) rather than at 1246.3 m (4089 ft), as depicted on Figure 32.1. The lower position is preferable because this allows the placement of sandy carbonates within the upper, rather than middle, part of the Cass Fjord Formation; comparable sandy carbonates are known to occur in similar stratigraphic position on Devon Island (Christie, 1977). Equally tentative is the lower boundary of the Cass Fjord Formation. In the present study the formation has been extended to the base of the Phanerozoic succession and lies unconformably on the Precambrian Aston Formation. The dolomite below the 1291.1 m (4236 ft) level, however, may be correlative with the lower part of the Bear Point Formation on eastern Devon Island.

The unnamed Ordovician carbonate strata are nonevaporitic equivalents of the Baumann Fiord Formation, and were incorrectly correlated with the Eleanor River Formation by Mayr (1978).

The contact between the Thumb Mountain and Bay Fiord formations is disconformable. This possibility was suggested earlier by Mayr (1978) and subsequent field work on Devon Island (Mayr and Thorsteinsson, unpublished information) confirmed the existence of a disconformity between the Thumb Mountain and Bay Fiord formations on the eastern part of the island.

¹ Visiting Post-Doctoral Fellow

² University of Waterloo, Waterloo, Ontario

Table 32.1

Stratigraphic nomenclature and ages of the lower Paleozoic succession of the Arctic Platform encountered in four wells.

Age		Murphy Alminex et al Victoria Isl. F-36	Sun Panarctic Russell E-82	KMG Decalta Young Bay F-62	Panarctic Deminex Garnier O-21
Devonian	Early	Dalejan	Eids (part)		
		Zlichovian			
		Pragian			
		Lochkovian		upper mbr.	Peel Sound
Silurian	Late	Pridolian	Read Bay C ?	lower mbr.	
		Ludlovian	Read Bay B ?	B	Read Bay (undivided)
			Read Bay A ?	A	
			Cape Storm	Cape Storm	Cape Storm
Mid.	Wenlockian				
E.	Llandoveryan	Allen Bay	Allen Bay	Allen Bay	
Ordovician	Late	Ashgillian			Irene Bay
		Caradocian			Thumb Mountain
	Middle	Llandeillian	Bay Fjord		Bay Fjord
		Llanvirnian			Eleanor River
		Arenigian			unnamed carbonates
	Early	Tremadocian			Cape Clay
					Cape Clay
Cambrian	F.			Cass Fjord	
	Mid. f.			(may include lower Bear Point Fmn.)	
	E.				
Precambrian				Aston (part)	

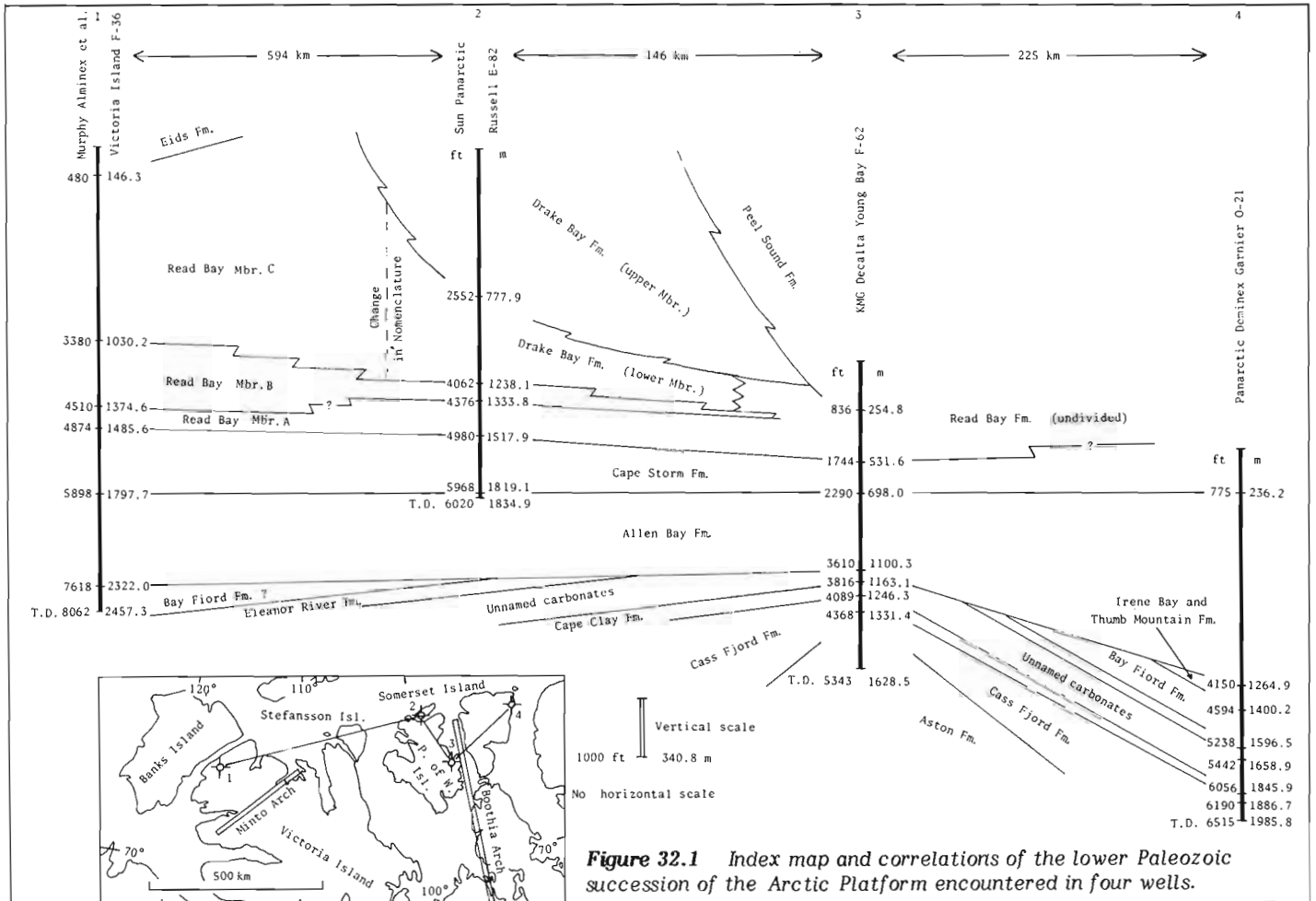


Figure 32.1 Index map and correlations of the lower Paleozoic succession of the Arctic Platform encountered in four wells.

Correlation of the rocks underlying the Allen Bay Formation in the Victoria Island well is uncertain; they contain anhydrite and shale, and thus belong to one of the formations of restricted origin. Sandy strata, which are characteristic of the Cass Fjord Formation and the unnamed carbonate rocks in the east, were not reported and consequently the Victoria Island strata are tentatively assigned to the Bay Fiord Formation.

The oldest conodont fauna in this study was derived from the Cape Clay Formation, in the interval 1847.1-1865.4 m (6060-6120 ft) of the Garnier well. The fauna includes the new genus of Repetski and Ethington (1977), and "*Acontiodus*" cf. "*A.*" *staufferi* Furnish. The new genus, as presently understood, is known to be restricted to Fauna C of Ethington and Clark (1971). Fauna C, of late Tremadocian age, has also been found in the uppermost Copes Bay Formation on Grinnell Peninsula on Devon Island.

The overlying unnamed carbonates yielded conodonts in the interval 1127.8-1158.2 m (3700-3800 ft) of the Young Bay well. Among the conodonts are "*Acodus*" *oneotensis* Furnish, *A.* cf. *A. brevis* Branson and Mehl sensu Lindström (in Ziegler, 1977), "*Drepanodus*" *parallelus* Branson and Mehl, "*Scolopodus*" *gracilis* Ethington and Clark, and cf. "*S.*" *quadruplicatus* Branson and Mehl. "*Acodus*" *brevis* and "*Scolopodus*" *quadruplicatus* are common constituents of Fauna D of Ethington and Clark (1971). This fact, together with the general affinities of the accompanying conodonts, suggests a post-Tremadocian Early Ordovician age (i.e., late, but not latest, Canadian). Elements similar to "*Acodus*" *oneotensis* are known to occur in post-Tremadocian age rocks (Lindström in Ziegler, 1977, p. 429-431).

A single sample from the Bay Fiord Formation, in the interval 2435.4-2450.6 m (7990-8040 ft) of the Victoria Island well failed to yield any conodonts.

The interval 1396.6-1400.3 m (4582-4592 ft) in the Garnier well contained, among other species, *Appalachinathus delicatulus* Bergström et al., *Belodella* n. sp. and *Polyplacognathus ramosus* Stauffer. Both the belodelliform and oistodiform elements of *Belodella* n. sp. are close to, but probably not identical with, those of *Belodella jemtlandica* Löfgren (Löfgren, 1978). The age of the fauna is late Chazy to mid-Barneveld (early Caradocian), representing Faunas 6-7 of Sweet et al. (1971).

The youngest collection from the pre-Allen Bay sequence was obtained from an interval regarded as ranging from Irene Bay Formation to the lowermost part of the Allen Bay Formation. This occurs in the Garnier well, in the interval 1249.7-1280.2 m (4100-4200 ft), and the fauna consists of *Panderodus* cf. *P. panderi* (Stauffer). The probable age of the interval is late Middle to Late Ordovician.

Allen Bay and Cape Storm Formations

The Ordovician formations discussed are overlain disconformably by Late Ordovician-Early Silurian age dolomites of the Allen Bay Formation. The existence of an unconformity at the base of the Allen Bay Formation has been demonstrated on the east side of the Boothia Arch by Miall and Kerr (in press). In the Victoria Island, Russell, and Young Bay wells the contact between the Allen Bay Formation and overlying silty dolomites of the Cape Storm Formation is sharp and probably disconformable. If this interpretation is correct, the nature of the contact could reflect the first pulse of the Cornwallis Disturbance (Kerr, 1977). In the Garnier well the contact is gradational.

The Allen Bay Formation was sampled at eight intervals in three wells: Victoria Island, Young Bay and Garnier. Of these intervals, only two, both from the Garnier well, yielded conodonts other than *Panderodus* spp. The first is interval 664.5-670.6 m (2180-2200 ft) with a peculiar greilingiform element that is closely similar to the Sb element of *Ozarkodina plana* (Walliser). The second is from 295.7-313.9 m (970-1030 ft), that yielded a slightly asymmetrical trichonodelliform element similar to the Sa element of *Oulodus jeannae* Schönlaub. Both taxa were previously reported from the Western Karawanken Alps in Austria, where they occur in the *celloni* Zone of Llandovery age (Sweet and Schönlaub, 1975, p. 49-53).

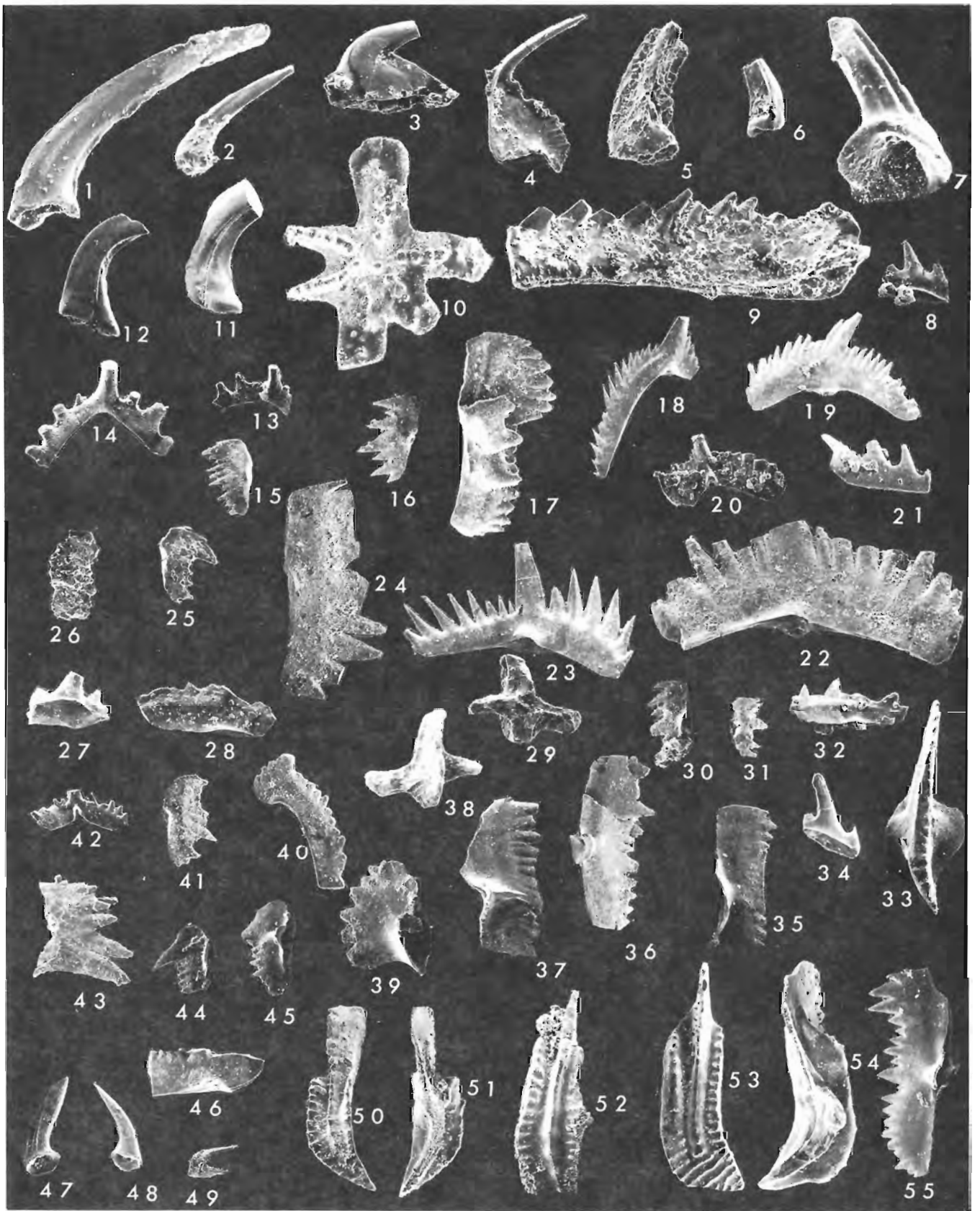
The overlying Cape Storm Formation was sampled at four intervals in three wells: Garnier, Young Bay and Victoria Island. The interval 73.2-82.3 m (240-270 ft) in the Garnier well did not yield any conodonts. The collection from the interval 566.9-597.4 m (1860-1960 ft) of the Young Bay well includes *Ozarkodina* n. sp. B of Klapper and Murphy (1975) and Apparatus B of Uyeno (in press). Both have been found previously in the Dourou Formation and its lateral equivalent, member A of the Read Bay Formation, with the former occurring on Cornwallis and Prince of Wales islands, and Boothia Peninsula, and the latter on Boothia Peninsula only (Uyeno, 1977, in press). These conodonts are assignable to the *siluricus* Zone of Ludlovian age.

The Cape Storm Formation was sampled in the intervals 1630.7-1661.2 m (5350-5450 ft) and 1524.0-1554.5 m (5000-5100 ft) of the Victoria Island well. The lower interval yielded a single fragmentary Pa element that can be referred to only as *Ozarkodina* cf. *O. confluens* (Branson and Mehl). The fauna from the higher interval includes *O. confluens* gamma morphotype of Klapper and Murphy (1975), and the peculiar spathognathodontan element that has been referred previously to *O.* cf. *O.* n. sp. B of Klapper and Murphy (1975). Its known occurrences are the upper part of the Cape Storm Formation at Goodsir Creek, eastern Cornwallis Island (Uyeno, 1977) and near the top of the Allen Bay/Read Bay carbonate unit in the Panarctic ARCO et al. Blue Fiord E46 well on Bjorne Peninsula, Ellesmere Island (Mayr et al., 1978). The age of the fauna from the higher interval is regarded as Ludlovian.

Read Bay-Drake Bay-Peel Sound Complex

The lithology of these partly correlative formations documents the rise of the Boothia Arch during Late Silurian and Early Devonian time. The formations grade from the offshore marine carbonates of member C of the Read Bay Formation, through the nearshore carbonates of the upper member of the Drake Bay Formation, into the nonmarine sandstones of the Peel Sound Formation. The dolomite of the lower member of the Drake Bay Formation is similar to that of the Read Bay member C in the Victoria Island well and the separation of the two units is a matter of stratigraphic convenience, as indicated by a vertical dashed line of Figure 32.1. Mayr (1978) assigned the interval 1238.1-1333.8 m (4062-4376 ft) in the Russell well to member A of the Read Bay Formation, but recent field evidence from Devon Island (Mayr and Thorsteinsson, unpublished information) suggests that this unit in fact is correlative with member B. The three members of the Read Bay Formation in the Victoria Island well may be broadly correlative with units 11a, 11b and 11c of the Read Bay Group (Thorsteinsson and Tozer, 1962) on Stefansson Island. Member B thickens westward, but it is not known which parts of the carbonate units are replaced by shale.

- Figures 1-7, 9, 10 are x60, remainder are x50. All figures are lateral views unless otherwise noted. Refer to Figure 32.1 for stratigraphic assignment.
- Figures 1, 2, 5, 7, 8, 16-24, 27, 36, 40, 43, 46-48. From the KMG Decalta Young Bay F-62 well, east-central Prince of Wales Island, GSC loc. C-83486.
- Figure 1. "*Drepanodus*" *parallelus* Branson and Mehl. GSC 62966 (1127.8-1158.2 m, 3700-3800 ft).
- Figure 2. "*Scolopodus*" *gracilis* Ethington and Clark. GSC 62967 (1127.8-1158.2 m, 3700-3800 ft).
- Figure 5. "*Acodus*" *oneotensis* Furnish. GSC 62968 (1127.8-1158.2 m, 3700-3800 ft).
- Figure 7. cf. "*Scolopodus*" *quadruplicatus* Branson and Mehl. GSC 62969 (1127.8-1158.2 m, 3700-3800 ft).
- Figures 8, 21, 27. Apparatus B of Uyeno (in press). 8, 21, GSC 62970 and 62971 (566.9-597.4 m, 1860-1960 ft); 27, GSC 62972 (487.7-518.2 m, 1600-1700 ft).
- Figures 17-20. *Ozarkodina* n. sp. B of Klapper and Murphy (1975). Pa, M, Pb and Sa elements, GSC 62973-62976, respectively (566.9-597.4 m, 1860-1960 ft).
- Figures 16, 22-24, 36. *Ozarkodina confluens* (Branson and Mehl). 16, 23, 24, Pa, Pb and Pa elements, GSC 62977-62979, respectively (487.7-518.2 m, 1600-1700 ft); 22, 36, Pb and Pa elements, GSC 62980 and 62981 (274.3-304.8 m, 900-1000 ft).
- Figures 40, 46. *Ozarkodina?* sp. M and Pa elements, GSC 62982 and 62983 (182.9-213.4 m, 600-700 ft).
- Figures 43, 47, 48. *Pelekysgnathus* n. sp. C of Uyeno (in press). I, M₂ and M₂ elements, GSC 62984-62986, respectively (182.9-213.4 m, 600-700 ft).
- Figures 3, 4, 6, 9-14. From the Panarctic Deminex Garnier 0-21 well, north-eastern Somerset Island, GSC loc. C-30875.
- Figures 3, 4. *Belodella* n. sp. Oistodiform and belodelliform elements, GSC 62987 and 62988, respectively (1396.6-1400.3 m, 4582-4594 ft).
- Figure 6. New genus of Repetski and Ethington (1977). GSC 62989 (1396.6-1400.3 m, 4582-4594 ft).
- Figure 10. *Polyplacognathus ramosus* Stauffer. Upper view of amorphognathiform element, GSC 62991 (1396.6-1400.3 m, 4582-4594 ft).
- Figure 11, 12. *Panderodus* cf. *P. panderi* (Stauffer). GSC 62992 and 62993 (1249.7-1280.2 m, 4100-4200 ft).
- Figure 13. ?*Ozarkodina plana* (Walliser). Sb element, GSC 62994 (664.5-670.6 m, 2180-2200 ft).
- Figure 14. ?*Oulodus jeanae* Schönlaub. Sa element, GSC 62995 (295.7-313.9 m, 970-1030 ft).
- Figures 15, 25, 26, 28, 29, 38, 41, 42. From the Murphy Alminex Victoria Island F-36 well, northwestern Victoria Island, GSC loc. C-39595.
- Figure 15, 25. *Ozarkodina confluens* (Branson and Mehl), gamma morphotype of Klapper and Murphy (1975). Pa elements, GSC 62996 and 62997 (1524.0-1554.5 m, 5000-5100 ft).
- Figure 26. *Ozarkodina* cf. O. n. sp. B of Klapper and Murphy (1975). Pa element, GSC 62998 (1524.0-1554.5 m, 5000-5100 ft).
- Figure 28. *Ozarkodina excavata excavata* (Branson and Mehl). Pa element. GSC 62999 (1402.1-1432.6 m, 4600-4700 ft).
- Figure 29, 38. Cruciform element, GSC 63000 (1402.1-1432.6 m, 4600-4700 ft).
- Figures 41, 42. *Ozarkodina confluens* (Branson and Mehl). Pa and Sb elements, GSC 63001 and 63002 (1402.1-1432.6 m, 4600-4700 ft).
- Figures 30-32, 34, 37. From the Sun Panarctic Russell E-82 well, Russell Island, GSC loc. C-30870.
- Figure 32. *Ozarkodina excavata excavata* (Branson and Mehl). Pa element, GSC 63003 (1402.1-1426.5 m, 4600-4680 ft).
- Figure 34. Apparatus B of Uyeno (in press). GSC 63004 (1402.1-1426.5 m, 4600-4680 ft).
- Figure 37. *Kockelella variabilis* Walliser. Pa element, GSC 63005 (1310.6-1328.9 m, 4300-4360 ft).
- Figure 30. *Ozarkodina remscheidensis?* (Ziegler). Pa element, GSC 63006 (707.1-719.3 m, 2320-2360 ft).
- Figure 31. *Ozarkodina remscheidensis remscheidensis* (Ziegler). Pa element, GSC 63007 (585.2-621.8 m, 1920-2040 ft).
- Figures 33, 35, 39, 44, 45. From Drake Bay Formation, upper member, from an outcrop located about 10 km west of the Russell E-82 well site, Russell Island, GSC loc. C-82456.
- Figures 33, 35. *Eognathodus sulcatus sulcatus* Philip. Upper and lateral views of two Pa elements, GSC 63008 and 63009.
- Figure 39. *Pelekysgnathus* n. sp. C of Uyeno (in press). I element, GSC 63010.
- Figures 44, 45. *Pandorinellina* sp. or *Ozarkodina* sp. Pa elements, GSC 63011 and 63012.
- Figures 49-52. From Eids Formation, from an outcrop located about 24 km west-southwest of the Victoria Island F-36 well site, Victoria Island, GSC locs. C-30547 and C-30548.
- Figure 49. ?*Pandorinellina expansa* Uyeno and Mason. Pb element, GSC 63013.
- Figure 50, 51. *Polygnathus* sp. Upper and lower views of a Pa element, GSC 63014.
- Figure 52. ?*Polygnathus costatus* Klapper. Upper view of a Pa element, GSC 63015.
- Figures 53-55. From Blue Fiord Formation, from an outcrop on the larger of the Princess Royal Islands, located about 32 km west of the Victoria Island F-36 well site, Victoria Island, GSC locs. C 30544 and C-30545.
- Figure 53, 54. *Polygnathus inversus* Klapper and Johnson. Upper and lower views of a Pa element, GSC 63016.
- Figure 55. *Pandorinellina* sp. Pa element, GSC 63017.



The Read Bay Formation is divided in the Young Bay well, and was sampled for conodonts in three intervals: 487.7-518.2 m (1600-1700 ft), 347.5-378.0 m (1140-1240 ft) and 274.3-304.8 m (900-1000 ft). The lowermost of these intervals yielded *Ozarkodina confluens* and Apparatus B of Uyeno (in press); the middle, *Ozarkodina* n. sp. B; and the highest, *Pelekysgnathus* n. sp. C of Uyeno (in press) and *O. confluens* alpha morphotype of Klapper and Murphy (1975). As discussed previously in this paper, the age of the lowest and middle faunas can be regarded as Ludlovian, whereas the highest fauna may be as young as Pridolian. *Pelekysgnathus* n. sp. C has been found previously in the lower part of the Peel Sound Formation on eastern Prince of Wales Island (Uyeno, in press).

Conodonts of member A of the Read Bay Formation were obtained from the Victoria Island and Russell wells. In the latter, *Ozarkodina* n. sp. B was found in the interval 1432.6-1456.9 m (4700-4780 ft), *Ozarkodina excavata excavata* (Branson and Mehl), Apparatus B, and *Ancoradella ploeckensis* Walliser at 1402.1-1426.5 m (4600-4680 ft), and *Ozarkodina excavata* at 1380.7-1399.0 m (4530-4590 ft). The Ludlovian age of *O. n. sp. B* has been discussed previously. The presence of *A. ploeckensis*, below the first occurrence of *Polygnathoides siluricus* Branson and Mehl, indicates the *ploeckensis* Zone of mid-Ludlovian age. In the Victoria Island well, member A was sampled in the intervals 1402.1-1432.6 m (4600-4700 ft) and 1377.7-1392.9 m (4520-4570 ft). In the lower interval, *Ozarkodina excavata excavata* and *O. confluens* were recovered, as well as a peculiar cruciform element, of undetermined taxonomic assignment. Only *O. confluens* was obtained from the upper interval. The age of these faunas cannot be stated more precisely than as Late Silurian.

Kockellella variabilis Walliser was found in member B of the Read Bay Formation in the interval 1310.6-1328.9 m (4300-4360 ft) of the Russell well. The species has been found also in member B at its type section on Goodsir Creek, eastern Cornwallis Island (Uyeno, 1977), and in the upper part of the Douro Formation on Ellesmere Island (Uyeno, in press). The species is relatively long-ranging, but its upper limit is in the *siluricus* Zone (Walliser, 1964). In view of the occurrence of *ploeckensis* Zone conodonts in the underlying member A, this fauna is assigned to the *siluricus* Zone of late Ludlovian age. Member B in the Victoria Island well, in the interval 1280.2-1298.4 m (4200-4260 ft), yielded fragmentary specimens that can only be assigned to *Ozarkodina?* sp.

In the wells included in this study, member C of the Read Bay Formation only occurs in the Victoria Island well. Three samples were taken from it in this succession, but only the interval of 999.7-1033.3 m (3280-3390) yielded any conodonts and these are referable to *Ozarkodina confluens*. The fauna can only be dated as Late Silurian.

Only the upper member of the Drake Bay Formation was sampled for conodonts. In the Russell well, these conodonts are from the intervals 707.1-719.3 m (2320-2360 ft) and 658.4-688.8 m (2160-2260 ft), and are identifiable as *Ozarkodina remscheidensis?* (Ziegler). The highest interval, from 585.2-621.8 m (1920-2040 ft), yielded *O. remscheidensis remscheidensis*. The lowest and middle intervals, therefore, can only be dated as Pridolian-Lochkovian, whereas the highest is probably of Lochkovian age.

To supplement the data from the upper part of the Russell well, conodonts from the upper member of the Drake Bay Formation were obtained from an outcrop located some 10 km west of the well (GSC loc. C-82456). Mayr (1978, p. 52) estimated that the beds of this outcrop fall within the upper 30 m (100 ft) or so of the stratigraphic succession of the well. The conodonts include *Eognathodus sulcatus sulcatus* Philip, *Pelekysgnathus* n. sp. C of Uyeno (in press), and *Pandorinellina* sp. or *Ozarkodina* sp. As stated earlier, *Pelekysgnathus* n. sp. C has been found previously in the lower part of the Peel Sound Formation. In Nevada, the first-mentioned subspecies is restricted to the *sulcatus* Zone (Klapper, 1977, Fig. 3), but may range higher in the Arctic Island (Uyeno in McGregor and Uyeno, 1972, Table 1). The age of the fauna is Pragian.

In this study, the Peel Sound Formation was encountered only in the Young Bay well. There the formation was sampled at two intervals, the lower 182.9-213.4 m (600-700 ft) of which yielded *Pelekysgnathus* n. sp. C and *Ozarkodina?* sp. The age of the fauna cannot be stated unequivocally, but it is probably about Lochkovian to Pragian.

Eids Formation

The dolomites of the Read Bay Formation are overlain disconformably by a sequence of calcareous shales with minor limestones that is here assigned to the Eids Formation. This formation was found to occur only in the Victoria Island well. The same shale occurs in an isolated outcrop about 24 km west-southwest of the Victoria Island well-site (Thorsteinsson and Tozer, 1962), and was tentatively included in the Blue Fiord Formation. Miall (1976) assigned the shale to the Orksut Formation. Laterally equivalent limestones of the Blue Fiord Formation are present 32 km west of the well-site on Princess Royal Islands. The age of the disconformity between the Read Bay and Eids formations coincides with that of pulse 3 of the Cornwallis Disturbance (Kerr, 1977).

The Eids conodonts from the Victoria Island well were obtained from intervals 115.8-134.1 m (380-440 ft) and 61.0-91.4 m (200-300 ft). The specimens were small and fragmented, and only *Belodella* sp. was identified from the lower interval. Other constituents include pyritized radiolarians and sponge spicules. A.W. Norris (personal communication, September, 1979) identified *Nowakia* cf. *N. cancellata* (Richter) and *Styliolina* sp. from the interval 88.4-118.9 m (290-390 ft). The fauna was dated as Dalejan.

Because of the sparsity of the above data, supplementary materials were sought from outcrops located relatively close to the well-site. The first of these originated from the isolated outcrops of the Eids Formation mentioned above. These samples were collected by A.D. Miall (1976, p. 30; GSC locs. C-30547, C-30548). The Eids conodonts include a Pb element similar to those previously assigned to *Pandorinellina expansa* Uyeno and Mason. The polygnathan element is more difficult to identify; the development of the wide basal cavity is somewhat like that in *Polygnathus inversus* Klapper and Johnson, but the moderately large pit is located far more anteriorly. In some of these features this element approaches more closely to *P. n. sp. A* of Klapper and Johnson (1975). Another polygnathan element, which is badly fragmented, is somewhat similar to that of *Polygnathus costatus* Klapper; the critical free blade is missing, however, and a more precise assignment cannot be made. Based on this limited fauna, the age of the outcropping beds can only be regarded as probably Dalejan to Couvinian.

The second supplementary collection was derived from the Blue Fiord Formation which outcrops on the larger of the Princess Royal Islands. The collecting was done by A.D. Miall (GSC loc. C-30544, C-30545). The conodonts from these beds include **Polygnathus inversus** and a spathognathodontan element that is superficially similar to that of **Pandorinellina optima** (Moskalenko). The fauna can be assigned to the **inversus** Zone, which spans the Zlichovian-Dalejan boundary (Klapper and Ziegler, 1979, Text-fig. 2).

References

- Christie, R.L.
 1967: Bache Peninsula, Ellesmere Island, Arctic Archipelago; Geological Survey of Canada, Memoir 347.
 1977: Stratigraphic reconnaissance of lower Paleozoic rocks, eastern Devon Island, Arctic Archipelago; in Report of Activities, Part B, Geological Survey of Canada, Paper 77-1B, p. 217-225.
- Ethington, R.L. and Clark, D.L.
 1971: Lower Ordovician conodonts in North America; in Symposium on Conodont Biostratigraphy, W.C. Sweet and S.M. Bergström, ed., Geological Society of America, Memoir 127, p. 63-82 [imprint 1970].
- Kerr, J.Wm.
 1977: Cornwallis fold belt and the mechanism of basement uplift; Canadian Journal of Earth Sciences, v. 14, p. 1374-1401.
- Klapper, G. (with contributions by D.B. Johnson)
 1977: Lower and Middle Devonian conodont sequence in central Nevada; in Western North America: Devonian, M.A. Murphy et al., ed.; California University, Riverside, Campus Museum Contribution no. 4, p. 33-54.
- Klapper, G. and Johnson, D.B.—
 1975: Sequence in conodont genus **Polygnathus** in Lower Devonian at Lone Mountain, Nevada; *Geologica et Palaeontologica*, v. 9, p. 65-83.
- Klapper, G. and Murphy, M.A.
 1975: Silurian-Lower Devonian conodont sequence in the Roberts Mountains Formation of central Nevada; University of California Publications in Geological Sciences, v. 111 [imprint 1974].
- Klapper, G. and Ziegler, W.
 1979: Devonian conodont biostratigraphy; in The Devonian System, M.R. House et al., ed.; Special Papers in Palaeontology, no. 23, p. 199-224.
- Löfgren, A.
 1978: Arenigian and Llanvirnian conodonts from Jämtland, northern Sweden; *Fossils and Strata*, no. 13.
- Mayr, U.
 1978: Stratigraphy and correlation of lower Paleozoic formations, subsurface of Cornwallis, Devon, Somerset and Russell Islands, Canadian Arctic Archipelago; Geological Survey of Canada, Bulletin 276.
- Mayr, U., Uyeno, T.T. and Barnes, C.R.
 1978: Subsurface stratigraphy, conodont zonation and organic metamorphism of the Lower Paleozoic succession, Bjorne Peninsula, Ellesmere Island, District of Franklin, in Current Research, Part A, Geological Survey of Canada, Paper 78-1A, p. 393-398.
- McGregor, D.C. and Uyeno, T.T.
 1972: Devonian spores and conodonts of Melville and Bathurst Islands, District of Franklin; Geological Survey of Canada, Paper 71-13.
- Miall, A.D.
 1976: Proterozoic and Paleozoic geology of Banks Island, Arctic Canada; Geological Survey of Canada, Bulletin 258.
- Miall, A.D. and Kerr, J.Wm.
 Cambrian to Upper Silurian stratigraphy, Somerset Island and north-eastern Boothia Peninsula, District of Franklin, N.W.T.; Geological Survey of Canada, Bulletin 315 (in press).
- Repetski, J.E. and Ethington, R.L.
 1977: Conodonts from graptolite facies in the Ouachita Mountains, Arkansas and Oklahoma; in Symposium on the Geology of the Ouachita Mountains, Arkansas Geological Commission, v. 1, p. 92-106.
- Sweet, W.C., Ethington, R.L. and Barnes, C.R.
 1971: North American Middle and Upper Ordovician conodont faunas; in Symposium on Conodont Biostratigraphy, W.C. Sweet, and S.M. Bergström, ed.; Geological Society of America, Memoir 127, p. 163-193 [imprint 1970].
- Sweet, W.C. and Schönlaub, H.P.
 1975: Conodonts of the genus **Oulodus** Branson and Mehl, 1933; *Geologica et Palaeontologica*, v. 9, p. 41-59.
- Thorsteinsson, R. and Tozer, E.T.
 1962: Banks, Victoria and Stefansson Islands, Arctic Archipelago; Geological Survey of Canada, Memoir 330.
- Uyeno, T.T.
 1977: Summary of conodont biostratigraphy of the Read Bay Formation at its type sections and adjacent areas, eastern Cornwallis Island, District of Franklin; in Report of Activities, Part B, Geological Survey of Canada, Paper 77-1B, p. 211-216.
 The conodonts of Upper Silurian and Lower Devonian rocks in central parts of the Canadian Arctic Archipelago and Boothia Peninsula; Geological Survey of Canada, Bulletin 292, Part 2 (in press).
- Walliser, O.H.
 1964: Conodonten des Silurs; *Abhandlungen des Hessischen Landesamtes für Bodenforschung*, Heft 41.
- Ziegler, W. (ed.)
 1977: Catalogue of Conodonts; E. Schweizerbart'sche Verlagsbuchhandlung, Stuttgart, v. 3.

H. Williams¹ and S.C. Godfrey¹
Precambrian Geology Division

Williams, H. and Godfrey, S.C., *Geology of Stephenville map area, Newfoundland*; in *Current Research, Part A, Geological Survey of Canada, Paper 80-1A*, p. 217-221, 1980.

Abstract

Rocks of the map area consist of an autochthonous Cambrian-Ordovician carbonate sequence overlain structurally by a variety of transported rocks of the Humber Arm Allochthon. Lower structural slices of the allochthon consist of sedimentary rocks and include the Summerside, Irishtown and Cooks Brook formations of mainly Cambrian age in the east, and chaotic sedimentary rocks and Lower Ordovician Blow Me Down Brook greywackes in the west. A wide zone of chaotic sedimentary rocks with huge volcanic blocks can be traced across the map area and it is continuous northward with the Companion Mélange. The highest structural slices of the allochthon consist of ophiolitic assemblages, some interpreted as pristine oceanic crust and others as oceanic crust that was deformed and metamorphosed at an oceanic fracture zone.

Carbonate slivers within the assembled allochthon are interpreted as parautochthonous shelf carbonates incorporated among farther-travelled rocks during their final emplacement.

Introduction

The Serpentine (12 B/16) and Shag Island (12 B/15 E) areas were mapped in 1979 as part of the program to remap the Stephenville map area (12 B). Emphasis was placed on the distinction and delineation of autochthonous and allochthonous rocks, and subdivision of the sedimentary, volcanic and plutonic rocks that constitute the Humber Arm Allochthon. Most of the area was mapped in reconnaissance fashion by the first author. The second author mapped a corridor across the Humber Arm Allochthon from Serpentine Lake westward to the coast. The geology of the central part of the Lewis Hills is adapted from Karson (1979) and that of Lewis Brook and southward from Schillereff and Williams (1979). The following report summarizes the results of this work.

General Geology

The Serpentine and Shag Island map areas are underlain by an autochthonous sequence of mainly Lower to Middle Ordovician carbonate rocks. These are overlain by a variety of transported sedimentary and volcanic rocks of late Precambrian to Early Ordovician age, in turn overlain by the ophiolitic complexes in the highest structural slices of the Humber Arm Allochthon. The youngest group in the map area is the Middle Ordovician Long Point Group that forms Long Ledge (Fig. 33.1). These rocks were deposited after the emplacement of the Humber Arm Allochthon (Rodgers, 1965; Schillereff and Williams, 1979).

The eastern part of the area is a rugged heavily wooded upland, much of which is now accessible by a network of logging roads. The western part of the area is dominated by the barren highlands of Lewis Hills and Blow Me Down. Exposure is fair to poor in the wooded areas and good to excellent across the western barren highlands. Except for a few riverbed outcrops, there are no rocks exposed in the valley of Serpentine River.

The carbonate sequence is exposed in the southeastern part of the area and the rocks form two anticlinal structures farther west near Spruce Brook and Blue Hill. Similar carbonates form conspicuous slivers within the Humber Arm Allochthon at Serpentine Lake and Fox Island River. Transported sedimentary rocks underlie most of the eastern part of the area, the Serpentine River lowlands and the coastal lowlands between Serpentine River and Lewis Brook. Transported ophiolitic complexes constitute the highlands of Lewis Hills and Blow Me Down, as well as the highlands at Coal River Head.

For purposes of description, the rocks of the map area are subdivided into an autochthonous sequence (units 1 and 2, Fig. 33.1), transported sedimentary and volcanic rocks (units 3 to 7), transported ophiolitic complexes (units 8 to 17) and neautochthonous rocks (unit 18).

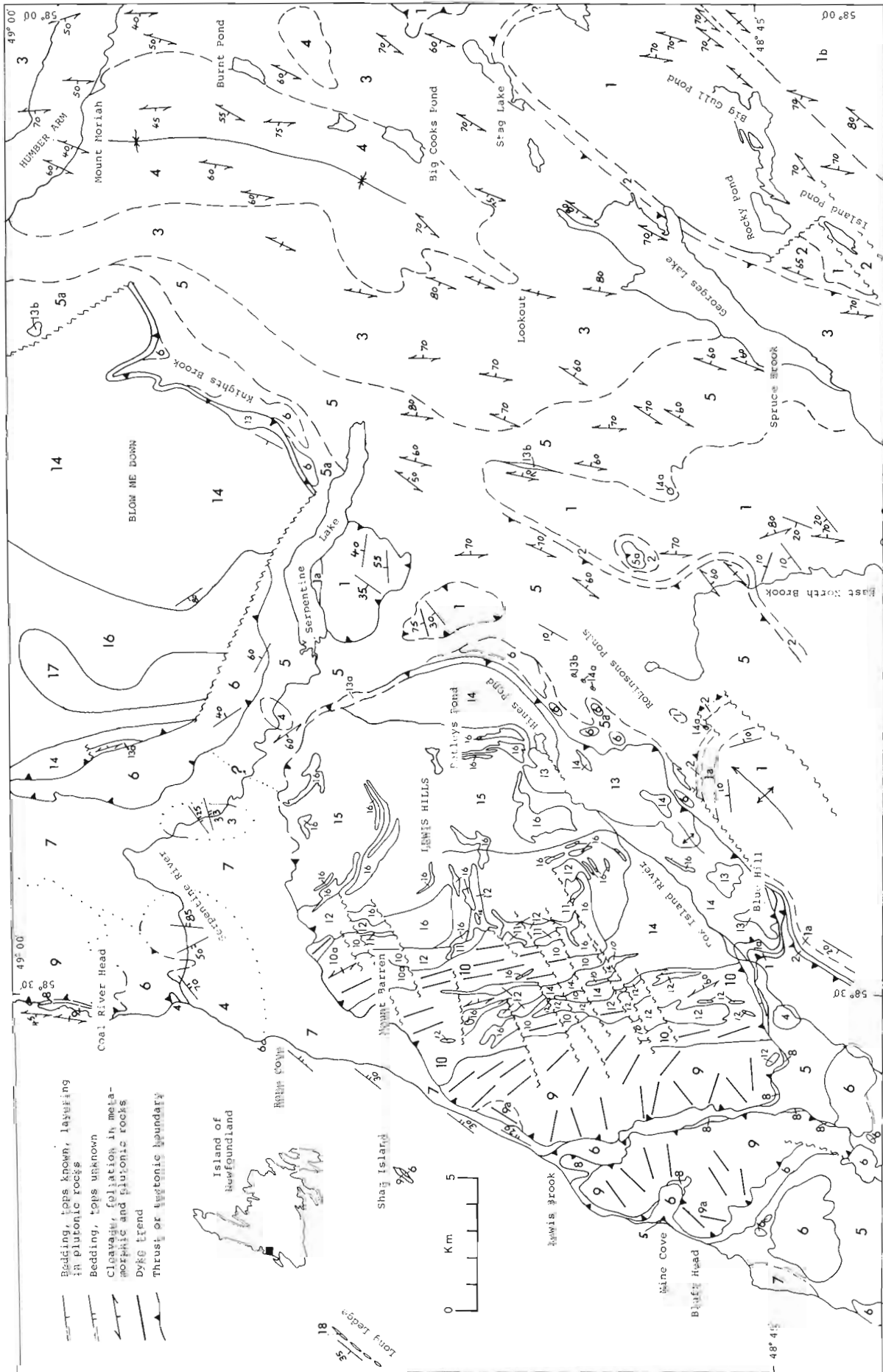
Autochthonous Rocks

Autochthonous rocks of the map area are mainly limestone and dolomite with thin shale units. They are assigned to the St. George Group (Late Cambrian to Early Ordovician; Kindle and Whittington, 1965) and the Table Head Formation (early Middle Ordovician), although fossils are rare, especially in easterly exposures. The St. George Group consists of medium to thick bedded grey limestone, dense white to grey and buff dolomitic limestone, dolomite, and minor shale and chert. The Table Head Formation consists of monotonous thick bedded grey mottled limestone that is overlain by limestone breccia and shales at its top. In the nearby Port au Port area, the limestone breccia and shale were assigned informally to the Caribou Brook formation (Schillereff and Williams, 1979).

Toward the west near Blue Hill and Robinsons Ponds, the distinction between the St. George Group (unit 1) and the Table Head Formation (unit 1a) is relatively clear; farther east the distinction is difficult because of structural complexity and increasing metamorphism. Carbonate rocks of both the St. George Group and Table Head Formation occur within the parautochthonous slivers at Serpentine Lake and Fox Island River. A single outcrop of limestone south of Robinsons Ponds may represent an anticlinal dome or a detached block in shale mélangé.

A section through the top of the autochthonous sequence and its contact with transported rocks (unit 5) is exposed with only a few gaps in East North Brook. Gently north-dipping Table Head limestone is followed upstream by limestone breccia and then grey shale. Across a narrow exposure gap, the autochthonous sequence is followed northward by chaotic black and green shales with limestone breccia blocks up to 3 m in diameter. A similar contact is poorly exposed in a river south of Robinsons Ponds. Farther south near Blue Hill, Table Head limestones are overlain by grey shale and the limestone breccia unit is missing. Limestone breccias occur locally at the top of the autochthonous sequence near Spruce Brook, although farther north the autochthonous limestone breccia and shale units are absent. East of Georges Lake, thin bedded steeply-dipping limestones are overlain directly by dark grey to black pyritic

¹Department of Geology, Memorial University of Newfoundland, St. John's, Newfoundland, A1B 3X5



- 2 Dark grey shale, siltstone and limestone breccia (west) and grey shale (east); Middle Ordovician
- 1 Limestone, dolomite, shale, Table Head Formation and St. George Group; Ordovician to Cambrian; Table Head Formation; 1b, crystalline limestone or marble

- 7 Greenwacke, dark grey shale and red shale; Blow Me Down Brook Formation; Early Ordovician
- 6 Red to purple and green pillow lava, massive lava, agglomerate, tuff and limestones; structural slices and blocks in melange
- 5 Chaotic sedimentary rocks, mainly dark shale with blocks of limestone, Blow Me Down Brook Formation and local serpentinite and amphibolite blocks; Cambrian to Early Ordovician blocks; 5a, zone of abundant volcanic blocks
- 4 Thin bedded limestone and shale with prominent limestone breccia units, Cooks Brook Formation; Middle Cambrian to Early Ordovician
- 3 Dark grey shale with thick white quartzite units, locally includes quartz pebble conglomerate units, mainly Irishtown Formation, minor Summerside Formation; late Precambrian to Middle Cambrian

- 17 Mafic sheeted dyke complex; Bay of Islands Complex (Upper Cambrian to Early Ordovician)
- 16 Mainly gabbroic rocks, includes wehrlite, clinopyroxenite, troctolite and feldspathic dunite as interlayers or megacrysts in dunite (15) of Lewis Hills Massif
- 15 Mainly serpentinized dunite with pyroxene-bearing units, feldspathic units and chromite-rich units
- 14 Mainly serpentinized harzburgite with dunitic units; 14a, blocks in sedimentary melange
- 13 Greenschist to amphibolite facies metamorphic rocks, basal aureole, mainly amphibolite of alabroic protolith; 13a, psammatic schist; 13b, amphibolite blocks in sedimentary melange

- 18 Fossiliferous limestone, Long Point Formation; Middle Ordovician (Casadean)

Figure 33.1. Geology of the Serpentine (12 B/16) and Shag Island (12 B/15E) map areas, western Newfoundland. Geology of Lewis Hills after Karson (1979) with slight modifications.

shales, whereas northeast of Stag Lake limestone breccia is again common. These local stratigraphic variations at the top of the autochthon are interpreted to reflect a rugged topography across a disturbed carbonate bank with the omission of parts of the section across positive areas.

Transported Sedimentary and Volcanic Rocks

Transported sedimentary rocks of the Humber Arm Supergroup (Stevens, 1970) underlie about one half of the map area. These range in age from late Precambrian to Early Ordovician and their stratigraphic sequence has been determined previously, viz. the Summerside, Irishtown, Cooks Brook, Middle Arm Point and Blow Me Down Brook formations (Lilly, 1967; Stevens, 1970; Williams, 1973). In general the oldest formations occur in the east with successively younger formations represented westward. In the east, the rocks are essentially intact, although tightly folded with penetrative cleavage. In the central part of the area along the southeast margins of Lewis Hills and Blow Me Down, the rocks are chaotic with large blocks surrounded by shale. Farther west along the coast, intact younger formations occur between Serpentine River and Lewis Brook, although folding is complex. Tremadocian graptolites and Upper Cambrian trilobites occur in the Cooks Brook shale and limestone south of Serpentine River (Kindle and Whittington, 1965) and similar graptolites occur at Rope Cove in black shale of Middle Arm Point type.

The contact between allochthonous and autochthonous rocks is defined with relative ease west of Spruce Brook where chaotic sedimentary rocks (unit 5) are easily separated from nearby autochthonous shale (unit 2). In the Georges Lake-Stag Lake area the contact is difficult to define because of the general similarity between grey shale at the top of the autochthon and transported shale of the Irishtown Formation. Intense deformation in this easterly area also serves to confuse rock relationships.

The transported sedimentary rocks exhibit significant lithic and structural variation across the map area. Most of the rocks in the east are grey shales with prominent white quartzite units (Irishtown) overlain by thin bedded shale-limestone and limestone breccias of the Cooks Brook Formation. A major synclinal axis is defined by the occurrence of the Cooks Brook Formation between Mount Moriah and the Lookout, flanked on both sides by the older Irishtown Formation.

Sedimentary rocks of the Humber Arm Supergroup in the central part of the area from Fox Island River to Knights Brook are chaotic and represent a major zone of disruption. Most of these rocks are grey, black and green shales with larger resistant blocks of greywacke, limestone breccia, volcanic rocks, and local serpentinite, gabbro and amphibolite blocks. Sedimentary blocks are dominant in the east and include the most easterly exposures of the Blow Me Down Brook Formation (unit 7). This zone is bounded westward by chaotic shales with numerous large volcanic blocks (unit 6) and local blocks derived from the ophiolite suite of rock units. A large serpentinite block, 5 km northwest of Spruce Brook (unit 14a), is host to the Bond asbestos prospect (Walthier, 1949) and other serpentinite and amphibolite blocks occur at the top of the autochthon nearby.

The chaotic zone (units 5, 5a), traceable northeastward across the map area, is continuous with the Companion Melange to the north. The same zone appears to continue all the way northward to Bonne Bay. Its extent and continuity implies a major disruption during the emplacement of the allochthon.

The order of sedimentary units from north to south along the coast between Serpentine River and Lewis Brook, i.e. Cooks Brook to Blow Me Down Brook formations,

suggests a stratigraphic sequence, and this is supported by the occurrence of graptolitic shales of Middle Arm Point type at Rope Cove. These rocks are complexly folded but lack penetrative cleavage, so that the folds are most likely emplacement structures.

Volcanic rocks (unit 6) are mainly pillow lavas and agglomerates with associated limestones that resemble the Skinner Cove Formation to the north of the map area (Williams, 1973). The volcanic rocks occur as boulders to discrete tabular masses several kilometres in diameter, surrounded or underlain by chaotic sedimentary rocks. The volcanic rocks along the southwest margin of the Blow Me Down massif form a distinct slice structurally above chaotic sediments (unit 5) and overlain by the Bay of Islands Complex. Similarly at Mine Cove, volcanic rocks (unit 6) overlie chaotic sediments (unit 5) and are in turn overlain by gabbro (unit 9) at Bluff Head. Between Blue Hill and Robinsons Ponds, a chaotic mixture of volcanic rocks and shale suddenly shows greenschist metamorphism and folded schistosity from east to west toward the Lewis Hills. The deformed rocks possibly grade westward into aureole rocks (unit 13) of the Bay of Islands Complex. In most places however there is a sharp contact and a clear metamorphic and structural contrast between aureole rocks (unit 13) and nearby sedimentary and volcanic rocks (units 5a, 6).

Transported Ophiolitic Complexes

Ophiolitic rocks of the Bay of Islands Complex (units 13-17) and possibly related assemblages (Mount Barren, Little Port, and Bluff Head, units 8 to 12) form the highest structural slices of the Humber Arm Allochthon.

All of the rocks of the Blow Me Down massif are assigned to the Bay of Islands Complex and these consist of a nearly complete ophiolite suite, from basal dynamothermal aureole (unit 13) to ultramafic rocks (unit 14), gabbro (unit 16) and sheeted dykes (unit 17). The order of rock units defines an open synclinal structure with the youngest dyke unit (unit 17) nestled in its axial zone. An apparent thinning of ultramafic and gabbroic units westward suggests structural complications or an original thinning of ophiolitic units from east to west. The aureole of the Bay of Islands Complex is mainly amphibolite of gabbroic protolith along the eastern flank of Blow Me Down. Toward the west, rocks depicted as aureole (unit 13a) are psammitic schists of greenschist metamorphic facies. Similar schists occur nearby on the south side of Serpentine River in the northernmost exposures of the Lewis Hills aureole.

Ophiolitic rocks of the Lewis Hills massif show significant variation with respect to those of Blow Me Down. The former were assigned to the Bay of Islands Complex (Cooper, 1936; Smith, 1958) but recent detailed mapping has distinguished three plutonic assemblages (Karson, 1979). From east to west these are the Bay of Islands, Mount Barren, and Bluff Head assemblages. Rocks assigned to the Bay of Islands Complex at Lewis Hills (Karson, 1979) resemble correlatives to the north at Blow Me Down, except for a greater abundance of dunitic rocks (unit 15) with gabbroic megalenses (unit 16) toward its top. A much wider aureole in the vicinity of Blue Hill and northeastward is interpreted as the result of folding and faulting of an initially thin unit.

The Mount Barren assemblage (Karson, 1979) occupies a steep zone of intensely deformed mainly gabbroic rocks, and includes an extensive lherzolitic megadyke that is less deformed and cuts the Bay of Islands Complex to the east. The Bluff Head assemblage (informal) to the west is gradational with the Mount Barren assemblage and consists mainly of gabbro. Correlation of the rocks at Bluff Head (unit 9) with the Little Port Complex (Williams, 1973) to the

north, and the continuity among all three assemblages in the Lewis Hills massif, is interpreted to provide an important genetic link between the Bay of Islands and Little Port Complexes that occur in separate structural slices elsewhere. The Bay of Islands Complex is interpreted as oceanic crust and mantle. The Bluff Head assemblage (Little Port correlative) is interpreted as oceanic crust that was deformed and metamorphosed in an oceanic fracture zone as it moved away from a spreading centre to be eventually juxtaposed with newer crust represented by the Bay of Islands Complex (Karson and Dewey, 1978; Karson, 1979). The interpretation is attractive as it explains the variations in metamorphic and structural style among the plutonic rocks of the Lewis Hills massif.

The Little Port Complex at Coal River Head consists of deformed gabbro and broken mafic dykes. It includes a conspicuous serpentinite mélangé zone (unit 8) that contains sedimentary lithologies and may represent an abortive dismemberment of this structural slice.

Serpentine and serpentinite mélangé are represented in most places at the base of the Bluff Head slice. These serpentinites are host to the Lewis Brook asbestos occurrence (Walthier, 1949) and abundant asbestos fibre occurs in the same setting north of Mine Cove.

Neoautochthonous Rocks

The Long Point Group constitutes the islands of Long Ledge, a continuation of the morphologic Long Point 10 km southwestward. Its fossiliferous limestone is of Caradocian age (Bergström et al., 1974) and its deposition is interpreted to postdate the arrival of the Humber Arm Allochthon (Rodgers, 1965).

Structural Geology

A regional foliation in ultramafic rocks of the Bay of Islands Complex and intricate deformation and metamorphism of the ophiolitic assemblages at Mount Barren are structures that are confined to the highest structural slices of the Humber Arm Allochthon. They record deformation within the oceanic tract and predate the first expulsion of the ophiolitic suites from their place of origin.

The formation of a dynamothermal aureole at the stratigraphic base of the Bay of Islands Complex records the earliest transport of hot ophiolitic material. After formation of the aureole, some of the ophiolitic rocks such as those that presently constitute Blow Me Down were folded into a broad syncline that was later truncated by the present horizontal tectonic base of the slice.

Sedimentary and volcanic rocks (units 3 to 7) do not exhibit pre-emplacement structures, but their chaotic co-mingling and discordant fold styles in sedimentary units are directly attributable to surficial processes of assembly and final emplacement.

Parautochthonous carbonate slivers at Serpentine Lake and Fox Island River structurally overlie chaotic sedimentary rocks and they are overlain or dip toward the higher ophiolitic slices. The carbonate rocks are therefore part of the assembled allochthon. Their presence among the farther travelled rocks of the allochthon implies that final assembly and the latest movements of the ophiolitic slices involved local stripping and detachment of upper parts of the autochthonous carbonate sequence. The common absence of carbonate breccia and shale units at the top of the autochthon implies considerable local relief across the disturbed carbonate shelf before emplacement of the allochthon, so that positive areas may have been kneaded and detached from their substrate to become incorporated in the allochthon.

A steeply-dipping northeast-trending cleavage that affects both transported and autochthonous rocks increases in intensity from west to east across the area. It is recognized in subhorizontal autochthonous sedimentary rocks as far west as Fox Island River, but it does not appear to affect transported sedimentary rocks in more westerly coastal exposures. Across the eastern part of the map area between Serpentine Lake and Stag Lake, the cleavage forms a fan with easterly dips in the west and westerly dips in the east. The steep axial zone of the cleavage fan is nearly coincident with the axis of the major syncline containing the Cooks Brook Formation, but this relationship may be fortuitous. The steep cleavage is superposed on local recumbent folds in the Cooks Brook Formation at Humber Arm, implying early recumbent structures related to emplacement and later post-emplacement upright folds with steep cleavage. A penetrative cleavage of the same orientation is axial planar to tight upright folds in easterly exposures of the metamorphosed carbonate terrane (unit 1b) in the southeast corner of the map area. The carbonate terrane and rocks farther east are the subject of a report by Kennedy (1980).

Economic Geology

The Stephenville area contains a large number of mineral deposits and prospects. These include gypsum, limestone, asbestos, chromite, magnetite, base metals, etc. A map that displays the known mineral occurrences within the Stephenville area has recently been released by the Newfoundland Department of Mines and Energy (Mercer and Andrews, 1979). It distinguishes the size and significance of the occurrences, from mere indications to present producers, and the legend lists the name, status and minerals present in each occurrence. The map is accompanied by a chronological precis of exploration activity and an assessment of mineral potential of the area.

Acknowledgments

The authors acknowledge the field assistance of Alex Pittman and Craig Wheeler, and the many hospitalities shown by our neighbours, the Mitchells of Pasadena and the Barnes' of Mount Moriah. We also express thanks to Bowaters Paper Company for the use of their private roads.

The first author acknowledges support of field work through EMR Research Agreement 2239-4-48/79 and N.S.E.R.C. Operating Grant A5548. The second author acknowledges financial support through a Memorial University of Newfoundland Fellowship.

References

- Bergström, S.M, Riva, J., and Kay, M.
1974: Significance of conodonts, graptolites, and shelly faunas from the Ordovician of western and north-central Newfoundland; *Canadian Journal of Earth Sciences*, v. 11, p. 1625-1660.
- Cooper, J.R.
1936: Geology of the southern half of the Bay of Islands igneous complex; Newfoundland Department of Natural Resources, Bulletin 4.
- Karson, J.A.
1979: Geological map and descriptive notes of Lewis Hills Massif, western Newfoundland; Geological Survey of Canada, Open File 628.

- Karson, J.A. and Dewey, J.F.
1978: Coastal complex, western Newfoundland: An Early Ordovician oceanic fracture zone; *Geological Society of America Bulletin*, v. 89, p. 1037-1049.
- Kennedy, D.P.
1980: Geology of the Corner Brook Lake area, western Newfoundland; in *Current Research, Part A*, Geological Survey of Canada, Paper 80-1A, report 36.
- Kindle, C.H. and Whittington, H.B.
1965: New Cambrian and Ordovician fossil localities in western Newfoundland; *Geological Society of America Bulletin*, v. 76, p. 683-688.
- Lilly, H.D.
1967: Some notes on stratigraphy and structural styles in central-west Newfoundland; in Neale, E.R.W. and Williams, H., (ed.), *Geology of the Atlantic Region*; Geological Association of Canada, Special Paper 4, p. 201-212.
- Mercer, N. and Andrews, K.
1979: Mineral occurrence map Stephenville Newfoundland; Mineral Development Division, Newfoundland Department Mines and Energy, Map 79-123.
- Rodgers, John
1965: Long Point and Clam Bank Formations, western Newfoundland; *Geological Association of Canada Proceedings*, v. 16, p. 83-101.
- Schillereff, S. and Williams, H.
1979: Geology of Stephenville map area, Newfoundland; in *Current Research, Part A*, Geological Survey of Canada, Paper 79-1A, p. 327-332.
- Smith, C.H.
1958: Bay of Islands igneous complex, western Newfoundland; Geological Survey of Canada, Memoir 290.
- Stevens, R.K.
1970: Cambro-Ordovician flysch sedimentation and tectonics in west Newfoundland and their possible bearing on a Proto-Atlantic Ocean; in *Flysch sedimentology in North America*, Lajoie, J. (editor); Geological Association of Canada, Special Paper 7, p. 165-177.
- Walthier, T.N.
1949: Geology and mineral deposits of the area between Corner Brook and Stephenville, western Newfoundland (Part I), and Geology and mineral deposits of the area between Lewis Hills and Bay St. George, western Newfoundland (Part II); Newfoundland Geological Survey, Bulletin 35.
- Williams, H.
1973: Bay of Islands map area, Newfoundland; Geological Survey of Canada, Paper 72-34.

**ON THE RELATIVE AGE OF THE MUSKOX INTRUSION AND
THE COPPERMINE RIVER BASALTS, DISTRICT OF MACKENZIE**

Project 770019

P.F. Hoffman
Precambrian Geology Division

Hoffman, P.F., On the relative age of the Muskox Intrusion and the Coppermine River basalts, District of Mackenzie; in Current Research, Part A, Geological Survey of Canada, Paper 80-1A, p. 223-225, 1980.

Abstract

If the main northward extension of the Canoe Lake Fault, which displaces the Muskox Intrusion (middle Proterozoic), follows the east branch, rather than the west branch as has previously been assumed, the arguments that the Muskox Intrusion must predate the Dismal Lakes Group are circumvented. The east branch requires a sharp bend in the fault, but this is typical of rift faulting today. Therefore, it is possible that the Muskox Intrusion is coeval, even comagmatic, with the Coppermine River basalts.

Introduction

The Muskox Intrusion (Irvine and Smith, 1967; Irvine and Baragar, 1972) is a layered, mafic-ultramafic, igneous body of middle Proterozoic age. In cross-section, it has the form of an oblate funnel, and was intruded along and just beneath the unconformity separating early Proterozoic rocks of Wopmay Orogen from middle Proterozoic cover rocks (Irvine, 1971). The cover sequence comprises, in ascending order, the Hornby Bay Group (mostly sandstone), Dismal Lakes Group (mostly dolomite but with a basal sandstone) and Coppermine River Group (mostly basalt flows).

It was initially thought that the Muskox Intrusion was younger than, or coeval with, the Coppermine River Group basalts (Smith, 1962; Smith et al., 1966). However, detailed mapping led Irvine (1970) to the conclusion that the intrusion predates the Dismal Lakes Group and therefore must be older than the basalts. This view is followed by Baragar and Donaldson (1973). Irvine (1970) advanced two essential arguments:

1. The Canoe Lake Fault has a throw of about 500 m, west side down, where it displaces the intrusion but, where it cuts the Dismal Lakes Group, its throw is much less and is of the opposite sense.
2. The Dismal Lakes Group dolomite is unmetamorphosed, even within 300 m of the roof of the intrusion.

Northward Extension of the Canoe Lake Fault

Both Irvine (1970) and Baragar and Donaldson (1973) show the Canoe Lake Fault dividing northward into two branches as it passes through the Dismal Lakes Group (Fig. 34.1). The junction of the two branches is heavily drift covered. The northwest branch deviates only 13 degrees from the trend of the stem fault, whereas the northeast branch deviates by 38 degrees. This is apparently the reason why Irvine (1970) considers only the northwest branch as the principal extension of the Canoe Lake Fault.

Although transcurrent faults are generally straight or gently curved (eg. Hoffman, 1980), this is not generally true of normal faults. Normal faults related to continental rifts commonly display a "zigzag" or "gridded" pattern (Freund and Merzer, 1976). This has been documented in such diverse rifts as the Rhine graben (Illies, 1970), the east African rifts (Baker et al., 1972; Moore and Davidson, 1978) and the Basin and Range province (Stewart, 1971). Ramberg and Smithson (1975) invoke pre-existing oblique fractures to account for "gridded" fault patterns in the Rio Grande Rift and Oslo Graben. Just 4 km west of the Canoe Lake Fault (Fig. 34.1) is a narrow graben, in which the "gridded" fault pattern may

reflect pre-existing oblique transcurrent faults (Hoffman, 1980). There is, therefore, no reason to reject a priori the northeast branch as the principal extension of the Canoe Lake Fault.

Unlike the northwest branch, the northeast branch is comparable to the main Canoe Lake Fault in both sense (west side down) and throw. Near the Muskox North drill hole (Fig. 34.1), lower Hornby Bay Group sandstone is faulted against the upper part of Unit 14 (Baragar and Donaldson, 1973) Dismal Lakes Group dolomite, a stratigraphic separation crudely estimated to be 400-600 m. However, where the fault transects the base of the Coppermine River basalts the throw appears less, although still of the requisite sense. This, plus the apparent thickening of the Dismal Lakes Group dolomite westward across the fault, suggests that most of the fault movement may have occurred near the end of Dismal Lakes Group deposition. If so, there is no need to postulate pre-Dismal Lakes Group displacement and no reason why the Muskox Intrusion must pre-date the Dismal Lakes Group.

The outcrops of unmetamorphosed Dismal Lakes Group dolomite, reported by Irvine (1970, Fig. 2), are separated from the Muskox Intrusion by the northeast branch of the Canoe Lake Fault, which has greatly reduced the apparent vertical distance between them. Because the Hornby Bay Group is not exposed between the two branch faults, the original vertical distance between the roof of the intrusion and those outcrops of dolomite is not accurately known. Assuming a thickness of 200 m for the Hornby Bay Group, the dolomite is estimated to have been 800 m above the roof of the intrusion. This is far greater than the 300 m mentioned by Irvine (1970) as being close enough to expect a metamorphic effect.

Conclusion

By recognizing that the northeast branch is the principal extension of the Canoe Lake Fault, both arguments advanced by Irvine (1970) for a pre-Dismal Lakes Group age for the Muskox Intrusion are circumvented. Therefore, it is possible to reconsider a direct and genetic link between the intrusion and the Coppermine River basalts. However, detailed stratigraphic work is needed in the Dismal Lakes Group to pin down the age(s) of fault movement.

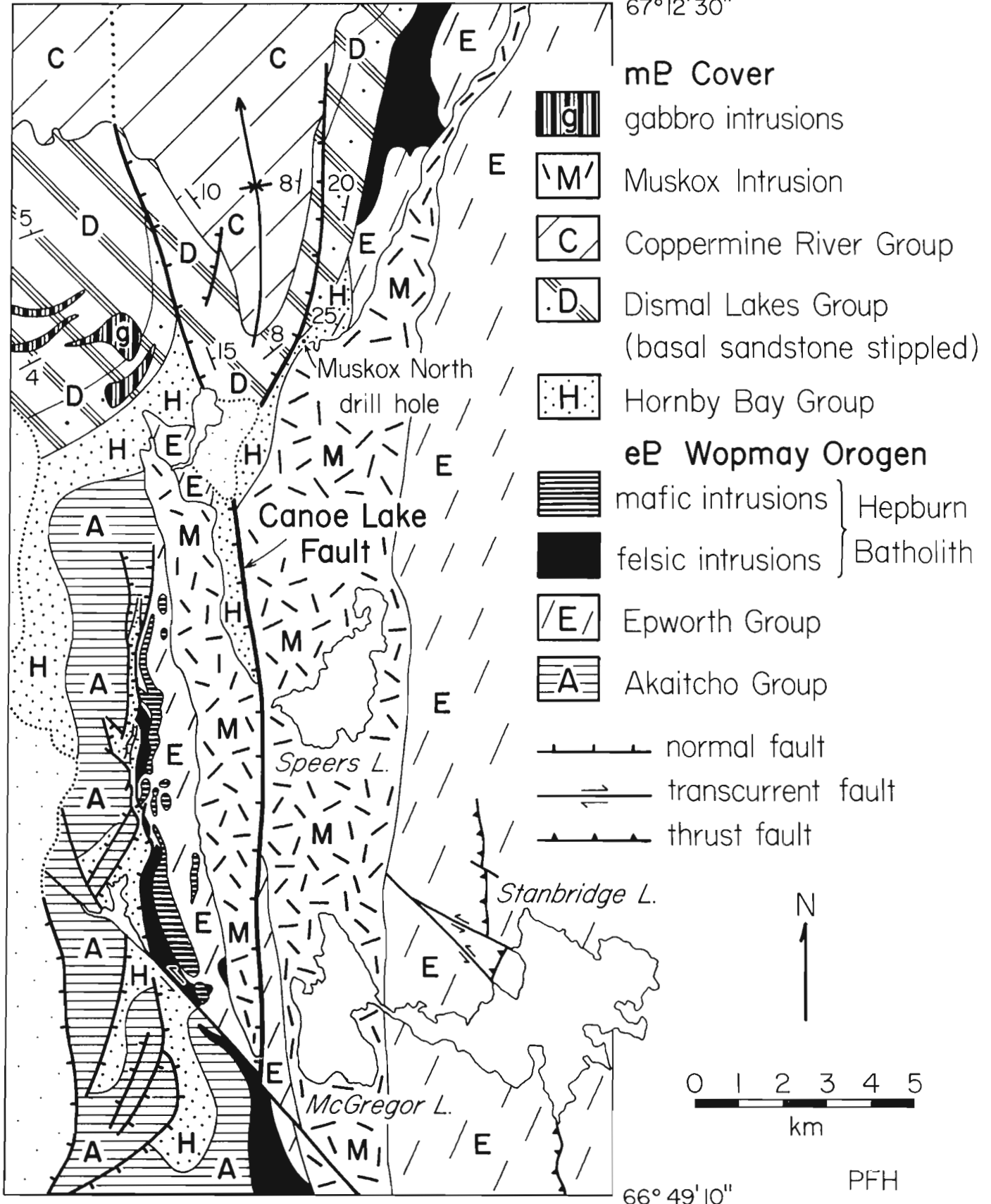
Acknowledgments

I am grateful to J.A. Donaldson (Carleton University) and his doctoral students C. Kerans and G. Ross for discussions and knowledge of their unpublished work on the Hornby Bay and Dismal Lakes Groups.

115° 30'

115° 00'

67° 12' 30"



66° 49' 10"

Figure 34.1. Geological relations near the roof of the Muskox Intrusion. Mapping north of 67°00' is by Smith et al. (1966), Irvine (1970), and Baragar and Donaldson (1973).

References

- Baker, B.H., Mohr, P.A., and Williams, L.A.J.
1972: Geology of the western rift system of Africa; Geological Society of America, Special Paper 136, 67 p.
- Baragar, W.R.A. and Donaldson, J.A.
1973: Coppermine and Dismal Lakes map-areas; Geological Survey of Canada, Paper 71-39, 20 p. with Maps 1337A and 1338A.
- Freund, R. and Merzer, A.M.
1976: The formation of rift valleys and their zigzag fault patterns; Geological Magazine, v. 113, p. 561-568.
- Hoffman, P.F.
1980: Conjugate transcurrent faults in north-central Wopmay Orogen (early Proterozoic) and their dip-slip reactivation during post-orogenic extension, Hepburn Lake map area, District of Mackenzie; in Current Research, Part A, Geological Survey of Canada, Paper 80-1A, report 29.
- Illies, J.H.
1970: Graben tectonics and relation to crust-mantle interaction; in Graben Problems, J.H. Illies and S. Mueller, ed., Schweizerbart, Stuttgart, p. 4-27.
- Irvine, T.N.
1970: Geologic age and structural relations of the Muskox Intrusion; in Report of Activities, Part A, Geological Survey of Canada, Paper 70-1A, p. 149-153.
1971: Emplacement of the Muskox Intrusion; in Report of Activities, Part A, Geological Survey of Canada, Paper 71-1A, p. 112-114.
- Irvine, T.N. and Baragar, W.R.A.
1972: Muskox Intrusion and Coppermine River lavas, Northwest Territories; XXIV International Geological Congress, Field Excursion A29 Guidebook, Canada, 70 p.
- Irvine, T.N. and Smith, C.H.
1967: The ultramafic rocks of the Muskox Intrusion; in Ultramafic and Related Rocks, P.J. Wyllie, ed., John Wiley and Sons, New York, p. 38-49.
- Moore, J.M., Jr. and Davidson, A.
1978: Rift structure in southern Ethiopia; Tectonophysics, v. 46, p. 159-173.
- Ramberg, I.B. and Smithson, S.B.
1975: Gridded fault patterns in a late Cenozoic and a Paleozoic continental rift; Geology, v. 3, p. 201-205.
- Smith, C.H.
1962: Notes on the Muskox Intrusion, Coppermine River area, District of Mackenzie; Geological Survey of Canada, Paper 61-25, 16 p.
- Smith, C.H., Irvine, T.N., and Findlay, D.C.
1966: Geologic maps of the Muskox Intrusion; Geological Survey of Canada, Maps 1213A and 1214A.
- Stewart, J.H.
1971: Basin and Range structure: a system of horsts and grabens produced by deep-seated extrusion; Geological Society of America Bulletin, v. 82, p. 1019-1044.

Project 770026

G.R. Dunning¹ and R.K. Herd
Precambrian Geology Division

Dunning, G.R. and Herd, R.K., The Annieopsquotch ophiolite complex, southwest Newfoundland, and its regional relationships; in Current Research, Part A, Geological Survey of Canada, Paper 80-1A, p. 227-234, 1980.

Abstract

The Annieopsquotch ophiolite complex is divided into five units. From base to top these are: (1) layered series, including troctolite, norite, gabbro, anorthosite, and mafic granulite; (2) massive gabbro, cut by diabase dykes; (3) a unit transitional from massive gabbro to sheeted dykes; (4) a sheeted dyke complex; and (5) pillow lava, cut by diabase dykes and including volcanic breccia.

Mafic and intermediate volcanics conformably overlie these units and an elongate, biotite- and hornblende-bearing granite intrudes the top of the ophiolite complex.

Block faulted red sediments and felsic volcanics of probable Silurian age occur south and southwest of the ophiolite suite.

Smaller occurrences of ophiolitic rocks have been recognized at Star Lake, on the eastern shore of Padille Pond and southwest of Puddle Pond, and south of Little Grand Lake. Harzburgite associated with gabbro and anorthosite occurs within granite and gneiss, northwest of the Lloyds River. These ophiolite fragments resemble parts of the Bay of Islands, Annieopsquotch, and other ophiolite complexes.

Introduction

Mapping in 1978 at 1:50 000 scale in the Puddle Pond area (NTS 12 A/5) revealed that the Annieopsquotch Mountains in the southeast part of the map area are underlain by an ophiolite complex (Herd and Dunning, 1979). Gabbro, cut by diabase dykes, occurs on the northwest side of the mountains, sheeted dykes through the centre, and pillow lavas cut by dykes on the southeast side. The strike of the contacts between these units is approximately northeast, parallel to the mountain ridges.

June to August 1979 was spent mapping the ophiolite complex in further detail. A granite, which intrudes the ophiolite complex, and a sequence of red sediments and associated felsic volcanic rocks, which occur south and southwest of the ophiolite, were also mapped. A few days were spent mapping mafic and intermediate volcanics south of the ophiolite. These are likely an extension, to the southwest, of the Victoria Lake group (Kean, 1977).

Regional mapping and reconnaissance continued north of the Annieopsquotch Mountains.

Access

The recently completed Burgeo Road (Route 480) passes near the southwest end of the ophiolite complex and excellent exposures of redbeds and mafic volcanics occur in new roadcuts. However, most mapping was done from flycamps in the mountains, supported by helicopter and fixed wing aircraft.

Annieopsquotch Ophiolite Complex

Five units have been distinguished in the igneous rocks of the ophiolite complex, namely the layered series, massive gabbro, a transition zone, sheeted dykes, and pillow lava (Figure 35.1). The transition zone boundaries are arbitrary and have been placed at 25 and 75 per cent diabase dykes in gabbro. The pillow lava unit is marked by the appearance of screens of pillow lava in the sheeted dykes. The highest stratigraphic level noted in the ophiolite is pillow lava cut by approximately 50 per cent diabase dykes.

Layered Series

Layered igneous rocks displaying cumulate textures occur in two areas along the northwest side of the mountains. These are separated by equigranular gabbro and may represent two discrete intrusions into the base of the gabbro, or may be remnants of a once more extensive unit. The layers strike 160-180° in both bodies and are steeply dipping, similar to dyke trends in the sheeted dyke zone. Parallelism of igneous layering and dykes, although unusual, has been observed in the Oman ophiolite (J. Smewing, personal communication, 1979).

Cumulus minerals in the layered series are olivine, orthopyroxene, clinopyroxene, and plagioclase, and in some outcrops dramatic compositional variations are apparent between adjacent layers, for example mafic troctolite next to anorthosite (Figure 35.2). Bright green chrome diopside occurs as large crystals in some layers. Magmatic-sedimentary features such as graded bedding, trough structures and slumped blocks are present but rare.

The layered rocks appear fresh in hand specimen but anorthosite, felsic gabbro and gabbro layers in the southern part of the northeastern body have been recrystallized; porphyroblasts of a mafic mineral are evident growing across layer contacts. Mafic granulites associated with the southwestern body of layered rocks are medium grained, granular, two pyroxene metamorphic rocks, commonly cut by raised, amphibole-bearing veinlets. Also associated with the southwestern unit are several brown weathering dykes one to several metres wide with chilled margins, containing both olivine and plagioclase phenocrysts. They may be either feeders or offshoots of the layered unit.

Massive Gabbro

The gabbro zone occurs along the northwest edge of the mountains, and gabbro occurs as screens in the transition zone and sheeted dyke zone. The gabbro is predominantly coarse grained and equigranular, composed of near equal amounts of plagioclase and clinopyroxene, and is correlated with "high-level" gabbro described from other ophiolite complexes. Many varieties of this gabbro occur along the mountain range and some may represent discrete intrusions.

¹Department of Geology, Memorial University of Newfoundland, St. John's, Newfoundland A1B 3X5.

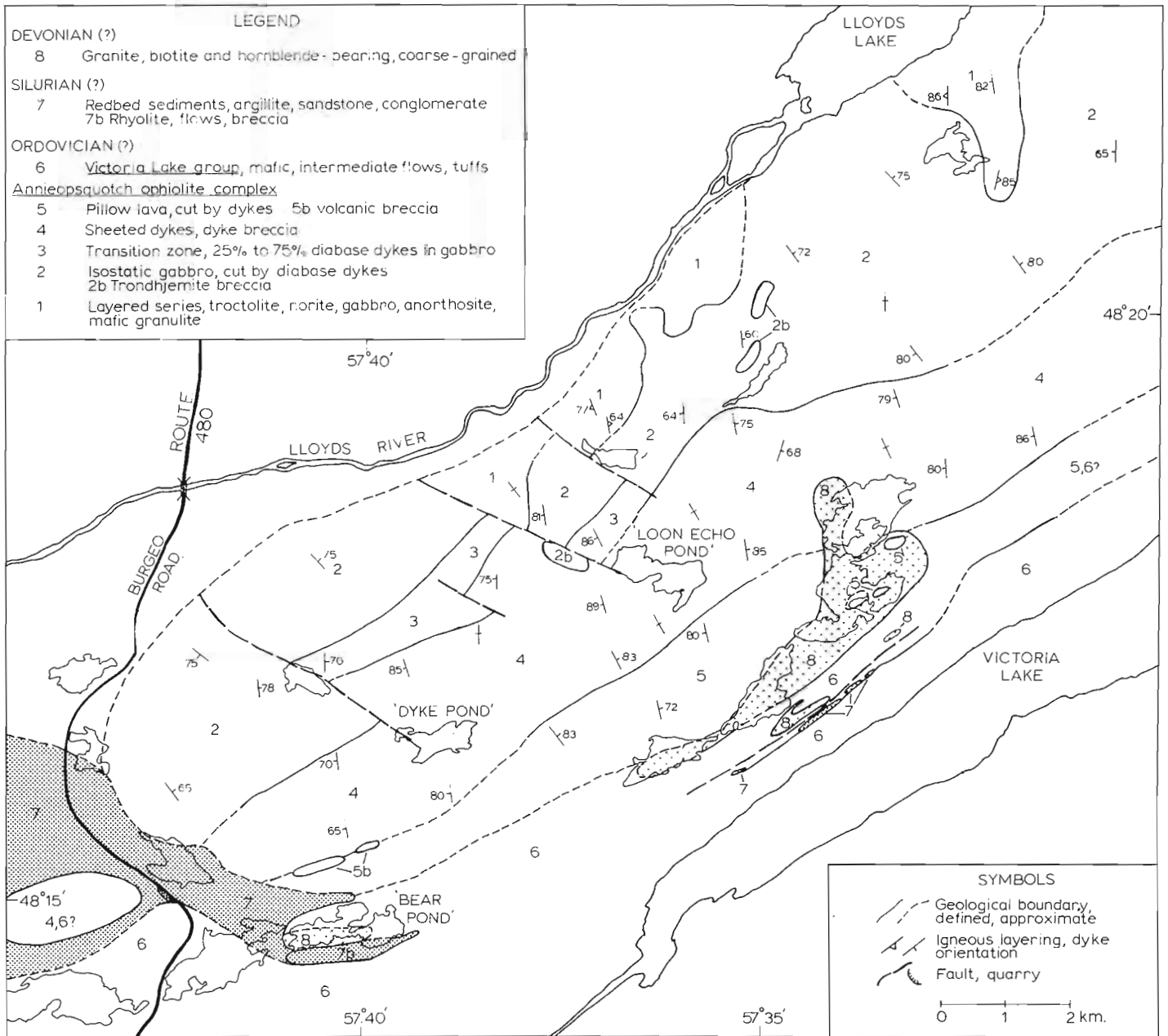


Figure 35.1. Geological sketch-map of the Annieopsquotch ophiolite (informal names are in quotation marks).

In some areas the gabbro is cut by hundreds of crisscrossing, raised, amphibole-rich veinlets which may represent hydrothermal fluid pathways (Figure 35.3). Occasionally, plagioclase is bleached along the veinlets. Pegmatitic pods are locally abundant within the gabbro, containing crystals of hornblende up to 15 cm in length.

At 'Loon Echo Pond' (informal name), the gradation from gabbro to transition zone is well exposed. The gabbro becomes increasingly magnetite-rich to the south (stratigraphic top) and is cut by increasing numbers of diabase dykes. Screens of gabbro in this zone may contain 5 to 10 per cent magnetite. Elsewhere the gabbro is magnetite-poor and the gradation to the transition zone is marked by breccia with trondhjemite matrix. The trondhjemite is composed of approximately 90 per cent plagioclase, the remainder being amphibole, chlorite, quartz, epidote, apatite, sphene and accessory zircon and prehnite. Blocks of both gabbro and diabase, some partially digested,

occur in the breccia (Fig. 35.4), which commonly extends into the transition zone. Trondhjemite breccia also occurs in the fault zone northwest of 'Loon Echo Pond'.

Transition Zone

The transition zone is of variable thickness along the length of the mountains and may be very narrow or absent in some areas. In such places gabbro, cut by only a few dykes grades over 100 m or less into 100 per cent sheeted dykes. There is no evidence of faulting where the transition zone is absent.

Many dykes in the transition zone are 5 to 10 m wide with coarse grained cores and chilled margins. Evidence for both dykes intruding gabbro and gabbro intruding dykes is present. Within the transition zone there is a gradual increase in the percentage of diabase dykes from northwest to southeast.



Figure 35.2. Troctolite, norite and anorthosite of the northwest body of the layered series. GSC 203551-S.



Figure 35.3. Isostatic gabbro cut by raised amphibole-bearing alteration veinlets. GSC 203551-G.



Figure 35.4. Trondhjemite breccia with angular blocks of diabase and gabbro. GSC 203551-O.



Figure 35.5. Coarse volcanic breccia from southwest corner of the ophiolite; all blocks are diabase. GSC 203551-H.

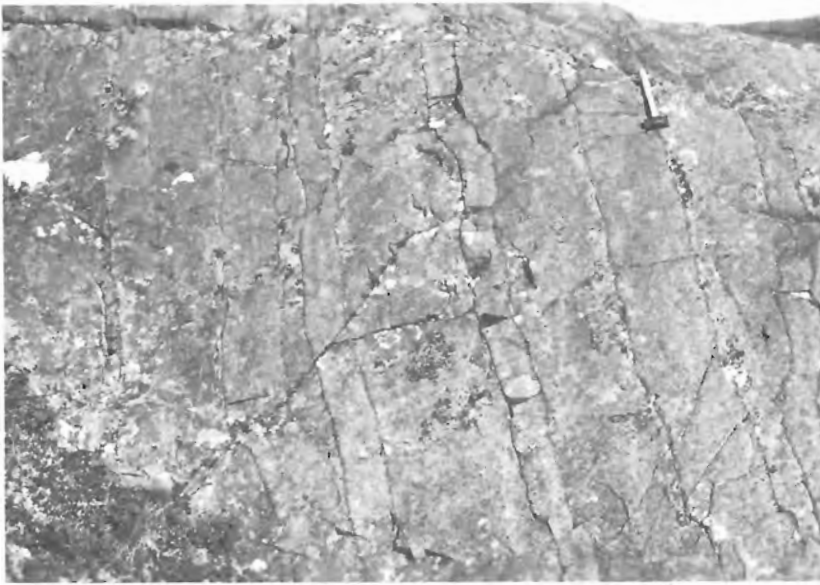


Figure 35.6.

Sheeted diabase dykes southeast of 'Loon Echo Pond' at boundary with pillow lava zone. GSC 203064-V.



Figure 35.7. *Pillow lava with interpillow aphanitic basalt southeast of 'Loon Echo Pond' 100 m from sheeted dykes of Figures 35.6. GSC 203551-B).*

Sheeted Dykes

The sheeted dyke zone of the Annieopsquotch ophiolite complex comprises approximately 30 per cent of its areal extent. The dykes strike between 160° and 190° and are steeply dipping. They vary in width from 1 cm to 10 m with the majority between 0.5 and 3 m. Many dykes have aphanitic chilled margins, with well developed cooling fractures, and grade to fine to coarse grained cores depending on their width.

Plagioclase is the most common phenocryst phase in the diabase dykes but less than 10 per cent of the dykes contain phenocrysts or inclusions. Phenocrysts of olivine, orthopyroxene, clinopyroxene and hornblende occur, and diabase and gabbro fragments have been noted. A few dykes with pale grey fresh surface and quartz phenocrysts are likely intermediate in composition. Some late-intrusive rhyolite dykes occur southeast of 'Loon Echo Pond'.

Several breccia dykes are present; the best exposed is at the east end of 'Dyke Pond' and is parallel to the regional dyke trend. It is composed of subangular fragments of diabase in a matrix of fine grained diabase. At the southwest corner of the ophiolite several poorly exposed outcrops of coarse breccia occur (Fig. 35.5) south of a group of breccia dykes within the sheeted dyke zone.

In some areas, near the contact with the pillow lava zone, many closely-spaced, narrow, fine grained diabase dykes intrude into earlier thick diabase dykes. They are well exposed on the ridge south of 'Loon Echo Pond' (Fig. 35.6).

Pillow Lava

The maximum thickness of this zone is approximately 1 km and the highest ratio of pillow lava to diabase dykes noted is 1:1.

South of 'Loon Echo Pond' at the level where screens of pillow lava first occur in the sheeted dykes, some diabase dykes bud to form pillows and some dykes pass upward into breccia.

Pillows are round to elongate. Their orientations do not indicate an obvious top direction. They vary from 0.2 to 1 m in length and some contain plagioclase phenocrysts. The interpillow material is aphanitic basalt and all pillows appear to be mafic in composition (Fig. 35.7).

The pillows are aphanitic, nonvesicular and most do not have distinct chilled margins. Isotropic glass shards are present in the pillow rims with abundant alteration products which include actinolite, chlorite, albite and pumpellyite.

Mafic and Intermediate Volcanics

Volcanic rocks, which may in part be ophiolitic and in part equivalents of the Victoria Lake group (Kean, 1977) occur north and south of the main granite body, along the northern part of the King George IV Lake map area and in numerous roadcuts along Route 480. They consist of bedded tuffs, mafic flows and pillow lava with interpillow chert. One volcanic breccia horizon occurs with bedded tuffs, southwest of the ophiolite. A few outcrops of strongly sheared chlorite and sericite-rich tuffs were observed. Most units seem to be lensoid. One 100 m long body of coarse grained gabbro, which is interpreted to be a synvolcanic sill, is present within the mafic volcanic sequence.

Redbed - Felsic Volcanic Sequence

Excellent exposures of red sediments occur in roadcuts and in a quarry on the new road. They dip shallowly southeast in the northern roadcuts and are near vertical but overturned in the quarry, suggesting the presence of fault-bounded blocks. The rocks vary from argillite to coarse sandstone with pebble horizons. Crossbeds in sandstone in the quarry (Fig. 35.8) indicate that the sequence faces north. Sedimentary features noted are mudcracks, ripple marks, load casts, and mud-chip beds; detrital muscovite occurs. These sedimentary rocks bear a striking resemblance to those of the Botwood Group exposed near Bishops Falls.

Within the sequence in the quarry is a 10 m thick unit composed of angular to subrounded blocks of felsic volcanics in an aphanitic red-brown matrix (Fig. 35.9). Primary volcanic features such as flow banding and fiamme are well preserved in the blocks. This unit is interpreted as a laharic breccia. It overlies massive volcanic rocks and is overlain by the sandstone-argillite sequence.

Southeast of the quarry, a several hundred metre thick pile of felsic volcanics occurs within the redbed sequence. Flow banded and massive feldspar-phyric rhyolite flows form two prominent hills in the area and locally a rhyolite breccia is present. Many of the redbed sandstones have a volcanic component, and pumice clasts up to 3 cm in diameter are present in one bed.



Figure 35.8. Crossbedded sandstone from the redbed sequence. Tops to right (north). GSC 203551-E.

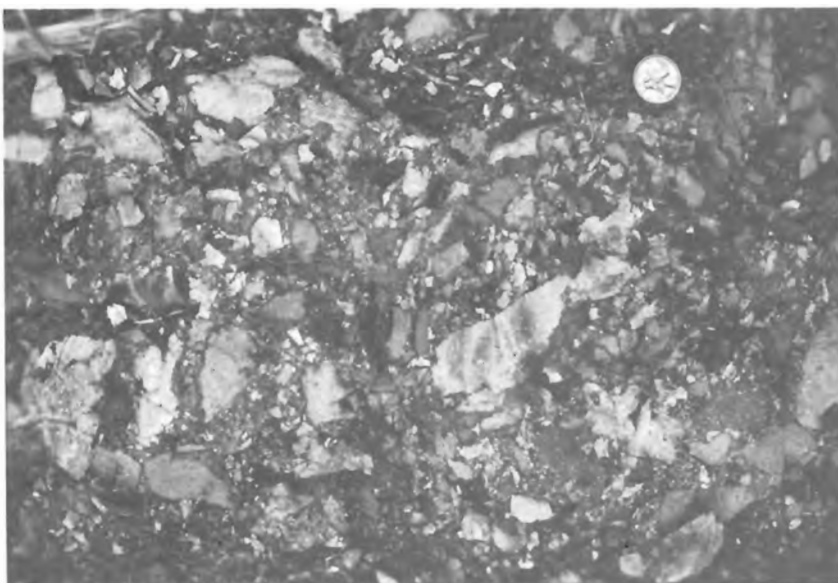


Figure 35.9.

Laharic breccia of felsic volcanic rocks in red brown matrix. Note angularity and poor sorting. GSC 203551-T.

In one stream valley north of 'Bear Pond' a 10 m thick exposure of grey siltstone-argillite, bedded at centimetre scale, occurs between two outcrops of red sandstones but the actual contacts were not observed. Within the argillite, one bed 0.5 m thick contains brachiopods, some recrystallized to coarse grained calcite.

This redbed sequence is probably an extension to the northeast of that described by DeGrace (1974) immediately adjacent to King George IV Lake. There he described sandstone and a conglomerate in which 40 per cent of the coarse clasts are felsic volcanics.

Because of its similarity in appearance to redbeds of the Botwood Group and the presence of a significant proportion of felsic volcanic flows and sediments similar to those of the Springdale Group this redbed sequence is likely to be of Silurian age, rather than Carboniferous as previously thought (Herd and Dunning, 1979).

On the ridge immediately northwest of Victoria Lake, red siltstone, sandstone and conglomerate occur in a 2 to 3 m thick horizon which is discontinuous along strike, dips steeply southward and is bounded on the north by a major mylonite zone. These sedimentary rocks contact mafic volcanic flows to the south. The contact, as observed in several outcrops, appears to be conformable, with clasts of red sediment included in the mafic volcanics. The majority of pebbles in the conglomerate are of other redbed lithologies, chert and diabase.

One roadcut southwest of 'Bear Pond' contains a 1 m thick red shale horizon interbedded with mafic volcanics. This shale may be related to the redbeds north of Victoria Lake. It is uncertain whether these small lenses of redbeds are related to the thick redbed-felsic volcanic sequence described above.

Granite

Coarse grained biotite- and hornblende-bearing granite occurs along a chain of lakes in the valley south of the ophiolite complex. It contains large inclusions of fine grained mafic rock and pillow lava, which are likely part of the ophiolite complex. The granite forms the matrix of an intrusion breccia at its margins; many of the included mafic blocks are now amphibolite, and it has a faulted intrusive contact with mafic volcanics to the south. Isolated, probably fault-bounded, pods of granite occur southeast of the major body.

Faulting

Within the ophiolite complex faults have been noted crosscutting and locally offsetting the stratigraphy, for example west-northwest of 'Loon Echo Pond'. No major faults have been noted parallel to the stratigraphy, however many narrow shear zones are present oriented northeasterly. One fault in the layered series with an apparent displacement of 4 m contains coarse grained undeformed gabbro intruded along it, suggesting that it was formed in the oceanic environment rather than during emplacement.

The structural geology south of the ophiolite is only poorly known. Some northeast-trending faults are present in the ridge northwest of Victoria Lake and one major fault, marked along its length by sheared and mylonitized rocks, separates redbed sediments and overlying mafic volcanics from granite and mafic volcanics to the northeast.

As noted above, block faulting may be responsible for the variation in dip of the redbeds in adjacent outcrops along the Burgeo Road.

Economic Geology

Cu-Ni-Fe sulphides occur in small amounts in all rock types of the Annieopsquotch ophiolite and in amounts up to 10 per cent in sheared and altered volcanic flows and tuffs, in roadcuts in the northern part of the King George IV Lake map area. Asbestos fibres up to 3 mm long are present along with massive serpentine and magnetite in alteration veinlets cutting a troctolite layer in the eastern layered body.

Pink stained surfaces in the redbed sequence in the quarry may be due to the presence of Mn and/or Co mineralization. Scintillometer counts of three times background were obtained from a crossbedded sandstone layer just above the contact with the lahatic breccia, in the quarry.

Regional Correlations

Mafic and ultramafic rocks in the region northwest of the Lloyds River - Red Indian Lake valley have been examined and several areas of rocks with ophiolite affinities have been recognized. The areas referred to below can be found by reference to Riley (1957).

Star Lake

A massif of similar topographic relief and appearance to the Annieopsquotch ophiolite region, occurs on the northeast side of Star Lake. Part of this massif has been mapped as intrusive gabbro (Kean, 1978). The area was examined briefly during reconnaissance and two units distinguished. The northwest side of the massif is underlain by cumulate troctolite, norite, two-pyroxene gabbro and minor anorthosite, locally well layered (Fig. 35.10); the layering strikes northwest and dips steeply. These rocks are identical to those of the layered series of the Annieopsquotch ophiolite (unit 1). The second unit of the massif is massive gabbro cut by a few diabase dykes, and can be correlated with the basal part of the Annieopsquotch massive gabbro (unit 2). Minor trondhjemite was noted in both the layered series and in the gabbro. The contact between the units at Star Lake, as in the Annieopsquotch ophiolite, runs roughly northeast.

Padille Pond and Puddle Pond

Mapping by D.P. Kennedy in connection with the present project has revealed a small area of poorly exposed mafic-ultramafic rocks on the southeast side of Padille Pond. Lithologically, these rocks are identical to mafic layers in the Annieopsquotch ophiolite layered series. They show cumulate plagioclase in a pyroxene-olivine matrix, and large bronzite oikocrysts can be distinguished in hand specimen. They are intruded by massive and foliated granite.

South and southwest of Puddle Pond occur anorthosite and gabbroic anorthosite, thought previously to resemble Grenvillian anorthosites (Herd, 1978). Closer examination now shows that these rocks are troctolitic, and identical to rocks from the layered series of the Annieopsquotch ophiolite. Olivine-plagioclase reactions have occurred and altered olivine cores are surrounded by greenish rims against the feldspar.

Little Grand Lake

The Glover Formation (Riley, 1957) occupies much of the area of western Grand Lake and Little Grand Lake. Mapping northeast of Island Pond has revealed a fault contact between ophiolitic rocks along Little Grand Lake, and granitic gneisses to the south. The ophiolitic rocks are massive gabbro-norite, overlain by sheeted dykes. Ophiolites have previously been reported from the Glover Formation, on Glover Island (Knapp et al., 1979).

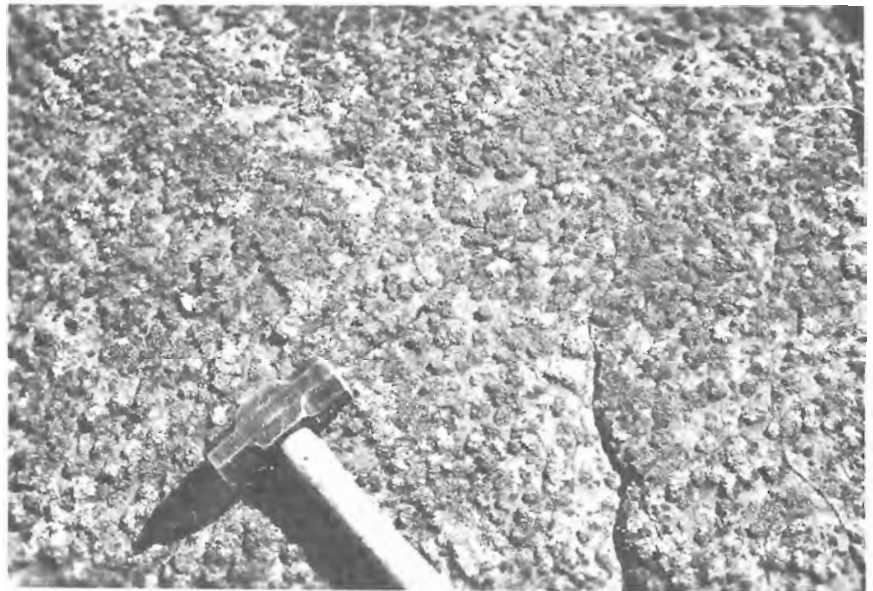


Figure 35.10.

Layered series rocks at Star Lake. GSC 203064-Z.

Figure 35.11.

Layering in harzburgite west of Silver Pond. The large oikocrysts are altered bronzite. GSC 203546-E.



East of Little Barachois Brook

Metamorphosed gabbro, anorthosite, and pyroxenite cut by granite and foliated granite were mapped previously, southwest of Silver Pond, northwest of Lloyds River, and south of Southwest Brook (unit 8 of Herd and Dunning, 1979). Further mapping has revealed associated ultramafic rocks, locally interlayered with gabbro, and gabbroic anorthosite, all cut by granite and gneiss. The most compelling evidence that these rocks have ophiolitic affinities, is the lithologic character of the ultramafics. They are harzburgites, with serpentinized olivine matrix, and bronzite oikocrysts in layers (Fig. 35.11); the bronzite may be altered to chlorite, and the contained olivine serpentinized, but the essential texture remains. They resemble harzburgites from the Lewis Hills and from the Troodos complex, Cyprus.

Long Range Mafic-Ultramafic Complex

Near Port aux Basques, ophiolitic rocks have been mapped by Brown (1976). A basal thrust sheet composed of dunite with pods of harzburgite, lherzolite, and wehrlite, and

an upper sheet of well layered troctolite, olivine gabbro, norite and anorthosite, passing into gabbro, occur, overlying tonalitic gneiss. The description of the upper sheet is reminiscent of the layered series of the Annieopsquotch ophiolite.

Summary and Implications

The Annieopsquotch ophiolite is of regional importance in unravelling the complex history of the southern Long Range in Newfoundland, and its detailed study will provide important information about the upper portions of ophiolite suites (cf. Malpas and Stevens, 1978). Relationships to the red sediments and volcanics imply that an oceanic environment was succeeded in the Silurian by continental conditions. Scattered ophiolite fragments northwest of the Lloyds River valley provide links with other western Newfoundland ophiolites. The fact that some of these fragments are intruded by granite and foliated granite implies considerable plutonic activity after ophiolite emplacement.

Acknowledgments

Detailed work on the Annieopsquotch ophiolite complex constitutes the basis of a Ph.D. thesis study by the first author, while regional correlations are the task of the second author. The detailed mapping is a fully supported part of the program to revise the mapping of NTS map sheet 12 A (W/2), begun in 1977; this program is proceeding in conjunction with mapping by the Mineral Development Division, Department of Mines and Energy, Newfoundland, under terms of the Canada-Newfoundland Mineral Development Subsidiary Agreement (1976-1981).

D. Kennedy did independent mapping as part of the project. Field assistance was also ably provided by K. Cameron, R. Jackson, and M. Thomson. Base camp facilities and aircraft support at Pasadena were as previously provided and appreciated. J. Malpas and K. Currie read drafts of the manuscript and suggested improvements. J. MacManus helped prepare the sketch map. Field discussions with many visitors are hereby acknowledged.

References

- Brown, P.A.
1976: Ophiolites in south-western Newfoundland; *Nature* (London), v. 264, p. 712-715.
- DeGrace, J.R.
1974: Notes on the geology of the King George IV Lake area, southwest central Newfoundland; in *Report of Activities, 1973*, Mineral Development Division, Newfoundland Department of Mines and Energy, p. 43-49.
- Herd, R.K.
1978: Geology of Puddle Pond area, Red Indian Lake map-sheet, Newfoundland; in *Current Research, Part A*, Geological Survey of Canada, Paper 78-1A, p. 195-197.
- Herd, R.K., and Dunning, G.R.
1979: Geology of Puddle Pond map area, southwestern Newfoundland; in *Current Research, Part A*, Geological Survey of Canada, Paper 79-1A, p. 305-310.
- Kean, B.F.
1977: Geology of the Victoria Lake map area (12A/6), Newfoundland; Mineral Development Division, Newfoundland Department of Mines and Energy, Report 77-4.
1978: Geology of the Star Lake east half sheet (12A/11E), Newfoundland; in *Report of Activities for 1977*, Mineral Development Division, Newfoundland Department of Mines and Energy, Report 78-1, p. 129-134.
- Knapp, D., Kennedy, D., and Martineau, Y.
1979: Stratigraphy, structure, and regional correlation of rocks at Grand Lake, western Newfoundland; in *Current Research, Part A*, Geological Survey of Canada, Paper 79-1A, p. 317-325.
- Malpas, J. and Stevens, R.K.
1978: The origin and emplacement of the ophiolite suite with examples from western Newfoundland; *Geotectonics, English Translation*, v. 11, (1977), p. 453-466.
- Riley, G.C.
1957: Red Indian Lake (west half), Newfoundland; Geological Survey of Canada, Map 8-1957.

Denis P. Kennedy¹
Precambrian Geology Division

Kennedy, Denis P., *Geology of the Corner Brook Lake area, western Newfoundland; in Current Research, Part A, Geological Survey of Canada, Paper 80-1A, p. 235-240, 1980.*

Abstract

Precambrian basement rocks are faulted against cover rocks, which range in age from Hadrynian to Carboniferous. A polydeformed metasedimentary sequence of Hadrynian to Ordovician age consists of feldspathic psammites and semipelites in basal parts and quartz-rich and calcareous rocks in upper parts. These metasediments are possible equivalents of the Fleur de Lys Supergroup; in places they are thrust against basement rocks as well as against lower parts of a Cambro-Ordovician carbonate platform sequence. At least three deformation events have affected the area. The first two events are probably equivalents of the Taconic and Acadian orogenies. The intensity of both deformation and metamorphism decreases westward, and a lower amphibolite facies metamorphic peak may have been reached in the metasedimentary sequence between the first two deformation events. Thrust faults may have been initiated during the early deformation; associated with one thrust are rocks of possible ophiolitic affinity.

Introduction

Reconnaissance mapping in the Corner Brook Lake area, immediately west of Grand Lake, western Newfoundland, was completed during the 1979 field season. The map area (Fig. 36.1) is bounded by Grand Lake and South Brook valley on the south and east, by the Trans-Canada Highway and Humber River valley on the west and north, and includes parts of NTS map sheets 12 A/12, 13, 12 B/9, 16, 12 H/4. The area consists of an eastern highland area, which is part of the Long Range Mountains, and an area of lower, gently rolling hills to the west.

The aim of the study was to sketch the major stratigraphical and structural features, particularly in the eastern part of the area. The following is a progress report of this work.

Stratigraphy

The area is underlain by a variety of deformed and variably metamorphosed rocks ranging in age from Precambrian to Carboniferous. Fourteen lithologic units are recognized, eleven of which are divided among three geographically and stratigraphically distinct terranes: a basement terrane (units 1 to 3); a metasedimentary terrane (units 4 to 8); and a carbonate terrane (units 9 to 11). Each of these major stratigraphic divisions is discussed in turn. The remaining three lithologic units (12 to 14) are considered separately.

Basement Terrane

Rocks of the basement terrane are found in three fault-bounded blocks in the south-central part of the map area. The basement terrane comprises granitoid gneisses with amphibolite, paragneisses and foliated granite.

The granitoid gneisses include medium grained, green, tonalitic gneiss and migmatite (unit 1a), and well layered pink, granite gneiss (unit 1b). Both units contain amphibolite layers and lenses, generally up to one metre thick. Locally discordant contacts suggest that the amphibolites are metamorphosed basic dykes. A single exposure of garnet amphibolite was noted. Abundant green biotite, epidote and saussuritized plagioclase in the tonalitic gneiss indicate strong retrogression. On the basis of their distinctive textures and lithologies the granitoid gneiss units are interpreted to be correlatives of the Long Range Complex (Baird, 1960; Neale and Nash, 1963), and thus Precambrian in age.

The paragneiss unit (2) is dominantly fine grained, buff coloured, psammitic to semipelitic gneiss and schist with scattered thin layers of garnetiferous, pelitic schist. Green calc-silicate schist and grey, pure quartzite are minor components. The paragneiss unit is interpreted to be an integral part of the Precambrian basement complex.

Foliated, medium grained, pink granite (unit 3) outcrops in the middle of the basement terrane. On one side, the granite intrudes rocks of the paragneiss unit, while on three sides it is faulted against paragneiss or granite gneiss. Deformed granite veins, common in all units of the basement terrane, and pink granite neosome in locally developed lit-par-lit migmatite, may be apophyses of the granite. A Precambrian age is suggested by the granite's restriction to the basement terrane.

Metasedimentary Terrane

The eastern half of the map area is underlain by a variety of polydeformed, dominantly metasedimentary, schists and gneisses collectively referred to as the metasedimentary terrane. Four major lithologic units are recognized.

The first unit (4), composed of a variety of feldspathic schists and gneisses, outcrops along the eastern margin of the area in a belt that widens considerably from south to north. The unit is dominated by medium- to coarse-grained albite-quartz-mica schist, which varies in texture from gneissic to slaty, mainly as a function of the phyllosilicate content. Pink porphyroblasts of albite are conspicuous and range in size from 1 mm to 1 cm. The feldspathic schists are intensely sheared in the southeast corner of the map area, and are commonly strongly lineated elsewhere. Quartzite and quartz-rich schistose layers are common.

The second unit (5) consists of quartzofeldspathic schists and gneisses, locally garnetiferous, with scattered pure quartzite and albite schist layers, and minor garnet amphibolite layers. Unit 5 is distinguished from unit 4 by its higher proportion of quartz and significantly lower proportion of albite schist. The structurally lower part of this unit contains two distinctive lithologic associations: a quartzofeldspathic gneiss cut by amphibolite layers containing up to 20 per cent, large (1 cm) biotite porphyroblasts, and a metaconglomerate consisting of mainly quartz and feldspar clasts, with a few flattened quartz clasts as long as 20 cm.

¹Department of Geology, Memorial University of Newfoundland, St. John's, Newfoundland, A1B 3X5

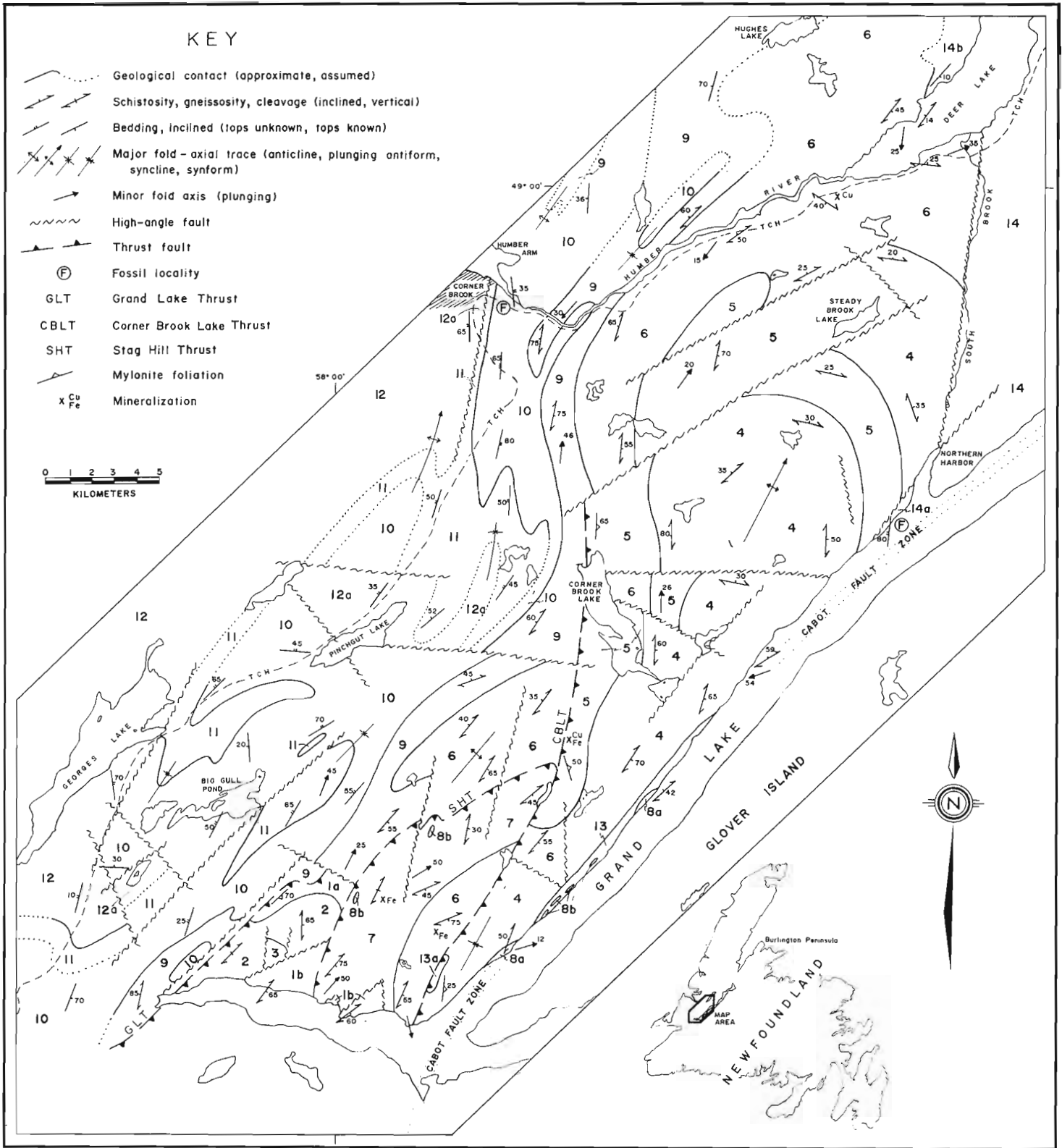


Figure 36.1. Geology, Corner Brook Lake area.

LEGEND FOR FIGURE 36.1

CARBONIFEROUS AND OLDER

- 14 Carboniferous sediments: 14a – Anguille Group, plant-bearing, grey sandstone and siltstone; 14b – Deer Lake Group, red conglomerate
- 13 Granite: medium grained, foliated and brecciated, pink granite; 13a – foliated granite and felsic volcanics
- 12 Humber Arm Supergroup: 12a – mainly black shale, minor gray sandstone

CAMBRIAN TO ORDOVICIAN (CARBONATE TERRANE)

- 11 Table Head Formation: grey marble and limestone, black shale, minor limestone breccia
- 10 St. George Group: buff and pink, dolomitic and calcitic marble, limestone and dolomite
- 9 Grand Lake Brook Group (includes Reluctant Head Formation): grey, sericitic marble, phyllite, interbedded phyllite and marble, marble breccia, phyllitic schist, minor quartzite

HADRYNIAN TO ORDOVICIAN (METASEDIMENTARY TERRANE)

- 8 Rocks of possible ophiolitic affinity: 8a – mafic rocks: amphibolite and greenschist; 8b – ultramafic rocks: mainly serpentinite
- 7 Calcareous schist and marble: actinolite-garnet-calcite-mica schist, grey and white marble, schistose (micaceous) marble, minor quartz-mica and garnet-quartz-mica schist
- 6 Quartz-rich psammitic rocks (includes Mount Musgrave Formation): quartz-mica and garnet-(tourmaline)-quartz-mica schists, quartzite, and minor mica-feldspar-quartz schist and meta-arkose
- 5 Quartzofeldspathic psammites: quartz-feldspar-mica and garnet-quartz-feldspar-mica schist and gneiss, minor quartzite, garnet amphibolite and biotite amphibolite
- 4 Feldspathic schist and gneiss: medium and coarse grained albite-quartz-mica schist and gneiss, minor quartzite and quartz-mica schist

PRECAMBRIAN (BASEMENT TERRANE)

- 3 Granite: medium grained, foliated, pink granite
- 2 Paragneiss: buff, fine grained, quartz-feldspar-mica gneiss and schist, locally garnetiferous, minor calc-silicate schist and quartzite
- 1 Granitoid gneisses and amphibolite: 1a – green, tonalitic gneiss, migmatite and amphibolite; 1b – pink, well layered, granitic gneiss and amphibolite

The third lithologic unit (6) comprises a variety of quartz-rich psammitic rocks. The dominant lithologies are quartz-mica and garnet-quartz-mica schists, and gray to white quartzite. Garnet porphyroblasts (1 cm or less) are ubiquitous, and small (1 cm), black, tourmaline crystals are relatively common. Minor amounts of mica-albite-quartz schist, quartz-feldspar-calcite-mica schist and orange-coloured, meta-arkose are found locally in this unit, also. Rocks of unit 6 outcropping in the northwestern part of the map area have been previously referred to as the Mount Musgrave Formation by McKillop (1963) and Lilly (1963).

The fourth major lithologic unit in the metasedimentary terrane is a very distinctive sequence of calcareous schist and marble (unit 7), restricted in distribution to the southern

part of the map area. The unit is immediately recognizable by the presence, in calcareous schists, of acicular actinolite porphyroblasts ranging in length from 1 to 15 cm. Red garnet porphyroblasts up to 4 cm in diameter are common, and in many cases both garnet and actinolite are found in the same rock. These calcareous schists are interlayered with variably micaceous, grey and white, coarse grained marbles. Pink marble, associated with garnet-mica schist and micaceous quartzite containing blue quartz grains, was noted at two localities. Mica, quartz-mica, and garnet-quartz-mica schists are common in the western, structurally lower part of this unit.

These four lithologic units (4 to 7) are interpreted as a metamorphosed sequence of dominantly metasedimentary rocks. The age of the sequence is uncertain, and stratigraphic relations within it are not clear due largely to the degree of deformation and metamorphism, and to the scarcity of facing criteria.

Correlations have previously been made between the metasediments in the map area and rocks of the Fleur de Lys Supergroup on the Burlington Peninsula (Church, 1969; Williams et al., 1972, 1974; Williams and Stevens, 1974). Preliminary results from the present study support this correlation, based on the similarities in lithology, structural style, metamorphic grade and tectonic setting.

Recent work on the stratigraphy of the Fleur de Lys Supergroup (Hibbard, 1979; Bursnall, 1979; Bursnall and de Wit, 1975) indicates that lower parts of the sequence (e.g., Seal Cove group) include feldspathic psammities, semipelites, amphibolite and metaconglomerate, and upper parts of the sequence (e.g., Rattling Brook Group) include psammitic, semipelitic and calcareous rocks. Based on correlation with the Fleur de Lys Supergroup, metasediments in the map area are interpreted to be Hadrynian to Ordovician in age, with basal parts of the sequence represented by the coarse feldspathic and quartzofeldspathic rocks of units 4 and 5, and upper parts represented by the more quartz-rich psammities and calcareous rocks of units 6 and 7. Further work will likely refine the stratigraphy of the metasedimentary terrane, and thereby sharpen correlation with the Fleur de Lys Supergroup.

A variety of deformed and metamorphosed mafic and ultramafic rocks (unit 8) constitutes an areally minor portion of the metasedimentary terrane. The ultramafic rocks are massive to schistose serpentinites with patches and veins of magnesite. Picrolite, talc and anthophyllite were also noted. Schistose serpentinite in the Cabot Fault zone is cut by granite (unit 13), and two bodies of serpentinite are located in the Stag Hill Thrust zone. Mafic rocks outcrop on the shore of Grand Lake and include slaty greenschist and medium grained amphibolite, the latter cut by granite.

The lithologies of unit 8, their setting along structural discontinuities, and their proximity to ophiolitic rocks of the Glover Island complex (Knapp et al., 1979) all suggest that they are of ophiolitic affinity.

Carbonate Terrane

The carbonate terrane underlies an area of low, rolling hills west of the basement and metasedimentary terranes. The carbonate terrane consists of three, previously named, lithologic units: the Grand Lake Brook Group (Walthier, 1949), the St. George Group and the Table Head Formation (Schuchert and Dunbar, 1934; Walthier, 1949; Riley, 1962).

The Grand Lake Brook Group (unit 9) comprises phyllite, thinly interbedded phyllite and marble, grey sericitic marble, marble breccia, and minor phyllitic schist and quartzite. The marble breccia commonly consists of flattened clasts with long dimensions of 5 to 10 cm; locally, flattened or rounded clasts up to 30 cm are found. At two localities, grey marbles of the Grand Lake Brook Group grade westward into buff and pink marble of the overlying St. George Group (unit 10). North of the Humber River valley, lithologies similar to those of the Grand Lake Brook Group have been referred to as the Reluctant Head Formation by Lilly (1963). These lithologies are also stratigraphically beneath the St. George Group (Lilly, 1963; Brückner, 1966).

Within the map area, the St. George Group is represented by thickly bedded, buff, pink and white, calcitic and dolomitic marbles with a few silty layers. The degree of

recrystallization of the carbonates decreases westward; exposures on the Trans-Canada Highway are limestones and dolomites. One unidentified brachiopod was found in marble in a highway exposure near Corner Brook.

Where the Table Head Formation (unit 11) outcrops in the map area, it consists of grey, knobby-weathering limestone or marble, shaly limestone, black shale and minor limestone breccia. Only the more easterly exposures of limestone are crystalline. The contact with the underlying St. George Group has been interpreted as locally disconformable (Riley, 1962).

The St. George Group, the Table Head Formation and underlying Cambrian clastics and carbonates exposed west of the map area have been interpreted as a Cambrian to early Middle Ordovician carbonate platform sequence (Williams et al., 1972, 1974; Williams and Stevens, 1974). Grand Lake Brook Group lithologies, and their stratigraphic position beneath the St. George Group, suggest they are an eastern, metamorphosed and deformed, facies equivalent of Cambrian rocks exposed to the west. Marble breccia in the Grand Lake Brook Group and the Table Head Formation may indicate deposition near the edge of a carbonate bank.

Other Lithologic Units

Other lithologic units in the map area include rocks of the Humber Arm Supergroup (unit 12), a unit of felsic plutonic and volcanic rocks (unit 13), and terrestrial sediments of Carboniferous age (unit 14).

The Humber Arm Supergroup (Stevens, 1970) is represented along the western margin of the map area by mainly black shale or slate (unit 12a), locally containing grey sandstone beds and lenses (H. Williams, personal communication).

Felsic plutonic and volcanic rocks (unit 13) outcrop near the southeastern margin of the area, and include medium grained, brecciated and locally foliated, pink granite, as well as minor intermediate to acid, porphyritic volcanics. The granite appears to be localized in the Cabot Fault zone (Knapp et al., 1979), and in shoreline exposures on Grand Lake it displays intrusive contacts with mafic and ultramafic rocks (unit 8). The felsic volcanics (unit 13a) contain 1 per cent K-feldspar phenocrysts, and outcrop as intensely weathered, orange and grey layers in foliated granite. The age and significance of both the granite and the volcanics are as yet uncertain; however, they may be phases of the Middle to Late Paleozoic Topsails Batholith (Williams et al., 1974; Williams, 1978) initially intruded into a pre-Carboniferous zone of weakness and later caught up in the Cabot Fault zone deformation.

Carboniferous rocks outcrop at two localities in the northern part of the area. Dark grey, fine grained, plant-bearing sandstone and siltstone (unit 14a) (Anguille Group; Hyde 1979) are faulted against metasediments on the west shore of Grand Lake at Northern Harbor, while red, boulder conglomerate and interbedded red sandstone (unit 14b) (Deer Lake Group; Hyde, 1979) unconformably overlie metasediments on the west shore of Deer Lake.

Structure

At least three distinct phases of deformation have so far been recognized in the map area, the first two of which were major structural events. The overall tectonic evolution of the area, however, was undoubtedly considerably more complex.

The early, most intense deformation (D1) affected all Ordovician and older rocks in the area and is characterized by northeast trending, tight to isoclinal folding (F1), which transposed an earlier foliation (probably bedding) to produce the dominant planar structure (S1) in the area. F1 is generally represented by hand-specimen-scale closures, which are particularly well displayed in phyllitic marble of the Grand Lake Brook Group and in calcareous and semipelitic rocks of the metasedimentary terrane. This suggests proximity of parts of the carbonate and metasedimentary terranes during the early deformation.

Major, east-dipping thrust faults may have been initiated during D1, since mylonite foliations associated with the thrusts are generally parallel to S1, and are locally folded by F2(?). The Grand Lake Thrust (Williams, 1978) defines the western margin of the basement terrane, and juxtaposes basement gneiss (units 1 and 2) and St. George Group marble (unit 10) across a very narrow (< 500 m), topographically marked, high strain zone. The development of the thrust zone appears to have involved early (D1?) mylonite formation and later (D2?) more brittle shearing. The northern extension of the Grand Lake Thrust, as initially defined by Williams (1978) and later discussed by Knapp et al. (1979), is indefinite at this point in the study. The western boundary of unit 7 is also marked by a thrust zone, here referred to as the Stag Hill Thrust, which has associated with it two elongate, deformed bodies of serpentinized ultramafic rock (unit 8b) as well as a contrast in metamorphic grade between similar lithologies on either side. The Corner Brook Lake Thrust (Walthier, 1949; Kennedy, 1978; Knapp et al., 1979), extending from the southeastern corner of the map area to Corner Brook Lake, is a topographically visible feature and is marked locally by mylonitized feldspathic rocks and, in places, by contrasts in metamorphic grade.

The second deformation phase (D2) is recorded in all lithologic units in the map area with the exception of the Carboniferous rocks (unit 14). Deformation associated with D2, as well as with D1, is most intense in the east and decreases westward. D2 was apparently nearly coaxial with D1, and it is characterized by northeast-trending, open to tight folds (F2), generally having vertical to steep, southeast-dipping axial planes. Fold axes plunge moderately, and mainly to the northeast. Reorientation of S1 by F2 produced the steep, southeast-dipping, northeast-trending foliation which dominates the structural pattern of the area. F2 is common on all scales, and macroscopic folds are particularly well developed in the carbonate terrane where they are visible on air photographs. Macroscopic F2 folds are likely major contributors to the structural complexity of the metasedimentary terrane as well, as is suggested by outcrop patterns and S1 trends. In fact, the entire northern part of the metasedimentary terrane is thought to be the core of a gently northeast-plunging, F2 antiform.

The sequence and style of the D1 and D2 events, and the ages of the rocks they affect, suggest they may be correlatives of the regionally recognized Taconic and Acadian orogenies, respectively (Williams et al., 1972, 1974). The third deformation phase D3 is relatively minor by comparison and may represent a closing phase of the Acadian Orogeny. D3 is only locally recorded in outcrop, and it is identified by generally northwest-trending, inclined, open folds.

The most recent deformation in the map area is related to faulting. Relatively intense deformation related to movement on the Cabot Fault is clearly recorded in the steeply-dipping Carboniferous sediments adjacent to the fault. The sense of displacement on the Cabot Fault is unknown, and its age is indefinite (Carboniferous or younger). Numerous, high-angle faults have dissected the map area as well, and fault trends vary from west, through north, to northeast, with northwest trends dominant.

Metamorphism

Metamorphic grade in the map area decreases westward with local discontinuities at thrust faults. Mineral assemblages indicate upper greenschist to lower amphibolite facies conditions (Miyashiro, 1973) were reached in the metasedimentary terrane, while conditions in the carbonate terrane were at most those of the lower greenschist facies. The basement terrane appears to have experienced amphibolite facies metamorphism, and this likely during the Precambrian.

A variety of porphyroblasts are found in the metasedimentary terrane, including: albite, actinolite, biotite, zoisite, garnet and tourmaline. Relations between porphyroblasts and rock fabrics suggest that a major period of porphyroblast growth occurred between the D1 and D2 structural events. This may have coincided with peak metamorphism, since retrograde metamorphism appears to have accompanied the D2 event, as evidenced by, for example, chloritized garnet, actinolite and biotite.

Economic Geology

Small amounts of hematite and malachite were found in one outcrop of quartzofeldspathic gneiss (unit 5) in the southeastern part of the area. Minor chalcocopyrite was noted in quartz-rich psammite at one locality in the north. Magnetite is common throughout the metasedimentary and basement terranes, and locally constitutes about 5 per cent of some semipelites in units 6 and 7 in the southern part of the map area.

In the Corner Brook area, limestone and dolomite of the St. George Group (unit 10) and Table Head Formation (unit 11) are quarried for local cement production.

Acknowledgments

The author thanks R.K. Herd, H. Williams, W.H. Poole, J. Hibbard, and D. Knapp for their helpful discussion on various aspects of the work, and R. Jackson, K. Cameron, M. Thomson, J. Elkins and S. Hicks for their capable and cheerful assistance in the field.

Financial support for this work has been provided by E.M.R. Research Agreement 2239-4-48/79 to H. Williams, and field support in 1979 through G.S.C. Project 770026 of R.K. Herd. Other phases of the study are funded by an N.S.E.R.C. Postgraduate Scholarship to the author.

References

- Baird, D.M.
1960: Sandy Lake (west half), Newfoundland; Geological Survey of Canada, Map 47-1959.
- Brückner, W.D.
1966: Stratigraphy and structure of west-central Newfoundland; in *Guidebook - geology of parts of the Atlantic provinces*, Geological Association of Canada, p. 137-151.
- Bursnell, J.T.
1979: Geology of part of the Fleur de Lys map area (12 I/1), Newfoundland; in *Report of Activities for 1978*, Mineral Development Division, Newfoundland Department of Mines and Energy, Report 79-1, p. 68-74.
- Bursnell, J.T. and de Wit, M.J.
1975: Timing and development of the orthotectonic zone in the Appalachian Orogen of northwest Newfoundland; *Canadian Journal of Earth Sciences*, v. 12, p. 1712-1722.

- Church, W.R.
1969: Metamorphic rocks of Burlington Peninsula and adjoining areas of Newfoundland, and their bearing on continental drift in the North Atlantic; in Kay, M., (editor), North Atlantic - geology and continental drift, American Association of Petroleum Geologists, Memoir 12, p. 212-233.
- Hibbard, J.
1979: Geology of the Baie Verte map area (12 H/16 W), Newfoundland; in Report of Activities for 1978, Mineral Development Division, Newfoundland Department of Mines and Energy, Report 79-1, p. 58-63.
- Hyde, R.S.
1979: Geology of portions of the Carboniferous Deer Lake basin, western Newfoundland; in Report of Activities for 1978, Mineral Development Division, Newfoundland Department of Mines and Energy, Report 79-1, p. 11-17.
- Kennedy, D.P.
1978: The geology of a section of the Corner Brook Lake Thrust, western Newfoundland; unpublished B.Sc. thesis, Memorial University, Newfoundland, 81 p.
- Knapp, D., Kennedy, D.P., and Martineau, Y.
1979: Stratigraphy, structure and regional correlation of rocks at Grand Lake, western Newfoundland; in Current Research, Part A, Geological Survey of Canada, Paper 79-1A, p. 317-325.
- Lilly, H.D.
1963: Geology of Hughes Brook-Goose Arm area, west Newfoundland; Memorial University of Newfoundland, Geology Report No. 2.
- McKillop, J.H.
1963: Geology of the Corner Brook area, Newfoundland, with emphasis on the carbonate deposits; unpublished M.Sc. thesis, Memorial University of Newfoundland.
- Miyashiro, A.
1973: Metamorphism and Metamorphic Belts; George Allen and Unwin Ltd., London; 492 p.
- Neale, E.R.W. and Nash, W.A.
1963: Sandy Lake (east half) map-area, Newfoundland; Geological Survey of Canada, Paper 62-28.
- Riley, G.C.
1957: Red Indian Lake (west half); Geology Survey of Canada, Map 8-1957.
1962: Stephenville map-area, Newfoundland; Geological Survey of Canada, Memoir 323.
- Schuchert, C. and Dunbar, C.O.
1934: Stratigraphy of western Newfoundland; Geological Society of America, Memoir 1.
- Stevens, R.K.
1970: Cambro-Ordovician flysch sedimentation and tectonics in west Newfoundland and their possible bearing on a Proto-Atlantic Ocean; in Lajoie, J. (editor), Flysch sedimentology in North America, Geological Association of Canada, Special Paper 7, p. 165-177.
- Walthier, T.N.
1949: Geology and mineral deposits of the area between Corner Brook and Stephenville, western Newfoundland; Newfoundland Geological Survey, Bulletin 35, Part 1.
- Williams, H.
1978: Tectonic lithofacies map of the Appalachian Orogen; Memorial University of Newfoundland, Map No. 1.
- Williams, H., Kennedy, M.J., and Neale, E.R.W.
1972: The Appalachian structural province; in Price, R.A. and Douglas, R.J.W. (editors), Variations in tectonic styles in Canada; Geological Association of Canada, Special Paper 11, p. 182-261.
1974: The northeastern termination of the Appalachian Orogen; in Nairn, A.E. and Stehli, F.G. (editors), The Ocean Basins and Margins, v. 2, Plenum Publishing Corp., New York, p. 79-123.
- Williams, H. and Stevens, R.K.
1974: The ancient continental margin of eastern North America; in Burk, C.A. and Drake, C.L. (editors), The Geology of Continental Margins, Springer-Verlag, New York, P. 781-796.

Project 720102

Suzanne M. Costaschuk¹
Terrain Sciences Division

Costaschuk, S.M., Heavy mineral analysis of southern Beaufort Sea sediments; in *Current Research, Part A, Geological Survey of Canada, Paper 80-1A, p. 241-252, 1980.*

Abstract

Fluvial erosion and transportation, shoreline retreat, denudation of relict arenaceous sediments, and ice-related phenomena are processes presently causing the influx of coarser grained sediments into the southern Beaufort Sea coastal and shelf sediments. The fine terrigenous sands are poorly sorted mineralogically and texturally. Limited authigenic mineralization is occurring on the seafloor at present. Heavy mineral analyses that were carried out on southern Beaufort Sea sands (0.06-0.25 mm fraction) indicate that the sands are derived from pre-existing sedimentary beds as well as from igneous and metamorphic rocks.

Ultrastable and metastable transparent minerals form the bulk of the heavy mineral residue. Zircon, tourmaline, and rutile constitute the former and least abundant group, and clinopyroxene, clinoamphibole, garnet, staurolite, kyanite, sillimanite, andalusite, mica, and heavy carbonates are the most commonly encountered minerals of the latter group. A variety of opaque iron and titanium oxides are also present. The minerals and mineraloids recognized under reflected light are magnetite, ilmenite, leucosene, limonite, goethite, hematite, and pyrite.

Two distinct heavy mineral provinces are recognized in the southern Beaufort Sea: (1) an area characterized by clinopyroxene-clinoamphibole lies to the west of Mackenzie Bay and (2) one with clinopyroxene-clinoamphibole-garnet lies to the east. West of Mackenzie Delta the source of sediment is the Cordillera; east of the delta much of the coarse sediment is believed to have originated from both the Canadian Shield and the sedimentary rocks of the northern Interior Plains.

Introduction

This work is an extension of the sedimentological work undertaken in 1970 by the Marine Sciences Directorate (of the former Department of the Environment) and subsequently by the Geological Survey of Canada. The field work began with the **Hudson 70** cruise into the Beaufort Sea and was supported with sampling from other vessels: **CSS Baffin**, **CSS Parizeau**, **CSS Richardson**, **M/V Theta**, **M/V Pandera**, and several smaller craft. A helicopter was provided for several seasons through the Polar Continental Shelf Project. Much of the early work was augmented by the multidisciplinary program of the Beaufort Sea Project undertaken jointly in 1974 and 1975 by the petroleum industry and the Department of the Environment. It was designed to provide essential baseline data from research and survey programs in order to evaluate environmental hazards related to exploratory and production drilling by the petroleum industry. From this work, Pelletier (1975), dealing with bottom sediments, and Bornhold (1975), working on suspended sediments, were able to demonstrate a sediment dispersal pattern in the southern Beaufort Sea.

This study is based on an analysis of the heavy mineral fraction of bottom sediments collected during these early cruises and operations from helicopters over the ice. This report describes the mineral species and shows their distribution and origin in order to give a more complete history of sediment deposition in the region.

Acknowledgments

I thank Dr. B.R. Pelletier for having made this study possible, for his continued encouragement throughout its duration, and for his contribution to my knowledge of the marine area. I would also like to thank Drs. H. Baadsgaard, O.L. Hughes, J.F. Lerbekmo, T. Poulton, and N.W. Rutter who provided essential background information on the geology of the surrounding area and discussion on the interpretation of the sediments. Appreciation is expressed to

R.N. Delabio and A.C. Roberts of the Geological Survey of Canada for X-ray identification of minerals and to Dr. H. Rimsaite, J. Kempt, and J. White for helping with photography of the minerals.

Geological Framework

The Ancient Setting

The geology of the Beaufort Basin (Yorath et al., 1975) and the adjacent land areas is composed of variously inundated sedimentary strata of Paleozoic, Mesozoic, and Cenozoic age. West of Mackenzie Bay, gently folded Tertiary and Cretaceous marine sequences, which are overlain by unconsolidated sediments, become deformed and faulted in association with the Richardson Mountains and Romanzof Uplift of the Cordilleran tectonic province (Yorath, 1973). East of Mackenzie Delta, the formations comprising the Anderson Plain and the Coppermine Arch dip westward and extend relatively undisturbed into the Beaufort Basin (Yorath, 1973).

The Modern Setting

The marine depositional environments encountered in the study area are of three types: (1) a shallow sea continental shelf generally less than 100 m deep comprising most of the western and eastern regions, (2) a trough, 500 m deep, created in Tertiary time by the Mackenzie River system, northwest from the present delta, and (3) a continental slope margin parallel to the present shoreline (see Fig. 37.1).

Sediment discharged from Mackenzie River accumulates in the gently sloping deltaic plain which is presently advancing north and northeastward from the river system (Pelletier, 1975). The suspended silt- and clay-sized sediments transported by Mackenzie River derive primarily from Liard River, an important tributary originating in the Mackenzie Mountains, which joins Mackenzie River some 1120 km south of the delta (Mackay, 1970).

¹AMOCO Canada Ltd., Calgary, Alberta.

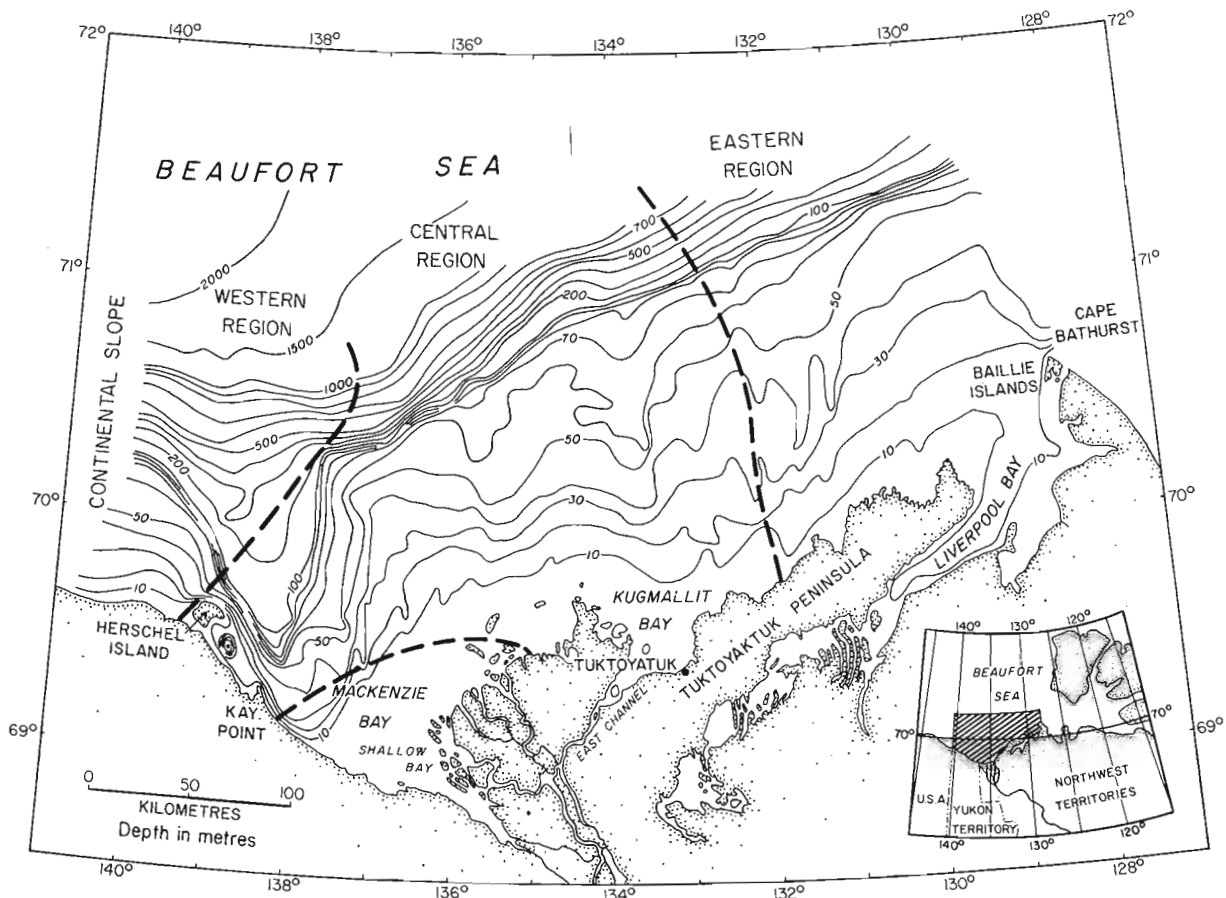


Figure 37.1. Bathymetric map showing location of six regions of heavy mineral occurrences.

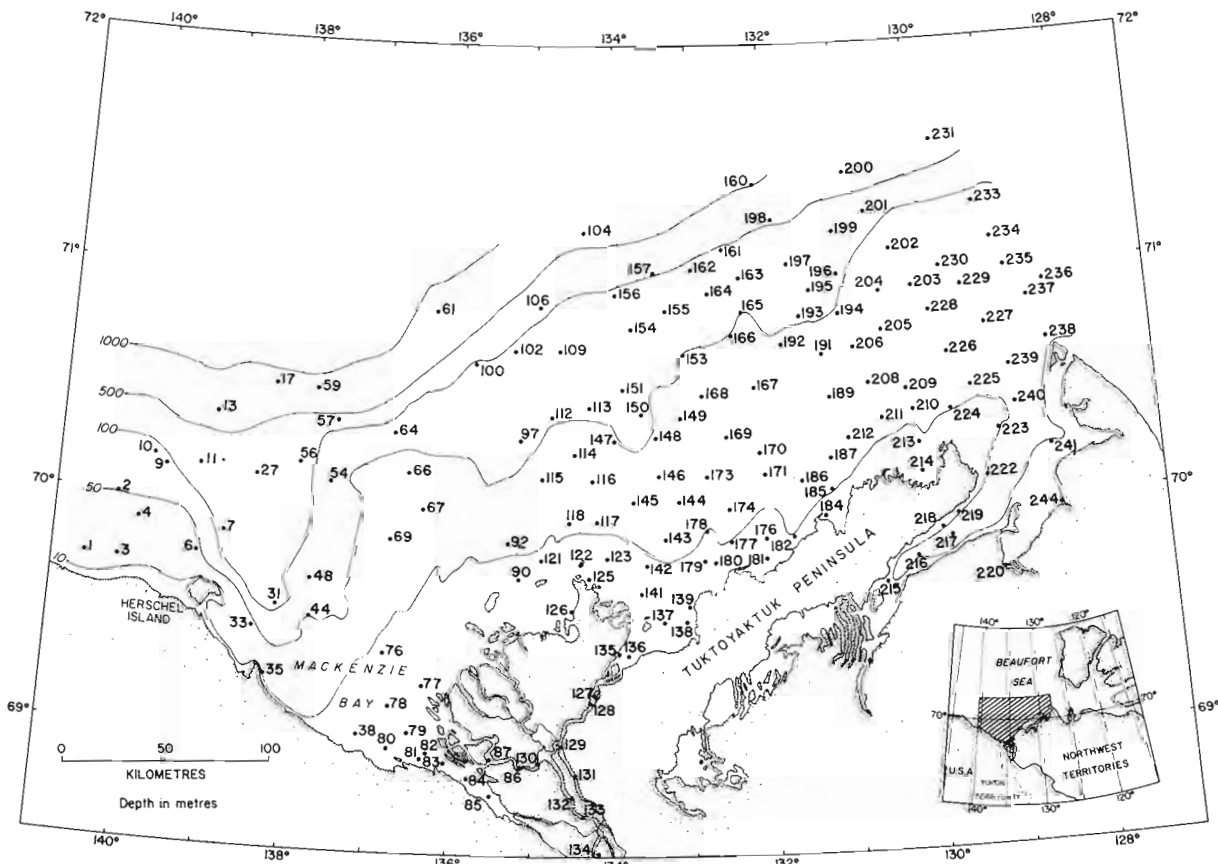


Figure 37.2. Stations where sediment samples were collected (after Pelletier, 1975, Fig. 2).

Retreat of the Arctic Coastal Plain (Bostock, 1969) is occurring rapidly along much of the coastline in the study area. This is particularly so in areas where sedimentary cover is laden with a high ice content (Rampton, 1975). Shoreline deterioration is a result both of the action of waves and permafrost degradation. Because of a southerly migration of the Coastal Plain at a rate of 0.3 to 5 m/year, the volume of sediment accumulating in the Beaufort Sea is considerable. In addition, relict Cenozoic beach sands are being exposed at a faster rate in the eastern part of the study area because of a faster rate of isostatic rebound here (Andrews, 1970).

Recent sediments underlie most of the coast areas adjacent to the southern Beaufort Sea (Lewis and Forbes, 1975; Norris, 1973; Yorath, 1973). Deposits of mud, sand, and gravel comprising the Arctic Coastal Plain vary in width from narrow stretches occurring along the more steeply dipping northern Yukon slopes, to regions that extend as much as 240 km inland; the present Mackenzie Delta and the Kugaluk Homocline exemplify the latter types (Norris, 1973).

The flat-lying sediments that outcrop on the Arctic Coastal Plain are of varying ages and origins (L.V. Hills, personal communication, 1976; Norris, 1973; Rampton, 1975). Glacial drift lies to the east of the contemporary active delta. South of Liverpool Bay, unconsolidated nonmarine mature eolian sands from the Tertiary Beaufort Formation, which also are present on Banks Island, outcrop in a few scattered localities. These deposits cover the consolidated Tertiary, Cretaceous, and Paleozoic sediments of the Northern Interior Platform and the metamorphic and igneous Proterozoic assemblages of the Coppermine Arch Complex (Law, 1971; Yorath, 1973). West of Mackenzie Delta the Quaternary sediments of the Coastal Plain are derived primarily from the Phanerozoic sedimentary rocks of the Cordillera (Lewis and Forbes, 1975; Norris, 1973).

Method

The sediments analyzed were taken from six areas of the southern Beaufort Sea as follows: (1) the western region west and north of Herschel Island including the Mackenzie Canyon; (2) the Kay Point region lying between Herschel Island and Mackenzie Bay; (3) the central region extending north from Kugmallit Bay; (4) the eastern region seaward from Liverpool Bay; (5) the Mackenzie Bay and Shallow Bay area and adjacent part of the Mackenzie Delta; and (6) East Channel of the Delta (Fig. 37.1, 37.2). The regions were chosen for convenience of reporting the results of the heavy mineral study. The modern depositional environments of the study area overlap several of these arbitrary regions.

Heavy mineral separations of the seabottom sediments from 166 sample sites (Figure 37.2) were carried out on the fine sand (0.0625-0.25 mm) fractions and were isolated by wet and dry sieving. After mineral separation with bromoform (specific gravity 2.85) was completed, the magnetic component was removed from the heavy residue with a hand magnet.

The weights of the light, heavy nonmagnetic, and heavy magnetic fractions were recorded, and these values were used to calculate component percentages. Some of the heavy mineral fractions were treated with boiling 10 N HCl in order to dissolve the bulk of the carbonates in the heavy mineral assemblage. Mineral counts were made on the remainder of the residue.

The identification of heavy minerals was aided by the use of X-ray diffractometry, which required the examination of nearly 100 mounts in order to recognize the majority of the mineral phases and their varieties. Examinations of

heavy minerals and counts of loose grains were made in reflected light under a binocular microscope. As further aids in mineral identification, X-ray fluorescence and autoradiography techniques were used. These minerals are shown in Plates 37.1 and 37.2.

Minerals

The light minerals, identified from a few geographically representative samples, include quartz, feldspar, mica, and primarily dolomitic carbonates. Organic matter, in the form of decayed organisms and coal, is present in varying amounts in most light mineral fractions. As mica and heavy carbonates are present in both the light and heavy mineral fractions, they represent mineral classes that are not completely separated by bromoform.

The magnetic component is composed principally of black equidimensional magnetite and ilmenite grains. Rock fragments possessing magnetic character form a significant proportion, comprising up to 30 per cent of the heavy magnetic fraction. The magnetic rock fragments generally consist of fine grained magnetite embedded in grains of quartz and less commonly in amphibole, pyroxene, or epidote. The latter originates from coarse grained metamorphic and igneous rocks or from immature sediments derived from these rock types. The nonmagnetic heavy fraction is composed of undifferentiated clinopyroxenes and clinoamphiboles, as well as garnet, kyanite, sillimanite, andalusite, apatite, epidote, mica, orthoamphibole, staurolite, zircon, tourmaline, rutile, lazulite, limonite, pyrite, ilmenite, and hematite.

The characteristic features of the minerals found in the heavy fractions are listed in Table 37.1, including comments on relative size, shape, roundness, purity, and colour of the transparent and opaque minerals. Colour numbers (Rock-Colour Chart 1951) are included in order that correlations may be made with results from other heavy mineral studies in the area.

Results

Heavy Mineral Distribution

The heavy mineral fraction ranges from a low of 0.13 per cent (Station 231) to a high 8.1 per cent (Station 2) (Fig. 37.2, 27.3). In calculating the heavy to total (heavy plus light) mineral ratio, the value used for the entire heavy residue includes the magnetic fraction, the heavy carbonates (some of which were dissolved in boiling HCl), and the remaining heavy minerals.

The coastal and shelf sediments are mainly sands whose heavy residue content ranges from 0.1 to 5.0 per cent. Patches of more texturally and mineralogically mature sands contain from 3.0 to 5.0 per cent heavy mineral residue. This is probably a reflection of the variation in the rate of uncovering of marine and coastal Cenozoic arenaceous strata in the Beaufort-Mackenzie Basin (Norris, 1973; Pelletier, 1975). Increased uplift (Andrews, 1970) and hydrodynamic vigour (Pelletier, 1975) in the shallow shelf environment of the eastern district are inhibiting factors to the deposition of fine particles derived from Mackenzie River. However, in the central region where scouring by ocean waves and currents is less intense, the quiet deposition of suspended matter continues as in the protected embayments bordering the coast.

Low concentrations of heavy minerals are observed in lutites extending beyond 100 m depth. Their occurrence lies in an area that extends northwest from Mackenzie Bay to Mackenzie Canyon as well as continuing northeastward along the continental shelf-slope boundary.

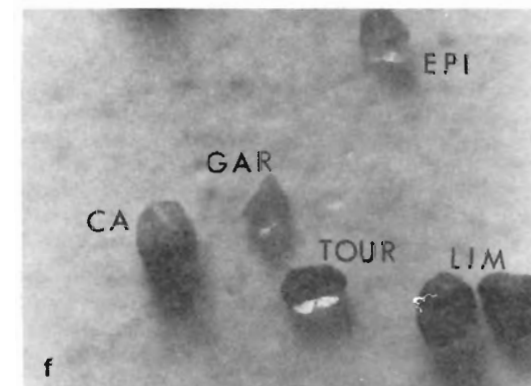
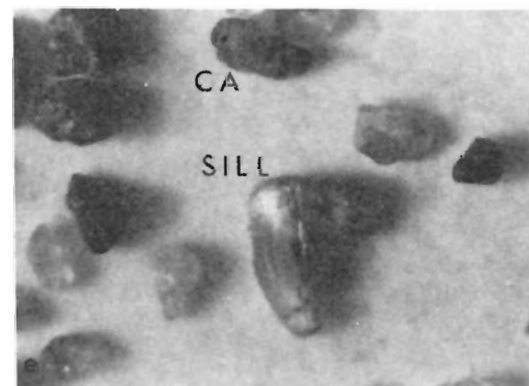
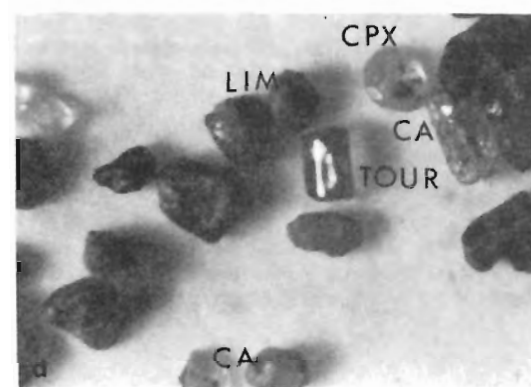
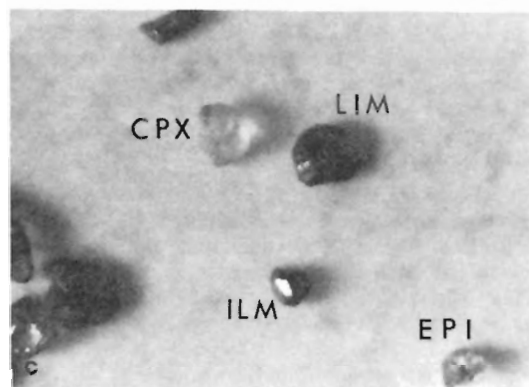
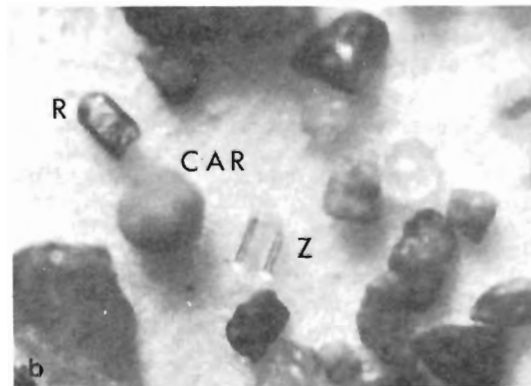
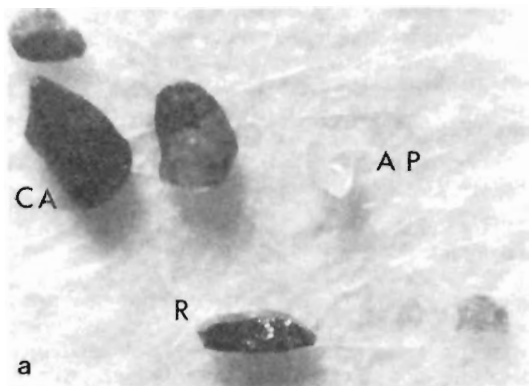


PLATE 37.1

- a. STATION 238. rutile (R), light coloured apatite (AP), clinoamphibole (CA). (x80).
- b. STATION 238. zircon (Z), rutile (R), dolomite-ankerite carbonate (CAR). (x80).
- c. STATION 182. ilmenite (ILM), limonite (goethite) (LIM), clinopyroxene (CPX), epidote (EPI). (x80).
- d. STATION 182. olive-grey tourmaline (TOUR), limonite (LIM), clinopyroxene (CPX), clinoamphibole (CA). (x80).
- e. STATION 182. sillimanite (SILL), clinoamphibole (CA). (x80).
- f. STATION 182. blue-green tourmaline (TOUR), epidote (EPI), garnet (GAR), clinoamphibole (CA), limonite (LIM). (x80).

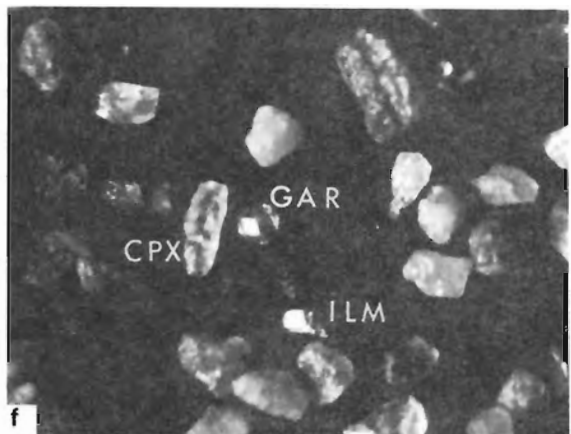
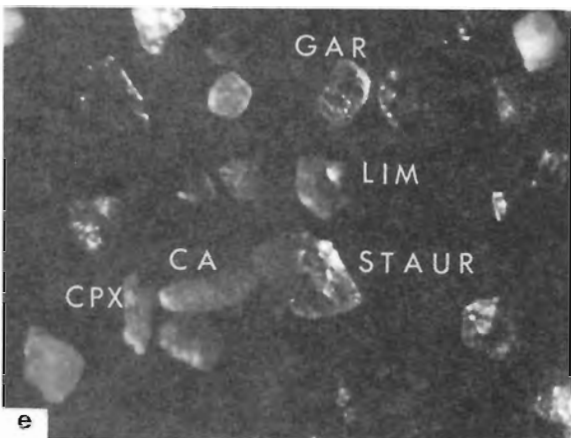
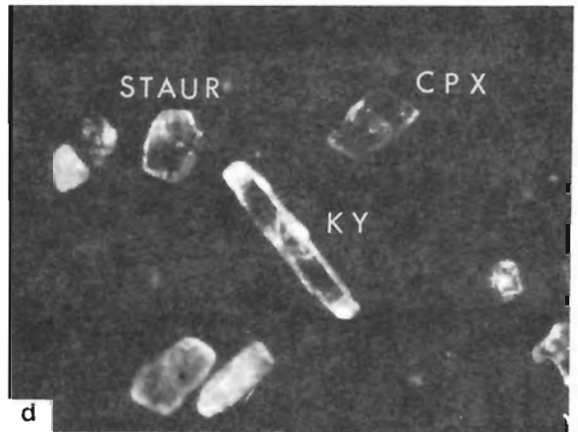
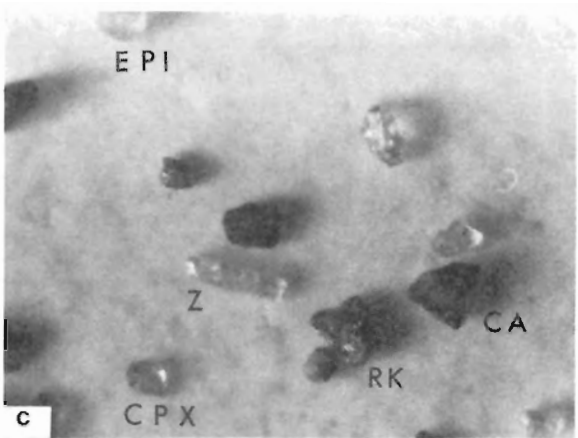
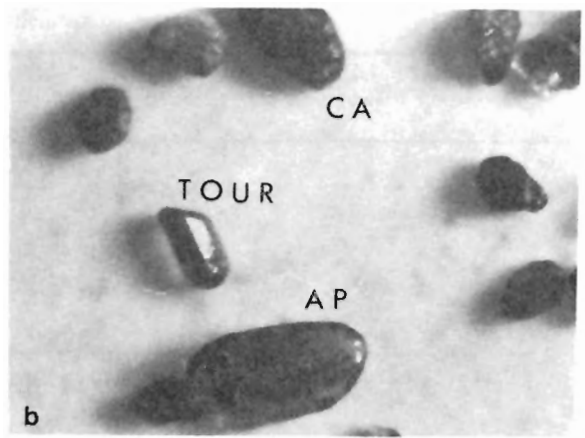
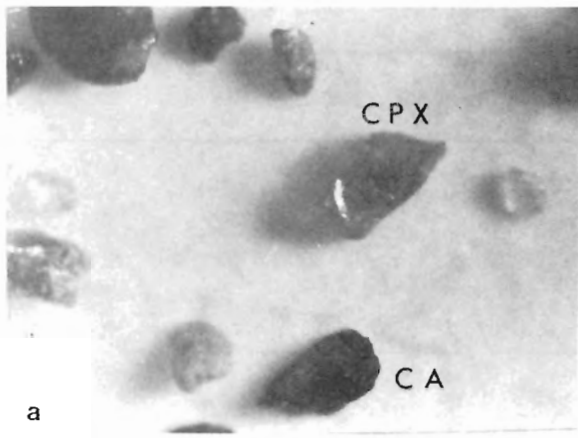


PLATE 37.2

- a. STATION 1. clinopyroxene (CPX), clinoamphibole (CA). (x80).
- b. STATION 182. olivine-grey tourmaline (TOUR), reddish brown apatite (AP), clinoamphibole (CA). (x80).
- c. STATION 182. zircon (Z), clinoamphibole (CA), rock fragment (RK), epidote (EPI), clinopyroxene (CPX). (x80).
- d. STATION 122. kyanite (KY), clinopyroxene (CPX), staurolite (STAUR). (x80).
- e. STATION 122. staurolite (STAUR), limonite (LIM), garnet (GAR), clinoamphibole (CA), clinopyroxene (CPX). (x80).
- f. STATION 122. garnet (GAR), clinopyroxene (CPX), ilmenite (ILM). (x80).

Table 37.1.
Mineral Descriptions

Station (see Fig. 37.2)	Rock Fragments	Clino- amphibole (ca)	Clino- pyroxene (cpx)	Garnet + Andalusite	Mica	Dark Apatite	Light Apatite	Epidote	Staurolite	Kyanite
1	22	15	27	2	2	1		1	0.5	
2	21	14	40	6	0.5	0.5		0.5	0.5	
3	19	15	23	TR	3	0.5		0.5	TR	
4	13	16	37	5	5	0.5		0.5	0.5	
6	14	16	44	2	0.5	0.5		TR	TR	
9	9	16	42	9	2	1	0.5	0.5	0.5	
10	6	21	40	7	0.5	1		0.5	TR	
13	15	21	31	3	1	1	0.5	TR	TR	
29	26	4	20	0.5	14	TR	0.5	2		
31	13	12	36	2	13	TR		1		
33	28	6	25	3	5	TR	0.5	TR		
35	14	7	21	6	10	0.5		1	1	
77	1	11	17	2	61	1		0.5		
84	1	20	36	6	10	3		3	1	
61	7	12	17	6	TR	1		1	0.5	
100	2	36	35	5	4	2		1	0.5	
97	4	30	28	16	2	2		2	2	
115	2	30	31	22	TR	0.5	0.5	1	2	
118	4	14	31	2	2	1		0.5	0.5	
122	7	23	21	6	4	2		2	0.5	0.5
125	5	22	22	8	4	1	0.4	2	0.5	
127	8	2	26	3	4	2		3	2	
231	7	11	22	8	2	4	2	2	TR	
233	4	14	32	11	14	1	1	0.5	TR	
234	4	16	41	9	7	2	0.5	3	1	
235	16	7	37	13	0.5	TR		1	TR	
236	8	11	48	14	TR	TR		1	2	
237	9	13	32	15	0.5	1		TR	TR	
238	6	17	33	16	TR	1		1	0.5	0.5
239	6	19	38	11	1	2		2	1	

Magnetic Fraction

Weight percentages of magnetic to total heavy residue are shown in Figure 37.4. The percentages vary from trace amounts, in the Mackenzie Bay and Mackenzie River areas, to 29.2 per cent in the western region. Other areas of low magnetic components exist in an area extending north from Kugmallit Bay to the east and northeast of Tuktoyaktuk Peninsula. The remaining western, central, and eastern regions show gradations from low (1.2 per cent) to high (19.6 per cent) values.

Anomalously high magnetic to heavy residue percentages, but an overall low heavy mineral content, are shown in the fine grained sediments of Mackenzie Canyon and the northeastern slope areas. The precipitation of magnetite from sea water is not known to occur in marine environments that are not influenced by igneous activity, but it may have occurred in the Beaufort Sea area in Paleozoic time (Miall, 1976). The limited evidence for the formation of authigenic magnetite makes the interpretation of these results difficult. Under mildly reducing conditions, magnetite is known to form (Folk, 1974; Garrels and Christ, 1975), and glauconite is commonly an associated authigenic mineral (Folk, 1974). Hence, below the surface sediments, magnetite may be forming. An analysis of the bulk samples taken from the deeper water should follow in order to clarify this paragenetic problem. Alternatively, the origin of the magnetic fraction could be inferred from chemical analysis.

The large percentage of magnetic grains may be a reflection of relict Cenozoic beach sand that has a high percentage of heavy minerals. If the arenaceous sediments found in the deeper waters (Vilks et al., 1979) represent either original Cenozoic strata or sediments formed from the slumping of shelf sediments, magnetite and ilmenite would be of a detrital nature. Continuous inundation in arctic waters may have created a thermodynamically stable regime for the preservation of these ferric oxides (Garrels and Christ, 1975). Upwelling observed along the upper margin of the continental slope may also be responsible for the preservation of greater volumes of magnetite (B.R. Pelletier, personal communication, 1975).

Mineral Counts

Mineral counts (Table 37.2) have been made on 30 bottom samples. Rock fragments, clin amphiboles, clinopyroxenes, garnets, andalusite and micas comprise the majority of transparent minerals. Less common minerals such as apatite, epidote, staurolite, kyanite, sillimanite, zircon, rutile, tourmaline, and lazulite never appear in concentrations greater than 4 per cent. Limonite, ilmenite, and hematite constitute the majority of the nonmagnetic opaques. Pyrite, found locally, comprises 43 per cent of the heavy mineral fraction found at station 61.

Rock fragments range from 1 to 28 per cent of the heavy residue (Table 37.2). Several rock types are

Table 37.1 (cont'd)

Silli- manite	Zircon	Rutile	Tour- maline	Lazulite	Lim- onite	Pyrite	Ilmen- ite	Hema- tite	Other	(ca cpx)	Region (see Fig. 37.1)
	0.5			0.5	20		1	2	8	0.56	Western
	0.5	0.5		0.5	9		TR	2	6	0.35	
	TR				29		0.5	4	5	0.65	
	TR				15		TR	0.5	7	0.43	
	0.5				13		2	1	7	0.36	
	1	0.5	0.5		10		3	2	6	0.38	
	0.5				14		1	3	5	0.53	
	2	1			16		4	1	3	0.68	
	TR		0.5		7		0.5	TR	25	0.20	Kaypoint
	0.5		0.5		5			0.5	17	0.33	
	0.5		0.5	0.5	16		0.5	3	13	0.24	
	0.5	2	3	2	15		1	TR	14	0.33	
	TR	0.5	1	0.5	4				2	0.65	Mackenzie Bay
	0.5		0.5	0.5	10				9	0.56	
0.5	1		0.5		2	43	2	1	5	0.71	Central
	TR		0.5		4	2		3	7	1.03	
	1	0.5			7	0.5	2	2	5	1.07	
0.5	3		0.5		2		0.5	2	4	0.97	
	2				21		1	2	2	0.45	
	TR	0.5	2		21			3	8	1.10	
	0.5		1		20		1	4	6	1.00	
	1		2		14			0.5	8	0.08	
	2	TR	1		28		2	6	3	0.50	Eastern
	1	TR	TR	TR	13		0.5	6	3	0.44	
	TR	0.5	0.5		8		3	3	3	0.39	
	TR	2	TR		7		1	14	2	0.19	
	TR	1	TR		6		2	8	1	0.23	
0.5	2	TR	TR		10		10	7	TR	0.41	
	TR	0.5	0.5		13		0.5	5	4	0.52	
0.5	1	0.5	0.5		5		7	3	3	0.50	

recognized, the most important being feldspar and shale. In the eastern and central districts, hematite-rich argillaceous rock fragments are abundant. These are thought to be derived from Upper Cretaceous shales on the Anderson Plain (Bostock, 1969).

Rock fragments are more abundant in the western region. These are likely derived from consolidated rocks in northern Alaska and Yukon Territory and in the northwestern part of the District of Mackenzie. Tertiary flysch and molasse sediments outcropping along the north slope of Yukon Territory are probable sources of these various rock fragments (Young, 1973). Their preservation in recent coastal sediments east of Herschel Island is partly a consequence of a steeply sloping shelf area (Fig. 37.1). With rapid deposition in deeper waters, mechanical erosion of sediments by waves and currents would be minimized. Poor sorting, increased angularity, and arenite-rich sediments in this area are also suggestive of rapid sedimentation.

Transparent Minerals The heavy minerals encountered in this study include those which, according to Folk's classification (1974), fall into the ultrastable and metastable groups of transparent minerals. Zircon, tourmaline, and rutile fall into the former, and most other transparent minerals are grouped into the latter.

Clinopyroxenes (cpx) and clin amphiboles (ca) are the predominant heavy minerals in the arenitic shelf sediments.

The clinopyroxenes are more abundant than the clin amphiboles, ranging from 17 to 48 per cent of the nonmagnetic heavy minerals. Their concentrations are slightly higher in the western and eastern regions, though this finding may not be truly representative because of insufficient sampling. Clin amphibole concentrations comprise from 2 to 36 per cent of the heavy residue content, with the lowest amounts found in the fine sediments of the Mackenzie Delta area. The distributions in the western (14 to 21 per cent) and the eastern (11 to 19 per cent) regions are approximately equal, but in the central region higher levels are found (12 to 36 per cent).

Offshore, the proportion of clinopyroxenes varies inversely to that of clin amphiboles. The ca/cpx ratios were calculated in order to detect subtle changes in heavy mineral content. Higher ca/cpx values are observed for sands in the central region as compared with those in the western and eastern regions (see Table 37.2).

According to the Mineral Reaction Series (after Goldich, see Krumbein and Pettijohn, 1938) clin amphiboles should be more stable than clinopyroxenes in oxidizing surface conditions. Hence, higher ca/cpx ratios for the central region may be indicative of sands that are mineralogically more mature than sands in the bordering districts. Conversely, sediments in the western and eastern districts may be younger due to the influx of coarse material which either is very immature or is derived from formations with an initially high content of clinopyroxene.

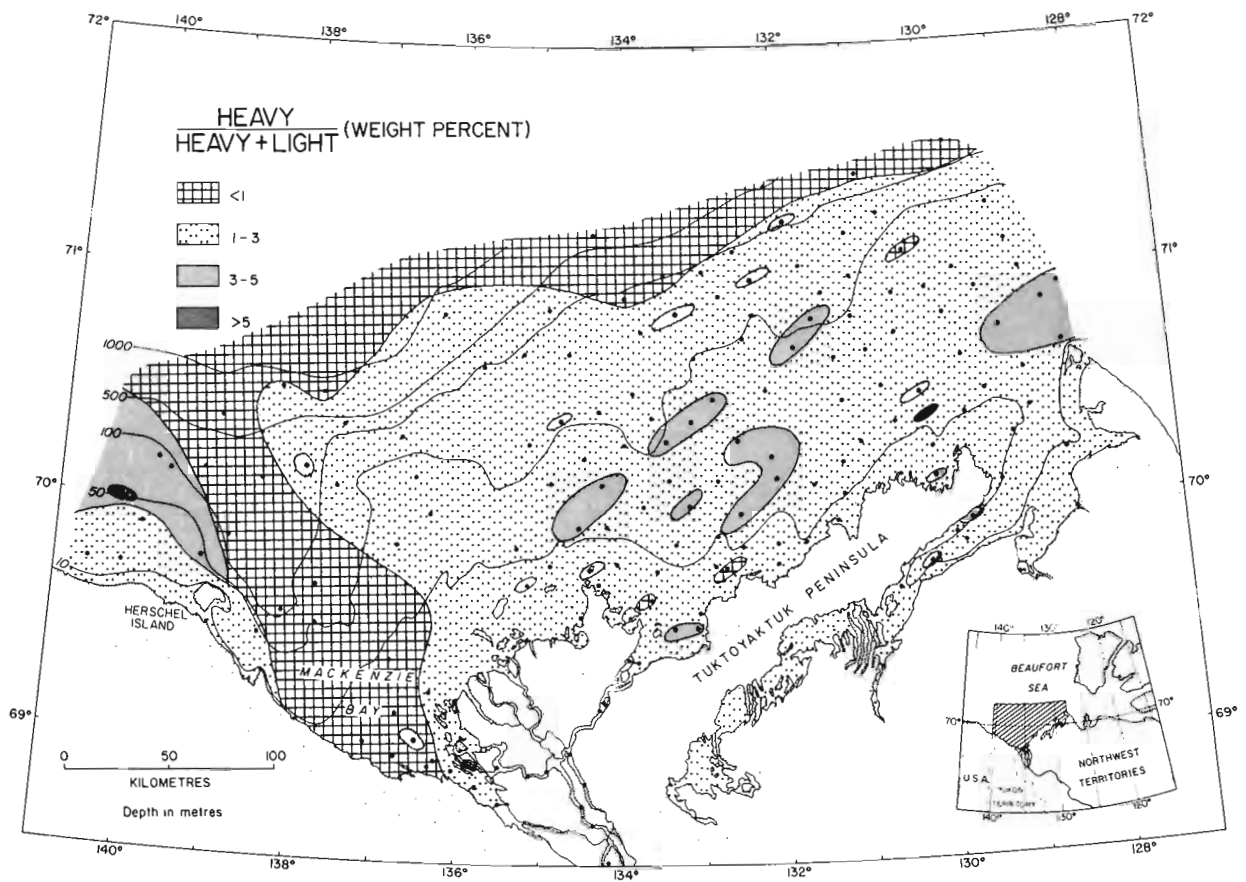


Figure 37.3. Map showing distribution of heavy minerals to total minerals.

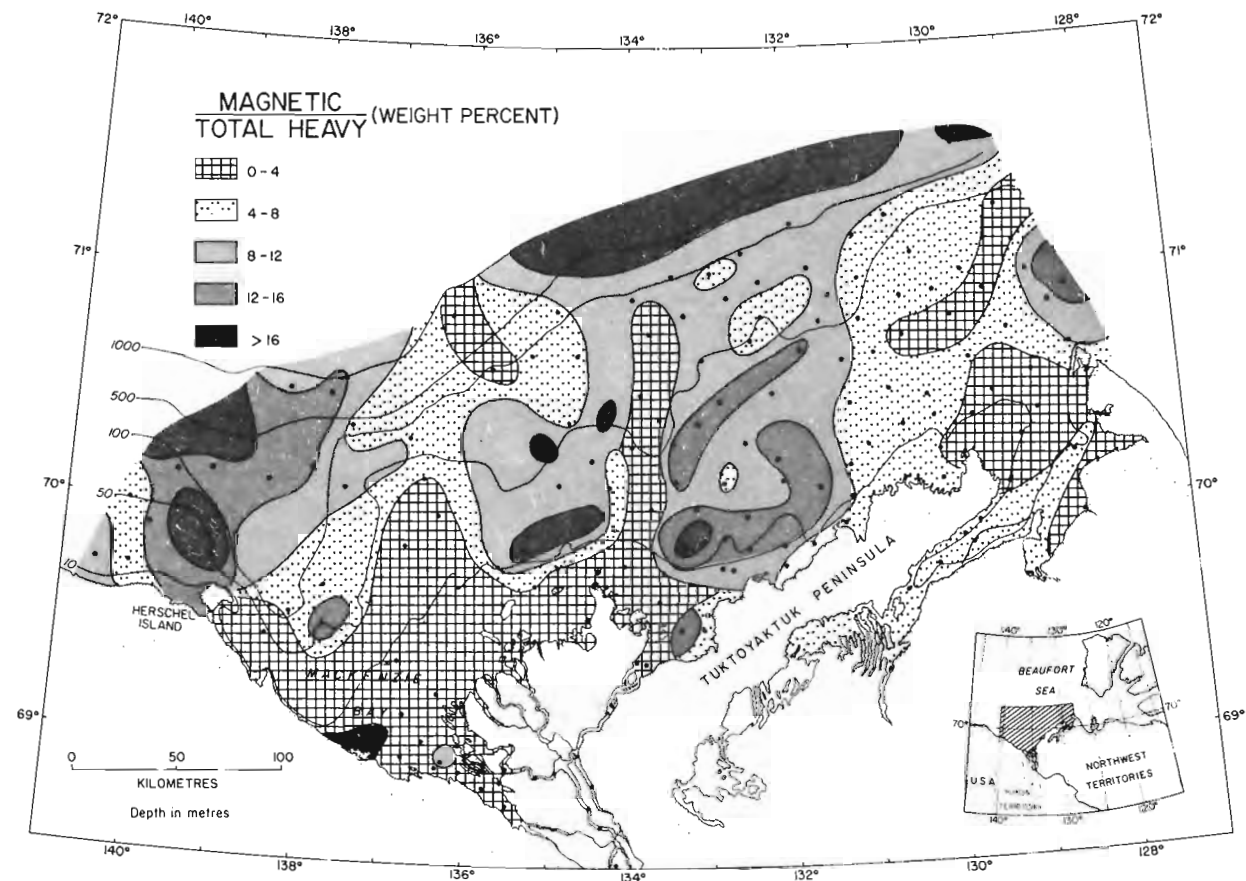


Figure 37.4. Map showing distribution of magnetic residue to total heavy residue.

Igneous assemblages generally contain higher percentages of pyroxenes than their equivalent metamorphic rocks (Deer et al., 1966). Although igneous rocks do not outcrop in or near the Beaufort Basin, their presence in the Northern Cordillera and Proterozoic rocks of Alaska and northern Canada is of importance (Brosge and Dutro, 1973; Douglas, 1970). In the western region, granitic and ultramafic intrusives of the Northern Cordillera are the most likely source of clinopyroxenes found in the heavy mineral fractions (Brosge and Dutro, 1973; Gleeson, 1963; Monger et al., 1972). In the eastern region, where glaciofluvial material is being eroded, mafic intrusions associated with sills and Mackenzie dyke swarms in the Precambrian Shield are probably the source of some of the clinopyroxenes (Douglas, 1970; Norris, 1973).

Garnet and andalusite grains have been grouped as one mineral type (Table 37.2) because they could not be distinguished from one another under reflected light; their colour, grain shape, and purity were not distinctive enough to permit their separation. X-ray analysis of pink grains from several localities indicates that andalusite forms a very small percentage of grains encountered.

Andalusite has been found at only two nearshore eastern and central sampling sites which indicates that it probably has been recently incorporated into Beaufort Sea sediments. Because of its low specific gravity it should be winnowed out to the deeper portions of the continental shelf. It possibly originates from the mineralogically immature sedimentary horizons that underlie the northern Interior Plains bordering the Beaufort Sea. Since andalusite is a less stable and less common metamorphic mineral than garnet (Krumbein et al., 1938), its low relative abundance compared with garnet is expected; hence, it is felt that data obtained on their combined percentages remains meaningful.

A range of only 0 to 9 per cent garnet (gr), together with traces of andalusite, is obtained for sands in and west of Mackenzie Bay (Table 37.2). Proportions as high as 22 per cent in the central and eastern regions, however, indicate a change in source material. The provenance of this material is undoubtedly igneous and high grade metamorphic terranes to the east, certainly for the sands found in the cpx-ca-gn heavy mineral province in the central and eastern regions (Douglas, 1970).

Mica content in the Mackenzie Bay lutites is high; mica forms up to 61 per cent of the heavy residue. Because of differences in relative grain size, mica flakes carried by Mackenzie River likely are deposited in nearshore environments, whereas clay- and silt-sized particles are transported farther offshore. Impure carbonates and shales of the northern Interior Plains are probably sources of mica in surface sediments of the southern Beaufort Sea (Douglas, 1970; Noble and Ferguson, 1971; Yorath, 1973). The erosion of subsurface lutites underlying Mackenzie Delta also may cause an increase in mica concentrations.

The remaining metastable heavy minerals appear in concentrations forming up to 4 per cent of the heavy fraction. Apatite, epidote, staurolite, kyanite, and sillimanite are more common in the central and eastern regions, in both nearshore and offshore environments. Igneous and high grade metamorphic rocks to the east or southeast of the Beaufort Basin are required as sources of the angular, metastable assemblages described above.

Zircon, rutile, and tourmaline are present in concentrations of less than 3 per cent. These ultrastable minerals are more common in the eastern region and in the coastal areas bordering the seaward side of Tuktoyaktuk Peninsula. The characteristics of these heavy minerals change to the west. Large, well rounded zircons (especially hyacinth) and brown tourmalines are found in the well sorted

arenaceous-rich sediments northwest of Cape Bathurst (see Fig. 37.1). The occurrence of rounded hyacinth zircons in sedimentary formations is thought to indicate incorporation of material derived from Precambrian rocks (Poldervaart, 1955). These could be derived from plutonic igneous intrusions in the Slave and Churchill provinces and transported by Pleistocene glaciers (Douglas, 1970; Prest, 1969).

Opaque Minerals Iron oxides and sulphides form a significant part of the heavy arenaceous sediment, with limonite, hematite, and pyrite being most important (see Table 37.2). They are commonly diagnostic of the thermodynamic conditions prevailing at the time of their formation.

The occurrence of the iron-oxides is suggestive of near-surface oxidizing conditions. The presence of limonite in the coastal and shelf environments is expected, as materials from decomposing soil horizons constitute a significant proportion of the bottom sediments; however, limonite in the deeper slope sediments likely results both from the winnowing effects existing in the shallower waters and from sediment slumping in the shelf-slope area. In the eastern shelf sediments, higher hematite concentrations probably are caused by the influx of sediment derived from the oxidized iron-rich Cretaceous strata underlying the Anderson Uplift (Yorath, 1973). On the other hand, pyrite found locally in the deeper slope sediment is an indicator of reducing environments.

Opaque titanium-bearing oxides are mainly associated with the eastern shelf sediments. Ilmenite concentrations reach as high as 10 per cent off Cape Bathurst (Fig. 37.1, Table 37.2). As ilmenite is derived from metamorphic and basic igneous rocks, it is abundant in the eastern region because here sediments originate mainly from the Precambrian Shield. Leucoxene (see ilmenite and rutile, Table 37.2), a titanium-bearing mineraloid, is restricted to the easternmost coastal sands. Leucoxene forms somewhat elongated and well rounded grains whose shapes bear a striking resemblance to both fresh and altered rutile grains; however, they are beige to white opaque grains with surfaces that are rough but polished. Leucoxene forms from rutile and other titanium-bearing minerals and is representative of oxidized horizons (Krumbein and Pettijohn, 1938; Milner, 1962). The areal distributions both of leucoxene and rutile are in agreement as each is found in larger concentrations in coastal sands bordering the eastern region.

Discussion

The presence of ultrastable well rounded minerals such as zircon, tourmaline and rutile is indicative of older sediments as source material. Such mature sediments have undergone either several cycles of sedimentation or prolonged periods of mechanical erosion. Conversely, the abundance of metastable minerals such as garnet, amphibole, and pyroxene is suggestive of crystalline and high metamorphosed rocks as sources. This implies that voluminous supplies of sedimentary material having undergone possibly but one cycle of sedimentation have been incorporated into the Beaufort Sea bottom sediments. Also, significant percentages of both heavy carbonates and hematitic argillaceous grains found in the sediment indicate a source of material from sedimentary formations other than mature detrital sands.

Several sources of rounded, ultrastable minerals are possible, such as submerged relict beach deposits presently being eroded. Similarly, terrestrial Phanerozoic clastic sediments associated with the Cordilleran and western Canadian Shield are contributing material to the Beaufort Sea. Although only limited heavy mineral research on strata

Table 37.2
Percentage of heavy minerals

TRANSPARENT MINERALS			TRANSPARENT MINERALS		
MINERAL DESCRIPTION	COLOUR	ROCK COLOUR CHART NO.	MINERAL DESCRIPTION	COLOUR	ROCK COLOUR CHART NO.
<u>CLINOAMPHIBOLES</u>			<u>ZIRCON</u>		
large elongated, angular to well rounded rough with dull to polished surfaces; inclusions common in light-coloured varieties.	pale yellowish green, greyish green, dusty yellowish green, dark yellowish green, dusty green, greyish green, dusty blue-green, black	10GY 7/2 10GY 5/2 10GY 3/2 10GY 4/4 5G 3/2 10G 4/2 5BG 3/2 N-2	medium to small, elongated to short prismatic, polished smooth surfaces, euhedral to rounded; inclusions frequent in coloured varieties; colourless zircons commonly perfect euhedral; pink and red zircons well rounded, clear.	colourless pale pink, pale red-purple pale brown, very pale orange, greyish orange, pale yellowish orange	5RP 8/2 5RP 6/2 5YR 5/2 10YR 8/2 10YR 7/4 10YR 8/6
<u>CLINOPYROXENES</u>			<u>RUTILE</u>		
large, elongated to equant, angular to well rounded, vitreous to dull with rough surfaces; inclusions common; small olive-grey euhedral crystals, vitreous, inclusions frequent.	colourless, white, yellowish grey, yellowish grey, pale yellowish orange, greyish orange, light olive-grey, olive-grey, pale olive, moderate olive brown	5Y 8/1 5Y 7/2 10YR 8/6 10YR 7/4 5Y 5/2 5Y 3/2 10Y 6/2 5Y 4/4	small, elongated, prismatic, adamantine lustre; grey variety well rounded with dull rough surfaces.	medium light grey, black metallic, blackish red	N6 N2 5R 2/2
<u>APATITE</u>			<u>TOURMALINE</u>		
large elongated, well rounded, vitreous, polished smooth surfaces, clear; light coloured apatite commonly smaller, equant grains.	very dark red, moderate reddish brown, dark reddish brown, dark yellowish orange, dusty yellowish brown, pale blue-green, colourless	5R 2/6 10R 4/6 10R 3/4 10YR 6/6 10YR 2/2 5BG 7/2	large to small, euhedral, vitreous to well rounded, polished smooth grains, clear; blue-green variety, lath-like conchoidal fracture, vitreous, clear.	greyish olive, light olive-grey, olive-grey, dusty blue-green	10Y 4/2 5Y 5/2 5Y 3/2 5BG 3/2
<u>EPIDOTE</u>			<u>MICA</u>		
medium to small, equant, vitreous, well rounded, polished smooth, clear.	moderate yellow, moderate yellow green	5Y 8/2 5GY 7/4	large broken flakes, bent, some pseudo-hexagonal; mica books rare.	dark reddish brown, pale greenish yellow, dark yellowish orange, light olive-grey	10R 3/4 10Y 8/2 10YR 6/6 5Y 5/2
<u>GARNET</u>			<u>ORTHOAMPHIBOLE</u>		
large to small, euhedral crystals to angular crystal fragments, vitreous, commonly clear.	greyish pink, greyish orange-pink, pinkish grey, moderate orange-pink, moderate reddish orange, moderate reddish brown	5R 8/2 10R 8/2 5YR 8/1 10R 7/4 10R 6/6 10R 4/6	medium sized, lath shaped clear.	colourless	
<u>ANDALUSITE</u>			<u>LAZULITE</u>		
small, anhedral with conchoidal fracture, cloudy.	very pale-orange, greyish pink, pale reddish brown	10YR 8/2 5R 8/2 10R 5/4	small, anhedral, vitreous, rough surfaces.	moderate blue	5B 5/6
<u>STAUROLITE</u>			<u>CARBONATES (dolomite, ankerite, siderite)</u>		
large to small, slightly elongated, conchoidal fracture, vitreous, inclusions frequent.	dark yellowish orange, moderate reddish brown	10YR 6/6 10YR 4/6	large to small, euhedral clear crystals to spherical polished rough grains.	light brown, moderate brown, moderate yellowish brown, medium grey, yellowish grey, colourless	5YR 6/4, 5/6 5R 4/4 10YR 5/4 N6, N5, N4 5Y 8/1
<u>KYANITE</u>			<u>OPAQUE MINERALS</u>		
small, elongated euhedral, vitreous, clear.	colourless		<u>LIMONITE (GOETHITE)</u>		
<u>SILLIMANITE</u>			large to small, irregular shapes to well rounded spheres, commonly polished with smooth or rough surfaces.		
large, elongated, bent, fibrous, aggregated; colour generally not uniform.	colourless, white, very pale green, pale brown, greenish grey	5G 9/2 5YR 5/2 5GR 6/1	moderate brown, dark yellowish brown, dusty yellowish brown, light brown, dark yellowish orange		
			<u>PYRITE</u>		
			small, equant, dull rough surfaces.		
			medium dark grey		
			N4		
			<u>ILMENITE</u>		
			small, equant to elongated, metallic lustre.		
			greyish black		
			N2		
			<u>HEMATITE</u>		
			medium to small rounded fine grained rock fragments.		
			dark grey, dusty red, moderate red		
			N3 5R 3/4 5R 4/6		

in the western Arctic has been conducted, examination of the equivalent formations to the south has revealed the presence of highly rounded ultrastable minerals (Douglas, 1970). Rounded zircons are predominantly derived from pre-existing sediments, but evidence of such zircons in crystalline rocks has been documented (Poldervaart, 1956). Nearly equidimensional, anhedral zircons, reported to be in several intrusions in northern Yukon Territory, are thought to be the source of similarly shaped zircons in the western part of the study area.

Generally metastable heavy minerals, such as clinopyroxene, clinoamphibole, and garnet, associated with young sediments conceivably are derived from various sources. In the western region of the Beaufort Shelf, coarser sediments are transported to the coastal plain through fluvial processes. Here, detrital sands and gravels are also accumulating because of continuing coastal erosion. In the eastern and central regions, mineralogically immature sands with abundant accessory metastable minerals derived from a receding arctic coastline are being accumulated. Consequently, widespread glaciofluvial sediments derived from the Canadian Shield are being incorporated into the Beaufort Sea sediments.

Presumably, mixing of materials derived from both the reworked beach deposits and the commonly immature, terrestrial sediments occurs following deposition in the Beaufort Sea. Bars and spits shaped by the action of waves and longshore currents are redistributing the sand principally into lineaments parallel with the coast (Lewis and Forbes, 1975; Pelletier, 1975).

The direction and distance that arenaceous sediment is transported in the Beaufort Sea is variable and is not completely understood (Carsola, 1954; Forbes, 1976; Lewis, 1975; Pelletier, 1975). The limited evidence for drift direction is likely a reflection of the complexity of this deltaic-marine environment. In most cases, distinctive dispersal patterns of each mineral are not developed due to thorough mixing of sediments from various sources. Furthermore, heavy residue provinces hosting characteristic mineral associations are not sufficiently distinct to be utilized in detailed studies of sediment transport. Nevertheless, the recognition of two discrete heavy mineral provinces to the west and east of Mackenzie Canyon, cpx-ca and cpx-ca-gn respectively, can serve to determine broad, sediment dispersal trends.

In nearshore environments, movement is known to occur parallel to the present shoreline. An east-west trend of sediment dispersal is apparent in the eastern and central region, which may prove to be a result of differential rate of exposure of submerged relict beaches. West of Mackenzie Delta, no general trends prevail. Certainly, a comparison of the heavy mineral assemblages in the shelf sediments extending off Alaska and Yukon Territory would confirm the direction of transport. Evidence for the movement of material offshore is lacking although this may become apparent with further studies concentrating on the hydrodynamic factors existing in shelf waters.

Lazulite, probably originating in the Mount Fitton area in northern Yukon Territory, is found in marine deposits in the Herschel Island and Kay Point area (Campbell, 1962). Ancient river systems that drained the Mount Fitton area and Richardson Mountains could also be responsible for the increased spatial distribution of this relatively rare phosphate mineral in the western Arctic Coastal Plain. As indicated in Table 37.2, lazulite is restricted to an area both immediately west and east from its proposed site of egress to the sea near Kay Point.

The influx of coarse grained material to the Beaufort Sea sediments generally is restricted to coastal areas where retreat of the shoreline is occurring. Ocean waves and

currents scouring the coastal sands are likely effective dispersing agents. Waves and currents redistribute the material into variously oriented bars and spits. Consequently, in shoreline districts, the mineral assemblages are continuously being modified as new material is added and submerged arenaceous sediments become exposed. Hydrodynamic factors, causing the heavier minerals to deposit in nearshore environments while lighter minerals (quartz, feldspars, carbonates, and micas) may be winnowed out and redeposited in deeper low-energy regimes, are not apparent from dispersal patterns reported here. A more detailed study of all the sand-sized fractions, however, could establish the magnitude of hydrodynamic factors operating in the shallow water environments.

Pack and shore-fast ice found in areas within 50 m water depth (Pelletier and Shearer, 1972) disturb and redistribute bottom sediments. Sediment emplaced in sea ice may be transported considerable distances before being dislodged from the melt ice. Consequently, even bottom sediments in deeper waters conceivably can receive material from melting sediment-laden ice. The trace amount of lazulite found in the bottom sediments at one eastern sampling site is probably the result of ice rafting. Such processes are also thought to be responsible for the development of poorly sorted coarser sediment near Herschel Island (Pelletier, 1975).

Conclusions

The heavy mineral distributions of the Beaufort Sea include minor concentrations of ultrastable minerals such as zircon, tourmaline, and rutile. Metastable minerals such as clinopyroxene, clinoamphibole, garnet, staurolite, kyanite, sillimanite, andalusite, mica, and heavy carbonates are in greater abundance. Other minerals identified under reflected light include: magnetite, ilmenite, leucosene, limonite, goethite, hematite, and pyrite.

At least two provenances have been distinguished for the heavy mineral suite occurring in the Beaufort Sea sediments: (1) the Cordillera is the source of the heavy minerals west of Mackenzie Delta, based on an examination of the clinopyroxene-clinoamphibole suite and (2) the Canadian Shield and the rocks of the northern Interior Plains are sources of the coarse sediments found in the east, characterized by the clinopyroxene-clinoamphibole-garnet suite.

The heavy mineral distributions of the Beaufort Sea sands have been described and subsequently related to the local and regional geology of the Beaufort Basin. The shelf sediments have developed mostly through the reworking of relict beach material and the deterioration of the sedimentary horizons in the immediate coastal regions. These predominantly detrital, immature marine sands are derived from sediments of differing provenances, including various stratigraphic horizons underlying and bordering the coastal region. In the northern Interior Plains, recent glacial fluvial sands originating from the Precambrian igneous metamorphic rocks to the east have been the major source of material to the eastern and central shelf sediments. Mesozoic and Paleozoic rocks underlying the Quaternary sediments are believed to be the source of carbonates as well as other minerals characteristic of sedimentary regimes. West of Mackenzie Delta, coarse grained sediments derived from Mesozoic and Paleozoic sedimentary and igneous rocks from northern Yukon Territory comprise the Arctic Coastal Plain which at present is being eroded through permafrost degradation and wave action. The resulting debris is being incorporated into the western Beaufort Shelf sediments. Only to the western shelf region, where sand and gravel material is originating from young rivers draining the Cordilleran hinterland, is there an active fluvial source of coarse grained material.

References

- Andrews, J.T.
1970: A geomorphological study of postglacial uplift with particular reference to Arctic Canada; Institute of British Geographers, Special Publication 2, London.
- Bornhold, B.D.
1975: Suspended matter in the southern Beaufort Sea; Beaufort Sea Project, Department of the Environment, Technical Report No. 25a, 30 p.
- Bostock, H.S.
1969: Physiographic regions of Canada; Geological Survey of Canada, Map 1254A, scale 1:5 000 000.
- Brosge, W.P. and Dutro, J.R.
1973: Paleozoic rocks of northern and central Alaska; in *Arctic Geology*, ed. M.G. Pitcher; American Association of Petroleum Geologists, Memoir 19.
- Campbell, F.A.
1962: Lazulite from Yukon, Canada; *American Mineralogist*, v. 47.
- Carsola, A.J.
1954: Recent marine sediments from Alaskan and northwest Canadian Arctic; *American Association of Petroleum Geologists, Bulletin* 38.
- Deer, W.A., Howie, R.A., and Zussman, J.
1966: *An Introduction to the Rock Forming Minerals*; Longman Group Ltd., London.
- Douglas, R.J.W. (ed.)
1970: *Geology and economic minerals of Canada*; Geological Survey of Canada, Economic Geology Report No. 1, 5th edition, 838 p.
- Folk, R.L.
1974: *Petrology of Sedimentary Rocks*; Hemphill Publishing Co., Austin, Texas.
- Forbes, D.L.
1976: Sedimentary processes and sediments, Babbage River delta, Yukon coast: a progress report; in *Report of Activities, Part C*; Geological Survey of Canada, Paper 76-1C, p. 165-168.
- Garrels, R.M. and Christ, C.L.
1975: *Solutions, Minerals and Equilibria*; Harper and Row, New York.
- Gleeson, C.F.
1963: Reconnaissance heavy-mineral study in northern Yukon Territory; Geological Survey of Canada, Paper 63-62, 10 p.
- Krumbein, W.C. and Pettijohn, F.J.
1938: *Manual of Sedimentary Petrography*; D-Appleton-Century Comp. Inc., New York.
- Law, J.
1971: Regional Devonian geology and oil and gas possibilities, Upper Mackenzie River area; *Canadian Petroleum Geology, Bulletin*, v. 19.
- Lewis, C.P. and Forbes, D.L.
1975: Beaufort Sea coast sediments and sedimentary processes; Beaufort Sea Project, Technical Report No. 24; Department of Environment, Victoria.
- Mackay, J.R.
1970: Lateral mixing of the Liard and Mackenzie River downstream from their confluence; *Canadian Journal of Earth Sciences*, v. 7, p. 111.
- Miall, A.D.
1976: Devonian geology of Banks Island, Arctic Canada, and its bearing on the tectonic development of the Circum-Arctic region; *Geological Society of America, Bulletin*, v. 87.
- Milner, H.B.
1962: *Sedimentary Petrology*, Ruskin House, George Allen and Unwin Ltd., London.
- Monger, J.W.H., Souther, J.G., and Gabrielse, H.
1972: Evolution of the Canadian Cordillera: A plate tectonic model; *American Journal of Science*, v. 272.
- Noble, J.P.A. and Ferguson, R.D.
1971: Facies and faunal relations at edge of early mid-Devonian carbonate shelf, South Nahanni River area, N.W.T., *Canadian Petroleum Geology, Bulletin*, v. 19, no. 3, p. 570.
- Norris, D.K.
1973: Tectonic styles of northern Yukon Territory and northwestern District of Mackenzie, Canada; in *Arctic Geology*; American Association of Petroleum Geologists, Memoir 19, v. 23.
- Pelletier, B.R.
1975: Sediment dispersal in the southern Beaufort Sea; Beaufort Sea Project, Technical Report No. 25a; Department of the Environment, Victoria.
- Pelletier, B.R. and Shearer, J.M.
1972: Sea bottom scouring in the Beaufort Sea of the Arctic Ocean; in *Proceedings of the 24th International Geological Congress (Montreal)*, Section 8, p. 251-261.
- Poldervaart, A.
1955: Zircons in rocks. 1. Sedimentary rocks; *American Journal of Science*, v. 253.
1956: Zircons in rocks. 2. Igneous rocks; *American Journal of Science*, v. 254.
- Prest, V.K.
1969: Retreat of Wisconsin and Recent ice in North America; Geological Survey of Canada, Map 1257A, scale 1:5 000 000.
- Rampton, V.N. and Bouchard, M.
1975: Surficial geology of Tuktoyaktuk, District of Mackenzie; Geological Survey of Canada, Paper 74-53, 17 p.
- Rock-Color Chart
1951: Geological Society of America, New York.
- Vilks, G., Wagner, F.J.E., and Pelletier, B.R.
1979: The Holocene marine environment on the Beaufort Shelf; Geological Survey of Canada, Bulletin 303.
- Yorath, C.J.
1973: Geology of Beaufort-Mackenzie Basin and eastern part of Northern Interior Plains; in *Arctic Geology*; Proceedings, 2nd International Symposium on Arctic Geology; American Association of Petroleum Geologists.
- Yorath, C.J., Myhr, D.W., and Young, F.G.
1975: The geology of the Beaufort-Mackenzie Basin; Geological Survey of Canada, Open File 251, 23 p.
- Young, F.G.
1973: Mesozoic epicontinental flyschoid and molasse depositional phases of Yukon's north slope; in *Proceedings, Symposium on the Geology of the Canadian Arctic*; Geological Association of Canada, Canadian Society of Petroleum Geologists.

**MINERALOGY OF RADIOACTIVE OCCURRENCES IN THE GRENVILLE STRUCTURAL PROVINCE,
BANCROFT AREA, ONTARIO: A PROGRESS REPORT**

Project 770061

J. Rimsaite
Economic Geology Division

Rimsaite, J., Mineralogy of radioactive occurrences in the Grenville structural province, Bancroft area, Ontario: A progress report; in Current Research, Part A, Geological Survey of Canada, Paper 80-1A, p. 253-264, 1980.

Abstract

This report summarizes results of laboratory studies of specimens from selected radioactive occurrences in the Bancroft area, Ontario, described in 1978 in a preliminary report by the author. The studies include atomic absorption spectrometric analyses of mineral concentrates for REE, Th and Pb; optical microscope, scanning electron microscope and electron microprobe studies of radioactive and associated minerals; and preliminary results of isotopic studies of Pb, U and Th in heterogeneous zircon, uraninite, pyrochlore and allanite provided by Dr. G.L. Cumming of the University of Alberta. Mineral assemblages and sequence of crystallization of uranium, thorium and REE (rare-earth elements)-bearing minerals are discussed under the following ore types:

1. "melanocratic ore" at the contact of metapyroxenite, metasediments, anhydrite and syenite pegmatite;
2. "leucocratic ore" in a pink aplitic rock composed dominantly of albite, microcline and quartz with accessory pyroxene, amphibole, fluorite and calcite;
3. radioactive REE-bearing pegmatite composed of allanite, titanite, zircon, uraninite, thorite, amorphous minerals, minor tourmaline and biotite in an albite-microcline groundmass;
4. radioactive pyrochlore-bearing pegmatite in which rare-earth elements exceed the uranium content.

Radioactive and host minerals are present in complex intergrowths illustrated in scanning electron images at high magnifications. Mineral relationships and isotope studies indicate remobilization of radioactive and radiogenic compounds.

Introduction

Samples collected in the Bancroft area in 1977 (Rimsaite, 1978) were studied using rapid chemical, spectrographic, mass-spectrometric, X-ray diffraction, electron microprobe, scanning electron microscope, neutron activation and atomic absorption analyses. Samples are identified by the neutron activation analysis number in a preliminary report (Rimsaite, 1978, Table 9.1). The purpose of the present progress report is to illustrate and interpret heterogeneous mineral textures and to describe selected uranium ore samples from the Bancroft area. Samples are from the underground mining area of the Madawaska mine and from trenches of adjacent closed mines. A map showing localities that were sampled and data on uranium concentrations in the principal rock types and selected minerals from the Bancroft area are presented by Rimsaite (1978, Fig. 9.2 and Table 9.1).

Mineralogical studies discussed here are based on petrological studies of polished thin sections of selected ore samples and on analytical results of individual minerals and mineral concentrates. Most of the minerals were identified by their physical and X-ray properties during selection and concentration of samples for analyses. Mineral concentrates were prepared by the author using heavy liquids ranging in specific gravity from 2.2 to 3.3. The homogeneity of the concentrates was checked by X-ray diffractometer analyses and in oil immersion mounts under a petrographic microscope. The concentrates were studied by atomic absorption spectrometric analyses for REE, Y, Th and Pb (Table 38.1). Isotope ratios Pb/U; Pb/Th and Pb/Pb and apparent ages of heterogeneous zircon (cyrtolite), allanite, uraninite and pyrochlore were provided by Dr. G.L. Cumming of the University of Alberta (research contracts 0SU77-00353 and 0SU78-00319 (see Table 38.2 and Fig. 38.7).

Heterogeneous minerals selected in polished thin sections were studied by scanning electron microscope coupled with an energy dispersive spectrometer. Complex textures were recorded in electron micrographs which provided better resolution and clearer images of the mineral intergrowths and of microfractures than the photomicrographs. Diverse mineral phases in heterogeneous grains were studied by an energy dispersive spectrometer at sites one micron in diameter. The principal U-, Th- and REE (rare-earth elements)-bearing minerals and their intergrowths (some submicroscopic in size) are illustrated in scanning electron micrographs and chemical differences between the mineral phases in these intergrowths are illustrated in characteristic spectra obtained using an energy dispersive spectrometer (Fig. 38.1 to 38.6). Quantitative electron microprobe analyses of diverse mineral phases in heterogeneous grains and X-ray identification of minerals removed from polished thin sections continue and will be discussed later.

Much of the radioactive material is isotropic (metamict) and occurs in fine grained intergrowths of several submicroscopic mineral phases, too fine grained for conventional identification by X-ray diffraction and by optical microscopy. Clean separation of such minerals is technically impossible, thus electron microprobe and scanning electron microscope analyses are the most useful methods to study chemical composition, habit and size of these radioactive intergrowths. Because of heterogeneity and chemical complexity of minerals, the predominant mineral defines the grain (e.g. "tourmaline" is probably a tourmaline with minute impurities of other minerals). Only chemically analyzed grains with the confirmed presence of uranium are referred to as "uranothorite". The term "thorite" is used for optically identified thorite of unknown chemical composition.

Table 38.1

Distribution of some rare-earth elements, minor and trace elements in selected minerals from uranium deposits in the Bancroft area, Ontario*

Mineral concentrate	Concentrations in ppm												
	La	Ce	Nd	Sm	Eu	Dy	Ho	Er	Tm	Yb	Y	Th	Pb
Concentrates from high grade uranium ore RF-1, Madawaska mine, 30-62 Mesh fractions													
Biotite	2000	3200	1000	300	20	502	140	650	150	950	2450	1400	130
Albite	447		70	15	1	8	3	8	1	10	84	110	
Microcline	124		25	7	1	3	1	3	< 1	3	30	33	128
Tourmaline	9500	15000	2800	300	30	350	100	420	100	700	2550	2200	1900
Titanite	7200	11000	3400	600	100	600	13	470	100	540	4050	2100	1300
Allanite, l**	50000	>50000	3600	800	100	130	46	64	6	100	1000	7500	100
Allanite, r***	1000	1085	250	30	2	4	6	5	1	8	42	118	3
Cyrtolite, l**	450	606	225	39	8	37	8	34	6	40	300	169	4300
Cyrtolite, r***	20	40	14	7	1	21	10	71	19	152	520	70	500
<u>Concentrates from pyrochlore ore</u>													
Pyrochlore	1900	5700	4450	3700	70	9140	1650	6400	1200	10700	820	4800	2600
Apatite	4100		5000	1000	130	1100	230	800	100	530	700	1900	
Albite			< 3	3	< 1	3	1	3	1	7	36	9	18
Microcline			4	3	< 1	4	1	4	1	11	45	4	27
Sericite			17	18	1	51	10	55	13	121	533	13	19
Muscovite			6	7	< 1	3	2	2	< 1	3	21	14	9
<u>Concentrate from fluorite-calcite bands</u>													
Fluorite			5	4	< 1	2	1	1	< 1	20	118	19	δ

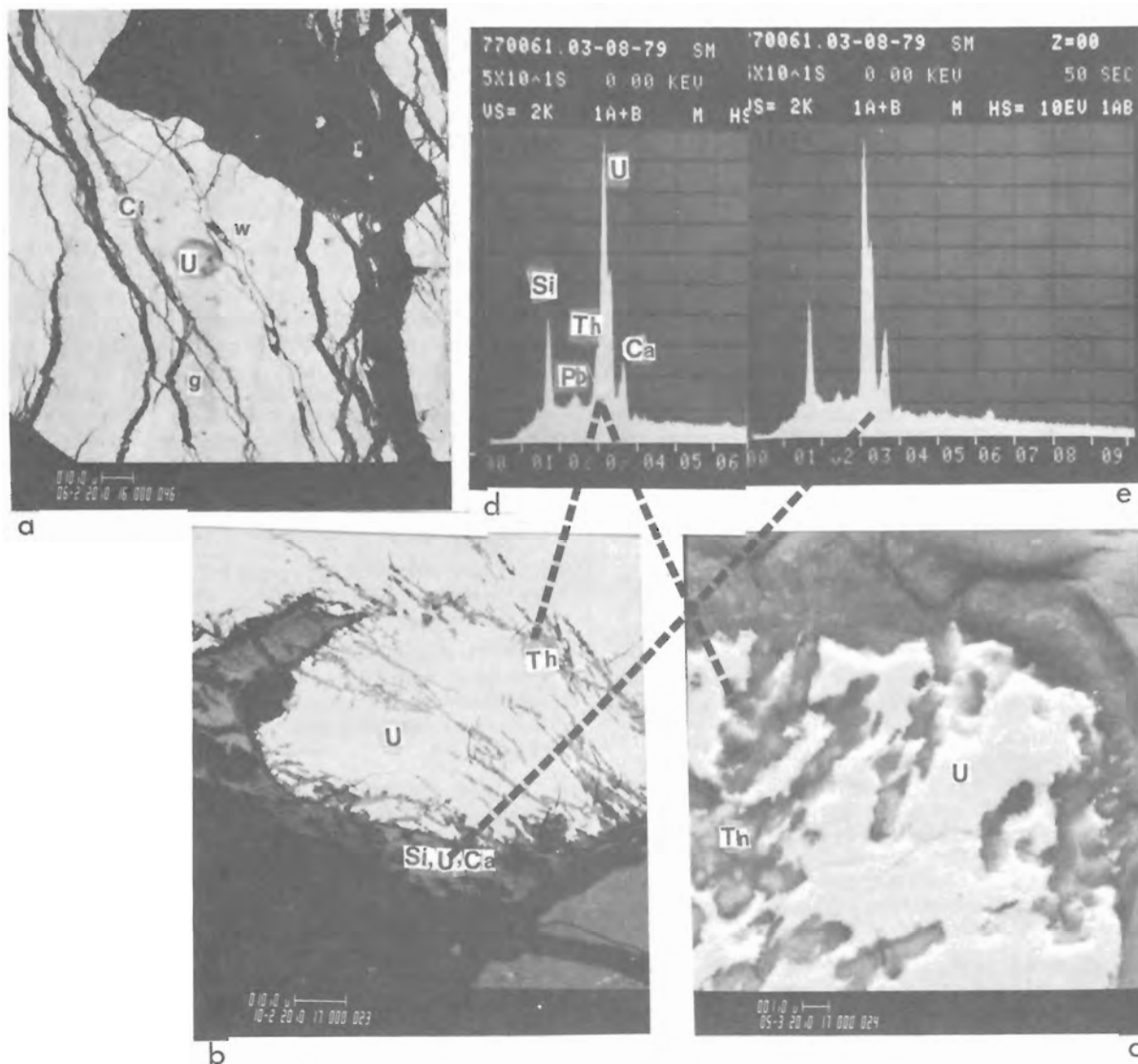
* Atomic absorption spectrometric analysis by J.G. Sen Gupta (for method used see Sen Gupta, 1976 and 1977).
 **l - HNO₃ leach.
 ***r - residue from HNO₃ leach.

Table 38.2

Uranium, thorium and lead concentrations, Pb/U, Pb/Th and Pb/Pb isotope ratios and apparent ages of mineral concentrates from uranium mines in the Bancroft area*

Specimen No.****	1U	2Z	3Z	4UZ	5A	6A	7B	8B
Weight (grams)	0.0182	0.0654	0.0597	0.0668	0.2164	0.3941	0.2624	0.2254
U%	54.6	0.613	0.567	44.0	1.44	1.27	14.96	11.3
Th%	15.5	N.D.**	N.D.	N.D.	N.D.	0.654	N.D.	0.479
Pb%	9.71	0.0658	0.0667	6.92	0.133	0.192	0.150	0.190
Common Pb%	0.25	0.37	0.27	0.34	3.07	1.52	0.58	0.36
²⁰⁷ Pb/ ²⁰⁶ Pb***	0.07493	0.07373	0.07222	0.07299	0.07703	0.07766	0.05191	0.05154
²⁰⁸ Pb/ ²⁰⁶ Pb***	0.09090	0.10139	0.05206	0.13332	0.26320	0.27537	0.03909	0.03483
²⁰⁴ Pb/ ²⁰⁶ Pb***	0.00004	0.00006	0.00004	0.00005	0.00025	0.00028	0.00009	0.00005
²⁰⁷ Pb/ ²³⁵ U	1.818	1.066	1.202	1.508	0.7538	1.310	0.08516	0.1256
²⁰⁸ Pb/ ²³⁸ U	0.1773	0.1106	0.1217	0.1515	0.07918	0.1289	0.01219	0.01794
²⁰⁸ Pb/ ²³² Th	0.0539	N.D.	N.D.	N.D.	N.D.	0.06468	N.D.	0.01350
<u>Apparent ages (Ma)</u>								
²⁰⁷ Pb/ ²⁰⁶ Pb	1051.7	1011.2	975.8	991.9	900.1	1033.1	225.0	230.6
²⁰⁷ Pb/ ²³⁵ U	1051.9	736.7	801.4	933.7	570.4	850.2	83.0	120.1
²⁰⁶ Pb/ ²³⁸ U	1051.9	649.7	740.1	909.3	491.2	781.2	78.1	114.6
²⁰⁸ Pb/ ²³² Th	1061.1	N.D.	N.D.	N.D.	N.D.	1266.1	N.D.	271.1

* Analytical data from Cumming (1978, 1979), analytical procedure as by Cumming & Rimsaite (1979)
 **N.D. = Not determined.
 ***Ratios abbreviated to fifth decimal place.
 ****Specimens: 1U = uraninite separated from fluorite;
 2Z = fine-grained zircon (cyrtolite) separated from sample RF-1 illustrated by Rimsaite (1978, Fig. 9.5);
 3Z = coarse-grained cyrtolite from same sample as 2Z, residue after HNO₃ leaching, details in Figures 38.6 and 38.7 and Rimsaite (1978, Fig. 9.6);
 4UZ = uraninite leached from zircon (cyrtolite) 3Z, Figure 38.6.
 5A and 6A = heterogeneous allanite from the same sample as 1U, 2Z, 3Z and 4UZ, Rimsaite (1978, Fig. 9.5).
 7B and 8B = pyrochlore separated from muscovite (Rimsaite, 1978, Table 9.1, analysis 28).
 All mineral concentrates prepared by Rimsaite.



- a. Backscattered electron image (BEI) of striated uraninite (U) at the contact of pyroxene, anhydrite and albite. Lighter streaks (white = w) consist of U and Pb, darker streaks (d) consist of U, minor Ce, Y and Pb. The uraninite is transected by fractures, some filled with U-Si coffinite-like crusts.
- b. BEI of fractured uraninite, partly replaced by Si-Pb-Th-U-Ca bearing material along fractures (spectrum 1d) and rimmed by red bands composed of Si, U and Ca (spectrum 1e).
- c. BEI of corroded uraninite, partly replaced by uraniferous phase composed of Si, Pb, Th, U and Ca (spectrum 1d).

Figure 38.1. Illustration of uraninite in melanocratic radioactive rock, polished thin section RF-731. (GSC 203532-U)

The chemically complex niobates and titanates are referred to using general group names, such as pyrochlore or niobate until chemical analyses are completed to justify a more precise nomenclature of mineral species.

Tables summarizing results of rapid chemical and semiquantitative spectrographic analyses of minerals, rocks and heavy mineral concentrates of samples described in the preliminary report (Rimsaite, 1978, Tables 9.1 and 9.2) and additional mineral spectra and electron micrographs are available from the author upon request.

The following selected ore types are discussed on the basis of preliminary analytical results:

1. "melanocratic ore" at the contact of paragneisses, metapyroxenite, anhydrite and syenite pegmatite containing variable concentrations of uranium, analyses No. 2 and 6 (U = 119 ppm and 16 920 ppm);
2. "leucocratic ore" in a pink aplitic rock composed dominantly of albite, microcline and quartz with accessory pyroxene, amphibole, fluorite, calcite, titanite, uraninite, thorite and amorphous REE-bearing minerals with a relatively homogeneous distribution of uranium (U = 927 ppm and 4090 ppm), sample analyses No. 5 and 13;
3. high grade ore composed of allanite, titanite, zircon (cyrtolite), amorphous REE minerals, tourmaline, biotite, uraninite and thorite, all in feldspar matrix. Minor quartz, sulphides and arsenides were detected in microfractures within mineral grains and along grain boundaries. Sample RF-1, analysis No. 27 (U = 23 440 ppm);
4. radioactive pyrochlore-bearing pegmatite composed of alkali feldspar, muscovite, apatite and accessory uraninite, xenotime, galena and bismuth in fine grained intergrowths.

Acknowledgments

Microscopic studies by the author were supported by X-ray identification of minerals by A.C. Roberts; rapid chemical analyses of rocks by G.R. Lachance, J.-L. Bouvier and staff of the Analytical Chemistry Section; spectrographic analysis by R.A. Meeds; atomic absorption spectrometric analysis for REE by J.G. Sen Gupta; scanning electron microscope studies and spectra of mineral phases using an energy dispersive spectrometer were provided by D.A. Walker and electron microprobe analyses by A.G. Plant of the Central Laboratories and Administrative Services Division. Photographic plates were prepared by the staff of the Photographic Section, Geological Survey of Canada. Their assistance is gratefully acknowledged. The author thanks Dr. G.L. Cumming and Mr. D. Krstic of the University of Alberta for providing isotope analyses (research contracts OSU77-00353 and OSU78-00319) and Messers R.L. Alexander and D.R. Wilson of the Madawaska Mines Limited for specimens and guidance in the mine.

1. "Melanocratic" Ore (contains more than 50% mafic minerals)

High grade ore samples having erratic uranium concentrations, between 500 ppm (cut off value) and 16 920 ppm U, consisted dominantly of green pyroxene (80-90%) transected by fractures filled with Na and K feldspars, anhydrite, quartz, calcite, accessory zircon, titanite, apatite, uraninite, uranothorite, amorphous REE grains, and locally garnet, fluorite and gypsum.

Pyroxene is massive, coarse grained, reaching several centimetres in length, locally replaced by blue-green amphibole and green to orange-brown patches of fine grained serpentine- and montmorillonite-like aggregates. The major constituent in "melanocratic" ore is clinopyroxene (GSC X-ray pattern 61859) that consists mainly of Si, Ca, Fe and minor Mg, Mn and Na. Pyroxene has inclusions of magnetite, pyrite, uraninite and uranothorite.

In the Madawaska mine, amphibole that locally replaces pyroxene in mineralized rocks, contains more iron, sodium, fluorine and rubidium than amphibole from nonradioactive paragneiss.

Wedge-shaped crystals of titanite and associated coarse grained apatite have crystallized along contacts between metapyroxenite and invading feldspar-anhydrite pegmatite. Some titanite crystals exhibit polysynthetic twinning and consist of REE-bearing, niobian and common titanite intergrowths.

Anhydrite is twinned and fills wide fractures in amphibole adjacent to albite. Calcite is associated with anhydrite and fills narrow fractures in amphibole.

Zoned crystals of coarse grained cyrtolite, reaching several millimetres in diameter, are euhedral and almost isotropic (metamict). Some crystals are overgrown by anisotropic zircon and contain rusty reddish patches of fibrous material in some bands. Cyrtolite crystals occur in groups in albite and quartz matrix and are usually associated with uraninite and uranothorite. Cyrtolite grains are heterogeneous and exhibit several episodic growths. Groups of small (pre-metamorphic?) zircons in the core are overgrown by numerous concentric bands of grey, almost isotropic and weakly anisotropic cyrtolite.

Uraninite crystals reach 1mm in size and have red and rusty brown rims, some resembling the serpentine-like alteration observed in pyroxene fractures. Uraninite crystallizes: along fractures in pyroxene; at the contact between pyroxene, anhydrite and albite (Fig. 38.1a); in titanite and cyrtolite; as overgrowths on titanite (Fig. 38.2a)

and in association with uranothorite in microcline. Coarse crystals of uraninite appear striated on backscattered electron image (BEI) and are made up of light grey and darker grey lamellae that vary in REE contents (Fig. 38.1a). Uraninite is traversed by numerous fractures, some filled with coffinite-like crusts. Some of the uraninite crystals appear to be resorbed along the fractures and replaced by a complex uraniferous phase containing Si, Pb, Th, U and Ca (Fig. 38.1b and 38.1c, spectrum in Fig. 38.1d).

Red and orange-brown rims surrounding uraninite are heterogeneous and consist of Si-Fe-rich crusts in intergrowths with a Si-U-Ca-bearing phase (Fig. 38.1b and spectrum 38.1e). Uraninite overgrown on titanite (Fig. 38.2a and 38.2c) contains a pyrite-rich rim adjacent to pyroxene. Euhedral pyrite crystals are in Si-Fe-rich matrix. The coexistence of sulphate (anhydrite) and sulphide (pyrite) in the same sample is interesting. The sulphide-sulphate association implies differences in environmental conditions, on a microscopic scale, during crystallization of pyrite and anhydrite. The oxidation of uraninite might have produced a local reducing environment and produced favourable conditions of crystallization for pyrite.

Isotropic REE-bearing grains are rare in "melanocratic" ore samples. When present, they contain small uraninite inclusions overgrown by Si^- , Th^- , U^- , Fe^- bearing rims.

Thorite crystals, associated with uraninite occur in pyroxene, microcline and in cyrtolite. Thorite grains have resorbed edges enclosed in prominent red Si-Fe rims containing disseminated specks rich in Fe, Sn, V and Mn (Fig. 38.2b).

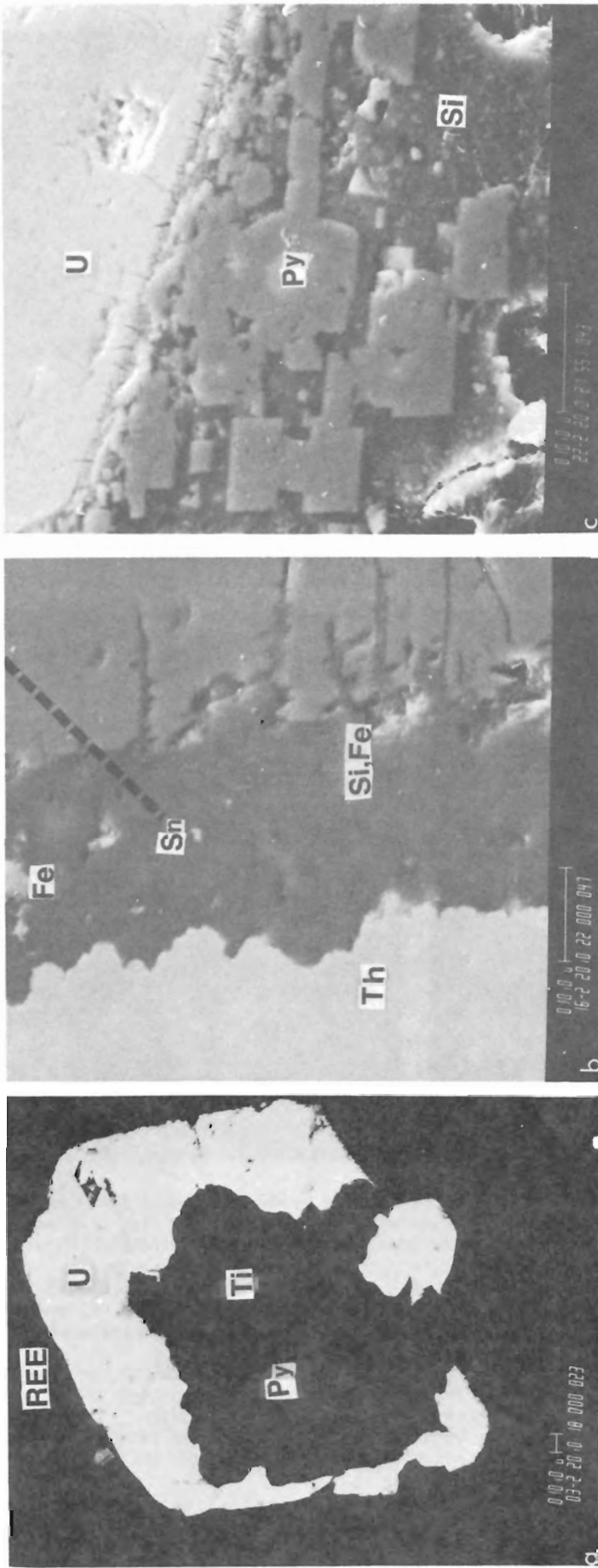
The following sequence of crystallization was interpreted in "melanocratic" ore samples: pyroxene, followed by Fe^3 -rich amphibole, titanite, REE-rich allanite, albite, microcline, anhydrite, quartz, calcite, locally fluorite, uranothorite, uraninite, Si-U and Si-U-Th-Ca compounds, accessory magnetite and pyrite, Sn-, Fe-, V-rich specks in rims surrounding uraninite and uranothorite and serpentine- and montmorillonite-like alteration products locally replacing pyroxene and forming crusts on pyroxene fractures and on uraninite grains.

2. "Leucocratic" Ore (contains less than 5% mafic minerals)

Pink aplitic rocks constitute more homogeneous and more abundant ore material and have uranium contents between 0.1 and 0.4% U_3O_8 over larger areas than the "melanocratic" ore samples. Locally the pink quartz-feldspathic radioactive rocks extend vertically more than 50 m. The host rocks are made up of a medium- to coarse-grained mosaic of albite, microcline and quartz with minor accessories consisting of pyroxene-amphibole intergrowths (1-2%), purple fluorite, calcite, uraninite, uranothorite and allanite.

The remnant intergrowths of pale green pyroxene and bright green amphibole are partly replaced by quartz and resemble in texture residual graphic granite or micropegmatite. Radioactive minerals are present at contacts between microcline and albite, or between albite and quartz, and enclosed in purple fluorite haloes.

Small uraninite grains surrounded by complex multiple rims or haloes have crystallized in fractures in quartz and at the contact between potassic feldspar and albite. The uraninite grains appear heterogeneous on backscattered electron images and consist of bright white and darker grey lamellae (Fig. 38.3a, 38.3b and 38.3c). The uraninite consists of Pb-rich and Pb-depleted, Si-bearing phases with or without Th. They represent residual uranium and REE which precipitated along fractures and grain boundaries after crystallization of major mineral phases and accessory fluorite

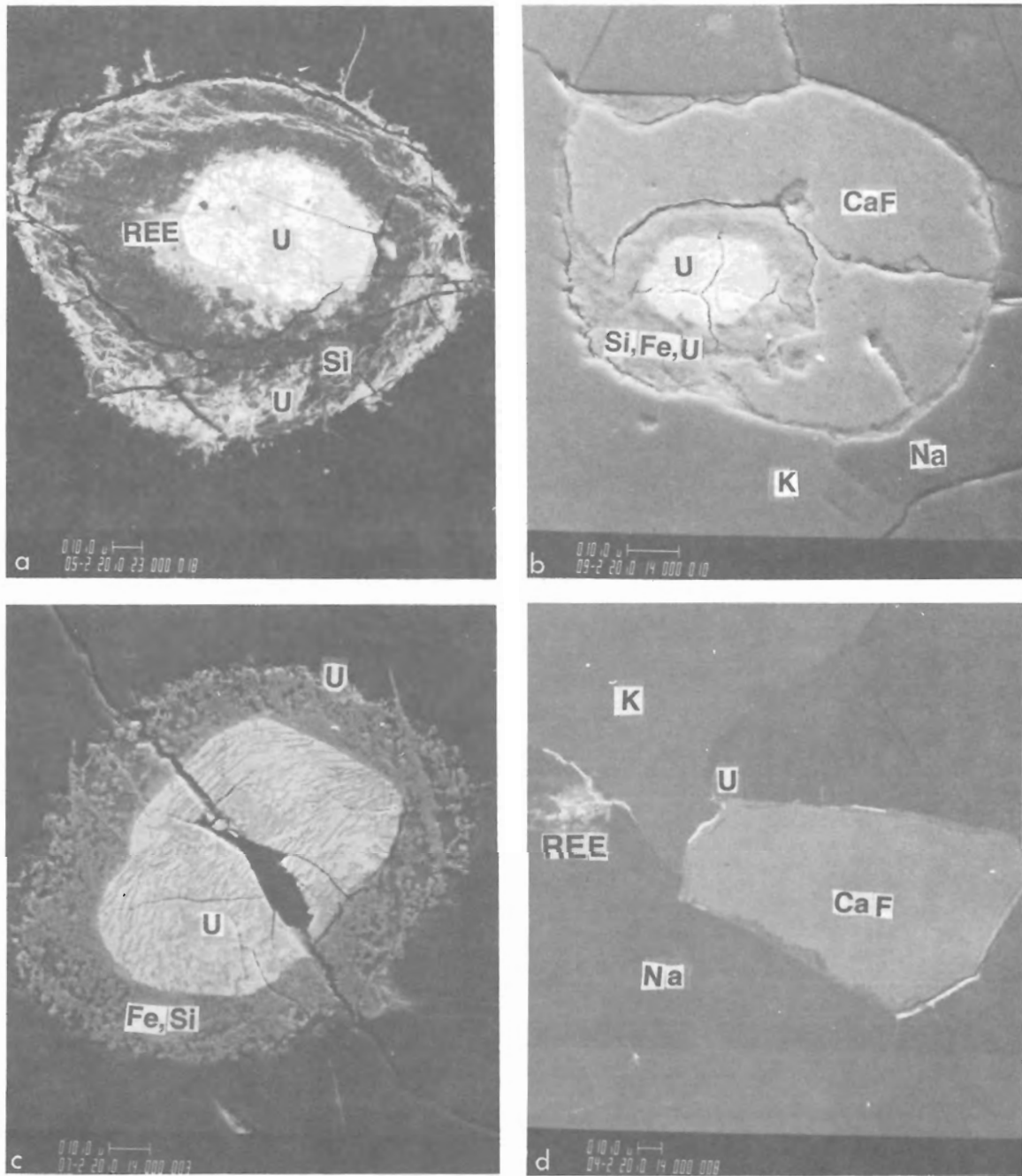


a. Uraninite (U) overgrown on titanite (Ti) at the pyroxene-microcline contact. Titanite has pyrite (Py) in fractures.

b. BEI of resorbed edge of thorite (Th) surrounded by Si-Fe-rich rim adjacent to pyroxene. Grey specks in the rim contain high concentrations of Fe and Sn. Rims surrounding uraninite and thorite extend into fractures of host pyroxene.

c. BEI of uraninite (U) that adjacent to pyroxene is surrounded by Si-Fe-rich rim (Si) containing euhedral pyrite (Py). Rims adjacent to isotropic portions of allanite contain REE, Si, Th, U, and Ca. Mineral spectra obtained using an energy dispersive spectrometer are available for grains marked with a dotted line.

Figure 38.2. Illustration of uraninite and thorite in metacratitic rock, polished thin section RF-731. (GSC 203532-S)



- Uraninite composed of U and Pb (white) is partly replaced by darker irregular bands composed of Si, Th, U, Ca, Pb and Fe and enclosed in heterogeneous REE-bearing inner rim, a wider Si-rich (Si) central rim, and a radioactive U-bearing outer rim that overlaps with a marked circular fracture. The uraniferous rim extends into the radial fractures of adjacent albite and quartz.
- Heterogeneous uraninite (U) surrounded by Si, Fe, U-bearing rims, all enclosed in fluorite (CaF) and a narrow isotropic outermost rim of feldspar at the contact between microcline (K) and albite (Na). The uraninite is transected by marked radial fractures and surrounded by haloes separated by circular fractures.
- Heterogeneous micrographic uraninite consists of brighter U-Pb phase that is corroded and partly replaced by Pb-poor U-Si phase, enclosed in Si-Fe-bearing rims. Outer edges of the rim contain uranium (U). The uraninite and adjacent minerals are transected by fractures.
- Thin uraniferous crusts and REE-filled fractures at grain boundaries between fluorite (CaF), microcline (K) and albite (Na). Uranium (U) and REE-filled fractures appear white.

Figure 38.3. Illustration of heterogeneous uraninites enclosed in multiple rims or haloes in "leucocratic ore" samples (all illustrations are backscattered electron images, BEI) obtained using scanning electron microscope by D.A. Walker), polished thin section RF-721. (GSC 203532-H)

(Fig. 38.3d). As can be seen in Figure 38.3, rims overgrown on uraninite resemble pleochroic haloes in the distance from the radioactive source. The spectra of some uraninite rims indicated the presence of Po. The haloes consist of REE; Fe-, Si-rich compounds with or without uranium; fluorite; and locally of isotropic (or metamict) outer rim of host feldspar. Some of the rims are separated by marked circular fractures. In some rims, uranium is enriched in the outer portion of the rim, suggesting a still later episode of uranium crystallization.

Uraninite crystals are transected by radial fractures and surrounded by circular fractures that coincide with some outer uraniferous haloes and might have been caused by radiation from uraninite and expansion of isotropic (metamict) mineral phases as a result of structural damage.

3. Radioactive Rare-Earth Elements-Bearing Pegmatite RF-1

Of the samples studied, the REE-bearing pegmatite, represented by sample RF-1 from Madawaska mine contains the highest concentration of uranium, 23 440 ppm U. The sample is chemically and mineralogically complex. It consists of allanite; titanite; zircon; amorphous Y-U and radioactive REE-bearing grains enclosed in and associated with tourmaline, biotite, albite, microcline and quartz. Common rock-forming minerals, such as feldspar, quartz and mica are interstitial constituents in this rock and are present in variable, although minor, amounts.

Uraninite is associated with uranothorite and crystallizes in various minerals, including tourmaline (Fig. 38.4), feldspar, allanite, cyrtolite and mica (Rimsaite, 1978, Fig. 9.5). Uraninite is surrounded by complex multiple rims, composed of galena (Fig. 38.4c); REE-bearing specks (Fig. 38.4d, spectrum in Fig. 38.4e); pyrite (Fig. 38.4g); and Fe-Si-U-Ca-bearing minerals (spectrum in Fig. 38.4f). Uraninite crystals are heterogeneous and enclose grains of quartz, Na and K feldspars, REE-bearing inclusions and sulphides.

Zircon (isotropic cyrtolite) is a common host for the uraninite (Fig. 38.5 and Rimsaite, 1978, Fig. 9.6). Cyrtolite crystals were hand-picked for isotope studies and merit more detailed description. Cyrtolite grains reach several millimetres in diameter and consist of isotropic (metamict) central portions and shattered anisotropic zones, usually at the periphery. In some cyrtolite grains, the core portion is stained red and appears different from the overgrowth of pale and dark grey zones. Large cyrtolite crystals grow around a nucleus composed of several small (pre-metamorphic?) zircon or quartz fragments (Fig. 38.5c, Si) and enclose uraninite at the contact between the isotropic core and anisotropic rim (Fig. 38.6a). Other enclosed grains in cyrtolite are K-feldspar in the outer shattered rim and intergrowths of REE-bearing grain and iron arsenide. FeAs, plates (Fig. 38.6a, 38.6b and spectrum in Fig. 38.6c), and galena in fractures (Fig. 38.5a and 38.5b). Chemical analysis indicated ca 4 wt. % H₂O in cyrtolite concentrates. According to electron microprobe analysis, small chemical differences exist between the core (SiO₂ = 30.7%; ZrO₂ = 62.3%; CaO = 1.3%; FeO = 0.2%) and the rim (SiO₂ 29.7%; ZrO₂ = 58.4%; CaO = 2.3%; FeO = 1.5%). The cleanest portions of cyrtolite contained SiO₂ = 32.7% and ZrO₂ = 66.1%. These cyrtolite varieties yielded the same "cyrtolite" X-ray diffraction patterns.

Allanite is one of the major constituents in the pegmatite. It crystallizes in crystals several millimetres long that in transmitted light vary in colour from green to yellow and red-brown. Allanite is intergrown with epidote, a uraniferous REE-bearing phase and amorphous Y-Th-U-bearing grains that contain variable proportions of iron, silica, radioactive elements and disseminated grains of galena.

Feldspar in the groundmass of radioactive minerals is fractured and stained brownish yellow by fracture-fillings made up of Si, Fe, REE, Ca and U compounds that extend from rims surrounding uraninite into fractures of the adjacent feldspar host (Fig. 38.4, pyrite and REE-bearing rims).

Minerals from specimen RF-1 were hand-picked and purified in heavy liquids for REE and isotopic analyses (Tables 38.1 and 38.2). Relatively high concentrations of REE and Pb in biotite and feldspar (first three analyses in Table 38.1) can be accounted for by the presence of radioactive REE-bearing fracture-fillings in these minerals.

Because cyrtolite and allanite enclose uraninite, galena and other impurities, acid-leach and residues after leaching were analyzed in an attempt to determine REE contents in these mineral concentrates after removing leachable contaminants (analyses "l" and "r" in Table 38.1). With the exception of cyrtolite residue "r" that contained more Y and Yb, all REE, Th and Pb were found to be enriched in the acid-leach fraction. Tourmaline concentrate that yielded X-ray diffraction pattern of "tourmaline" contains higher concentrations of Dy, Ho, Er, Tm, Y and Pb than the concentrate of associated allanite. Table 38.1 provides data on concentration sites of REE in the rock, including Nd and Sm, which are important for the selection of samples for isotopic dating and isotope research.

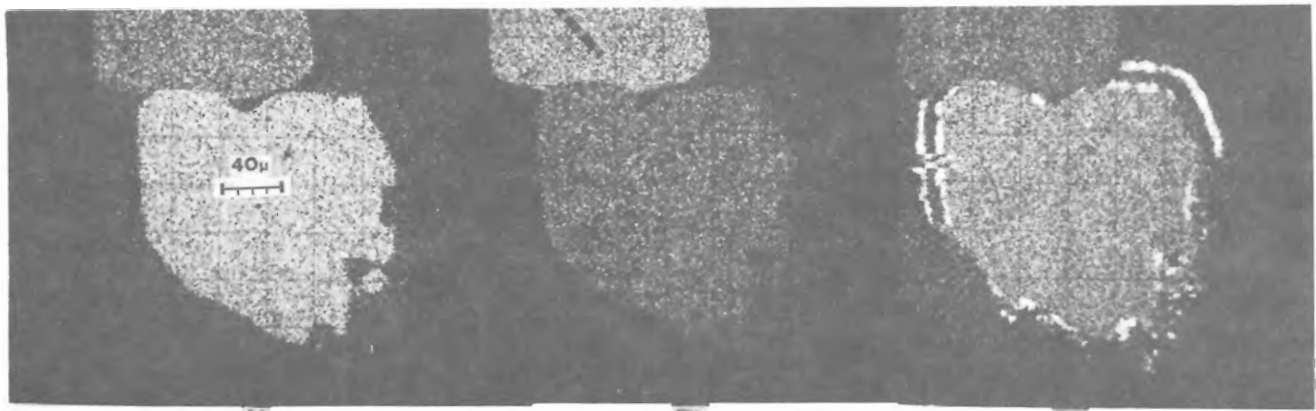
4. Pyrochlore-bearing Pegmatite, Uraniferous Niobate-Tantalate-Titanate and Yttrian Ore

Uraniferous niobian titanates and tantalum-bearing niobates associated with less abundant uraninite were observed in specimens from Bicroft, Greyhawk, Dyno and Silver Crater mines. In the Madawaska mine niobium concentrations are relatively scarce, however, some titanites are heterogeneous, intergrown with niobian phases and contain small quantities of uranium and REE.

The niobian ore contains pyrochlore crystals in coarse grained feldspar pegmatite. Pyrochlore is isotropic (metamict) and appears shiny black in hand specimen. It crystallized in fractures in red albite and is overgrown by muscovite. In thin sections pyrochlore appears heterogeneous. It varies in colour from pale yellow to deep orange. It has a speckled appearance due to disseminated bismuth and heterogeneous distribution of U and REE, and in this respect resembles heterogeneous euxenite (Rimsaite and Lachance, 1966). Pyrochlore crystals are mottled, heterogeneous and very impure along the edges and fractures. Pyrochlore contains rows of fine grained black plates resembling graphite along fractures, shattered grains of apatite cemented by U-Nb-Si fracture fillings, uraninite, REE grains and galena. Uraninite, enclosed in Nb-Fe-bearing and yttrian grains, surrounded by disseminated cubes of galena, crystallized along the edges of pyrochlore.

Pyrochlore was separated for REE and isotope analyses (Table 38.1 and 38.2). The pyrochlore concentrate contained very high concentrations of Yb (10 000 ppm), Dy (9140 ppm) and Er (6400 ppm).

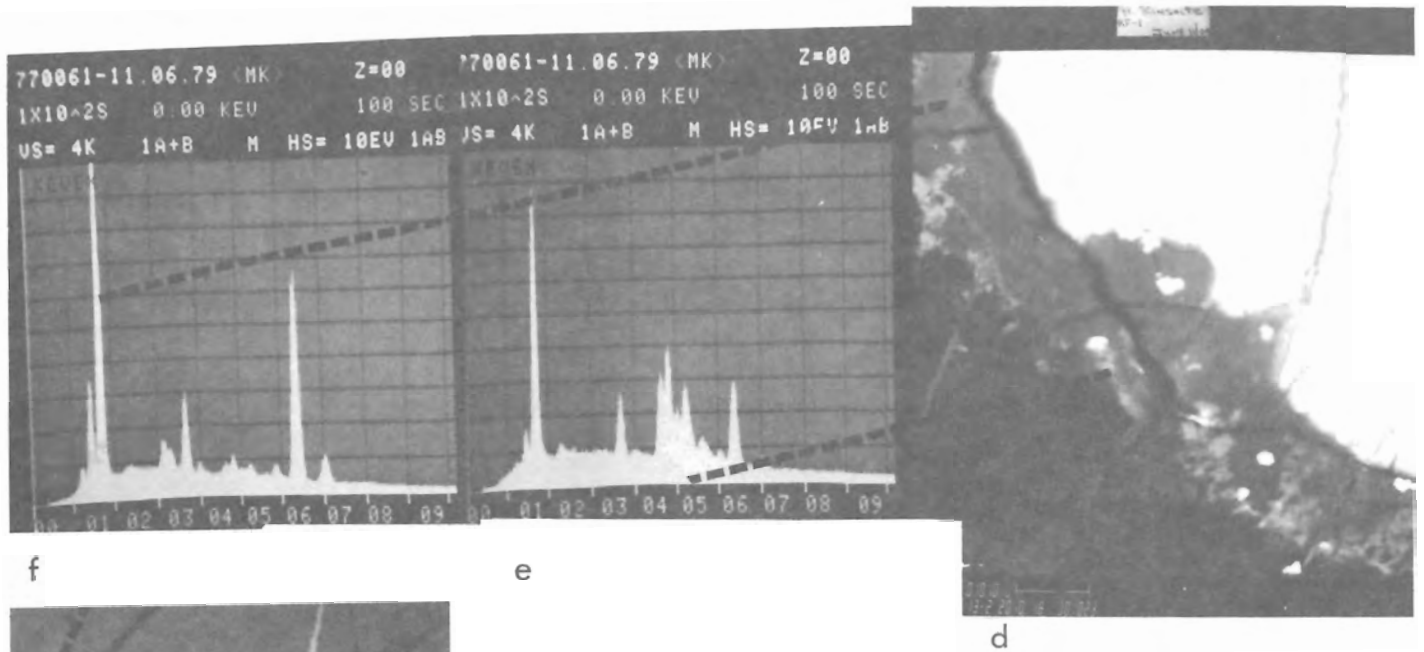
Chemically complex niobate from "leucocratic" ore at Bicroft mine was studied by scanning electron microscope and an energy dispersive spectrometer. The niobate is isotropic (metamict) and occurs in intergrowths with small grains of uraninite. The niobate appears heterogeneous reddish brown to opaque in transmitted light and is amorphous to X-rays. The Nb-rich specimens contain also small crystals of uraninite enclosed in purple fluorite haloes, and in this respect resemble the mineral assemblage (uraninite-fluorite) in "leucocratic" ore from Madawaska mine illustrated in Figure 38.3b.



a

b

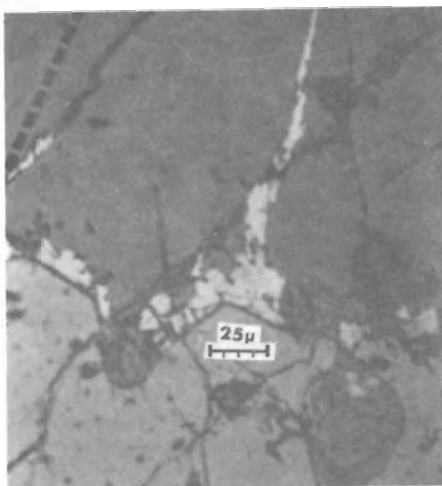
c



f

e

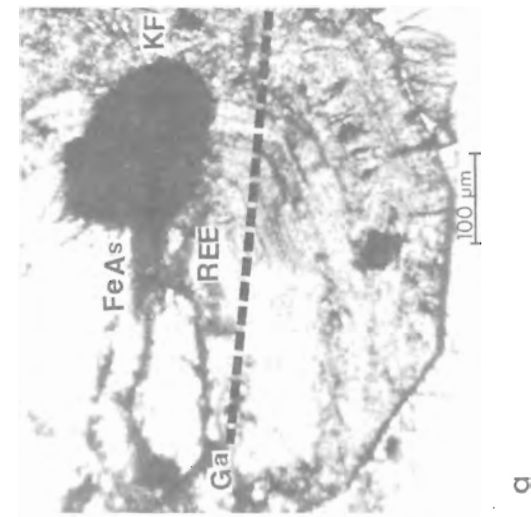
d



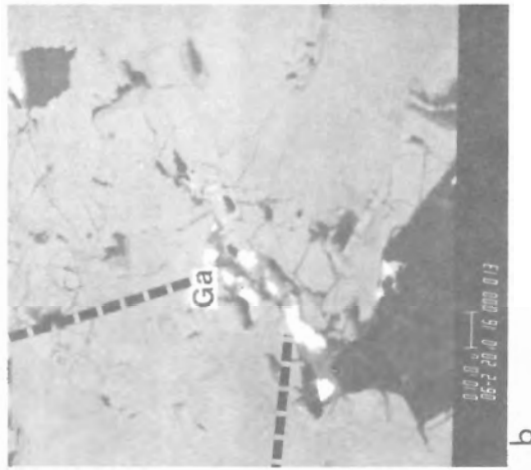
g

- a,b,c. X-ray scanning images for U, Th and Pb, showing distribution of uraninite and uranothorite grains in tourmaline. Uraninite is rimmed by double rim of galena. The rim between two galena rims contain REE (electron microprobe analysis by G.A. Plant).
- d. BEI of resorbed edges of uraninite (white, right) that is surrounded by red Si, U, Ca, Fe-bearing rim with disseminated galena (white crystals) and REE-bearing spots (spectra in Fig. 38.4e and 38.4f).
- e. Spectrum of REE-bearing spots in rim illustrated in Figure 38.4d. Element peaks are identified in Fig. 38.1 and 38.6.
- f. Spectrum of Si-Fe-rich rim on uraninite shown in Figure 38.4d. The rim contains also U and Ca.
- g. Photomicrograph (reflected light) of an edge of uraninite rimmed by pyrite (white) that extends into feldspar fractures. The uraninite contains inclusions of quartz, feldspar and REE-bearing grains.

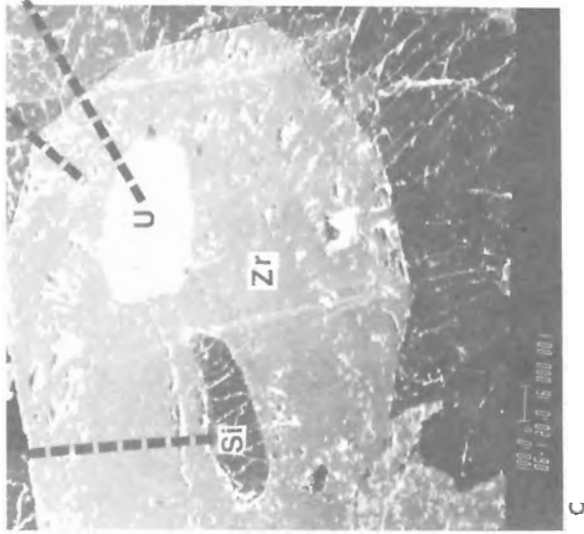
Figure 38.4. Illustrations of radioactive minerals in U, Th, REE ore sample RF-1, polished thin section RF-1. (GSC 203532-F)



a. Photomicrograph (transmitted light) of zoned zircon (cyrtolite) that consists of isotropic and anisotropic zones overgrown on quartz fragment (white). Cyrtolite encloses uraninite (black), potassic feldspar (KF) near shattered rim, a grain made up of REE and iron arsenide (FeAs) in fine-grained intergrowths, and galena (Ga) along fractures. For details see Figures 38.5b and 38.6.

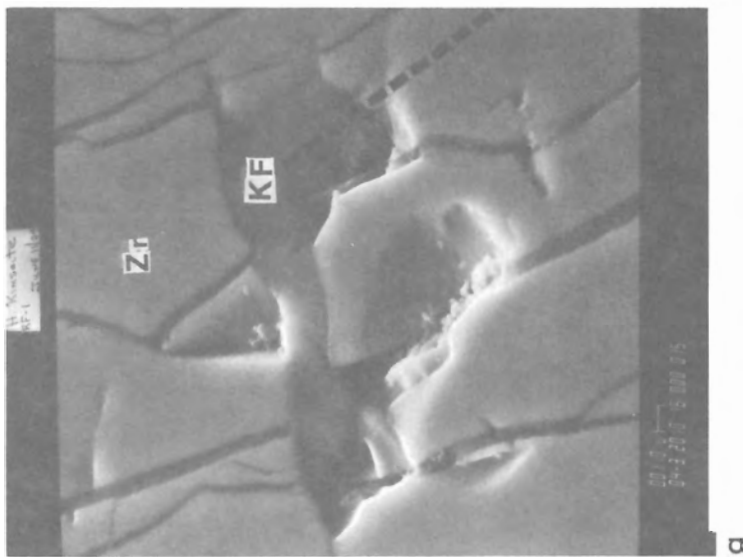


b. BEI of cyrtolite with white specks of galena, same cyrtolite as in Figure 38.5a.

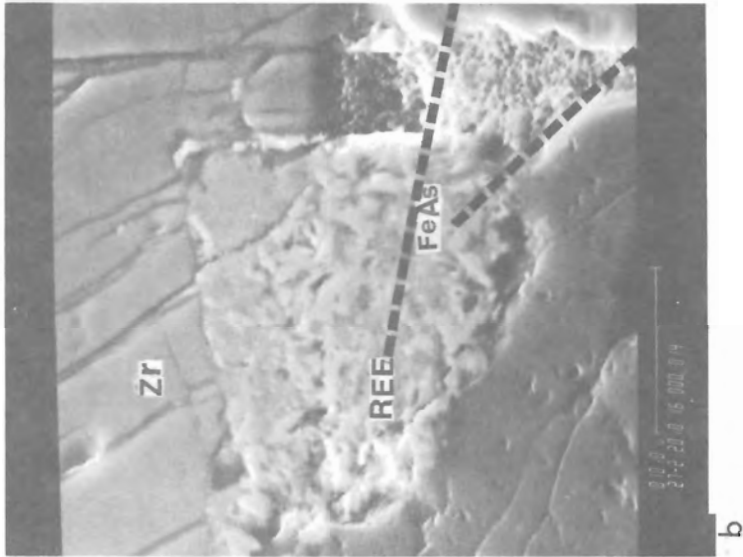


c. Secondary electron image (SEI) of cyrtolite (Zr) in Figure 38.5a showing numerous microfractures, enclosed quartz (Si) and uraninite (U).

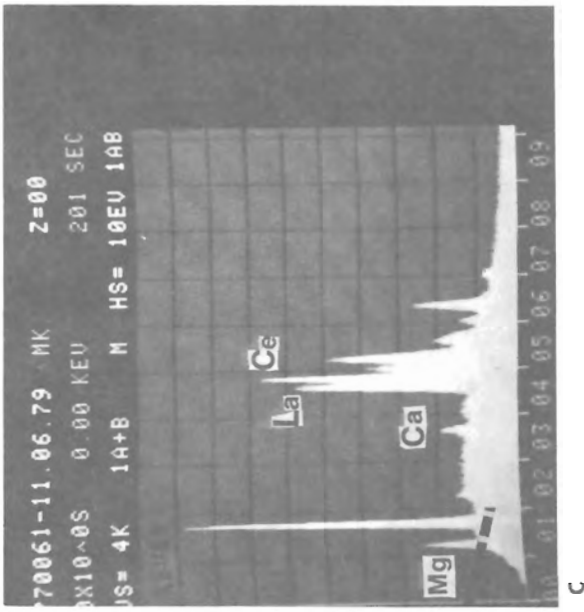
Figure 38.5. Illustrations of heterogeneous zircon (cyrtolite) in high grade uranium ore RF-1. (GSC 203532-L)



a. SEI of K-feldspar in fractured rim of cyrtolite (Zr).



b. SEI showing fine grained intergrowths of REE-bearing grain in intergrowths with iron arsenide (FeAs) plates, and clay-filled fracture (right) in fractured cyrtolite (Zr). White crusts on fractures of REE-bearing grains contain uranium.



c. Spectrum of REE-bearing grain in cyrtolite illustrated in Figure 38.6b.

Figure 38.6. Illustrations of heterogeneous zircons, enlarged portions of grain in Figure 38.5. (GSC 203532-B)

Isotope Studies

Results of isotope studies are summarized in Table 38.2 and in Figure 38.7. The oldest concordant age was obtained on uraninite concentrate separated from fluorite (1050 Ma, specimen 1U). Fine grained zircons and coarse grained cyrtolite containing visible uraninite inclusions (Rimsaite, 1978, Fig. 9.6) yielded a discordia line having an upper intersection with the concordia curve at 1000 Ma and lower intersection at 90 Ma. The discordia line suggests remobilization of radiogenic and/or radioactive elements. Uranium leached by acid from cyrtolite, sample 4UZ, plots below the concordia curve, and near the intersection of the zircon discordia line with the concordia. The lowest point that appears to lie on the discordia line (near 90 Ma intersection with the concordia curve) was obtained for a pyrochlore concentrate (7B). A repeated pyrochlore analysis (8B) confirmed relatively low apparent Pb/U ages and suggested that the pyrochlore analyses may lie on a second discordia that intersects the concordia at about 230 Ma. Also, pyrochlore 8B yielded a Pb/Th age (271 Ma) twice as high as the Pb/U ages (120 Ma and 114 Ma), and this supports the suggested discordia. The relatively low and apparently discordant ages of pyrochlore confirm those obtained by Robinson et al. (1963) on euxenite concentrates. The niobates are apparently very susceptible to environmental changes and their radiogenic and radioactive components are readily mobilized and redeposited.

The Pb/Th age of allanite (6A) is also higher than the discordant apparent Pb/U ages of allanites (5A and 6A), but in reasonable agreement with the uraninite age.

The concordant Pb/U age of uraninite 1U (1051 Ma) agrees well with Pb/U ages of uraninite from Madawaska (former Faraday) mine (1045 Ma) and from Cardiff uranium mine (1070 Ma) and K/Ar ages of associated biotite (analysis 59-51 = 1035 Ma) and phlogopite (analysis 59-49 = 1060 Ma) reported by Robinson (1960).

Some of the radiogenic lead apparently migrated from the structure of radioactive minerals and at least some of it recrystallized as galena specks and rims in and around radioactive minerals (Fig. 38.4 and 38.5; and Rimsaite and Lachance, 1966, Figs. V and VI). However, some of the radiogenic lead was probably entirely removed from the radioactive minerals, especially from Pb-depleted phases of uranothorite and uraninite. Because of the corrosion and replacement of radioactive minerals and their apparent depletion in radiogenic lead, the measured ages are probably only lower limits to the original age of crystallization. The markedly lower U/Pb ages of allanite and pyrochlore can probably be accounted for by enhanced migration, diffusion and losses of radiogenic lead and susceptibility of these minerals to environmental changes and alteration.

Isotopic study of "old", probably detrital, zircons from meta-sedimentary rocks, especially from silty impurities in limestones would be warranted in an attempt to establish temporal relationships between sedimentation and complex metamorphic events.

Summary and Conclusions

In an attempt to characterize ore mineralogy, uranium, thorium and REE minerals have been studied using the scanning electron microscope and energy dispersive spectrometer, and their host rocks studied by optical and chemical methods. The chemically complex intergrowths and replacements of radioactive mineral phases from the ore grade specimens have been illustrated in backscattered (BEI) and secondary electron images (SEI) and chemical variations shown in mineral spectra obtained by energy dispersive spectrometer. The relationship between uranium and

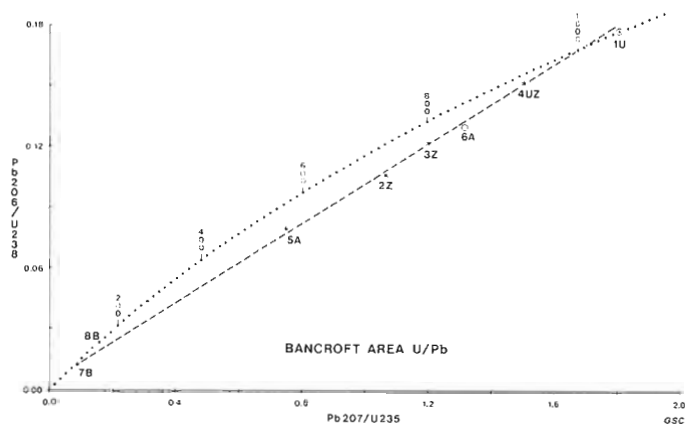


Figure 38.7. Concordia diagram for Pb/U data on samples from the Bancroft area, Ontario. Crosses are samples plotted on discordia line; circles are additional samples analyzed also for Pb/Th (see Table 38.2 and text). Isotope data are from Cumming (1978, 1979).

thorium-bearing phases in uraninite and the heterogeneous distribution of lead in zircons (cyrtolite) and in radioactive minerals are illustrated by high resolution scanning electron microscopy. Ore-forming minerals illustrated include uraninite, uranothorite, allanite, titanite, and isotropic radioactive Y, REE and Nb-bearing mineral aggregates.

The preliminary mineralogical, chemical and isotope studies of radioactive samples from the Bancroft area indicate more than one episode of crystallization and apparent remobilization of radioactive and radiogenic elements.

The following sequence of crystallization of radioactive and associated minerals is interpreted: uraniferous thorite was succeeded by crystallization of uraninite and the latter by REE minerals. "Secondary" uraninite and galena crystallized along the edges of pyrochlore from mobilized uranium and radiogenic lead from radioactive niobate. Uraninite occurs in several chemically and temporally different phases, commonly intergrown, e.g.: pure uraninite that consists of U and Pb and uraninite containing Th and/or REE and Si. The uraninite and uranothorite are corroded and partly replaced by a Pb-poor, Si-rich phase containing uranium and thorium. Some grains of uranothorite and uraninite have corroded or resorbed edges and are surrounded by Si-, Fe- and REE-bearing rims that locally contain high concentrations of As, Fe, Mn, Sn, Ti, secondary Th, U, Pb, Po and V.

In the rims and fracture-fillings, REE postdate crystallization of rock-forming minerals, euhedral uraninite and uranothorite. The mobilized or residual uranium and REE crystallize at the outer edges of the rims and in mineral interstices as thin crusts after crystallization of all other minerals, being the latest phase to precipitate.

The most common radioactive mineral associations include: pyroxene-uraninite-uranothorite; pyroxene-anhydrite-uraninite; biotite-uraninite; titanite-uraninite; albite-zircon-uraninite-uranothorite-quartz; albite-microcline-uranothorite-uraninite; allanite-uraninite-amorphous Y-U-bearing grains; uraninite-niobate-tantalate and uraninite-fluorite-calcite.

Zircon (cyrtolite) is commonly isotropic (metamict) and indicates several growth zones around nuclei of several fine grained (pre-metamorphic ?) zircons or quartz fragments.

With the exception of one concordant Pb/U age for uraninite separated from fluorite (1051 Ma), all mineral concentrates yielded discordant ages, apparently as a result of postcrystallizational alterations and losses of radiogenic lead from the structures of the radioactive minerals. Some of the mobilized lead remained in the radioactive host as disseminated specks of galena and Pb-rich rims, but much of it was probably entirely removed. Pyrochlore apparently lost essentially all of its radiogenic lead at about 270 to 225 Ma.

References

- Cumming, G.L.
1978: Isotope analyses for Geological Survey of Canada, Contract No. 0SU77-00353. Final Report, March 15, 1978, 14 p. (Available from the author).
1979: Isotope analyses for Geological Survey of Canada, Contract No. 0SU78-00319. Final Report, March 15, 1979, 21 p. (Available from the author).
- Cumming, G.L. and Rimsaite, J.
1979: Isotopic studies of lead-depleted pitchblende, secondary radioactive minerals and sulphides from the Rabbit Lake deposit, Saskatchewan; Canadian Journal of Earth Sciences, v. 16, No. 9, p. 1702-1715.
- Rimsaite, J.
1978: Mineralogy of radioactive occurrences in the Grenville Structural Province Ontario and Quebec: A Preliminary Report; in Current Research, Part B, Geological Survey of Canada, Paper 78-1B, p. 49-58.
- Rimsaite, J. and Lachance, G.R.
1969: Illustrations of heterogeneity in phlogopite, feldspar, euxenite and associated minerals; in Mineralogical Society of India, IMA Volume 1966, International Mineralogical Association, Papers, Fourth General Meeting, 1964, p. 209-229.
- Robinson, S.C.
1960: Note on the interpretation of the U-Pb, Th-Pb and K-Ar ages in the Bancroft, Ontario Region; in Age determinations by the Geological Survey of Canada, Report 1, Isotopic ages; Geological Survey of Canada, Paper 60-17, p. 41-51.
- Robinson, S.C., Loveridge, W.D., Rimsaite, J. and van Peteghem, J.
1963: Factors involved in discordant ages of euxenite from a Grenville pegmatite; Canadian Mineralogist, v. 7, part 3, p. 533-546.
- Sen Gupta, J.G.
1976: Determination of lanthanides and yttrium in rocks and minerals by atomic absorption and flame-emission spectrometry; Talanta, v. 23, p. 343-348.
1977: Determination of traces of rare-earth elements, yttrium and thorium in several international geological reference samples and comparison of data with other published values; Geostandards Newsletter, v. 1, No. 2, October 1977, p. 149-155.

Projects 750077, 780034

P.A. Egginton
Terrain Sciences Division*Egginton, P.A., Determining river ice frequency from the tree record; in Current Research, Part A, Geological Survey of Canada, Paper 80-1A, p. 265-270, 1980.***Abstract**

At some sites along Mackenzie River the frequency with which river ice reaches a given bank elevation can be determined using tree age. In the lower seres where ice thrusting occurs, the process limits tree age. During breakup Mackenzie River ice may break into blocks 2 m or more in thickness; ice movement on shore is capable of crushing or uprooting trees. The maximum tree age at a given bank elevation is indicative of the amount of time that has elapsed since ice of sufficient magnitude to kill or uproot the tree has reached that elevation. In this manner approximate return periods of ice events can be determined.

Introduction

At certain locations between Fort Simpson and Norman Wells trees, which line Mackenzie River, increase in size and age with distance and elevation from the river (Fig. 39.1). In many of these areas the size and age of the trees do not appear to be related solely to channel migration or degradation; rather tree age appears to be limited by ice activity. The following study was undertaken to investigate this occurrence.

Acknowledgments

The data presented here were collected during a study of river hydraulics and stability of selected rivers crossed by the proposed Mackenzie Highway. Funding for this work was provided in part by the Department of Indian and Northern Affairs. The author would like to acknowledge the helpful comments made by J. Anderson, D.K. MacKay and D.E. Sherstone, Environment Canada, on an earlier draft of this paper.

Methodology

A series of sites was chosen for study at the confluence of Mackenzie River and some tributary streams (Fig. 39.2). The tributaries were chosen to facilitate river hydraulics and stability studies. A general trend of increasing tree age with increasing elevation above river level was observed at these sites. It must be stressed, however, that between Fort Simpson and Norman Wells, areas with obvious trends of tree

age increase with elevation are limited to those which have moderate to gentle slopes; a large proportion of Mackenzie river banks are steep or are cutbanks. In some areas banks are scoured so frequently by ice that boulder pavements relatively free of vegetation are produced (MacKay and MacKay, 1977).

The sites described here are located on the banks of Mackenzie River, but for convenience they are referred to by the tributary name (Fig. 39.2). At each site a series of transects was run up the bank of Mackenzie River. The transects were chosen to cover the variety of bank configurations present. At distances from the river where there seemed to be a marked change in tree diameter and age, cores from three to five trees at that specific elevation were collected using an increment borer, the object being to obtain the maximum tree age at a given elevation. Where tree age was constant with height and distance from the river, only the leading edge of the trees was sampled. Both live and dead trees were sampled. The only limiting criterion was that the tree be firmly rooted to ensure that the trees sampled could not have been shoved or have drifted to their present elevations. The ages of the trees were subsequently dated by counting growth rings. When individual rings were indistinct or difficult to count in the field, the cores were returned to the office, mounted on a grooved board, smoothed with successively finer grades of sandpaper, and the rings counted with the aid of a binocular magnifier; some 200 trees were dated. The positions of the dated trees on each bank profile were fixed by surveying techniques using a theodolite and stadia rod.



Figure 39.1 Tree age increasing with elevation above Mackenzie River at the mouth of Saline River, 1979. (GSC 203165-L)

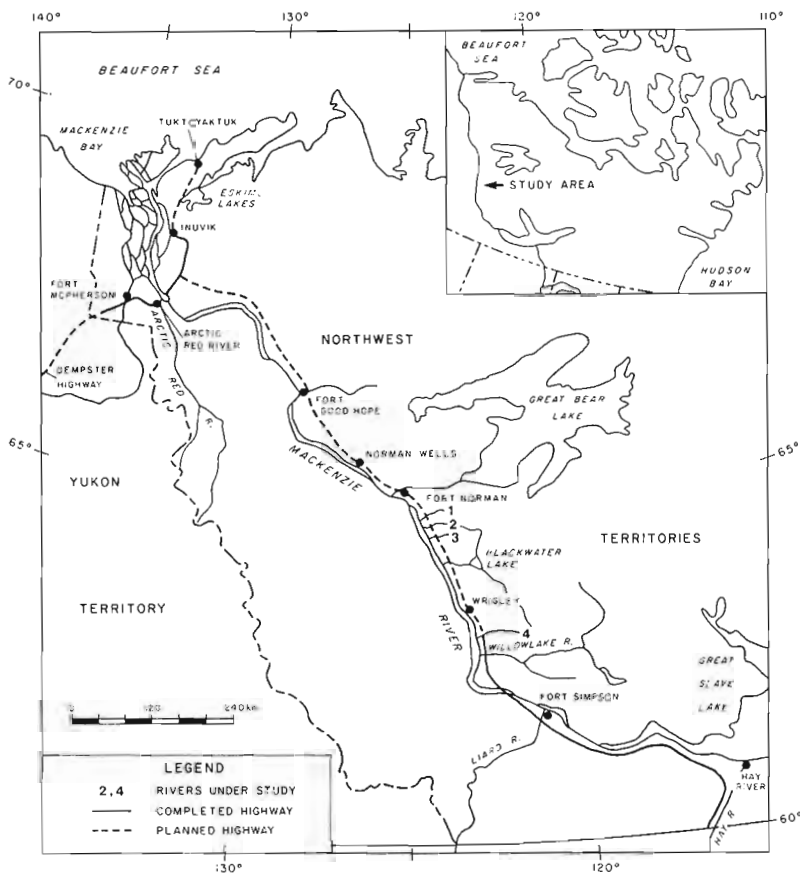


Figure 39.2

The location of Mackenzie River study sites at the confluence of 1) Little Smith Creek, 2) Saline River, 3) Steep Creek, and 4) River Between Two Mountains.

Tree Profiles

The age and location of the oldest tree at a given height on each transect (termed a tree profile) are presented for several bank configurations at the four study sites along Mackenzie River (Fig. 39.3). The generalized trend of increasing tree age with increasing height above Mackenzie River (O datum, Fig. 39.3) is readily apparent. Variations from this trend, however, occurred in places; vegetation islands, where stands of older trees are surrounded by younger trees, were found (for example L-2, Steep Creek). Another complicating factor was forest fires which are common in the area and which limit tree growth. Areas of burn generally were avoided or, if sampled, were identified as such.

Processes Controlling Tree Age

Mackenzie River in the vicinity of the study sites is downcutting and is laterally mobile. Evidence of recent downcutting includes well vegetated islands which are no longer part of the active floodplain, newly emergent bars, and the presence of numerous terraces at the mouths of rivers tributary to Mackenzie River. The presence of cutbanks and meanders indicates lateral mobility. Given such an environment, simple succession could produce transects with a trend of increasing tree age with elevation above the river; however, simple succession does not explain the considerable change in elevations with tree age observed. In some cases, Mackenzie River would have to downcut at rates of 4 m every 10 years to produce the transects observed (Fig. 39.3). Nor does simple succession explain why trees approximately the same age, and on different transects within hundreds of yards of each other, are found at such varied elevations and distances from Mackenzie River. Succession associated with downcutting would be expected to progress uniformly over a limited reach, that is, points at the same elevation above the

river would be exposed and revegetated at approximately the same time. Finally, simple succession does not explain the presence of 'vegetation islands' of older trees surrounded by younger trees found on some transects along the banks of Mackenzie River (Fig. 39.3).

During spring breakup large ice blocks weighing many tonnes are thrust on shore, crushing or uprooting trees in their path (Fig. 39.4). Uprooted trees up to 100 years old have been observed (Fig. 39.5). In a given year the elevation that the ice reaches depends upon a variety of factors: ice strength, bank geometry, and flow conditions, including local velocities and the presence or absence of backwater. Thus there is a substantial variation in the elevations reached by ice and subsequently, the position of uprooted trees over relatively short distances along the banks of Mackenzie River. Furthermore, ice can be thrust obliquely onto shore and if local bank configuration is suitable, the ice may bypass stands of vegetation giving rise to the 'vegetation islands' discussed above.

Gill (1973) has suggested that allogenic processes such as flooding and sedimentation are dominant successional forces in the lower seres in Mackenzie Delta. Ice thrusting can limit tree growth and scour distinct ice trimlines. In some areas ice thrusting recurs with such frequency that trees do not survive for more than a few years before being crushed or uprooted.

It is clear that ice thrusting is an allogenic process that may limit or influence the successional progression; as such, it should be included in any model of succession of the lower seres. In this context, the tree profiles described result from succession; however, the dominant factor limiting tree age and the main process responsible for the observed trend of increasing maximum tree age with increasing elevation above river level is ice thrusting.

Figure 39.3 Tree profiles, Mackenzie River at Saline River, Steep Creek, River Between Two Mountains, and Little Smith Creek. The numbers under the stylized trees refer to the maximum tree age at that location. Note the development of a 'vegetation island' at L-2, Steep Creek, resulting from ice moving obliquely onto the bank uprooting trees but by-passing the 'island'.

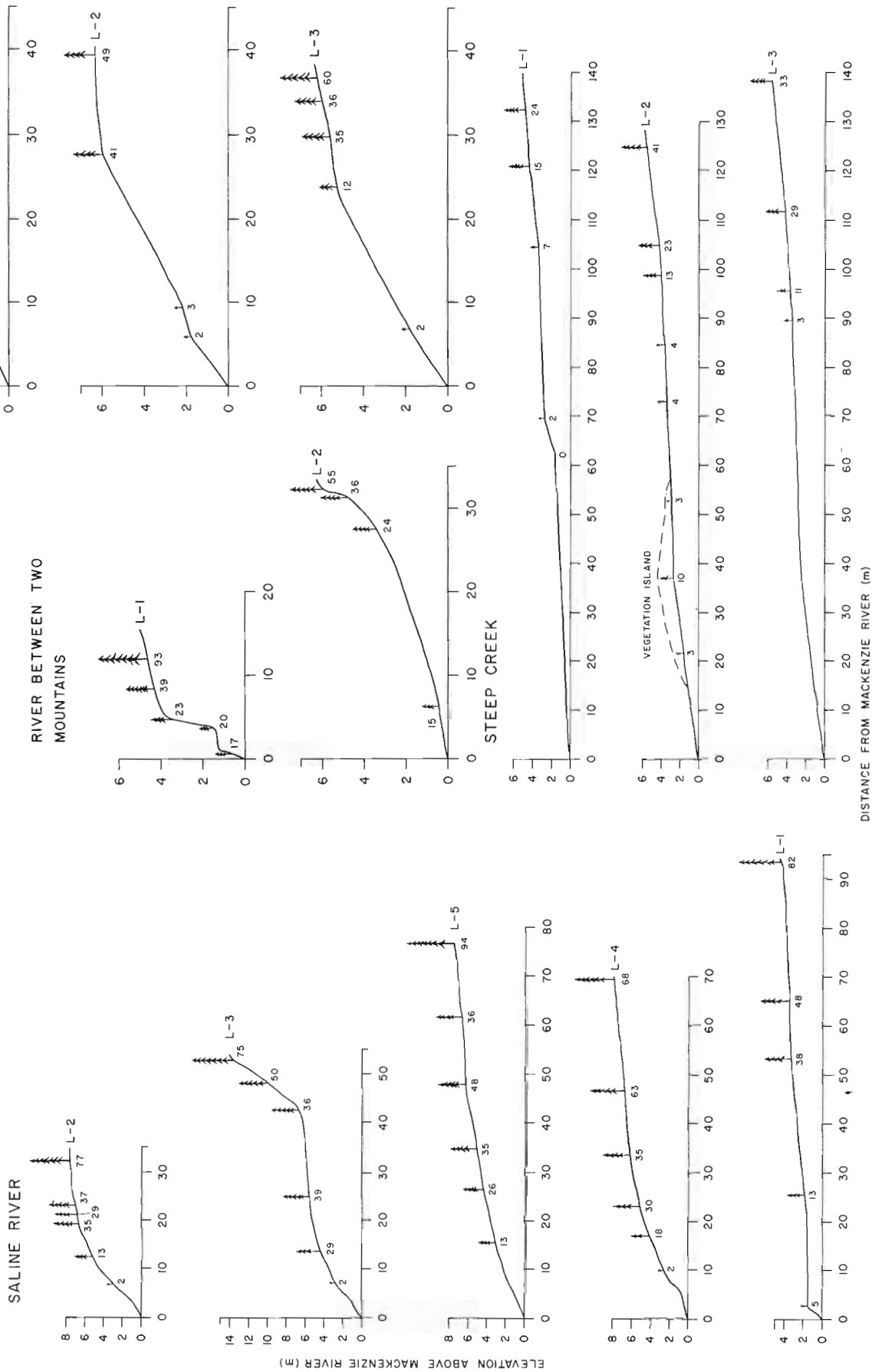




Figure 39.4

Ice control of tree age, Mackenzie River at Little Smith Creek, 1977. The area has been overridden by ice. Ice thrusting was limited to the immediate vicinity of the river. Note the person for scale. (GSC 203165-K)

Figure 39.5

Crushed trees, Little Smith Creek, 1977. Trees up to 100 years of age were crushed or uprooted by this particular event. In this case the bank configuration was such that ice thrust more than 100 m inland. (GSC 203165-J)



Ice Frequency

Graphs of maximum tree age versus elevation for each study site suggest that ice activity is not random but ordered (Fig. 39.6). For example, the maximum age of trees uprooted by ice activity in 1975 at Saline River was found to be constant at 35 to 39 years for five profiles spread over 500 m in spite of considerable elevation differences between the bases of the uprooted trees. The maximum elevation of trees uprooted at Steep Creek and Little Smith Creek was also found to be constant at 35 to 39 years for the 1975 ice event. As is common in frequency analysis, it is postulated that another event of this magnitude probably will not occur for another 35 to 39 years, that is, the event would have a return period of 35 to 39 years. This approach is similar to one used by Stewart and LaMarche (1964) to determine the return period of flood events on Coffee Creek, California. The maximum tree age at each location on a tree profile similarly is assumed to approximate the return period for ice events of sufficient magnitude to uproot or crush trees at and below the respective elevations. For the most part, vegetation at elevations below the maximum reached by the ice was uprooted; however, some of the smaller, more supple trees did survive the 1975 and 1977 ice events.

The return periods for ice events at different locations along Mackenzie River are shown in Figure 39.6 and 39.7. (the lines were fitted to the data by eye). The graphs may be used to determine the expected elevation for ice events of a given return period. For some locations all transects plot as an individual line or curve, for others distinct curves are produced. At Saline River for example where multiple lines are produced, the one-in-fifty year event occurs at an elevation 4 m higher on transect L-1 than on transect L-2 located 400 m downstream. The form of the curve and the presence or absence of multiple curves are thought to depend largely upon bed and bank configuration. Where bank shape varies greatly with distance, multiple frequency curves are produced.

Over the 1975-79 period of observation field evidence, including the deposition of silt and ice on tributary streams hundreds of metres from Mackenzie River, indicates that the uprooting of trees by ice observed for 1975 and 1977 was associated with backwater events. Ice jams recur regularly at a number of sites along Mackenzie River and water can back up behind these jams as much as 9 to 14 m above normal midsummer stage (MacKay and Mackay, 1973; Egginton and Day, 1977). Ice moving downstream during periods of backwater therefore is able to reach substantial elevations on

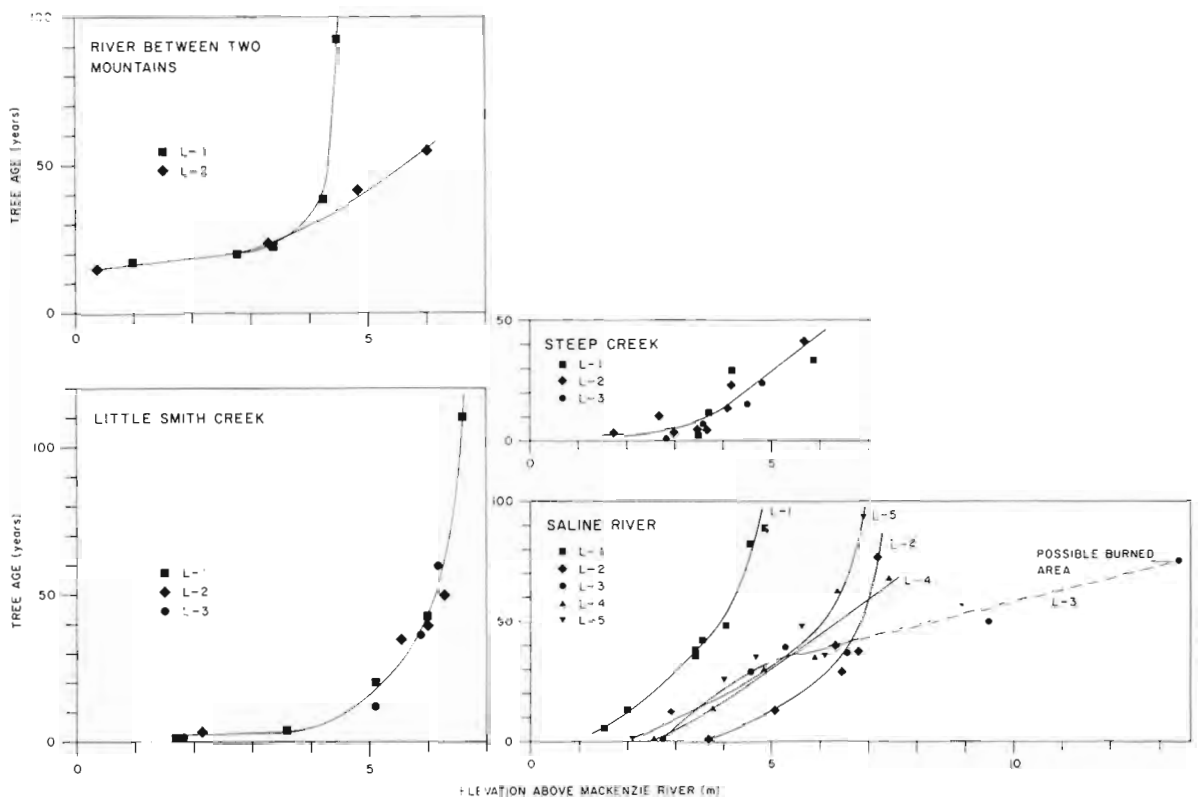


Figure 39.6. Maximum tree age at a point along a transect versus elevation (field datum) above Mackenzie River at Saline River, Steep Creek, River Between Two Mountains, and Little Smith Creek. The curves are drawn by eye. L-3, Saline River, is the site of a possible fire and is excluded from further analysis.

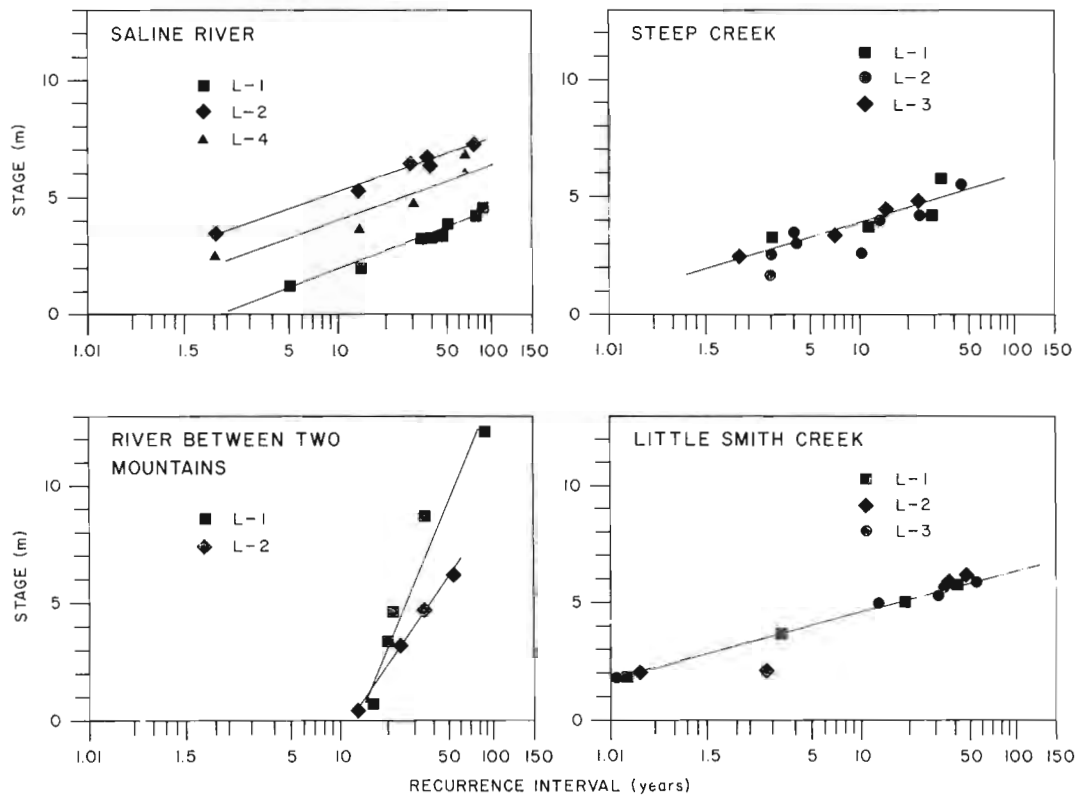


Figure 39.7. Expected ice frequency for transects on Mackenzie River at Saline River, River Between Two Mountains, Steep Creek, and Little Smith Creek. The scatter of points on the frequency curve for Steep Creek may, in part, result from the fact that ice characteristically moves obliquely onto shore at this site; however, the transects were run perpendicular to the river.

the banks of the river. River velocities are reduced during backwater; however, ice thrusting still occurs. This is borne out by the fact that in 1975 and 1977 ice reached different elevations even within the same limited reach.

At exposed sites where the thalweg is directed towards shore, ice may be thrust to considerable elevation simply as a result of spring flooding (Mackay and MacKay, 1977). At sheltered sites where the main flow is directed away from shore, it seems reasonable that most ice movement on shore would occur in association with backwater. Observations at Fort Simpson during breakup in 1978, however, suggest that the process may be more complex. The left bank of Mackenzie River at Fort Simpson is relatively sheltered from Liard ice moving into Mackenzie River. In 1978, however, Liard River ice piled onto the right bank and subsequently sheared in such a manner that ice was thrust onto the left bank at the Fort Simpson townsite (D.E. Sherstone, personal communication, 1979).

With the limited information available it is not possible to evaluate any relationship that may exist between ice frequency and other hydrologic variables. Attempts to compare the ice frequency curve derived from the tree record at Fort Simpson with historic backwater frequency curves for the town failed. Due to lumbering activities the tree record was not adequate, nor was the historic record. Traditionally backwater elevations have not been recorded at Water Survey of Canada observation sites.

Summary

At some locations between Fort Simpson and Norman Wells where the bank slopes are moderate, trees which line Mackenzie River increase in size and age with elevation above the river. The limiting factor for tree age is the thrusting of ice blocks onto shore during breakup, thereby destroying existing trees. The trees provide a means of determining the frequency of ice events at a given location. At the relatively sheltered sites studied, ice movement on shore to elevations in excess of a few metres was associated with backwater. Even in these cases, however, ice was thrust to varying elevations. Observations at Fort Simpson indicate that even in sheltered sites where the main flow of the river and ice is away from a given bank, ice can still be thrust onto that bank to a considerable elevation as a result of a simple spring flood event.

Data are lacking to make a meaningful evaluation of the interrelationships between ice frequency and other parameters. The process is certainly complex. Irrespective of such interrelationships, the ice frequency curves presented are useful for estimating the frequency with which ice reaches a given elevation. Mackenzie River may be somewhat unique in that ice thickness, ice quantity, and breakup characteristics are such that ice can dominate the lower series. Other rivers experiencing a different breakup regime may not exhibit the same degree of ice control of tree age as does Mackenzie River.

References

- Egginton, P.A., and Day, T.J.
1977: Dendrochronologic investigations of high-water events along Hodgson Creek, District of Mackenzie; in Report of Activities, Part A, Geological Survey of Canada, Paper 77-1A, p. 381-384.
- Gill, D.
1973: Floristics of a plant succession sequence in the Mackenzie Delta, Northwest Territories; Zeitschrift der Deutschen Gesellschaft für Polarforschung Münster (Westf.) 43. Jahrgang, Nr. 1/2, p. 55-65.
- MacKay, D.K. and Mackay, J.R.
1973: Breakup and ice jamming on the Mackenzie River, N.W.T.; in Hydrologic Aspects of Northern Pipeline Development, Task Force on Northern Oil Development, Environmental-Social Program, Department of Indian Affairs and Northern Development, Report 73-3, p. 223-232.
- Mackay, J.R. and MacKay, D.K.
1977: The stability of ice push features, Mackenzie River, Canada; Canadian Journal of Earth Sciences, v. 14, p. 2213-2215.
- Stewart, J.H. and LaMarche, U.C.
1964: Erosion and deposition in the flood of December 1964 on Coffee Creek, Trinity County, California; United States Geological Survey, Professional Paper 422-K, 22 p.

**ELEMENTAL ASSOCIATIONS WITHIN APHEBIAN CLASTIC REDBEDS,
NORTHERN HALF OF THE RICHMOND GULF AREA, NEW QUEBEC**

Project 750010

A.R. Miller and J.A. Kerswill
Economic Geology Division

Miller, A.R. and Kerswill, J.A., Elemental associations within Apebian clastic redbeds, northern half of the Richmond Gulf area, New Quebec; in Current Research, Part A, Geological Survey of Canada, Paper 80-1A, p. 271-279, 1980.

Abstract

The principal elemental association within Apebian red arkosic sediments of the Richmond Gulf area is U-Th-Ti-Zr-Y-Cr-V-Ce-La. Relationships between and among elements as well as differences in concentrations of elements among different rock types suggest paleoplacer processes were operative during terrestrial braided river deposition. Anomalous radioactivity in the redbeds can be related to accumulations of monazite and thorite that occur with magnetite, titanomagnetite and zircon in the heavy mineral rich coarsest fractions of the Pachi and Richmond Gulf arkoses.

Introduction

This report is a continuation of the uranium reconnaissance study conducted on Apebian redbeds in the northern Richmond Gulf area, NTS area 34C/8, 9 (Miller, 1978, 1979). The purpose is to document the elemental associations that accompany the U and Th anomalies within the red sediments of the Richmond Gulf area.

This paper reports and discusses:

- i. the U, Th, Ti, Zr, Y, Ce, La, B, Ba, Sr, Rb, Ni, Co, Cu, V, Cr abundances of the redbeds, volcanic rocks, and basement complex.
- ii. the associations between and among elements and the relationship of the geochemical associations to the sedimentological character of the hosting sediments.
- iii. a comparison of the elemental associations and geological environment of the Richmond Gulf red clastic sediments to other fluvial sequences.

General Geology

Geology and stratigraphic nomenclature follow that of Chandler (1978) and Woodcock (1960). The Apebian supra-crustal sequence rests unconformably upon an Archean granitic to granodioritic gneiss complex.

Sedimentary rocks of the Pachi clastic unit, varying from ortho- and paraconglomerate to fine grained sandstone (arkose), represent a sequence of braided fluvial sediments. Thin basal sediments of the Pachi clastic unit include white quartz and granitoid gneiss cobble to boulder conglomerate overlain by a sericitic arkose. The sericitic unit is overlain by a thick sequence of coarse- to medium-grained pink to red crossbedded arkose which contains minor thin interbeds of cobble to pebble sized conglomerates and red mudstone-siltstone. Subaerial alkali basalt flows, the Pachi volcanic unit, overlie the clastic sediments (Chandler, 1979).

Fluvial sediments of the Richmond Gulf Formation disconformably overlie the Pachi volcanic unit. A basal volcanic conglomerate overlies the volcanic flows and is overlain by three successive members: i) a red arkose-siltstone unit, ii) a pink arkosic unit and iii) a grey pyritic arkosic unit.

Black heavy mineral concentrates are present throughout the Pachi clastic sequence and occur within the conglomeratic beds at the Archean-Proterozoic unconformity

as well as within the fining upward cycles consisting of conglomerate, pebbly arkose, and coarse to medium grained arkose. Within the Richmond Gulf Formation, black heavy mineral concentrates occur as laminae along trough crossbed stratifications. Heavy mineral-rich laminae are primarily confined to the redbed member with minor concentrations in the pink member. Heavy mineral sands are composed of magnetite, titanomagnetite, zircon, apatite, thorite, and rare earth bearing monazite (Miller, 1978).

Age of the Supracrustal Rocks

An approximate age using the Rb-Sr whole rock method on argillites from the Richmond Gulf Formation is 1800 ± 160 Ma (Hews, 1976). Paleomagnetic data on the redbeds indicate an Apebian depositional age ranging from 1850 to 2000 Ma (K. Clark, personal communication, 1979, preliminary data). Thus the redbeds of the Richmond Gulf area are interpreted to have an Apebian depositional age which corresponds with ages obtained from various areas in the Circum-Ungava Geosyncline (Fryer, 1972; Dressler, 1975).

Statistical Methodology

As a first step in the statistical analysis, frequency distributions of both untransformed and logarithmically transformed data were evaluated for each element in each rock type. Standard tests for normality were applied. In samples with contents of Y, Ce, La, B, Sr, Ni, Co, Cu, U, and Cr that were below the detection limit, values equal to half the lowest reported values for the appropriate elements were used in the statistical analysis. For Th, values of 1.0 were used when the content was reported to be less than 3.0 ppm. It is believed that the use of such values is appropriate and will not adversely affect the validity of the statistical results.

Associations between and among elements were investigated by a variety of methods for each rock type and for a composite population containing the Pachi (P1, P2 and P3) and Richmond (R) samples. Pearson product moment correlation coefficients were calculated and variation diagrams (scattergrams) were plotted for all possible combinations of element pairs. R-mode factor analysis using the Oblimin method of oblique factor rotation was performed to enhance the interpretability of the relatively cumbersome correlation matrices. Squared multiple correlation coefficients were used as initial communality estimates in computation of the factor matrices.

Multivariate analysis of variance (MANOVA) and discriminant analysis were used to statistically evaluate the presence or absence of geochemical differences among the rock types in terms of element content.

All computations related to the statistical procedures were done at the Computer Science Centre of the Department of Energy, Mines and Resources using the Control Data Corporation version of the Statistical Package for the Social Sciences (SPSS) as developed by the Vogelback Computing Centre at Northwestern University.

Geochemistry of the Redbeds

Elemental concentrations for each sample collected in the study area are listed in Table 40.1 along with the respective lithological descriptions. Uranium contents were determined by neutron activation-delayed neutron counting at Atomic Energy of Canada Ltd. Thorium, titanium, zirconium, yttrium, cerium, lanthanum, barium, strontium and rubidium were analyzed by X-ray fluorescence and boron, nickel, cobalt, copper, vanadium and chromium by emission spectroscopy at the Geological Survey of Canada. An unusually high iron content in Sample 21 from the Richmond Gulf formation prevented determinations for those elements analyzed by emission spectroscopy.

Sample numbers in Table 40.1 are keyed to the sample location map, Figure 25.1, that appeared in the previous report by the senior author (Miller, 1978, p. 112). Samples from the Pachi clastic unit have been subdivided into four distinct lithologies termed for the purposes of this paper P1, P2, P3 and P4. Group P1 (n=7) contains generally medium- to coarse-grained arkoses devoid of heavy mineral concentrations, Group P2 (n=8) consists principally of coarse to granular heavy mineral laminated arkose, Group P3 (n=12) is largely made up of quartz pebble arkose and granite-quartz pebble conglomerate both of which contain abundant heavy minerals. The single sample of Group P4 is distinct from the other Pachi arkose samples in that it is from the arkosic matrix of a quartz cobble granite boulder conglomerate at the Archean-Proterozoic unconformity (Fig. 25.2, Miller 1978, p. 113). Sample 20 from the Richmond Gulf Formation represents a black heavy mineral crossbed from rock sample 21 and thus has a somewhat different nature than the other Richmond Gulf samples. It is however lithologically similar to a number of Pachi samples from the P2 and P3 groups. The evaluation of frequency distributions indicates all elements except Rb and Y are best described as being lognormally distributed. In light of this, a logarithmic ($\log_{10}x$) transformation was applied to all elements except Rb and Y during the statistical operations described in this paper.

Arithmetic means for Rb and Y and geometric means for the other elements in the principal rock types of the study area are listed in Table 40.2. For most elements the geometric means that appear in the table are considerably less than the corresponding arithmetic means that are not shown. Two sets of averages are given for the Richmond Gulf Formation, one in which the number of samples equals the total number analyzed (n=25), and the other for all samples except Sample 20 (n=24). It follows that two sets of averages, based on 62 and 61 samples, are given for the composite redbed sample population made up of Pachi (P1, P2, P3) and Richmond Gulf arkoses (R). In each set the averages for those elements determined spectrographically are the same. Comparisons between the two sample populations for the Richmond Gulf Formation and between the two composite populations indicate only subtle if any differences. The inclusion or elimination of Sample 20 from the Richmond Gulf population either because it was incompletely analyzed or because it is lithologically different

than the other Richmond Gulf samples does not seem to have a profound effect upon the estimated average contents. A number of differences in element concentrations among the various sample populations are apparent when the averages of Table 40.2 are compared. Results of the statistical evaluation of such possible differences are given following presentation of the results from the study of elemental associations.

Correlation matrices computed for the Pachi clastic unit, the Richmond Gulf Formation and the composite redbed population are reproduced in Tables 40.3, 40.4, and 40.5. The matrices were calculated using pairwise instead of listwise deletion to make maximum use of the data. This means correlation coefficients for the elements analyzed by X-ray fluorescence were computed on sample populations of 25 and 62 for the Richmond Gulf and composite population respectively, whereas coefficients for the elements analyzed spectrographically were based on sample populations of 24 and 61. This approach to a difficult problem is considered more appropriate than completely discarding Sample 20 from the correlation analysis. Correlation coefficients for any pairs containing Ni, Co or Cu must be viewed with caution because of the large percentage of samples with contents below the detection limit.

A number of correlation coefficients are worthy of note. These include from Table 40.3 (Pachi) and Table 40.5 (Composite redbed population) the strong positive coefficients between U and Th; the strong positive coefficients between all pairs of the elements U, Ti, Zr and Y; and the substantially weaker positive coefficients between Th and the elements Ti, Zr and Y. In Table 40.4 (Richmond Gulf) the coefficients are generally similar except that both U and Th, not just U, have strong positive correlations with Ti, Zr and Y.

Scattergrams of U against Th and Zr are illustrated in Figure 40.1 and scattergrams of Ti against U, Y, and Zr are presented in Figure 40.2 for the samples of the Pachi arkose (P1+P2+P3, N=37). Figure 40.3 contains similar diagrams plotting U against Th and Zr, Ce against Zr and Y, and Ti against Y for the composite redbed population (P1+P2+P3+R, N=62). These particular scattergrams were selected from the great number that were computed because they appear to contribute most to an understanding of the interrelationships among elements. In all diagrams, samples of the Pachi arkose have been given different symbols so the P1, P2 and P3 groups can be differentiated. The best fitting straight lines as determined by linear regression analysis (dependent variable along the vertical axis) are also plotted on the scattergrams.

The scattergrams clearly illustrate the strengths of the correlations between selected element pairs and are more effective than consideration of the coefficients by themselves. In most cases the lines representing the regression equations appear to be lines of best fit but in Figure 40.1 (left) and Figure 40.3 (bottom) the positions of the lines are distorted by the samples containing Th contents that were below the detection limit. For each of these scattergrams the relationship between U and Th may indeed be stronger than that reflected by the correlation coefficients.

Examination of the diagrams also suggests the highest contents of U and Th, in particular, but also of Zr, Y and Ce occur within the heavy mineral enriched conglomerates of the Pachi arkose (P3). It is also evident that within the Pachi sediments the coarse- to medium-grained arkoses (P1) contain the least amounts of these elements. Samples of the Richmond Gulf arkose are generally similar in element contents to the finer grained less heavy mineral enriched samples of the Pachi arkose (P1 and P2).

Table 40.1

Trace element abundances of various lithologies from the Richmond Gulf area.
 Sample numbers are keyed to map Figure 25.1 (Miller, 1978). Rock units include:

B = Basement complex; P = Pachi clastic unit with varying degrees of coarseness (P1, P2, P3, P4);

V = Pachi volcanic unit; R = Richmond Gulf Formation; NA = Not analyzed

Rock unit	Sample number	U ppm	Th ppm	Ti wt%	Zr ppm	Y ppm	Ce ppm	La ppm	B ppm	Bo ppm	Sr ppm	Rb ppm	Ni ppm	Co ppm	Cu ppm	V ppm	Cr ppm	Lithology
B	5	2.0	21	.18	189	5	35	10	58	1209	239	124	<10	<10	<8	<33	<5	AUGEN GRANITIC GNEISS
B	8	2.1	21	.11	108	5	<3	<2	<50	830	222	124	<10	<10	<8	<20	<5	HEMATITIC LEUCOCRATIC GRANITE
B	2	2.7	39	.06	111	9	42	26	72	832	148	141	10	<10	<8	<20	<5	LEUCOCRATIC GRANITE
B	4	4.2	25	.26	297	19	95	63	72	484	230	109	<10	<10	<8	<27	<5	FOLIATED HEMATITIC GRANITE
B	1	5.9	50	.15	190	18	75	43	55	645	127	155	<10	<10	<8	<24	<5	HEMATITIC CHLORITIC GRANITE
P1	13	2.0	20	.02	31	2	13	<2	<50	1201	115	94	<10	<10	<8	<20	<5	PINK COARSE ARKOSE
P1	26	3.3	31	.07	61	14	7	<2	132	1075	89	72	<10	<10	<8	<20	<5	PINK MEDIUM GRAINED ARKOSE
P1	29	3.3	21	.03	64	3	<3	<2	147	1181	114	95	<10	<10	<8	<20	<5	PINK MEDIUM GRAINED ARKOSE
P1	34	6	43	.05	76	<2	<3	<2	106	1087	101	106	<10	<10	<8	<76	<5	COARSE PINK ARKOSE
P1	33	6	21	.06	104	6	24	<2	<50	768	65	53	<10	<10	<8	<20	<5	GRANULAR LIGHT PINK SERICITIC ARKOSE
P1	12	7	16	.09	182	<2	<3	<2	78	1038	94	77	13	11	10	<20	10	PINK COARSE ARKOSE
P1	32	8	23	.12	252	7	90	42	75	1056	108	88	<10	<10	<8	<20	<5	GRANULAR PINK ARKOSE
P1	25	1.0	23	.06	110	2	87	48	84	919	86	91	<10	<10	<8	<20	<5	MOTTLED PINK GRANULAR ARKOSE
P1	37	1.0	25	.05	100	15	<3	<2	93	1010	91	83	<10	<10	<8	<20	<5	COARSE PINK ARKOSE
P1	28	1.2	33	.10	270	8	5	<2	89	1108	111	81	<10	<10	12	<20	7	SERICITIC GRANULAR ARKOSE
P1	31	1.7	47	.13	40	3	<3	<2	167	1343	87	128	<10	<10	<8	41	31	MARON LAMINATED MUDSTONE
P1	36	2.3	42	.31	565	22	25	9	77	1755	79	139	<10	<10	<8	33	10	COARSE PINK ARKOSE
P1	19	3.4	14	.10	156	2	11	<2	69	863	71	107	<10	<10	<8	66	5	SERICITIC PEBBLY ARKOSE
P1	23	6.6	<3	.06	101	6	<3	<2	85	892	86	105	<10	<10	<8	<20	5	GRAY GRAINED GRAY ARKOSE
P2	30	1.8	26	.06	98	11	4	<2	73	839	137	61	<10	<10	<8	<20	8	GRANULAR HEAVY MINERAL LAMINATED ARKOSE
P2	17	2.6	35	.16	351	26	17	3	14	1738	1375	57	<10	<10	<8	<20	18	MARON HEAVY MINERAL LAMINATED ARKOSE
P2	14	3.8	74	.14	304	5	36	11	56	1366	110	67	<10	<10	<8	<20	<5	PINK HEAVY MINERAL LAMINATED ARKOSE
P2	21	4.0	35	.13	334	3	35	2	84	893	80	75	<10	<10	<8	39	13	GRANULAR HEAVY MINERAL LAMINATED ARKOSE
P2	16	4.2	52	.08	251	8	<3	<2	743	3190	403	69	<10	<10	<8	<20	11	MARON HEAVY MINERAL LAMINATED ARKOSE
P2	35	4.4	43	.12	358	11	85	32	122	1098	86	97	<10	<10	<8	44	19	GRANULAR HEAVY MINERAL LAMINATED ARKOSE
P2	38	2.3	29	.07	167	6	89	49	60	992	99	76	<10	<10	<8	<20	26	GRANULAR SERICITIC HEAVY MINERAL LAMINATED ARKOSE
P2	3	5.0	39	.11	307	9	29	2	410	1266	145	105	<10	<10	<8	<20	<5	QUARTZ PEBBLY ARKOSE
P2	10	1.0	189	.05	498	25	185	89	170	1254	327	50	<10	<10	<8	19	11	GRANITE-QUARTZ PEBBLE CONGLOMERATE
P3	1	1.0	124	.11	426	25	43	13	318	1843	128	136	<10	<10	12	58	30	GRANITE-QUARTZ PEBBLE CONGLOMERATE
P3	7	1.6	229	.06	129	9	24	<2	304	1496	258	103	<10	<10	12	58	30	GRANITE-QUARTZ PEBBLE CONGLOMERATE
P3	18	2.0	62	.14	577	20	12	9	277	4878	269	84	<10	<10	<8	<20	52	QUARTZ PEBBLY ARKOSE
P4	27	71.4	23	.05	77	7	<5	<2	<50	848	184	88	<10	<10	<8	<20	6	MARON COARSE GRAINED ARKOSE AT UNCONFORMITY
V	1	1	<3	.75	79	20	25	<2	50	384	129	53	<10	<10	35	18	128	AMYGDALOIDAL APHANTIC
V	3	1	43	.41	35	14	10	<2	125	189	136	53	<10	<10	37	19	225	APHANTIC PORPHYRITIC
V	4	<3	<35	.35	35	38	14	<2	71	211	28	69	<10	<10	17	18	95	AMYGDALOIDAL APHANTIC
V	2	3	43	.60	81	23	29	<2	40	522	<53	67	70	43	55	98	142	AMYGDALOIDAL APHANTIC PORPHYRITIC
R	28	4	<3	.05	97	5	<3	<2	50	1410	130	35	<10	<10	<8	<20	<5	MEDIUM GRAINED MARON ARKOSE
R	6	4	43	.03	76	2	18	8	27	985	84	54	<10	<10	<8	<20	<5	COARSE WHITE ARKOSE
R	4	14	48	.08	109	6	<3	<2	<50	1005	82	75	<10	<10	<8	<20	<5	COARSE GRAY ARKOSE
R	5	43	85	.05	129	5	17	9	49	1390	95	102	<10	<10	<8	<20	<5	COARSE WHITISH GRAY ARKOSE
R	11	6	26	.19	99	9	34	13	77	1052	99	102	<10	<10	<8	28	7	MEDIUM GRAINED MARON ARKOSE
R	16	7	10	144	11	7	17	7	207	1152	130	111	<10	<10	3	3	24	MARON HEAVY MINERAL LAMINATED ARKOSE
R	15	8	43	.15	152	10	31	19	134	1101	117	96	<10	<10	17	8	19	COARSE HEAVY MINERAL LAMINATED ARKOSE
R	17	8	43	.21	282	10	35	11	82	1082	134	106	<10	<10	<8	28	9	COARSE HEAVY MINERAL LAMINATED ARKOSE
R	10	8	43	.18	398	10	55	13	171	1027	187	110	<10	<10	<8	36	8	COARSE HEMATITE MOTTLED ARKOSE
R	5	9	43	.10	198	6	6	9	45	1110	75	73	<10	<10	<8	28	<5	COARSE GREENISH GRAY ARKOSE
R	16	9	43	.24	237	12	67	37	594	1713	176	120	<10	<10	<8	38	16	MEDIUM GRAINED HEAVY MINERAL LAMINATED ARKOSE
R	9	1.0	32	.30	316	28	22	2	274	803	101	99	<10	<10	10	8	46	MARON LAMINATED SILTSTONE
R	2	1.0	32	.23	359	13	36	11	79	1168	130	124	<10	<10	10	8	11	MARON LAMINATED SILTSTONE
R	7	1.0	43	.15	203	2	3	12	91	1189	137	104	<10	<10	<8	25	9	COARSE PINK ARKOSE
R	22	1.0	23	.15	178	7	24	<2	178	879	103	68	<10	<10	<8	<20	8	COARSE PINK ARKOSE
R	3	1.2	23	.07	179	2	20	13	56	1100	96	78	<10	<10	8	28	7	LIGHT PINK ARKOSE
R	15	1.3	18	.12	222	5	29	6	73	943	84	78	<10	<10	13	23	8	COARSE HEMATITE MOTTLED ARKOSE
R	13	1.3	43	.15	260	<2	38	3	83	999	92	68	<10	<10	8	2	11	GRANULAR HEMATITE MOTTLED ARKOSE
R	24	1.3	32	.23	360	10	38	5	91	1132	126	105	<10	<10	8	4	9	COARSE PINK HEAVY MINERAL LAMINATED ARKOSE
R	25	1.3	43	.34	407	20	73	36	3870	1119	340	119	<10	<10	14	7	25	COARSE RED HEAVY MINERAL LAMINATED ARKOSE
R	16	1.5	43	.29	464	17	37	21	1980	1349	310	92	<10	<10	<8	43	15	MEDIUM GRAINED PINK HEAVY MINERAL LAMINATED ARKOSE
R	10	4.2	54	.52	1199	34	32	21	79	1089	121	98	14	11	<8	10	46	COARSE HEMATITE MOTTLED HEAVY MINERAL LAMINATED ARKOSE
R	21	5.5	35	.69	1714	40	109	38	200	950	119	111	25	12	10	14	62	COARSE HEMATITE MOTTLED HEAVY MINERAL LAMINATED ARKOSE
R	20	62.5	496	.98	5103	65	647	398	NA	93	70	NA	NA	NA	NA	NA	NA	BLACK HEAVY MINERAL CROSSBED FROM SPECIMEN 21

Table 40.2

Arithmetic means for Rb and Y and geometric means for other elements
in the principal rock types of the Richmond Gulf area.

	B (N=5)	P1 (N=17)	P2 (N=8)	P3 (N=12)	V (N=4)	R (N=24)	R (N=25)	P1+P2+P3 (N=37)	P1+P2+P3+R (N=61)	P1+P2+P3+R (N=62)
U	3.1	1.0	2.8	7.7	0.2	1.0	1.1	2.4	1.7	1.8
Th	29.3	8.5	20.4	82.4	1.0	4.2	5.1	21.4	11.3	12.0
Ti	0.14	0.085	0.12	0.12	0.54	0.15	0.16	0.10	0.12	0.12
Zr	166.0	138.0	285.8	292.8	52.9	238.8	269.9	206.2	218.5	229.9
Y	11.2	8.1	9.5	12.3	23.8	11.6	13.8	9.7	10.5	11.4
Ce	25.4	8.3	12.5	25.4	20.7	20.0	23.0	13.0	15.4	16.4
La	14.8	3.2	4.2	7.4	1.0	8.2	9.6	4.4	5.6	6.0
Ba	764.2	1001.6	1629.5	1384.1	235.1	1060.7	962.3	1241.4	1166.9	1120.3
Sr	195.7	93.9	154.0	149.5	38.6	118.8	116.3	121.5	120.4	119.4
Rb	130.6	96.8	69.9	90.1	58.5	95.6	91.9	88.8	91.5	90.0
B	42.8	95.4	146.6	294.7	74.7	116.5	116.5	150.9	136.3	136.3
V	21.2	15.4	19.1	39.6	109.3	30.2	30.2	21.9	24.9	24.9
Cr	2.0	4.0	11.4	18.4	140.4	9.3	9.3	8.3	8.7	8.7
Ni	5.7	5.9	5.0	6.8	74.7	7.2	7.2	5.9	6.4	6.4
Co	5.0	5.5	5.0	6.6	47.1	5.4	5.4	5.7	5.6	5.6
Cu	5.7	4.7	4.0	6.3	23.3	5.5	5.5	5.0	5.2	5.2

Table 40.3

Matrix of correlation coefficients for samples of the Pachi arkose (P1 + P2 + P3, N = 37). Critical values for significance at the .001, .01 and .05 levels are 0.51, 0.41 and 0.32 respectively

	U	TH	TI	ZR	Y	CE	LA	BA
U	1.00000	.55777	.50099	.66623	.40127	.26950	.29499	.23863
TH	.55777	1.00000	.19535	.29968	.35363	.35865	.19836	.17258
TI	.50099	.19535	1.00000	.84323	.69958	.48351	.51255	-.02144
ZR	.66623	.29968	.84323	1.00000	.55559	.41227	.45282	.10774
Y	.40127	.35363	.69958	.55559	1.00000	.30839	.27719	.13364
CE	.26950	.35865	.48351	.41227	.30839	1.00000	.75423	-.39524
LA	.29499	.19836	.51255	.45282	.27719	.75423	1.00000	-.11313
BA	.23863	.17258	-.02144	.10774	.13364	-.39524	-.11313	1.00000
SR	.28049	.28838	.00303	.12130	.18634	-.32981	-.23091	.84791
RB	.16784	-.03711	.49610	.28299	.45535	.28739	.32049	-.25085
B	.48574	.31833	.31725	.30332	.32438	-.16524	-.13286	.49477
V	.62033	.35918	.59857	.60593	.43324	.33120	.37728	.14440
CR	.74079	.49958	.64516	.67561	.43940	.27832	.35485	.37138
NI	.24146	.15570	.30344	.15172	.26517	-.04045	.19330	.26483
CO	.29147	.19495	.25336	.19420	.23548	-.11523	.14874	.34272
CU	.35463	.35494	.07357	.22863	.12166	-.06647	-.13185	.17137
	B	V	CR	NI	CO	CU	SR	RB
U	.48574	.62033	.74079	.24146	.29147	.35463	.28049	.16784
TH	.31833	.35918	.49958	.15570	.19495	.35494	.28838	-.03711
TI	.31725	.59857	.64516	.30344	.25336	.07357	.00303	.49610
ZR	.30332	.60593	.67561	.15172	.19420	.22863	.12130	.28299
Y	.32438	.43324	.43940	.26517	.23548	.12166	.18634	.45535
CE	-.16524	.33120	.27832	-.04045	-.11523	-.06647	-.32981	.28739
LA	-.13286	.37728	.35485	.19330	.14874	-.13185	-.23091	.32049
BA	.49477	.14440	.37138	.26483	.34272	.17137	.84791	-.25085
SR	.76639	.07176	.38828	.11858	.18256	.26355	1.00000	-.29838
RB	.00008	.39941	.13107	.01577	-.01872	-.16096	-.29838	1.00000
B	1.00000	.32392	.54217	.25256	.28031	.37804	.76639	.00008
V	.32392	1.00000	.73297	.36122	.38740	.25625	.07176	.39941
CR	.54217	.73297	1.00000	.46552	.48219	.38521	.38828	.13107
NI	.25256	.36122	.46552	1.00000	.95924	.47311	.11858	.01577
CO	.28031	.38740	.48219	.95924	1.00000	.55871	.18256	-.01872
CU	.37804	.25625	.38521	.47311	.55871	1.00000	.26355	-.16096

Table 40.4

Matrix of correlation coefficients for samples of the Richmond Gulf arkose (N = 25 for coefficients among all pairs of elements except those including B, V, Cr, Ni, Co and Cu where N = 24). Critical values for significance at the .001, .01 and .05 levels are 0.63, 0.52 and 0.40 respectively

	U	TH	TI	ZR	Y	CE	LA	BA
U	1.00000							
TH	.60626	1.00000						
TI	.79352	.42127	1.00000					
ZR	.93512	.49210	.88494	1.00000				
Y	.88029	.51979	.81674	.88623	1.00000			
CE	.69499	.35255	.69620	.70627	.63505	1.00000		
LA	.65210	.29210	.55527	.63874	.60641	.71417	1.00000	
BA	-.78194	-.54493	-.44966	-.61351	-.73794	-.52471	-.48069	1.00000
SR	-.07118	-.34244	.28203	.08560	.00643	.10921	.19422	.39758
RB	-.48879	-.38732	.02026	-.23868	-.34212	-.15836	-.15104	.77479
B	.37976	-.20588	.59098	.43331	.43659	.55878	.42590	.13117
V	.67663	.16033	.84191	.71409	.77742	.65777	.54272	-.07673
CR	.74196	.24869	.88601	.71568	.78066	.66593	.41629	-.21212
NI	.40162	.10463	.55208	.35339	.69052	.38498	.31615	-.32377
CO	.77518	.43687	.56806	.74368	.78255	.28253	.33924	-.11586
CU	.28403	.12578	.32141	.16462	.34865	.37632	.19092	-.31489
	B	V	CR	NI	CO	CU	SR	RB
U	.37976	.67663	.74196	.40162	.77518	.28403	-.07118	-.48879
TH	-.20588	.16033	.24869	.10463	.43687	.12578	-.34244	-.38732
TI	.59098	.84191	.88601	.55208	.56806	.32141	.28203	.02026
ZR	.43331	.71409	.71568	.35339	.74368	.16462	.08560	-.23868
Y	.43659	.77742	.78066	.69052	.78255	.34865	.00643	-.34212
CE	.55878	.65777	.66593	.38498	.28253	.37632	.10921	-.15836
LA	.42590	.54272	.41629	.31615	.33924	.19092	.19422	-.15104
BA	.13117	-.07673	-.21212	-.32377	-.11586	-.31489	.39758	.77479
SR	.84993	.43165	.40693	.24166	.00823	.13287	1.00000	.57326
RB	.46750	.63577	.53619	.28537	.16687	.12483	.57326	1.00000
B	1.00000	.58030	.60511	.36393	.02442	.30519	.84993	.46750
V	.58030	1.00000	.93342	.71477	.52094	.54901	.43165	.63577
CR	.60511	.93342	1.00000	.71592	.53059	.49934	.40693	.53619
NI	.36393	.71477	.71592	1.00000	.45893	.73223	.24166	.28537
CO	.02442	.52094	.53059	.45893	1.00000	.09802	.00823	.16687
CU	.30519	.54901	.49934	.73223	.09802	1.00000	.13287	.12483

Table 40.5

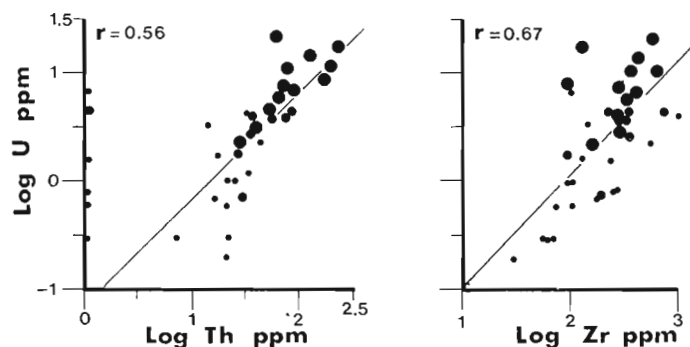
Matrix of correlation coefficients for samples of the composite redbed population (P1 + P2 + P3 + R, N = 62 for coefficients among all pairs of elements except those including B, V, Cr, Ni, Co and Cu where N = 61). Critical values for significance at the .001, .01 and .05 levels are 0.41, 0.33 and 0.25 respectively

	U	TH	TI	ZR	Y	CE	LA	BA
U	1.00000							
TH	.62014	1.00000						
TI	.46270	.15181	1.00000					
ZR	.67127	.29813	.86014	1.00000				
Y	.50654	.32803	.75496	.74285	1.00000			
CE	.32365	.25106	.57569	.53107	.45157	1.00000		
LA	.30293	.11381	.55620	.53492	.43647	.75100	1.00000	
BA	-.00916	-.00717	-.23381	-.19670	-.30983	-.45522	-.26653	1.00000
SR	.18971	.08938	.07396	.09671	.08144	-.22122	-.12644	.72248
RB	-.07268	-.18930	.30014	.07093	.03149	.14803	.17079	.06985
B	.43708	.13612	.38856	.34025	.36115	.06038	.02766	.38910
V	.47785	.16683	.70501	.64827	.58511	.43998	.44416	.07504
CR	.64061	.34087	.71867	.68995	.57427	.39020	.37267	.27036
NI	.16744	.03639	.44592	.25095	.50675	.14175	.25445	.10390
CO	.38632	.28047	.30040	.33172	.39255	-.03754	.16518	.36284
CU	.23696	.17423	.20741	.20819	.24727	.10319	.00639	.06839
	B	V	CR	NI	CO	CU	SR	RB
U	.43708	.47785	.64061	.16744	.38632	.23696	.18971	-.07268
TH	.13612	.16683	.34087	.03639	.28047	.17423	.08938	-.18930
TI	.38856	.70501	.71867	.44592	.30040	.20741	.07396	.30014
ZR	.34025	.64827	.68995	.25095	.33172	.20819	.09671	.07093
Y	.36115	.58511	.57427	.50875	.39255	.24727	.08144	.03149
CE	.06038	.43998	.39020	.14175	-.03754	.10319	-.22122	.14803
LA	.02766	.44416	.37267	.25445	.16518	.00639	-.12644	.17079
BA	.38910	.07504	.27036	.10390	.30284	.06839	.72248	.06985
SR	.76101	.15907	.38668	.14419	.14813	.20625	1.00000	-.05901
RB	.12191	.47049	.23862	.12769	.00486	-.04674	-.05901	1.00000
B	1.00000	.39553	.55273	.28112	.20234	.32748	.76101	.12191
V	.39553	1.00000	.79639	.52937	.39069	.38923	.15907	.47049
CR	.55273	.79639	1.00000	.55969	.48232	.42834	.38668	.23862
NI	.28112	.52937	.55969	1.00000	.68517	.61479	.14419	.12769
CO	.20234	.39069	.48232	.68517	1.00000	.36887	.14813	.00486
CU	.32748	.38923	.42834	.61479	.36887	1.00000	.20625	-.04674

A variety of factor analysis solutions were computed for the individual rock types and the composite rebedded population to shed more light on the associations among elements. The number of factors and the number of elements included in the computations were varied in an effort to gain a relatively stable solution containing the fewest factors that would still be able to account for at least 70 percent of both the overall data variability and the variability of each element. Only a brief summary of the results is presented in this paper. Complete factor solutions will be made available upon request.

Three consistent associations were indicated by the factor analyses of the Pachi arkose, Richmond Gulf Formation and the composite sample populations. These were in order of decreasing importance: 1) Ti-Zr-Y-Ce-La-V-Cr-U, 2) Sr-Ba-B, and 3) Th-U-Ce-La. Greater than 50 percent of the total variation explained by these three factors was related to the first factor. The elements in each association are listed in order of relative importance as indicated by factor loadings. Ce and La appear in the first and third factors but are most important in the first factor. Uranium was about evenly split between the first and third association. Thorium appears with the first association in only the Richmond Gulf arkose. However, correlations between the first and third associations were consistently positive at a moderate level. When Ni, Co and Cu were included in the factor analysis they formed a separate association. Rubidium achieved low communalities in most of the factor solutions but was most closely related to the first association. In retrospect, the associations revealed by factor analysis were those that could have been deduced from careful study of the correlation matrices in Tables 40.3, 40.4, and 40.5.

The strong positive correlation between U and Th, the moderately strong positive correlation between the Ti-Zr-Y-Ce-La-V-Cr-U association and the Th-U-Ce-La association, and the occurrence of Th in the former association for the Richmond Gulf arkose indicate that U, Th, Ti, Zr, Y, Ce, La, V and Cr can be considered as elements belonging to a single association that dominates the geochemistry of the redbeds in the Richmond Gulf area.



- Coarse to medium grained arkose
- Granule to coarse heavy mineral laminated arkose
- Granitoid & quartz pebble conglomerate; pebbly arkose

Figure 40.1. Scattergrams of U against Th and Zr for samples of the Pachi arkose (P1 + P2 + P3, N = 37).

Multivariate analysis of variance (MANOVA) and discriminant analysis statistically confirmed the geochemical differences in element contents among rock types that were suggested earlier by the apparent variation among means of Table 40.2 and the distribution of samples in the scattergrams of Figures 40.1, 40.2, and 40.3. Two tests capable of indicating statistical difference among populations were used in this study: 1) the commonly employed statistic, Wilk's Lambda, a measure of the amount of variance within groups being compared relative to the total variation among all samples, and 2) the number of correct classifications of samples into groups based on computed discriminant functions. Results of three comparisons using all 16 elements in the analyses are summarized in Table 40.6. The low values for Wilk's Lambda and the high percentage of correct classifications for each comparison suggest the groups included in each analysis have distinct geochemical signatures in terms of element content. However, the table also shows that only certain elements are effective discriminators. This is particularly true in the comparison between the Pachi and Richmond Gulf arkoses (Comparison 2). U and Th are virtually the only elements that are greatly different between the two sample populations.

The discussion of differences among sample populations would not be complete without consideration of the variation in the Th to U ratio among the rock types. It is interesting to note that the ratio calculated using the average contents listed in Table 40.2 has a similar value of about 10 in the basement gneisses (N=5) and the Pachi arkose (N=37) but has a lesser value of between 4 and 5 for the Richmond Gulf arkose. The ratio is also relatively constant in the P1, P2, and P3 subgroups of the Pachi arkose but the concentration of Th and U becomes greater than in the basement gneisses only in the P3 group where the average enrichment is on the order of two to three times.

Discussion

It has been clearly demonstrated that the elements included in this study can be grouped into a number of well defined interrelated associations and that different lithologies have distinct geochemical signatures in terms of element abundances. A paleoplacer model can be constructed that relates the U and Th anomalies within the Pachi and Richmond Gulf arkoses to the coarser heavy mineral enriched portions of the clastic sequence. It is postulated that the radioactive minerals were concentrated by the same process and along with the nonradioactive heavy minerals.

Such a model is reasonable because the elements of the principal U-Th-Ti-Zr-Y-Ce-La-V-Cr association clearly reflect the chemistry of the heavy minerals known to occur in the redbeds. Ti, Cr and V can be reasonably connected with magnetite and titanomagnetite, the most abundant heavy minerals; Ce, La, Y, U and Th with thorite and monazite and Zr with zircon. Furthermore, the differences in abundance of these elements from one rock sample to the next can be directly related to the varying degree of coarseness in the clastic sediments which in turn influences the extent of heavy mineral concentration.

The Sr-Ba-B association and variations in content of these elements are less easily explained because a relationship between tourmaline, the most probable source of B, and the sericite, biotite, feldspar or barite that could contribute the Sr and Ba has not been documented. Anomalous concentrations of boron are associated with black heavy mineral rich basal polymictic conglomerates north of the North River (Miller, 1978, Figure 25.1) and reflect locally intensive epigenetic tourmalinization of the basal conglomerates. The few high values of Ba suggest the possible local presence of barite cement.

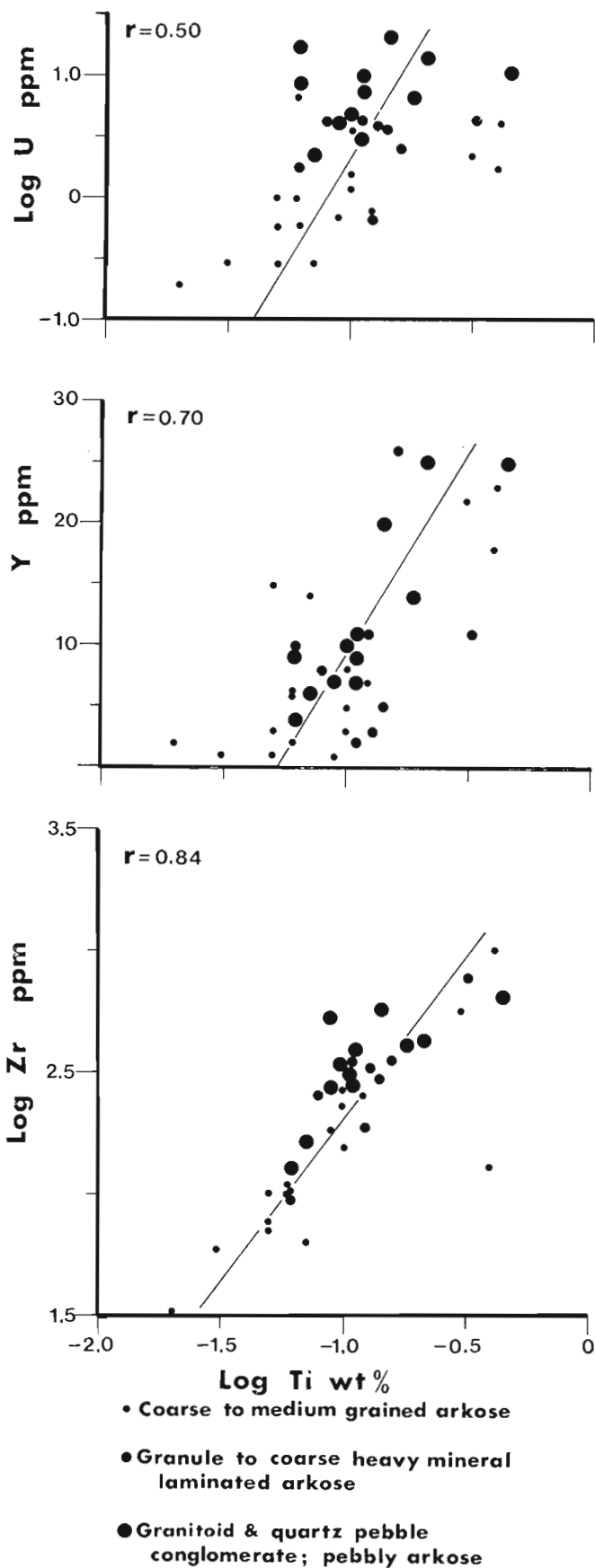


Figure 40.2. Scattergrams of Ti against U, Y and Zr for samples of the Pachi arkose (P1 + P2 + P3, N = 37).

Table 40.6

Summary of multivariate analysis of variance (MANOVA) and discriminant analysis results for three comparisons among rock types

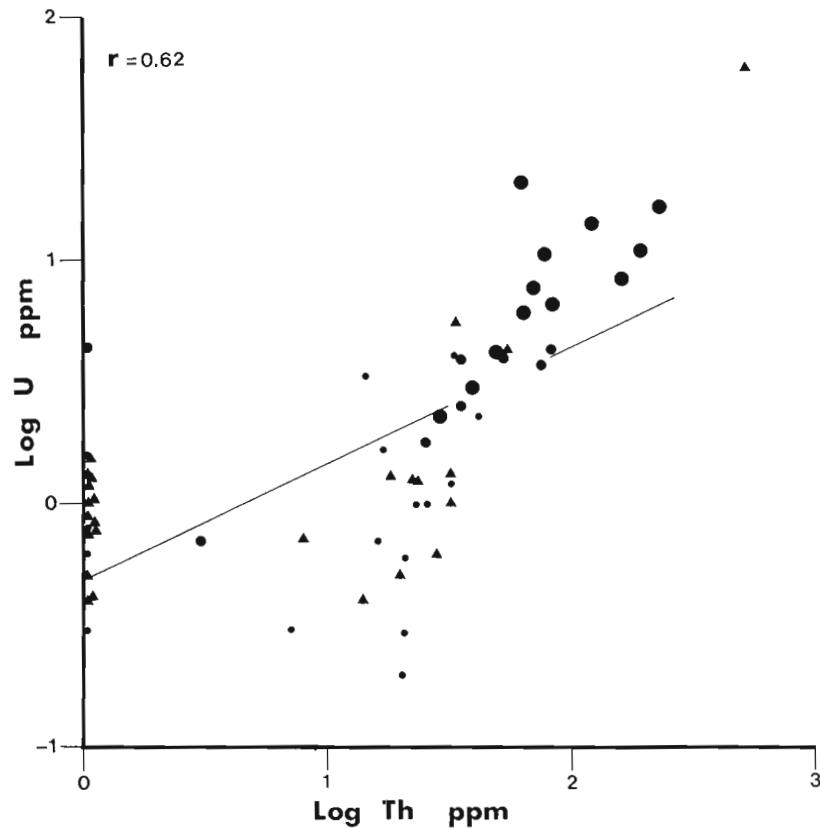
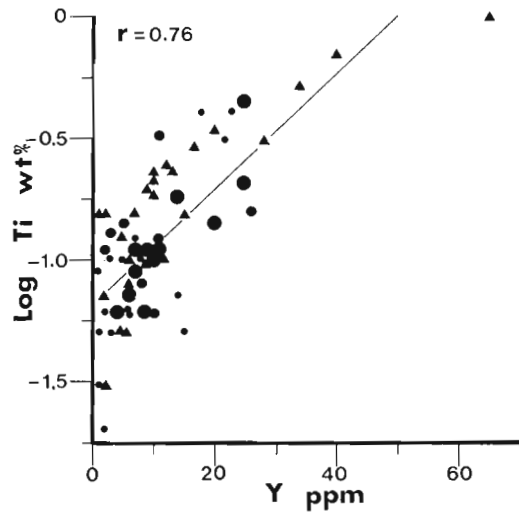
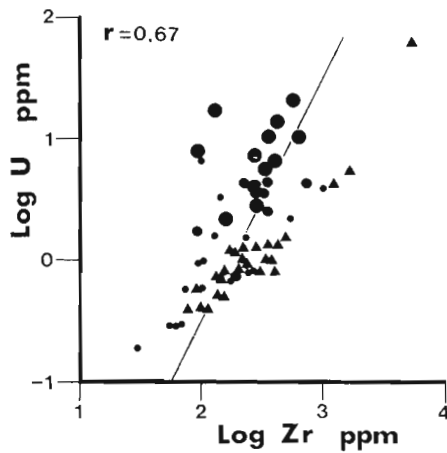
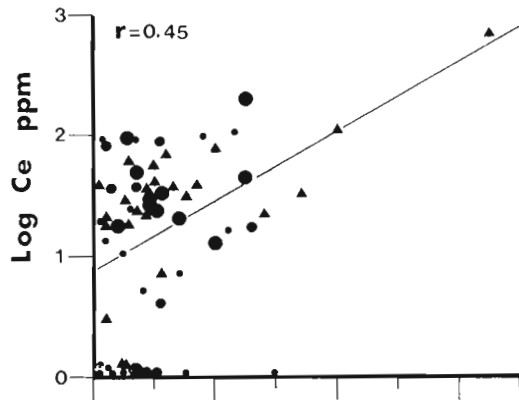
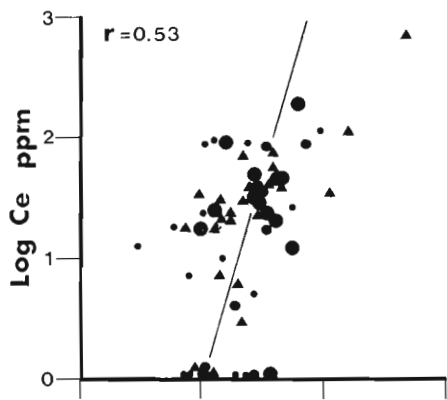
	Sample populations included in analysis	Wilk's Lambda	Percentage of correct classifications	Elements most effective in discriminant analysis
1	Pachi arkose groups (P1 vs P2 vs P3)	.0882	94.6	U, Th, Cr, V
2	Pachi and Richmond arkoses (P1+P2+P3) vs (R)	.4459	90.2	Th, U
3	All principal rock types (P1 vs P2 vs P3 vs R vs B vs V)	.0018	88.6	U, Th, Co, Ni, Cr

The greater amount of U and Th in the Pachi arkose relative to the Richmond Gulf arkose is a function of the greater concentration of heavy minerals in the Pachi arkose. This phenomenon is most likely the result of a greater topographic relief and thus greater hydraulic gradient and faster depositional rate during Pachi sedimentation. The somewhat greater contents of Ti, V, Cr and Ni in the Richmond Gulf arkose relative to the Pachi arkose can be related to the presence of the Pachi volcanic unit as a source for the Richmond Gulf arkose. The volcanic unit is enriched in Ti, V, Cr and Ni relative to the basement gneisses which were the source for the Pachi clastic sediments. A similarity in Th to U ratios for the Richmond Gulf arkose and the Pachi volcanic unit, though suggestive of a link between them, may be coincidental.

Chandler (1978) concluded the Richmond Gulf Formation represents the continuation of fluvial arkosic sedimentation begun during Pachi sedimentation but interrupted by a period of subaerial basaltic volcanism. The similarities in elemental associations between the Pachi and Richmond Gulf clastic sequences combined with the above mentioned differences in relative abundance of certain elements support Chandler's hypothesis.

The geochemical relationships that have been presented and the model that has been proposed to explain the U and Th anomalies of the Richmond Gulf area can be compared to the situation at Elliot Lake, Ontario where Early Apehbian uraniferous conglomerates have been interpreted as paleoplacer deposits (Roscoe, 1969). Theis (1978, 1979) documented in detail the geochemical and sedimentological characteristics of the ore reefs. Correlations among the elements U, Th, Zr and Ce and between these elements and pebble size were used to demonstrate that the heaviest detrital mineral, uraninite, was concentrated within the coarsest conglomerates whereas the thorite, monazite and zircon fraction of the river sediment remained within the river load until the appropriate hydraulic conditions permitted deposition (Theis, 1978). The elemental variation within the ore reefs was interpreted to result from the accumulation of heavy minerals interstitial to the framework clasts (Theis, 1978).

The elemental associations in the Apehbian redbeds of the Richmond Gulf area are somewhat similar to those documented for the Elliot Lake ores and have led to the construction of a paleoplacer model. However, there is a very important difference even though the process of



Richmond Gulf Fm

▲ Coarse to medium grained arkose with heavy mineral laminae

Pachi arkose

- Coarse to medium grained arkose
- Granule to coarse heavy mineral laminated arkose
- Granitoid & quartz pebble conglomerate; pebbly arkose

Figure 40.3.

Scattergrams of U against Th, Zr against Ce and U, and Y against Ce and Ti for the composite redbed population (P1 + P2 + P3 + R, N = 62).

formation may have been comparable. Uraninite occurs as an ore mineral in the pyritic conglomerates of the Elliot Lake camp but has not been identified in the redbeds of the Richmond Gulf area. The Th to U ratios and low concentrations of uranium in the samples of the study area do not support even the possibility that uraninite will be found. The placers of the Richmond Gulf area are more typical of the non-uraniferous hematite type than the anoxic potentially uraniferous pyritic types as discussed by Roscoe (1969, p. 82, 83).

Conclusions

This study effectively documents the direct correspondence between U-Th anomalies and monazite-thorite bearing heavy mineral concentrations within the Proterozoic redbeds of the Richmond Gulf area. Consideration of associations among elements and of differences in element contents were useful in modelling the geochemistry. Similar studies in other environments containing anomalous radioactivity would be beneficial in constructing appropriate genetic models for use as guides to exploration or as essential aids in resource evaluation.

Acknowledgments

The authors acknowledge the Geochemical Section, Geological Survey of Canada: R. Rousseau for the X-ray fluorescence analyses and the staff of the spectrographic laboratory for the photospectrographic analyses.

References

- Chandler, F.W.
1979: Geology of the Manitounuk Supergroup, Lac Guillaume Delisle (Richmond Gulf) area, New Quebec; Geological Association of Canada/Mineralogical Program with Abstracts, Annual Meeting, Quebec City, p. 42 (abstract).
1978: Geological environment of Archean redbeds of the north half of Richmond Gulf, New Quebec; in Current Research, Part A; Geological Survey of Canada, Paper 78-1A, p. 107-110.
- Dressler, B.
1975: Lamprophyres of the north-central Labrador Trough, Quebec, Canada; Neues Jahrbuch fuer Mineralogie, Monatshefte, H6, p. 67-79.
- Fryer, B.J.
1972: Age determinations in the Circum-Ungava geosyncline and the evolution of Precambrian banded iron formations. Canadian Journal of Earth Sciences, v. 9, p. 652-663.
- Hews, P.C.
1976: A Rb-Sr whole rock study of some Proterozoic rocks, Richmond Gulf, Nouveau Quebec; unpublished M.Sc. thesis, Carleton University, Ottawa, 64 p.
- Miller, A.R.
1979: Geochemical expression of Proterozoic Uranium occurrences, Richmond Gulf area, New Quebec and Baker Lake area, N.W.T., Canada; Geological Association of Canada/Mineralogical Association of Canada, Annual Meeting, Quebec City, Program with Abstracts, p. 67.
1978: Uranium reconnaissance of the northern Richmond Gulf area, New Quebec; in Current Research, Part A, Geological Survey of Canada, Paper 78-1A, p. 111-117.
- Roscoe, S.M.
1969: Huronian rocks and uraniferous conglomerates in the Canadian Shield; Geological Survey of Canada, Paper 68-40.
- Theis, N.J.
1979: Uranium-bearing and associated minerals in their geochemical and sedimentological context, Elliot Lake, Ontario; Geological Survey of Canada, Bulletin 304, 50 p.
1978: Mineralogy and setting of Elliot Lake deposits; in Uranium Deposits: Their Mineralogy and Origin, ed. M.M. Kimberley, Mineralogical Association of Canada Short Course, p. 331-338.
- Woodcock, J.R.
1960: Geology of the Richmond Gulf Area, New Quebec; Proceedings of the Geological Association of Canada, v. 12, p. 21-39.

A STUDY OF INITIAL MOTION CHARACTERISTICS OF PARTICLES IN GRADED BED MATERIAL

Project 750080

T.J. Day
Terrain Sciences Division

Day, T.J., A study of initial motion characteristics of particles in graded bed material; in Current Research, Part A, Geological Survey of Canada, Paper 80-1A, p. 281-286, 1980.

Abstract

An analysis of size fraction thresholds as defined by P. Ackers and W.R. White indicates that shielding and protrusion effects exhibited by bed mixtures with a wide range of particle sizes are similar. The expected trend for higher thresholds of motion for smaller sizes and lower thresholds for larger sizes within mixtures, compared to thresholds for similarly sized uniform sediments, is illustrated. Furthermore, the results indicate that the threshold of the D_{50} size of a mixture is similar to the threshold for a uniform sediment of the same size.

Introduction

Water flowing over a bed composed of noncohesive sediment exerts forces on the grains that tend to move or entrain them. The forces resisting entrainment differ according to the grain size and grain size distribution of the sediment. When the hydrodynamic force acting upon a grain of sediment has reached a value that, if increased even slightly, will put the grain into motion, critical or threshold conditions are said to have been reached. Under critical conditions, a stream is said to be competent to move its sediment.

For beds of coarse uniform sediments such as sand and gravel, the forces resisting motion are caused mainly by the weight of the particles. If the bed is composed of a heterogeneous material, however, the initial movement of any specific size fraction depends not only on its weight but also upon the variation in stability caused by the relative size of surrounding particles. On average in a uniform sediment, exposures of individual grains are equal. In a mixed bed, however, particles of fine size are shielded by larger ones, thereby increasing stability; as the larger sized particles are more exposed, they should exhibit less stability than their uniform counterparts.

Experimental results, for example by Rakoczi (1975) and Fenton and Abbott (1977), field studies by Church (1972), and theoretical work by Egiazaroff (1965) all offer support for the expected trend in particle stabilities. Rakoczi was able to illustrate larger thresholds for particles of smaller size and smaller thresholds for larger ones, and in particular that the D_{50} size of sandy gravel mixtures have the same threshold as uniform sediments as predicted by the Shields' curve (cf. Graf, 1971, p. 127-128, Fig. 6, 7). This feature was not found for sand or gravel mixtures alone, however. Fenton and Abbott's (1977) study of the effect of protrusion height on threshold conditions illustrated, for example, that coarse sediments with large protrusions exhibited threshold conditions (as defined by a small rate of transport) one sixth that of the Shields' value. Church's (1972) results from field studies of coarse bed material streams indicated that over-loose sediments (those lying on the bed surface and protruding into the flow) exhibited threshold conditions less than the Shields' value and similar to Fenton and Abbott's results. Also, from measurements at low bed load rates, Church was able to illustrate the possible magnitude of change in the Shields' parameters for particles incorporated within the stream bed material. Where structural strengthening, such as

imbrication occurs, coarse particles (≈ 3 mm) can require threshold conditions 25% greater than the expected Shields' parameter.

Using a theoretical approach Egiazaroff (1965) presented a relationship for threshold conditions for any particle size in a mixture, providing that the size distribution of the transported material was known. This analysis also supported the previously mentioned shielding effects on threshold conditions. Egiazaroff's work led to the conclusion that the D_{50} size of a mixture would be expected to move at a higher threshold than the same size as a uniform material. There is, however, some criticism of this work. Neill (1968) questioned its validity, as the theoretical velocity profile extended below the peaks of some of the larger particles; he argued that the physical picture in this area must be confused and the interaction between the flow and the smaller grains must be dependent to a large extent upon the relative height and spatial distribution of the larger grains. Furthermore, the requirement for the shape of the transport curve is almost prohibitive, particularly as it is this precise information which is needed to compute the amount of and size particle in transport.

This report presents another approach to the definition of size fraction thresholds. Using the approach to sediment transport developed by Ackers and White (1973), initial movement as defined by a small rate of transport is determined from established motion characteristics. Also, the initial motion relationships for uniform sediment developed by Ackers and White are used to identify the magnitude of differences between uniform and graded sediments.

Acknowledgments

The support and continuing assistance of Dr. W.R. White's Section of the Hydraulics Research Station, Wallingford, England is gratefully acknowledged.

Ackers-White Approach

Ackers and White (1973) have described the movement of sediment in terms of three dimensionless groups: (1) particle mobility, F_{gr} ; (2) sediment transport, G_{gr} ; and (3) a dimensionless particle size, D_{gr} .

The particle mobility number is a ratio of shear forces and immersed weights. For coarse beds where bed forms are assumed to be small, sediment transport is considered a bed

process. The relationship between effective shear stress and the mean stream velocity can be described by the rough turbulent equation

$$\sqrt{\frac{\tau}{\rho}} = \frac{V}{\sqrt{32 \log\left(\alpha \frac{d}{D}\right)}} \quad (1)$$

where τ shear stress
 ρ mass density of fluid
 V mean velocity of flow
 d mean depth of flow
 D particle size
 α coefficient of rough turbulent equation

A fine sediment is considered to be transported in the main body of the flow, where it is suspended by turbulence. As the intensity of turbulence is dependent upon the total energy degradation, rather than on a net grain resistance, for fine material

$$\sqrt{\frac{\tau}{\rho}} = v_* = \sqrt{gdi} \quad (2)$$

where v_* shear velocity
 g acceleration due to gravity
 i hydraulic gradient

For coarse sediments the equation for particle mobility is

$$Fgr = \frac{V}{\sqrt{gD(s-1)}} \cdot \frac{1}{\sqrt{32 \log\left(\alpha \frac{d}{D}\right)}} \quad (3)$$

and for fine sediments

$$Fgr = \frac{V}{\sqrt{gD(s-1)}} \quad (4)$$

where s is mass density of sediment.

An extensive analysis of flume data led to the definition of $Dgr \geq 60$ for coarse sediments and $Dgr \leq 1.0$ for fine sediments. Sizes transitional between these two limits can exhibit both fine and coarse sediment behaviour, and which form of behaviour is dominant depends upon the size relative to either limit. A general equation for particle mobility is then

$$Fgr = \frac{v_*^n}{\sqrt{gD(s-1)}} \cdot \left[\frac{V}{\sqrt{32 \log\left(\frac{\alpha d}{D}\right)}} \right]^{1-n} \quad (5)$$

where n is a transitional exponent ranging from 1.0 for fine sediment to 0 for coarse. The value of n between 0 and 1 depends upon Dgr . The transitional range includes particle sizes approximately between 0.04 and 2.5 mm as Dgr ranges from 1 to 60.

The dimensionless particle diameter Dgr is defined as the cube root of the ratio of immersed weight to viscous forces or

$$Dgr = D \left(\frac{g(s-1)}{\nu^2} \right)^{1/3} \quad (6)$$

where ν is viscosity.

The expression for sediment transport was based on the stream power concept, in the case of coarse sediments using the product of net grain shear and stream velocity as the power per unit area of bed, and for fine sediments using the total stream power. By combining the efficiency of transport with the mobility number a transport parameter is:

$$Ggr = \frac{Xd}{sD} \left(\frac{v_*}{V} \right)^n \quad (7)$$

where X is the sediment transport as mass flux per unit mass flow rate.

For coarse sediments ($n = 0$) Eq. 7 reduces to

$$Ggr = \frac{Xd}{sD} \quad (8)$$

and for fine sediments ($n = 1$)

$$Ggr = \frac{Xd}{sD} \left(\frac{v_*}{V} \right) \quad (9)$$

In functional terms Eq. 7 is

$$Ggr = f(Fgr; Dgr) \quad (10)$$

and the generalized transport equation is

$$Ggr = C \left(\frac{Fgr}{A} - 1 \right)^m \quad (11)$$

where C and m are the coefficient and exponent of the sediment transport function, and A is the initial motion parameter for uniform bed material or the value of Fgr when Ggr equals 10^{-4} , which no significant transport is considered to take place.

On the basis of more than 1000 sets of experimental flume data, the parameters C , m , and A were determined as single value functions of Dgr (Fig. 41.1). The initial motion parameter, A , was defined as Fgr when Ggr equals 10^{-4} . The authors argued that as there will always be small and isolated movements due to the statistical nature of the fluctuating fluid forces, a definition of A for a small transport rate is reasonable. This choice is particularly useful as its application is objective and consistent even though the choice of 10^{-4} is somewhat subjective.

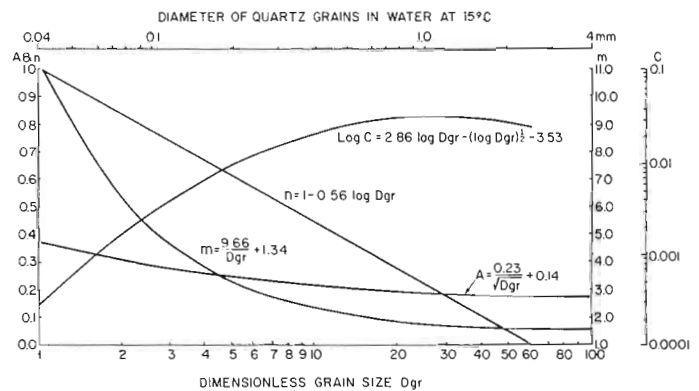


Figure 41.1. Comparison of parameters in Ackers and White's Equation 11.

Table 41.1
Summary of Bed Materials and Hydraulic and Transport Measurements

Bed Material No.	Source	D ₅₀ (mm)	$\sqrt{D_{84}/D_{16}}$	Range of Sizes (mm)	No. of Runs	Mean Depth (m)	Mean Velocity (m/s)	Shear Velocity (m/s)	Transport Rates ¹ (kg/s)	Concentration (ppm)
1	USWES Sand No. 1 (1935)	0.42	1.82	0.153 - 2.86	17	0.019 - 0.067	0.271 - 0.549	0.017 - 0.036	0.00006 - 0.00953	7.14 - 353.74
2	USWES Sand No. 2 (1935)	0.44	1.51	0.153 - 2.03	19	0.022 - 0.126	0.262 - 0.555	0.021 - 0.043	0.00003 - 0.01925	6.91 - 374.44
3	USWES Sand No. 9 (1935)	4.10	1.45	0.925 - 5.56	17	0.074 - 0.107	0.558 - 0.732	0.047 - 0.069	0.00003 - 0.01516	0.98 - 274.82
4	Gibbs and Neill (1972, 1973)	4.75	2.28	1.20 - 14.2	6	0.165 - 0.177	0.810 - 1.088	0.057 - 0.0913	0.0333 - 0.25197	234.51 - 1483.10
5	Cecen and Bayazit (1973)	13.90	1.68	2.18 - 18.0	7	0.098 - 0.140	0.816 - 1.143	0.098 - 0.117	0.01117 - 0.12850	279.25 - 1606.25
6	HRS A	1.75	4.28	0.153 - 11.11	11	0.169 - 0.107	0.479 - 0.745	0.033 - 0.062	0.00175 - 0.16100	8.90 - 834.85
7	HRS B	1.55	3.24	0.153 - 4.06	9	0.189 - 0.115	0.189 - 0.722	0.029 - 0.058	0.00033 - 0.22218	1.62 - 1089.95

¹Dry weights used in all calculations.

Experimental Data

The method developed by Ackers and White (1973) for determining the parameter A from established motion characteristics requires a considerable range of transport rates for adequate definition of the Ggr-Fgr functions. Experimental studies of graded sediment motion are neither as numerous nor as extensive as those performed with uniform materials. An added disadvantage for this analysis is that the size distribution, as well as the amount of transported material, must be known.

The following discussion is based upon the results of seven experimental series representing bed materials of diverse grading and coarseness. There is sufficient overlap of the sizes within the mixtures to enable direct comparisons of particle behaviour. A summary of size distribution parameters describing these five mixtures is listed in Table 41.1. Bed materials 6 and 7 are unpublished data courtesy of Hydraulics Research Station, Wallingford, England.

The number of transport measurements (here referred to as runs) for each experimental series is listed in Table 41.1. The ranges of hydraulic conditions and transport rates are included in this table as well. The data for bed material 4 and 5 are not extensive enough to determine accurately the initial motion parameter, A', for graded materials; however, these are included to support, through illustrated association, the trends in the remaining data sets.

Analysis

The size fractions chosen for analysis represent the sieve sizes used in the definition of bed materials 6 and 7. For the five mixtures considered here the sizes range from 0.153 to 11.1 mm. In all, 20 different sizes were considered, although no one mixture contained more than 18 size fractions. The size fraction diameters represent the mean size between two successive sieve diameters and therefore more accurately reflect the character of all materials passing through the upper sieve and remaining on the next lower one. A list of the size fractions is found in Table 41.2.

From the measured transport rates and the size distribution of the materials in transport, the amount of transport for each size fraction in motion was computed. The observed transport parameter, Ggr, was determined by using Eq. 7 with $X = (\text{kg/s})/(\text{Discharge (m}^3/\text{s)} \times 1000 \text{ kg/m}^3)$. These values of Ggr, however, are not compatible with uniform sediment transport studies. For the same mobility the observed Ggr for any size varies with the composition of the bed material. In uniform sediment transport studies a single size represents all the sediment in motion whereas the same size in mixture will simply be a fraction of the total load. To adjust the transport rate for any size fraction (D_i), each Ggr value was multiplied by (100%/Δp_i) where Δp_i refers to the observed percentage by weight of D_i in the total load.

A comparison of the observed Ggr and the adjusted or totalized Ggr is shown in Figures 41.2 and 41.3, respectively, for six size fractions. The higher transport rates associated with the totalized data are well illustrated.

The Initial Motion Parameter, A'

Definition of the initial motion parameter, A', for size fractions within graded sediments was done according to the 10⁻⁴ Ggr threshold value as used for uniform transport. For all but mixtures 4 and 5, the totalized Ggr-Fgr functions extended to and below 10⁻⁴ Ggr. These two mixtures could not be extended accurately as the transport functions are not well defined. The observed A' values are listed in Table 41.2, along with the Dgr and uniform A values for each D_i.

Table 41.2
Summary of Particle Sizes and Initial Motion Parameters

Particle Size D_i (mm)	USWES No. 1			USWES No. 2			USWES No. 9			HRS A			HRS B		
	Dgr	A	A'	Dgr	A	A'	Dgr	A	A'	Dgr	A	A'	Dgr	A	A'
0.153	4.22	0.252	0.380	4.22	0.252	0.320				3.24	0.265	0.400	3.24	0.265	0.500
0.215	5.92	0.235	0.300	5.92	0.235	0.280				4.55	0.245	0.370	4.55	0.245	0.395
0.275	-	-	-	-	-	-				-	-	-	5.82	0.235	0.365
0.303	8.35	0.220	0.245	8.35	0.220	0.260				6.70	0.229	0.305	-	-	-
0.328	-	-	-	-	-	-				-	-	-	6.94	0.227	0.350
0.390	10.75	0.210	0.230	10.75	0.210	0.230				8.26	0.218	0.280	8.26	0.218	0.300
0.463	12.76	0.204	0.215	12.76	0.204	0.210				9.80	0.212	0.262	9.80	0.212	0.277
0.550	15.15	0.199	0.200	15.15	0.199	0.200				11.64	0.206	0.242	11.64	0.206	0.252
0.655	18.05	0.194	0.192	18.05	0.194	0.180				13.87	0.200	0.225	13.87	0.200	0.237
0.780	21.49	0.190	0.185	21.49	0.190	0.175				16.51	0.195	0.215	16.51	0.195	0.230
0.925	25.49	0.186	0.165	25.49	0.186	0.170	22.27	0.189	0.320	19.58	0.191	0.200	19.58	0.191	0.212
1.200	33.06	0.180	0.160	33.06	0.180	0.140	28.89	0.183	0.280	25.41	0.185	0.170	25.41	0.185	0.190
1.550	42.71	0.175	0.150	42.71	0.175	0.140	37.32	0.178	0.255	32.82	0.179	0.165	32.82	0.179	0.170
2.030	55.93	0.171	0.143	55.93	0.171	0.130	48.88	0.173	0.230	42.98	0.174	0.140	42.98	0.174	0.155
2.860	78.80	0.170	0.135				68.80	0.170	0.205	60.55	0.170	0.160	60.55	0.170	0.137
4.060							98.65	0.170	0.185	89.80	0.170	0.135	89.80	0.170	0.125
5.560							135.10	0.170	0.170	117.70	0.170	0.135			
7.180										152.00	0.170	0.125			
9.730										184.80	0.170	0.127			
11.100										235.20	0.170	0.122			

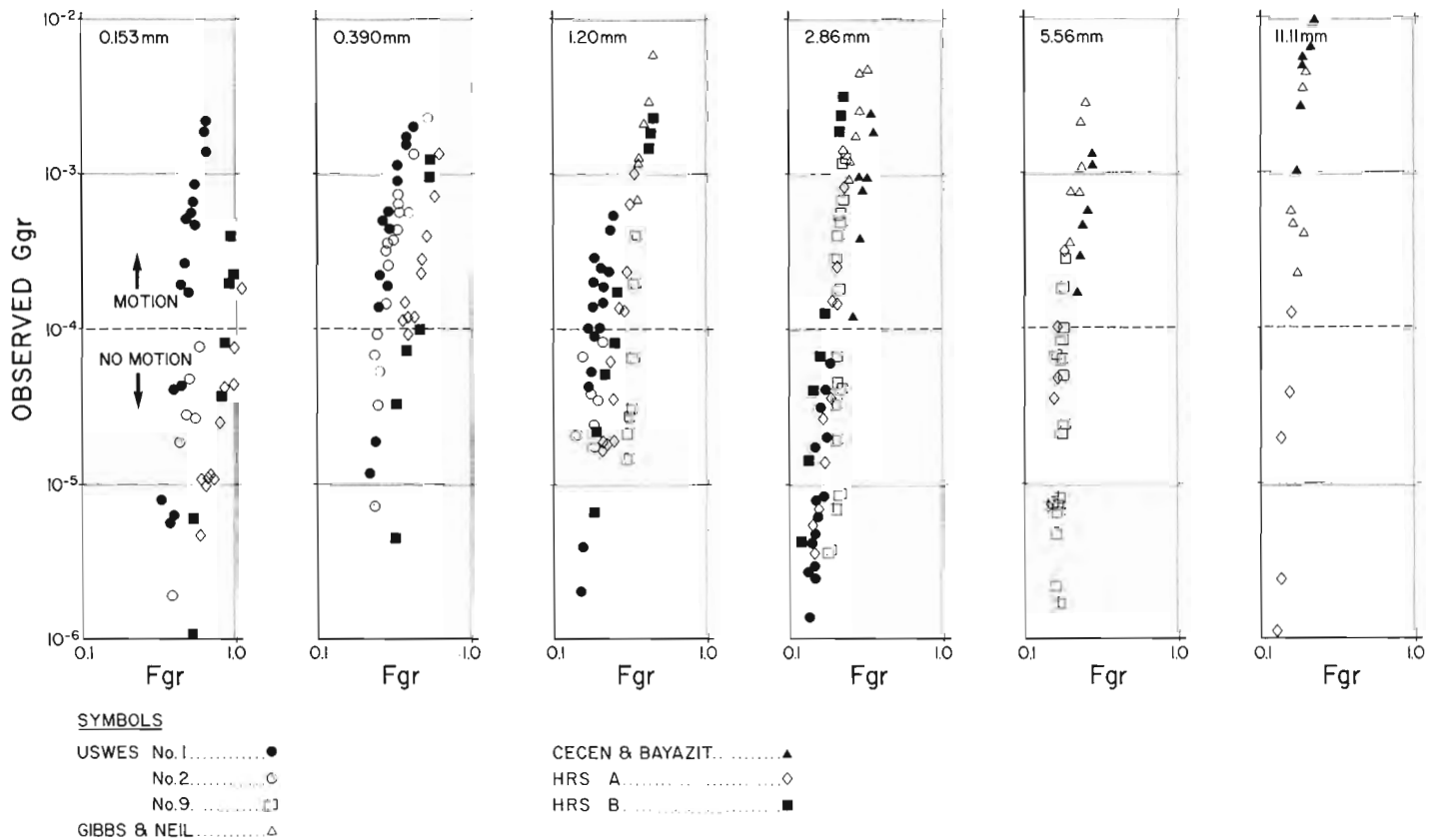


Figure 41.2. Ggr-Fgr functions for six size fractions in seven mixtures.

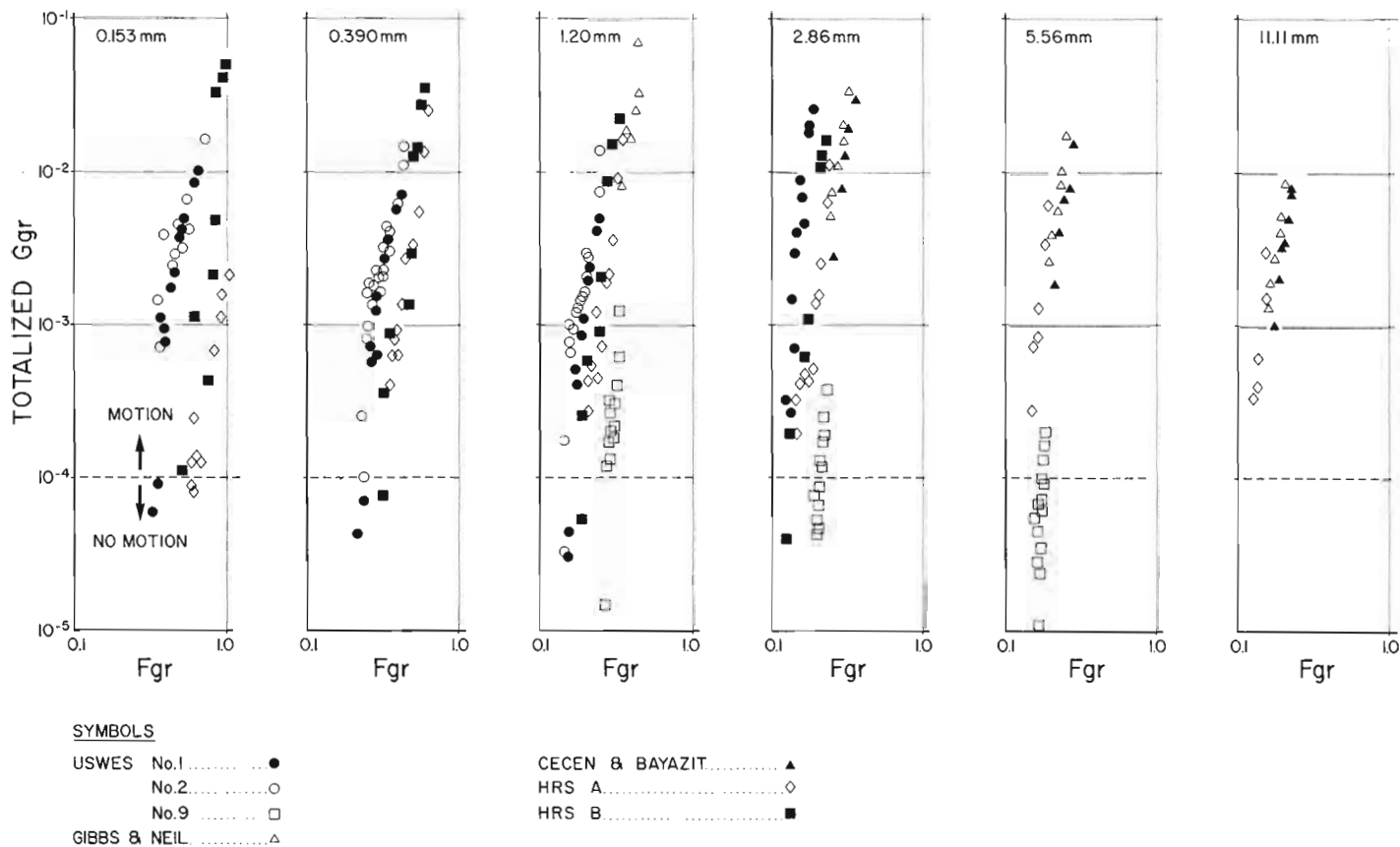


Figure 41.3. Totalized Ggr-Fgr functions for the same six size fractions shown in Figure 41.2.

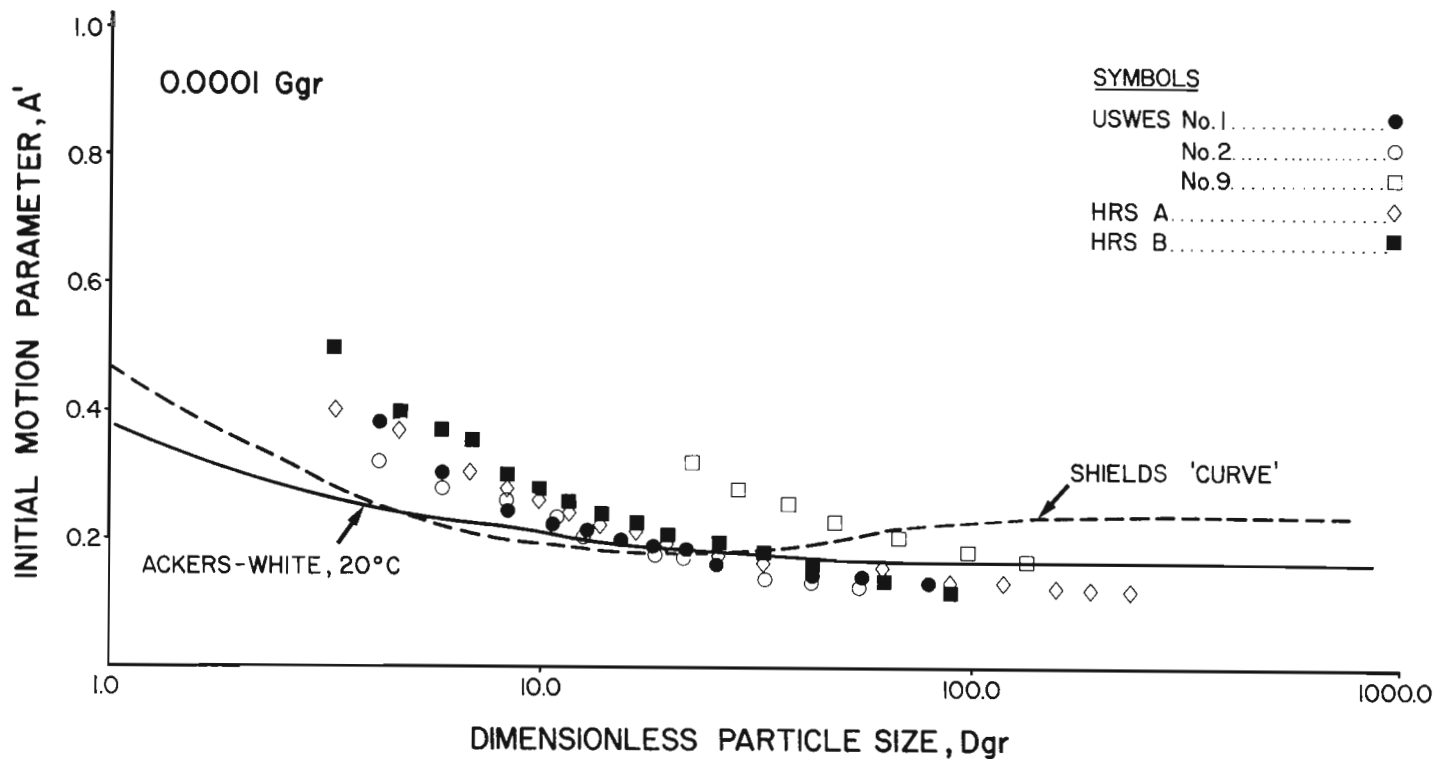


Figure 41.4. Initial motion parameter, A' , as function of dimensionless particle size, D_{gr} .

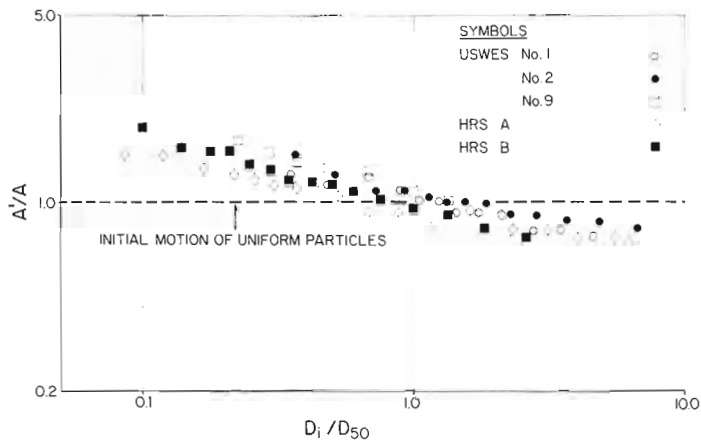


Figure 41.5. Ratio of graded and uniform initial motion parameters as a function of a particle ratio.

In Figure 41.4 the observed A' values are plotted as functions of D_{gr} and against both the Ackers-White uniform A relationship and the Shields curve. These data clearly illustrate the higher initial motion values associated with the shielding of the finer sizes, and the lower thresholds required for the more exposed larger sizes. All A' - D_{gr} relationships, although separated on the basis of mixture coarseness (fine mixtures plot systematically to the left of coarse mixtures), are similar in form, and all but mixture 6 coincide with the unique A - D_{gr} relationship near where their D_{gr} equivalents of D_{50} occur.

The largest differences between A and A' occur for particle sizes less than D_{50} , where shielding dominates. A' values for $D_i > D_{50}$, i.e. below the A - D_{gr} relationship, continue to follow an asymptotic trend which appears to continue beyond $D_{gr} = 60$, where Ackers and White (1973) believed that A became constant at 0.170. For large values of D_{gr} , the differences amongst the initial motion parameters for graded sediments decrease; although the present data are limited for large particle sizes, data sets 4 and 5 support this trend (cf. Fig. 41.3).

These observations on A' mean that these mixtures exhibit similar initial motion characteristics, and their D_{50} sizes begin to move near to the same value of F_{gr} as their uniform counterparts. The former observation supports previous work and presents it in a more thorough and systematic way. The latter observation is in agreement with Rakoczi's (1975) work and at odds with that of Egiazaroff (1965).

The similarity amongst the initial motion characteristics of the mixtures, and their dependence upon mixture coarseness, is best illustrated in Figure 41.5, where A' is plotted as a ratio of A against D_i/D_{50} . When supplemented with more data; this type of diagram should lead to a method for predicting the initial motion parameters for any particle size within a graded sediment.

Summary

An analysis of initial motion characteristics of a wide range of particle sizes from various mixtures illustrated the effect on particle stabilities caused by shielding of particles of fine size and the increased exposure of larger ones. Furthermore, the median size (D_{50}) of the bed material behaves as if it was in a uniform bed composed of the same diameter particles. Although these results are developed from experiments on only five bed materials, their systematic nature suggests that similar trends are to be expected for other bed materials. Extension of experimental studies to include different particle sizes, particularly larger sizes, and grades are recommended.

References

- Ackers, P. and White, W.R.
1973: Sediment transport: new approach and analysis; American Society of Civil Engineers, Journal of the Hydraulics Division, v. 99, HY11, p. 2041-2060.
- Church, M.
1972: Baffin Island sandurs; Geological Survey of Canada, Bulletin 216, 207 p.
- Cecen, K. and Bayazit, M.
1973: Critical shear stress of armoured beds; Proceedings XV, International Association of Hydraulic Research (Istanbul), p. 493-500.
- Egiazaroff, I.V.
1965: Calculation of nonuniform sediment concentration; American Society of Civil Engineers, v. 91, HY4 July, p. 225-247.
- Fenton, J.D. and Abbott, J.E.
1977: Initial movement of grains on a stream bed: the effect of relative protrusion; Proceedings of Royal Society of London, Series A, v. 352, p. 523-537.
- Gibbs, C.J. and Neill, C.R.
1972: Interim report on laboratory study of basket-type bed-load samplers; Research Council of Alberta, REH/72/2, 5 p.
1973: Laboratory testing of model VUV bed-load samples; Research Council of Alberta, REH/73/2, February, 5 p.
- Graf, W.H.
1971: Hydraulics of Sediment Transport, McGraw-Hill, New York, 513 p.
- Neill, C.R.
1968: A re-examination of the beginning of movement for coarse granular bed materials; Hydraulics Research Station, Report No. 68, 37 p.
- Rakoczi, L.
1975: Influence of grain-size composition on the incipient motion and self-pavement of bed materials; International Association For Hydraulic Research, Proceedings of the 16th Congress (San Paulo), p. 150-157.
- United States Waterways Experiment Station (USWES)
1935: Studies of river bed materials and their movement, with special references to the lower Mississippi River; Paper 17, January, 161 p.

Project 680047

J. Ross Mackay¹
Terrain Sciences Division

Mackay, J. Ross, *Deformation of ice-wedge polygons, Garry Island, Northwest Territories; in Current Research, Part A, Geological Survey of Canada, Paper 80-1A, p. 287-291, 1980.*

Abstract

In 1966 twenty-five steel tubes were inserted vertically into holes in an area of low centre polygons. Long term (1966-79) measurements of the changes in distance between the steel tubes, changes in tilt of the tubes, and the development of cavities preferentially on one side of the tubes show that the active layer of low centre polygons moves past the tubes. Because the cavities are confined to the active layer and movement tends to be radially outward from polygon centres, the movement is attributed to summer thermal expansion. Differential movement has implications for the interpretation of stratigraphies based upon ice-wedge sections. In view of the strong evidence for thermally induced movement in flat areas, thermally induced movement of the active layer may also occur on slopes.

Introduction

Ice-wedge polygons are widely distributed in areas of continuous permafrost. In tundra regions, ice-wedge polygons are commonly referred to as low or high centred depending upon whether they are saucer or dome shaped. Low centre polygons are bounded by ridges (Fig. 42.1) and as the centres become higher, low centre polygons can evolve into high centre polygons. However, high centre polygons cannot become low centre polygons. Ice-wedge polygons are of broad interest because of their widespread distribution, sensitivity to natural and artificial disturbances, and extensive use as paleoclimatic indicators. Numerous radiocarbon dates and palynological stratigraphies have been based upon studies of ice-wedge polygons. In this paper are discussed some long term (1966-1979) field measurements of deformation of ice-wedge polygons at Garry Island, Northwest Territories, at a site 160 km northwest of Inuvik, Northwest Territories.

Theoretical Considerations

Ice wedges grow by the opening of thermal contraction cracks in winter with infilling by water in spring to form an incremental ice veinlet (Fig. 42.2). At Garry Island, the cracks usually open between mid January and mid March and infill in May. Repeated cracking over several thousand years can result in the growth of ice wedges 1 m or more wide at the top and 5 to 8 m deep. The general theory of ice-wedge cracking and polygon growth is well known. In brief, there is broad agreement that thermal contraction from winter cooling builds up tension in the active layer and the top of permafrost, and when the tension exceeds the strength of the ground, vertical cracks will open (Fig. 42.2a). In summer, thermal expansion compresses both the ground and the ice wedge (Fig. 42.2b). In addition to the preceding changes, other factors to be considered include: the strain produced when water in the vertical crack freezes; the space problem

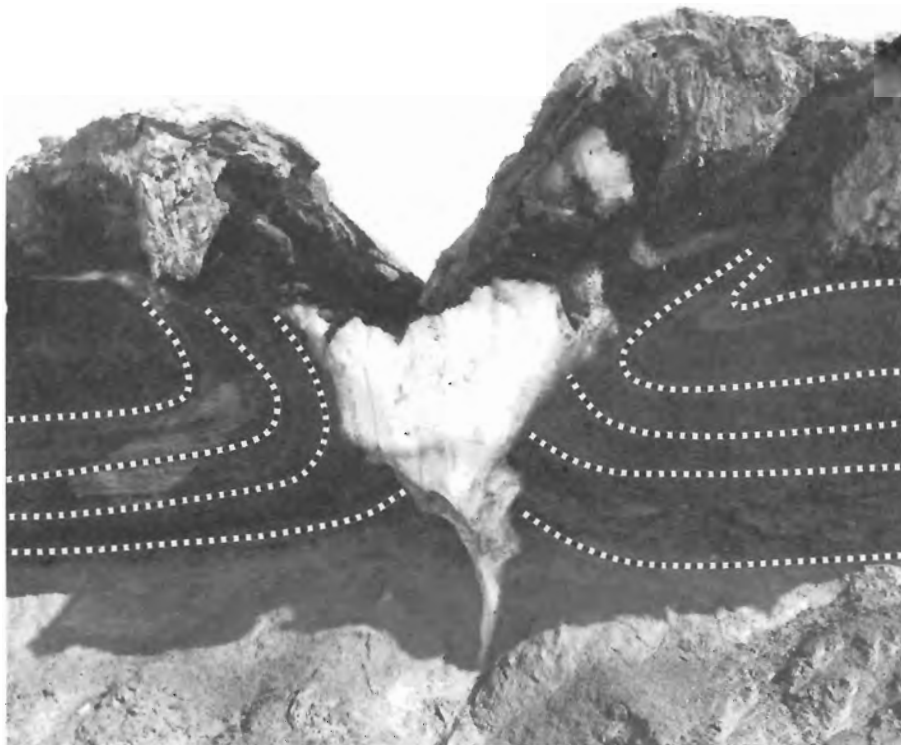


Figure 42.1

Coastal exposure across the trough of a low centre polygon, Pelly Island, Northwest Territories. The ice wedge is about 3 m wide at the top. Note the deformed beds on each side of the ice wedge.

¹ Department of Geography, University of British Columbia, Vancouver, British Columbia V6T 1W5.

created by an ever-growing ice wedge; the unequal accumulation of peat; the upward and downward squeezing of mineral soil and organic matter; the disruption of drainage; and thermal changes which accompany polygon growth. The end result is that the ground adjacent to an ice wedge becomes deformed (Fig. 42.1) but just why and how is uncertain.

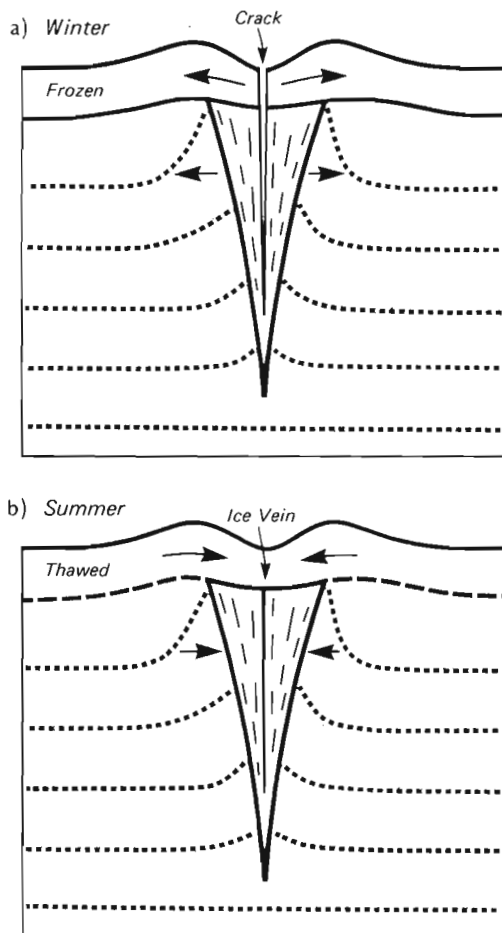
The development of the ridges of low centre polygons is poorly understood. Ridge formation has been attributed to: the lateral thrust of growing ice wedges which create a space problem; peat growth; summer expansion of the ground; cryostatic pressure and the lateral movement of water in the freeze-back period (Jahn, 1972); and partly to lateral compression which squeezes up both some of the ground and ice-wedge ice (Konishchev and Maslow, 1969).

Field Investigations

In 1966, an ice-wedge polygon site at Garry Island, Northwest Territories (Mackay 1974, Fig. 3, Site C) was instrumented for study. Twenty five steel tubes 1.5 m long were inserted into holes augered into permafrost (Fig. 42.3)

to surround completely one low centre polygon. In subsequent years, a variety of other types of measurement were added. The distances between pairs of steel tubes have been taped in a detailed triangulation system; the frequency, width, depth, closing, infilling, and propagation of ice-wedge cracks have been recorded; and measurements have been made on ground temperatures, snow depth, and changes in tilt of the 25 steel tubes.

The changes in separation of representative steel tubes for the 1966-1979 period are shown in Table 42.1 and Figure 42.4. Contrary to what might be expected, most distances between steel tubes on opposite sides of the ice-wedge troughs progressively decreased, even though the intervening ice wedges frequently cracked and therefore were growing. Conversely, distances from polygon centres to ridges usually increased when they might be expected to decrease. As the 1966-1979 total change in distance between steel tubes 1 and 13, in the centres of two polygons, was only +0.6 cm (Fig. 42.4), which is small relative to changes from the centres to the ridges (Table. 42.1), these two centres are then assumed to be fairly stable.



- a) an open crack which forms as a result of thermal contraction in winter;
- b) an ice vein which forms by infilling of the winter crack; summer expansion deforms the ground adjacent to the icewedge.

Figure 42.2. Schematic diagram of ice-wedge and polygon growth.



Figure 42.3. Steel tube number 8 located on the ridge of a low centre polygon. Note the cavity which has developed since 1966. The tiltmeter, on top of the tube, has been used to measure changes in tilt.

The tilt measurements (Fig. 42.3) of the 25 steel tubes show that most of those which are on ridges have been tilting towards the adjacent ice-wedge troughs and thus away from the polygon centres. When the measurements of tilt and distance change are combined, the majority of tubes appear to be pivoting with the tops moving towards the ice-wedge troughs, the bottoms towards the polygon centres. In addition, the pivot point of some tubes is moving towards the troughs.

Table 42.1

Change in separation of steel tubes for the 1966-1979 period

Tube Numbers	Change in Separation (cm)	Comment
1 to 2	+2.2	Change from centre to polygon ridge
1 to 3	+1.3	Change from centre to polygon ridge
1 to 4	+1.0	Change from centre to polygon ridge
2 to 5	-4.0	Change across ice wedge trough
3 to 6	-2.0	Change across ice wedge trough
4 to 7	-1.4	Change across ice wedge trough
5 to 13	+2.3	Change from centre to polygon ridge
6 to 13	+1.3	Change from centre to polygon ridge
7 to 13	+1.6	Change from centre to polygon ridge
8 to 13	+1.3	Change from centre to polygon ridge
9 to 13	+0.2	Change from centre to polygon ridge
10 to 13	-1.0	Change from centre to polygon ridge
12 to 13	+0.4	Change from centre to polygon ridge
1 to 3 to 6 to 13	+0.6	Change between two polygon centres

When the tubes were first inserted into augered holes in the summer of 1966, most tubes had small gaps around them at ground level. After a few years, however, some gaps closed and new ones opened until there gradually developed a preferred gap orientation which tended to remain on the same side of a tube in both summer and winter (Fig. 42.5). The gaps have since enlarged into cavities (Fig. 42.3, 42.5) which are widest at ground level and are confined in depth to the active layer. The cavities are not caused by heating or cooling of the ground by the tubes because the orientations are not dependent upon compass direction; nor are the cavities formed by slumping because some are on the upslope side of tubes and the cavities are not oriented downslope. There is excellent evidence to show that the cavities are formed by a differential movement of the active layer and tubes with respect to each other, a conclusion supported also by the common occurrence of a small bulge on the side of a tube opposite the cavity. Since the cavities are confined to the active layer and decrease in size from the surface downwards, cavity development would appear to be in summer. The cavities are best developed on polygon ridges with a movement of the active layer radially outward from the centres (Fig. 42.6). The movement, as shown by the cavities, is usually inclined to the contour and can be both upslope and downslope. Since the cavities face, in general, towards the ice-wedge troughs in the direction in which the tops of the tubes are moving, it seems evident that the cavities grow by the active layer moving past the tubes. As the active layer is frozen in winter when there is contraction, and thawed in summer when there is expansion, cavity growth doubtless takes place in summer.

Mass Transport and Ridge Growth

The existence of cavities in the lee of the tubes indicates considerable mass transport of the active layer past the tubes. Figure 42.6 has been drawn on the assumption that the mean annual twelve year 1966-1978 movement of the ground surface is 1/12 the diameter of the cavity as measured on 19 July 1978. The rate (cm/year) is conservative, because the added movement of the tubes is omitted. For the 1966-1979 period, the mean outward movement of the tubes for the polygon with centre at tube 13 was 0.3 cm and the mean cavity diameter at the ground surface was 2.3 cm, for a total movement of 3.2 cm. (Note: the distance between tubes 11 and 13 is excluded, because it was not measured due to intervening higher ground). The average movement of the top of the active layer past the tubes was then 3.2 cm in 13 years or about 0.25 cm/year. A movement of 0.25 cm/year at the top of the active layer amounts to 2.5 m/1000 years, a rate sufficient to create substantial ridges in low centre

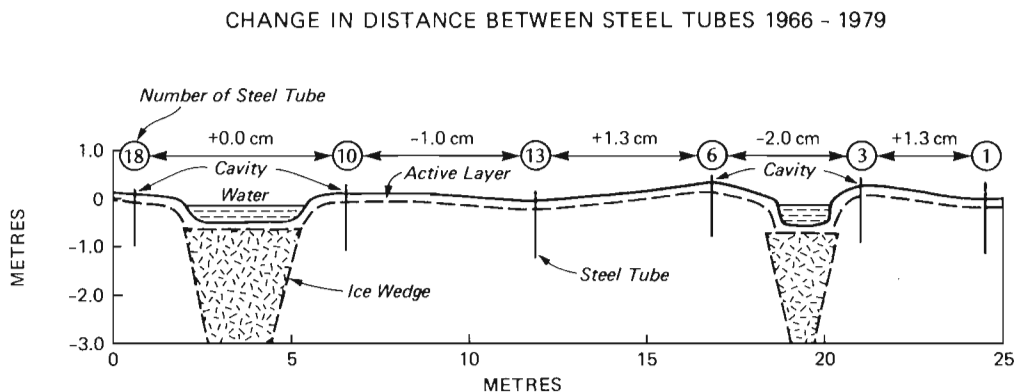


Figure 42.4. The diagram shows a cross-section between tubes 1 and 18. Note the locations of the cavities with reference to the steel tubes.

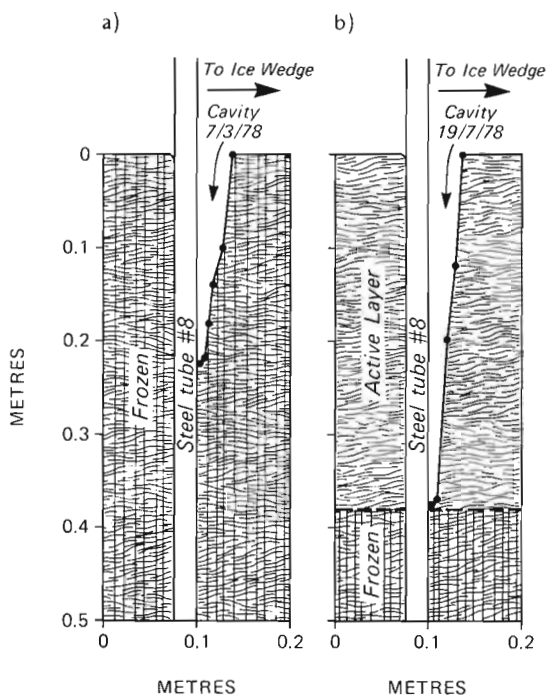


Figure 42.5. The cavity of tube 8 (Fig. 42.3) as measured in March and July 1978. Note that the vertical extent of the cavity in winter and summer is confined to the active layer.

polygons, many of which are at least a few thousand years old. Ridge growth is aided by the fact that outward expansion from a polygon centre is essentially unimpeded because of the existence of a "free face" bordering the ice-wedge troughs.

Coefficient of Thermal Expansion

A rough estimate of the coefficient of thermal expansion can be made based upon the 0.25 cm/year residual movement of the active layer, viz:

$$\alpha = \frac{\delta}{L \Delta T}$$

where α is the coefficient of thermal expansion

δ is the observed expansion

L is the length over which the expansion occurs

ΔT is the temperature change from the mean

Using $\delta \approx 0.25$ cm; $L = 7.5$ m for the polygon; $\Delta T = 20^\circ\text{C}$ for the polygon site, then $\alpha \sim 1.7 \times 10^{-5}/^\circ\text{C}$. Although the value for α is only an approximation, it seems to be of the right order of magnitude.

Thermally Induced Mass Transport

The combined evidence from the changes in separation of the tubes, the tilt, and cavity growth all suggest movement of the active layer past the tubes as a result of summer warming of the active layer and the upper part of permafrost. In other words, mass transport is due to thermal effects and not to freeze-thaw or gravity slumping. If this conclusion is correct, then it seems reasonable to infer that thermally

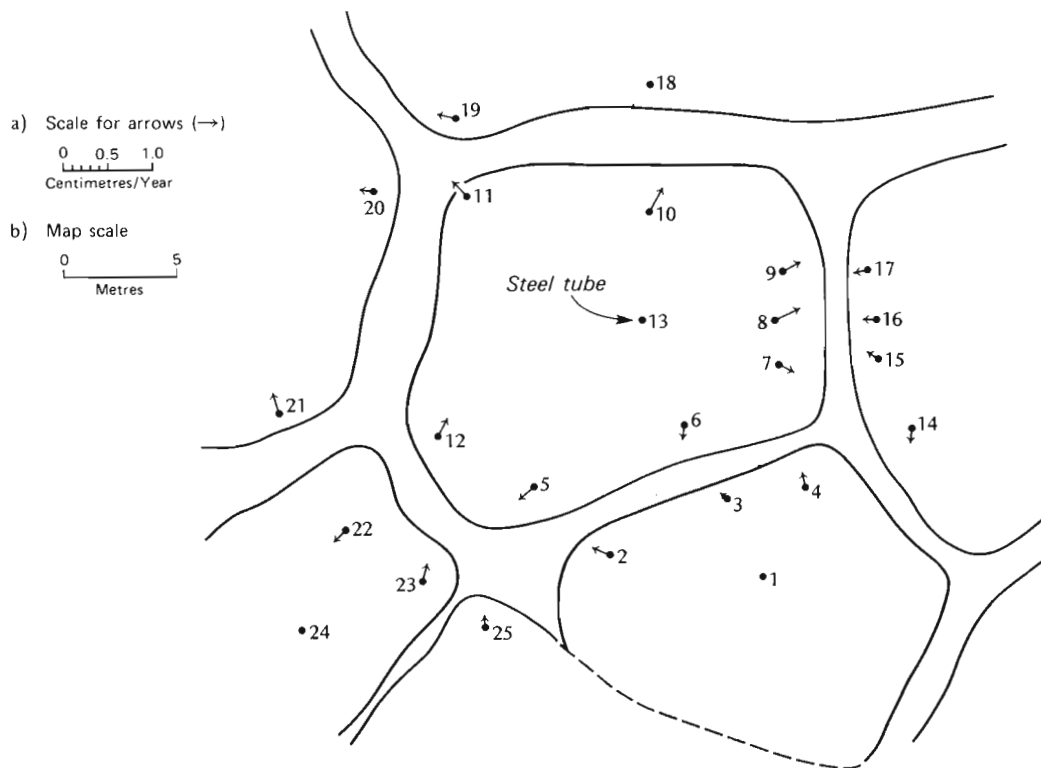


Figure 42.6

The experimental site at Garry Island, showing the locations of the 25 steel tubes. The 1966-1978 rate and direction of movement of the active layer, with reference to the tubes, is shown by the lengths of the arrows and their trend.

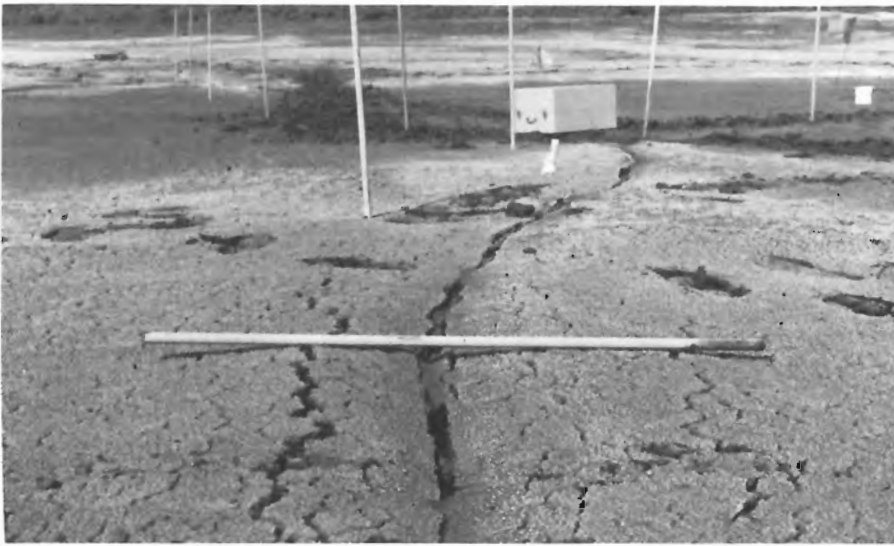


Figure 42.7

A frost crack formed in the period January to March 1979 in the bottom of a lake which was drained in August 1978. The photo, taken on June 20, 1979, shows that raised ridges had already developed. The rod is 1.75 m long.

induced mass transport can also occur elsewhere as, for example, in high centre polygons and hillslopes. On a hillslope, with an undulating earth hummock slope such as is present at Garry Island, there are no "free faces" corresponding to those of ice-wedge polygon troughs. Nevertheless, if some thermal expansion of the active layer does occur in summer on a hillslope, a net downslope movement should be favoured over an upslope movement because of gravity effects. Since thermally induced movement of the active layer seems to have been demonstrated for low centre polygons at a surface rate that can equal or exceed 0.25 cm/year, the probability of appreciable thermally induced slope movements seems very real. It seems possible that thermally induced downslope mass movement may help to explain why measured movement rates often exceed those which can be attributed to frost creep in periglacial areas.

Other Supporting Evidence

The preceding discussion has been based upon data for one instrumented site at Garry Island. Similar and also additional supporting data have been obtained for the 1968-1979 period for a second site instrumented with 30 steel tubes. Furthermore, a study of frost cracks which formed in the winter of 1978-1979 on a lake which was drained in August 1978 shows that some small ridges formed in the summer of 1979, presumably by summer expansion (Fig. 42.7).

Conclusion

Measurements made during 1966-1979 at an ice-wedge polygon site at Garry Island, Northwest Territories, show that thermally induced deformation has occurred in the active layer. The movement appears to result from summer

expansion, and it is generally radially outwards from the middle of low centre polygons. A rate of 0.25 cm/year has been estimated for the ridges of one polygon and the thermal coefficient of expansion at about $1.7 \times 10^{-5}/^{\circ}\text{C}$. Adjacent to the ice wedges, the upper part of permafrost may move inward in the opposite direction to that of the summer active layer so that some shearing may take place. This deformation poses problems for stratigraphic analyses and dating of peat in ice-wedge polygons. Since thermal expansion of the active layer appears to take place in polygon flats, it seems probable that thermal expansion on a hillslope may also contribute to downhill movement. The thermal expansion measured in low centre polygons, if it took place on a hillslope, would be difficult to separate from frost heave and gelifluction in cold environments, but it seems possible that it may be a so far unmeasured component of downslope movement.

References

- Jahn, A.
1972: Tundra polygons in the Mackenzie Delta area; Göttinger Geographische Abhandlungen, v. 60, p. 285-292.
- Konishchev, V.N. and Maslov, A.D.
1969: Physical causes of the frontal growth of syngenetic polygonal-veined ice; in Problems of Cryolithology, ed. A.I. Popov; v. 1, Moscow University Press, p. 24-33.
- Mackay, J.R.
1974: Ice-wedge cracks, Garry Island, Northwest Territories; Canadian Journal of Earth Sciences, v. 11, p. 1366-1383.

ELECTROMAGNETIC RESISTIVITY MAPPING OF THE AREA AROUND ALFRED, ONTARIO, WITH GEONICS EM 34 SYSTEM

Project 730004

Ajit K. Sinha
Resource Geophysics and Geochemistry Division

Sinha, Ajit K., Electromagnetic resistivity mapping of the area around Alfred, Ontario, with Geonics EM 34 System; in Current Research, Part A, Geological Survey of Canada, Paper 80-1A, p. 293-300, 1980.

Abstract

Electromagnetic resistivity¹ mapping of the area around Alfred, Ontario, was carried out during the summer of 1979 using the newly developed Geonics EM 34 instrument. Geonics EM 34 is a two man, portable, rapid reconnaissance instrument from which apparent conductivity of the ground may be read off directly at three possible coil separations. Much of the Alfred area is characterized by the presence of highly conductive Champlain Sea clays. These are underlain by resistive sand and dolomite horizons of Ordovician age, which, in turn, are underlain by highly resistive Precambrian rocks.

A total of 134 stations were used to map the area. Two corrections were applied to the raw data obtained in the field to take care of errors arising out of the presence of highly conducting ground. The instrument was able to delineate the high and low conductivity grounds very well, thereby indicating regions where the clay is thick and shallow and where it is absent or very thin. The results agree very well with known drift thickness data and with D.C. Schlumberger resistivity sounding data obtained from the same area.

Introduction

The area around Alfred, Ontario, lying about 65 km east of Ottawa on Highway 17 has been mapped by several geophysical methods in the last twelve years. The geological setting for the area has been described by Wilson (1946). From ground ground geophysical point of view, the area was first studied in 1968 by P. Andrieux who performed sixty-two D.C. Schlumberger soundings in the area both north and south of Alfred. The area was also mapped by two airborne electromagnetic systems, the INPUT system in 1967 (Dyck et al., 1974) and the Tridem three-frequency system in 1974 (Becker and Roy, 1977). The Maxi-Probe multifrequency ground electromagnetic system (Sinha, 1979) was also tested in the area in 1977.

Recently Geonics Ltd., Toronto, has introduced a new ground electromagnetic resistivity mapping system called EM 34 for rapid reconnaissance mapping of the ground. This system was tested in the Alfred area during the summer of 1979 to determine its effectiveness as a mapping tool. This paper presents the results obtained from that survey and compares that with some D.C. resistivity data obtained by P. Andrieux as well as with a drift thickness map of the area (Gwyn and Thibault, 1973). It should, however, be mentioned here that the depth of investigations of these systems are different and hence total correlation between the data sets from the surveys should not be expected.

Geology of the Area

The general geological characteristics of the area have been described adequately by Wilson (1946). The area lies just south of the Canadian Shield and south of Ottawa River. Figure 43.1 shows the location of the survey area. The bedrock in the area is similar to that described for the Ottawa area (Wilson, 1946) which consists of Precambrian granitic rocks and Grenville type metasedimentary gneisses and crystalline limestones. These rocks are overlain in most areas by rocks of Ordovician age. The lower Ordovician sediments, comprising sequences of sandstone and dolomite or dolimitic sandstones, were deposited in a shallow sea transgressing from the east. The middle Ordovician sediments were mainly limestones. The upper Ordovician sediments in the area consist of shale with interbedded limestone with shale at the base and 33 m from the top.

An immense hiatus ensued between the deposition of upper Ordovician sediments and the beginning of the glacial period. The area was then invaded by the Champlain Sea which deposited sand and marine clay which are very conductive. After the Champlain Sea receded, freshwater river currents deposited alluvium in several areas. The erosion of the older rocks led to deposition of freshwater, nonfossiliferous, rust-mottled clay beds. The physical differences between the sea clay and freshwater clay horizons may be explained by assigning the older one to marine or brackish water environment - the Champlain Sea, and the younger one to a freshwater lacustrine of fluvial environment of deposition - the ancestral Ottawa River (Gadd, 1963).

To summarize, therefore, we have recent sediments and soil at the top which are not very conductive. These are underlain by very conductive Champlain Sea clays which are, in turn, underlain by resistive sandstone and dolomite horizons of Ordovician age. Very resistive Precambrian rocks lie at the bottom of the sequence. Bedrock is, however, quite shallow in several places and is exposed at the surface in several places north of Alfred and in the southern part of the area.

In this area, it is generally accepted that the high conductivity of the ground is almost always due to the presence of conducting clay beds. The high resistivity grounds, on the other hand, are generally due to the presence of dry sand beds or where the resistive bedrock is very shallow or is exposed at the surface. Therefore, a rapid reconnaissance resistivity survey of the area should indicate the presence and the extent of the clay beds and also areas where the bedrock is very shallow.

Description of Geonics EM 34

Geonics EM 34 is a portable, two-man, direct conductivity reading instrument. The principle of operation of EM 34 is straightforward. Figure 43.2 shows the configuration of the system schematically. A portable transmitter console (powered by 8 D cells and weighing 3 kg) generates alternating current and is fed to the transmitter loop Tx via a shielded cable. The alternating current flowing through the transmitter loop (Tx) creates a primary oscillating magnetic field around it. The primary field interacts with any

¹ resistivity indicates the property of a material which resists the flow of electrical current. The reciprocal of resistivity is conductivity.

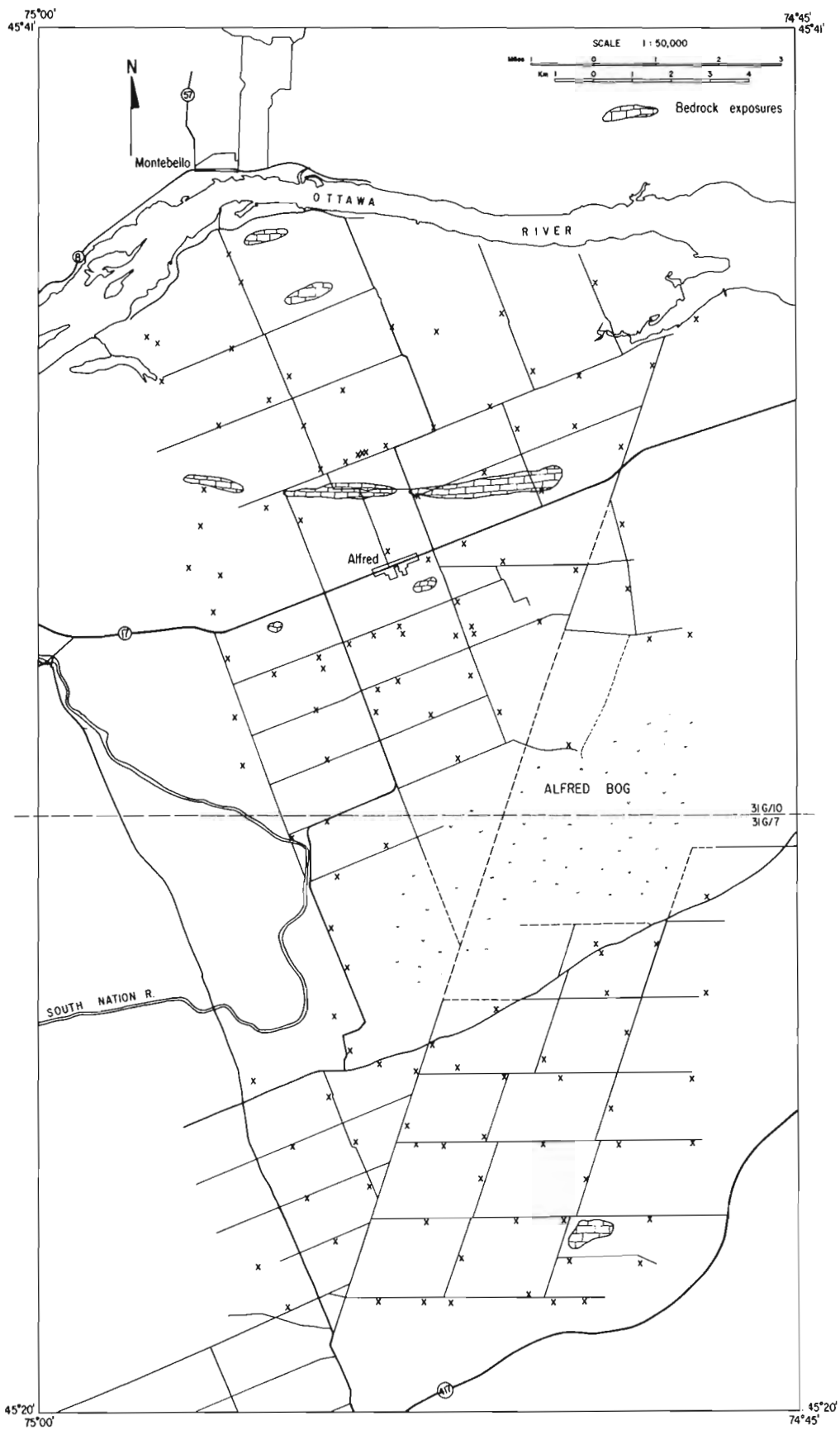


Figure 43.1 Location map for the Geonics EM 34 survey in the Alfred area along with station positions.

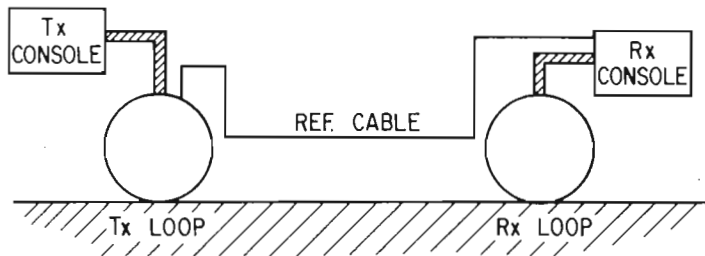
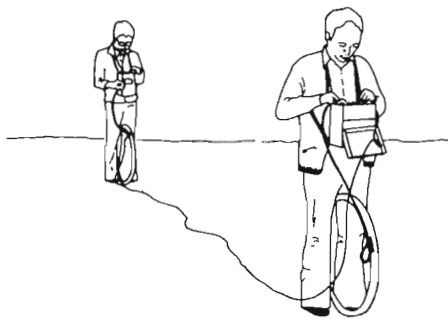


Figure 43.2 Schematic representation of the EM 34 system in the vertical coplanar mode.

conducting material in the ground producing eddy currents in the conductors. The eddy currents, in turn, generate secondary magnetic fields which may be picked up by a receiver coil (Rx) along with the primary field. The secondary field (which usually has a phase difference from the primary field) may be split into two components, namely, the real or the in-phase component which is in phase with the primary field and the quadrature or the out-of-phase component which is 90 degrees out of phase with the primary field. Both coils are, in general, placed on the ground in the vertical coplanar mode. A reference cable (the cable may be 10, 20 or 40 m long depending on the desired coil separation) is connected between the Tx loop and the receiver console for precise measurement of the distance between the Tx and the Rx loops. This will be explained later in detail.

The output from the receiver coil Rx which consists of the sum of primary and secondary field contributions is fed to the receiver console. There the in-phase and the quadrature components are separated and since the quadrature part is directly related to ground conductivity, the apparent conductivity of the ground may be read off the instrument directly. The transmitter frequencies are 6.5 kHz, 1.6 kHz and 0.4 kHz for the three coil separations of 10 m, 20 m and 40 m, respectively. Although the system is generally used with the coils in the vertical coplanar mode, they may also be used in the horizontal coplanar mode. The receiver console is powered by 8 C batteries and weighs 3.1 kg. The transmitter and the receiver loops weigh 7 kg and 3.2 kg respectively, while both of them have the same diameter of 63 cm.

Since this is an inductive system, no ground contacting probes are needed for the survey. This is specially advantageous over dry, resistive and frozen terrain, where it is difficult to send sufficient current into the ground using D.C. resistivity methods. There is also no need to carry measuring tapes or chains for survey work since the intercoil spacing is determined electronically. The system is quite portable too, the shipping weight of the system being 51 kg which fits into a small wooden box with lengths and breadths of 74 cm and depth of 23 cm and which is supplied by the manufacturer. Thus it may be carried in the field easily by two operators. The batteries for the transmitter and the receiver consoles last 7 and 20 hours of continuous operation which is good for resistivity measurements at several hundred stations.

The receiver console is calibrated to read the ground conductivity directly in millimho/m. If the ground is homogeneous, the recorded conductivity will be the true conductivity of the ground. In the case of a layered ground, the recorded value will be the apparent conductivity. The receiver console has five conductivity ranges of 3, 10, 30, 100 and 300 mmho/m. Once the apparent conductivity has been obtained in mmho/m, one may obtain the apparent resistivity of the ground in ohm-m by dividing that number into 1000. Thus an apparent conductivity value of 20 mmho/m is equivalent to 50 ohm-m.

Before beginning a survey, the battery levels of the transmitter and the receiver consoles and the zeros of the two meters in the receiver console (used for coil separation adjustment and for conductivity measurement) are checked. To operate the instrument, the coils are placed in a vertical coplanar mode by the two operators and the necessary connections are made. For surveying with 20 m coil separation, for example, the 20 m cable (the cable is somewhat longer than 20 m to permit some flexibility in the movement of coils) is used as the reference cable, which serves as a crude measure of the distance. Once the two consoles are switched 'on' the receiver operator adjusts the distance between the coils till the 'real' dial in the receiver console reads zero which indicates that the distance between the two coils has been correctly set. The idea behind this technique of distance measurement by the use of the 'real' dial is based on the following: for a particular coil separation chosen, the reference cable carries a signal which would be identical to the real part of the electromagnetic field received by the receiver coil for that coil separation. This reference signal is compared to the real part of the total field that is measured by the receiver coil. When they are identical, the 'real' dial in the receiver console reads zero, indicating that the distance between the two coils is correctly set. When the distance between the coils is not the same as the prescribed value, the 'real' dial will indicate either a positive or a negative reading depending on whether the distance is less or more than the prescribed value. The assumption in this method is that the ground is relatively resistive such that the real part of the secondary field is small. When this assumption is violated, a correction must be applied to the measured conductivity value.

When the two coils are placed at the correct separation (as measured by zero value in the 'real' dial), the quadrature part of the secondary field may be used for determining ground conductivity. It may be shown theoretically that when the ratio of the coil separation and the electrical skin depth¹ in the ground is much smaller than 1, the quadrature part of the secondary field contains all the essential information about the ground. Furthermore, the quadrature part of the response is almost linearly related to ground conductivity, thus permitting the instrument to be calibrated to read ground conductivity directly. In addition, under the above condition, the effective depth penetration of the system is determined by the intercoil separation only, and is independent of the skin depth, or ground conductivity. Therefore, electromagnetic sounding may be performed by varying the coil separation, analogous to the way the D.C. resistivity soundings are done.

Thus, the real part of the total field is used for determining the correct separation between the coils while the quadrature part is used in conductivity determination. A consequence of using the quadrature part for conductivity determination is that the system is relatively insensitive to small variation in coil separation. A system using the real part for conductivity determination would, on the other hand, be extremely sensitive to changes in coil separation. The field survey is quite fast with this system and takes only a few minutes to get the ground conductivity value for each

¹ Skin depth is the depth inside the earth at which the amplitude of a plane wave is attenuated to 37 per cent of its surface value. It is controlled by the ground conductivity and the frequency of the alternating field.

separation. If all three coil separations are used at each station, we have three different depth penetrations and, thus, in effect, we have electromagnetic sounding.

Results and Discussions

A total of 134 stations were occupied in the area. Figure 43.1 shows the location of the survey area and the X marks indicate station positions. The area is generally flat farmland with several good access roads. There are several exposures of bedrock in the area as shown in Figure 43.1 north of Alfred and in the southern part. The main access to the area from Ottawa is by highways 17 and 417. Electric power lines are present along most of the roads but it was observed that their influence is minimal if the readings are taken 80-100 m away from them. In the case of high voltage power lines, the station locations were taken at least 400-500 m away from the lines.

In the beginning, all three coil separations were tried, but after a trial survey it was decided to take measurements with the 20 m coil separation only since the depth penetration is small with 10 m separation and the noise levels, specially sferic noises (natural electromagnetic noises caused by lightning discharges) were high at 40 m separation. The time constraint also played a part in deciding to stick with one coil separation of 20 m for the whole area.

In general, the station locations were taken at about 1.6 km intervals except when power line influences were too strong or where access was difficult. In areas where conductivity values changed rapidly, stations were chosen as close as 100 m apart. Generally, the area exhibits high ground conductivity (low resistivity) because of the presence of conductive Champlain clay layers which are present in most of the area beneath a thin veneer of soil. But there are also areas characterized by very high resistivity caused either by the presence of resistive sand layers or when the bedrock is very shallow or is exposed at the surface.

Two corrections were applied to the raw apparent conductivity data obtained by EM 34. First, although the instrument has been designed for use over a wide variety of terrain, the instrument response departs from linearity for highly conductive ground. Figure 43.3 is a plot of the correction diagram which shows the relation between the true and measured apparent conductivity values for a homogeneous ground. The correction diagram is obtained theoretically and is supplied by the manufacturer of the instrument. When the ground is poorly conducting, the true and apparent conductivity values are very close. However, for good conducting ground, the divergence between the two becomes significant. Therefore, all observed apparent conductivity values were corrected using Figure 43.3. The second correction arises because of an error in setting the coil separation value by using the 'real' dial in the receiver console when the ground is conductive. The previously described method of setting distance works quite well over resistive ground when the secondary in-phase (real) field component is small. However, over conductive ground, the in-phase component of the field recorded by the receiver would contain contributions from both the primary and the secondary fields. However, since the reference cable only carries a predetermined amount of signal for comparison at any particular coil separation, trying to match these two fields will result in an error in distance measurement. That, in turn, will produce an error in measuring the quadrature part of secondary field, which is used in estimating ground conductivity. It has been estimated (D.J. McNeill, personal communication, 1979) that for ground resistivity values of 20 and 10 ohm-m, the errors in distance measurement would be of the order of 3 and 7.5 per cent, respectively, and so, similar order of error in conductivity estimates. Therefore,

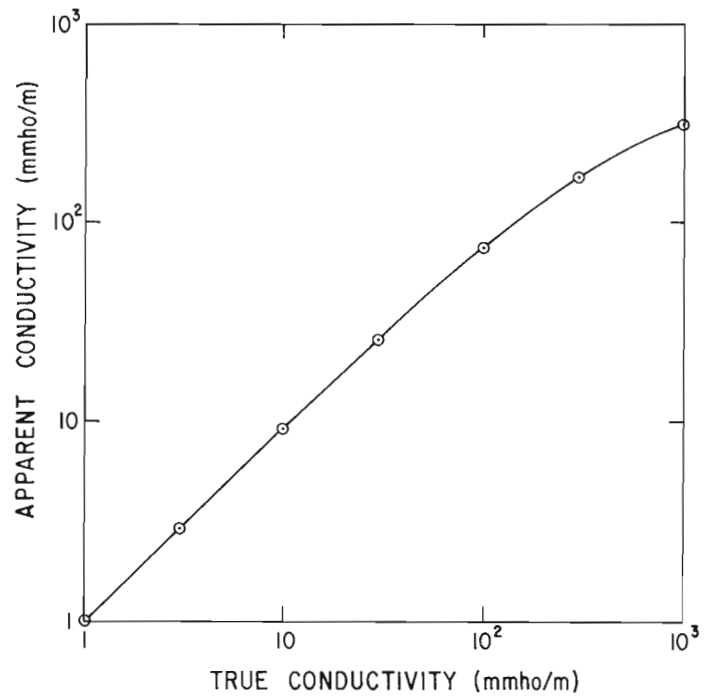


Figure 43.3 EM 34 correction diagram for a homogeneous ground for the nonlinear response of the instrument for conductive media.

all measured apparent conductivity values were corrected for the two above-mentioned errors before attempting any analysis of the data.

From the geophysical point of view, the dominant horizon in the region so far as electromagnetic anomalies are concerned is the highly conductive Champlain Sea clays. Therefore, their presence and extent would be indicated by high conductivity grounds. Similarly, the presence of highly resistive bedrock or dry sand beds close to the surface would be indicated by the high resistivity zones in an equiresistivity plot of the area obtained from EM 34 results. Figure 43.4 shows a plot of the apparent resistivity of the ground in ohm-m obtained from the EM 34 survey with a coil separation of 20 m. The central area south of Alfred is characterized by low resistivity ground which indicates that thick clay layers are possibly present. Some low resistivity ground is present north of Alfred as well, although the resistivity values there are somewhat higher than on the south side. This is presumably because the clay layers are not so thick and/or not as conductive north of Alfred. There are several high resistivity areas north and west of Alfred and in the southern part of the area where the apparent resistivity values reach 500 ohm-m or greater. Comparing the high resistivity areas with the bedrock exposure locations shown in Figure 43.1, there seems to be an excellent correlation between them. Only in the area west of Alfred, is the high resistivity ground not so well correlated with bedrock exposure indication presumably because the bedrock is covered by a thin veneer of soil. This view is confirmed by resistivity sounding results which are shown in Figure 43.5.

The diagram shows a contour map of the apparent resistivity of the ground obtained by D.C. Schlumberger soundings conducted in 1968 for a current electrode separation of 20 m. Since there were only 62 resistivity soundings in the area compared to 134 EM 34 stations, the density of coverage is much greater in the case of EM 34 survey. Hence, Figure 43.4 shows much greater detail about resistivity variations in the area. The areas designated by H in Figure 43.5 indicate regions where the apparent resistivity values were very high.

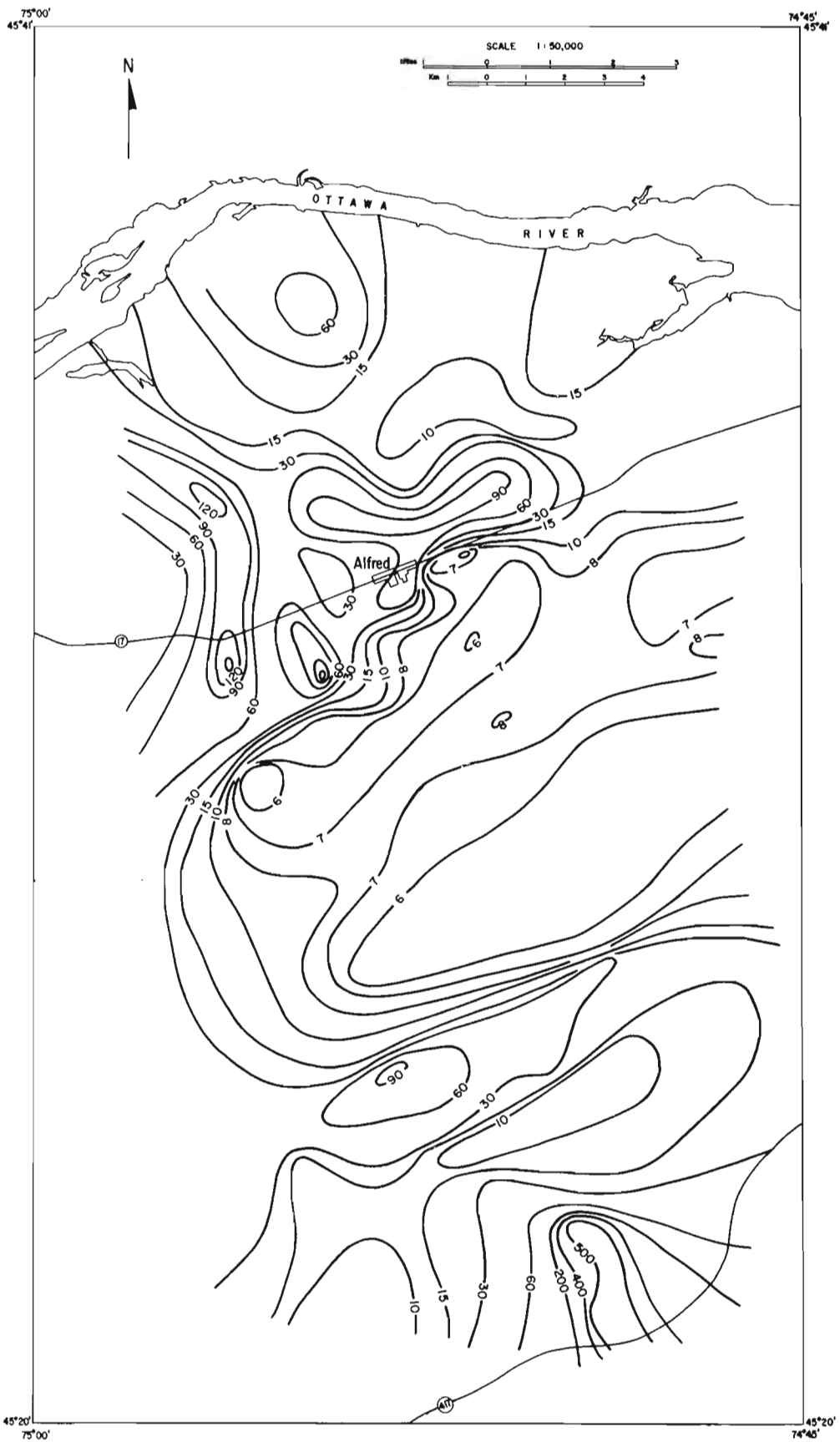


Figure 43.4 Apparent resistivity of the ground in ohm-m in the Alfred area obtained with the EM 34 system for a coil separation of 20 m.

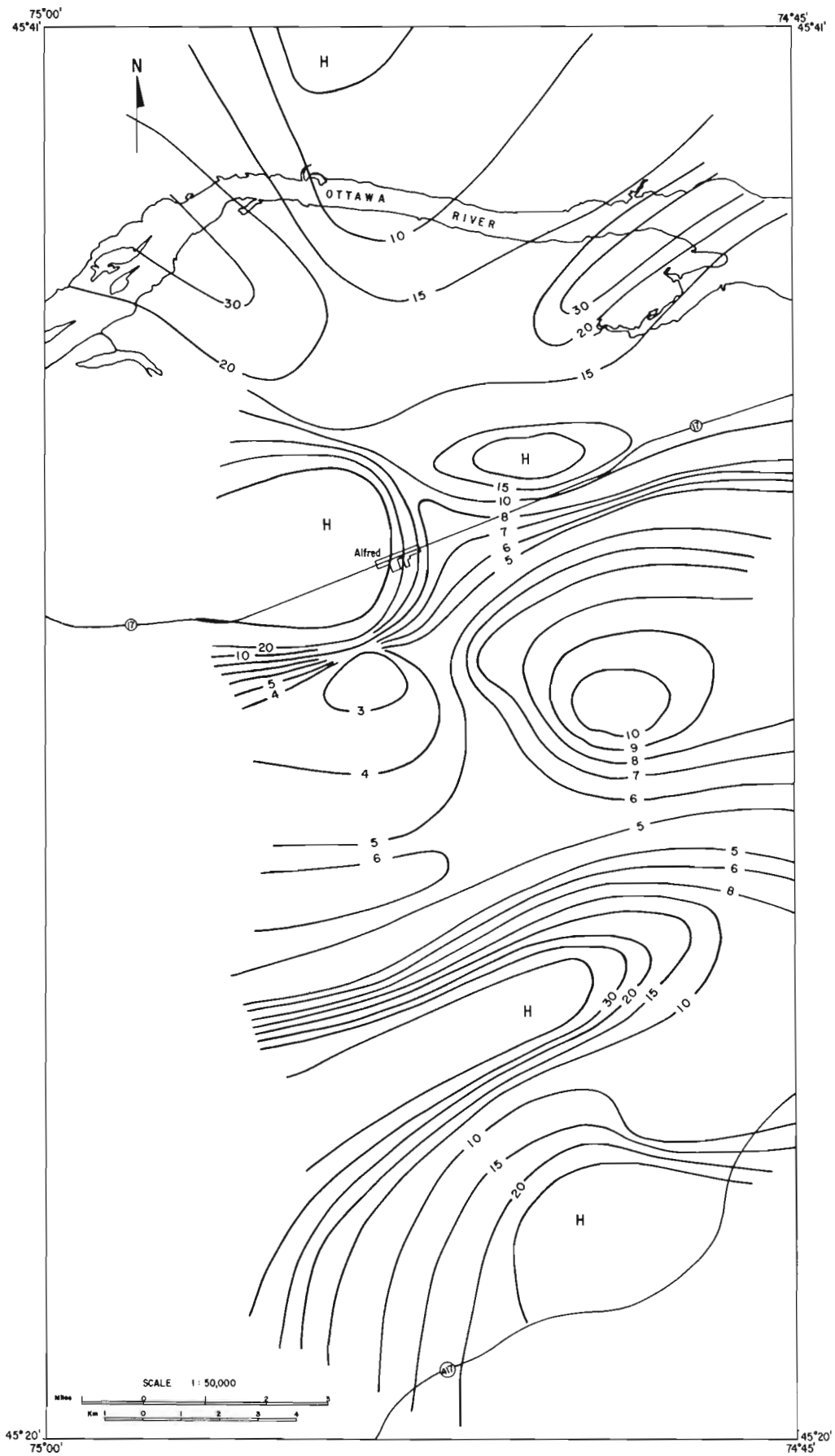


Figure 43.5 Apparent resistivity of the ground in ohm-m in the Alfred area obtained from D.C. Schlumberger resistivity data with current electrode separation of 20 m.

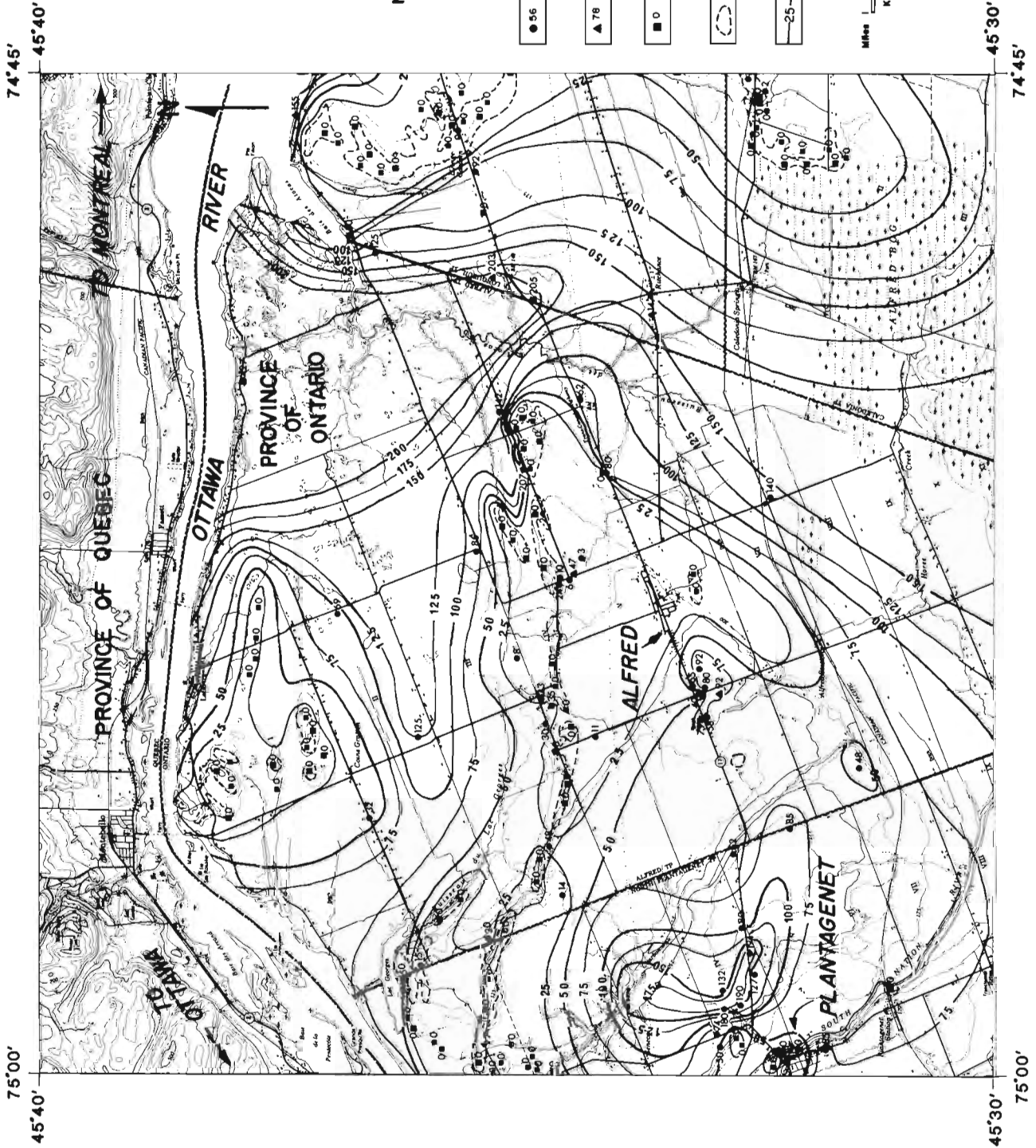


Figure 43.6 Drift thickness map of the northern part of the Alfred area (from Gwyn and Thibault, 1973).

The general similarities in Figures 43.4 and 43.5 are striking considering the fact that these two systems have different depth penetrations and the methods are based on two different principles. The high and low resistivity grounds match very well although the absolute values of the apparent resistivity obtained by the two systems may differ. That is understandable since the ground is multilayered and because the two systems have different depth penetrations. A detailed analysis of the D.C. sounding data will be published in forthcoming publication (Sinha, in prep.).

A detailed lithological map of the area is unavailable at present. However, a drift thickness map has been published by the Ontario Geological Survey (Gwyn and Thibault, 1973) for the north side of the map area. Figure 43.6 shows the drift thickness map for the northern half of the area and has been plotted based on information from well data in the area. Although the parameters plotted in Figure 43.4 (apparent resistivity) and Figure 43.6 (drift thickness) are different, they may still be used for some comparative study. The areas with large drift thickness values, shown south of Alfred, may be identified in this region with thick clay layers and hence of low resistivity. Ground with high apparent resistivity generally indicates areas where the bedrock is exposed or is very shallow. These areas should generally coincide with very low drift thickness values. Looking at Figures 43.4 and 43.6, it is clear there is a distinct correlation between the areas of high resistivity and low drift thickness. On the other hand, the low resistivity areas south of Alfred seem to coincide with areas of thick clay (high drift thickness values).

Therefore, a reconnaissance survey with Geonics EM 34 should be able to detect and delineate conductive Champlain clay layers in the area and also regions where the drift thickness is small. A survey with EM 34 may also be compared to a D.C. resistivity survey. While it takes 15 to 30 minutes (in the case of very dry ground) and at least three operators to obtain the apparent resistivity of the ground for each electrode separation in a Schlumberger array, an EM 34 can provide a rough idea about the presence and extent of the clay layers (from apparent resistivity values) in about five minutes for each coil separation, requiring only two operators. Another advantage of the EM 34 system is that being an inductive system, there is no need for ground contacting probes. This speeds up the field survey considerably specially over resistive and frozen ground. In fact, if apparent conductivity values are determined at all three coil separations with EM 34, one may be able to perform some preliminary interpretation with regard to the thickness and conductivity of the ground for simple models.

Acknowledgments

I am thankful to Mr. S. Wardlaw, a summer student, for his help with the field work and some preliminary interpretation of the data.

References

- Becker, A. and Roy, J.
1977: Interpretation of frequency domain airborne electromagnetic data; Unpublished Report, prepared for Geological Survey of Canada by IREM-MERI, Montreal.
- Dyck, A.V., Becker, A., and Collett, L.S.
1974: Surficial conductivity mapping with the airborne INPUT system; Canadian Institute of Mining and Metallurgy Bulletin, v. 77, no. 4, p. 1-6.
- Gadd, N.R.
1963: Surficial geology of the Ottawa map-area, Ontario and Quebec, 31G/5; Geological Survey of Canada, Paper 62-16, 4 p.
- Gwyn, Q.H.J. and Thibault, J.
1973: Drift thickness of the Hawkesbury-Lachute area, Southern Ontario; Ontario Division of Mines, Preliminary Map P. 909, Drift Thickness Series 1:50 000.
- Sinha, A.K.
1979: Maxiprobe EMR-16: A new wide-band multi-frequency ground EM system; in Current Research, Part B, Geological Survey of Canada, Paper 79-1B, p. 23-26.
- Sinha, A.K.
1979: Overburden characteristics of the area around Alfred, Ontario, obtained from D.C. electrical soundings; (in prep.)
- Wilson, A.E.
1946: Geology of the Ottawa-St. Lawrence lowland, Ontario and Quebec; Geological Survey of Canada, Memoir 241.

Project 770074

T.M. Gordon
Precambrian Geology Division

Gordon, T.M., *Manipulation and display of digital cartographic data; in Current Research, Part A, Geological Survey of Canada, Paper 80-1A, p. 301-307, 1980.*

Abstract

A digital file of topographic data has been transferred from XCM, the Surveys and Mapping Branch cartographic system, to the departmental computer. Programs written locally, as well as POLYVRT, SYMAP, and CALFORM from the Laboratory for Computer Graphics of Harvard University, have been used to manipulate and display the data. The feasibility of transferring such information to a variety of file structures and display devices has been established. Work is planned to process and merge other types of digital map data with digital topographic files.

Introduction

Since 1973, a series of pilot studies have examined the use of computer technology for the production of geological maps (Debain, 1974; Junginger-Frohberg et al.¹; Martin and Gordon²). These were encouraging and, as a result, this project was established to examine the feasibility of using digital cartographic data for scientific applications as well as map production. This study has examined the nature of the data available from various digitizing systems, the data structures required for various applications, and tests have been made of commercially available software for manipulation and display of map information.

Digital Cartographic Data

It should be appreciated at the outset that the maps of interest here portray regional bedrock or surficial geology. Digital processing for the production of single parameter maps (for example of uninterpreted geochemistry) has not been considered. Geological maps require considerable intellectual input and manual compilation. Computer processing of such data therefore must always involve the conversion of the analogue data on a scientist's manuscript map to digital form.

Although there are various devices for automatic line following or scanning a manuscript document, they are relatively expensive and often do not provide the resolution required for map production (Boyle³; van Zuijlen, 1975; P. Burrough, personal communication, 1978). It is therefore probable that any cartographic system used by the Geological Survey will involve manual line following. This type of digitizing produces strings of x-y co-ordinates approximating the lines on a manuscript map.

At present, digital data are used by cartographers at the Geological Survey to produce selected high quality plots. This requires only that the digitized line segments be labelled with a line type (for scribecoat symbolization) and with identifiers of the two map units separated by the line (for peelcoat colour separation.) This information can be produced by large scale digitizing systems (Young, 1978) as

well as mini computer systems (Ellwood⁴, Martin, 1978) and devices as simple as a digitizer console (Gordon et al.⁵). Such cartographic files do not contain explicit labelling of nodes (junctions of line segments) nor do they identify the map units as being to the right or left of the direction of digitizing.

The lines and points in Geological Survey cartographic files represent only geological data. These must be superimposed on a topographic base for final publication. Until topographic data are routinely available in digital form, photomechanical techniques will be required to combine geological and topographic data for production of final plates.

Data Structures for Scientific Applications

It is generally accepted that computer assisted cartography is rarely cost effective for map production alone (Rhind, 1977). For this reason, cartographic systems should provide facilities for a variety of uses. As the number of digital maps grows, this will have the additional benefit of ensuring that different researchers use a common geological base.

Data structures used in processing digital map data have evolved into two main types: topologic structures (Chrisman, 1977) in which spatial data are manipulated as polygons, lines, and points; and gridded structures (Dutton, 1976) in which the data are processed as a matrix of (usually) equally sized cells.

Topologic structures provide two advantages of particular interest to this study. First, the resolution of the original digitizing can be economically retained. Displays of the data may show all of the details of the original line work and hence be esthetically pleasing. More importantly, this resolution may be required by a particular scientific study (e.g. Sproll and Dietz, 1969). Second, spatial relationships in the data are explicit. A single polygon (map unit) or line (contact) can be referenced and manipulated as a complete entity. This is particularly useful for applications in which spatial coherence is important, for example computer simulation of plate motion or axial projection of deformed bodies (e.g. Stockwell, 1950). Polygons also form the basis of retrieval from many archival files. Digital outlines of structural provinces or metamorphic zones, for example, may be used to select data indexed only by geographic co-ordinates.

Grid or raster structures are commonly used where the data to be processed have no *a priori* domain structure. In fact the objective in studying such data is often to discover spatial correlations when such relationships are unknown, assumed not to exist, or ignored. The enormous investment in processing of satellite imagery has resulted in a large number of algorithms and systems for grid and raster processing.

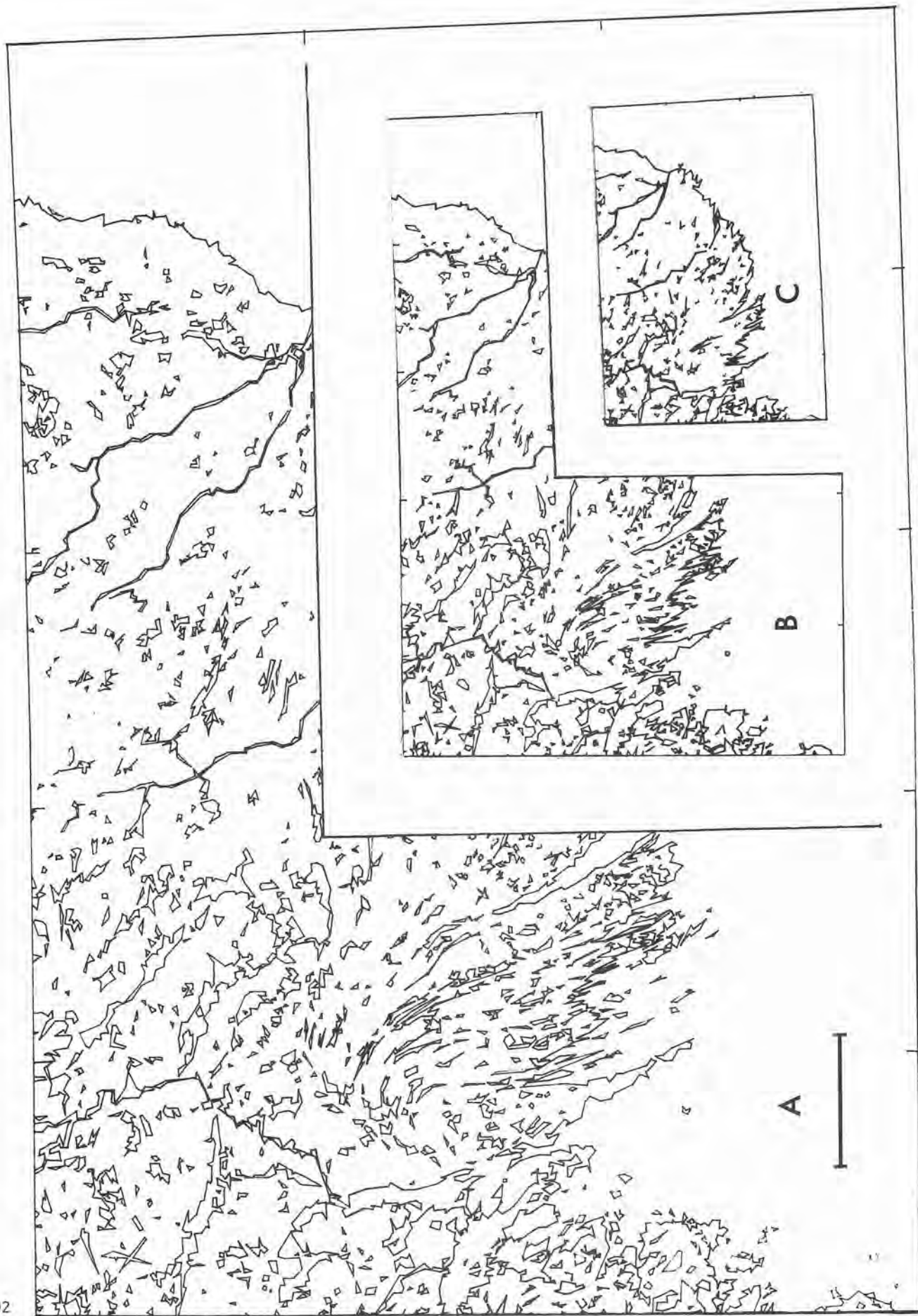
¹ XCM feasibility study interim report; Nov., 1977, internal report.

² Preliminary evaluation of systems for computer-assisted cartography in the Geological Survey of Canada, May, 1977, internal report.

³ A report on tests carried out on the Calspan automatic line digitization system for the Geological Survey of Canada; May, 1976, internal report.

⁴ Computer program FINGER. Internal report 1975.

⁵ Lineament measurement system; Sept. 1978, internal report.



A. 8646 points B. 3730 points C. 1414 points
 Figure 44.1 Generalization and scale reduction. Scale bar originally 2.5 cm.

Gridded data are used in the statistical analysis of geological variables (e.g. Agterberg et al., 1971) and special systems have been developed to process geological map data in matrix form (Fabbri et al., 1978). Another important use of grid structures occurs in the production of computer graphics whether the data originate as topologically defined polygons or as matrices. Plots produced by line printers or the colour plotter visibly show their gridded origin, while symbolization and shading routines used on pen plotters and CRT devices require conversion of data to scan-line (raster) forms.

Software for Data Transformation

It is apparent that the successful application of digital cartographic files in a variety of scientific uses requires that the original labelled line segments be restructured to both topological and gridded forms.

Fortunately, algorithms and programs exist that will perform many of the operations required. POLYVRT (Peucker and Chrisman, 1975; Laboratory for Computer Graphics, 1974) is a program which transforms files between various topologic structures as well as providing projection and generalization subroutines. The venerable SYMAP program (Dougenik and Sheehan, 1977), widely used for production of line printer maps, optionally produces a file containing a gridded representation of input polygons. CALFORM (Latham and White, 1978), a program for producing shaded maps on pen plotters and CRT devices, along with POLYVRT and SYMAP, are commercially available products of the Laboratory for Computer Graphics and Spatial Analysis of the Graduate School of Design at Harvard University.

These programs, modified where necessary, as well as several locally written routines, have been used in the test study described below.

Test Study

Input Data

Digital processing of geological map data will ultimately require the incorporation of digital topographic data, especially water features. Both data types originate as labelled line segments. Because of these factors, it was decided to begin the study with a topographic file. The area chosen includes the southern portion of NTS 56 A as well as parts of adjoining map sheets. A 1:250 000 map of water features was expertly digitized by Geological Survey staff members S. Junginger-Frohberg, J.A. King, and B. Mainville. The software used was the Surveys and Mapping Branch cartographic system XCM, which will eventually contain a digital topographic base for Canada (Young, 1978).

The digital information, obtained as a Digital Equipment binary tape file, was transferred to the departmental Control Data Cyber 74 using a program written by G.M. Martin. The resulting file consisted of a series of sequentially numbered lines, represented by their x-y co-ordinates, and labelled as topographic features (lakeshore, river, coastline, etc.).

Topological relationships in the test file are simple. There are two main polygon types – water and mainland – each containing outliers of the other (lakes within the land mass, islands within water). In turn some of the lakes themselves contain islands.

Pre-processing

POLYVRT requires that input data contain polygon identifiers and node labels. The program checks the topological consistency of the input to ensure the map is

made of closed polygons, and assembles internal tables of pointers between polygons, nodes, and chains (lines). The original digitizing deliberately used the procedure for a standard topographic map and hence did not have all the required data. It was thus necessary to perform the following series of pre-processing operations.

1. Some linear features, such as streams, did not contribute to the polygon structure of the file. Although POLYVRT will handle such features, they were deleted to save processing costs.
2. The number of points in the original file was determined by digitizing system and the resolution required for map production. The algorithm of Douglas and Peucker (1973) was used to reduce this number while retaining a resolution of one mil. This decreased the number of points from 122728 to 80413 and provided a proportional reduction in subsequent costs.
3. Preliminary plots of various feature types were made to ensure consistent labelling. The line defining an island in a river, for example, originally might be correctly identified either as an island or as a river boundary. Where necessary, labels in the original file were changed.
4. Intersections of the map neatline with topographic features were identified on preliminary plots. These points were used to divide the digitized neatline into a series of segments each of which was labelled as bounding water, land, or an island. This ensured closure of polygons on the periphery of the map.
5. Codes for the polygon types on opposite sides of each line were generated by a subroutine which also labelled each node with an identifier based on its x-y co-ordinates. This effectively gives adjacent line end points (nodes) identical identifiers. It is a tribute to the expertise of the digitizing team that the co-ordinates of only 5 nodes of a total of 1938 required modification.

Manipulation

Once the file was in POLYVRT format, it became possible to perform the following operations:

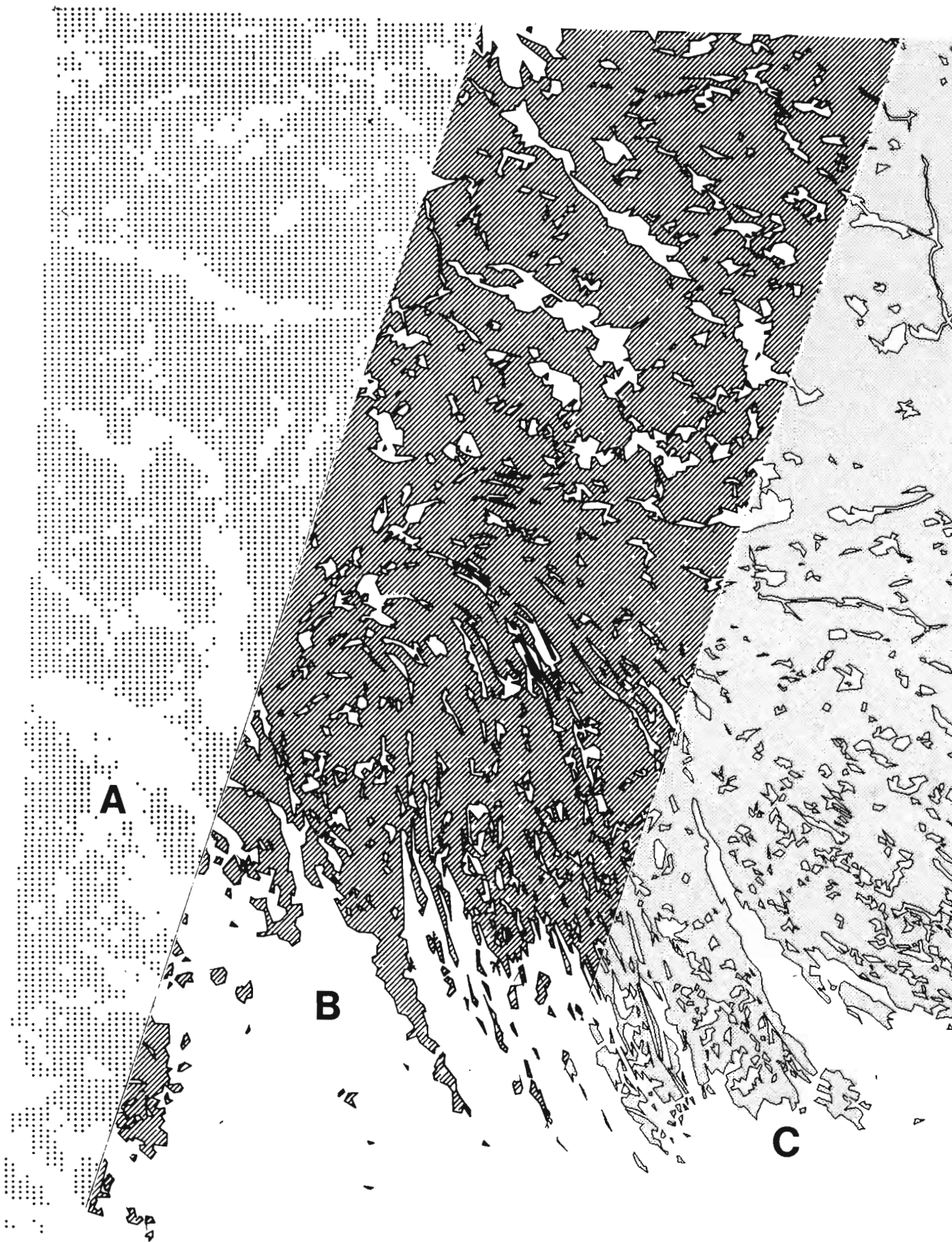
1) Transformation of the data at any scale to any mathematical map projection; 2) reduction of the number of points using the Douglas-Peucker algorithm; and 3) output of the data directly as a plot or in a form accepted by either SYMAP (for grid conversion and line printer plots) or CALFORM (for pen plotter and CRT plots).

Figure 44.1 illustrates the results of applying the generalization algorithm and plotting at proportionally reduced scales. The device used for these drawings was the Geological Survey of Canada EAI flat bed plotter. The detail level of each point is stored in the POLYVRT internal file, making it possible to gain considerable savings in plotter time on retrievals that do not require the resolution of the original data.

Display

In addition to the EAI plotter, there are several commonly used display devices available to the Geological Survey. In-house these are an Applicon colour ink jet plotter and several Tektronix CRT terminals. The Departmental Computer Science Centre supports a Calcomp 1051 pen plotter and line printers and maintains the Tektronix and Applicon software.

Each of these devices was used to produce a plot of the data. To reduce costs the map was generalized to a resolution of 0.01 inches. Results, excluding Tektronix output, are shown in Figure 44.2.



A

B

C



- A. Software - SYMAP; device - line printer
- B. Software - SLICE, CALFORM; device - Calcomp 1051
- C. Software - FLASH; device - Applicon
- D. Software - POLYVRT; device - EAI
- E. Software - XCM; device - Surveys and Mapping plotter

Figure 44.2. Output from various devices. Scale bar originally 5 cm.

The line printer map was produced at double scale using a file generated by POLYVRT and passed directly to SYMAP. Photo reduction was required to produce the final map. The symbol used was a single period, although SYMAP permits any combination of up to four superimposed printer symbols. The optionally available digital grid was not produced, but would contain a value for each grid point on the map. Such a file would be easily processable by most grid manipulation programs.

The Calcomp 1051 was used to produce the shaded line plot, with CALFORM generating the plotter commands. Because of memory constraints in CALFORM, the input file was not obtained directly from POLYVRT. Instead, an intermediate program was used to "slice" a SYMAP formatted file into strips and generate a CALFORM input file for each strip. Again, the full range of available symbolization is not illustrated by the figure.

Because colour cannot be reproduced in this publication, Figure 44.2 illustrates part of a grey-scale plot obtained from the Applicon colour plotter. D. Ellwood of the Geological Survey developed this procedure as part of a comprehensive map production system.

The software for this device includes a subroutine that allows the plotting of closed polygons, with the restriction that the x-y co-ordinates must all be in fast memory. The strategy used for the test map was to cover the complete plot area with the symbolization for land area; to then superimpose the symbolization for water (in this case a blank); and finally to plot the islands.

A portion of an EAI plot, directly produced by POLYVRT is also illustrated by Figure 44.2, along with a scribe of the original data produced by the Survey and Mapping Branch cartographic system. The full EAI plot contains only 22 per cent of the original data points, but has a satisfactory resolution for many applications.

Costs

For this study, modifications to the Harvard programs were kept to a minimum. Processing costs could be considerably reduced by making the programs data dependent and tailoring them to a particular application. Nonetheless, the relative costs are instructive. Exclusive of discounts for overnight and weekly turnaround, they were:

Line printer	\$23.09
Calcomp	\$124.69
Applicon	\$128.67
EAI	\$9.03

It is clear that shading or symbolization of polygons is relatively expensive when compared with line drawing. Line printer maps offer an important alternative to other forms of polygon display and are adequate for many applications.

Conclusions

1. It is feasible to transfer a file from Surveys and Mapping cartographic system to the departmental computer and restructure the data to forms useful in other applications.
2. Such restructuring presently involves some manual intervention to ensure topological consistency of the data.
3. Various devices may be used to display the data, although the line printer offers adequate results at low cost.

Future Work

Software has been acquired that will permit the merging of other digital files with a topographic base. Tests of these programs will be carried out during the next year.

Acknowledgments

This study would not have been possible without the assistance of many people. In addition to those mentioned in the text, I would like to thank T. Scaga, K. Kneisly, G. Leclerc, and G. Fahey for their skill in obtaining useable plots from often recalcitrant hardware.

References

- Agterberg, F.P., Chung, C.F., Fabbri, A.G., Kelly, A.M., and Springer, J.S.
1971: Geomathematical evaluation of copper and zinc potential of the Abitibi area, Ontario and Quebec; Geological Survey of Canada, Paper 71-41, 55 p.
- Chrisman, N.R.
1977: Concepts of space as a guide to cartographic data structures; in *An Advanced Study Symposium on Topological Data Structures for Geographic Information Systems: Papers Volume 2*. Laboratory for Computer Graphics and Spatial Analysis, Harvard University, no pagination.
- Debain, P.
1974: Auto-cartography in the Geological Survey of Canada — development in automation; in *Computer Use in Projects of the Geological Survey of Canada*, ed. T. Gordon and W.W. Hutchison; Geological Survey of Canada, Paper 74-60, p. 101-106.
- Dougenik, J.A. and Sheehan, D.E.
1977: SYMAP User's Reference Manual; Laboratory for Computer Graphics and Spatial Analysis, Harvard University, 187 p.
- Douglas, D.H. and Peucker, T.K.
1973: Algorithms for the reduction of the number of points required to represent a digitized line or its caricature; *The Canadian Cartographer*, v. 10, p. 112-122.
- Dutton, G.
1976: Minority report on gridded data; Internal Reports, 1976, Laboratory for Computer Graphics and Spatial Analysis, Harvard University, p. 76-11/1-76/11-4.
- Fabbri, A.G., Kasvand, T., and Stray, J.H.
1978: Implementation of an interactive system for computer processing of geological images; in *Current Research, Part C*, Geological Survey of Canada, Paper 78-1C, p. 123-124.
- Laboratory for Computer Graphics
1974: POLYVRT User's Manual; Laboratory for Computer Graphics and Spatial Analysis, Harvard University, 128 p.
- Latham, C.A. and White, D.
1978: CALFORM Manual; Laboratory for Computer Graphics and Spatial Analysis, Harvard University, 66 p.
- Martin, G.M.
1978: Branch Facilities for Digitizing Operations; internal report; Data Systems Group Technical Note 10, Geological Survey of Canada, 15 p.

- Peucker, T.K. and Chrisman, N.
1975: Cartographic data structures; *The American Cartographer*, v. 2, p. 55-69.
- Rhind, D.H.
1977: Computer-aided cartography; *Transactions of the Institute of British Geographers New Series*, v. 2, p. 71-97.
- Sproll, W.P. and Dietz, R.S.
1969: Morphological continental drift fit of Australia and Antarctica; *Nature*, v. 217, p. 345-348.
- Stockwell, C.H.
1950: The use of plunge in the construction of cross-sections of folds; *Proceedings of the Geological Association of Canada*, v. 3, p. 96-121.
- van Zijl, L.
1975: Automation in cartography; in *Soil Information Systems*, ed. S.W. Bie, Centre for Agricultural Publication and Documentation, Wageningen, The Netherlands, p. 52-60.
- Young, M.E.H.
1978: The automated cartography system of the Department of Energy, Mines and Resources; in *Recent trends in geographic information processing systems in the National Capital Region*, ed. D.R.F. Taylor, Department of Geography, Carleton University, Ottawa, p. 1-11.

**PETROGRAPHIC AND GEOCHEMICAL INVESTIGATION OF IRON FORMATION
AND OTHER IRON-RICH ROCKS IN BATHURST DISTRICT, NEW BRUNSWICK**

S.I. Saif¹
Economic Geology Division

Saif, S.I., Petrographic and geochemical investigation of iron formation and other iron-rich rocks in Bathurst District, New Brunswick; in Current Research Part A, Geological Survey of Canada, Paper 80-1A, p. 309-317, 1980.

Abstract

The Tetagouche Group, a metamorphosed volcano-sedimentary complex of Middle Ordovician age, underlies much of the Bathurst-Newcastle district. It hosts numerous massive sulphide deposits which may be a facies of iron formation, and some of these deposits are of great economic significance. Extreme structural and stratigraphic complexities, poor exposure and the occurrence of a variety of iron-rich rocks at different stratigraphic levels, have combined to make correlation of the ore horizons and the other associated iron formations difficult.

Five different types of iron-rich rocks have been identified on the basis of field, petrographic and chemical investigation. Their geochemical characteristics may ultimately be used to distinguish the type of iron-rich rocks associated with the massive sulphide bodies in the Tetagouche Group.

Introduction and Sample Localities

Fieldwork, carried out in October, 1978, was mainly aimed at collecting, for petrographic and geochemical purposes, samples of iron formation and other iron-rich rocks in the Tetagouche Group of the Bathurst-Newcastle area. Due to extreme structural and stratigraphic complexities, the relative stratigraphic positions of these rocks are unknown although some of the iron formations are genetically related to the numerous massive sulphide deposits found within the group.

A total of 167 samples were collected from outcrops, diamond drill cores and underground mines from the following areas (Fig. 45.1):

1. Key Anacon mine
2. Brunswick no. 6 mine
3. Brunswick no. 12 mine
4. Heath Steele mine
5. Austin Brook iron mine
6. Sabena mining property
7. The Narrows
8. Bathurst mine
9. The new trench area of Atlantic Coast Copper
10. Area about 13 km west of Caribou mine on Caribou road.

General Geology of Bathurst Mining Camp

The Bathurst-Newcastle district was described by Smith and Skinner (1958) as geologically constituted of the following three regional units (Fig. 45.1):

3. The Pennsylvanian – Mississippian Cover
2. The Silurian-Devonian Folded Belt
1. The Ordovician Folded Belt

1. The Ordovician Folded Belt

The Ordovician Folded Belt consists of highly deformed interlayered metavolcanic and metasedimentary rocks which underlie the central part of the district. These volcano-sedimentary strata comprise the Tetagouche Group and are generally considered to be Ordovician.

As noted below several attempts have been made to subdivide the Tetagouche Group.

The earlier distinction of different rock units within the Tetagouche Group led Boyle and Davies (1964) to arrange the rocks of the Austin Brook and Brunswick No. 6 area into a tentative stratigraphic sequence with a thick metasedimentary unit at the base, overlain by felsic and mafic volcanic units. Stockwell and Tupper (1966) interpreted the rock sequence near the Brunswick No. 6 mine as younging in a westerly direction on the basis of graded beds in the drill core, a conclusion which was compatible with Boyle and Davies' interpretation. Smith and Skinner (1958) and Skinner (1974) compiled most of the previous work in a large part of the Bathurst district and suggested, mostly on the basis of the sedimentary structures, that the volcanic and argillaceous metasedimentary rocks are younger than the siliceous metasedimentary rocks. Poole (1963, 1967) suggested an orthoquartzitic substratum for the entire Bathurst complex because of the lithological similarity of its quartzitic rocks to those that occur apparently at the base of the Ordovician sedimentary sequence in central New Brunswick.

Apart from the metasedimentary rocks at the base of the sequence, Rutledge (1972) noted a large proportion of metasedimentary rocks overlying and interbedded with the volcanic rocks and iron formation in the Brunswick No. 12 mine area. Helmstaedt (1973) also distinguished two metasedimentary rock units, one at the base of the Tetagouche Group and predating the volcanic sequence, and the other interlayered with and overlying the volcanic rocks. Recent work (Saif, 1977; Saif et al., 1978) has also identified two major metasedimentary rock units, one at the bottom and the other at the top of the stratigraphic sequence at each of the Key Anacon and Brunswick No. 6 mine areas.

In spite of these intensive efforts, no stratigraphic sequence has yet been agreed upon for the entire Tetagouche Group. This may be due to scarcity of outcrops, varied lithological characteristics, and intense deformation which has produced isoclinal folds and obliterated primary sedimentary structures. It may be also due to the fact that the stratigraphic sequence varies from place to place because of abrupt facies changes in a volcanic environment.

These rocks are intruded by Ordovician, and possibly also Silurian and Devonian, gabbro, diabase and diorite, and by Devonian granitic masses.

¹ Natural Sciences and Engineering Research Council, Canada

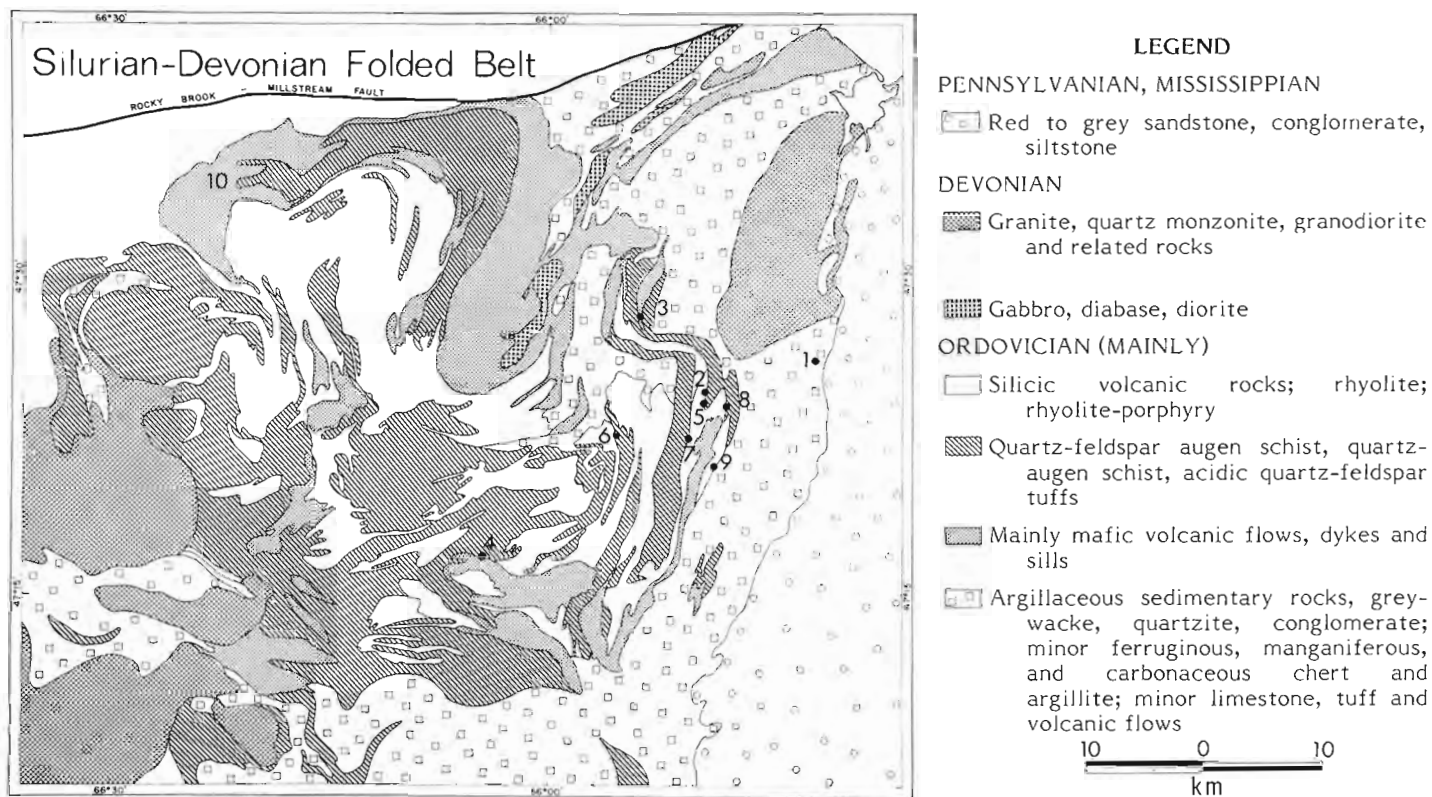


Figure 45.1. Geology of the Bathurst-Newcastle area, New Brunswick (after Davies, 1972). See 'Introduction' for sample localities Nos. 1 to 10.

The Tetagouche Group was subjected to several phases of deformation. The complicated structural features, absence of good marker horizons and poor exposure have so far prevented a coherent structural interpretation for the entire group, but it is generally regarded as part of a Taconic folded belt that has been refolded during the Acadian Orogeny (Smith and Skinner, 1958; Neale, et al. 1961; Poole, 1967; Davis, 1972).

This structurally and stratigraphically complex group contains economically significant massive sulphide bodies, as well as the iron formation and other iron-rich rocks that are the subject of this report.

2. The Silurian-Devonian Folded Belt

This structural unit, of Late Silurian and Early and Middle Devonian age, occurs north of a major fault known as the Rocky Brook-Millstream 'break' (Fig. 45.1) and consists mostly of greywacke, argillite, slate and interbedded volcanic rocks. Gabbro, diabase, diorite, quartz-feldspar porphyry aplite dykes and sills and granitic stocks have intruded the belt. These rocks are generally less deformed than those in the Ordovician Folded Belt. A number of small sulphide veins and lenses occur, some of which are of economic significance.

3. The Pennsylvanian - Mississippian Cover

Flat-lying sedimentary rocks of Pennsylvanian age which unconformably overlie the Tetagouche Group, cover the eastern part of the district (Fig. 45.1), and their outliers occur in other places such as Tetagouche Lukes and Clearwater Stream. They have been divided into the Bathurst Formation of red sandstone, shale, grit and conglomerate, and the Clifton Formation of grey and brown mudstone, shale, siltstone and conglomerate.

Geology and Petrology

Apart from sulphide facies iron formation, which was not included in this study, the following five types of iron-rich rocks have been identified:

1. Cherty magnetite iron formation (oxide facies)
2. Iron-rich chloritic rocks (silicate facies)
3. Iron-rich carbonate rocks (carbonate facies)
4. Basic iron formation
5. Iron-rich maroon shales

Cherty Magnetite Iron Formation

This is the most important type of iron formation in the area because it is considered to be genetically associated with the massive sulphide deposits. Its occurrence with several sulphide bodies has been clearly documented (e.g. Boyle and Davies, 1964; Davies, 1972; Goodfellow, 1975; Lea and Rancourt, 1958; Luff, 1975; McAllister, 1960; McBride, 1976; Pertold, 1972; Rutledge, 1972; Saif, 1977; Saif et al., 1978; Stockwell and Tupper, 1966; Whitehead, 1973).

The rocks are generally black, dark grey, light and dark red, and brown. They are usually massive and extremely hard, but a flaggy variety, due to local concentration of specular hematite, is present. Banding is the most conspicuous feature of these rocks, with individual bands varying from thin laminae to about 2 cm thick (Fig. 45.2, 45.3, 45.4). The bands consist of alternate magnetite-hematite and quartz or quartz- and jasper-rich layers. The bands are either even and continuous or streaky and discontinuous, and are considered to represent primary bedding as they are conformable with the contacts.



Figure 45.2. Fine laminae of chert alternate with magnetite-rich bands; cherty magnetite iron formation, Austin Brook iron mine area. GSC 202229-N



Figure 45.3. Fine laminae and thick bands of jasper alternate with magnetite-rich laminae and bands; cherty magnetite iron formation, Austin Brook iron mine area. Length = 13 cm. GSC 202229-Q

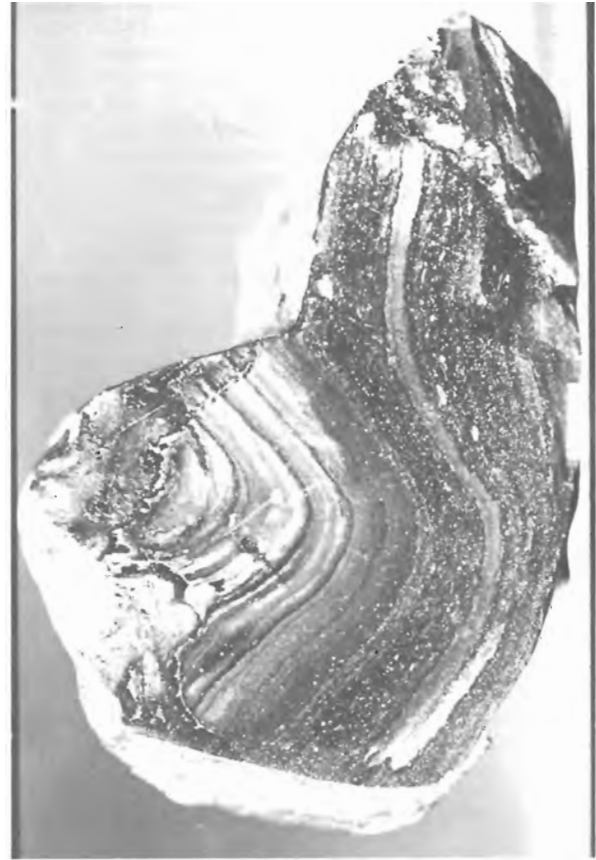


Figure 45.4. Folded laminae and bands of chert alternate with magnetite-rich bands and laminae; cherty magnetite iron formation, Brunswick No. 12 mine area. Length = 12 cm. GSC 202229-T



Figure 45.5. Folded and refolded (by two different phases of deformation) bands and laminae of chert alternate with magnetite-rich bands and laminae; cherty magnetite iron formation, Brunswick No. 12 mine area. Length 13 cm. GSC 202229-W

The rocks consist mostly of magnetite and quartz; hematite, jasper, chlorite and carbonate (calcite or siderite) and biotite are other major constituents. Feldspar is present in most of the rocks and is fairly abundant in some samples; it has been identified by electron microprobe to be mostly albite. The feldspar occurs as elongated coarse laths and as fine grains in the matrix (Fig. 45.6). K-feldspar is present but only in minor amounts. Apatite occurs in most of these rocks; some samples contain as much as 10 to 12 per cent. Other accessory minerals are muscovite, epidote, piemontite, zircon, sphene, titanomagnetite, ilmenite, rutile, pyrite, arsenopyrite, ferroan cobaltite, chalcopyrite, pyrrhotite, sphalerite and galena. Grunerite (Fig. 45.7) has been identified in only one thin section, in which it amounts to about 30 per cent. That sample was collected from an outcrop close to a huge mass of rhyolite, so the grunerite is considered to be a local phenomenon due to contact metamorphism by the overlying rhyolite.

Iron-rich Chloritic Rocks

Iron-rich chloritic rocks are closely associated with, and most often interbedded with, the cherty magnetite iron formation in many places such as at Austin Brook iron mine, Key Anacon mine, Bathurst mine locality and the new trench of Atlantic Coast Copper. The boundary between the oxide and silicate facies is sharp in places and gradational in others.

The rocks are dark green, schistose and usually friable but some are relatively hard. Texturally, the rocks are fine-grained with well to poorly developed fine bands and laminae of chlorite-magnetite and chert of green, pink or grey colours. The laminae and bands of chert vary in thickness from 1 mm to about 1 cm (Fig. 45.8).

Mineralogically, the rocks consist mostly of chlorite, magnetite and quartz. Chlorite content is as high as 65 per cent in some samples but on average it is approximately 30 per cent. Magnetite and quartz contents are, on average, 15 and 20 per cent, respectively. Other main constituents are biotite and carbonates (Fe-Mn carbonates with some Zn and Mg in solid solution). Feldspar is found in many samples and is mainly albite (Fig. 45.9) but minor amounts of K-feldspar have also been detected in a few samples. The grains of K-feldspar that were analyzed with the electron microprobe contain small amounts of Ba. Apatite is present but is not as abundant as in the oxide facies. A few monazite grains have been detected and these contain small amounts of thorium. Other accessory minerals are zircon, ilmenite, pyrite, chalcopyrite, pyrrhotite, sphalerite and galena. Sericite is present as an accessory mineral but in some samples it is found in great abundance (Fig. 45.8).

Iron-rich Carbonate Rocks

Carbonate facies is the least abundant of the facies of iron formation in the Bathurst region. The carbonate-rich rocks have been found in the Brunswick No. 6, Key Anacon mine and Brunswick No. 12 areas, with a maximum development in the latter two areas. In the Key Anacon area the carbonate is dominantly calcite with a little siderite, but in the other two areas it is predominantly siderite. In both areas, thin bands and laminae of carbonate occur within the oxide and chlorite facies but in Brunswick No. 12 area beds of carbonate rocks about 5 m thick are also found.

The rocks are generally light grey and buff colour, show striking thin light and dark laminae (about 0.5 mm thick) and bands up to 1 cm thick (Fig. 45.10). The rocks are massive, hard, and have a cherty appearance. They mainly consist of a very fine cryptocrystalline mixture of carbonate and quartz;

the carbonate is dominantly Fe-carbonate with subordinate Mn, Ca, and Mg in solid solution. Iron-rich chlorite ranges from a small amount to about 20 per cent of the carbonate rock.

Apatite and biotite are present in variable amounts in the carbonate rocks and are abundant in some samples. The accessory minerals include muscovite, K-feldspar (some of which contains Ba), pyrite, sphalerite and galena.

A green rock which is present in the Brunswick No. 12 mine area and at the Bathurst mine locality, locally referred to as 'spotted iron-formation', is an iron chlorite-rich rock with light grey patches (Fig. 45.11). The patches are either fine grained aggregates or individual coarse crystals of carbonate, consisting mostly of iron carbonate with a little Mn, Ca and Mg. Some of the coarse carbonate crystals are zoned. The probe investigation has revealed that the cores of the zoned crystals are rich in Fe and Mn and that Fe and Mg increase, and Mn decreases, toward the margins; Ca is constant throughout.

Basic Iron Formation

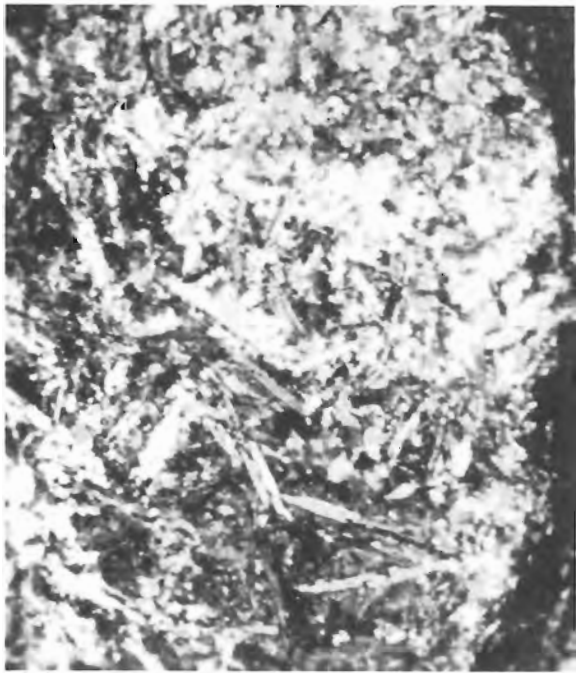
The term basic iron formation has been used locally for thin bands and lenses of magnetic rocks that occur within the mafic volcanic unit of the Tetagouche Group in the Brunswick No. 12 mine area. These bands and lenses are light and dark grey and range in thickness from about 2 to 50 cm. The basic iron formation has not been found to be as closely associated, spatially, with the massive sulphide deposits as has the cherty magnetite iron formation. Layers of similar iron formation have been also found in greenstone along the east side of Pabineau River (Sidwell, 1952; Skinner, 1956) and in the Grand Brook spilite body (Skinner, 1974). According to Gross (1967), similar material is common in belts of volcanic rocks, and represents an uncommon facies of some Algoma type iron formations.

The rocks are very fine grained, massive and hard. Most of them generally show primary bands and laminae consisting of alternating magnetite-rich and chlorite-, quartz- or carbonate-rich material (Fig. 45.12). Mineralogically, the important constituents are magnetite, chlorite (iron-rich), carbonate (calcite and siderite with low contents of Mn and Mg), quartz and feldspar (mostly albite but some is K-feldspar). Other important minerals are sphene, apatite, sericite, epidote and hematite. Sphene is found as rounded or oval ooliths most of which have a distinct core of iron-rich chlorite (Fig. 45.13). Another type of oolith is larger, more irregular in outline, less common and consists of a mixture of rutile, quartz, calcite and chlorite (Fig. 45.14). The accessory minerals are titanomagnetite, ilmenite, pyrite and galena.

Iron-rich Maroon Shales

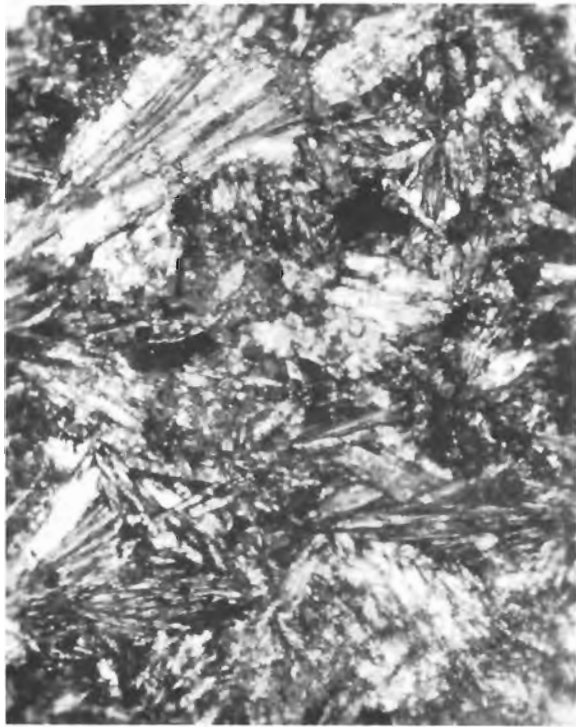
Red and maroon argillite, shale and slate occur in abundance in the Tetagouche Group. They were generally thought to contain Mn; pink nodules of rhodochrosite and veinlets of manganite are found in them at Tetagouche Falls (Skinner, 1974). Their colour has been attributed to hematite, but detailed work has not been done on these rocks. A few samples were collected for the present study.

The shales are very fine grained and include varieties such as cherty, hard and massive, laminated, friable and fractured. In places they have slaty cleavage. Their mineralogy is rather simple, most consist of very fine quartz and hematite with subordinate chlorite, sericite and carbonate. The quartz and hematite are generally uniformly distributed but in some cases they are concentrated in distinct fine laminae.



1 mm

Figure 45.6. Photomicrograph showing laths and fine grains of albite, other minerals are magnetite, chlorite, quartz and carbonate; cherty magnetite iron formation, Key Anacon mine area.



250 μ m

Figure 45.7. Photomicrograph showing grunerite and magnetite; cherty magnetite iron formation, from the new trench of Atlantic Coast Copper.



Figure 45.8. Fine laminae and bands of green chert alternate with laminae and bands of chlorite speckled with flakes of sericite; iron-rich chloritic rocks, Austin Brook iron mine area. Length = 13 cm. GSC 202229-Y

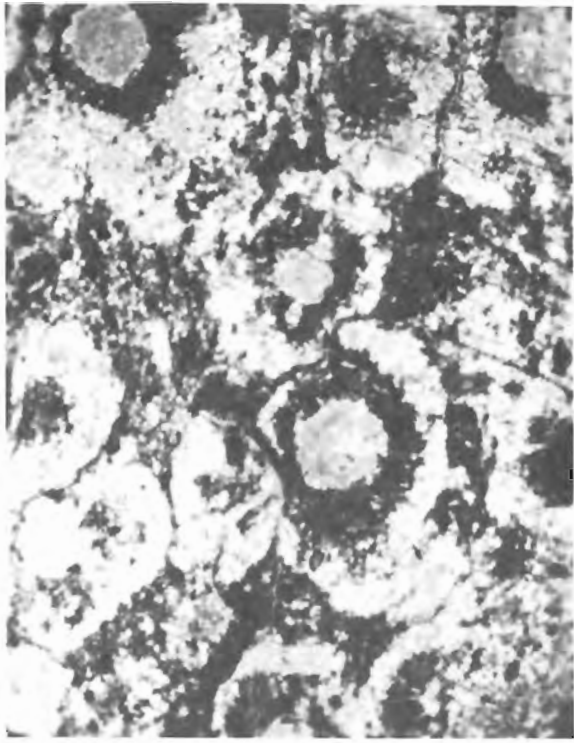


250 μ m

Figure 45.9. Photomicrograph showing laths and fine grains of albite, other minerals are magnetite, chlorite, and carbonate; chlorite and carbonate-rich rock, Key Anacon mine area.



Figure 45.10. Chert- and carbonate-rich laminae and bands in iron-rich carbonate rocks; Brunswick No. 12 mine area. Length = 8 cm. GSC 202229-R



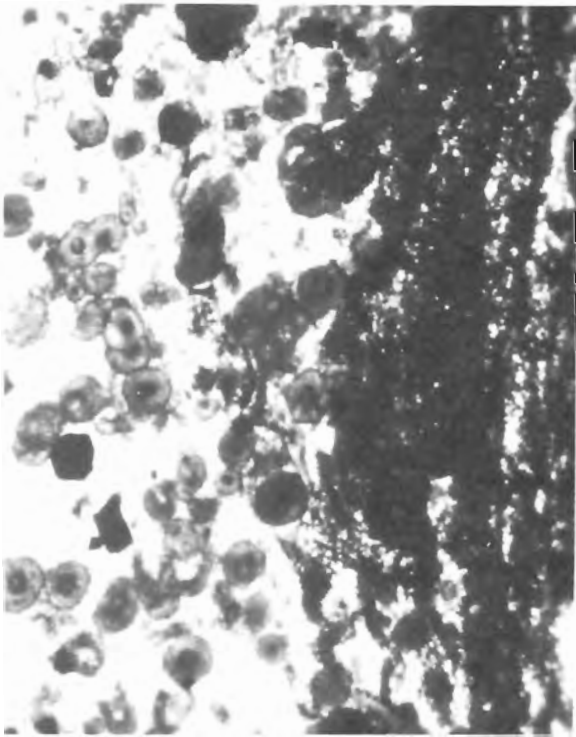
1 mm

Figure 45.11. Photomicrograph showing patches and ooliths of carbonate surrounded by groundmass rich in chlorite and biotite; 'spotted iron-formation', Bathurst mine locality.



250 μ m

Figure 45.12. Photomicrograph showing fine laminae of magnetite alternate with laminae rich in carbonate, quartz and chlorite; basic iron formation, Brunswick No. 12 mine area.



250 μ m

Figure 45.13. Photomicrograph showing ooliths of sphene most of which have a distinct core of iron-rich chlorite, the groundmass is carbonate, quartz, chlorite and magnetite; basic iron formation, Brunswick No. 12 mine area.

Table 45.1

Mean and variation in the major oxide composition of the 5 types of iron-rich rocks

Oxides	Cherty Magnetite Iron-Formation		Chloritic Iron-Formation		Carbonate Iron-Formation		Basic Iron-Formation		Maroon Shales	
	Variation	Mean	Variation	Mean	Variation	Mean	Variation	Mean	Variation	Mean
SiO ₂	4.30 - 80.00	29.98 (72)	27.10 - 53.50	45.66 (13)	11.00 - 43.30	30.32 (19)	25.30 - 53.70	43.26 (8)	42.6 - 79.4	62.93 (10)
Al ₂ O ₃	0.20 - 17.10	4.22 (72)	4.80 - 16.60	10.22 (13)	0.40 - 13.90	6.73 (19)	9.80 - 16.30	13.59 (8)	5.00 - 12.90	7.34 (10)
TiO ₂	.01 - 3.12	0.33 (72)	0.20 - 2.84	0.73 (13)	0.05 - 3.13	1.10 (19)	2.68 - 9.21	4.16 (8)	0.25 - 0.70	0.40 (10)
Fe ₂ O ₃	N.D. - 77.00	31.01 (71)	2.30 - 18.70	11.05 (13)	1.30 - 33.80	12.98 (19)	3.30 - 15.90	6.99 (8)	4.10 - 38.61	19.07 (10)
FeO	N.D. - 38.80	18.10 (68)	5.70 - 21.80	14.26 (13)	N.D. - 36.50	16.84 (18)	6.30 - 17.40	10.18 (8)	N.D. - 2.30	1.47 (3)
MnO	0.10 - 12.32	2.88 (72)	0.10 - 5.04	1.18 (13)	0.09 - 10.62	3.26 (19)	0.16 - 0.48	0.31 (8)	0.09 - 10.40	2.13 (10)
MgO	0.07 - 3.43	1.53 (72)	1.37 - 13.14	4.42 (13)	0.48 - 4.91	1.82 (19)	2.50 - 10.71	5.56 (8)	0.32 - 3.66	1.83 (10)
CaO	N.D. - 10.94	3.72 (71)	0.19 - 10.75	2.69 (13)	1.02 - 17.69	9.24 (19)	3.39 - 11.39	5.87 (8)	0.02 - 1.85	0.59 (10)
Na ₂ O	N.D. - 5.30	0.89 (17)	N.D. - 5.10	4.00 (2)	N.D. - 5.80	3.49 (8)	N.D. - 5.90	3.44 (7)	N.D. - 2.80	1.08 (5)
K ₂ O	N.D. - 5.05	0.65 (55)	N.D. - 2.47	0.75 (11)	N.D. - 3.82	0.94 (15)	0.38 - 3.35	0.99 (8)	0.32 - 2.96	1.69 (10)
P ₂ O ₅	0.02 - 4.64	1.77 (72)	0.04 - 2.65	0.84 (13)	N.D. - 5.83	1.42 (19)	0.63 - 2.94	1.10 (8)	0.09 - 1.22	0.44 (10)
S	N.D. - 11.70	0.77 (68)	N.D. - 0.57	0.12 (12)	N.D. - 6.50	0.86 (17)	0.01 - 0.11	0.05 (8)	N.D. - 0.03	0.03 (5)
CO ₂	N.D. - 16.7	4.39 (70)	N.D. - 8.50	4.26 (9)	6.50 - 21.80	11.65 (19)	0.20 - 1.10	0.58 (8)	0.10 - 4.50	0.58 (10)
H ₂ O	N.D. - 6.30	2.69 (63)	2.60 - 9.00	4.54 (13)	N.D. - 7.00	2.41 (17)	1.00 - 8.40	4.25 (8)	0.50 - 3.20	2.00 (10)

The number of samples with detectable amount of oxide is shown in parentheses below every mean value.

N.D. = Not detectable

Percentage error for various oxides in plus or minus is: SiO₂ & Al₂O₃ = 0.3; TiO₂, MnO₂, K₂O, P₂O₅ & S = 0.02;Fe₂O₃, FeO & CO₂ = 0.1; MgO & Na₂O = 0.2; CaO = 0.05; H₂O = 0.08.

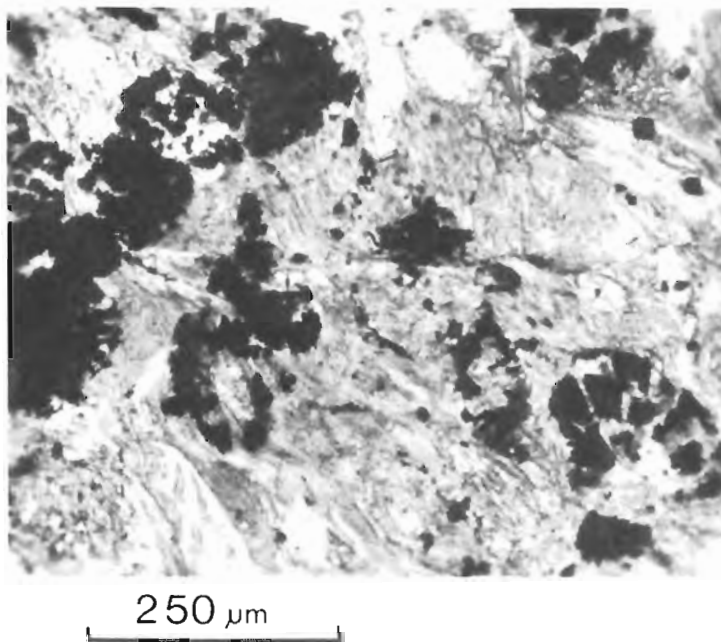


Figure 45.14. Photomicrograph showing oolites with irregular outline and consist of a mixture of rutile, quartz, calcite and chlorite, the groundmass also consists of the latter three minerals; basic iron formation, Brunswick No. 12 mine area.

Geochemistry

The mineralogy of the rocks investigated is faithfully reflected in their major oxide composition which is shown in Table 45.1. SiO_2 , Fe_2O_3 and FeO constitute between 47.1 and 99.1% of these rocks. Al_2O_3 varies greatly, its minimum value is 0.20% in the oxide facies of the Brunswick No. 6 mine area, and maximum value is 17.1% in the mixed oxide and chlorite facies of the Key Anacon mine area. The maroon shales have an average of 7.34% of Al_2O_3 . Na_2O is high in the oxide and chlorite facies of the Key Anacon rocks and in the basic iron formation of the Brunswick No. 12 mine. Its average in the two areas is 3.46 and 3.44% respectively. K_2O is generally very low (less than 1%) in all these rocks but in a few samples representing all the types examined, is as high as 3.45%; and in the case of one oxide facies sample from Key Anacon, the K_2O content is 5.05%. The basic iron formation has an average of 0.99% of K_2O .

Most of these iron-rich rocks are also rich in P_2O_5 ; a maximum of 5.83% is present in a sample of iron carbonate from the Brunswick No. 12 mine area. The high P_2O_5 content is attributed to the abundant apatite found in these rocks. Some of the rocks are also very high in TiO_2 (maximum 9.21% in a basic iron formation sample) and this is due to the presence of various titanium bearing minerals mentioned above. MnO values also vary greatly from less than 1% to as high as 12.32%. The highest value was obtained for an oxide facies sample from the Sabena mining property. MnO contents in the maroon shales range from 0.09 to 10.4%. Rocks which are richest in MgO are the basic iron formation (from 2.5 to 10.71%) and the chlorite facies (from 1.37 to 13.14%). As expected, the carbonate iron-formation is the richest in CO_2 , analyses indicated contents of 6.5 to 21.80% CO_2 .

Remarks

Structural and stratigraphic complexities as well as poor exposure have combined to create problems in exploration for massive sulphide deposits in the Bathurst mining

district. Geophysical techniques are useful, particularly aeromagnetic and ground-magnetic surveys which are utilized to locate the iron formation horizons along which sulphides are expected to occur since they are considered to be one of the four facies of the iron formation. Problems in the use of magnetic techniques are created by the basic iron formation which is also somewhat magnetic and therefore gives a false indication of the favourable horizon. The basic iron formation cannot be distinguished from the cherty magnetic iron formation in hand specimen and even under the microscope.

Table 45.1 shows that in certain aspects the basic iron formation appears to be chemically distinct from the other facies. It is quite high in TiO_2 and MgO relative to the other iron-rich rocks, but is very low in MnO , S and CO_2 . These chemical characteristics may be utilized to distinguish between the cherty magnetic and basic iron formation. Further interpretation of the chemical data is in progress which may provide an answer to this problem.

Acknowledgments

The author is thankful to the Natural Sciences and Engineering Research Council, Canada for the award of a Visiting Research Fellowship for one year during which this work has been completed. Thanks are due to D.F. Sangster for his supervision of the project, for scientific discussions and, with R.I. Thorpe, for critical reading of the manuscript. The author is also thankful to the management and staff of the Geological Survey of Canada for providing funds for the fieldwork, office accommodation and help in analytical, lapidary, photographic, computer, drafting and typing work. The geologists of Brunswick Mining and Smelting Corp. Ltd., Heath Steele Mines Ltd., and J.L. Davies of the New Brunswick Department of Natural Resources are also thanked for their co-operation.

References

- Boyle, R.W. and Davies, J.L.
1964: Geology of the Austin Brook and Brunswick No. 6 sulphide deposits, Gloucester County, New Brunswick; Geological Survey of Canada, Paper 63-24.
- Davies, J.L.
1972: The geology and geochemistry of the Austin Brook area, Gloucester County, New Brunswick with special emphasis on the Austin Brook iron formation; unpublished Ph.D. thesis, Carleton University, Ottawa, Ontario.
- Davis, G.H.
1972: Deformational history of the Caribou strata-bound sulphide deposits, Bathurst, New Brunswick, Canada; *Economic Geology*, v. 67, p. 634-655.
- Goodfellow, W.D.
1975: Rock geochemical exploration and ore genesis at Brunswick No. 12 deposit, New Brunswick; unpublished Ph.D. thesis, University of New Brunswick, Fredericton, New Brunswick.
- Gross, G.A.
1967: Geology of iron deposits in Canada, Iron deposits in the Appalachian and Grenville Regions of Canada; Geological Survey of Canada Economic Geology Report No. 22, v. 2.
- Helmstaedt, H.
1973: Structural geology of the Bathurst Newcastle district; in *Geology of New Brunswick*, ed., Rast, N., N.E.I.G.C. Field Guide to Excursions, p. 34-46.

- Lea, E.R. and Rancourt, C.
1958: Geology of the Brunswick Mining and Smelting orebodies, Gloucester County, New Brunswick; Canadian Institute of Mining and Metallurgy Bulletin, v. 51, no. 551, p. 167-177.
- Luff, W.M.
1975: Structural geology of the Brunswick No. 12 open pit; Canadian Institute of Mining and Metallurgy Bulletin, v. 68, no. 758, p. 64-74.
- McAllister, A.L.
1960: Massive sulphide deposits in New Brunswick; Canadian Institute of Mining and Metallurgy Bulletin, v. 53, no. 573, p. 88-98.
- McBride, D.
1976: Geology of Heath Steele Mines, New Brunswick; unpublished Ph.D. thesis, University of New Brunswick, Fredericton, New Brunswick.
- Neale, E.R.W., Beland, J., Potter, R.R., and Poole, W.H.
1961: A preliminary tectonic map of the Canadian Appalachian region based on age of folding; Canadian Institute of Mining and Metallurgy Bulletin, v. 54, no. 593, p. 687-694.
- Pertold, Z.
1972: Surface plan and cross section, Brunswick No. 6 orebody; in Mineral deposits of southern Quebec and New Brunswick, eds., McAllister, A.L. and Lamarche, R.Y., 24th International Geological Congress, Field Excursion A58-C58 Guidebook, p. 60-61.
- Poole, W.H.
1963: Hayesville, New Brunswick; Geological Survey of Canada Map 6-1963.
1967: Tectonic evolution of the Appalachian region of Canada; in Geology of the Atlantic Region, ed., Neale, E.R.W. and Williams, H., Geological Association of Canada Special Paper No. 4, p. 9-51.
- Rutledge, D.W.
1972: Brunswick Mining and Smelting Corporation, No. 6 and 12 Mines; in Mineral deposits of southern Quebec and New Brunswick, eds., McAllister, A.L. and Lamarche, R.Y., 24th International Geological Congress; Field Excursion A58-C58 Guidebook, p. 58-67.
- Saif, S.I.
1977: Identification, correlation and origin of the Key Anacon-Brunswick mines ore horizon, Bathurst, New Brunswick; unpublished Ph.D. thesis, University of New Brunswick, Fredericton, New Brunswick.
- Saif, S.I., McAllister, A.L., and Murphy, W.L.
1978: Geology of the Key Anacon mine area, Bathurst, New Brunswick; Canadian Institute of Mining and Metallurgy Bulletin, v. 71, no. 791, p. 161-168.
- Sidwell, K.O.J.
1952: Anomalies in the Bathurst Iron Mines area; New Brunswick Resources Development Board, Fredericton, New Brunswick.
- Skinner, R.
1956: Geology of the Tetagouche Group, Bathurst, New Brunswick; unpublished Ph.D. thesis, McGill University, Montreal, Quebec.
1974: Geology of Tetagouche Lakes, Bathurst, and Nepisiguit Falls map areas, New Brunswick; Geological Survey of Canada Memoir 371.
- Smith, C.H. and Skinner, R.
1958: Geology of the Bathurst-Newcastle mineral district, New Brunswick; Canadian Institute of Mining and Metallurgy Bulletin, v. 51, no. 551, p. 150-155.
- Stockwell, C.H. and Tupper, W.M.
1966: Geology of Brunswick No. 6 and No. 12 mining areas, Gloucester County, New Brunswick; Geological Survey of Canada Paper 65-13.
- Whitehead, R.E.
1973: Application of rock geochemistry to problems of mineral exploration and ore genesis at Heath Steele Mines, New Brunswick; unpublished Ph.D. thesis, University of New Brunswick, Fredericton, New Brunswick.

RIFT-RELATED LATE PROTEROZOIC SEDIMENTATION AND VOLCANISM ON
NORTHERN BAFFIN AND BYLOT ISLANDS, DISTRICT OF FRANKLIN

Project 770013

G.D. Jackson, T.R. Iannelli¹, and B.J. Tilley²
Precambrian Geology Division

Jackson, G.D., Iannelli, T.R., and Tilley, B.J., Rift-related late Proterozoic sedimentation and volcanism on northern Baffin and Bylot Islands, District of Franklin; in Current Research, Part A, Geological Survey of Canada, Paper 80-1A, p. 319-328, 1980.

Abstract

More than 5600 m of late Proterozoic quartzarenites, shales, stromatolitic and biohermal carbonates, arkoses, greywackes and conglomerates, were deposited in environments ranging from fluvial to subtidal on northern Baffin and Bylot islands. A delta-fan complex occurs in the lower part of the succession, coastal sabkha-type evaporites in the middle part, and an alluvial fan complex in the upper part. As much as 80 m of tholeiitic plateau basalts occur near the base of the succession.

Syndepositional faulting had a significant effect on the sedimentation pattern. Paleocurrent trends are varied, but most indicate northwesterly transport in central graben areas and in some horst areas. Transport away from fault zones active during sedimentation and toward central graben areas, is indicated in marginal trough areas. Rifting was probably related to a late Proterozoic ocean opening event to the northwest; perhaps an early phase of the Franklinian Geosyncline.

Introduction

The 1979 field season was the third on the project and the second in which a full-sized party was active. The major goals of the project continue to be the study of the several thousand metres of strata present in the Eequalulik and Uluksan groups. Early work is well documented by Lemon and Blackadar (1963) and by Blackadar (1970). More recent studies include those by Galley (1978), Geldsetzer (1973a, b), Iannelli (1979), Jackson and Davidson (1975), Jackson et al. (1975, 1978), and Olson (1977).

About 19 400 km² (7500 sq. miles) remained to be examined in 1979 during a 2 1/2 month field season (48 D, eastern two-thirds of 48 A, northern 37 G, western 38 B, northern 38 C). Because of poor weather relatively little work was carried out on the basement gneisses, and several large patches of late Proterozoic strata on northern Borden Peninsula and Bylot Island remain to be studied (Fig. 46.1, 46.2).

A Bell 206 B helicopter from Aerotrades Ltd. was used by the 9-man party headed by G.D. Jackson, and also provided support for W.F. Fahrig and K. Christie in their paleomagnetic studies. Excellent Twin Otter support was provided periodically by Polar Continental Shelf Project.

This preliminary report for the most part summarizes data gathered during the 1979 field season. Most of the work in the Eequalulik Group and the overlying Arctic Bay Formation was carried out by Iannelli (Contract No. 95704) who is responsible for those rocks in this report (Table of Formations). Jackson and Tilley worked chiefly in the Uluksan Group. Tilley provided a résumé of her work and a preliminary draft of the paleocurrent diagrams (Fig. 46.1, 46.2).

Basement Complex

A variable complex assemblage of Archean-Aphebian gneisses and igneous rocks is separated from the overlying late Proterozoic strata by a nonconformity. Most of the gneisses are irregularly banded migmatites which are commonly intruded by two or more generations of granitic rocks. Upper amphibolite metamorphic grade predominates but granulite grade occurs in several places and seems to have superseded late granitic emplacement.

Regolithic material up to 6 m thick is preserved beneath the Proterozoic strata at several localities. Basement rocks grade upward into poorly consolidated varicoloured rocks containing kaolinized feldspar, granular quartz and fine chlorite-sericite matrix and partings. The contact with overlying Nauyat and Adams Sound strata is undulatory and disconformable.

Nauyat Formation

The Nauyat Formation outcrops chiefly from south of Adams Sound southeast to south of Tremblay Sound (Fig. 46.1), east of Elwin Inlet and on northern Bylot Island. It is the basal formation of the late Proterozoic succession, nonconformably overlies the basement complex, ranges from 16 to over 90 m thick, and has been divided informally into two conformable members, N₁ and N₂ (Jackson et al., 1978).

Rb-Sr and K-Ar ages recently completed by the Geochronology Section of the Geological Survey of Canada range from 762 to 1060 Ma. Preliminary considerations of the results suggest that an age of 917 to 1032 Ma is most likely for the formation.

N₁ Member

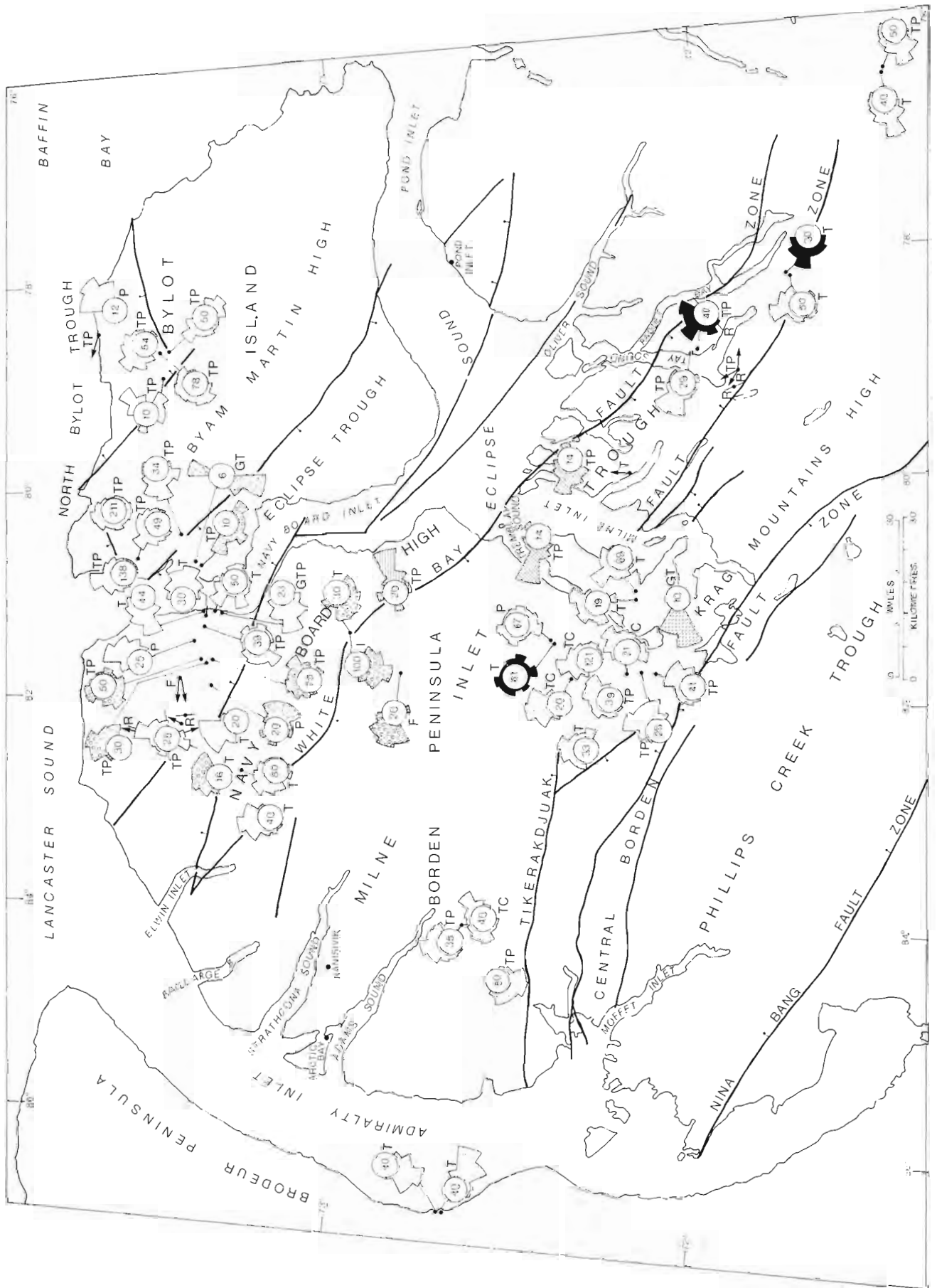
The lower (N₁) member consists chiefly of thin- to medium-bedded, grey-white to pink, dark red, buff and brown quartzarenite. Thin layers of quartz-granule to quartz-pebble conglomerate occur as basal units of fining upward cycles in the lower part of the member. Sedimentary structures include trough- and planar-crossbeds, wave and current ripple marks, load casts, and synaeresis cracks. Crossbeds indicate unimodal northwesterly paleocurrent trends. The member ranges from 8 to 20 m in thickness.

N₂ Member

Nauyat volcanics overlie basement gneisses nonconformably where the N₁ member is absent. The flows occur in a single sequence containing 1 to 5 flows of fine grained, massive, amygdaloidal tholeiitic plateau basalt with alkaline affinities (Galley, 1978; Jackson et al., 1978). Some layers on northern Bylot Island are fine- to medium-grained, olive green, ultramafic, and may be ultrabasic sills. Thin, baked quartzarenite, siltstone, dolosiltite and chert beds are interbedded with the flows locally.

¹ Department of Geology, University of Western Ontario, London, Ontario, N6A 5B7

² Alberta Research Council, 11315 - 87th Avenue, Edmonton, Alberta, T6G 2C2



The flows contain amygdules filled with quartz, agate, calcite, and dolomite. Columnar joints and flow banding occur locally. Small pillows occur south and southwest of Tremblay Sound. Individual flows range from 2.5 to 20 m thick. The sequence thickens to the northwest, ranging from 8 to 16 m thick near the Central Borden Fault zone to over 80 m thick east of Elwin Inlet.

Interpretation

Deposition of N_1 quartzarenite in a braided fluvial environment was interrupted by extrusion of chiefly subaerial basalt. Continued sedimentation buried the flows before they could be eroded. The flows are spatially related to major fault zones and were probably extruded along them.

Adams Sound Formation

Adams Sound strata are exposed along the southern edge of the study area, east of Elwin Inlet, and on northwestern Bylot Island. The formation consists chiefly of thin- to thick-bedded quartzarenite with minor shale and siltstone. Quartz-pebble conglomerate occurs mostly in the lower and upper parts of the formation. Sedimentary structures include trough- and planar-crossbeds (Fig. 46.1), current ripple marks, scours, channels, load casts, graded beds, synaeresis and dessication cracks, microfaults and small vugs. Pyrite and marcasite occur locally.

The formation is about 65 m thick from Tremblay Sound east to Paquet Bay and 340 m thick on northwest Bylot Island. It thickens toward the north and northwest. Adams Sound Formation is conformable with the Nauyat Formation and rests conformably on basement gneisses where the Nauyat is absent. The contact with the overlying Arctic Bay Formation is gradational. The Adams Sound Formation has been divided into three intergradational members on Borden Peninsula (AS_1 , AS_2 , AS_3), two members in the Paquet Bay area (AS_4 , AS_5) and into a lower and upper member (AS_L , AS_U) on Bylot Island (Jackson and Davidson, 1975).

AS_1 Member

This member is mostly pink, purple-red to cream-brown quartzarenite with pebble- to cobble-polymictic conglomerate interbeds at the base of fining upward cycles. Paleocurrent trends are unimodal and northwest to northeast (Fig. 46.1). Thicknesses range from 8 to 16 m near Tremblay Sound to over 30 m east of Elwin Inlet.

AS_2 Member

AS_2 strata are chiefly buff-white, pink-white to purple-grey quartzarenites that contain fining upward cycles. Unimodal northwest to northeast paleocurrent trends predominate. Southeast trends are less common. The member is 33 m thick at Tremblay Sound and over 100 m thick east of Elwin Inlet.

Figure 46.1. Location map and rose diagrams showing crossbed measurements. The radius of the centre circle is 20 per cent. Single determinations are indicated by a straight line or arrow.

- | | |
|------------------------------|------------------------------|
| - Adams Sound Formation | C - channels |
| - Arctic Bay Formation | F - flutes |
| - Fabricius Fiord Formation | G - giant trough crossbeds |
| - Society Cliffs Formation | I - imbricate clasts |
| - Victor Bay Formation | P - planar crossbeds |
| - Athole Point Formation | R - ripple marks |
| - Strathcona Sound Formation | S - stromatolite elongations |
| VEES - Elwin Formation | T - trough crossbeds |

AS_3 Member

White and grey to grey-brown quartzarenite with interbeds and lenses of pebbly quartzarenite and quartz-pebble conglomerate dominate the AS_3 member. Minor shale and siltstone interbeds occur in the uppermost part. Fining upward cycles occur in some sections. Most paleocurrent trends are polymodal to bimodal, although some are unimodal northwest to northeast. The member is 16 m thick near Tremblay Sound and over 70 m thick east of Elwin Inlet.

AS_4 , AS_5 Members (see Iannelli, 1979)

These strata are grey-white to buff-grey quartzarenite. Minor quartz-pebble conglomerate occurs chiefly at the base. Paleocurrents are unimodal and trend north-northwest. These strata are 45-65 m thick in the Paquet Bay area.

AS_L Member

The AS_L member is chiefly pink, buff-orange to purple-red quartzarenite with interbeds of pebbly quartzarenite and pebble conglomerate. Siltstone and shale beds occur in the upper part. Poorly defined fining upward cycles are present. Bipolar-bimodal northwest and southeast trending paleocurrents predominate. Polymodal trends and northwest to southwest unimodal trends occur locally. Thicknesses of 88 to over 200 m occur on northern Bylot Island, but the member is absent locally on central western Bylot Island.

AS_U Member

This member is composed of buff-grey, white to pink-grey quartzarenite with thin interlayers of siltstone, and quartz-pebble conglomerate. Fining upward cycles are seen in some sections. Paleocurrent trends are unimodal to the northwest and bimodal southwest to west. Thicknesses range from over 70 m on central west Bylot Island to 140 m on northeast and 196 m on northwest Bylot Island.

Interpretation

During early Adams Sound time braided fluvial sediments were deposited in the southern and southeastern parts of the map area, whereas mixed fluvial and intertidal sediments were deposited in the northern part. Regional basin transgression ended this fluvial deposition, which was followed by intertidal to shallow subtidal deposition.

Arctic Bay Formation

The Arctic Bay Formation outcrops in the same general areas as does the Society Cliffs Formation. The strata are chiefly laminated shale and thin- to medium-bedded siltstone, quartzarenite, dolosiltite, doloarenite and stromatolitic dolostone. Structures include cone-in-cone, concretions, soft sediment folds, load casts, microfaults, convoluted beds, wave and current ripples, trough- and planar-crossbeds, scours, rip-up clasts, synaeresis and dessication cracks, dewatering structures, and vugs filled with carbonates, quartz, and bituminous material. White gypsum efflorescence is common on the shales. Some beds emit a strong petroliferous odour and others contain disseminated pyrite and marcasite.

The Arctic Bay Formation exceeds 260 m in thickness west of Tremblay Sound, and 600 m east of Elwin Inlet. It is 466 m thick at the head of Tremblay Sound and is more than 414 m thick west of Tay Sound. The formation rests nonconformably on basement gneisses at several places. The contact with the overlying Society Cliffs Formation ranges from conformable to erosional. Four intergradational and regionally variable members have been identified (Iannelli, 1979).

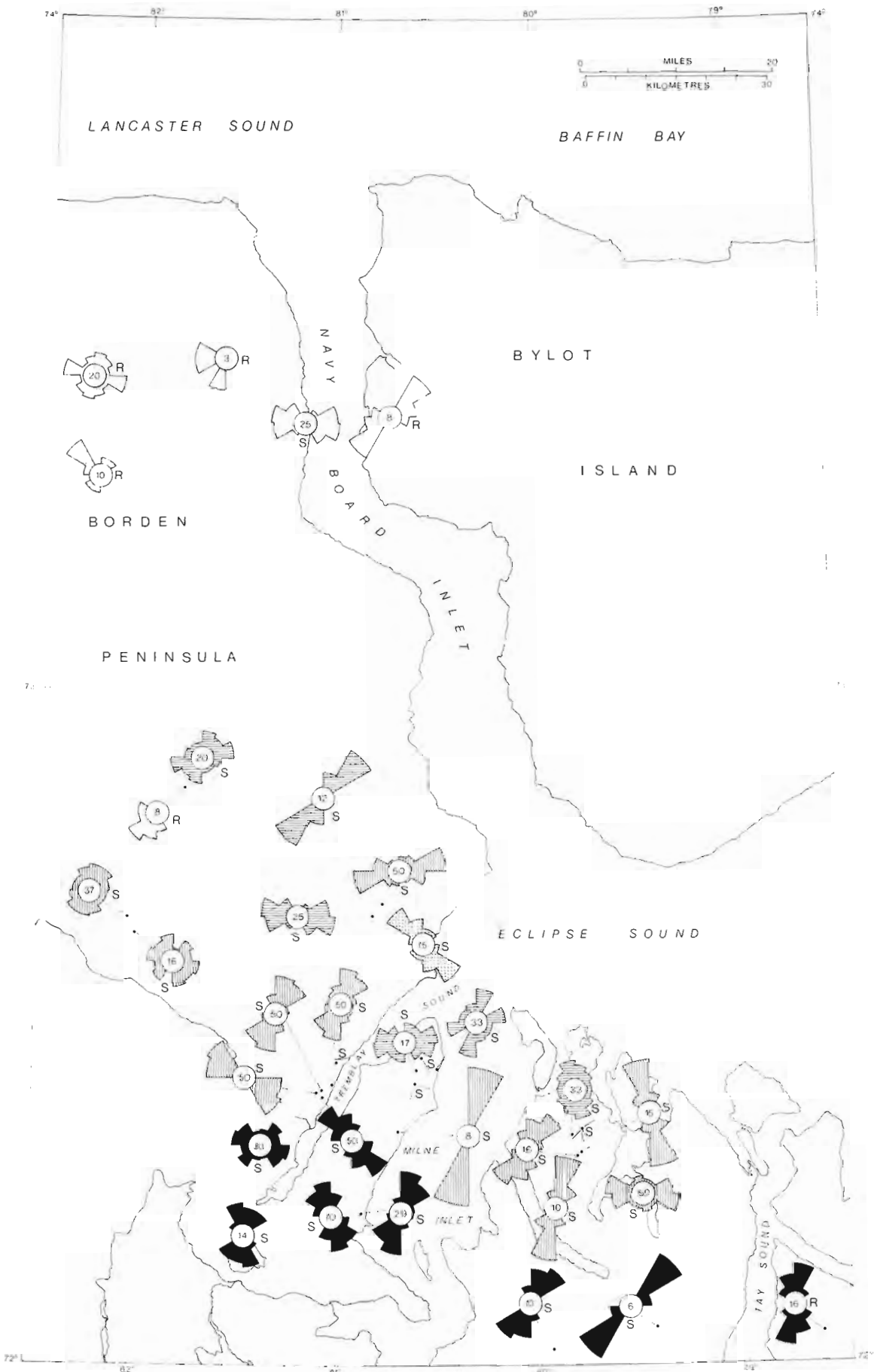


Figure 46.2. Rose diagrams showing measurements for ripplemarks and stromatolites. See Figure 46.1 for legend.

TABLE OF FORMATIONS

HADRYNIAN	Franklin Intrusions: Diabase			
	Intrusive Contact			
	Elwin Fm. (700 m+): Siltstone, quartzarenite, siltstone			
	Gradational			
	Strathcona Sound Fm. (870 m+): Arkose, conglomerate, shale, greywacke			
	Gradational			
	Athole Point Fm. (585 m): Limestone, sandstone, shale			
	Gradational		Gradational to unconformable	
	Victor Bay Fm. (724 m):		VB ₂ : Limestone, dolostone, flat pebble conglomerate VB ₁ : Shale, siltstone, sandstone	
	Gradational?			
ULUKSAN GROUP	Society Cliffs Fm. (825 m+):		SC ₂ : Stromatolitic and massive dolostone	
	Unconformable			
	Fabricius Fiord Fm. (1500 m+)		SC ₁ : Stromatolitic dolostone, shale, sandstone, gypsum	
	FF ₄ : Conglomerate, dolostone			
	FF ₃ : Subarkose		Gradational to unconformable	
	FF ₂ : Shale, quartzarenite		Arctic Bay Fm. (600 m)	
	FF ₁ : Sandstone, shale		AB ₄ : Shale, dolostone AB ₃ : Shale AB ₂ : Shale, quartzarenite AB ₁ : Siltstone, quartzarenite	
	Gradational			
	NEOHELIKIAN?	EQALULIK GROUP	Adams Sound Fm. (340 m):	
			AS ₃ : Quartzarenite, conglomerate	AS _{4,5} : Quartzarenite, conglomerate
AS ₂ : Quartzarenite			AS _U : Quartzarenite AS _L : Quartzarenite, conglomerate	
		AS ₁ : Quartzarenite		
Conformable				
Nauyat Fm. (90 m+)		N ₁ : Basalt N ₂ : Quartzarenite		
Nonconformity				
ARCHEAN-APHEBIAN	Granitic gneiss basement complex			

AB₁ Member

Throughout most of the area this member consists of interbedded green-grey siltstone and quartzarenite and pink-red or grey to white quartzarenite. At the southeast corner of the map area the member is composed of a basal quartz-cobble conglomerate which grades up into interbedded purple-orange to brown-grey quartzarenite, subarkose, quartz-feldspar pebble conglomerate and siltstone. Bimodal-bipolar northwest to southeast paleocurrent trends predominate. Polymodal trends also occur. Thicknesses range from 12 m southeast of Paquet Bay to 36 m west of Tremblay Sound and 15 m east of Elwin Inlet.

AB₂ Member

This member is composed of 5 to 15 coarsening upward cycles, up to 20 m thick each, which are shale dominated west of Milne Inlet and quartzarenite dominated east of Milne Inlet. The lower parts of the cycles are chiefly grey-black shale. The upper parts are green-grey, buff-white, and pink interlayered quartzarenite, subarkose, siltstone, dolostone, and quartz pebble-cobble conglomerate. Paleocurrents include unimodal southwest to northwest trends and polymodal patterns. Thicknesses west of Milne Inlet range from 150 to 261 m and to the east from 65 to more than 100 m.

AB₃ Member

This member comprises black to grey shale. Minor interlayers of dolosiltite, siltstone, and quartzarenite increase in amount of the south and southeast. However, the member increases in thickness from 200 m west of Tremblay Sound to 285 m on the west side of Milne Inlet and more than 400 m east of Elwin Inlet.

AB₄ Member

West of Milne Inlet this member consists chiefly of black-grey shale with thin interbeds of buff-grey to orange-brown siltstone, dolosiltite, stromatolitic dolostone and limestone. Locally, the top 10 m is stromatolitic dolostone. The stromatolites include planar, small mounds, and branching columnar types. Mound and stromatolite elongations indicate paleocurrent trends ranging from northwest-southeast to north, northeast to south and southwest. The member contains more than 112 m on the west side of Milne Inlet. It is 152 m thick at the head of Tremblay Sound, 25 m thick just west of it, and 132 m about 50 km northwest of the head of the Sound. More than 30 m occur east of Elwin Inlet.

East of Milne Inlet the AB₄ member constitutes most of the Arctic Bay Formation. It consists chiefly of over 30, 3-15 m thick, coarsening up cycles whose lower parts are composed of black-grey shale which grades into the upper part composed of interbedded green-grey and orange-buff to brown siltstone, quartzarenite, dolosiltite, stromatolitic dolostone and flat pebble conglomerate. Coarsening-upward arkose-rich wedges or fans occur along the White Bay Fault Zone. Elongate stromatolites indicate northeast to southwest paleocurrent trends. The AB₄ member is over 130 m thick in the Tay Sound area and may be 414 m thick between Tay Sound and Milne Inlet.

Interpretation

Basin transgression initiated in late Adams Sound time continued throughout most of Arctic Bay time. Deposition west of Milne Inlet was under mixed intertidal and subtidal environments. East of Milne Inlet alluvial and delta fans accumulated adjacent to active fault zones and interfingered basinward with alluvial plain and intertidal sediments.

Fabricius Fiord Formation

Fabricius Fiord strata outcrop locally north of the Central Borden Fault Zone. Similar strata outcrop locally south of the White Bay Fault Zone west of Eclipse Sound. Only two of the four subdivisions were examined in 1979.

FF₂ strata consist of about 12 coarsening up cycles in which black-grey shale grades up into interlayered siltstone, and quartzarenite. The FF₂ member grades up into FF₃ interbedded quartzarenite, subarkose and conglomerate which contain trough-crossbeds, current ripples, and synaeresis cracks. Three-metre high crossbeds southwest of Milne Inlet indicate southwest transport. Incomplete sections range from 30 to more than 100 m thick.

Interpretation

The FF₂ and FF₃ strata were deposited in marine influenced delta fan complexes that prograded northward. These strata pass laterally northward into AB₂ to AB₄ basinward facies equivalents.

Society Cliffs Formation

Society Cliffs strata outcrop in a belt from Adams and Strathcona sounds southeast to Tremblay Sound and Paquet Bay. They also outcrop west of southern Navy Board Inlet, east and southeast of Elwin Inlet, and on western and northern Bylot Island. In all of these areas, except for the first-mentioned belt, it is difficult to differentiate Society Cliffs from Victor Bay strata because of the general absence of the lower Victor Bay member (VB₁). Therefore, total thicknesses at these localities are for strata between the Arctic Bay and Strathcona Sound formations.

Laminated to thin bedded, commonly stromatolitic and thick bedded to massive (faintly internally bedded) dolostones predominate in units up to 40 m thick. Thin, flat pebble conglomerate beds are common. Most stromatolites are individual to laterally linked low domal and hemispheroidal types, and columnar types are also present. Cryptalgal laminites are abundant. Bioherms of various sizes are common and varieties 30 to 60 m across are locally abundant. Most elongations of stromatolites and bioherms indicate northeast to southwest paleocurrent trends. Chert has commonly replaced the carbonate rocks and is particularly abundant on Bylot Island where red varieties are common, and east of Milne Inlet where brown and black varieties are common. Dolomitization and brecciation has obscured primary structures in much of the rock. Petroliferous odours and specks of black bituminous material are common. Disseminated pyrite occurs locally. Sedimentary structures include tepees, molar tooth, wave ripple marks, synaeresis and dessication cracks, convoluted to disrupted beds, dewatering structures, load casts, scours, local unconformities, soft sediment deformation, vugs, and microfaults.

The Society Cliffs Formation is about 665 m thick at the head of Tremblay Sound. Partial sections indicate thicknesses of 825 m near the mouth of Tremblay Sound, 345 m east of Milne Inlet, 450 m thick east of Elwin Inlet, and about 750 m on western Bylot Island. The formation is conformable with the overlying Victor Bay Formation. Two members have been differentiated.

SC₁ Member

West of Milne Inlet a 10 to 15 m thick lower unit contains pebbly calcareous quartzarenite to sublitharenite interlayered with stromatolitic dolostone, limestone, and flat pebble conglomerate. This unit is overlain by two 120 m thick internally cyclic shallowing upward sequences containing shale, brown-grey stromatolitic dolostone and flat

pebble conglomerate or breccia. This member thins abruptly northwestward and ranges from 165 to more than 315 m in the vicinity of Tremblay Sound, to 45 m west of Tremblay Sound, and 15 m east of Elwin Inlet.

East of Milne Inlet and on Bylot Island the SC₁ member is relatively thick due to the presence of black shale and redbed sequences interbedded with grey to brown-grey, black-grey, green-grey and pale pink dolostones. The shaly units contain interbedded purple to red, green, black, brown and grey shale, dolostone, calcareous quartzarenite and subarkose. A few white gypsum beds occur east of Milne Inlet and are extensively developed on Bylot Island. The gypsum rarely occurs in beds more than 1 m thick. At one locality on western Bylot Island gypsum is abundant throughout the lower 240 m of the formation and occurs interbedded with shales and dolostones in units up to 40 m thick. Salt casts occur locally. East of Milne Inlet measured thicknesses, most incomplete, range from 75 to 165 m. On western Bylot Island the gypsiferous zone, which may contain as much as 20 per cent gypsum, is over 240 m thick and the SC₁ member may be at least 380 feet thick.

SC₂ Member

This member consists chiefly of grey to brown-grey dolostones as already described for the formation. Beds of red and green shale, siltstone and arkose, occur throughout the member on Bylot Island and in the Tay Sound area, and are accompanied by hematite staining of the associated strata. About 250 m are present in the Tay Sound area. Elsewhere, incomplete sections indicate thicknesses of 660 m west of Milne Inlet, 370 m on western Bylot Island and west of Tremblay Sound, and 450 m east of Elwin Inlet.

Interpretation

West of Milne Inlet the formation was deposited in shallow subtidal to intertidal environments, whereas to the east of the inlet and on Bylot Island it originated in an environment that varied from alluvial plain to shallow subtidal. The gypsiferous units probably represent coastal sabkha evaporites.

Victor Bay Formation

The Victor Bay Formation outcrops in the same general areas as the Society Cliffs Formation. It is about 460 to 640 m thick 50 m northwest of Tremblay Sound, 724 m east of Milne Inlet, and 423 m west of southern Navy Board Inlet. It is divisible into two members in the southern part of the area. The lower member (VB₁) is absent west of Eclipse Sound and in most of the northern part of the area. In these localities it is very difficult to separate the SC₂ from the VB₂ member.

VB₁ Member

Grey to black and brownish grey laminated to very thin bedded shale, calcareous to dolomitic shale, siltstone, dololomite and dolosiltite predominate in this member. Minor graphitic shale, quartzwacke, quartzarenite and subarkose, flat pebble carbonate conglomerate and pyrite laminae, occur locally. Scour channels, soft sediment deformation, crossbeds, ripple marks, syneresis cracks; and molar tooth, load, and ball and pillow structures are rare.

The VB₁ member is 170 to 370 m thick 50 km northwest of Tremblay Sound, 100 to 140 m 15 km west of Tremblay Sound, 15 m along northern Tremblay Sound, 120 m west of Eclipse Sound and 44 m east of Milne Inlet.

VB₂ Member

This member is composed of various light to dark grey and black limestone and dolostone lithologies that occur in 1 to 20 m thick units (rarely as thick as 55 m). East of Milne Inlet, for example, the lower 200 m are chiefly limestones, the upper 260 m are chiefly dolomites, and the middle 220 m contain both. Petroliferous odours are most common in the limestone. Major lithologies are flat pebble-boulder conglomerate, laminated to very thick bedded carbonates, stromatolitic carbonate, cryptalgal laminites, lumpy bedded carbonate, evenly nodular carbonate, and vuggy carbonate. Minor round clast conglomerate, "turbidite" units, shale and replacement chert, are common. Lenses of quartzarenite, quartzwacke and subarkose occur locally.

Stromatolites occur individually and in bioherms up to 1.5 km in length. Individual and laterally linked hemispheroidal and columnar and digitate columnar types are the most common. Hemispheroidal stromatolites are elongated in predominantly east-west to northeast-southwest directions at several localities (Fig. 46.2). Other common structures are molar tooth, teepee, rip-up clasts, scour channels, syneresis and desiccation cracks, load casts, convoluted beds, soft sediment folds, dewatering structures, birds eye structures, ripple marks, crossbeds, and microfaults.

Thickness for the VB₂ member are: about 290 m 50 km west of Tremblay Sound, 470 m 15 km west of Tremblay Sound, 680 m east of Milne Inlet, 300 m west of Eclipse Sound and 450 m east of Elwin Inlet. VB₁ and VB₂ members are conformable and interfinger at most localities. However, a local disconformity may occur at the contact 50 km west of Tremblay Sound where 10 m of round clast limestone conglomerate occurs at the base of VB₂.

Interpretation

Most of the VB₁ member was probably deposited under subtidal conditions. Influx of fine terrigenous clastic material probably prevented algal growth. The upper (VB₂) member was probably deposited under chiefly shallow subtidal to intertidal conditions.

Athole Point Formation

Athole Point Formation outcrops from east of Milne Inlet to about 50 km northwest of Tremblay Sound. Medium to dark grey and black laminated to medium bedded limestones, cryptalgal laminites and stromatolitic limestones predominate in units 2 to 40 m thick. Minor lithologies include lumpy bedded carbonates and flat-pebble and round-clast conglomerates. At least one "debris-flow" carbonate breccia bed occurs near the base of the formation east of Milne Inlet. Orange-weathered 1 to 10 m thick siliceous carbonate beds occur sparsely throughout the formation. Stromatolites other than planar types are relatively uncommon, but include low domal hemispheroidal and small columnar types as well as bioherms. Carbonate-cemented sandstone, quartzarenite, sublitharenite, subarkose, shale, siltstone, and flat-pebble conglomerate occur chiefly in the upper part of the formation in fining upward turbidite sequences, and become increasingly abundant northwestward. Observed structures include graded beds, flutes, load casts, flame structures, small scale crossbeds, syneresis and desiccation cracks, soft sediment deformation channels, scours, birds eye structures, convoluted beds, molar tooth, tepees, concretionary structures, and microfaults. Unimodal crossbeds indicate west-northwesterly transport.

Athole Point Formation may be divided into a lower member containing abundant cryptalgal laminites and an upper member in which turbidite sequences are common. The formation is probably about 500-585 m thick in the vicinity of Milne Inlet and thins westward and abruptly northward. It is conformable with both the underlying Victor Bay and overlying Strathcona Sound Formation.

Interpretation

Most of the strata were probably deposited in intertidal to subtidal environments with relatively deep water lying to

the south. The formation is considered to be the seaward equivalent of the lower and possible middle parts of the Strathcona Sound Formation with which it interfingers laterally.

Strathcona Sound Formation

This formation outcrops chiefly in a broad belt south of the White Bay Fault Zone west of Eclipse Sound. It also underlies small areas between Elwin Inlet and northern Navy Board Inlet and on western Bylot Island.

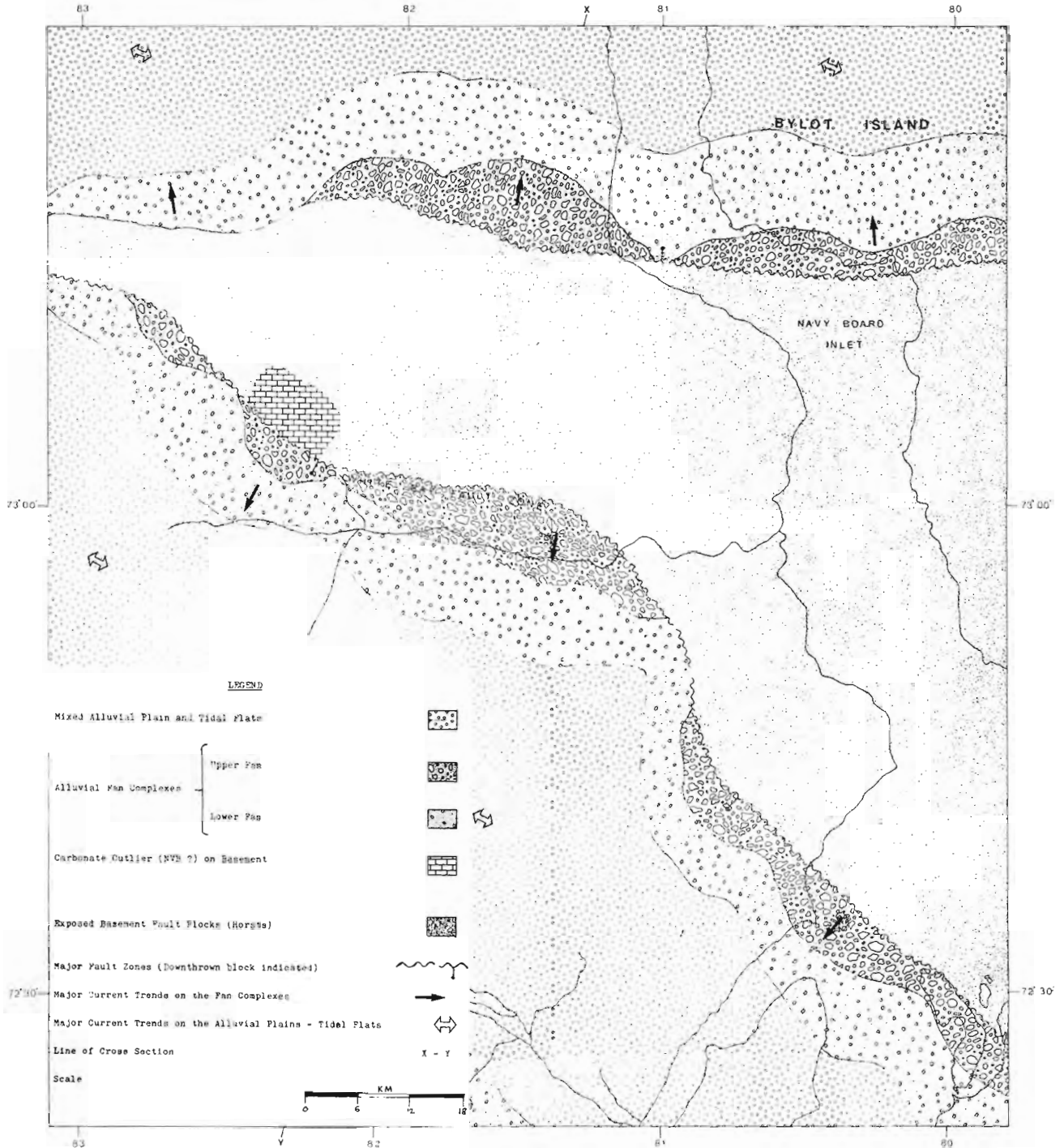


Figure 46.3. Tentative reconstruction of facies distribution around basement fault blocks during the early depositional history of the Strathcona Sound Formation.

Most of the strata are laminated to thin bedded, although many are medium to very thick bedded. The various lithologies occur chiefly in alternating units from 1 to 20 m thick, but which range to more than 100 m thick. These units may contain a single lithology or may contain several interbedded lithologies. Fining upward sequences predominate. Sedimentary structures include graded bedding, trough, planar and herringbone crossbeds, ripple marks, imbricated clasts, soft sediment folds, slump features, convoluted and disrupted beds, scours, channels, flutes, sphaeresis cracks, and microfaults.

Paleocurrent trends adjacent to and south of the White Bay Fault Zone are moderately unimodal and indicate chiefly southerly to westerly transport. North of the fault they range from unimodal to bimodal and polymodal, and indicate chiefly northerly to easterly transport west of Navy Board Inlet and southwesterly transport on western Bylot Island.

More than 110 m of grey interlayered siltstone, sandstone, fine calcareous clastics, and limestone form the basal member of the Strathcona Sound Formation about 50 km west of Eclipse Sound. This unit thins northward to about 40 m locally near the White Bay Fault Zone. It seems to be absent north of the fault zone. It represents a transition zone between the Victor Bay, Athole Point and Strathcona Sound sediments.

In the same region west of Eclipse Sound these strata are overlain by more than 400 m of grey, brown, green and chiefly red shale, siltstone, feldspathic wacke, and arkose. The sandstones commonly have a calcareous matrix. One or more beds or lenses of oligomictic angular clast carbonate breccia in the lower part of this member probably are debris flow breccias. These strata are overlain by grey-green, coarse calcareous feldspathic wacke and minor polymictic conglomerate.

Northward, adjacent to the White Bay Fault Zone, more than 870 m of Strathcona Sound strata are composed chiefly of red arkoses and polymictic conglomerates that contain carbonate clasts and clasts from the basement complex in varying proportions. Flat pebble conglomerate and oligomictic carbonate conglomerate clasts occur locally (Fig. 46.3, 46.4). The conglomerates are absent from the lower 170 m in some places but in others are interbedded throughout the formation. At one locality more than 186 m of chiefly oligomictic carbonate conglomerate rests directly on the Society Cliffs-Victor Bay Formation and contains clasts up to 10 m across. The upper part of the formation is chiefly conglomerate as described above.

Strathcona Sound strata west of northern Navy Board Inlet are similar to the strata west of Eclipse Sound above the basal grey siltstone member and includes a debris-flow breccia in the lower part of the section. Bylot Island strata are also similar, but red arkose predominates in the basal part, and contains crossbeds more than 3 m high. Orange weathering, locally stromatolitic carbonate beds range up to 10 m thick and occur sparsely throughout the Bylot Island strata which are more than 365 m thick.

Interpretation

The boulder conglomerates and arkoses adjacent to the White Bay Fault Zone probably represent alluvial fan complexes that were deposited rapidly along an active fault (Fig. 46.3, 46.4). These deposits interfinger with the shales, siltstones and sandstones to the south, which represent alluvial plain and mixed alluvial and intertidal to shallow subtidal deposition. The alluvial deposits may include minor channel deposits.

Elwin Formation

These strata outcrop from northern Navy Board Inlet west to Elwin Inlet. In the east they consist chiefly of red to minor green arkose, siltstone and shale interbedded with buff sandstone, white quartzarenite and grey to buff and light red sandy to stromatolitic dolostone. Stromatolites include planar, low domal and hemispheroidal types. Some dolostone beds are brecciated at the top. The strata are laminated to medium bedded and occur in lithological units 1 to 20 m thick. Most of the redbed strata occur in sequences 5-130 m thick separated by 8-50 m thick sequences of grey to green strata. Both sequences are cyclic. Carbonate strata seem to decrease in abundance upward as well as toward the west, whereas the proportion of white quartzarenite and buff sandstone seems to increase westward. Frosted sand grains are common in the sandstones and dolostones.

Cycles within the redbed sequences are 2-40 m thick and commonly consist of lower arkose-shale that grades upward into dolostone. A less common cycle contains basal arkose that grades upward into quartzarenite which grades into dolostone. Shale may occur above or below the latter dolostone as part of the cycle. Cycles in the grey to green sequences include arkose or quartzarenite grading upward into siltstone or dolostone.

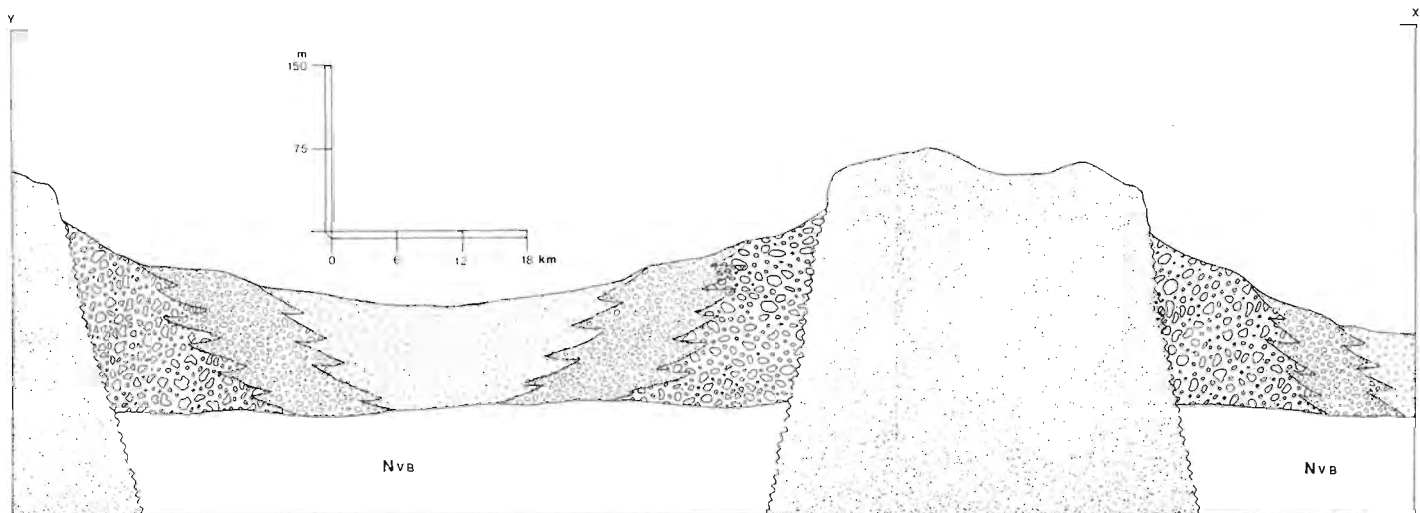


Figure 46.4. Cross-section along the line X-Y in Figure 46.3. Legend as in Figure 46.3.

Sedimentary structures include trough crossbeds (some 2 m), planar crossbeds, ripple marks, synaeresis and desiccation cracks, local unconformities, microfaults, tepees, dewatering structures, birds eye structure, channels, stylolites, oolites and pisolites, shale chips and rip-up clasts, ball and pillows, flutes, soft sediment folds and convoluted beds. Crossbed measurements indicate unimodal to bimodal and weakly bipolar patterns which indicate chiefly westerly and northerly transport. Stromatolite and ripple measurement indicate chiefly east-west paleocurrents.

The Elwin Formation is at least 470 m thick on the west side of Navy Board Inlet. The lower contact with the Strathcona Sound Formation is conformable and possibly gradational. A low-angle unconformity separates the Elwin from overlying Lower Paleozoic strata.

Interpretation

Most of the strata were probably deposited in locales that ranged from alluvial plain to intertidal. Some channel deposits are present and some aeolian deposits may be present in both the Elwin and Strathcona formations.

Notes

There is little evidence that Adams Sound deposition was significantly affected by contemporaneous faulting, although the association of Nauyat basalt with major fault zones suggests that some rifting had already occurred in early Adams Sound time. The onlap of Arctic Bay strata onto basement gneisses in the Tay Sound region supports this. Faulting was active during Arctic Bay sedimentation, at which time the effects of movement along the Central Borden Fault Zone were greater than for the White Bay Fault Zone. The reverse seems to have been true in Strathcona Sound time. Also, the Byam Martin Mountain High does not seem to have been significantly uplifted until late or post Society Cliffs time.

Paleocurrent measurements crudely outline portions of the Milne Inlet and Eclipse troughs. The facies changes in the Milne Inlet area, and the fact that the known westerly extent of Society Cliffs gypsiferous redbeds is a north-northwesterly trending line, suggest that some syndepositional faulting may have occurred in a north-south direction and that the Borden Peninsula component of the Navy Board High may have been an island. This is supported by a few paleocurrent measurements.

Acknowledgments

Excellent assistance in the field was provided by L.M. Cumming of the Geological Survey of Canada, Valerie Gislason of Toronto University, Leslie MacLaren of Queen's University, John McEwen of Atomic Energy of Canada Limited, and Beverlee McLean of Georgian College.

The authors are grateful to Polar Continental Shelf for their excellent logistical support. We are also grateful to John Rogers, Project Manager for Nanisivik Mines Ltd., and Lionel Thorpe, the company's geologist, for making maps and drill core available and for supporting a brief examination of mine geology.

References

- Blackadar, R.G.
1970: Precambrian geology northwestern Baffin Island, District of Franklin; Geological Survey of Canada, Bulletin 191, 89 p.
- Galley, A.
1978: The petrology and chemistry of the Nauyat Formation volcanics, Borden Peninsula, Northwestern Baffin Island; unpublished B.Sc. Thesis, Carleton University, 53 p.
- Geldsetzer, H.
1973a: Syngenetic dolomitization and sulfide mineralization; in *Ores in Sediments*, G.G. Amstutz and A.J. Bernard, ed., Springer-Verlag, p. 115-127.
1973b: The tectono-sedimentary development of an algal-dominated Helikian succession on northern Baffin Island, N.W.T.; in *Symposium on Arctic Geology*, Geological Association of Canada, Memoir 19, p. 99-126.
- Iannelli, T.R.
1979: Stratigraphy and depositional history of some upper Proterozoic sedimentary rocks on northwestern Baffin Island, District of Franklin; in *Current Research, Part A*, Geological Survey of Canada, Paper 79-1A, p. 45-56.
- Jackson, G.D. and Davidson, A.
1975: Bylot Island map-area, District of Franklin; Geological Survey of Canada, Paper 74-29 12 p.
- Jackson, G.D., Davidson, A., and Morgan, W.C.
1975: Geology of the Pond Inlet map-area, Baffin Island, District of Franklin; Geological Survey of Canada, Paper 74-75, 33 p.
- Jackson, G.D., Iannelli, T.R., Narbonne, G.M. and Wallace, P.J.
1978: Upper Proterozoic sedimentary and volcanic rocks of northwestern Baffin Island; Geological Survey of Canada, Paper 78-14, 15 p.
- Lemon, R.R.H. and Blackadar, R.G.
1963: Admiralty Inlet area, Baffin Island, District of Franklin; Geological Survey of Canada, Memoir 328, 84 p.
- Olson, R.A.
1977: Geology and genesis of zinc-lead deposits within a late Precambrian dolomite, northern Baffin Island, N.W.T.; unpublished Ph.D. Thesis, University of British Columbia, 371 p.

Project 760058

S.A. Edlund
Terrain Sciences Division

Edlund, S.A., *Vegetation of Lougheed Island, District of Franklin; in Current Research, Part A, Geological Survey of Canada, Paper 80-1A, p. 329-333, 1980.*

Abstract

The nature of the flora and the relationships between plant communities and the surficial materials on Lougheed Island were studied. Thirty-three vascular species were identified. Most communities are dominated by monocotyledons. Several *Luzula*-based communities occur on sandy materials; grass-based communities, primarily dominated by *Alopecurus alpinus* and *Puccinellia* species occur on fine grained materials. *Saxifraga oppositifolia*-based communities are restricted to materials with significant calcareous components. For each type of material, moisture content determines which type of community is present.

Introduction

Three weeks (mid July to early August 1979) were spent on Lougheed Island, in the northwestern Queen Elizabeth Islands (Fig. 47.1), studying the interrelationships between plant communities and the various surficial materials. This project was carried out in conjunction with mapping of surficial materials by D.A. Hodgson.

Travel about the island was on foot and by Honda 90 ATC. Seventy-five sites were reached from two camps.

Lougheed Island is a north-south elongated, low-lying island (70 km long, 20 km average width) developed on poorly consolidated Cretaceous sandstone, siltstone, and shale (Balkwill et al., 1977). The central part of the island has gently rolling topography (maximum elevation ca. 140 m). The coastal margins are generally gently sloping and of low relief.

The island shows evidence of Quaternary glaciation, including an esker in the southeastern part of the island, drumlinoid features on the west side, and the widespread presence of erratics, including limestone, igneous, and metamorphic granule to boulder sized materials.

The island was largely submerged during higher sea levels of the late Pleistocene and early Holocene, for marine deposits occur over much of the island and marine shells have been collected at elevations of more than 100 m.

Acknowledgments

The logistical support of Polar Continental Shelf Project is gratefully acknowledged. Appreciation is also extended to F.M. Nixon and D.A. Hodgson for plant observations, collections, and discussions in the field.

Previous Biological Studies

Little has been written on the vegetation or wildlife of Lougheed Island. Stephansson (1921) noted that the vegetation was abundant on the southern and western parts of the island and that this vegetation supported a sizeable caribou population. Macpherson (1961) recorded estimates made by R. Thorsteinsson in 1955 and 1959 of 300 caribou on Lougheed Island; Miller and Russell (1974) saw only 30 caribou. During the three weeks we travelled around the island, only four caribou were seen together with numerous well picked-over carcasses.

Glenister and Thorsteinsson (1963) reported that the vegetation was primarily grasses, lichens, and mosses; they observed no shrubs. Savile (1961) stopped briefly on the

northeastern part of the island and observed *Alopecurus alpinus* and *Saxifraga oppositifolia*. These were the first species recorded for the island and until the present study the only species information available.

General Remarks on Vegetation

The vascular flora of Lougheed Island is small, only 33 species in total, all present at both ends of the island (Appendix I; taxonomic nomenclature follows Porsild, 1964). Grass-like species dominate the vascular plant component of most plant communities, namely the rushes *Luzula confusa* and *L. nivalis* and the grasses *Alopecurus alpinus* and *Puccinellia* species. Caryophyllaceae and Saxifragaceae are the most abundant and diverse dicotyledonous families. No shrubs, Cyperaceae, or aquatic species were found.

Despite the low number of vascular species, the per cent cover of vegetation can be high (greater than 75 per cent cover, Fig. 47.1), where dark soil lichens (patina) and a few mosses are present. From the air this nearly continuous lower stratum gives the terrain a dark appearance. Areas without this lower cryptogamic stratum are generally poorly vegetated, usually less than 20 per cent cover. This "all or nothing" phenomenon of vegetation cover occurs on other high arctic islands as well. Vegetation cover between 20 and 75 per cent is too localized to be shown on Figure 47.1.

The reduced vascular flora and the absence of shrubs that are present on similar materials on southern Amund Ringnes, Cornwall and Graham islands (Hodgson and Edlund, 1975, 1978) and southern Sabine Peninsula (Barnett et al., 1975) indicate that this island belongs entirely in Zone I, the most severe of the high arctic bioclimatic subdivisions described by Hodgson and Edlund (1978).

Surficial Materials and Plant Communities

Though the island is underlain by Cretaceous rocks, a substantial area is covered by Quaternary glacial, glacio-marine, fluvial, and eolian material. Soil development is minimal in this region so that the plants are rooted directly in unaltered or physically weathered material. The nature and composition of the materials, therefore, have a great influence on the vegetation.

Bedrock

Weathered and unweathered rock is commonly exposed at higher elevations, and in stream cuts and in headwalls of nivation hollows at lower elevations. Vegetation is generally sparse, but there are definite patterns to the plant groups found on the various rock types.

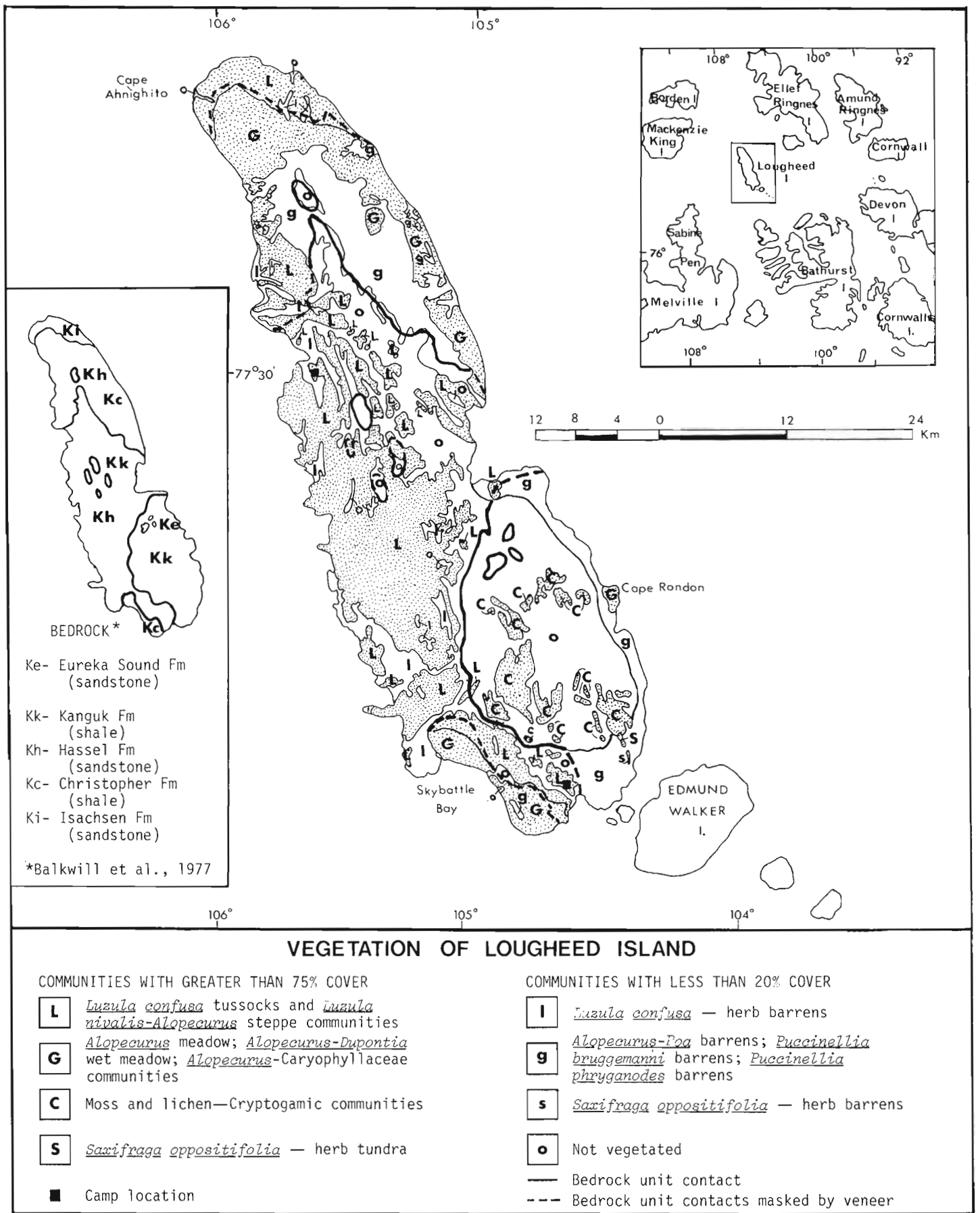


Figure 47.1. Vegetation of Lougheed Island.

Shale. One of the most striking illustrations of the influence of bedrock composition on vegetation can be seen by comparing vegetation on shales of the Christopher and Kanguk formations.

Christopher Formation weathers into fine silts and clays and supports grass communities. Sparse *Alopecurus alpinus*, *Colpodium vahlianus*, and *Poa* species are the most common plants on well drained materials. On lower slopes and in valleys and depressions where drainage is poor, *Alopecurus* is the dominant grass (usually less than 5 per cent cover). A lower stratum of patina and mosses is commonly found. Caryophyllaceae, Saxifragaceae, and *Papaver radicum* are sporadic associates. This assemblage of plants is also found on the Christopher Formation on Sabine Peninsula, Melville Island (Barnett et al., 1975), and on the Ringnes Islands (Hodgson and Edlund, 1978).

Fine grained Kanguk Formation is unvegetated, regardless of the moisture regime; this was also observed on Kanguk Formation on Amund Ringnes Island. The shale is extremely acidic and probably inhibits plant growth; only where there is a marine or glaciomarine veneer over the bedrock do plants grow.

Sandstone. The Hassel Formation is predominantly a poorly consolidated sandstone which includes thin shale beds. Unconsolidated sand weathered from the Hassel Formation is present on hilltops and ridges in the central part of the island. The sand is generally well drained and prone to deflation. Some of the weathered surface is covered by a thin, red-weathering sandstone and siltstone lag deposit. Although the sands are commonly unvegetated, the lichen *Cornicularia divergens* attaches to the lag pebbles in a few places. Locally *Luzula confusa*, *Papaver radicum*, and other herbs occur sporadically. Only in sheltered locations where moisture is retained, such as snowmelt seepage slopes, are there places with continuous vegetation. Such areas are dominated by *Luzula*-patina communities described in greater detail below.

In a few places where fine grained material is present at the surface, sparse grasses and a variety of Caryophyllaceae occur, including *Alopecurus*, *Puccinellia* species, *Poa glauca*, *Stellaria longipes*, *Cerastium arcticum*, *C. regelii*, *Arenaria rossii*, *Saxifraga caespitosa*, and *Papaver radicum*.

Sandstones from the Isachsen and Eureka Sound formations were not visited. It is probable, however, that these outcrops are extremely poorly vegetated or unvegetated, as is the case on Sabine Peninsula and the Ringnes Islands. Communities present are probably *Luzula* based.

Quaternary Deposits

Much of the bedrock of Loughheed Island is masked by a variety of unconsolidated Quaternary materials from several metres to less than a metre thick. Included are fine to coarse grained glacial deposits, silt and clay of glaciomarine and offshore marine sediments, beach sands, sand to fine grained deltaic deposits, and modern fluvial sediments. These materials are generally moderately or poorly drained. Saturated soils are common; however, ponding is rare and extremely localized.

Sands. Sandy Quaternary materials, including fluvial and some deltaic and nearshore deposits, are derived primarily from Hassel Formation sandstone. These deposits are among the most heavily vegetated materials on the island where depositional processes are not currently active. Communities are primarily *Luzula* based, with a nearly

continuous lower stratum of patina and *Polytrichum* moss. *Luzula confusa* is the dominant vascular plant of moderately to well drained sites; *Luzula* cover is typically drained 5 to 15 per cent. *Potentilla hyparctica*, *Luzula nivalis*, *Alopecurus alpinus*, *Papaver radicum*, *Draba* species, and *Stellaria longipes* are common associates. *Luzula confusa* tussocks can be extremely dense (25 to 50 per cent cover) in areas adjacent to current eolian activity.

On imperfectly drained sands, *Luzula nivalis* is the dominant vascular plant and *Alopecurus alpinus* is a common associate. The moss component of the nearly continuous lower stratum is thicker and includes *Polytrichum*, *Rhacomitrium lanuginosum*, and *Aulacomnium*.

Standing water is rare on Quaternary sand, but in the few areas where it is present, there are pure bryophytic communities and *Alopecurus* - *Dupontia fisheri* communities with a dense bryophytic lower stratum. Other vascular species are rare.

Silty sand, particularly common as a fluvial deposit overlying the Kanguk Formation, appears barren; however, close examination commonly revealed small clumps of *Puccinellia bruggemanni* (1 to 10 per cent cover) partially masked by a layer of fine eolian sand. The only other vegetation rarely observed on this material was *Papaver radicum*.

On sand and silty sand near the modern shoreline, sparse, sporadic *Puccinellia phryganodes* halophytic communities occur. In zones where ice thrust is common this community may occur immediately inshore of the ice thrust features.

Silt and Clay. Silt and loamy clay, commonly including granule or larger sized clasts are widespread. These materials of marine, glaciomarine, and glacial origin are commonly covered by continuous vegetation. They are poorly drained for the most part, and where relief is slight, such as on broad ridge tops, the materials are frequently saturated. Only on moderate and steep slopes do materials appear to be moderately to well drained.

Where this veneer overlies Kanguk Formation shale, communities are essentially cryptogamic. Vascular plants are poorly represented (usually less than 5 per cent) by *Alopecurus alpinus* and *Puccinellia bruggemanni* and rarely *Luzula nivalis*. Scattered thermokarst ponds commonly are surrounded by dense bryophytic mats; *Alopecurus alpinus* and *Dupontia fisheri* can be found locally on raised moss hummocks at the pond edges, along with rarer *Saxifraga nivalis*, *S. tenuis*, and *S. cernua*. On moderate to steep slopes, the vegetation is much more varied; *Saxifraga oppositifolia*, the above Saxifrages, *Papaver radicum*, *Stellaria longipes*, and *Cerastium arcticum* appear in conjunction with *Alopecurus alpinus*.

Over Hassel Formation sandstone, poorly drained silt and clay veneers support *Luzula nivalis* communities, with *Alopecurus* usually co-dominant. *Juncus biglumis*, *Puccinellia bruggemanni*, *Saxifraga nivalis*, *S. tenuis*, *S. cernua* and *S. caespitosa* are common associates. On saturated materials *Puccinellia bruggemanni* and *Alopecurus alpinus* are commonly the only vascular plants. A moss-patina lower stratum is nearly continuous on such materials. On better drained slopes of fine grained material, the highest diversity of vascular plants on the island occurs. In addition to the expected *Luzula* species and *Alopecurus*, six saxifrages, *Potentilla hyparctica*, *Cochlearia officinalis*, *Cardamine bellidifolia*, *Draba* species, *Papaver radicum*, four Caryophyllaceae, and two *Ranunculus* species commonly occur.

Alopecurus alpinus is the dominant vascular plant where marine silt and clay overlie Christopher Formation shale,

Table 47.1

Relationships between plant communities, moisture regime, and surficial materials

Dominant Plant Community	Surficial Material	Moisture Regime
<u>BEDROCK</u>		
1. <i>Alopecurus-Poa</i> barrens	Shale (Kc)	Dry
2. <i>Luzula confusa</i> barrens	Sandstone (Kh, Ke, Ki)	Dry
3. Unvegetated	Shale (Kk)	Dry to wet
<u>QUATERNARY DEPOSITS</u>		
4. <i>Luzula confusa</i> barrens	Sand	Dry
5. <i>Luzula nivalis</i> - <i>Alopecurus</i> steppe	Sand	Moderately to imperfectly drained
6. <i>Alopecurus-Poa</i> barrens	Silt and clay	Dry
7. <i>Alopecurus-Caryophyllaceae</i> tundra	Silt and clay	Moderately drained
8. <i>Alopecurus-Puccinellia</i> steppe	Silt and clay	Imperfectly drained to saturated
9. <i>Alopecurus-Dupontia</i> wet meadow	Sand, silt, and clay	Saturated; around ponds and seepage slopes
10. <i>Puccinellia phryganodes</i> barrens	Sand and silty sand	Imperfectly drained shoreline
11. <i>Saxifraga oppositifolia</i> barrens	Calcareous gravelly sand	Dry
12. <i>Saxifraga oppositifolia</i> moss tundra	Calcareous gravelly sand	Imperfectly drained

regardless of the moisture regime. Imperfectly and poorly drained materials are the most common and these support *Alopecurus* meadows with a nearly continuous moss-patina lower stratum. *Luzula nivalis* is a rare component of this community. *Puccinellia bruggemanni* appears on the saturated materials with *Alopecurus*. Moderately well drained materials have *Alopecurus-Caryophyllaceae* communities. *Cerastium regelii* and *Stellaria longipes* are common associates, along with scattered clumps of *Saxifraga oppositifolia*. The driest materials have a sparse *Alopecurus-Poa* barrens similar to that on Christopher Formation outcrop.

Gravel and Gravelly Sand. An esker-like ridge at the southeast extremity of the island is composed of gravelly sand armoured with granule to boulder sized materials of local and exotic lithologies; there is a substantial limestone component. Fine grained glaciomarine deposits overlap all but the ridge crest and are vegetated with *Luzula* and *Alopecurus* communities; however, on the ridge crest *Saxifraga oppositifolia* communities appear. The driest materials support *Saxifraga oppositifolia* - herb barrens with *Luzula confusa*, *Poa abbreviata*, *Alopecurus alpinus*, *Ranunculus sabinei*, *Potentilla hyparctica*, *Draba* species, and *Papaver radiculatum* as associates. On the moderately to imperfectly drained materials *Saxifraga oppositifolia* (5 to 25 per cent cover) is the dominant vascular plant component, and there is a dense moss-patina lower stratum.

These gravels are the only materials on the island that support purple saxifrage communities. This is probably due to the presence of calcareous erratics, for purple saxifrage communities are common on slightly to moderately calcareous materials on other high arctic islands.

Table 47.1 summarizes the interrelationships between plant community and surficial materials. For a given material, the moisture regime determines which community dominates.

Luzula-based communities are the most common plant communities on Loughed Island. These are found primarily on sandy sediments derived from Hassel Formation sandstone and on veneers of Quaternary sediments over sandstone. *Luzula confusa* communities occur on the drier aspects, whereas *Luzula nivalis* - *Alopecurus* communities favour less well drained sites.

Grass-based communities are found on fine grained Christopher Formation shale and glaciomarine deposits. Sparse *Alopecurus-Poa* barrens occur on dry silt and clay. On moderately drained surfaces *Alopecurus-Caryophyllaceae* communities occur. *Alopecurus* meadows dominate the poorly drained materials.

Alopecurus - Puccinellia bruggemanni communities occur on both saturated sands and saturated fine grained materials. In the few places that ponding occurs, *Alopecurus-Dupontia* wet meadow communities, with a dense bryophytic lower stratum, occur near the water margin.

Kanguk Formation shale is devoid of vegetation, regardless of the moisture regime. In regions where material derived from this shale are mixed with sand, and eolian processes are active, sparse *Puccinellia bruggemanni* tussocks occur.

Purple saxifrage (*Saxifraga oppositifolia*) communities occur on the probable glacial deposits where there are significant calcareous erratics.

Puccinellia phryganodes halophytic communities occur sporadically on sand and sandy silt at the coast.

The plant communities and variety of vascular plant species on Loughheed Island are similar to adjacent islands, notably northern Amund Ringnes Island, northern Sabine Peninsula, and King Christian Island, where similar surficial materials occur. On Loughheed Island, however, there is a higher total per cent cover than on these other islands; this is probably due to the extent to which glaciomarine and marine veneers blanket the island.

References

- Balkwill, H.P., Hopkins, W.S., Jr., and Wall, J.H.
1977: Loughheed Island and neighboring small islands, District of Franklin; in Report of Activities, Part B, Geological Survey of Canada, Paper 77-1B, p. 181-183.
- Barnett, D.M., Edlund, S.A., Dredge, L.A., Thomas, D.C. and Prevett, L.S.
1975: Terrain classification and evaluation, Melville Island, N.W.T.; Geological Survey of Canada, Open File 252.
- Glenister, B.F. and Thorsteinsson, R.
1963: Southern Loughheed Island; in Geology of the North-central Part of the Arctic Archipelago, Northwest Territories (Operation Franklin), Y.O. Fortier, et al.; Geological Survey of Canada, Memoir 320, p. 571-575.
- Hodgson, D.A. and Edlund, S.A.
1975: Surficial materials and biophysical regions, eastern Queen Elizabeth Islands: Part I; Geological Survey of Canada, Open File 265.
1978: Surficial materials and vegetation, Amund Ringnes and Cornwall islands, District of Franklin; Geological Survey of Canada, Open File 541.
- Macpherson, A.H.
1961: On the abundance and distribution of certain mammals in the western Canadian Islands in 1958-59; Arctic Circular, no. 14, p. 1-17.
- Miller, F.L. and Russell, R.H.
1974: Aerial survey of Peary caribou and muskoxen on western Queen Elizabeth Islands, N.W.T.; Canadian Wildlife Service Progress Notes 40; 18 p.
- Porsild, A.E.
1964: Illustrated Flora of the Canadian Arctic Archipelago; National Museum of Canada Bulletin 146, 2nd edition, 218 p.
- Savile, D.B.O.
1961: The botany of the northwestern Queen Elizabeth Islands; Canadian Journal of Botany, v. 39, p. 909-942.
- Stefansson, V.
1921: The Friendly Arctic; New York, MacMillan Co., 784 p.

APPENDIX I

Vascular species of Loughheed Island

Alopecurus alpinus, *Poa abbreviata*, *P. alpigena*, *P. hartzii*, *P. glauca*, *Colpodium vahlium*, *Puccinellia angustata*, *P. phryganodes*, *P. bruggemanni*, *Dupontia fisheri*, *Juncus biglumis*, *Luzula confusa*, *L. nivalis*, *Oxyria digyna*, *Papaver radicum*, *Arenaria rossii*, *Cerastium arcticum*, *C. regelii*, *Stellaria longipes*, *Cochlearia officinalis*, *Cardamine bellidifolia*, *Draba bellii*, *D. oblongata*, *Ranunculus nivalis*, *R. sabinei*, *Saxifraga caespitosa* ssp. *uniflora*, *S. cernua*, *S. flagellaris*, *S. nivalis*, *S. oppositifolia*, *S. rivularis*, *S. tenuis*, *Potentilla hyparctica*.

PETROLOGICAL STUDIES ON THE RAINY LAKE GRANITOID COMPLEX,
NORTHWESTERN ONTARIO: A PRELIMINARY EVALUATION

EMR Research Agreement 222-4-79

R.H. Sutcliffe¹ and J.J. Fawcett¹
Precambrian Geology Division

Sutcliffe, R.H. and Fawcett, J.J., *Petrological studies on the Rainy Lake granitoid complex, northwestern Ontario, a preliminary evaluation; in Current Research, Part A, Geological Survey of Canada, Paper 80-1A, p. 335-338, 1980.*

Abstract

Three suites of granitoid rocks as well as their origins were identified in the complex: (1) An early suite of foliated to gneissic biotite tonalite-granodiorite which may have formed by partial melting of rocks of basaltic composition at mantle depths; (2) Diorites, monzodiorites, and monzonites of the Jackfish Lake-Weller Lake Pluton appear to be derived by partial melting of a mafic source at crustal depths; and (3) A late suite of biotite granite which represents a partial melt of the earlier gneissic tonalite-granodiorite.

Introduction

This report is a further evaluation of petrological models for the genesis of magmas in the Archean Rainy Lake Granitoid Complex. Potential magma sources for the granitoids have been primarily modelled by trace element chemistry. The field relations, petrography, and major element chemistry have been used to provide constraints on these models.

The Archean Rainy Lake Granitoid Complex is located approximately 15 km north of the town of Fort Frances, Ontario. It is situated in the southwestern portion of the Wabigoon volcanic-plutonic subprovince of the Superior Province. To the north the complex is intrusive into meta-volcanic rocks of the Wabigoon belt, and its southern boundary has been placed at the Quetico Fault Zone.

The complex is composed of four structurally and lithologically distinct elements including three suites of granitoid rocks (Sutcliffe and Fawcett, 1979). These are: 1) an early suite of highly foliated to gneissic tonalite-granodiorite, 2) amphibolite facies supracrustal rocks which form septa within the tonalite-granodiorite, 3) foliated to massive diorite-monzodiorite-granodiorite of the Jackfish Lake-Weller Lake Pluton, and 4) a late granite suite of foliated to massive biotite granite and pegmatite. The field relations, structure and petrography of these rocks were summarized by (Sutcliffe and Fawcett, 1979).

The lithological elements present in the Rainy Lake Complex are repeatedly observed in other granitoid complexes of northwestern Ontario (Sage et al., 1973; Schwerdtner and Sutcliffe, 1978). Models for the genesis of the granitoid rocks at Rainy Lake may therefore be applicable to granitoid rocks in other parts of the Superior Province.

Chemistry

The three groups of granitoids are chemically distinct. This is evident from the major elements plots in Figures 48.1 and 48.2 and from the selected analyses in Table 48.1.

The tonalite-granodiorite gneiss has a restricted range in composition and is characterized by generally higher Na₂O than the other granitoids. The gneiss typically has moderate to high strontium, low rubidium, moderately enriched light rare earth elements (REE), depleted heavy REEs, and no europium anomaly. These characteristics are comparable to the Northern Light Gneiss of northeastern Minnesota (Arth and Hanson, 1975) and to the high Al₂O₃-type tonalites (Barker and Arth, 1976).

The diorites, monzodiorites, and monzonites of the Jackfish-Weller Lakes Pluton are characterized by a calc-alkalic trend, generally high Na₂O (Mol. Na₂O/K₂O greater than 1.5) and are metaluminous. The group is consistently higher in CaO, FeO², MgO, TiO₂ and P₂O₅ than other granitoids of the complex. The rocks of the pluton typically have low Rb, high Sr, enriched light REEs, moderately depleted heavy REEs and a slight negative to absent europium anomaly. Longstaffe (1977) identified a granodioritic suite in the southwestern portion of the Pluton characterized by higher abundances of large ion lithophile elements, but comparable rocks were not identified elsewhere in the body.

The late granites are relatively restricted in composition and have the highest K₂O of the Rainy Lake Granitoids. They are peraluminous, corundum normative and low in CaO, MgO and TiO₂. The granites have enriched light REEs, depleted heavy REEs and a negative europium anomaly.

Representative REE patterns for the three groups of Rainy Lake granitoids are shown in Figure 48.3.

Petrogenesis

Recent experimental studies (Winkler and Breitbart, 1978; Wyllie, 1977) and geochemical studies on granitoids (White and Chappell, 1977) indicated that many granitoid melts contain solid residual material from the source region. White and Chappell (1977) suggested that this model can be used to explain many of the chemical and mineralogical characteristics of granitoid rocks. They further indicated that the nature of the source region of a melt may be deduced through the identification of residual material.

We believe that residual material ranging from enclaves to clotty mafic minerals and xenocrysts can be identified in the Rainy Lake granitoids. Accordingly, we have used trace and REE element concentrations to test genetic models developed by this approach.

1. Late Granite Suite

The REE patterns for the biotite granites can be used to test a partial melting model involving crustal material. Differentiation of one of the older granitoid suites to produce the granites is not considered as there is no apparent geochemical continuity between the biotite granites and either of the older granitoid suites.

Mafic metavolcanics, metasediments, and the gneissic tonalite-granodiorite are locally available rocks which by

¹Department of Geology, University of Toronto, Toronto, Ontario

²total Fe as FeO

partial melting at greater depths may have been the source of the biotite granite. Partial melting of basaltic rocks under hydrous conditions gives melts of granitic composition (Helz, 1976). However, producing the degree of REE fractionation observed in the biotite granites requires a residuum with bulk distribution coefficients dominated by garnet. This would be incompatible with the observed negative europium anomaly. Similarly, partial melting of Archean sediments implies unrealistic amounts of residual garnet to produce the heavy REE depletion.

If the source is geochemically evolved with fractionated REE abundances, there is no need for large amounts of residual garnet. A locally available source rocks fulfilling this requirement is the tonalite-granodiorite gneiss.

A model REE pattern based on partial melting of the tonalite-granodiorite gneiss is shown in Figure 48.4. This model assumes a 20 per cent partial melt and a mixing of melt with residue in a ratio of 2:1. This ratio is compatible with field and petrographic observations if material such as andesine cores in plagioclase and clotty biotite grains are residual.

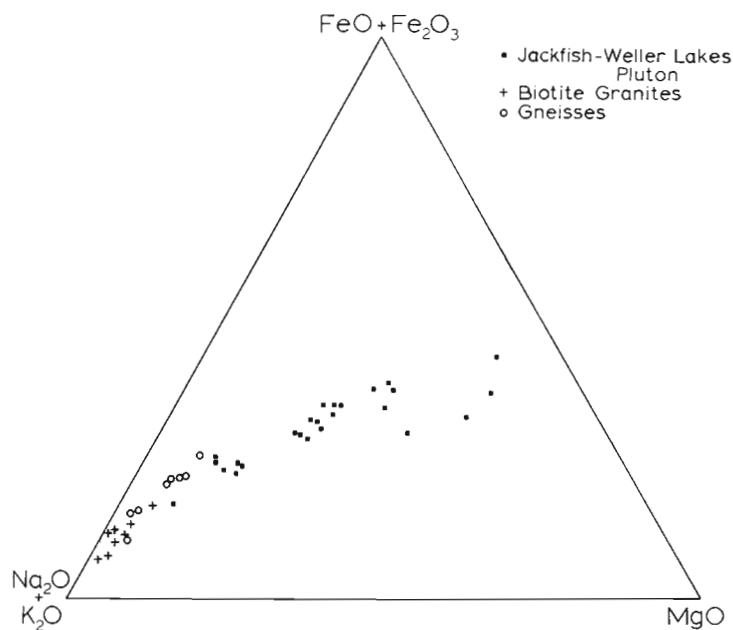


Figure 48.1. AFM (wt.%) diagram for granitoid rocks of the Rainy Lake Granitoid Complex.

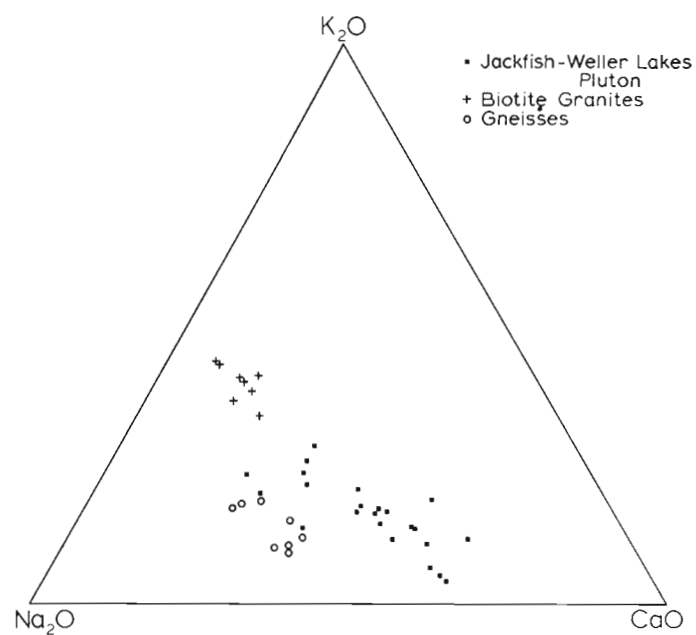


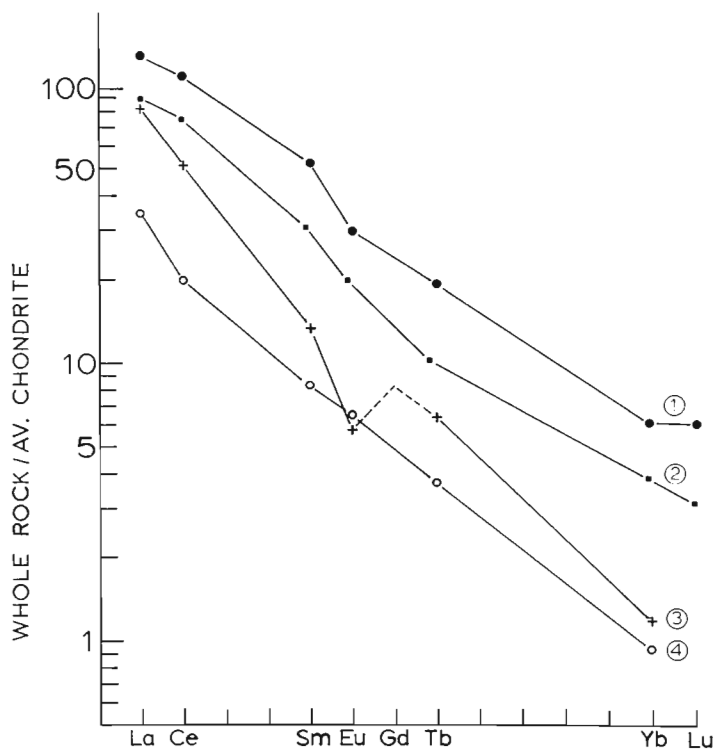
Figure 48.2. Na₂O-K₂O-CaO (mol.%) diagram for granitoid rocks of the Rainy Lake Granitoid Complex.

Table 48.1
Selected analyses of granitoid rocks from the Rainy Lake Granitoid Complex

	1	2	3	4	5
wt.%					
SiO ₂	53.97	60.76	73.82	71.80	72.42
TiO ₂	0.79	0.58	0.10	0.25	0.20
Al ₂ O ₃	16.00	15.70	14.03	15.42	15.53
Fe ₂ O ₃	2.57	2.36	0.48	0.94	0.08
FeO	4.69	2.96	0.55	0.88	0.86
MnO	0.16	0.07	0.03	0.03	0.04
MgO	5.72	3.70	0.30	0.52	0.41
CaO	7.79	5.44	0.95	2.72	2.01
Na ₂ O	4.87	4.76	3.85	4.60	5.31
K ₂ O	1.48	2.74	5.08	2.04	2.50
P ₂ O ₅	0.46	0.27	0.00	0.08	0.04
Loss	1.11	0.74	0.43	0.46	0.40
TOTAL	99.61	100.08	99.62	99.74	99.80
ppm					
Rb	22	58	233	45	62
Sr	1297	1011	221	526	895
La	42	30	28	14	9
Ce	93	65	43	21	12
Sm	10.5	6.2	2.4	1.6	1.6
Eu	2.2	1.5	0.4	0.4	0.5
Tb	1.0	0.5	0.3	-	0.2
Yb	1.27	0.78	0.25	0.09	0.08
Lu	0.21	0.10	-	-	-

Major elements by XRF, except FeO (titration and Na₂O (flame photometry). Rb, Sr by XRF. REE by INAA. Analysts: major elements and Rb, Sr by M.P. Gorton and R.H. Sutcliffe; REE by J. Hancock and R.H. Sutcliffe.

- 1 Hornblende diorite, Jackfish Lake-Weller Lake Pluton (76-36).
- 2 Biotite hornblende monzodiorite, Jackfish Lake-Weller Lake Pluton (78-25).
- 3 Biotite granite, late granite suite (77-36).
- 4 Biotite tonalite, gneissic suite (76-30).
- 5 Biotite granodiorite, gneissic suite (77-101).



1. Hornblende diorite, Jackfish Lake-Weller Lake Pluton (76-36).
2. Biotite hornblende monzodiorite, Jackfish Lake-Weller Lake Pluton (78-25).
3. Biotite granite, late granite suite (77-36).
4. Average tonalite-granodiorite, gneissic suite.

Figure 48.3. Chondrite normalized REE abundances in representative samples from the Rainy Lake Granitoid Complex. Chondrite values used for normalizing the data are those of the Leedy chondrite divided by 1.20 (cf. Taylor and Gorton, 1978).

Model major element compositions assuming the same 20 per cent partial melting of the average tonalite-granodiorite gneiss and a melt to residue mix of 2:1 are shown in Table 48.2.

2. Jackfish Lake-Weller Lake Pluton

The Jackfish Lake-Weller Lake Pluton displays many of the characteristics of the I-type granitoids of White and Chappell (1977). These features include relatively high Na/K and Na+K+Ca/Al, hornblende and clinopyroxene as the predominant mafic minerals, and numerous hornblende or mafic granulite enclaves.

The mafic minerals of the Jackfish Lake-Weller Lake Pluton occur primarily as clotty aggregates and the mineralogy of the clots is similar to that of the enclaves. Mafic granulite enclaves with the assemblage hypersthene-augite-hornblende are contained within a hypersthene-biotite-augite phase of the pluton. The enclaves have no systematic association with the mafic wall rocks and they are interpreted as unmodified residuum from partial melting of a mafic source. Major element variation within the pluton is consistent with mixing of a leucocratic melt and the residual mafic enclaves.

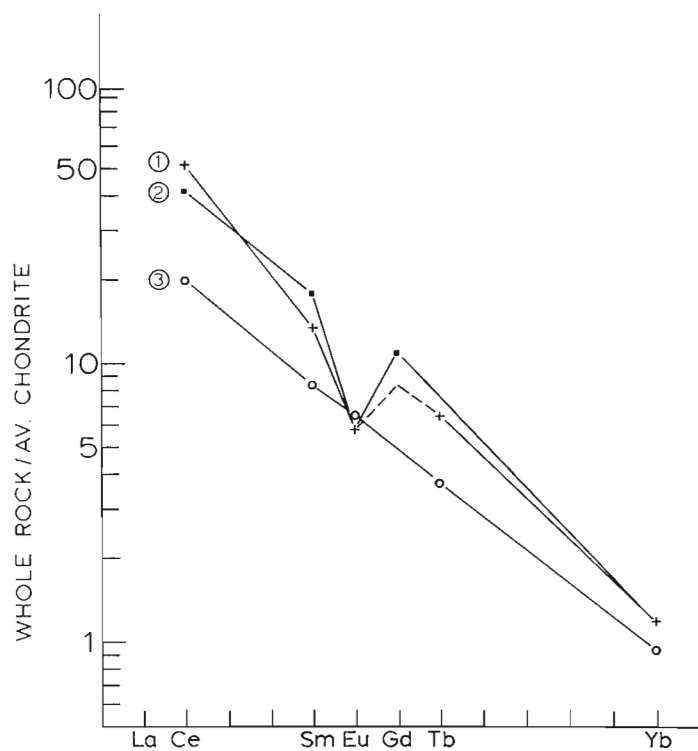


Figure 48.4. Chondrite normalized REE abundances in

1. the biotite granite (77-36),
2. average tonalite-granodiorite, and a model magma
3. based on 20 per cent melt of the average tonalite-granodiorite with a melt to residue mix of 2:1,

Model assumes modal batch melting using formula and partition coefficients in Arth (1976).

Table 48.2

Major element model for the biotite granites

	1	2	3
SiO ₂	74.42	73.50 - 76.00	76.29
TiO ₂	0.10	0.08 - 0.16	0.11
Al ₂ O ₃	14.14	13.60 - 14.30	13.23
FeO*	1.03	0.07 - 1.50	0.75
MnO	0.03	0.02 - 0.04	0.01
MgO	0.30	0.14 - 0.40	0.23
CaO	0.96	0.60 - 1.20	1.11
Na ₂ O	3.88	3.80 - 3.90	3.86
K ₂ O	5.12	4.90 - 5.20	4.39
P ₂ O ₅	0.00	0.00 - 0.04	0.03

- 1 Biotite granite (77-36), recalculated on an anhydrous basis.
- 2 Range of composition in biotite granites from the Rainy Lake Complex.
- 3 Model composition based on 20 per cent melt of the average tonalite-granodiorite with a melt to residue mix of 2:1. Melt is assumed to be the 4 Kb minimum melt in the system Plag-Or-Qtz-H₂O with Ab/An = 2.9 (Winkler, 1976).

Longstaffe (1977) has modelled REE patterns obtained from the hornblende diorites and monzodiorites of the south-western portion of the pluton. He interpreted the pluton as being derived from partial melting of an eclogite source with subsequent modification of the magma by hornblende fractionation. Although this hypothesis is a valid interpretation of the REE data, field evidence in the vicinity of the mafic enclaves indicates that segregation of the mafic minerals was taking place during magma emplacement and therefore the enclaves cannot be regarded as cumulates.

As an alternative hypothesis, the Jackfish Lake-Weller Lake Pluton may be derived by partial melting of a mafic crustal source, leaving a mafic granulite residuum with the assemblage hypersthene-augite-hornblende. The absence of significant europium anomalies, and high strontium of the granitoids is compatible with the absence of plagioclase in the residue. If the granulite is a residue, the observed REE fractionation in the granitoids indicates that the source must have been moderately fractionated. Therefore, although a mafic crustal source is postulated, geochemically unmodified Archean metabasalts are not a probable source from which the pluton was derived.

3. Tonalite-Granodiorite Gneiss

The genesis of tonalitic rock types has recently received considerable attention. This stems largely from the recognition of tonalitic rocks as a possible key to understanding the Earth's early sialic crust (Barker and Peterman, 1974) and a recognition of the significance of the heavy REE depletion in these rocks (Hanson and Goldrich, 1972).

The strong deformation and metamorphism of the tonalite-granodiorite gneiss of the Rainy Lake Complex obliterates many of the primary features which may have provided clues to the genesis of the suite. As a consequence, we have not attempted to refine existing models for the genesis of the tonalitic rock types based on the interpretation of REE data. Hanson and Goldrich (1972) and Arth and Hanson (1975) have proposed partial melting of rocks of basaltic composition, such as quartz eclogite to produce the tonalites. Calculations by Longstaffe (1977) showed that a 20-25 per cent melt of light REE-enriched quartz eclogite can be used to model REE distributions in the tonalites of the Footprint Lake area in the western part of the Rainy Lake Complex.

Summary

Three distinct suites of granitoid rocks are present in the Rainy Lake Complex. Their origin can be summarized as follows:

1. An early suite of foliated to gneissic biotite tonalite-granodiorite which may have formed by partial melting of rocks of basaltic composition at mantle depths.
2. Diorites, monzodiorites, and monzonites of the Jackfish Lake-Weller Lake Pluton appear to be derived by partial melting of a mafic source at crustal depths. The dioritic to monzodioritic magmas are composed of both melt and residual granulite material.
3. A late suite of biotite granite which represents a partial melt of the earlier gneissic tonalite-granodiorite.

References

- Arth, J.G.
1976: Behavior of trace elements during magmatic processes - A summary of theoretical models and their applications; *Journal of Research, U.S. Geological Survey*, v. 4, no. 1, p. 41-47.
- Arth, J.G. and Hanson, G.N.
1975: Geochemistry and origin of the early Precambrian crust of northeastern Minnesota; *Geochimica et Cosmochimica Acta*, v. 39, p. 325-362.
- Barker, F. and Arth, J.G.
1976: Generation of trondhjemitic-tonalitic liquids and Archean bimodal trondhjemite-basalt suite; *Geology*, v. 4, no. 10, p. 596-600.
- Barker, F. and Peterman, Z.E.
1974: Bimodal tholeiitic-dacitic magmatism and the early Precambrian crust; *Precambrian Research*, v. 1, p. 1-12.
- Hanson, G.N. and Goldrich, S.S.
1972: Early Precambrian rocks in the Saganaga Lake-Northern Light Lake area, Minnesota-Ontario, Part II: Petrogenesis; *Geological Society of America, Memoir 135*, p. 179-192.
- Helz, R.T.
1976: Phase relations of basalts in their melting ranges at $P_{H_2O} = 5 \text{ Kb}$, Part II: Melt Compositions; *Journal of Petrology*, v. 17, part 2, p. 139-163.
- Longstaffe, F.J.
1977: The oxygen isotope and elemental geochemistry of Archean rocks from northern Ontario; unpublished Ph.D. Thesis, McMaster University, 564 p.
- Sage, R.P., Breaks, F.W., Stott, G.W., and McWilliams, G.M.
1973: Operation Ignace-Armstrong; in *Summary of Field Work*, Milne, V.G., Hewitt, D.F., and Wolfe, W.J., ed., Ontario Division of Mines, Miscellaneous Paper 56, p. 38-70.
- Schwerdtner, W.M. and Sutcliffe, R.H.
1978: Structure and lithology of two Archean granitoid complexes, Ontario (Abst.); *Geological Society of America, Abstracts with Programs*, 1978.
- Sutcliffe, R.H. and Fawcett, J.J.
1979: Petrological and geochronological studies on the Rainy Lake Granitoid Complex, northwestern Ontario: A progress report; in *Current Research, Part A*, Geological Survey of Canada, Paper 79-1A, p. 377-380.
- Taylor, S.R. and Gorton, M.P.
1978: Geochemical application of spark source mass spectrography - III. Element sensitivity, precision and accuracy; *Geochimica et Cosmochimica Acta*, v. 41, p. 1375-1380.
- White, A.J.R. and Chappell, B.W.
1977: Ultrametamorphism and granitoid genesis; in *Experimental Petrology Related to Extreme Metamorphism*, D.H. Green, ed., *Tectonophysics*, v. 43, p. 7-22.
- Winkler, H.G.F.
1976: *Petrogenesis of Metamorphic Rocks*; 4th Edition, Springer-Verlag Publishers, New York, 334 p.
- Winkler, H.G.F. and Breitbart, R.
1978: New aspects of granitic magmas; *Neues Jahrbuch fuer Mineralogie, Monatshefte*, h. 10, p. 463-480.
- Wyllie, P.J.
1977: Crustal Anatexis: An experimental review; in *Experimental Petrology Related to Extreme Metamorphism*; D.H. Green, ed., *Tectonophysics*, v. 43, p. 41-71.

GEOLOGY OF THE TEBESJUAK LAKE MAP AREA, DISTRICT OF KEEWATIN: A PROGRESS REPORT WITH NOTES ON URANIUM AND BASE METAL MINERALIZATION

Project 780008

A.N. LeCheminant, A.R. Miller, G.W. Booth¹,
M.J. Murray² and G.A. Jenner³
Precambrian Geology Division

LeCheminant, A.N., Miller, A.R., Booth, G.W., Murray, M.J., and Jenner, G.A., Geology of the Tebesjuak Lake map area District of Keewatin: A progress report with notes on uranium and base metal mineralization; in Current Research, Part A, Geological Survey of Canada, Paper 80-1A, p. 339-346, 1980.

Abstract

Southern and eastern parts of the Tebesjuak Lake map area contain faulted successions of sediments and volcanics of the Dubawnt Group that overlie an irregular basement of Archean and Apebian granitoid gneisses. Dubawnt Group rocks consist of basal successions of sheared and altered stream-channel and fluvial deposits that are unconformably overlain by subaerial alkaline flows and volcanoclastic sediments of the Christopher Island Formation. The thick successions of volcanics are succeeded by wedges of red alluvial fan sediments and Pitz Formation rhyolitic flows and intercalated quartz-rich sediments. Poorly exposed black, amygdaloidal basalt overlies the Pitz Formation rocks. Stocks and plutons of syenite and granite and northeast trending dyke-like gabbroic intrusions cut the Dubawnt Group rocks.

Epigenetic fracture-controlled uranium mineralization is spatially related to basal formations of the Dubawnt Group. Anomalous radioactive syenites are confined to southeastern parts of the map area. High uranium and thorium contents are due to disseminated thorite, monazite, and zircon.

Volcanic and sedimentary rocks of the Christopher Island Formation have been subjected to widespread alteration, veining and/or contact metamorphism. Base-metal mineralization (Cu, Pb-Cu and Pb-Cu-Ag-Bi-Cd-Zn) has developed in a few of the vein systems. Acid magmatic events associated with Pitz Formation volcanism and the emplacement of granite plutons may be responsible for the base metal mineralization.

Introduction

The Tebesjuak Lake map area (65 O) contains basins filled with continental sediments and volcanics of the Paleohelikian or Late Apebian Dubawnt Group. These rocks unconformably overlie or are in fault contact with granitoid gneisses of Archean and Apebian ages and are intruded by syenite and granite plutons and small basic intrusions. Southern and eastern parts of map area 65 O were mapped at a scale of 1:250 000 during the 1979 field season (Fig. 49.1). Previous work in map area 65 O was confined to reconnaissance helicopter traverses during Operation Baker (Wright, 1955, 1967), and LeCheminant et al. (1979a) described the stratigraphy of the Dubawnt Group in two small parts of the area.

Archean and Apebian Granitoid Gneisses

Gneisses of granodioritic to granitic composition inter-layered with thin units of paragneiss and amphibolite form the basement to the Dubawnt Group. In the Nutarawit Lake area the basement consists of poorly exposed cataclastic felsic and mafic gneisses, augen granite gneiss and gneissic granite similar to rocks of the Thirty Mile domain to the northeast (LeCheminant et al., 1979b). The gneisses are intruded by diabase and younger biotite lamprophyre and syenite dykes and are transected by numerous northeasterly and northwesterly faults. Near the basal Dubawnt unconformity and adjacent to fault zones the gneisses are intensely fractured and brecciated. Chlorite, epidote, quartz and carbonate veining and alteration are prominently developed within these rocks.

Two breccia zones, interpreted as diatremes, are exposed on small islands near the southwest shore of Nutarawit Lake in map area 65 O/1. The zones contain angular to subrounded fragments of various gneiss lithologies, amphibolite and metadiabase, up to 2 m in diameter in a matrix of pulverized gneiss and biotite lamprophyre. A foliation, due to primary orientation of fragments, is locally developed within the lamprophyre. Both breccias are unmineralized and are similar to diatremes in map area 56 D/1 (Schau and Hulbert, 1977) and to a mineralized pipe in map area 56 D/2 (Miller, in press).

A 10-15 km wide domain of northeasterly trending granodioritic orthogneiss underlies an area north and west of 'P.O.' Lake. To the southeast the domain is in fault contact with a wedge of Dubawnt Group rocks along a northeasterly trending cataclastic zone that has been intruded by syenite. To the north and northwest the gneisses are unconformably overlain by rocks of the Dubawnt Group or are intruded by a complex suite of syenites. To the west the gneisses are intruded by the Pamiutuq Granite. The gneisses consist mainly of white-weathering granodioritic orthogneiss with minor grey layered biotite-hornblende-plagioclase gneiss, biotite- (garnet)- paragneiss and amphibolite. They are intruded by feldspar porphyry and younger quartz-feldspar porphyry dykes; however dykes are significantly less numerous and lack the compositional diversity of dykes in the Nutarawit Lake area.

Isolated exposures of basement gneisses are located along the Kunwak River and on the shores of Tulemalu Lake. These gneisses are (1) overlain unconformably by all formations of the Dubawnt Group with which they are in

¹University of Toronto, Toronto, Ontario.

²Carleton University, Ottawa, Ontario.

³University of Tasmania, Hobart, Tasmania.

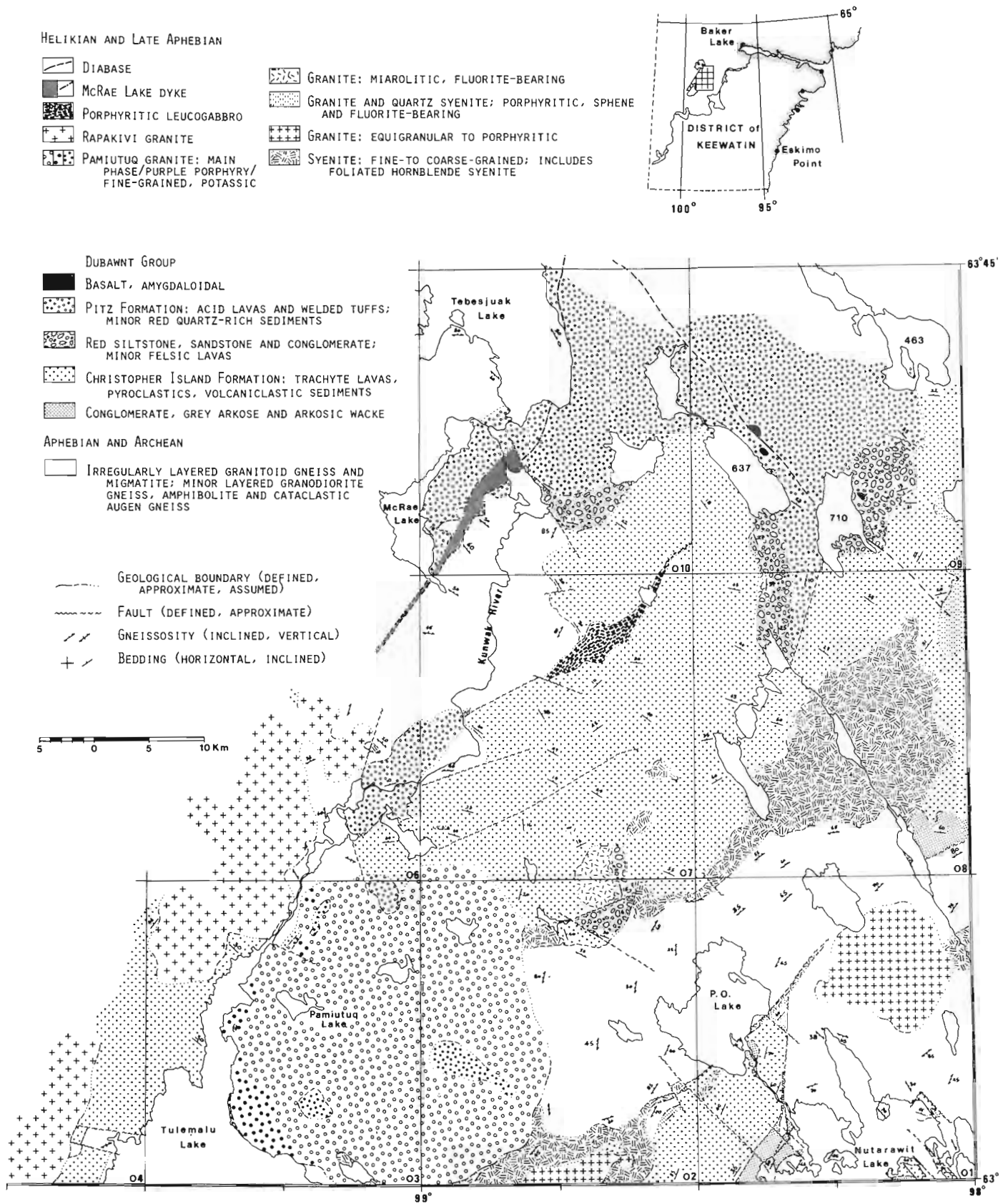


Figure 49.1. Simplified geological map of southeastern parts of the Tebesjuak Lake (65 O) map area.

contact; (2) faulted against Dubawnt Group rocks; or (3) intruded by dyke-like basic intrusions and granitic plutons. The basement rocks are mainly granodioritic orthogneisses similar to the gneisses exposed near 'P.O.' Lake. East of McRae Lake gneissosity trends are consistently northwesterly with moderate northeasterly dips. Elsewhere trends are highly variable. On the western shore of Tulemalu Lake a coarse grained quartz-poor K-feldspar augen gneiss is in fault contact with rocks of the Christopher Island Formation. The gneisses are intruded by syenite dykes and small plugs and by easterly trending biotite lamprophyre dyke swarms.

Dubawnt Group

Regional Setting

Dubawnt Group rocks in the map area consist of a basal succession of sheared and altered stream-channel and fluvial sediments that are overlain by alkaline flows and volcanoclastic sediments of the Christopher Island Formation. The thick successions of volcanic rocks are succeeded by wedges of alluvial fan sediments and Pitz Formation rhyolitic lavas and pyroclastics. Stocks and plutons of syenite and granite and northeast trending dyke-like basic intrusions cut the Dubawnt Group rocks.

In the north half of the area the Dubawnt Group rocks fill part of a northeast trending structural depression, the Baker Lake Basin, that can be traced more than 300 km from the east end of Baker Lake to Tulemalu Lake (LeCheminant et al., 1979b). Southeast of the Baker Lake Basin near Nutarawit Lake isolated fault blocks preserve basal formations of the Dubawnt Group in homoclinal successions with different attitudes.

Basal Sedimentary Successions

Successions of polymictic conglomerate and pink to grey arkose and arkosic wacke are the lower units of the Dubawnt Group within fault blocks in map area 65 O/1, and in the southeastern corners of map areas 65 O/2 and O/8. Sediments near the base of these successions are poorly bedded polymictic conglomerates containing subrounded clasts of grey and pink granitoid gneiss, foliated mafic rocks and quartz. Overlying arkosic rocks are well-indurated with sericite, chlorite and quartz and contain channel scours, trough crossbedded or laminar fining-upward cycles and heavy mineral laminations. The most complete section is exposed west of Nutarawit Lake where a continuous succession of conglomerate and arkose, made up in part of overlapping clastic wedges, unconformably overlies cataclastic gneisses (LeCheminant et al., 1979a).

The successions are unconformably or disconformably overlain by volcanics of the Christopher Island Formation, intruded by hornblende syenite or in fault contact with basement gneisses. They are correlated with the South Channel and Kazan formations (Donaldson, 1965) on the basis of lithology and stratigraphic position.

Isolated exposures in a zone extending from the southern limit of the map area in map area 65 O/2 through to the east side of 'P.O.' Lake and northeast to the corner of map area 65 O/8 are intensely altered and locally deformed. The sediments are deformed in narrow zones adjacent or parallel to northeast and north trending faults. Stretch-peggle conglomerates show a range of pebble shapes due to initial shape variation and competence difference during deformation. The plane of flattening is steeply dipping and pebble elongations are parallel to adjacent faults. The major northeast trending fault zone along which these deformed sediments are preserved was the locus for later intrusions of hornblende syenite. Northwest trending faults with a predominant dip-slip component transect the northeast structures and truncate several of the sedimentary successions.

Christopher Island Formation

Alkaline flows and volcanoclastic sediments of the Christopher Island Formation comprise thick homoclinal successions which lie unconformably on or are faulted against basement gneisses and the basal clastic successions. The formation comprises mafic and felsic trachyte lavas and breccias, associated pyroclastics and volcanoclastic wackes and epiclastic breccias. Phlogopite (biotite)- and clinopyroxene-phyric mafic trachyte lavas and breccias are the dominant rock type. Pyroclastic rocks include crystal and crystal-lithic tuffs with minor agglomerates, tuff-breccias and welded tuffs. Interflow sediments are, for the most part, immature, poorly sorted volcanoclastic conglomerates and wackes that contain lithic and crystal fragments derived from the trachytes. Minor argillite and siltstone containing desiccation features occur as thin well bedded units that, along with graded crystal-rich tuffs, provide the best stratigraphic control within the formation. Descriptions of these rocks and detailed stratigraphic sections from the Nutarawit Lake area and from fault blocks near the southwestern end of the Baker Lake Basin were presented by LeCheminant et al. (1979a). They concluded that the lavas and tuffs were erupted in a subaerial environment with cycles of volcanism beginning with vent clearing explosions followed by effusions of mafic and then felsic alkaline lavas.

The 1979 mapping confirmed that similar patterns of volcanism and sedimentation characterize the Christopher Island Formation throughout the southwestern end of the Baker Lake Basin. Homoclinal successions are exposed in fault blocks bounded by northeasterly faults that are locally truncated by northwesterly faults. Within the successions shallow northerly dips of 20-40° predominate although dips as steep as 70°, apparently related to the proximity of faults or intrusions, have been recorded. No overturned beds were encountered. Changes of bedding trends of up to 70° over distances as short as a few hundred metres in the southeastern corner of map area 65 O/9 and in map area 65 O/7 may indicate open folds, perhaps related to the emplacement of intrusive rocks. However, no minor folds were noted and many of the changes are abrupt. In most cases they probably reflect overlapping of series of units derived from different eruptive centres, changes in original bedding on the flanks of a stratovolcano complex, or local faulting.

Throughout the area the volcanics and sediments of the Christopher Island Formation have been subjected to alteration, veining and/or contact metamorphism. Whereas this alteration has rarely affected original igneous and sedimentary textures or igneous phenocrysts, the matrix of most rocks is replaced by a mat of secondary phases including quartz, chlorite, carbonates, albite, epidote, tremolite, talc and phlogopite. In mafic lavas a fibrous blue amphibole coats fracture surfaces or occurs with quartz in thin veinlets. Weakly foliated biotite and biotite-hornblende hornfels has developed adjacent to syenite, quartz syenite and fluorite-sphene-bearing granite in map area 65 O/8. West of Tulemalu Lake in map area 65 O/4 an unusual 15 m wide adularia-wollastonite vein has formed within sheared K-feldspar augen gneiss parallel to a 010° fault contact with mafic lavas and tuffaceous sediments of the Christopher Island Formation.

White vuggy quartz veins and stockworks up to 10 m wide, with minor fluorite and epidote, have developed throughout the Christopher Island Formation and some can be traced for more than 2 km. Quartz-epidote-fluorite-garnet veinlets, which may contain copper or lead-copper mineralization (see economic geology section), occur within all lithologies of the formation. They are common in the northwest corner of map area 65 O/3 and the southeast corner of map area 65 O/9 where the formation is intruded by plutons of fluorite-bearing granite.

Red Volcaniclastic Successions

Wedges of alluvial fan sediments consisting of red volcaniclastic conglomerates, lithic sandstones, siltstone and mudstone unconformably overlie the Christopher Island Formation. The successions are generally shallow dipping and poorly exposed. The sediments have a scattered distribution peripheral to the main outcrop area of the Christopher Island Formation. Clastic components for the most part are derived from the immediately underlying lavas or from basement gneiss terrane.

The most complete stratigraphic sequence is exposed south of 637' Lake. A north-south trending, east dipping homoclinal succession up to 1000 m thick comprises basal conglomerates, red felsic lavas and fine grained red sediments. Basal conglomerates contain mainly feldspar trachyte clasts (maximum 30 cm) in parallel bedded units up to 2 m in thickness and are interbedded with medium-to coarse-grained lithic sandstones. The coarse clastics are overlain by red dacite lavas intercalated with volcaniclastic and tuffaceous sandstones and siltstones. Dacites contain small K-feldspar and plagioclase phenocrysts and apatite microphenocrysts set in an aphanitic quartzofeldspathic matrix. The lavas are strikingly vesicular and/or amygdaloidal with amygdules to 3 cm filled by various combinations of chlorite, epidote, quartz, chalcedony, fluorite and specularite. These lavas are unique to this sequence and have not been found in other red clastic wedges. The dacites are conformably overlain by laminated to thin bedded mudstones, siltstones and sandstones. Minor structures within the pink, red and maroon sediments include graded bedding, desiccation cracks, reduction spots and ripple marks.

The red clastic units are interpreted primarily as stream-channel deposits with some mudflow deposits near the base of the successions. On the basis of lithology and stratigraphic position they are correlated with the Kunwak Formation (LeCheminant et al., 1979b).

Pitz Formation Rhyolitic lavas and associated sediments of the Pitz Formation underlie northern parts of areas 65 O/9 and O/10 and occur as isolated remnants to the southwest. They unconformably overlie basement gneisses and volcanics of the Christopher Island Formation. The distribution of red clastic successions and the Pitz Formation suggests these units may be locally separated by a slight angular unconformity, however the few observed contacts are concordant.

Exposures along the eastern shore of Tulemalu Lake and east of Kunwak River in map area 65 O/6 are mainly red sparsely porphyritic flow-banded rhyolite lavas and welded crystal-lithic tuffs. Mauve and purple quartz-feldspar-phyric dacites and rhyolites intercalated with rhyolite-cobble conglomerate and red sandstones are dominant lithologies in map areas 65 O/9, 10, and west of the Kunwak River. The sequences dip gently to the north or northwest and exceed 200 m in thickness north of 637' Lake. The large island in 463' Lake has excellent cliff exposures of sparsely porphyritic flow-banded fluorite- and topaz-bearing rhyolites 75 m thick that overlie a rhyolite-boulder conglomerate. Interflow conglomerate and sandstone lenses record mass-wasting and stream-channel activity contemporaneous with volcanism.

Pink and red conglomerates and crossbedded sandstones on the north shore of 637' Lake resemble basal lithologies of the Thelon Formation (Donaldson, 1965) but their restricted development suggests they are interflow sediments. Poorly bedded quartz-rich grit and conglomerate in map area 65 O/6 tentatively correlated with the Thelon Formation (LeCheminant et al., 1979a) are similar to conglomerates intercalated with quartz-feldspar-phyric rhyolites north of the Kunwak River and are therefore reassigned to the Pitz Formation.

Basalt

Limited exposures of black, amygdaloidal basalt overlie conglomerates correlated with the Kunwak Formation and lavas and sediments of the Pitz Formation. The basalt contains aligned plagioclase microphenocrysts and microlites in an altered matrix of epidote, chlorite and opaques. Pipe vesicules to 3 cm are lined with chlorite and filled by epidote and calcite. North of 637' Lake the basalt is intercalated with thinly laminated green siltstone and has a maximum observed thickness of 10 m. Here the basalt fills low-lying areas south of ridge-forming Pitz Formation lavas whereas east of 710' Lake it caps hills. A similar thin basalt unit, also extruded over an irregular surface, unconformably overlies Thelon Formation sandstone southwest of Lookout Point on the Thelon River (Donaldson, 1969). Basalt has not previously been reported from the Dubawnt Group within the Baker Lake Basin.

Intrusive

Syenite

Stocks and composite plutons of fine- to coarse-grained red syenites occur in map areas 65 O/1, 2, and 8. They have intruded along both the northwest and southeast contacts of the Christopher Island Formation and the orthogneiss domain north and west of 'P.O.' Lake. Most have sharp intrusive contacts although reactivation along northeasterly faults has locally resulted in sheared and foliated marginal phases. A strong northeasterly foliation has developed in a fine- to medium-grained hornblende syenite on the south boundary of map area 65 O/2 that is intruded by porphyritic pink granite to the east and the Pamiutuq Granite to the west.

Syenites along the southern boundary of the Baker Lake Basin in map areas 65 O/2 and O/8 range from very coarse grained syenite stocks to microsyenite dykes. Anomalous radioactivity within some of these bodies is discussed briefly in the economic geology section. An irregular-shaped composite pluton underlies more than 150 km² in the central part of map area 65 O/8. The poorly exposed intrusion consists of fine- to medium-grained hornblende and biotite-hornblende syenite and northeastern parts contain quartz-bearing phases. Quartz-feldspar porphyry dykes intrude the syenite complex.

Granite

Granite stocks and plutons that postdate the Christopher Island Formation have been subdivided into five units based on texture, accessory minerals and contact relations. Plutons of massive equigranular to porphyritic pink granite that intrude basement gneisses and syenites in map areas 65 O/1 and O/2 are similar to plutons exposed near Forde Lake. (LeCheminant et al., 1979b) and resemble variants of the rapakivi granites that underlie large areas west of Tulemalu Lake. Two stocks of miarolitic fluorite-bearing alkali-feldspar granite intrude the Christopher Island Formation and the overlying red clastic successions in map areas 65 O/2 and O/7.

A stock of porphyritic biotite-hornblende granite, containing fluorite and rich in accessory sphene, intrudes mafic lavas and biotite-rich tuffs of the Christopher Island Formation in the northeast corner of map area 65 O/8. The stock has syenitic border phases and probably is part of a composite syenitic-granitic intrusion exposed to the northeast in map area 65 P/12 (LeCheminant et al., 1979b). Border phases resemble quartz-bearing variants of the syenite intrusion exposed to the southwest. All rocks within the intrusion have an anomalous radiometric signature and contact aureoles are locally mineralized (see economic geology section).

The Pamiutug Granite, a large circular pluton, underlies approximately 700 km² east of Tulemalu Lake, and is in sharp intrusive contact with all surrounding rock types. The main phase of the pluton is homogeneous and contains perthitic orthoclase, plagioclase and rimmed quartz phenocrysts set in a fine grained micrographic matrix. Mafic minerals are clinopyroxene, amphibole and chloritized biotite. A high proportion of plagioclase, both in phenocrysts and in perthite, places this main phase in the granite-B field of the IUGS classification scheme (Streckeisen, 1973), whereas other granites in the area typically fall within the granite-A or rarely the alkali-feldspar granite fields. Xenoliths are common throughout the pluton and consist predominantly of granitoid gneiss, mafic hornblende syenite and a plagioclase porphyritic fine grained mafic rock that has no known analogous lithology adjacent to the intrusion. Plagioclase megacrysts to 5 cm are sparsely distributed.

A purple porphyritic phase with a very fine grained to aphanitic matrix forms a narrow chill margin along most contacts except on the west side where the pluton is in contact with flow-banded rhyolites of the Pitz Formation. Here the purple phase is a wide unit that in part appears to overlie the main phase. Sharp intrusive contacts exist between purple porphyry and rhyolite although at one location an apparent gradational contact between rhyolite and porphyry was observed.

Several stocks of fine grained red equigranular granite intrude the main phase of the pluton. These more potassic granites are irregular in shape and are associated with compositionally and texturally similar aplite dykes that are concentrated within southern and western parts of the pluton. Quartz-feldspar porphyry dykes intrude all phases of the pluton.

Granite plutons west of Tulemalu Lake and the Kunwak River intrude granitoid gneisses and volcanic rocks of the Christopher Island Formation. The largest of these plutons exceeds 1000 km² and underlies a large part of 65 O/4, the northwest corner of 65 J (Eade and Blake, 1977) and the northeast corner of 65 K (Eade, personal communication 1979). This pluton is a coarse grained rapakivi granite characterized by K-feldspar ovoids (2-6 cm) mantled by plagioclase. Mantled and unmantled K-feldspar phenocrysts occur together. Within the ovoids concentric patterns of quartz and biotite inclusions are common and repetition of mantling can occur. Typical accessory minerals are biotite, hornblende, fluorite, and zircon. Rapakivi granite grades into variants that contain only unmantled phenocrysts and rarely grades into fine- and medium-grained equigranular granite. These latter variants are the predominant rock type of smaller plutons that underlie areas of 65 O/3 and O/6. Mantled phenocrysts, where present, are smaller (0.5-2 cm) and less abundant than within the main pluton. The smaller plutons are circular to multilobate in plan and are separated by Christopher Island volcanic rocks and granitoid gneiss. Intrusive contacts are sharp and discordant. The granites lack foliation and in sharp contrast to the Pamiutug Granite they contain no xenoliths.

Quartz-feldspar porphyry dykes, irregular in shape and trend, ranging up to 50 m in width intrude all formations of the Dubawnt Group in southwestern parts of the Baker Lake Basin. The porphyry contains abundant phenocrysts of ovoid K-feldspar, which may be mantled, and round quartz eyes set in a dark reddish grey matrix. The dykes intrude the syenite suite, miarolitic fluorite granites and the Pamiutug Granite. Mantled phenocrysts and absence of xenoliths suggests they are comagmatic with the rapakivi granites and are not a late phase of the Pamiutug Granite as proposed by LeCheminant et al. (1979a).

Basic Intrusions

A 045° trending dyke-like intrusion of spectacular porphyritic leucogabbro in map area 65 O/7 intrudes flows and sediments of the Christopher Island Formation and a northeasterly fault zone between basement gneisses and the Christopher Island Formation. The dyke has been traced for almost 20 km and ranges in width from 0.5-5.5 km. The grey to greenish grey leucogabbro contains up to 70 per cent closely packed, aligned labradorite laths (0.5-2 cm with megacrysts to 8 cm) with interstitial clinopyroxene, magnetite-ilmenite and apatite. Thin sections show pale green amphibole rimming clinopyroxene, skeletal apatite needles to 4 mm and minor interstitial micrographic alkali feldspar and quartz. Alteration consists of patches of epidote, chlorite and prehnite. The leucogabbro is homogeneous in texture and composition throughout the intrusion. Plagioclase phenocrysts and megacrysts are strongly aligned subparallel to contacts and only interstitial phases show chill effects at the margin of the intrusion. Unusually high concentrations of magnetite-ilmenite (3-5%) and apatite (1%) suggest the intrusion is rich in FeO, TiO₂ and P₂O₅. It appears to have formed as the result of a single injection of a plagioclase-rich crystal mush. The leucogabbro is cut by a quartz-feldspar porphyry dyke of the swarm that is thought to be comagmatic with the rapakivi granites.

A composite gabbroic dyke, here named the McRae Lake dyke, intrudes rhyolite flows of the Pitz Formation and granodiorite gneiss in map area 65 O/10. The 035° trending dyke has been mapped for 14 km east of McRae Lake where it widens from 450 m in the southwest to 1.8 km in the northeast. In Figure 49.1 the dyke is shown to extend another 9 km to the southwest of McRae Lake on the basis of a reconnaissance helicopter traverse and the continuity of a pronounced aeromagnetic high. To the northeast the dyke is truncated by a 150° fault. A probable continuation of the dyke to the north is shown in Figure 49.1 as a dash-dot line which traces a well-defined but narrower aeromagnetic anomaly. No outcrop of the dyke was encountered northeast of the fault.

The dyke is a composite intrusion consisting of a medium grained grey-green gabbroic phase that is intruded by the major phase, a brick red, pink to grey glomeroporphyritic quartz monzodiorite. The gabbroic phase contains labradorite and clinopyroxene with accessory biotite, amphibole, magnetite-ilmenite, apatite and up to 3 per cent micrographic alkali feldspar and quartz. The main phase is leucocratic with plagioclase phenocrysts to 1 cm, commonly in clusters, set in a fine grained micrographic matrix. Accessory mafic minerals are amphibole and biotite. Xenoliths of country rock and rimmed quartz eyes (xenocrysts?) are common near the northwest end of the dyke. The gabbroic phase ranges in width from 100-200 m and is chilled against country rocks along either the west or the east side of the dyke. The main phase has sharp intrusive contacts both with country rocks and the gabbroic phase.

A major 130° to 140° trending diabase dyke has been traced from map area 65 O/10 through to the northeast corner of map area 65 O/8. The dyke has vertical contacts and is 100 m thick north of 637' Lake. Contacts against Pitz Formation lavas have a 2-3 cm aphanitic chill margin containing plagioclase and clinopyroxene microphenocrysts. This glassy margin passes into a transitional chill zone up to 1 m wide that contains aligned plagioclase microlites. Microlites increase in size and number across the transitional zone towards the interior of the dyke. The central phase of the dyke is a medium- to coarse-grained gabbro or quartz gabbro. The continuity of the dyke is confirmed northwest of 710' Lake by a prominent aeromagnetic anomaly. Southeast of 710' Lake the dyke is 35 m thick and thins to only 3 m in map area 65 O/8.

Table 49.1

Uranium and base metal mineralization in map areas 65 O and P

	Location	Map Sheet	Host Rock	Element Association	Ore Minerals	Secondary Minerals	Gangue Minerals	Brief description (* additional comments in text)
1.	545300 E (98°06'27" N) 6985800N (63°00'08" E)	65 O/1 SE	Volcaniclastic wacke Christopher Island Fm.	U	pitchblende	present	chlorite	Fracture 140cm by 0.5cm parallel to adjacent NW fault
2.	548450 E (98°02'42" N) 6986600N (63°00'30" E)	65 O/1 SE	Granitoid gneiss	U-Cu	pitchblende chalcocopyrite	none observed	calcite pyrite hematite	*Anomalous zone approximately 150m NW by 60m NE within microfractured gneiss in fault contact with Christopher Island Fm. volcaniclastic sediments
3.	534300 E (98°19'39" N) 6987800N (63°01'14" E)	65 O/1 SW	Granitoid gneiss	U	pitchblende	present	hematite chlorite	Veinlet 3m by 1cm in chloritic gneiss, 60m from basal Dubawnt Group unconformity
4.	549300 E (98°01'12" N) 7013300N (63°14'52" E)	65 O/1 NE	Paragneiss	U	pitchblende	present	chlorite hematite	Discontinuous mineralization 4m by 1-2cm in epidote-chlorite-biotite paragneiss band in granodiorite gneiss
5.	528500 E (98°25'39" N) 7025550N (63°21'37" E)	65 O/8 SW	Mafic trachyte lava Christopher Island Fm.	U	pitchblende	present	quartz calcite chlorite	Trachyte lavas and breccias intruded by feldspar porphyry dykes, cross-cutting quartz stockworks, mineralization in tight fractures
6.	546650 E (98°04'03" N) 7029400N (63°23'35" E)	65 O/8 NE	Fluorite-sphene- biotite quartz syenite	U-Cu	pitchblende chalcocopyrite	cuprosklo- owskite	quartz	*Veinlet 3m by 2-3cm in marginal phase of a syenite intrusion; limited exposure
7.	554650 E (97°54'00" N) 7036000N (63°27'02" E)	65 P/5 NW	Mafic trachyte lava Christopher Island Fm.	U-Pb	pitchblende galena	bolwoodite	chlorite hematite	*Mafic lavas intruded by quartz-fluorite bearing feldspar porphyry dykes. Mineralization in several discontinuous 0.5-1cm wide veinlets
8.	483100 E (99°20'06" N) 7006500N (63°11'25" E)	65 O/3 NW	Mafic trachytes and volcaniclastic wackes Christopher Island Fm.	Cu	digenite? bornite covellite chalcocopyrite	malachite azurite brochantite	garnet epidote calcite quartz	*Discontinuous veins up to 10cm wide of massive and disseminated sulphides
9.	517300 E (98°39'09" N) 7040700N (63°29'54" E)	65 O/7 NE	Mafic trachyte lavas Christopher Island Fm.	Pb-Cu- Ag-Bi- Cd-Zn- U	galena chalcocopyrite bornite digenite? covellite sphalerite greenockite pitchblende	malachite azurite anglesite kasolite	quartz Sr-barite barite fluorite magnetite chlorite sphene K-Mg mica?	*Intersecting 070° and 110° vein systems; massive and disseminated sulphides with related alteration developed in trachyte lavas; crosscut by fluorite-quartz-pitchblende veins
10.	530600 E (98°22'57" N) 7045700N (63°32'30" E)	65 O/9 SW	Mafic trachyte lavas Christopher Island Fm.	Pb-Cu	Galena	malachite azurite	quartz calcite specularite	Disseminated sulphide in vuggy quartz vein system

Economic Geology

Table 49.1 lists uranium and base metal occurrences located during 1979 mapping in map area 65 O and western parts of map area 65 P. Research is continuing to augment the interim assemblage data reported in this table.

Most uranium occurrences listed in Table 49.1 are small zones of limited mineralization and/or exposure that are spatially related to basal formations of the Dubawnt Group. They are similar to other occurrences of epigenetic fracture-controlled mineralization within and adjacent to the Baker Lake Basin (Miller, 1979; in press). Occurrences 1 and 2 are associated with fracture zones adjacent to northwest faults. The host granitic gneiss at occurrence 2 is intensely fractured and hematitized and contains disseminated pyrite and epidote-chlorite veins. A frost-shattered area of 150 m by 60 m has anomalous radioactivity and contains a few discontinuous tight pitchblende-bearing fractures up to 15 cm long by 1-2 mm wide and minor quartz-pink calcite-chalcopryrite veinlets.

Chalcopryrite-pitchblende mineralization at occurrence 6 is hosted in a medium grained quartz syenite containing accessory purple fluorite, euhedral sphene and magnetite. At occurrence 7, contact metamorphosed lavas of the Christopher Island Formation are intruded by quartz-fluorite-bearing feldspar porphyry dykes. Irregular, discontinuous pitchblende veinlets up to 1 cm in width occur in the altered lavas. The occurrence is located within the thermal aureole of a composite syenite-granite pluton that is exposed north of the mineralized zone. Occurrences 6 and 7 appear to be genetically related to the syenitic-granitic intrusions and are similar to contact aureole U-Cu mineralization in map area 65 P/12 (LeCheminant et al., 1979b).

Syngenetic thorium-uranium mineralization within northwest trending bostonitic dykes and small stocks of syenite in southeastern parts of the map area have been discussed by Miller (1979) and Beaudry (1979). Anomalously radioactive syenites intrude basement gneisses near Nutarawit Lake and Dubawnt Group rocks in map area 65 O/1 and along the southern margin of the Baker Lake Basin in map areas 65 O/2 and O/8. The leucocratic fine- to medium-grained syenites are characterized by a pink to cherry red colour and aligned alkali feldspar laths. High uranium and thorium contents are due to disseminated thorite, monazite and zircon (variety cyrtolite). Some bostonite dykes contain disseminated sulphides and/or discontinuous thin fractures that are coated with assemblages that include pyrite, chalcopryrite, bornite, galena, molybdenite and sooty pitchblende.

Occurrences 8-10 represent base metal mineralization that has developed in vein systems within the Christopher Island Formation. Several smaller occurrences of malachite or chalcopryrite in quartz-epidote-fluorite-garnet veinlets have not been tabulated. Occurrence 8 consists of east to northeast trending discontinuous veins up to 10 cm in width that cut biotite trachyte lavas and intercalated volcanoclastic wackes. The veins contain bornite-chalcopryrite and bornite-digenite(?) intergrowths partly replaced by covellite with a gangue assemblage of garnet, epidote, calcite, and quartz. The mineralized zone lies approximately 1 km east of a contact between Christopher Island Formation lavas and rapakivi granite. This occurrence was previously investigated in 1966 and 1967 by Hudson Bay Exploration and Development Co. Ltd. (Caine et al., 1979).

Sulphide mineralization at occurrence 9 is located at the intersection of 070° and 110° trending quartz vein systems and is hosted in altered mafic trachyte lavas and breccias of the Christopher Island Formation. Pb-Cu-Ag mineralization is exposed within a 20 m by 7 m outcrop that

Table 49.2.

Geochemical analyses¹ (ppm) of a massive sulphide pod from a vein in trachytes of the Christopher Island Formation (occurrence 9, Table 49.1)

	1	2
Pb (%)	60.8*	64.8*
Cu (%)	5.18*	4.72*
Fe (%)	2.70	3.25
Ag	332** (10.64 oz/ton)	51** (1.65 oz/ton)
Bi	300	343
Cd	175	175
Zn	80	145
Se	50	52
Mn	74	38
Ni	9	6
Co	4	3
Mo	2	2
Sb	11	1
As	N.D.	N.D.
Te	N.D.	N.D.
Au (ppb)	<5	10

¹ Bondar-Clegg & Co. Ltd., Ottawa.

* Assay

** Fire assay (confirms similar atomic absorption results)
N.D. = Not detected

contains a heavily mineralized 6 m by 4 m zone. Sulphide-rich veins and pods up to 0.5 m in width and 4 m long contain more than 90 per cent sulphides, primarily galena, bornite with exsolved chalcopryrite-digenite(?), and chalcopryrite. Trace sulphides include sphalerite (ZnS with a trace of Cd), greenockite (CdS with a trace Zn), and minor covellite replacing chalcopryrite, bornite and greenockite. The gangue assemblage is quartz, fluorite, chlorite, sphene magnetite, a K-Mg-Al-Si phyllosilicate and barite (two varieties - one Sr-bearing). This mineralogy was determined by ore microscopy, powder X-ray diffraction data and preliminary energy dispersive electron microprobe study. Two analyses of the massive sulphides are listed in Table 49.2. The elements Pb, Cu, Fe, Cd and Zn are accounted for by the above mineralogy; however, to date no Ag- or Bi-bearing phases have been identified.

Southern and western sides of the main mineralized outcrop contain carbonate-quartz-purple fluorite stockworks that are younger than the sulphide-rich veins. Fractures within these stockworks are anomalously radioactive and contain disseminated pitchblende. Disseminated Pb-Cu mineralization occurs up to 40 m west of the main zone in intensely altered mafic trachytes that are completely replaced by mica-chlorite-albite assemblages with variable proportions of quartz, fluorite, magnetite, galena, chalcopryrite, bornite and pyrite.

The 070° vein system consists of quartz stockworks and veins up to 15 m wide that can be traced discontinuously for 350 m east-northeast and 750 m west-southwest of the mineralized zone. The 110° system contains quartz stockworks up to 5 m wide and is expressed as a 10-20 m wide topographic linear that exceeds 350 m east-southeast and 1900 m west-northwest of the intersection of the two systems. Veins up to 10 cm wide containing galena, bornite and/or chalcopryrite are erratically distributed along the limbs of the vein systems up to 750 m from the main mineralized zone. These occurrences are associated with purple fluorite and have developed within altered trachytes adjacent to barren quartz stockworks.

A red quartz-eye porphyry dyke has intruded along the east-southeast limb of the 110° vein system. This dyke is rich in purple fluorite and disseminated sulphides (mainly pyrite). The dyke rock closely resembles sparsely porphyritic fluorite-bearing rhyolite lavas of the Pitz Formation and sulphide-fluorite-bearing chill margins of miarolitic granite stocks in map areas 65 O/2 and O/7. Acid magmatism and associated fluorine- and sulphur-bearing hydrothermal systems are probably responsible for the base metal vein mineralization. Subaerial alkaline flows of the Christopher Island Formation are notably deficient in both sulphur and fluorine.

Acknowledgments

The authors thank T. Garagan and G. Tannis for their capable field assistance. A.L. Littlejohn and A.C. Roberts provided X-ray identification of secondary mineral assemblages and A.G. Plant was particularly helpful with electron microprobe energy dispersive investigations.

References

- Beaudry, C.
1979: A study of uranium-thorium bearing syenite intrusions from the District of Keewatin, N.W.T.; unpublished B.Sc. Thesis, University of Ottawa, 56 p.
- Caine, T.W., Debicki, R.L., Goodwin, J., and Smith, B.
1979: Index to Mining Assessment Reports; Document Numbers 019539, 061289, p. 70.
- Donaldson, J.A.
1965: The Dubawnt Group, Districts of Keewatin and Mackenzie; Geological Survey of Canada, Paper 64-20.
1969: Descriptive notes (with particular reference to the Late Proterozoic Dubawnt Group) to accompany a geological map of central Thelon Plain, Districts of Keewatin and Mackenzie (65 M, N, W½, 66 B, C, D, 75 P E½, 76 A, E½); Geological Survey of Canada, Paper 68-49.
- Eade, K.E. and Blake, D.H.
1977: Geology of the Tulemalu Lake map-area, District of Keewatin; in Report of Activities, Part A, Geological Survey of Canada, Paper 77-1A, p. 209-211.
- LeCheminant, A.N., Lambert, M.B., Miller, A.R., and Booth, G.W.
1979a: Geological studies: Tebesjuak Lake map area, District of Keewatin; in Current Research, Part A, Geological Survey of Canada, Paper 79-1A, p. 179-186.
- LeCheminant, A.N., Leatherbarrow, R.W., and Miller, A.R.
1979b: Thirty Mile Lake map area, District of Keewatin; in Current Research, Part B, Geological Survey of Canada, Paper 79-1B, p. 319-327.
- Miller, A.R.
1979: Uranium geology in the central Baker Lake Basin; in Current Research, Part A, Geological Survey of Canada, Paper 79-1A, p. 57-59.
Uranium geology of the eastern Baker Lake Basin; Geological Survey of Canada, Paper. (in prep)
- Schau, Mikkel and Hulbert, L.
1977: Granulites, anorthosites and cover rocks northeast of Baker Lake, District of Keewatin; in Report of Activities, Part A, Geological Survey of Canada, Paper 77-1A, p. 399-407.
- Streckeisen, A.
1973: IUGS Subcommittee on the Systematics of Igneous Rocks, classification and nomenclature of plutonic rocks. Recommendations; Neues Jahrbuch fuer Mineralogie, Monatshefte, v. 4, p. 149-164.
- Wright, G.M.
1955: Geological notes on central District of Keewatin; Geological Survey of Canada, Paper 55-17.
1967: Geology of the southeastern barren grounds, parts of the Districts of Mackenzie and Keewatin (Operation Keewatin, Baker, Thelon); Geological Survey of Canada, Memoir 350.

SCIENTIFIC AND TECHNICAL NOTES

NOTES SCIENTIFIQUES ET TECHNIQUES

OPERATION DEASE

Project 770016

H. Gabrielse
Cordilleran Geology Division, Vancouver

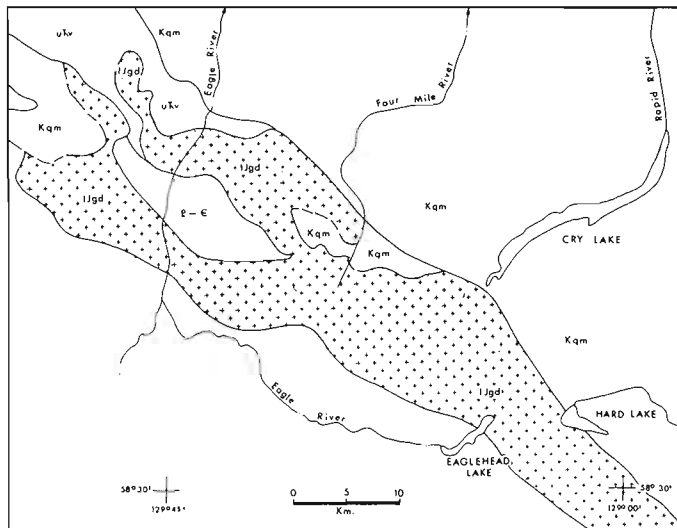
Introduction

Regional mapping accompanied by selected detailed studies was continued in Cry Lake (104 I), Dease Lake (104 J) and Spatsizi (104 H) map areas in 1979. T.N. Irvine of the Geophysical Laboratory, Washington, D.C. spent two and one-half weeks examining an Alaskan type ultrabasic body along Turnagain River northeast of the mouth of Hard Creek (Gabrielse, 1979). R.G. Anderson completed field work on a thesis project dealing with the Hotailuh Batholith and related rocks. Linda Thorstad completed a thesis study of the "Kutcho Formation" which hosts a massive copper-zinc deposit east of Kutcho Creek. J.L. Mansy concluded a study of Upper Proterozoic stratigraphy and structural style in the Omineca and Cassiar mountains. S. Leaming continued investigations of ultramafic rocks in the Cry Lake and Dease Lake map areas with emphasis on alteration mineral assemblages. Logistic support was provided for several biostratigraphic studies: by W.H. Fritz on Lower Cambrian strata in Cassiar and northern Rocky Mountains; by B.S. Norford on Ordovician and Silurian strata in Cassiar and northern Rocky Mountains; by J.W.H. Monger on Upper Triassic and Lower Jurassic volcanogenic rocks in Tulsequah (104 K) and Dease Lake map areas; and by H.W. Tipper on Jurassic strata in Tulsequah and Spatsizi map areas.

Stratigraphy

North of the easterly flowing of Turnagain River, between the valley leading to Major Hart River and longitude 128°20' (see Gabrielse, 1979) strata of Late Devonian(?) age appear to rest unconformably on Cambro-Ordovician strata of the Kechika Group. Farther west and northwest fetid carbonate, 10 to 15 m thick, of probable Middle Devonian age occurs beneath the fine grained black slate of the Late Devonian sequence.

Just southeast of Serpentine Creek in central Cry Lake map area near longitude 130°00' strata of the Inklin Formation, 'Kutcho formation', and Cache Creek Group are well exposed. Contacts are offset by left-handed northeast-trending faults. The Cache Creek Group near the contact with conglomerate of the 'Kutcho formation' is typical fine grained green-weathering volcanic rock. No evidence was found for structural discontinuity between the three assemblages and contacts appear to be depositional with unconformities below the Inklin and Kutcho strata. Thus, the Nahlin Fault is of little importance in this area relative to the southern margin of the Cache Creek rocks. J.W.H. Monger (personal communication, 1979) noted similar relationships west of Dease Lake.



- E-E** - Upper Proterozoic(?) and Lower Cambrian metamorphosed clastic rocks;
- uTv** - Upper Triassic andesitic volcanics;
- IJgd** - Lower Jurassic(?) diorite and granodiorite;
- Kqm** - mid-Cretaceous quartz monzonite.

Figure 1. Sketch map showing distribution of Lower Jurassic(?) hornblende diorite and biotite-hornblende granodiorite in northwestern Cry Lake map area.

Granitic Rocks

A batholith comprising medium- to coarse-grained hornblende diorite and hornblende-biotite granodiorite, commonly foliated, was mapped in a terrane formerly included in the Cassiar Batholith which is characterized by biotite quartz monzonite (Fig. 1). The diorite and granodiorite are identical to that underlying large areas in Toodoggone River map area to the southeast and are tentatively considered to be of Early Jurassic age. It includes stocks and plugs of fine- to medium-grained quartz monzonite probably related to the Cassiar Batholith.

Reference

- Gabrielse, H.
1979: Geological map of Cry Lake map-area; Geological Survey of Canada, Open File Report 610.

OPERATION FINLAY

Project 700047

H. Gabrielse

Cordilleran Geology Division, Vancouver

Devono-Mississippian and Upper Triassic strata were examined briefly between the headwaters of Joe Poole Creek and Warneford River in Ware west half (94E W1/2) map area. There a previously unrecognized sequence of fossiliferous Upper Triassic rocks is preserved in a syncline with a klippe of clastic Devono-Mississippian strata forming the core (Fig. 1, 2). The Upper Triassic sequence comprises about 150 m of dark grey calcareous siltstone and shale with resistant beds of buff weathering argillaceous limestone overlain by about 150 m of recessive weathering platy calcareous shale and siltstone. The Upper Triassic beds overlie a resistant well bedded unit, as much as 100 m thick, of black cherty argillite, porcellanite and chert. The age of the cherty unit is in doubt although it has been included in the Devono-Mississippian clastic assemblage.



Figure 2. View southerly to klippe of Devono-Mississippian clastic rocks on Upper Triassic strata southeast of headwaters of Joe Poole Creek.

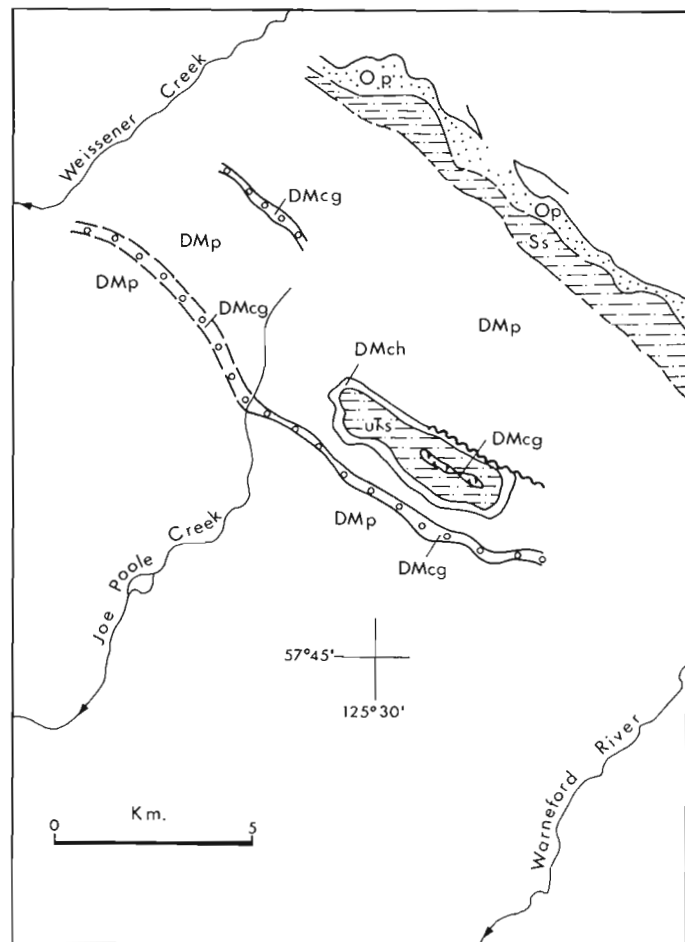


Figure 1. Sketch map of geology near headwaters of Joe Poole Creek.

- | | |
|---|--|
| Op - Ordovician graptolitic shale and argillaceous limestone; | DMcg - chert-pebble conglomerate; |
| Ss - Silurian siltstone and dolomitic siltstone; | DMch - chert and siliceous shale; |
| DMp - Upper Devonian and (?) Lower Mississippian black shale; | UTs - Upper Triassic siltstone, shale and limestone. |

Study of a small area south of Kwadacha River and on trend with rocks host to barite-lead-zinc deposits revealed the presence of a system of northeasterly directed imbricated thrust faults. Commonly the hanging walls comprise resistant tan weathering Silurian siltstone and dolomitic siltstone underlain by a variable thickness of Ordovician black shale and calcareous shale. The footwall strata generally are incompetent Upper Devonian slates or Ordovician shales. The Upper Devonian strata, previously included in the Road River Formation (Gabrielse, 1977), are exposed with older rocks in a belt as much as 3 km wide extending southeasterly from northeast of Mount Alcock to beyond the head of Paul River.

The thrust plates exposed west of a prominent Middle Devonian carbonate formation do not include the carbonate indicating that this unit was either not deposited or was eroded farther west. Examination of the Middle Devonian carbonate formation suggests that much of its deposition was in situ rather than of olistostromal origin.

Reference

Gabrielse, H.
1977: Geological map of Ware W1/2 and Toodoggone River map-areas; Geological Survey of Canada, Open File Report 483.

From: Scientific and Technical Notes in Current Research, Part A; Geol. Surv. Can., Paper 80-1A.

**STUDIES OF ULTRAMAFIC ROCKS IN DEASE LAKE AREA,
BRITISH COLUMBIA**

Project 490038

S. Leaming
Cordilleran Geology Division, Vancouver

Introduction

During the 1979 field season further investigations in the eastern part of the Atlin terrane (Monger, 1975) were carried out from a base camp near Dease Lake, British Columbia. About two months were spent studying rocks of the Cache Creek Group centred on King Mountain in Cry Lake map area (104 I) and about a month in the Dease Lake map area (104 J) at Tachilta Lakes and along Thibert Creek.

King Mountain Ultramafic and Related Rocks

The King Mountain area is underlain by several rock types including serpentized ultramafics, mafic rocks, both intrusive and extrusive, and marine sediments, mainly chert, pelite and minor crystalline limestone (Fig. 1). They form a tectonic mélange bounded on the south by the Nahlin fault, and on the north by Kutcho fault.

The ultramafic rocks are pervasively serpentized but are not everywhere deformed. They consist of peridotite and minor dunite; some of the peridotite may include harzburgite or wehrlite. Where deformation is intense, the rocks are black, fine grained, and highly slickensided, and commonly weather light green. Where deformation is weak, the rocks are massive and tough and weather to shades of reddish brown.

The mafic rocks are predominantly well to weakly layered amphibole-plagioclase-epidote group rocks thought to be gabbro but which may be amphibolite later affected by greenschist facies metamorphism. The layering is most pronounced in the cirque on the north side of King Mountain but it is not entirely absent elsewhere. In general the rocks are medium- to fine-grained with few minerals larger than 2-3 mm across. For this reason these rocks were mapped as greenstone (i.e. altered volcanics) in previous field seasons. Some of the fine grained phases may be dykes or sills.

In a few places, pyroxenite and peridotite masses appear within the gabbro. These appear to be cumulates.

In a few places, dark coloured, fine grained rocks show poorly developed pillow structure. In the absence of this criterion, it is difficult to recognize them as volcanics.

Chert and cherty pelites form a large proportion of the Cache Creek Group in the King Mountain area. They are generally schistose rocks; the regional schistosity trends northwest and dips steeply. In places, especially along the south side of King Mountain, northwest-trending folds in the cherts plunge nearly vertically. These folds are evidence of deformation earlier than that which produced the schistosity and are probably unrelated to movement along the Nahlin fault.

Limestone units of the Cache Creek Group are recrystallized to marble or crystalline limestone, and where in contact with serpentinite may give rise to contact reaction zones.

The King Mountain area has been disrupted along at least four major and many minor faults. The King Salmon fault is a major thrust which has carried the Cache Creek Group over the Takwahoni Formation. The surface trace of this fault lies about 12 km south of King Mountain and dips under it. The thrust may extend to the Kutcho fault which marks the northern limit of the Cache Creek Group in this area. The Nahlin fault is a vertical fault in the vicinity of King Mountain and brings together the Cache Creek Group and rocks of the Inklin Formation.

Between the Nahlin and Kutcho faults the Cache Creek Group has been affected by two other major faults. The King fault is marked by intensely sheared serpentinite and is interpreted as a normal fault in which the north side moved up to expose the overlying gabbro to erosion. The other fault, called the Letain fault, is assumed to underlie the lineament occupied by Letain Lake, and serves to explain the presence of gabbroic rocks overlying the ultramafics north of Letain Lake. Within the serpentinite bodies, slickenside zones, sheared disrupted bodies of limestone and chert, and peridotite nodules testify to the complex tectonic history of the area. The peridotite nodules are hard and tough with one or more sole marks thought to be the result of rotation and crushing of angular blocks of serpentized peridotite within a shear zone. The largest nodules are roughly spherical and about 20-25 cm across, but some as small as 3-4 cm have been seen.

Further evidence of the great stress involved in serpentinite deformation is the presence of foliation and fractures in many of the nephrite deposits commonly found in this area. Such deposits are entirely worthless for lapidary purposes because of foliation and close-spaced fractures. These structures reflect the tectonic history of these rocks since their formation as contact reaction zones to their final emplacement as tectonic inclusions of heavy rocks (S.G. = 3.0) in light serpentinites (S.G. = 2.6).

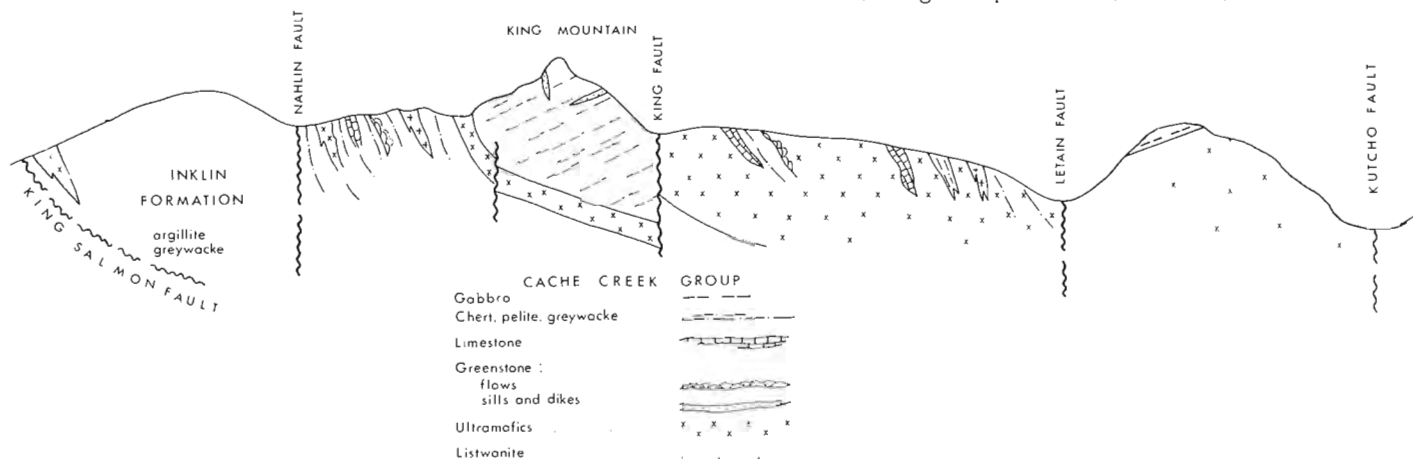


Figure 1. Diagrammatic cross-section through King Mountain (looking west).

From: *Scientific and Technical Notes
in Current Research, Part A;
Geol. Surv. Can., Paper 80-1A.*

The King Mountain succession may represent a dismembered ophiolite but it lacks the sheeted-dyke complex and pillow lavas are rare.

Ultramafic Rocks at Tachilta Lakes

The ultramafic rocks at Tachilta Lakes, 65 km west of Dease Lake, investigated around the shoreline and on short traverses inland, were found to be largely undeformed and much less serpentinized than those around King Mountain. They are massive brown weathering peridotites with few if any alteration zones, and are cut rarely by serpentinized shears. An interesting phenomenon associated with these rocks is the production of "alligator skin" in which a wrinkled effect is produced by weathering along two or more intersecting cracks. Souther (1971) noted these in ultramafic rocks in the Tulsequah area and explained them as shrinkage cracks due to the replacement of olivine by pyroxene.

Much of the Tachilta Lakes ultramafic rocks are in contact with granitic rocks assigned to Triassic and later by Gabrielse (1962). A sample for radiometric age determination was obtained.

There is no significant magnetic anomaly over the Tachilta ultramafic rocks in marked contrast to the magnetic highs which mark those centred on King Mountain. It might be therefore that the magnetite normally associated with serpentinization, has been incorporated into regenerated olivine because of the heat from the granitic rocks which intrude the ultramafics.

Carbonate Rocks Associated with Ultramafics

Carbonatized zones within the ultramafic rocks are numerous throughout the area, and in fact are found in alpine ultramafic rocks elsewhere in the world. Commonly these zones also contain quartz, talc, chlorite, limonite and mariposite in various proportions. In the King Mountain area, however, such zones are marked by small bodies consisting mainly of quartz, magnesite and mariposite. The largest bodies seen are about 100 m long and 5 m wide.

Soviet geologists call similar rocks listwanites and the term listwanitization is used to describe this type of alteration, but the terms are rarely used in North America. Whatever the name, such rocks are auriferous in some parts of the U.S.S.R., and the possibility that this might apply to some of the bodies in the King Mountain area is being investigated.

References

- Gabrielse, H.
1962: Geology of Dease Lake map-area; Geological Survey of Canada, Map 21-1962.
- Monger, J.W.H.
1975: Upper Paleozoic rocks of the Atlin Terrane, northwestern British Columbia and south-central Yukon; Geological Survey of Canada, Paper 74-47.
- Souther, J.G.
1971: Geology and mineral deposits of Tulsequah map-area, British Columbia; Geological Survey of Canada, Memoir 362.

**STRUCTURE OF THE TURNAGAIN RIVER PENDANT
IN NORTHEASTERN CRY LAKE MAP AREA,
BRITISH COLUMBIA**

Project 770016

J.L. Mansy¹
Cordilleran Geology Division, Vancouver

Introduction

Cursory examination in 1977 of an area enclosed on the west, south and east by granitic rocks south of Turnagain River led to the tentative conclusion that recumbant, westerly overturned folds were major elements in the structure (Gabrielse and Mansy, 1978). Detailed work in 1979 shows that large folds are not evident but that intraformational faults are important.

Stratigraphy

In the pendant area south of Turnagain River a sequence typical of the miogeoclinal assemblage west of Kechika Fault includes strata ranging from the Swannell Formation of the Proterozoic Ingenika Group to the carbonates of the Middle Devonian McDame Group (see Fig. 1; Gabrielse, 1979). Locally, formations may be thin or absent because of deformation.

Structure

No large recumbent structures are present but recumbent folds on scales of from 10 cm to 10 m involving transposition of bedding are abundant (Fig. 1). Although the formations are essentially in normal stratigraphic order, lithological units are commonly separated by flat to gently dipping faults that truncate underlying beds (Fig. 3, 2).

Figure 1.

Folded beds of Stelkuz Formation in hanging-wall of flat fault south of Turnagain River. Slab is about 20 cm long.

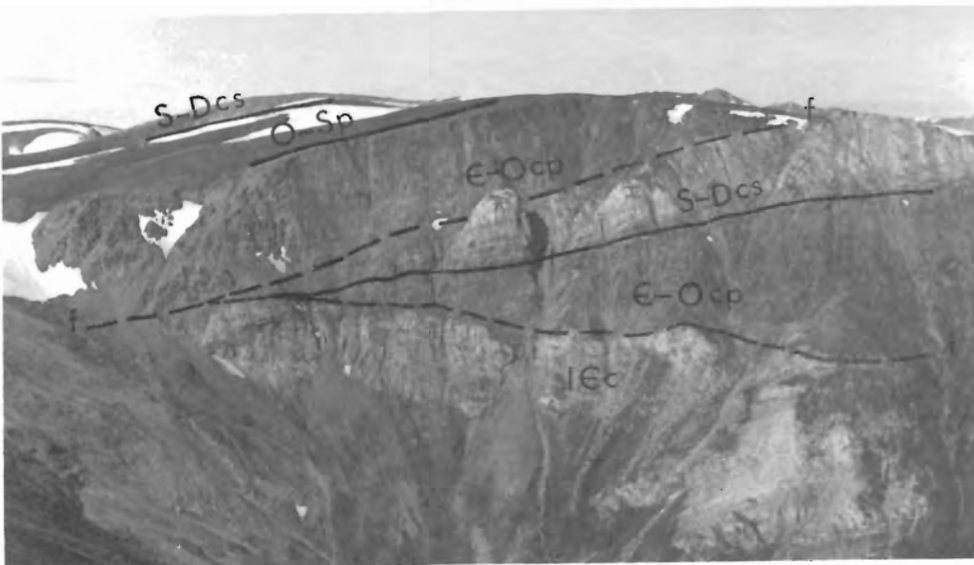
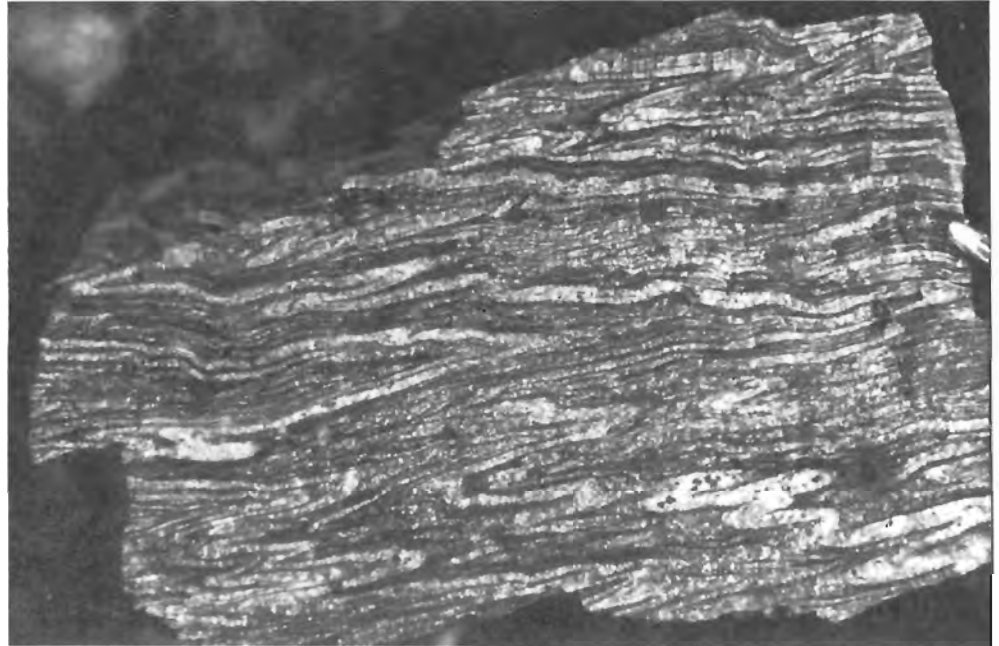


Figure 2.

View southerly south of Turnagain River.

- 1Ec Atan Formation limestone
 - E-Ocp Kechika Group shale and argillaceous limestone
 - O-Sp graptolitic shale and siltstone
 - S-Dcs dolomite, sandy dolomite, limestone
- Lower fault (f) is gently dipping whereas upper one is nearly vertical.

¹ University of Lille, France

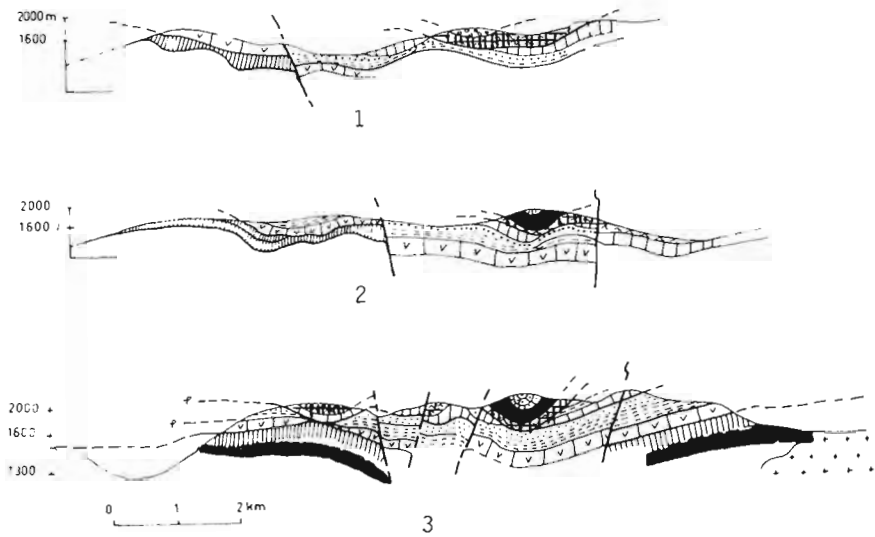
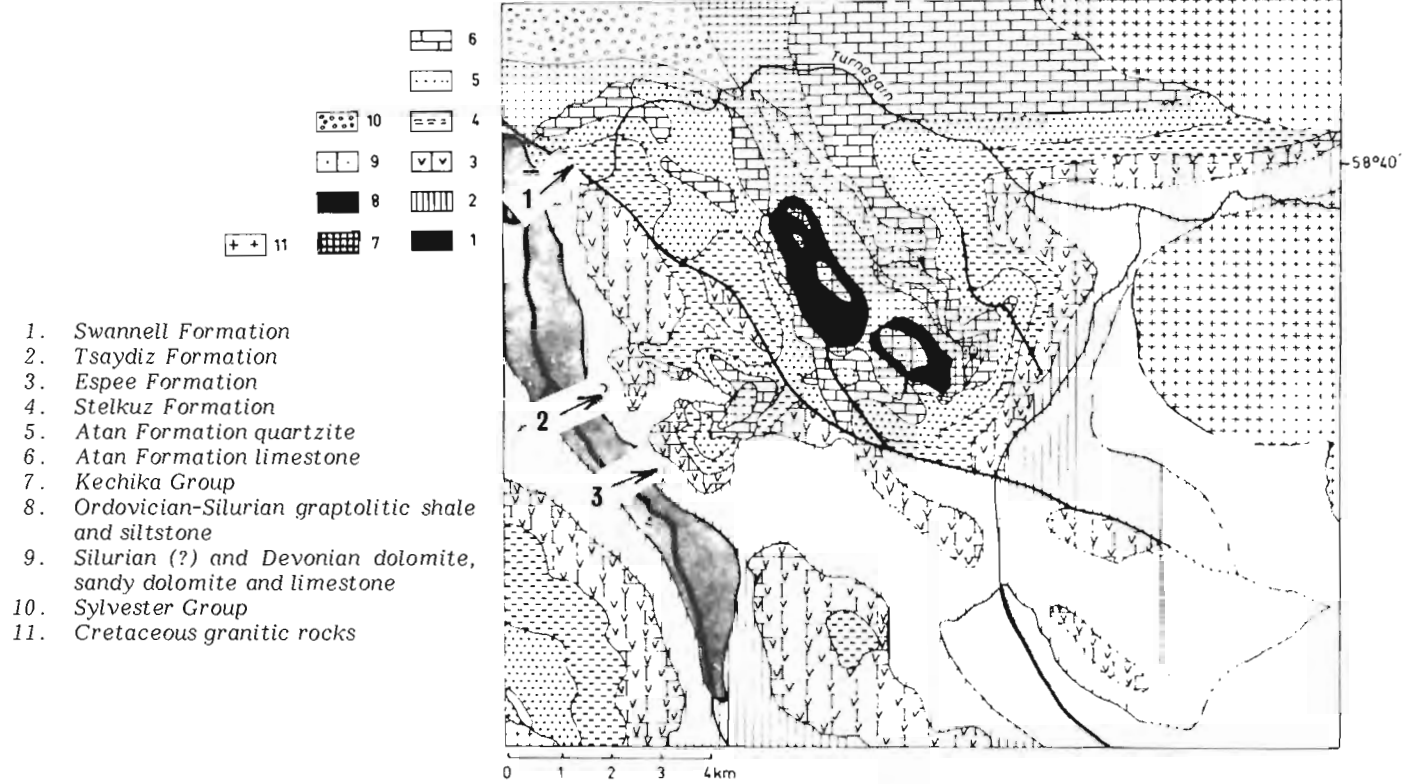


Figure 3. Sketch map and diagrammatic cross-sections for Turnagain pendant area.

Incompetent units including the Tsaydiz Formation, Kechika Group and graptolitic Silurian rocks are disharmonically folded and greatly variable in thickness. Polyphase folding, characteristic of Cassiar and Omineca mountains, is not as easily discerned as in similar terranes elsewhere but is clearly evident locally. The earliest phase produced the tight small isoclinal folds in conjunction with the development of southwesterly-directed, flat thrusts. A second phase produced fairly open folds trending northwesterly and was mainly responsible for the present map pattern. The third phase resulted in kink folds trending slightly south of east.

On regional evidence the three phases of deformation are considered, tentatively, to be mid-Jurassic, Late Jurassic to mid-Cretaceous and early Cenozoic (Gabielse, personal communication, 1979).

Metamorphism

Andalusite and staurolite are conspicuous near contacts of clastic rocks with granitic rocks of the Cassiar Batholith. Biotite and possibly garnet formed during the first phase of deformation and garnet, andalusite, staurolite and sillimanite accompanied the second phase.

References

Gabielse, H.
 1979: Geological map of Cry Lake map-area; Geological Survey of Canada, Open File Report 610.

Gabielse, H. and Mansy, J.L.
 1978: Structure style in northeast Cry Lake map-area, north-central British Columbia; in Current Research, Part A, Geological Survey of Canada, Paper 78-1A, p. 33-34.

**STRATIGRAPHIC CROSS-SECTION,
SELWYN BASIN TO MACKENZIE PLATFORM,
NAHANNI MAP AREA, YUKON TERRITORY AND
DISTRICT OF MACKENZIE**

Project 790007

S.P. Gordey
Cordilleran Geology Division, Vancouver

Introduction

Nahanni map area is underlain by sedimentary rocks ranging in age from Late Proterozoic to Devonian-Mississippian that change facies rapidly across generally northwest-trending hinge lines. Stratigraphic relations of northeastern platformal carbonate units (Mackenzie Platform) have been investigated this past field season as part of a regional mapping program refining the bedrock geology of Nahanni map area at a scale of 1:250 000 and locally at a scale of 1:50 000. Others of the Geological Survey currently working in the area include W. Goodfellow and I. Jonasson doing a preliminary geochemical study of the Howard's Pass deposit and laterally equivalent unmineralized rocks, J. Lydon studying the ore deposit mineralogy, textures, and structures, and K.M. Dawson investigating major showings. W.H. Fritz and B.S. Norford examined sections of Lower Cambrian and Ordovician-Silurian strata. This preliminary report describes the stratigraphic relationships of the northeastern platformal carbonate units and, along with earlier reports on the westerly basinal facies (Selwyn Basin) (Gordey, 1978, 1979), forms a preliminary account of the stratigraphy of Nahanni map area. Figure 1 summarizes this knowledge to date. In the following text numbers in brackets, e.g. (unit 2), refer to the map units of the 1:250 000 scale Nahanni geologic map by Blusson et al. (1968). The writer is grateful for the logistical assistance of Welcome North Mines and particularly Riocean Exploration.

Proterozoic and Lower Cambrian

The oldest strata in northeastern Nahanni map area are dark brown weathering siltstone, shale, and green quartz sandstone (unit 3), fine grained and probably deeper water equivalents of the Backbone Ranges Formation mapped by Gabrielse et al. (1973) in Glacier Lake map area to the east. To the southwest equivalent strata (unit 2) are finer grained, consisting of siltstone, shale and minor sandstone and merge with distinctive maroon and blue-black weathering shale of the upper part of the Grit Unit (unit 1a). Southeast of area C clastics of the upper Backbone Ranges, at least 950 m thick, overlie buff weathering dolomite equivalent to the middle carbonate member of the Backbone Ranges Formation in the type area (Gabrielse et al., 1973, p. 34). Tracks and trails are abundant in the upper part of the formation which is overlain conformably by Lower Cambrian carbonate of the Sekwi Formation.

The Sekwi Formation consists of a lower carbonate member (unit 4), overlain by quartz arenite, dolomite, and shallow water maroon shale (unit 5). Both of these members exist to the northeast (unit 5a), although they are thinner, and the quartz arenite is less abundant. The regional 'swiss-cheese' nodular limestone member of the basal Sekwi (unit 4a) is minor in northeastern sections (section D). To the southwest the Sekwi is equivalent to buff weathering shale and grey mudstone which rest above local archeocyathid-bearing limestone conglomerate debris flows.

Middle Cambrian

The Middle Cambrian Rockslide Formation (unit 6) overlies the Sekwi Formation with sharp and presumably conformable contact. The upper part of the Sekwi is poorly fossiliferous and a faunal break between Middle and Upper Cambrian strata has not been documented in the Nahanni area (Fritz, personal communication). Gabrielse et al. (1973) reported a regional disconformity between Middle and Lower Cambrian strata in Glacier Lake map area to the east. If the contact is disconformable it is likely that little of the upper Sekwi has been removed.

The Rockslide Formation contains mostly dark brown weathering thin bedded fossiliferous silty limestone overlain locally by medium bedded grey weathering dolomite (Fritz, 1979). Southeast of area C dolomite progressively replaces the upper part of the Rockslide to a thickness of at least 140 m. Strata of Middle Cambrian age have been removed in Selwyn Basin by sub-Cambro-Ordovician erosion.

Cambro-Ordovician

At the base of the Franconian (middle Upper Cambrian) is an important regional unconformity which in Selwyn Basin cuts down as low as the maroon shale of the upper Grit Unit, the Rabbitkettle Formation (unit 7b) resting directly above. In area C the beds above the unconformity are shallow water, mudcracked and ripple marked mudstone, sandstone and orange dolomite about 100 m thick (unit 7a) which are in sharp contact with the underlying Middle Cambrian Rockslide Formation. To the northeast where there is no appreciable faunal break between lithologically similar Rabbitkettle and Rockslide formations (Fritz, personal communication) the time horizon is marked by an influx of fine grained quartz sand (section D).

In contrast to older units which show similar facies over large areas, lithologies of Cambro-Ordovician age are varied. In the northeast the Rabbitkettle Formation consists of thin bedded orange weathering argillaceous locally nodular limestone. Its time equivalent, the Broken Skull Formation is grey weathering, medium- to thick-bedded grey dolomite (section C). In section C the unfossiliferous Broken Skull - Sunblood Formation forms a single thick carbonate unit that includes rocks as young as Silurian (Whittaker Formation equivalents). In Cambro-Ordovician time the relatively shallow water facies of area C were deposited on a northwest-trending arch separating equivalent relatively deeper water Rabbitkettle Limestone to the northeast and southwest.

Ordovician and Silurian

The predominantly Ordovician and Silurian Road River Formation (unit 10) comprises an assemblage of various facies. In the southwest a distinctive orange weathering mudstone, a good stratigraphic marker in Selwyn Basin, is equivalent on the platform to tan weathering thin bedded limy siltstone and argillaceous limestone. In the northeast (sections D, E) the Silurian part of the section is a porcelain blue-grey weathering thin bedded limestone. The overlying dark tan to buff silty limestone, containing a vague wispy lamination similar to the bioturbated orange mudstone, may range up to Lower Devonian. Blue-grey porcelaneous limestone of Early Ordovician age forms a tongue of Road River Formation in area D.

The sub-Whittaker (sub-Upper Ordovician) unconformity recognized to the northeast continues as far southwest as section D. It is likely present in sections C and E, but cannot be recognized within the monotonous unfossiliferous dolomite sequence.

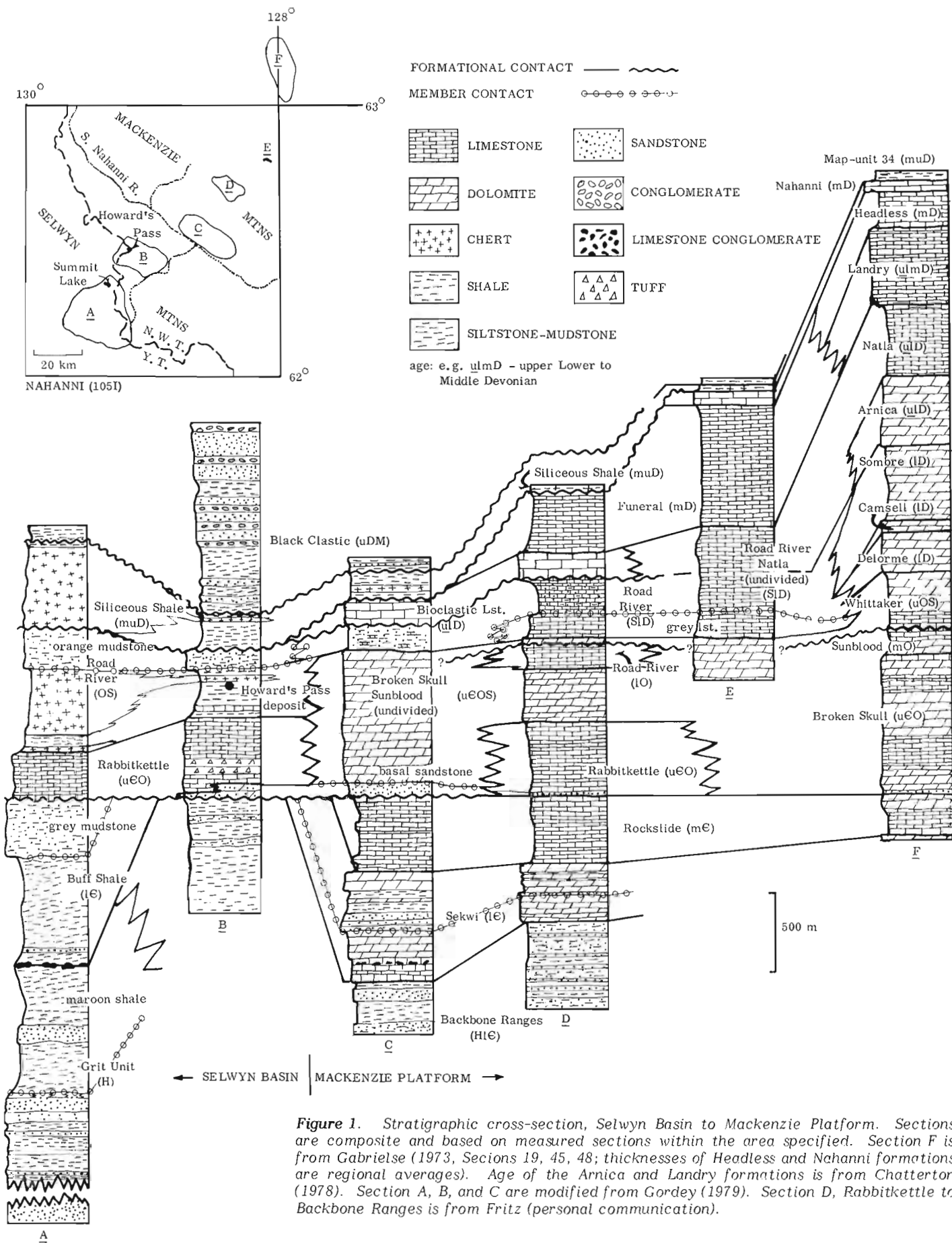


Figure 1. Stratigraphic cross-section, Selwyn Basin to Mackenzie Platform. Sections are composite and based on measured sections within the area specified. Section F is from Gabrielse (1973, Sections 19, 45, 48; thicknesses of Headless and Nahanni formations are regional averages). Age of the Arnica and Landry formations is from Chatterton (1978). Section A, B, and C are modified from Gordey (1979). Section D, Rabbitkettle to Backbone Ranges is from Fritz (personal communication).

Lower and Middle Devonian

In northeastern Nahanni map area blue-grey weathering thin-bedded to massive limestone and crinoidal limestone (units 18 and 16b) forms a prominent unit up to 175 m thick. Locally well preserved coralline faunas indicate a latest Early Devonian age. It sits unconformably on the Road River Formation so that locally in area C it rests directly upon Silurian dolomite. Crinoid-stem fragments with twin axial canals are numerous and characteristic of this unit. Northeasterly, presumably through facies changes, the bioclastic limestone loses its entity as a mappable unit and is partly equivalent to dark weathering thin-bedded limestone of the Natla Formation, which also contains 2-hole crinoids in abundance (sections D, E).

The Middle Devonian Funeral Formation (unit 16a) overlies the bioclastic limestone and Road River - Natla (undivided) formations (unit 15) with sharp contact; the orange weathering thin bedded silty limestone of the Funeral forms a sharp contrast with underlying blue-grey to black weathering strata. The Funeral is mostly equivalent to buff and orange weathering thin- to thick-bedded limestone of the Landry and Headless formations to the northeast (section F). It thins rapidly southwesterly due to erosion beneath overlying Middle and Upper Devonian siliceous shale and chert.

Upper Devonian to Mississippian

The siliceous shale (base of unit 18) is a distinctive gun-blue, black, or steel grey weathering unit of siliceous shale and thin-bedded black chert sitting in sharp unconformable contact on underlying units. In the vicinity of section D mid-Devonian fossils have been collected at the top of the underlying Funeral, and at two localities in area B upper Devonian conodonts have been recovered from thin limestones in the unit just below the contact with overlying black clastic shales. If the extrapolation of the unconformity beneath this Middle and Upper Devonian unit southwestward above the orange mudstone is correct, there may be little or no Lower Devonian strata preserved in this part of Selwyn Basin. The rapid changes of thickness and abrupt contact that suggest unconformable relations between the siliceous shale and black clastic (Section B) in the southwest persist into northeastern Nahanni area. Farther east in Mackenzie Mountains the Nahanni Formation maintains a relatively constant thickness, and the contact with overlying shales is reported to be sharp and apparently conformable (Gabrielse et al., 1973, p. 92). In the northeastern part of the area the brown weathering shales of the black clastic (unit 18) contain only minor amounts of sand in contrast to the coarse conglomerate found to the southwest.

Mineral Exploration Guide

The stratigraphic position of the Howard's Pass stratiform lead-zinc deposit and its relationship to facies boundaries is shown in Figure 1. The stratigraphic position of the Vulcan property, currently being evaluated by RioCanex Exploration is at the lower contact of the bioclastic limestone. However, the age of the Vulcan lead-zinc-iron massive sulphide and associated fluorite, and even whether it is stratigraphically controlled remain uncertain. Small showings of sphalerite occur in other places in Nahanni at this stratigraphic level. South-southeast of area C volcanic flows, tuffs, and intercalated dolomite up to 340 m thick occur in mid-Ordovician dolomite. These contain abundant pyrite, but are older and unrelated to the Vulcan mineralization. The volcanics are similar to those in the Rabbittkettle Formation in the Howard's Pass area and are probably of like age or slightly younger. The siliceous shale is host in its upper part of the Upper Devonian regional barite horizon equivalent to the lead-zinc-barite mineralization at Macmillan Pass. The unconformity beneath the black clastic may be responsible for its local absence.

References

- Blusson, S.L., Green, L.H., and Roddick, J.A.
1968: Nahanni, District of Mackenzie and Yukon Territory; Geological Survey of Canada, Map 8-1967.
- Chatterton, B.D.E.
1978: Aspects of late Early and Middle Devonian conodont biostratigraphy of western and northwestern Canada; in *Western and Arctic Canadian Biostratigraphy*, Stelck, C.R. and Chatterton, B.D.E., ed., Geological Association of Canada, Special Paper 18, p. 161-231.
- Fritz, W.H.
1979: Cambrian stratigraphic section between South Nahanni and Broken Skull rivers, southern Mackenzie Mountains; in *Current Research, Part B*, Geological Survey of Canada, Paper 79-1B, p. 121-125.
- Gabrielse, H., Blusson, S.L. and Roddick, J.A.
1973: Geology of Flat River, Glacier Lake, and Wrigley Lake map-areas, District of Mackenzie and Yukon Territory; Geological Survey of Canada, Memoir 366.
- Gordey, S.P.
1978: Stratigraphy and structure of the Summit Lake area, Yukon and Northwest Territories; in *Current Research, Part A*, Geological Survey of Canada, Paper 78-1A, p. 43-48.
1979: Stratigraphy of southeastern Selwyn Basin in the Summit Lake area, Yukon Territory and Northwest Territories; in *Current Research, Part A*, Geological Survey of Canada, Paper 79-1A, p. 13-16.

**SUMMARY OF THE PETROLOGY OF THE
HEART PEAKS VOLCANIC CENTRE,
NORTHWESTERN BRITISH COLUMBIA**

EMR Research Agreement 121-4-79

J.J. Casey¹ and C.M. Scarfe¹
Cordilleran Geology Division

The late Cenozoic Heart Peaks Plateau of northwestern British Columbia (Casey and Scarfe, 1978; Casey, 1979) is broadly subdivided into flat-lying basaltic to intermediate rocks of the Level Mountain Group and rhyolite and trachyte domes of the Heart Peaks Formation.

The compositions of the Level Mountain Group lavas range from ankaramite to andesite and trachyte; alkali basalt and hawaiite are the dominant rock types. Major and trace element variations support the derivation of these lavas by a process of fractional crystallization from an alkali basalt parent. Textural and compositional similarities exist between Level Mountain Group lavas at Heart Peaks and at Level Mountain 16 m to the east (Hamilton and Scarfe, 1977; Hamilton, in preparation).

The rhyolite and trachyte domes of the Heart Peaks Formation appear to be closely related to the plateau lavas and probably erupted contemporaneously from different vents. The lack of peralkaline compositions contrasts with the distinctly peralkaline nature of silicic rocks present at Level Mountain and at Edziza (Souther, 1970).

Strontium and oxygen isotope data support a mantle origin for alkali basalt (see also Hamilton et al., 1978) and high abundances of large-ion lithophile elements are compatible with models that have small degrees of partial melting of peridotite. The origin of the rhyolites is more obscure, however, and requires further work.

Evidence from the Heart Peaks area supports Souther's (1970, 1977) model of a tensional tectonic environment for late Cenozoic volcanism in the Stikine belt of northern British Columbia.

References

- Casey, J.J.
1979: Geology of the Heart Peaks volcanic center, north-western British Columbia; M.Sc. thesis, University of Alberta, 116 p.
- Casey, J.J. and Scarfe, C.M.
1978: Geology of the Heart Peaks volcanic center, northwestern British Columbia; in *Current Research, Part A*, Geological Survey of Canada, Paper 78-1A, p. 87-89.
- Hamilton, T.S.
Petrology of the Level Mountain volcanic centre, northwestern British Columbia; Ph.D. thesis, University of Alberta (in prep).
- Hamilton, T.S. and Scarfe, C.M.
1977: Preliminary report of the petrology of the Level Mountain volcanic center, northwest British Columbia; in *Report of Activities, Part A*, Geological Survey of Canada, Paper 77-1A, p. 429-434.
- Hamilton, T.S., Baadsgaard, H., and Scarfe, C.M.
1978: Petrogenesis of late Cenozoic alkaline volcanics, Level Mountain, northern British Columbia; *Geological Society of America, Abstracts with Programs* 10, No. 7, 414 p.
- Souther, J.G.
1970: Volcanism and its relationship to recent crustal movements in the Canadian Cordillera; *Canadian Journal of Earth Sciences*, v. 7, p. 553-568.
- Souther, J.G.
1977: Volcanism and tectonic environments in the Canadian Cordillera - a second look; *Geological Association of Canada, Special Paper* 16, p. 3-24.

¹ Department of Geology, University of Alberta, Edmonton, T6G 2E3

HIGHLIGHTS OF FIELD WORK IN LABERGE AND CARMACKS MAP AREAS, YUKON TERRITORY

Project 770017

Dirk Tempelman-Kluit
Cordilleran Geology Division, Vancouver

Introduction

The geology of Laberge and Carmacks map areas was first investigated nearly fifty years ago when little was known of the geology of the Canadian Cordillera in general and of southern Yukon is particular. Reports of this early work (Bostock and Lees, 1938; Bostock 1936) constitute the first systematic geological information in Yukon. Since that study much new information has become available on the geology of the northern Cordillera and the present investigation was carried out in the context of this new understanding. Field re-examination was begun in Carmacks map area in 1974 (Tempelman-Kluit, 1974a, 1975) and in Laberge map area in 1977 (Tempelman-Kluit, 1978a, 1978b), and these areas were systematically remapped during the summer of 1979.

Field Work and Related Studies

Field work from base camps at Fox Lake and Carmacks was co-ordinated with independent special studies in the region by several individuals. Darrel Long (GSC, Calgary) studied the Tantalus Formation in detail. Terry Poulton (GSC, Calgary) examined fossiliferous sections of the Laberge Group to compare the fauna with that in equivalent strata elsewhere. Steve Hopkins (GSC, Calgary) examined selected sections of the Tantalus Formation and Carmacks Group, collecting material for palynological study. Steve Morrison (GSC, Calgary) examined the surficial geology of Laberge and Carmacks map areas and O.L. Hughes (GSC, Calgary) carried out similar studies in Mayo and Aishihik Lake map areas.

Philippe Erdmer, Helen Grond, Sheila Churchill, Pam Reid and Tim England provided able assistance in the field and began independent studies of certain strata for their graduate or undergraduate theses. Erdmer, a Ph.D. candidate at Queen's University, examined the fabric and metamorphic mineral assemblages in cataclastic rocks of Teslin Suture Zone to determine the physical conditions under which they were deformed. Reid (Ph.D. candidate at the University of Miami) collected material from the Upper Triassic carbonate reefs, in order to study their algal flora and associated fauna for comparison with carbonates of like age elsewhere. England collected samples from the Triassic reefs and intends to compare their conodonts with those of the now adjacent, and time equivalent, but paleogeographically remote Omineca Belt. Grond and Churchill studied sections of the Mount Nansen and Carmacks groups (Eocene) and collected material to determine by isotopic dating whether or not these strata are coeval. Mike Duff, pilot, and Janet Souther, cook, provided expert support.

General Geology

Carmacks and Laberge map areas in south central Yukon lie within the Intermontane Belt except for a small part of eastern Laberge map area which lies within the bounding Omineca Belt (Fig. 1). In the project area the Intermontane Belt is subdivided into three elements, the Yukon Cataclastic Complex, including Teslin Suture Zone, Whitehorse Trough and Yukon Crystalline Terrane. Yukon Cataclastic Complex and Teslin Suture Zone are developed in Upper Paleozoic basalt and Mesozoic sedimentary rocks whose relations and stratigraphy are obscured by Mesozoic

penetrative strain. Whitehorse Trough comprises Upper Triassic volcanics capped by carbonate reefs (Lewes River Group) and Lower Jurassic greywacke, shale and conglomerate, derived from the underlying Lewes River Group and Upper Triassic granitic rocks (Laberge Group). Yukon Crystalline Terrane includes quartz mica schist with quartzite, marble and amphibolite, and is possibly Early Paleozoic, although later metamorphosed.

The Mesozoic strata of Whitehorse Trough may rest depositionally on the Yukon Crystalline Terrane and on certain strata in Yukon Cataclastic Complex, but where exposed the contacts are faults. Relations between Yukon Cataclastic Complex and Yukon Crystalline Terrane are unknown; younger plutonic rocks intrude the contact and Tertiary volcanic rocks cover it. The contact between Teslin Suture Zone and Omineca Belt is a southwest dipping thrust fault locally modified by younger faults.

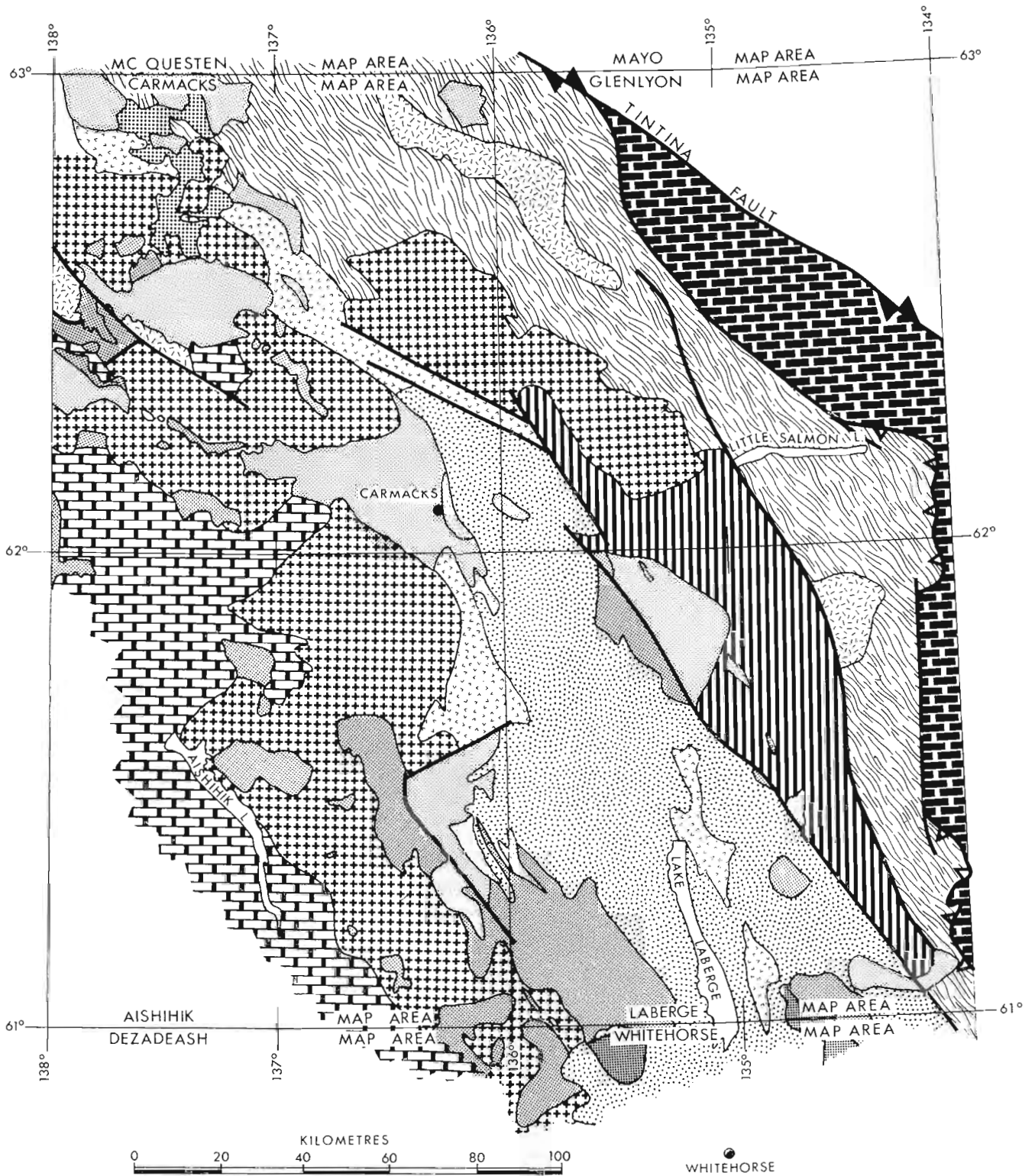
Results of Present Work

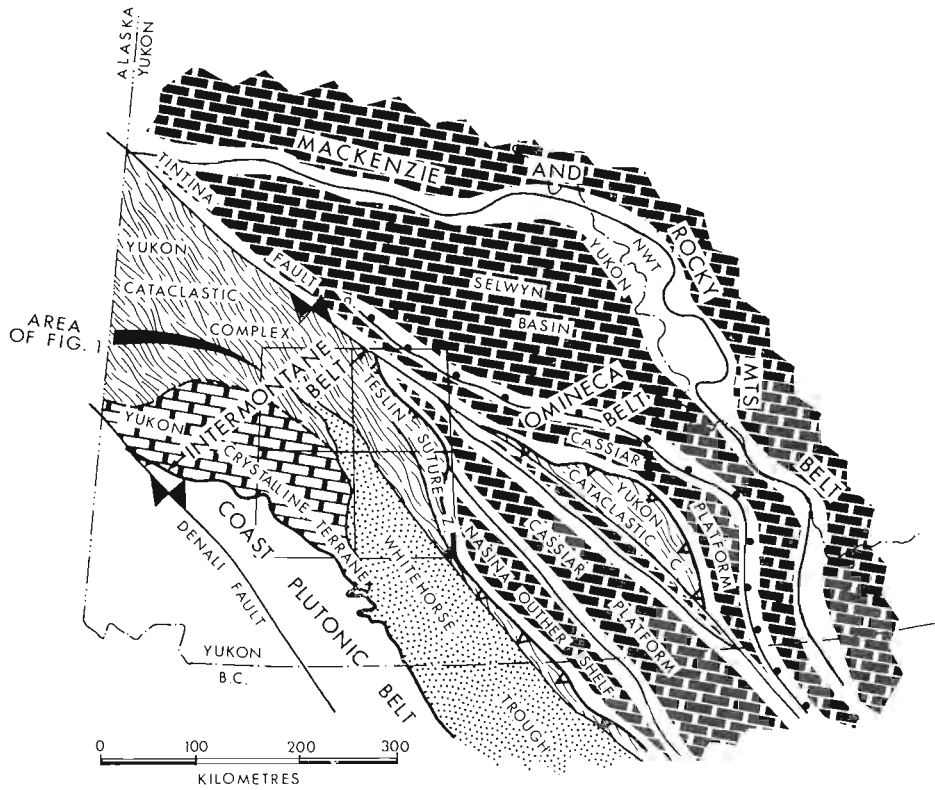
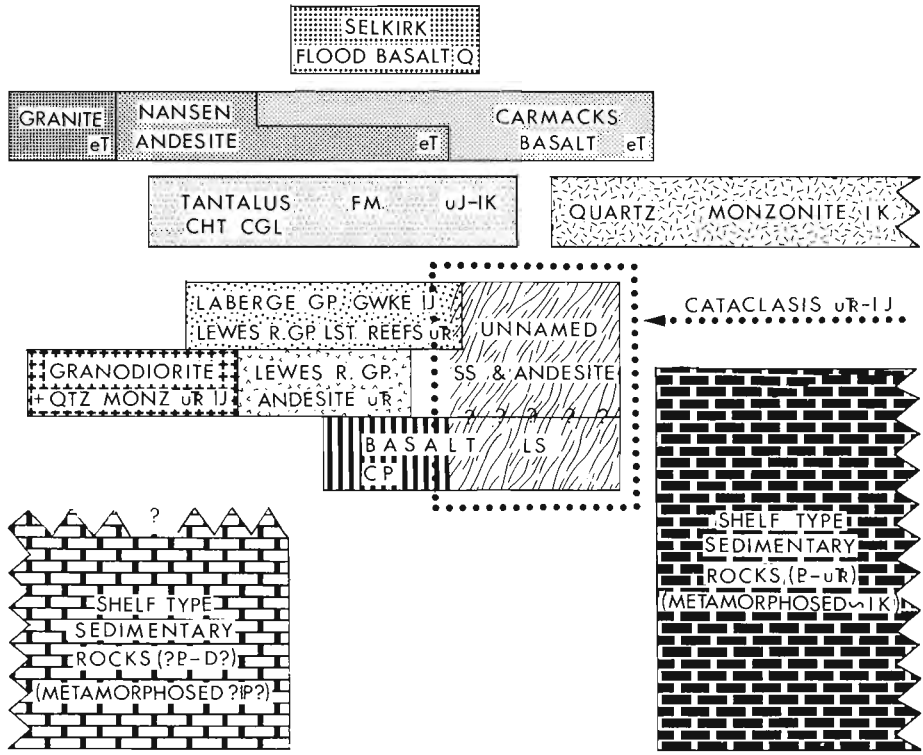
Fusulinids (tentatively considered Middle or Late Pennsylvanian by J.W.H. Monger) and other fossils were discovered in limestone and limy tuff at six localities in the Semenof Hills and on Boswell Mountain. This implies that the belt of basalt, tuff and chert which extends northwest diagonally across Laberge map area from Boswell Mountain to Moose Mountain, Mount Peters and the Semenof Hills, and with which the limestone is interbedded, is Late Paleozoic. Previously these rocks were assigned to the Mesozoic (Unit uTlJw of Tempelman-Kluit, 1978b) although Lees had discovered poorly preserved fossils that he considered Late Paleozoic in a limestone of this belt near Big Salmon (Bostock and Lees 1938, p.11). The Upper Paleozoic volcanics continue northwestward in Glenlyon map area (included with other rocks in Campbell's (1967) map unit 16a), and probably correspond to Mulligan's (1963) map unit 7. The fossiliferous volcanic, chert and limestone unit can be followed laterally into amphibolite and marble with related other rocks and imply a Late Paleozoic age for the amphibolite. Specifically, the amphibolite and marble included in Campbell's (1967) units 6 and 7 and their strike extension in northern Carmacks map area, (unit PPs_n of Tempelman-Kluit, 1974b) are probably the sheared and metamorphosed equivalents of the Upper Paleozoic Cache Creek Group in the Atlin Terrane. Amphibolite in Teslin Suture Zone is likewise considered Late Paleozoic.

The structure of the Lewes River and Laberge groups consists of fairly tight, slightly asymmetrical, northwest trending, faulted anticlines with the steeper limb on the southwest separated by comparatively open synclines. The wave length of the folds is about 15 km. Faults do not dominate the structure to the degree implied in Tempelman-Kluit (1978b). The main structure is an irregular anticline or culmination that can be followed northwest from near Lime Peak through Povoas Mountain and Frank Lake to Mandanna Lake. The Lewes River Group is exposed along much of its length.

The Mount Nansen and Carmacks groups are Tertiary volcanic rocks of acid to intermediate, and basaltic composition, respectively. They were thought to be depositionally separate; although the Mount Nansen Group is Eocene the Carmacks was considered to be possibly as young as Miocene. In Carmacks map area south of Prospector Mountain, on the south flank of Mount Pitts, and on the northeast side of Victoria Mountain the Carmacks Group overlies the Mount Nansen Group conformably. This suggests they are not greatly different in age and, although compositionally distinctive, may form one volcanic assemblage of Eocene age. The different relations at the base of the two groups (Tempelman-Kluit, 1974b, p. 44 and p. 52) are thought to reflect their different chemistry and

Figure 1. Map of the distribution of the main rock units in Laberge and Carmacks map areas showing the proposed correlations with adjacent areas. The inset shows the location of the map in relation to Cordillera wide subdivisions.





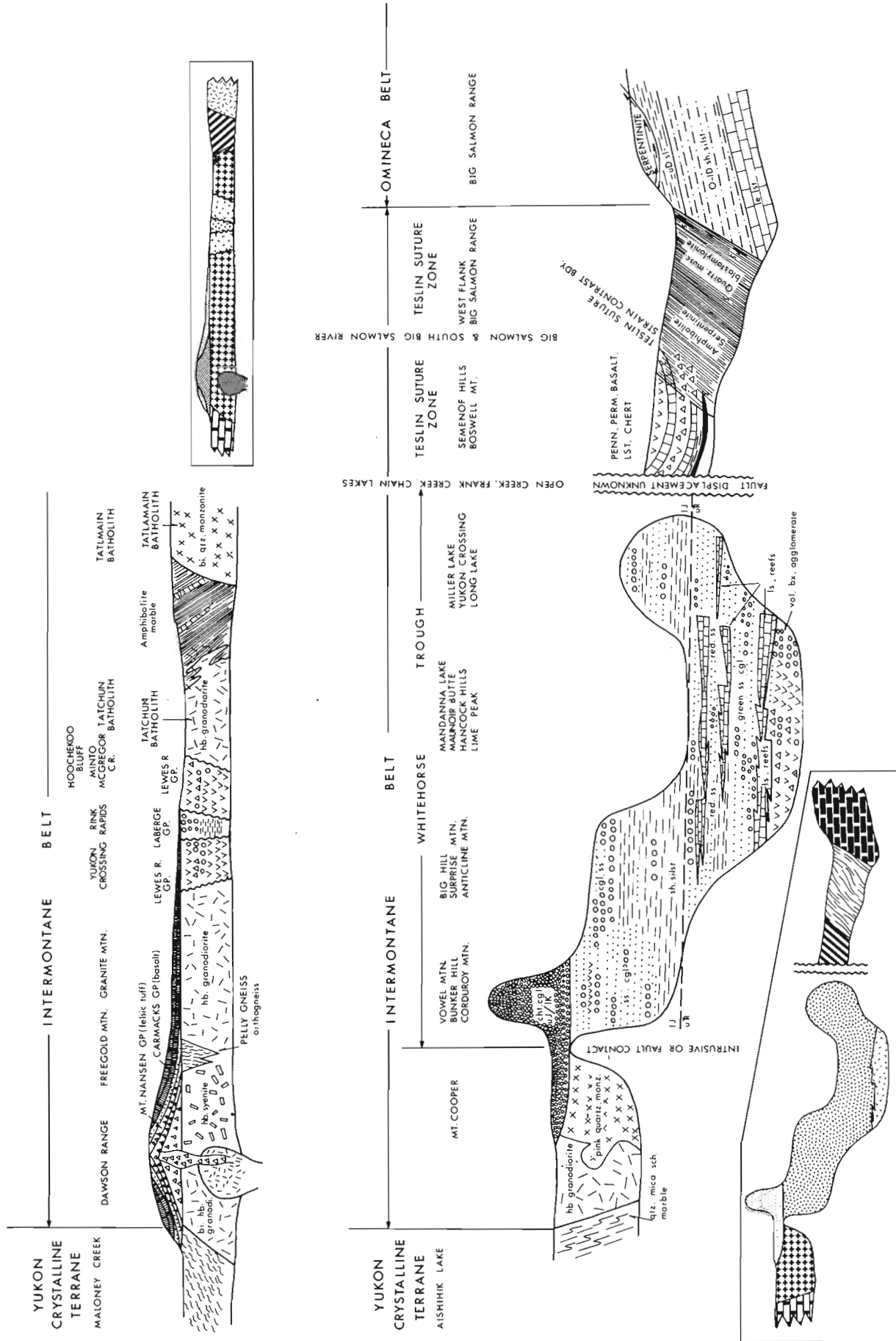


Figure 2. Schematic cross-sections (no scale; northeast on right to southwest on left) of Laberge and Carmacks map areas to show the relations of the rock units. The insets show how subdivisions of the cross-sections correspond to the units of Figure 1.

fluidity. Whereas the Mount Nansen Group is relatively restricted and preserved as plug domes in high parts of the Dawson Range, the Carmacks Group is a more extensive flood basalt which filled depressions in the surrounding topography. The Mount Nansen Group was interpreted to lie on remnants of an eroded upland surface and the Carmacks on an incised surface of greater relief similar to the present. Instead the topographic surface beneath the Carmacks and Mount Nansen groups may have been the same upland with a relief near 1000 m.

Feldspar porphyry dykes and plugs occur in a belt that trends northwest diagonally across Laberge map area. They are probably subvolcanic equivalents of the Mount Nansen Group and Eocene in age. The volcanics on Packers Mountain include flow-banded rhyolite and other felsic types and are considered of like affinity and age. Felsic volcanic rocks near the mouth of Boswell River appear fresher than the Carmacks and Mount Nansen groups. They are more extensive than shown in Tempelman-Kluit (1978b) and occupy a considerable area on the west side of Open Creek.

Of five fault blocks of conglomerate in the northeast half of Laberge map area included in map unit LKT or eTcg in Tempelman-Kluit (1978b) four are chert conglomerate and equivalents of the Tantalus Formation. The block astride the lower part of Walsh Creek contains conglomerate made up entirely of locally derived pebbles and boulders of graphitic quartzite (Nasina), quartz muscovite schist (Klondike), fresh intermediate volcanics (from Solitary Mountain), biotite quartz monzonite (Big Salmon Range) and quartz mica schist (Big Salmon Range). This conglomerate is interbedded with siltstone and peat deposits and is probably the remains of a fan built westward from Solitary Mountain. Strata closely similar to the finer grained parts of the Walsh Creek unit also occur in the upper part of the Carmacks Group on the west side of Five Finger Mountain.

The vast bulk of clasts in the Tantalus Formation are grey chert, most likely derived from the Cache Creek Group. Several clasts of muscovite quartz blastomylonite and one of amphibolite (from Teslin Suture Zone) were also discovered in the unit and this supports a general eastern or northeastern source for the Tantalus Formation.

Two distinct units of different age are included in syenite (map unit My; Tempelman-Kluit, 1974a) in the Dawson Range. The more spectacular rock is a coarse grained hornblende syenite with euhedral hornblende and pink K-feldspar phenocrysts. It is locally sheared and altered and is probably Mesozoic, possibly Late Triassic or Early Jurassic. The other rock is fine- to medium-grained equigranular biotite hornblende granite, the subvolcanic equivalent of the Mount Nansen Group and probably Eocene in age. The latter type predominates near Klaza Mountain and Prospector Mountain and the former is commonest east of there.

The Tatchun and Tatmain batholiths (Fig. 1) differ. Tatchun Batholith contains foliated biotite hornblende granodiorite that is likely Triassic or Jurassic but Tatmain Batholith is coarse grained biotite quartz monzonite without fabric, and grades locally into rhyolite and felsic tuff. These rocks are probably Cretaceous and correlatives of the Coffee Creek quartz monzonite (Fig. 1). The Tatmain Batholith clearly intrudes the surrounding strata but relations at the margins of Tatchun Batholith are ambiguous and modified by strain.

A sheet of serpentinized peridotite, 500 m thick, is interfoliated with quartz mica schist in the southwest corner of Carmacks map area 1 km south of peak 5269. The rock is an alpine ultramafic like those in the Pelly Mountains but its relations and association are unlike those and its age is unknown. Most of the bodies mapped as ultramafic in Carmacks map area (Tempelman-Kluit, 1974a) are mafic phases of the surrounding rocks and do not form mappable units.

The White Mountains in McQuesten map area were briefly examined to compare their geology, as mapped by Bostock (1964), with that in Finlayson Lake map area. The two main peaks, Flat Top and Rough Top, expose two klippen of near-horizontal serpentinized peridotite that lie structurally above muscovite quartz blastomylonite with a horizontal fabric and mapped as Klondike Schist by Bostock (1964). The rocks and their relations are identical with those in the Simpson Range in Finlayson Lake map area and because these two areas are about 420 km apart and on opposite sides of Tintina Fault they support the concept of right lateral movement of that magnitude on the fault.

A reconnaissance was also made of Dromedary Mountain in northern Glenlyon map area to examine the upper part of the Earn Group (unit 13 of Campbell, 1967). The rocks on Dromedary Mountain are a sequence of southwest dipping hornfels with alternate whitish laminae of quartz diopside skarn and purplish brown biotite hornfels. The rock is unlike Upper Paleozoic strata in the region and is probably correlative with Lower Paleozoic rocks in the Anvil Range (i.e., unit 2 of Tempelman-Kluit, 1972). If this interpretation is correct the unit and the overlying volcanics (unit 16 of Campbell, 1967) are comparable to strata that contain zinc-lead mineralization in the Anvil Range and should be prospected for like occurrences. Further, if correct, an important fault that has telescoped equivalent facies must separate the strata on Dromedary Mountain from the Kalzas Formation to the north. This fault probably can be traced northwest into the structure mapped in the Kalzas Range by Campbell (1967) and farther along Grey Hunter Creek by Bostock (1947). Southeastward it may continue across Earn Lake to the fault mapped on the south flanks of Mount Menzie and Two Peter Mountain (Tay River map area; Roddick and Green, 1961).

Implications for Mineral Exploration

The Upper Paleozoic unit of basalt, limestone, chert and slate in the Semenof Hills contains four small copper occurrences in Laberge map area (Cassiar Bar, Semenof, Sylvia and Loon; Tempelman-Kluit, 1978a). None of these appear exciting and the Cache Creek Group with which the host rocks are correlated generally contain no economic concentrations of copper in the northern Cordillera. Strained rocks in Teslin Suture Zone, partly the cataclastic equivalents of this Upper Paleozoic unit, contain no known mineral showings in Laberge map area, but in Carmacks map area they host the small Braden's Canyon copper occurrence. More generally these cataclastic rocks envelop several occurrences (e.g., the Fetish and Fyre in Finlayson Lake map area and the Lucky Joe in Ogilvie map area), but these showings also appear unpromising. Generally the cataclastic rocks of Teslin Suture Zone and their less strained equivalents, do not hold much promise for exploration.

Upper Triassic carbonate reefs of the Lewes River Group, a potentially interesting host to mineralization, were examined at many localities in Laberge map area, but no mineralization was discovered. Similarly none was noted in the Laberge Group.

The feldspar porphyry bodies (correlated with the Mount Nansen Group) that trend diagonally across Laberge map area contain several copper occurrences (e.g., Packers, Tuv). Traces of chalcopyrite can be seen in these rocks at many places and pyrite is widely disseminated in them. The Mount Nansen Group and its various related subvolcanic rocks include a variety of felsic lithologies ranging from miarolitic granite plutons, crowded porphyry dykes and plugs, quartz-feldspar porphyry dyke swarms, to breccia pipes and felsic tuff. It is favourable as a host for vein and disseminated gold occurrences and for porphyry copper molybdenum accumulations; several showings of both types are known in the unit.

Chalcopyrite is common as scattered small grains in volcanics of the Lewes River Group (map unit Fvb, Tempelman-Kluit, 1974b) in Laberge and Carmacks map areas and concentration are known at the Bonanza King. The unit appears a promising exploration target although parts have been examined before.

References

- Bostock, H.S.
1936: Carmacks district, Yukon; Geological Survey of Canada, Memoir 189.
1947: Mayo, Yukon Territory; Geological Survey of Canada, Map 890A with descriptive notes.
1964: Geology, McQuesten, Yukon Territory; Geological Survey of Canada, Map 1143A with descriptive notes.
- Bostock, H.S. and Lees, E.J.
1938: Laberge map-area, Yukon; Geological Survey of Canada, Memoir 217.
- Campbell, R.B.
1967: Reconnaissance geology of Glenlyon map-area, Yukon Territory; Geological Survey of Canada, Memoir 352.
- Mulligan, R.
1963: Geology of Teslin map-area, Yukon Territory; Geological Survey of Canada, Memoir 326.
- Roddick, J.A. and Green, L.H.
1961: Tay River, Yukon Territory; Geological Survey of Canada, Map 13-1961.
- Tempelman-Kluit, D.J.
1972: Geology and origin of the Faro, Vangorda, and Swim concordant zinc-lead deposition, central Yukon Territory; Geological Survey of Canada, Bulletin 208.
1974a: Carmacks, Yukon Territory; Geological Survey of Canada, Open File 200.
1974b: Reconnaissance geology of Aishihik Lake, Snag and part of Stewart River map-areas, west-central Yukon; Geological Survey of Canada, Paper 73-41.
1975: Carmacks map-area, Yukon Territory; in Report of Activities, Part A, Geological Survey of Canada, Paper 75-1A, p. 41-44.
1978a: Reconnaissance geology, Laberge map-area, Yukon; in Current Research, Part A, Geological Survey of Canada, Paper 78-1A, p. 61-66.
1978b: Laberge map-area (NTS 105 E); Geological Survey of Canada, Open File 578.

**EARLY AND MIDDLE ORDOVICIAN CONODONT FAUNA
FROM THE MOUNTAIN DIATREME, NORTHERN
MACKENZIE MOUNTAINS, DISTRICT OF MACKENZIE**

Project 500029

M.L. McArthur¹, R.S. Tipnis², and C.I. Godwin³
Institute of Sedimentary and Petroleum Geology, Calgary

Introduction

Mafic diatremes cutting lower Paleozoic rocks in the northern Mackenzie Mountains are probable feeders for volcanoclastic strata described within basin facies rocks of the Misty Creek Embayment by Cecile (1978). Identification of conodonts in the xenoliths of the diatreme was undertaken to establish the maximum age of the diatreme and to aid in correlating the diatreme with equivalent volcanic strata. Conodonts figured in this report are from GSC loc. C-85901; see sample M1 (Fig. 2).

Locality and Sample Data

The Mountain Diatreme is located in the Sayunei Range of the northern Mackenzie Mountains in the southwestern part of the Mount Eduni map area, NTS 106 A/3 W (64°14'N, 129°28'W) (Fig. 1). It is accessible by helicopter from Norman Wells, District of Mackenzie, 195 km northeast or from Ross River, Yukon Territory, 305 km south-southwest. The diatreme is exposed in a southwest trending, U-shaped valley at an elevation of approximately 1680 m. Although above treeline, outcrop is limited to less than 25 per cent because of both glacial and talus cover.

The diatreme is located on the edge of Misty Creek Embayment described by Cecile (1978) and intrudes Upper Cambrian to Lower and lower Middle Ordovician transitional facies (silty limestones) up to the unconformity at the base of the Upper Ordovician to Lower Silurian Mount Kindle Formation. In the adjacent strata of the basin embayment there are several volcanic horizons of Late Cambrian to Early Devonian age with the largest volume of volcanic rocks associated with Ordovician and Silurian sedimentary strata (Cecile, 1978, and personal communication). Cecile (1978) recognized a volcanic centre with volcanic breccia, feeder dykes and sills 40 km southwest of the Mountain Diatreme.

The Mountain Diatreme is subcircular in plan and averages 600 m in diameter. It consists of an outer rusty weathering zone and an inner green breccia (Fig. 2). Breccia fragments are angular to subrounded, less than 1 cm to over 30 cm in size and are highly carbonatized and chloritized. Many of the fragments are autoliths which characteristically contain cores of phlogopite and rarely pyroxene. Volcanic strata in the Misty Creek embayment typically contain megacrysts of biotite (Cecile, personal communication).

In the central part of the diatreme are several large blocks of light grey weathering limestone breccia. Breccia bed fragments are altered most conspicuously around their margins. Samples of this limestone breccia were dissolved in acetic acid to obtain conodonts in order to determine the origin (provenance) of the blocks. Only one of the five samples of limestone breccia (Fig. 2) yielded conodonts.

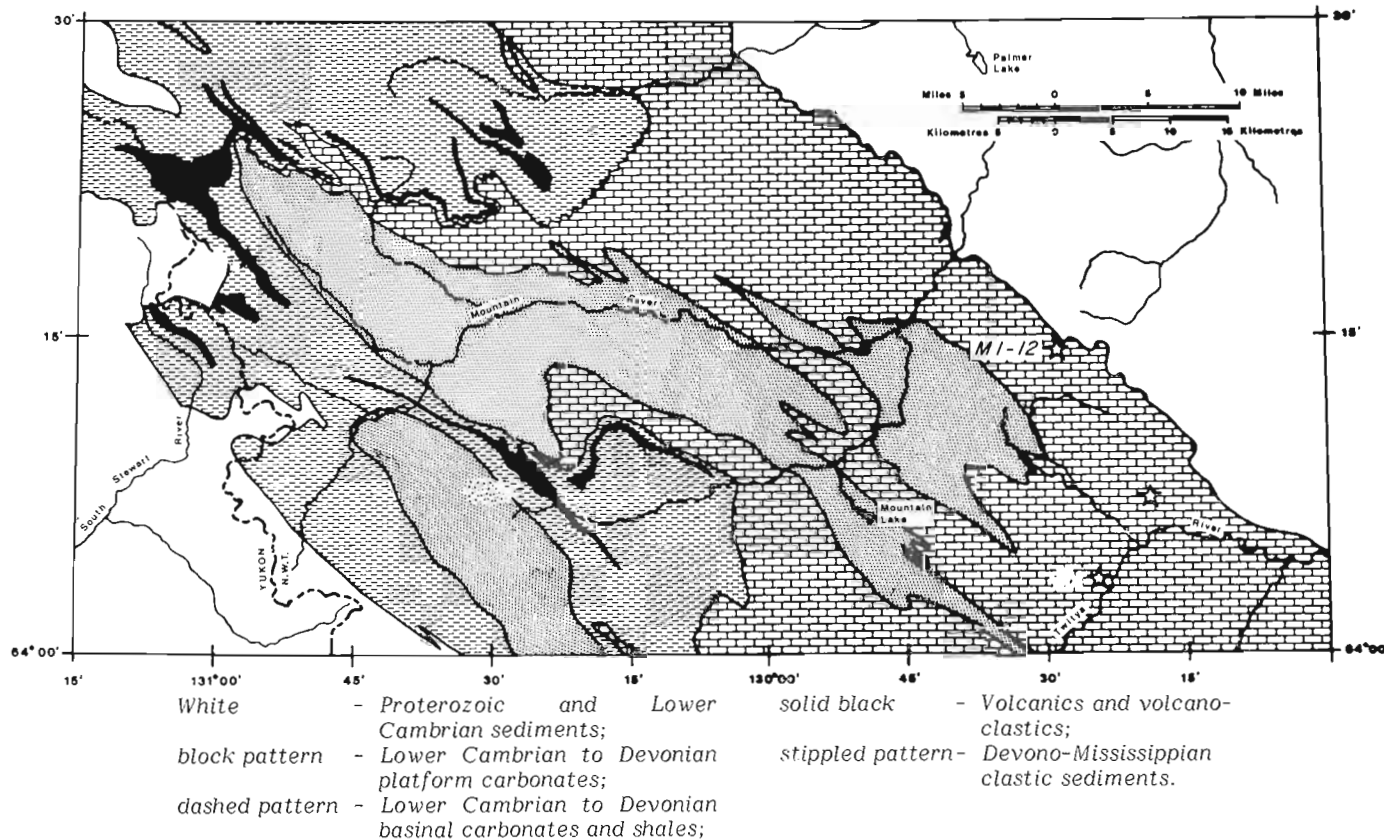


Figure 1. Generalized geological map of the Mackenzie Mountains in the vicinity of Mountain Diatreme (M1-12).

¹Amoco Canada Petroleum Company, Alberta
²Visiting Fellow, Institute of Sedimentary and Petroleum Geology, Calgary, Alberta
³University of British Columbia, Vancouver, B.C.

From: *Scientific and Technical Notes in Current Research, Part A; Geol. Surv. Can., Paper 80-1A.*

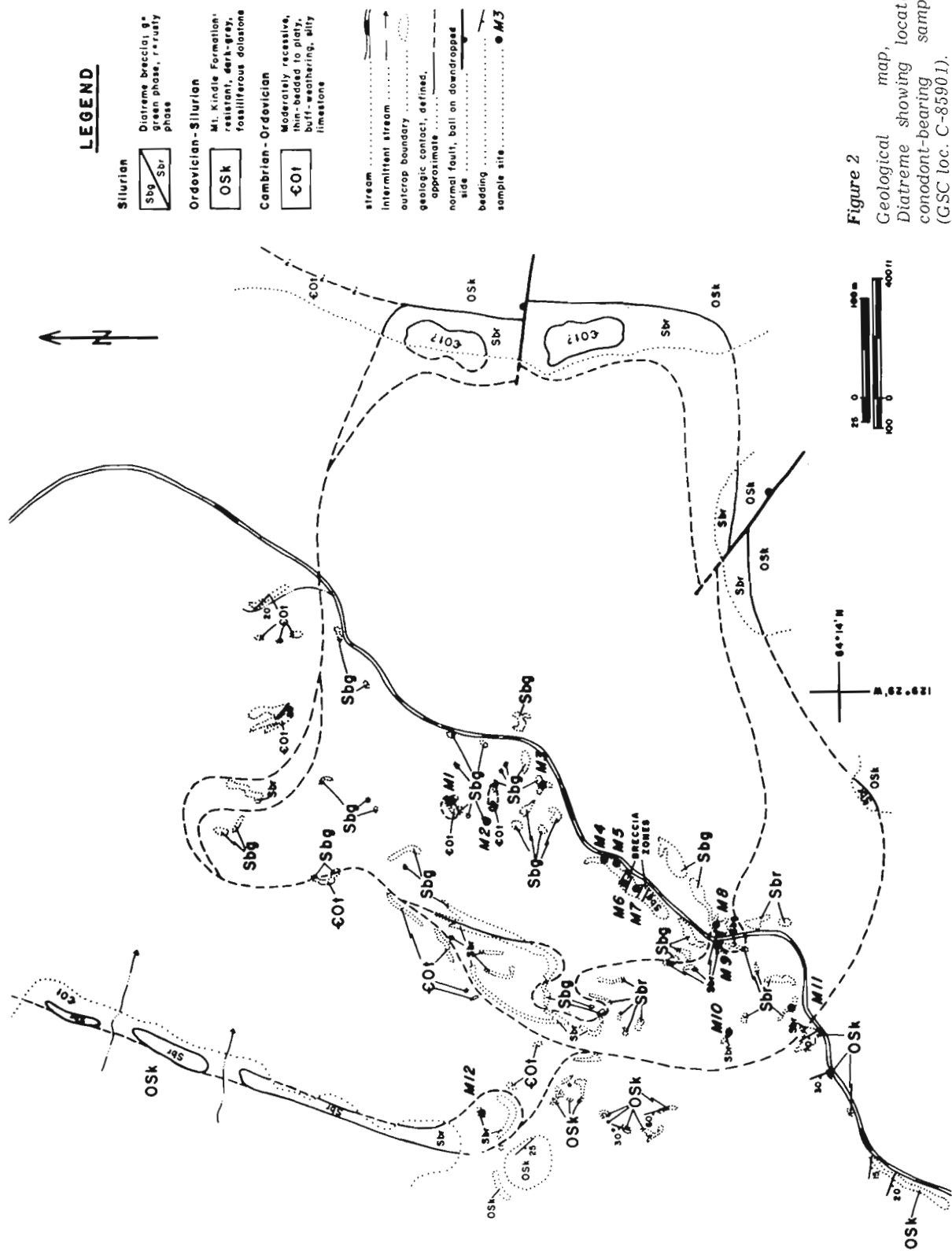


Figure 2
 Geological map, Mountain Diatreme showing location of conodont-bearing sample M1. (GSC loc. C-85901).

Table 1

List of conodont taxa, ages, biogeographic affinity, and other occurrences

Figure Numbers from Plate 1	Names of the Taxa	Age Indicated	Bonnet Plume Sections 31 and 54	Biogeographic Affinity ¹
1, 5	Walliserodus australis Serpagli	early Arenigian	X	NA ?
2	Drepanoistodus forceps (Lindström)	early middle to middle Arenigian	X	
3	aff. Scandodus mysticus	late Arenigian ? early Llanvirnian	X	
4	Walliserodus ethingtoni (Fåhreaus)	Late Arenigian ? Llanvirnian	X	NA
6	Ruetterodus andinus Serpagli	late Arenigian early Llanvirnian	?	MC
7, 13	New Genus A Sweet et al., 1971	late Arenigian early Llanvirnian	?	MC
8, 14	Paroistodus pallelus (Pander)	Arenigian Early Llanvirnian	X	
9, 12	Drepanoistodus basiovalis (Sergeeva)	Arenigian ? early Llanvirnian	X	
10	Walliserodus cf. W. ethingtoni (Fåhreaus) sensu Löfgren	middle to late Arenigian	?	NA
15	Protopanderodus cooperi (Sweet and Bergström)	Llanvirnian	X ?	NA
11, 16	Oepikodus evae (Lindström)	early – Middle Arenigian	X	NA
17	aff. Walliserodus iniquis Löfgren	Middle Ordovician		NA
18	Periodon flabellum (Lindström)	late Arenigian	X	NA
21 – 23	Periodon aculeatus Hadding	Llanvirnian	X	NA
19, 20	Oepikodus sp.	Arenigian ?		NA ?

¹ NA – North Atlantic
MC – Mid-Continent

Conodonts as Thermal Indicators

Epstein et al. (1977) developed a general relationship between conodont colours, depicted as Colour Alteration Index (CAI), and the thermal history of enclosing sedimentary strata. The underlying argument of these workers, that the change in the colour of conodonts is primarily attributable to the heat accompanying their depth of burial, was corroborated by comparing the various colours of lower Paleozoic conodonts through a cross-section of the Appalachian basin (Epstein et al., 1977). Conodonts, however, can also be affected by heat generated through other geological activities such as igneous intrusions, as demonstrated by this study.

Conodonts from several localities adjacent to the Mountain Diatreme (by R.S.T.) have CAI values of 4 or less. These samples are from equivalent Upper Cambrian to Lower and lower Middle Ordovician transition facies rocks along the edge of the Misty Creek embayment, 5 km southeast and 60 km northwest of the Mountain Diatreme (sections 54 and 31, respectively, of Cecile, 1978, Fig. 1). In fact, coeval conodont faunas from the two localities have CAI values of 2 and 3 only. Conodonts from the xenolith, however, have significantly higher and more variable CAI values. Most conodonts exhibit colours that may be grouped between CAI 6 and 7 but a few extreme values of 4+ and 7+. These values suggest that limestone blocks were in the diatreme fluid long enough to have undergone some degree of thermal

metamorphism. This is also indicated by chloritization of fragments. This observation is also consistent with that of Epstein et al. (1977, p. 8) who noted that conodonts obtained from carbonate rocks that were intruded by dykes and sills (or were in contact with lava flows), change in colour from "white to black to brown to pale yellow with increasing distance from the igneous body".

Usually conodonts possessing high CAI values show breakage, corrosion and surficial damage (see Fig. 7 of Epstein et al., 1977). On the other hand, a majority of the conodonts from the diatreme sample, although showing similarly high CAI values, are surprisingly smooth and undamaged. This difference might be attributed to the fact that in the present case conodonts were rapidly cooked because of the heat (and pressure?) generated by the intrusion as against a possibly gradual heating effect operating over a significant period of time in the case of conodonts found in metamorphosed strata.

Conodonts as Indicators of the Age of the Diatreme

Beside dating the strata intruded by the Mountain Diatreme, conodonts also give a maximum date for the diatreme, in the sense that the age of the volcanic activity must postdate the youngest conodont present. Although many conodonts are broken, the majority are sufficiently well preserved to be recognized at the generic and, in many



All illustrated specimens are from the same sample. (GSC loc. C-85901). Magnifications are approximate. All views lateral, unless otherwise noted.

- Figs. 1, 5 – *Walliserodus australis* Serpagli l. postero-lateral view, three costate element, x 65, GSC 50999. 5, five costate element, x 65, GSC 51000.
- Fig. 2 – *Drepanoistodus forceps* (Lindström). homocurvatiiform element, x 65, GSC 51001.
- Fig. 3 – aff. *Scandodus mysticus* Barnes and Poplawski. x 65, GSC 51002.
- Fig. 4 – *Walliserodus ethingtoni* (Fåhreaus). x 65, GSC 51003.
- Fig. 6 – *Reutterodus andinus* Serpagli. cone-like element, x 92, GSC 51004.
- Figs. 7, 13 – New genus A. Sweet et al., 1971. 7. ramiform element, x 139, GSC 51005. 13. oistodiform element, x 139, GSC 51006.
- Figs. 8, 14 – *Paroistodus parallelus* (Pander). 8. oistodiform element, x 65, GSC 51007. 14. drepanodiform element, x 139, GSC 51008.
- Figs. 9, 12 – *Drepanoistodus basiovalis* (Sergeeva). 9. subterectiform element, x 65, GSC 51009. 12. drepanodiform element, x 139, GSC 51010.
- Fig. 10 – *Walliserodus* cf. *W. ethingtoni* (Fåhreaus) sensu Lofgren? Postero-lateral view, x 139, GSC 51011.
- Figs. 11, 17 – *Oepikodus evae* (Lindström). 11. oistodiform element, x 65, GSC 51012. 17. prioniodiform element, x 65, GSC 51013.
- Fig. 15 – *Protopanderodus cooperi* (Sweet and Bergstrom). x 33, GSC 51014.
- Fig. 16 – aff. *Walliserodus iniquis* Löfgren? x 139, GSC 51015.
- Fig. 18 – *Periodon flabellum* (Lindström)? prioniodiniform element, x 139, GSC 51016.
- Figs. 19, 20 – *Oepikodus?* sp. 19. oepikodiform element, x 139, GSC 51017. 20. prioniodiform element, x 139, GSC 51018.
- Figs. 21-23 – *Periodon aculeatus* Hadding. 21. multi-ramiform element, x 924, GSC 51019. 22. oistodiform element, x 139, GSC 51020. 23. antero-lateral view, toritiliform element, x 139, GSC 51021.

specimens, at the specific levels. The age determinations and identification are primarily based on the works of Serpagli (1974), Tipnis (1978a), Tipnis et al. (1979), Löfgren (1977) and on unpublished studies of conodont faunas from adjacent areas by Tipnis.

Illustrations of most of the conodonts obtained from the sample are shown on Plate I. The list of taxa, their tentative ages, biogeographic affinities (NA = North Atlantic, MC = Mid-Continent) and geographic occurrences from sections 54 and 31 of Cecile (1978) are given on Table 1. A large number of the taxa belong to North Atlantic province. Several studies have shown that Early-Middle Ordovician strata marginal to the North American craton commonly contain significant proportions of North Atlantic type

conodonts (Tipnis, 1978a or Tipnis et al., 1979, amongst others). Thus finding such fauna close to the margin of Misty Creek Embayment is consistent with their distribution noted in other parts of the North America craton.

Early Arenigian species include *Walliserodus australis* Serpagli, *Drepanoistodus forceps* (Lindström) and aff. *Scandodus mysticus* Barnes and Poplawski. Taxa of late Early Arenigian age and younger include Midcontinent forms, *Reutterodus andinus* Serpagli and New Genus A Sweet Ethington and Barnes 1971, and several North Atlantic forms such as *Oepikodus evae* (Lindström), regarded as the index species for late Early/early Middle Arenigian, *Protopanderodus cooperi* (Sweet and Bergström), aff. *Walliserodus iniquis* Löfgren and *Periodon aculeatus* Hadding. Some of the latter taxa range into early Middle Ordovician (possibly Llanvirnian).

Although conodonts obtained from the xenolith indicate some sort of stratigraphic "mixing", the average indicated age falls within a fairly short time span, that is mostly Arenigian, possibly extending into the Llanvirnian.

The diatrema itself must have intruded sometime during or after the Llanvirnian interval.

Cecile (1978) noted that the largest volume of volcanic rocks are interbedded with basin facies rocks of early Middle Ordovician to Early Silurian age (Cecile, personal communication). If the volcanic activity associated with this particular diatrema reflects a period of contemporaneous volcanism through the region, then conodonts can be used to provide a reasonably accurate measure of the timing of such an event.

Conclusion

The conodonts have aided in dating the volcanic activity responsible for the intrusion of the diatrema as early Middle Ordovician or later. Further, some insight into the thermal history of surrounding strata may also be accomplished by interpreting the conodont colour data.

Acknowledgments

The samples used for conodont extraction were collected by M.L.M. while employed by Welcome North Mines Ltd. of Vancouver, British Columbia. SEM photographs were taken with the aid of research grants to C.I.G. (U.B.C. Arctic and Alpine Research Grant) and R.S.T. (GSC, Calgary). We are grateful to the late David Perry (U.B.C.) for his enthusiasm and help during the early part of this project, to M.P. Cecile and T.T. Uyeno for reading and commenting on the manuscript.

References

- Cecile, M.P.
1978: Report on Road River stratigraphy and the Misty Creek Embayment, Bonnet Plume and surrounding map-areas, Northwest Territories; in Current Research, Part A, Geological Survey of Canada, Paper 78-1A, p. 371-377.
- Epstein, A.G., Epstein, J.B., and Harris, L.
1977: Conodont color alteration – an index to organic metamorphism; U.S. Geological Survey Professional Paper 995.
- Löfgren, A.
1978: Arenigian and Llanvirnian conodonts from Jamtland, Northern Sweden; Fossils and Strata, No. 13, p. 1-29.

Serpagli, E.

1974: Lower Ordovician conodonts from Precordilleran Argentina (Province of San Juan); *Bollettino Societa Paleonologica Italiana*, No. 9, p. 17-98.

Tipnis, R.S.

1978a: Biostratigraphy and paleontology of the Late Cambrian to Late Middle Ordovician conodonts from southwestern Mackenzie Mountains, Northwest Territories; Unpublished Ph.D. dissertation, Department of Geology, University of Alberta, Edmonton.

Tipnis, R.S. (cont'd)

1978b: Early Middle Ordovician conodonts of North Atlantic Province from northeastern Ellesmere Island, Arctic Canada; in *Current Research, Part C, Geological Survey of Canada*, Paper 78-1C, p. 75-79.

Tipnis, R.S., Chjatterton, B.D.E., and Ludvigsen, R.

1979: Biostratigraphy of Ordovician conodonts from southern Mackenzie Mountains; in C.R. Stelck and B.D.E. Chatterton, ed., *P.S. Warren Biostratigraphy Symposium, Geological Association of Canada, Special Paper 18*, p. 39-91 (in print 1978).

FRACTURE FILLING MATERIAL IN THE ATIKOKAN AREA, NORTHWESTERN ONTARIO

D.C. Kamineni¹, P.A. Brown¹, and Denver Stone¹
Terrain Sciences Division

Introduction

During the summer of 1979 the geological research program for radioactive waste disposal, being conducted by Geological Survey of Canada in co-operation with Atomic Energy of Canada Limited, began work in the Eye-Dashwa lakes granite and surrounding gneiss at Atikokan, northwestern Ontario. The work reported here on fracture filling materials forms part of that program.

The Eye-Dashwa lakes granite, located 15 km northeast of Atikokan, is a massive, medium- to coarse-grained hornblende-biotite granite which is intrusive into a series of tonalitic gneisses – the Dashwa gneiss (Schwerdtner, 1976; Simpson, 1976). The gneissic complex encompasses a wide spectrum of lithologies ranging from tonalitic to granitic to amphibolitic gneiss. The pluton and the gneiss show different degrees of fracturing. In general, the fractures in the area have the following physical characteristics: 1) fractures filled with or coated by mineral matter; 2) fractures without any appreciable filling or coating but which show alteration of minerals in the wall rock i.e., sericitization of feldspars; and 3) fractures devoid of the above two features.

It is not possible to assess the different proportions of the three types of fractures with the available data. From surface investigations it appears that types 1 and 2 predominate over type 3. In view of their abundance and their importance in inferring the fluid activity along the fractures and their potential to act as pathways for present day fluids, the mineralogy and textures of the fracture fillings are examined in detail.

The fracture filling material can be divided into three general categories: pre-granite emplacement, syn to late granite emplacement, and post-granite emplacement. The pre-granite emplacement fillings are present only in the gneiss and include amphibolite dykes, granodiorite dykes, and minor sulphides. The syn emplacement fillings include two types of pegmatite, muscovite, and lamprophyre dykes. The post emplacement filling material ranges from epidote, quartz, fluorite and chlorite to zeolite, hematite-goethite, and diabase to late stage (recent?) carbonate, gypsum and clays.

Acknowledgments

Glen McCrank, John Misuira, John Psutka, Nate Rey, and Robert Thivierge contributed to this project significantly by participating in the geological mapping of the Eye-Dashwa lakes pluton. Dr. Edgar Froese critically reviewed the manuscript.

Pre-emplacement Fracture Fillings

The pre-emplacement fillings are present only within the gneiss and include amphibolite dykes, quartz veins, granodiorite dykes, and sulphides. They are recognized as pre-emplacement by the fact that the pegmatite-aplite dykes (which are syn emplacement fracture fillings) consistently crosscut fractures containing these materials. The age sequence within the pre-emplacement fillings is also defined by crosscutting relationships.

¹ Atomic Energy of Canada Limited,
601 Booth Street, Ottawa, Ontario

Amphibolite Dykes

Amphibolite dykes are one of the oldest filling materials recognized in the gneiss. They are fine- to medium-grained amphibolites with a variably developed tectonic fabric and are generally less than 50 cm in width. The amphibolites, however, appear to have acted as the locus for later shear or flattening zones, and their original width could not be determined.

The schistose amphibolite dykes are crosscut by quartz veins, granodiorite dykes, pegmatite dykes, and epidote filled veins.

Quartz Veins

Quartz veins are locally abundant within the gneiss. In general they are parallel to subparallel with the gneissosity, are less than 1 cm in width, and locally show minor isoclinal folding. The veins crosscut the amphibolite dykes and are crosscut by granodiorite and pegmatite dykes.

Granodiorite Dykes

Granodiorite dykes are sporadically developed throughout the area. They fill various fracture directions and are generally less than 5 cm wide. Characteristically they are fine- to medium-grained granodiorite and contain euhedral crystals of magnetite. These dykes crosscut the amphibolite dykes and the quartz veins and are crosscut by pegmatites of granitic composition and epidote filled fractures.

Sulphides

A sulphide fracture filling (comprising pyrrhotite and pyrite) locally occurs as thin (<4 mm) veins within the gneiss. The sulphide veins are crosscut by syn emplacement pegmatite dykes.

Syn to Late Emplacement Fracture Fillings

The syn to late granite emplacement fracture fillings are present both within the gneiss and the granite and include two ages of pegmatite dykes, muscovite, and lamprophyre dykes. The separation of late emplacement and post-emplacement fillings is arbitrary. For convenience, epidote (which is definitely a post-emplacement filling) is taken as a readily recognizable time horizon. The syn to late emplacement fillings are all crosscut by epidote filled fractures.

Early Formed Pegmatite Dykes

East-west trending coarse-grained (quartz, albite, microcline, muscovite-bearing) pegmatite dykes crosscut both the gneiss and the granite. They range in width from a few centimetres to one metre and locally show a grain size zonation with the coarse-grained material concentrated at the margins. The dykes present up to 1 km from the granite-gneiss contact and show an increase in frequency towards the contact zone. They are relatively sparse within the granite itself and are crosscut by the late formed pegmatite dykes.

Late Formed Pegmatite Dykes

The late formed pegmatite to aplite dykes generally contain quartz, albite, microcline, biotite, and opaques, are more mafic than the early formed pegmatite dykes, and locally show flow features. Their occurrence is restricted largely to the contact zone between gneiss and granite although they are also present throughout the granite. They are crosscut by muscovite filled fractures and lamprophyre dykes.

Muscovite

Muscovite fillings are common in fractures both within the gneiss and around the margins of the pluton. This mineral occurs as a fracture filling and is restricted to fractures trending 120°. In thin section, the muscovite displays little penetration into the wall rock, and flakes are randomly oriented indicating growth under relatively stress-free conditions.

Lamprophyre Dykes

Lamprophyre dykes displaying porphyritic texture (phenocrysts of hornblende and plagioclase in feldspar matrix) fill major fractures; commonly this intrusion is accompanied by faulting against granite. Epidote filled microfractures crosscut the lamprophyre dykes.

Post-emplacement Fracture Fillings

The post-emplacement fracture fillings can be crudely separated into relatively high temperature minerals: epidote, quartz, fluorite, chlorite, adularia, zeolite, hematite-goethite, and diabase, and relatively low temperature filling materials: carbonate, gypsum, and clay. The age sequence of filling materials is defined, whenever possible, by crosscutting relationships. These relationships confirm that, in general, the high temperature minerals predate the low temperature minerals. Due to the number of fracture filling materials and to their sparse development throughout the area, much of this study relies on petrographic observation to complement the field data.

Epidote

Epidote occurs throughout the area as a fracture filling material in association with large faults. It is, however, most prevalent close to the contact zone between the granite and gneiss. The epidote filled fractures crosscut the pegmatite and lamprophyre dykes and are crosscut by chlorite filled fractures and diabase dykes. A hand specimen and thin section study of the epidote filled fractures indicates that

the epidote has crystallized under variable stress conditions resulting in variable growth patterns. The major growth patterns determined (to date) are outlined below.

1. Highly deformed crystals elongated along a lepidoblastic fabric in a cataclastic matrix (Fig. 1). The fabric is made up of oriented sericitic matrix. The orientation of the sericitic fabric as well as the sigmoidal epidote crystals may vary locally when warped and wrapped around feldspar and quartz crystals. Undeformed epidote crystals are locally well developed and represent a 'post cataclastic growth' indicating that crystallization of epidote outlasted the faulting.
2. Acicular oriented crystals commonly associated with quartz and locally with chlorite occur as slickensides on fault surfaces. This type of occurrence is restricted to fault planes.
3. Fillings containing a mixture of deformed epidote crystals in the wall rock show (a) a mixture of randomly arranged coarser epidote and calcite as a vug (Fig. 2) and (b) acicular crystals grown perpendicular to the vein wall. Prehnite may also be present and shows acicular growth.
4. Veins containing elongated epidote crystals show evidence of recrystallization, i.e., elongated domains contain subgrains of epidote with 120° interfacial angles between the grain boundaries (Fig. 3).
5. Fine crystals of epidote occupying the interstitial space between fragmental quartz and feldspar crystals represent fault breccia (Fig. 4); some epidote crystals are elongated.
6. Fine veinlets of epidote arranged approximately at 30 to 35° angle to 'shear or fault zones' (Fig. 5). These veinlets possibly define the tensional fractures complementary to the shears. In thin section the shear veinlets contain broken crystals of epidote, quartz, and feldspars whereas the tensional fractures are filled with prisms of randomly oriented crystals. This mode of occurrence demonstrates clearly that growth occurred both under shear and tensional conditions.

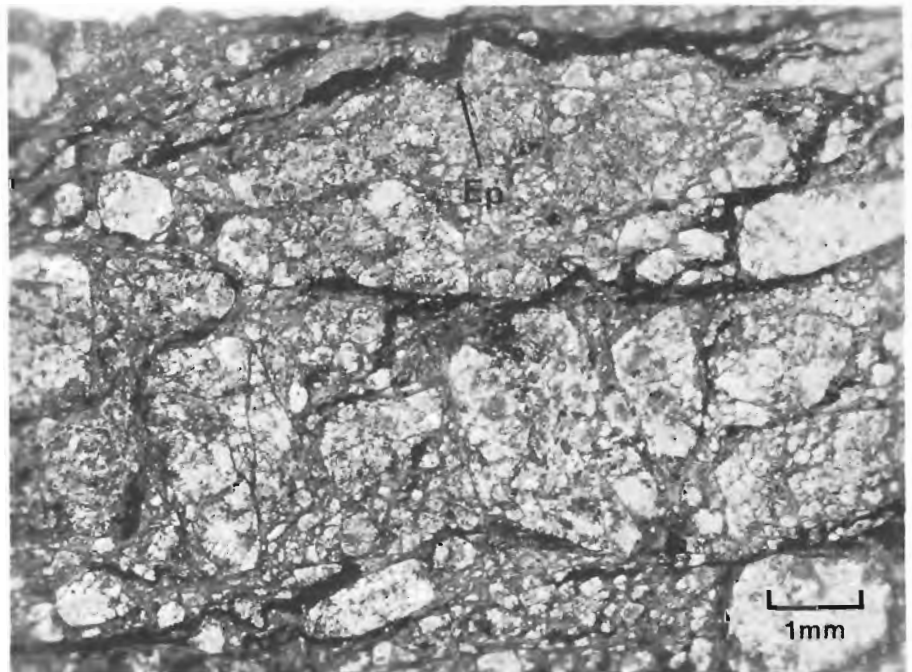
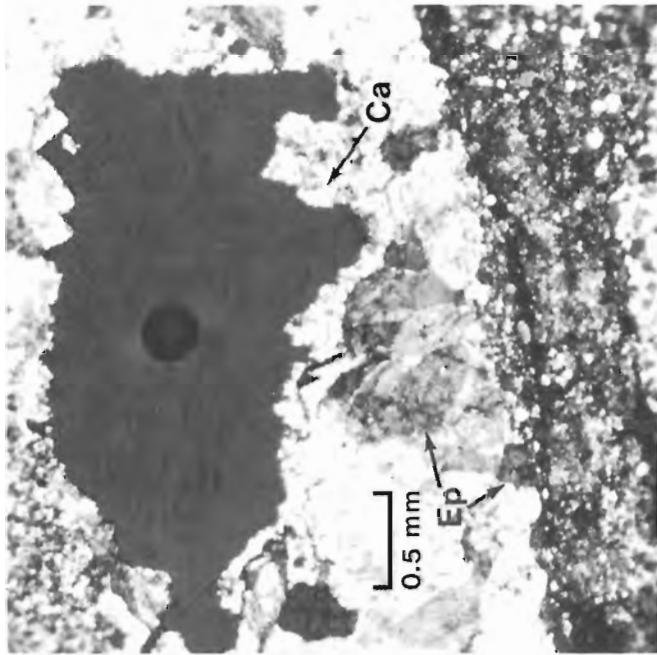


Figure 1.

Highly deformed epidote crystals in a cataclastic matrix. (GSC 203357-C).

Ep = epidote



Ca = calcite Ep = epidote

Figure 2. Composite epidote filling; deformed crystals near the wall rock and randomly arranged crystals and calcite-bearing vug towards the centre. (GSC 203357-Y).

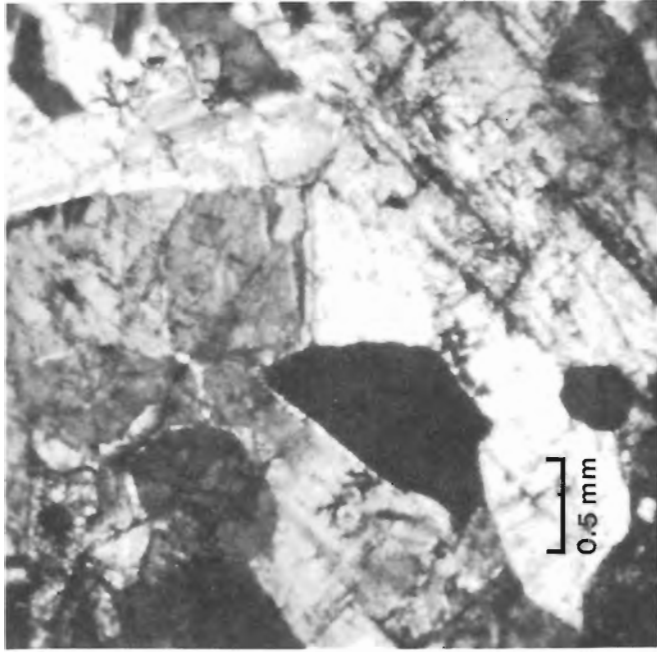


Figure 3. Recovered epidote crystals displaying interfacial angles around 120° . All the grains comprise epidote (GSC 203357-X).

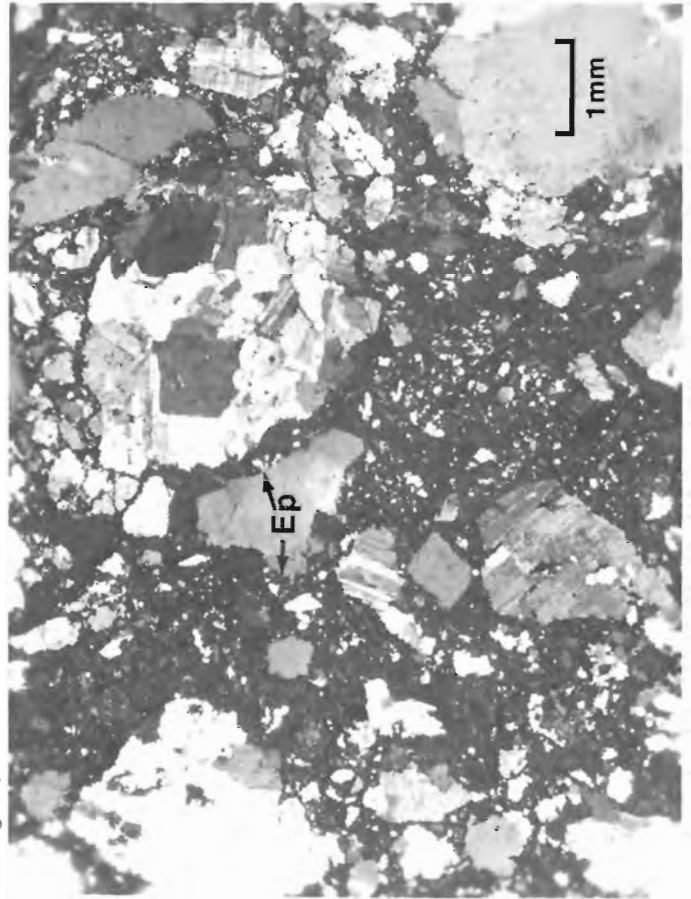


Figure 4.

Epidote crystals filling the interstitial space between fragmental feldspar-quartz matrix representing fault breccia. (GSC 203357-D).

Ep = epidote

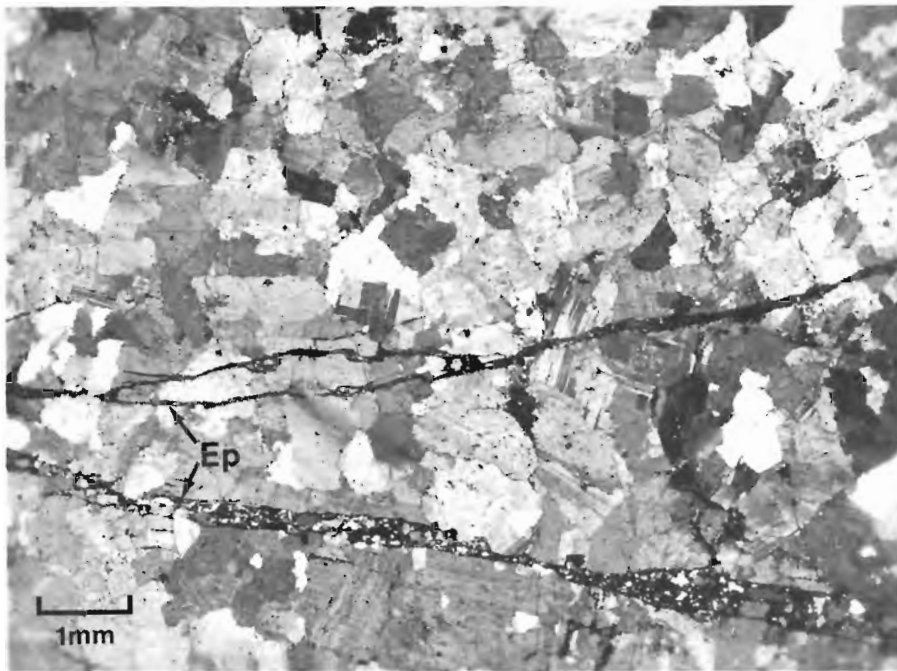


Figure 5.

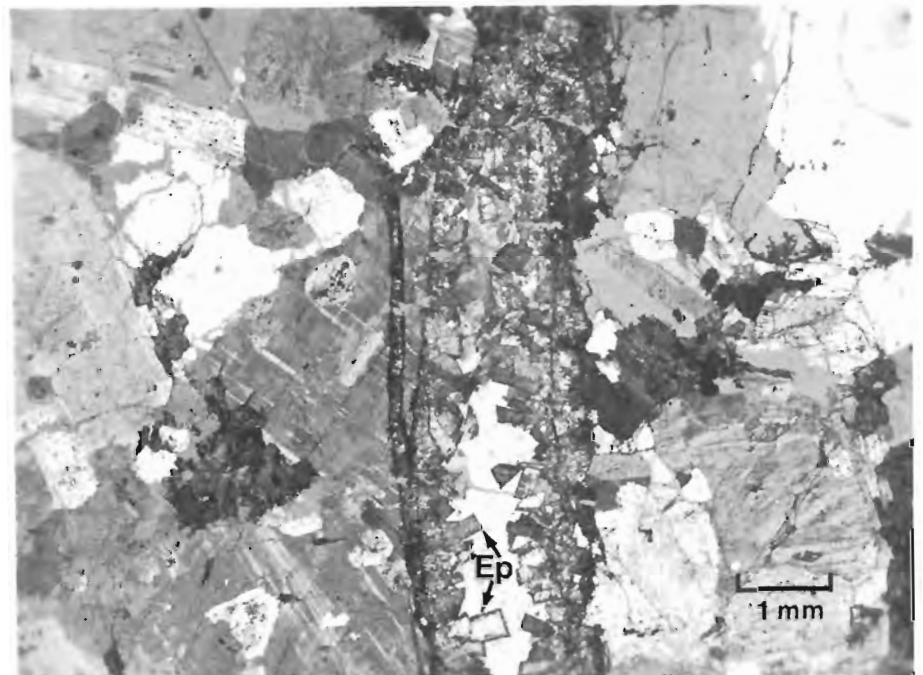
Epidote crystals filling shear and tensional types of fractures. (GSC 203357-I)

Ep = epidote

Figure 6.

Randomly oriented prisms of epidote displaying optical zoning. (GSC 203357-G).

Ep = epidote



7. Fibrous epidote with sigmoidal shape arranged across the vein wall. This type of occurrence suggests growth in an overall extensional environment associated with faulting identified in the pluton. The epidote crystals close to the wall rock record some strain. Those towards the centre of the vein show tensional characteristics. This texture conforms to the interpretation that the vein growth is of composite character, i.e. shear forces were dominant during the initial growth of the vein and they were followed by dilation due to extension.
8. Highly randomly oriented epidote crystals with a well developed prismatic form. These crystals display optical zoning and well developed growth steps (Fig. 6). The random arrangement emphasizes that they crystallized in a stress free environment.

The growth patterns of epidote described above demonstrate their development under different conditions – essentially under stress or stress free environments. These conditions can be related to faulting within the Eye-Dashwa lakes pluton. The growth of epidote was initiated prior to faulting and continued after faulting ceased. Three broad groups of growth patterns are recognized:

1. Pre- to syn? fault epidote comprising growth style 1;
2. Syn to late fault epidote comprising growth styles 2, 3, 4, 5, 6;
3. Post-fault epidote comprising growth styles 7 and 8;

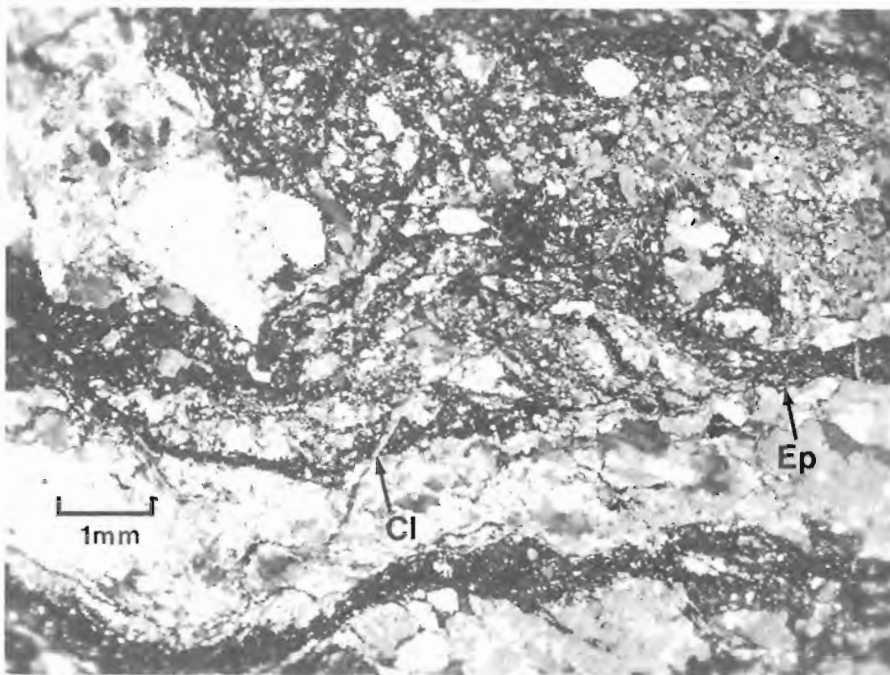


Figure 7.

Fine chlorite-quartz fillings developed across deformed epidote fillings. (GSC 203357-P).

Ep = epidote Cl = chlorite

The epidote development, which may be attributed to concentration of fluids at the contact, was manifested during the hydrothermal stage (probably 200-500°C) of pluton development and accompanied the major fault events recorded in the Eye-Dashwa lakes granite.

Coexisting Minerals with Epidote

A variety of minerals coexist with epidote, including sphene, fluorite, and chlorite. Fluorite is present in relatively few fractures implying that the activity of fluorine was high in certain local horizons. Texturally, chlorite and epidote appear to have developed at the same time, but in places chlorite crystals cut across epidote crystals, indicating a later growth.

Other Fillings

Chlorite occurs predominantly on fault surfaces. It is also found in joints developed at a high angle to major fault zones and commonly has iron oxides associated with it. Most chlorite fillings appear to have formed later than epidote growth, i.e., chlorite fills fractures developed across epidote prisms (Fig. 7). Hematite and/or hydrous iron oxide (goethite?) also cuts across epidote crystals implying it also developed at a later stage.

Quartz veins are extensively developed in fractures formed by faulting. The granite near these faults is characterized by a reddish brown colour and shows textural changes involving mylonitization and elongation of grains. These relationships probably indicate that material has been redistributed by faulting, including extraction of silica to develop quartz veins in the form of fillings in extensional joints.

Adularia which is a low temperature polymorph of potash feldspar (Deer et al., 1963), is observed as a filling in some fractures. Like quartz, adularia also is localized around fractures developed in the vicinity of faults, indicating its genesis is due to redistribution of elements, particularly mobilization of potash from the fault zones.

A few occurrences of zeolites (natrolite) have been noted in the Eye-Dashwa lakes granite; all show a radial habit and extend into the wall rock (Fig. 8) indicating an extensional type of growth.

East-west trending diabase dykes, with well developed ophitic texture, crosscut both the granite and the gneiss. The dykes represent a late tensional fracture filling. In many cases they follow an echelon type fractures spatially related to fault zones. Unlike the lamprophyre dykes, the diabase dykes are unaffected by epidotization and crosscut epidote-filled fractures; therefore, the diabase dykes are definitely post-epidote fillings.

Calcite, gypsum, and clay are noted in some fractures. In the majority of cases these minerals occur as coatings on early-formed high temperature fillings such as epidote and chlorite. Calcite is found as an exclusive filling in some fractures.

Conclusions

The faults and fractures in the Eye-Dashawa lakes granite and surrounding gneiss formed over considerable periods of time, i.e., Archean to Recent and can be divided into three age sequences (Table 1):

1. pre-granite emplacement fractures developed only within gneiss and presumably related to tectonic activity;
2. syn to late granite emplacement fractures developed within both gneiss and granite and related to the intrusive event and subsequent cooling; and
3. post-granite emplacement fractures related to tectonic activity and erosional unloading.

By careful examination of the fracture filling material a relative time sequence of fractures and fracture filling material can be outlined (Table 1) based on two criteria: 1) crosscutting relationships and 2) temperature of formation of the fracture filling material.

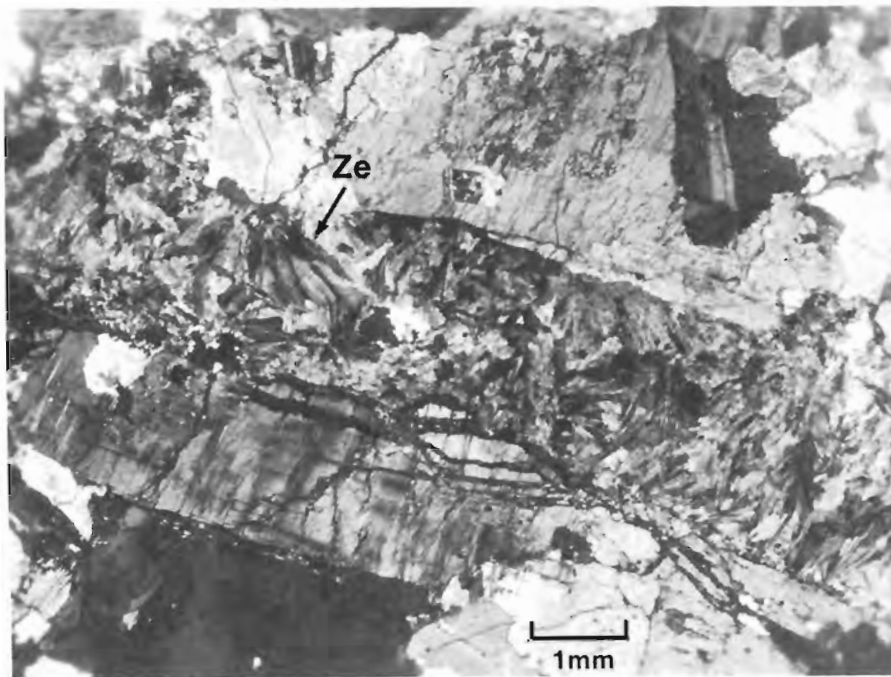


Figure 8.

Zeolite fracture-filling with radial habit; note the arrangement of prisms perpendicular to the wall. (GSC 203357-A).

Ze = zeolite

Table 1
Relative chronological sequence of fracture fillings in the Eye-Dashawa lakes pluton

Time	Type of filling	Temperature (approx.) °C
Pre-granite emplacement	1. Amphibolite	700-800
	2. Quartz veins	300-500
	3. Granodiorite	700
	4. Sulphides	300-400
	5. Early formed pegmatites	500-600
Syn to late granite emplacement	6. Late formed pegmatites	500-600
	7. Muscovite	300-400
	8. Lamprophyre dykes	600-700
	9. Epidote	200-500
	10. Prehnite	200-400
	11. Quartz	300-500
	12. Chlorite	200-400
	Post-granite emplacement	13. Adularia
14. Zeolite (Natrolite)		200-300
15. Hematite-goethite		200-300
16. Diabase		600-700
17. Carbonate		20-100
18. Gypsum		20-50
19. Clays		20-50

The pre-granite emplacement fractures are only developed within the gneisses. The syn to late granite emplacement fractures are developed in both granite and the surrounding gneiss and are related to the cooling of the pluton and possibly to subsequent tectonic events. The post-emplacement fractures are also developed in both granite and the surrounding gneiss and were formed by 1) tectonic activity and 2) erosional unloading. The epidote to hematite-goethite sequence is developed within and close to all major discontinuities in the area, i.e., it is related to tectonic (fault) activity.

Diabase dykes crosscut this sequence, and their occurrence is not restricted to defined faults. It is suggested that these dykes were intruding during a tensile event which postdates the major fault tectonic activity observed in the area.

Carbonate, gypsum, and clay constitute the youngest fracture filling material and occur as coatings and vugs in pre existing filled fractures. It is suggested that they are a relatively recent filling, and that they are related to late tectonic events, i.e., erosional unloading. As such these materials may have precipitated from groundwater systems and are indicators of relatively recent flow paths.

References

- Deer, W.A., Howie, R.A., and Zussman, J.
1963: *Rock Forming Minerals*, Longmans, London.
- Schwerdtner, W.M.
1976: *Lithology and structure of Irene-Etrut lakes granite complex between Atikokan and Ignace*; progress report, Geotraverse Conference, University of Toronto.
- Simpson, E.L.
1976: *Eye and Ear Lake Plutons, Atikokan Region, northwest Ontario*; progress report, Geotraverse Conference, University of Toronto.

**ICE FLOW PATTERNS, MONTREAL-OTTAWA
LOWLAND AREAS**

Project 780017

Nelson R. Gadd
Terrain Sciences Division

Introduction

Field reconnaissance during late May to mid-August 1979 was carried out mainly in the St. Lawrence Lowland area of the 1:500 000 scale Ottawa-Montreal map sheet, National Topographic System 31 SE. Most observations were made within the area enclosed by Ottawa, Montreal, Lake Champlain, and Cornwall (Fig. 1). Brief excursions were made into the highland areas both north (Laurentians) and south (Adirondacks) of this principal area of study.

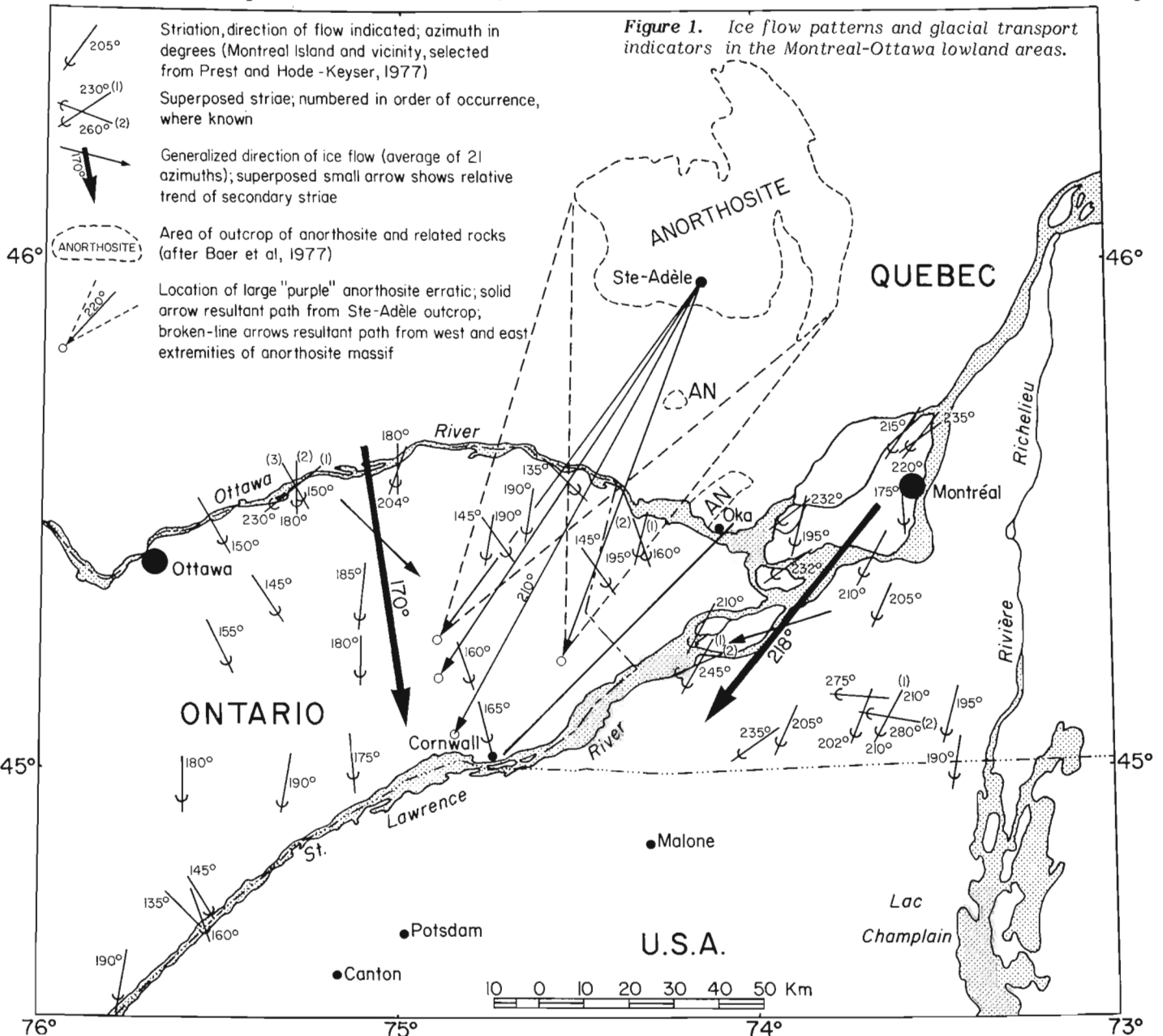
Regional flow patterns for glaciation of this region have not been clearly shown by previous mapping. It was known from previous work (e.g. Terasmae, 1965; Richard, 1975;

Gadd, 1976) that much of the region is drift covered and has relatively little bedrock outcrop from which only a few striae have been recorded. The purpose of this study therefore was 1) to re-examine the bedrock terrain, particularly new exposures, for additional direct evidence of glacial movement (flutings, striae, streamlined phenomena) and 2) to seek and examine other criteria, such as direction of transport of erratics and provenance of till materials, to supplement the evidence for glacial abrasion. The evidence assembled, though sparse, forms interesting regional patterns.

Field Observations

Primary Striae Patterns

Figure 1 shows two basic groupings of striae (both primary and secondary). Northwest of a line passing through Oka and Cornwall, striae trend southerly to southeasterly. The orientation of the large arrow, 170°, is the numerical average of azimuths of 21 sets of striae in the northwest sector. Southeast of the Oka-Cornwall line, striae trend southwesterly to westerly. The orientation of the large



From: Scientific and Technical Notes
in Current Research, Part A;
Geol. Surv. Can., Paper 80-1A.

arrow, 218°, is the numerical average of 21 sets of striae in the southeast sector.

In both sectors the flow direction is clearly indicated on most outcrops by crescentic tension cracks, crescentic percussion cracks, and miniature crag-and-tail and other glacial shadow phenomena.

The bulk of the striae recorded are characterized by long, deep grooves ranging from a few millimetres to about 10 cm wide and several centimetres deep. These are classed here as primary striae that represent regional flow.

Secondary Striae Patterns

In a relatively small number of localities there are glacial abrasion phenomena that are visible as a light polish of the surface and that are made up of shallow striae generally less than 1 mm in width and depth. These striae commonly are superimposed on primary striae. The secondary striae represent late movement of ice, probably the last ice movement in the region.

Within the area shown in Figure 1, secondary striae, where superimposed on primary striae, have a consistent relationship to them: in the northwest sector, secondary striae trend more easterly than primary ones; in the southeast sector, secondary striae trend more westerly than primary striae.

Displacement of Erratics

Previous observations in the area by the writer and colleagues indicated that erratics from distant sources are concentrated in the surface materials, possibly through ablation. Although no regional significance can be derived from the limited data collected to date, it is thought worthwhile to report on one aspect of the findings.

Small open circles in Figure 1 identify the locations of four selected large erratics (1.5-3.0 m diameter) of a distinctive anorthosite whose plagioclase is purple to maroon on fresh crystal surfaces and mauve to purple on weathered surfaces. Hand specimens taken from field erratics have been compared with those taken from outcrops in the Laurentian Highlands; rocks that outcrop in the town of Sainte-Adèle are sufficiently like the four erratics to be a probable source. Solid lines have been drawn on Figure 1 from this probable source to the present locations of the erratics. Similar rocks, however, are known to occur elsewhere (Emslie, 1975) within the easternmost massif of anorthosite mapped by Baer et al. (1977). Eastern and western limiting paths are shown in Figure 1 for movement of erratics from this larger possible source area. The resultant path for the azimuth of the various paths shown, 210°, coincides with the one path from Sainte-Adèle to the vicinity of Cornwall. This direction is similar to the arithmetic mean for striae in the southeast sector but is at angles of 40-75° with early and late flow directions in the sector where the erratics are found.

Despite this apparent anomaly between the resultant directions for displacement of erratics (210°) and that of the most commonly observed primary striae in the sector (170°), the 'purple' anorthosite erratics appear to be abundant in the northwest sector but are rare or absent in the southeast sector. Granitoid rocks (granulites?) of greenish grey to greenish brown colour on fresh surfaces that weather grey to pink are common in the southeast sector. Similar rocks are found as large erratics (about 3 m diameter) in areas south and east of Canton and Potsdam, New York. It is assumed that their provenance is from the Canadian Shield terrane north and northeast of the study area.

Comment

The comments made above differ from the MacClintock and Stewart (1965) concept of an early ice flow from the northeast (Malone glaciation) followed by a later ice flow from the northwest (Fort Covington glaciation). Although

several authors previously have related glacial chronologies in this region to that concept (e.g., Terasmae, 1965; Richard, 1975), I do not feel that my more recent observations, particularly those of westerly flow in the southeast sector, are in accord. Therefore, for the present, and recognizing the limited amount of new data presented here, that concept of ice movement is laid aside. It should be emphasized that although the principal elements of northeasterly and northwesterly flow are present in the study area, they do not appear to be superimposed but rather to occupy different sectors of the area. Further, the lithologies of erratics in the two sectors appear to be significantly different. Superimposed secondary striae in both sectors indicate that there were changes in flow direction within what would appear to be two lobes, rather than indicating a sequence of separate glaciations.

Conclusions

1. Patterns of ice flow as revealed by grouping of striae in this limited study area allow for a working hypothesis that the last major glaciation comprised two lobes: a south to southeasterly flow in the area between Ottawa and St. Lawrence valleys, and a southwest to westerly flow in and south of St. Lawrence Valley. It is not known whether movements in these lobes were contemporaneous.

2. A sequential relationship is assumed to exist between primary and secondary striae, which is based in part on their order of superposition. The corresponding change in size from major to minor striae is interpreted as representing a change from regional to local, or residual, ice flow. The younger striae emphasize the bilobate configuration of the ice by their consistent swing towards the area thought to mark an interlobate position.

3. Further study of the distribution of the distinctive anorthosite may help to understand the late glacial distribution of ice and its lobations. For example, it should be possible to verify or disprove the statement that these erratics are limited to the northwest sector of the study area.

References

- Baer, A.J., Poole, W.H., and Sanford, B.V.
1977: Rivière Gatineau, Quebec and Ontario: Sheet 31; Geological Survey of Canada, Map 1334A.
- Emslie, R.F.
1975: Major rock units of the Morin Complex, southwestern Quebec; Geological Survey of Canada, Paper 74-48, Map 2-1974.
- Gadd, N.R.
1976: Surficial geology and landslides of Thurso-Russell map-area, Ontario; Geological Survey of Canada, Paper 75-35.
- MacClintock, P. and Stewart, D.P.
1965: Pleistocene geology of the St. Lawrence Lowland; New York State Museum and Science Service, Bulletin 394; Albany.
- Prest, V.K. and Hode-Keyser, J.
1977: Geology and engineering characteristics of surficial deposits, Montreal Island and vicinity, Quebec; Geological Survey of Canada, Paper 75-27, Map 1426A.
- Richard, S.H.
1975: Surficial geology mapping: Ottawa Valley Lowlands (Parts of 31 G, B, F); in Report of Activities, Part B, Geological Survey of Canada, Paper 75-1B, p. 113-117.
- Terasmae, J.
1965: Surficial geology of the Cornwall and St. Lawrence Seaway Project areas, Ontario; Geological Survey of Canada, Bulletin 121, Map 1175A.

**EXISTENCE OF A CENTRAL NEW BRUNSWICK ICE CAP
BASED ON EVIDENCE OF NORTHWESTWARD-MOVING
ICE IN THE EDMUNDSTON AREA,
NEW BRUNSWICK**

Project 760008

Claude Gauthier¹
Terrain Sciences Division

Introduction

The interpretation of the origin of glacial Lake Madawaska presented by Chalmers (1885) has remained unchallenged until now. Several striated outcrops indicating a northwestward glacial flow in the region of Edmundston have lead to a reevaluation of this interpretation. Because of the regional significance of this discovery, a brief description and a preliminary interpretation of the implications of this new find are presented here.

Chalmers (1885, p. 41-42 GG) described "chains of lakes" formed in Saint John Valley behind drift dams (the most prominent one is a frontal moraine at Grand Falls). Breaching of the drift in the valley gradually lowered the lake levels and re-established the normal drainage. Kiewiet de Jonge (1951) traced the extent of this lake up to Lac Témiscouata (Fig. 1) and gave it the name: "Glacial Lake Madawaska"; he recognized only one single phase related to the existence of the lake. Lee (1935, 1955) confirmed this interpretation and traced the extent of the shoreline deposits in the region of Edmundston. Martineau (1979) observed rhythmite deposits in the Lac Témiscouata area; he also reported the existence of two opposite glacial flows in the area: an early flow towards the southeast (Laurentide ice) followed by a flow with reversed direction (Appalachian ice). Martineau did not present the potential regional implications of his finding.

Glacial Flow in the Edmundston Area

During a one day field excursion in the area around Edmundston with J. Thibault, several striation sites were observed. Convincing evidence of striated and polished outcrops was collected to demonstrate that glacial flow was active towards the west and the northwest, controlled by the orientation Saint John Valley and some tributaries to it. Sites were observed along Madawaska and Iroquois valleys (six sites with northwest flow) as well as along Saint John River near the city of Edmundston (three sites indicated a westward flow). No other flow direction was noted, and all striated outcrops reflected a single ice flow direction (with variations of the order of 20 degrees at most). Sense of flow was obtained from numerous and distinctive characters: on a microscale, crag-and-tail and nailhead features, and plucking of lee sides of outcrops; on a macroscale, well developed stoss-and-lee relationships on outcrops, producing whalebacks and roches moutonnées. Although the number of sites observed is limited because of 1) the uniformity of the various observations, 2) the intensity of the erosional features, and 3) the absence of other movements, it is believed that they represent the last glacial flow, and that this flow was channelled by the major valleys of the area. Since some of these sites are recorded by Lee (1955), it is unclear to me how Lee could have suggested a reversed flow direction.

Implications of the New Observation

The present observation forces me to reject the previous interpretation of the mode of deglaciation of Saint John Valley and of the origin of glacial lake Madawaska. In order to generate a northwestward-moving ice mass, the glacier would have had to be centred in the highlands of central New Brunswick (and Maine?) and would have had to flow radially in several directions. At one time, the frontal position of the ice was located in the Grand Falls area, forming so-called glacial Lake Madawaska by ice damming the valley. Lee (1953) determined the altitude of the lake to be 167 m a.s.l. in the Edmundston area; Martineau (1979) established its level at 195 m in the vicinity of Lac Témiscouata. Both authors based their observations on the beaches, deltas, and terraces observed along valleysides. If these observations correspond to the highest level of the same lake phase, the glacial lake presents a minimal glacial-isostatic deformation of 28 m over a distance of 50 km (a gradient of 0.56 m/km, oriented north-northwest - south-southeast) with an apparent dip towards the south-southeast.

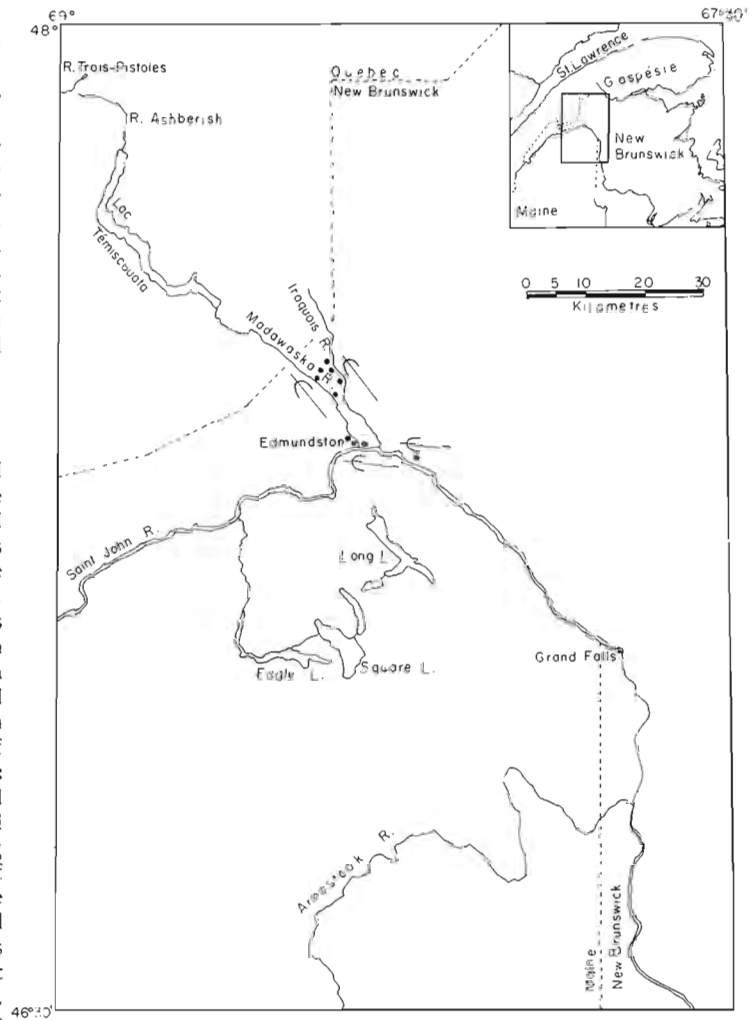


Figure 1. Map showing the study area; black circles mark sites of striated bedrock.

¹Department of Geology, University of Western Ontario, London, Ontario

From: *Scientific and Technical Notes
in Current Research, Part A;
Geol. Surv. Can., Paper 80-1A.*

The region of Plaster Rock (28 km east-southeast of Grand Falls) presents a set of discontinuous moraines, with a relief locally greater than 60 m. From limited evidence gathered in the field (one transversal section) glaciofluvial stratification in the moraines (beds dipping at 5-20 degrees towards the west) indicates: 1) ice localized to the east side of the moraines and 2) an aquatic mode of deposition. The ice contact ridges, in spite of their high relief (greater than 60 m), have no regional extent; nevertheless, they seem to represent a position of an ice cap centred in the New Brunswick Highlands, succeeding the retreat from the Grand Falls ice dam of Chalmers.

The damming of Saint John Valley by ice in the Grand Falls area forced glacial Lake Madawaska to drain into the St. Lawrence. The outlet corresponds to the divide between Trois-Pistoles and Ashberish rivers, at an elevation of 190-200 m, which precisely corresponds to the highest strandlines described by Martineau (1979). According to this concept, glacial Lake Madawaska is a dammed lake of truly glacial nature. As a result, the Saint John could not serve as an efficient drainage system during the melting of a local late glacier(s?), as assumed in the original model.

On a regional basis, it is significant to point out that striae in northwestern New Brunswick (National Topographic System map area 21 O, Campbellton) present a regular and uniform trend towards the east (Gauthier, 1979). In central New Brunswick (National Topographic System map area 21 J, Woodstock), a variety of flow directions have been recorded by previous workers. No trends or chronology can be defined from data on hand, which seem to reflect a fluctuating flow pattern during the last phase of deglaciation. This central New Brunswick area corresponds to the region where Alcock (1948) believed the New Brunswick ice cap to have been located. Such a phenomenon would have resulted in the damming of Saint John Valley during the southward retreat towards the ice centre. The westward and northwestward striae sites relate to protuberances of ice lobes into tributary valleys of the Saint John and in Saint John Valley. Kame terraces (Thibault, 1979) on valleysides in these areas also would relate to this system.

Unexplained Problems

Although the glacial flow in Saint John Valley in the Edmundston area convincingly reflects a westward direction, many aspects of the glacial geology remain to be studied before a coherent picture of the deglaciation can be presented. The new working hypothesis has far reaching implications over a large area and represents an entire revision of the previous ideas. Many aspects of the new problems need to be studied, the most significant of which are:

1. the presence of large outwash plains extending from the Grand Falls "drift dam", upon which the original definition of glacial Lake Madawaska was based;
2. the interrelation between the Appalachian ice (northward flow) in the Quebec Appalachian Mountains and a) the eastern flow of northwestern New Brunswick, b) the local ice cap of central New Brunswick, and c) ice retreat in Maine; and
3. glacial Lake Madawaska would have covered an extensive area in Maine if the region had been deglaciated at that time. Large lake basins in northeastern Maine (Eagle, Square, and Long lakes) and Aroostook Valley all may have lain within the basin of glacial Lake Madawaska.

References

- Alcock, F.J.
1948: Problems of New Brunswick geology; Transactions of the Royal Society of Canada, v. XLII, series III, section 4, p. 1-15.
- Chalmers, R.
1885: Report on the Surface Geology of Western New Brunswick; Geological Survey of Canada, Report of Progress, 1882-1884, part XI, GG, 47 p.
- Gauthier, R.C.
1979: Aspects of the glacial history of the north-central highlands of New Brunswick; in Current Research, Part B, Geological Survey of Canada, Paper 79-1B, p. 371-377.
- Kiewiet de Jonge, E.J.C.
1951: Glacial water levels in the Saint John River Valley; unpublished Ph.D. thesis, Clark University, Worcester, Mass., 116 p.
- Lee, H.A.
1953: Two types of till and other glacial problems in the Edmundston-Grand Falls region, New Brunswick, Quebec and Maine; unpublished Ph.D. thesis, University of Chicago, Chicago, Illinois, 113 p.
1955: Surficial geology of Edmundston, Madawaska, and Temiscouata counties, New Brunswick and Quebec; Geological Survey of Canada, Paper 55-15, 13 p.
- Martineau, G.
1979: Géologie des dépôts meubles de la région du Lac Temiscouata; Ministère des richesses naturelles du Québec; DPV-618; 18 p.
- Thibault, J.
1979: Granular aggregate resources of Edmundston; Department of Natural Resources of New Brunswick, Plate 79-35.

GENERAL GEOLOGY OF THE EYE-DASHWA LAKES PLUTON, ATIKOKAN, NORTHWESTERN ONTARIO

P.A. Brown¹, C. Kamineni¹, D. Stone¹, and R.H. Thivierge¹
Terrain Sciences Division

Introduction

During the summer of 1979 the geological research program for radioactive waste disposal, being conducted by Geological Survey of Canada in co-operation with Atomic Energy of Canada Limited, began work on the Eye-Dashwa lakes pluton at Atikokan, northwestern Ontario. This work involved 1) geological mapping, 2) detailed mapping of faults and fractures, and 3) outlining the mineralogy and distribution of fracture filling material. This report deals primarily with the broad geological synthesis rather than the detailed analyses of fractures and fracture filling materials.

The Eye-Dashwa lakes pluton (Fig. 1), located 15 km north-northwest of Atikokan, northwestern Ontario, is an egg-shaped medium- to coarse-grained hornblende-biotite granite which intrudes a tonalitic to amphibolitic gneiss complex – the Dashwa Gneiss. The gneiss shows a complex and protracted tectonic and metamorphic history (including faulting, shearing, and fracturing) which predates the intrusion of the granite.

The intrusion of the granite appears to have occurred in three distinct phases. An early medium- to coarse-grained syenodioritic phase (locally showing igneous layering) occurs both as a separate tadpole-shaped intrusion at Volcano Bay and as a border phase to the main granite. The second phase, a fine- to medium-grained leucogranite, is restricted to the southern and eastern margins of the main granite body. The third, and last major phase, comprises the bulk of the Eye-Dashwa lakes pluton and is a medium- to coarse-grained biotite-hornblende granite. Three 'intrusive centres' are recognized, the early syenodioritic phase at Volcano Bay, the Dashwa Lake 'centre' with a large roof pendant, and the Forsberg Lake-Eye Lake mass.

Subsequent to the main intrusive event the region was subjected to further faulting and fracturing, followed by the intrusion of diabase dykes. These events affected both the granite and the gneiss and in part were accompanied by remobilization of the early discontinuities within the gneiss. The faults and fractures contain a variety of filling material including amphibolite, quartz, granodiorite, pegmatite, aplite, muscovite, lamprophyre dykes, epidote, hematite-goethite, fluorite, chlorite, diabase dykes, calcite, gypsum, and clay minerals.

Acknowledgments

Valuable mapping contributions by geologists Glen McCrank, John Misiura (Dashwa Lake area), and Nate Rey and John Psutka are gratefully acknowledged.

Dashwa Gneiss Complex

The gneiss surrounding, and included as xenoliths within, the Eye-Dashwa lakes pluton form a heterogeneous group of predominantly sodic to locally amphibolitic gneiss (Schwerdtner, 1977; Fenwick, 1976) which display a complex and protracted tectonic and metamorphic history. The sodic rocks are generally tonalitic to quartz dioritic and are either well banded or strongly foliated. Pegmatitic segregations of granitic material are locally abundant. The amphibolites are medium grained equigranular rocks with a well developed composite fabric and occur as isolated bands, lenses, and xenoliths within the tonalitic gneiss.

¹ Atomic Energy of Canada Limited,
601 Booth Street, Ottawa, Ontario

Textures vary from equigranular to subporphyritic with the local development of augen gneiss. Cataclastic and blastomylonitic textures locally overprint the gneiss textures.

The general trend of the gneissic banding varies around the Eye-Dashwa lakes granite and is subparallel to the contact (Fig. 1). Present data indicate that the gneiss to the west dips under the pluton and that to the north and east dips away from the pluton. Insufficient data are available to determine the general dip of the gneissic banding to the south of the body.

Eye-Dashwa Lakes Pluton

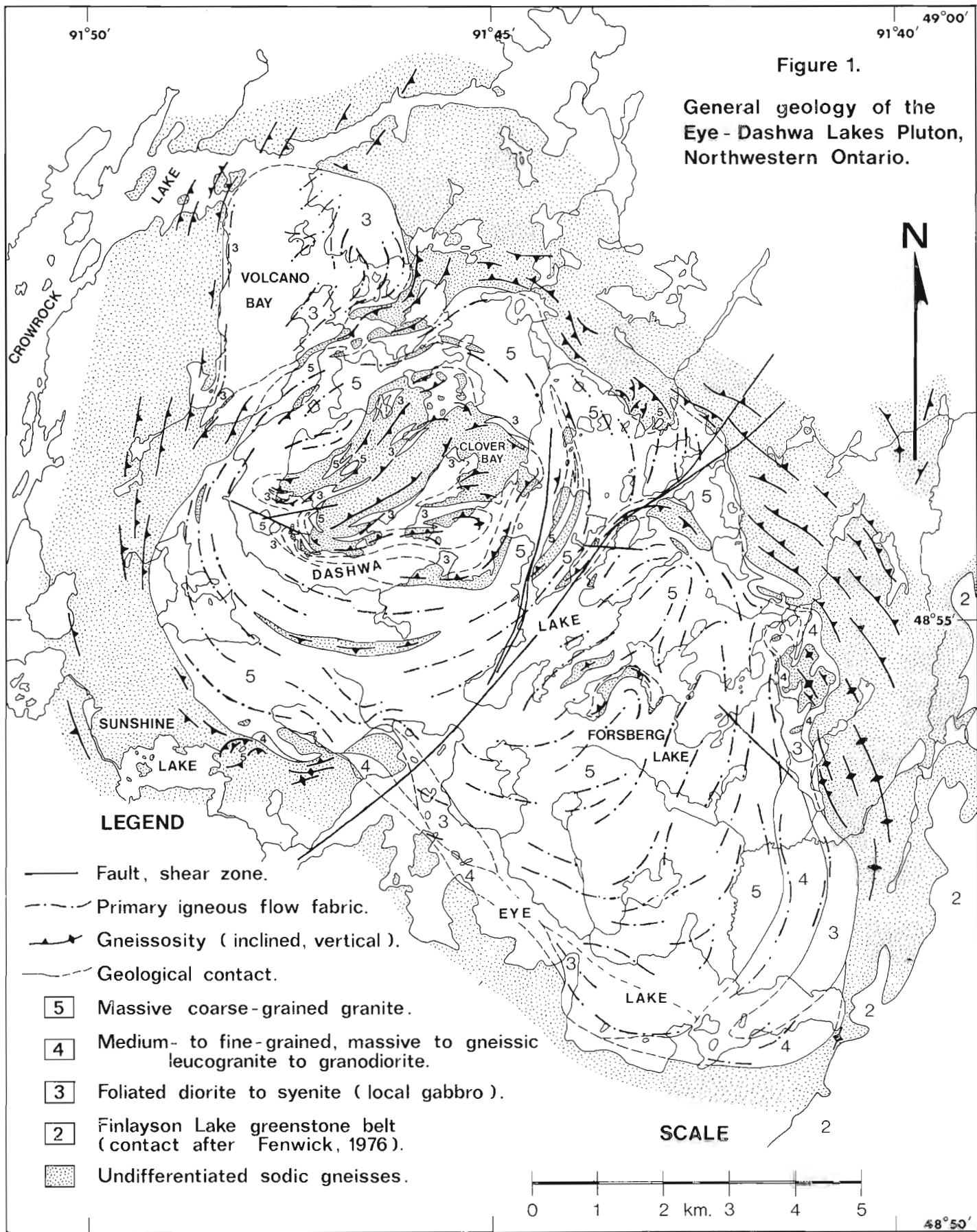
The Eye-Dashwa lakes pluton intrudes the Dashwa Gneiss Complex (Schwerdtner, 1977; Simpson, 1977). It can be separated into three distinct compositional phases, an early coarse grained syenodioritic phase, a fine- to medium-grained leucogranite, and a late medium- to coarse-grained subporphyritic granite. This latter phase constitutes the main mass of the pluton.

The syenodioritic phase is a coarse grained foliated to locally banded rock which occurs both as a border phase to the main Eye-Dashwa lakes granite and as an isolated stock underlying Volcano Bay, which is separated from the main body by a thin sliver of gneiss (Fig. 1). In composition it ranges from a quartz-free to quartz-rich hornblende monzonitic rock through to a more sodic hornblende dioritic phase. Texturally the rock varies from an equigranular, medium- to coarse-grained rock syenodioritic phase with a moderately strong flow fabric to a coarse grained, massive, subporphyritic rock (monzonitic phase). The latter is gradational to the later coarse grained granitic phase. Locally a felsic-mafic igneous layering is well developed. The mafic layers are defined by an increase in hornblende content. Both mafic and felsic bands are wavy, discontinuous and pinch out along strike. The layering is conformable with the surrounding gneissic banding and consistently dips at a steep angle to the southwest, i.e., this sequence structurally underlies the main Eye-Dashwa lakes granite.

Small subrounded hornblende clots (1-3 cm) and small angular foliated to finely banded amphibolite xenoliths (1-5 cm) are common throughout the mass. Locally, in the Clover Bay area, larger xenolithic blocks of a mostly textured medium- to coarse-grained hornblende gabbro are found within the syenodioritic phase. The hornblende clots and hornblende gabbro may represent relicts of the earliest phase of the intrusion. The banded xenoliths probably represent mafic remnants derived from the gneiss or possibly the metavolcanic rocks. The syenodioritic phase is locally crosscut by, and contained as xenoliths within, the leucogranite.

The leucogranite is a massive to gneissic, pink to white, medium- to fine-grained, equigranular homogeneous leucocratic granitic to granodioritic rock. It is largely restricted in occurrence to the southern and eastern margins of the main Eye-Dashwa lakes pluton where it is present as a border zone, locally up to 1.5 km in width. Elsewhere, within the main body, it is locally developed as narrow discontinuous zones adjacent to gneissic enclaves and xenoliths.

The main mass of the Eye-Dashwa lakes pluton is composed of a pink, massive to foliated, coarse grained to subporphyritic granite. For the most part it is a remarkably homogeneous rock, with the quartz and feldspar ratios varying little throughout the body. Close to the contact with the gneiss the quartz content may decrease with an increase in the plagioclase and hornblende contents. Hornblende is the major mafic mineral although biotite, which also occurs throughout the body, is locally dominant.



The primary foliation in the rock is defined by aligned feldspars and orientated mafic minerals. Close to the margin, and to gneiss enclaves, the foliation becomes well developed and is generally conformable to the gneissic banding. At Sunshine, Eye, and northeast Dashwa lakes the granite crosscuts the gneissic banding. The contact is generally marked by a xenolith-rich zone which may be up to 100 m wide.

Structurally the Eye-Dashwa lakes pluton can be separated into three 'intrusive centres' (Fig. 1). The early syenodioritic phase occurs as a separate tadpole-shaped body underlying Volcano Bay to the northwest of the main granite body. The fabric and igneous banding in this body are largely conformable with the surrounding gneissic banding and show a moderate to steep dip to the southeast, i.e., under the Eye-Dashwa lakes granite. This body is separated by a sliver of gneiss from a second 'intrusive centre' at Dashwa Lake. In this latter region the flow fabric in the granite wraps around a large central gneiss xenolith, 6-7 km in diameter, which is probably a roof pendant. Elongate slivers of gneiss conform to the flow fabric in the granite and help outline the circular pattern.

The main mass of the granite, to the southeast, is separated from the second 'intrusive centre' by a marginal xenolith-rich zone and a zone of cataclasis which runs parallel to the eastern shore of Dashwa Lake. (This demarcation line is coincident with an aerial photograph lineament which is of the order of 100 km long). The flow pattern in the southeastern area is much more irregular than in the other two areas. A crude arcuate domal structure, however, can be outlined (Fig. 1).

These structural centres conform, in part, to the compositional variation within the granite. The centre underlying Volcano Bay is composed of the early syenodioritic rock and probably represents an early phase of intrusion of the pluton. Minor injection of this phase is represented by the border zone in the southeastern part of the body.

The leucogranite is present only in the southern and eastern part of the body. This is a minor phase which locally separates the early syenodioritic phase from the later granite intrusion.

It is suggested that the main southeastern mass of granite was emplaced immediately after the leucogranite and that this was followed by, or synchronous with, the emplacement of the Dashwa 'centre'. The large xenolith, which may represent a roof pendant, and the numerous gneiss xenoliths suggest that this is an upper, late phase of the intrusion.

Faults and Fractures

The fault and fracture patterns developed in the Eye-Dashwa lakes granite and surrounding gneiss were examined at various scales by

- a. aerial photograph analyses,
- b. regional groundwork covering both the granite and the gneisses,
- c. detailed groundwork covering an area of approximately 2 km², and
- d. detailed grid scale work covering a cleared area 200 by 50 m.

Preliminary observations and results from the aerial photograph and regional work are presented here. Results from the analyses of the regional, detailed, and grid scale work are incomplete to date.

Aerial photograph lineament analyses of the Eye-Dashwa lakes granite and surrounding gneiss indicate that the gneiss contains a higher density of lineaments than the granite and also that the lineaments in the gneiss are more regularly orientated than those in the granite (Fig. 2). Only one major lineament was defined in the area. This feature trends northeast and defines the eastern shore of Dashwa Lake. It can be traced to the northeast and southwest for about 100 km. Ground followup has shown that this feature has relatively little surface expression. Neither the granite nor the gneiss shows evidence of intense faulting, and the granite-gneiss contact is not displaced. The separation of the main granite body into two domal structures, however, is coincident with the lineament.

A length weighted histogram of the lineaments in the granite and surrounding gneiss (Fig. 3A) indicates that the dominant trends are 035° and 115-120° with well developed but subordinate peaks at 000°, 020°, 050°, 060°, 090°, and minor peaks at 135°, 150°, 160° and 170°.

The regional groundwork covered both the granite and the surrounding gneiss, and fracture data have been collected from some 1300 localities throughout the area. In addition four small 'control areas' (some tens of kilometres outside the study area) were examined in order to evaluate the regional fracture setting. At each outcrop the fractures present were separated into fracture sets according to their attitude and character, and, for each set, the orientation, frequency, length, continuity, width, and type of filling material and/or alteration was recorded in coded computer compatible form. These data are presently being processed.

Preliminary evaluation of the field observations indicates that within the granite two to four fracture sets are generally developed at any one outcrop. The fractures tend to be straight and regular, long, relatively evenly spaced, and outline a somewhat regular intersecting fracture network. Close to major faults the fractures show a decrease in spacing and additional fracture sets can be identified. This increase in fracturing is generally accompanied by pronounced fracture filling and fracture-wall rock alteration.

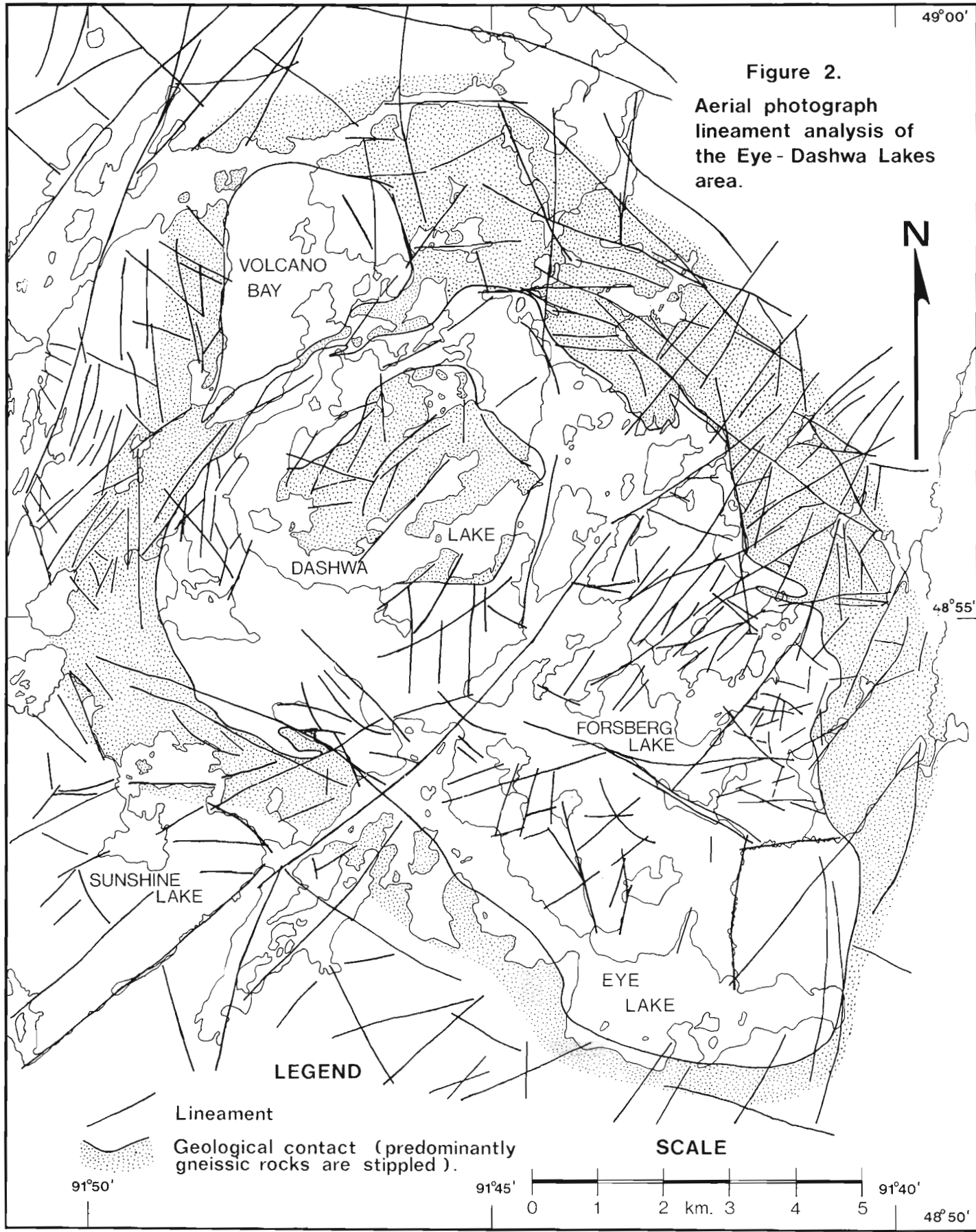
Within the gneiss the fracture systems show a wide range of development. As in the granite several fracture sets are generally developed at any one outcrop; however, the fractures are somewhat irregular, short, unevenly spaced, and outline a less regular pattern than in the granite. Close to the faults the fracture patterns become chaotic with numerous fracture sets being developed. At the other extreme, local outcrops well away from any faults contain few fractures, and those that are present are short, irregular, and discontinuous and do not form an intersecting fracture network.

Preliminary compilations of the fracture data are presented as frequency-weighted histograms (Fig. 3). These indicate that the dominant fracture directions over the entire area, including both granite and gneiss (Fig. 3B), trend 000°, 090°, and 105° with subordinate peaks at 020°, 040°, 140°, 150°, 160°, and 170°. The general trends correspond well with the lineament trends (Fig. 3A).

Within the granite (Fig. 3C) the dominant fracture trends are at 000°, 090°, 105°, and 160° with subordinate peaks at 015° and 115°, and minor peaks at 045°, 075°, 140°, and 170°. Detailed analyses will show whether these peaks represent discrete fracture sets or whether there is a reorientation of fracture sets throughout the body. Evaluation of the fracture sets with reference to the type and nature of the filling material will allow a sequential history of fracture development to be evaluated.

49°00'

Figure 2.
Aerial photograph
lineament analysis of
the Eye - Dashwa Lakes
area.



VOLCANO
BAY



DASHWA
LAKE

FORSBERG
LAKE

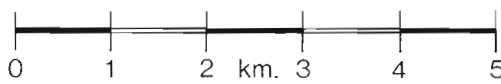
SUNSHINE
LAKE

EYE
LAKE

LEGEND

-  Lineament
-  Geological contact (predominantly gneissic rocks are stippled).

SCALE



91°50'

91°45'

91°40'

48°50'

48°55'

Within the gneiss (Fig. 3D) the dominant fracture trends are at 000° , 040° , 105° and 150° , with subordinate peaks at 020° , 090° and 140° . Some fractures formed prior to the intrusion of the granite, some formed during the intrusion event, and others formed after the pluton had cooled and

solidified. The type and nature of the fracture filling material allows the segregation of the fractures into three broad groups (discussed below).

Fracture Filling Material

A variety of filling materials and minerals is present in the fractures both within the gneiss and the granite (Famineni et al., 1980). These materials can be arranged into a relative age sequence based on crosscutting relationships. This sequence falls naturally into three categories: pre-granite emplacement, syn to late granite emplacement, and post-granite emplacement.

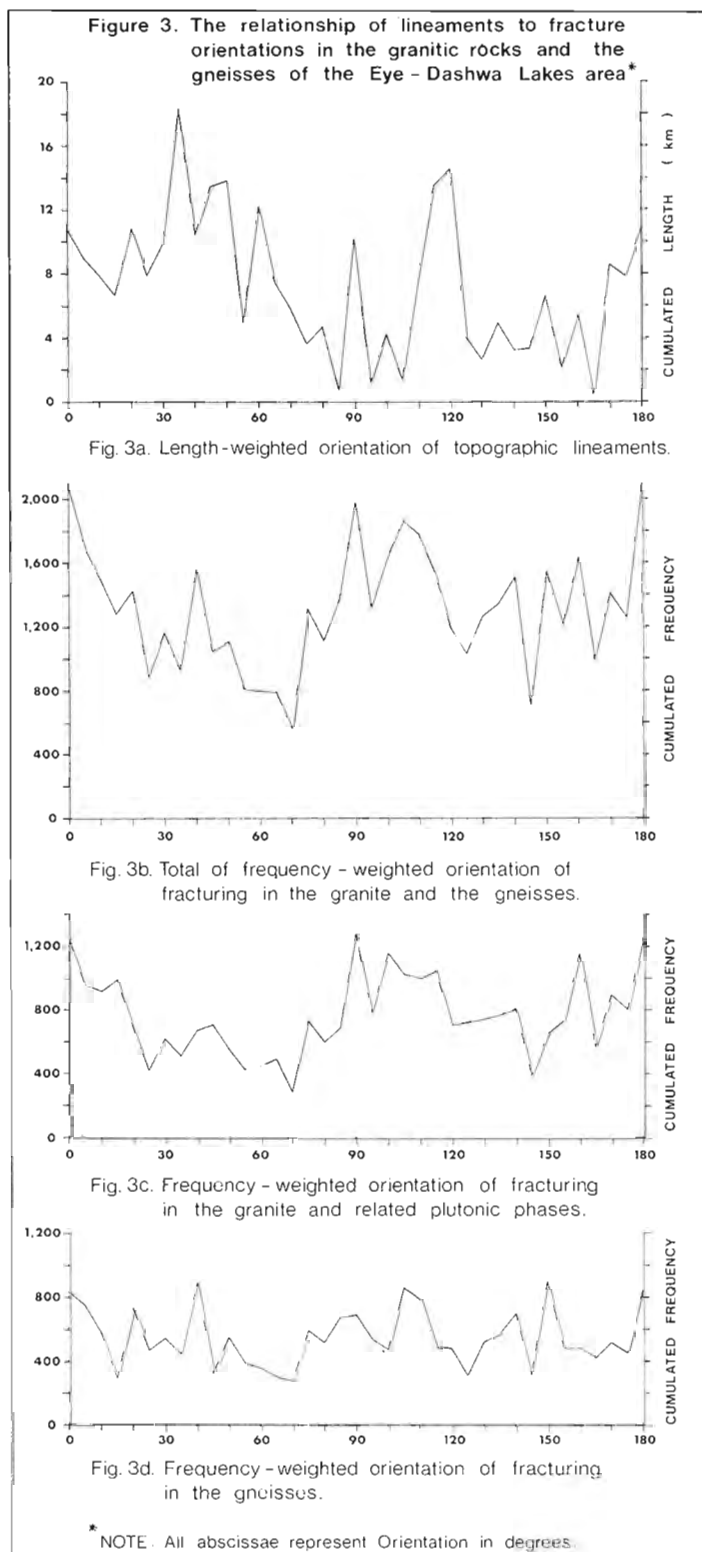
The pre-emplacement fillings are only present within the gneiss and include amphibolite dykes, quartz veins, granodiorite dykes, and sulphides. They are recognized as being pre-emplacement because they are consistently crosscut by syn emplacement pegmatite dykes. Fine to medium grained amphibolite dykes which have been affected by late shearing are the earliest recognized filling material. Quartz veins crosscut the dykes and are not affected by the shearing. These, in turn, are crosscut by a network of fine grained magnetite-bearing granodioritic dykes. The sulphides (pyrrhotite and pyrite) are only locally developed, and at present it is uncertain how they fit into the sequence; they are crosscut by the pegmatite dykes and are thus part of the pre-emplacement fillings.

The syn to late emplacement fillings are present in both the granite and gneiss and include two ages of pegmatite dykes, muscovite, and lamprophyre dykes. The separation of late and post-emplacement fillings is somewhat arbitrary. For convenience, epidote, which is definitely post-emplacement, is taken as a readily recognizable time-event horizon. The syn to late emplacement fillings are all crosscut by the epidote-filled fractures. The early formed pegmatites are coarse grained muscovite-bearing dykes which crosscut the granite and extend at least 1 km into the surrounding gneiss. They are crosscut by later formed, finer grained, more mafic pegmatites, which in turn are crosscut (locally) by muscovite-filled fractures. Lamprophyre dykes, characterized by phenocrysts of hornblende, crosscut the muscovite- and pegmatite-filled fractures.

The post-emplacement fracture fillings can be separated into a relatively high temperature sequence: epidote, quartz, fluorite, chlorite, zeolite, and hematite-geothite, and a relatively low temperature sequence: carbonate, gypsum, and clay. The intrusion of east-west trending diabase dykes acts as a marker horizon between the two sequences. The distribution of the high temperature sequence indicates that minerals are fault-related with the mineral-bearing fluids being injected at various stages in the faulting process. Detailed work on this sequence is in progress and is providing considerable information on the history and development of the fault-related fracture systems.

The diabase dykes are not spatially related to known fault systems within the area and it is suggested that these dykes represent a post-faulting tensional event. Similar dykes have been recognized in the Kashbowie area (40-50 km to the east) indicating that this may be a regional event (W.M. Schwerdtner, personal communication, 1979).

The minerals in the low temperature sequence occur in vugs and as coatings on pre-existing fracture filling minerals. The type of occurrence and the low temperature of crystallization suggest that these minerals may have precipitated from the groundwater system and, as such, are indicators of relatively recent flow paths.



Summary

The Eye-Dashwa lakes granite is a composite granite pluton intruded into a sequence of tonalitic to amphibolitic gneisses. The gneiss shows a complex and protracted tectonic-metamorphic history (including faulting and fracturing) prior to the injection of the granite. Three 'intrusive centres', which partially conform to the compositional changes, i.e. the syenodioritic phase, the leucogranite and the granite, can be recognized. Syn to post-intrusive tectonic events include the development of fractures which are subsequently filled by pegmatite dykes, muscovite, and lamprophyre dykes.

Post-emplacement tectonism involves extensive faulting and fracturing accompanied by the injection of fluids along the fault and fracture planes. The fluids show a time-temperature sequence from early formed, relatively high temperature epidote to low temperature hematite-geothite. These fractures and their filling materials are crosscut by east-west trending diabase dykes which may represent a regional(?) tensional event. The final events involve the remobilization of the existing fracture system and the deposition of low temperature minerals (calcite, gypsum, clays) on the pre-existing fracture filling minerals. This is probably related to the present groundwater flow system.

References

- Fenwick, W.G.
1976: Geology of the Finlayson Lake area, District of Rainy River; Ontario Division of Mines, Geoscience, Report no. 145, 86 p.
- Kamineni, D.C., Brown, P.A., and Stone, D.
1980: Fracture filling material in the Atikokan area, northwestern Ontario; in Current Research, Part A; Geological Survey of Canada, Paper 80-1A, note.
- Schwerdtner, W.M.
1976: Lithology and structure of the Irene-Eltrut Lakes Granitic Complex between Atikokan and Ignace - a progress report; Geotraverse Conference, University of Toronto, p. 22-27.
1977: Origin of the tonalitic and granodioritic gneisses in the Wabigoon and Shebandowan super belts with special emphasis on the Irene-Eltrut Lakes Granitic Complex; Geotraverse Conference, University of Toronto, p. 34-40.
- Simpson, E.L.
1977: Eye Lake and Ear Lake Plutons, Atikokan Region, northwest Ontario; Geotraverse Conference, University of Toronto.

MINERAL ASSEMBLAGE POLARITY IN MAGMATIC SULPHIDE BLEBS IN A KOMATIITIC NICKEL DEPOSIT

Project 630037

O.R. Eckstrand
Economic Geology Division

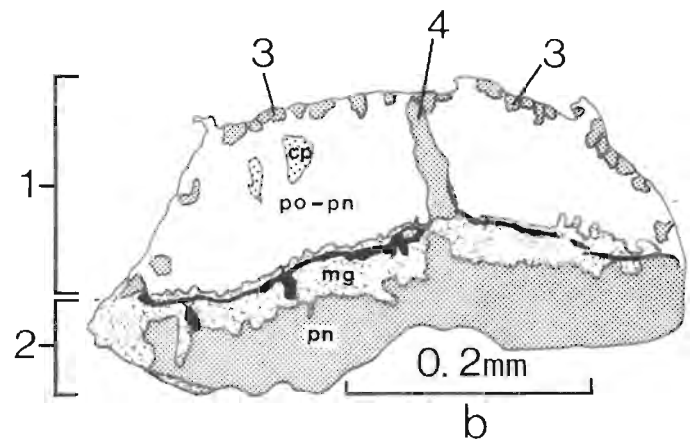
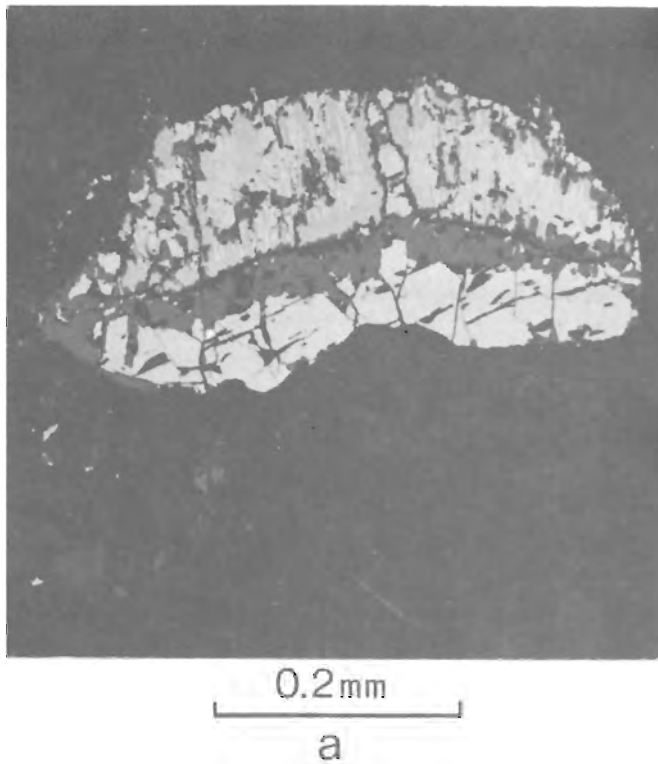
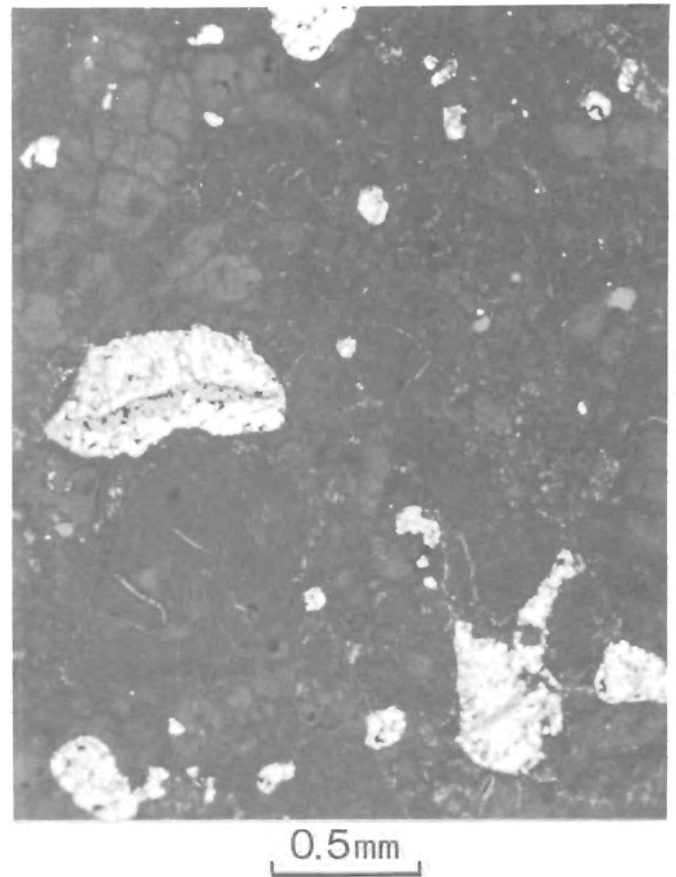
Introduction

A rather remarkable mineral assemblage polarity (MAP) in small nickeliferous sulphide blebs has been encountered in a sample from the komatiite-hosted Dundonald deposit, about 50 km northeast of Timmins. The purpose of this note is to describe the feature which is basically a segregation within individual blebs into a pyrrhotite zone and a pentlandite zone. The pyrrhotite zones consistently occupy the same side of every bleb, so that the sample displays a polarity analogous to that of a magnet and its constituent dipoles. Some preliminary speculations on interpretation and significance of the MAP are presented.

Acknowledgments

I am grateful to Falconbridge Nickel Mines Limited for permission to obtain samples, to R.D. Lancaster and S. Green for preparation of photomicrographs and the diagram, and to J.M. Duke for useful discussion and suggestions.

Figure 1. Photomicrograph illustrating distribution of sulphide blebs and their size and shape, Dundonald nickel sulphide deposit. Mineral zones are apparent in the largest bleb, left centre; details are shown in Figure 2. This and all succeeding photomicrographs are from the same plane surface and all are oriented in the same direction.



b. Principal textural features in the bleb of Figure 2a.

- (1) = pyrrhotite zone. Note exsolution lamellae of pentlandite in pyrrhotite, Figure 2a.
- (2) = pentlandite zone
- (3) = fringe of pentlandite grains peripheral to pyrrhotite at bleb margin
- (4) = pentlandite septum
- po = pyrrhotite
- pn = pentlandite
- cp = chalcopyrite
- mg = magnetite

Black areas in bleb are pits in the polished surface.

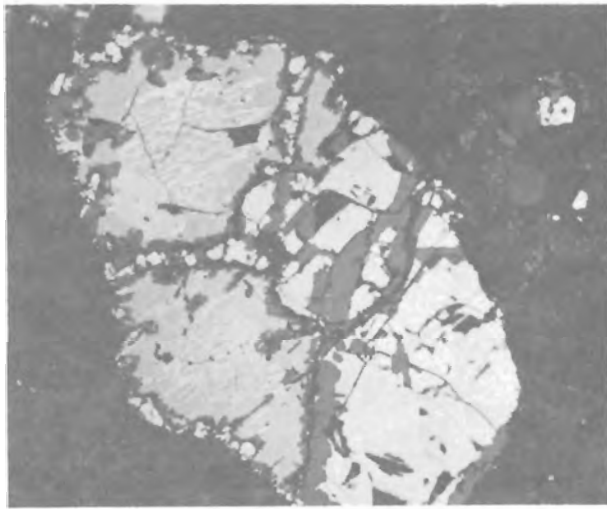
a. Photomicrograph of a typical sulphide bleb showing mineral assemblage polarity (MAP), Dundonald nickel deposit

Figure 2



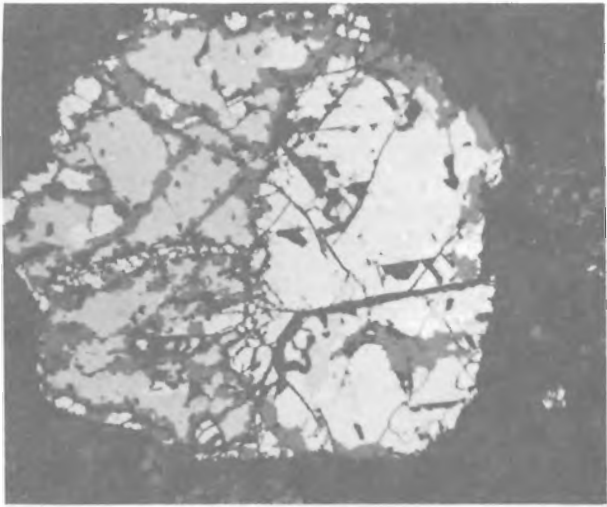
3

0.2mm



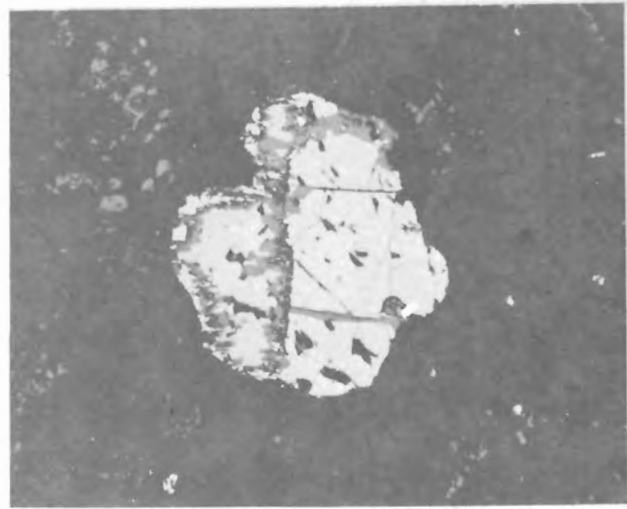
4

0.2mm



5

0.2mm



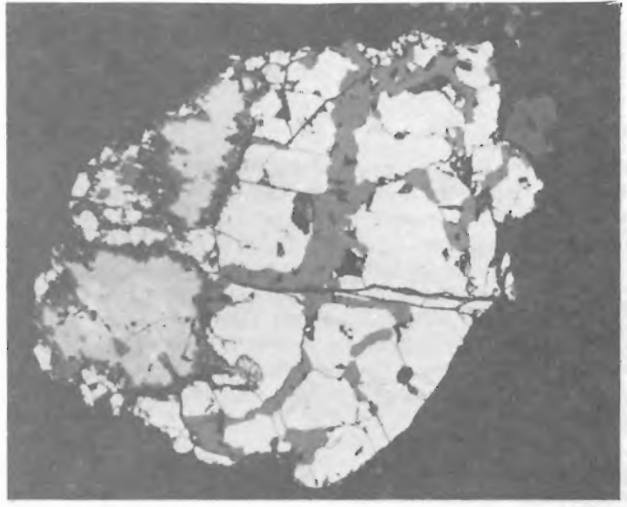
6

0.2mm



7

0.2mm



8

0.2mm

Figures 3 to 8. Photomicrographs of sulphide blebs showing typical development of .MAP, fringing pentlandite grains, pentlandite septa between pyrrhotite individuals. Dundonald deposit. See text for additional comments.

General Description of Deposit

The Dundonald deposit has been described by Comba (1972), and by Muir and Comba (1979) from which the following summary is extracted. It is a small, undeveloped nickel sulphide deposit in the Abitibi greenstone belt, and has an average grade of 1.50 per cent Ni and 0.03 per cent Cu. It is hosted in an east-west striking steeply-dipping sequence of spinifex-textured pyroxenitic and peridotitic komatiite flows. The sulphide mineralization occurs as 1) basal conformable zones in some of the flows, comprising intercumulate disseminated blebs and continuous networks of sulphides, mainly pentlandite, and 2) "interflow" ore, highly mineralized horizons between flows, characterized by nodules and fragments of graphite, volcanic clasts and a pentlandite-pyrrhotite assemblage. The latter mineralization is in some cases intercalated with tuffaceous carbon-rich beds that locally contain bands and nodules of pyrite replaced to varying degrees by pyrrhotite.

Description of sulphide blebs

Representative drill core samples of the Dundonald deposit were obtained from Falconbridge in 1972. Recent re-examination of polished sections made from these samples resulted in recognition of the MAP within the sulphide blebs of one specimen. This rock is a cumulate-textured peridotite, consisting of 1 to 2 mm equant olivine and tabular clinopyroxene crystals, and a finer grained intercumulate matrix consisting mainly of radiating bundles of lath-like clinopyroxene, and minor plagioclase. Chromite occurs as dispersed 0.1 mm equant crystals. Alteration has converted much of the olivine and some of the clinopyroxene to mixtures of serpentine, magnetite, tremolite and chlorite.

The sulphide blebs are dispersed through the intercumulate material as rounded to ovoid "droplets" (Fig. 1*). Bleb outlines tend to be sharply defined against surrounding silicate minerals. Some blebs have concave portions to their peripheries (Fig. 3) and apparently have been molded against cumulative olivine or clinopyroxene crystals. One bleb is enclosed within a clinopyroxene crystal. The blebs range from less than 0.1 mm to somewhat more than 1 mm in diameter.

The majority of blebs show a mineral assemblage polarity (MAP) comprising a pyrrhotite zone consistently on the same side of each bleb, and a pentlandite zone on the other (Fig. 2 to 9). The terms "top" and "bottom" come to mind in describing this polarity, although it is not known whether the feature is related to a vertical direction. In any case, true top and bottom in the sample are not known. From one-half to two-thirds of those blebs greater than about 0.3 mm in size show clearly recognizable MAP, and probably more than 90 per cent of the blebs greater than about 0.5 mm in size show MAP. Little if any MAP has been recognized in blebs less than 0.3 mm.

The principal features of the sulphide blebs that show MAP are illustrated in Figure 2. The pyrrhotite zone consists mainly of pyrrhotite, but also contains abundant pentlandite in two or three distinct habits, a moderate amount of magnetite, and commonly chalcopyrite. The pentlandite zone contains no pyrrhotite, a moderate amount of magnetite, and rarely chalcopyrite. In a survey of 265 blebs (mostly larger than 0.3 mm), chalcopyrite was observed in 135 (51%), and in 125 (92%) of these chalcopyrite was in the pyrrhotite zone, and in 11 (8%), it was in the pentlandite zone.

*All photomicrographs are from the same polished plane surface of one sample, all oriented in the same direction.

† mss = monosulphide solid solution, the high temperature phase in the Fe-Ni-S system that shows complete solid solution between Fe_{1-x}S and Ni_{1-x}S .

The pyrrhotite zone consists mainly of one or more pyrrhotite grains with borders of granular pentlandite. In Figure 2, two pyrrhotite grains, separated by a septum of pentlandite, have slightly different orientations indicated by pentlandite exsolution lamellae paralleling (0001). Similarly, two or more pyrrhotite grains are evident in the pyrrhotite zones of Figures 4 and 8.

The pyrrhotite grains tend to be free of pentlandite exsolution lamellae around their peripheries, but at the same time to have a border of granular pentlandite, either as fringing grains at the margins of the bleb, or as more continuous septa, separating pyrrhotite grains. Both fringing grains and septa of pentlandite are clearly displayed in Figures 2, 4, 5, 8, 9, and 12. These relations suggest that the fringing grains and septa of pentlandite, like the lamellae, are also the result of exsolution out of pyrrhotite, and subsequent migration to the periphery of the pyrrhotite grains.

The pentlandite zone consists of one or a few grains of pentlandite and some borders and veins of magnetite. A minor part of this pentlandite might represent exsolution out of pyrrhotite.

Magnetite generally constitutes 10 to 20 per cent of each of the sulphide blebs. It occurs in both pyrrhotite and pentlandite zones with no clear preference, but does tend to be associated with fringing grains and septa of pentlandite within the pyrrhotite zone.

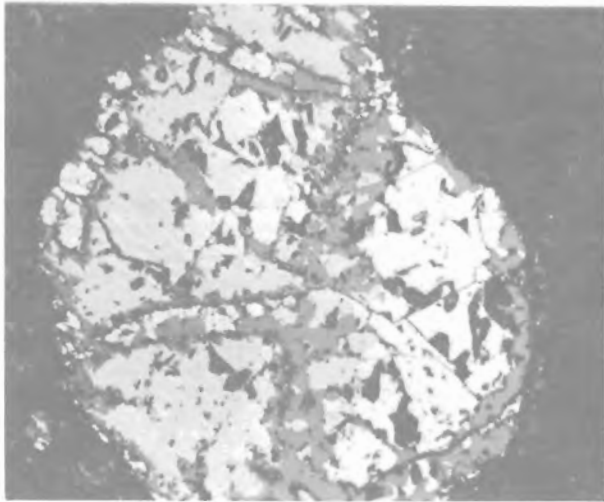
Variations in the MAP feature are seen in some grains. The anchor-shaped bleb in Figure 10 may result from two coalesced blebs, each with its distinct pyrrhotite and pentlandite zones. In others (Fig. 11, 12, 13) the existence of a pentlandite zone is somewhat conjectural but likely. In Figure 12, the rather abundant pentlandite with surrounding pyrrhotite grains in the centre of the bleb could possibly be accounted for by exsolution from the pyrrhotite.

The bleb in Figure 14 typifies one of the two types of blebs that do not show MAP, and consists of just a pyrrhotite zone with only the fringing and septal varieties of pentlandite (plus magnetite, chalcopyrite). Conversely the other type of bleb that does not show MAP consists only of pentlandite with magnetite, i.e. a pentlandite zone. Both of these cases could be explained as statistically expectable sections through the extremities of blebs. For example, pyrrhotite alone only would result from a section near the right end of the bleb in Figure 4, and pentlandite zone only from the left end of the bleb in Figure 8.

Interpretation

The textural features and MAP of these sulphide blebs suggest at least a three stage genesis:

1. **Bleb formation.** The sharp boundaries, rounded shape, and intercumulus location of the blebs suggest that at a magmatic stage the blebs are immiscible sulphide droplets in partly crystallized peridotitic magma (a komatiitic flow).
2. **Formation of MAP.** The formation of pyrrhotite and pentlandite zones displaying a consistent polarity indicates some kind of oriented segregation mechanism within the droplets. This is discussed further in subsequent comments.
3. **Exsolution.** The material of the pyrrhotite zone crystallized into one or a few grains (presumably mss† with a significant Ni and minor Cu content) and subsequently exsolved pentlandite to form lamellar intergrowths, fringing grains, and septa which separated the pyrrhotite grains. The last pyrrhotite-pentlandite exsolution equilibration probably took place below 300°C.



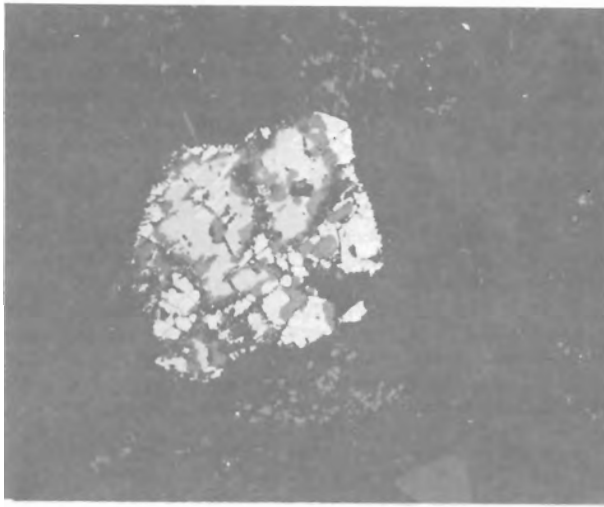
9

0.2mm



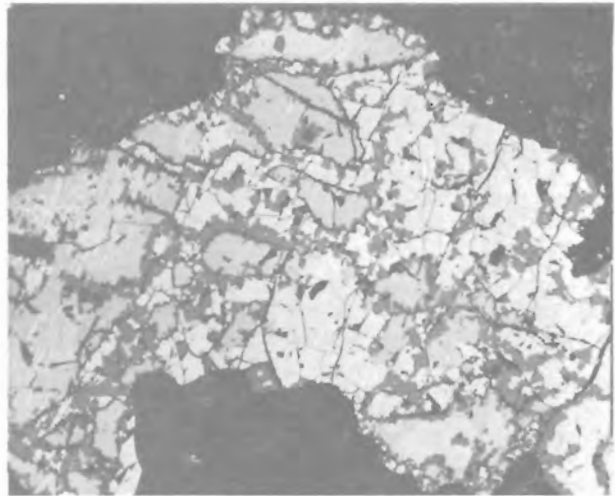
10

0.2mm



11

0.2mm



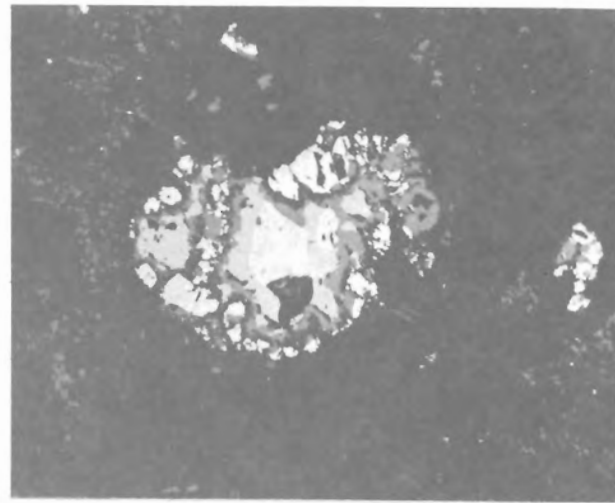
12

0.2mm



13

0.2mm



14

0.2mm

Figures 9 to 14. Photomicrographs of sulphide blebs, Dundonald deposit. Figure 9, typical. Figure 10, two coalesced blebs, Figures 11 to 13, pentlandite zone not well defined but probably present. Figure 14, pyrrhotite zone only, with pentlandite fringe and septum, central grain of chalcopyrite. See text for additional comments.

The segregation mechanism that produced MAP is not understood. The most obvious interpretation is that during crystallization of the sulphide liquid in the bleb, the first solid phase, presumably a Ni-bearing mss phase, sank in the residual sulphide liquid to form a gravitational cumulate. However at this point, a dilemma is encountered. According to experimentally observed phase relations in the Ni-Fe-Cu-S system (Craig and Kullerud, 1969; Kullerud et al., 1969), the mss that crystallizes from a S-poor sulphide liquid should have a Fe/Ni ratio higher than that of the liquid, and therefore, the pyrrhotite zone should represent the cumulate phase in the blebs. However, the same experimental studies also suggest that Cu should be enriched in the residual liquid, eventually crystallizing as chalcopyrite. This would seem to suggest that the pyrrhotite zone with its attendant chalcopyrite represents the residual liquid phase, rather than the cumulate phase. It is not obvious at present whether and how this dilemma can be resolved.

Another possible explanation (J.M. Duke, personal communication) is that the blebs have developed their MAP by diffusion under the steep thermal gradient which might be expected in a cooling lava flow. After complete crystallization of the sulphide droplet to a virtually monomineralic assemblage of mss, nucleation and exsolution of pentlandite would begin at the cool end of each bleb (presumably the top). With continued cooling, the constituents of pentlandite contained in mss at the hot end of the bleb, rather than nucleating in situ, would diffuse toward, and precipitate on the previously nucleated pentlandite at the cool end of the bleb. The end result of this high temperature diffusion-exsolution would be blebs consisting of mainly pentlandite at the cool end and mss at the hot end. By this model, the chalcopyrite observed in the pyrrhotite zone could be explained as an exsolution product from mss which is known to dissolve significant amounts of Cu (about 5% at 700°C in the Cu-Fe-S system, Yund and Kullerud, 1966).

Other potential gradients (beside gravitational and thermal), e.g., magnetic or electrical, seem rather unlikely mechanisms of reproducing the observed MAP.

The genesis of magnetite in the sulphide blebs is not clear. It could result from crystallization of an original oxide component in the sulphide liquid, or it could represent a subsequent alteration of the crystallized sulphide (or some combination). The relatively constant proportion of magnetite in the blebs might argue weakly for an original sulphide-oxide liquid, whereas the similar proportions of magnetite in both pyrrhotite and pentlandite zones could support an alteration origin.

Further Work

Attempts should be made to identify more such blebs with MAP in drill core from this deposit that can be oriented with respect to recognizable stratigraphic facing. It is hoped that this will demonstrate whether it is the pyrrhotite zone or the pentlandite zone that represents the tops of the blebs.

On the experimental side, a more detailed knowledge of phase relations should permit a firmer genetic interpretation of the MAP in the sulphide blebs that is also consistent with the field evidence for stratigraphic facing.

References

- Comba, C.D.A.
1972: The Dundonald deposit of nickel sulphides; B.Sc. thesis, Queen's University, Kingston, Ontario.
- Craig, J.R. and Kullerud, G.
1969: Phase relations in the Cu-Fe-Ni-S system and their application to magmatic ore deposits; in Magmatic Ore Deposits, ed. H.D.B. Wilson, Economic Geology Monograph 4, p. 344-358.
- Kullerud, G., Yund, R.A., and Moh, G.H.
1969: Phase relations in the Cu-Fe-S, Cu-Ni-S, and Fe-Ni-S systems; in Magmatic Ore Deposits ed. H.D.B. Wilson, Economic Geology Monograph 4, p. 323-343.
- Muir, J.E. and Comba, C.D.A.
1979: The Dundonald deposit: an example of volcanic-type nickel-sulfide mineralization; Canadian Mineralogist, v. 17, p. 351-359.
- Yund, R.A. and Kullerud, G.
1966: Thermal stability of assemblages in the Cu-Fe-S system; Journal of Petrology, v. 7, p. 454-488.

THEORETICAL ASPECTS OF ENHANCEMENT COEFFICIENTS IN X-RAY SPECTROMETRY

Project 600307

G.R. Lachance and R.M. Rousseau
Central Laboratories and Administrative Services Division

The search for simpler algorithms to correct for inter-element effects using influence coefficients that retain maximum physical meaning is continuing. Although alpha coefficients can deal adequately with absorption situations, strong enhancement in multi-element systems continue to present minor but annoying difficulties. A most promising solution to this problem is envisaged and is currently being investigated.

The application of the single alpha coefficient model, in which enhancement is treated as negative absorption, to complex systems covering wide ranges of concentration led to the introduction of second order coefficients and also to "crossed" coefficients. The latter, based on corrections involving the products of weight fractions taken in pairs, have been viewed with reluctance by most X-ray analysts. Another approach, the introduction of separate empirical coefficients to deal exclusively with enhancement, has met a similar fate. It was subsequently shown (Tertian, 1973) that crossed coefficients are negligible in cases involving absorption only, provided the binary alpha coefficients are computed at the proper level. A comprehensive algorithm based on this premise was proposed by Lachance and Claisse (1979).

In reviewing the derivation of coefficient models that involve the least approximations, the following equation (Rousseau, 1970)

$$W_i = R_i \left[\frac{1 + \sum_j W_j \alpha_{ij}}{1 + \sum_j W_j \rho_{ij}} \right] \quad (1)$$

- where W_i = weight fraction analyte
- R_i = relative intensity versus pure analyte
- W_j = weight fraction matrix element
- α_{ij} = a coefficient quantifying absorption effects
- ρ_{ij} = a coefficient quantifying enhance effects

represents what might be considered a "natural" form for inter-element corrections. The effect of absorption and enhancement is separated, ρ is equal to zero if there is no enhancement, the derivation is strictly rigorous, and a very simple form is retained. The stumbling block at the practical level rests in the fact that, even in binary systems, ρ coefficients vary over a fairly wide range of values and cannot be approximated by a constant.

Considering the processes involved, it is possible to infer that if the absorption portion of the effect is "isolated" when dealing with a binary system in which the analyte i is enhanced by element j , the remaining enhancement portion (as a first approximation) should be related to intensity of the enhancer, R_j . This indicates that the enhancement corrections in equation (1) may be more amenable if presented as products of coefficients times relative intensities, and leads to the simple transformation whereby the influence coefficient model takes the form

$$W_i = R_i \left[\frac{1 + \sum_j W_j \alpha'_{ij}}{1 + \sum_j R_j \rho'_{ij}} \right] \quad (2)$$

where α'_{ij} was defined (Lachance and Claisse, 1979) and ρ'_{ij} is the bracketed term in the expression

$$1 + \sum_j \left(\frac{W_j \rho_{ij}}{R_j} \right) R_j$$

Preliminary investigations do indicate that ρ' coefficients remain virtually constant for the complete range of concentrations. A comprehensive study is underway to establish the overall application of this concept and to evaluate the mode and extent of the variation of ρ' in going to complex systems involving absorption/enhancement and enhancement/enhancement.

References

Lachance, G.R. and Claisse, Fernand
1979: A comprehensive alpha coefficient algorithm, in Abstracts Twenty-Eight Annual Conference Applications of X-ray Analysis, July 29-August 3, Denver, Colorado.

Rousseau, Richard M.
1970: Correction numérique de l'effet de rehaussement en fluorescence X; M.Sc. Thesis, Université Laval, Québec, Canada.

Tertian, R.
1974: Concerning interelement crossed effects in X-ray fluorescence analysis; X-Ray Spectrometry, v. 3, p. 102.

DISCUSSIONS AND COMMUNICATIONS

DISCUSSIONS ET COMMUNICATIONS

A THEORETICAL ESTIMATION OF ION MOBILITIES THROUGH GLACIOLACUSTRINE SEDIMENTS – DIFFUSION DOWN A CONCENTRATION GRADIENT: DISCUSSION

J.S. Colville
Soils Division
CSIRO
Private Bag No. 2,
P.O. Glen Osmond, South Australia 5064

Smee (1979) discussed the upward migration of ions from a mineral sulphide formation buried beneath a layer of clay. This note concerns his mathematical formulation and suggests that much less migration occurs.

Following Smee the convection of ions by water moving down the clay profile is neglected in comparison with diffusion. This would be valid if the particle size and water flux are sufficiently small. The water in the clay profile can then be regarded as almost in static equilibrium. Let θ be the volumetric water content of the soil and let c be the ionic concentration in the soil water at a height z above the till layer which acts as a reservoir for the ions released by the sulphide formation. Following Olsen and Kemper (1968) the approximate linearized description of the system is

$$b \frac{\partial c}{\partial t} = (b' + \theta) \frac{\partial c}{\partial t} = D_p \frac{\partial^2 c}{\partial z^2} \quad (1)$$

where t is the time, b' is the soil 'capacity factor' and D_p is the diffusion coefficient in the porous material.

The term b' represents the influence of ionic adsorption by the clay minerals. Numerical values of b' are obtained from the slope of the isothermal adsorption curves and will depend upon the nature of the ion as well as the mineral type, its particle size and the presence of other ions, especially hydrogen ions. Only approximate values therefore can be quoted, but for most cations $b' \gg \theta$.

Tiller et al. (1972) published adsorption isotherms for zinc in a range of soils, from which values of b' between 6 and 250 can be calculated. Udo et al. (1970) used slightly more concentrated solutions for which $b' \approx 10$ for a loam soil. Phillips et al. (1972) measured the adsorption of copper on kaolinite and montmorillonite, for which $b' \approx 10$ and 50 respectively.

The diffusion coefficient D_p will depend upon θ and hence upon z . For a heavy clay θ will be very close to the saturation value for any water tension less than 10 m of water. Here the maximum clay height L is only 500 cm. For lighter clays θ could decrease significantly e.g. at only 3 m of water tension. Therefore it would be prudent to use throughout the clay a constant value D_p appropriate for the top of the clay horizon because this region will limit the whole diffusion process.

Porter et al. (1960) measured the diffusivity of chloride ions in several clays. Chloride ions are adsorbed very slightly by clay and hence their data can be interpreted as $D_p/(\theta D_0)$ where D_0 is the diffusion coefficient in free water.

Using $\theta=0.2$ in their results for a clay loam, $D_p \approx 2 \times 10^{-2} D_0$, and using $\theta=0.35$ for a clay, $D_p \approx 7 \times 10^{-2} D_0$. It is assumed that this holds for all ions. Their is insufficient information to justify any modification of equation (1) to include the change of D_p with z .

For a solution of equation (1), Smee quoted Garrels et al. (1949) who in turn had taken a solution derived for the conditions

$$C(z,0) = C_0 \quad \left. \begin{array}{l} -\infty < z < 0 \\ = 0 \quad 0 < z < \infty \end{array} \right\} \quad (2)$$

and accordingly the height L of the clay above the till layer does not occur explicitly in Smee's equation 3. There is the further complication that Garrels et al. (1949) had misquoted their source and their version could predict negative concentrations. The correct solution of equation (1) with equation (2) is given by Crank (1975, p. 14).

In his discussion Smee assumes firstly, that when the clay layer was deposited over the till it held none of the ions, secondly, that the till layer contains a constant concentration of the various ions, and thirdly, that any ions which reach the top of the clay are adsorbed by the A horizon as some insoluble compound. Hence the relevant boundary conditions are

$$\left. \begin{array}{l} C(z,0) = 0 \quad z > 0 \\ C(0,t) = C_0 \quad t \geq 0 \\ C(L,t) = 0 \quad t \geq 0 \end{array} \right\} \quad (3)$$

The solution of equation (1) subject to equation (3) is

$$\frac{C(z,t)}{C_0} = \frac{L-z}{L} + \frac{2}{\pi} \sum_{n=1}^{\infty} \frac{(-1)^n}{n} \sin\left(\frac{n\pi(L-z)}{L}\right) \exp\left(-\frac{n^2\pi^2 t D_p}{L^2} \frac{1}{b}\right) \quad (4)$$

which approaches the steady state asymptotically with time.

The calculation of flux at the top of the clay has better physical basis than has any calculation of range of migration. From equation (4) the instantaneous flux will be

$$\frac{D_p C_0}{L} \left[1 + 2 \sum_{n=1}^{\infty} (-1)^n \exp(-n^2\pi^2 t D_p / (bL^2)) \right]$$

and hence the total adsorption of ions from zero time to t will be

$$Q = t D_p C_0 f(\eta) / L \quad (5)$$

$$\text{where } f(\eta) = 1 - \frac{2}{\pi^2 \eta} \sum_{n=1}^{\infty} \frac{(-1)^n}{n^2} \left\{ \exp(-n^2\pi^2 \eta) - 1 \right\}$$

and the dimensionless variable $\eta \equiv t D_p / (bL^2)$. For large η this reduces to $Q \approx t D_p C_0 / L - b C_0 L / 6$. For small η , $f(\eta)$ converges slowly and becomes very small as shown in Table 1.

Table I

η	f
0.010	5.93×10^{-12}
0.015	2.94×10^{-8}
0.020	2.14×10^{-6}
0.025	2.85×10^{-5}
0.030	1.61×10^{-4}
0.035	5.61×10^{-4}
0.040	1.44×10^{-3}
0.045	2.99×10^{-3}
0.050	5.39×10^{-3}
0.060	1.31×10^{-2}
0.080	4.01×10^{-2}
0.100	7.89×10^{-2}
0.200	3.07×10^{-1}
0.300	4.79×10^{-1}
0.400	5.93×10^{-1}
0.500	6.70×10^{-1}
0.600	7.23×10^{-1}
0.800	7.92×10^{-1}
1.000	8.33×10^{-1}
5.000	9.67×10^{-1}

Assuming $D_p = 2 \times 10^{-2} D_o$ and using the given information that $t = 2.5 \times 10^{11}$, $L = 5 \times 10^2$ and that the A horizon is 100 cm thick and has a density of 1 gm/cm^3 , then the average or uniform concentration of the adsorbed ion in the A horizon becomes

$$\bar{c} = 10^5 C_o D_o f(2 \times 10^4 D_o/b).$$

Values of C_o and D_o are given by Smee (1979) in Tables 55.2 and 55.1 respectively but values of b must be assumed. The calculated concentrations are

Copper $\bar{c} = 3 \times 10^{-14}$ ppm if $b = 10$ cf. Smee 1.14 ppm
 Zinc $\bar{c} = 1.5 \times 10^{-13}$ ppm if $b = 10$ cf. Smee 3.65 ppm
 Chloride $\bar{c} = 12$ ppm if $b = 0.5$ cf. Smee 123 900 ppm

For a heavy clay, using $D_p = 7 \times 10^{-2} D_o$ the concentrations will increase to 1×10^{-5} ppm, 5×10^{-5} ppm, and 60 ppm respectively.

The conclusion is that diffusion cannot supply the quantities of ions calculated by Smee (1979) in Tables 55.7 and 55.8. Even smaller values of \bar{c} would be obtained if larger, but quite reasonable values of b were assumed. Smee's values must be queried because they exceed the limit $t D_p C_o / L$.

If the clay was thinner there would be an explicit increase in the final concentration gradient and η . Also for a light clay there would be an increase in the minimum value of θ and hence in D_p . Using $L = 250$ (cm) and $D_p = 0.1 D_o$ then $\bar{c} = 10^6 C_o D_o f(4 \times 10^5 D_o/b)$ and with the same values of b as before, the concentrations of copper, zinc and chloride become 0.015 ppm, 0.075 ppm and 196 ppm, respectively.

References

- Crank, J.
 1975: The Mathematics of Diffusion; Clarendon Press Oxford.
- Garrels, R.M., Dreyer, R.M., and Howland, A.L.
 1949: Diffusion of ions through intergranular spaces in water-saturated rocks; Geological Society of America Bulletin, v. 60, no. 12, p. 1809-1828.
- Olson, S.R. and Kemper, W.D.
 1968: Movement of nutrients to plant roots; Advances in Agronomy, v. 20, p. 91-151.
- Phillips, R.E., Barnhisel, R.J., and Ellis, J.H.
 1972: Percentage of copper diffusing in the adsorbed and electrolytic solution phase in kaolinite and montmorillonite; Soil Science Society of America Proceedings, v. 36, p. 35-39.
- Porter, L.K., Kemper, W.D., Jackman, R.D., and Stewart, B.A.
 1960: Chloride diffusion in soils as influenced by moisture content; Soil Science Society of America Proceedings, v. 24, p. 460-463.
- Smee, B.W.
 1979: A theoretical estimation of ion mobilities through glaciolacustrine sediments: Diffusion down a concentration gradient; in Current Research, Part A, Geological Survey of Canada, Paper 79-1A, p. 367-374.
- Tiller, K.G., Honeysett, J.L. and de Vries, M.P.C.
 1972: Soil zinc and its uptake by plants; Australian Journal of Soil Research, v. 10, p. 165-182.
- Udo, E.J., Bohn, H.L. and Tucker, T.C.
 1970: Zinc adsorption by calcareous soils; Soil Science Society of America Proceedings, v. 34, p. 405-407.

NOTE TO CONTRIBUTORS

Submissions to the *Discussion* section of *Current Research* are welcome from both the staff of the Geological Survey and from the public. Discussions are limited to 6 double-spaced typewritten pages (about 1500 words) and are subject to review by the Chief Scientific Editor. Discussions are restricted to the scientific content of Geological Survey reports. General discussions concerning branch or government policy will not be accepted. Illustrations will be accepted only if, in the opinion of the editor, they are considered essential. In any case no redrafting will be undertaken and reproducible copy must accompany the original submissions. Discussion is limited to recent reports (not more than 2 years old) and may be in either English or French. Every effort is made to include both *Discussion* and *Reply* in the same issue. *Current Research* is published in January, June and November. Submissions for these issues should be received not later than November 1, April 1, and September 1 respectively. Submissions should be sent to the Chief Scientific Editor, Geological Survey of Canada, 601 Booth Street, Ottawa, Canada, K1A 0E8.

Avis aux auteurs d'articles

Nous encourageons tant le personnel de la Commission géologique que le grand public à nous faire parvenir des articles destinés à la section discussion de la publication Recherches en cours. Le texte doit comprendre au plus six pages dactylographiées à double interligne (environ 1500 mots), texte qui peut faire l'objet d'un réexamen par le rédacteur en chef scientifique. Les discussions doivent se limiter au contenu scientifique des rapports de la Commission géologique. Les discussions générales sur la Direction ou les politiques gouvernementales ne seront pas acceptées. Les illustrations ne seront acceptées que dans la mesure où, selon l'opinion du rédacteur, elles seront considérées comme essentielles. Aucune retouche ne sera faite aux textes et dans tous les cas, une copie qui puisse être reproduite doit accompagner les textes originaux. Les discussions en français ou en anglais doivent se limiter aux rapports récents (au plus de 2 ans). On s'efforcera de faire coïncider les articles destinés aux rubriques discussions et réponses dans le même numéro. La publication Recherches en cours paraît en janvier, en juin et en novembre. Les articles pour ces numéros doivent être reçus au plus tard le 1^{er} novembre, le 1^{er} avril et le 1^{er} septembre respectivement. Les articles doivent être renvoyés au rédacteur en chef scientifique: Commission géologique du Canada, 601, rue Booth, Ottawa, Canada, K1A 0E8.

AUTHOR INDEX

	Page		Page
Anderson, R.G.	37	Jackson, G.D.	319
Armstrong, R.L.	27	Jenner, G.A.	339
Atkinson, M.L.	119	Kamineni, D.C.	369,379
Attoh, K.	101	Kennedy, D.P.	235
Baragar, W.R.A.	89	Kerswill, J.A.	271
Barnes, C.R.	209	Lachance, G.R.	390
Beakhouse, G.P.	57	Lamontagne, C.G.	89
Bell, I.	157	Leaming, S.	349
Bielecki, J.	95	LeCheminant, A.N.	339
Booth, G.W.	339	Lichtblau, A.P.	69
Bostock, H.H.	153	Mackay, J. Ross	287
Brown, P.A.	369,379	Mansy, J.L.	33,351
Brown, R.L.	47	Maurice, Y.T.	125
Card, K.D.	61	Mayr, Ulrich	209
Casey, J.J.	356	McArthur, M.L.	363
Chandler, F.W.	125	McIntyre, D.J.	197
Charbonneau, B.W.	125	McNutt, R.H.	57
Ciesielski, A.	125	Miller, A.R.	271,339
Coe, Kenneth	61	Murray, M.J.	339
Colville, J.S.	391	Owen, Victor	137
Conaway, J.G.	77	Pajari, G.E., Jr.	115
Costachuk, S.M.	241	Percival, J.A.	61
Cousens, B.	95	Pickerill, R.K.	115
Currie, K.L.	115	Poulton, T.P.	187
Day, T.J.	281	Read, P.B.	19
Dimroth, E.	69,137	Rimsaite, J.	253
Dunning, G.R.	227	Rousseau, R.M.	390
Easton, R.M.	171	Saif, S.I.	309
Eckstrand, O.R.	385	St-Onge, M.R.	171,179
Edlund, S.A.	329	Scarfe, C.M.	356
Egginton, P.A.	265	Schulze, D.E.	171
Emslie, R.F.	95	Sinha, A.K.	293
Erdman, L.R.	27	Souther, J.G.	1
Fawcett, J.J.	335	Stone, Denver	369,379
Fritz, W.H.	41	Sutcliffe, R.H.	335
Froese, E.	53	Tempelman-Kluit, Dirk	357
Gabrielse, H.	27,33,347,348	Thivierge, R.H.	379
Gadd, N.R.	375	Thompson, P.H.	165
Gauthier, Claude	377	Tilley, B.J.	319
Godfrey, S.C.	217	Tipnis, R.S.	209,363
Godwin, C.I.	363	Tippett, C.R.	147
Gordon, T.M.	301	Tirrul, R.	157
Gordey, S.P.	353	Tozer, E.T.	107
Grasty, R.L.	133	Uyeno, T.T.	209
Grotzinger, J.	171	Wanless, R.K.	27
Hamblin, C.	95	Watkinson, D.H.	119
Harper, J.R.	13	White, S.	125
Henderson, J.B.	165	Williams, H.	217
Henderson, J.R.	147	Woussen, Gerard	137
Herd, R.K.	227		
Hoffman, P.F.	171,179,183,223		
Iannelli, T.R.	319		
Ioannides, N.S.	197		

